

Cumulative Habilitation
Faculty of Science, University of Bern

Spatio-Temporal Dynamics and Drivers of Flood Risk Change

Perspectives of Coupled Component Models

Andreas Paul Zischg
Dr.rer.nat.

Bern, October 2018

Contents

Summary	1
1 Introduction	5
2 Overview and structure	11
3 Spatio-temporal dynamics and drivers of flood risk change	15
3.1 <i>Data-driven analyses of environmental and socio-economic change</i>	15
3.1.1 Analyzing environmental changes related to flood risk	15
3.1.2 Analyzing socio-economic changes related to flood risk	18
3.2 <i>Paving the ground: Model development</i>	23
3.3 <i>Synthesizing: Model coupling</i>	27
4 Concluding remarks: Perspectives of coupled component models	33
4.4 <i>Perspectives of model coupling across scales for analyzing the spatio-temporal dynamics and drivers of flood risk change</i>	33
4.5 <i>Perspectives of coupled component models for simulating interactions between humans and the natural environment</i>	35
4.6 <i>Perspectives of coupled component models in hydrology</i>	37
4.7 <i>Outlook for future research: The human dimension of hydrological change</i>	39
5 Papers	43
5.1 <i>Data-driven analyses of environmental and socio-economic change</i>	43
5.2 <i>Paving the ground: Model development</i>	199
5.3 <i>Synthesizing: Model coupling</i>	365
5.4 <i>Concluding remarks: Perspectives of coupled component modelling</i>	513
6 References	549

Summary

Spatio-Temporal Dynamics and Drivers of Flood Risk Change. Perspectives of Coupled Component Models

Extreme floods are one of the most damaging natural hazards, accounting for the majority of all economic losses from natural hazards worldwide. Several intertwined natural and anthropogenic drivers influence flood risk and its change: global warming, precipitation patterns, flood triggering processes, river morphology, river engineering works, population and values at risk, and flood risk reduction strategies. Sustainable flood risk management requires understanding all aspects of flood risk and its change in space and time. Thus, flood risks must be analyzed from a dynamic rather than a static perspective. However, methods to analyze and quantify environmental and socio-economic changes related to flood risk, both in space and time, are nearly not existent.

The main motivation of this cumulative habilitation thesis has been to examine and develop methods that allow the analysis of past and future changes in both the natural and human environment with a spatially explicit perspective, and methods that allow disentangling the different drivers of change that are mostly interwoven and have opposing effects on flood risk evolution. The cumulative habilitation extends the frontiers of research on flood risk changes with three main methodological approaches: (1) data-driven analyses of environmental and socio-economic change, (2) development of models for specific aspects of flood risk, and (3) model coupling.

Data-driven analyses of environmental and socio-economic change

In the first section, the thesis summarizes publications about empirical and data-driven analyses of ongoing environmental and socio-economic changes related to flood risk. The main focus is on the use of newly available spatio-temporal data. Regarding the analyses of environmental changes, the summarized work shows that changes in the periglacial high alpine environment are relevant for the evolution of flood risks in the valley floors, even though the hazard triggering areas are remote from the flooded locations. Beside the environmental changes that alter the disposition and triggering of natural hazards, the increasing values at risk play an important role in the evolution of flood risk. For the analyses of socio-economic changes, I provide a summary of my research related to long- and short-term changes in the elements at risk. The data-driven analyses clearly show that newly available data such as the residential register and insurance claim data proved to be a valuable basis for analyzing the effects of socio-economic change on flood risk. However, data-driven approaches do not allow the disentanglement of co-evolutionary dynamics in both environmental and socio-economic changes.

Paving the ground: Model development

In the second section, methods are applied to develop models for analyzing specific aspects of the spatio-temporal dynamics of flood risk change. I developed and evaluated specialized models that provide the basis for a full model chain for flood risk research: models for estimating the values at risk, models for linking the outcomes of inundation models with exposed buildings, vulnerability functions, models for simulating surface water floods and pluvial floods, and models for predicting large wood volumes and dynamics in rivers. Secondary aspects were the development of validation methods based on insurance claim data and sensitivity analyses.

Model coupling

The main contribution of this habilitation thesis is the evaluation of the coupled component modelling approach. Coupled component models are composed of specialized disciplinary models (components) representing the parts of a studied system. Coupled models integrate these specialized models to form a model chain that represents a whole system.

One presented example is a coupled component model that represents physical processes in the atmosphere and hydrosphere as well as processes leading to damages to the elements at risk. This coupled component model covers the Aare River basin upstream of Bern, Switzerland. This model chain was set up in a multi-model framework at the component level, enabling us to analyze uncertainties of the full model chain and disentangle the effects of selected drivers of flood risk change. This can be achieved by exchanging one specific disciplinary model at component level with another model. With variations of this coupled component model, we analyzed the effects of the spatio-temporal rainfall pattern, the effects of downscaling methods, the effects of the model coupling setup, the effects of the vulnerability functions, the effects of scale, and the effects of river engineering measures on the estimation of flood losses. Two further coupled component models were presented, one for analyzing the spatio-temporal dynamics of large wood recruitment, transport and deposition in rivers during flood events and another for analyzing social justice of flood risk management strategies. The simulation model for wood dynamics in rivers bases on coupling an inundation model with a tree detection model using remote sensing techniques and a model for simulating wood transport in rivers. The coupled component model for strategy assessment provides the basis for evaluating the long-term effects of different philosophies for prioritizing investments in flood risk prevention on social justice.

Concluding remarks: Perspectives of coupled component models

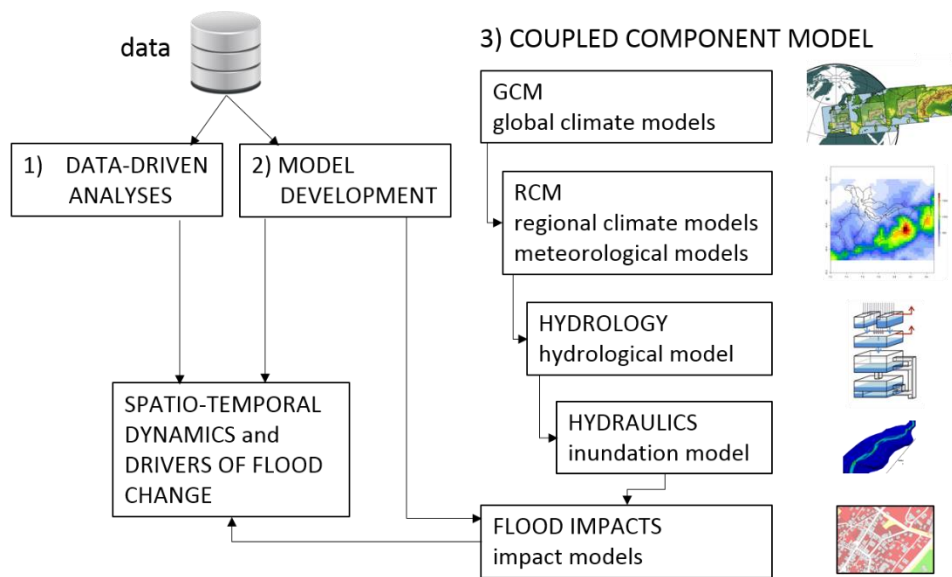
The presented examples of coupled component models allow the analysis of flood risks in their full breadth—from rainfall to damage—and the analysis of isolated effects of selected drivers of flood risk change. The model experiments show that human impacts on hydrology and river morphology increasingly dominate over natural causes of flood risk change over centuries. All

presented model chains connect several temporal and spatial scales. Moreover, coupled component models are able to couple raster-based with vector-based modelling approaches. These two main benefits, coupling across scales and coupling of different modelling approaches into hybrid modelling frameworks, together with the multi-model and multi-temporal approach at component level, allow new study designs for analyzing flood risk change. Only with this setup, is it possible to analyze spatio-temporal dynamics and drivers of flood risk. In the presented cases, this is mainly the human dimension of hydrological change. The multi-model approach at component level leads to a higher interpretability of the results in that it highlights the most sensitive component of a model chain. The targeted high spatial resolution avoid the aggregation and parametrization of local small-scale processes at a coarser spatial resolution required by earth system models. The sensitivity analyses of the presented coupled component models show that the uncertainties do not necessarily propagate decidedly throughout the model chain. This effect can be traced but is not as relevant as suggested by previous work.

Thus, the main hypothesis of this habilitation thesis—that coupled component models provide a robust and reliable framework for analyzing spatio-temporal dynamics and drivers of flood risk change—could be verified. Coupled component models are able to model flood risk change in a spatially-explicit way compared to system dynamics models, that are in most cases spatially lumped models. In contrast to integrated assessment models and earth system models, coupled component models do not require bringing all submodules and processes to common spatial and temporal resolution and can be validated at the component level. Already validated models can be coupled together. As such, coupled component models, even if highly complex, offer a higher level of transparency and reproducibility than integrated assessment models.

The main concluding remark of this habilitation thesis is that coupled component models provide an interesting approach for analyzing flood risk change, for modelling feedback mechanisms between human activities and the natural environment, and for the regionalization of global environmental and socio-economic changes. The habilitation thesis gives an outlook for enabling coupled model frameworks to predict and evaluate the effects of different adaptation strategies on flood risk evolution. Here I showed how model experiments can test alternative pathways of flood risk evolution by assuming specific management strategies. This is supporting the search for robust and sustainable risk management strategies in the context of adaptation to global changes.

Finally yet importantly from a personal perspective, a modelling framework that couples specialist models toward whole-system models offers the potential for obtaining an universalist view and unifying several approaches in geography. Such a holistic approach is supporting the search for sustainable solutions for the complex and interconnected problems we are facing today.



Graphical abstract: Data-driven approaches are used to analyze specific aspects of flood risk change and to develop sub-modules for the model chain. The coupled component model is representing atmospheric, hydrologic, and hydraulic processes and is used to analyze flood impacts and flood risks, as well as spatio-temporal dynamics and drivers of flood risk change.

1 Introduction

Floods are one of the most damaging natural hazards, accounting for the majority of all economic losses from natural hazards worldwide (UNISDR, 2015). Risk resulting from floods is defined as a function of the probability of a flood event or scenario, and its related extent of damage (Fuchs et al., 2005). The latter is computed as a function of the monetary value of the object affected by the flood and its vulnerability against process magnitude.

However, the single factors of the risk formula are evolving in space and time, as is the resulting risk. Consequently, flood risks are being more frequently analyzed from a dynamic rather than from a static perspective (Mazzorana et al., 2012; Merz et al., 2010). Several studies have addressed changes in natural risks over recent decades and centuries (Himmelsbach et al., 2015; Hufschmidt et al., 2005; Paprotny et al., 2018), and research on climate change and its impacts have focused on future changes in risks (Alfieri et al., 2018; Alfieri et al., 2016a; Alfieri et al., 2016b; Alfieri et al., 2015b; Alfieri et al., 2015a; Arnell and Gosling, 2016; Dottori et al., 2018; Feyen et al., 2012; Hirabayashi et al., 2013; Hundecha and Merz, 2012; Kundzewicz et al., 2014). However, most studies focused solely on the future increase in flood hazard. Only few studies consider both the impacts of climatic changes to river flows and the future dynamics in the elements at risk (Bouwer et al., 2010; Jongman et al., 2012; Liu et al., 2015; Löschner et al., 2016; Winsemius et al., 2015). Closer examinations of the spatio-temporal dynamics and the actual rate of change are rather rare. Knowledge about hazardous processes and their impacts, as well as about the trajectories of flood risk changes is essential for the sustainable management of flood risks.

Several intertwined natural and anthropogenic drivers influence the spatio-temporal evolution of flood risk (Zischg et al., 2018d). In this thesis, the following drivers of flood risk change that are related to environmental changes are considered:

- Floods are either caused by direct rainfall on the floodplain (pluvial floods and surface water floods) or rainfall on river catchments resulting in catchment outflow. The latter causes floods in downstream floodplains (riverine floods and lake floods). Consequently, changes in flood processes, i.e., changes in frequency and magnitude of floods in a floodplain, are determined by changing precipitation.
- In mountainous areas, flood hazards are influenced by sediment transport and deposition processes and debris flows. Debris flows are influenced by environmental changes, such as melting of glaciers and permafrost, or changes in weathering processes and mass movements.
- River morphology changes over time, including natural and gradual changes in the river morphology, or disruptive changes by flood events. An important aspect of river morphology changes are anthropogenic interventions, which are relevant drivers of flood risk in a floodplain, for example, the construction of flood defenses such as levees and dams or river restoration projects. However, the construction of levees as flood pro-

tection measures in one floodplain can have adverse effects in the downstream floodplains and can result in flooding trade-offs between upstream and downstream floodplains.

Beside changes in the natural environment, flood risk is also changing due to variations in the exposed elements at risk and their vulnerability. From this aspect, the following drivers of change are considered here (for full references see Zischg et al., 2018d; Zischg, 2018):

- The increase in the elements at risk change due to socio-economic development (Elmer et al., 2012; Fuchs et al., 2015). The growth of settlements and thus the increase of residential buildings is related to population growth.
- Infrastructure is increasing in parallel with population growth. This has wider impacts on the socio-economic system. For example, in economically active areas, floodplains are increasingly occupied by production facilities, as these require relatively flat areas for their construction. With economic development, the elements at risk and the infrastructure in floodplains are increasing both in terms of quantity and monetary value.
- Increasing values at risk compete with opposing drivers of flood risk reduction measures implemented by individuals and the public. Hence, changes in exposure and vulnerability are influenced by governmental interventions and regulations and by the actions of individuals.

The built environment in floodplains, whether the settlement area or the river channel, is subject to changes and co-evolutionary dynamics in both society and nature (Di Baldassarre et al., 2015; Di Baldassarre et al., 2013a). As Vitousek (1997) postulated, the human impact on nature is now considerably larger than at any point in history. This is true for the floodplains, as humans are shaping landscapes with the built environment. These impacts on society on nature influences past and future risk pathways. The spatio-temporal development of these drivers of change in flood risk leads to difficulties in predicting future flood risk. Consequently, recent studies have extended the framework of risk analysis toward a spatio-temporal framework as drivers for flood risk changes are varying in space and time (Ahmad and Simonovic, 2013; Fuchs et al., 2017).

Scope of the cumulative habilitation and research questions

Methods to visualize and quantify changes, both in space and time, are lacking. Thus, the main research questions here include which methods allow analysis of past and future changes in both the natural and human environment with a spatially explicit perspective, and which methods disentangle the different drivers of change that are mostly intertwined and have opposing effects on flood risk evolution (Jonkman, 2013). Therefore, the main problem addressed in this thesis is how to consider the relationship between humans and the natural environment and its change. The main scope of this work was to develop methods for analyzing the spatio-temporal dynamics and drivers of flood risk change.

From the overall research question, additional research questions arose on a more detailed level:

- How can we quantify the effects of environmental changes and socio-economic changes on flood risk?
- Is flood risk constant over time or is flood risk varying in the long-term (centuries) or in the short term (days, hours)?
- Which data and methods are required to analyze past and future developments of flood risk?
- What are the main drivers of changing flood risks?
- Is model coupling suitable for analyzing the spatio-temporal dynamics and drivers of flood risk change?
- Can model coupling overcome the problems of spatially-explicit modelling of processes in dynamical systems?
- Is the coupling of models across spatial and temporal scales feasible?
- How are the uncertainties propagating through the full model chain?
- What is the benefit of coupled component models in a multi-modelling framework?
- Must a coupled model be calibrated as a whole or can the validated submodules be coupled together without a recalibration of the integrated model?
- Does object-based modelling enable considering the connections between geographically distant but teleconnected processes?
- How can human adaptation to floods be integrated in coupled component models for assessing future risk development?

Methods applied

As this thesis focuses on flood risk changes, human-environment relationships and feedback processes had to be considered. Methodologically, there are two main approaches that can be used for analyzing spatio-temporal patterns of flood risk change. One is the empirical and data-driven approach. From these analyses, regression models are produced to project future behavior of coupled human and natural systems from data describing the past. The other is the modelling approach.

As flood risk is composed of many processes and factors, the modelling approach must consider a certain level of complexity. This can be completed using different ways (Kelly et al., 2013; Werner and McNamara, 2007):

Probably the most common approach in modelling coupled human and natural systems is integrated assessment models. In these models, all processes and submodules are incorporated into one model. Integrated assessment models have a common spatial and temporal resolu-

tion for all submodules and processes. This is one of the main limitations of integrated models, as disaggregation and aggregation approaches are needed to convert different processes to the same spatial and temporal scale, complicating validation and calibration. Furthermore, the uncertainties are assumed to propagate through the submodels (Voinov and Shugart, 2013). Earth system models (ESM) (Donges et al., 2018b) are the most prominent representative of this kind of model. ESM are global climate models with the added capability to explicitly represent biogeochemical processes that interact with the physical climate, thereby altering its response to forcing, such as that associated with human-caused emissions of greenhouse gases (Flato, 2011). Giorgi and Avissar (1997) stated that the spatial resolution of ESM is too coarse to capture local heterogeneity effects. Thus, most processes need to be parametrized or considered as sub-grid processes. In addition, surface heterogeneity can lead to dynamic errors in coarse models. This is especially important for the representation of water fluxes (Clark et al., 2015; Nazemi and Wheeler, 2015a, 2015b). Several attempts have extended earth system models with the ability to consider the actions of humans on natural systems (Donges et al., 2018a; Donges et al., 2017; Müller-Hansen et al., 2017; Palmer and Smith, 2014). An overview and future directions of integrated human-earth system modelling was produced by Calvin and Bond-Lamberty (2018).

Another approach for modelling coupled human and natural systems is the system dynamics (SD) approach. This is a computer simulation problem-solving approach with a foundation in the concept of system feedback used to gain insight into real-world system behavior (Neuwirth et al., 2015). SD are based on the first computational experiments of Forrester (1969) and on Luhmann's (1987) system theory. These approaches have been used for conceptualizing human-flood interactions (Di Baldassarre et al., 2013b), vulnerability analyses (Rougé et al., 2015), modelling the feedbacks between flooding and economic growth (Grames et al., 2015), and analysing upstream-downstream trade-offs in the internalization and externalization of flood risks (Roos et al., 2017). However, system dynamic models are, in most cases, lumped models. The ground processes, that is, the spatiotemporal dynamics, are not spatially explicitly modelled. Thus, the outcome is quantitative but aggregated in a lumped variable. Only a few recent studies addressed the spatial discretization of system dynamic models (Neuwirth, 2017; Wingo et al., 2017). In flood risk research, these models either focus on structural changes in flood risks in general (Neuwirth et al., 2015), the management of flood risk (Simonovic, 2009), or disaster management (Simonovic, 2011). These approaches provide a potential for system conceptualization and thus a holistic analysis of floodplains. However, methods are still for incorporating physically-based process models and linking them with other modules towards more complex models.

A third alternative is the coupling of different models. Coupled component models (CCM) are composed of specialized disciplinary models representing parts or processes of a studied system. Coupled models integrate sub-models to form a model chain that represents a whole system (Blair and Buytaert, 2016). CCMs have been hypothesized to be flexible regarding the level of integration, and relatively transparent because the sub-models have mostly been validated in their specific discipline. However, the sub-models often use different spatial and temporal scales, so the bridging of different scales in model coupling is challenging. Another ad-

vantage is that CCM can potentially combine both lumped and spatially explicit models. However, integrating process-based models with socio-environmental models are lacking.

As newly available data arise and disciplinary models advance, I focus here on (1) empirical methods for analyzing environmental and socio-economic changes, (2) the development of models representing specific aspects of flood risk, and (3) the coupling of different disciplinary models for disentangling the effects of selected drivers of flood risk change. Data-driven analyses provide the basis for developing specific models. This is especially true for the development of flood impact models, which consist of models for the values at risk, vulnerability functions, and models for attributing hazard parameters to the values at risk. The coupling of models aims to represent the full chain of natural processes from atmospheric and meteorological processes to hydrologic and hydraulic processes, and finally to the drivers of flood risk change.

A further personal motivation for this thesis is the need for approaches that synthesize relevant scientific progress in the different disciplines of flood risk. Under a reductionist philosophy, all the subdisciplines of hydrology and flood risk research have made relevant progress in developing reliable models for specific and narrow purposes. From a universalist view, this fragmented knowledge has to be compiled and incorporated to meet the requirements of holistic thinking in solving our actual problems, which are often interconnected, complex, and interdisciplinary. Thus, a more philosophical hypothesis is that coupled component modelling frameworks have the potential to unify specialist knowledge and to bring together experts or knowledge from different disciplines for holistically analyzing human and natural systems.

Definitions

Throughout this thesis and the compiled papers, a few terms are repeatedly used. Since these terms are often used in different meanings and frameworks, some definitions are given here.

One of the most used terms is *flood risk*. Flood risk here is defined as the risk resulting from flood hazards and is quantified by the probability of occurrence of a dangerous process and the related degree of damage of objects at risk. The latter is specified by the damage potential (i.e., the monetary and non-monetary value) and the vulnerability of the endangered object (United Nations 2004).

$$R_{ij} = p_{si} * A_{Oj} * p_{Oj,si} * v_{Oj,si} \quad (1)$$

According to this definition, the specifications for the probability of the defined scenario (p_{si}), the monetary value of the object affected by this scenario (A_{Oj}), the probability of exposure of object j to scenario i ($p_{Oj,si}$) and the vulnerability of object j in dependence on scenario i ($v_{Oj,si}$) are required for the quantification of risk (R_{ij}).

As *flood hazards*, the following processes are considered here: riverine floods, lake flooding, floods with sediment transport, debris flows, pluvial floods, and surface water floods.

Elements at risk are defined here as the population, buildings, infrastructure and utilities, economic activities, and environmental values in the area potentially affected by floods. If the values of the elements at risk are quantified, the term *values at risk* is used. The sum of all objects exposed to floods are defined as *exposure*.

Vulnerability is defined here as the degree of loss to a given element at risk resulting from the occurrence of a flood hazard of a given frequency and magnitude. It is expressed on a scale from 0 (no damage) to 1 (total loss) (Fuchs et al., 2007).

Flood risk is changing in space and time. Regarding the temporal scale, I am defining the “*long-term*” time horizon as a centennial scale, ranging from several decades up to three centuries. As “*short-term*” I regard a time scale ranging from minutes to 72 hours, i.e., the intra-event time scale including a short lead time before the triggering of the flood event.

Coupled component models are composed of specialized disciplinary models representing the parts of a studied system. Coupled models integrate sub-models to form a model chain that represents a whole system.

After Tobin and Montz (1994), natural risks are resulting from the interactions between humans and their environment. In several chapter and papers, I am therefore mentioning “coupled human–natural systems” (CHANS). I am using this term in the sense of Liu et al. (2007a), Liu et al. (2007b) and Werner and McNamara (2007), the CHANS approach focuses on simulations of changes in systems by considering feedback mechanisms between human activities and the natural environment.

2 Overview and structure

The cumulative habilitation is structured along three main methodological approaches.

In the first section, the thesis summarizes publications about empirical analyses of ongoing environmental changes and socio-economic changes. Herein, the main focus is the creation and use of newly available spatio-temporal data. For analyses of environmental changes, I summarize work on changes in the periglacial high alpine environment. I studied the relevance of environmental changes in mountainous areas for flood risk in the valley floors. For analyses of socio-economic changes, I summarize studies on the relevance of long- and short-term changes in the elements at risk.

In the second section, data-driven methods are applied to develop models for analyzing specific aspects of the spatio-temporal dynamics of flood risk change. I develop submodules for a full model chain for flood risk research. The developed models are validated and sensitivity analyses are completed.

In the third section, the coupling of different disciplinary models is summarized. The main outcome is a coupled component model that represents physical processes in the atmosphere and in the hydrosphere, as well as processes leading to damage to the elements at risk.

In the conclusion, the limitations and the potential of coupled component modelling frameworks are summarized and discussed. Moreover, an outlook is outlined for extending coupled component models with models that consider human interactions with the environment.

The structure of this thesis can also be viewed from the perspective of the risk formula, beginning with environmental factors leading to changes in hazards and socio-economic factors that are relevant for changes in exposure and vulnerability. Figure 1 provides an overview of the structure of the cumulative habilitation thesis.

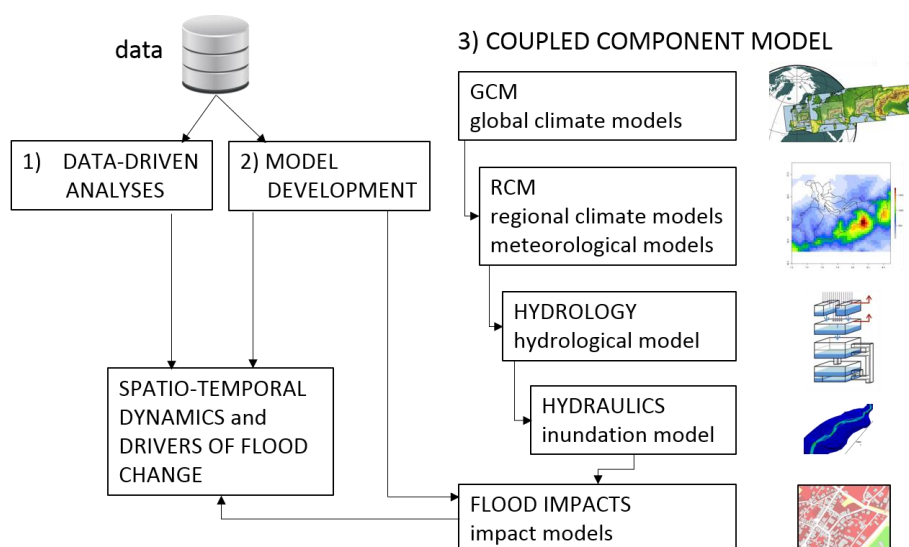


Figure 1: Data-driven approaches are used to analyze specific aspects of flood risk change and to develop sub-modules for the model chain. The coupled component model is representing atmospheric, hydrologic, and hydraulic processes and is used to analyze flood impacts and flood risks, as well as spatio-temporal dynamics and drivers of flood risk change.

The following list provides an overview of the publications contributing to the cumulative habilitation thesis. The publications are ordered along the structure described above.

#	paper	contribution	citations
1. Data-driven analyses of environmental and socio-economic change			
1	Cremonese, E., Gruber, S., Phillips, M., Pogliotti, P., Boeckli, L., Noetzli, J., Suter, C., Bodin, X., Crepaz, A., Kellerer-Pirklbauer, A., Lang, K., Letey, S., Mair, V., Morra di Cella, U., Ravelin, L., Scapozza, C., Seppi, R., Zischg , A., 2011. Brief Communication: "An inventory of permafrost evidence for the European Alps". <i>The Cryosphere</i> 5, 651–657. 10.5194/tc-5-651-2011.	project management, writing, method development	Google Scholar: 38 Scopus: 24
2	Kenner, R., Chinellato, G., Iasio, C., Mosna, D., Cuozzo, G., Benedetti, E., Visconti, M.G., Manunta, M., Phillips, M., Mair, V., Zischg , A., Thiebes, B., Strada, C., 2016. Integration of space-borne DInSAR data in a multi-method monitoring concept for alpine mass movements. <i>Cold Regions Science and Technology</i> 131, 65–75. 10.1016/j.coldregions.2016.09.007.	analysis, writing	Google Scholar: 3 Scopus: 3
3	Sattler, K., Keiler, M., Zischg , A., Schrott, L., 2011. On the Connection between Debris Flow Activity and Permafrost Degradation: A Case Study from the Schnalstal, South Tyrolean Alps, Italy. <i>Permafrost and Periglacial Processes</i> 22, 254–265. 10.1002/ppp.730	data preprocessing, supervision	Google Scholar: 30 Scopus: 20
4	Röthlisberger, V., Zischg , A., Keiler, M., 2017. Identifying spatial clusters of flood exposure to support decision making in risk management. <i>Science of The Total Environment</i> 598, 593–603. 10.1016/j.scitotenv.2017.03.216.	method development, supervision	Google Scholar: 19 Scopus: 17
5**	Fuchs, S., Keiler, M., Zischg , A., 2015. A spatiotemporal multi-hazard exposure assessment based on property data. <i>Natural Hazards and Earth System Sciences</i> 15, 2127–2142. 10.5194/nhess-15-2127-2015.	data proc., analysis, method dev., writing	Google Scholar: 51 Scopus: 39
6	Röthlisberger, V., Zischg , A., Keiler, M., 2016. Spatiotemporal aspects of flood exposure in Switzerland. <i>E3S Web Conf.</i> 7, 8008. 10.1051/e3sconf/20160708008.	method dev., data proc., supervision	Google Scholar: 8 Scopus: 5

Overview and structure

7**	Fuchs, S., Röthlisberger, V., Thaler, T., Zischg, A. , Keiler, M., 2017. Natural Hazard Management from a Coevolutionary Perspective: Exposure and Policy Response in the European Alps. <i>Annals of the American Association of Geographers</i> 107, 382–392. 10.1080/24694452.2016.1235494.	data proc., analysis, method dev., writing	Google Scholar: 32 Scopus: 24
8	Armbruster, S., Hintermann, B., Zischg, A. , 2018. The effects of flood events on land and housing value: Evidence from the Swiss real estate market: SURED 2018 - Monte Verità Conference on Sustainable Resource Use and Economic Dynamics, June 3-7, 2018, Ascona/Switzerland. ETH Zurich, Zurich, 39 pp.	data proc., analysis, writing	Google Scholar: 0 Scopus: 0
9	Keiler, M., Zischg, A. , Fuchs, S., Hama, M., Stötter, J., 2005. Avalanche related damage potential - changes of persons and mobile values since the mid-twentieth century, case study Galtür. <i>Natural Hazards and Earth System Sciences</i> 5, 49–58. 10.5194/nhess-5-49-2005.	method development, data processing	Google Scholar: 62 Scopus: 45
10**	Zischg, A. , 2016. River corrections and long-term changes in flood risk in the Aare valley, Switzerland. <i>E3S Web Conf.</i> 7, 11010. 10.1051/e3sconf/20160711010.	method dev., analysis, writing	Google Scholar: 2 Scopus: 2

** key publications of this thesis

2. Paving the ground: Model development			
11	Röthlisberger, V., Zischg, A. , Keiler, M., 2018. Comparison of building value models for flood risk analysis. <i>Natural Hazards and Earth System Sciences</i> 18, 2431–2453. 10.5194/nhess-2017-442.	supervision, co-writing	Google Scholar: 0 Scopus: 0
12	Papathoma-Köhle, M., Zischg, A. , Fuchs, S., Glade, T., Keiler, M., 2015. Loss estimation for landslides in mountain areas – An integrated toolbox for vulnerability assessment and damage documentation. <i>Environmental Modelling & Software</i> 63, 156–169. 10.1016/j.envsoft.2014.10.003.	analysis, method dev., co-writing	Google Scholar: 54 Scopus: 43
13	Mosimann, M., Frossart, L., Keiler, M., Weingartner, R., Zischg, A. , in revision. A robust and transferable model for the prediction of flood losses on household contents. <i>Water</i> .	supervision, co-writing	Google Scholar: 0 Scopus: 0
14**	Zischg, A.P. , Mosimann, M., Bernet, D.B., Röthlisberger, V., 2018. Validation of 2D flood models with insurance claims. <i>Journal of Hydrology</i> 557, 350–361. 10.1016/j.jhydrol.2017.12.042.	method dev., analysis, writing	Google Scholar: 6 Scopus: 6
15**	Bermúdez, M., Zischg, A. , 2018. Sensitivity of flood loss estimates to building representation and flow depth attribution methods in micro-scale flood modelling. <i>Natural Hazards</i> 92, 1633–1648. 10.1007/s11069-018-3270-7.	method dev., analysis, writing	Google Scholar: 4 Scopus: 3
16	Bernet, D.; Zischg, A. ; Prasuhn, V.; Weingartner, R., 2018. Modeling the extent of surface water floods in rural areas: lessons learned from the application of various uncalibrated models. <i>Environmental Modelling & Software</i> 109, 134–151, doi:10.1016/j.envsoft.2018.08.005.	method dev., supervision, co-writing	Google Scholar: 0 Scopus: 0
17	Mazzorana, B., Zischg, A. , Largiader, A., Hübl, J., 2009. Hazard index maps for woody material recruitment and transport in alpine catchments. <i>Natural Hazards and Earth System Sciences</i> 9, 197–209. 10.5194/nhess-9-197-2009.	method dev., analysis, writing	Google Scholar: 59 Scopus: 44
18	Mazzorana, B., Hübl, J., Zischg, A. , Largiader, A., 2011. Modelling woody material transport and deposition in alpine rivers. <i>Natural Hazards</i> 56, 425–449. 10.1007/s11069-009-9492-y.	method dev., analysis, writing	Google Scholar: 71 Scopus: 47

** key publications of this thesis

Overview and structure

3. Synthesizing: Model coupling			
19	Zischg, A., Felder, G., Weingartner, R., Gómez-Navarro, J.J., Röthlisberger, V., Bernet, D., Rössler, O., Raible, C., Keiler, M., Martius, O., 2016. M-AARE - Coupling atmospheric, hydrological, hydrodynamic and damage models in the Aare river basin, Switzerland, in: 13th Congress INTERPRAEVENT 2016, 30 May to 2 June 2016, Lucerne, Switzerland. Conference proceedings, 444–451.	principal investigator, method dev., writing	Google Scholar: 2 Scopus: 0
20	Felder, G., Zischg, A., Weingartner, R., 2017. The effect of coupling hydrologic and hydrodynamic models on probable maximum flood estimation. <i>Journal of Hydrology</i> 550, 157–165. 10.1016/j.jhydrol.2017.04.052.	method dev., analysis, co-writing	Google Scholar: 6 Scopus: 6
21**	Zischg, A., Felder, G., Weingartner, R., Quinn, N., Coxon, G., Neal, J., Freer, J., Bates, P., 2018. Effects of variability in probable maximum precipitation patterns on flood losses. <i>Hydrology and Earth System Sciences</i> 22, 2759–2773. 10.5194/hess-22-2759-2018.	method dev., analysis, writing	Google Scholar: 4 Scopus: 2
22**	Zischg, A., Felder, G., Mosimann, M., Röthlisberger, V., Weingartner, R., 2018. Extending coupled hydrological-hydraulic model chains with a surrogate model for the estimation of flood losses. <i>Environmental Modelling & Software</i> , 108, 174–185, doi:10.1016/j.envsoft.2018.08.009.	method dev., analysis, writing	Google Scholar: 1 Scopus: 1
23**	Felder, G., Gómez-Navarro, J.J., Zischg, A., Raible, C.C., Röthlisberger, V., Bozhinova, D., Martius, O., Weingartner, R., 2018. From global circulation to local flood loss: Coupling models across the scales. <i>Science of The Total Environment</i> 635, 1225–1239. 10.1016/j.scitotenv.2018.04.170.	method dev., analysis, writing	Google Scholar: 4 Scopus: 3
24**	Zischg, A., Hofer, P., Mosimann, M., Röthlisberger, V., Ramirez, J.A., Keiler, M., Weingartner, R., 2018. Flood risk (d)evolution: Disentangling key drivers of flood risk change with a retro-model experiment. <i>Science of the Total Environment</i> 639, 195–207. 10.1016/j.scitotenv.2018.05.056.	method dev., analysis, writing	Google Scholar: 1 Scopus: 2
25**	Zischg, A., Galatioto, N.; Deplazes, S.; Weingartner, R.; Mazzorana, B., 2018: Modelling spatiotemporal dynamics of large wood recruitment, transport and deposition at river reach scale during extreme floods. <i>Water</i> 10, 9, 1134. 10.3390/w10091134.	method dev., analysis, writing	Google Scholar: 0 Scopus: 0
26	Staffler, H., Pollinger, R., Zischg, A., Mani, P., 2008. Spatial variability and potential impacts of climate change on flood and debris flow hazard zone mapping and implications for risk management. <i>Natural Hazards and Earth System Sciences</i> 8, 539–558. 10.5194/nhess-8-539-2008.	method dev., analysis, lead author	Google Scholar: 19 Scopus: 12
27	Zischg, A., Schober, S., Sereinig, N., Rauter, M., Seymann, C., Goldschmidt, F., Bäk, R., Schleicher, E., 2013. Monitoring the temporal development of natural hazard risks as a basis indicator for climate change adaptation. <i>Natural Hazards</i> 67, 1045–1058. 10.1007/s11069-011-9927-0.	method dev., analysis, writing	Google Scholar: 20 Scopus: 10

** key publications of this thesis

4. Concluding remarks: Perspectives of coupled component modelling			
28**	Thaler, T., Zischg, A., Keiler, M., Fuchs, S., 2018. Allocation of risk and benefits—distributional justices in mountain hazard management. <i>Regional Environmental Change</i> 18, 353–365. 10.1007/s10113-017-1229-y.	method dev., analysis, writing	Google Scholar: 3 Scopus: 2
29	Zischg, A., 2018. Floodplains and Complex Adaptive Systems—Perspectives on Connecting the Dots in Flood Risk Assessment with Coupled Component Models. <i>Systems</i> 6, 9. 10.3390/systems6020009.	review, writing	Google Scholar: 1 Scopus: 1

** key publications of this thesis

3 Spatio-temporal dynamics and drivers of flood risk change

3.1 Data-driven analyses of environmental and socio-economic change

This section summarizes publications on empirical analyses of ongoing environmental changes and socio-economic changes. Hence, this section is divided in two subsections: the first subsection focuses on environmental changes, and the second subsection focuses on socio-economic changes.

3.1.1 Analyzing environmental changes related to flood risk

Global warming has relevant and visible effects on the high alpine environment (Beniston et al., 2018). The most evident effect is the melting of glaciers. The mostly invisible ground ice in permafrost areas is melting due to climate change. This affects mass movements (Stoffel et al., 2014) and, as a consequence, the sediment delivery of mountain torrents is changing the probability of occurrence and the magnitude of debris flows. Thus, debris flows are expected to increase. However, the effects of a changing cryosphere on floods and debris flows and on flood risks is only partially known. The following papers aim to contribute to closing this gap.

- **Paper 1:** Cremonese, E., Gruber, S., Phillips, M., Pogliotti, P., Boeckli, L., Noetzli, J., Suter, C., Bodin, X., Crepaz, A., Kellerer-Pirklbauer, A., Lang, K., Letey, S., Mair, V., Morra di Cella, U., Ravanel, L., Scapozza, C., Seppi, R., Zischg, A., 2011. Brief Communication: "An inventory of permafrost evidence for the European Alps". *The Cryosphere* 5, 651–657. 10.5194/tc-5-651-2011.
- **Paper 2:** Kenner, R., Chinellato, G., Iasio, C., Mosna, D., Cuzzo, G., Benedetti, E., Visconti, M.G., Manunta, M., Phillips, M., Mair, V., Zischg, A., Thiebes, B., Strada, C., 2016. Integration of space-borne DInSAR data in a multi-method monitoring concept for alpine mass movements. *Cold Regions Science and Technology* 131, 65–75. 10.1016/j.coldregions.2016.09.007.
- **Paper 3:** Sattler, K., Keiler, M., Zischg, A., Schrott, L., 2011. On the Connection between Debris Flow Activity and Permafrost Degradation: A Case Study from the Schnalstal, South Tyrolean Alps, Italy. *Permafrost and Periglacial Processes* 22, 254–265. 10.1002/ppp.730

Paper 1 (Cremonese et al., 2011) described a method for inventorying and harmonizing observations of permafrost occurrence in the European Alps. We developed a standard data model and compiled a unique data set of mapped permafrost evidence for the European Alps. This collection of permafrost evidence not only synthesizes existing data and allows new analyses

based on larger data sets, but also provides complementary information for an improved interpretation of monitoring results. The dataset provided a basis for the development of a geo-statistical model for simulating the spatial distribution of permafrost in the European Alps (Boeckli et al., 2012a, 2012b).

Paper 2 (Kenner et al., 2016) compared different methods for monitoring slope movements in the periglacial environment. In an experimental application at different test sites in the Italian and Swiss Alps, a multi-method measurement and monitoring concept was developed. The following monitoring methods were applied: satellite-borne differential interferometric synthetic aperture radar (DInSAR), terrestrial laser scanning (TLS), and the Global Navigation Satellite System (GNSS). The results of the selected monitoring techniques were compared. TLS proved to be the most reliable and accurate method for monitor an area with a certain extent. The monitoring methods were temporally repeated. Thus, they were able to provide spatio-temporal data for slope movements.

Paper 3 (Sattler et al., 2011) analyzed the role of permafrost degradation in debris flow activity. Based on historic aerial photographs, changes in debris flow initiation areas over time were mapped and the congruence with a modelled permafrost distribution map was analyzed. In the decades from 1980 to 2010, the detected debris flow activity did not appear to be markedly influenced by permafrost degradation. However, debris flow activity increased in steep proglacial areas where the glacier recently retreated. This study shows that environmental changes have to be analyzed over a long time period to reliably assess their effects on natural hazards.

In a further publication (Zischg et al., 2012a), the above-presented methods were synthesized and the relevance of the changing cryosphere for flood risks was estimated. The combination of monitoring results with models for simulating the permafrost distribution and the triggering and runout of debris flows, as well as data for the values at risk (houses and traffic infrastructure), showed that, in a characteristic region of the central Alps, debris flow processes triggered in permafrost areas potentially affect around 1-2% of the settlement area. A total of 20% of all torrent catchments are partially located in permafrost areas. Hence, environmental changes in the high alpine environment are relevant for the evolution of flood risks in the valley floors.

In addition to the literature, the three papers mentioned above provided a basis for the formulation of several outreach documents (Mair et al., 2011; Probst et al., 2013) and guidelines (Zischg et al., 2012b) for managing natural hazards in a changing climate.

Further publications of the author on this section topic:

Bollmann, E., Rieg, L., Spross, M., Sailer, R., Bucher, K., Maukisch, M., Monreal, M., Zischg, A., Mair, V., Lang, K., and Stötter, J.: Blockgletscherkataster in Südtirol - Erstellung und Analyse. In: Stötter, J., Sailer, R. (Eds.), Permafrost in Südtirol. Institut für Geographie Universität Innsbruck, Innsbruck, 147-172, 2012.

Chinellato, G., Iasio, C., Mair, V., Strada, C., Mosna, D., Phillips, M., Kenner, R., and Zischg, A.: Remote and Terrestrial Ground Monitoring Techniques Integration for Hazard Assessment

- and Prediction in Densely Populated Mountain Areas, in: Engineering Geology for Society and Territory - Volume 2: Landslide Processes, Lollino, G., Giordan, D., Crosta, G. B., Corominas, J., Azzam, R., Wasowski, J., and Sciarra, N. (Eds.), Springer International Publishing, Cham, s.l., 379–383, 2015. 10.1007/978-3-319-09057-3_59.
- Kork, J., Mayer, B., Rudolf-Miklau, F., Greminger, P., and Zischg, A.: Climate adaptation and natural hazard management in the Alpine Space. AdaptAlp final report. Bavarian State Ministry of the Environment and Public Health, Munich, 2011.
- Mair, V., Lang, K., Zischg, A., Tonidandel, D., 2012. PROALP und die Erforschung des Permafrosts in Südtirol. In: Stötter, J., Sailer, R. (Eds.), Permafrost in Südtirol. Institut für Geographie Universität Innsbruck, Innsbruck, 45-66.
- Mair, V., Zischg, A., Lang, K., Tonidandel, D., Krainer, K., Kellerer-Pirklbauer, A., Deline, P., Schoeneich, P., Cremonese, E., Pogliotti, P., Gruber, S., and Boeckli, L.: PermaNET - Permafrost Long-term Monitoring Network. Synthesis report., INTERPRAEVENT Journal series 1, 3, International Research Society INTERPRAEVENT, Klagenfurt, 2011.
- Probst, T., Wicki, W., Zischg, A., and Pichler, A.: Alpine strategy for adaptation to climate change in the field of natural hazards: Developed by the Platform on Natural Hazards of the Alpine Convention PLANALP, Alpine Convention, Innsbruck, 2013.
- Schoeneich P., Dall'Amico M., Deline P., and Zischg A.: Hazards related to permafrost and to permafrost degradation. PermaNET project - state-of-the-art report WP6.2. ADRA - Association pour la diffusion de la recherche alpine, Grenoble, 2011.
- Sattler, K., Keiler, M., Zischg, A., and Schrott, L., 2007. Development of debris flow activity influenced by climate change in periglacial high mountain areas: Schnalstal, Italy. In: Kellerer-Pirklbauer, A., Keiler, M., Embleton-Hamann, C., Stötter, H. (eds.), Geomorphology for the future, Obergurgl, Austria. Innsbruck University Press, 169-176.
- Stötter, J., Zischg, A., Sailer, R., 2012. Entwicklung des Permafrosts in Südtirol. In: Stötter, J., Sailer, R. (Eds.), Permafrost in Südtirol. Institut für Geographie Universität Innsbruck, Innsbruck, 1-45.
- Zilger, J., Marks, F., Mair, V., Belitz, K., Zischg, A. 2006. PROALP - Kartierung und Überwachung von Permafrost-Phänomenen in den Alpen mit Hilfe Differentieller Radar-Interferometrie. In: Strobl, J., Blaschke, T. & G. Griesebner (eds.): Angewandte Geoinformatik 2006. Beiträge zum 18. AGIT-Symposium Salzburg, Heidelberg, 783-792.
- Zischg, A., Mair, V., 2011. Case studies in the European Alps - Upper Sulden Valley, Ortler Mountains, Italian Alps. In: Kellerer-Pirklbauer, A., Lieb, G., Schoeneich, P., Deline, P., Pogliotti, P. (eds.), Thermal and geomorphic permafrost response to present and future climate change in the European Alps, Graz, pp. 159-169.
- Zischg, A., Mair, V., Tondidandel, D., Lang, K., 2012. Berücksichtigung von Permafrost in der Gefahrenzonenplanung in Südtirol. In: Stötter, J., Sailer, R. (Eds.), Permafrost in Südtirol. Institut für Geographie Universität Innsbruck, Innsbruck, 173-186.

- Zischg, A., Flury, C., Costa, R., Huber, B., Berger, S.: Auswirkungen der landwirtschaftlichen Bewirtschaftung auf die Naturgefahren. Nationale Plattform für Naturgefahren PLANAT, Bern. 154 pp, 2011.
- Zischg, A., Mair, V., and Lang, K.: PROALP - Kartierung und Monitoring von Permafrost in der Autonomen Provinz Bozen Südtirol, Italien. In: Koboltschnig, G., Hübl, J., Braun, J. (Eds.), INTERPRAEVENT 2012 - Proceedings. INTERPRAEVENT, Klagenfurt, 1–12, 2012.
- Zischg, A., Mair, V., Lang, K., Deline, P., Ravanel, L., Schoeneich, P., Kellerer-Pirklbauer, A.: Consideration of permafrost and permafrost degradation in natural hazards assessment. In: Koboltschnig, G., Hübl, J., Braun, J. (Eds.), INTERPRAEVENT 2012 - Proceedings. INTERPRAEVENT, Klagenfurt, 237-246, 2012.
- Zischg, A., Mair, V., Lang, K., 2012. PROALP - Kartierung und Monitoring von Permafrost in der Autonomen Provinz Bozen Südtirol, Italien. In: Koboltschnig, G., Hübl, J., Braun, J. (Eds.), INTERPRAEVENT 2012 - Proceedings. INTERPRAEVENT, Klagenfurt, 421-432.
- Zischg, A., Costa, R., Flury, C., Schild, A., 2012. Einfluss der landwirtschaftlichen Bewirtschaftung auf alpine Naturgefahren - eine zusammenfassende Betrachtung. In: Koboltschnig, G., Hübl, J., Braun, J. (Eds.), INTERPRAEVENT 2012 - Proceedings. INTERPRAEVENT, Klagenfurt, 833-846, 2012.

3.1.2 Analyzing socio-economic changes related to flood risk

Beside the above-mentioned environmental changes that alter the disposition and triggering of natural hazards, the increasing values at risk play an important role in the evolution of flood risk. How fast these changes occur in the values at risk and at which temporal scale these changes have to be studied are rarely known. The following papers focused on the spatio-temporal dynamics of changes in the values at risk. We looked at both the long- and short-term changes in the values at risk. Moreover, the compilation of these papers shows the added value of newly available datasets, such as residential registers and insurance data for answering this research question on the dynamics of change.

- Paper 4: Röthlisberger, V., Zischg, A., Keiler, M., 2017. Identifying spatial clusters of flood exposure to support decision making in risk management. *Science of the Total Environment* 598, 593–603. 10.1016/j.scitotenv.2017.03.216.
- Paper 5: Fuchs, S., Keiler, M., Zischg, A., 2015. A spatiotemporal multi-hazard exposure assessment based on property data. *Natural Hazards and Earth System Sciences* 15, 2127–2142. 10.5194/nhess-15-2127-2015.
- Paper 6: Röthlisberger, V., Zischg, A., Keiler, M., 2016. Spatiotemporal aspects of flood exposure in Switzerland. *E3S Web Conf.* 7, 8008. 10.1051/e3sconf/20160708008.
- Paper 7: Fuchs, S., Röthlisberger, V., Thaler, T., Zischg, A., Keiler, M., 2017. Natural Hazard Management from a Coevolutionary Perspective: Exposure and Policy Response in

the European Alps. *Annals of the American Association of Geographers* 107, 382–392. 10.1080/24694452.2016.1235494.

- Paper 8: Armbruster, S., Hintermann, B., Zischg, A., 2018. The effects of flood events on land and housing value: Evidence from the Swiss real estate market: SURED 2018 - Monte Verità Conference on Sustainable Resource Use and Economic Dynamics, June 3-7, 2018, Ascona/Switzerland. ETH Zurich, Zurich, 39 pp.
- Paper 9: Keiler, M., Zischg, A., Fuchs, S., Hama, M., Stötter, J., 2005. Avalanche related damage potential - changes of persons and mobile values since the mid-twentieth century, case study Galtür. *Natural Hazards and Earth System Sciences* 5, 49–58. 10.5194/nhess-5-49-2005.
- Paper 10: Zischg, A., 2016. River corrections and long-term changes in flood risk in the Aare valley, Switzerland. *E3S Web Conf.* 7, 11010. 10.1051/e3sconf/20160711010.

Papers 4-9 (Röthlisberger et al., 2017; Fuchs et al., 2015; Röthlisberger et al., 2016) have been based on newly available spatio-temporal data: the public official residents register, insurance claim data, and data of changes in properties (selling of land and houses). These data are usually restricted by privacy regulations. However, in an anonymized form, these datasets can be analyzed for scientific research. The data contain the addresses of properties and thus can be georeferenced. Moreover, the data contain information about the type of building, age, and number of residents. Thus, these datasets provide unique opportunities to analyze the spatio-temporal dynamics of exposure to floods by overlaying these data with flood hazard maps.

In paper 4 (Röthlisberger et al., 2017), methods for identifying clusters and hot spots of flood exposure were developed. The identification of hot spots is important for setting national and regional priorities in flood risk management. In this paper, we showed that the aggregation method influences priority setting. As the search for hot spots of exposure in absolute monetary values preferred dense areas in the Swiss Plateau, hot spots of relative exposure, in terms of the share of exposed population to the absolute number of population in aerial units, were mostly found in Alpine and remote areas. In this study, we contribute to the discussion about the prioritization schemes for investments in flood protection.

In contrast to paper 4, paper 5 (Fuchs et al., 2015) provided a methodological basis for analyzing these data from a spatial and a spatio-temporal perspective. Flood exposure was not considered a constant in time, but the temporal dynamics of change in the exposure was the main focus of this research. As a requirement for this analysis, the official data of the residential registers had to be enriched with auxiliary information. In this study, we added further information to these data using data-mining approaches. A crucial point was modelling the values at risk, i.e., the monetary value of each building. While paper 5 used data from Austria, paper 6 (Röthlisberger et al., 2016) used similar data from Switzerland.

In paper 7 (Fuchs et al., 2017), both the Austrian and Swiss datasets were harmonized and the spatio-temporal dynamics of the increasing values at risk were compared for both countries.

Both countries exhibited similar trends in the increase in settlements exposed to floods although having different legislative frameworks for restricting land use in areas at risk. Moreover, paper 7 highlighted the influence of policies on the long-term evolution of flood exposure.

Paper 8 (Armbruster et al., 2018) analyzed the effect of flood hazard information on the prices of houses and land. In this study, we developed a hedonic price model for testing the hypothesis of a fully rational and informed decision of houses prices in relation to the exposure to floods. This paper showed that house prices in hazard areas decline after the occurrence of a flood event with regional relevance. Moreover, the introduction of flood hazard maps into legally binding land use plans increases property prices. These findings provide relevant information for developing models for simulating the long-term effects of adaptation options.

In addition to the focus on long-term dynamics of flood exposure, paper 9 (Keiler et al., 2005) examined short-term fluctuations in values at risk, i.e., diurnal (hourly), weekly, and seasonal fluctuations of persons and mobile values such as cars in hazard areas. This study was based on different datasets: census data, tourism statistics, employment and commuter statistics, and on own mappings and statistics of motor vehicles. It was noted that a long-term increase in the values at risk is overlaid by remarkably short-term fluctuations in the number of persons and cars. Hence, the impact of a natural hazard event depends strongly on the time of day and season. Although this study was related to snow avalanche risk, the findings can be transferred to flood risk research.

Paper 10 (Zischg, 2016) analyzed both the effects of environmental change and socio-economic change (i.e., settlement growth). However, the latter considers the anthropogenic impacts on the river system due to river regulation and river engineering. In a case study of the Aare River basin upstream of Bern, I reconstructed the historic natural states of the rivers before any river engineering measures had been constructed and implemented the resulting digital terrain models in a multi-temporal flood model that represents the historic and the actual state of the river courses. On both hydraulic models, the same flood events were simulated. The extent of the flooded areas and the number of affected houses and inhabitants were compared. Without river corrections, the flooded areas and the number of exposed residential housings would be remarkably higher than observed. This case study shows that the effects of the main river corrections are remarkable for today's economic activities in the floodplains. Hence, the maintenance of the river engineering works is of fundamental importance in flood risk management.

Further Publications by the author on this section topic:

Fuchs, S., Keiler, M., Zischg, A., and Bründl, M., 2005. The long-term development of avalanche risk in settlements considering the temporal variability of damage potential, *Natural Hazards and Earth System Sciences*, 5, 893–901, 2005. 10.5194/nhess-5-893-2005.

Fuchs, S., Keiler, M., Zischg, A., 2008. Multitemporale skalenabhängige Schadenpotenzialanalyse. *Wildbach- und Lawinenverbau*, 158: 149-157.

- Fuchs, S., Zischg, A., and Keiler, M., 2016. Räumliche und zeitliche Exponiertheit von Gebäuden in Österreich, in: 13th Congress INTERPRAEVENT 2016, 30 May to 2 June 2016, Lucerne, Switzerland. Conference proceedings, 503–512.
- Fuchs, S., Keiler, M., and Zischg, A., 2014. A regional analysis of elements at risk exposed to mountain hazards in the Eastern European Alps. In: N. Kazakov (ed.): Third international conference on debris flows: disasters, risk, forecast, protection. Yuzhno-Sakhalinsk: Russian Academy of Sciences. 114-117.
- Keiler, M., Fuchs, S., Zischg, A., Stötter, J., 2004. The adaptation of technical risk analysis on natural hazards on a regional scale. *Zeitschrift für Geomorphologie. Supplementband* 135, 95–110.
- Keiler, M., Sailer, R., Jörg, P., Weber, C., Fuchs, S., Zischg, A., and Sauermoser, S., 2006. Avalanche risk assessment; a multi-temporal approach, results from Galtür, Austria *Natural Hazards and Earth System Sciences*, 6, 637–651, 2006. 10.5194/nhess-6-637-2006.
- Mosimann, M., Thomi, L., Röthlisberger, V., Keiler, M.; Zischg, A., 2017. 1.1 Millionen Menschen leben in der Schweiz in Hochwassergebieten. *Wasser Energie Luft*, 109(3), pp. 191-196. Schweizerischer Wasserwirtschaftsverband.
- Suter, H., Thomi, L., Kern, R., Künzler, M., Gusterer, C., Zischg, A., Weingartner, R., Martius, O., and Keiler, M., 2016. Was macht Hochwasserschutzprojekte erfolgreich? Eine Evaluation von Projektablauf und Risiko basierend auf den Perspektiven Schweizer Gemeinden, in: 13th Congress INTERPRAEVENT 2016, 30 May to 2 June 2016, Lucerne, Switzerland. Conference proceedings, 159–167.
- Thomi, L., Zischg, A., and Suter, H., 2015. Was macht Hochwasserschutzprojekte erfolgreich?: Eine Evaluation der Risikoentwicklung, des Nutzens und der Rolle privater Geldgeber, Geographisches Institut, Bern, 91 S.
- Zischg, A., Macconi, P., Pollinger, R., Sperling, M., Mazzorana, B., Marangoni, N., Berger, E., Staffler, H., 2007. Historische Überschwemmungs- und Murgangereignisse in Südtirol. Erhebung und Dokumentation. *Der Schlern* 3/2007, 4-16, Bozen.
- Zischg, A., 2012. Participative Planning Processes in Flood Risk Management and in Integrated Watershed Management, in: Wong, T.S.W. (Ed.), *Flood risk and flood management*. Nova Science Publishers, Hauppauge, N.Y., 45–66.

3.2 Paving the ground: Model development

This section summarizes publications describing the process of developing, testing, and validating models. The developed models provided the basis (the sub-modules) for the coupled component models described in the next chapter. All the models described here simulate natural processes or describe relationships between natural processes and values at risk. The papers in this section are organized as follows. The first three (11-13) addressed building models and vulnerability functions. The next two in this section (papers 14 and 15) focused on methods for overlaying the outcomes of inundation models with the objects at risk. Paper 16 evaluated different modes for simulating surface water floods and pluvial floods. The last two in this section developed models for predicting large wood volumes and dynamics in rivers.

- Paper 11: Röthlisberger, V., Zischg, A., Keiler, M., 2018. Comparison of building value models for flood risk analysis. *Natural Hazards and Earth System Sciences* 18, 2431–2453. 10.5194/nhess-2017-442.
- Paper 12: Papathoma-Köhle, M., Zischg, A., Fuchs, S., Glade, T., Keiler, M., 2015. Loss estimation for landslides in mountain areas – An integrated toolbox for vulnerability assessment and damage documentation. *Environmental Modelling & Software* 63, 156–169. 10.1016/j.envsoft.2014.10.003.
- Paper 13: Mosimann, M., Frossart, L., Keiler, M., Weingartner, R., Zischg, A., submitted. A robust and transferable model for the prediction of flood losses on household contents. *Water*.
- Paper 14: Zischg, A.P., Mosimann, M., Bernet, D.B., Röthlisberger, V., 2018. Validation of 2D flood models with insurance claims. *Journal of Hydrology* 557, 350–361. 10.1016/j.jhydrol.2017.12.042.
- Paper 15: Bermúdez, M., Zischg, A., 2018. Sensitivity of flood loss estimates to building representation and flow depth attribution methods in micro-scale flood modelling. *Natural Hazards* 92, 1633–1648. 10.1007/s11069-018-3270-7.
- Paper 16: Bernet, D.; Zischg, A.; Prasuhn, V.; Weingartner, R., 2018: Modeling the extent of surface water floods in rural areas: lessons learned from the application of various uncalibrated models. *Environmental Modelling & Software* 109, 134–151, doi:10.1016/j.envsoft.2018.08.005.
- Paper 17: Mazzorana, B., Zischg, A., Largiader, A., Hübl, J., 2009. Hazard index maps for woody material recruitment and transport in alpine catchments. *Natural Hazards and Earth System Sciences* 9, 197–209. 10.5194/nhess-9-197-2009.
- Paper 18: Mazzorana, B., Hübl, J., Zischg, A., Largiader, A., 2011. Modelling woody material transport and deposition in alpine rivers. *Natural Hazards* 56, 425–449. 10.1007/s11069-009-9492-y.

Paper 11 (Röthlisberger et al., 2018) laid the basis for flood exposure and flood risk analyses. We evaluated five different approaches for modelling the values at risk. Four approaches re-

ferred to individual buildings, whereas one was based on values per surface area, differentiated by land use category. The model parameters were estimated using a database of more than half a million building insurance contracts in Switzerland, which were provided by cantonal insurance companies for buildings that operate under a monopoly within the respective Swiss cantons. Comparing the five model results with the directly applied spatially referenced insurance data suggested that models based on individual buildings produce better results than models based on surface area, but only if they include the individual building's volume. In summary, the paper shows the added value of an exposure analysis at the scale of individual objects.

Paper 12 (Papathoma-Köhle et al., 2015) and paper 13 (Mosimann et al., in revision) described the development of vulnerability functions. Paper 12 was based on loss data from several regions in the European Alps and focused on the impacts of debris flows on building structure. The result was a vulnerability function describing the relationship between the magnitude of debris flow and the degree of loss. Instead, paper developed a vulnerability function for household content exposed to floods. This analysis was based on data from a private insurance company. These data provided information about both the loss of building structure and the loss of household content. Thus, this paired dataset provided a unique opportunity for studying the relationship between both types of losses.

As papers 11-13, paper 14 (Zischg et al., 2018e) was also based on insurance claim data. In contrast to the previous papers, the focus here was validating inundation models with insurance data. As the main purpose of coupling meteorological models with hydrologic and hydraulic models is to assess potential flood impacts, a validation method that targets the impact assessment is required. Hence, in this study, we validated the BASEMENT inundation model with insurance data. This is the first time model chains or sub-modules of a model chain for flood impact assessment have been validated with indicators that best represent the main purpose of flood impact analyses, i.e., the identification of objects exposed to a flood scenario. The validation metrics were calculated with two different datasets: a dataset of event documentations reporting flooded areas and a dataset of insurance claims. The model fit relating to insurance claims was slightly lower than the model fit computed based on the observed inundation areas. This comparison between two independent validation data sets suggested that validation metrics using insurance claims can be compared to conventional validation data, such as the flooded area. However, validation on the basis of insurance claims is more conservative in cases where model errors are more pronounced in areas with a high density of values at risk.

Paper 15 (Bermúdez and Zischg, 2018) analyzed the uncertainties that arise when estimating flood impacts at the single house scale. In contrast to the hypothesis which states that a very high spatial resolution (at the sub-meter scale) eliminates uncertainties given by the parametrization of models at coarser scales, the study showed that flood loss analyses at very high spatial resolution introduces new uncertainties. We showed that the method for attributing flow depths from the inundation model to the geographically represented objects at risk (houses) introduced new uncertainties into the whole flood impact estimation process. The spatial representation of the objects at risk (houses) in the computational mesh for the flood

simulation is also important. Overall, flood impact analyses at a high spatial resolution are subject to uncertainties that have to be considered.

Paper 16 (Bernet et al., 2018) evaluated the applicability and reliability of several approaches for modelling surface water floods. As a basis for this validation, a unique dataset that documents the extent of several surface water flood events was elaborated. The data for validating pluvial floods in rural areas were missing. The data were published so other research groups could continue with testing and evaluating surface water floods. Models for simulating surface water floods have not been able to reliably represent the natural processes, so further research is needed in the development of models for this process.

Papers 17 (Mazzorana et al., 2009) and 18 (Mazzorana et al., 2011) focused on the development of models for estimating the amount of large wood and simulating the transport of large wood in rivers during flood events. Paper 17 (Mazzorana et al., 2009) described a method for estimating the potential amount of large wood for all mountain torrent catchments in an alpine region in case of extreme floods. This provides the basis for assessing potential flood hazards that are influenced by large wood dynamics, e.g., due to clogging at bridges and subsequent flooding of the nearby areas. In contrast, paper 18 (Mazzorana et al., 2011) presents an approach for modelling the transport of large wood in rivers during a flood event. Both models provide the basis for the development of a coupled component model for assessing the dynamics of large wood during a flood at river reach scale.

Further Publications by the author on this section topic:

Felder, G.; Paquet, E., Penot, E., Zischg, A., Weingartner, R., accepted. Consistency of extreme flood estimation approaches. *Journal of Hydrologic Engineering*.

Schober, S., Zischg, A., and Sereinig, N., 2010. "Flood risk tools" - GIS-based Method on the determination of flood according to the requirements of the EU Floods Directive, *Österreichische Wasser- und Abfallwirtschaft*, 62, a28-a32. 10.1007/s00506-010-0205-2.

Zischg, A., Fuchs, S., Keiler, M., Meißl, G., 2005. Modelling the system behaviour of wet snow avalanches using an expert system approach for risk management on high alpine traffic roads, *Natural Hazards and Earth System Sciences*, 5, 821–832, 2005. 10.5194/nhess-5-821-2005.

Zischg, A., Fuchs, S., Keiler, M., and Stötter, J., 2005. Temporal variability of damage potential on roads as a conceptual contribution towards a short-term avalanche risk simulation, *Natural Hazards and Earth System Sciences*, 5, 235–242, 2005. 10.5194/nhess-5-235-2005.

3.3 Synthesizing: Model coupling

This section synthesizes the empirical research and the developed models described in the previous sections. The main outcome and highlight of the research summarized in this cumulative habilitation is a coupled component model for analyzing flood impacts at river basin scale at very high spatial resolution to analyze individual objects at risk, such as single houses. An important aspect of this model chain is the multi-model and multi-temporal approach at sub-module level. Only this aspect allowed the analyses of spatio-temporal dynamics in changing flood risks. Whereas the multi-model approach is relatively common in flood risk research, the combination of this approach with a multi-temporal approach is, to the best of my knowledge, rare. Hence, this combination is probably the most significant contribution of this thesis to the progress of flood impact research. The following papers summarize the development of the coupled component model.

- Paper 19: Zischg, A., Felder, G., Weingartner, R., Gómez-Navarro, J.J., Röthlisberger, V., Bernet, D., Rössler, O., Raible, C., Keiler, M., Martius, O., 2016. M-AARE - Coupling atmospheric, hydrological, hydrodynamic and damage models in the Aare river basin, Switzerland, in: 13th Congress INTERPRAEVENT 2016, 30 May to 2 June 2016, Lucerne, Switzerland. Conference proceedings, 444–451.
- Paper 20: Felder, G., Zischg, A., Weingartner, R., 2017. The effect of coupling hydrologic and hydrodynamic models on probable maximum flood estimation. *Journal of Hydrology* 550, 157–165. 10.1016/j.jhydrol.2017.04.052.
- Paper 21: Zischg, A., Felder, G., Weingartner, R., Quinn, N., Coxon, G., Neal, J., Freer, J., Bates, P., 2018. Effects of variability in probable maximum precipitation patterns on flood losses. *Hydrology and Earth System Sciences* 22, 2759–2773. 10.5194/hess-22-2759-2018.
- Paper 22: Zischg, A., Felder, G., Mosimann, M., Röthlisberger, V., Weingartner, R., 2018. Extending coupled hydrological-hydraulic model chains with a surrogate model for the estimation of flood losses. *Environmental Modelling & Software* 108, 174–185, doi:10.1016/j.envsoft.2018.08.009.
- Paper 23: Felder, G., Gómez-Navarro, J.J., Zischg, A., Raible, C.C., Röthlisberger, V., Bozhinova, D., Martius, O., Weingartner, R., 2018. From global circulation to local flood loss: Coupling models across the scales. *Science of The Total Environment* 635, 1225–1239. 10.1016/j.scitotenv.2018.04.170.
- Paper 24: Zischg, A., Hofer, P., Mosimann, M., Röthlisberger, V., Ramirez, J.A., Keiler, M., Weingartner, R., 2018. Flood risk (d)evolution: Disentangling key drivers of flood risk change with a retro-model experiment. *Science of The Total Environment* 639, 195–207. 10.1016/j.scitotenv.2018.05.056.
- Paper 25: Zischg, A., Galatioto, N., Deplazes, S., Weingartner, R., Mazzorana, B., 2018. Modelling spatiotemporal dynamics of large wood recruitment, transport and deposi-

tion at river reach scale during extreme floods. *Water* 10, 9, 1134. 10.3390/w10091134.

- Paper 26: Staffler, H., Pollinger, R., Zischg, A., Mani, P., 2008. Spatial variability and potential impacts of climate change on flood and debris flow hazard zone mapping and implications for risk management. *Natural Hazards and Earth System Sciences* 8, 539–558. 10.5194/nhess-8-539-2008.
- Paper 27: Zischg, A., Schober, S., Sereinig, N., Rauter, M., Seymann, C., Goldschmidt, F., Bäk, R., Schleicher, E., 2013. Monitoring the temporal development of natural hazard risks as a basis indicator for climate change adaptation. *Nat Hazards* 67, 1045–1058. 10.1007/s11069-011-9927-0.

Paper 19 (Zischg et al., 2016) described the aim of the project “M-AARE - Coupling atmospheric, hydrological, hydrodynamic, and damage models in the Aare river basin, Switzerland”. The project was one of the flagship projects with which the Mobiliar Lab for Natural Risks was started in 2014. The Mobiliar Lab for Natural Risks is a common research initiative by the Oeschger Centre for Climate Change Research at the University of Bern and Swiss Mobiliar. The M-AARE project aimed at developing a coupled component model covering atmospheric and meteorological processes to hydrological and hydraulic processes and models for estimating flood impacts.

The first step in coupling hydrologic and hydraulic models was described in paper 20 (Felder et al., 2017). This study assessed the potential benefits and constraints of coupled modelling compared to standard deterministic hydrologic modelling when for the estimation of the probable maximum flood (PMF). Two modelling approaches were applied using a set of 100 spatio-temporal probable maximum precipitation (PMP) distribution scenarios. The resulting hydrographs, the resulting peak discharges, as well as the reliability and plausibility of the estimates were evaluated. The results showed that coupling hydrologic and hydrodynamic models substantially improves the physical plausibility of PMF modelling, although both modelling approaches led to PMF estimations for the catchment outlet that fell within a similar range. Using a coupled model is particularly suggested in cases where considerable flood-prone areas are situated within a catchment, so relevant flood retention effects have to be expected. This appraisal is especially important for hydrologic models that are calibrated with observed data that should produce reliable discharge predictions in the range of extreme flood events not observed in the observation period. As runoff processes are probably not stationary in the case of a PMF where discharge greatly exceeds observed flood peaks, coupling hydrologic with one-dimensional hydrodynamic models and using them to build coupled hydrologic hydrodynamic models can potentially improve the plausibility of PMF estimations. A comparison between hydrologic models of different complexities with the aim of estimating the probable maximum flood of the Aare River in Bern, Switzerland was further complemented by Felder and Weingartner (2017).

Paper 21 (Zischg et al., 2018c) expanded on the work of paper 20 as the coupled hydrologic/hydrodynamic model was extended with a two-dimensional (2D) flood inundation model and a flood loss estimation module. Paper 21 analyzed the effects of rainfall pattern on flood losses and the key factors of uncertainty in the full model chain. We showed that the spatio-temporal pattern of rainfall is the most relevant contribution to the overall model uncertainty, measured in terms of flood losses. The rainfall pattern is even more important than the vulnerability functions for the considered overall uncertainty, which is hitherto stated to be the most relevant uncertainty in flood impact model chains.

Paper 22 (Zischg et al., 2018b) evaluated the propagation of uncertainties through the model chain. This study showed that the validation of the flood impact model differed when considering observed discharges or observed precipitation as the model input. The approach of paper 14 was used for validation, validating the outcome of reconstructed flood events in terms of the number of exposed buildings. However, the difference between the two types of input data used for model validation was shown to be not as relevant as hypothesized by Voinov and Shugart (2013). Paper 22 developed and tested a new method for extending coupled hydrologic and hydraulic models with a surrogate model or a meta-model for flood impact analyses. A relationship between peak discharge and flood loss that was valid for a specific floodplain was coupled with a one-dimensional hydrodynamic model. This relationship—the floodplain’s loss footprint—was established by a number of flood simulations with a range of magnitudes and by computing flood losses for each scenario. This approach thus reduced the complexity in flood-risk modeling at the river basin scale. The surrogate model for flood-loss estimation can be coupled with a hydrological-hydraulic model cascade, allowing the computing of a high number of flood scenarios for whole river basins. Hence, this approach offers new possibilities for stress test analyses and Monte-Carlo simulations for analyzing the system behavior under different system loads or for analyzing weather simulations of long time periods.

Paper 23 (Felder et al., 2018) presented an approach for the coupled hydrologic-hydrodynamic-flood impact model chain, i.e., the coupled component model M-AARE, which could be driven by long-term climate simulations with a global climate model and dynamic downscaling with a regional climate model. The model chain setup incorporated a global and regional climate model to simulate atmospheric processes, a hydrological model to estimate the catchment’s runoff reaction to precipitation inputs, a hydrodynamic model to identify flood-affected areas, and a damage and loss model to estimate flood losses requires building interfaces between the individual models. The submodels were coupled across several scales in terms of spatial and temporal resolution and so several pre- and post-processing steps for the individual models were required. The results showed that a coupled model chain allows for reliable representation of runoff for both long-term runoff characteristics and extreme events, as long as a bias correction on the precipitation input is applied. Although coupled models have been established, and coupling two to three of these models has been successful, no assessment had been conducted of a full and comprehensive model chain from the atmospheric models to the local scale flood loss models. Hence, paper 23 was one of the first coupled component models that covered a spatial scale from global climate models to the sub-

meter scale of the flood impact module and a temporal scale ranging from several centuries of the climate simulation to the seconds scale of flood inundation models.

Paper 24 (Zischg et al., 2018d) extended the developed coupled component model with a multi-temporal approach. The submodules of the inundation model and the data for the values at risk were represented by selected timestamps of the river morphology and the status of the settlements. This study aimed to analyze how flood risks dynamically change over time. Over decades and centuries, the main drivers for flood risk change are influenced either by perturbations or slow alterations in the natural environment or, more importantly, by socio-economic development and human interventions. However, changes in the natural and human environment are intertwined. Thus, the analysis of the main drivers for flood risk changes requires disentangling the individual risk components. In paper 24, a method for isolating the individual effects of selected drivers of change and selected flood risk management options were developed. The study design was based on a model experiment. We used this model setup to analyze the temporal evolution of the flood risk for an ex-post evaluation of the key drivers of change, and for analyzing possible alternative pathways for flood risk evolution under different governance settings. We show that the construction of lateral levees and the consecutive river incision were the main drivers for decreasing flood risks since the early 1900s in the study region. A rebound effect in flood risk was observed following an increase in settlements since the 1960s. This effect was not as relevant as the river engineering measures, but will become increasingly so in the future with continued socio-economic growth. The presented approach provides a methodological framework for studying pathways for future flood risk evolution and for the formulation of narratives for adapting governmental flood risk strategies to the spatio-temporal dynamics in the built environment.

Paper 25 (Zischg et al., 2018a) was based on papers 17 and 18 in that both approaches were coupled for modelling the large wood available for recruitment during a flood event and modelling recruitment, transport, and deposition of large wood in rivers and floodplains. The resulting coupled component model for simulating large wood dynamics (recruitment, transport, and deposition) was connected with a 2D hydrodynamic model. Overall, the simulation results of the large wood dynamics, both the temporal and spatial dynamics in a river reach during an extreme flood event, provided important information for flood risk management. The developed coupled component model allowed the expected volume of large wood at a certain point in the river basin to be assessed by considering the actual conditions of vegetation and a specific flood scenario. This provided a basis for the design of bridges or wood-retention structures and for quantitatively assessing large wood dynamics during a worst-case flood. Analyzing the trade-off between the ecological benefits of wood in rivers and flood risk management, another reason was found for using coupled component models for simulating large wood dynamics in rivers. With the presented model, the areas from which large wood is recruited and transported toward the lower system boundary, and those from which the recruited large wood is not transported downstream, can be identified. With this, areas that are important for ecology and for flood discharge improvement can be prioritized based on a transparent and reproducible method. Therefore, the unnecessary use of wood cuts as a flood prevention measure can be avoided.

In addition, papers 26 (Staffler et al., 2008) and 27 (Zischg et al., 2013) used coupled component models for analyzing the sensitivity of floodplains to the effects of climate change in terms of flood losses. Paper 26 (Staffler et al., 2008) described a model experiment that analyzed the potential effects of a general increase in rainfall intensity on the losses to buildings and infrastructure due to a subsequent increase in the magnitudes of floods and debris flows. The study aimed to identify the alpine torrent catchments that are sensitive to climatic changes and to assess the robustness of the methods for the elaboration of flood and debris flow hazard zone maps to specific effects of climate changes. The selected case studies showed a remarkable increase in the areas affected by floods and debris flow when considering possible future precipitation intensities in hazard mapping. However, the torrent and river catchments showed high spatial variability in their sensitivity to climate changes. This knowledge about the spatial patterns of sensitivity could eliminate speculative and unnecessary measures against the impacts of climate changes like a general enlargement of hazard zones or a general over dimensioning of protection structures for the whole territory. Paper 27 (Zischg et al., 2013) described a framework for monitoring changes in flood risks and capturing the drivers of these changes.

4 Concluding remarks: Perspectives of coupled component models

4.4 Perspectives of model coupling across scales for analyzing the spatio-temporal dynamics and drivers of flood risk change

The presented examples of coupled component models prove the applicability of this approach for analyzing the spatio-temporal dynamics of flood risk change. The research questions could have been answered and the main hypothesis—that coupled component models provide a suitable, robust and reliable framework for analyzing spatio-temporal dynamics and drivers of flood risk change—could be verified. The presented coupled component models, namely the model chain from global climate models to flood impact models, the model chain for simulating large wood dynamics in rivers, and the model chain for analyzing social justice of flood risk management strategies, all connect several temporal and spatial scales. Coupled component models are also able to couple raster-based with vector-based modelling approaches.

These two benefits, coupling models across scales and coupling different modelling approaches into hybrid modelling frameworks, together with the multi-model and multi-temporal approach at submodule level, allow new study designs for analyzing flood risk change. Only with these setups, is it possible to analyze spatio-temporal dynamics and isolate the effects of different drivers of flood risk.

The targeted local scale of the flood and flood impact submodels (single house level) avoids the aggregation and parametrization of local small-scale processes at a coarser spatial resolution, as required by earth system models. The sensitivity analyses of the coupled component models furthermore show that the uncertainties do not necessarily propagate through the model chain. This effect can be traced but is not as relevant, as suggested by Calvin and Bond-Lamberty (2018), Voinov and Shugart (2013), and Verburg et al. (2016). In contrast to integrated assessment models, coupled component models can be validated at the submodule level, or robust and validated models can be coupled together. As such, coupled component models offer a higher level of transparency and reproducibility than integrated assessment models even with a high complexity. Moreover, the multi-model approach at submodule level leads to a higher interpretability of the results as the most sensitive submodules of a model chain are highlighted.

Overall, the concluding remark of this habilitation thesis is that coupled component models provide an interesting approach for modelling feedback mechanisms between human activities and the natural environment and for the regionalization of global trends in environmental and socio-economic change (figure 2). A modelling framework that couples specialist's models toward system models offers potential for re-gaining a universalist viewpoint and unifying several approaches in geography.

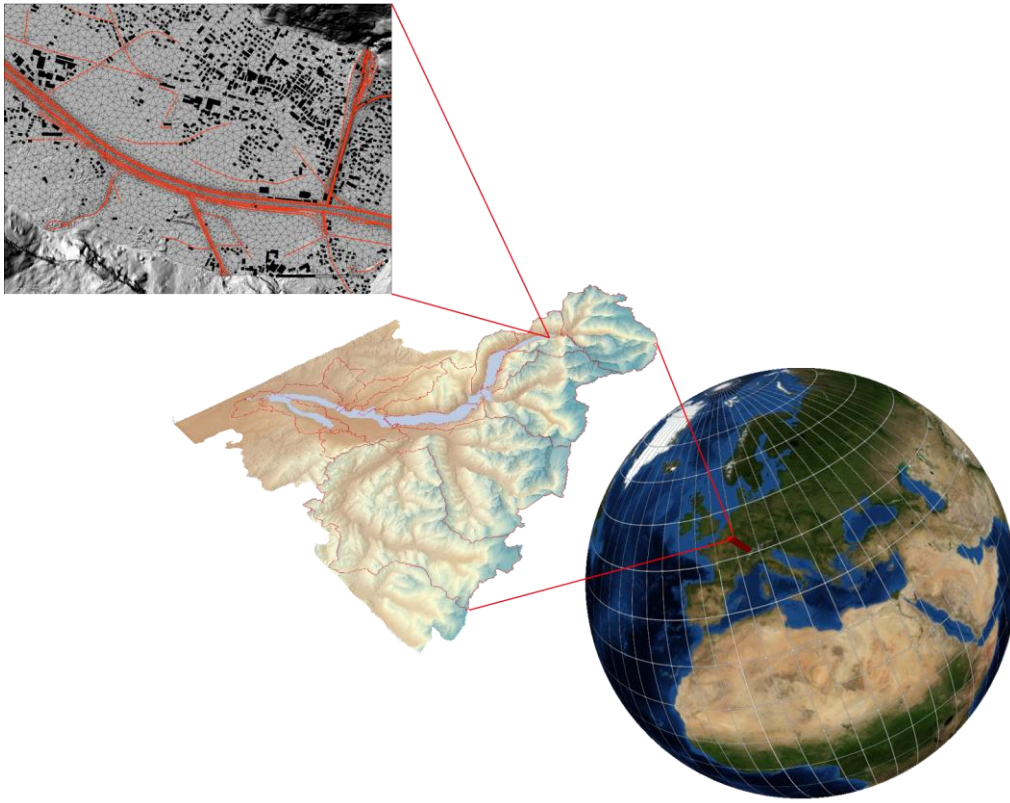


Figure 2: Schematic representation of the concept for coupling models across scales. Coupled component models provide an interesting approach for the regionalization of global trends in environmental and socio-economic change.

4.5 Perspectives of coupled component models for simulating interactions between humans and the natural environment

Two papers highlighted and summarized the benefits of coupled component modelling for simulating interactions between human activities and the natural environment. One described a method that allows studying the potential future long-term effects of different philosophical schools in prioritizing investments in flood risk prevention, and the second reviewed approaches for modelling interactions between humans and the natural environment. The latter discusses the pros and cons of coupled component models in comparison with other approaches.

- Paper 28: Thaler, T., Zischg, A., Keiler, M., Fuchs, S., 2018. Allocation of risk and benefits—distributional justices in mountain hazard management. *Regional Environmental Change* 18, 353–365. 10.1007/s10113-017-1229-y.
- Paper 29: Zischg, A., 2018. Floodplains and Complex Adaptive Systems—Perspectives on Connecting the Dots in Flood Risk Assessment with Coupled Component Models. *Systems* 6, 9. 10.3390/systems6020009.

Paper 28 (Thaler et al., 2018) discussed the dilemma that potentially emerges when following one strategy for prioritizing investments in flood prevention at the national scale. Depending on the philosophy of this prioritization strategy, some local governments and individuals gain from natural hazard protection schemes, whereas others lose. Decisions on whom to protect often cause contradicting concepts of political understanding, which differ in interpretations of fair resource allocation and distribution. This paper analyzed the impact of different philosophical schools of social justice on mountain hazard management in Austria. Based on spatially explicit, object-based data of elements at risk and a coupled component modelling approach, we compared potential distributional effects of three political jurisdictions over the future four decades. The implementation of a utilitarian policy approach would cause high income communities in hazard-prone areas to mainly benefit from investments in flood prevention. Consequently, this policy direction would encourage the public administration to ignore their own failure in past natural hazards management and prevention. Following a Rawlsians approach, peripheral communities would mainly gain from new policy direction who often experience, besides natural hazards problems, large and mainly socio-economic challenges. Finally, the most radical change would include the strict implementation of a liberalism policy, whereabouts the state only provides hazard information, but no further mitigation measures. These findings highlight the distributional consequences of future flood risk management strategies and point to the crucial selection of policy direction in navigating the selection of various adaptation schemes.

Paper 29 (Zischg, 2018) interpreted floodplains as co-evolving natural and human systems. As the previous papers in this habilitation thesis showed, both flood processes and the values at risk dynamically change over time and influence each other. These changes influence future risk pathways. The co-evolution of all these drivers of changes in flood risk could lead to emergent behavior. Hence, complexity theory and systems science can provide a sound theoretical

framework for flood risk management in the 21st century. Paper 29 reviewed selected approaches for modelling coupled human and natural systems and finally provided an outlook on potential future coupled component modeling approaches for modelling the interactions between humans and the environment. Especially, the coupling of process models with spatially explicit agent-based models offers remarkable potential for future research in coupled human and natural systems and in particular for coupled human-water systems.

4.6 Perspectives of coupled component models in hydrology

Human activities related to water are challenged by both climatic changes and anthropogenic influences to the water systems. Hence, sustainable adaptation in the water sector requires an understanding of hydrology in its full complexity. I summarized studies that are showing how changing human and natural systems are shaping hydrology and how changing hydrology is framing human activities and ecosystem services. Extending process models, such as climate models and weather forecast models, coupled with hydrologic/hydraulic models with socio-economic impact and loss models, is a way to integrate modelling frameworks. This coupled component modelling framework enables considering the impacts that a technological society could have on natural systems when reacting to extreme events. This requires an analysis of driving forces that shape water systems and the analysis of feedback processes between hydrology and socio-economy. Thus, coupled component models provide an approach for studying both the context for hydrology and hydrology as a context.

Context for hydrology

In studying the changing context for hydrology, often a top-down approach of analyzing the effects of global environmental changes to the hydrology of rivers is followed. This includes changes in the climate, in the natural environment, and in the human footprints on the river systems (hydromorphology). The analysis of changing contexts for hydrology is based on the coupling of process models in combination with data-driven analyses. The main focus herein lays on the regionalization of the impacts, i.e. predicting the spatio-temporal dynamics of global changes on selected river basins at regional to local scale. This requires bridging spatial scales from global climate models to local impacts, and temporal scales from centennial to sub-hourly flood dynamics.

Hydrology as a context

In contrast, the analysis of hydrological conditions as context for society must follow a bottom-up approach of studying the vulnerability of human activities and socio-economic systems related to water. In this approach, hydrology is a main context for their future evolvement and changes in hydrology affect their functioning. The main focus in this research topic must be laid on changes in the river systems and their special role for society. Rivers are remarkable modified by flood protection works, dams, and water/energy infrastructure. Thus, heavily modified river systems act as a crucial framework for settlement development or even as life-lines in the Anthropocene. Changes in hydrology markedly drive future pathways of socio-economic development. The research question in studying hydrology as context is the sensitivity of water systems to hydrological changes. Furthermore, studying future pathways of evolving water systems in the Anthropocene requires a comparison between natural and engineered river systems. Examples of this comparison were shown in selected papers of this cumulative habilitation thesis.

Feedbacks: unifying top-down and bottom-up modelling approaches

Finally, top-down and bottom-up approaches have to be brought together and bi-directional feedback mechanisms between rivers and society have to be implemented in integrated modelling frameworks. This means that coupled component models for studying the impacts of hydrometeorological extremes and global changes on water systems have to be extended with capabilities for capturing the effects of adaptation measures. The adaptation strategies of governments and individuals must be implemented into impact models. The habilitation thesis presented approaches for enabling coupled model frameworks to predict and evaluate the effects of different adaptation strategies. This is supporting the search for robust and sustainable risk management strategies in the context of global changes. It requires first to study feedback mechanisms empirically or theoretically. One main foundation for this are model experiments. Herein, different states of the environment and the human system are represented in multi-temporal models. With this, model experiments can test alternative pathways of flood risk evolution by assuming specific management strategies.

4.7 Outlook for future research: The human dimension of hydrological change

A short outlook is provided for new study designs that are facilitated by coupled component models. One is the question of quantifying the human dimension of hydrological change. Several studies have stated that engineering measures for flood risk prevention in the upper river reaches have negative effects for downstream river reaches (Pinter et al., 2009, 2008; Pinter et al., 2006). Such research questions are hardly answerable with empirical approaches, as anthropogenic interventions introduce relevant system changes and non-linearity in the discharge regime of rivers and are superimposed by long-term climate variabilities (Munoz et al., 2018; Munoz and Dee, 2017). This is even more pronounced when considering the effects of long-term changes in the values at risk on flood risk evolution. Hence, only a multi-temporal coupled component model is able to disentangle the drivers of flood risk.

The coupled component model for the Aare River basin was extended with multi-temporal submodules of river morphology and elements at risk. This enabled the isolation and study of the human dimension of hydrological change in the Aare River. For this goal, I simulated the outflow at Bern for a historic natural situation of the river system, before any anthropogenic interventions occurred. I used two different approaches for modelling precipitation. In the first step, I used time series of observed precipitation for the years 2005-2015 as the input for the coupled hydrologic-hydraulic model using the natural state of the river system for hydrodynamic modelling. For the second step, I analyzed the aerial precipitation of the river basin for several return periods. As suggested by (Zischg et al., 2018c), the effects of the variability in the rainfall pattern on discharge at the catchment outlet had to be considered to quantify the human impacts on hydrological change. Figure 3 compares the observed discharge with the modelled natural discharge that would occur if no river engineering measures had been constructed in the catchment. The peak flows would have been remarkably higher in a natural state than in the present state of the river system. This effect is mainly caused by the increase of flood retention volume after the deviation of the Kander River into Lake Thun in 1714. This is one of the first geoenvironmental measures in the European Alps.

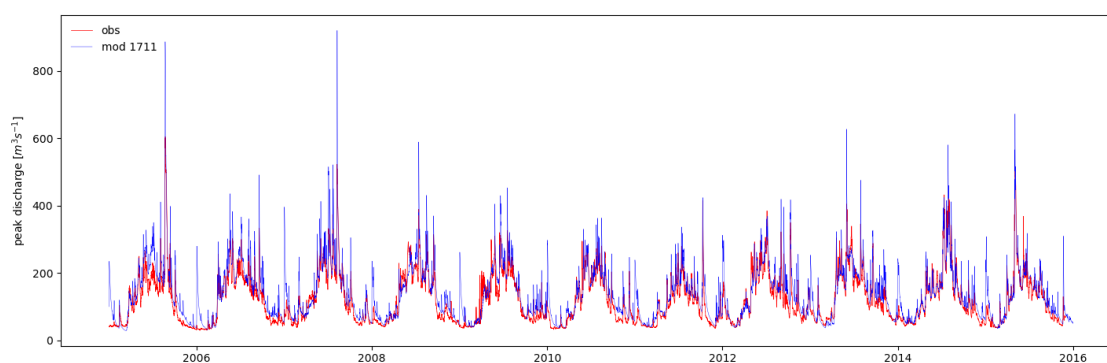


Figure 3: Comparison of the observed peak discharge at Bern and a modelled natural discharge prior to any anthropogenic modifications of the river morphology. The modelled discharge bases on the observed precipitation in the river basin in the years 2005-2015.

The second analysis focused on changes in the discharge at higher return periods. Figure 4 shows that the effect of the increasing retention volume of Lake Thun is relevant for all considered return periods. The peak discharges in Bern would be remarkably higher in a natural state of the river system. However, this decrease in flood hazard in Bern was achieved at the cost of a higher flood hazard in Thun. The level of Lake Thun remarkably increased in the case of floods.

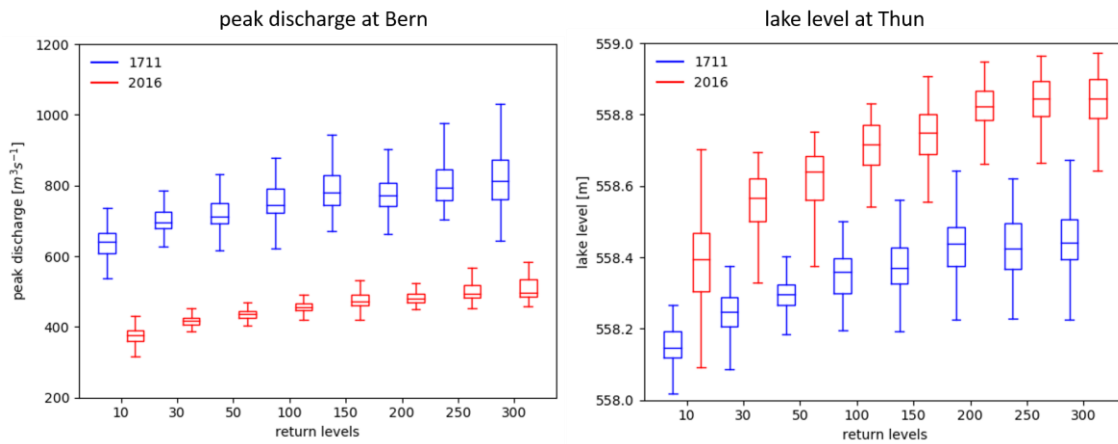


Figure 4: Modification of the discharges (left) and lake levels (right) of several return periods by the cumulative effect of all river engineering works in the Aare River basin upstream of Bern, Switzerland. This analysis takes into account the uncertainty related to the spatio-temporal rainfall pattern as proposed by (Zischg et al., 2018c). The peak discharge in Bern decreased after the Kander correction with the cost of increasing lake levels in Lake Thun.

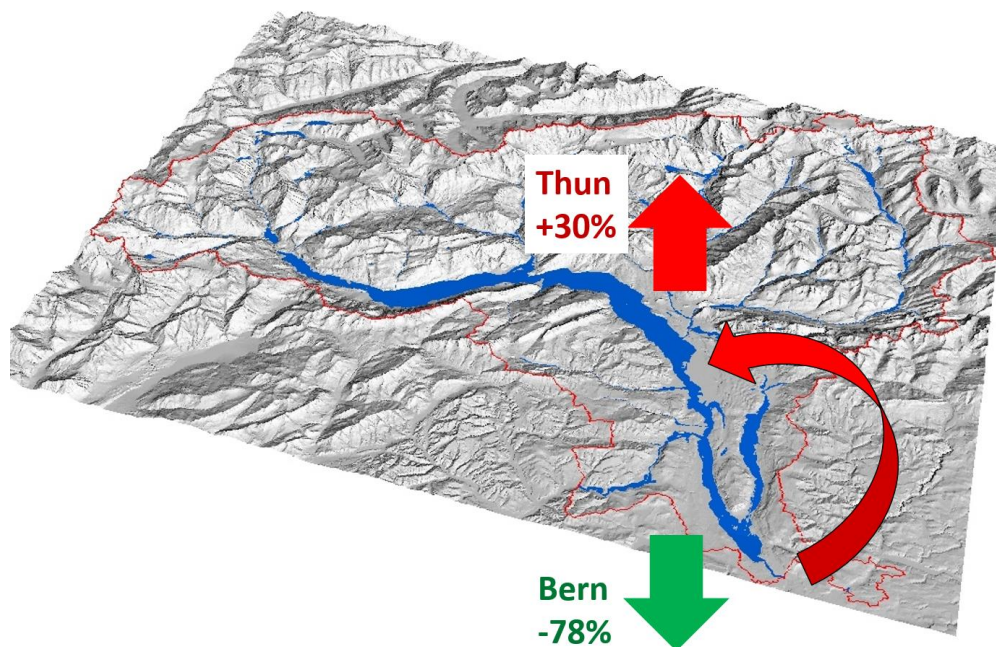


Figure 5: Quantification of the flood risk transfer from Bern to Thun. After the Kander correction in 1714, flood risk in Bern is 78 % less than in the natural state while it is about 30 % higher in Thun. This case study is one example of showing the potential of coupled component models for analyzing the spatio-temporal dynamics and drivers of flood risk change at river basin scale.

These changes in flood hazard also affect flood risks. The calculation of the flood risk with the coupled component model M-AARE showed that the flood risk in Bern decreased by 78% after the deviation of the Kander River into Lake Thun, whereas the flood risk for the city of Thun increased by 30%. This risk transfer was computed based on the present values at risk.

This outlook shows how coupled component models allow the analysis of isolated effects of selected drivers of change—in this case, the human dimension of hydrological change. Further potential lays in analyzing the long-term effects of adaptation strategies in terms of flood risk and water resources management.

5 Papers

5.1 Data-driven analyses of environmental and socio-economic change

Paper 1: Cremonese, E., Gruber, S., Phillips, M., Pogliotti, P., Boeckli, L., Noetzli, J., Suter, C., Bodin, X., Crepaz, A., Kellerer-Pirklbauer, A., Lang, K., Letey, S., Mair, V., Morra di Cella, U., Ravel, L., Scapozza, C., Seppi, R., Zischg, A., 2011. Brief Communication: "An inventory of permafrost evidence for the European Alps". *The Cryosphere* 5, 651–657. 10.5194/tc-5-651-2011.

Brief Communication:

“An inventory of permafrost evidence for the European Alps”

E. Cremonese¹, S. Gruber², M. Phillips³, P. Pogliotti¹, L. Boeckli², J. Noetzli², C. Suter³, X. Bodin⁴, A. Crepez⁵, A. Kellerer-Pirklbauer^{6,7}, K. Lang⁸, S. Letey¹, V. Mair⁸, U. Morra di Cella¹, L. Ravanel⁴, C. Scapozza⁹, R. Seppi¹⁰, and A. Zischg¹¹

¹Environmental Protection Agency of Aosta Valley, ARPA Valle d’Aosta, Saint Christophe, Italy

²Glaciology, Geomorphodynamics and Geochronology, Department of Geography, University of Zurich, Zurich, Switzerland

³WSL Institute for Snow and Avalanche Research SLF, Davos, Switzerland

⁴Laboratoire EDYTEM, CNRS, Université de Savoie, Le Bourget du Lac, France

⁵Arabba Avalanche Center, Environmental Protection Agency of Veneto, ARPAV, Arabba di Livinalongo, Italy

⁶Department of Geography and Regional Science, University of Graz, Graz, Austria

⁷Institute of Remote Sensing and Photogrammetry, Graz University of Technology, Graz, Austria

⁸Autonomous Province of Bolzano, Geological Service, Bolzano, Italy

⁹Institute of Geography, University of Lausanne, Lausanne, Switzerland

¹⁰Earth Science Department, University of Pavia, Pavia, Italy

¹¹Abenis Alpinexpert Srl, Bozen/Bolzano, Italy

Received: 28 March 2011 – Published in The Cryosphere Discuss.: 18 April 2011

Revised: 3 August 2011 – Accepted: 4 August 2011 – Published: 22 August 2011

Abstract. The investigation and modelling of permafrost distribution, particularly in areas of discontinuous permafrost, is challenging due to spatial heterogeneity, remoteness of measurement sites and data scarcity. We have designed a strategy for standardizing different local data sets containing evidence of the presence or absence of permafrost into an inventory for the entire European Alps. With this brief communication, we present the structure and contents of this inventory. This collection of permafrost evidence not only highlights existing data and allows new analyses based on larger data sets, but also provides complementary information for an improved interpretation of monitoring results.

1 Introduction

In mountain areas, permafrost distribution is spatially heterogeneous and there is a scarcity of direct permafrost measurements and observations. In the European Alps, numerous local permafrost distribution models have been devel-

oped (e.g. Keller, 1992; Hoelzle, 1996; Imhof, 1996; Gruber and Hoelzle, 2001; Lambiel and Reynard, 2001), but are usually based on a small number of data points (often proxies) from rather restricted regions. Similarly, statistical analyses of permafrost distribution patterns taking into account topography, mean annual air temperature (MAAT) or precipitation face the challenge of assembling heterogeneous data. In order to make the most of the potential of existing data, an Alpine-wide standardized collection of permafrost evidence has been carried out and is described here. We define a permafrost evidence to be a point or an area where permafrost is known to be present during a certain time or where the absence of permafrost can be ascertained. The wide variety of relevant field measurements and observations (e.g. temperature in boreholes or near the ground surface, rock glacier mapping, geophysics), and their different spatial scale of reference, make the process of data standardization challenging. Permafrost experts from several European Alpine countries have contributed to the inventory presented here (Appendix B). It was compiled within the framework of the project PermaNET and combines results obtained by many researchers and data assembled by national or regional monitoring programmes such as PERMOS (Noetzli and Vonder Muehll, 2010), PermaFRANCE (Schoeneich et al., 2010)



Correspondence to: E. Cremonese
(e.cremonese@arpa.vda.it)

or PROALP (Mair et al., 2008). With this brief communication we aim to present the first version of the concept, structure and data of the inventory. In addition, we hope this brief communication will also contribute to the further improvement of the inventory through peer-review, to widen its usage and to improve its integration in the context of national and international monitoring and measurement programs.

2 Structure and organization of the inventory

The design and implementation of the inventory is based on the following principles: the inventory has to be simple in structure and technical implementation and the number of parameters must be kept small. This allows researchers to register their existing data within the newly standardized scheme in a user-friendly manner. For important variables, at least a qualitative uncertainty is assigned. After insertion, data are verified in order to remove obvious errors. Basic information on the origin of each evidence point is required, such as a published reference or the measurement method applied. The inventory contains the following types of evidence: borehole temperature (BH), ground surface temperature (GST), rock fall scar (SC), trench or construction site (TR), surface movement (SM), geophysical prospecting (GP), other indirect evidence (OIE) and rock glaciers (RG). SC and TR are considered to be evidence of permafrost only if ice has been seen (e.g. on photographs or in-situ) and can be excluded to be seasonal. The criterion to exclude seasonal ice is a depth exceeding five meters from the surface. SM is usually based on field observations, terrestrial surveys, photogrammetric analyses or DInSAR data. GP include primarily geoelectrics, seismics, ground penetrating radar and electromagnetic prospecting. OIE provides room for further types of evidence such as thermokarst depressions.

For all types of evidence, general information concerning for example location and the person responsible are required. Additionally, contributors can use the optional fields available for comments and further specification of criteria. BH, GST and SM have additional specific data fields. The complete list and description of information contained in the inventory are presented in Appendix A.

The rock glacier inventory (RG) is managed separately from the point types of evidence. Individual RG inventories are supplied as a collection of polygons and/or centroids (shapefiles) in local coordinate systems and then transformed to the common coordinate system WGS84. The contribution of an inventory requires the addition of common data fields into the GIS attribute table and supplying separate meta-information about the inventory. The estimation of RG activity is based on field observation or image interpretation (e.g. aerial photography, satellite imagery) of typical morphological characteristics (e.g. steepness of the front, absence of vegetation) and then classified as being “intact” (i.e. active or inactive landform with permafrost) or “relict” (i.e. without

permafrost) and minimal information explaining the grounds for this assessment is included (Appendix A).

3 Data collection, verification and homogenization

The inventory was completed using four “calls for evidence” accompanied by a spreadsheet and detailed instructions. Thirty-five individuals or institutions provided data. Contributors provided information from their own research areas, consisting of existing data and knowledge adapted to the common data format used in this inventory. This was complemented by specific investigations in collaboration with regional/local geological services, ski resort operators, engineering companies or alpine guide societies. The design and administration of the inventory was carried out jointly by ARPA Valle d’Aosta (Italy), the WSL Institute for Snow and Avalanche Research SLF and the Department of Geography of the University of Zurich (Switzerland).

To avoid errors in spatial positioning introduced during data entry or coordinate transformation, the assembled inventory was sent as a KML file to all contributors for visual verification of the provided information using Google Earth. An updated version of the inventory was released using the feedback from the contributors after verification.

As the dataset is characterized by a high degree of heterogeneity, the issue of data homogenization is very important and still under development. A first step towards homogenization has been made for GST data measured on steep rock walls: as their inter-annual variation is similar to that of MAAT, a normalization procedure (Allen et al., 2009) to estimate mean annual ground surface temperature (MAGST) for the period 1961–1990 has been applied to make measurements from differing years comparable. Based on the resulting temperatures and considering possible mechanisms of thermal offset, GST points were classified into the categories “presence” or “absence” of permafrost with differing degrees of certainty (permafrost presence: $MAGST < -2^{\circ}\text{C}$ medium certainty; $-2^{\circ}\text{C} < MAGST < 0^{\circ}\text{C}$ low certainty; permafrost absence: $0^{\circ}\text{C} < MAGST < 2^{\circ}\text{C}$ low certainty; $MAGST > 2^{\circ}\text{C}$ medium certainty).

4 Content of the inventory

The total number of point type permafrost evidence is 408 (October 2010), extending from 44.29 to 47.47° N and from 5.91 to 14.88° E and covering all Alpine countries except Monaco, Liechtenstein and Slovenia. The rock glacier dataset includes seven inventories from Italy, Austria, Switzerland and France with a total of 4795 rock glaciers (Fig. 1). The seven inventories are regional (Valle d’Aosta, Piemonte, Veneto, Trentino Alto Adige in Italy, Massif du Combeynot in France, Ticino in Switzerland and central and eastern Austria) and thus do not cover the entire European Alps.

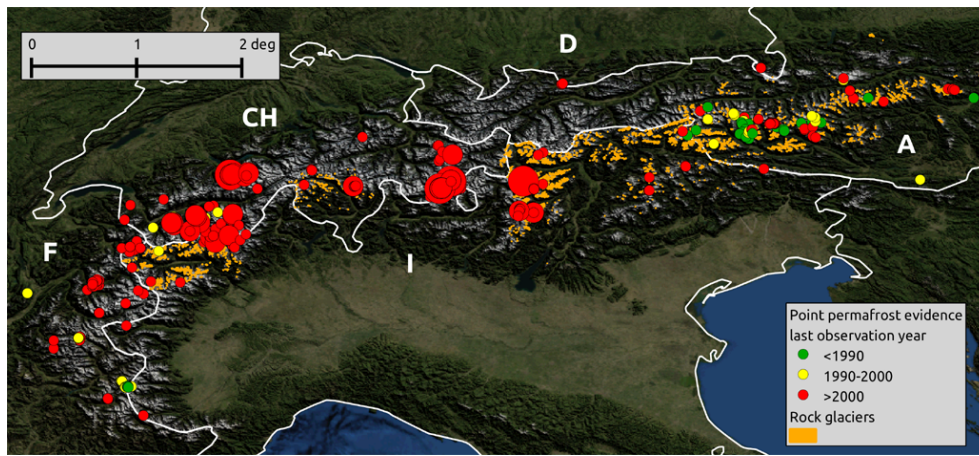


Fig. 1. Map of the permafrost evidence acquired in the Alps. The dots represent point permafrost evidence. The colors of dots represent the classes of last observation dates confirming permafrost state (before 1990, between 1990 and 2000, after 2000). The size of the dots indicates 3 classes (<3 yr, 3–8 yr, >8 yr) representing the length of observations/measured data associated with each evidence. Orange polygons represent rock glacier inventories.

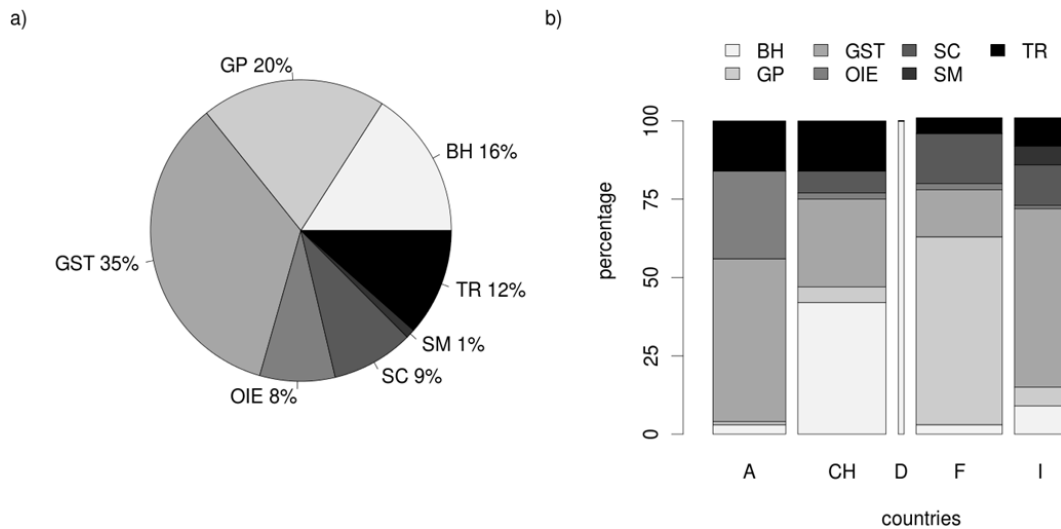


Fig. 2. (a) Relative amounts of point evidence types (borehole (BH), geophysical prospecting (GP), ground surface temperature (GST), other indirect evidence (OIE), rock fall scar (SC), surface movement (SM), trench or construction site (TR)) in the entire inventory and (b) by country. Bar width represents the relative abundance of evidence in each country: A–24 %, CH–29 %, D–0.5 %, F–28 %, I–17 %; for graphical reasons, Germany bar width has been increased (tripled).

GST, BH and GP are the most common types of point evidence. Most of the points are located in Switzerland, France and Italy (Fig. 2). The elevation of the permafrost evidence ranges from 1000 m a.s.l. in a cold talus slope in central Austria (Toteisboden) to 4120 m a.s.l. for a GST point in the Mont Blanc Massif (Grandes Jorasses); however, the majority (>60 %) are situated between 2500 and 3000 m a.s.l. (Fig. 3). Most of the points have slope angles in the range 10–45°. GST and SC also exist in near-vertical conditions and even some BH (Zugspitze (D), Aiguille du Midi (F), Gemsstock (CH), Grawand (IT)) are located in steep rock

faces. GP, TR and SM mostly occur on gently inclined slopes. The distribution of slope aspects is slightly biased towards the North (36 %) and West (24 %) with fewer points (20 % each) in the South and East. The majority (85 %) of points have no or only sparse vegetation cover and few have partial or complete coverage (15 %, mostly of type TR). Most (44 %) of the evidence are located in coarse debris, the others are in bedrock (33 %) and in fine material (23 %). Evidently, types such as SC and TR are biased towards a certain surface type. About 20 % of BH and GST are situated on plateaus or ridges, while 10–15 % of TR are located in depressions.

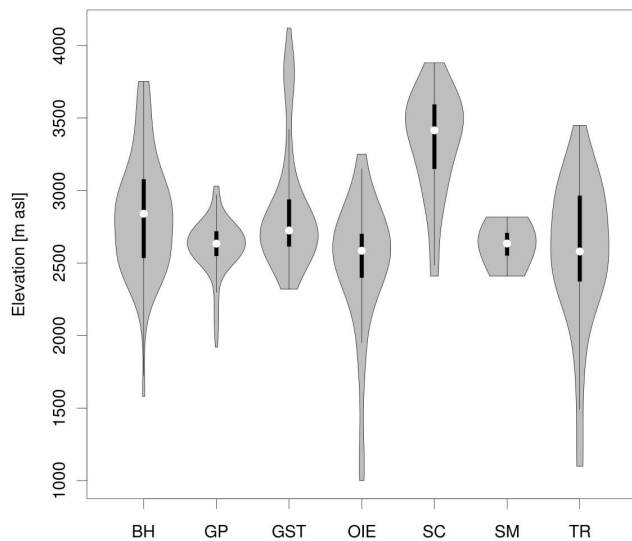


Fig. 3. Elevation range of each type of evidence (except rock glaciers). The plot shown is a combination of a box plot (the white dot is the median, the black boxes range from the lower to upper quartile, and the thin black lines represent the whiskers) and a kernel density plot super-imposed in a mirror image fashion (grey shaded areas).

The depth of BH ranges from 5 to 133 m with a mean of 33 m. Most boreholes are equipped with temperature sensor chains and data loggers but some require manual measurements. For each BH, active layer depth as well as mean annual ground temperature (MAGT) of the coldest sensor is reported as the mean of all available measurement years. As BH have variable depths, the MAGT of the coldest sensor is used as an indication for permafrost conditions. GST is mostly measured at a depth of around 10 cm (55 %), with some measurements being shallower (25 % at 0–2 cm) and others deeper (20 % at 15–55 cm). GST is reported as the mean of all full measurement years with durations ranging from 3 to 5 yr.

Evidence of the absence of permafrost is also relevant: whilst 75 % of the rock glaciers presented in the inventory are relict forms, only 23 % of the point types of evidence indicate the absence of permafrost. 61 % of point evidence where permafrost absence has been ascertained are ground surface temperature, 17 % are boreholes and 22 % are represented by geophysical investigations and trenches. Points of permafrost absence have a mean elevation of 2600 m a.s.l. but can reach also elevations higher than 3500 m a.s.l. in particularly unfavourable conditions (e.g. south exposed rock walls).

5 Data access

The October 2010 version of the inventory is available digitally at www.geo.uzh.ch/microsite/cryodata/. A compressed version of the inventory can be downloaded containing point types of evidence in ASCII format. Since the rationale behind the inventory is data sharing, point evidence publication policy are classified in two categories: “Usage without restriction” and “Inform before publication”. Data belonging to the first category can be downloaded without any feedback to the owner while in the latter case, an automatic email reporting the contact person and the intended use of the data, will be sent to the owner when a download occurs.

6 Conclusions

We have established an inventory of permafrost evidence for the Alps and made its contents freely available to other scientists and practitioners. This inventory complements monitoring programmes in which changes in permafrost terrain are measured at individual locations with great precision and over long time spans (e.g. PERMOS, PermaFRANCE or NorPerm, Juliussen et al., 2010) by providing a solid basis to advance the understanding of the spatial distribution of permafrost and its evolution in heterogeneous mountain environments. While the homogenized contents and public availability of the inventory increase the value of the data contained, the synopsis of data over a larger region additionally enables analyses that were previously not possible, as larger environmental gradients are covered and more data points available. Future experience with data homogenization, scientific analyses, gathering of evidence, re-interpretation of existing data for inclusion in the inventory and with merging differing inventories and monitoring systems into higher-level products will likely require or inspire changes to the structure and strategy outlined here. In addition, the provision of proper user interfaces for the input, validity checking and output of data as well as strategies to ensure correct scientific governance and data stewardship are important to maximize the acceptance and utility of inventories such as the one presented here.

Appendix A

Inventory structure

1. General Information (required for all types of evidence)
 - Evidence Type: Borehole (BH), Geophysics (GP), Rock fall scar (SC), Ground surface temperature (GST), Surface movement (SM), Trench or construction site (TR), Other indirect evidence (OIE);
 - Country ID: Austria (A), Germany (D), France (F), Italy (I), Switzerland (CH), Liechtenstein (FL), Slovenia (SLO);

- Evidence ID: progressive code to identify the single evidence;
 - Site name: established name for site;
 - Responsible name: first and last name of responsible person/data owner. This person is to be contacted for any questions and also for impending publications;
 - Responsible email: e-mail address of responsible person/data owner;
 - Longitude: coordinates of the evidences (WGS84, decimal degrees);
 - Latitude: coordinates of the evidences (WGS84, decimal degrees);
 - Coordinate accuracy: approximate accuracy of coordinates (m);
 - Position method: method used for locating site (e.g. GPS, MAP, Google Earth, others);
 - Orientation method: method used for determining slope and aspect (e.g. field, GIS, other);
 - Elevation: elevation of the evidence point (m);
 - Slope: slope, expressed in degrees, of the evidence point (°);
 - Aspect: aspect, expressed in degrees, of the evidence point (90° for East, 180° for South, 270° for West, 360° for North);
 - Vegetation: degree of vegetation cover: none, sparse, partly covered, complete coverage;
 - Surface type: coarse debris (no fines at surface), fine grained debris (fines at surface) or bedrock;
 - Permafrost YES/NO: permafrost presence or absence (Yes/No);
 - Permafrost certainty: degree of certainty related to permafrost presence or absence: high certainty (i.e. definite proof), medium certainty, low certainty;
 - Justification: explanation and justification of the permafrost degree of certainty given;
 - Ice: indication of the presence of ice below active layer depth or visible in rock fall scar (Yes/No/Unknown);
 - Ice depth: depth of visible ice (m);
 - Date last: last observation confirming permafrost state;
 - Permafrost comments: any additional comments on permafrost;
 - Terrain characteristics: indication of the type of terrain: slope, ridge, peak, plateau, depression, slope base;
 - Source type: source of the information related to the evidence: literature, field observation, personal communication;
 - Source comment: any additional comment on the source type;
 - Publication policy: Usage without restriction, Inform before publication.
2. Additional information (not obligatory)
 - Additional data: indication of any additional measurement existing at this site (e.g. snow depth, air temperature, ...);
 - Comments general: any other information about the site that may be important;
 - Publications: indication of publications where the site and its permafrost condition are discussed (specifically).
 3. Boreholes (specific information required for boreholes)
 - Borehole name: established local borehole name;
 - Borehole depth: maximum depth of the borehole (m);
 - Borehole ALT: mean of maximum annual active layer thickness (m);
 - Borehole ALT years: years used for the calculation of average active layer depth;
 - Borehole MAGT min: minimum mean annual temperature in the borehole (i.e. the mean annual temperature of the coldest sensor) (°C);
 - Borehole MAGT min depth: depth of the sensor used for the minimum mean annual temperature (m);
 - Borehole MAGT period: years used for the calculation of the minimum mean annual temperature;
 - Borehole MAGT accuracy: accuracy of the temperature sensors installed in the borehole;
 - Borehole GST: mean annual ground surface temperature; indicates if a measurement is available near the borehole not in the same thermistor chain (°C);
 - Borehole comments: any additional information: e.g. borehole with/without tubing, depth of Zero-annual amplitude (ZAA), angle of drilling (relative to ground surface) if borehole is not vertical.
 4. Ground Surface Temperatures (specific information required for GST)
 - GST mean: mean ground surface temperature (°C);
 - GST period: years used for the calculation of the mean ground surface temperature;

- GST measurement depth: maximum depth of measurement from surface (cm);
 - GST accuracy: accuracy of the temperature sensors;
5. Surface Displacement (specific information required for SD)
- Displacement method: indication of the method used to measure displacement: field observation, air photo observation, photogrammetric analysis, terrestrial survey, InSAR, ...;
 - Movement rate: cm day^{-1} , cm month^{-1} or cm yr^{-1} ;
 - Movement date: date of measurement.
6. Rock glacier inventory (required for each rock glacier inventory)
- RGI ID: number of the rock glacier inventory;
 - RGI name: name of the inventory;
 - RGI file name: filename of the corresponding shapefile;
 - RGI coordinate system: coordinate system of the inventory;
 - RGI delineation base: specification of the delineation method used (e.g. air photo, map, field observation etc.);
 - RGI mapping strategy: specification of the mapping strategy used to compile the inventory (e.g. random sample of rock glaciers/all rock glaciers/only large rock glaciers etc.);
 - RGI year: date of the rock glacier inventory;
 - RGI responsible name: first and last name of responsible person/data owner;
 - RGI responsible email: e-mail address of responsible person/data owner;
 - RGI publication: indication of publications where the rock glacier inventory is discussed (specifically).
7. Rock glacier (required for each rock glacier)
- Degree of activity: definition of the degree of activity using two classes: Intact (Active/inactive) or Relict;
 - RG field evidence: presence of field evidence for the rock glacier (e.g. Measurements)? Yes/No;
 - RG activity data: presence of InSAR (A), geodetic (B), photogrammetric (C), GPS (D) or other (E) data for the rock glacier: no data, activity, no activity;
 - RG vegetation front: presence of vegetation on the front of the rock glacier: Yes, No, Unknown;
 - RG glacier above: presence of a glacier or perennial snow field in the root zone of the rock glacier: Glacier, Perennial snow field, No.

Appendix B

List of contributing institutions

- Austria
 1. ZentralAnstalt für Meteorologie und Geodynamik – ZAMG
 2. Universität Graz
- France
 1. Conservatoire National des Arts et Métiers – CNAM
 2. Université Joseph Fourier
 3. Université de Savoie
 4. Centre national de la recherche scientifique – CNRS
- Germany
 1. Bayerisches Landesamt für Umwelt – LfU
- Italy
 1. Agenzia Regionale per la Protezione dell’Ambiente del Piemonte – ARPA Piemonte
 2. Agenzia Regionale per la Protezione dell’Ambiente della Valle d’Aosta – ARPA VdA
 3. Fondazione Montagna Sicura
 4. Provincia Autonoma di Bolzano
 5. Provincia Autonoma di Trento
 6. Regione Veneto
- Switzerland
 1. Bundesamt für Umwelt – BAFU
 2. Université de Lausanne – UNIL
 3. Universität Freiburg
 4. WSL Institute for Snow and Avalanche Research – SLF
 5. Universität Zürich – UZH

Acknowledgements. The project PermaNET is part of the European Territorial Cooperation and is co-funded by the European Regional Development Fund (ERDF) in the scope of the Alpine Space Programme (<http://www.alpine-space.eu>). We are grateful to all data contributors: Broccard A., Crittin C., Curtaz M., Delaloye R., Fabre D., Garcia S., Hölzle M., Keusen H. R., Kroisleitner C., Krysiacki J. M., Lambiel C., Lieb G., Mari S., Monnier S., Paro L., Riedl C., Rovera G., Schoeneich P., Springman S., Walcher J., Zampedri G., as well as the Swiss Permafrost Monitoring Network (PERMOS). Alexander Brenning has contributed to designing the initial structure of the inventory.

Edited by: R. Rigon

References

- Allen, S., Gruber, S., and Owens, I.: Exploring steep bedrock permafrost and its relationship with recent slope failures in the Southern Alps of New Zealand, *Permafrost Periglac.*, 20, 345–356, 2009.
- Gruber, S. and Hoelzle, M.: Statistical modelling of mountain permafrost distribution: local calibration and incorporation of remotely sensed data, *Permafrost Periglac.*, 12, 69–77, 2001.
- Hoelzle, M.: Mapping and modelling of mountain permafrost distribution in the Alps, *Norsk Geogr. Tidsskr.*, 50, 11–15, 1996.
- Imhof, M.: Modelling and verification of the permafrost distribution in the Bernese Alps (Western Switzerland), *Permafrost Periglac.*, 7, 267–280, 1996.
- Juliussen, H., Christiansen, H. H., Strand, G. S., Iversen, S., Midttømme, K., and Rønning, J. S.: NORPERM, the Norwegian Permafrost Database – a TSP NORWAY IPY legacy, *Earth Syst. Sci. Data*, 2, 235–246, doi:10.5194/essd-2-235-2010, 2010.
- Keller, F.: Automated mapping of mountain permafrost using the program PERMAKART within the geographical information system ARC/INFO, *Permafrost Periglac.*, 3, 133–138, 1992.
- Lambiel, C. and Reynard, E.: Regional modelling of present, past and future potential distribution of discontinuous permafrost based on a rock glacier inventory in the Bagnes-Hérémence area (Western Swiss Alps), *Norsk. Geogr. Tidsskr.*, 55, 219–223, 2001.
- Mair, V., Zischg, A., Krainer, K., Stötter, J., Zilger, J., Belitz, K., Schenk, A., Damm, B., Kleindienst, H., Bucher, K., Lang, K., Tagnin, S., and Munari, M.: PROALP Rilevamento e monitoraggio dei fenomeni permafrost. Esperienze della Provincia di Bolzano, *Neve e Valanghe*, 64, 50–59, 2008.
- Noetzli, J. and Vonder Muehl, D. (Eds.): PERMOS 2010. Permafrost in Switzerland 2006/2007 and 2007/2008, *Glaciological Report Permafrost No. 8/9*, Cryospheric Commission of the Swiss Academy of Sciences, 2010.
- Schoeneich, P., Bodin, X., Krysiacki, J., Deline, P., and Ravelin, L.: Permafrost in France. Report No. 1, *Institute of Alpine Geography*, University of Grenoble, 2010.

Paper 2: Kenner, R., Chinellato, G., Iasio, C., Mosna, D., Cuzzo, G., Benedetti, E., Visconti, M.G., Manunta, M., Phillips, M., Mair, V., Zischg, A., Thiebes, B., Strada, C., 2016. Integration of space-borne DInSAR data in a multi-method monitoring concept for alpine mass movements. *Cold Regions Science and Technology* 131, 65–75. [10.1016/j.coldregions.2016.09.007](https://doi.org/10.1016/j.coldregions.2016.09.007).



Integration of space-borne DInSAR data in a multi-method monitoring concept for alpine mass movements



Robert Kenner^{a,*}, Giulia Chinellato^b, Christian Iasio^b, David Mosna^c, Giovanni Cuzzo^b, Elisa Benedetti^d, Maria Grazia Visconti^e, Michele Manunta^f, Marcia Phillips^a, Volkmar Mair^c, Andreas Zischg^g, Benni Thiebes^b, Claudia Strada^c

^a WSL Institute for Snow and Avalanche Research SLF, Switzerland

^b European Academy of Bolzano/Bozen (EURAC), Italy

^c Office for Geology and Building Materials Testing, Autonomous Province of Bolzano, Italy

^d Sapienza University of Rome, Italy

^e Politecnico di Milano, Italy

^f National Research Council of Italy, Institute for Electromagnetic Sensing of the Environment (IREA), Italy

^g University of Bern, Institute of Geography, Oeschger Centre for Climate Change Research, Mobiliar Lab for Natural Risks, Switzerland

ARTICLE INFO

Article history:

Received 21 August 2015

Received in revised form 17 August 2016

Accepted 3 September 2016

Available online 9 September 2016

Keywords:

Monitoring

Remote sensing

Alpine mass movements

Terrestrial laser scanning

DInSAR

GNSS

ABSTRACT

This study presents the results of an experimental application of a multi-method measurement concept for the monitoring of alpine mass movements. Satellite-borne differential interferometric synthetic aperture radar (DInSAR) was applied as the key technology. To improve the information contents of the DInSAR displacement data for an individual mass movement, a complementary measurement was carried out with a three dimensional measurement system. The information on the 3D movement characteristics obtained by this complementary measurement was used to extrapolate subsequent DInSAR measurements to 3D. Terrestrial laser scanning (TLS) and Global Navigation Satellite System (GNSS) data were tested as complementary 3D measurement systems. The deviations between the single measurement systems were mainly controlled by the error budgets of the different methods. An exception were short term GNSS single point time series which included small scale surface movements that were not captured by the other methods. TLS proved to be the most suitable complementary method. A single TLS repeat measurement was sufficient to create a mask, which enables the projection of DInSAR displacement data to 3D. The application of satellite-borne DInSAR in alpine terrain is challenging; signal decorrelation is a problem due to fast terrain movements and snow coverage and can cause failure of the measurement system.

© 2016 Elsevier B.V. All rights reserved.

1. Introduction

The densification of infrastructure and settlement areas in the European Alps requires careful consideration of natural hazards and the activity of geomorphological processes, in particular in the light of climate change. Alpine mass movements like landslides, permafrost creep or rock slope failures are the source of potentially hazardous processes. They can show a low activity for decades or even centuries without being seriously hazardous – before unexpectedly accelerating. Some of these accelerations can be forecasted or at least detected in real time if the mass wasting zone is monitored on a long term basis. These include for example rock glacier creep surges (Delaloye et al., 2013; Kenner et al., 2014), accelerations of landslides and deep seated

gravitational slope deformations (Angeli et al., 2000) or rock fall events (Abellán et al., 2010; Kenner et al., 2011).

However, decision makers in natural hazard prevention are confronted with a considerable number of critical mass movement processes in alpine environments, which are often insufficiently documented. Long term monitoring tasks using classical monitoring methods are in many cases associated with high costs. This may force the natural hazard managers into a mode of reactionary operation. In many cases potentially dangerous mass movements are only focused on after the occurrence of larger events, which is suboptimal in terms of hazard prevention (Tobler et al., 2012). A cost-efficient long term monitoring system, mostly working in a self-operating mode over regions of hundreds of square kilometers, with cm accuracy and capturing changes in existing mass movement processes or even detecting new ones, would clearly help decision makers. This is the point on which the current study was based on. Our aim was to develop a measurement

* Corresponding author.

E-mail address: kenner@slf.ch (R. Kenner).

concept that enables a supra-regional, long term monitoring of as many individual mass movements as possible.

Numerous measurement technologies are currently used for monitoring tasks in alpine terrain (Table 1). They can be classified into in-situ and remote sensing methods but also into single point tracking systems or those enabling data acquisition over wide areas. The information content of the data obtained varies substantially according to the measurement system. Mass movement processes were traditionally monitored using total stations (Veulliet et al., 2009). Air-borne photogrammetry has been used for several decades for long term monitoring tasks (Fabris et al., 2005; Kääh, 1999; Kaufmann and Ladstädter, 2003). In recent years, this method has been applied more frequently and facilitated by the development of air-borne digital sensors (ADS), the availability of drone-borne photogrammetry (Bühler et al., 2012; Eisenbeiß, 2009) and software improvements. Meanwhile GNSS measurements have become a widely used additional method to the classical surveying techniques (Lambiel and Delaloye, 2004; Wirz et al., 2015). Since the beginning of the 2000s, laser scanning technology has developed rapidly and allowed the terrestrial and air-borne acquisition of widespread 3D terrain data (Bauer et al., 2003; Kenner et al., 2014; Sailer et al., 2012). This was a notable development, especially for monitoring inaccessible and steep terrain areas. Simultaneously, radar technology proved to be a very powerful method for high accuracy applications in mass movement monitoring (Colesanti and Wasowski, 2006; Gischig et al., 2009; Kos et al., 2013; Strozzi et al., 2005), allowing to monitor millimeter scale deformations of the ground surface over areas of up to hundreds of square kilometers. Table 1 gives an overview of the characteristics of these technologies. Several of the methods have been applied by Strozzi et al. (2010) for the monitoring of a rock slide in high alpine terrain. This study provides additional information about the characteristics of the methods and differences between them.

Based on this evaluation of measurement systems, our study focuses on satellite-borne differential interferometric synthetic aperture radar (DInSAR) as a key technology to realize the aim of a self-operating large scale monitoring concept providing centimeter accuracy. Space-borne DInSAR is an established method to detect and monitor large scale surface displacements. Similarly it can be used to monitor numerous small scale displacements distributed over areas of several hundred square kilometers (Pritchard and Simons, 2002). In the last decade, a

large number of case studies successfully applied DInSAR methods for detecting and monitoring ground deformations in alpine environments, and in particular in permafrost-affected areas (Barboux et al., 2012, 2015; Echelard et al., 2013; Strozzi et al., 2004). A comprehensive overview of differential InSAR and the application of the method to alpine environments and the detection of ground deformations is provided by Barboux et al. (2015).

However all these studies also underline several limitations of DInSAR, making it difficult to rely exclusively on DInSAR data when analyzing and monitoring a mass movement; the one-dimensionality of movement measurements has to be mentioned here in particular. We tried to overcome this weakness by embedding DInSAR measurements into a monitoring concept that can implement the results of a complementary measurement system if necessary. A locally and temporally limited application of such complementary data provide 3D movement information on individual mass movements to understand their general movement characteristics. The complementary data should enable the operator to draw clear conclusions from further DInSAR measurements and also monitor complex movement processes using DInSAR only.

2. Study site

The study was carried out at a test site located above Pontresina in the Upper Engadin valley, Grisons (Switzerland). The monitoring area includes three individual active rock glaciers in a West oriented mountain cirque called Foura da l'amd Ursina. The rock glacier complex henceforth referred to as Ursina (Fig. 1) ranges between 2700 and 2900 m asl. The steep surrounding ridges and rock walls reach elevations over 3000 m and are subject to intermittent rock fall. The lowest rock glacier has a steep front in the top of the Val Giandains gully, which is the source area of potential debris flows. A protection dam was built at the base of the gully above Pontresina in 2003.

3. Methods

3.1. Monitoring concept

Satellite-borne differential interferometric synthetic aperture radar (DInSAR) (Bamler and Hartl, 1998; Skolnik, 1980) provides data on

Table 1
Most frequently applied monitoring technologies for mass movements in alpine terrain.

	GNSS	Total station	Terrestrial laser scanning	Air-borne laser scanning	Air-borne photogrammetry	Terrestrial Radar	Space-borne SAR
Platform	Terrestrial: on site	Terrestrial: on site	Terrestrial: ground base close to site	Remote: aeroplane/helicopter	Remote: aeroplane/drone	Terrestrial: ground base close to site	Remote: satellite
Highest achievable spatial resolution	Single point measurement	Single point measurement	Few cm	>50 cm	>25 cm	>1 m @ 1 km	>1 m
Spatial coverage	Local	Local	Local	Regional	Supra-regional	Local	Supra-regional
Dimensionality	Direct 3D point coordinates	Direct 3D point coordinates	Direct 3D surface coordinates	Direct 3D surface coordinates	Indirect 3D surface coordinates	Direct 1D coordinate differences	Direct 1D coordinate differences
Highest achievable accuracy	>mm	mm	>cm	dm	sub-dm	mm	mm
Image information	Not available	Not available	Referenced images	Not available	Multiband image information	Not available	Not available
Natural radiation	Independent	Independent	Independent	Independent	Dependent	Independent	Independent
Topographical effects	Satellite shadowing	Surface shadowing	Surface shadowing	No influence	In steep terrain	Surface shadowing and layover	Surface shadowing and layover
Vegetation	No influence	No influence	Influence	Influence	Influence	Influence	Influence
Effort (time for data acquisition, logistics, costs)	High, manual measurement on every single point	High, manual measurement on every single point	Medium, remote sensing over long ranges, close to site access required	High, long flight time, expensive	Medium, efficient area coverage, expensive	Medium, automatic operation, heavy equipment,	Low, automatic operation, efficient, reasonable prices

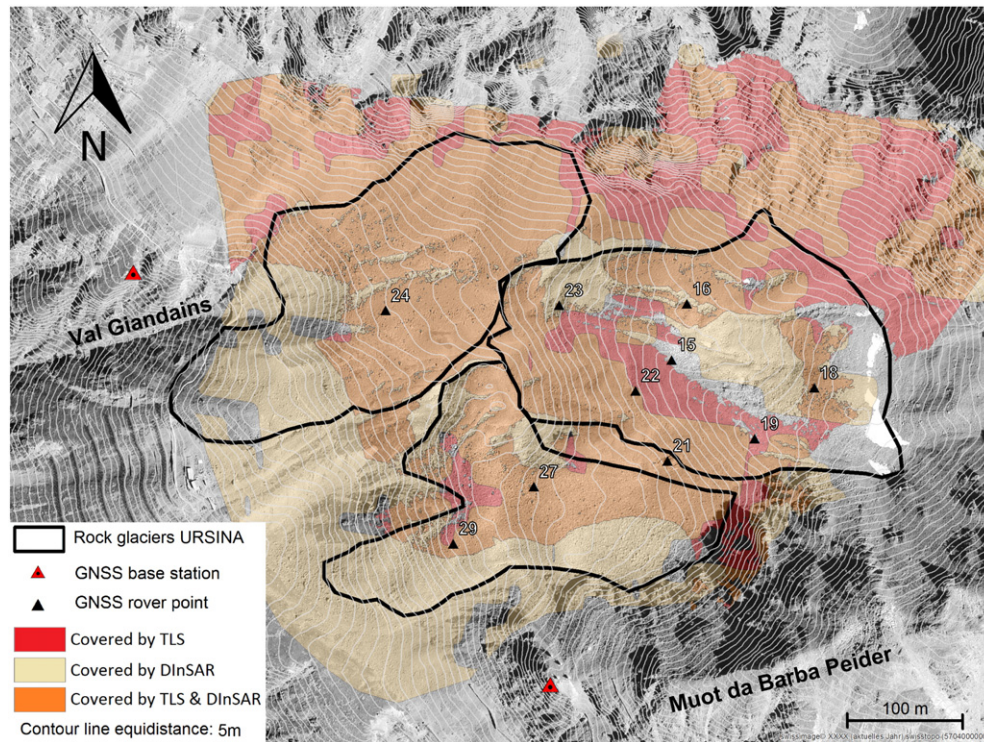


Fig. 1. Study site Ursina with measurement configurations. The area covered by DInSAR includes only these regions in which displacement rates or a proof of stability could be deduced from DInSAR data.

surface changes over areas of several hundred square kilometers with up to mm accuracy and a minimum of effort for the recipient of the data.

However, there are also considerable problems using DInSAR. The InSAR-specific effects regarding overlay, foreshortening and shadowing (Speck et al., 2007) prevent the complete surface coverage. Fast surface movements can lead to a decorrelation of multi-temporal InSAR images (Bingyuan et al., 2008). Closed snow- and dense vegetation cover entirely prevent the capture of surface movements using DInSAR. However, the major disadvantage of DInSAR is that surface changes are only displayed one dimensionally along the line of sight (LOS) of the satellite, making it difficult to infer the type of movement and its exact kinematic characteristics. Additional information is therefore necessary to correctly interpret DInSAR data. This information can be obtained via a spatially and temporally limited reconnaissance campaign using a different measurement system that provides information on the 3D surface kinematics. The three dimensional interpretability of the DInSAR signal can thus be established for individual sites by referencing it to the reconnaissance campaign. Ideally DInSAR measurements, supported by process information obtained from such local reconnaissance campaigns can then be used to perform an autarkical long term monitoring and provide estimations of the 3D kinematics. The complementary measurement system applied for the reconnaissance campaign must be embedded in the measurement geometry of DInSAR and be suitable to acquire information on the unknown detailed process kinematics. We therefore defined requirements for the complementary measurement system:

- The reconnaissance campaign is temporally limited, so a high accuracy is required to capture even slow movements
- Measurement results should be provided in direct 3D
- If not already available, a digital elevation model (DEM) should be derivable from the measurement data to determine slope and to project the DInSAR data onto

- In some cases the moving terrain is not accessible and must be monitored remotely

Terrestrial laser scanning (TLS) offers adequate solutions for all these issues but depends on an unchanging surface structure for creep detection (see 3.4) and its accuracy is limited to a few cm. These limitations can be narrowed, if necessary, using single point measurements such as GNSS or terrestrial surveying with a total station. Both provide a higher accuracy - up to mm (Table 1) and capture movements based on the tracking of individual points. Their disadvantages include the need for accessible terrain and the spatially sporadic data records in contrast to the area-covering TLS method. In our pilot study we tested both TLS and GNSS as complementary methods to DInSAR.

3.2. Reference framework

Each of the measurement systems used has its own reference system. GNSS and DInSAR operate within the World Geodetic System 1984 (WGS84) but their registration can differ due to satellite orbit uncertainties. The TLS data are referenced in a local frame of control points. To create coherence between the measurements these reference frames must be linked. We therefore installed two local terrestrial control points. Theoretically a third linking point would be necessary to join the reference frames exactly; however, due to the limited spatial extent of the study site and the high temporal stability of the reference frames we could neglect the remaining deviations between the reference frames. The linking reference points were set on stable bedrock and were equipped with an artificial InSAR reflector, a GNSS antenna base and a TLS reflector (Fig. 2). The linking points acted as stable reference points for the TLS and DInSAR measurements and the GNSS base stations were located on them. The InSAR corner reflectors consist of an orthogonal open aluminium trihedral with a short edge length of 57 cm (Mair et al., 2016). This size results in a theoretical radar cross section



Fig. 2. Example of a multi-functional control point. The TLS reflector target (bottom right), the InSAR Corner and on it the basement for the GNSS reference station with attached GNSS antenna.

of approximately 20 dB for the COSMO-SkyMed® X-band data used. To reduce the weight of the reflector and to facilitate snow melt, a regular grid of circular holes was drilled in the 3 mm aluminium plates. The hole diameter of 6 mm does not interfere with the wavelength used by the satellite system. The TLS reflectors consist of metal plates laminated with retro-reflecting foil. In addition to the linking points four other reflectors were used to define the TLS reference frame. They were mounted on stable bedrock at various distances from the scan position, i.e. shorter distances for the positioning and longer ones for the orientation of the scanner.

3.3. GNSS

Relative GNSS measurements were carried out using two base stations in stable terrain and one rover for the data acquisition in the mass wasting zone. The double frequency sensors Leica Viva GS10 and Leica GS530 were used. A network of GNSS measurement platforms was installed, taking into account the expected surface kinematics and the geometrical GNSS requirements (i.e. satellite visibility, baseline length). The platforms consisted of measurement poles mounted on large boulders; 14 measurement points were defined in addition to the base stations (Fig. 1). One GNSS campaign was carried out in summer 2012 and three during the summers 2013 and 2014 (Table 2). To obtain highly accurate results, each point was measured in static mode for at least 30 min with a 5 second sampling rate.

The post-processing of the collected GNSS data was performed using the 'Leica Geo Office' software, by Leica Geosystems. Baselines of all rover points to both base stations were calculated and the relative coordinates of these points were defined. The comparison of the baselines from two different base stations allowed the identification of large errors. Random errors of single points were minimized by calculating a least squares adjustment of the GPS network baselines. In order to refer the local net to the global reference system the base stations were connected to permanent reference stations belonging to the Swiss geodetic network (SWIPOS). The results of two measurement campaigns A and B were referred against each other by correcting the

point coordinates of the repeat measurement B by the deviation A-B of the Barycenter between the local reference stations. The degree of precision between two measurement campaigns is equivalent to the accuracy of the displacement values. This precision was equivalent to the remaining deviation of the reference station coordinates between two measurement campaigns, after they have been corrected by Barycenter bias (accuracy specifications are given in the Results section).

For calculating displacement velocities from the GNSS data we carried out a pre-selection of rover points. A few of these rover points

Table 2
Dates of the measurement campaigns.

	TLS	GNSS	DInSAR
2009	Sep, 11	–	–
2010	Aug, 04	–	–
2011	Aug, 18	–	–
2012	Sep, 18	Sep, 18	Jul, 21 Aug, 06 Aug, 22 Sep, 07 Sep, 23
2013	Aug, 29	Jul, 24–25 Aug, 29 Sep, 23	Jul, 24 Aug, 09 Aug, 22 Aug, 25 Sep, 07 Sep, 10 Sep, 14 Sep, 09
2014	Aug, 15	Jul, 09 Aug, 18–19 Sep, 30	Jul, 15 Jul, 23 Aug, 16 Aug, 25 Aug, 28 Sep, 13 Sep, 29 Oct, 03 Oct, 12

showed movements below the level of significance, a few others could not be measured during each campaign due to logistic reasons and thus show data gaps. Both types of rover points were therefore excluded from the calculation. For the remaining points a mean velocity per measurement interval was defined.

3.4. TLS

Annual TLS measurements have been carried out for the entire site since 2009. Shorter measurement intervals showed no significant movement results. The instruments used were a Riegl LPM321, and from 2013 onwards a Riegl VZ6000. Both scanner systems are specified for long range applications (for technical details see: www.riegl.com). Measurements were carried out from a single fixed scan platform on the mountain ridge Mout da Barba Peider (Fig. 1). The scans were performed with a resolution of <10 cm (range dependent). Referenced images of the scan areas were taken using the camera integrated in the scanners. To reference the data, six retro-reflecting reference points including the reference frame linking points were scanned at a very high resolution. The absolute coordinates (WGS84) of the reference points were defined in advance, using a Leica TPS1200 total station.

The point clouds acquired were filtered to remove outliers and to homogenize the spatial resolution. To achieve an optimal relative referencing of the multi-temporal scans, the iterative closest point (ICP) algorithm was applied to match unchanged terrain parts in the scan (Chen and Medioni, 1991). Subsequently the set of relative registered point clouds was transformed into global coordinates using the least squares adjustment of all observations on reference points carried out for the single scans. The point clouds were then transformed into grid based digital elevation models (DEM) with 20 cm resolution. Small data gaps were filled using a 3×3 cell mean interpolation.

Horizontal 2D displacements (i.e. rock glacier creep) were derived from the multi-temporal DEM using the surface structure of the blocky terrain. The DEM grids were filtered using a high pass filter which removed information about the raw topography from the grid and only conserved the high frequency surface structure (blocks and boulders). These surface models were grey value scaled to visualize the surface pattern and saved as images. Subsequently image patches of 10×10 m were matched using the particle imaging velocimetry correlating method introduced by Roesgen and Totaro (1995). This algorithm produced a 2D displacement vector for each patch. The resulting vector field was filtered to eliminate faulty correlations (Kenner et al., 2014).

Regarding the vertical component of the displacement, a simple difference DTM would show the surface change on a specified location in the reference system. The GNSS and DInSAR methods track the movement of a single surface point or surface patch instead. This methodical difference would not allow a direct comparison of the vertical displacement components between the different measurement systems. An additional processing step was therefore applied to the TLS data. Initially, the DEMs of the first measurement t_1 and a repeat measurement t_2 and the horizontal 2D displacement vector field between both measurements were used. For the initial position of each horizontal 2D displacement vector, the elevation value was defined by calculating a weighted average between the four closest cell centres of DEM t_1 surrounding the point. Subsequently the displacement value was added to the initial positions of the displacement vectors and the elevation calculation was applied to this second set of points using the DEM t_2 . Both elevations were subtracted to define the change in elevation for each point pair. This elevation difference represents the dZ component of the final 3D displacement vector field. Fig. 3 summarizes this procedure.

An accuracy analysis of the TLS measurements at this site was previously carried out by Kenner et al. (2014), detailing a methodical approach to define accuracy specifications for TLS displacement measurements in position and elevation (accuracy specifications are given in the Results section below).

3.5. DInSAR

The spatial and temporal resolution of space-borne SAR imagery were important characteristics on which the selection of a satellite system was based on. Additional analyses were carried out including a topographical analysis, applying distortion masks to simulate the layover, shadowing and foreshortening effects. Based on this, the satellite platform COSMO-SkyMed, operated by the Italian Space Agency and the Italian Ministry of Defense was selected. It consists of four satellites with a revisit time of 8–16 days. To capture the West oriented mountain cirque, descending orbits were used with a resulting off-nadir angle of 30.620 degrees. The SAR acquisition was carried out in stripmap mode with a nominal spatial resolution of 3 m.

Multi-temporal DInSAR uses stacks of SAR images acquired with the same geometry and exploits the redundant information of phase difference to measure ground displacements. The available techniques can be grouped in two main classes: Persistent Scatterers (PS; Ferretti et al., 2001) and Small Baseline Subsets (SBAS; Berardino et al., 2002). Both methods can deliver displacements along the line of sight (LOS) direction with accuracy in the order of a few millimetres per year (Pasquali et al., 2014). In a recent paper, Barboux et al. (2015) applied PS and SBAS interferometry based on TerraSAR-X for the monitoring of Swiss rock glaciers. One central finding of the aforementioned study was that SBAS interferometry was able to detect maximum displacements ten times larger than PS interferometry (3.5 cm/a versus 35 cm/a for SBAS) but inaccurate measurements due to phase unwrapping errors were already observed for velocity rates larger than 20 cm/a. Referring to the creep velocities of up to 25 cm/a we chose the SBAS technique developed by CNR IREA of Naples (Lanari et al., 2004) for our data analysis. This technique uses the surface structure as natural scatter and allows an analysis of the study area with a high spatial resolution. The study site, showing a complete absence of vegetation and widespread rocks and boulders, was particularly suited for the application of this algorithm.

The influence of atmospheric distortions such as refraction in SAR images declines with an increasing number of images. To achieve a high accuracy, multi-interferometry of SAR data requires a minimum of 20 images to effectively remove the distortions by applying spatial and temporal filtering operations (Colesanti et al., 2003). The implementation of our concept showed that due to the short snow free period at this elevation, only 5 images could be captured in 2012, 8 in 2013 and 9 in 2014. This not only affected the accuracy of the results, but also the resolution of spatially differential movements. The spatial resolution of the generated surface velocity maps was thus adapted to the significance of the data and lowered to $15 \text{ m} \times 21 \text{ m}$.

Geometrical or electrical changes in the properties of the Earth's surface between data acquired at different times are potential sources of temporal decorrelation. If the temporal decorrelation between two consecutive images is high (usually a threshold of 0.7 is used), no reliable interferogram or deformation map can be created. Moreover, if the deformation along the LOS is greater than half the wavelength (i.e. 1.55 cm in the COSMO-SkyMed data) aliasing problems can occur. Similar problems arise for parts of a scene covered by snow. In our study area, the snow-free period only lasted for 3–4 months each year and thus hindered the determination of interannual displacements.

3.6. Integration of multi-methodical measurement results

To compare the results acquired with GNSS and TLS, each GNSS displacement vector was linked to the mean of all TLS displacement records in its $15 \text{ m} \times 15 \text{ m}$ surroundings. The deviation between both solutions was calculated for each data pair in all three spatial components. Subsequently the mean absolute error deviation was specified for each directional component.

To allow a comparison of the DInSAR monitoring results and the results obtained from TLS and GNSS, the 3D movement information of the

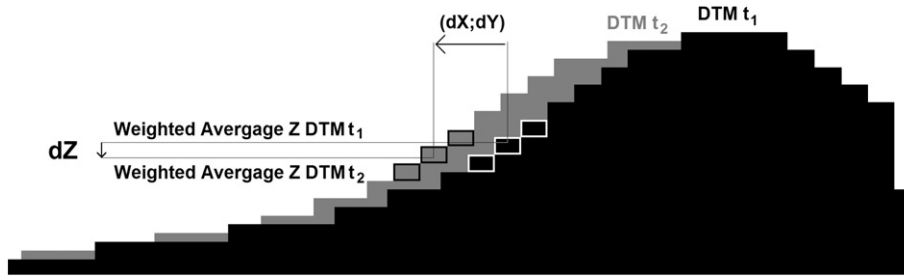


Fig. 3. Sketch showing the mode of extracting the z component of a movement from two TLS DTMs.

latter had to be projected on the line of sight (LOS) of the SAR satellite. In a Cartesian coordinate system both the displacement and the LOS of the radar sensor are represented by a 3D vector. The scalar product of the displacement vector $\vec{a} = (a_x, a_y, a_z)$ and the unit vector $\hat{b} = (b_x, b_y, b_z)$ of the radar LOS results in the projection of \vec{a} on \hat{b} . The TLS and GNSS displacement vectors were projected on the SAR LOS to achieve comparability between the different datasets.

The GNSS measurements were carried out with a similar temporal resolution as the DInSAR measurements and were used as comparative data. All DInSAR displacement values in a 15 m radius around each GNSS point were averaged and linked to the GNSS displacement result. These values were normalized by time and then directly compared to define the absolute accuracy of DInSAR monitoring results.

So far, data from different measurement systems were only compared with each other. In the next step the three dimensional information of a TLS reference measurement is linked to DInSAR results of another measurement period, to extrapolate these DInSAR results into 3D. The information content of the DInSAR is thus clearly improved. To do this, TLS displacement data were transformed into an extrapolation mask for DInSAR in the following way: TLS displacement vectors \vec{a} for the monitoring period 2013–14 were projected onto the LOS of the SAR sensor. This projection is called \vec{c} . Subsequently all three spatial displacement components of \vec{a} were expressed as a fraction of the length of the vector \vec{c} (Eqs. (1–3)).

$$a_x = u \cdot [\vec{c}] \quad (1)$$

$$a_y = v \cdot [\vec{c}] \quad (2)$$

$$a_z = w \cdot [\vec{c}] \quad (3)$$

Using the vector specific fraction parameters u , v and w a 1D DInSAR displacement value can be extrapolated to 3D under the assumption that the creep directions remain constant. We extrapolated the DInSAR displacements in summer 2013 to 3D by splitting each DInSAR displacement value into the components dx , dy and dz by multiplication with the mean fraction parameters of all TLS vectors in their 15×15 m vicinity.

In a following step, the reliability of the DInSAR derived 3D dataset was tested. Although TLS and DInSAR datasets were now both available in 3D, they could not be compared directly due to their different temporal resolution. TLS measurements were taken with an annual resolution, whereas no interannual DInSAR processing was possible. However, the relative spatial distribution of the creep velocity was assumed to be similar between the different but temporally close observation periods of both datasets. This implies that the ratio in velocity between a fast moving zone and a slow moving zone should be approximately the same for both methods. Although the relative velocity pattern remained constant, the absolute displacement values differed between different observation periods due to: a) temporal creep velocity differences and b) different durations of the monitoring intervals.

To eliminate this scale difference between both datasets, the TLS displacement vectors were scaled on the DInSAR vectors. The scaling factor was defined using the ratio of the mean norm of all DInSAR displacement vectors and the mean norm of all TLS displacement vectors. Subsequently root mean square error and mean absolute deviation between the datasets were calculated.

4. Results

4.1. Results and comparability of GNSS and TLS

The individual results of GNSS and TLS measurements were plausible and coherent. TLS captured highly differential surface movements with a high area covering resolution (Fig. 4). GNSS single point measurements confirmed the vector field obtained by TLS and provided a higher temporal resolution during the summer months (Fig. 5).

The 3D mean absolute error (MAE) between displacement records of GNSS and TLS was found to be 3.7 cm and the root mean square error (RMSE) 3.4 cm. There is no significant difference in the deviation for the single directional components. The deviations are slightly higher than the TLS precision of 3.3 cm for the position, and 3 cm for the elevation and clearly greater than the GNSS precision of 2 mm on the East-, 0.8 mm on the North- and 6 mm on the elevation component.

4.2. Results, validation and integration of DInSAR measurements

The rock glacier movement at Foura da l'amd Ursina could also be verified with the satellite-borne DInSAR measurements. As mentioned in the method section the DInSAR displacement solutions only exist for individual summer seasons and not on a full annual basis. A first comparison shows that the zones of mass movements detected by DInSAR are almost the same as the zones detected by terrestrial laser scanning. These zones correspond to the geomorphologically defined spatial extent of the rock glaciers (Fig. 6). DInSAR captured the mass movement area with a similar reliability as TLS at this site, yet with a lower spatial resolution. Unfortunately, movement rates could not be quantified in some of the fast moving zones of the rock glacier complex by DInSAR. No correlation between the limited number of SAR images could be established here by the DInSAR processing. As a couple of GNSS basements are located in these fast moving zones the comparison of GNSS and DInSAR displacement results is based on a small statistical baseline. This comparison was intended to give an estimation of accuracy and reliability on the DInSAR results. However, we obtained differences between both methods that cannot be explained by the error budgets alone. Fig. 7 shows the differences of GNSS and DInSAR displacement records projected on the LOS of the radar sensor. The values are given in mm per day and are based on the monitoring period 2013 (61 days for GNSS and 76 days for DInSAR) (Table 2). Although the 3D GNSS displacements include larger error influences compared to the 2D solutions, they are probably more relevant in this figure, as the elevation component of the movement is disproportionately strong represented in the LOS projection. Parts of the differences between GNSS and DInSAR are related to measurement errors. The error bars for the GNSS

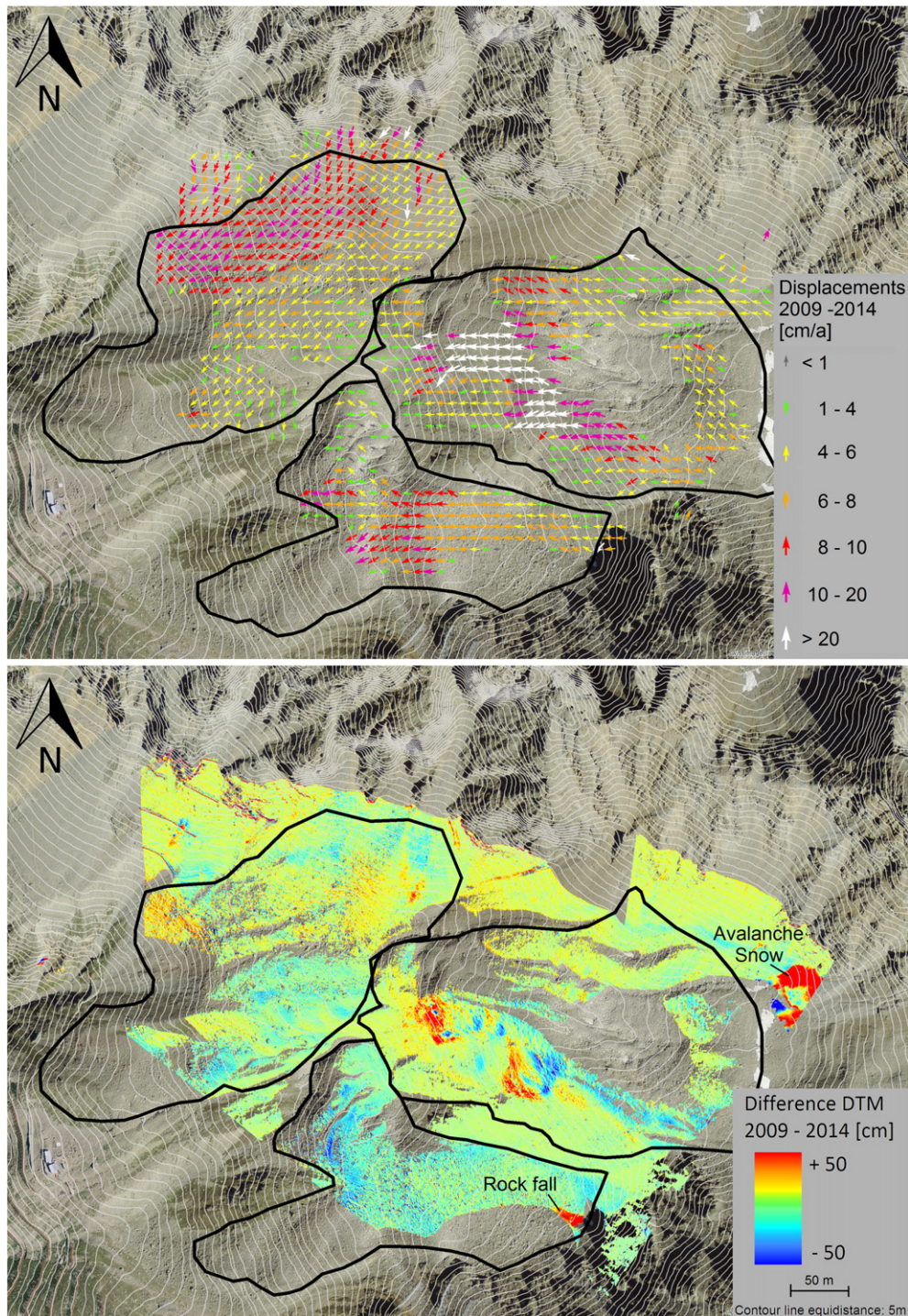


Fig. 4. Results of the TLS measurements between 2009 and 2014. Horizontal 2D creep rates are shown for visualization. The vertical differences represent the differences between the DTMs.

measurements are included in the figure. Certainly also the DInSAR results show sub-optimal accuracy. This is likely due to the relatively low number of available acquisitions; as a rule of thumb, an accurate SBAS analysis requires 20–25 images – however, for our analyses, a lower number of images was available. Another problematic issue is the uneven distribution of the images over time. Moreover, the analysed deformation phenomena are characterised by fast ground displacements (i.e. in relation to the X-band wavelength) and high spatial (Fig. 4) and temporal (Fig. 5) heterogeneity. These conditions are not ideal for DInSAR applications and lead to errors in the phase unwrapping, particularly in fast moving areas. Another error source contributing to

the deviations between GNSS and DInSAR in Fig. 7, is the spatial averaging of the DInSAR displacements over a 15 m radius around each GNSS monitoring point. While the GPS value represents the displacement of one point, DInSAR represents the displacement of a large area surrounding this point. However, also GNSS points that are surrounded by homogeneous DInSAR displacement values (Fig. 6, e.g. point 18 and 27) show high deviations (Fig. 7). Another explanation for the deviations is therefore, that the GNSS single point measurements include small scale surface movements that superimpose the large scale rock glacier creep and disturb the creep signal, especially for short measurement periods (Wirz et al., 2014). These small scale effects e.g. the toppling or

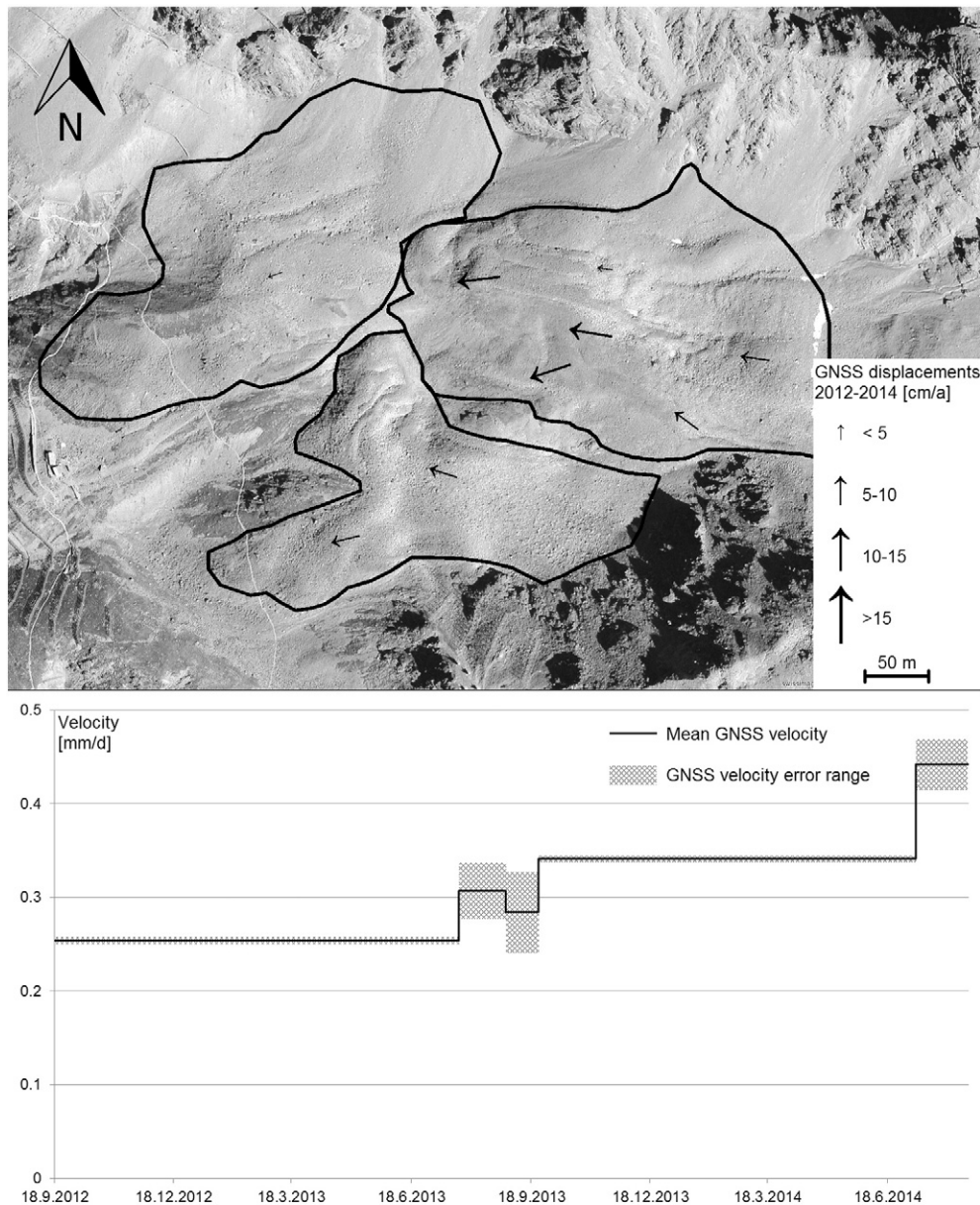


Fig. 5. Velocities of the GPS point displacements during the monitoring period 2012–2014, in spatial resolution (top) and temporal resolution (bottom).

subsiding of single rocks are not included in the DInSAR signal that is achieved by the correlation of larger surface patches. An accuracy assessment using single point measurements is therefore only reasonable for a longer monitoring period.

The 3D vector field extrapolated from DInSAR displacement values with the help of the TLS extrapolation mask showed visually plausible results (Fig. 8). Unfortunately, large parts of the moving area are not included in the dataset: on the one hand the areas of DInSAR decorrelation and on the other the areas in the TLS shadow. The comparison with the scaled TLS 3D vectors resulted in an MAE of 1.1 cm and a RMSE of 1.5 cm. The highest displacement values within the reference period, i.e. the DInSAR monitoring period of 2013, were around 6 cm. We can therefore consider the relative velocity pattern of TLS and DInSAR as significantly coherent.

5. Discussion

Space-borne DInSAR is an established method to detect and monitor large scale surface displacements or numerous small scale displacements

that are distributed over large areas. One aim of this pilot study was to identify an appropriate complementary method for large scale DInSAR data at local scales and for a limited time period to provide 3D movement information of individual mass movements. TLS and GNSS were tested as complementary methods. When comparing TLS and GNSS directly, we found consistent results; the deviations between both were mainly controlled by the measurement precision of the TLS system. Static GNSS showed the higher precision, thus providing the possibility of a higher temporal measurement resolution or rather shorter significant monitoring intervals. When comparing GNSS to DInSAR deviations of different magnitude and algebraic sign occurred. Phase unwrapping errors might be one explanation for these deviations. As the comparison period of both methods corresponds to time scales of weeks to a couple of months, short term surface movements, which are not captured by DInSAR might also contribute to the deviations. Small scale surface movements of the blocky surface (toppling, subsidence or acceleration of single boulders) induced by the creep process may have distorted the signal of the large scale creep process in the GNSS single point measurements (Wirz et al., 2014). The differing algebraic sign of the

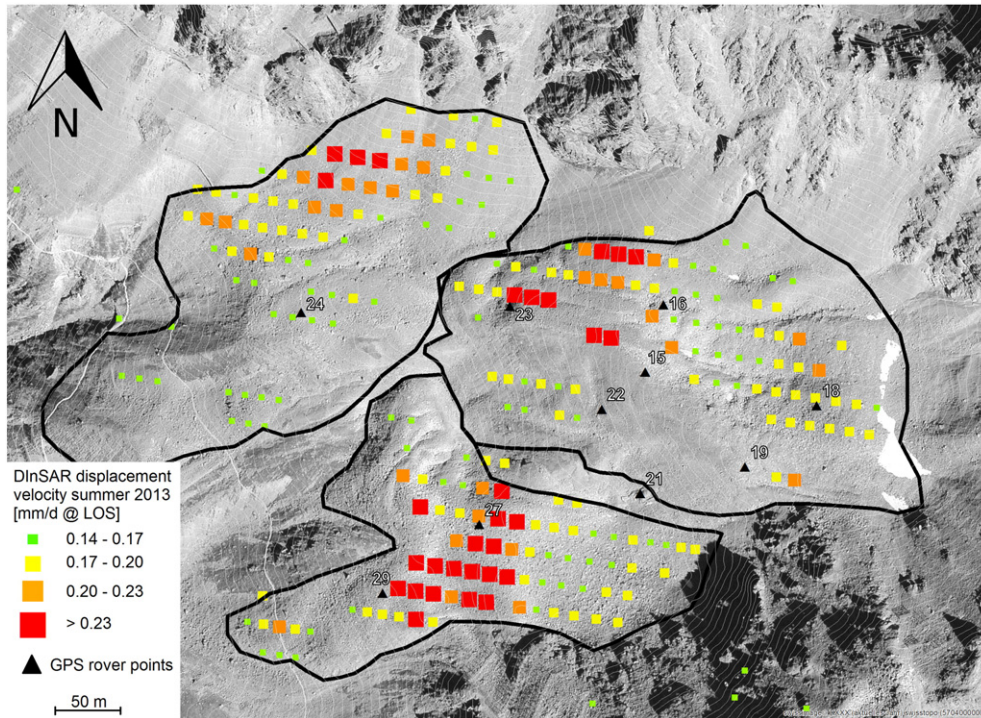


Fig. 6. Mean velocity of the rock glaciers in the direction of the line of sight of the SAR sensor. Additionally the locations of the GNSS rover points are mapped.

deviations supports this second hypothesis. In the short term, the deviations between both measurement systems occasionally reached magnitudes higher than the creep process itself and caused a total misalignment with the DInSAR results. An accuracy analysis of the DInSAR results using GNSS data was difficult due to the unknown origin of these deviations. However these deviations are random and become less significant with increasingly long measurement periods. Therefore the phenomenon was not observed in the comparison of GNSS and TLS, as these results were compared over a much longer time span. The GNSS advantage of high accuracy associated with higher temporal resolution was nevertheless almost invalid. Instead, the weakness of GNSS in relation to TLS became more relevant: this is mainly the very low spatial

resolution of the data. It is highly improbable that meaningful conclusions can be drawn from the GNSS displacements mapped in the upper section of Fig. 5 regarding the rest of the rock glacier complex. Nevertheless, it is still possible to derive an overview of the seasonal creep velocity signal for the entire site out of the GNSS data by using the spatial redundancy of multiple GNSS monitoring points to filter out the small-scale distortions (lower section of Fig. 5).

TLS was the more convincing complementary method to DInSAR in this study. It allowed the creation of an area-wide 3D extrapolation mask for the DInSAR displacements and showed a high degree of relative conformity with them. This is due to the similar procedure of displacement tracking of these methods. Both correlate surface patterns

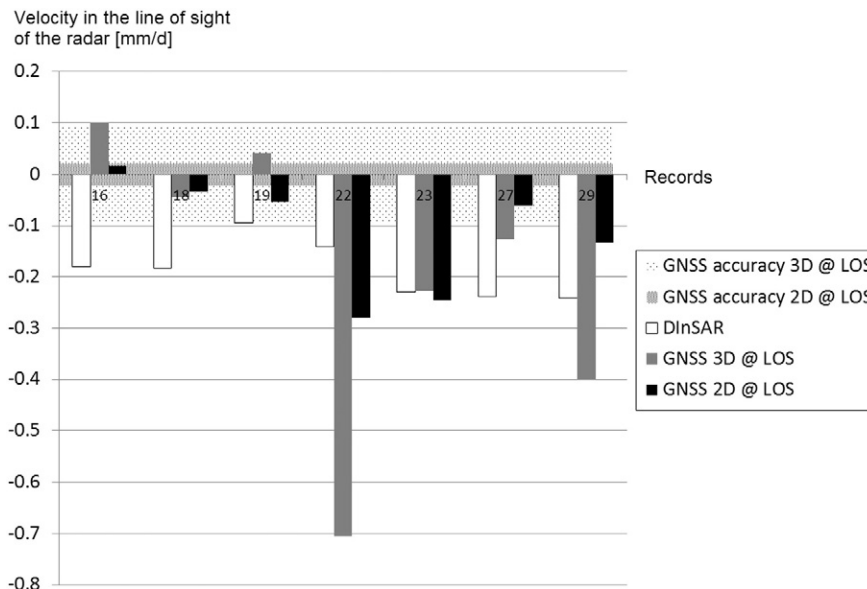


Fig. 7. Differences between GNSS displacements projected in the line of sight of the radar and the surrounding DInSAR displacement values; the values are based on the summer monitoring period 2013 (61 days for GNSS and 76 days for DInSAR). Systematic deviations are evident.

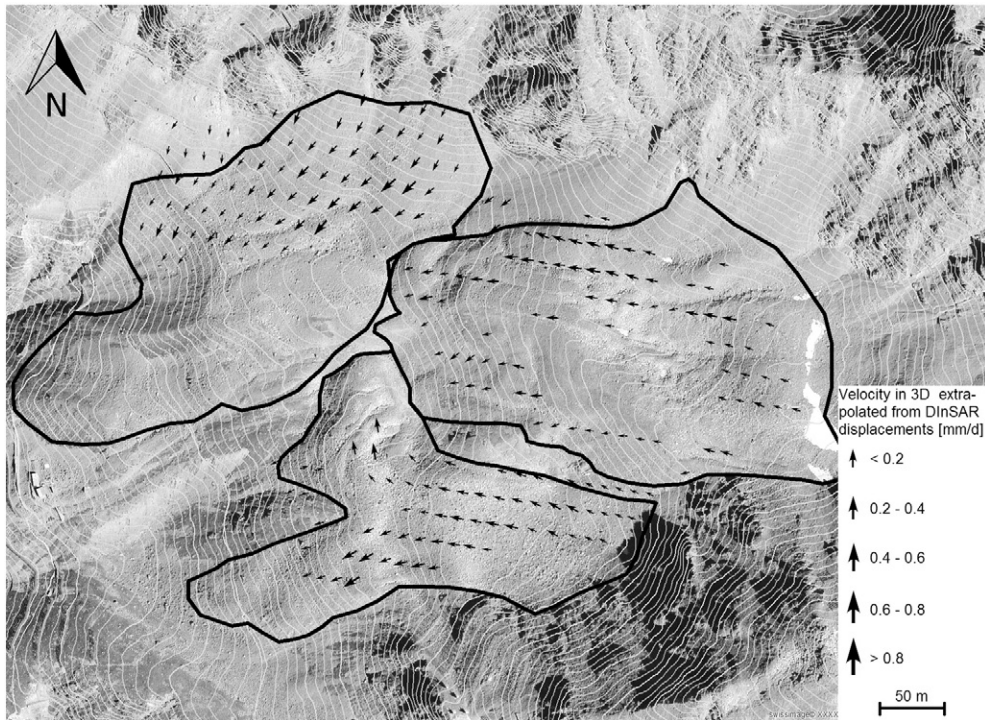


Fig. 8. 3D Vector field extrapolated from DInSAR measurements using a TLS extrapolation mask.

of several square meters to detect movements. In contrast to GNSS measurements, small-scale surface movements were therefore not captured; the movement signal rather represents the movement of the entire rock glacier body instead. Moreover, TLS has the great advantage of being a remote sensing method avoiding time consuming and potentially dangerous work directly on the difficult terrain of the monitored object. However, in contrast to GNSS, TLS fails due to visibility disruptions by cloudage, fog, snow coverage or terrain shadows.

For this study site, space-borne DInSAR measurements did not meet all the expectations of our study. This was mainly due to the loss of SAR image correlation caused by a) the long period of snow coverage and b) the too low frequency of SAR image acquisitions in relation to the rock glacier movement. As both issues are valid for many high alpine mass movement zones, this must be considered as being a characteristic limitation of the method. The long snow period not only prevents the capture of inter-annual deformation time series, it also lowers the spatial resolution and accuracy of intra-seasonal results. The decorrelation in fast moving terrain parts can theoretically be limited with shorter measurement intervals. However, the planning of data acquisition is subject to restrictions by the provider and this study used the highest temporal resolution available. Our study area is small and not representative for all alpine mass movements. It is therefore likely, that other problems and restrictions may occur when applying this concept to other alpine sites. In particular, shadow effects inherent to the remote techniques TLS and DInSAR might play a much more important role at other sites.

Apart from these limitations, DInSAR delivered reliable and plausible results and was in general suitable for our measurement concept. The common reference frame proved to be stable for all three methods and allowed data comparability. The DInSAR extrapolation mask created using the 3D TLS information allowed a simple 3D projection of the radar data. In contrast to the original DInSAR deformations, these 3D vector fields can be interpreted intuitively and allow a rapid recognition of potentially hazardous accelerations: Depending on the SAR geometry, the raw DInSAR displacements results show sometimes just a small fraction of the actual movement; the movement velocity and so the absolute magnitude of a possible acceleration are strongly underestimated. This can lead to misinterpretations regarding the risk

assessment. The 3D extrapolation allows the estimation of the real velocity and acceleration values. Moreover, the comparison with the TLS monitoring results showed that the DInSAR method captured spatial velocity differences with a similar reliability as TLS.

6. Conclusions

Summarising, the applied measurement concept is a sufficient way of rationalising the monitoring efforts for selected mass movements. This selection is mainly based on the applicability of spaceborne DInSAR measurements regarding overlay, foreshortening and shadowing as well as the duration of Snow coverage and the continuous availability of SAR images in a sufficient frequency. Furthermore the movement directions of the mass movement have to stay constant and the application of TLS or other terrestrial measurement systems must be feasible. Apart from this limitations the initially defined requirements cost-efficiency, long term monitoring, self-operating mode and large scale application with cm accuracy are fulfilled.

Additionally we can draw the following conclusions:

- Referring to the initially defined requirements, TLS was shown to be the more suitable complementary measurement method for DInSAR. The reasons are the similar tracking method for surface displacements, the high spatial resolution and the efficient remote sensing. It should be noted that there may be different results for other sites.
- On short time scales up to months, GNSS and DInSAR displacement values show large deviations. They are probably the result of small scale surface movements included in the GNSS signal or originate from error sources which could not be identified within this study.
- Space-borne DInSAR showed considerable limitations in alpine terrain due to a short measurement season (long snow coverage), spatially differential creep velocities and complex terrain. This led to spatial and temporal data gaps and a reduced accuracy and spatial resolution.
- Nevertheless, reliable and valid 3D results could be extrapolated from the DInSAR records with the help of a single TLS repeat

measurement. These results are easy to interpret and include considerably more information.

- Considering its limitations, a suitable practical application for space-borne DInSAR in combination with a complementary reconnaissance method is the monitoring of extensive, slightly active, long term mass movements that require observation. Furthermore, the area wide acquisition and analysis of DInSAR data allows to detect hitherto unknown mass movements which can then be investigated using the presented monitoring concept to facilitate the early recognition of hazardous areas.

Acknowledgements

The village of Pontresina is thanked for allowing the installation of the measurement setup. This project was funded by Interreg (project no. 13.2011.1180.5), with joint funding from Canton Graubünden, the Swiss Confederation and the European Union. Natascha Maria Gruber is thanked for her support in the field. Helibernina is thanked for logistic support.

References

- Abellán, A., Calvet, J., Vilaplana, J.M., Blanchard, J., 2010. Detection and spatial prediction of rockfalls by means of terrestrial laser scanner monitoring. *Geomorphology* 119 (3–4), 162–171.
- Angeli, M.-G., Pasuto, A., Silvano, S., 2000. A critical review of landslide monitoring experiences. *Eng. Geol.* 55 (3), 133–147.
- Bamler, R., Hartl, P., 1998. Synthetic aperture radar interferometry. *Inverse Prob.* 14.
- Barboux, C., Delaloye, R., Strozzi, T., Lambiel, C., Collet, C., Raetzo, H., 2012. Monitoring active rock glaciers in the Western Swiss Alps: challenges of Differential SAR Interferometry and solutions to estimate annual and seasonal displacement rates. *Geoscience and Remote Sensing Symposium (IGARSS)*, 2012. IEEE International, pp. 5210–5213.
- Barboux, C., Strozzi, T., Delaloye, R., Wegmüller, U., Collet, C., 2015. Mapping slope movements in Alpine environments using TerraSAR-X interferometric methods. *ISPRS J. Photogramm. Remote Sens.* 109, 178–192.
- Bauer, A., Paar, G., Kaufmann, V., 2003. Terrestrial laser scanning for rock glacier monitoring. In: Phillips, Springman, Arenson (Eds.), 8th International Conference on Permafrost. Swets & Zeitlinger, Zurich, Switzerland, pp. 55–60.
- Berardino, P., Fornaro, G., Lanari, R., Sansosti, E., 2002. A new algorithm for surface deformation monitoring based on small baseline differential SAR interferograms. *IEEE Trans. Geosci. Remote Sens.* 40 (11), 2375–2383.
- Bingyuan, H., Chao, M., Guifang, Z., Lixun, K., 2008. Analyzing decorrelation of multi-temporal SAR data on InSAR. *Image and Signal Processing*, 2008. CISP '08. Congress on, pp. 452–461.
- Bühler, Y., Marty, M., Ginzler, C., 2012. High resolution DEM generation in high-alpine terrain using airborne remote sensing techniques. *Trans. GIS* 16, 635–647.
- Chen, Y., Medioni, G., 1991. Object Modeling by Registration of Multiple Range Images, Robotics and Automation, 1991. Proceedings., 1991 IEEE International Conference on vol. 3, pp. 2724–2729.
- Colesanti, C., Wasowski, J., 2006. Investigating landslides with space-borne Synthetic Aperture Radar (SAR) interferometry. *Eng. Geol.* 88 (3–4), 173–199.
- Colesanti, C., Ferretti, A., Prati, C., Rocca, F., 2003. Multi-image satellite SAR interferometry: state of the art and future trends, Radar Conference, 2003. Proceedings of the International, pp. 239–244.
- Delaloye, R., Morard, S., Barboux, C., Abbet, D., Gruber, V., Riedo, M., Gachet, S., 2013. Rapidly moving rock glaciers in Mattertal. In: Graf, C. (Ed.), Mattertal - ein Tal in Bewegung. Eidg. Forschungsanstalt WSL, St. Niklaus, pp. 21–31.
- Echelard, T., Krysiwicki, J., Gay, M., Schoeneich, P., 2013. Détection des mouvements de glaciers rocheux dans les Alpes françaises par interférométrie radar différentielle (D-InSAR) dérivée des archives satellitaires ERS (European Remote Sensing). *Geomorphology* 3, 231–242.
- Eisenbeiß, H., 2009. UAV Photogrammetry, ETH Mitteilungen Nr.105. ETH Zurich, Zurich, Switzerland.
- Fabris, M., Dipartimento di Fisica, S.G. Università degli Studi di Bologna, Italy, Pesci, A., Istituto Nazionale di Geofisica e Vulcanologia, S.B., Bologna, Italia, 2005. Automated DEM Extraction in Digital Aerial Photogrammetry: Precisions and Validation for Mass Movement Monitoring.
- Ferretti, A., Prati, C., Rocca, F., 2001. Permanent scatterers in SAR interferometry. *IEEE Trans. Geosci. Remote Sens.* 39 (1), 8–20.
- Gischig, V., Loew, S., Kos, A., Moore, J., Raetzo, H., Lemy, F., 2009. Identification of active release planes using ground-based differential InSAR at the Randa rock slope instability, Switzerland. *Nat. Hazards Earth Syst. Sci.* 9 (6), 2027–2038.
- Kääb, A., 1999. Photogrammetry for early recognition of high mountain hazards: new techniques and applications. *Phys. Chem. Earth* 25, 765–770.
- Kaufmann, V., Ladstädter, R., 2003. Quantitative analysis of rock glacier creep by means of digital photogrammetry using multi-temporal aerial photographs: two case studies in the Austrian Alps. In: Phillips, Springman, Arenson (Eds.), 8th International Conference on Permafrost. A.A. Balkema Publishers, Zurich, Switzerland, pp. 525–530.
- Kenner, R., Phillips, M., Danioth, C., Denier, C., Zraggen, A., 2011. Investigation of rock and ice loss in a recently deglaciated mountain rock wall using terrestrial laser scanning: Gemsstock, Swiss Alps. *Cold Reg. Sci. Technol.* 67, 157–164.
- Kenner, R., Bühler, Y., Delaloye, R., Ginzler, C., Phillips, M., 2014. Monitoring of high alpine mass movements combining laser scanning with digital airborne photogrammetry. *Geomorphology* 206 (0), 492–504.
- Kos, A., Strozzi, T., Stockmann, R., Wiesmann, A., Werner, C., 2013. Detection and Characterization of Rock Slope Instabilities Using a Portable Radar Interferometer (GPRI), *Landslide Science and Practice*. Springer Berlin, Heidelberg, pp. 325–329.
- Lambiel, C., Delaloye, R., 2004. Contribution of real-time kinematic GPS in the study of creeping mountain permafrost: examples from the Western Swiss Alps. *Permafrost. Periglac. Process.* 15, 229–241.
- Lanari, R., Mora, O., Manunta, M., Mallorqui, J.J., Berardino, P., Sansosti, E., 2004. A small-baseline approach for investigating deformations on full-resolution differential SAR interferograms. *IEEE Trans. Geosci. Remote Sens.* 42 (7), 1377–1386.
- Mair, V., Mulas, M., Chinellato, G., Corsini, A., Iasio, C., Mosna, D., Strada, C., Thiebes, B., 2016. Developing X-band corner reflectors for multi-technological monitoring of ground displacement in alpine environments. 13th Congress INTERPRAEVENT Luzern, pp. 336–344.
- Pasquali, P., Cantone, A., Riccardi, P., Defilippi, M., Ogushi, F., Gagliano, S., Tamura, M., 2014. Mapping of Ground Deformations with Interferometric Stacking Techniques, *Land Applications of Radar Remote Sensing In: Closson, Damien Dr. (Ed.) InTech* <http://dx.doi.org/10.5772/58225> Available from: <http://www.intechopen.com/books/land-applications-of-radar-remote-sensing/mapping-of-ground-deformations-with-interferometric-stacking-techniques>.
- Pritchard, M.E., Simons, M., 2002. A satellite geodetic survey of large-scale deformation of volcanic centres in the central Andes. *Nature* 418 (6894), 167–171.
- Roesgen, T., Totaro, R., 1995. Two-dimensional on-line particle imaging velocimetry. *Exp. Fluids* 19, 188–193.
- Sailer, R., Bollmann, E., Hoinkes, S., Rieg, L., Sproß, M., Stötter, J., 2012. Quantification of geomorphodynamics in glaciated and recently deglaciated terrain based on airborne laser scanning data. *Geogr. Ann.: Ser. A Phys. Geogr.* 94 (1), 17–32.
- Skolnik, M., 1980. Introduction to Radar Systems. McGraw-Hill Kogakusha Ltd., New York NY.
- Speck, R., Turchi, P., Süß, H., 2007. An End-to-End Simulator for High-resolution Spaceborne SAR Systems (pp. 65680H–65680H-8).
- Strozzi, T., Kääb, A., Frauenfelder, R., 2004. Detecting and quantifying mountain permafrost creep from in situ inventory, space-borne radar interferometry and airborne digital photogrammetry. *Int. J. Remote Sens.* 25 (15), 2919–2931.
- Strozzi, T., Farina, P., Corsini, A., Ambrosi, C., Thüring, M., Zilger, J., Wiesmann, A., Wegmüller, U., Werner, C., 2005. Survey and monitoring of landslide displacements by means of L-band satellite SAR interferometry. *Landslides* 2 (3), 193–201.
- Strozzi, T., Delaloye, R., Kääb, A., Ambrosi, C., Perruchoud, E., Wegmüller, U., 2010. Combined observations of rock mass movements using satellite SAR interferometry, differential GPS, airborne digital photogrammetry, and airborne photography interpretation. *J. Geophys. Res. Earth Surf.* 115 (F1) (n/a-n/a).
- Tobler, D., Kull, I., Hählen, N., 2012. Gefahrenmanagement der Murgänge im Spreitgraben, Guttannen. *Swiss Bull. Angew. Geol.* 17 (2), 53–61.
- Veulliet, E., Stötter, J., Weck-Hannemann, H., 2009. Sustainable Natural Hazard Management in Alpine Environments. Springer-Verlag, Berlin, Heidelberg (403 pp.).
- Wirz, V., Beutel, J., Gruber, S., Gubler, S., Purves, R.S., 2014. Estimating velocity from noisy GPS data for investigating the temporal variability of slope movements. *Nat. Hazards Earth Syst. Sci.* 14 (9), 2503–2520.
- Wirz, V., Geertsema, M., Gruber, S., Purves, R., 2015. Temporal variability of diverse mountain permafrost slope movements derived from multi-year daily GPS data, Mattertal, Switzerland. *Landslides*, pp. 1–17.

Paper 3: Sattler, K., Keiler, M., Zischg, A., Schrott, L., 2011. On the Connection between Debris Flow Activity and Permafrost Degradation: A Case Study from the Schnalstal, South Tyrolean Alps, Italy. *Permafrost and Periglacial Processes and Landforms* 22, 254–265. [10.1002/ppp.730](https://doi.org/10.1002/ppp.730).

On the Connection between Debris Flow Activity and Permafrost Degradation: A Case Study from the Schnalstal, South Tyrolean Alps, Italy

K. Sattler,^{1,2*} M. Keiler,¹ A. Zischg³ and L. Schrott⁴

¹ Department of Geography and Regional Research, University of Vienna, Vienna, Austria

² School of Geography, Environment and Earth Sciences, University of Wellington, Wellington, New Zealand

³ Abenis Alpinexpert GmbH/srl, Bozen, Italy

⁴ Department of Geography and Geology, University of Salzburg, Salzburg, Austria

ABSTRACT

The possible influence of permafrost degradation on the formation of debris flows in an area of the South Tyrolean Alps, Italy, was examined by comparing debris flow activity since 1983 with the modelled contemporary permafrost distribution. The study focused on the spatial congruence of new initiation zones and potentially marginal permafrost, which should be especially sensitive to climatic change and is presumed to be currently degrading. The results show that distinct changes in the spatial position of debris flow initiation areas mainly occurred at elevations above this marginal zone. Consequently, the changes detected in debris flow activity do not appear to have been influenced by atmospheric warming-induced degradation of permafrost. However, a link may exist to the thickening of the active layer caused by the melting of a glacier. Copyright © 2011 John Wiley & Sons, Ltd.

KEY WORDS: periglacial debris flows; mapping; permafrost degradation; spatial modelling

INTRODUCTION

Areas of mountain permafrost are expected to be significantly affected by current climate warming (Haeberli and Gruber, 2009). Mountainous areas are also subject to increasingly intense use and development (Haeberli *et al.*, 1997). Thus, the possible increase in hazard potential—especially in the European Alps—has generated considerable research on the links between atmospheric warming, permafrost degradation and slope instability (e.g. Schlyter *et al.*, 1993; Davies *et al.*, 2001; Harris *et al.*, 2001; Kneisel *et al.*, 2007; Noetzli *et al.*, 2007; Allen *et al.*, 2010; Keiler *et al.*, 2010). The present study focuses on debris flows, which are common mass-wasting processes in the changing alpine environments and thus pose significant hazards to life and infrastructure.

Recent progress in measurement techniques and modelling has improved our knowledge of the relationship between permafrost and rock face stability (e.g. Harris *et al.*, 2009), but the possible role of climatically induced permafrost degradation in the initiation of debris flows is not yet well

understood. One reason for this is an inadequate comprehension of the evolution of permafrost beneath moderately inclined slopes where debris and snow cover act as complex interfaces between the atmosphere and the subsurface (Luetsch *et al.*, 2004; Gruber and Haeberli, 2009). This creates a significant challenge for modelling the thermal condition and spatial distribution of permafrost. Furthermore, permafrost in unconsolidated materials generally has high ice contents, which retard potential thawing by the uptake of latent heat (Noetzli *et al.*, 2007). Permafrost soils thus may respond to climate forcing over several decades to centuries (cf. Haeberli, 1992) and the effects of permafrost degradation on debris flows may be difficult to detect within one or two decades. Finally, debris flows themselves are highly complex geomorphic processes. Our understanding of their initiation, resulting from the temporal and spatial concurrence of several highly variable factors including debris availability and the occurrence of transient triggering events, and their overall sensitivity to changes in climatic parameters, is still incomplete (cf. Rebetz *et al.*, 1997; Zimmermann *et al.*, 1997; Jomelli *et al.*, 2004, 2007). Yet, climatically induced thawing of alpine permafrost is expected to significantly affect the hydraulic and geotechnical properties of perennially frozen unconsolidated

Received 28 January 2010

Revised 13 May 2011

Accepted 15 May 2011

* Correspondence to: K. Sattler, School of Geography, Environment and Earth Sciences, University of Wellington, PO Box 600, Wellington, New Zealand. E-mail: katrin.sattler@vuw.ac.nz

debris and may therefore result in a transient increase in debris flow formation (cf. Zimmermann and Haerberli, 1992; Zimmermann *et al.*, 1997).

Permafrost slopes are particularly prone to slips and slides as the permafrost table at depth acts as an aquiclude and hence as a potential failure plane during periods of elevated pore pressure, such as after summer rainfall events or extreme thaw periods (cf. Larsson, 1982). Furthermore, the co-existence of frozen and unfrozen moisture in voids close to the seasonally shifting thawing plane increases the probability of active-layer failure (Nater *et al.*, 2008). Active-layer detachment failures are common in arctic fine-grained soils (cf. Harris and Lewkowicz, 2000; Lewkowicz and Harris, 2005) but have been rarely observed on coarse and generally better-drained alpine debris slopes (cf. Zimmermann and Haerberli, 1992; Rist, 2007). However, the progressive lowering of the permafrost table may increase the susceptibility of such slopes for instabilities and thus the occurrence of debris flows. The thickening of the active layer can increase sediment availability in potential debris flow initiation zones. In addition, changes may occur in the frequency of rainfall-related triggering events at high elevations (e.g. due to a rise in the level at which snow falls in the summer and consequently an increase in triggering rainfall events; cf. Beniston, 2006).

Lowering of the thaw front within permafrost soils beyond average active-layer depths may also reduce the shear strength of debris. Rist (2007) found in a laboratory experiment that active-layer instability was not triggered by the oversaturation of material at the base of the active layer but by the release of fine-grained material formerly fixed in the ice matrix. However, the potentially destabilising effect of permafrost degradation is thought to be temporally restricted. As the permafrost table progressively descends, permafrost bodies are also likely to decrease in size due to lateral melting and thermal erosion-related disintegration. The probability of slope instability related to permafrost degradation, therefore, may decrease in the long term as the slope adjusts to new conditions.

During the inferred critical thawing period, instabilities appear most likely to occur in localities near the lower limit of contemporary permafrost distribution, where permafrost bodies are thin and have temperatures close to 0°C (cf. Haerberli, 1992). These are assumed to be especially sensitive in terms of climate warming and therefore may be experiencing slow thaw. High sensitivity of relatively warm permafrost to thermal forcing has been shown in the case of permafrost creep (Kääb *et al.*, 2007). Average creep velocities have increased for a large number of rock glaciers in the European Alps since the 1990s, which is believed to be the result of increases in air temperature (Kääb *et al.*, 2007; Roer *et al.*, 2008). As increased deformation rates equate to higher material transport, accelerated permafrost creep may lead to increased sediment availability in existing debris flow initiation zones or to sediment accumulation in new process-susceptible locations and thus may also enhance debris flow activity in certain locations (cf. Pontresina/Schafberg, Hoelzle *et al.*, 1998).

The hypothesised connection between permafrost degradation in non-creeping slope material and enhanced debris flow activity has not yet been proven. Field studies of debris flow-triggering mechanisms on thawing slopes remain a challenge given the difficulties to predict where and when slope instabilities will occur (Harris, 2005). Observations of large numbers of debris flows originating in areas presumed to be at the margin of contemporary permafrost distribution lend support to the hypothesis (e.g. Zimmermann and Haerberli, 1992; Stötter, 1994; Damm and Felderer, 2008), but these are typically made following an exceptional heavy rainfall event or refer to a specific year of geomorphological mapping. The goal of the present paper is to examine debris flow activity through time in a periglacial area, which might allow for a better-informed evaluation of the influence of permafrost degradation on the initiation of debris flows.

STUDY AREA

The study area is located on the southern flank of the main divide of the European Alps and comprises the head area of the Schnalstal (Val Senales) in the northwestern part of the Autonomous Province Bozen - South Tyrol, Italy (Figure 1). The lithology is dominated by the old crystalline schistose gneiss of the Ötztaler Alps (Purtscheller, 1971) and the topography is steep with a relative relief of up to 1000 m. Some sites have only recently been deglaciated and rates of geomorphic activity are high throughout the area.

The climate is continental with an annual monthly temperature range of 16.5°C and low precipitation due to rain shadow effects (cf. Fliri, 1975). The mean annual precipitation at the Kurzras climate station (2012 m a.s.l., records since 1990; Figure 1c) is 711 mm (Autonomous Province Bozen - South Tyrol, Department of Hydrology, 2007). Mean maximum snow depth for the month of March is 90 cm at the Lazauner Alm (2427 m a.s.l., records since 1987; Autonomous Province Bozen - South Tyrol, Department of Hydrology, 2008).

The climatic conditions and the steep relief that is unsuitable for widespread glaciation favour the development and preservation of alpine permafrost, as indicated by the presence of numerous rock glaciers and protalus ramparts in the valley head area. Measurements of the basal temperature of the snow cover (BTS) indicate that the Lazaun rock glacier (Figures 1 and 5) is active and temperatures measured within a borehole drilled recently through the summit of the Grawand also show the presence of permafrost (Mair *et al.*, in preparation).

Debris flow activity in the last two decades was examined in three sub-areas (Figure 1c; Tables 1 and 2):

1. The Langgrub sub-area (Figure 2A) is in the south of the Langgrub Valley in the western part of the study area. According to a historical topographic map of the Italian Military Cartography Institute, the slope was covered by a glacier as recently as the 1960s. The glacier is no longer present and a large part of the area is mantled by

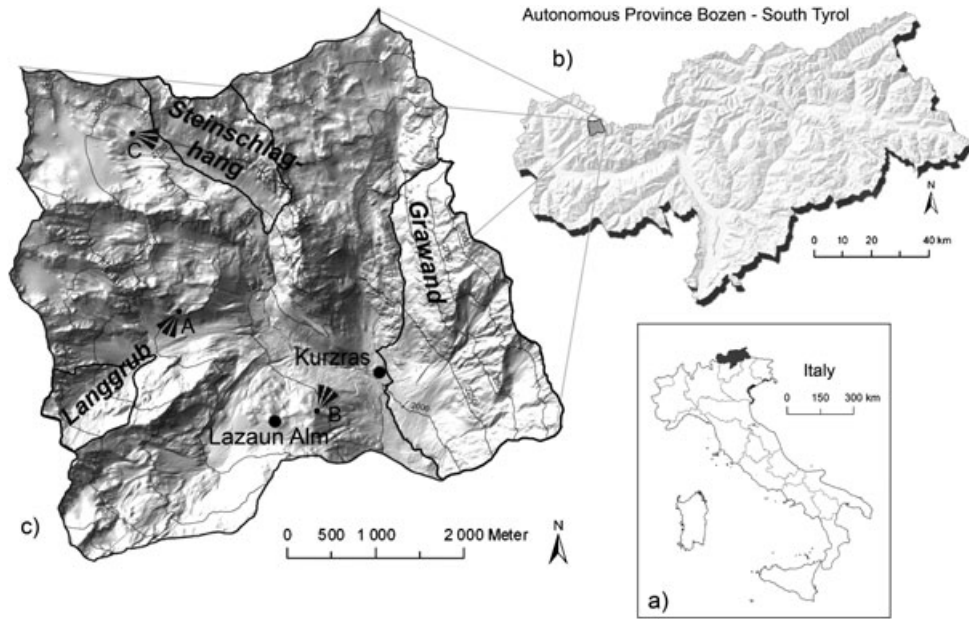


Figure 1 (a, b) Location of the study area; (c) hill shade of the study area showing sub-areas under further investigation regarding the development of debris flow activity since 1983 (outlined using a solid line), location of climate stations referred to in the text and viewpoints of photographs shown in Figure 2. (Cartographic basemap: LIDAR DEM, Autonomous Province Bozen - South Tyrol, Department of Regional Planning, 2008.)

Table 1 Basic characteristics of the investigated sub-areas.

Area	Size (ha)	Altitudinal range (m a.s.l.)	Predominate aspect	Debris-covered area (% of total area)
Langgrub	73	2504 – 3194	N – NE	75
Grawand	410	1898 – 3251	W – SW	54
Steinschlaghang	127	2434 – 3227	S – SW	50

Table 2 Characteristics of debris flow activity in the investigated sub-areas (as of 2006).

Area	Number of initiation zones	Type of debris flows (% of total number)		Material in source areas (% of total number)		
		Landslide type	Mobilised type	Rockfall debris	Morainic material	Rock glacier
Langgrub	67	36	64	22	78	—
Grawand	272	9	91	94	5	1
Steinschlaghang	125	6	94	80	20	—

morainic material, which can be easily remobilised by debris flows. Initiation zones are mainly located beneath prominent rock convexities. The debris flows are therefore predominantly of the ‘mobilised’ type, where the local concentration of water drainage is the decisive initiating factor (see Takahashi, 1981). Given the abundance of glaciogenic sediment, it is assumed that the occurrence of suitable rainfall events is the primary factor controlling their frequency. The generally long runout distances (> 500 m) observed in the sub-area support this assumption.

2. The Grawand sub-area (Figure 2B) lies in the east of the study area and comprises the whole slope-rock face complex from the Hochjoch glacier lake in the north to the Korbeck peak in the south. Initiation zones are mainly located at the mouths of steep rock channels where they meet talus slopes and are also of the mobilised type. Talus slopes below active rock walls, representing recent debris storages, are mainly of moderate size and the availability or re-accumulation of rockfall debris is hence an important factor for process initiation. The magnitude of these events is

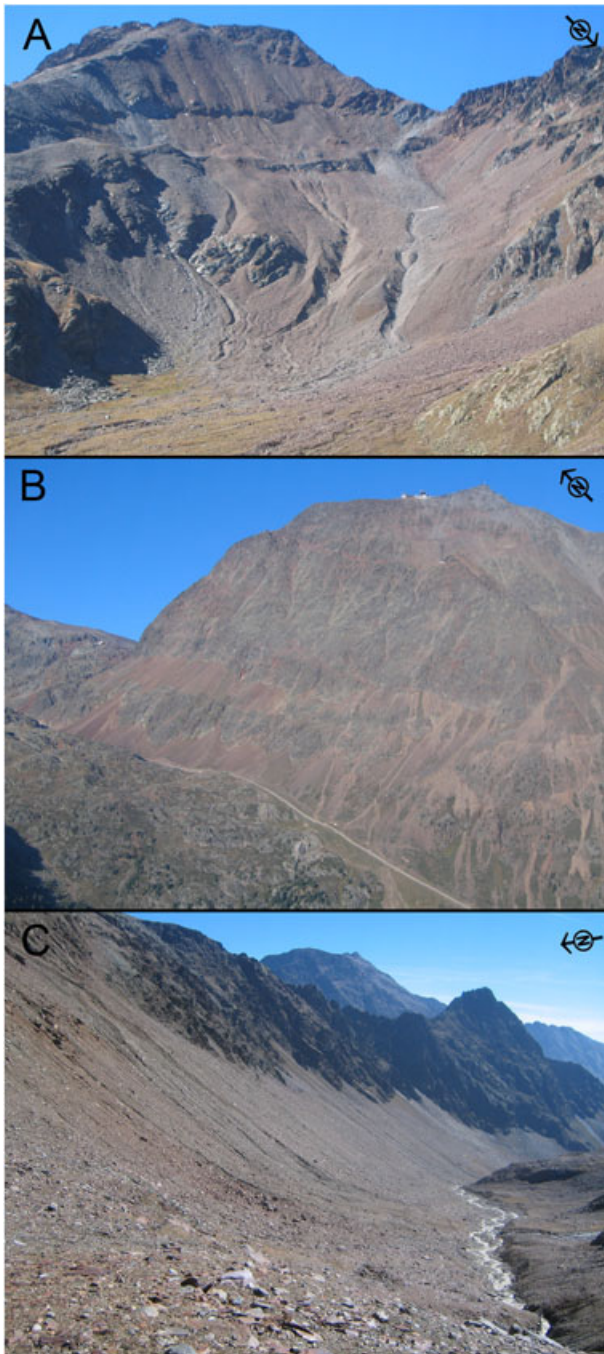


Figure 2 Photographs of the sub-areas, taken September 2006, showing different debris flow environments: (A) Langgrub, (B) Grawand and (C) Steinschlaghang. This figure is available in colour online at wileyonlinelibrary.com/journal/ppp

smaller than in the Langgrub sub-area, and source areas, travel paths and depositional areas of the debris flows are generally limited to the talus slopes (runout distances mainly < 200 m). Debris flows originating from a fossil rock glacier at the exit of the southernmost gully

system are notable exceptions as this old debris storage provides abundant material for the rainfall-dependent debris flows and slides emanating from the frontal lobe.

3. The Steinschlaghang sub-area (Figure 2C) is located in the northwest of the study area in the Steinschlag Valley. The lower part was covered by a valley glacier during the Little Ice Age, which reached its last maximum extent around 1850 AD (cf. Grove, 1988; Stötter, 1994) as evidenced by well-preserved left lateral and terminal moraines and a highly consolidated ground moraine. Debris flow initiation zones are predominantly located at the mouths of steep rock channels. The talus accumulations beneath, however, are small compared to those in the Grawand sub-area and their volume is thought to be only due to the blocking effect of the lateral moraine. Given their small size, it is assumed that the formation of debris flows in this sub-area is particularly supply dependent. Process magnitudes are small and runout distances are short (~ 250 m).

METHODS AND DATA

Geomorphological Mapping

The geomorphology of the valley head area was first mapped using analogue colour aerial photographs taken in 2004. These were examined stereoscopically and information was digitised in a GIS using a standardised group of symbols for mapping natural hazards (Bundesamt für Wasser und Geologie, 2002; see Sattler *et al.*, 2007, and Sattler, 2008). Digital orthophotographs from 1997 and 1999 and an extended field survey in September 2006 allowed for verification and updating of the digitally mapped geomorphology.

Multi-temporal Analysis of Debris Flow Activity

The geomorphological mapping and a distinct spatial concentration of debris flows led to differentiation of the three investigated sub-areas (Figure 1c). Since the absolute age of debris flow deposits and the resultant frequency of individual debris flow events are not known, a spatial clustering of process traces was taken to be indicative of a high level of debris flow activity. In the following, the term 'activity' mainly refers to the spatial occurrence of debris flows and not to magnitude-frequency relations.

The three sub-areas were analysed for changes in debris flow activity from 1983 (the earliest aerial photographs available) to 1997 and on to 2006 (including field survey observations). The low quality of the oldest aerial photographs, arising from their small scale and photographic overexposure of the slopes of interest, prevented a detailed evaluation of antecedent geomorphic situations in the sub-areas. Hence, the multi-temporal analysis involved only a visual assessment of changes in the spatial position

of debris flow initiation zones such as spatial enlargement of existing initiation zones, or the development of new initiation zones at higher elevations and/or on previously stable slopes.

Estimation of Contemporary Permafrost Distribution

Contemporary permafrost distribution in the study area was modelled using an empirical-statistical approach based on 'the rules of thumb for potential permafrost distribution in the Alps' (Haeberli, 1996). These guidelines include a list of numeric threshold values for the lower boundary, differentiating between zones of probable and possible permafrost occurrence (Table 3). The values incorporate aspect-dependent radiation effects, elevation-dependent changes in air temperature and influences of relief-controlled snow cover variation (Haeberli, 1975). Although the values were regionally calibrated in the Swiss Alps, they are thought to be applicable to the study area owing to comparable climatic conditions.

Areas bounded by the threshold values were demarcated within a GIS (ArcGIS 9.2) using a Digital Elevation Model (DEM) (2.5-m high-resolution LIDAR (light detection and ranging) DEM, Autonomous Province Bozen - South Tyrol, Department of Regional Planning, 2008) following the approach of the programs PERMAKART for slopes $\geq 11^\circ$ (Keller, 1992) and PERM (Imhof, 1996) for less-inclined areas. Gentle slopes where avalanche deposits might accumulate were omitted from the distribution predictions

Table 3 Threshold values (m a.s.l.) used for modelling the potential contemporary distribution of alpine permafrost in the study area, slightly modified after Haeberli (1996).

	Permafrost	
	Possible	Probable
Steep areas ($\geq 11^\circ$)		
N	2400	2600
NE	2450	2600
E	2600	3000 ^a
SE	2850	3000 ^a
S	3000	3175 ^b
SW	2700	2900
W	2500	2600
NW	2350	2400
Flat areas ($< 11^\circ$)		
Wind exposed	2600	2700
Wind sheltered	2650	3000 ^a

Note: Additional to probable and possible permafrost occurrence, steep areas where local permafrost distribution is primarily determined by radiation and thus aspect and flat areas where next to air temperature the existence of snow cover has significant influence are distinguished. The limit value of 11° was taken from Haeberli *et al.* (1999).

^aHaeberli (1996) indicates these values with higher uncertainty (see text).

^bValue derived from the averaged differences of adjacent orientation classes to the 'possible permafrost' threshold value.

as preliminary identification of foot-slope areas showed that they do not accumulate deep snow. Furthermore, the focus of this study is on potential debris flow initiation zones, which excludes these gently sloping sites.

Occurrences of permafrost are assumed to be extensive in the zone of 'probable permafrost' and sporadic in the 'possible permafrost' zone where they are linked to specific topo-climatic conditions (Keller and Hoelzle, 1996). Predictions in this latter category are presumed to be only 50 per cent accurate and therefore considerable spatial uncertainty exists (Haeberli, 1975). Furthermore, it is inferred that ground temperatures in the zone of 'possible permafrost' as well as areas close to the lower boundary of the 'probable permafrost' zone are close to 0°C and therefore are especially sensitive in terms of climatic change. Consequently, for this study, the zone of 'possible permafrost' and the lower 50 m of the 'probable permafrost' elevational zone were grouped as 'sensitive permafrost'.

RESULTS

Debris Flow Activity Since 1983

Distinctive shifts in the spatial position of debris flow initiation zones within the last two decades were only observed in the Langgrub sub-area where almost half of the initiation zones mapped in 2006 developed after 1983 (Table 4). Numbers of initiation zones particularly increased above 2850 m a.s.l. (Figure 3) and three out of the seven elevation classes showed disproportionately high spatial concentrations. Approximately three-quarters of the new initiation zones developed between 1983 and 1997 (Figure 4) with almost all of these located in formerly glaciated, till-covered areas. The number of initiation zones doubled above 2900 m a.s.l. from 1983 to 1997 and those that developed between 1997 and 2006 also formed predominantly in this upper slope area. No trends were observed in the type of debris flow initiation zones for the two periods.

Only minor changes in debris flow activity were observed within the Grawand sub-area. A mere 3 per cent of the debris flow initiation zones mapped in 2006 developed after 1983 (Table 4). These were predominantly in rock-debris contact zones and slightly more new initiation zones developed between 1983 and 1997 than in the subsequent period. However, in view of the limited number of changes, no conclusions can be reached regarding their spatial occurrence and type.

Changes in the spatial position of the debris flow initiation zones could not be evaluated for the Steinschlaghang sub-area owing to the poor quality of the 1983 aerial photographs.

Estimation of Contemporary Permafrost Distribution

A validation of the model output using the distribution of rock glaciers and perennial snow patches as direct and

Table 4 Number and location of new initiation zones in the sub-areas since 1983 (% of total in 2006).

	1983–97			1997–2006				
	% new initiation zones	Probable permafrost	Sensitive permafrost	Improbable permafrost	% new initiation zones	Probable permafrost	Sensitive permafrost	Improbable permafrost
Langgrub	34	31	3	0	12	11	1	0
Grawand	2	0	0	2	1	0	0	1
Steinschlaghang	—	—	—	—	—	—	—	—

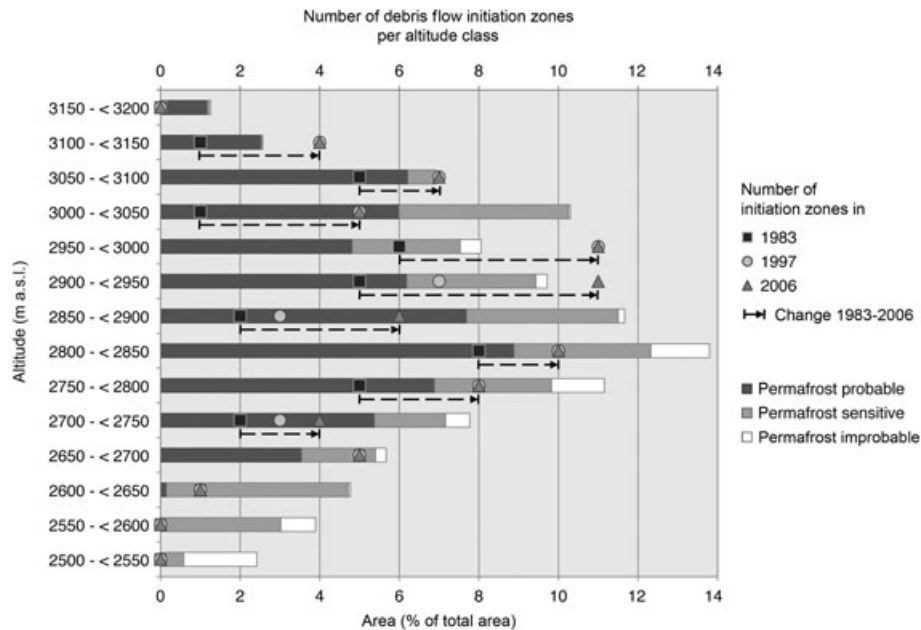


Figure 3 Changes in the number of debris flow initiation zones through time in the Langgrub sub-area in relation to observed altitude. Bars show the area of each altitudinal class and the proportional extent of modelled classes of contemporary permafrost distribution. (Numbers of debris flow initiation zones in 1997 resp. 2006 are cumulative, i.e. initiation zones that were e.g. visible in the 1983 photograph but not identifiable in the 1997 photograph (e.g. due to refilling by rockfall debris or upward shift) were also included in the 1997 count in order to illustrate the observed changes.)

indirect permafrost indicators, respectively, showed that the empirical threshold values of Haeberli (1996) produced reasonable results (Figure 5). All of the active rock glaciers inventoried lie within the modelled permafrost extent. The distribution of perennial snow patches, however, which were mapped by Zischg (2006) from orthophotographs and which comprises a synthesis of observations from 1996, 1999 and 2003, shows less accordance with the modelled permafrost distribution, especially on south-facing slopes. This may indicate an incorrect choice of threshold value for this aspect category, supporting the uncertainty originally indicated by Haeberli (1996) (Table 3). Alternatively, it relates to particularly extensive snow in 1999, perhaps due to summer snowfall or other exceptional meteorological conditions. As a result, the accuracy of permafrost modelling for south-facing slopes cannot be evaluated. However, as the modelled permafrost distribution is otherwise in good agreement with the permafrost indicators, the model is thought to be reasonable.

According to the model, approximately half of the head area of the Schnalstal has possibly permafrost and about one-third probably permafrost (Figure 5). The latter includes steep rock faces at high elevations as well as large areas of debris accumulations on north- and northeast-facing slopes in the western tributary valleys, where the permafrost extends to lower elevations. Sensitive permafrost, which may be experiencing significant degradation due to ongoing climate warming, occupies 23 per cent of the area. Information on potential permafrost distribution in the sub-areas is listed in Table 5.

Spatial Correlation of Process Initiation Zones and Permafrost Occurrence

All but one of the debris flow initiation zones mapped in 2006 for the Langgrub sub-area are situated in areas where permafrost is currently probable or possible (Table 6). This is not surprising given that these zones cover 93 per cent of

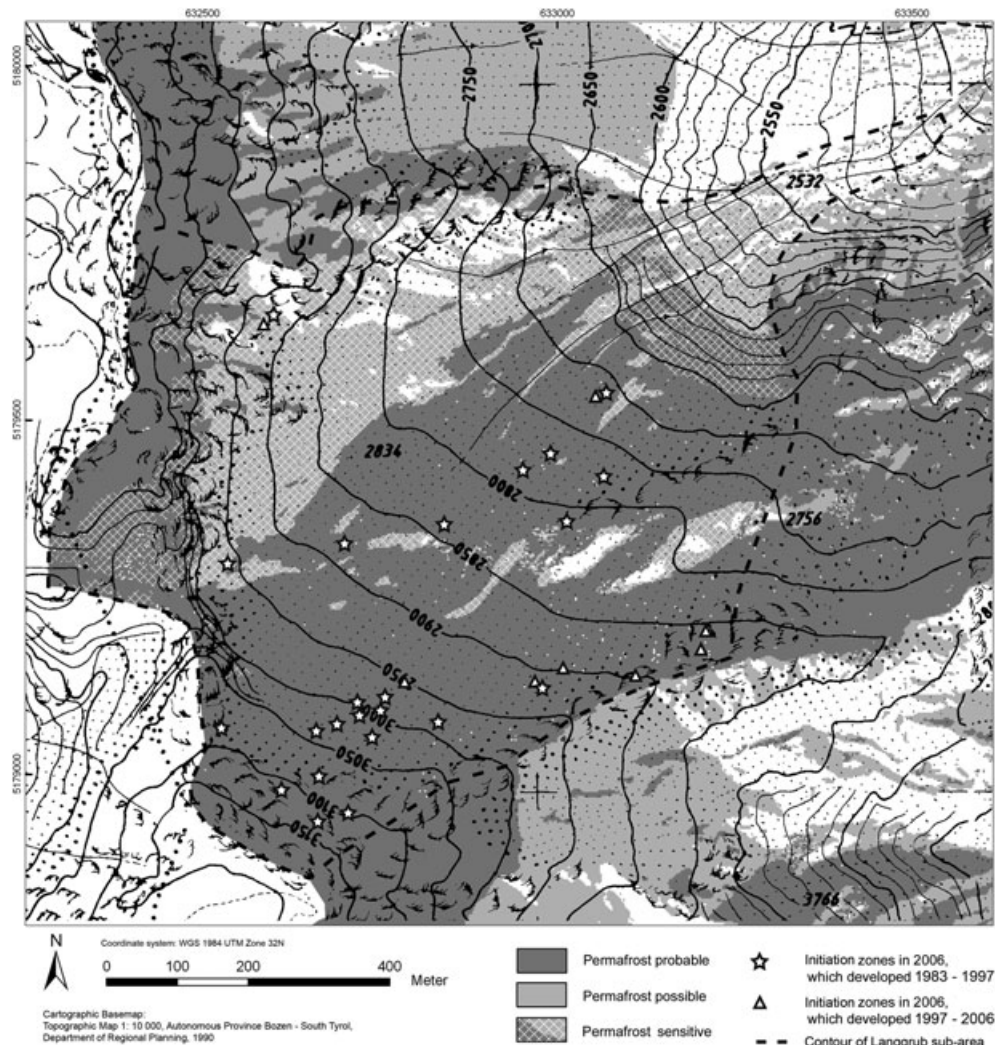


Figure 4 Location of debris flow initiation zones that developed after 1983 in the Langgrub sub-area in relation to modelled permafrost distribution.

the area. Approximately one-fifth of the initiation zones are located in areas with sensitive permafrost, predominantly at the contact zone of the western rock faces and their debris slopes. Almost all (90%) of the initiation zones that developed after 1983, however, formed in areas of probable permafrost (Figure 4).

In the Grawand sub-area, slightly more than one-third of the initiation zones observed in 2006 lie in areas of probable or possible permafrost occurrence. Three-quarters of these are in areas categorised as sensitive permafrost, predominantly at rock-debris contact zones. However, all but one of the initiation zones that developed after 1983 were below the assumed lower boundary of contemporary permafrost.

Approximately 80 per cent of the process initiation zones mapped in 2006 in the Steinschlaghang sub-area are in areas where permafrost occurrences are currently probable or possible, and here also nearly three-quarters of these are in areas of sensitive permafrost. Two-thirds of debris flows mapped as

comparatively recent, owing to the light colour of the deposits and the distinctiveness of the process traces, originated in these areas.

As none of the investigated sub-areas showed any indications of active permafrost creep, the possible influence of accelerated creep processes on debris flow activity is not regarded as significant.

DISCUSSION

Distinct changes in debris flow activity over the last two decades could be detected only in the Langgrub sub-area. Nearly half the initiation zones mapped in 2006 developed after 1983, with many of these in the upper slope area. However, almost all of these formed in areas where the probability of extensive permafrost occurrence is assessed as high and which are therefore considered to be well above the

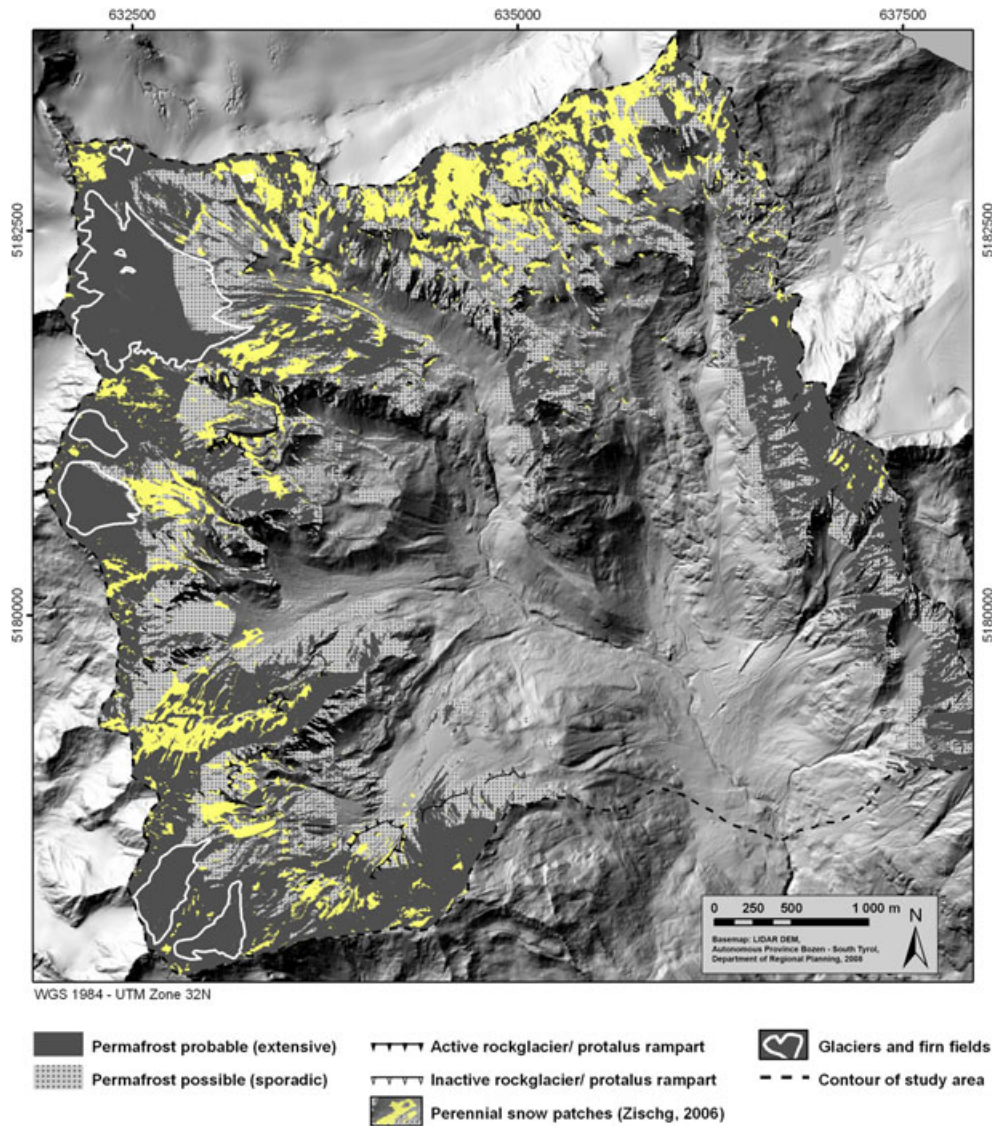


Figure 5 Map showing potential contemporary permafrost distribution in the study area as modelled according to the empirical threshold values of Haeberli (1996), as well as the distribution of permafrost indicators used for model validation. Today's extent of glaciers and firn fields are included to indicate those areas that may be only partly underlain by permafrost due to the polythermal character of ice bodies in permafrost environments (cf. Suter *et al.*, 2001; Etzelmüller and Hagen, 2005). This figure is available in colour online at wileyonlinelibrary.com/journal/ppp

Table 5 Potential contemporary permafrost distribution in the investigated sub-areas according to the modelling categories (% of total sub-area).

Area	Probable permafrost	Possible permafrost	Improbable permafrost	Sensitive permafrost
Langgrub	67	26	7	33
Grawand	25	12	63	15
Steinschlaghang	25	24	51	29

margin of contemporary permafrost distribution. Based on the theoretical framework outlined above, a correlation between the development of the new initiation zones and climate change-induced degradation of permafrost is thus unlikely.

Given that most of the recent debris flows formed in areas that were formerly covered by ice, they may be connected to the melting of the eastern Langgrub glacier. A possible explanation is the paraglacial adaption of over-

Table 6 Location of debris flow initiation zones in the sub-areas within the modelled potential permafrost distribution (% of total number).

Area	Location of debris flow initiation zones		
	Probable permafrost	Possible permafrost	Sensitive permafrost
Langgrub	81	18	21
Grawand	21	17	27
Steinschlaghang	34	47	58

steepened morainic material to unglaciated conditions (cf. Ballantyne, 2002). These sediments may have been in a geomorphodynamic unstable or metastable state and were especially susceptible to erosion and hence debris flow formation. However, increased debris flow activity was only observed for 1983–97. This tends to invalidate the concept of increased geomorphic activity after deglaciation, since this normally commences shortly after ice retreat. Furthermore, in the course of the multi-temporal mapping a progressive increase in debris cover was noted in the analysed aerial photographs. These observations suggest another possible explanation connected to permafrost degradation: Slope gradient and elevation suggest that the Langgrub Glacier was polythermal (cf. Suter *et al.*, 2001; Etzelmüller and Hagen, 2005) or at least to some extent frozen to the rock, especially in the higher, steep slope areas close to the bergschrund. Temperatures at the glacier base in these localities may have been below 0°C and the permafrost table hence directly at the surface. The loss of ice cover, which is thought to have occurred in the late 1960s or 1970s, triggered thawing of the permafrost. As an active layer developed and *in-situ* weathering occurred, loose material became available which was easily mobilised by erosive processes given the steep slope gradient. The marked development of debris flow initiation zones can thus also be interpreted as a sign of the paraglacial adaption of near-surface permafrost to modern unglaciated conditions. A possible increase in debris flow activity due to exceptional rainfall events could not be clarified owing to a lack in climate data.

It is doubtful that even the few debris flow initiation zones that developed in the Langgrub sub-area after 1983 in areas of sensitive permafrost relate to its recent degradation. They are mainly located at the rock-debris contact zone and the debris flows themselves are of the ‘mobilised’ type. Process initiation in these cases is highly dependent on the rocky topography above, which can be considered to be stable and thus process-triggering concentrated flow within rock channels is likely to have occurred repeatedly in the past. The *ab-initio* development of these initiation zones in recent years is therefore improbable. More likely is the refilling of existing initiation zones prior to 1983 by rockfall debris from the active rock walls above so that their existence was hidden on the 1983 aerial photographs but

was revealed by subsequent reactivation. It is possible that the degradation of permafrost within the debris slopes promoted their recurrence through an increased supply of loose material with a thaw plane providing a sliding surface, but this cannot be demonstrated. Even if magnitude-frequency data were available, correlation between process activity and permafrost degradation would remain challenging as a wide range of interacting factors, such as the natural variability of debris flows, unknown lag and reaction times of alpine permafrost to climate change, and the re-accumulation time of debris storage under stable as well as changing climatic conditions, would have to be considered.

The findings for the Langgrub sub-area demonstrate the limitations of the study’s methodological approach not only in terms of the interpretability of results but also regarding its significance. For example, the dependence of observed changes in debris flow activity on the type of initiation zones is apparent. As a consequence of restricting the multi-temporal analysis to an assessment of spatial displacement in the formation of initiation zones, changes regarding debris flows originating at rock-debris contact zones were generally not registered. Since the location of these initiation zones is primarily controlled by topography, the formation of new zones or a change in position is unlikely. Changes in process activity at these sites would be better revealed by changes in the magnitude and frequency of events rather than by the formation of new initiation zones. However, only a few new initiation zones could be observed in the Grawand sub-area where ‘mobilised’ debris flows represent the prevailing process type. In view of the low number and uncertainties associated with their identification as described above, an interpretation of the results of the multi-temporal analysis is not justified in this case. Results for the Steinschlaghang sub-area may have been similar, given the similarity in debris flow characteristics.

Comparing the location of debris flow initiation zones and the potential distribution of permafrost, it is notable that a high proportion of initiation zones in the Grawand and Steinschlag sub-areas are situated in the sensitive permafrost zone (Tables 5 and 6). There may be a connection between process activity and permafrost degradation, especially given that two-thirds of the debris flows mapped as comparatively recent events in the Steinschlaghang sub-area originated in these areas. A coincidental juxtaposition of the topographically determined, most active zones and the potential marginal occurrences of contemporary permafrost distribution is, however, a more likely explanation. Furthermore, an interpretation of the spatial concurrence of debris flow initiation zones and the potential permafrost distribution has to consider uncertainties in the permafrost modelling approach. The ‘rules of thumb’ were originally designed for a scale of 1: 25 000 and a spatial resolution of 50–100 m (Haerberli *et al.*, 1996). The lower limits of particular zones therefore represent a fringe rather than a sharp line, and especially in the case of the lower boundary of the possible permafrost zone mark only the presumed

border between potential permafrost areas and likely permafrost-free areas. Permafrost occurrences developed due to particular micro-climatic conditions (such as extremely shadowed locations) can also exist below this elevation.

The use of a high-resolution elevation model as data input implies an unjustified degree of spatial accuracy, as shown by the highly fragmented model output on some slopes due to localised changes in aspect. An interpretation of the concurrence of debris flow initiation zones and permafrost areas is thereby impeded or leads to outliers such as the one in the Langgrub sub-area. To counteract this fragmentation effect and reduce uncertainties, debris flow initiation zones were treated as polygons with a 10-m diameter rather than as points.

Furthermore, the permafrost model's uncertainties differed with aspect. Haerberli (1996) marked probable permafrost thresholds for eastern and south-eastern aspects as doubtful and did not develop thresholds for south-facing slopes (Table 3). The southern value was therefore derived mathematically from the adjacent orientation classes. As these values and the model predictions have not been verified in the field using geophysics, conclusions regarding a possible correlation between process activity and permafrost degradation can only be made with caution.

CONCLUDING REMARKS

Observed changes in the spatial distribution of debris flow activity over the past two decades are not thought to have been influenced by atmospheric warming-induced thawing of perennially frozen debris in the process source areas. Although situated at high enough elevations, debris flows predominantly started at sites that are not predicted to be at the margin of contemporary permafrost distribution, and thaw of permafrost at these locations in reaction to current

changes in climatic conditions is therefore unlikely. However, a connection between the development of new initiation zones in the Langgrub sub-area and the thickening of the active layer as a reaction to the melting of a former glacier is thought to be possible.

In assessing the links between permafrost degradation and debris flow initiation, attention has to be paid to the type of initiation zones analysed, as permafrost thawing-related changes may manifest themselves differently depending on the initiation type. The nature of the source area (old vs recent debris storage) and the triggering mechanism (rainfall dependent vs sediment-supply dependent) may also be decisive factors in the response of debris flows to permafrost-related changes in the spatial distribution of initiation zones. Straightforward research approaches, such as the one used, help clarify associations among contributing factors and can identify suitable study sites for more intensive geophysical research at the slope scale.

ACKNOWLEDGEMENTS

Geomorphological mapping and associated fieldwork were funded by Abenis Alpinexpert GmbH within the project Un metodo innovativo per la valutazione del pericolo di frane nelle Alpi basato su interferometria satellitare e GIS, partially co-financed by the innovation programme Applied Spatial Management of the Autonomous Province of Bolzano and the EU (Fondo Europeo di Sviluppo Regionale (FESR) 2000–06). We would like to thank the two referees, Andreas Käab and Christian Huggel, as well as the Editor for their helpful and very much appreciated comments, and Jan Thompson for her constructive remarks on an earlier version of this paper.

REFERENCES

- Allen S, Cox S, Owens I. 2010. Rock avalanches and other landslides in the central Southern Alps of New Zealand: a regional study considering possible climate change impacts. *Landslides* **8**(1): 33–48. DOI: 10.1007/s10346-010-0222-z
- Autonomous Province Bozen - South Tyrol, Department of Hydrology. 2007. Temperature and precipitation data of the meteorological station at Kurzras for the period 1990 to 2006. (Unpublished data).
- Autonomous Province Bozen - South Tyrol, Department of Hydrology. 2008. Snow cover observations from the Lazaun Alpe (1986–2007). (Unpublished data).
- Autonomous Province Bozen - South Tyrol, Department of Regional Planning. 1990. Topographic Map 1: 10 000, Sheet 1201, 1202, 1205 and 1206. <http://www.provinz.bz.it/raumordnung/kartografie/469.asp>. [24 February 2008].
- Autonomous Province Bozen - South Tyrol, Department of Regional Planning. 2008. DTM Lidar Data. <http://www.provinz.bz.it/raumordnung/kartografie/469.asp>. [17 February 2008].
- Ballantyne CK. 2002. Paraglacial geomorphology. *Quaternary Science Reviews* **21** (18–19): 1935–2017. DOI: 10.1016/S0277-3791(02)00005-7
- Beniston M. 2006. August 2005 intense rainfall event in Switzerland: Not necessarily an analog for strong convective events in a greenhouse climate. *Geophysical Research Letters* **33**(5): L05701. DOI: 10.1029/2005GL025573
- Bundesamt für Wasser und Geologie (ed). 2002. *Naturgefahren, Symbolbalkasten zur Kartierung der Phänomene, EDV-Legende, Version 1.0*. Bern. (Unpublished data).
- Damm B, Felderer A. 2008. Identification and assessment of natural hazards in relation to permafrost degradation in the Ahrn Valley area in South Tyrol (Italy). *Geophysical Research Abstracts*, Vol. 10, EGU2008-A-05439.
- Davies MCR, Hamza O, Harris C. 2001. The effect of rise in mean annual temperature on the stability of rock slopes containing ice-filled discontinuities. *Permafrost and Periglacial Processes* **12**(1): 137–144. DOI: 10.1002/ppp378
- Etzelmueller B, Hagen JO. 2005. Glacier-permafrost interactions in arctic and alpine environments with examples from southern Norway and Svalbard. In *Cryospheric Systems: Glaciers and Permafrost*, Harris C, Murton JB (eds). Special Publications V. 242. Geological Society: London; 11–27.
- Fliri F. 1975. *Das Klima der Alpen im Raume von Tirol*. Universitätsverlag Wagner: Innsbruck; 454 pp.
- Grove JM. 1988. The Little Ice Age in the Oetztal, Eastern Alps. In *The Little Ice Age*, Grove JM. Routledge: London: 134–166.

- Gruber S, Haeberli W. 2009. Mountain permafrost. In *Permafrost Soils*, Margesin R (ed). Soil Biology V. 16, Springer: Berlin; 33–44. DOI: 10.1007/978-3-540-69371-0
- Haeberli W. 1975. *Untersuchungen zur Verbreitung von Permafrost zwischen Flüelapass und Piz Grialetsch (Graubünden)*. Mitteilungen der Versuchsanstalt für Wasserbau, Hydrologie und Glaziologie, **17**. Eidgenössische Technische Hochschule Zürich: Zürich; 221 pp.
- Haeberli W. 1992. Possible effects of climate change on the evolution of Alpine Permafrost. *Catena Supplement* **22**: 23–35.
- Haeberli W. 1996. Die 'Permafrost-Faustregeln' der VAW/ETHZ - einige grundsätzliche Bemerkungen. In *Simulation der Permafrostverbreitung in den Alpen mit geographischen Informationssystemen*, Haeberli W, Hoelzle M, Dousse JP, Ehrler C, Gardaz JM, Imhof M, Keller F, Kunz P, Lugon R, Reynard E (eds). vdf Hochschulverlag an der ETH: Zürich; 13–18.
- Haeberli W, Gruber S. 2009. Global warming and mountain permafrost. In *Permafrost Soils*. Margesin R (ed). Soil Biology V. 16. Springer: Berlin; 205–218. DOI: 10.1007/978-3-540-69371-0
- Haeberli W, Hoelzle M, Dousse JP, Ehrler C, Gardaz JM, Imhof M, Keller F, Kunz P, Lugon R, Reynard E. 1996. *Simulation der Permafrostverbreitung in den Alpen mit geographischen Informationssystemen - Diskussion*. Arbeitsheft NFP **31**. vdf Hochschulverlag ETHZ: Zürich; 47–48.
- Haeberli W, Käab A, Hoelzle M, Bösch H, Funk M, Vonder Mühl D, Keller F (eds). 1999. *Eisschwund und Naturkatastrophen im Hochgebirge, Schlussbericht NFP 31*. vdf Hochschulverlag ETHZ: Zürich; 190.
- Haeberli W, Wegmann M, Vonder Mühl D. 1997. Slope stability problems related to glacier shrinkage and permafrost degradation in the Alps. *Ecologiae Geologicae Helvetiae* **90**(3): 407–414.
- Harris C. 2005. Climate change, mountain permafrost degradation and geotechnical hazard. In *Global Change and Mountain Regions*. Advances in Global Change Research V. 23, Huber UM, Bugmann HKM, Reasoner MA (eds). Springer: Dordrecht; 215–224. DOI: 10.1007/1-4020-3508-X_22
- Harris C, Lewkowicz AG. 2000. An analysis of the stability of thawing slopes, Ellesmere Island, Nunavut, Canada. *Canadian Geotechnical Journal* **37**(2): 449–462.
- Harris C, Davies MCR, Eitzelmüller B. 2001. The assessment of potential geotechnical hazards associated with mountain permafrost in a warming global climate. *Permafrost and Periglacial Processes*, **12**(1): 145–156. DOI: 10.1002/ppp376
- Harris C, Arenson LU, Christiansen HH, Eitzelmüller B, Frauenfelder R, Gruber S, Haeberli W, Hauck C, Holzle M, Humlum O, Isaksen K, Käab A, Kern-Lutschg MA, Lehning M, Matsuoka N, Murton JB, Nozli J, Phillips M, Ross N, Seppala M, Springman SM, Muhll DV. 2009. Permafrost and climate in Europe: Monitoring and modelling thermal, geomorphological and geotechnical responses. *Earth-Science Reviews*, **92**(3–4): 117–171. DOI: 10.1016/j.earscirev.2008.12.002
- Hoelzle M, Wagner S, Käab A, Vonder Muehl D. 1998. Surface movement and internal deformation of ice-rock mixtures within rock glaciers in the Upper Engadin, Switzerland. In *Proceedings of the 7th International Conference on Permafrost*, Lewkowicz AG, Allard M (eds). Collection Nordicana V. 55, Université Laval: Québec; 465–471.
- Imhof M. 1996. PERM - ein Programm für die automatisierte Kartierung von Permafrost in den Schweizer Alpen. In *Simulation der Permafrostverbreitung in den Alpen mit geographischen Informationssystemen*, Haeberli W, Hoelzle M, Dousse JP, Ehrler C, Gardaz JM, Imhof M, Keller F, Kunz P, Lugon R, Reynard E (eds). vdf Hochschulverlag an der ETH: Zürich; 25–33.
- Jomelli V, Pech P, Chochillon C, Brunstein D. 2004. Geomorphic Variations of Debris Flows and Recent Climatic Change in the French Alps. *Climatic Change*, **64**(1): 77–102. DOI: 10.1023/B:CLIM.0000024700.35154.44
- Jomelli V, Brunstein D, Grancher D, Pech P. 2007. Is the response of hill slope debris flows to recent climate change univocal? A case study in the Massif des Ecrins (French Alps). *Climatic Change*, **85**(1–2): 119–137. DOI: 10.1007/s10584-006-9209-0
- Käab A, Frauenfelder R, Roer I. 2007. On the response of rockglacier creep to surface temperature increase. *Global and Planetary Change*, **56**(1–2): 172–187. DOI: 10.1016/j.gloplacha.2006.07.005
- Keiler M, Knight J, Harrison S. 2010. Climate change and geomorphological hazards in the eastern European Alps. *Philosophical Transactions of the Royal Society A - Mathematical Physical and Engineering Sciences*, **368**(1919): 2461–2479. DOI: 10.1098/rsta.2010.0047
- Keller F. 1992. Automated mapping of mountain permafrost using the program PERMAKART within the geographical information system Arc/Info. *Permafrost and Periglacial Processes*, **3**(2): 133–138.
- Keller F, Hoelzle M. 1996. PERMAKART und PERMAP. In *Simulation der Permafrostverbreitung in den Alpen mit geographischen Informationssystemen - Arbeitsheft NFP 31*, Haeberli W, Käab A, Hoelzle M, Bösch H, Funk M, Vonder Mühl D, Keller F (eds). vdf Hochschulverlag ETHZ: Zürich; 37–48.
- Kneisel C, Rothenbühler C, Keller F, Haeberli W. 2007. Hazard assessment of potential periglacial debris flows based on GIS-based spatial modelling and geophysical field surveys: a case study in the Swiss Alps. *Permafrost and Periglacial Processes*, **18**(3): 259–268. DOI: 10.1002/ppp.593
- Larsson S. 1982. Geomorphological Effects on the Slopes of Longyear Valley, Spitsbergen, after a Heavy Rainstorm in July 1972. *Geografiska Annaler. Series A, Physical Geography*, **64**(3/4): 105–125.
- Lewkowicz AG, Harris C. 2005. Morphology and geotechnique of active-layer detachment failures in discontinuous and continuous permafrost, northern Canada. *Geomorphology*, **69**(1–4): 275–297. DOI: 10.1016/j.geomorph.2005.01.011
- Luetschg M, Stoeckli V, Lehning M, Haeberli W, Ammann W. 2004. Temperatures in two boreholes at Flüela Pass, Eastern Swiss Alps: the effect of snow redistribution on permafrost distribution patterns in high mountain areas. *Permafrost and Periglacial Processes* **15**: 283–297. DOI: 10.1002/ppp.500
- Mair V, Lang K, Krainer K, Stötter J, Zischg A. Permafrost in Südtirol. *Innsbrucker Geographische Studien*. In preparation.
- Nater P, Arenson L, Springman S. 2008. Choosing geotechnical parameters for slope stability assessments in alpine permafrost soils. In *Proceedings of the Ninth International Conference on Permafrost*, V. 2, Kane DL, Hinkel KM (eds). Institute of Northern Engineering, University of Alaska: Fairbanks; 1261–1266.
- Noetzli J, Gruber S, Kohl T, Salzmann N, Haeberli W. 2007. Three-dimensional distribution and evolution of permafrost temperatures in idealized high-mountain topography. *Journal of Geophysical Research-Earth Surface*, **112**(F2). DOI: 10.1029/2006jg000545
- Purtscheller F. 1971. *Ötztaler und Stubai Alpen*. Sammlung Geologischer Führer, **53**. Gebrüder Borntraeger: Berlin; 128 pp.
- Rebetez M, Lugon R, Baeriswyl PA. 1997. Climatic change and debris flows in high mountain regions: the case study of the Ritigraben torrent (Swiss Alps). *Climatic Change*, **V36**(3): 371–389. DOI: 10.1023/A:1005356130392
- Rist A. 2007. Hydrothermal processes within the active layer above alpine permafrost in steep scree slopes and their influence on slope stability. Unpublished PhD thesis, Swiss Federal Institute for Snow and Avalanche Research and University of Zurich, Zurich; 168 pp.
- Roer I, Haeberli W, Avian M, Kaufmann V, Delaloye R, Lambiel C, Käab A. 2008. Observations and considerations on destabilizing

- active rock glaciers in the European Alps. In *Proceedings of the Ninth International Conference on Permafrost*, V. 1, Kane DL, Hinkel KM (eds). Institute of Northern Engineering, University of Alaska: Fairbanks; 1505–1510.
- Sattler K. 2008. Murgangaktivitaet und Permafrostverbreitung in einem periglazialen Hochgebirgsraum – eine Fallstudie im Schnalstal, Suedtirol. Unpublished diploma thesis, University of Vienna, Vienna, 145 pp.
- Sattler K, Keiler M, Zischg A, Schrott L. 2007. Development of debris-flow activity influenced by climate change in periglacial high mountain areas: Schnalstal, Italy. In *Proceedings of the Geomorphology for the Future*, Kellerer-Pirklbauer A, Keiler M, Embleton-Hamann C, Stötter J (eds). Innsbruck University Press, Innsbruck; 169–176.
- Schlyter P, Jonsson P, Nyberg R, Persson P, Rapp A, Jonasson C and Rehn J. 1993. Geomorphic Process Studies Related to Climate-Change in Karkevage, Northern Sweden - Status of Current Research. *Geografiska Annaler. Series A, Physical Geography*, **75**(1–2): 55–60.
- Stötter J. 1994. Veränderungen der Kryoshäre in Vergangenheit und Zukunft sowie Folgeerscheinungen - Untersuchungen in ausgewählten Hochgebirgsräumen im Vinschgau. Unveröffentlichte Habilitationsschrift, Ludwig-Maximilians-Universität, München; 264 pp.
- Suter S, Laternser M, Haeberli W, Frauenfelder R, Hoelzle M. 2001. Cold firn and ice of high-altitude glaciers in the Alps: measurements and distribution modelling. *Journal of Glaciology*, **47**(156): 85–96.
- Takahashi T. 1981. Estimation of potential debris flows and their hazardous zones: Soft counter measures for a disaster. *Journal Natural Disaster Science*, **3**(1): 57–89.
- Zimmermann M, Haeberli W. 1992. Climatic change and debris flow activity in high-mountain areas. A case study in the Swiss Alps. *Catena Supplement*, **22**: 59–72.
- Zimmermann M, Mani P, Gamma P, Gsteiger P, Heiniger O, Hunziker G. 1997. *Murganggefahr und Klimaänderung - ein GIS-basierter Ansatz*. Schlussbericht NFP 31. vdf Hochschulverlag an der ETH: Zürich; 161 pp.
- Zischg A. 2006. Kartierung der perennierenden Schneeflecken aus den Orthofotokarten der Jahre 1996, 1999, 2003. PROALP – Konsortium Geo-IM – Tätigkeitsbericht WP4.

Paper 4: Röthlisberger, V., Zischg, A., Keiler, M., 2017. Identifying spatial clusters of flood exposure to support decision making in risk management. *Science of The Total Environment* 598, 593–603. [10.1016/j.scitotenv.2017.03.216](https://doi.org/10.1016/j.scitotenv.2017.03.216).



Identifying spatial clusters of flood exposure to support decision making in risk management



Veronika Röthlisberger^{a,b,*}, Andreas P. Zischg^{a,b,c}, Margreth Keiler^a

^a University of Bern, Institute of Geography, Hallerstrasse 12, CH-3012 Bern, Switzerland

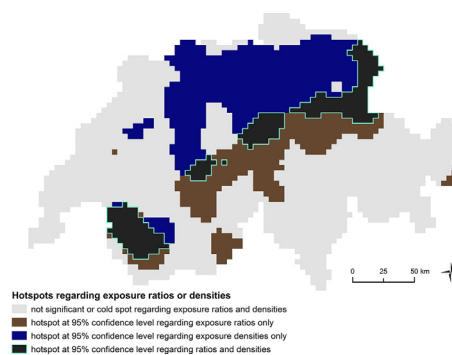
^b University of Bern, Oeschger Centre for Climate Change Research, Mobililar Lab for Natural Risks, Falkenplatz 16, CH-3012 Bern, Switzerland

^c University of Bristol, School of Geographical Sciences, University Road, BS8 1SS Bristol, United Kingdom

HIGHLIGHTS

- Evaluation of methods and parameters pertinent to flood exposure analyses
- Spatial exposure analyses support prioritization in flood risk management.
- Feasible detection of hotspots at national scale based on spatially explicit data
- Complementary spatial distribution of exposure densities and ratios in Switzerland
- Data aggregation scheme (i.e. by municipalities or grids) influences the results.

GRAPHICAL ABSTRACT



ARTICLE INFO

Article history:

Received 31 October 2016

Received in revised form 8 March 2017

Accepted 22 March 2017

Available online xxxx

Editor: R. Ludwig

Keywords:

Flood exposure
Flood risk management
Prioritization strategies
Spatial cluster analysis
MAUP
Switzerland

ABSTRACT

A sound understanding of flood risk drivers (hazard, exposure and vulnerability) is essential for the effective and efficient implementation of risk-reduction strategies. In this paper, we focus on 'exposure' and study the influence of different methods and parameters of flood exposure analyses in Switzerland. We consider two types of exposure indicators and two different spatial aggregation schemes: the density of exposed assets (exposed numbers per km²) and the ratios of exposed assets (share of exposed assets compared to total amount of assets in a specific region) per municipality and per grid cells of similar size as the municipalities. While identifying high densities of exposed assets highlights priority areas for cost-efficient strategies, high exposure ratios can suggest areas of interest for strategies focused on the most vulnerable regions, i.e. regions with a low capacity to cope with a disaster. In Switzerland, the spatial distribution of high exposure densities and exposure ratios tend to be complementary. With regards to the methods, we find that the spatial cluster analysis provides more information for the prioritization of flood protection measures than 'simple' maps of spatially aggregated data represented in quantiles. In addition, our study shows that the data aggregation scheme influences the results. It suggests that the aggregation based on grid cells supports the comparability of different regions better than aggregation based on municipalities and is, thus, more appropriate for nationwide analyses.

© 2017 The Authors. Published by Elsevier B.V. This is an open access article under the CC BY-NC-ND license (<http://creativecommons.org/licenses/by-nc-nd/4.0/>).

* Corresponding author at: University of Bern, Institute of Geography, Hallerstrasse 12, CH-3012 Bern, Switzerland.

E-mail addresses: veronika.roethlisberger@giub.unibe.ch (V. Röthlisberger), andreas.zischg@giub.unibe.ch (A.P. Zischg), margreth.keiler@giub.unibe.ch (M. Keiler).

1. Introduction

Flood risk has been increasing during the last decades on a global scale (IPCC, 2012); this is exemplified by the occurrence of flood events associated with high losses in Europe (e.g. 2002 Danube, Elbe and Vltava catchments, 2007 United Kingdom, 2014 Southeast Europe, 2016 Northwest Europe). The flood events prompted political actions with a focus on the generation of flood risk maps and enhanced national risk management strategies, e.g. the European Parliament's Floods Directive (2007) or the respective frameworks in Switzerland (Bründl et al., 2009; PLANAT, 2005). Flood risk analysis combines information about the hazard (i.e. the frequency and magnitude of floods), exposure (i.e. the population and assets located in flood-prone areas) and vulnerability (i.e. the susceptibility of the exposed elements to the hazard) (Klijn et al., 2015; Merz and Thielen, 2004; Papathoma-Köhle et al., 2011; UNISDR, 2015a). These three main factors of the risk analysis show spatiotemporal patterns (Aubrecht et al., 2013; Black and Burns, 2002; Fuchs et al., 2013; Mazzorana et al., 2012; Winsemius et al., 2016). In particular, several studies and reports identify increasing in exposure as the main driver of increasing risk (Hallegatte et al., 2013; IPCC, 2012; de Moel et al., 2011). In the future, flood risk will continue to increase because of socio-economic development and climate change (Visser et al., 2014; Winsemius et al., 2015). Consequently, effective and efficient strategies for risk reduction are essential for the future (Jongman et al., 2014; Rojas et al., 2013) and a sound understanding of relevant risk drivers is a prerequisite for the implementation of risk-reduction strategies (IPCC, 2012; UNISDR, 2015b).

In this paper, we focus on exposure and how the associated data analysis can influence decisions in different risk-based strategies. Exposure analysis is strongly dependent on availability, resolution and quality of data, namely data on assets (i.e. including affected people, buildings and infrastructure) and on the nature of the hazards (i.e. flood extent and magnitude). Asset data characteristics, in particular the spatial resolution and the aggregation level, also influence the choice of methods for exposure analysis. Examples of exposure analysis approaches include intersecting flood areas with average asset values based on aggregated land-use classification (e.g. Cammerer et al., 2013; Jonkman et al., 2008; Muis et al., 2015) and spatially explicit intersections of building polygons (Figueiredo and Martina, 2016; Fuchs et al., 2015). The latter approach generates high quality and spatially explicit information on exposure, thereby reducing uncertainties if up-scaled to a larger spatial entity. Merz (2006) compares different exposure analysis approaches and de Moel et al. (2015) provide an overview concerning spatial scales. Additionally, the levels at which exposed assets are aggregated are dependent on data privacy restrictions, data availability and study objectives. Aggregation levels can range from municipality level (Fuchs et al., 2015; Hallegatte et al., 2013; Huttenlau et al., 2010; Staffler et al., 2008) to NUTS levels for European studies (Lugeri et al., 2010; Lung et al., 2013) and aggregation based on countries (and 'food producing units') for global studies (Jongman et al., 2012; UNISDR, 2015a). However, due to limited data availability, comprehensive object-based and therefore spatially explicit analyses are generally restricted to local and regional levels (Huttenlau et al., 2010; Zischg et al., 2013). Since additional information has become increasingly available (e.g. on building stock, i.e. existing buildings within a defined environment) throughout Europe based on new European regulations, more accurate information on exposed elements can be obtained (e.g. Figueiredo and Martina, 2016; Fuchs et al., 2015) and will be used as a basis for decision-making in risk management.

In Switzerland, object-specific information about the building stock and flood hazards map are available nationwide. In this study, we investigate and test the application of different aggregation and normalization methods on these datasets and highlight their impact on resultant differences to build awareness among relevant decision makers. The legislative framework and the limited funds for protection measures oblige authorities to prioritize the most efficient and effective risk

reduction schemes. Thus, decision makers need to know "which region should risk reduction focus on?" or alternatively, "where are the flood exposure hotspots located?". To answer these questions, we propose an approach of spatial cluster analysis based on the aggregation of point data with respect to different spatial units. Spatial cluster analyses are well established in many disciplines (crime, health, archeology, with Snow's (1855) publication on the 1854 cholera outbreak in Soho district of London being to our knowledge the first work on spatial clusters), but with limited applications in natural risk analysis and management to date. The few studies on natural hazards that apply spatial cluster analyses (e.g. Borden and Cutter, 2008; Fuchs et al., 2012; Kazakis et al., 2015; Su et al., 2011; van der Veen and Logtmeijer, 2005) often use aggregated data and rarely consider the influence of the shape and size of the data aggregation units. In our study, we investigate if and to what extent the aggregation scheme influences the results. In other words, we examine the relevance of the still unresolved and thus often ignored Modifiable Areal Unit Problem (MAUP) (Openshaw, 1984; cf. also Section 2.4 in this paper).

We further consider two types of exposure indicators: the density of exposed assets (exposed number of assets per km²) and the share of exposed assets (share of exposed assets compared to the total number of assets in a specific region). The first indicator, the exposure density, supports risk management strategies that follow the concept of utilitarianism (Mill, 2007). Utilitarianism in natural hazard and risk management means to choose the most cost-efficient measures. Numerous factors influence a measure's efficiency, i.e. the ratio of resource input to the risk reduction output. The density of exposed assets is an example of the aforementioned factors. Provided that all factors are the same except the exposure density, the efficiency of a measure is higher in areas with high densities of exposed assets than in areas with low exposure densities. That is, the density of exposed assets is a meaningful criterion for the selection of measures with respect to cost efficiency. The second exposure indicator, the share of exposed assets, informs strategies which comply with Rawls' concept of justice (Rawls, 1971). The application of this concept in risk management implies the prioritization of the most vulnerable areas and people (Johnson et al., 2007). The term 'vulnerable' in this context does not refer to the individual physical susceptibility of assets in a region, but to the missing capacity of a region to cope with a disaster. We assume an inverse relationship between the share of affected assets and a region's coping capacity. Consequently, we propose that the share of exposed assets in a given spatial unit is used as an indicator of the unit's vulnerability.

The proposed approach of spatial cluster analysis is generally applicable, i.e. for different regional and national flood exposure surveys. In this paper it is applied and illustrated with the case study of Switzerland.

2. Material and methods

For the analysis of flood exposure, we overlay spatially explicit information about buildings and inhabitants with data describing flood prone areas. Based on different aggregations of the exposed assets we search for statistically significant hotspots of flood exposure. The following sections outline the methods applied and describe the datasets used in the Switzerland case study.

2.1. Data on buildings and inhabitants

Two datasets are extracted from (1) a topographic landscape model and (2) from point data on residential buildings and combined to obtain a comprehensive and homogenous, country-wide database of buildings polygons and of residents in Switzerland.

The feature group 'buildings' from the 'Topographic Landscape Model' (TLM) (swisstopo, 2016a, 2016b) contains footprints of all buildings currently in Switzerland. The TLM building data is highly accurate (10⁻¹ m), however, the spatial subsets of the data are not updated

simultaneously, but regionally in phases between the years 2009–2015. In addition, the change of the building data from 2D to 3D representation is completed only for approximately half of the area (swisstopo, 2016c). Consequently, there are regional differences, e.g. in the degree of division and overlaps of building polygons and the date of underlying aerial images. We address the shortcoming regarding the spatially different stages of 2D to 3D conversion by merging all adjoining or overlapping building polygons, so that terraced houses or apartment blocks are homogeneously represented as one single polygon. Furthermore, we correct invalid geometries. After these preprocessing steps, our dataset includes 2,086,411 non-overlapping building polygons with a total areal footprint of 540 km².

The federal 'Buildings and Dwellings statistic' (Gebäude- und Wohnungsstatistik (GWS)) contains point-referenced data of all buildings (entrances) for residential use in Switzerland (Federal Statistical Office FSO, 2016). The number of inhabitants (main residence) at the end of 2012 is used in our study. The dataset contains 1,670,054 points with slightly over 8 million (8,057,480) inhabitants assigned to them.

We assign the number of inhabitants to the building footprints by intersecting the GWS point data with building footprint polygons and applying a snapping distance of ≤ 2 m. Within this distance, 97.7% of all points in the GWS can be attributed to a neighboring building polygon. For the total number of inhabitants per building, we total the number of inhabitants of all points associated to a specific building polygon.

2.2. Flood maps

We combine two different types of flood maps to define the areas potentially prone to inundation. The main source of data is a compilation of all available communal flood hazard maps, which are complemented by a nationwide floodplain model called 'Aquaprotect'.

The communal flood hazard maps are generated at the local municipal or cantonal level with respect to Swiss national guidelines (Borner, 1999; Loat and Petrascheck, 1997) and include information from historical events, 2D flood simulations and expert knowledge. Within the perimeter of the communal flood hazard maps, five different hazard classes ('high', 'medium', 'low', 'residual' and 'no or negligible') are defined by a specific combination of intensity and probability of events. The communal flood hazard maps are widely accepted and used, especially in the planning process of flood protection measures at communal and cantonal levels (Bundesamt für Umwelt BAFU, 2016a). In our study, we use the March 2016 versions available from the 26 Swiss cantons (federal states) and consider the hazard classes 'high', 'medium' and 'low' as flood prone areas (i.e. we include areas affected by events up to a return period of 300 years).

67% (1,390,382) of the building polygons (70% of footprint areas, 77% of residents) are located within the perimeters of the communal flood hazard maps. For the buildings located partially or completely outside of these perimeters (i.e. buildings without flood assessment at the local level), the Aquaprotect dataset provided by the Federal Office for the Environment (Federal Office for the Environment, 2008) is used complementarily. This dataset defines inundation areas based on a "geomorphologic regression" approach (Feyen et al., 2003); this approach has been applied in Switzerland on a 25 m \times 25 m grid. Technical flood control facilities and catchment areas below 10 km² are not considered by Aquaprotect (Federal Office for the Environment, 2008). Aquaprotect includes four different layers with recurrence periods of 50, 100, 250 and 500 years. We use the layer with the 250 year return period in addition to the communal flood hazard map's areas of events with a return period of up to 300 years.

2.3. Exposure analysis

The two datasets – of building footprints and of flood prone areas – are spatially intersected within a GIS to assess the flood exposure of buildings and residents. A building (and its inhabitants) is classified as

exposed if the (partial or whole) footprint polygon overlaps with a flood prone area according to the communal flood hazard maps (classes 'high', 'medium' and or 'low'). If the building footprint is located outside of the perimeter (i.e. it is without flood assessment at the local level), it is exposed if it overlaps with the considered Aquaprotect layer. Buildings that are located on the fringes of the perimeter of the communal flood hazard maps (i.e. partially inside and outside the perimeter) are classified as exposed if they overlap with one of the three considered classes of the flood hazard maps and/or with the respective Aquaprotect layer.

2.4. Spatial aggregation of data and density calculation

We aggregate the number of exposed buildings, associated footprint and inhabitants based on the currently defined Swiss municipal districts. The values are then normalized by the area of the respective polygon to determine the resultant densities of exposed assets. The Swiss municipalities dataset (swisstopo, 2016d) consists of 2312 entities, covering the entire national territory of 41,290 km². 2294 of these entities are actually territories of municipalities, 16 are cantonal territories (coinciding mainly with lake areas) and two are 'comunanzas' or public areas managed communally by farmers. The sizes of the 2312 polygons range from 0.1 km² to 439 km² with a mean value of 18 km². With reference to motivation stated in the introduction, we are interested in investigating whether data aggregation by municipal districts influences data analysis results. That is, we want to determine if the 'Modifiable Areal Unit Problem' (MAUP) impacts the analysis of flood exposure of Swiss municipalities. The MAUP includes two aspects, (1) the scaling and (2) the zonation effect (Openshaw, 1984; cf. also Charlton, 2008). The scaling effect describes the observation that analytical results change based on the level of data aggregation (e.g. block census vs municipal districts vs county level). The zonation effect describes inconsistencies in results when the number of areal units (and thus their average size) remains constant, while boundary positions are shifted. In our study, we focus on the zonation effect by creating an arbitrary grid of 4.23 km \times 4.23 km cells, covering the entire Swiss territory. The comparison of the results based on these grid cells (2533 cells, each 17.8929 km²) with the results based on aggregation by municipalities (2312 polygons with an areal average of 17.8592 km²) supports the assessment of how relevant the MAUP zonation effect is. To calculate the densities of exposed buildings, footprint areas and inhabitants in each grid cell, we apply the quadratic kernel function described by Silverman (1986) with a window 6.345 km wide.

We apply the same density calculation procedures to the total building stock (exposed and unexposed buildings) and divide the densities of exposed buildings by the densities of the total building stock. We obtain relative exposure ratios of building numbers, footprint areas and inhabitants per municipality and per grid cell, respectively.

To determine the robustness of the results based on grid cells we shift the arbitrarily set grid by half of its cell width in each direction, i.e. by 2115 m in north-south and east-west respectively, and repeat the described density calculations. The resulting densities and their distributions within this second grid are very similar to ones in the first grid. Thus, we proceed solely with the first grid.

2.5. Detection of spatial clusters

'Hotspots' and 'spatial clusters' are defined differently and many relevant techniques can be applied to detect these spatial patterns (see Getis, 2008 for a historical outline, and Legendre and Legendre, 2012 for a topical overview and mathematical details). From the available range of interpretations, Levine's definition of a hotspot as an "extreme form of spatial autocorrelation" (Levine, 2008) and Knox's definition of spatial clusters as "geographically ... bounded group[s] of occurrences ... of sufficient size and concentration to be unlikely to have occurred by chance" (Knox, 1989) are of particular interest.

We apply the local spatial autocorrelation statistic $G_i^*(d)$, by Getis and Ord (Getis and Ord, 1992; Ord and Getis, 1995), to identify hotspots of flood exposure in Switzerland. In other words, the aim is to detect statistically significant clusters of high values in terms of densities of exposed buildings (numbers, footprint areas and inhabitant), as well as in terms of relative exposure ratios. The confidence level is set at 95%, and for d , we use fixed distance bands. We set the first distance band just above the maximal distance between centroids of neighbors (i.e. at 21 km for municipalities and at 4.25 km for grid cells) to assign to each municipality or grid cell at least one neighbor. We investigate the effect of the size of d by increasing it for municipalities to 31.5 km and 42 km and for grid cells to 8.5 km, 12.75 km, 17 km and 21.25 km.

The evaluation of the $G_i^*(d)$ statistical framework reveals additional issues with both spatial dependence and multiple testing. While the spatial dependence violates the test requirement of independent features, the multiple testing leads to a high number of false type I errors, i.e. incorrect rejections of the null hypothesis. Therefore, it is necessary to adjust the critical values of the G_i^* statistics. We use the method proposed by Caldas de Castro and Singer (2006).

3. Results and discussion

The data resulting from the assignment of point data on inhabitants (GWS dataset) to building footprints (TLM dataset) are presented in Section 3.1, together with the national level results from the flood exposure analysis. In Section 3.2, we discuss selected outcomes of the spatial aggregation investigation and of the density and ratio calculations. Section 3.3 describes the results of the spatial clusters analysis. The relevance of the MAUP is addressed in Section 3.4, and in Section 3.5, we discuss the implications of our findings for the prioritization of flood risk reduction measures. The annex presents supplementary results to the selected outcomes described in Section 3.2.

3.1. Exposed assets: buildings and residents

A total of 97.7% (1,631,531) of the GWS data points are assigned to a building footprint polygon (i.e. 93.7% are located within a TLM building footprint polygon and 4% within a distance of ≤ 2 m). These assigned GWS data points represent 98.2% (7,909,191) of the Swiss residents. The high percentage of residents assigned to buildings reflects the high spatial accuracy of both the GWS points and the TLM footprints datasets.

Overall, 320,509 buildings in Switzerland are identified as exposed to floods up to a return period of 250 to 300 years (see Table 1). This is equivalent to an exposure ratio of 15.4%. This ratio is in agreement with results from previous studies conducted with Switzerland as a study site (Bundesamt für Umwelt BAFU, 2016b; Fuchs et al., 2017) and is in line with findings about other mountainous regions in Europe (Chen et al., 2016; Fuchs et al., 2015; Url and Sinabell, 2008). The exposure ratios of the building footprint areas and of the number of residents are higher (20.4% and 17.1%, respectively) but still comparable to the ratio regarding the numbers of buildings. This indicates that the average footprint area of exposed buildings is greater than the average footprint area of unexposed buildings in Switzerland (343 m² for exposed versus 244 m² for unexposed, cf. Table 1). The same comparison is valid for the number of residents. However, the relative difference between the average number of inhabitants in exposed buildings (4.2 persons per

building) and in unexposed buildings (3.7 persons per building) is smaller. Fuchs et al. (2015) obtain similar findings with respect to larger buildings located inside of flood prone areas and explain that larger buildings require more flat terrain. Consequently, they are preferably built on floodplains. A second explanation for the higher exposure ratios associated with larger buildings is related to the applied method. It scores any building overlapping with flood prone areas as “exposed”, regardless of the percentage of the building footprint that intersects with the flood area feature. As a result, large building polygons are more likely to be scored as “exposed” than small ones.

The last column in Table 1 presents the exposed elements normalized by the total area of Switzerland (41,290 km²). An average of eight buildings (2,700 m² footprint area, 33 inhabitants) are exposed per square kilometer. These normalized figures are revisited in the following section, where we present the densities of exposed assets based on spatial aggregations with different spatial units.

3.2. Spatial aggregates, densities and ratios of exposed assets

Fig. 1 presents the aggregation of the number of exposed buildings per municipality normalized per square kilometer in five 20%-quantiles. The limit between the middle and the second highest class coincides with the average value of eight exposed buildings per square kilometer considering all of Switzerland (cf. Table 1). Consequently, 60% of the municipalities (the three lower classes) have densities that are less than or equal to the nationwide average. Furthermore, the mean of the density values of all municipalities is approximately 13 exposed buildings per square kilometer, which is >50% higher than the nationwide density. In other words, the density distribution per municipality is not symmetrical but right-skewed and small municipalities are generally associated with higher densities than large ones. Considering the spatial distribution of the densities, low values are generally concentrated in the south-eastern part of Switzerland. In contrast, many municipalities with high densities are located in the central and the northern parts of the country, with the exception of two lines of high values in the south (areas A and B in Fig. 1).

Fig. 2 also presents densities of the number of exposed buildings, but per 4.23 km × 4.23 km grid cells. The thresholds used to define the five plotted classes are the same as in Fig. 1. Overall, the spatial distribution pattern of the densities per grid cell in Fig. 2 is similar to Fig. 1, but the high density values in area B (in Fig. 1) are less prominent. Here, the high values of some small municipalities ($\ll 18$ km²) are smoothed out when the densities are calculated per grid cell. This smoothing effect of high and low density values affects all regions, where the areas of municipalities are considerably smaller than the areas of the grid cells. Additionally, the applied kernel density estimation with a window width of 6.345 km smoothens the resultant values. However, this smoothing effect of the kernel density estimation is cancelled out in regions where the municipal areas are notably larger than the grid cell areas. Consequently, in regions with large municipalities, the variability of the underlying exposure data is more evident in the density maps organized per grid cell (e.g. area C in Fig. 2) than per municipality.

In principal, the exposure density in a particular spatial unit is the result of two underlying features, (1) the density of assets (number of buildings, footprints or inhabitants per square kilometer of this spatial unit) and (2) the proportion of flood prone area to the total area of this spatial unit. While the high exposure density in the northern part

Table 1
Flood exposure in Switzerland. Norm. = normalized per km², surface of Switzerland: 41,290 km².

Asset type	All	Not exposed	Exposed	Ratio [%]	Norm. [10 ⁶ m ²]
	[N] or [10 ⁶ m ²]	[N] or [10 ⁶ m ²]	[N] or [10 ⁶ m ²]		
Number of buildings [N]	2,086,411	1,765,902	320,509	15.4	8
Footprint area of buildings [10 ⁶ m ²]	540	430	110	20.4	0.0027
Number of residents [N]	7,909,191	6,556,486	1,352,705	17.1	33

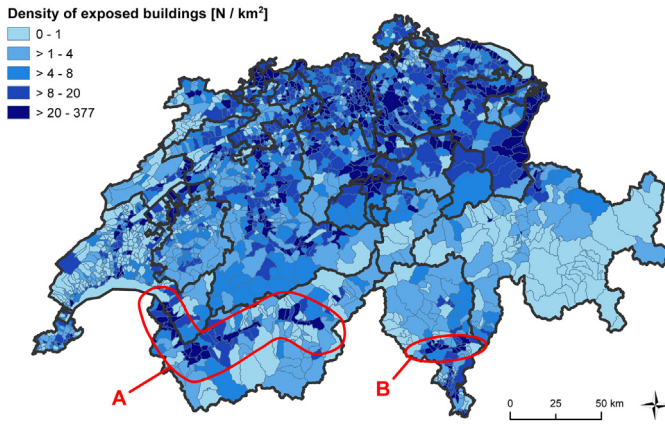


Fig. 1. Densities of flood exposed buildings per Swiss municipality, numbers per km². Data classes are (rounded) 20% quantiles. Fine lines represent municipal boundaries and thick lines represent cantonal boundaries. Areas A and B highlight two lines of high values in the south of Switzerland.

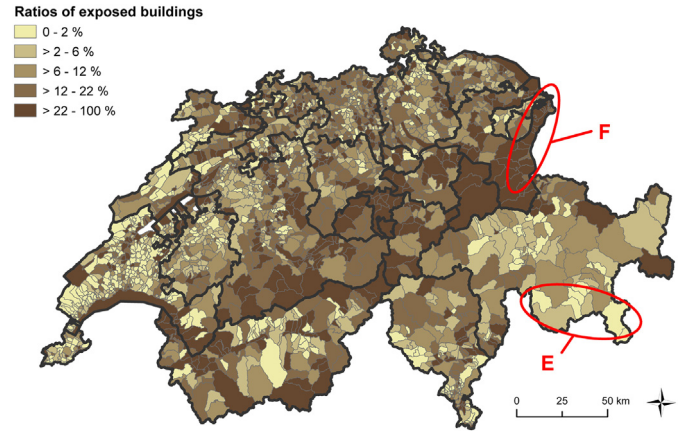


Fig. 3. Ratios of flood exposed buildings per Swiss municipality [numbers of exposed buildings/numbers of all buildings]. Data classes are (rounded) 20% quantiles. Fine lines represent municipal boundaries and thick lines represent cantonal boundaries. Area E highlights an example, where low values are observed in all four maps with 20% quantile representation (Figs. 1 to 4), and area F is characterized by high values in all four maps.

of Switzerland is attributed to an overall high density of assets in these lowlands and hilly regions, the high exposure densities in the mountainous south correspond with the high settlement concentrations located on the main alpine river floodplains that extend across the entire valley bottom (Zimmermann and Keiler, 2015).

The spatial distributions of the building exposure ratios per municipality are shown in Fig. 3, classified in five quantiles of 20%. The 15.4% nationwide exposure ratio (see Table 1), as well as the mean of the exposure ratios of all municipalities (13.9%) belong to the second highest class, indicating a right-skewed distribution. However, unlike the density values per municipality, the exposure ratios per municipality do not show a correlation to the areal size of municipality. Considering the spatial distribution of the exposure ratios per municipality, we identify a narrow area of high ratios from the southwest to the northeast of Switzerland, which coincide with the northern and pre-alpine regions of the Swiss Alps. Otherwise, low to medium ratios dominate, with the exception of some isolated high values.

Finally, Fig. 4 presents the exposure ratios per grid cell with the same thresholds of the five classes as in Fig. 3. Compared with Fig. 3 (municipalities) an equivalent spatial distribution of the exposure ratios appears in Fig. 4 (grids). As in the case of the exposure ratios per municipality, the exposure ratios per grid cell are generally higher in a broad strip that stretches from the southwest to the northeast.

in addition, we identify an accumulation of high values in the west (area D in Fig. 4), which does not appear in Fig. 3 (ratios per municipalities) due to the presence of some polygons without data. These polygons represent parts of lakes that are not assigned to municipalities and that do not contain buildings; thus, no exposure ratios are calculated. Finally, in the northern part of Switzerland, the map of exposure ratios per grid cells (Fig. 4) is easier to interpret than the map per municipalities (Fig. 3). This is mainly due to the smoothing effects caused by larger grids cells than municipalities and by the kernel density estimation procedure.

The prominent concentration of high exposure ratios in the narrow region that spans from the southwestern to the northeastern parts coincides with the northern and central parts of the Swiss Alps. This is a region that includes both concentrated settlements and wide areas characterized by relatively sparse populations. The main settlements here are concentrated in the few relatively flat areas, which are mainly floodplains, alluvial fans and debris cones.

When comparing exposure densities with exposure ratios (both sets of values organized per municipality or per grid cell), the extreme values (in the highest and the lowest classes) are found to be largely complementary. There are only a few major areas that are consistent.

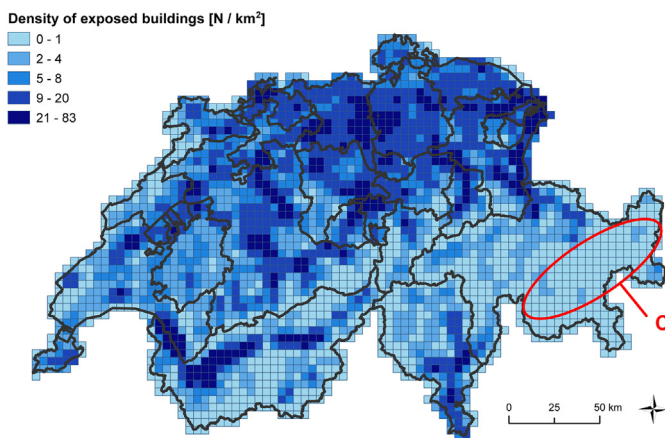


Fig. 2. Densities of flood exposed buildings in Switzerland per 4.23 × 4.23 km² grid cell, numbers per km². Thresholds of classes are identical to Fig. 1 (densities per municipalities). Fine lines represent grid cells and thick lines represent cantonal boundaries. Area C highlights an example, where the variability of exposure is more evident in density maps per grid cell than per municipality.

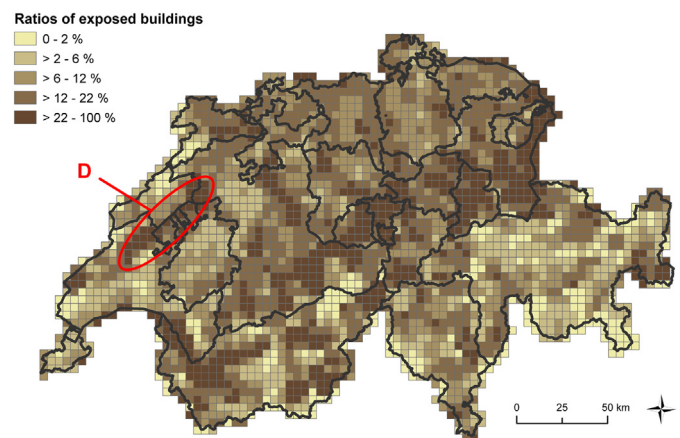


Fig. 4. Ratios of flood exposed buildings in Switzerland per 4.23 × 4.23 km² grid cell [numbers of exposed buildings/numbers of all buildings]. Thresholds of classes are identical to Fig. 3 (ratios per municipalities). Fine lines represent grid cells and thick lines represent lines cantonal boundaries. Area D highlights an accumulation of high values, which does not appear in Fig. 3 (ratios per municipalities).

Two examples are highlighted in Fig. 3: Area E is a region where low values are observed in all four maps (Figs. 1 to 4, see for a better overview Fig. A1 in Appendix) and area F is characterized by high values in all four maps. Overall, areas with high values in all four maps correspond with the relatively wide valleys of the main rivers connecting the high alpine regions with the foothills of the Alps, in particular, the Rhine river valley upstream of Lake Constanze (area F in Fig. 3) and the Rhone valley upstream of Lake Geneva (area A in Fig. 1). Both are considered to be densely populated areas surrounded by rather sparsely populated mountain areas. The large region of low values in the south-east observed in all four maps (Fig. A1 in Appendix) is almost congruent with the territory of Canton Graubünden. Authorities of Canton Graubünden pioneered the consideration of natural hazard aspects in the spatial planning processes in Switzerland. Legally binding hazard maps were introduced as early as 1963.

The aforementioned statements regarding the numbers of buildings also generally apply to the results describing the areal building footprints, and to a lesser degree, to the inhabitants. To provide an overview of the spatial distributions, the appendix presents the aggregations of the numbers of buildings (Fig. A1), of the areal building footprints (Fig. A2), and of the number of inhabitants (Fig. A3).

3.3. Hotspots of flood exposure

The results of the hotspot analyses are summarized in Figs. 5 and 6. The dark colored areas in all of the maps represent clusters of high values, based on the $G_i^*(d)$ statistic (Getis and Ord, 1992, Ord and Getis, 1995) and on a 95% confidence level. Fig. 5 provides an overview of 30 maps based on the five distance bands d (applied on data aggregated on grid cells, see columns in Fig. 5) and on the six analyzed exposure indicators (rows in Fig. 5) aggregated per grid cells. The results show (Fig. 5) that an increasing distance band value results in larger and more generalized hotspots, but does hardly change the position of these areas. The 18 maps in Fig. 6 provide a comparable overview to the one presented in Fig. 5 and are based on the same six indicators (rows in Fig. 6), but aggregated per municipalities and based on three distance bands d (columns in Fig. 6). In contrast to the grid cell aggregation, the results of the municipality-based aggregation highlight that an increasing distance band not only changes the size and shape of hotspot areas but, also their position under some circumstances (e.g. in the central northern part in the first row in Fig. 6). Thus, due to the spatially more stable results obtained, the grid cell approach is considered to be more appropriate for hotspot analyses. In addition, we consider the

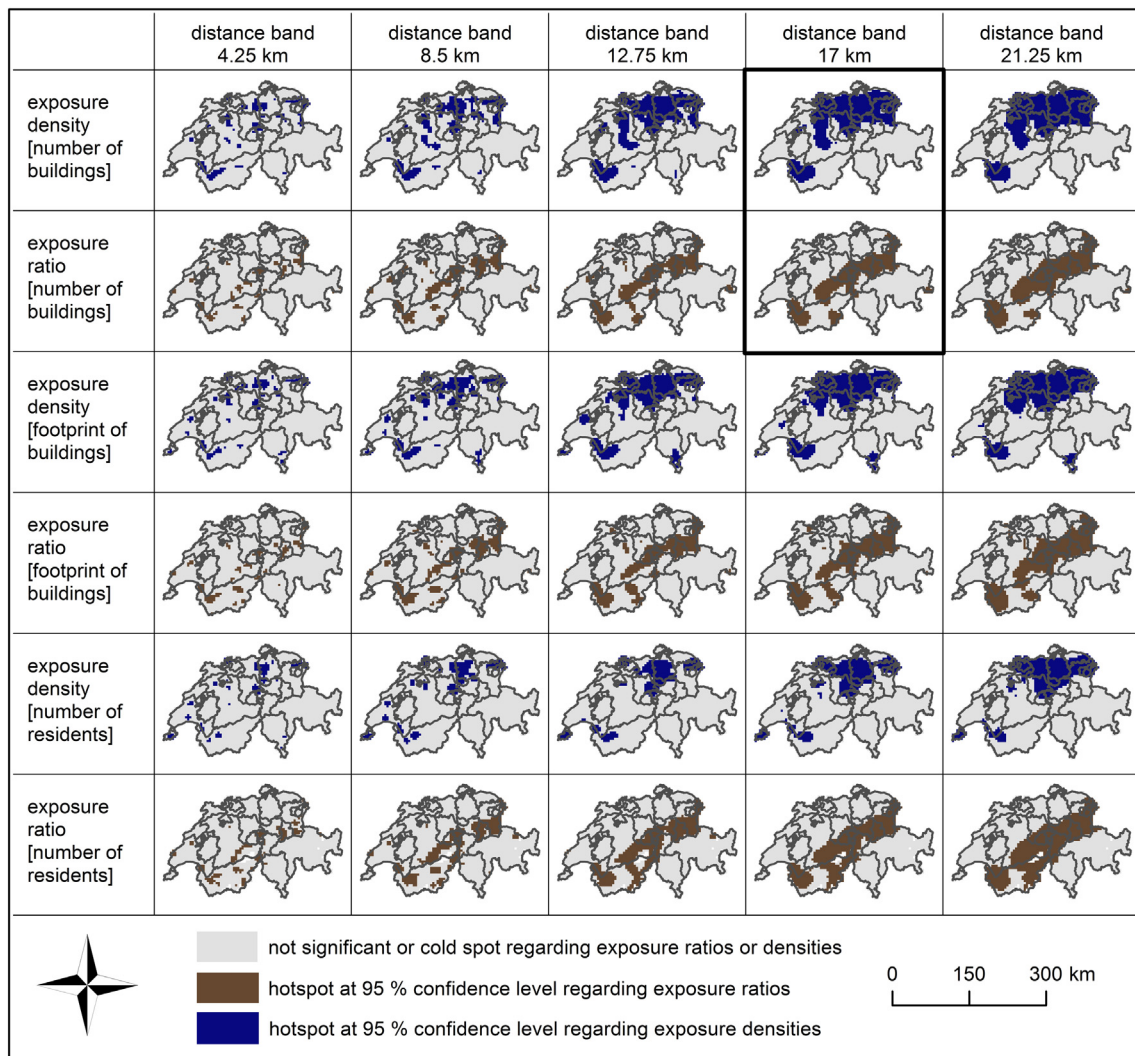


Fig. 5. Hotspots of flood exposure in Switzerland, based on data aggregated on $4.23 \times 4.23 \text{ km}^2$ grid cells. The dark colored areas show statistically significant clusters of high values (see legend) based on the local spatial autocorrelation statistic $G_i^*(d)$ by Getis and Ord (references see text), for five different fixed distance bands (columns) and six different types of indicators (rows). Confidence level at 95%, correction of false discovery rate applied. Details on the applied method described in Section 2.5. The two maps, which are replicated in Fig. 7, are highlighted by a bold frame. Gray lines represent cantonal boundaries.

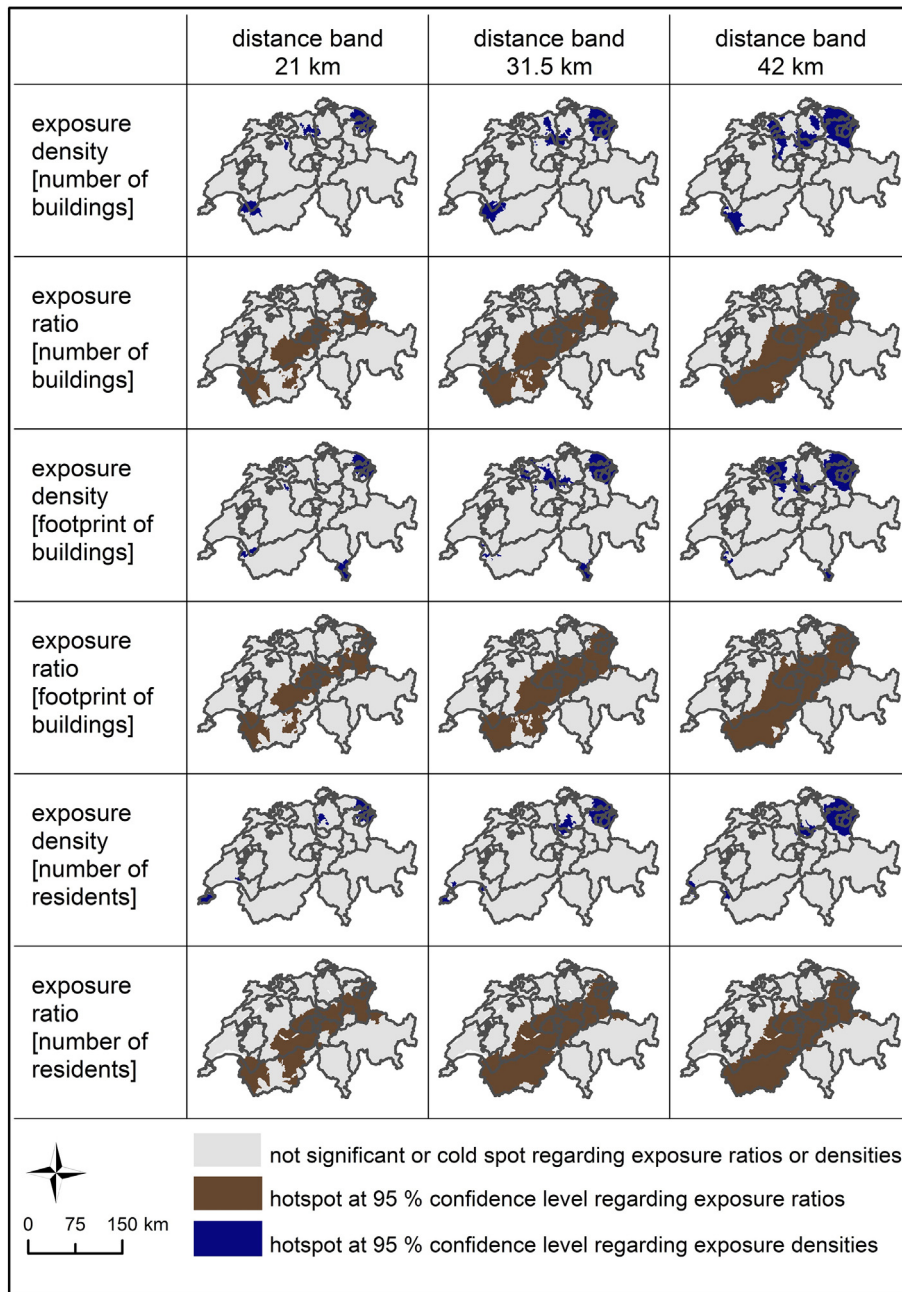


Fig. 6. Hotspots of flood exposure in Switzerland, based on data aggregated on municipalities. The dark colored areas show statistically significant clusters of high values (see legend) according to local spatial autocorrelation statistic $G_i^*(d)$ by Getis and Ord (references see text), for three different fixed distance bands (columns) and six different types of indicators (rows) Confidence level at 95%, correction of false discovery rate applied. Details on the applied method described in Section 2.5. Gray lines represent cantonal boundaries. (For interpretation of the references to color in this figure legend, the reader is referred to the web version of this article.)

analyses based on grid cells as 'spatially more consistent' in the sense that the sizes of the cells are all identical. Consequently, the size factor does not influence the result the way that variable sizes of municipalities do. For instance, the high exposure ratio (numbers of buildings) in the most eastern municipality of Switzerland is not identified as a part of a cluster (see first row with brown colored maps in Fig. 6), simply because this municipality is comparably large and has no neighboring municipalities with high exposure ratios (see Fig. 3). If the underlying data of the same municipality are aggregated on smaller areal units (e.g. grid cells of approximately 18 km²), the same hotspot analysis shows significant clusters of high exposure ratios (see first row with brown colored maps in Fig. 5). While the reason that data aggregation on grid cell is to prefer over the aggregation based on administrative boundaries is generally valid, the optimal size of the distance band d is dependent on the

purpose of the spatial cluster analysis. It represents a compromise between producing continuous areas (by increasing d) and maintaining spatial differentiations (by decreasing d). Based on the evaluation of the parameters, we consider hotspot analyses based on grid cells and with a distance band of 17 km (second last column in Fig. 5). The selected parameters are optimal for providing a nationwide overview. Further analysis follows this optimal approach.

Fig. 7 presents hotspots of the number of exposed buildings, based on data aggregated on 4.23 km × 4.23 km grid cells and with a distance band of 17 km. It can be observed that the hotspots based on density values are highly complementary to the hotspots based on exposure ratios. While the hotspots based on density values are mainly located in the northern part of Switzerland (with some additional spots in the southwest), the majority of the ones based on exposure ratios are

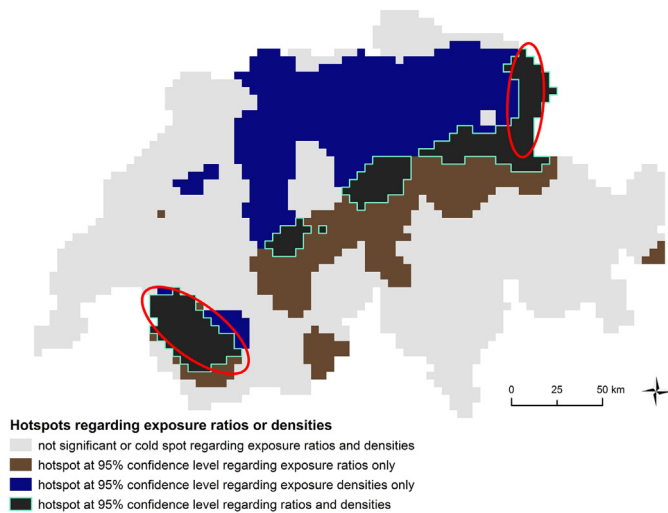


Fig. 7. (Selection and intersection of the two highlighted maps in Fig. 5): Hotspots of numbers of flood exposed buildings in Switzerland, based on data aggregated on 4.23×4.23 km² grid cells. The dark colored areas show statistically significant clusters of high values (see legend) according to local spatial autocorrelation statistic $G_i^*(d)$ by Getis and Ord (references see text). Confidence level at 95%, fixed distance band at 17 km, correction of false discovery rate applied. Details on the applied method described in Section 2.5. Red ellipses highlight the location of two major flood protection project in Switzerland. (For interpretation of the references to color in this figure legend, the reader is referred to the web version of this article.)

located within a broad strip from the southwestern to the northeastern parts of the country. Additionally, there are two small and isolated hotspots of exposure ratios, one located in the west and another in the east. Dark gray colored areas in Fig. 7 are areas where hotspots based on exposure densities and hotspots based on exposure ratios overlap. These dark gray areas are comparatively small and limited to the intermediate zones between the high alpine regions and the foothills of the Alps.

The spatial distributions of hotspots based on building footprint or on inhabitants respectively are similar to the distribution of hotspots based on the number of buildings (see Figs. 5 and 6).

3.4. Relevance of the MAUP

Our results show that the MAUP is relevant. The aggregation scheme influences both groups of results, namely, the spatial aggregates (see Section 3.2) and the hotspots (see Section 3.3) of flood exposed assets.

In particular, the aggregation scheme does not influence the general spatial distributions of flood exposure densities or ratios with respect to spatial aggregates. They remain the same whether the data is aggregated based on municipality districts or regular grids. However, upon further detailed inspection, they differ due to the effects of smoothing and coarsening (see Section 3.2). These effects illustrate the scaling aspect of the MAUP. In relation to MAUP, there are two reasons why aggregation based on grid cells is considered to be more appropriate for nationwide analyses. Firstly, aggregation based on (regular) grid cells supports the comparability of different regions better than the aggregation based on (irregularly shaped and sized) municipalities. Secondly, in regions with (very) small municipal districts (e.g. in the northwestern parts or in the very south of Switzerland), the visualization of aggregated values based on grid cells provides a more usable overview of the situation at the presented scale.

The comparison of the respective hotspots based on the two different aggregation schemes shows that they differ not so much with regards to exposure ratios (brown colored maps in Figs. 5 and 6), but remarkably when looking at exposure densities (blue colored maps in Figs. 5 and 6). The two different aggregation schemes using similar numbers and average sizes of spatial units, result in different areas of

flood exposure hotspot densities in Switzerland. That is, the results of these hotspot analyses are inconsistent when applying the two aggregation schemes, which vary in border locations. In other words, it matters where the borders of the spatial units are drawn. Consequently, the MAUP, especially the zonation aspect, should not be neglected.

3.5. Prioritization in risk reduction and risk management strategies

The dark colored areas in all presented maps (i.e. in the maps with 20% quantiles and in the hotspots maps) address the initial question pertaining to where flood protection measures should be prioritized. The dark blue areas (of exposure densities) indicate priorities for strategies following the concept of utilitarianism (Mill, 2007), whereas the dark brown ones (of high exposure ratios) identify priority areas for strategies which comply with Rawls' concept of justice (Rawls, 1971). In risk management, utilitarianism requests prioritization of the most cost efficient measures. High cost efficiency in turn is linked to high density of exposed assets, which is represented by the dark blue areas in this study. In contrast to utilitarianism, Rawls' concept on justice is focused on the most vulnerable areas and people. Vulnerable means to have low capacity to cope with a disaster. In this study, we use the share of exposed assets as an indicator for vulnerability, represented by brown colors in our maps. The maps with 20% quantile representation (of exposure densities and ratios, Figs. A1 to A3) are limited to the single spatial units of data aggregation, which are municipal districts or grid cells in our study. However, flood protection measures are often more effective when covering more than a single municipal district or a grid cell of 4.23 by 4.23 km (Thaler et al., 2016). Consequently, for strategy prioritization, there is less interest in the high values of single spatial units and greater interest in clusters of high values, i.e. in hotspots. As hotspots represent statistically significant spatial clusters (in our case at 95% confidence level) of high values, they support an evidence-based prioritization of regions for protection measures. Hence, the dark colored areas in Fig. 7 suggest regions of national priority for protection measures.

Switzerland's flood risk management strategy is still mainly driven by the reaction after large damaging flood events (Suter et al., 2016). The same reaction was observed by Thielen et al. (2016) after the 2013 flood in Germany and also in other countries. However, the number of preventive risk reduction projects in Switzerland are increasing with an emphasis on areas, which our study identifies as hotspots based on exposure densities. This emphasis reflects a commonly recommended strategic focus on cost efficiency (Meyer et al., 2013; Mori and Perrings, 2012). It is implemented into the decision making process on the allocation of federal subsidies by a respective tool to provide evidence of cost efficient measures (Bründl et al., 2009). Only measures with evident cost efficiency are supported by national funds. Currently, there is increasing awareness about certain regions indicated in our study as the most vulnerable territories within Switzerland. However, the focus in these areas is on their capacity to cope with floods (and other natural hazards), rather than on the reduction of their exposure ratios. Thus, it would be beneficial to determine whether current risk management strategies e.g. intervention or risk transfer by extensive insurance systems (Gretener, 2011; von Ungern-Sternberg, 2004) in these vulnerable areas are sufficient in the case of the occurrence of an event (as discussed within the Austrian context by Holub and Fuchs, 2009).

Nevertheless, within Switzerland's strategic focus on cost efficiency, the most vulnerable regions identified in our study are not neglected. For instance, the federal authorities support precisely two current technical flood protection projects, with a dedicated contact person. These projects are the 'Alpenrhein Expansion Project' conducted on the river Rhine upstream of Lake Constance and the 'Third Rhone Correction' upstream of Lake Geneva (Federal Office for the Environment, 2016). These two projects are not only operating within identified hotspots based on density values, but also within hotspots based on exposure ratios. As a result, the aforementioned projects lay within the dark gray

colored areas in Fig. 7 (see red ellipses in Fig. 7) that indicate areas where the hotspots based on density values and on ratios overlap. This means that the prioritization of these two projects at the national level is in line with our insights. Our findings suggest that the prioritization of these regions of overlapping hotspots is required to support the realization of both types of strategies focused on cost efficiency and on the most vulnerable regions.

4. Conclusions and outlook

The preceding sections illustrate the utility and pitfalls of spatial statistics applied on flood exposure data in Switzerland. We show that the detection of hotspots, i.e. of statistically significant clusters of high values, is feasible at the national scale and based on the use of spatially explicit data. We find that spatial cluster analyses support the generation of more informative databases, which can be used to prioritize flood protection measures, especially compared with the limited information from 'simple' maps of spatially aggregated data represented in quantiles. However, the analysis results into more than one single answer to the question 'where are the hotspots of flood exposure?', at least in the case of Switzerland. Thus, the proposed analysis provides a broad basis for decisions on different types of prioritization strategies in flood risk management.

First of all, the answer depends on the type of the indicator. The results of our case study suggest largely complementary hotspots based on exposure densities and exposure ratios. This means that priority areas for protection measures following cost efficient strategies (utilitarianism) and for measures focusing on the most vulnerable regions (Rawls' concept on justice) hardly overlap in Switzerland. Identifying these differences on a national level could already be an important step towards evaluating prioritization strategies. The prioritization of cost efficient measures is a well-established strategy with respective tools and criteria supporting the decision process in Switzerland and elsewhere. The density of exposed assets is a key determinant of cost efficiency. In contrast, the focus on vulnerability is less common and the development of the respective concepts and tools is still at a very early stage. The term vulnerability is already subject to ongoing academic discussions (cf. Birkmann et al., 2013), even more diverse are the existing concepts of vulnerability assessments upon which flood management decisions are based. The exposure ratio, used in this study, is one of all conceivable criteria for vulnerability assessments.

Secondly, there may be differences in the answer when considering different kinds of assets. However, only minor differences between the results regarding the number or footprint or inhabitants of exposed buildings are identified in Switzerland. More importantly, the way data aggregation is conducted influences the results. That is, the MAUP is relevant and must not be neglected in any spatial cluster analysis based on aggregated flood exposure data. By presenting hotspots based on different distance bands, we further exemplify the influence of parameter settings on the results of a hotspot test statistic. Not only the parameter setting influence the identification of spatial clusters, but already the type of the test statistic that is applied does. In future studies, it might be interesting to apply other spatially explicit local statistics and to compare them with the presented approaches, e.g. procedures presented by Aldstadt and Getis (2006), Anselin (1995) or Tango and Takahashi (2005). Data aggregation based on small catchment areas (instead of grid cells or municipalities), combined with the use of connectivity indices (instead of Euclidean distance) as the neighborhood criteria, would be another promising approach for future improvements.

Regardless of the data and the methods used, it is essential to select them based on the questions to be answered for flood risk management. Furthermore, we emphasize the utility of publishing hotspots of flood exposure in combination with notes on their dependency on the parameters of the applied method. This way, flood exposure hotspot analyses

provide added value to evidence-based decisions making pertaining to the prioritization of flood risk reduction measures.

Supplementary data to this article can be found online at <http://dx.doi.org/10.1016/j.scitotenv.2017.03.216>.

Acknowledgments

Funding from the Swiss Mobiliar ('die Mobiliar AG') supported the completion of this research. We thank the natural hazards group at the Swiss Mobiliar for acquiring and compiling the communal flood hazard maps; Candace Chow for editorial assistance; Sven Fuchs for proofreading and Markus Mosimann for his support with the design of the figures. We like to thank the anonymous reviewer and the editor for their inputs which substantially improved this manuscript.

References

- Aldstadt, Jared, Getis, Arthur, 2006. Using AMOEBA to create a spatial weights matrix and identify spatial clusters. *Geogr. Anal.* 38 (4):327–343. <http://dx.doi.org/10.1111/j.1538-4632.2006.00689.x>.
- Anselin, Luc, 1995. Local indicators of spatial association - LISA. *Geogr. Anal.* Vol 27 (2), 93–115.
- Aubrecht, Christoph, Fuchs, Sven, Neuhold, Clemens, 2013. Spatio-temporal aspects and dimensions in integrated disaster risk management. *Nat. Hazards* 68 (3): 1205–1216. <http://dx.doi.org/10.1007/s11069-013-0619-9>.
- Birkmann, Jörn, Cardona, Omar D., Carreño, Martha L., Barbat, Alex H., Pelling, Mark, Schneiderbauer, Stefan, et al., 2013. Framing vulnerability, risk and societal responses. The MOVE framework. *Nat. Hazards* 67 (2):193–211. <http://dx.doi.org/10.1007/s11069-013-0558-5>.
- Black, Andrew R., Burns, John C., 2002. Re-assessing the flood risk in Scotland. *Sci. Total Environ.* 294 (1–3):169–184. [http://dx.doi.org/10.1016/S0048-9697\(02\)00062-1](http://dx.doi.org/10.1016/S0048-9697(02)00062-1).
- Borden, Kevin A., Cutter, Susan L., 2008. Spatial patterns of natural hazards mortality in the United States. *Int. J. Health Geogr.* 7:64. <http://dx.doi.org/10.1186/1476-072X-7-64>.
- Borner, Patricio, 1999. Risikoanalyse bei gravitativen Naturgefahren. Methode. Edited by Bundesamt für Umwelt, Wald und Landschaft (BUWAL) (Umwelt-Materialien, Nr. 107/1). Available online at: <http://www.bafu.admin.ch/publikationen/publikation/00131/index.html?lang=de> (checked on 7/21/2016).
- Bründl, Michael, Romang, Hans E., Bischof, Nicole, Rheinberger, Christoph M., 2009. The risk concept and its application in natural hazard risk management in Switzerland. *Nat. Hazards Earth Syst. Sci.* 9, 801–813.
- Bundesamt für Umwelt BAFU, 2016a. Von der Risikoanalyse zur Massnahmenplanung. Arbeitsgrundlage für Hochwasserschutzprojekte Bern (Umweltwissen, 1606).
- Bundesamt für Umwelt BAFU, 2016b. Umgang mit Naturgefahren in der Schweiz - Bericht des Bundesrates.
- Caldas de Castro, Marcia, Singer, Burton H., 2006. Controlling the false discovery rate: a new application to account for multiple and dependent tests in local statistics of spatial association. *Geogr. Anal.* 38, 180–208.
- Cammerer, Holger, Thieken, Annegret H., Verburg, Peter H., 2013. Spatio-temporal dynamics in the flood exposure due to land use changes in the Alpine Lech Valley in Tyrol (Austria). *Nat. Hazards* 68 (3):1243–1270. <http://dx.doi.org/10.1007/s11069-012-0280-8>.
- Charlton, Martin, 2008. Modifiable areal unit problem (MAUP). In: Kemp, Karen K. (Ed.), *Encyclopedia of Geographic Information Science*. SAGE Publications, Inc., pp. 289–290.
- Chen, Lixia, van Westen, Cees J., Hussin, Haydar, Ciurean, Roxana L., Turkington, Thea, Chavarro-Rincon, Diana, Shrestha, Dhruva P., 2016. Integrating expert opinion with modelling for quantitative multi-hazard risk assessment in the Eastern Italian Alps. *Geomorphology* 273:150–167. <http://dx.doi.org/10.1016/j.geomorph.2016.07.041>.
- de Moel, Hans, Aerts, Jeroen C.J.H., Koomen, Eric, 2011. Development of flood exposure in the Netherlands during the 20th and 21st century. *Glob. Environ. Chang.* 21 (2): 620–627. <http://dx.doi.org/10.1016/j.gloenvcha.2010.12.005>.
- de Moel, Hans, Jongman, Brenden, Kreibich, Heidi, Merz, Bruno, Penning-Rowsell, Edmund, Ward, Philip J., 2015. Flood risk assessments at different spatial scales. *Mitig. Adapt. Strateg. Glob. Chang.* 20 (6):865–890. <http://dx.doi.org/10.1007/s11027-015-9654-z>.
- European Parliament, 2007. Directive 2007/60/EC of the European Parliament and of the Council of 23 October 2007 on the assessment and management of flood risk. 2007/69/EC. *Off. J. Eur. Union* 288, 27–34.
- Federal Office for the Environment FOEN, 2008. Terms of Use Aquaprotect. Available online at: <http://www.bafu.admin.ch/naturgefahren/14186/14801/16598/16600/index.html?lang=en> (checked on 9/26/2016).
- Federal Office for the Environment FOEN, 2016. Flood Protection Section. Responsibilities of Staff. Available online at: <http://www.bafu.admin.ch/org/organisation/00180/00188/index.html?lang=en> (checked on 10/2/2016).
- Federal Statistical Office FSO, 2016. Buildings and Dwellings Statistic (Since 2009). Factsheet - Surveys, Sources. Neuchâtel. Available online at: <https://www.bfs.admin.ch/bfs/en/home/statistics/construction-housing/surveys/gws2009.html> (checked on 1/9/2017).
- Feyen, Hans, Mehlhorn, Jens, Menzinger, Ivo, 2003. Invention: Method for Evaluating Flood Plain Risks (Patent Application in the United States Patent and Trademark Office).

- Figueiredo, Rui, Martina, Mario L.V., 2016. Using open building data in the development of exposure data sets for catastrophe risk modelling. *Nat. Hazards Earth Syst. Sci.* 16 (2): 417–429. <http://dx.doi.org/10.5194/nhess-16-417-2016>.
- Fuchs, Sven, Keiler, Margreth, Sokratov, Sergey, Shnyarkov, Alexander, 2013. Spatiotemporal dynamics. The need for an innovative approach in mountain hazard risk management. *Nat. Hazards* 68 (3):1217–1241. <http://dx.doi.org/10.1007/s11069-012-0508-7>.
- Fuchs, Sven, Keiler, Margreth, Zischg, Andreas P., 2015. A spatiotemporal multi-hazard exposure assessment based on property data. *Nat. Hazards Earth Syst. Sci.* 15 (9): 2127–2142. <http://dx.doi.org/10.5194/nhess-15-2127-2015>.
- Fuchs, Sven, Orntsmüller, Christine, Totschnig, Reinhold, 2012. Spatial scan statistics in vulnerability assessment. An application to mountain hazards. *Nat. Hazards* 64 (3): 2129–2151. <http://dx.doi.org/10.1007/s11069-011-0081-5>.
- Fuchs, Sven, Röthlisberger, Veronika, Thaler, Thomas, Zischg, Andreas P., Keiler, Margreth, 2017. Natural hazard management from a co-evolutionary perspective: exposure and policy response in the European Alps. *Ann. Am. Assoc. Geogr.* 107 (2).
- Getis, Arthur, Ord, John K., 1992. The analysis of spatial association by use of distance statistics. *Geogr. Anal.* Vol. 24 (3), 189–206.
- Getis, Arthur, 2008. A history of the concept of spatial autocorrelation: a geographer's perspective. *Geogr. Anal.* 40, 297–309.
- Greterer, Max, 2011. Die Versicherung von Elementarschäden durch die privaten Sachversicherer in der Schweiz. Schweizerischer Versicherungsverband, Zürich Available online at: <http://www.svv.ch/de/publikationen/die-versicherung-von-elementarschaeden-durch-die-privaten-sachversicherer-der-schweiz> (checked on 8/22/2014).
- Hallegette, Stephane, Green, Colin, Nicholls, Robert J., Corfee-Morlot, Jan, 2013. Future flood losses in major coastal cities. *Nat. Clim. Chang.* 3 (9):802–806. <http://dx.doi.org/10.1038/nclimate1979>.
- Holub, Markus, Fuchs, Sven, 2009. Mitigating mountain hazards in Austria – legislation, risk transfer, and awareness building. *Nat. Hazards Earth Syst. Sci.* 9 (2):523–537. <http://dx.doi.org/10.5194/nhess-9-523-2009>.
- Huttenlau, Matthias, Stötter, Johann, Stiefelmeyer, Heinz, 2010. Risk-based damage potential and loss estimation of extreme flooding scenarios in the Austrian Federal Province of Tyrol. *Nat. Hazards Earth Syst. Sci.* 10 (12):2451–2473. <http://dx.doi.org/10.5194/nhess-10-2451-2010>.
- IPCC, 2012. Managing the Risks of Extreme Events and Disasters to Advance Climate Change Adaptation. A Special Report of Working Groups I and II of the Intergovernmental Panel on Climate Change. With assistance of Field, C.B., V. Barros, T.F. Stocker, D. Qin, D.J. Dokken, K.L. Ebi, M.D. Mastrandrea, K.J. Mach, G.-K. Plattner, S.K. Allen, M. Tignor, P.M. Midgley. IPCC. Cambridge University Press, Cambridge, UK and New York, NY, USA.
- Johnson, Clare, Penning-Rowsell, Edmund, Parker, Denis, 2007. Natural and imposed injustices: the challenges in implementing 'fair' flood risk management policy in England. *Geogr. J.* 173:374–390 <http://www.jstor.org/stable/30130632>.
- Jongman, Brenden, Hochrainer-Stigler, Stefan, Feyen, Luc, Aerts, Jeroen C.J.H., Mechler, Reinhard, Botzen, Wouter W.J., et al., 2014. Increasing stress on disaster-risk finance due to large floods. *Nat. Clim. Chang.* 4 (4):264–268 Available online at: <http://www.nature.com/nclimate/journal/v4/n4/full/nclimate2124.html> (checked on 7/2/2014).
- Jongman, Brenden, Ward, Philip J., Aerts, Jeroen C.J.H., 2012. Global exposure to river and coastal flooding. Long term trends and changes. *Glob. Environ. Chang.* 22 (4): 823–835. <http://dx.doi.org/10.1016/j.gloenvcha.2012.07.004>.
- Jonkman, Bas S.N., Bočkarjova, Marija, Kok, Matthijs, Bernardini, Patrizia, 2008. Integrated hydrodynamic and economic modelling of flood damage in the Netherlands. *Ecol. Econ.* 66 (1):77–90. <http://dx.doi.org/10.1016/j.ecolecon.2007.12.022>.
- Kazakis, Nerantzis, Kougiyas, Ioannis, Patsialis, Thomas, 2015. Assessment of flood hazard areas at a regional scale using an index-based approach and Analytical Hierarchy Process: application in Rhodope-Evros region, Greece. *Sci. Total Environ.* 538:555–563. <http://dx.doi.org/10.1016/j.scitotenv.2015.08.055>.
- Klijn, Frans, Kreibich, Heidi, de Moel, Hans, Penning-Rowsell, Edmund, 2015. Adaptive flood risk management planning based on a comprehensive flood risk conceptualisation. *Mitig. Adapt. Strateg. Glob. Chang.* 20 (6):845–864. <http://dx.doi.org/10.1007/s11027-015-9638-z>.
- Knox, E. George, 1989. Detection of clusters. In: Elliott, Paul (Ed.), *Methodology of Enquiries Into Disease Clustering*, pp. 17–22 Workshop. Papers and discussions. (London).
- Legendre, Pierre, Legendre, Louis, 2012. *Numerical Ecology*. 3rd English ed. Elsevier, Amsterdam (Chapters 8 and 13).
- Levine, Ned, 2008. CrimeStat: a spatial statistical program for the analysis of crime incidents. In: Shekhar, Shashi, Xiong, Hui (Eds.), *Encyclopedia of GIS*. Springer, New York, pp. 187–193.
- Loat, Roberto, Petrascheck, Armin, 1997. Consideration of Flood Hazards for Activities with Spatial Impact. Edited by Bundesamt für Wasserwirtschaft (BWW) Federal Office for Water Management, Bundesamt für Raumplanung (BRP) Federal Office for Spatial Planning, Bundesamt für Umwelt, Wald und Landschaft (BUWAL) Federal Office for the Environment, Forests and Landscape. Biel. Available online at: <http://www.bafu.admin.ch/publikationen/publikation/00786/index.html?lang=en> (checked on 7/21/2016).
- Lugeri, Nicola, Kundzewicz, Zbigniew W., Genovese, Elisabetta, Hochrainer, Stefan, Radziejewski, Maciej, 2010. River flood risk and adaptation in Europe—assessment of the present status. *Mitig. Adapt. Strateg. Glob. Chang.* 15 (7):621–639. <http://dx.doi.org/10.1007/s11027-009-9211-8>.
- Lung, Tobias, Lavallo, Carlo, Hiederer, Roland, Assio, Alessandro, Bouwer, Laurens M., 2013. A multi-hazard regional level impact assessment for Europe combining indicators of climatic and non-climatic change. *Glob. Environ. Chang.* 23 (2):522–536. <http://dx.doi.org/10.1016/j.gloenvcha.2012.11.009>.
- Mazzorana, Bruno, Levaggi, Laura, Keiler, Margreth, Fuchs, Sven, 2012. Towards dynamics in flood risk assessment. *Nat. Hazards Earth Syst. Sci.* 12 (11):3571–3587. <http://dx.doi.org/10.5194/nhess-12-3571-2012>.
- Merz, Bruno, 2006. *Hochwasserrisiken: Grenze und Möglichkeiten der Risikoabschätzung*. Schweizerbart'sche Verlagsbuchhandlung, Stuttgart.
- Merz, Bruno, Thielen, Annegret H., 2004. Flood risk analysis: concepts and challenges. *Österreichische Wasser- und Abfallwirtschaft* 56 (3–4), 27–34.
- Meyer, Volker, Becker, Nina, Markantonis, Vasileios, Schwarze, Reimund, van den Bergh, Jeroen C.J.M., Bouwer, Laurens M., et al., 2013. Review article: assessing the costs of natural hazards – state of the art and knowledge gaps. *Nat. Hazards Earth Syst. Sci.* 13 (5):1351–1373. <http://dx.doi.org/10.5194/nhess-13-1351-2013>.
- Mill, John Stuart, 2007. *Utilitarianism, Liberty and Representative Government*. Wildside Press.
- Mori, Koichiro, Perrings, Charles, 2012. Optimal management of the flood risks of flood-plain development. *Sci. Total Environ.* 431:109–121. <http://dx.doi.org/10.1016/j.scitotenv.2012.04.076>.
- Muis, Sanne, Gunalp, Burak, Jongman, Brenden, Aerts, Jeroen C.J.H., Ward, Philip J., 2015. Flood risk and adaptation strategies under climate change and urban expansion: a probabilistic analysis using global data. *Sci. Total Environ.* 538:445–457. <http://dx.doi.org/10.1016/j.scitotenv.2015.08.068>.
- Openshaw, Stan, 1984. The Modifiable Areal Unit Problem. *Geo Abstracts Univ. of East Anglia, Norwich (Catmog: concepts and techniques in modern geography)*.
- Ord, John K., Getis, Arthur, 1995. Local spatial autocorrelation statistics: distributional issues and an application. *Geogr. Anal.* Vol. 27 (4), 286–306.
- Papathoma-Köhle, Maria, Kappes, Melanie, Keiler, Margreth, Glade, Thomas, 2011. Physical vulnerability assessment for alpine hazards: state of the art and future needs. *Nat. Hazards* 58 (2):645–680. <http://dx.doi.org/10.1007/s11069-010-9632-4>.
- PLANAT, 2005. *Protection Against Natural Hazards in Switzerland - Vision and Strategy (Executive Summary)*.
- Rawls, John, 1971. *A theory of justice*. Harvard University Press, Cambridge.
- Rojas, Rodrigo, Feyen, Luc, Watkiss, Paul, 2013. Climate change and river floods in the European Union. Socio-economic consequences and the costs and benefits of adaptation. *Glob. Environ. Chang.* 23 (6):1737–1751. <http://dx.doi.org/10.1016/j.gloenvcha.2013.08.006>.
- Silverman, Bernard W., 1986. *Density Estimation for Statistics and Data Analysis*. Chapman and Hall, New York, p. 76 (Monographs on statistics and data analysis). (equation 4.5).
- Snow, John, 1855. *On the Mode of Communication of Cholera*. second ed. Churchill, London.
- Staffler, Hanspeter, Pollinger, Rudolf, Zischg, Andreas P., 2008. In: *Interpraevent (Ed.), Prioritisation in the planning of permanent protection structures against floods and debris flows on the regional scale in the autonomous province of Bolzano - South Tyrol*, pp. 323–334 Conference Proceedings.
- Su, Wei, Zhang, Xiaodong, Wang, Zhen, Su, Xiaohui, Huang, Jianxi, Yang, Siqian, Liu, Sanchao, 2011. Analyzing disaster-forming environments and the spatial distribution of flood disasters and snow disasters that occurred in China from 1949 to 2000. *Math. Comput. Model.* 54 (3–4):1069–1078. <http://dx.doi.org/10.1016/j.mcm.2010.11.037>.
- Suter, Hannes, Thomi, Luzius, Kern, Raoul, Künzler, Matthias, Gusterer, Conny, Zischg, Andreas P., et al., 2016. What makes a successful flood control project? An evaluation of project procedure and risk based on the perspective of Swiss communes. In: *Koboltschnig, Gernot (Ed.), Interpraevent 2016. Living With Natural Risks. Proceedings of the 13th Congress*. Lucerne, pp. 159–167.
- swisstopo, 2016a. *swisTLM3D, The Topographic Landscape Model TLM (of Switzerland) Version 1.x as per March 2016*. (Description and acquisition online at, checked on 9/27/2016).
- swisstopo, 2016b. *Objektkatalog swisTLM3D 1.4*. Available online at: https://www.swisstopo.admin.ch/content/swisstopo-internet/de/home/products/landscape/tlm3d/_jcr_content/contentPar/tabs/items/dokumente/tabPar/downloadlist/downloadItems/759_1464676126625.download/201603swisTlm3d14okd.pdf (checked on 7/20/2016).
- swisstopo, 2016c. *swisTLM3D Nachführungsinfo 2016*. Available online at: https://www.swisstopo.admin.ch/content/swisstopo-internet/de/home/products/landscape/tlm3d/_jcr_content/contentPar/tabs/items/dokumente/tabPar/downloadlist_159209046/downloadItems/760_1464676201314.download/swisTlm3drelease2016dedefbarrierefrei.pdf (checked on 7/20/2016).
- swisstopo, 2016d. *swisBOUNDARIES3D. Grenzen Schweizweit 3D*. Available online at: https://www.swisstopo.admin.ch/content/swisstopo-internet/de/home/products/landscape/boundaries3d/_jcr_content/contentPar/tabs/items/dokumente/tabPar/downloadlist/downloadItems/793_1464683261852.download/201602sboundinfodbarrierefrei.pdf (checked on 8/4/2016).
- Tango, Toshiro, Takahashi, Kunihiko, 2005. A flexibly shaped spatial scan statistic for detecting clusters. *Int. J. Health Geogr.* 4:11. <http://dx.doi.org/10.1186/1476-072X-4-11>.
- Thaler, Thomas A., Priest, Sally J., Fuchs, Sven, 2016. Evolving inter-regional cooperation in flood risk management. Distances and types of partnership approaches in Austria. *Reg. Environ. Chang.* 16 (3):841–853. <http://dx.doi.org/10.1007/s10113-015-0796-z>.
- Thielen, Annegret H., Kienzler, Sarah, Kreibich, Heidi, Kuhlicke, Christian, Kunz, Michael, Mühr, Bernhard, et al., 2016. Review of the flood risk management system in Germany after the major flood in 2013. *E&S* 21 (2). <http://dx.doi.org/10.5751/ES-08547-210251>.
- UNISDR, 2015a. *Global Assessment Report on Disaster Risk Reduction. Making Development Sustainable: The Future of Disaster Risk Management*. Geneva, Switzerland.
- UNISDR, 2015b. *Sendai Framework for Disaster Risk Reduction 2015–2030*. Geneva, Switzerland.
- Url, Thomas, Sinabell, Franz, 2008. Flood risk exposure in Austria - options for bearing risk efficiently. *Schmollers Jahrbuch*. vol. 128, pp. 593–614.

- van der Veen, Anne, Logtmeijer, Christian, 2005. **Economic hotspots: visualizing vulnerability to flooding.** *Nat. Hazards* 36, 65–80.
- Visser, Hans, Petersen, Arthur C., Ligtoet, Willem, 2014. On the relation between weather-related disaster impacts, vulnerability and climate change. *Clim. Chang.* 125 (3–4): 461–477. <http://dx.doi.org/10.1007/s10584-014-1179-z>.
- von Ungern-Sternberg, Thomas, 2004. *Efficient Monopolies. The Limits of Competition in the European Property Insurance Market.* Oxford University Press, New York.
- Winsemius, Hessel C., Aerts, Jeroen C.J.H., van Beek, Ludovicus P.H., Bierkens, Marc F.P., Bouwman, Arno, Jongman, Brenden, et al., 2016. Global drivers of future river flood risk. *Nat. Clim. Chang.* 6 (4):381–385. <http://dx.doi.org/10.1038/nclimate2893>.
- Zimmermann, Markus, Keiler, Margreth, 2015. International frameworks for disaster risk reduction. Useful guidance for sustainable mountain development? *Mt. Res. Dev.* 35 (2):195–202. <http://dx.doi.org/10.1659/MRD-JOURNAL-D-15-00006.1>.
- Zischg, Andreas P., Schober, Stephan, Sereinig, Norbert, Rauter, Marina, Seymann, Christof, Goldschmidt, Franz, et al., 2013. Monitoring the temporal development of natural hazard risks as a basis indicator for climate change adaptation. *Nat. Hazards* 67 (3):1045–1058. <http://dx.doi.org/10.1007/s11069-011-9927-0>.

Paper 5: Fuchs, S., Keiler, M., Zischg, A., 2015. A spatiotemporal multi-hazard exposure assessment based on property data. *Natural Hazards and Earth System Sciences* 15, 2127–2142. [10.5194/nhess-15-2127-2015](https://doi.org/10.5194/nhess-15-2127-2015).



A spatiotemporal multi-hazard exposure assessment based on property data

S. Fuchs¹, M. Keiler², and A. Zischg^{2,3}

¹University of Natural Resources and Life Sciences, Institute of Mountain Risk Engineering, Vienna, Austria

²University of Bern, Institute of Geography, Bern, Switzerland

³University of Bern, Oeschger Centre for Climate Change Research, Mobiliar Lab for Natural Risks, Bern, Switzerland

Correspondence to: S. Fuchs (sven.fuchs@boku.ac.at)

Received: 23 March 2015 – Published in Nat. Hazards Earth Syst. Sci. Discuss.: 10 April 2015

Revised: 6 September 2015 – Accepted: 16 September 2015 – Published: 25 September 2015

Abstract. The paper presents a nation-wide spatially explicit object-based assessment of buildings and citizens exposed to natural hazards in Austria, including river flooding, torrential flooding, and snow avalanches. The assessment was based on two different data sets, (a) hazard information providing input to the exposure of elements at risk, and (b) information on the building stock combined from different spatial data available on the national level. Hazard information was compiled from two different sources. For torrential flooding and snow avalanches available local-scale hazard maps were used, and for river flooding the results of the countrywide flood modelling eHORA were available. Information on the building stock contained information on the location and size of each building, as well as on the building category and the construction period. Additional information related to the individual floors, such as their height and net area, main purpose and configuration, was included for each property. Moreover, this data set has an interface to the population register and allowed, therefore, for retrieving the number of primary residents for each building. With the exception of sacral buildings, an economic module was used to compute the monetary value of buildings using (a) the information of the building register such as building type, number of storeys and utilisation, and (b) regionally averaged construction costs.

It is shown that the repeatedly stated assumption of increasing exposure due to continued population growth and related increase in assets has to be carefully evaluated by the local development of building stock. While some regions have shown a clearly above-average increase in assets, other regions were characterised by a below-average development. This mirrors the topography of the country, but also the dif-

ferent economic activities. While hotels and hostels are extraordinarily prone to torrential flooding, commercial buildings as well as buildings used for recreational purposes are considerably exposed to river flooding. Residential buildings have shown an average exposure, compared to the number of buildings of this type in the overall building stock. In sum, around 5 % of all buildings are exposed to torrential flooding, and around 9 % to river flooding, with around 1 % of the buildings stock being multi-exposed. The temporal assessment of exposure has shown considerable differences in the dynamics of exposure to different hazard categories in comparison to the overall property stock. In conclusion, the presented object-based assessment is an important and suitable tool for nation-wide exposure assessment and may be used in operational risk management.

1 Introduction

World-wide data on natural disasters suggest an increasing number of reported events, of people affected and economic losses, but – in the most-developed countries – a decreasing number of reported fatalities since around 1900 (e.g. CRED, 2014; Munich Re, 2014). Regional analyses supplement these global data, but these regional data are not easily available because they are often not collected in global databases due to relatively low event magnitudes only affecting society on a regional or even local scale (United Nations, 2013). A review of Fuchs et al. (2013) has shown that overall conclusions on the dynamics of natural hazards, including

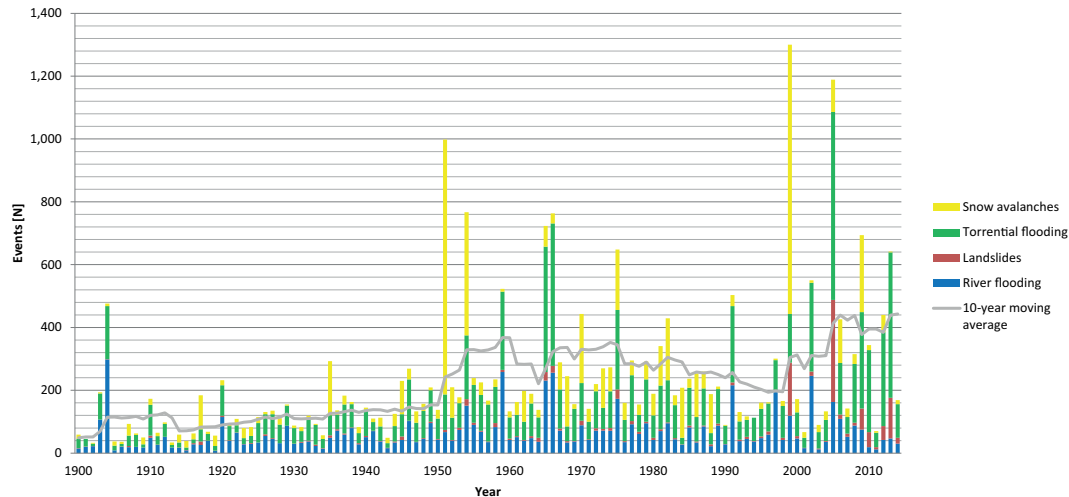


Figure 1. Annual number of documented natural hazards causing losses in Austria. Data source: Austrian Federal Ministry of Agriculture, Forestry, Environment and Water Management, 12/2014.

floods, landslides and snow avalanches, may be challenging due to the inherent complexity behind data.

Focusing on mountain regions, an increase in hazardous events and associated losses is repeatedly claimed (a) as a result of increasing exposure of elements at risk (Mazzorana et al., 2009; Preston, 2013), (b) due to natural fluctuations in flood frequencies (Schmocker-Fackel and Naef, 2010), and (c) due to the effects of climate change (e.g. Huggel et al., 2012; Korup et al., 2012). In Fig. 1, the annual number of natural hazards triggering losses in the Eastern European Alps (Republic of Austria) is shown. The underlying event documentation focused on different types of hazards but no further detailed information on individual losses or loss pattern is provided. The data for the period 1900–2014 describes snow avalanches, torrential flooding, landslides and river flooding, as well as the 10 years moving average of the total number per year. While between 1900 and 1959 an increase in the annual number of hazard events of around a factor of four can be concluded – presumably also due to an improved event observation – between 1960 and 1964 a decrease of around 50 % is traceable, followed by an increase due to the excessive events in 1965 and 1966. Since then, the 10 years moving average is steadily decreasing again, which is in line with the increasing efforts into technical mitigation measures since the mid-1960s (Fuchs, 2009; Holub and Fuchs, 2009). Due to the high number of hazard events in 1999, 2002, 2005 and 2009, however, the curve is again increasing to around 440 events per year. During the period of investigation, specific years with an above-average occurrence of individual hazard types can be traced as for example snow avalanches in 1951, 1954, 1999 and 2009, torrential flooding in 1965, 1966, 2005 and 2013, and river flooding in 1904, 1959, 1966 and 2002. The trend reported in Fig. 1 is in clear contrast to the trends repeatedly presented for

world-wide data and indicating an exponential increase in the number of events since the 1950s (e.g. Keiler, 2013). Apart from hazard dynamics (the natural frequency and magnitude of events), decreasing dynamics in mountain hazard losses may result from (a) increased efforts into technical mitigation (Keiler et al., 2012), (b) an increased awareness of threats being consequently considered in land-use planning (Wöhler-Alge, 2013; Thaler, 2014), both leading to less exposure, and (c) a decline in vulnerability (Fuchs et al., 2007; Jongman et al., 2015) which will not be further considered in the following sections. Apart from the ongoing discussion of the effects of climate change influencing the hazard trigger (e.g. Auer et al., 2007; Keiler et al., 2010; Lung et al., 2013), the effects of dynamics in exposure have so far not been sufficiently studied in the context of a possible influence on dynamics of damaging events suggested by Fig. 1. Since spatially explicit data on the dynamics of exposure remained fragmentary, data on the temporal dynamics of natural hazard events resulted in misleading conclusions with respect to the underlying causes and effects (Pielke Jr., 2007), and studies on dynamics in loss data may therefore have over-emphasized the effects of climate change (Barredo, 2009).

Focusing on exposure, the effectiveness of natural hazard risk management depends on the availability of data and in particular an accurate assessment of elements at risk (Jongman et al., 2014), which also requires a temporal and spatial assessment of their dynamics. It has been repeatedly claimed with respect to flood hazards in Europe that the main driver of increases in observed losses over the past decades is increased physical and economic exposure (Bouwer, 2013; Hallegatte et al., 2013; Jongman et al., 2014). Until now, however, in mountain regions of Europe such conclusions remain fragmentary since property data have only been available on the local scale as a result of individual case stud-

ies. These – often conceptual – studies related to the temporal dynamics of exposure to multiple types of mountain hazards include both the long-term and the short-term evolution. Long-term changes were found to be a result from the significant increase in numbers and values of properties endangered by natural hazard processes, and can be observed in both rural and urban mountain areas of Europe (Keiler, 2004; Fuchs et al., 2005; Keiler et al., 2006a; Shnyparkov et al., 2012). Short-term fluctuations in elements at risk supplemented the underlying long-term trend, in particular with respect to temporary variations of people in hazard-prone areas and of vehicles on the road network (Fuchs and Bründl, 2005; Keiler et al., 2005; Zischg et al., 2005). These results suggest that the spatial occurrence of losses is not so much dependent on the occurrence of specifically large events with high hazard magnitudes but more a result of an increased number of elements at risk in endangered areas (Fuchs et al., 2012). Most of the recent works, however, rely on local object-based studies (Zischg et al., 2004; Fuchs et al., 2012) or aggregated land use data (Bouwer et al., 2010; de Moel et al., 2011; Cammerer et al., 2013), leading to substantial uncertainties if up-scaled to a larger spatial entity (de Moel and Aerts, 2011; Jongman et al., 2012a). Because of the limited data availability, comprehensive object-based and therefore spatially explicit analyses have thus not been extended beyond the local or regional level (Kienberger et al., 2009; Huttenlau et al., 2010; Zischg et al., 2013), and studies focusing on the national level in mountain regions using such data remain fragmentary (Fuchs et al., 2013).

To contribute to this gap, we show how detailed property level data can be used to improve the understanding of trends in hazard exposure on a national level. We will explicitly focus on dynamics in elements at risk, neglecting (a) any changes in the process dynamics due to underlying changes in the natural system including the effects of climate change, (b) any shifts in exposure due to the implementation of technical mitigation measures, and (c) any changes in vulnerability. This allows for the assessment of dynamics in property exposure, and will provide insights elements at risk may have on changing risk in mountain environments leaving other risk-contributing factors constant.

2 Methods

This study is based on two different data sets, (a) hazard information providing input to the exposure of elements at risk, and (b) information on the building stock combined from different spatial data available on the national level. We consider hazard information for river flooding, torrential flooding including debris flows, and snow avalanches since these hazard types are responsible for the majority of damages in the European Alps (Sinabell and Url, 2007; Hilker et al., 2009). In the following, the composition and preparation of data sets is described.

2.1 Hazard information

Two different sources provide the base for compiling hazard information. For mountain hazards accessible local-scale hazard maps are used, and for river flooding the results of a nation-wide flood modelling are available. This combination of data sets was necessary because (a) for mountain hazards, no nation-wide modelling is available in Austria and (b) for river flooding, no nation-wide compilation of hazard maps exists in contrast to mountain hazards due to the fact that river flooding lies within the competency of the individual Federal States.

In Austria, the method for hazard mapping is regulated by a national legal act (Republik Österreich, 1975) and an associated decree (Republik Österreich, 1976). The implementation of these regulations is assigned to the Federal Ministry of Agriculture, Forestry, Environment and Water Management (BMLFUW) and administrated by the governmental departments of the Austrian Service for Torrent and Avalanche Control (WLV). Since the mid-1970s, these governmental departments have been progressively compiling hazard maps for the communities affected by mountain hazards based on available data and information on hazards as well as modelling exercises (Holub and Fuchs, 2009). These hazard maps are mostly compiled on a detailed local scale of 1:2000 to 1:10000 in order to decide whether or not individual plots are affected by the different hazard types. Hazard maps usually refer to individual catchments within individual communities, and depict the area affected by a design event with a return period of 1 in 150 years. So far, 92 % of all communities with an obligation for hazard mapping in Austria do have a legally valid hazard map. According to the Decree on Hazard Zoning (Republik Österreich, 1976), red hazard zones indicate those areas where the permanent utilisation for settlement and traffic purposes due to the exposure to the design event is not possible or only possible with extraordinary efforts for mitigation measures. Already existing buildings in these areas are not allowed to be expanded or to be used for other purposes than the existing one. Yellow hazard zones indicate those areas where a permanent utilisation for settlement and traffic purposes is impaired by the design event. Red and yellow hazard zones of different catchments and multiple hazard types may overlap, and as a result elements at risk may be exposed to more than one hazard type (multi-exposure, Kappes et al., 2012a, b). While in some catchments there may be a temporal differentiation of processes affecting the same elements at risk (snow avalanches during winter and torrential processes in summer), in other catchments there may be a temporal overlap of different processes occurring in the same period of time (debris flows from the tributary and flooding in the receiving channel), both affecting the same elements at risk. The available red and yellow hazard zones were provided digitally by the Austrian Federal Ministry of Agriculture, Forestry, Envi-

ronment and Water Management in March 2013 in order to select exposed property.

For river flooding data from the digital eHORA platform (<http://www.hochwasserrisiko.at/>) was used. This platform provides information on the flooding extent using web-GIS techniques, and has been jointly implemented by the Federal Ministry of Agriculture, Forestry, Environment and Water Management and the Austrian Insurance Association in terms of a public-private partnership on more than 25 000 of a total of 39 300 river kilometres (Stiefelmeyer and Hlatky, 2008). By using a hydrological model probabilistic runoff data for a 1 in 30, 100, and 300 year event was computed and converted into water levels and flood zones based on a nationwide DEM and a digital slope model. Following an ongoing discussion on the harmonisation of hazard mapping in Austria (Rudolf-Miklau and Sereinig, 2009), the 1 in 100 year event was provided by the Austrian Insurance Association in terms of a vector representation of flood plain boundaries and taken for our analysis.

2.2 Data on the building stock

Since the implementation of the Federal Law related to the Building Register (Republik Österreich, 2009), municipalities in Austria are responsible for the collection and digital processing of specified information related to the entire building stock. This information is centrally stored in a database and contains information on the location and size of each building, as well as on the building category and the construction period (1919–2000) and year of construction (since 2001), respectively (Statistik Austria, 2012). The latter information is related to the existing building stock. However, even though a building will be destroyed, the information and property attributes will be archived in the database and can be separately queried in order to provide a full overview on the construction history. Additional information related to the individual floors, such as their height and net area, main purpose and configuration, is included for each property. Moreover, this data set has an interface to the population register and allows, therefore, for retrieving the number of primary residents per accommodation unit for each building. Because this information contains x and y coordinates based on the address it can be processed within a GIS environment. Each building is characterized by the main use, which is assessed by the net area of used space for different purposes of every floor. If a minimum 50 % of the total net area of the building is for residential purpose, the building is characterized as a residential building. If the total sum of net areas for residential use is below 50 %, the main use is derived from the use with the largest total net area. If the net area of different types of use is the same, the main use is hierarchically classified in decreasing order by (1) hostels and hotels, (2) office buildings, (3) commercial buildings, (4) communication and transportation buildings, (5) industrial buildings, (6) buildings for cultural activities

and leisure, (7) agricultural buildings, (8) sacral buildings. Building categories were taken from the classification within the data set (Statistik Austria, 2012). Since the amendment of the respective law (Republik Österreich, 2013) the data may be used by the Federal administration for research purposes, and as such the information was made available through the Federal Ministry of Agriculture, Forestry, Environment and Water Management.

2.3 Exposure analysis

In exposure analysis, the building data set was intersected with the hazard information. The hazard information was represented as polygon, and the address location in terms of x and y coordinates by a point. A relational database composed from different modules was created.

With the exception of sacral buildings, an economic module was used to compute the monetary value of buildings using (a) the information of the building register such as building type, number of storeys and utilisation, and (b) regionally averaged construction costs following a method outlined in Fuchs and Zischg (2013) based on Keiler et al. (2006b) and Kranewitter (2002). The construction costs were based on replacement values instead of market values following general insurance principles (Fuchs and McAlpin, 2005), and were adjusted to inflation using the respective index of construction costs (Statistik Austria, 2013).

An exposition module was applied to connect the spatially defined information from the building register (x and y coordinates) to the hazard information in order to achieve information whether or not a building is exposed. In this step, an auxiliary data set on the building footprint of every building retrieved from the digital cadastral map was used to test whether or not the spatial location of a building corresponds to the point information of the digital building register and to assign the information of the hazard map to the address points. If the location of the x and y coordinates of the building did not match exactly with the location of the building, they were snapped to the border of the nearest building footprint available within a distance of ≤ 15 m around a polygon. Address information inside a polygon or in a distance exceeding 15 m were not changed, the first was included in the analyses as point information, the latter was excluded due to missing preciseness in geographic location. Assuming that hazards may damage buildings also if just parts are affected, an intersection between the building footprint and the hazard information was made. Thereby, any building was computed as being part of the highest hazard intensity level it was intersecting with.

Using information of the population register, the number of exposed citizens (principal residences) was calculated on the level of individual buildings.

The spatial and temporal analyses were relying on the information in the digital building register, i.e. on the construction period and construction year, respectively. As a result,

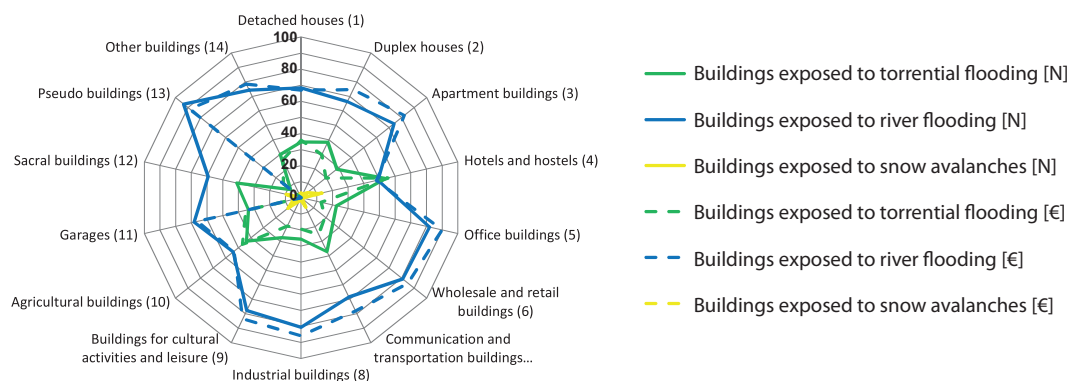


Figure 2. Radar chart of exposure (percentage of numbers and reconstruction values) to river flooding, torrential flooding and snow avalanches for different building categories.

the analysis of the dynamics of elements at risk is based on present-day monetary values and actual numbers of citizens, and can neither be used to deduce the historical composition of society, nor the historical value distribution. However, this approach can be used to indicate the temporal and spatial dynamics beyond the economic development in the country, and may therefore serve as a proxy for the absolute development of exposure.

3 Results

In the following sections results from the analyses are presented, focusing on the number of exposed buildings and citizens. Both the spatial and temporal analyses resulted in considerable heterogeneities among the communities and among different building categories. In Sect. 3.1 the results of the spatial analysis are provided, and in Sect. 3.2 the results of the temporal analysis are presented.

3.1 Results of spatial analysis

In Austria, 2 399 500 buildings are located, 319 026 of which (13.3 %) are exposed to natural hazards (Table 1). Of these almost 2.4 million buildings, 9 % (219 359) are exposed to river flooding, and 5 % to mountain hazards (torrential flooding 111 673 and snow avalanches 9009). Altogether, 298 248 buildings (93.5 % of exposed buildings and 12.4 % of the entire building stock in Austria) are exposed to one hazard type, and 20 778 buildings (6.5 % of exposed buildings and 0.9 % of the entire building stock in Austria) are exposed to more than one hazard type: 18 089 buildings are exposed to river and torrential flooding, 2595 to torrential flooding and snow avalanches, 568 to snow avalanches and river flooding, and 237 to river and torrential flooding as well as snow avalanches.

Citizens exposed were defined as primary residents according to the compulsory residency registration. When comparing the building stock with the number of primary resi-

dents, a slightly higher percentage (9.7 % versus 9.1 %) of citizens is exposed to river flooding, while to mountain hazards, a lower percentage (5.0 % versus 4.3 %) is affected. In total, 1 125 601 citizens are exposed to natural hazards, 1 058 594 (94.0 % of the exposed residents and 13.3 % of the entire population) to one type of hazard and 67 007 (5.95 % of the exposed residents and 0.8 % of the entire population) to more than one hazard type (Table 2).

Analysing the data set according to the type of building, a considerable part of the building stock is composed from residential buildings (category 1–3), but also a high number of hotels (category 4) and commercial buildings (category 5–8) is exposed (Table 3):

- a total of 2 056 322 residential buildings represent 85.7 % of the entire buildings stock in the country, but only 12.62 % of them (259 687) are exposed;
- a total of 140 470 commercial buildings represent 5.86 % of the entire buildings stock in the country, and 21.06 % of them (29,593) are exposed;
- a total of 37 272 hotels and hostels represent 1.55 % of the entire buildings stock in the country, and 23.04 % of them (8589) are exposed.

Analysing Fig. 2 it becomes evident that – with the exception of hostels and hotels – the percentage of buildings exposed to torrential flooding is below the percentage of buildings exposed to river flooding. A relatively high share of buildings from the category of residential buildings and commercial buildings is exposed to river flooding, whereas apart from hostels and hotels a considerable percentage of sacral buildings and agricultural buildings is exposed within the hazard type of torrential flooding. The percentage of hotels exposed to torrential flooding is even higher than the percentage of hotels exposed to flooding, which is exceptional: the other building categories exposed to torrential hazards fall relatively below the river flooding exposure. Only a minority of buildings is exposed to snow avalanches. Moreover,

Table 1. Information on non-exposed buildings and buildings exposed to river flooding, torrential flooding and snow avalanches, aggregated on the level of Federal States in Austria. Additionally, information on multi-exposed buildings is given.

Federal state	Buildings [N]	Non-exposed buildings [N]	Exposed buildings [N]	Exposed buildings [%]	Single exposure				Multi-exposure			
					River flooding [N]	Torrential flooding [N]	Snow avalanches [N]	River flooding and torrential flooding [N]	Torrential flooding and snow avalanches [N]	River flooding and snow avalanches [N]	Torrential flooding, river flooding and snow avalanches [N]	
Burgenland	133 482	123 905	9577	7.2	9439	140	0	2	0	0	0	0
Carinthia	185 693	161 782	23 911	12.9	17 012	8466	188	1660	95	10	10	10
Lower Austria	648 693	569 085	79 608	12.3	73 239	8381	6	2018	0	0	0	0
Upper Austria	425 718	378 307	47 411	11.1	37 836	12 471	137	2950	22	71	10	10
Salzburg	139 377	99 662	39 715	28.5	20 360	23 800	594	4684	319	128	92	92
Styria	381 484	331 065	50 419	13.2	27 953	25 695	460	3530	130	52	23	23
Tyrol	192 381	141 735	50 646	26.3	25 635	24 631	4465	2975	924	276	90	90
Vorarlberg	106 098	91 910	14 188	13.4	4334	8089	3159	270	1105	31	12	12
Vienna	186 574	183 023	3551	1.9	3551	0	0	0	0	0	0	0
Sum	2 399 500	2 080 474	319 026	13.3	219 359	111 673	9009	18 089	2595	568	237	237

Table 2. Information on non-exposed principal residents and principal residents exposed to river flooding, torrential flooding, and snow avalanches, aggregated on the level of Federal States in Austria. Additionally, information on multi-exposure is given.

Federal state	Single exposure					Multi-exposure				
	Principal residents [N]	Non-exposed residents [N]	Exposed residents [N]	Exposed residents [%]	River flooding [N]	Torrential flooding [N]	Snow avalanches [N]	River flooding and torrential flooding [N]	River flooding and snow avalanches [N]	Torrential flooding, river flooding and snow avalanches [N]
Burgenland	284 735	267 378	17 357	6.1	17 092	266	0	0	0	0
Carinthia	556 248	478 721	77 527	13.9	58 784	23 057	367	4478	203	20
Lower Austria	1 621 951	1 393 880	228 071	14.1	212 713	21 155	9	5806	0	0
Upper Austria	1 422 853	1 257 724	165 129	11.6	137 850	38 117	307	10 917	57	199
Salzburg	535 671	356 248	179 423	33.5	111 614	85 265	1621	18 008	969	424
Styria	1 212 345	1 044 934	167 411	13.8	105 888	70 219	913	9296	249	115
Tyrol	719 304	495 781	223 523	31.1	144 072	80 218	13 376	10 901	2542	918
Vorarlberg	373 566	328 682	44 884	12.0	16 363	24 749	6976	848	2318	56
Vienna	1 759 940	1 737 664	22 276	1.3	22 276	0	0	0	0	0
Sum	8 486 613	7 361 012	1 125 601	13.3	826 652	343 046	23 569	60 255	6338	1732

Table 3. Buildings exposed to natural hazards according to different building categories. Building category 13 (pseudo buildings) includes mobile and temporary accommodation facilities such as mobile homes and barracks if persons are living there, and building category 14 includes all other buildings not included in categories 1–13 (Statistik Austria, 2012).

Building categories	Buildings [N]	Buildings [%]	Single exposure										Multi-exposure				
			Non-exposed buildings [N]	Exposed buildings [N]	Exposed buildings [%]	River flooding [N]	Torrential flooding [N]	Snow avalanches [N]	River flooding and torrential flooding [N]	Torrential flooding and snow avalanches [N]	River flooding and snow avalanches [N]	Torrential flooding, river flooding and snow avalanches [N]					
Detached houses (1)	1 510 151	62.94	1 335 938	174 213	11.54	119 189	60 424	4607	8600	1280	221	94					
Duplex houses (2)	542 118	22.59	457 359	84 759	15.63	56 195	32 477	2308	5421	681	177	58					
Apartment buildings (3)	4053	0.17	3338	715	17.64	528	204	38	37	18	3	3					
Hotels and hostels (4)	37 272	1.55	28 683	8589	23.04	4217	4622	994	895	302	82	35					
Office buildings (5)	31 420	1.31	25 551	5869	18.68	4815	1325	63	315	17	5	3					
Wholesale and retail buildings (6)	32 583	1.36	25 646	6937	21.29	5612	1761	73	481	25	5	2					
Communication and transportation buildings (7)	4319	0.18	3525	794	18.38	544	295	53	73	24	9	8					
Industrial buildings (8)	72 148	3.01	56 155	15 993	22.17	12 874	4113	248	1139	86	30	13					
Buildings for cultural activities and leisure (9)	21 082	0.88	17 041	4041	19.17	3142	1113	90	264	35	11	6					
Agricultural buildings (10)	18 496	0.77	17 341	1155	6.24	624	501	121	66	24	4	3					
Garages (11)	48 819	2.03	43 412	5407	11.08	3686	1811	136	193	31	5	3					
Sacral buildings (12)	4384	0.18	3896	488	11.13	289	200	47	33	15	2	2					
Pseudo buildings (13)	4 536	0.19	3 683	853	18.81	797	71	3	18	0	0	0					
Other buildings (14)	68 119	2.84	58 906	9213	13.52	6847	2756	228	554	57	14	7					
Sum	2 399 500	100	2 080 474	319 026	13.30	219 359	111 673	9009	18 089	2595	568	237					

it can be deduced from Fig. 2 that the exposed values are higher for buildings exposed to river flooding in almost all building categories, and lower for buildings exposed to torrential flooding. The exception is again within the group of hostels and hotels, as well as agricultural buildings, garages, pseudo buildings and detached houses. Sacral buildings were not considered during economic analysis.

If queried spatially on a municipal level, considerable differences would manifest throughout the country, as shown in Fig. 3 by using a bipolar representation. The reference for Fig. 3 (left column panels) was the number of buildings which are affected by the respective hazard. Communities with no hazard data available are shown in grey colours and were not considered during the set of computations. The reference for Fig. 3 (right column panels) was the number of primary residents exposed to the respective hazard, and again grey colours show communities which were not considered because of missing hazard information.

- Regarding snow avalanches, the mean number of exposed buildings is 30.4 per municipality focusing on avalanche-prone municipalities, and the mean number of exposed principal residents is 79.6. The highest exposure is found in those municipalities next to the main chain of the Alps in western Austria (Federal States of Vorarlberg and Tyrol).
- The mean number of buildings exposed to torrential processes is 87.7 per municipality focusing on torrent-prone municipalities, and the mean number of exposed principal residents is 269.3. Apart from some outliers the highest exposure can be found in the Federal State of Salzburg as well as in municipalities of adjacent Federal States.
- River flooding is a threat to almost the entire country, and a mean number of 97.1 buildings is exposed per municipality. Due to the considerable number of buildings exposed to river flooding in the larger Vienna agglomeration, the highest exposure can be found in this area. Moreover, communities along the larger rivers show an above-average exposure. The mean number of exposed principal residents is 365.9 per municipality.

To summarise the nation-wide spatial assessment, around 13 % of the entire building stock and 13 % of the principal residents are exposed to the considered natural hazard scenarios in Austria, while considerable regional differences are manifested: While in the Federal States of Salzburg and Tyrol, 28.5 and 26.3 % of the entire building stock as well as 33.5 and 31.1 % of the residents are exposed, in Vienna it is only 1.9 and 1.3 %. While only around 5 % of all buildings and 4.3 % of the residents in Austria are exposed to mountain hazards (torrential flooding and snow avalanches), around 9 % of all buildings and almost 10 % of the residents are exposed to river flooding. Above-average exposure to mountain

hazards can be found in the Federal States of Salzburg, Tyrol and Vorarlberg, and buildings in Salzburg, Tyrol and Lower Austria are exceptionally prone to river flooding (Tables 1 and 2). Almost 1 % of the entire properties and 0.8 % of the residents have to be classified as being multi-exposed, which is, according to the topography of the country, a very low value.

3.2 Results of temporal analysis

In Fig. 4 the temporal analysis of the building stock in Austria is presented. There is evidence that the absolute number of buildings exposed to individual hazard types steadily increases in the country, which means that over the study period there were no exceptional construction activities traceable in either flood-prone areas or areas prone to torrential hazards (Fig. 4a). In contrast, a considerable increase of non-exposed buildings is evident for the period since the 1950s. Additionally, it can clearly be shown that exposure to snow avalanches is relatively low compared to other hazard categories, even if individual events occurred leading to considerable economic losses in recent decades (Fuchs et al., 2013). Since 1919, the total number of properties in Austria has increased by 643 % from 373 067 to 2 399 500 buildings. For 4.25 % of buildings, however, a year of construction was missing in the data and they were therefore excluded from further analysis. The total number of properties exposed to river flooding has increased by 650 % from 33 697 to 219 359 buildings (4.16 % excluded due to missing information on the year of construction). The total number of properties exposed to torrential flooding has risen by 594 % from 18 797 to 111 673 buildings (3.35 % excluded due to missing information on the year of construction). The total number of properties exposed to snow avalanches has risen by 433 % from 2081 to 9009 buildings (2.9 % excluded due to missing information on the year of construction). Based on absolute figures it has to be concluded that the growth rate is almost the same for buildings exposed to river flooding and non-exposed buildings, whereas for torrential flooding the growth rate is slightly lower and for snow avalanches the rate is considerably lower.

In Fig. 4b, the growth rate is shown for the building stock exposed to torrential and river flooding as well as snow avalanches, based on the respective construction period 1919–2012. Additionally, the growth rate of the overall building stock is provided. While the growth rate of the buildings exposed to river flooding is above the overall growth rate over the entire time period, the growth rate of buildings exposed to torrential flooding is below this rate for the period prior to 1960 and after 1980. For the period 1960–1980, both rates are almost the same. The growth rate of buildings exposed to snow avalanches is clearly below over the entire time span.

In Fig. 4c, the average annual number of newly constructed buildings is shown for the different hazard cate-

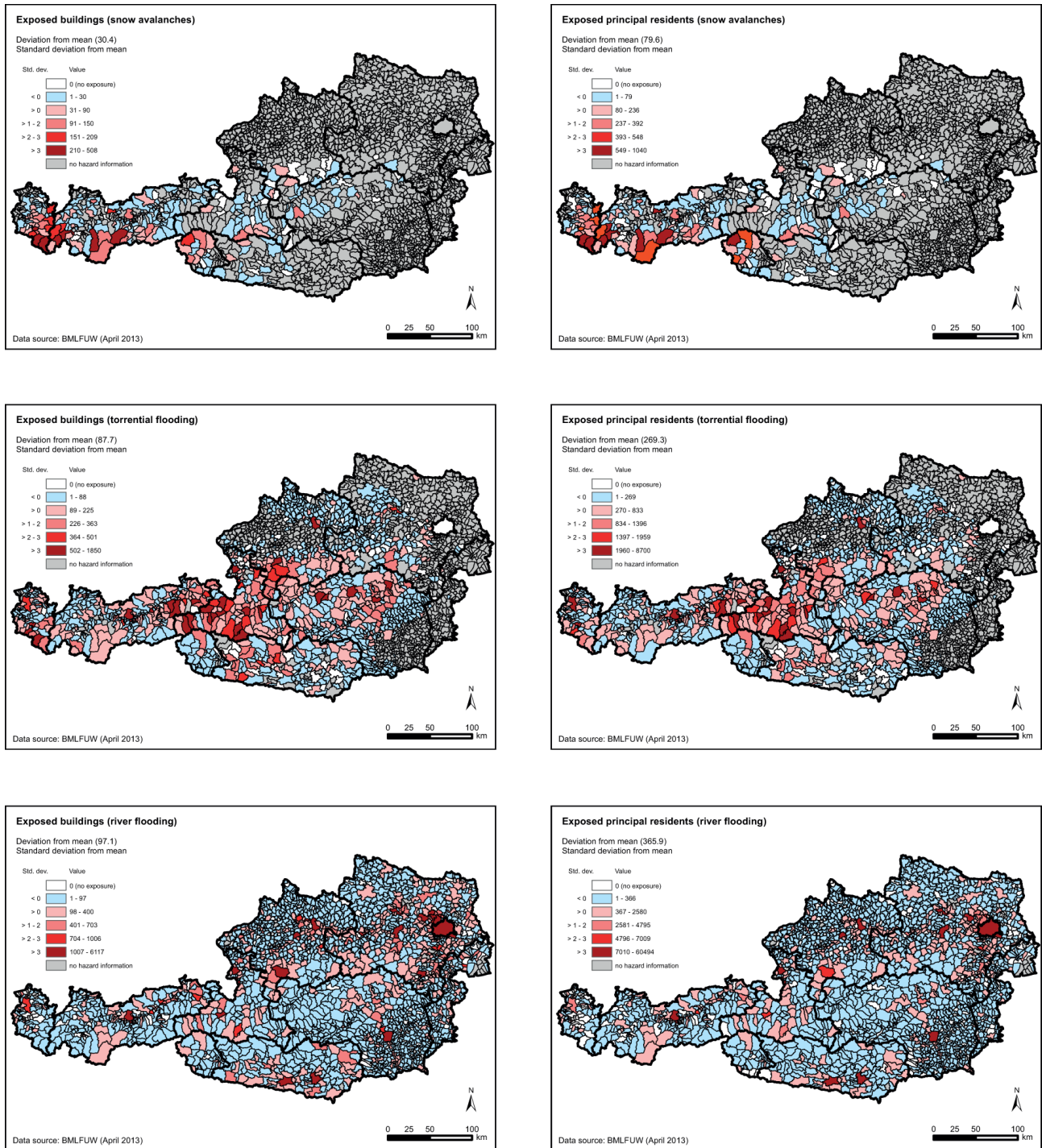


Figure 3. Number of buildings and primary residents exposed to snow avalanches, torrential flooding and river flooding in Austria, shown as deviation from mean.

gories. Until the 1970s, this number has risen remarkably and since then, the number of new constructions is decreasing. Since 2000, however, there is again a slight increase detectable. What is evident, however, that the curves for river flooding and torrential flooding follow the same pattern over

the study period. The annual growth was lowest in the period 1919–1944 (snow avalanches: 19, torrential flooding: 286, river flooding: 731 new buildings per year, for comparison annual growth for the entire building stock: 6894 buildings per year) and highest in the period 1971–1980 (snow

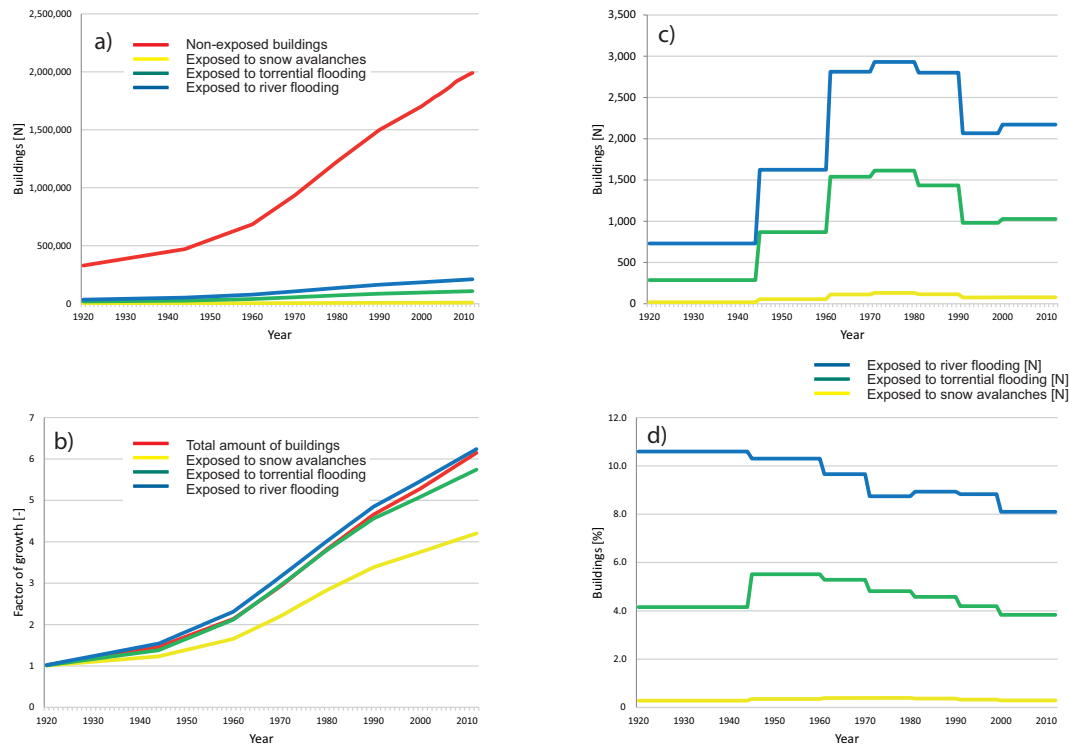


Figure 4. Temporal development of building stock in Austria. In (a) the cumulative absolute increase in the number of buildings is shown for non-exposed buildings and buildings exposed to snow avalanches, torrential as well as river flooding. In (b) the relative increase of the building stock is shown for the total number of buildings and buildings exposed to snow avalanches, torrential as well as river flooding, 1919 = 1. In (c) the average annual number of newly constructed buildings is shown for buildings exposed to snow avalanches, torrential as well as river flooding. In (d) the annual number of newly constructed exposed buildings versus the total number of newly-constructed buildings is shown for buildings exposed to snow avalanches, torrential as well as river flooding.

avalanches: 132, torrential flooding: 1614, river flooding: 2931 new buildings per year, for comparison annual growth for the entire building stock: 33 515 buildings per year). Currently, 78 buildings are constructed each year in avalanche-prone areas, 1028 in areas prone to torrential flooding, and 2172 in areas prone to river flooding, while 26 814 buildings are constructed annually throughout the country.

If these data are related to the annual construction activities only, neglecting the high number of already existing buildings, a reverse trend becomes obvious (Fig. 4d): the annual number of newly constructed exposed buildings versus the total number of newly constructed buildings regardless of the exposure is decreasing since the 1940s, but with different rates. The only exception is a decade of 1981–1990, where the percentage of buildings exposed to river flooding is slightly increasing, and the period between 1919–1944 and 1945–1960 with an increase from 4.2 to 5.5 % for torrential flooding. For river flooding, the percentage of new development in exposed areas decreased from 10.6 to 8.1 % for the period under investigation, while for torrential flooding the decrease is from 4.2 to 3.8 %. For snow avalanches, the percentage is within a range of 0.3–0.4 % only.

The results of a cumulative analysis including the entire building stock and focusing on inter-annual changes in the construction activity between exposed buildings and the total building stock are shown in Fig. 5 by the relation between annual dynamics in new constructions per year against the respective entire building stock at each time step. Because of the relatively low number of exposed buildings in the country (cf. Table 1), the resulting percentage is low. For river flooding, a slight increase in the share of elements at risk exposed from 9 to 9.8 % is detectable until the 1960s and since then a slight decrease to 9.2 % can be proven. In contrast, with respect to torrential flooding, the percentage of share of elements at risk is slightly decreasing from 5 to 4.8 % for the period 1919–1944, subsequently increasing to 5.1 % until 1970, and decreasing again to 4.7 %. For snow avalanches, the values are slightly decreasing over the entire period under investigation from 0.6 to 0.4 %. The buildings exposed to river flooding and torrential flooding are increasing in value compared to the non-exposed buildings, in particular during the period 1944–1990. The number of residents exposed is following a similar increase than the value of buildings from 7.2 to 9.7 % for river flooding. For torrential flooding, the increase is from 3.2 to 4.0 %, whereas since 1980 this rate

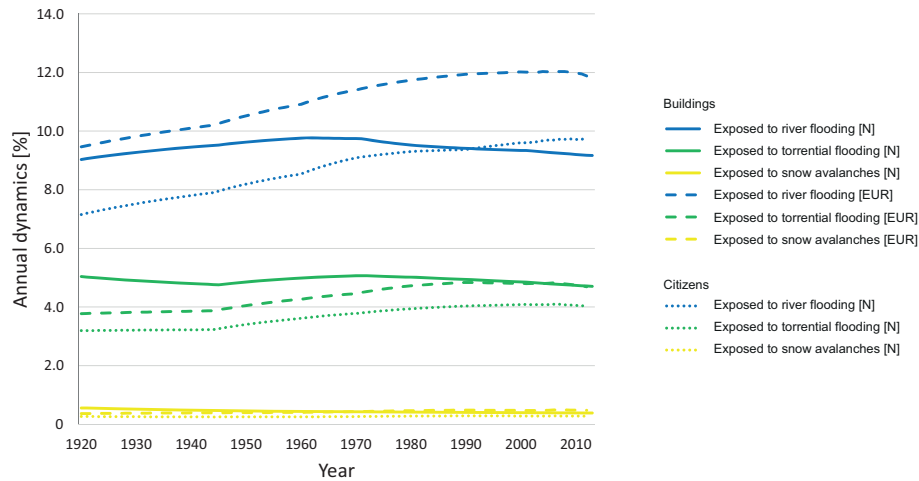


Figure 5. Relation between exposed buildings and residents and the total building stock and total number of residents. The numbers are based on average annual construction activities based on the available construction periods.

is almost constant around 4 %. The increase of residents exposed to snow avalanches is constant with a factor of 0.3 %. The overall dynamics, however, are within percent range.

4 Discussion

Whereas so far a general increase in the building stock could only be proven for selected case studies if data are analysed object-based (Keiler, 2004) or aggregated in terms of land-use classes (Cammerer and Thielen, 2013), the presented results provide more diversified insights in exposure. To give an example, previous studies with respect to exposure concluded that in some villages the property has increased above-average compared to the regional-scale development (Keiler 2004; Fuchs and Bründl, 2005). Taking the findings presented above it was shown that hazard-dependent above- and below-average dynamics are evident throughout the country both for the number of buildings and citizens. In some rural test sites, the total number of endangered buildings had been reported to having increased by a factor of approximately 2.5 since 1950, most of this increase being due to the category of accommodation facilities, such as hotels and guest houses (Keiler et al., 2006a) and residential buildings (Fuchs et al., 2005). By means of the nation-wide building register it was shown that the exposure of different building categories – as well as citizens exposed – is variable in dependence on the hazard type. Cammerer and Thielen (2013) concluded with respect to a possible future development of exposure until 2030 that if built-up areas expand along the valley bottom in the neighbourhood to existing settlements, a considerable increase in exposure will result. However, these projected changes in areas at risk vary strongly between the individual land-use scenarios applied (Cammerer and Thielen, 2013). By extrapolation of the temporal dynamics it can be shown that if a further development

of construction activity in Austria following the numbers of the period 1919–2012 is assumed, a continued increase of buildings exposed to river flooding of 2 % per year – compared to the entire building stock – would result in a number of 530 000 exposed buildings until 2100 (increase of 2.5 compared to 2012 which would be 8.1 % of the entire building stock in 2100). If new constructions would be banned immediately in areas exposed to flooding and the annual growth rate of the new constructions is assumed as 2 %, in the year 2100 still 3.4 % of the entire building stock would be exposed to river flooding, and 1.7 % to torrential flooding. This shows the considerable time lag as a result of previous land-use decisions and therefore clearly highlights the importance of risk management actions in terms of structural prevention measures.

Most communities with an extraordinary share of buildings prone to mountain hazards are located in the mountainous part of Austria, communities with an above-average exposure to river flooding are cities or centred on agglomerations in the alpine foreland. Given the economic structural change from the primary to the tertiary sector within the country, a high number of hotels is located in mountain tourist-spots, which explains the high exposure to mountain hazards. In turn, in regions with an emphasis on the secondary sector, a considerable share of commercial buildings, which are usually space-requiring, is located in flood plains of larger rivers or – historically grown – along mountain torrents because of the demand for hydropower. The category of buildings for cultural activities also requires space, and is therefore also often located in the flood plains. These areas were traditionally also used for agricultural purposes, which explains the above-average presence of agricultural buildings in these areas. Hence, since information on the building stock became increasingly available throughout Europe (e.g. Jongman et al., 2012b), more accurate information on

values exposed can be obtained contributing to strategic hazard and risk management (Mazzorana et al., 2009, 2012). Moreover, the results allow for adjusting adaptation strategies (Rojas et al., 2013). Small-scale differences in exposure can be precisely shown, which allows for more differentiated management strategies such as increasing community awareness (Fuchs et al., 2009; Meyer et al., 2012), implementing local structural protection (Holub et al., 2012) or fostering tailored insurance solutions (Paudel et al., 2013; Carina et al., 2014). Future investments into risk management are encouraged in particular for those communities with an above-average exposure to individual hazard types. As a result, public investments in mitigation measures can be targeted at regions with higher values at risk, which follows the axiom of spending public funding with the highest return of investments (Meyer et al., 2013).

The results also proved that the number of documented hazard events as shown in Fig. 1 should not directly be used to assess the development of losses and exposure: while the overall stock of exposed buildings as well as the non-exposed buildings increased by a factor of 2.3 between 1960 and 2000, the number of damaging hazard events was almost decreased by 50%. With respect to the annual growth rate of non-exposed and exposed buildings, the total building stock as well as the buildings exposed to river flooding and torrential flooding show similar characteristics and a rate of around a factor of six. The buildings exposed to snow avalanches again have a below-average rate (around 4.2). The total number of new constructions, in contrast, increased since 1944 and culminated in the period 1971–1980 followed by a sharp decrease and an additional increase since 2000 (Fig. 4c). As such, factors other than exposure may be responsible for temporal dynamics of natural hazard loss, such as (a) changes in the natural process activity resulting from the effects of climate change, and (b) the implementation of technical mitigation measures leading to less exposure or vulnerability. These factors were explicitly neglected during the present study in order to get the signal of dynamics in peril exposure in mountain environments.

Comparing the ratio between new constructions and the existing building stock (Fig. 5) and the annual ratio of new constructions inside hazard-prone areas and the total new constructions (Fig. 4d), a time lag between actual planning decisions and their effects on exposure becomes evident. While the ratio of buildings exposed to river flooding compared to the cumulative development of buildings stock is increasing until the 1960s, the ratio of annual constructions inside endangered areas is already decreasing starting with 1945 due to the relatively higher number of non-exposed buildings in Austria (almost 87% of the entire stock). With the exception of the decade 1981–1990, where a slight increase in this annual ratio is detectable, both the annual ratio of exposed to non-exposed buildings and the ratio between exposed buildings and the entire stock is decreasing. This may be interpreted as success of land-use planning activi-

ties (namely hazard mapping and the related ban of new constructions inside red hazard zones), even if a clear relation between new constructions and the implementation of hazard maps cannot be deduced. Because fewer buildings are exposed to torrential flooding, this pattern cannot be followed in this category of exposure: for torrential flooding both the annually constructed number of buildings exposed compared to the entire building stock (Fig. 5) and the annual number of constructions inside endangered areas (Fig. 4d) is decreasing until 1944, followed by an increase until 1970 and 1960, respectively. Since then, both ratios are continuously decreasing. This clearly shows the dependency of success in land-use planning on the initial situation, and in turn reveals the challenge in exposure in a different light: even if the ratio of annual new development inside and outside endangered areas is decreasing, the effects will be unveiled decades later. More precisely, the fewer buildings are exposed in comparison to the entire buildings stock, the longer land-use regulations enacted today will take to show success.

Nevertheless, some limitations of the data have to be addressed. While this study relies on a building inventory providing detailed information on the characteristics and types of the current building functionality, dimension and residents, historical information on the population composition as well as information on former population registers would enhance the significance of the results with respect to exposed citizens. Furthermore, exposure analysis is only possible for those buildings where information in the building register is available. Minor auxiliary buildings and remote agricultural buildings without addresses are not considered. Furthermore, around 8% of the communities with an obligation for hazard mapping is not considered because of missing hazard information – the mandatory hazard map has not yet been compiled and set effective in law, respectively. Despite these limitations, the results demonstrate advantages in comparison to local-scale case studies, and provide valuable information for decisions in natural hazard mitigation.

5 Conclusions

A detailed and spatially explicit object-based assessment of buildings exposed to natural hazards in Austria was undertaken, including elements at risk to river flooding, torrential flooding, and snow avalanches. While some regions have shown a clearly above-average increase in assets, other regions were characterised by a below-average development. This mirrors the topography of the country, but also the different economic activities: as such, hotels and hostels were found to be extraordinarily prone to mountain hazards, and commercial buildings as well as buildings used for recreational purposes to river flooding. Residential buildings have shown an average exposure, compared to the number of buildings of this type in the overall building stock.

In conclusion, a nation-wide and object-based assessment has advantages compared to the traditional approaches based on individual case studies: exposure to natural hazards is heterogeneous, and follows small-scale patterns which cannot necessarily be satisfyingly modelled by only assessing one hazard type within a specific local environment. The accuracy of such information may be used – together with down-scaled climate projections and combined with appropriate hazard models – to provide valuable risk estimates on a national scale. As a result, such approaches may also be valuable for the implementation of the European Floods Directive. The presented method together with the results may be used for similar assessments focusing on hazards other than those covered by the Directive, and may enable for a more precise overview on exposure and possible losses. This may link the development of risk to socio-economic development indicators, and improve available risk management options facing the challenge of global environmental change.

Acknowledgements. This study was supported by the Austrian Federal Ministry of Agriculture, Forestry, Environment and Water Management. The authors kindly acknowledge data provision by Thomas Hlatky, Austrian Insurance Association. The authors are grateful to Brendan Jongman, Daniela Molinari and Thomas Thaler as well as the anonymous referees for their comments on an earlier version of this manuscript.

Edited by: H. Kreibich

Reviewed by: B. Jongman, D. Molinari, and two anonymous referees

References

- Auer, I., Böhm, R., Jurkovic, A., Lipa, W., Orlik, A., Potzmann, R., Schöner, W., Ungersböck, M., Matulla, C., Briffa, K., Jones, P., Efthymiadis, D., Brunetti, M., Nanni, T., Maugeri, M., Mercalli, L., Mestre, O., Moisselin, J.-M., Begert, M., Müller-Westermeier, G., Kveton, V., Bochnicek, O., Stastny, P., Lapin, M., Szalai, S., Szentimrey, T., Cegnar, T., Dolinar, M., Gajic-Capka, M., Zaninovic, K., Majstorovic, Z., and Nieplova, E.: HISTALP – Historical instrumental climatological surface time series of the Greater Alpine Region, *Int. J. Climatol.*, 27, 17–46, 2007.
- Barredo, J. I.: Normalised flood losses in Europe: 1970–2006, *Nat. Hazards Earth Syst. Sci.*, 9, 97–104, doi:10.5194/nhess-9-97-2009, 2009.
- Bouwer, L. M.: Projections of future extreme weather losses under changes in climate and exposure, *Risk Analysis*, 33, 915–930, 2013.
- Bouwer, L. M., Bubeck, P., and Aerts, J. C. J. H.: Changes in future flood risk due to climate and development in a Dutch polder area, *Global Environ. Change*, 20, 463–471, 2010.
- Cammerer, H. and Thielen, A. H.: Historical development and future outlook of the flood damage potential of residential areas in the Alpine Lech Valley (Austria) between 1971 and 2030, *Reg. Environ. Change*, 13, 999–1012, 2013.
- Cammerer, H., Thielen, A. H., and Verburg, P. H.: Spatio-temporal dynamics in the flood exposure due to land use changes in the Alpine Lech Valley in Tyrol (Austria), *Nat. Hazards*, 68, 1243–1270, 2013.
- Carina, E., Keskitalo, H., Vulturius, G., and Scholten, P.: Adaptation to climate change in the insurance sector: examples from the UK, Germany and the Netherlands, *Nat. Hazards*, 71, 315–334, 2014.
- CRED – Centre for Research on the Epidemiology of Disasters: The OFDA/CRED international disaster database EM-DAT, Université Catholique de Louvain, Brussels, <http://www.emdat.net>, last access: 1 December 2014.
- de Moel, H. and Aerts, J.: Effect of uncertainty in land use, damage models and inundation depth on flood damage estimates, *Nat. Hazards*, 58, 407–425, 2011.
- de Moel, H., Aerts, J. C. J. H., and Koomen, E.: Development of flood exposure in the Netherlands during the 20th and 21st century, *Global Environ. Change*, 21, 620–627, 2011.
- Fuchs, S.: Susceptibility versus resilience to mountain hazards in Austria – paradigms of vulnerability revisited, *Nat. Hazards Earth Syst. Sci.*, 9, 337–352, doi:10.5194/nhess-9-337-2009, 2009.
- Fuchs, S. and Bründl, M.: Damage potential and losses resulting from snow avalanches in settlements of the canton of Grisons, Switzerland, *Nat. Hazards*, 34, 53–69, 2005.
- Fuchs, S. and McAlpin, M. C.: The net benefit of public expenditures on avalanche defence structures in the municipality of Davos, Switzerland, *Nat. Hazards Earth Syst. Sci.*, 5, 319–330, doi:10.5194/nhess-5-319-2005, 2005.
- Fuchs, S. and Zischg, A.: Vulnerabilitätslandkarte Österreich, Report 152, Universität für Bodenkultur, Institut für alpine Naturgefahren, Wien, 2013.
- Fuchs, S., Keiler, M., Zischg, A., and Bründl, M.: The long-term development of avalanche risk in settlements considering the temporal variability of damage potential, *Nat. Hazards Earth Syst. Sci.*, 5, 893–901, doi:10.5194/nhess-5-893-2005, 2005.
- Fuchs, S., Heiss, K., and Hübl, J.: Towards an empirical vulnerability function for use in debris flow risk assessment, *Nat. Hazards Earth Syst. Sci.*, 7, 495–506, doi:10.5194/nhess-7-495-2007, 2007.
- Fuchs, S., Spachinger, K., Dorner, W., Rochman, J., and Serrhini, K.: Evaluating cartographic design in flood risk mapping, *Environ. Hazards*, 8, 52–70, 2009.
- Fuchs, S., Ornetsmüller, C., and Totschnig, R.: Spatial scan statistics in vulnerability assessment – an application to mountain hazards, *Nat. Hazards*, 64, 2129–2151, 2012.
- Fuchs, S., Keiler, M., Sokratov, S. A., and Shnyparkov, A.: Spatiotemporal dynamics: the need for an innovative approach in mountain hazard risk management, *Nat. Hazards*, 68, 1217–1241, 2013.
- Hallegatte, S., Green, C., Nicholls, R. J., and Corfee-Morlot, J.: Future flood losses in major coastal cities, *Nat. Clim. Change*, 3, 802–806, 2013.
- Hilker, N., Badoux, A., and Hegg, C.: The Swiss flood and landslide damage database 1972–2007, *Nat. Hazards Earth Syst. Sci.*, 9, 913–925, doi:10.5194/nhess-9-913-2009, 2009.
- Holub, M. and Fuchs, S.: Mitigating mountain hazards in Austria – legislation, risk transfer, and awareness building, *Nat. Hazards Earth Syst. Sci.*, 9, 523–537, doi:10.5194/nhess-9-523-2009, 2009.

- Holub, M., Suda, J., and Fuchs, S.: Mountain hazards: reducing vulnerability by adapted building design, *Environ. Earth Sci.*, 66, 1853–1870, 2012.
- Huggel, C., Clague, J., and Korup, O.: Is climate change responsible for changing landslide activity in high mountains?, *Earth Surf. Proc. Land.*, 37, 77–91, 2012.
- Huttenlau, M., Stötter, J., and Stiefelmeyer, H.: Risk-based damage potential and loss estimation of extreme flooding scenarios in the Austrian Federal Province of Tyrol, *Nat. Hazards Earth Syst. Sci.*, 10, 2451–2473, doi:10.5194/nhess-10-2451-2010, 2010.
- Jongman, B., Kreibich, H., Apel, H., Barredo, J. I., Bates, P. D., Feyen, L., Gericke, A., Neal, J., Aerts, J. C. J. H., and Ward, P. J.: Comparative flood damage model assessment: towards a European approach, *Nat. Hazards Earth Syst. Sci.*, 12, 3733–3752, doi:10.5194/nhess-12-3733-2012, 2012a.
- Jongman, B., Ward, P. J., and Aerts, J. C. J. H.: Global exposure to river and coastal flooding: Long term trends and changes, *Global Environ. Change*, 22, 823–835, 2012b.
- Jongman, B., Koks, E. E., Husby, T. G., and Ward, P. J.: Increasing flood exposure in the Netherlands: implications for risk financing, *Nat. Hazards Earth Syst. Sci.*, 14, 1245–1255, doi:10.5194/nhess-14-1245-2014, 2014.
- Jongman, B., Winsemius, H. C., Aerts, J. C. J. H., de Perez, E. C., van Aalst, M. K., Kron, W., and Ward, P. J.: Declining vulnerability to river floods and the global benefits of adaptation, *P. Natl. Acad. Sci. USA*, 112, E2271–E2280, doi:10.1073/pnas.1414439112, 2015.
- Kappes, M., Keiler, M., von Elverfeldt, K., and Glade, T.: Challenges of analyzing multi-hazard risk: a review, *Nat. Hazards*, 64, 1925–1958, 2012a.
- Kappes, M., Ppathoma-Köhle, M., and Keiler, M.: Assessing physical vulnerability for multi-hazards using an indicator-based methodology, *Appl. Geogr.*, 32, 577–590, 2012b.
- Keiler, M.: Development of the damage potential resulting from avalanche risk in the period 1950–2000, case study Galtür, *Nat. Hazards Earth Syst. Sci.*, 4, 249–256, doi:10.5194/nhess-4-249-2004, 2004.
- Keiler, M.: World-wide trends in natural disasters, in: *Encyclopedia of natural hazards*, edited by: Bobrowski, P., Springer, Dordrecht, 1111–1114, 2013.
- Keiler, M., Zischg, A., Fuchs, S., Hama, M., and Stötter, J.: Avalanche related damage potential – changes of persons and mobile values since the mid-twentieth century, case study Galtür, *Nat. Hazards Earth Syst. Sci.*, 5, 49–58, doi:10.5194/nhess-5-49-2005, 2005.
- Keiler, M., Sailer, R., Jörg, P., Weber, C., Fuchs, S., Zischg, A., and Sauermoser, S.: Avalanche risk assessment – a multi-temporal approach, results from Galtür, Austria, *Nat. Hazards Earth Syst. Sci.*, 6, 637–651, doi:10.5194/nhess-6-637-2006, 2006a.
- Keiler, M., Zischg, A., and Fuchs, S.: Methoden zur GIS-basierten Erhebung des Schadenpotenzials für naturgefahreninduzierte Risiken, in: *GIS und Sicherheitsmanagement*, edited by: Strobl, J. and Roth, C., Wichmann, Heidelberg, 118–128, 2006b.
- Keiler, M., Knight, J., and Harrison, S.: Climate change and geomorphological hazards in the eastern European Alps, *Philos. T. Roy. Soc. Lond. A*, 368, 2461–2479, 2010.
- Keiler, M., Kellerer-Pirklbauer, A., and Otto, J.-C.: Concepts and implications of environmental change and human impact: studies from Austrian geomorphological research, *Geograf. Ann. A*, 94, 1–5, 2012.
- Kienberger, S., Lang, S., and Zeil, P.: Spatial vulnerability units – expert-based spatial modelling of socio-economic vulnerability in the Salzach catchment, Austria, *Nat. Hazards Earth Syst. Sci.*, 9, 767–778, doi:10.5194/nhess-9-767-2009, 2009.
- Korup, O., Görüm, T., and Hayakawa, Y.: Without power? Landslide inventories in the face of climate change, *Earth Surf. Proc. Land.*, 37, 92–99, 2012.
- Kranewitter, H.: *Liegenschaftsbewertung*, Gescow, Wien, 327 pp., 2002.
- Lung, T., Lavallo, C., Hiederer, R., Dosio, A., and Bouwer, L. M.: A multi-hazard regional level impact assessment for Europe combining indicators of climatic and non-climatic change, *Global Environ. Change*, 23, 522–536, 2013.
- Mazzorana, B., Hübl, J., and Fuchs, S.: Improving risk assessment by defining consistent and reliable system scenarios, *Nat. Hazards Earth Syst. Sci.*, 9, 145–159, doi:10.5194/nhess-9-145-2009, 2009.
- Mazzorana, B., Comiti, F., Scherer, C., and Fuchs, S.: Developing consistent scenarios to assess flood hazards in mountain streams, *J. Environ. Manage.*, 94, 112–124, 2012.
- Meyer, V., Kuhlicke, C., Luther, J., Fuchs, S., Priest, S., Dorner, W., Serrhini, K., Pardoe, J., McCarthy, S., Seidel, J., Palka, G., Unnerstall, H., Viavattene, C., and Scheuer, S.: Recommendations for the user-specific enhancement of flood maps, *Nat. Hazards Earth Syst. Sci.*, 12, 1701–1716, doi:10.5194/nhess-12-1701-2012, 2012.
- Meyer, V., Becker, N., Markantonis, V., Schwarze, R., van den Bergh, J. C. J. M., Bouwer, L. M., Bubeck, P., Ciavola, P., Genovese, E., Green, C., Hallegatte, S., Kreibich, H., Lequeux, Q., Logar, I., Papyrakis, E., Pfuertscheller, C., Poussin, J., Przyłuski, V., Thieken, A. H., and Viavattene, C.: Review article: Assessing the costs of natural hazards – state of the art and knowledge gaps, *Nat. Hazards Earth Syst. Sci.*, 13, 1351–1373, doi:10.5194/nhess-13-1351-2013, 2013.
- Munich Re: *Topics Geo*, in: *Natural catastrophes 2013*, edited by: Munich Reinsurance Company, München, 60 pp., 2014.
- Paudel, Y., Botzen, W. J. W., and Aerts, J. C. J. H.: Estimation of insurance premiums for coverage against natural disaster risk: an application of Bayesian Inference, *Nat. Hazards Earth Syst. Sci.*, 13, 737–754, doi:10.5194/nhess-13-737-2013, 2013.
- Pielke Jr., R. A.: Mistreatment of the economic impacts of extreme events in the Stern review report on the economics of climate change, *Global Environ. Change*, 17, 302–310, 2007.
- Preston, B. L.: Local path dependence of U.S. socioeconomic exposure to climate extremes and the vulnerability commitment, *Global Environ. Change*, 23, 719–732, 2013.
- Republik Österreich: *Forstgesetz 1975*, BGBl 440/1975, 1975.
- Republik Österreich: *Verordnung des Bundesministers für Land- und Forstwirtschaft vom 30. Juli 1976 über die Gefahrenzonenpläne*, BGBl 436/1976, 1976.
- Republik Österreich: *Bundesgesetz, mit dem das Registerzahlungsgesetz, das Bundesgesetz über das Gebäude- und Wohnungsregister, das Bundesstatistikgesetz 2000 und das E-Government-Gesetz geändert werden*, BGBl 125/2009, 2009.
- Republik Österreich: *Bundesgesetz über das Gebäude- und Wohnungsregister (GWR-Gesetz)*, BGBl 9/2004 i.d.F. 1/2013, BGBl 1/2013, 2013.

- Rojas, R., Feyen, L., and Watkiss, P.: Climate change and river floods in the European Union: Socio-economic consequences and the costs and benefits of adaptation, *Global Environ. Change*, 23, 1737–1751, 2013.
- Rudolf-Miklau, F. and Sereinig, N.: Festlegung des Bemessungshochwassers: Prozessorientierte Harmonisierung für Flüsse und Wildbäche, Österreich. Wasser Abfallwirts., 61, 27–32, 2009.
- Schmocker-Fackel, P. and Naef, F.: Changes in flood frequencies in Switzerland since 1500, *Hydrol. Earth Syst. Sci.*, 14, 1581–1594, doi:10.5194/hess-14-1581-2010, 2010.
- Shnyparkov, A. L., Fuchs, S., Sokratov, S. A., Koltermann, K. P., Seliverstov, Y. G., and Vikulina, M. A.: Theory and practice of individual snow avalanche risk assessment in the Russian arctic, *Geogr. Environ. Sustain.*, 5, 64–81, 2012.
- Sinabell, F. and Url, T.: Effizientes Risikomanagement für Naturgefahren am Beispiel von Hochwasser, WIFO Monatsberichte 6/2007, Österreichisches Institut für Wirtschaftsforschung, Wien, 537–547, 2007.
- Statistik Austria: Adress-GWR Online Handbuch, Teil C, Anhang 2: Merkmalskatalog, Statistik Austria, Wien, 134 pp., 2012.
- Statistik Austria: Baupreisindex für den Hoch- und Tiefbau, Statistik Austria, Wien, 2013.
- Stiefelmeyer, H. and Hlatky, T.: HORA – An Austrian platform for natural hazards as a new way in risk communication, in: Internationales Symposium Interpraevent, Dornbirn, May 26–30, 2008, edited by: Mikoš, M., Hübl, J., and Koboltschnig, G., Internationale Forschungsgesellschaft Interpraevent, Klagenfurt, 229–236, 2008.
- Thaler, T.: Developing partnership approaches for flood risk management: implementation of inter-local co-operations in Austria, *Water Int.*, 39, 1018–1029, 2014.
- United Nations: Global assessment report on disaster risk reduction, UNISDR, Geneva, 246 pp., 2013.
- Wöhler-Alge, M.: Landslides management in Austria with particular attention to hazard mapping and land use planning, in: *Landslide Science and Practice*, Vol. 7, edited by: Margottini, C., Canuti, P., and Sassa, K., Springer, Berlin, 231–237, 2013.
- Zischg, A., Fuchs, S., and Stötter, J.: Uncertainties and fuzziness in analysing risk related to natural hazards – a case study in the Ortles Alps, South Tyrol, Italy, in: *Risk Analysis IV, WIT Transactions on Ecology and the Environment 77*, edited by: Brebbia, C., WIT, Southampton, 523–532, 2004.
- Zischg, A., Fuchs, S., Keiler, M., and Meißl, G.: Modelling the system behaviour of wet snow avalanches using an expert system approach for risk management on high alpine traffic roads, *Nat. Hazards Earth Syst. Sci.*, 5, 821–832, doi:10.5194/nhess-5-821-2005, 2005.
- Zischg, A., Schober, S., Sereinig, N., Rauter, M., Seymann, C., Goldschmidt, F., Bäk, R., and Schleicher, E.: Monitoring the temporal development of natural hazard risks as a basis indicator for climate change adaptation *Nat. Hazards*, 67, 1045–1058, 2013.

Paper 6: Röthlisberger, V., Zischg, A., Keiler, M., 2016. Spatiotemporal aspects of flood exposure in Switzerland. E3S Web Conf. 7, 8008. [10.1051/e3sconf/20160708008](https://doi.org/10.1051/e3sconf/20160708008).

Spatiotemporal aspects of flood exposure in Switzerland

Veronika Röthlisberger^{1,2,a}, Andreas Zischg^{1,2} and Margreth Keiler²

¹ University of Bern, Institute of Geography, Hallerstrasse 12, CH-3012 Bern, Switzerland

² University of Bern, Oeschger Centre for Climate Change Research, Falkenplatz 16, CH-3012 Bern, Switzerland

Abstract. While flood hazard mapping in Switzerland is close to completion, only a limited number of studies have been specifically conducted on exposure and vulnerability. We fill this knowledge gap by conducting a nation-wide study of flood exposure of buildings in Switzerland. Therefore, we generate a country-wide comprehensive and homogenous data set of polygons of residential buildings and their period of construction and overlay these building polygons with compiled and harmonized flood hazard maps provided by the Swiss cantons. In this paper we present first results of spatiotemporal analyses, namely the evolution of exposure from 1919 to 2012. Surprising is the increase in the share of exposure of new constructed buildings since the 1980s which contradicts the intended effects of the Swiss flood risk management strategies and calls for further investigations.

1 Introduction

Floods are one main hazard type in the world-wide event and loss database on natural disasters. The data highlight an increasing number of reported events, of people affected and of economic losses, but a decreasing number of reported fatalities since around 1900, especially in the most developed countries [1, 2]. The IPCC [3] identified exposure and vulnerability as key determiners of disaster risk. Furthermore, there is high confidence that “increasing exposure of people and economic assets has been the major cause of long-term increases in economic losses from weather- and climate-related disasters” [3:7]. Being aware of these important drivers – beside the challenge of climate change – efficient flood risk management strategies are strongly related to the availability of data and the assessment of elements at risk [4]. Investigations on the long-term evolution of exposure and the effects on flood risk is still rare, and most studies focus only on the local scale with individual case studies. However, the first nation-wide projects indicate important insights [5, 6].

In line with international standards, the main components of risk assessments in Switzerland are hazard mapping, exposure and vulnerability analyses. While flood hazard mapping in Switzerland is close to completion [7], only a limited number of studies have been specifically conducted on exposure and vulnerability. Several Swiss cantons have investigated their exposure and/or vulnerability to floods, and many insurance companies continue to use hazard maps for the risk management of their portfolio. However, these studies are either limited in space (e.g. to the area of a canton) or in content (e.g. based only on the assets

insured by a single company), and findings are rarely published. An exception is a publication by SwissRe with countrywide sums on insured property losses in Switzerland for different return periods based on their in-house flood risk model [8]. Yet, the description of the model and the results are rather generic, without data about elements at risk. To summarise, there is a lack of nation-wide exposure analysis to floods scenarios. Furthermore, all exposure or risk assessments are based on the analysis of the current status, which neglects the long-term evolution of exposure or risk. Consequently, the analysis regarding the long-term evolution of the key driver of exposure is missing in Switzerland too. Both analyses are very important to gain insights into the effectiveness of risk management strategies (such as land-use planning, which has been applied in Switzerland since the 1970s) and to design future flood risk management strategies based on these insights. In this paper, we focus on following main questions and discuss the possible relation to flood risk management:

- How have residential buildings exposed to flood evolved temporally?
- Do exposure ratios at the different hazard levels mapped show different temporal patterns?

2 Data and Methods

To analyse flood exposure, we link data on flood hazardous areas with spatially explicit information on buildings. In the following sections, the data sets and the methods used are described.

^a Corresponding author: veronika.roethlisberger@giub.unibe.ch

2.1 Flood hazard maps

For the determination of flood endangered areas, we use flood hazard maps provided by the Swiss cantons and elaborated according to national guidelines [9, 10]. Flood hazard is thereby defined by a combination of intensity and probability of events (see Fig. 1) with thresholds in terms of intensity at 0.5 m (water depth) or 0.5m/s^2 (water depth x velocity), for the differentiation between ‘weak’ and ‘medium’ intensity, and at 2 m or 2m/s^2 , respectively, to differentiate between ‘medium’ and ‘strong’ intensity. The probabilities of occurrence investigated correspond to return periods of 30 (high), 100 (medium), 300 (slight) and above 300 (very slight) years, respectively. The spatial representation and combination of events of different return periods lead to the mapping of five hazard classes: ‘high’ (red coloured areas), ‘medium’ (blue), ‘low’ (yellow), ‘residual’ (yellow-white striped) and ‘no or negligible’ (white) threat (see Fig. 1). In this paper, we focus on three classes - ‘high’, ‘medium’ and ‘low’ - i.e. on areas endangered by flood events up to a return period of 300 years. The flood hazard maps as of June 2015 are harmonized and compiled in a geodatabase by the Mobiliar insurance company.

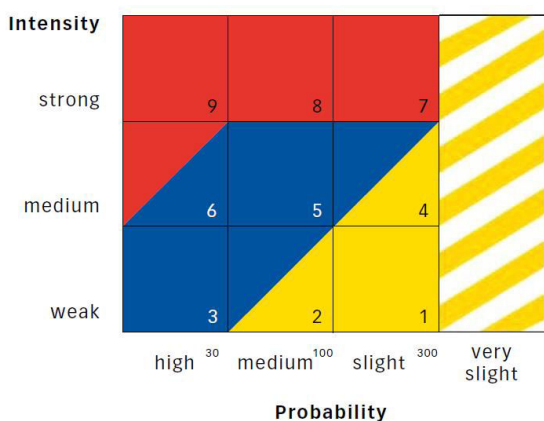


Figure 1. Assessment matrix for the identification of hazard levels in Switzerland (red = high; blue = medium; yellow = low, yellow-white striped = residual, white = no or negligible) [11]

2.2 Data on buildings

We generate a country-wide comprehensive and homogenous data set of polygons of residential buildings and their period of construction by combining two data sets of (a) a topographic landscape model and (b) point data on residential buildings. From the ‘Topographic Landscape Model TLM3D’ provided the Federal Office of Topography ([12], version 1.1, 2012, TLM hereafter), we extract the feature group ‘buildings’, which contains footprints of all present buildings in Switzerland. These over two million footprint polygons “are not cartographically generalized and provide an accuracy of between 0.2 and 1.5m” [12]. The information on residential use and period of construction as of the end of 2012 is taken from the federal register of residential buildings and dwellings, also known as the ‘Gebäude-

und Wohnungsregister (GWR)’. This register is provided by the Swiss Federal Statistical Office and contains nearly 1.7 million point-referenced records of buildings (entrances) with residential use [13]. The lengths of the 12 construction periods in the GWR differ considerably (from 2 to 27 years). In order to minimize these differences, we combine the seven shortest periods (of lengths between two and five years) to three (of lengths of ten and twelve years), obtaining the following eight periods: (1) before 1919; (2) 1919 – 1945; (3) 1946 – 1960; four ten-years periods (4-7) between 1961 and 2000; and (8) 2001 – 2012.

We intersect the point data of GWR with the building footprint polygons in order to assign the information on construction periods to the building footprints. Points that do not match a building polygon exactly are snapped to the nearest polygon within a distance of $\leq 5\text{m}$. In this way, every building polygon contains the features ‘numbers of associated GWR points’ and ‘construction periods of the associated GWR points’. We reduce the polygon data set to buildings with residential utilization, i.e. to polygons with at least one associated GWR point and thus with information on construction period. We further delete polygons with inhomogeneous construction periods, and finally reduce the data set to polygons with a construction period of determined length (i.e. 1919 onwards).

2.3 Exposure analysis

The building footprint polygons – pre-processed and selected as described above – are intersected with the compiled and harmonized flood hazard maps as defined by Fuchs et al. [6]. Every building is thereby classified to the highest hazard level it is intersecting with. For each of the eight time periods analysed, the total number (and annual average) of the constructed buildings and the share of exposed buildings (at hazard levels ‘low’, ‘medium’ and ‘high’) are calculated. We thus define ‘share of exposed buildings’ as the ratio of the number of ‘newly constructed building that are exposed to floods (at respective hazard level)’ to the number of ‘total newly constructed buildings for which a flood hazard map exists.’ We compute the ratio separately for each time period. Furthermore, we compare the exposure ratios of the three most recent time periods (1981-1999, 1991-2000, 2001-2012) to the ones of the 1971 – 1980 time period. Finally, we present the results on timelines, indicating temporal evolution of flood exposure. For the analysed time period, we therefore assume that no building has been demolished nor replaced, and that the flood hazardous areas remained unchanged.

3 Results

The numbers resulting in the pre-processing of building data are presented in section 3.1, followed by the results of the flood exposure analyse in section 3.2.

3.1 Data set of building polygons including period of construction

1,464,978 of the total 1,670,540 data points of residential buildings and dwellings in GWR lay within a TLM building footprint polygon, and an additional 131,622 are within a distance of ≤ 5m. Consequently, 1,596,600 (or 95.6% of the total 1,670,540) data points are associated to a building footprint polygon.

Among the 2,053,539 TLM building footprint polygons 1,268,553 (61.7%) are classified as buildings with residential utilization, i.e. at least one GWR data point is associated to them. The deletion of the 50,270 polygons with inhomogeneous construction periods reduces the data set further to 1,218,283 polygons. Finally, the 239,619 polygons from the construction period ‘before 1919’ are removed, resulting in a data set of 978,664 footprint polygons of buildings with residential utilization and homogenous construction periods between 1919 and 2012. These 978,644 building footprint polygons are used for the exposure analysis.

3.2 Flood exposure

In Switzerland, a flood hazard map exists for 691,529 (70.7% of total 978,664, see Tab. 1) residential buildings constructed between 1919 and 2012. That is, the areas where these buildings are located were part of the study areas of the cantonal hazard mapping procedures. Therefore, these buildings were assessed with respect to flood exposure. Of the assessed buildings, 110,745 (16.01%) are exposed to floods. The exposure is mainly at hazard level ‘low’ (63,318 buildings or 9.16%). But some are also exposed considerably at level ‘medium’ (41,007 buildings or 5.93% respectively), whereas their exposure at hazard level ‘high’ is comparatively low with just 6,420 buildings (0.93%) at that level.

In terms of annual newly constructed buildings, the period 1971-1980 shows the highest amounts, in ‘all analysed buildings’ (column 1 in Tab. 1) as well as in ‘all buildings assessed in a flood hazard map’ (column 2 in Tab. 1 and grey dashed line in Fig. 2). Yet, all exposure ratios (i.e. the number of newly constructed buildings within hazardous areas compared to the total number of newly constructed buildings within the perimeter of a flood hazard map) during this period of construction are lower than in any other period. Generally, it is remarkable that the amount of annual newly constructed buildings and the share of exposed buildings show a negative correlation (Fig. 2). When interpreting the data of consecutive time periods as time series, one detects a decrease in exposure ratios at hazard levels ‘low’ and ‘medium’ (and consequently summarized over all hazard levels) from 1919 to 1970, whereas from 1981 to 2012 the same exposure ratios increase.

Comparing the exposure of the three time periods between 1981 and 2012 to the exposure rates of the time period 1971-1980, we notice remarkable differences between the three hazard levels considered (Fig. 3 and the last for columns in Tab. 1). While the exposure rates at hazard levels ‘low’ and ‘medium’ show comparable increases by factors 1.06 to 1.16, the change at hazard level ‘high’ is strikingly higher up to factor 1.5 for the period 2001-2012, resulting from exposure ratios at hazard level ‘high’ of 1.11 (period 2001-2012) compared to 0.74 (period 1971-1980).

Construction period		Flood exposure of newly constructed buildings													
		Newly constructed buildings [N]							Share of new buildings exposed [%]				Change in exposure compared to period 1971-1980		
		All	Assessed in a flood hazard map						At hazard level				At hazard level		
			Total	Exposed to hazard level			L/M/H			Low	Medium	High	L/M/H		
		Low	Medium	High	L/M/H		Low	Medium	High	L/M/H	Low	Medium	High	L/M/H	
1919-1945	Total	146'711	101'115	10'711	6'939	970	18'620	10.59	6.86	0.96	18.41	1.31	1.35	1.29	1.33
	Per year	5'434	3'745	397	257	36	690								
1946-1960	Total	151'192	106'966	10'633	6'782	1'000	18'415	9.94	6.34	0.93	17.22	1.23	1.25	1.26	1.24
	Per year	10'079	7'131	709	452	67	1'228								
1961-1970	Total	142'476	96'368	8'648	6'015	994	15'657	8.97	6.24	1.03	16.25	1.11	1.23	1.39	1.17
	Per year	14'248	9'637	865	602	99	1'566								
1971-1980	Total	156'929	111'031	8'977	5'630	823	15'430	8.09	5.07	0.74	13.9	1	1	1	1
	Per year	15'693	11'103	898	563	82	1'543								
1981-1990	Total	149'937	107'461	9'191	5'986	963	16'140	8.55	5.57	0.9	15.02	1.06	1.1	1.21	1.08
	Per year	14'994	10'746	919	599	96	1'614								
1991-2000	Total	122'288	91'651	8'284	5'140	814	14'238	9.04	5.61	0.89	15.54	1.12	1.11	1.2	1.12
	Per year	12'229	9'165	828	514	81	1'424								
2001-2012	Total	109'131	76'937	6'874	4'515	856	12'245	8.93	5.87	1.11	15.92	1.11	1.16	1.5	1.15
	Per year	9'094	6'411	573	376	71	1'020								
Total 1919 to 2012		978'664	691'529	63'318	41'007	6'420	110'745	9.16	5.93	0.93	16.01	1.13	1.17	1.26	1.15
Per year		10'411	7'357	674	436	68	1'178								

Table 1. Information on flood exposure of Swiss residential buildings constructed between 1919 and 2012. Hazard levels are explained in text, section 2.1. L/M/H = total exposure, sum of exposure to hazard level ‘low’ (L), ‘medium’ (M) and ‘high’ (H). The ‘share of exposed buildings’ (and the absolute number of annual newly built buildings assessed in terms of flood exposure, column 2) are additionally shown in Fig. 2, whereas the changes in exposure of time periods 1981-2012 compared to period 1971-1980 (last four columns) are illustrated in Fig. 3.

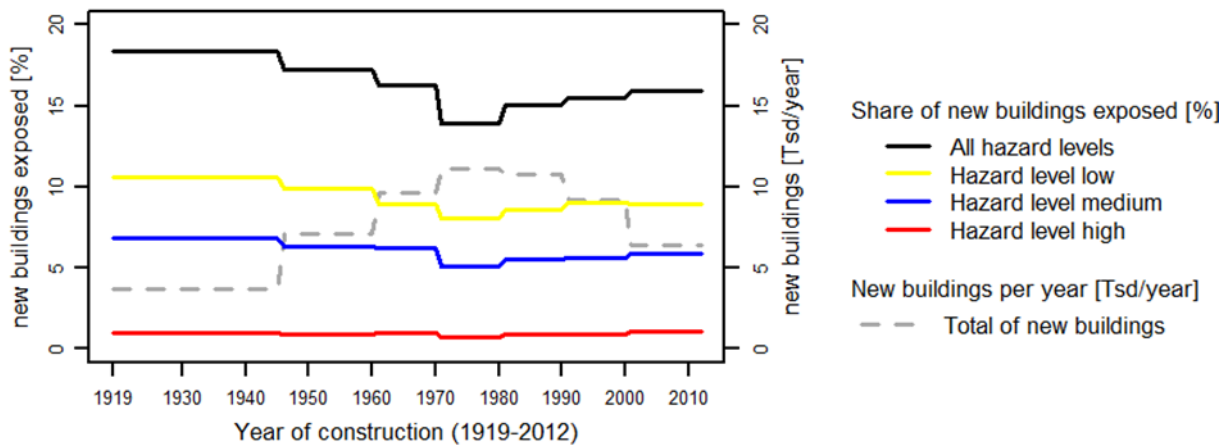


Figure 2. Newly constructed buildings per construction period. The ‘share of new buildings exposed’ is the ratio of the number of ‘newly constructed building that are potentially exposed to floods (at respective hazard level)’ to the number of ‘total newly constructed buildings for which a flood hazard map exists’. The ‘new buildings per year’ are calculated by dividing the total number of buildings newly constructed within a particular time period by the length of the respective time period, figures are presented in thousands of buildings per year.

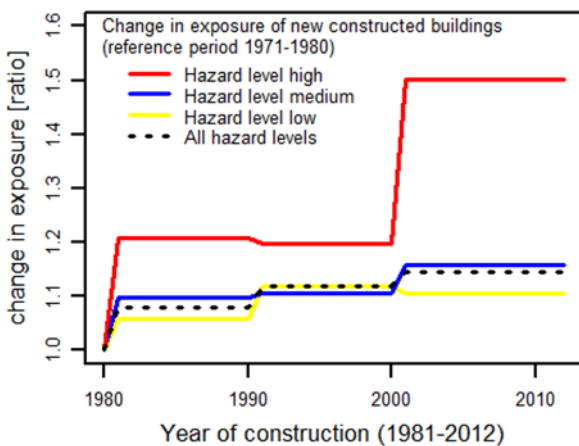


Figure 3. Relative change of the exposure ratios of the three most recent time periods (1981-1999, 1991-2000, 2001-2012) compared to the ones of 1971 – 1980.

4 Discussion and Conclusion

When interpreting this study’s results, one needs to keep in mind that we derive a development in the *past* from *current* data. Therefore, we assume that (a) flood threat areas remained constant and (b) no building was demolished nor replaced during the analysed periods of time.

Concerning the first assumption, it can be stated that extensive river trainings in Switzerland were completed by the end of the 19th century, i.e. before the time period investigated in this study. Further on, recent structural protection measures are designed for events up to a 100-year return period. That means that 300-year events (and thus the encasing area of the analysed hazardous zones at levels ‘low’, ‘medium’ and ‘high’) are not influenced by these protection measures. However, the lines between areas of different hazard levels may be shifted. Therefore, temporal changes in the exposure to one specific hazard level must not be over-interpreted. In addition, the reliability of temporal comparisons of exposure ratio at different hazard levels decrease with the length of time period considered.

The second assumption (no demolition nor replacement of buildings) is less problematic in Switzerland than in other countries because Switzerland has (a) not been involved in any wars since the middle of the 19th century and (b) standards in building construction and maintenance are comparatively high resulting in long times of use. As discussed in other publications [5, 6], however, studies on temporal dynamics that are based on current data records of construction year should focus on relative trends rather than on absolute values. Nevertheless, the presented absolute figures of (annual) newly constructed buildings and especially their relative changes over time are plausible. While the increase up to the 1970s may be explained by demographic parameters, the decrease after 1990 may be caused by the global financial crisis of the 1990s.

Looking at exposure rates, our findings of increasing rates since the 1980s do not mirror the Switzerland-wide declared paradigm change “from protection against hazard to the management of risk” [14, front page] in the aftermath of the 1987 floods. It implies spatial planning as an imported part of risk management. In particular, the relatively high increase at hazard level ‘high’ is surprising as, for areas of this hazard level, the

federal recommendations (and many cantonal and communal regulations) foresee a ban on construction of new buildings [11]. We see two possible explanations for this mismatch: time lag and obstacles to the enforcement in spatial planning processes. Thus, at national level, regulations on spatial planning (including the consideration of natural hazards) were introduced in the 1970s [15]. More details on natural hazards are regulated in the national laws on forest and on water [16, 17], which were totally revised and passed in the early 1990s. However, ten years later the federal extra-parliamentary commission for natural hazard PLANAT noted that “their implementation encounters very difficult conditions” [14:6].

Another remarkable result of the present study is the negative correlation between number of annual newly constructed buildings and the share of exposure. Sound statistical analyses as well as exploration of the underlying reasons of this phenomenon go beyond the scope of this paper, but are definitively worth examining in the future.

In conclusion, this study shows that nation-wide analysis of flood exposure at single building level is possible, and it derives new insights for the evaluation of risk management strategies. The temporal evolution of flood exposure ratios, with its lowest values in the 1970s, calls into question the effects of the risk management strategies introduced during the past decades and indicates a need for further investigation. Studies on exposure as one risk driver help to evaluate our risk management strategies and provide one basis for the improvement of risk management policies and practice. A comparison between different nation-wide exposure data and their development would add even more value to flood risk management.

5 References

- Keiler M. (2013). World-wide trends in natural disasters. *Encyclopedia of Natural Hazards, edited by: Bobrowsky, P., Springer*, 1111-1114.
- CRED [Centre for Research on the Epidemiology of Disasters] (2016). The OFDA/CRED international disaster database EM-DAT, Université Catholique de Louvain, Brussels, www.emdat.net, last access 26 February 2016.
- IPCC [Intergovernmental Panel on Climate Change] (2012). Managing the Risks of Extreme Events and Disasters to Advance Climate Change Adaptation. A Special Report of Working Groups I and II of the Intergovernmental Panel on Climate Change, edited by: Field C. B., Barros V., Stocker T. F., Qin D., Dokken D. J., Ebi K. L., Mastrandrea M. D., Mach K. J., Plattner G.-K., Allen S. K., Tignor M., and Midgley P. M. Cambridge, UK, and New York, NY, USA, 582 pp.
- Jongman B., Ward P.J. and Aerts J.C.J.H. (2012). Global exposure to river and coastal flooding: Long term trends and changes. *Global Environmental Change*, **22**, 823-835.
- Jongman B., Koks E.E., Husby T.G. and Ward P.J. (2014). Increasing flood exposure in the Netherlands: Implications for risk financing. *Natural Hazards and Earth System Sciences*, **14**, 1245-1255.
- Fuchs S., Keiler M., and Zischg A. (2015). A spatiotemporal multi-hazard exposure assessment based on property data. *Natural Hazards and Earth System Sciences*, **15**, 2127-2142.
- BAFU [Bundesamt für Umwelt] (2015). Naturgefahrenkartierung der ganzen Schweiz steht. Press release of 26 May 2014. <http://www.bafu.admin.ch/dokumentation/medieninformation/00962/index.html?lang=de&msgid=53122>, last access 26 February 2016.
- Hausmann P., Kunz Ch. and Rebuffoni G. (2012). Floods in Switzerland – an underestimated risk. Swiss Re Logistics Media Production. Zurich.
- BWW [Bundesamt für Wasserwirtschaft], Bundesamt für Raumplanung BRP, Bundesamt für Umwelt, Wald und Landschaft BUWAL (1997). Berücksichtigung der Hochwassergefahren bei raumwirksamen Tätigkeiten.
- BUWAL [Bundesamt für Umwelt, Wald und Landschaft] (1999): Risikoanalyse bei gravitativen Naturgefahren, Methode. Umwelt-Materialien Nr. 107/I.
- ARE [Bundesamt für Raumentwicklung], Bundesamt für Wasser und Geologie BWG, Bundesamt für Umwelt, Wald und Landschaft BUWAL (2005): Empfehlungen Raumplanung und Naturgefahren / Federal Office for Spatial Development, Federal Office for Water and Geology, Swiss Agency for the Environment, Forests and Landscape: Recommendation Spatial Planning and Natural Hazards.
- swisstopo [Federal Office of Topography] (2012). swissTLM3D, large-scale topographical landscape model of Switzerland. Version 1.1 as per 2012. Description and acquisition on <http://www.swisstopo.admin.ch/internet/swisstopo/en/home/topics/geodata/TLM.html>, last access 26 February 2016
- Bundesamt für Statistik BfS (2008): Gebäude und Wohnungsregister, Merkmalskatalog / Federal Register of Buildings and Dwellings, Catalogue of attributes, Version 3.4.
- National Platform for Natural Hazards PLANAT (2005). From protection against hazards to the management of risk. 19p.
- Schweizerische Eidgenossenschaft (1979). Bundesgesetz über die Raumplanung. SR 700.
- Schweizerische Eidgenossenschaft (1991a). Bundesgesetz über den Wald. SR 921.0.
- Schweizerische Eidgenossenschaft (1991b). Bundesgesetz über den Wasserbau. SR 721.100.

Paper 7: Fuchs, S., Röthlisberger, V., Thaler, T., Zischg, A., Keiler, M., 2017. Natural Hazard Management from a Coevolutionary Perspective: Exposure and Policy Response in the European Alps. *Annals of the American Association of Geographers* 107, 382–392. [10.1080/24694452.2016.1235494](https://doi.org/10.1080/24694452.2016.1235494).

Natural Hazard Management from a Coevolutionary Perspective: Exposure and Policy Response in the European Alps

Sven Fuchs ,* Veronika Röthlisberger ,† Thomas Thaler ,* Andreas Zischg ,† and Margreth Keiler 

**Institute for Mountain Risk Engineering, University of Natural Resources and Life Sciences*

†*Mobililar Lab for Natural Risks, Oeschger Centre for Climate Change Research, and Institute of Geography, University of Bern*

‡*Institute of Geography, University of Bern*

A coevolutionary perspective is adopted to understand the dynamics of exposure to mountain hazards in the European Alps. A spatially explicit, object-based temporal assessment of elements at risk to mountain hazards (river floods, torrential floods, and debris flows) in Austria and Switzerland is presented for the period from 1919 to 2012. The assessment is based on two different data sets: (1) hazard information adhering to legally binding land use planning restrictions and (2) information on building types combined from different national-level spatial data. We discuss these transdisciplinary dynamics and focus on economic, social, and institutional interdependencies and interactions between human and physical systems. Exposure changes in response to multiple drivers, including population growth and land use conflicts. The results show that whereas some regional assets are associated with a strong increase in exposure to hazards, others are characterized by a below-average level of exposure. The spatiotemporal results indicate relatively stable hot spots in the European Alps. These results coincide with the topography of the countries and with the respective range of economic activities and political settings. Furthermore, the differences between management approaches as a result of multiple institutional settings are discussed. A coevolutionary framework widens the explanatory power of multiple drivers to changes in exposure and risk and supports a shift from structural, security-based policies toward an integrated, risk-based natural hazard management system. *Key Words: coevolution, European Alps, exposure, natural hazard management, path dependency.*

本文採用共同演化的观点来理解欧洲阿尔卑斯地区暴露于山区灾害的动态。本文呈现奥地利和瑞士在1919年至2012年间,对山区灾害(洪泛、山洪暴发与泥石流)而言具有风险元素之特定空间且基于对象的时间评估。该评估是根据下列两组不同的数据集:(1)遵循具法律约束力的土地使用规划限制之灾害信息,以及(2)从不同的国家层级空间数据组合而成的建筑形态信息。我们探讨这些跨领域动态,并聚焦经济、社会与制度间的相互依赖,以及人类和物理系统的互动。曝险度在回应包括人口成长及土地使用冲突等多重驱动力时有所改变。研究结果显示,当若干区域资产与灾害曝险度的显著增加有关时,其他区域则以低于平均的曝险度为特徵。空间与时间的结果,显示出欧洲阿尔卑斯地区热点的相对稳定性。这些研究与各国家的地志学,以及各别的经济活动范围与政治环境相符。此外,本文探讨因多重制度环境所导致的管理方法差异。共同演化架构,扩张了多重驱动力之于曝险度和风险的改变的解释力,并支持从结构性、以安全为基础的政策转变为整合性的、以风险为基础的自然灾害管理系统。关键词:共同演化,欧洲阿尔卑斯地区,曝险,自然灾害管理,路径依赖。

Se adopta una perspectiva co-evolucionista para entender la dinámica de la exposición a los riesgos de montaña en los Alpes europeos. Se presenta una evaluación temporal espacialmente explícita y basada en objeto de los elementos de riesgo en catástrofes de montaña (inundaciones fluviales, inundaciones torrenciales y flujos de detritos) en Austria y Suiza, para el período de 1919 a 2012. La evaluación descansa en dos conjuntos de datos diferentes: (1) información de riesgos que adhiere a las restricciones de planificación de uso del suelo legalmente obligatorias, y (2) información combinada sobre tipos de construcciones desde diferentes fuentes de datos espaciales a nivel nacional. Discutimos estas dinámicas transdisciplinarias y nos enfocamos en interdependencias e interacciones económicas, sociales e institucionales entre sistemas humanos y físicos. La exposición

© S. Fuchs, V. Röthlisberger, T. Thaler, A. Zischg, and M. Keiler

This is an Open Access article. Non-commercial re-use, distribution, and reproduction in any medium, provided the original work is properly attributed, cited, and is not altered, transformed, or built upon in any way, is permitted. The moral rights of the named authors have been asserted.

cambia en respuesta a múltiples controles, incluyendo crecimiento de la población y conflictos por usos del suelo. Los resultados muestran que mientras algunas ventajas regionales están asociadas con un fuerte incremento en exposición a los riesgos, otras están caracterizadas por un nivel de exposición por debajo del promedio. Los resultados espaciotemporales indican puntos calientes relativamente estables en los Alpes europeos. Estos resultados coinciden con la topografía de los países y con el respectivo ámbito de actividades económicas y el contexto político. Adicionalmente, se discuten las diferencias entre los enfoques de administración como resultado de múltiples escenarios institucionales. Un marco co-evolucionario amplía el poder explicativo de múltiples controles a los cambios en exposición y riesgo, y soporta un cambio de políticas estructurales, basadas en seguridad, hacia un sistema integrado de manejo de catástrofes naturales basado en riesgo. *Palabras clave: co-evolución, Alpes europeos, exposición, manejo de catástrofes naturales, dependencia en la ruta.*

In Europe, approximately 40 percent of the total land area is mountainous and is home to almost 20 percent of the total population (Nordregio 2004). Consequently, mountain regions are characterized by a significant number of settlements and economic and recreational areas. Only about 17 percent of the European Alps is suitable for permanent settlement due to topographic constraints, however (Tappeiner, Borsdorf, and Tasser 2008). As a result, mountain region developments are inherently linked to natural hazard risk, as land development occurs in hazard-prone areas where many settlements are located on alluvial fans and in floodplains. Flood risk management differs remarkably between floodplains along large rivers (e.g., the Rhine in Europe or the Mississippi in the United States) and the floodplains of alpine rivers. Whereas large rivers are predominantly managed with flood retention and levee constructions (Remo, Carlson, and Pinter 2012; Theiling and Burant 2013), mountainous areas are primarily managed by restricting the development of settlements in floodplains. Consequently, spatiotemporal exposure and the vulnerability of elements at risk plays a dominant role in risk management.

The main drivers of natural hazard risk are high reliefs, hydroclimatology, and the effects of climate dynamics on hydrological hazards (Keiler, Knight, and Harrison 2010). Hydrological hazards constitute a major threat to communities and assets, even though they occur episodically (Fuchs et al. 2013), especially if exposure and vulnerability are not properly managed (Zimmermann and Keiler 2015). These two aspects have only received scientific attention relatively recently (Papathoma-Köhle et al. 2011; Totschnig and Fuchs 2013; Fuchs, Keiler, and Zischg 2015; Papathoma-Köhle et al. 2015), whereas the overall concept of risk that combines hazard, exposure, and vulnerability had already been introduced in operational risk management for decades (Keiler et al. 2004; Kienholz et al. 2004).

Despite the considerable efforts to reduce mountain hazard risk, particularly with the implementation of technical means such as levees and retention basins (Holub and Fuchs 2009), the losses due to hydrological hazards in Europe remain significant (Andres, Badoux, and Hegg 2015; Fuchs, Keiler, and Zischg 2015). Although there is some evidence of increasing losses, which can be found in the publications of large reinsurers (Munich Re 2016; Swiss Re 2016), some scholars stated that underlying trends should be carefully interpreted. Mudelsee et al. (2003) analyzed flood magnitudes and concluded that there is no evidence of recent upward trends describing the occurrence of large flood events in central Europe. Similarly, Barredo (2009) reported no clear positive trend in flood losses in Europe once the losses are normalized by socioeconomic development indicators. Furthermore, when flood data in the United States are presented in terms of damage per unit wealth, a slight and statistically insignificant downward trend is observed (Loucks and Stedinger 2007).

Besides hazard dynamics (i.e., changes in the natural frequency and magnitude of events due to climatic change), shifts in hazard losses could result from (1) changing exposure of elements at risk due to overall population migration and associated land development, (2) changing vulnerability due to the presence or absence of technical mitigation measures, and (3) a greater awareness of threats considered in land use planning. In the past, spatially explicit data on elements at risk in Europe were fragmentary; a spatiotemporal assessment of exposure was limited to studies using large-scale, aggregated data (Keiler 2004; Keiler et al. 2006; Fuchs et al. 2013) and neglected any small-scale but supraregional dynamics. Spatially inclusive and comprehensive analyses on national levels were undertaken, for example, on flood risk in The Netherlands (Jongman et al. 2014) and on mountain hazards in Austria (Fuchs, Keiler, and Zischg 2015) when such

data became recently available. In the following review, we focus on residential buildings (RBs) exposed to flood hazards in The European Alps, and we show how such data can be used to improve our understanding of hazard exposure and how a coevolutionary framework widens the explanatory power of multiple drivers in exposure dynamics. The coevolutionary framework provides a guideline for analyzing and explaining the linkage between exposure and policy.

Assessing Coevolution in Natural Hazard Management

We attempt to address challenges attributed to institutional changes in natural hazard management by focusing on the exposure of RBs in the European Alps from a coevolutionary perspective. Coevolution includes two or more interdependently evolving systems (Gual and Norgaard 2010). The aim is to analyze and understand the coevolutionary changes within the different interacting systems, where coevolutionary dynamics are path dependent (Kallis 2007). These dynamics include social adaptation to environmental change. A central theme inherent to coevolutionary thinking in social science is the analysis of institutional changes, especially with respect to the development of human behavior. Institutions are defined as a constant (formally legal and informally social) norm over a certain period of time (van den Bergh and Stagl 2003). Institutions are responsible for the organization of structures to optimize for social and economic behaviors (e.g., by minimizing uncertainty). Therefore, institutions have a direct influence on individuals and vice versa. Institutions influence the behavior of individuals (top down); their behavior and habitat are also key drivers for the development of new institutions or institutional changes (bottom up; Hodgson 2006). In summary, institutions define rules or procedures that support decision-making processes.

The aim is to interpret and to holistically explain exposure evolution in the European Alps with respect to policy responses and technological developments. The insights then support the valuation of natural hazard management policies. We identified two evolutionary systems:

- The first system is characterized by population pressures (i.e., demand for increased residences in hazard areas) associated with different behaviors, norms, beliefs, and physical attributes. Over time, the behavior and attributes of the populations in

Austria and Switzerland changed. This is exemplified by the increase of single households compared to multihouseholds starting in the 1960s or gradually more numerous requests for secondary residences over the last 100 years (Statistik Austria 2004). Changes were based on socioeconomic developments within the society and external drivers (e.g., influx of homeowners from abroad). Furthermore, societal attributes change (e.g., new designs and uses for RBs, the number of inhabitants from 16.57 people per RB in 1919 to 4.59 people in 2012).

- The second evolutionary system involves changes in natural hazard management policy. For decades since the 1890s, the focus was on the implementation of structural engineering measures (Holub and Fuchs 2009). From the 1970s onward, nonstructural measures (e.g., land use planning) supplemented these engineered structures. Over time, however, key strategies in natural hazard management were incapable of sufficiently addressing the magnitude of associated losses. Institutions and respective policymakers currently rely on a combination of structural and nonstructural measures to reduce natural hazard risk in the European Alps (Fuchs 2009) and beyond (Kubal et al. 2009). There is an evident shift in natural hazard discourse away from exclusively engineered solutions toward broader integrated management strategies. These include land use management and other incentives to discourage developments in high-risk areas (Fuchs 2009). Consequently, this shift has been identified as a key point of contention in policy discussions, especially toward the implementation of nonstructural measures (Wiering and Immink 2006). This was triggered by crises such as the Galtür avalanche event in 1999 (Keiler 2004) and flood events in 2002 and 2005 (Bard, Renard, and Lang 2012). These catastrophic events provide new opportunities for actors from all administrative levels to introduce new management systems. Despite these shifts, natural hazard management still predominantly considers the use of structural measures (Thaler, Priest, and Fuchs 2016). Additionally, the implementation of structural mitigation measures has encouraged increases in the number of buildings in hazard areas.

Assessing Flood Hazard Exposure

Two different data sets were used for this study. Information on flood hazards provided input for

the exposure assessment, in addition to data on building inventory in Austria and Switzerland (see Figure 1). Hazards such as river and torrential flooding (i.e., dynamic flooding with sediment transport and debris flows) in mountain rivers were assessed.

Available hazard maps were combined with nation-wide flood modeling results (see supplementary materials) to obtain spatial information on flood hazards. We defined a low- to medium-probability event as a source for the exposure assessment, in accordance with the requirements of the European Union Floods Directive (Commission of the European Communities 2007).

For the building exposure assessment, information on RBs was computed according to Fuchs, Keiler, and Zischg (2015), using specified information related to the entire building inventory. This information is available in a governmental database and contains details about the location and size of each building, the building category, and the year and period of construction (Bundesamt für Statistik 2012; Statistik Austria 2012).

Exposed buildings are defined as built structures that are susceptible to hydrological hazards. The hazard information was overlaid with building inventory data in a geographic information system. Each building was characterized by its main use, which was assessed by the net area of used space allotted for the different purposes of each floor.

Results

Analysis of Exposure Evolution

An overview on the number of RBs is provided in Table 1. A total of 3,574,198 RBs is located in Austria and Switzerland, of which 14.14 percent are exposed to hydrological hazards. The percentage exposed is slightly higher in Switzerland than in Austria. Almost two thirds (62.6 percent) of these buildings are single-family houses (SFHs), and slightly more than one third (37.4 percent) are apartment buildings (ABs). Between 1919 and 2012, the overall share of exposed RBs dropped around 2 percent, whereas the absolute number increased by a factor of 5. Similarly, the overall share of exposed SFHs dropped by around 2 percent, but the overall number of exposed SFHs increased by a factor of 5.6. Finally, the overall share of exposed ABs dropped by around 1.5 percent, but the overall number of exposed ABs increased by a factor of 4.2. In Switzerland, the exposure is generally slightly higher than in Austria.

The temporal development of the total RB stock is shown in Figure 2. Starting with an almost similar number of RBs in 1919 (Austria, 312,962; Switzerland, 307,751), the increase until 2012 was considerably higher in Austria (1,984,475) than in Switzerland (1,589,723). This increase followed a similar shape until 1960; thereafter, the increase was steeper in Austria than in Switzerland. A comparable pattern is observed for SFHs, starting

Residential buildings exposed to floods

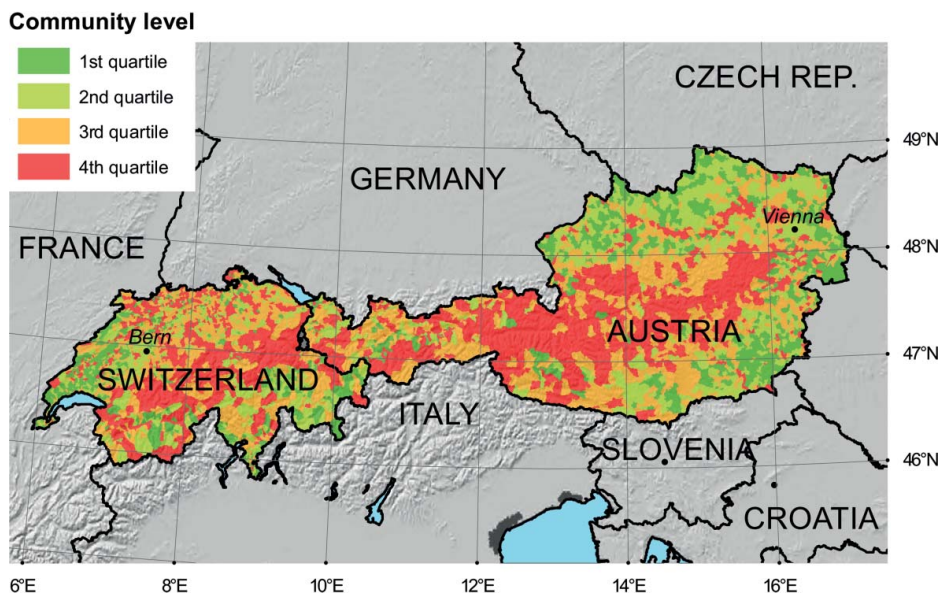


Figure 1. Exposure rate of residential buildings to hydrological hazards in Austria and Switzerland (exposed buildings to all buildings within a local authority, shown in terms of quartiles). (Color figure available online.)

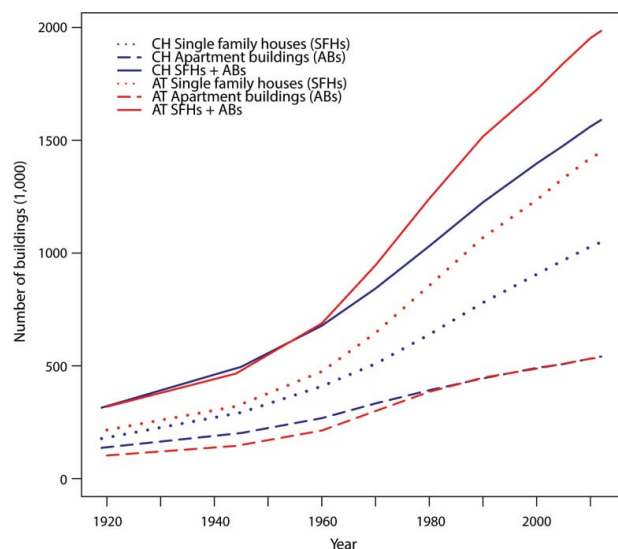


Figure 2. Absolute number of residential buildings in Austria and Switzerland (total number, single-family houses and apartment buildings) between 1919 and 2012. CH = Switzerland; AT = Austria; SFH= single-family house; AB = apartment building. (Color figure available online.)

from a total of 211,586 (Austria) and 173,309 (Switzerland), with a steeper increase in Austria than in Switzerland after 1960 and reaching totals of 1,447,144 (Austria) and 1,048,217 (Switzerland). In contrast, in 1919, there was a higher number of ABs in Switzerland (134,442) than in Austria (101,376). This number increased to almost the same amount for both countries (537,331 in Austria and 541,506 in Switzerland) in 2012.

Starting in 1919, there was a lower number of exposed RBs in Austria (42,219) than in Switzerland (58,446). These numbers increased until 2012, where the total numbers were higher in Austria (267,759) than in Switzerland (237,454). Similarly, the number of exposed SFHs increased from 26,473 (Austria) and

29,371 (Switzerland) to 179,257 (Austria) and 137,129 (Switzerland) between 1919 and 2012. In 1919, the number of exposed ABs started as a moderate amount in both countries (15,746 in Austria and 29,075 in Switzerland), which increased to 88,502 (Austria) and 100,325 (Switzerland) in 2012 (see Table 1).

Spatial analysis of the data reveals that hydrological hazards are an evident threat to municipalities, even if considerable differences between regions exist (Figure 1). In general, the exposure to hydrological hazards is defined as the share of exposed RBs to all existing RBs within a municipality. Exposure is low (first quartile) in communities located in the northern and southern alpine foreland and high (fourth quartile) in municipalities located in the high mountain areas around the main divide. The large river courses (Rhone, Aare, Rhine, Danube, and Mur) coincide with the higher levels of exposure in municipalities situated along these features. Moreover, some regions in the Central Alps are associated with low exposure values, even though there are above-average numbers of hazard events (Fuchs, Keiler, and Zischg 2015). This observation can be partially explained by a rigorous regional spatial planning policy (Thaler 2014; Thaler, Priest, and Fuchs 2016) and is discussed in the following section.

The temporal analysis reveals distinct differences between the Eastern and Western Alps. As shown in Figure 3, the share of exposed SFHs (number and value) compared to the entire number of SFHs decreased from 16.95 percent to 13.08 percent in Switzerland but was more or less constant in Austria (from 12.51 percent in 1919 to 12.39 percent in 2012). Hence, although the absolute number of exposed SFHs is higher in Austria than in Switzerland (Table 1), the relative distribution is reversed. The

Table 1. Overview of residential buildings in Austria and Switzerland

	Total RB N	Total RB exposed		Total SFH N	Total SFH exposed		Total AB N	Total AB exposed	
		N	%		N	%		N	%
CH 1919	307,751	58,446	18.99	173,309	29,371	16.95	134,442	29,075	21.63
CH 2012	1,589,723	237,454	14.94	1,048,217	137,129	13.08	541,506	100,325	18.53
AT 1919	312,962	42,219	13.49	211,586	26,473	12.51	101,376	15,746	15.53
AT 2012	1,984,475	267,759	13.49	1,447,144	179,257	12.39	537,331	88,502	16.47
CH + AT 1919	620,713	100,665	16.22	384,895	55,844	14.51	235,818	44,821	19.01
CH + AT 2012	3,574,198	505,213	14.14	2,495,361	316,386	12.68	1,078,837	188,827	17.50

Note. RB = residential buildings; SFH = single-family house; AB = apartment building; CH = Switzerland; AT = Austria.

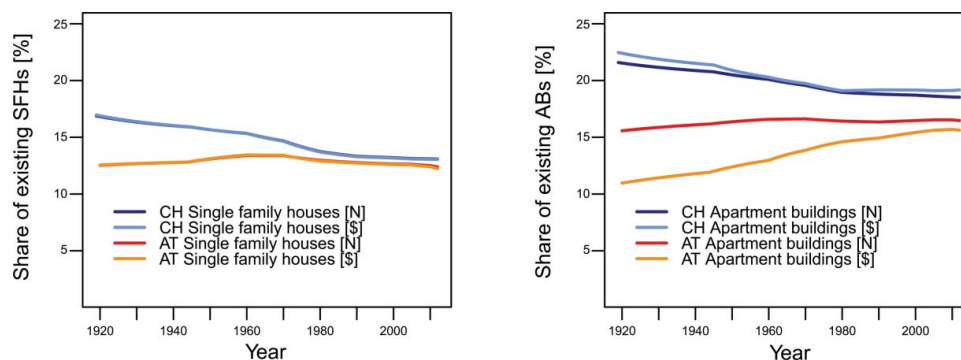


Figure 3. Share of exposed single-family houses (left) and apartment buildings (right) in Austria and Switzerland, relative to the total number of SFHs and ABs per country. The share of existing SFHs (left) is essentially identical in number and value for both Austria and Switzerland. This effect gives the appearance of only two graph lines when in fact there are four. CH = Switzerland; AT = Austria; SFH = single-family house; AB = apartment building. (Color figure available online.)

temporal ABs pattern is comparable to the one for SFHs and shows a slight decrease in the number of exposed ABs from 21.63 percent to 18.53 percent in Switzerland, with a similar progression for the values exposed. The Austrian data, in contrast, show a slightly increasing trend for the relationship between exposed ABs and the total ABs (from 15.53 percent in 1919 to 16.47 percent in 2012; the highest value is 16.62 percent in 1970) and a strong increase in the values. Hence, even if the increase in exposed buildings for the 1919 to 2012 period is lower in Switzerland than in Austria (factor of 4.67 vs. 6.77 for SFHs, 3.45 vs. 5.62 for ABs), the relative share of exposed SFHs and ABs remains higher in Switzerland than in Austria over 1919 to 2012. If the entire population is

considered, the share of RBs (number and value) slightly decreased from 1919 to 2012 (Figure 4), with a higher rate of decrease during the 1970s. If values and numbers are compared, the exposed SFHs and ABs were becoming more expensive since the 1970s.

Analysis of Policy Response in Natural Hazard Management

Strategies to prevent or to reduce the effects of natural hazards in settlement areas can be traced back to medieval times; official authorities were only founded in 1876 (Switzerland) and 1884 (Austria) as a result of legal regulation (Schweizerische Eidgenossenschaft 1876; Österreichisch-Ungarische Monarchie 1884). Since then, efforts to minimize detrimental impacts to civilians and society have been centered on silvicultural measures to prevent erosion and the introduction of engineering structures within the catchment, along channel systems, and in deposition areas. Starting in the 1950s, conventional mitigation concepts, which were aimed at decreasing both the magnitude and frequency of events, were increasingly complemented with technical mitigation measures. The amendment of respective legal regulations marks a turning point in responsibility sharing. Changes were observed in the following examples: the Hydraulic Engineering Assistance Act (Republik Österreich 1848), the Water Act (Republik Österreich 1959), the Disaster Act (Republik Österreich 1966), and the Forest Act (Republik Österreich 1975) in Austria and the Water Act and the Forest Act in Switzerland (Schweizerische Eidgenossenschaft 1991a, 1991b). As a result of these regulations, which were supplemented by multiple

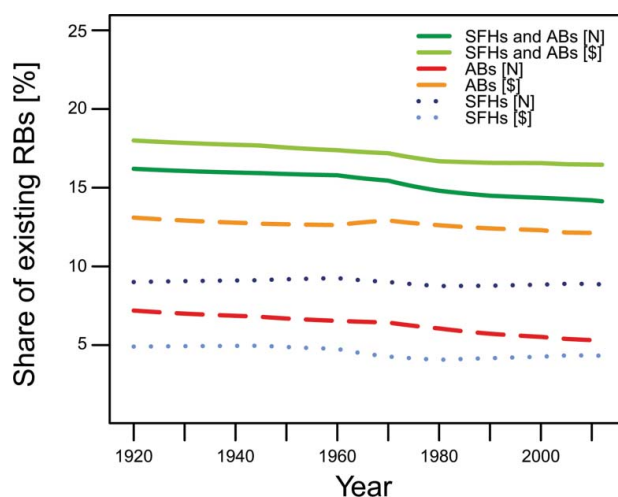


Figure 4. Share of exposed single-family houses and apartment buildings in relation to the total number of residential buildings. SFH = single-family house; AB = apartment building; RB = residential building. (Color figure available online.)

federal directives, protection against natural hazards became a governmental duty. Starting in the 1970s, with the Directive on Hazard Mapping in Austria (Republik Österreich 1976) and the National Spatial Planning Act in Switzerland (Schweizerische Eidgenossenschaft 1979), the use of nonstructural measures for natural hazard protection was implemented. As a result, spatial planning methods such as hazard maps aimed at reducing development activities in hazard-prone areas were introduced (Holub and Fuchs 2009). Multiple directives, such as the Directive on the Assessment of Flood Hazards in Spatial Planning (Bundesamt für Wasserwirtschaft, Bundesamt für Raumplanung, and Bundesamt für Umwelt, Wald und Landschaft 1997) in Switzerland and the Disaster Management Act (Republik Österreich 1996) in Austria supplemented these national laws, and further federal regulations from both countries were set into motion (Kanonier 2006). The European Union Floods Directive (Commission of the European Communities 2007) finally provided the basis for a risk-based management of flood hazards in European countries. In summary, we identified four key periods of natural hazard management in the European Alps, which are attributed to different hazard paradigms:

- In the 1870s and 1880s, a governmental system for natural hazard protection was introduced. The initial legal regulations that were focused on natural hazard management shifted to watershed management, forest-biological, soil bio-engineering measures, and technical measures (construction material: timber and stone masonry) for the first time.
- In the 1950s and 1960s, a shift toward engineering systems was observed. In the European Alps, the mitigation of mountain hazards was predicated on the implementation of structural engineering measures. These targeted the minimization of both the magnitude and frequency of events, which were increasingly complemented by more sophisticated technical mitigation measures.
- In the 1970s and 1980s, the system evolved to include a broader discussion on natural hazard management based on respective national laws. These laws served as responses to various natural hazard events. As a result, nonstructural measures supplemented engineering solutions. In particular, land use planning was introduced. Institutions and policymakers relied on a combination of structural

and nonstructural measures to reduce the negative impact of future events.

- Finally, the risk-based approach was introduced in the 1990s. The shift from hazard to risk required a completely different approach to effectively address outstanding management issues. Here, the concept of risk is defined as a function of hazard and consequences. Comprehensive experiences have been documented about the application of the risk concept to mountain hazard management, especially in Switzerland. The risk-based approach was focused on encouraging a discourse on risk within respective societies. By considering different scenarios (including the aspect of residual hazard), a greater focus is placed on stakeholder engagement and bottom-up initiatives, and the implementation of catchment-wide management concepts was observed.

Discussion and Conclusion

The aforementioned results clearly showed that effective exposure reduction has yet to be achieved. In fact, the evolution of new policy instruments in flood risk management has largely been unable to reduce increases in exposure for both countries. We observed that the new flood risk management strategies allowed continuous developments in floodplain areas. In particular, the expectation that engineered measures would protect floodplains had encouraged development instead. This resulted in increases in potential losses (White, Kates, and Burton 2001). In response, the public administration in Austria and Switzerland generated a situation of moral hazard within society (Tarlock 2012), because new buildings in hazard areas were secured by innovative defense strategies. For example, the Austrian housing subsidy system, which changed in 1958, led to an increase in public subsidies that are available for private house owners. As such, the total number of new RBs increased to 1,296,101 between 1960 and 2012, compared to the 375,412 new RBs between 1919 and 1960. Consequently, the availability of housing subsidies contributed to the development of SFHs; during the period of investigation, more than 115,687 were constructed in hazard-prone areas with financial support from the government. This effect is referred to as *perverse subsidies* (van Beers and Van Den Bergh 2001). Furthermore, the Austria Superior Administrative Court decided

against enforcing the production of hazard maps as a part of statutory regulation for spatial planning; instead they are only judged as an expert report (Verwaltungsgerichtshof 1995).

Because an absolute decrease in exposed RBs would only be possible if the original buildings are removed from identified hazard zones, we computed the hypothetical development of the buildings based on a scenario where a construction ban is enforced in endangered areas. To demonstrate the effectiveness of such a ban, associated legal regulations were assumed to be effective in the 1970s and the 1990s, respectively. If we hypothetically assume that starting in 1976, which coincides with the amendment to the Directive on Hazard Mapping in Austria, further development in hazard-prone areas would have been stopped, a total of 162,907 buildings would not have been constructed in exposed areas. This number equates to -32 percent of exposure. Similarly, after 1991, which coincides with the amendment of the Water Act and the Forest Act in Switzerland, a total of 102,935 buildings would not have been constructed in hazard-prone zones. This is equivalent to -20 percent exposure. Consideration for these scenarios also demonstrates the importance of time when investigating the effectiveness of nonstructural measures. For instance, it recommends that land use planning policies should be consistently implemented over longer temporal horizons.

The policy system encourages private homeownership, despite associated increases in vulnerability. Another driver that contributed to increased exposure was the interpretation of land use management regulations at local levels. In some of the regions belonging to the fourth quartile of exposure (Figure 1), the regional land use management act allowed the construction of houses outside of defined building zones in land use plans; consequently, around 7,000 out of a total of 12,000 new residential buildings were constructed due to this exemption. Furthermore, governmental organizations interpreted how land was protected by engineering structures differently. In Salzburg, for example, new buildings and settlements were built to create dense urban areas, resulting in an increase in exposure in high-risk areas. Moreover, the public administration seemed to have ignored the problem of exposure, as natural hazard management had little or no impact on the design of local land use plans and strategies. This is explained by the fact that economic growth within administrative boundaries is regularly prioritized above ecological concerns or

protection against hazards (Thaler 2014; Thaler, Priest, and Fuchs 2016).

The observations show that the exposure of RBs has considerably increased over the last ninety years. This rise has been observed despite the introduction of natural hazard management strategies in the European Alps. This development was heavily influenced by the occurrence of disasters, which led to an increased gravitation toward the dependency on technical mitigation measures but did not prevent further unsuitable land use developments. Moreover, acknowledging the levee effect, natural hazard management encouraged further development of hazard-prone areas with the consequence of an increase of exposure dynamics. As such, both systems (exposure dynamics and management paradigms) are profoundly interrelated, where increases in exposure necessitate further mitigation measures. These measures evolve from purely engineered solutions toward risk-based planning approaches. The implementation of key strategies in isolation, however, does not completely eliminate potential losses due to damages over time. Instead, a lock-in situation results, where the reliance on technical mitigation measures that dominate current risk management approaches continues to be more prominent than the perceived impact of land use planning.

To break away from the way exposure has been addressed to date, there is a need to set incentives to ensure responsible natural hazard management. This requires rigorous enforcement of land use planning legislation (e.g., reconsideration of *perverse subsidies* from a political perspective), which would foster the popularization of alternative hazard mitigation measures and promote the implementation of coherent policies. It would also support the development of further incentives to minimize risk. Natural hazard risk management will only be successful if the further development of construction in hazard-prone areas is restricted.

The aforementioned management approaches ensure the availability and accessibility of knowledge on natural hazard risk and how this can be effectively applied to a range of societal conditions. The result would be a paradigm shift in natural hazards management, which would result in decreased vulnerability and increased resilience for the affected population.

Funding

This study received funding from the Austrian Science Fund (FWF): P27400.

Supplemental Material

Supplemental data for this article can be accessed on the publisher's Web site at <http://dx.doi.org/10.1080/24694452.2016.1235494>.

ORCID

Sven Fuchs  <http://orcid.org/0000-0002-0644-2876>

Veronika Röhliberger  <http://orcid.org/0000-0003-1911-6268>

Thomas Thaler  <http://orcid.org/0000-0003-3869-3722>

Andreas Zischg  <http://orcid.org/0000-0002-4749-7670>

Margreth Keiler  <http://orcid.org/0000-0001-9168-023X>

References

- Andres, N., A. Badoux, and C. Hegg. 2015. Unwetterschäden in der Schweiz im Jahre 2014 [Swiss hazard losses in 2014]. *Wasser, Energie, Luft* 107 (1): 47–54.
- Bard, A., B. Renard, and M. Lang. 2012. Floods in the alpine areas of Europe. In *Changes in flood risk in Europe*, ed. Z. Kundzewicz, 362–71. Boca Raton, FL: CRC.
- Barredo, J. 2009. Normalised flood losses in Europe: 1970–2006. *Natural Hazards and Earth System Sciences* 9 (1): 91–104.
- Bundesamt für Statistik. 2012. *Eidgenössisches Gebäude- und Wohnregister, Merkmalskatalog* [Swiss federal building register, catalogue of characteristics]. Neuchâtel, Switzerland: Bundesamt für Statistik.
- Bundesamt für Wasserwirtschaft, Bundesamt für Raumplanung, and Bundesamt für Umwelt, Wald und Landschaft. 1997. *Berücksichtigung der Hochwassergefahren bei raumwirksamen Tätigkeiten* [Acknowledging flood hazards in spatial planning]. Biel und Bern, Switzerland: BWW, BRP, BUWAL.
- Commission of the European Communities. 2007. Directive 2007/60/EC of the European Parliament and of the Council of 23 October 2007 on the assessment and management of flood risks. *Official Journal of the European Union* 288:27–34.
- Fuchs, S. 2009. Susceptibility versus resilience to mountain hazards in Austria—Paradigms of vulnerability revisited. *Natural Hazards and Earth System Sciences* 9 (2): 337–52.
- Fuchs, S., M. Keiler, S. A. Sokratov, and A. Shnyarkov. 2013. Spatiotemporal dynamics: The need for an innovative approach in mountain hazard risk management. *Natural Hazards* 68 (3): 1217–41.
- Fuchs, S., M. Keiler, and A. Zischg. 2015. A spatiotemporal multi-hazard exposure assessment based on property data. *Natural Hazards and Earth System Sciences* 15 (9): 2127–42.
- Gual, M. A., and R. B. Norgaard. 2010. Bridging ecological and social systems coevolution: A review and proposal. *Ecological Economics* 69 (4): 707–17.
- Hodgson, G. 2006. What are institutions? *Journal of Economic Issues* 40 (1): 1–25.
- Holub, M., and S. Fuchs. 2009. Mitigating mountain hazards in Austria—Legislation, risk transfer, and awareness building. *Natural Hazards and Earth System Sciences* 9 (2): 523–37.
- Jongman, B., E. E. Koks, T. G. Husby, and P. J. Ward. 2014. Increasing flood exposure in the Netherlands: Implications for risk financing. *Natural Hazards and Earth System Sciences* 14 (5): 1245–55.
- Kallis, G. 2007. When is it coevolution? *Ecological Economics* 62 (1): 1–6.
- Kanonier, A. 2006. Raumplanungsrechtliche Regelungen als Teil des Naturgefahrenmanagements [Land use planning regulations as part of natural hazard management]. In *Recht im Naturgefahrenmanagement*, ed. S. Fuchs, L. Khakzadeh, and K. Weber, 123–53. Innsbruck, Austria: Studienverlag.
- Keiler, M. 2004. Development of the damage potential resulting from avalanche risk in the period 1950–2000, case study Galtür. *Natural Hazards and Earth System Sciences* 4 (2): 249–256.
- Keiler, M., S. Fuchs, A. Zischg, and J. Stötter. 2004. The adaptation of technical risk analysis on natural hazards on a regional scale. *Zeitschrift für Geomorphologie* 135 (Suppl.): 95–110.
- Keiler, M., J. Knight, and S. Harrison. 2010. Climate change and geomorphological hazards in the eastern European Alps. *Philosophical Transactions of the Royal Society of London A* 368: 2461–79.
- Keiler, M., R. Sailer, P. Jörg, C. Weber, S. Fuchs, A. Zischg, and S. Sauer Moser. 2006. Avalanche risk assessment—A multi-temporal approach, results from Galtür, Austria. *Natural Hazards and Earth System Sciences* 6 (4): 637–51.
- Kienholz, H., B. Krummenacher, A. Kipfer, and S. Perret. 2004. Aspects of integral risk management in practice—Considerations with respect to mountain hazards in Switzerland. *Österreichische Wasser- und Abfallwirtschaft* 56 (3–4): 43–50.
- Kubal, C., D. Haase, V. Meyer, and S. Scheuer. 2009. Integrated urban flood risk assessment—Adapting a multi-criteria approach originally developed for a river basin to a city. *Natural Hazards and Earth System Sciences* 9 (6): 1881–95.
- Loucks, D., and J. Stedinger. 2007. Thoughts on the economics of floodplain development in the U.S. In *Extreme hydrological events: New concepts for security*, ed. O. Vasiliev, P. van Gelder, E. Plate, and M. Bolgov, 3–19. Dordrecht, The Netherlands: Springer.
- Mudelsee, M., M. Börngen, G. Tetzlaff, and U. Grünewald. 2003. No upward trends in the occurrence of extreme floods in central Europe. *Nature* 425 (6954): 166–69.
- Munich Re. 2016. *Topics geo: Natural catastrophes 2015*. Munich, Germany: Munich Re.
- Nordregio. 2004. Mountain areas in Europe: Analysis of mountain areas in EU member states, acceding and other European countries. Final report, Nordregio, Stockholm, Sweden.

- Österreichisch-Ungarische Monarchie. 1884. *Gesetz, betreffend Vorkehrungen zur unschädlichen Ableitung von Gebirgswässern* [Law related to the nonhazardous discharge of mountain waters]. Wien, Austria: Kaiserlich-königliche Hof- und Staatsdruckerei.
- Papathoma-Köhle, M., M. Kappes, M. Keiler, and T. Glade. 2011. Physical vulnerability assessment for alpine hazards: State of the art and future needs. *Natural Hazards* 58 (2): 645–80.
- Papathoma-Köhle, M., A. Zischg, S. Fuchs, T. Glade, and M. Keiler. 2015. Loss estimation for landslides in mountain areas—An integrated toolbox for vulnerability assessment and damage documentation. *Environmental Modelling and Software* 63:156–69.
- Remo, J. W. F., M. Carlson, and N. Pinter. 2012. Hydraulic and flood-loss modeling of levee, floodplain, and river management strategies, Middle Mississippi River, USA. *Natural Hazards* 61 (2): 551–75.
- Republik Österreich. 1948. Wasserbautenförderungsgesetz [Federal Hydraulic Engineering Development Act]. BGBl 34/1948.
- . 1959. Wasserrechtsgesetz [Federal Water Act]. BGBl 215/1959.
- . 1966. Bundesgesetz vom 9. September 1966 über den Katastrophenfonds [Federal Act of 9 September 1966 on the Disaster Fund]. BGBl. Nr. 207/1966.
- . 1975. Forstgesetz [Federal Forest Act]. BGBl 440/1975.
- . 1976. Verordnung des Bundesministers für Land- und Forstwirtschaft vom 30. Juli 1976 über die Gefahrenzonenpläne [Decree of the Federal Minister for Agriculture and Forestry of 30 July 1976 related to hazard mapping]. BGBl 436/1976.
- . 1966. Bundesgesetz vom 9. September 1966 über den Katastrophenfonds [Federal Act of 9 September 1966 on the Disaster Fund]. BGBl. Nr. 207/1966.
- Schweizerische Eidgenossenschaft. 1876. Bundesgesetz betreffend die eidgenössische Oberaufsicht über die Forstpolizei [Federal law related to the confederate supervision of the Swiss Forest Police]. BS 9 521.
- . 1979. Bundesgesetz über die Raumplanung [Federal law on spatial planning]. SR 700.
- . 1991a. Bundesgesetz über den Wald [Federal Forest Act]. SR 921.0.
- . 1991b. Bundesgesetz über den Wasserbau [Federal Hydrography Act]. SR 721.100.
- Statistik Austria. 2004. *Gebäude- und Wohnungszählung 2001—Hauptergebnisse Österreich* [Census of buildings and flats 2001—Main results for Austria]. Wien, Austria: Statistik Austria.
- . 2012. *Adress-GWR Online Handbuch, Teil C, Anhang 2: Merkmalskatalog*. Wien, Austria: Statistik Austria.
- Swiss Re. 2016. *Natural catastrophes and man-made disasters in 2015*. Zurich: Swiss Re.
- Tappeiner, U., A. Borsdorf, and E. Tasser. 2008. *Alpenatlas* [Atlas of the Alps]. Heidelberg, Germany: Springer.
- Tarlock, A. D. 2012. United States flood control policy: The incomplete transition from the illusion of total protection to risk management. *Duke Environmental Law & Policy Forum* 23:151–83.
- Thaler, T. 2014. Developing partnership approaches for flood risk management: Implementation of inter-local co-operations in Austria. *Water International* 39 (7): 1018–29.
- Thaler, T., S. Priest, and S. Fuchs. 2016. Evolving interregional co-operation in flood risk management: Distances and types of partnership approaches in Austria. *Regional Environmental Change* 16 (3): 841–53.
- Theiling, C. H., and J. T. Burant. 2013. Flood inundation mapping for integrated floodplain management: Upper Mississippi River system *River Research and Applications* 29:961–78.
- Totschnig, R., and S. Fuchs. 2013. Mountain torrents: Quantifying vulnerability and assessing uncertainties. *Engineering Geology* 155:31–44.
- van Beers, C., and J. C. J. M. Van Den Bergh. 2001. Perseverance of perverse subsidies and their impact on trade and environment. *Ecological Economics* 36 (3): 475–86.
- van den Bergh, J. C. J. M., and S. Stagl. 2003. Coevolution of economic behaviour and institutions: Towards a theory of institutional change. *Journal of Evolutionary Economics* 13 (3): 289–317.
- Verwaltungsgerichtshof. 1995. Erkenntnis 91/10/0090 [Decision 91/10/0090] (27.03.1995) https://www.ris.bka.gv.at/Dokumente/Vwgh/JWT_1991100090_19950327x00/JWT_1991100090_19950327x00.pdf (last accessed 1 December 2015).
- White, G., R. Kates, and I. Burton. 2001. Knowing better and losing even more: The use of knowledge in hazards management. *Environmental Hazards* 3 (3–4): 81–92.
- Wiering, M., and I. Immink. 2006. When water management meets spatial planning: A policy-arrangements perspective. *Environment and Planning C: Government and Policy* 24 (3): 423–38.
- Zimmermann, M., and M. Keiler. 2015. International frameworks for disaster risk reduction: Useful guidance for sustainable mountain development? *Mountain Research and Development* 35 (2): 195–202.
- SVEN FUCHS is Senior Scientist in the Institute of Mountain Risk Engineering at the University of Natural Resources and Life Sciences, Vienna 1190, Austria. E-mail: sven.fuchs@boku.ac.at. His research interests include mountain hazard risk management, the study of coupled human–environment systems, and vulnerability assessment for natural hazards.
- VERONIKA RÖTHLISBERGER is a PhD candidate in the Institute of Geography at the University of Bern, Bern 3012, Switzerland. E-mail: veronika.roethlisberger@giub.unibe.ch. She is also member of the Mobiliar Lab for Natural Risks at the Oeschger Centre for Climate Change Research at the University of Bern. Her research interests include risk assessment and management of floods, spatial statistics, and the analysis of economic data in the context of flood risk.
- THOMAS THALER is a Research Fellow in the Institute of Mountain Risk Engineering at the University of Natural Resources and Life Sciences, Vienna 1190, Austria. E-mail: thomas.thaler@boku.ac.at. His research interests include policy issues in mountain hazards, focusing on national risk management and related policy strategies in different European countries.

ANDREAS ZISCHG is a Scientist in the Institute of Geography at the University of Bern, Bern 3012, Switzerland, and he is also affiliated with the Mobiliar Lab for Natural Risks of the Oeschger Centre for Climate Change Research at the University of Bern. E-mail: andreas.zischg@giub.unibe.ch. His research interests include flood risk modeling.

MARGRETH KEILER is Associate Professor in the Institute of Geography at the University of Bern, Bern 3012, Switzerland. E-mail: margreth.keiler@giub.unibe.ch. Her research interests include hazard assessment of floods, landslides and multihazards, vulnerability, risk and resilience in the context of natural disasters, risk evolution, coupled human–landscape systems, and complex system research.

Paper 8: Armbruster, S., Hintermann, B., Zischg, A., 2018. The effects of flood events on land and housing value: Evidence from the Swiss real estate market: SURED 2018 - Monte Verità Conference on Sustainable Resource Use and Economic Dynamics, June 3-7, 2018, Ascona/Switzerland. ETH Zurich, Zurich, 39 pp.

The effects of flood events on land and housing value: Evidence from the Swiss real estate market *

Stephanie Armbruster[†], Beat Hintermann[‡] and Andreas Zischg[§]

January 31, 2018

Abstract

If homeowners are fully rational and well aware of flood risks and related cost, there should be a reduction in land and housing values from a risky floodplain location. Previous research has indicated that price differentials reflecting the risk of flooding exist, but that they become much larger in the wake of a storm. This suggests that households may suffer from availability bias such that risks become more salient to buyers and sellers in the wake of a major flood. We apply a hedonic price model to Geographic Information System data on housing and land prices in Switzerland, combined with flood hazard maps and investigate the effect of the biggest floods of 2007, 2013 and 2015 on housing and land prices. Despite the presence of socialized insurance mandate for buildings we find evidence for a persistent availability bias. We further find that the introduction of flood hazard maps into legally binding land use plans increases property prices.

Keywords: *Flood risk, housing values, hedonic pricing, environmental amenities, availability bias*

*This research has been supported by the Swiss National Science Foundation under grant Nr. CRSII1-154404 (Sinergia).

[†]University of Basel, Peter-Merian-Weg 6, CH-4002 Basel, CH. stephanie.armbruster@unibas.ch

[‡]University of Basel, Peter-Merian-Weg 6, CH-4002 Basel, CH. b.hintermann@unibas.ch

[§]University of Bern, Institute of Geography, Oeschger Centre for Climate Change Research, Mobiliar Lab for Natural Risks, Hallerstrasse 12, CH-3012 Bern, Switzerland andreas.zischg@giub.unibe.ch

1 Introduction

About 21 million people are affected by river floods each year, and due to climate change and socio-economic development, the number of affected people is predicted to increase to 54 million in 2030 as the surface temperature continues to rise (Luo et al., 2015; Willner et al., 2018). Switzerland, which is the context of this paper, is no exception. In 2015, the damage to private property, infrastructure, forestry and agriculture caused by floods, debris flows, landslides and rock falls cause amounted to CHF 135 million, 92 per cent of which resulted from flooding (Hilker et al., 2009). Furthermore, both capital and people have been moving into floodplains and other high risk areas (Röthlisberger et al., 2016), despite the existence of hazard maps informing homeowners about the respective probability and intensity of potential flood risks.

To assess the value of environmental risks, hedonic theory has been the paradigm used to investigate the relationship between house prices and environmental disamenities.¹ A series of hedonic studies has estimated the effect of sea floods on housing values in the USA and the UK.² A common finding is that flooding in coastal areas lowers property values. This could be either due to differences in expected damages, or, equivalently, differences in insurance premia.

Standard hedonic price models show correlations which may suffer from omitted variable bias. In addition, there can be a sorting issue as households move to locations matching their preferences for amenities. One way to overcome this shortcoming is the use of a difference-in-differences (DiD) spatial hedonic model framework. One example is Davis (2004), who focuses on a county in Nevada where residents had recently experienced a severe increase in pediatric leukemia. Housing prices are compared before and after the increase with a nearby county acting as a control group. Billings and Schnepel (2017) estimate the benefits of lead-paint remediation on housing prices adopting a DiD estimator that compares values among remediated properties with those for which an inspection does not identify a lead paint hazard.

In this paper, we use a DiD-approach to investigate the responsiveness of housing and land

¹Significant negative effects on housing values have been found to be associated with hazardous waste sites (Gayer et al., 2000), earthquake/volcanic hazards (Bernknopf et al., 1990; Beron et al., 1997) water pollution (Leggett and Bockstael, 2000), and air pollution (Chay and Greenstone, 2005). For a survey, see Boyle and Kiel (2001).

²For the US context, see Bartosova et al. (2000); Shilling et al. (1985); MacDonald et al. (1987); Donnelly (1989); MacDonald et al. (1990); Speyrer and Ragas (1991); Harrison et al. (2001); Bin and Polasky (2004); Bin and Kruse (2006); Bin et al. (2008); Atreya et al. (2013). Daniel et al. (2009) carries out a meta-analysis and finds that there is a significant heterogeneity in flood risk-induced price differentials. For studies from the UK, see Lamond and Proverbs (2008); Belanger and Bourdeau-Brien (2017); Lamond et al. (2010).

prices to flood risk using data from Zurich Canton in Switzerland. Homeowners in Switzerland are required to buy a flat-rate building insurance, which covers monetary damages caused by flooding at a price that does not depend on the individual structure's risk. This should, in principle, remove any price differential due to flood risk, as the risk is effectively socialized. However, due to uninsurable costs such as the possibility of death or injury, damage to community infrastructure, hassle of being displaced or the loss of personal items with sentimental value, the willingness to pay for a property could nevertheless decrease in the flood risk, *ceteris paribus*, despite the presence of the insurance mandate.

There is evidence that flood risk may be subject to an “availability bias”, which describes a situation in which “people assess the frequency of a class or the probability of an event by the ease with which instances or occurrences can be brought to mind” (Kahneman et al., 1982). Flood becomes more salient to buyers and sellers in the wake of a hazard event (e.g. earthquake, flood, or hurricane) as reflected by increasing price differentials across hazard zones (Hallstrom and Smith, 2005; Kellens et al., 2013; Burningham et al., 2008). Bakkensen and Barrage (2017) find that around 40% of households substantially underestimate coastal flood risks. Bubeck et al. (2012) report that many individuals have no willingness-to-pay for insurance because they underestimate the (low) probability of flood risk, and that the demand for flood insurance is determined to an important degree by emotional fear. Risk mis-perception can result in spiking insurance take-up after a flood (Gallagher, 2014).

Bin and Landry (2013) examine the flood effects on price differentials of Hurricane Fran in 1996 and Hurricane Floyd in 1999 in North Carolina. The treatment group consists of houses within a flood plain and the respective control group are located outside the floodplain. Using data on property transactions before and after the floods, they detect no market risk premium for the presence in a flood zone in general, but significant price differentials after major flooding events. The effect is diminishing over time, essentially disappearing about 5 or 6 years after Hurricane Floyd. Similarly, Atreya et al. (2013) demonstrate in a DiD framework that property price differentials reflecting flood risk increase following a large flood event in 1994 in Dougherty County, Georgia diminishing after eight to nine years.

In this paper, we follow Bin and Landry (2013) and Atreya et al. (2013) by using a hedonic price model to assess the effect of the flash floods of 2007, 2013 and 2015 on the real estate

market of the canton of Zurich. Our treatment group consists of houses and land within areas that are labeled as subject to flood risk, whereas properties outside of flood zones serve as the control group. We investigate if (i) there is a price differential due to flood risk (difference), (ii) whether this differential increases after major floods (difference-in-difference), and (iii) if the effect differs between prices for houses and for land (triple difference). We further examine if the implementation of obligatory protective measures (cantonal land use plan) has an influence on real estate prices. To our knowledge, there no previous studies analyze the influence of relatively small-scale events such as river floods on both local housing and land markets. Furthermore, the Swiss setting is special due to the presence of a socialized insurance mandate and detailed maps informing potential home buyers about flood risks.

We find that being located in a risky zone has a significant and negative effect on housing prices, but the effect is not statistically significant for land prices. The advent of the flood in 2007 a negative and significant effect on the price for both housing and land located in flood zones. The effect is short-lived: It is strongest directly three months after the flood but becomes statistically insignificant already after six months. We interpret this finding as evidence for an availability bias. The effect for the floods of 2013 and 2015 has the same negative sign but is not statistically different from zero. The DDD estimation strategy confirms these results (again, with statistical significance only for the 2007 flood) and additionally shows that house prices were less negatively affected than land prices. Our results imply that an availability bias for flood risk exists even in the presence of socialized building insurance and detailed and public information about flood risk.

Evaluating the elaboration and implementation of the cantonal land use plan, we find that the implementation of obligatory hazard map compliance has a positive influence on housing and land prices relative to the no hazard group and can reduce the negative effect of risky building locations. In contrast, the mere creation of hazard maps without a mandatory implementation does not have an effect. These results highlight the value of better flood hazard information and can help to guide decisionmakers as they assess community-wide benefits from flood control and mitigation projects.

In a future version of this paper, which is work in progress, we will match insurance claim data to our dataset and examine whether prices for homes that were actually damaged react

differently to the occurrence of a flood than houses that are located in a risk area but escaped damage. Furthermore, we will include additional controls variables such as the distance to water (rivers or lakes), the amount of sun per day, distance to the woods and distance to Zurich. This will allow us to reduce the scope for unobserved heterogeneity, which is an issue especially for our first-difference results (i.e., the price differential for real estate located in flood zones). The required data will be available by the end of February.

The next section contains a brief theoretical model linking the demand for real estate to flood risk. Section 3 provides background information for the hazard maps, insurance scheme and major flood events in Switzerland and describes the data as well as the estimation strategy. The results are presented in Section (4) and robustness tests are discussed. Section (5) concludes.

2 A model of real estate demand and risk

We build on Bin et al. (2008) and use the following simple model to guide our empirical analysis. For now, we focus on housing prices but assume that the same logic applies for land prices as well, at least in the absence of a socialized insurance scheme. Households are perfectly rational and well informed. Following Rosen (1974), the hedonic price function is represented as:

$$P = P(s, n(t), r) \tag{1}$$

The price P for the market good that is used (in our case, houses and land) is a function of structural characteristics s , such as the number of rooms or the age of the house; community-specific public goods $n(t)$; and the risk r . The public goods are financed by linear community taxes t such that $\frac{\partial n(t)}{\partial t} > 0$. The function $P(\cdot)$ is assumed to be twice continuously differentiable in all arguments and will produce an estimate of the representative household's marginal willingness to pay for an additional unit of an attribute. Households' utility is strictly concave in all arguments and given by:

$$U(s, n(t), c), \tag{2}$$

with c representing a composite commodity that serves as the numeraire. Consumers are assumed to be informed about relatively safe and unsafe locations, hence the risk r , as hazard maps are publicly available. We further assume that flood adaptation measures are rather small

such that we refrain from modeling flood risk prevention as a public good.

Following (Brookshire et al., 1985), we use an expected utility framework in which consumers account for the risk information in their decision making. The observed discount on property in an area with high flood risk, relative to a safe area, thus reflects household's willingness to pay to avoid such risk. The consumer's problem is to maximize expected utility over two states of the world: the flood state and no flood, which occur with probabilities p and $1 - p$, respectively.

There exists insurance for the structure of the house and households have to pay a deductible. In addition, floods can cause monetary and non-monetary losses which are not covered by insurance such as personal injury, hassle of being displaced by flood damage, damage to community infrastructure, the effort to contact insurance, destruction of items excluded from insurance (such as damages to garden structures or vegetation) and loss of personal items with sentimental value. The parameter m^L represents the expected income in the loss state i.e. income remaining for consumption of the numeraire, including any insurance settlement net of insurance payments, deductibles and uninsured losses, and m^{NL} represents expected income in the no-loss state, with $m^L < m^{NL}$. Expected Utility is given by

$$E[U] = p(r) \cdot U^L[s, n(t), m^L - \lambda \cdot P(s, n(t), r) - t] + (1 - p(r)) \cdot U^{NL}[s, n(t), m^{NL} - \lambda \cdot P(s, n(t), r) - t] \quad (3)$$

where $p(r)$ is the subjective probability of a flood event (based on available hazard maps) and the utility function is state dependent across loss (L) and no-loss (NL). λ is a parameter which converts the sales price to a yearly price.

Consumers take the hedonic price schedule $P(\cdot)$ as given and residual income is spend for consumption of a composite commodity. Differentiating (3) with respect to s , the optimal choice of housing characteristics is given by the first-order conditions:

$$\frac{\partial P}{\partial s} = \frac{p(r) \frac{\partial U^L}{\partial s} + (1 - p(r)) \frac{\partial U^{NL}}{\partial s}}{\lambda \cdot [p(r) \frac{\partial U^L}{\partial m} + (1 - p(r)) \frac{\partial U^{NL}}{\partial m}]} > 0 \quad (4)$$

The marginal "implicit hedonic price" for amenity s is equal to the ratio of expected amenity value and expected marginal utility of income. Taxes influence housing prices as follows:

$$\frac{\partial P}{\partial t} = \frac{p(r) [\frac{\partial U^L}{\partial n} \frac{\partial n(t)}{\partial t} - \frac{\partial U^L}{\partial m}] + (1 - p(r)) [\frac{\partial U^{NL}}{\partial n} \frac{\partial n(t)}{\partial t} - \frac{\partial U^{NL}}{\partial m}]}{\lambda \cdot [p(r) \frac{\partial U^L}{\partial m} + (1 - p(r)) \frac{\partial U^{NL}}{\partial m}]} \quad (5)$$

where we have applied the envelope theorem i.e. $\frac{\partial U^{L,NL}}{\partial m} \frac{\partial P}{\partial n(t)} \frac{\partial n(t)}{\partial t} = \frac{\partial U^{L,NL}}{\partial m} \frac{\partial P}{\partial t}$. If the marginal utility of income exceeds the marginal utility of a tax increase financing the community- public good, i.e., $\frac{\partial U^L}{\partial m} > \frac{\partial U^L}{\partial n} \frac{\partial n(t)}{\partial t}$, a tax increase has a negative effect on housing prices, and vice versa if the marginal utility of private consumption is below that of public consumption.

The marginal effect of (exogenous) risk on housing prices is given by

$$\frac{\partial P}{\partial r} = \frac{\frac{\partial p(r)}{\partial r} (U^L - U^{NL})}{\lambda \cdot [p(r) \frac{\partial U^L}{\partial m} + (1 - p(r)) \frac{\partial U^{NL}}{\partial m}]} < 0 \quad (6)$$

Equation (6) shows that the marginal price for risk is equal to the difference in utility by the two states, weighted by the marginal probability of risk $\frac{\partial p(r)}{\partial r} (U^L - U^{NL})$ and divided by the expected marginal utility of income. As $m^L < m^{NL}$ such that $U^L > U^{NL}$, an increase in flood risk will have a negative price effect. This constitutes our first hypothesis.

A finding of no price differential between risky and safe zones could be due to a small difference between U^L and U^{NL} , which is the case if the uninsurable costs are small, or to consumers underestimating flood risk at the time when they purchase a house. In the absence of flooding, buyers can become insensitive to some environmental risk factors, even in the presence of certain insurance requirements (availability bias). The occurrence of a flood may lead to a revision of the subjective likelihood as information is available. Therefore, our second hypothesis states that the price differential should become larger for properties located in risky areas shortly after a flood has been observed.

Finally, note that if the uninsurable costs are simply too small to matter empirically, then we should see no effect after a flood either.

3 Data and empirical strategy

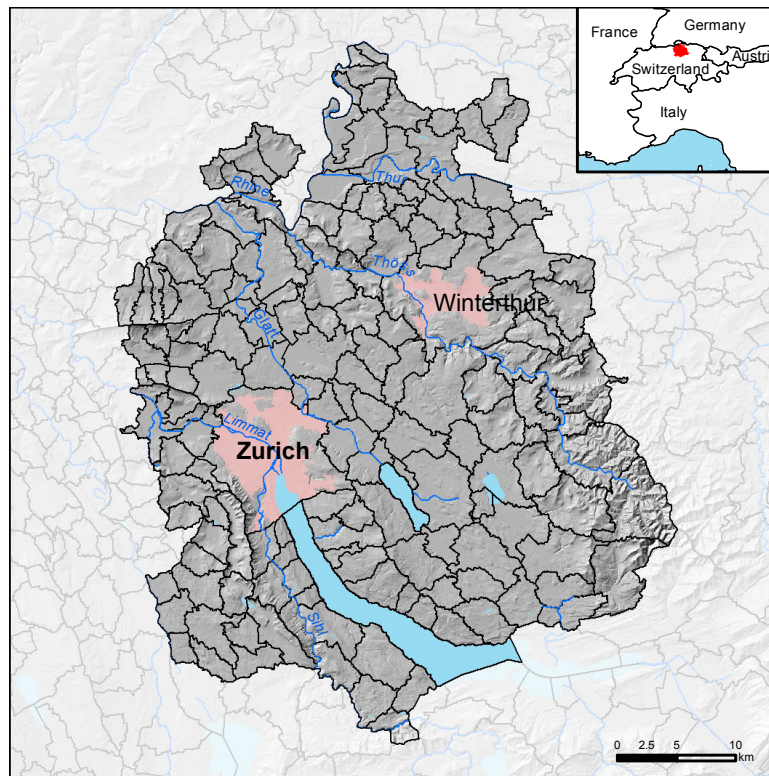
In this section, we provide some background information about the real estate market in the canton of Zurich and describe the data, before we present our empirical strategy.

3.1 Background

The canton of Zurich contains 168 political communities and a population of close to 1.5 million, which makes it the most populous canton in Switzerland. Due to its population and

the industrial concentration, it is one of the most important flood risk areas in terms of damages (Tages-Anzeiger, 2012). Figure 1 shows a map.

Figure 1: Overview of the Canton of Zrich



Notes: The overview presents the canton with the main cities Zurich & Winterthur. Map sources: SWISSTOPO (background map, reproduced by permission of SWISSTOPO)

The canton is characterized by its capital Zurich and its agglomeration, which occupies most of the canton. The largest body of water in the canton is the elongated Lake Zurich, and Greifensee and Pfaeffikersee are two other major lakes in the canton. The Tuerlersee, the Katzensee, the Luetzelsee and the Husemersee are smaller waters. Major rivers are Limmat, Sihl, Rhine, Glatt, Toess and Thur.³

All buildings in the canton with a value $> 5,000$ CHF have to be insured at the GVZ (“Gebaeudeversicherung Kanton Zurich”). Buildings are socially insured with the structure, the structural cover, the installations and the interior construction. Everyone pays the same price per building value independent of structural risk.⁴ In case of a damage, the GVZ covers

³The river Limmat leaves Zurich Lake in the city of Zurich, later uniting with the Reuss, the Aare river and with the Rhine. The Glatt, whose entire run is in the canton, drains the Glatt Valley and the Zurich Oberland and flows into the Rhine near Glattfelden in the Zurich Unterland. The Toess is also a mountain river, which rises in the Zurich Oberland and flows into the Rhine at the Tssegg. The Thur also flows through the canton of Zurich on the last few kilometers. The Sihl rises in the canton of Schwyz, flows through the Zurich Sihltal and flows into Zurich in the Limmat. The Reuss forms in the southwest a small section of the border to Aargau.

⁴In 2017, the insurance premium was CHF 0.32 cents (about USD 0.34) for every CHF 1,000 of the insurance value, which is an estimate of the cost to rebuild the house.

the cost of immediate and emergency measures and compensates for the effective demolition, clearing and disposal cost. Elementary damage by flooding as a result of rainfall (if water penetrates the building on the surface), avalanches, snow pressure and snowfall as well as rock fall and landslide are insured. The deductible is CHF 500 (see appendix 6 for more details) (Gebäudeversicherung Kanton Zurich (GVZ), 2017). For land properties within flood zones, there is no insurance.

Detailed flood maps indicating the precise location of each property and the respective flood hazard are available to residents. The flood maps are available online, and new homeowners are pointed towards them during the purchasing process (see section 3.2.2).

3.2 Data

For our empirical analysis, we use information about major floods, Geographic Information System data on housing and land prices, and tax data from the Zurich Statistical Office which we combine with data of hazard zones as well as insurance data from the GVZ. Our unique dataset contains data from 168 communities during 2007 - 2016.

3.2.1 Flood events

The Swiss flood and landslide damage database (BAFU, 2016) gives a detailed overview of the flood events between 2007 - 2016 and provides approximate aggregate damages (Table 1). We focus on the three biggest flood events in terms of caused damages during our sample period, which occurred in 2007, 2013⁵ and 2015. Since detailed data on monetary losses are confidential and not available, we rely on these aggregate data to quantify the size of the flood in terms of caused damage.

Include table 1 here

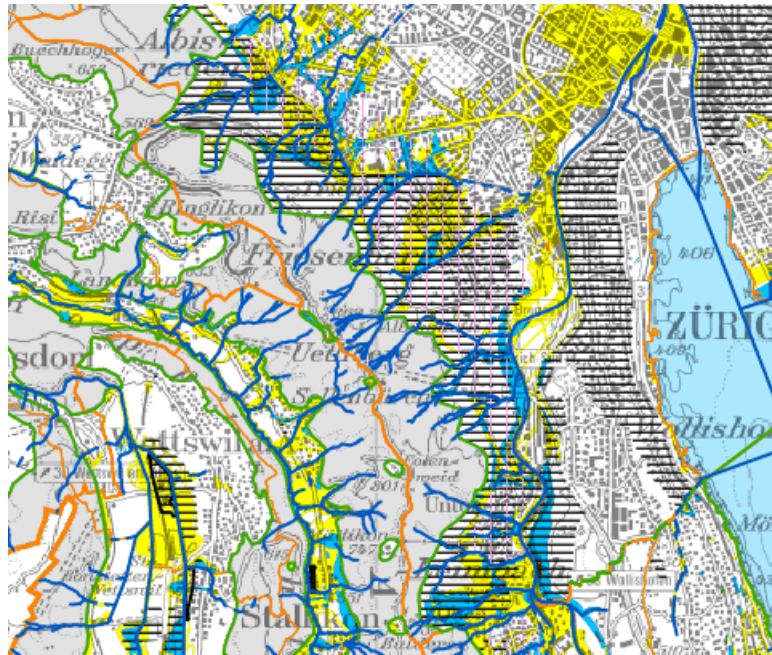
According to a report by the Federal Office for Water and Geology (BWG) and extrapolations by the Swiss Insurance Association concerning damage in the private sector, the damage to the buildings during the flooding of 2005 in June caused on average CHF 55,800 (Bundesamt fuer Wasser und Geologie (BWG), 2005).

⁵In 2013, two floods occurred on the second of May followed by a flash flood on the first of June. As both events are closely connected, we specify these two flood events by one event.

3.2.2 Hazard maps

In Switzerland, all municipalities are obliged to elaborate a hazard map. This hazard map classifies an examined area into five categories with respect to the magnitude and frequency of potential flood events (Fuchs et al., 2017). Red zones (high hazard) indicate areas where residents are at risk both inside and outside of buildings and sudden destruction of a building is possible upon impact with process-related forces. Blue zones (moderate hazard) indicate those areas where people are at risk outside of buildings and moderate destruction of buildings may be possible. Yellow zones (low hazard) delimit areas where flood hazard may lead to considerable monetary loss at buildings, but people are rarely at risk. Figure 2 illustrates the available hazard maps.

Figure 2: Online available hazard maps



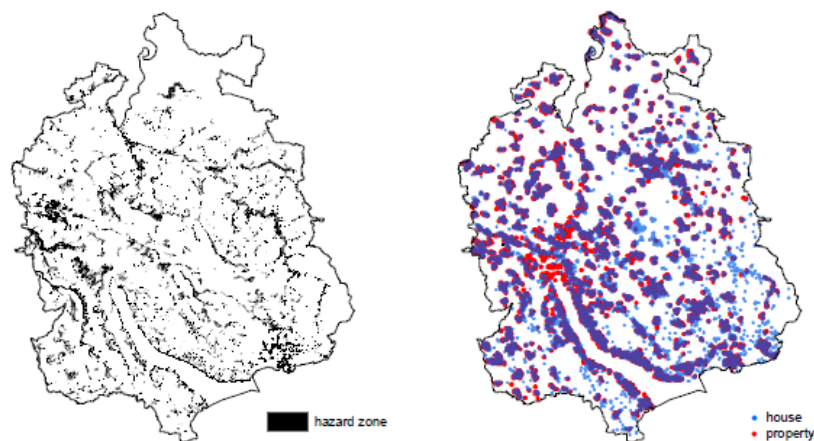
Notes: A map section of Zurich's hazard zones. Source: <http://maps.zh.ch>.

The main criteria for classification of the hazard is the flood intensity with thresholds at 0.5 m or $0.5 m^2/s$ (yellow and blue), between 0.5 m and 2.0 m or $0.5m^2/s$ and $2.0m^2/s$ (yellow and blue), or exceeding 2.0 m or $2.0 m^2/s$ (red). The probability of occurrence of the underlying flood hazard is used to further distinguish hazard zones for up to 30 year (blue and red), 30-100 year (yellow, blue and red) and 100 to 300 year (yellow and red) return periods. Areas within the investigation focus but without a potential hazard are colored as white. Areas susceptible to a residual risk are colored in yellow-white striped, i.e. areas in which the probability of

occurrence of a flood event is less than one in 300 years. The hazard maps were elaborated in a target scale of 1:2,000 to 1:10,000. Here, we focus on red, blue and yellow hazard zones since only one building is partially located in the red zone.

When implemented into the legally binding land use plan of the municipality, the hazard map becomes relevant for home- and landowners. The Guidelines for the Consideration of the Hydrological Hazards in Land-Use Planning Activities were approved in 1997 (BWW, BRP, and BUWAL, 1997). In red zones, the authorities are obliged to restrict any construction of new houses. Thus, land parcels within red zones cannot be sold with a value of land suitable for construction. Houses that are located in red zones before the implementation of the hazard map are not allowed to be extended. In blue zones, new houses are only permitted to be constructed if the owner guarantees to implement protection measures that prevent losses from flooding. Existing houses have to be adapted in case of a planned modification or extension. In yellow zones, the construction of critical buildings, e.g. schools and public buildings, is allowed only after a specific sensitivity analysis of the planned project (Kanton Zuerich, 2014).

Figure 3: Georeferenced overlay of real estate data and hazard maps



Notes: The map shows a combination of different datasets. Left: Map of hazard zones, map source: Canton of Zurich. Right: Location of the sold houses and land, map source: Canton of Zurich.

The attribution of the hazard to houses and land is done by georeferenced overlay (Fuchs et al., 2015; Röthlisberger et al., 2017). The houses are represented spatially by a point while the hazard zones are represented by polygons. Thus, the attribution of the hazard category to the houses can be done in two ways. The first is a direct attribution by the location of the point. This could underestimate the number of exposed buildings in the neighborhood of the

hazard zones, especially for large buildings. In a second way, we attributed the hazard zone to an auxiliary dataset of the building footprints, and consequently we used these categorized building footprints to attribute the hazard zone to the house represented by a point. Herein, the building footprint polygon act as a bridge for the information attribution (Zischg et al., 2013). In the latter approach, the situation in which a house is located with one edge in a flood zone but the centroid is located outside, is considered. For land, the hazard category with the highest share of the parcel's area is attributed (see figure 3).

The hazard maps are implemented continuously by the municipalities and by the canton. In the implementation process, there are two dates to consider. The first is the date when the hazard map has been elaborated and delivered to the municipality (further referred to as "elaboration date"). After this date, the information of the hazards is known by the authorities. The elaborated map is consequently implemented into the official land use plan (further referred to as "implementation date"). This process can take several months up to a few years. Thus, we attributed both dates to houses and land. The dates of elaboration and implementation were collected from the cantonal authorities in Switzerland (Bruchez, 2017).

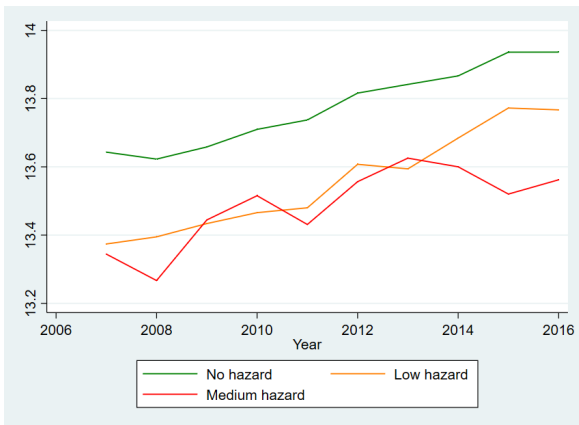
3.2.3 House prices and land prices

We use consistent geographic location data on housing and land prices for 2007 - 2016 provided by the Statistical Office Canton Zurich (2017b). The data contains information about the number of rooms, sales year, community, age of the building and the building zone. We convert the nominal prices to real prices using the CPI provided by the Federal Statistical Office (2017). We correct for outliers by excluding the bottom and top 5 % of transactions.

The DiD estimator requires a common trend for unbiased estimation. One way to (qualitatively) assess the validity of a non-risky group as a control is to visually compare the trends of housing and land prices in risky vs. non-risky zones. Figure 4 shows the annual price development by low, medium and no hazard group, as well as by hazard and no hazard group. The prices reflect annual average prices in real terms from 2007 - 2016 in the ninety-five percentile confidence interval without controlling for observables.

Figure (4a) suggests that there is no sharp differentiation between the low and medium hazard zones. Sample size might also play a role as we have only 330 observations in the

Figure 4: Housing price development



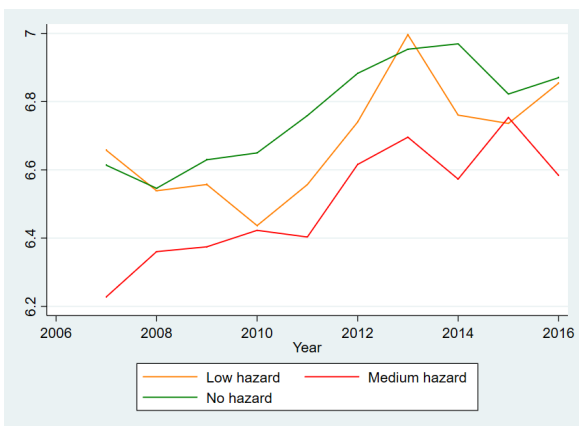
(a) Total ln real price development (ln) by low, medium and no hazard



(b) Total ln real price development (ln) by hazard and no hazard zone

medium hazard group and 1,173 in the low hazard group. We summarize the risky groups and use a hazard and no hazard group. Figure 4b shows that the price development of the risky zones is significantly below the no hazard zones following a roughly similar trend. We will control for further potential factors such that this lends support to the use of no hazard zones as a control group.

Figure 5: Land price development



(a) Total ln real price development (ln) by low, medium and no hazard



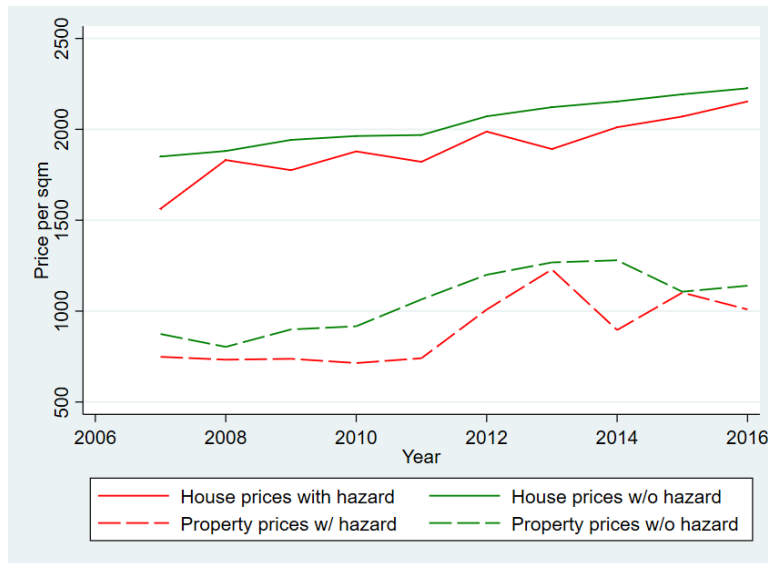
(b) Total ln real price development (ln) by hazard and no hazard zone

Concentrating on land values without controlling for observables, the pattern seems comparable to housing prices (see Figure 5). Figure 5a shows the yearly averages by the three hazard zones low, medium and no hazard. Risky zones sell on average for less than non-risky

zones, however, there is no clear distinction between low and medium hazard zones. Figure 5b indicates the yearly prices for hazard and no hazard zones. As for housing prices, there is a clear separation between no hazard and hazard zones.

Comparing house price and land price development (Figure 6), we see not only that land properties sell for less than houses, as would be expected, but also that land and house prices without hazard follow similar trends until 2015. In 2015, there was a sharp drop in land prices but housing prices remained stable.

Figure 6: Real house vs. land price per sqm development in CHF



The descriptive graphs show raw data without controlling for potential confounding factors. The framework described in section 3.3 controls for unobserved time-invariant differences across locations and unobserved time effects. For the analyses, the two datasets of the sold houses and land properties have been overlaid with auxiliary datasets. We have attributed the hazard category from the hazard maps and the date when the hazard map was produced and implemented into the legally binding land use plan.

3.2.4 Taxes

We use community-specific personal tax shifters provided by the Statistical Office Canton Zurich (2017a). These linear tax shifters are given in percent of the cantonal income tax schedule, which is progressive.

Figure (7) shows the average tax rate over all communities in the canton of Zurich. By 2011, there was a sharp downward trend overall communities and 2013, 35 of the 171 Zurich

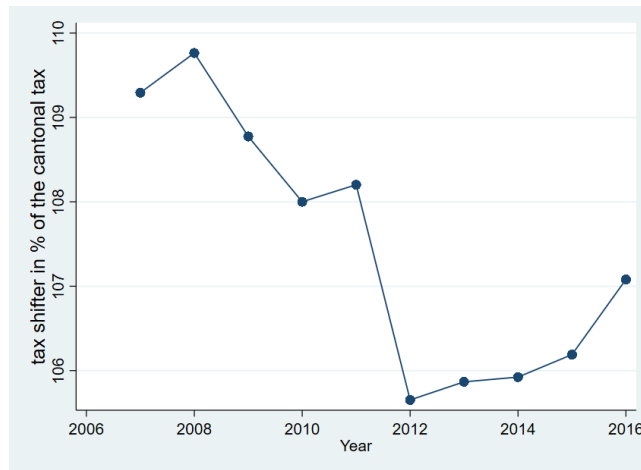


Figure 7: Average yearly tax shifter

municipalities cut their tax rate.

3.2.5 Insurance claims

There were 1,221 insurance claims as a result of the flood in August 2007, 458 of which were paid, with 240 claims above the long-term median (Gebäudeversicherung Kanton Zurich (GVZ), 2018). In the 2013, 329 claims were in May and June, 107 were paid and 54 claims were above the median. The flood of 2015 caused 722 notifications of claims, 443 were paid with 245 damages above the median.

In a future version of the paper, we will match our dataset with binary GVZ insurance claims (yes/no) and conduct a further DiD analysis of actually damaged buildings vs. risky buildings according to the hazard maps.

3.2.6 Additional controls

Daniel et al. (2009) argue that "previous studies often fail to adequately take into account the positive effect of a location close to the water and that the literature would benefit from alternative methodologies that better incorporate this confounding variable."

We will control for positive amenities as distance to water, the amount of sun per day, distance to the woods and distance to Zurich in the future. Calculations are currently running.

3.3 Empirical strategy

To investigate our main hypotheses, we use two different estimation strategies: A hedonic property price method, and a triple-difference analysis to compare housing and land prices.

3.3.1 DiD hedonic property price method

We apply a DiD hedonic price model and separately estimate the effect of flooding on housing and on land prices. Figure (4b) shows similar trends and adding the additional covariates in the regression, we argue that the control group is appropriate for calibrating flood risk premiums in property prices over time. The underlying identifying assumption is that the any confounding omitted variables affect both treatment and control groups similarly.

The treatment group is composed of housing or land sales in flood-prone areas during 2007 through 2016. The control group in the first estimation includes houses or land located outside of floodplains, i.e. without flood hazard. We use data of housing or land transactions before and after the floods for both flood-prone and non-flood-prone locations.

We control for time-invariant unobserved characteristics by including community fixed effects. The estimated equation for housing prices takes the following form:

$$\ln(P_{ijym}) = \beta_0 + \beta_1 \ln L_{jy} + \beta_2 S_{ik} + \beta_3 hazard_i + \beta_4 Flood_{iym} + \beta_5 hazard_i \times Flood_{iym} \quad (7) \\ + \delta_y + \phi_m + \lambda_j + \epsilon_{iym}$$

The dependent variable is the price per square meter of the sold property i , in community j , in the year y and month m . The independent variables are:

- neighborhood and location characteristics, L (community taxes)
- S_{ik} measures k different structural characteristics such as number of rooms, the actual size of the house, the defined building zone and the age of the building
- dummy variables to indicate the hazard zones: $hazard_i$
- $Flood_{iym}$ captures the effects of the flood: it is a dummy variable equal to 1 if the sale happened after the flood (2007 / 2013)

- δ_y year FE are included to capture annual shocks, potential business cycles and interest rate effects
- ϕ_m month FE capture seasonality
- λ_j are the community FE

Standard errors are clustered on the community level. β_3 represents systematic differences between flood-prone and other properties i.e. the possible difference between the treatment and control group before the flood events corresponding to hypothesis 1.

The coefficient related to hypothesis 2, β_5 , multiplies the interaction term $hazard_i \times Flood_{iytm}$, which is equivalent to a dummy equal to one for those observations in the treatment group (risky locations) after the flood, and zero otherwise. To see how we can interpret β_5 , we follow Wooldridge (2010) and define \bar{y}_{h1} as the sample average of the treatment group (hazard) before a flood (state 1) and \bar{y}_{h2} after the flood. \bar{y}_{nh1} is the sample average of the control group (no hazard) in state 1 and \bar{y}_{nh2} in state 2. The average treatment effect on the treated (ATT) can be expressed as:

$$\beta_5 = ATT = (\bar{y}_{h2}|X_{h2} - \bar{y}_{h1}|X_{h1}) - (\bar{y}_{nh2}|X_{nh2} - \bar{y}_{nh1}|X_{nh1}).$$

where X refers to the vector of control variables on which the outcome is conditioned. We compare the time change in means for treatment and control group such that group-specific and time-specific trends are allowed for (see Wooldridge, 2010).

This framework allows us to isolate the effect from the flood from other contemporaneous characteristics (e.g. local housing market changes, macroeconomic shocks), since the control group experiences some or all of the contemporaneous influences that affect land values in the treatment group but offers lower flood risk. The equation for land prices includes lot size and the building zone as the structural characteristics.

Unbiased estimation still requires that the floods are not systematically related to other factors which affect ϵ_{it} . No anticipation is required to identify average counterfactual pre-treatment outcomes. We follow Gallagher (2014) and assume that, conditional on a community's geography and time trends, whether or not a community is flooded in a particular year is random and households do not anticipate the specific timing of the event.

3.3.2 Difference-in-difference-in-differences (DDD) estimation

To compare housing and land prices, and to obtain a more robust analysis, we conduct a Difference-in-Difference-in-Differences (DDD) estimation in a further step. We use both, different states of houses (sold before vs. after the flood) and a control group within the treatment state i.e. risky land prices sold after respective floods. Our three-group comparison, where we build on (7) incorporating the DDD estimate, takes the following form:

$$\begin{aligned}
 \ln(P_{ijym}) = & \beta_0 + \beta_1 \ln L_{jy} + \beta_2 S_{ik} + \beta_3 \text{hazard}_i + \beta_4 \text{Flood}_{iym} \\
 & + \beta_5 \text{hazard}_i \times \text{Flood}_{iym} + \beta_6 \text{hazard}_i \times \text{Flood}_{iym} \times \text{House}_i \\
 & + \delta_y + \phi_m + \lambda_j + \epsilon_{iym}
 \end{aligned} \tag{8}$$

Here, House_i is a dummy variable equal to one if the transaction is a house and equal to 0, if it is a land transaction. S_{ik} measures the defined building zone and the size of the property.

β_6 is the estimator of the triple interaction term, the DDD estimate. We can not only learn more about the difference between land and housing prices, but potential bias resulting from a violation of the common trends assumption can be addressed by the use of a DDD estimator. If the trend of the differential is similar in states (in the absence of floods), β_6 is a stable estimate of the flood effect (see Figure 6 for comparison of raw data).

Again, we follow Wooldridge (2010) and label the two states as 1 and 2. The control group is labeled nh (no hazard) and the treatment group is defined by the subscript h (hazard). The superscript h denote houses and p properties such that the differential DATT can be express by (suppressing conditioning on the observable variables):

$$\beta_6 = DATT = [(\bar{y}_{h2}^h - \bar{y}_{h1}^h) - (\bar{y}_{h2}^p - \bar{y}_{h1}^p)] - [(\bar{y}_{nh2}^h - \bar{y}_{nh1}^h) - (\bar{y}_{nh2}^p - \bar{y}_{nh1}^p)]$$

The first term in brackets would be the usual DD estimator if we concentrate only on the "treated" (hazard) prices using sold land properties as the control group. The second term in brackets gives us an estimate of the differential state of the non-treated i.e. non-risky house and land prices, which acts as a further control group.

3.4 Summary statistics

Table 2 and 3 present the summary statistics of the used variables.

Include Tables 2 and 3 here

To elaborate on the time profile of the flood effect, we specify the flood effect to last for three, four, five and six months until forever. We think that the time span of three month after the flood is a good starting point, as a property transaction takes some time until it is completed.⁶

The variables not previously described are the hazard dummy *hz1*; *elaboration date*, which is a dummy equal to one if the date when the hazard map has been elaborated and delivered to the municipality is in the past; and *implementation date* is a dummy equal to 1 if the implementation date is in the past.

4 Results

We start by discussing the DiD estimation results for housing and land transactions, followed by the results from the DDD approach and the investigation of the implemented cantonal land use plan.

4.1 DiD estimation

We estimate equation (7) separately for houses and land. The no hazard-group serves as the reference group.

Include Table 4 here

The results in Table 4 show that "hazard" i.e. being located in a risky zone has a significant negative effect on housing prices in all specifications (0.01 % level). This confirms *Hypothesis 1* - houses located in areas at risk sell at a discount relative to houses without flood risk. Although the social insurance covers losses related to the building structure, the uninsurable cost negatively affects housing prices. Note that since this estimator is based on a simple

⁶If required, credits by banks have to be granted, and the transaction has to be attested by a notary.

difference, rather than DiD, it may be subject to omitted variable bias if unobserved house price determinants are correlated with flood zones. This means that the trust we place in this estimator depends on the extent to which we can control for the most important determinants of house prices. In a future version of this draft, we will include additional control variables to further increase the variation in house prices explained by our model.

Concentrating on the biggest flood 2007, the causal effect of the flood (the DiD estimator) is reflected in the interaction term of the flood 2007 and risky location (hazard). The effect of the flood has a significant negative effect on housing prices compared to living in a "safe" location, throughout all specifications (regressions 1 - 5). After three months, i.e. directly after the flood, the effect is the strongest. The coefficient of the DiD estimator is constantly decreasing over time, looking at the specifications four to six months (regression 2 - 4). The coefficient is almost zero and insignificant in the "flood effect lasting forever" specification. We interpret this as evidence for a persistent availability bias (*Hypothesis 2*).⁷ This decreasing pattern is also true for the flood of 2013, however, the effect is not significant. For the smallest (in terms of caused damage) flood 2015, the coefficients of the flood dummies are not significant neither. From the estimation results, we conclude that only the biggest flood 2007 was large enough to make home owners and buyers more sensitive to flood risks, and only for a very short time. This could indicate, that the size of the flood in terms of caused damage is in fact of consequence.

The negative effect and the pattern of the flood 2007 is partially in line with the literature (Bin and Landry, 2013; Atreya et al., 2013; Gallagher, 2014). However, the time horizon of studied events as well as the setting is very different. "Forgetting" related to house prices of large scale events in the US, i.e. hurricanes and related floods, takes from six (Bin and Landry, 2013) to eight years (Atreya et al., 2013) and up to nine years concerning insurance take up Gallagher (2014). The setting in Zurich is quite different. There exists the social insurance program and the floods are very unlike compared to the US flood events in terms of caused damage. It would be interesting to differentiate whether this short time profile of "forgetting" is attributable to the flood size, the social insurance or rather that the Swiss population is substantially different than the US population.

Structural characteristics s , namely how new a house is (the negative of age) and the number

⁷One critique might be that pre-trend observations are too small, however, the sample contains 1300 observations before the flood, which seem to be sufficient to capture the pre-trend.

of bedrooms have a positive influence on housing prices as predicted by equation (4). Housing prices are decreasing with size. The sign of the tax effect (5) is ambiguous. Community-specific taxes have a significant negative effect on housing prices, but once we include year and month FE, the influence is not significant anymore.

Table 5 presents the DiD estimation results for land prices. In contrast to housing prices, being located in a risky zone does not significantly negative affect land prices. We reject *Hypothesis 1* for land prices. At time when a land property is purchased, there is no insurance and obligatory protective measures are not required neither. If we assume that property buyers are rational (perfect foresight) and plan to build a house on the acquired land, there should be no difference in discounts on risky locations between land and house prices. One explanation could be, that land buyers imperfectly foresee the process of construction and the related flood risks at the time of the purchase.

Include Table 5 here

In addition to the result of housing prices, we conclude that the availability bias is at play (*Hypothesis 2*). Estimates of the DiD estimator show that the flood 2007 has a negative and significant effect on risky land prices compared to unrisky land. The effect of the flood is the biggest after 4 months and decreases steadily (Table 5, regressions 1 through 5).⁸ The effect is not temporary as the coefficient is not significant anymore (regression 5). It seems that land buyers forget about flood risk. The coefficients of the negative discount of the flood 2007 on risky land is larger compared to the discount on housing prices. This finding seems plausible, as land prices are not insured.

The floods 2013 and 2015 did not have a significant and negative effect on land prices. In contrast to the results for housing prices, the size of a land significantly increases the price. Taxes have no significant influence on land prices.

4.2 DDD estimation

The estimates from the DDD model are presented in Table 6. Estimation result for the DiD ($Hazard \times Flood_i$) are similar then in the estimations for housing and land prices. The flood

⁸Note that the marginal effect of hazard is given by the sum of all Flood 2007 coefficients.

of 2007 has a significant and negative effect on housing and land prices, with a decreasing coefficient the further in the past of the flood 2007 (regressions 2 - 5).

Include Table 6 here

The interaction term of $House \times Hazard \times Flood_i$ is the coefficient of the DDD estimator. The coefficient is positive and highly significant in the first specification, directly after the flood (three months). The differential effect of the flood 2007 between risky compared to non-risky houses and risky and non-risky land was less negative. Stated differently, the differential treatment effect for houses compared to land was less negative. Houses are socially insured whereas for land properties, there is no insurance, which might explain this effect. This difference is only true for three to four months after the flood and then vanishes.

The flood of 2013 does not have a more negative effect on risky real estate compared to locations without flood risk. However, houses in general were more negative affected than land properties, and the effect was permanent. In this DDD specification, the flood 2015 did not seem to have an influence on land and housing prices neither. Only the coefficient of the interaction of the long-lasting flood dummy and houses is significant and positive, which potentially measures a different time effect.

4.3 Effect of creating and implementing hazard maps

As described in section 3.2.2, our dataset contains the community-specific date when hazard maps were implemented into the legally binding land use plan of the municipality and became obligatory for remodeled and newly constructed houses (implementation date). In addition, there is an elaboration date indicating when hazard maps are available to communities and binding for community planning only.

To test for the effect of the binding land use plan, we run an OLS regression where the dependent variable is the property price and available property-specific controls are included. To see whether the implementation and elaboration has a differential effect on risky and non-risky housing prices, we include an interaction term of $hazard \times obligatory$ as well as $hazard \times elaboration$.

Table 7 shows how the elaborated and implemented land use plan influences housing prices.

Include Table 7 here

The negative discount on risky housing values is reduced, once the land use plan is implemented in a community (regression 1). This suggests that protective building regulations (i.e. obligatory building regulations based on the hazard level) have a positive influence on housing prices relative to the no hazard group.⁹ One explanation for this positive effect could be that protective measures of newly build houses are almost costless.¹⁰ Once implemented, they reduce the risk of suffering from flood damages reducing the negative price discount.

The coefficient of the elaboration date of the provided hazard maps per community is insignificant. From regression 2, we conclude that mere elaboration of the official land use plan of the hazard map is not of consequence for the valuation of real estate in Switzerland.

The pattern for land prices is similar. Obligatory building restrictions have a positive and significant influence on housing prices (regression 1).

Include Table 8 here

Note that the total effect of implementation is the sum of both terms (the interaction term and the single term). The elaboration date is not significant neither (regression 2). The results indicate, that only once protective measures are obligatory, they will affect housing and land prices.

4.4 Robustness checks

Auto-correlation: We test for auto-correlated errors. We have performed the general specification test of serial correlation in a time series proposed by Cumby and Huizinga (Cumby and Huizinga, 1990).

⁹Remember that in high hazard zones (red), construction is entirely prohibited and in medium zones, new houses can only be constructed if their constructor guarantees to implement protection measures. Low hazard zones have to declare that they are well aware of the respective hazard, however, protection is voluntary (Kanton Zuerich, 2014).

¹⁰Housing protection measures include structural changes to the house, so that a certain water level, e.g. 0.5 m leads to no damage. This is e.g. sealing the building envelope, sealing windows and doors, increasing light wells in front of basement windows, installing electrical installations in the upper floor instead of in the waier, hanging down oil tanks so that they do not float up (which was already paid in the house purchase price). In new buildings, property protection can be planned in advance which eliminates the additional material cost. Architect are free from existing configurations and rarely needs special solutions. The same level of security per property protection is therefore much cheaper for a new building.

The null hypothesis of the test is that the time series is a moving average of known order q , which could be zero or a positive value. The test is general enough to test the hypothesis that the time series has no serial correlation ($q = 0$). The test considers the general alternative that auto-correlations of the time series are nonzero at lags greater than q .

(Cumby and Huizinga, 1990).

Include Table 9 here

We do not detect auto-correlated errors. Autocorrelation is not present at any lag orders (up to the six lags tested). Thus, we do not account for auto-correlation.

Other events: Between 2007 and 2017, several referenda took place. In September 2014, there was a cantonal referendum on the submission of planning and building law. Residents had to decide whether there should be a minimum share of reasonably priced housing. The referendum was accepted and municipalities should reserved a minimum proportion of specified building zones for low-cost apartments. We include a dummy which is one if the transaction took place after the referendum. The effect is not significant and does not change our results.

Attribution of hazard map: We have tried different forms of attribution of hazard maps to house and land transaction points. As a robustness check we have assigned the classification of the danger level to the point via a building polygon. If the point is in a building that is somehow affected by a danger level, but the point itself is just outside the zone, it is still classified as risky. Using this classification did not change the robustness of the results. Our primary estimation uses the exact danger level of the georeferenced points.

5 Conclusion

The cantonal government of Zurich government decided in 2017 to implement a new project against extreme flooding of the river Sihl which is expected to cost around 130 million CHF and would be completed in 2023 at the earliest (Amt fuer Abfall, Wasser, Energie und Luft, 2017). Without such adaptation investments, the number of people at risk due to flooding will increase dramatically the next 25 years (Willner et al., 2018). The estimates of our study provide valuable information necessary in the context of cost-benefit analyses of public investments in

flood protection measures or of mandatory insurance schemes, in which the price depends on the hazard rate.

The negative effect of disastrous hurricanes and floods on housing prices in the US is well established (Bartosova et al., 2000; Shilling et al., 1985; MacDonald et al., 1987; Donnelly, 1989; MacDonald et al., 1990; Speyrer and Ragas, 1991; Harrison et al., 2001; Bin and Polasky, 2004; Bin and Kruse, 2006; Bin et al., 2008; Atreya et al., 2013). In the US, insurance for the most risky flood zones is mandatory, which could explain the negative effect. However, less is known about a setting where socialized building insurance exist. Our results suggest, that houses within a flood zone sell on average for less than houses outside a flood zone, even though social insurance exists. However, this seems not to be the case for land. One explanation could be, that land buyers imperfectly foresee the construction process of houses and relevant flood risks, when they buy land.

We find that the discount on houses and land within a flood zone is increasing directly after the flood 2007 (three months) and steadily declines in magnitude back to baseline. We interpret this as evidence for an persistent availability bias. The DDD estimator confirms the robustness of the result and demonstrates that land and housing prices react differently to floods. The differential effect of the flood 2007 on risky vs. unrisky properties, was less negative for houses. This could be attributable to the social building insurance for houses.

Exploring the influence of the cantonal land use plan, we find that the negative discount on housing as well as land prices is reduced, once implemented. We conclude that the cantonal intervention of obligatory protective measures can reduce the negative effect of being located in a flood zone.

Comparing the different floods, it seems that the specific characteristic of the flood matters. Only the biggest flood of 2007 has an overall influence on land and housing prices. There remains work to be done assessing detailed geological characteristics of river floods and the link to housing and land prices. What is the critical threshold in terms of damages, such that a flood is of consequence for real estate prices? In addition, "forgetting" of past flood events is rather fast, compared to tremendous hurricanes in the US. It would be a fruitful task for future research to investigate whether social building insurance alone can explain this fast and persistent availability bias.

Acknowledgments

The authors want to thank the Canton of Zurich for providing the data on property prices, the public insurance company of the Canton of Zurich for providing the location of losses on houses, the Federal Institute for Forest, Snow and Avalanche Research for providing the data on damaging natural hazards events, the Federal Office for Topography SwissTopo for providing basic GIS data, and the Swiss Mobiliar for the harmonization of hazard maps over Switzerland. Suggestions of Ulrich Wagner improved the paper.

References

- Amt fuer Abfall, Wasser, Energie und Luft (2017). Hochwasserschutz an Sihl, Zuerichsee und Limmat: Gefaehrung und Massnahmen im Ueberblick. Technical report, Kanton Zuerich Baudirektion.
- Atreya, A., S. Ferreira, and W. Kriesel (2013). Forgetting the flood? An analysis of the flood risk discount over time. *Land Economics* 89(4), 577–596.
- BAFU (2016). Unwetterschadens-datenbank wsl.
- Bakkensen, L. and L. Barrage (2017). Heterogeneous climate beliefs and U.S. home price dynamics: Going under water? *Working paper*.
- Bartosova, A., D. E. Clark, V. Novotny, and K. S. Taylor (2000). Using GIS to evaluate the effects of flood risk on residential property values.
- Belanger, P. and M. Bourdeau-Brien (2017). The impact of flood risk on the price of residential properties: The case of England. *Housing Studies* 0(0), 1–26.
- Bernknopf, R. L., D. S. Brookshire, and M. A. Thayer (1990). Earthquake and volcano hazard notices: An economic evaluation of changes in risk perceptions. *Journal of Environmental Economics and Management* 18(1), 35–49.
- Beron, K. J., J. C. Murdoch, M. A. Thayer, and W. P. Vijverberg (1997). An analysis of the housing market before and after the 1989 Loma Prieta earthquake. *Land Economics*, 101–113.

- Billings, S. B. and K. T. Schnepel (2017). The value of a healthy home: Lead paint remediation and housing values. *Journal of Public Economics* 153(Supplement C), 69 – 81.
- Bin, O. and J. B. Kruse (2006). Real estate market response to coastal flood hazards. *Natural Hazards Review* 7(4), 137–144.
- Bin, O., J. B. Kruse, and C. E. Landry (2008). Flood hazards, insurance rates, and amenities: Evidence from the coastal housing market. *Journal of Risk and Insurance* 75(1), 63–82.
- Bin, O. and C. E. Landry (2013). Changes in implicit flood risk premiums: Empirical evidence from the housing market. *Journal of Environmental Economics and management* 65(3), 361–376.
- Bin, O. and S. Polasky (2004). Effects of flood hazards on property values: evidence before and after hurricane floyd. *Land Economics* 80(4), 490–500.
- Boyle, M. and K. Kiel (2001). A survey of house price hedonic studies of the impact of environmental externalities. *Journal of real estate literature* 9(2), 117–144.
- Brookshire, D. S., M. A. Thayer, J. Tschirhart, and W. D. Schulze (1985). A test of the expected utility model: Evidence from earthquake risks. *Journal of political economy* 93(2), 369–389.
- Bruchez, L. (2017). Effet des cartes de danger de crues sur la construction de nouveaux btiments dhabitation dans les communes de suisse. Master’s thesis, Master thesis at the Institute of Geography, University of Bern, Switzerland.
- Bubeck, P., W. J. W. Botzen, and J. C. J. H. Aerts (2012). A review of risk perceptions and other factors that influence flood mitigation behavior. *Risk Analysis* 32(9), 1481–1495.
- Bundesamt fuer Wasser und Geologie (BWG) (2005). Bericht ber die hochwasserereignisse 2005. Technical report.
- Burningham, K., J. Fielding, and D. Thrush (2008). it’ll never happen to me: understanding public awareness of local flood risk. *Disasters* 32(2), 216–238.

- BWW, BRP, and BUWAL (1997). Beruecksichtigung der hochwassergefahren bei raumwirk-samen taetigkeiten. Technical report, Biel und Bern: Bundesamt fr Wasserwirtschaft, Bun-desamt fr Raumplanung, Bundesamt fuer Umwelt, Wald und Landschaft.
- Chay, K. Y. and M. Greenstone (2005). Does air quality matter? evidence from the housing market. *Journal of political Economy* 113(2), 376–424.
- Cumby, R. E. and J. Huizinga (1990). Testing the autocorrelation structure of disturbances in ordinary least squares and instrumental variables regressions.
- Daniel, V. E., R. J. Florax, and P. Rietveld (2009). Flooding risk and housing values: An economic assessment of environmental hazard. *Ecological Economics* 69(2), 355–365.
- Davis, L. W. (2004). The effect of health risk on housing values: Evidence from a cancer cluster. *The American Economic Review* 94(5), 1693–1704.
- Donnelly, W. A. (1989). Hedonic price analysis of the effect of a floodplain on property values. *JAWRA Journal of the American Water Resources Association* 25(3), 581–586.
- Federal Statistical Office (2017). Swiss consumer price index in september 2017. Technical report, Federal Statistical Office.
- Fuchs, S., M. Keiler, and A. Zischg (2015). A spatiotemporal multi-hazard exposure assessment based on property data. *Natural Hazards and Earth System Sciences* 15(9), 2127–2142.
- Fuchs, S., V. Röthlisberger, T. Thaler, A. Zischg, and M. Keiler (2017). Natural hazard man-agement from a coevolutionary perspective: Exposure and policy response in the european alps. *Annals of the American Association of Geographers* 107(2), 382–392.
- Gallagher, J. (2014). Learning about an infrequent event: evidence from flood insurance take-up in the united states. *American Economic Journal: Applied Economics* 6(3), 206–233.
- Gayer, T., J. T. Hamilton, and W. K. Viscusi (2000). Private values of risk tradeoffs at superfund sites: housing market evidence on learning about risk. *The Review of Economics and Statistics* 82(3), 439–451.
- Gebaeudeversicherung Kanton Zurich (GVZ) (2018). Ueberschwemmungsschaeden der gvz vom 01.01.2006 bis zum 31.12.2016. Requested and received by the authors.

- Gebäudeversicherung Kanton Zurich (GVZ) (2017). Kundeninformation januar 2014.
- Hallstrom, D. G. and V. K. Smith (2005). Market responses to hurricanes. *Journal of Environmental Economics and Management* 50(3), 541–561.
- Harrison, D., G. T. Smersh, and A. Schwartz (2001). Environmental determinants of housing prices: the impact of flood zone status. *Journal of Real Estate Research* 21(1-2), 3–20.
- Hilker, N., A. Badoux, and C. Hegg (2009). The swiss flood and landslide damage database 1972-2007. *Natural Hazards and Earth System Sciences* 9(3), 913.
- Kahneman, D., P. Slovic, A. Tversky, et al. (1982). *Judgment under uncertainty*. Cambridge, UK: Cambridge University Press.
- Kanton Zuerich (2014). Gefahrenkarte kanton zrich lesehilfe. Technical report, Zuerich.
- Kellens, W., T. Terpstra, and P. De Maeyer (2013). Perception and communication of flood risks: A systematic review of empirical research. *Risk Analysis* 33(1), 24–49.
- Lamond, J. and D. Proverbs (2008). Flood insurance in the uk: a survey of the experience of floodplain residents.
- Lamond, J., D. Proverbs, and F. Hammond (2010). The impact of flooding on the price of residential property: A transactional analysis of the uk market. *Housing studies* 25(3), 335–356.
- Leggett, C. G. and N. E. Bockstael (2000). Evidence of the effects of water quality on residential land prices. *Journal of Environmental Economics and Management* 39(2), 121–144.
- Luo, T., A. Maddocks, C. Iceland, P. Ward, and H. Winsemius (2015). Worlds 15 countries with the most people exposed to river floods. *World Resources Institute*.
- MacDonald, D. N., J. C. Murdoch, and H. L. White (1987). Uncertain hazards, insurance, and consumer choice: evidence from housing markets. *Land Economics* 63(4), 361–371.
- MacDonald, D. N., H. L. White, P. M. Taube, and W. L. Huth (1990). Flood hazard pricing and insurance premium differentials: evidence from the housing market. *Journal of Risk and Insurance*, 654–663.

- Rosen, S. (1974). Hedonic prices and implicit markets: product differentiation in pure competition. *Journal of political economy* 82(1), 34–55.
- Röthlisberger, V., A. P. Zischg, and M. Keiler (2017). Identifying spatial clusters of flood exposure to support decision making in risk management. *Science of the total environment* 598, 593–603.
- Röthlisberger, V. E., A. P. Zischg, and M. Keiler (2016). Spatiotemporal aspects of flood exposure in switzerland. In *E3S Web of Conferences*, Volume 7. EDP Sciences.
- Shilling, J. D., J. D. Benjamin, and C. Sirmans (1985). Adjusting comparable sales for floodplain location. *The Appraisal Journal* 53(3), 429–436.
- Speyrer, J. F. and W. R. Ragas (1991). Housing prices and flood risk: an examination using spline regression. *The Journal of Real Estate Finance and Economics* 4(4), 395–407.
- Statistical Office Canton Zurich (2017a). Gemeindesteuerfuesse.
- Statistical Office Canton Zurich (2017b). Prices for residential land canton of zurich. Technical report, Statistical Office Canton Zurich.
- Tages-Anzeiger (2012, July). Stadt zrich ist eines der groessten risikogebiete der schweiz.
- Willner, S. N., A. Levermann, F. Zhao, and K. Frieler (2018). Adaptation required to preserve future high-end river flood risk at present levels. *Science advances* 4(1), eaao1914.
- Wooldridge, J. M. (2010). *Econometric analysis of cross section and panel data*. MIT press.
- Zischg, A., S. Schober, N. Sereinig, M. Rauter, C. Seymann, F. Goldschmidt, R. Bäk, and E. Schleicher (2013). Monitoring the temporal development of natural hazard risks as a basis indicator for climate change adaptation. *Natural hazards* 67(3), 1045–1058.

6 Tables and estimation results

Table 1: Floods in Zurich 2007 - 2016

	Name Date	Total damage in Mio CHF from Water	Total damage in Mio CHF from landslide	TOTAL
7.47	09.08.2007	10.78	0.12	10.9
2008.23	10.06.2008	1.85		1.85
2011.48	27.07.2011	1.91		1.91
2012.49	03.07.2012	1.75	0.01	1.76
2013.51	02.05.2013	5.75		5.75
2013.65	01.06.2013	0.74	1.45	2.19
2014.051	12.07.2014	1.04	0.04	1.08
2014.065	28.07.2014	0.51	0.16	0.67
2015.37	07.06.2015	8.34	0.02	8.36

Table 2: Summary statistics housing prices

<i>n</i> = 22270	mean	sd	min	max
lnprice_real	7.510	0.701	0.440	10.437
<i>Flood effect:</i>				
F07_forever	0.942	0.235	0.000	1.000
F07_3months	0.024	0.153	0.000	1.000
F07_4months	0.031	0.174	0.000	1.000
F07_5months	0.038	0.192	0.000	1.000
F07_6months	0.043	0.204	0.000	1.000
F13_forever	0.356	0.479	0.000	1.000
F13_3months	0.029	0.169	0.000	1.000
F13_4months	0.038	0.191	0.000	1.000
F13_5months	0.047	0.211	0.000	1.000
F13_6months	0.053	0.225	0.000	1.000
F15_forever	0.155	0.362	0.000	1.000
F15_3months	0.024	0.154	0.000	1.000
F15_4months	0.033	0.178	0.000	1.000
F15_5months	0.041	0.199	0.000	1.000
F15_6months	0.050	0.218	0.000	1.000
<i>Hazard:</i>				
hz1	0.055	0.228	0.000	1.000
<i>related Dates:</i>				
elaboration date	0.411	0.492	0.000	1.000
implementation date	0.964	0.187	0.000	1.000
<i>Housing Controls:</i>				
ln_tax	4.668	0.139	4.277	4.898
rooms	5.063	1.591	0.000	45.000
age	59.056	60.242	0.000	752.000
ln_size	6.252	0.698	3.466	12.823
zone	2.275	2.608	0.000	11.000
<i>Fixed effects:</i>				
community	148.947	79.951	1.000	298.000
month	6.675	3.332	1.000	12.000
year	2011.452	2.850	2007.000	2016.000

Table 3: Summary statistics Property prices

$n = 6588$	mean	sd	min	max
lnprice_real	6.701	0.568	5.838	8.411
<i>Flood effect:</i>				
F07_forever	0.915	0.279	0.000	1.000
F07_3months	0.033	0.178	0.000	1.000
F07_4months	0.042	0.200	0.000	1.000
F07_5months	0.055	0.229	0.000	1.000
F07_6months	0.067	0.250	0.000	1.000
F13_forever	0.199	0.399	0.000	1.000
F13_3months	0.022	0.146	0.000	1.000
F13_4months	0.027	0.161	0.000	1.000
F13_5months	0.031	0.172	0.000	1.000
F13_6months	0.036	0.187	0.000	1.000
F15_forever	0.076	0.264	0.000	1.000
F15_3months	0.015	0.121	0.000	1.000
F15_4months	0.021	0.142	0.000	1.000
F15_5months	0.024	0.152	0.000	1.000
F15_6months	0.027	0.162	0.000	1.000
<i>Hazard:</i>				
hz1	0.083	0.277	0.000	1.000
<i>related Dates:</i>				
elaboration date	0.355	0.479	0.000	1.000
implementation date	0.961	0.193	0.000	1.000
<i>Controls:</i>				
lntax	4.676	0.141	4.277	4.898
valid_land	0.928	0.405	0.000	6.000
lnsize	6.187	1.295	0.000	10.345
c_zone	2.693	2.948	1.000	11.000
<i>Fixed effects:</i>				
community	136	77.795	1	298
month	6.56	3.442	1	12
year	2010	2.595	2007	2016

Table 4: The effect of flooding on housing prices after 3, 4, 5, 6 months until forever

	(1)			(2)			(3)			(4)			(5)		
	<i>Dependent variable: LN-Price (real) in sqm</i>														
	3 months			4 months			5 months			6 months			forever		
	Coef.	Std. err.	p	Coef.	Std. err.	p	Coef.	Std. err.	p	Coef.	Std. err.	p	Coef.	Std. err.	p
Hazard	-0.044***	0.014	0.0020	-0.041***	0.014	0.0035	-0.044***	0.015	0.0030	-0.047***	0.015	0.0015	-0.051	0.061	0.4054
F 07	0.039*	0.020	0.0556	0.032*	0.018	0.0713	0.012	0.019	0.5296	0.007	0.017	0.6782	0.005	0.019	0.7821
Hazard # F 07	-0.149***	0.048	0.0021	-0.139**	0.057	0.0157	-0.116**	0.052	0.0280	-0.081*	0.045	0.0718	-0.007	0.057	0.8969
F 13	0.017	0.017	0.3228	0.015	0.016	0.3276	0.003	0.015	0.8237	-0.003	0.015	0.8381	0.004	0.017	0.8256
Hazard # F 13	-0.087	0.068	0.1990	-0.081	0.061	0.1850	-0.050	0.047	0.2901	-0.027	0.053	0.6194	-0.003	0.032	0.9245
F 15	0.015	0.016	0.3506	0.033**	0.015	0.0304	0.022	0.015	0.1445	0.014	0.015	0.3446	0.002	0.015	0.8753
Hazard # F 15	0.080	0.080	0.3189	0.026	0.073	0.7257	0.075	0.059	0.2012	0.085	0.054	0.1156	0.069**	0.032	0.0305
Intax	0.002	0.127	0.9896	0.004	0.127	0.9724	0.006	0.126	0.9629	0.008	0.126	0.9517	0.003	0.127	0.9784
Rooms	0.062***	0.006	0.0000	0.062***	0.006	0.0000	0.062***	0.006	0.0000	0.062***	0.006	0.0000	0.062***	0.006	0.0000
age	-0.002***	0.000	0.0000	-0.002***	0.000	0.0000	-0.002***	0.000	0.0000	-0.002***	0.000	0.0000	-0.002***	0.000	0.0000
LN Total size	-0.685***	0.013	0.0000	-0.685***	0.013	0.0000	-0.684***	0.013	0.0000	-0.684***	0.013	0.0000	-0.684***	0.013	0.0000
Constant	11.473***	0.610	0.0000	11.456***	0.610	0.0000	11.453***	0.610	0.0000	11.447***	0.610	0.0000	11.467***	0.612	0.0000
<i>Community FE</i>	<i>Yes</i>			<i>Yes</i>			<i>Yes</i>			<i>Yes</i>			<i>Yes</i>		
<i>Months FE</i>	<i>Yes</i>			<i>Yes</i>			<i>Yes</i>			<i>Yes</i>			<i>Yes</i>		
<i>Year FE</i>	<i>Yes</i>			<i>Yes</i>			<i>Yes</i>			<i>Yes</i>			<i>Yes</i>		
<i>R</i> ²	0.7546			0.7546			0.7546			0.7546			0.7545		
<i>N</i>	20652			20652			20652			20652			20652		

Note: * $p < 0.1$, ** $p < 0.05$, *** $p < 0.01$. We controll for the different type of building zones as well. Standard errors are clustered on the community level.

Table 5: The effect of flooding on land prices after 3, 4, 5, 6 months until forever

	(1)			(2)			(3)			(4)			(5)												
	<i>Dependent variable: LN-Price (real) land in sqm</i>									3 months			4 months			5 months			6 months			forever			
	Coef.	Std. err.	p	Coef.	Std. err.	p	Coef.	Std. err.	p	Coef.	Std. err.	p	Coef.	Std. err.	p	Coef.	Std. err.	p	Coef.	Std. err.	p	Coef.	Std. err.	p	
Hazard	-0.017	0.021	0.4242	-0.016	0.022	0.4835	-0.016	0.022	0.4636	-0.016	0.021	0.4622	-0.005	0.050	0.9149										
Flood 07	-0.028	0.034	0.4068	-0.035	0.036	0.3420	-0.033	0.036	0.3498	-0.024	0.028	0.3893	-0.045	0.034	0.1816										
Hazard # Flood 07	-0.229*	0.118	0.0536	-0.241**	0.095	0.0127	-0.201**	0.082	0.0157	-0.189*	0.097	0.0534	-0.017	0.049	0.7284										
Flood 13	0.049	0.048	0.3042	0.063	0.043	0.1422	0.047	0.041	0.2597	0.004	0.039	0.9222	-0.002	0.044	0.9552										
Hazard # Flood 13	0.092	0.102	0.3668	0.039	0.073	0.5968	0.066	0.074	0.3708	0.069	0.062	0.2631	-0.005	0.060	0.9354										
Flood 15	-0.026	0.048	0.5910	-0.040	0.044	0.3649	-0.057	0.041	0.1661	-0.013	0.041	0.7609	-0.021	0.047	0.6544										
Hazard # Flood 15	0.086	0.142	0.5448	0.091	0.134	0.5006	0.080	0.116	0.4918	0.064	0.117	0.5869	0.036	0.067	0.5945										
Intax	0.326	0.231	0.1599	0.321	0.231	0.1669	0.327	0.231	0.1585	0.324	0.232	0.1646	0.330	0.231	0.1544										
LN Total size	0.045***	0.008	0.0000	0.045***	0.008	0.0000	0.045***	0.008	0.0000	0.045***	0.007	0.0000	0.045***	0.008	0.0000										
Constant	5.069***	1.081	0.0000	5.100***	1.081	0.0000	5.072***	1.080	0.0000	5.087***	1.085	0.0000	5.055***	1.079	0.0000										
<i>Community FE</i>	<i>Yes</i>			<i>Yes</i>			<i>Yes</i>		<i>Yes</i>		<i>Yes</i>		<i>Yes</i>												
<i>Months FE</i>	<i>Yes</i>			<i>Yes</i>			<i>Yes</i>		<i>Yes</i>		<i>Yes</i>		<i>Yes</i>												
<i>Year FE</i>	<i>Yes</i>			<i>Yes</i>			<i>Yes</i>		<i>Yes</i>		<i>Yes</i>		<i>Yes</i>												
R2		0.6281			0.6283			0.6284			0.6282				0.6278										
N		6588			6588			6588			6588				6588										

Note: * $p < 0.1$, ** $p < 0.05$, *** $p < 0.01$. We controll for the different type of bulding zones as well. Standard errors are clustered on the community level.

Table 6: DDD estimation results

	(1)			(2)			(3)			(4)			(5)		
	<i>Dependent variable: LN-Price (real) in sqm</i>														
	3 months			4 months			5 months			6 months			forever		
	Coef.	Std. err.	p	Coef.	Std. err.	p	Coef.	Std. err.	p	Coef.	Std. err.	p	Coef.	Std. err.	p
House	0.960***	0.032	0.0000	0.962***	0.032	0.0000	0.961***	0.033	0.0000	0.962***	0.033	0.0000	0.961***	0.046	0.0000
Hazard	-0.063	0.042	0.1385	-0.069	0.044	0.1182	-0.072	0.045	0.1053	-0.075*	0.044	0.0931	0.033	0.084	0.6946
House # Hazard	0.039	0.045	0.3903	0.047	0.046	0.3070	0.047	0.047	0.3162	0.048	0.047	0.3126	-0.130	0.141	0.3562
Flood 07	0.008	0.045	0.8674	0.032	0.041	0.4427	0.002	0.037	0.9510	0.009	0.033	0.7947	-0.011	0.040	0.7858
House # Flood 07	0.023	0.051	0.6545	0.009	0.052	0.8682	0.019	0.047	0.6810	0.010	0.046	0.8241	0.023	0.039	0.5552
Hazard # Flood 07	-0.525***	0.176	0.0032	-0.390**	0.179	0.0302	-0.271*	0.163	0.0995	-0.267*	0.145	0.0674	-0.105	0.102	0.3057
House # Hazard # Flood 07	0.461**	0.188	0.0151	0.324*	0.191	0.0919	0.203	0.182	0.2653	0.212	0.159	0.1848	0.159	0.155	0.3054
Flood 13	0.187**	0.089	0.0369	0.188**	0.074	0.0122	0.079	0.076	0.3023	0.045	0.063	0.4814	0.083*	0.044	0.0586
House # Flood 13	-0.205**	0.085	0.0177	-0.213***	0.072	0.0037	-0.149*	0.077	0.0525	-0.121*	0.064	0.0608	-0.159***	0.035	0.0000
Hazard # Flood 13	-0.227	0.316	0.4731	-0.085	0.240	0.7229	-0.005	0.224	0.9813	0.101	0.193	0.6012	0.019	0.128	0.8828
House # Hazard # Flood 13	0.107	0.332	0.7481	0.001	0.260	0.9975	-0.033	0.242	0.8905	-0.127	0.212	0.5496	0.038	0.138	0.7864
Flood 15	0.000	0.087	1.0000	0.017	0.070	0.8058	0.029	0.064	0.6479	0.061	0.058	0.3009	-0.095*	0.057	0.0971
House # Flood 15	-0.003	0.089	0.9772	-0.008	0.070	0.9121	-0.029	0.064	0.6470	-0.054	0.059	0.3637	0.111**	0.055	0.0457
Hazard # Flood 15	-0.285	0.329	0.3883	-0.086	0.227	0.7047	-0.086	0.206	0.6752	-0.117	0.191	0.5425	-0.239	0.179	0.1847
House # Hazard # Flood 15	0.276	0.332	0.4066	0.022	0.231	0.9249	0.100	0.204	0.6259	0.155	0.188	0.4096	0.216	0.178	0.2264
Constant	6.463***	0.855	0.0000	6.456***	0.855	0.0000	6.452***	0.856	0.0000	6.447***	0.855	0.0000	6.422***	0.854	0.0000
<i>Community FE</i>	<i>Yes</i>			<i>Yes</i>				<i>Yes</i>						<i>Yes</i>	
<i>Months FE</i>	<i>Yes</i>			<i>Yes</i>				<i>Yes</i>						<i>Yes</i>	
<i>Year FE</i>	<i>Yes</i>			<i>Yes</i>				<i>Yes</i>						<i>Yes</i>	
<i>R</i> ²	0.5552			0.5552				0.5550						0.5551	
<i>N</i>	28721			28721				28721						28721	

Note: * $p < 0.1$, ** $p < 0.05$, *** $p < 0.01$. We control for the different type of bulding zones, taxes and size as well. Standard errors are clustered on the community level.

Table 7: Obligatory hazard map compliance, House prices

<i>Dependent Variable : LN-Price (real) in sqm</i>						
	(1)			(2)		
	Coef.	Std. err.	p	Coef.	Std. err.	p
Hazard	-0.070***	0.005	0.0000	-0.047***	0.016	0.0031
Implementation	0.052***	0.017	0.0020			
Hazard # implementation	0.028*	0.016	0.0847			
Elaboration				0.016	0.012	0.1696
Hazard # Elaboration				0.007	0.022	0.7424
Constant	10.936***	0.614	0.0000	10.946***	0.618	0.0000
R2	0.6578			0.6578		
N	18733			18733		
<i>Community FE</i>		<i>Yes</i>			<i>Yes</i>	
<i>Months FE</i>		<i>Yes</i>			<i>Yes</i>	
<i>Year FE</i>		<i>Yes</i>			<i>Yes</i>	

Note: * $p < 0.1$, ** $p < 0.05$, *** $p < 0.01$. Estimation controls for size, taxes, number of rooms, age and building zone as well. Standard errors are clustered on the community level.

Table 9: Cumby-Huizinga test for autocorrelation housing prices

H0: variable is MA process up to order q

HA: serial correlation present at specified lags $> q$

lags	chi2	df	p-val
1	3.176	1	0.0747
2	3.24	2	0.1979
3	3.24	3	0.3562
4	12.239	4	0.0157
5	12.564	5	0.0278
6	13.372	6	0.0375

Table 8: Obligatory hazard map compliance, land prices

	<i>Dependent Variable : LN-Price (real) in sqm</i>					
	(1)			(2)		
	Coef.	Std. err.	p	Coef.	Std. err.	p
Hazard	-0.110***	0.031	0.0006	-0.021	0.035	0.5422
Implementation	-0.064	0.075	0.3972			
Hazard # Implementation	0.115**	0.046	0.0132			
Elaboration				0.031	0.028	0.2633
Hazard # Elaboration				0.082	0.057	0.1512
Constant	5.187***	1.215	0.0000	5.087***	1.197	0.0000
r2		0.5806			0.5810	
N		6799			6799	
<i>Community FE</i>		<i>Yes</i>			<i>Yes</i>	
<i>Months FE</i>		<i>Yes</i>			<i>Yes</i>	
<i>Year FE</i>		<i>Yes</i>			<i>Yes</i>	

Note: * $p < 0.1$, ** $p < 0.05$, *** $p < 0.01$. We control for the different type of building zones, taxes and size as well. Standard errors are clustered on the community level.

Appendix

GVZ Insurance

What is insured?

- The building is insured with its structural shell, the supporting structure, the installations and the interior fittings.
- Co-insured are building structures that normally belong to the building and are secured or adjusted in such a way that they can not be removed without substantial damage to the building or substantial loss of its value; For example, kitchen equipment in homes, tiled stoves, wall cabinets, solar energy systems, lifts or escalators for passenger transport.

What is not insured?

- Excavation and environment work
- Work to reinforce the subsoil
- Outside the building envelope lying plants and lines
- Furniture and equipment

Paper 9: Keiler, M., Zischg, A., Fuchs, S., Hama, M., Stötter, J., 2005. Avalanche related damage potential - changes of persons and mobile values since the mid-twentieth century, case study Galtür. *Natural Hazards and Earth System Sciences* 5, 49–58. 10.5194/nhess-5-49-2005.

Avalanche related damage potential – changes of persons and mobile values since the mid-twentieth century, case study Galtür

M. Keiler^{1,*}, A. Zischg¹, S. Fuchs^{1,2}, M. Hama^{1,2}, and J. Stötter¹

¹Department of Geography, University of Innsbruck, Austria

²alpS Centre for Natural Hazard Management, Innsbruck, Austria

* now at: Department of Geography and Regional Research, University of Vienna, Austria

Received: 15 September 2004 – Accepted: 29 November 2004 – Published: 4 January 2005

Part of Special Issue “Multidisciplinary approaches in natural hazard and risk assessment”

Abstract. When determining risk related to natural hazard processes, many studies neglect the investigations of the damage potential or are limited to the assessment of immobile values like buildings. However, persons as well as mobile values form an essential part of the damage potential. Knowledge of the maximum number of exposed persons in an endangered area is of great importance for elaborating evacuation plans and immediate measures in case of catastrophes. In addition, motor vehicles can also be highly damaged, as was shown by the analysis of avalanche events. With the removal of mobile values in time as a preventive measure this kind of damage can be minimised.

This study presents a method for recording the maximum number of exposed persons and monetarily assessing motor vehicles in the municipality of Galtür (Tyrol, Austria). Moreover, general developments of the damage potential due to significant socio-economic changes since the mid-twentieth century are pointed out in the study area. The present situation of the maximum number of persons and mobile values in the official avalanche hazard zones of the municipality is described in detail. Information on the number of persons is derived of census data, tourism and employment statistics. During the winter months, a significant increase overlaid by strong short-term fluctuation in the number of persons can be noted. These changes result from a higher demand of tourism related manpower as well as from varying occupancy rates. The number of motor vehicles in endangered areas is closely associated to the number of exposed persons. The potential number of motor vehicles is investigated by means of mapping, statistics on the stock of motor vehicles and the density distribution. Diurnal and seasonal fluctuations of the investigated damage potential are pointed out. The recording of the number of persons and mobile values in endangered areas is vital for any disaster management.

1 Introduction

Avalanches pose a threat to settlements and infrastructure in Alpine environments; due to the catastrophic events in the winter 1999 the general public is more aware of this phenomenon. Yet these locations have always been confronted with natural hazards since they have been populated. Over centuries, hardly any change in dealing with natural hazards can be recognised. Accordingly, the relation of people to natural hazards was predominantly shaped by a conscious perception of the threat, acceptance of the risk and, if possible, by avoiding endangered areas. From the late nineteenth century onward, more permanent measures were constructed because of an increasing knowledge of avalanches processes and the development of appropriate techniques (Coaz, 1881). Since the beginning of the twentieth century, the Alps have been increasingly used as an area of settlement, economic activities and leisure (Bätzing, 1993). This resulted in an expansion of buildings and infrastructure in endangered areas. The avalanche winters of 1950/1951–1953/1954 with 296 casualties in Austria induced high investments of the public sector for the construction of permanent mitigation measures (BMLF, 1973). With responsibility shifting from the individual to the public authorities, the fear of natural hazards processes was replaced by a request for safety (Stritzl, 1980). Since the mid-twentieth century, the Alpine society has undergone enormous socio-economic changes from an agricultural society to a modern service industry- and leisure-oriented society (Bätzing, 1993). This economic upswing due to tourism led to an intensified building development in the confined areas of the valleys. As erecting protection measures is not feasible on an area-wide basis and financial resources are limited, hazard zone planning was introduced in the mid-1970s to coordinate the development of land-use (Kellermann, 1980; Weiss, 2002). Although investing in permanent mitigation measures has risen and spatial planning is applied, catastrophic avalanche events cannot be completely avoided. In February 1999, 55 persons died be-

Correspondence to: M. Keiler
(margreth.keiler@univie.ac.at)

cause of avalanche events in western Austria and in Switzerland (Heumader, 2000; SLF, 2000). Additionally, extensive direct damage of buildings and infrastructure as well as indirect damage occurred (Nöthiger et al., 2002). These events as well as decreasing public finances triggered a gradual change in dealing with natural hazards from the traditional process-oriented assessment of hazards to comprehensive risk assessment in the Alps (Heinimann et al., 1998; Bortler, 1999; Stötter et al., 2002a). In the field of natural hazards, risk is usually expressed as a function of probability of occurrence and damage potential. Due to the socio-economic development since the 1950s, the damage potential is the key factor of the changing risk related to avalanche processes (Fuchs and Bründl, 2005). Many studies neglect the investigation of the damage potential or are limited to the assessment of immobile values like buildings. However, persons as well as mobile values form an essential part of the damage potential.

The study area of Galtür is located in the inner Paznaun valley in the Tyrol, Austria. Galtür has always been an avalanche-prone area and has undergone a transformation from farming village to tourism resort, which is typical for the Eastern Alps. In this study, the changing probability of exposure of persons and mobile values in Galtür is presented for the period of 1951 to 2002. The study is conducted in decadal steps for the total community by differentiating between residents and tourists in the winter seasons. The development is pointed out in detail for 1951 and 2002, using the avalanche hazard zones for segmenting the community spatially. The probability of exposure of persons is not only subject to seasonal fluctuations of tourists but also to diurnal and hourly fluctuations of residents and tourists. The general movements of persons in and out of an endangered area are exemplified for a selected area on a diurnal and hourly basis in the winter season. For mobile values, the development of the value of passenger cars is presented for the study area as well as in detail for the avalanche hazard zones. Changes of the means of transport of tourists are discussed.

2 Methods

2.1 Persons

The development of the permanent population of Galtür since the mid-twentieth century was determined by using statistics (Gemeinde Galtür, 2003; Landesstatistik Tirol, 2004). Detailed information on the number of persons per building in 1951 is based on the statistical analysis of Böhm (1970) for 29 fractions of the municipality of Galtür.

The potential number of tourists in the endangered buildings was derived by using the official number of beds specified by the local tourist board in 1954 and 2002. The data represent values assuming a maximum occupancy rate of beds. The seasonal fluctuation of tourists was recorded by consulting official tourism statistics (Gemeinde Galtür, 2003; Landesstatistik Tirol, 2003a). In addition, the data was calculated on the basis of both the official period of the winter season

from November to April (181 days) and the local average period of the winter seasons (116 days). The winter season in Galtür starts a few days before Christmas and ends traditionally one week after Easter (ski lifts and most hotels close with this date). Depending on the weekday of Christmas day and the date of the Easter-weekend from 1970 to 2004, the average period of the winter season can be reduced to 116 days (10 days in December and 16 days in April).

A method was developed for analysing diurnal and hourly fluctuations of people. Moreover, it is incorporated in a newly designed model. The assumption for the fluctuation is deduced from information on the population (e.g. age group) and economic structure (activity rate, commuters) (Statistik Austria, 2004a) as well as on detailed tourism statistics in the municipality of Galtür (Gemeinde Galtür, 2003). For a detailed study, an area in the red and yellow hazard zones was selected close to the village centre. In this area, 36 buildings are located, which are composed of seven residential buildings, two hotels, 20 guesthouses or bed & breakfast businesses, and one restaurant. Three buildings consist of a residential part and a business part (sports outfitter, craftsman enterprise). One building was assigned to the category “public buildings” and five to “agricultural buildings” and garages. 112 people live in the selected area, 374 guest beds are rented out and approximately 45 persons commute from other areas of Galtür or other municipalities to the selected area.

Taking the pattern of the daily movements into consideration, the residents are divided into the groups of pupils (20 persons), permanent residents (including small children, residents who work in this area, retired persons; 80 persons), and outward-bound commuters (12 persons). Moreover, persons who commute to Galtür are split into the categories “inward-bound commuters/tourism industry” (20 persons) and “inward-bound commuters/other industries” (25 persons).

The potential number of tourists has to be calculated in a first step. For the periods of the main travel season (Christmas, carnival, Easter), the occupancy rate of beds is set at 95%, while a rate of 75% is assumed for the second highest peak (school holidays in several states of Austria, Germany and the Netherlands). For the rest of the season, the occupancy rate of beds was determined for each month corresponding to the remaining overnight stays. The movements of the residents and commuters are simulated depending on weekday, holiday and time of the day; for tourists merely on the time of the day. In Fig. 1, the changing exposure of persons (in %) from Monday to Friday is given for each group (Figs. 1a–1f). On Sundays and holidays, half of the pupils are not in the selected area from 10:00 a.m. to 05:00 p.m. For permanent residents and “inward-bound commuters/tourism industry” the same pattern of movements was assumed as during the week. Half of the outward-bound commuters are outside the selected area on Saturday, Sunday and holiday mornings (09:00–12:00 a.m.) and afternoons (02:00–05:00 p.m.). 60% of the group “inward-bound commuters/other industries” work also on Saturdays and follow

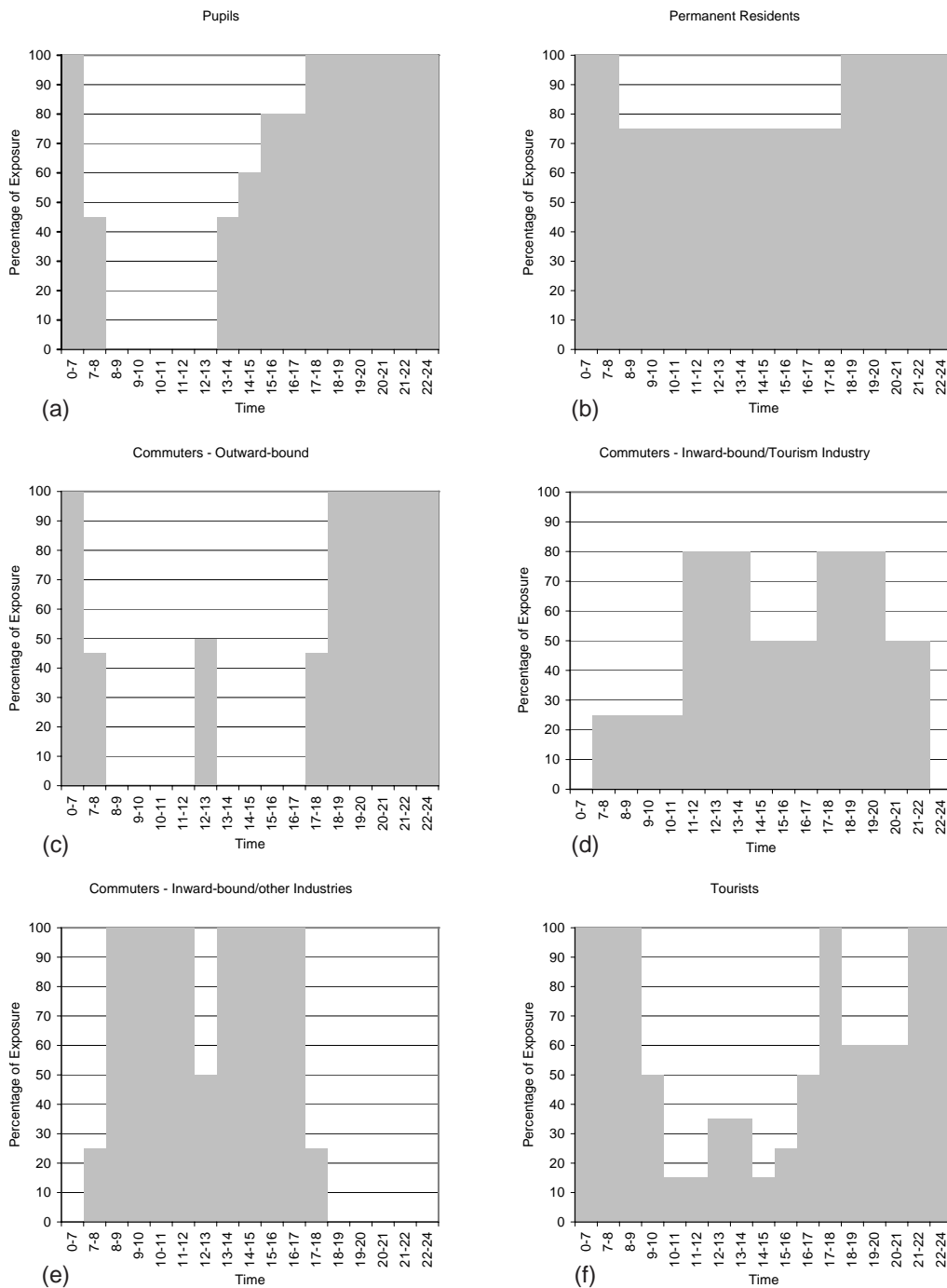


Fig. 1. Exposure of persons (in %) from Monday to Friday for pupils (a), permanent residents (b), commuters (outward-bound) (c), commuters (inward-bound/tourism industry) (d), commuters (inward-bound/other industries) (e), and tourists (f).

the same routine like during the week. On Sundays and holidays, this group is left out for the modelling. In the given examples, the permanent (residents, commuters) and temporary (tourists) population is considered as a whole.

2.2 Passenger cars

Collecting data on passenger cars is closely related to the investigations on potentially exposed persons. For estimating

the number of passenger cars per residents, the relationship between registered motor vehicle (Statistik Austria, 2004b) and the number of residents in the district of Landeck in 2002 was statistically analysed (Landesstatistik Tirol, 2003b).

The number of tourist passenger cars was calculated by employing information on the chosen means of transportation and the number of passengers per tourist car. A questionnaire-based survey conducted in the municipality of

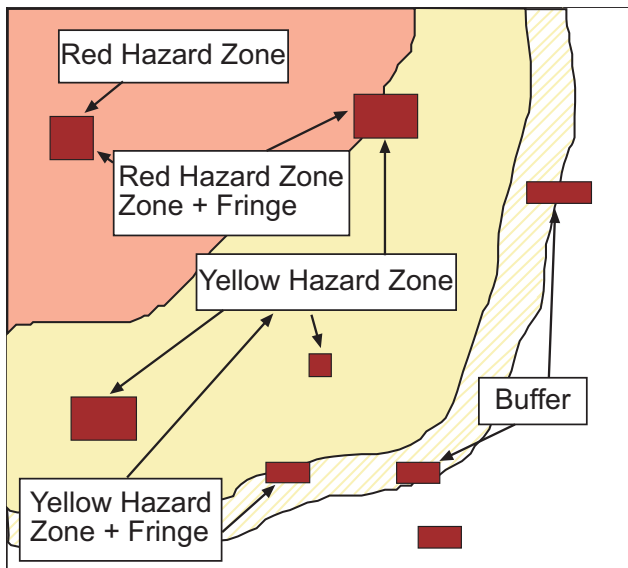


Fig. 2. Schematic diagram of the categories used for the spatial analysis (Keiler, 2004).

Galtür and the results of a study on arrivals and departures of tourists (ARGE Soft Mobility, 2003) show that 95% of the tourists arrived by car in 2002. In addition, 3–4% use private bus companies and 1–2% public transport in winter. Bed & breakfast businesses or small guesthouses register solely arrivals by private cars. Therefore, the number of beds is reduced by 5% for hotels; in all other businesses the total number of beds is considered for the calculations. In a next step, the number of the potential tourist passenger cars is calculated by applying the average number of passenger per car in leisure-time (2.34 persons) (BfS, 2004). In addition to the statistically analysed number of passenger cars, a survey on the existing underground parking in avalanche-prone areas was conducted. The number of parking spaces in underground parking was subtracted from the number of passenger cars. Furthermore, the number of parking spaces of public or ski lift parking areas was mapped in the field and added to the number of passenger cars.

The value of the passenger cars was determined using the price of the most popular brand (Volkswagen) and the most sold type of car in Austria since 1950 (Statistik Austria, 2004b). The car prices were provided by the general importer of Volkswagen in Austria and were adjusted to the price level of 2002. A middle price level is assumed, therefore, higher losses are possible.

2.3 Spatial analysis

When conducting the analysis, persons and passenger cars need to be allocated to buildings. The approach is incorporated in a Geographical Information System (GIS). Data of the Tyrolean state government forms the basis for the recording of the buildings and their location. The age of buildings was taken from descriptions, and thus it was possible to trace

the buildings back to their location in 1950 (Keiler, 2004). Public or ski lift parking areas are added to the GIS.

For pointing out the spatially differentiated development of the study area, the edited information was intersected with the avalanche hazard zones. As it has to be anticipated that buildings are destroyed and persons in buildings at the risk of their lives, any building activity is forbidden in the red zone. In the yellow zone, avalanches have an impact on the economic and individual use of the area and can damage buildings. When observing building requirements and restrictions, it is, however, unlikely that buildings are destroyed and people in buildings endangered (Fink, 1986).

The spatial analysis was conducted in five different categories, which are “red zone”, “yellow zone”, “red zone + fringe”, “yellow zone + fringe” and “10 m-buffer”:

- Buildings with their centre clearly located in a zone, are assigned to that zone (see Fig. 2)
- Buildings that are only partially located in a zone, are assigned to the categories “zone + fringe”; these categories include also the buildings of the respective zone.
- The zones were buffered by ten meters in the GIS, in order to be able to highlight developments in areas close to the zones. In this area, the buildings assigned to the categories “zone + fringe” are not included.

The development of the hazard zones is compared with the development of the whole area of the community. In order to describe the “hazard zones”, the categories “red zone” and “yellow zone + fringe” are added up.

3 Results

3.1 Persons

The population growth was about 68% between 1950 and 2000 (in 2000: 774 residents) (Landesstatistik Tirol, 2004). The out-migration of the population and a strong seasonal labour mobility in the nineteenth century were stopped by the onset of tourism in the beginning of the twentieth century (Böhm, 1970). Thus, new jobs were created in the municipality and affected a rise of the population number. The transformation from a farming community to tourism resort can be illustrated by the changed proportions of the economic sectors. In 1951, 72% of the Galtür-based labour force worked in agriculture, however, in the following ten years this proportion dropped already under 50% (ÖSTAT, 1963; Statistik Austria, 2004a). In the year 2001, the proportion of labour force in agriculture was less than 3%, while 41% of the labour could be found in tourism industry. This number is significantly higher than the average 12% in the state of Tyrol (Landesstatistik Tirol, 2004). The development in the employment structure started between 1950 and 1960. In 1964, 35 tourism businesses already existed, which represented 70% of the non-agricultural-businesses. 22% of the working population were employed in this field (Böhm,

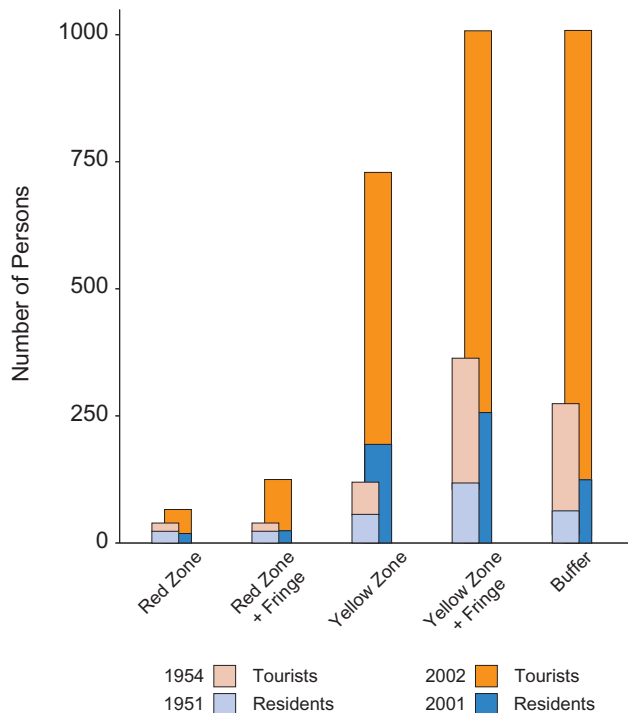


Fig. 3. Potentially exposed persons 1951/1954 and 2001/2002 in avalanche-prone areas in Galtür (Data source for the 1950s: Böhm, 1970).

1970). In 2001, 109 businesses were located in Galtür, 75% of which being assigned to tourism industry. The whole municipality and region shows a strong dependency on tourism, as 58% of the labour force work in this industry. Already in 1950, more commuters were inward-bound than outward-bound in Galtür. The commuters came mainly from nearby municipalities (Böhm, 1970). In 2000, the commuter ratio was still positive, however, 60% (69 persons) did not commute every day, but had their own seasonal accommodation. This seasonal manpower increases the permanent population rate during the winter season by 10% compared to the population rate at the reference date of the census (15 May). When adding the seasonal manpower to the number of residents for the spatial analysis of persons in avalanche-prone areas, following changes in the number of potentially exposed persons have taken place since 1950 (see Fig. 3).

23 of the 461 residents of Galtür lived in the red zone and there were no residential buildings partially located in the red zone (red zone + fringe) in 1951. In this area, 17 guest beds were rented out to tourists. In the yellow zone, the numbers of residents and guest beds rose to 58 and 60, respectively. If the fringe area (yellow zone + fringe) is taken into account, the numbers increase to 118 residents and 246 beds. 66 residents lived in the 10 m-buffer and 208 beds were rented out. In 1951, 141 residents (30.6% of the registered population) lived in the areas identified as hazards zones, and 33.5% (263) of all guest beds were located here. By 2002, the number of residents in the red zone dropped to 18, while

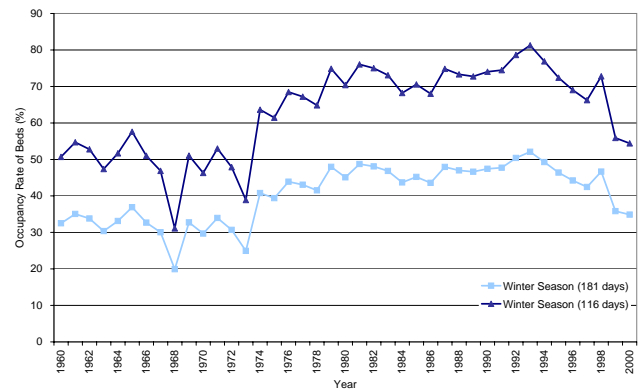


Fig. 4. Occupancy rates of guest beds in Galtür between 1960 and 2000, calculated with the official (181 days) and the average (116 days) period of the winter season (Data source: Landesstatistik Tirol, 2003a).

guest beds rose by a factor of 2.8 to 47 beds (Keiler, 2004). In the associated fringe area of the red zone, six residents and 54 guest beds are counted. In the yellow zone, the number of residents tripled to 197 and the number of guest beds increased to 532 (factor 8.9). Adding the fringe area, the numbers rise to 256 residents (factor 2.2) and 757 beds (factor 3.1). In the 10 m-buffer, a slight increase of residents by the factor 1.9 is registered while the number of beds more than quadrupled to 894 beds. In 2002, the proportion of the population living in the hazard zones (red zone and yellow zone + fringe) rose slightly to 31.3% in comparison to the total population of the municipality, whereas the percentage of guest beds located there decreased to 21.6% (804).

For the spatial analysis described above, a maximum occupancy rate of beds was assumed to show the maximum number of persons in endangered areas. The occupancy rate of beds, calculated with the official tourism period of winter (November to April), was between 30 and 40% from the 1960s to the mid-1970s (see Fig. 4). The low rate in 1968 results from successful advertisement campaigns by the neighbouring village Ischgl, which reduced the number of tourists in Galtür (Cimarolli, 1989). The decline in the winter 1973 is an effect of the oil crisis. Until 1998, the occupancy rate of beds fluctuated between 40 and 50% and attained a peak in the early 1990s with 52% (Landesstatistik Tirol, 2003a). The values declined after the avalanche event in February 1999 (Stötter et al., 2002b). These values differ when the average period of winter season is applied for estimating the average occupancy rate of beds, the rates change from 32% to 83% in December and from 32% to 60% in April.

The values in April show a greater deviation of the mean value as in December due to the changing dates of Easter and the end of season. The overnight stays in November and in the beginning of December as well as the end of April can be neglected because of an average occupancy rate of beds of 0.2 and four, respectively. Using the average period of the winter season by calculating the occupancy rate of beds, the values ranged around 50% until the mid-1970s, rose above

Table 1. Average number of tourists per day in decades, calculated with the official (181 days) and average (116 days) period of the winter season (Data source: Landesstatistik Tirol, 2003a).

Decade	Tourists per day in the winter season	
	Official period	Average period
1950s	170	269
1960s	507	791
1970s	863	1346
1980s	1321	2062
1990s	1436	2240

70% the late 1970s and attained their peak of more than 80% in 1993 before starting to decline (Fig. 4). Figure 5 shows the development of the tourist numbers per day in the winter season, determined for both the official and the average period of the winter season. Corresponding to the growing number of beds (Keiler, 2004) and the higher occupancy rate, the number of tourists per day increased from the 1950s to the 1990s by a factor of 8.3, with peaks of up to 2800 tourists (see Table 1 and Fig. 5).

Focusing on one season, the possible numbers of exposed persons show a strong fluctuation during the season as well as in daytime. Applying the described fluctuation approach in the selected area, the winter season 2001/2002 was modelled. The results of the general movements according to the population and economic structure of the municipality as well as to a winter tourist are illustrated as an overview in Fig. 6. On the abscissa, each day from 1 November to 30 April is shown, and on the ordinate each hour of the day is displayed. The number of persons is divided in steps of 50, which are colour-coded from light yellow to deep purple. The seasonal fluctuation is characterised by a strongly increasing number of tourists at Christmas time. After 6 January the numbers decline and gradually rise again up to the main travel season in February, followed by a reduction until the start of the Easter travel season. The end of the winter season is highlighted by a sharp decrease in the number of persons to nearly the amount of the permanent population one week after Easter. In November, the diurnal fluctuation of the permanent population is displayed with nearly no tourists and is characterised by a lower number in the early morning and at noon (see Fig. 6 and Figs. 1a–1e). In addition, the weekly structure can be recognised due to the absence of the commuters on Sundays and is displayed in light yellow. The minimum number of 86 persons in this period is modelled for 02:00 p.m.–04:00 p.m. on Sundays. During the week, the minimum rises to 91 persons and shifts to 08:00 a.m.–10:00 a.m. The maximum of 118 persons is attained between 07:00 a.m. and 08:00 a.m. on each day. From the beginning of the winter season on, these patterns are concealed by general movements of the tourists (see Fig. 1f). This results in a sharp decline of the number of persons at 10:00 a.m., followed by a slight increase at noon and a new

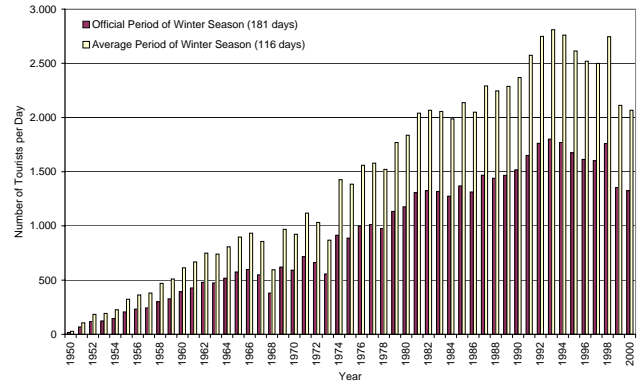


Fig. 5. Development of the number of tourists per day in Galtür between 1950 and 2000, calculated with the official (181 days) and the average (116 days) period of the winter season (Data source: Landesstatistik Tirol, 2003a).

reduction to the number of the late morning. The number of persons rises abruptly in the late afternoon and decreases lightly in the evening. After 09:00 p.m., the numbers of the nights are reached. Corresponding to the results of November, the maximum number of 472 persons is simulated between 07:00 a.m. and 08:00 a.m. because of more incoming commuters than persons leaving the area (see Fig. 6, February). In the period of the main season, 139 persons form the minimum on Sundays between 02:00 p.m. and 04:00 p.m. A minimum of 154 persons is found on weekdays and local school days from 10:00 a.m. to noon. In the second half of February, the bright purple illustrates a period in the main season where local children are at school. At Christmas and Easter, the period of the main season coincide with the school holidays.

3.2 Passenger cars

The numbers of passenger cars of the local residents rose from two cars in 1950 to 357 cars in 2000 (see Fig. 7). First, this strong increase is due to an abrupt fall of prices after suspending the monopoly in 1953. Afterwards, the car prices show merely a slight increase. Second, more and more people could afford to buy a car. In 1950, a passenger car cost the equivalent of 174 monthly salaries (Austrian average, ÖSTAT, 1963). This ratio was reduced to one car for 28 salaries in 1960, 23 salaries in 1970 and eleven salaries in 1980. Since 1990, the equivalent of seven monthly salaries has to be paid for one passenger car (Statistik Austria, 2004b). Consequently, the density of passenger cars in the district of Landeck increased from four passenger cars per 1000 residents in 1950 to 458 passenger cars per 1000 residents in 2000. The increasing motorisation made extending the existing roads mandatory after the mid-1950s (Cimarolli, 1989). This extension can be regarded as a further important impulse for the tourism industry (Lichtenberger, 2002). In 1950, the tourists travelled by public transport and were picked up at the train station, or arrived by a

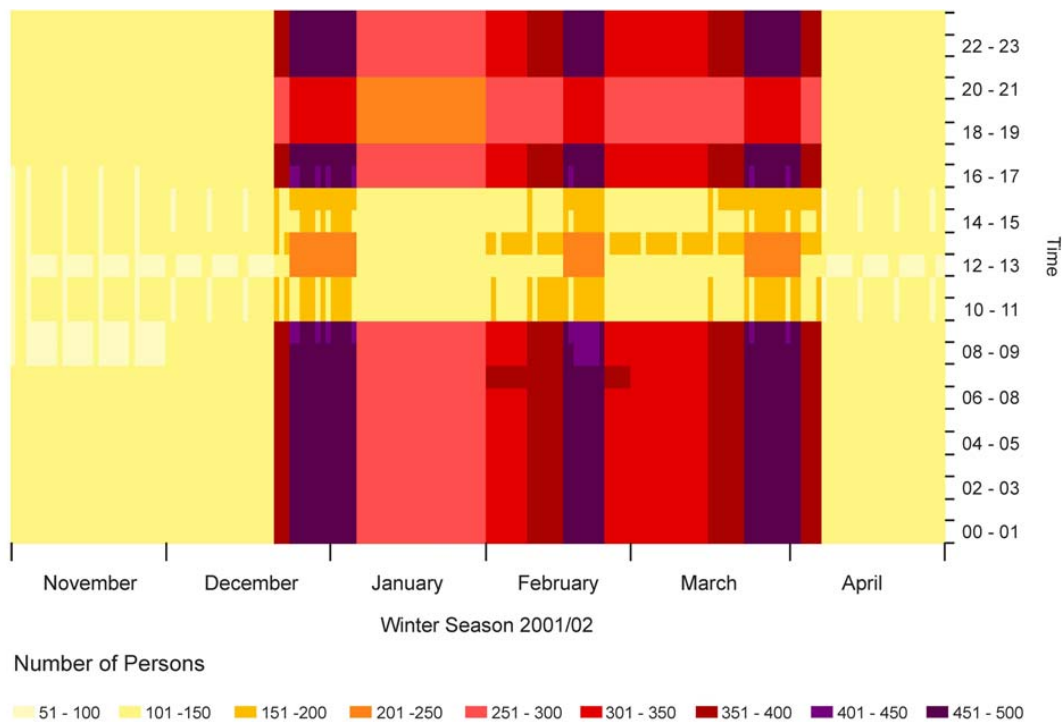


Fig. 6. Diurnal and hourly fluctuations of the number of exposed persons in a selected avalanche-prone area in Galtür (winter season 2001/2002).

daily operating bus in Galtür. In the beginning of the 1960s, the preferred means of transport of tourists were private busses and public transport in the Paznaun region (Cimarolli, 1989). Ten years later, offers for special trains in the travel season decreased while individual traffic rose instead above 55% (Cimarolli, 1989; Lichtenberger, 2002). In 2000, 95% of the tourists arrived by car (ARGE Soft Mobility, 2003).

Regarding the avalanche hazard zones in Galtür, it can be assumed that none of the two calculated passenger cars owned by residents were located in the endangered area and all tourists arrived by public transport. In 2002, the values of passenger cars in the red zones amounted to EUR 1.3 million (see Fig. 8). More than two thirds of these mobile values are attributed to potential passenger cars on public or ski lift parking areas. The remaining cars are determined on the basis of residents and tourists. Corresponding to the number of persons, the total value of passenger cars increased slightly in the fringe area of the red zone (red zone + fringe) (see Figs. 3 and 8). In the yellow zone, the value of the passenger cars added up to EUR 8.6 million, with more than the half of the cars belonging to tourists. The values of resident- and tourist-owned cars increased the total sum by EUR 0.7 million and EUR 0.9 million, respectively, when including the fringe area of the yellow zone. In the 10 m-buffer, the value of passenger cars totalled EUR 6.6 million, 82% of these values are associated to passenger cars of tourists. The numbers and values of passenger cars refer to parking spaces belonging to buildings or to parking areas. Additionally, nearly five kilometres of roads are endangered by avalanches in the mu-

nicipality. 1650 m of the main road are located in the red hazard zone and 2575 m in the yellow zone. In the latter, 700 m of community roads and 50 m of access roads are additionally endangered.

4 Discussion

In the municipality of Galtür, a significant change in the number of persons and mobile values has taken place due to tourism since the 1950s. The number of residents in Galtür has increased above average in comparison to the population of the district of Landeck and rose most between 1960 and 1970 (Landesstatistik Tirol, 2004). This local population growth is connected to rising numbers of jobs in tourism and tourism related businesses in the region. In particular, the tourism industry offered employment outside the agricultural sector. Thus, a higher and regular income of the residents lead to spatially increasing settlements due to more residential and guesthouse buildings (see Keiler, 2004).

In the hazard zones (red zone and yellow zone + fringe), the number of residents has almost doubled since the 1950s. In this context, the number of residents declined in the red zone, but tripled in the yellow zone. Thus, the increase in the yellow zone was slightly higher than in the community as a whole. The highest amount of tourists stays in the 10 m-buffer surrounding the yellow hazard zone. In this area, more guest beds exist than in the hazard zones. The highest increase of the number of beds has been registered in the yellow zone since 1950, while the slightest one was in the red

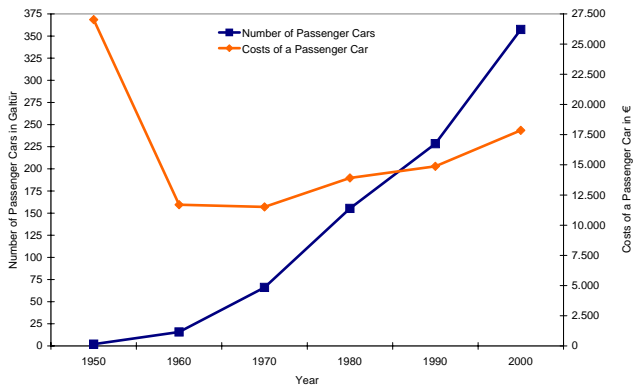


Fig. 7. Development of the number of passenger cars of the residents of Galtür and development of passenger car prices (Volkswagen) between 1950 and 2000 (Data source: ÖSTAT, 1963; Statistik Austria, 2004).

zone. The number of beds in the hazards zones rose less (factor 3) compared to the number of beds in the community, which quintupled. Altogether, the maximum number of persons in the hazard zones in 1950 was about 400 and increased until 2002 to 1080 persons (factor 2.7). The number of residents and tourists can be traced to a smaller number of persons per household, an increasing number of buildings and mainly to the change of the function of buildings from purely residential purposes to additional tourist purposes. The development per spatial category of both latter factors (Keiler, 2004) strongly correlates to the changes in the number of persons.

When using an average number of tourists corresponding to the occupancy rate of beds for determining the probability of exposure, the period of the winter season has to be considered. The official period of the winter season does not correspond with the shorter average season in Galtür and thus, causes a lower occupancy rate of beds and numbers of tourists per day. The occupancy rate of beds in December and April as well as in the season increase significantly, regarding this average period. As the durations of the official and average winter season differ strongly, both calculated numbers of tourists per day deviate by 1.6. In general, a gradually rising number of guest beds and higher occupancy rates cause an increasing number of tourists per day since the mid-1970s. Thus, the probability of exposure of persons between the year 1951 and 2002 increased by a factor of 4.2 in Galtür, taking the average number of tourists per day (average period) and the number of residents into account. In comparison, the factor 5.5 was calculated using the maximum number of tourists (Keiler, 2004).

By applying the fluctuation model, the changing numbers of persons over the seasons and during a day were pointed out. The beginning and the end of the winter season are characterised by a radical slump in the number of persons. From off-season to main season the maximum number of persons rises by a factor of 5.6, while the minimum number shows only a slight increase (factor 1.6). During the day, the num-

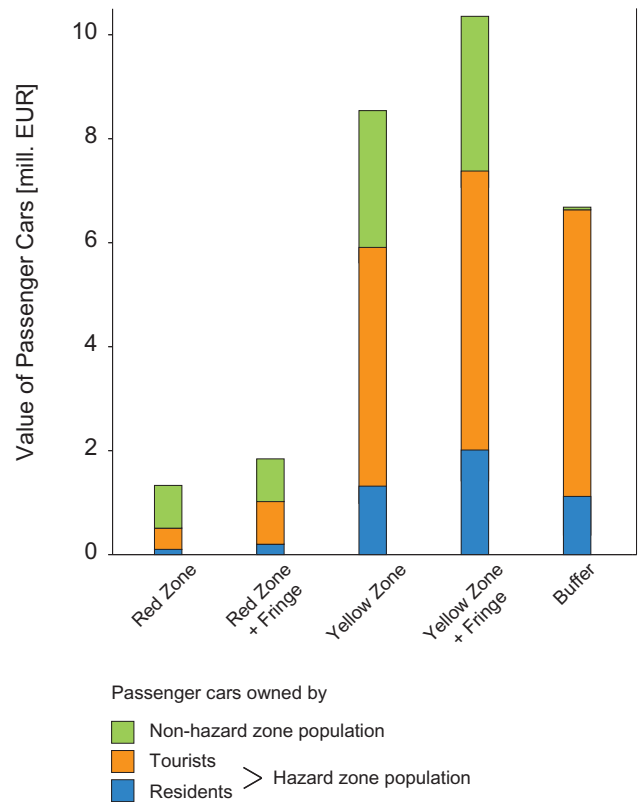


Fig. 8. Values of passenger cars in the avalanche-prone areas in Galtür in 2002.

ber of persons fluctuates by the factor 1.4 between minimum and maximum in the off-season, and by a factor of 3.4 in the period of the main season. These extreme changes of the number of persons can occur within one to two hours.

With the permanent population becoming more mobile and transport habits of the tourists having changed, a significant rise in the number of passenger cars and mobile values can be noticed. Damage of motor vehicles has been recorded since the 1960s and illustrated this development. 51 motor vehicles were destroyed by an avalanche in Galtür in 1967 (Fliri, 1998). About 118 passenger cars as well as agricultural equipment were totally damaged in the catastrophic avalanche events in Galtür and Valzur in February 1999 (Amt der Tiroler Landesregierung, 2000). Most of the cars in endangered areas (50%) are owned by tourists, while only 18% are associated to local residents. Up to one third of the passenger cars are owned by persons, who come from outside the hazard zones. These cars are located at public of ski lift parking areas.

5 Conclusion

Persons as well as mobile values form an essential and a special part of the damage potential. In contrast to the immobile damage potential (buildings and infrastructure, etc.), persons and mobile values can either leave or be removed

out of avalanche-prone areas in case of dangerous situations. For developing efficient and effective evacuation and emergency plans, information on numbers of persons and mobile values as well as their location and movements in the area is needed. The analysis conducted in this study points out the fluctuation of persons and mobile values in the community of Galtür, in order to possibly improve the understanding of mobile damage potential in time and space. Furthermore, following aspects have to be considered when dealing with avalanche related mobile damage potential.

This study focused on the changing numbers of persons and mobile values, but the probability of avalanche events undergoes seasonal and diurnal changes, too. Additionally, both factors are changing in space and form the base for a dynamic risk visualisation. This information may help to recognise high risk situations more easily and enables a situation-oriented and risk-based decision-making.

For devising or improving evacuation plans and immediate measures, the high numbers of tourists in endangered areas as well as possible escape routes in periods of high probability of avalanche release have to be regarded in order to guarantee an efficient and effective procedure in emergency cases. This is essential for efficient disaster risk reduction and contributes to the concept of resilience as part of proactive adaptation (UN/ISDR, 2004).

Persons and mobile values are not only in settlements at risk of avalanches, but are also exposed to high risk on roads to the tourism resorts. Due to the higher volume of traffic caused by increasing tourism and the high economic dependence on the road network, “safe” road connections become more and more important. Until 1999, 4 km of the 34 km long road to Galtür were protected by different mitigation measures. Since the avalanche event, protection for another 6 km was added and 1 km is under construction or planned for the next year (Tiroler Landesregierung, 2004). Regarding the limited financial resources of the public hand alternative ways in dealing with natural hazards should be more considered, like described in Wilhelm (1997) and Zischg and Stötter (2004).

The number of casualties and the height of damage of mobile values of the avalanche winter 1999 are, compared to former avalanche winters, relatively low, even though more persons and higher values are exposed in the Alpine environment than in the past. Combining the existing mitigations measures prevented a worse situation, but deficits still persist (SLF, 2000). In order to optimise dealing with natural hazards, methods of determining the risk, the economic assessment of the efficiency of mitigation measures as well as spatial planning have to be strengthened.

Acknowledgements. Many thanks go to the Federal Service for Torrent, Erosion and Avalanche Control, District Office Imst and Landeck, Tyrol as well as to A. Pasch, Porsche Austria, for making their data available. Furthermore, the authors would like to thank K. Walser and the community of Galtür for their help. The research for this paper was carried out with a grant from the MunichRe Reinsurance Company, Germany.

Edited by: T. Glade

Reviewed by: B. Braun and H. Staffler

References

- Amt der Tiroler Landesregierung (ed.): Schnee und Lawinen 1997/1998 und 1998/1999, Lawinenwarndienst Tirol, 7, 8, Innsbruck, 2000.
- ARGE Soft Mobility: <http://www.soft-mobility.com/members/EU-SANFTEMOBILITAET.pdf>, 5 February, 2003.
- Bätzing, W.: Der sozio-ökonomische Strukturwandel des Alpenraumes im 20. Jahrhundert, Geogr. Bernen., P26, 1993.
- BfS: Gesamtverkehrsfragen, <http://www.are.admin.ch/imperia/md/content/are/gesamtverkehr/personenverkehr/mz94.pdf>, 2 September, 2004.
- BMLF (ed.): Hochwasser, Muren, Lawinen – Information über Wasserwirtschaft und Katastrophenschutz, Schriftenreihe Wasserwirtschaft, 2, Wien, 1973.
- Böhm, H.: Das Paznauntal – Die Bodennutzung eines alpinen Tales auf geländeklimatischer, agrarökologischer und sozial-geographischer Grundlage, Forschungen zur Deutschen Landeskunde 190, Bonn, 1970.
- Bortler, P.: Risikoanalyse bei gravitativen Naturgefahren, Umwelt-Materialien, 107/I, II, BUWAL, Bern, 1999.
- Cimarolli, E.: Ischgl – Vom Bergbauerndorf zum internationalen Wintersportort, Eigenverlag, Landeck, 1989.
- Coaz, J.: Die Lawinen der Schweizer Alpen, Dalp’sche Buch- und Kunsthandlung, Bern, 1881.
- Fink, M. (ed.): Raumordnung und Naturgefahren, Österreichische Raumordnungskonferenz 50, Geschäftsstelle der Österr. Raumordnungskonferenz, Wien, 1986.
- Fliri, F.: Naturchronik von Tirol, Wagner, Innsbruck, 1998.
- Fuchs, S. and Bründl, M.: Damage Potential and Losses Resulting from Snow Avalanches in Settlements of the Canton of Grisons, Switzerland, Natural Hazards, 34, 53–69, 2005.
- Gemeinde Galtür: Statistik Galtür, <http://www.galtuer.tirol.gv.at/betten.htm>, 5 February, 2003.
- Heinimann, H., Hollenstein, K., Kienholz, H., Krummenacher, B., and Mani, P.: Methoden zur Analyse und Bewertung von Naturgefahren, Umwelt-Materialien, 85, BUWAL, Bern, 1998.
- Heumader, J.: Die Katastrophenlawinen von Galtür und Valzur am 23. und 24. Februar 1999 im Paznauntal/Tirol, Proc. Internationales Symposium Interpraevent – Villach, 26–30 June, 2, 397–410, 2000.
- Keiler, M.: Development of the Damage Potential Resulting from Avalanche Risk in the Period 1950–2000, Case Study Galtür, Nat. Haz. Earth Sc., 4, 249–256, 2004, **SRef-ID: 1684-9981/nhess/2004-4-249**.
- Kellermann, D.: Beziehungen zwischen den Gefahrenzonenplänen der Wildbach- und Lawinenverbauung und der örtlichen Raumplanung, Proc. Internationales Symposium Interpraevent – Bad Ischl, 8–12 September, 1, 23–32, 1980.
- Landesstatistik Tirol: Tourismus, <http://www.tirol.gv.at/themen/zahlenundfakten/statistik/tourismus.shtml>, 5 February 2003, 2003a.
- Landesstatistik Tirol: Tiroler Daten 2003, <http://www.tirol.gv.at/themen/zahlenundfakten/statistik/downloads/stat-fold03.pdf>, 15 May, 2003b.
- Landesstatistik Tirol: Landesstatistik Tirol, <http://www.tirol.gv.at/themen/zahlenundfakten/statistik/wohnbevoelkerung.shtml>, 5 February, 2004.

- Lichtenberger, E.: Österreich, Wissenschaftliche Buchgesellschaft, Darmstadt, 2002.
- Nöthiger, C., Elsasser, H., Bründl, M., and Ammann, W.: Indirekte Auswirkungen von Naturgefahren auf den Tourismus – Das Beispiel des Lawinenwinters 1999 in der Schweiz, *Geogr. Helv.*, 2, 91–108, 2002.
- ÖSTAT: Volkszählung 1951, Statistik Austria, Österreichisches Statistisches Zentralamt, Wien, 1963.
- SLF (ed.): Der Lawinenwinter 1999, Eidgenössisches Institut für Schnee- und Lawinenforschung, Davos, 2000.
- Statistik Austria: Census 2001, <http://www.statistik.gv.at/blickgem/vz5/g70606.pdf>, 18 March, 2004a.
- Statistik Austria: Stock on motor vehicle, <http://www.statistik.gv.at/gz/vz.shtml>, 13 January, 2004b.
- Stötter, J., Meißl, G., Ploner, A., and Sönsner, T.: Developments in Natural Hazard Management in Alpine Countries Facing Global Change, edited by Steininger, K. W. and Weck-Hannemann, H., *Global Environmental Change in Alpine Regions – Recognition, Impact, Adaptation and Mitigation*, 113–130, Edward Elgar, Cheltenham, 2002a.
- Stötter, J., Meißl, G., Rinderer, M., Keiler, M., and Fuchs, S.: Galtür – Eine Gemeinde im Zeichen des Lawinenereignisses von 1999, edited by Steinicke, E., *Geographischer Exkursionsführer Europaregion Tirol, Südtirol, Trentino, Spezialekursionen im Bundesland Tirol*, Eigenverlag, Innsbruck, Innsbrucker Geographische Studien, 33/2, 167–184, 2002b.
- Stritzl, J.: Sicherheit im alpinen Raum, *Proc. Internationales Symposium Interpraevent – Bad Ischl*, 8–12 September, 1, 17–22, 1980.
- Tiroler Landesregierung: Verkehr – Lawinenschutzbauten, http://www.tirol.gv.at/themen/verkehr/bauvorhaben/lawinenschutzbauten_lechtal_paznaun.shtml, 10 June, 2004.
- UN/ISDR: Living with Risk, A global review of disaster reduction initiatives, 2004 Version, 1, Geneva, 2004.
- Weiss, G.: The Political Practice of Natural Hazards Control in Austria and the Question of Global Change, edited by Steiniger, K. W. and Weck-Hannemann, H., *Global Environmental Change in Alpine Regions – Recognition, Impact, Adaptation and Mitigation*, 131–149, Edward Elgar, Cheltenham, 2002.
- Wilhelm, C.: Wirtschaftlichkeit im Lawinenschutz. *Mitt. Eidgenössisches Institut für Schnee- und Lawinenforschung*, 54, Davos, 1997.
- Zischg, A. and Stötter, J.: Objektorientierte Betrachtung des Lawinenrisikos, *Proc. Internationales Symposium Interpraevent – Riva del Garda*, 24–27 May, VI/217–VI/228, 2004.

Paper 10: Zischg, A., 2016. River corrections and long-term changes in flood risk in the Aare valley, Switzerland. E3S Web Conf. 7, 11010. [10.1051/e3sconf/20160711010](https://doi.org/10.1051/e3sconf/20160711010).

River corrections and long-term changes in flood risk in the Aare valley, Switzerland

Andreas Zischg^{1,a}

¹*Institute of Geography, Oeschger Centre for Climate Change Research, Mobililar Lab for Natural Risks, University of Bern, 3012 Bern, Switzerland*

Abstract. Flood risk is changing over time. Beside climatic changes, key drivers for changing flood risks are the modification of the river courses by flood defence structures and the increase in properties exposed to floods due to economic development. In this study, both effects – the modification of the river courses and the increase of economic assets – on the long-term evolution of flood risk were isolated and confronted. To this aim, two states of the river network were compared, one representing the river courses of today and another representing the river courses of the early 19th century before the river corrections took place. Selected observed and well documented flood events of the last decades were modelled on the historic states of the river reaches. The documented flood events were compared with the simulations in terms of inundated area and exposed buildings. Without river corrections, the flooded areas and the number of exposed residential housings would be remarkably higher than observed in recent flood events. The examples show that the effects of the main river corrections are remarkable for today's economic activities in the floodplains. Therefore, the maintenance of the former river correction works is an important part of today's risk management practice.

1 Introduction

Flood risk in terms of the probability of damages to persons, houses and infrastructure due to floodings is changing over time. The most important drivers for long-term changes (from decades to centuries) are climatic changes, changes in the runoff behaviour of the catchments, changes in the hydromorphologic state of the river courses and changes in the values at risk. For analysis of long-term changes in river systems, their historic states have to be reconstructed. This is done for many purposes. Historic floods are reconstructed for raising information about extreme events. The consideration of former extreme flood events can extend the time periods of discharge measurements and therefore improve flood frequency estimation (e.g. [1], [2], [3], [4], [5], [6], [7]). An overview of quantitative historical hydrology in Europe is given by [8]. Another use of reconstructed historical floods is the analysis of changes of the meteorological causes of floods (e.g. [9]). Other studies focus on the environmental changes in the river courses itself and their consequences for floods (e.g. [10], [11]). A third group is analysing the alteration of hydrologic regimes by reconstructing or “retro-modelling” historic states of the river channels and comparing them with the today's river channels (e.g. [12], [13]).

But, the question about the effect of the historic river corrections to the exposure of persons and values is rarely investigated. The aim of this study is therefore to quantify the effects of the river corrections in terms of the reduction of exposure of residential buildings to floods. The main hypothesis is that the actual morphology of the river courses as a sum of all anthropogenic modifications reduces the damage potential of rare floods remarkably. Thus, the main research question is to quantify this effect in terms of changes in number of exposed buildings to recent floods between the actual state and a historic state of the river morphology.

The study was carried out in the Aare river basin upstream of Bern, Switzerland. Most of the rivers in this catchment were regulated in the early 19th century. One important regulation, however, was realised as early as in the 18th century. The first river correction was the deviation of the Kander river into Lake Thun in 1714 ([14]). This deviation changed the hydrology and the flood frequency in Bern remarkably because of the retention effects of the lake. From 1814 on, the Aare river between Lake Thun and Bern was corrected with a uniform cross section and lateral dams [15]. These works were finished 1892. Since then, the Aare river course in this reach did not change remarkably, apart from incision into the riverbed. The Gürbe river was corrected and trained around 1850.

^a Corresponding author: andreas.zischg@giub.unibe.ch

2 Methods

In this study, both effects – the modification of the river courses and the increase of economic assets – on the long-term evolution of flood risk were isolated and confronted. In a first step, a historic state of the river course without any remarkable anthropogenic influences was implemented into a 2D hydrodynamic model. The historic states of the rivers Aare, Hasliaare and Gürbe before the river corrections were reconstructed by means of historic topographic maps and surveys. The historic terrain models were reconstructed by georeferencing and digitalizing historic maps and cross-sections combined with the mapping of the geomorphologic evidences of former river structures in areas not modified by anthropogenic activities ([16], [17], [18]).

In a second step, selected flood events of the last decades were modelled on the historic state of the river reaches. The results of these simulations were compared with the event documentation in terms of inundated area and number of exposed residential buildings. In a third step, the temporal development of residential buildings was quantified.

2.1 Reconstruction of historic river courses

The natural states of the river courses before the first relevant anthropogenic modifications took place were reconstructed on the basis of historic maps. The river corrections were planned on the basis of remarkably detailed topographic surveys. These surveys include plans and maps but also many mapped cross sections from different dates. The historic maps were georeferenced on the basis of the hillshade of the highly resolved digital elevation model. In this model, the former river beds and channel geometries are visible, especially in those areas which are covered now by alluvial forests. These evidences already visible in the terrain provide a useful base for verifying the accurateness of the historic maps and for the georeferencing. Afterwards, the recent anthropogenic modifications of the terrain were erased from the terrain model. In a next step, the digitized areas of the historic riverbeds were incised into the cleaned terrain model. The incision depth was delineated from the historic topographic surveys and the historic cross section geometries (see figure 1 for an example of a historic cross section). The reconstructed terrain model provided the basis for the creation of the computational mesh for the hydrodynamic model.

2.2 Hydrodynamic modelling

The historic situation of the river courses was implemented into a 2D flood simulation model. The computational mesh was generated on the basis of recent Lidar measurements with a resolution of 4 points/m² outside the anthropogenically modified areas. Within the modified areas, the mesh nodes were derived from the historic terrain model. For the hydrodynamic simulation,

the BASEMENT simulation model of ETHZ was used ([19]).

As flood scenarios, the flood hydrographs of the July 1990, August 2005 and October 2011 flood events were extracted from the time series of the gauging stations Gürbe at Burgistein, Aare at Thun, and Hasliaare at Brienzwiler respectively. The data was provided by the Federal Office for the Environment and the Canton of Bern.

2.3 Temporal development of residential buildings

Beside the changes in the river course, the number of exposed buildings is also changing over time. Therefore, this driver of changing exposure was analysed in a spatio-temporal framework following the approach of [20]. For this purpose, a dataset of the residential buildings with the year of construction was used. This dataset was provided by the Federal Office for Statistics. The classes of construction periods are: before 1919, 1919-1945, 1946-1960, 1961-1970, 1971-1980, 1981-1990, 1991-1995, 1996-2000, 2001-2005, 2006-2010, 2011-2014. For this study, it was assumed that the buildings constructed before 1919 represent more or less the state of the mid-19th century. The study areas were delimited on the basis of the floodplains morphology and the hillslopes of the valley bottom.

2.4 Quantification of the effects of river corrections

The historic state of the river course before the anthropogenic interventions was used as the terrain model for the hydrodynamic simulation. In this simulation, the observed hydrograph of the selected flood event was used as input for flood modelling. This hydrograph was measured by a gauging station. It was used as an inflow at the upper boundary of the floodplain. For the Aare river between Thun and Bern, the hydrograph of the August 2005 event measured in Thun was used. The peak discharge was 543 m³/s. For the Hasliaare river reach, the hydrograph of the October 2011 event with a peak discharge of 365 m³/s was used. For the Gürbe river, the hydrograph of the July 1990 event with a peak discharge of 85 m³/s was used for modelling the historic flood scenario.

The simulated flooded areas of the historic states were compared with the event documentation dataset of the Canton of Bern. In terms of exposed buildings, the comparison between the two states of the river courses was done in the following way: In a first step, the building stock of today was intersected with the documented flooded areas of the recent events (event documentation). In a second step, the actual building stock was intersected with the simulated flooded areas of the historic terrain model (hypothetic flood without flood defence structures). In a third step, the number of exposed buildings (actual building stock) located in the documented flooded areas was compared with the building stock of 1919 exposed to the hypothetic flooded

areas of the historic terrain model. Furthermore, the building stock of 1919 was intersected with the floodings of the historic state and the floodings of the actual state of the river course. Hence, this approach allowed to quantify a) the contribution of the river corrections to the reduction of the exposure of residential buildings, b) the effect of the growth in building stock to flood exposure, and c) the combination of both.

3 Results

The main results of this study are the reconstructed historic river courses. These represent a natural riverbed before the first anthropogenic interventions took place and provide the basis for further analyses of exposed residential buildings and their temporal development. With this, the basis for an analysis of the effects of the river corrections is provided.

3.1 Reconstructed historic river courses

Figure 2 shows an excerpt of the reconstructed terrain model of the Aare river around 1815. The river consisted of a network of channels with isolated temporary islands and occupied a width of 1000m with a braided character. The Hasliaare river showed a braided character in the upper part of the floodplain and a meandering character in the lower part before flowing into Lake Brienz. The Gürbe river showed in most parts a meandering character (figure 3). Table 1 shows the differences in mean flow length and table 2 shows the differences in the area of flowing water.

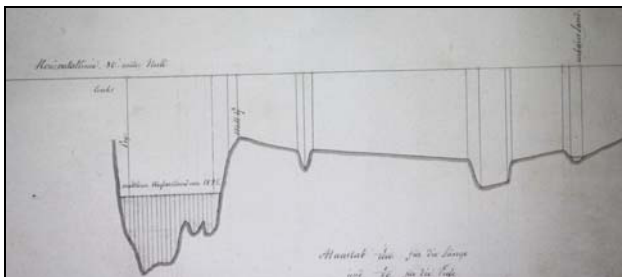


Figure 1. Example of a cross section of the Aare river 1826, near Jaberg

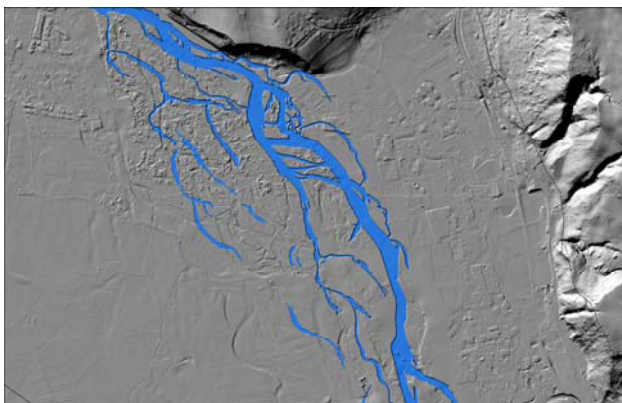


Figure 2. Extract of the reconstructed terrain model of the Aare river between Thun and Bern around 1815.

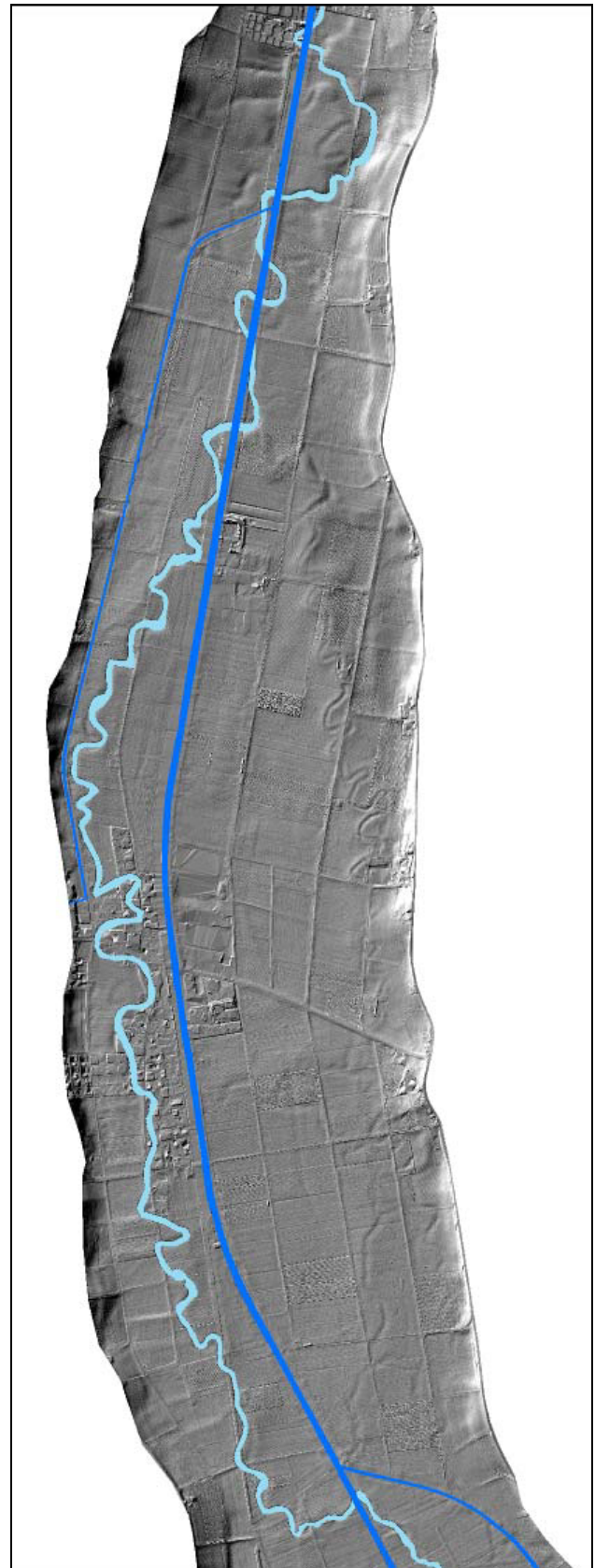


Figure 3. Reconstructed riverbed of the Gürbe river before the correction works (light blue) and the actual riverbed (dark blue).

River reach	early-19 th century [km]	actual state [km]	difference [%]
Aare Thun-Bern	34.0	27.2	-20
Hasliaare	27.2	13.5	-17
Gürbe	11.8	17.4	-32

Table 1. Differences in flow length

River reach	early-19 th century [km ²]	actual state [km ²]	difference [%]
Aare Thun-Bern	4.2	1.5	-64
Hasliaare	2.5	0.3	-88
Gürbe	0.4	0.3	-22

Table 2. Differences in flow area

The river corrections reduced the area covered by flowing water by 22-88% and the flow length by 17-32%.

3.2 Temporal development of exposed residential buildings

In total, 7505 residential buildings are located in 2012 in the study area of the Aare river between Thun and Bern. In the study area of the Hasliaare river reach, 1514 buildings are located and in the Gürbe study area 818 residential buildings. Between 1919 and 2012, the building stock increased by 837% in the Aare river reach, by 1428% in the Hasliaare study area and by 210% in the Gürbe valley.

River reach	early-19 th century [no.]	actual state [no.]	difference [%]
Aare Thun-Bern	896	7505	+837
Hasliaare	106	1514	+1428
Gürbe	389	818	+210

Table 3. Total number of residential buildings in the study areas (floodplains)

3.3 Effects of the river corrections

To compare the two states of the river reach of the Aare river between Thun and Bern, the August 2005 flood event was simulated on the basis of the historic terrain model. The inundated areas would be eight times higher in a status without any river corrections, resp. the flood defence structures reduce the flooded area about 88% (see table 4). If the building stock of 2012 is assumed to be as is in the historic flood scenario, then the number of exposed residential buildings to a flood similar to the August 2005 event but without any flood defence measures would be around forty times higher (see table 5). This means that the exposure of the actual building

stock is reduced by 97.5% by the river corrections in a flood event comparable to the August 2005 flood event. However, the reduction of exposure without taking into account the economic growth would be 93% (see table 6). But, taking into account the growth of buildings, this reduction of exposure is only 69% (see table 7). Therefore, the growth of the settlements in flood prone areas reduces the effectivity of the flood protection works remarkably over time.

The comparison of the two states of the Hasliaare river reach shows a similar picture. Here, the October 2011 flood event was taken for the comparison. The flooded area would be nearly eight times higher without any flood defence measures. Therefore, the river corrections reduce the flooded areas of this scenario by 87%. If the building stock is assumed as constant over the whole period (building stock of 2012), then the number of exposed buildings would be around 48 times higher in the historic scenario without the river corrections. This means that the exposure of the actual building stock is reduced by 98% in a flood event comparable to the October 2011 flood event. But, taking into account the growth of buildings, this reduction of exposure is only 87%.

In the Gürbe river reach, the results differ remarkably from the other cases. Here, the historic scenario affects less buildings than the actual scenario. From the building stock of 2012, 217 residential buildings are located within the documented flooded areas of the July 1990 flood event whereas only 182 are exposed to the same flood event but on the historic terrain model. If we consider the economic growth, the increase of exposure to this flood is about 700%. There are two main reasons for this. As shown in figure 3, the Gürbe river flows now in a totally different location than 1850. The corrected river course transports the water towards the villages Mühleturnen and Toffen. In these villages, the most damages occurred in 1990. In a historic terrain model, the flood flowed in the floodplains East of the villages. In these areas, no settlements are located. The second reason is, that the 1990 flood event was an event with a very short duration of less than 7 hours. Because of this short duration, most of the peak flow is absorbed in the floodplains of the upper part of the study area. Thus, in the lower part of the floodplain, the flood is remarkably attenuated. In contrast, the actual river course transports much more water in the lower parts of the floodplain where the most buildings are located.

River reach	early-19 th century [km ²]	actual state [km ²]	difference [%]
Aare Thun-Bern August 2005 flood	20.4	2.5	-88
Hasliaare October 2011 flood	8	1	-87
Gürbe	4.6	0.2	-96

Table 4. Sum of flooded area.

River reach	early-19 th century [no.]	actual state [no]	difference 1815-2012 [%]
Aare Thun-Bern August 2005 flood	2076	51	-97
Hasliaare October 2011 flood	242	5	-98
Gürbe	182	217	+19

Table 5. Sum of exposed buildings (building stock of 2012 for both states of the river courses)

River reach	early-19 th century [no.]	actual state [no]	difference 1815-2012 [%]
Aare Thun-Bern August 2005 flood	165	12	-93
Hasliaare October 2011 flood	39	2	-94
Gürbe	31	31	0

Table 6. Sum of exposed buildings (building stock of 1919 for both states of the river courses)

River reach	early-19 th century [no.]	actual state [no]	difference 1815-2012 [%]
Aare Thun-Bern August 2005 flood	165	51	-69
Hasliaare October 2011 flood	39	5	-87
Gürbe	31	217	+700

Table 7 Sum of exposed buildings (building stock of 1919 with historic terrain model vs. building stock of 2012 with recent events)

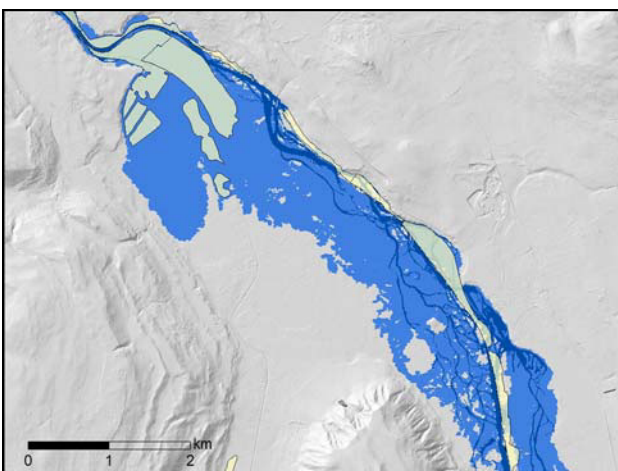


Figure 4. Comparison between the documented flooded areas of the August 2005 flood event (in yellow) in the Aare river and the hypothetical simulation of the same flood event in a historic state of the river course.

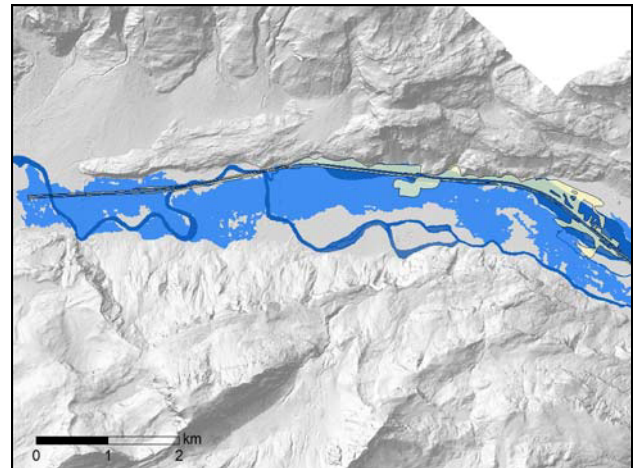


Figure 5. Comparison between the documented flooded areas of the October 2011 flood event (in yellow) in the Hasliaare river and the hypothetical simulation of the same flood event in a historic state of the river course.

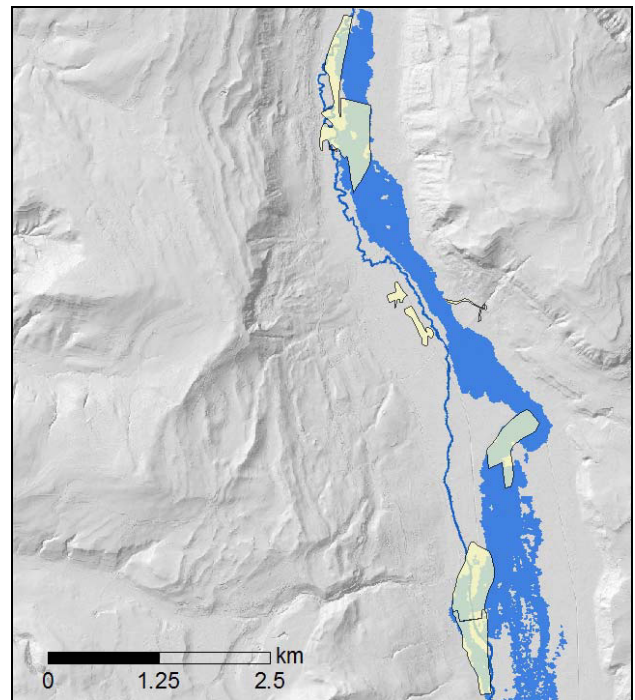


Figure 6. Comparison between the documented flooded areas of the July 1990 flood event (in yellow) in the Gürbe river and the hypothetical simulation of the same flood event in a historic state of the river course.

4 Discussion and conclusions

The results enable a first attempt to assess and quantify the effects of the river corrections of the 19th century for today's flood exposure. With the first two cases, the hypothesis could be verified while the Gürbe case study leads to a falsification. It is shown, that the range in reducing the flood exposure lays between 69 and 98%. But, also an increase is possible. The number of residential buildings exposed to the selected flood events would be up to forty times higher in a situation without any flood defence structures. It is also shown that the increase in the building stock reduces the effects of the

flood defence structures remarkably. Nevertheless, the positive effects of the flood defence structures in terms of exposure reduction outweigh these compensation effects of economic growth. The latter case shows that the loss of the retention effects of floodplains should be considered if assessing the effects of the river corrections in a holistic way. The special case of the July 1990 flood event in the Gürbe valley shows that the deviation of the river by the correction works is not reducing the exposure of buildings.

With this approach, arguments for the maintenance efforts could be formulated. Without a continuous maintenance of the meanwhile 150-year-old flood defence structures, the damages would be remarkably higher in case of a collapse. However, the example of the Gürbe river reach shows a differentiated view to this topic. Here, the flood defence structures increase the number of exposed buildings. The reasons are that the location of the actual river course totally differs from the historic river course and that the retention effect of the floodplain is lost. But, this example is only representative for flood events with a very short duration. In case of longer rain events, the floodplains may be filled also in their historic status and the peak discharge may be relevant also in the lower part of the floodplain. Nevertheless, this example shows that the re-allocation of the actual river course to the former place could be an interesting option in flood risk management.

The limitation of the presented approach lays in the restricted selection of the flood scenarios. For each study area, only one selected flood event was chosen for the assessment of the effectivity of the existing flood defence structures. This may lead to a constrained explanatory power. Especially, discharges below the transport capacity of the actual river reaches do not result in damages today. But, without any flood defence structures, also these discharges would result in damages. Therefore, it would be very interesting if the consideration of discharges with a medium frequency lead to other conclusions than drawn here. With more scenarios, the effectivity of the existing flood defence structures could be assessed in more detail. Another limitation of the presented approach is the validation of the hydrodynamic model of the historic status. The extents of historic floods are not known in detail. So, the reliability of the simulated flood events cannot be assessed and the uncertainties remain rather unknown. However, sensitivity analyses showed that the extent of the flooded areas are remarkably robust. Thus, - since the flow depths were not used - the simulations were assessed as valid for the purpose of this study. A further critical point is that the inflows of the tributaries into the floodplain were not considered. The inflows are not known, therefore the effects of this omission is hardly to assess.

However, the described examples show that the effects of the main river corrections are remarkable for today's economic activities in the floodplains. The effect of the river corrections for risk reduction is higher than the increasing risk due to the economic development in the studied time period. Therefore, the maintenance of the

former river correction works is an important part of today's risk management practice.

Acknowledgements: The author acknowledges the contributions of Sven Girod, Till Zaugg and Kevin Arnold for the collecting, compiling and georeferencing the historic data out of the historic maps and cross sections.

5 References

1. Kjeldsen T. R., Macdonald N., Lang M., Mediero L., Albuquerque T., Bogdanowicz E. et al. (2014). Documentary evidence of past floods in Europe and their utility in flood frequency estimation. *Journal of Hydrology* **517**, pp. 963–973.
2. Wetter O., Pfister C., Weingartner R., Luterbacher J., Reist T., Trösch J. (2011). The largest floods in the High Rhine basin since 1268 assessed from documentary and instrumental evidence. *Hydrological Sciences Journal* **56(5)**, pp. 733–758
3. Bodoque J. M., Díez-Herrero A., Eguibar M. A., Benito G., Ruiz-Villanueva V., Ballesteros-Cánovas J. A. (2015). Challenges in paleoflood hydrology applied to risk analysis in mountainous watersheds – A review. *Journal of Hydrology* **529**, pp. 449–467.
4. Herget J., Roggenkamp T., Krell M. (2014). Estimation of peak discharges of historical floods. *Hydrol. Earth Syst. Sci.* **18(10)**, pp. 4029–4037.
5. Zbinden E. (2011). Das Magdalenen-Hochwasser von 1342 – der «hydrologische Gau» in Mitteleuropa. *Wasser, Energie, Luft* **103(3)**, pp. 193–203.
6. Masoero A., Claps, P., Asselman N.E.M., Mosselman E., Di Baldassarre, G. (2013). Reconstruction and analysis of the Po River inundation of 1951. *Hydrol. Process.* **27(9)**, pp. 1341–1348
7. Schulte L., Peña J. C., Carvalho F., Schmidt T., Julià R., Llorca J., Veit, H. (2015). A 2600-year history of floods in the Bernese Alps, Switzerland: frequencies, mechanisms and climate forcing. *Hydrol. Earth Syst. Sci.* **19(7)**, pp. 3047–3072.
8. Benito G., Brázdil R., Herget J., Machado M. J. (2015). Quantitative historical hydrology in Europe. *Hydrol. Earth Syst. Sci.* **19(8)**, pp. 3517–3539.
9. Himmelsbach I., Glaser R., Schoenbein J., Riemann D., Martin, B. (2015). Reconstruction of flood events based on documentary data and transnational flood risk analysis of the Upper Rhine and its French and German tributaries since AD 1480. *Hydrol. Earth Syst. Sci.* **19(10)**, pp. 4149–4164
10. Sear D. A., Newson M. D. (2003). Environmental change in river channels: a neglected element. Towards geomorphological typologies, standards and monitoring. *Science of The Total Environment* **310(1-3)**, pp. 17–23.
11. Spaliviero M. (2003). Historic fluvial development of the Alpine-foreland Tagliamento River, Italy, and consequences for floodplain management. *Geomorphology* **52(3-4)**, pp. 317–333.
12. Remo J. W.F., Pinter N. (2007). Retro-modeling the Middle Mississippi River. *Journal of Hydrology* **337(3-4)**, pp. 421–435.

13. Pinter N., Heine R.A. (2005). Hydrodynamic and morphodynamic response to river engineering documented by fixed-discharge analysis, Lower Missouri River, USA. *Journal of Hydrology* **302(1-4)**, pp. 70–91.
14. Wirth S. B., Girardclos S., Rellstab C., Anselmetti, F. S. (2011). The sedimentary response to a pioneer geo-engineering project: Tracking the Kander River deviation in the sediments of Lake Thun (Switzerland). *Sedimentology* **58(7)**, S. 1737–1761.
15. Vischer D. (2003). Die Geschichte des Hochwasserschutzes in der Schweiz. Bundesamt für Wasser und Geologie. Bern
16. Girod, S. (2015). Rekonstruktion des historischen Flusslaufes der Aare zwischen Thun und Bern. Bsc Thesis. University of Bern, Bern. Institute of Geography.
17. Zaugg, T. (2015). Rekonstruktion des historischen Flusslaufes der Aare zwischen der Aareschlucht und dem Brienersee. Bsc Thesis. University of Bern, Bern. Institute of Geography.
18. Arnold, K. (2015). Rekonstruktion des historischen Flusslaufes der Gürbe. Bsc Thesis. University of Bern, Bern. Institute of Geography.
19. Vetsch D., Siviglia A., Ehrbar D., Facchini M., Gerber M., Kammerer S., Peter S., Vonwiller L., Volz C., Farshi D., Mueller R., Rousselot P., Veprek R., Faeh R. (2016). BASEMENT – Basic Simulation Environment for Computation of Environmental Flow and Natural Hazard Simulations. ETH Zurich. Zurich.
20. Fuchs S.; Keiler, M.; Zischg, A. (2015): A spatiotemporal multi-hazard exposure assessment based on property data. *Nat. Hazards Earth Syst. Sci.* **15(9)**, pp. 2127–2142.

5.2 Paving the ground: Model development

Paper 11: Röthlisberger, V., Zischg, A., Keiler, M., 2018. A comparison of building value models for flood risk analysis. *Natural Hazards and Earth System Sciences* 18, 2431–2453. [10.5194/nhess-2017-442](https://doi.org/10.5194/nhess-2017-442).



A comparison of building value models for flood risk analysis

Veronika Röthlisberger^{1,2,3}, Andreas P. Zischg^{1,2,3}, and Margreth Keiler^{1,2}

¹Institute of Geography, University of Bern, Hallerstrasse 12, 3012 Bern, Switzerland

²Mobilier Lab for Natural Risks, University of Bern, Hallerstrasse 12, 3012 Bern, Switzerland

³Oeschger Centre for Climate Change Research, University of Bern, Falkenplatz 16, 3012 Bern, Switzerland

Correspondence: Veronika Röthlisberger (veronika.roethlisberger@giub.unibe.ch)

Received: 13 December 2017 – Discussion started: 18 December 2017

Revised: 16 August 2018 – Accepted: 21 August 2018 – Published: 14 September 2018

Abstract. Quantitative flood risk analyses support decisions in flood management policies that aim for cost efficiency. Risk is commonly calculated by a combination of the three quantified factors: hazard, exposure and vulnerability. Our paper focuses on the quantification of exposure, in particular on the relevance of building value estimation schemes within flood exposure analyses on regional to national scales. We compare five different models that estimate the values of flood-exposed buildings. Four of them refer to individual buildings, whereas one is based on values per surface area, differentiated by land use category. That one follows an approach commonly used in flood risk analyses on regional or larger scales. Apart from the underlying concepts, the five models differ in complexity, data and computational expenses required for parameter estimations and in the data they require for model application.

The model parameters are estimated by using a database of more than half a million building insurance contracts in Switzerland, which are provided by 11 (out of 19) cantonal insurance companies for buildings that operate under a monopoly within the respective Swiss cantons. Comparing the five model results with the directly applied spatially referenced insurance data suggests that models based on individual buildings produce better results than the model based on surface area, but only if they include an individual building's volume.

Applying the five models to all of Switzerland produces results that are very similar with regard to the spatial distribution of exposed-building values. Therefore, for spatial prioritizations, simpler models are preferable. In absolute values, however, the five model results differ remarkably. The two simplest models underestimate the overall exposure, and even more so the extreme high values, upon which risk man-

agement strategies generally focus. In decision-making processes based on cost-efficiency, this underestimation would result in suboptimal resource allocation for protection measures. Consequently, we propose that estimating exposed-building values should be based on individual buildings rather than on areas of land use types. In addition, a building's individual volume has to be taken into account in order to provide a reliable basis for cost–benefit analyses. The consideration of other building features further improves the value estimation. However, within the context of flood risk management, the optimal value estimation model depends on the specific questions to be answered. The concepts of the presented building value models are generic. Thus, these models are transferable, with minimal adjustments according to the application's purpose and the data available. Within risk analyses, the paper's focus is on exposure. However, the findings also have direct implications for flood risk analyses as most risk analyses take the value of exposed assets into account in a linear way.

1 Introduction

Flood damage accounts for a large proportion of the economic losses due to natural hazards in developed countries, e.g. approximately one-third of losses over recent decades in Switzerland (Bundesrat, 2016) and Europe (European Environment Agency, 2017). Flood losses are expected to increase, not only due to ongoing anthropogenic climate change (IPCC, 2014) but also due to socio-economic development (Arnell and Gosling, 2016; Barredo, 2009; Kundzewicz et al., 2014; Liu et al., 2015). Future flood losses can be managed and ideally reduced with a wide range of

measures. Yet, measures entail costs, either in the form of direct construction expenditures or, indirectly, through lost profits due to restricted land use. However, budgets are generally limited and thus they require measures be prioritized. This prioritization is based on quantitative flood risk analyses in many countries (Bründl et al., 2009; European Parliament, 2007).

In this context, risk is commonly defined as a combination of hazard, exposure and vulnerability (see Birkmann, 2013 for an overview). It is usually expressed as the expected annual damage within a given area. There are different approaches with which to estimate this expected annual damage. While models based on absolute damage functions combine exposure and vulnerability into one model component (e.g. Penning-Rowsell et al., 2005; Zhai et al., 2005), studies applying relative damage functions explicitly consider both the value and the physical vulnerability of exposed assets (e.g. Glas et al., 2017; Hatzikyriakou and Lin, 2017). The latter approach has the advantage of being more transparent than risk models with absolute damage functions. Our paper focuses on exposure, in particular on the relevance of building value estimation schemes within flood exposure analyses on regional to national scales. However, as most risk analyses take the value of exposed assets into account in a linear way, this study's results have direct implications for flood risk analyses, too.

Different studies (e.g. de Moel and Aerts, 2011; Koivumäki et al., 2010) show that uncertainties in quantitative flood risk analyses are driven rather by uncertainties in the value of exposed assets than by uncertainties in area or frequency of floods. This is especially true on regional to national scales, where data availability limits the spatial resolution and differentiation of asset values within flood exposure analyses. Aggregated classes of land use have been the norm (Gerl et al., 2016), at least until recently, and the area-specific value of each land use class is derived from lumped economic data of administrative units (Merz et al., 2010). This transformation of values per administrative unit into values per spatial unit differentiated by land use class implies spatial data disaggregation, also referred to as dasymetric mapping (Chen et al., 2004; Thieken et al., 2006). While several case studies investigate the influence that different data sources of asset values have on flood loss estimation (e.g. Bubeck et al., 2011; Budiyo et al., 2015; Cammerer et al., 2013; Jongman et al., 2012), the effect of dasymetric mapping methods is only addressed in a few publications. For instance, Wunsch et al. (2009) and Molinari and Scorzini (2017) show in local case studies that, even though the way in which exposed assets are estimated influences the resulting flood loss and thus flood risk, the spatial resolution of the exposed assets is more important. In both cases, the validation with recorded losses suggests that finer resolution of asset data improves the modelling results. Yet, both research teams conclude that further research on the impact of data resolution and disaggregation is needed. In fact, based on the growing availability

of high-resolution data and increasing computational power, more and more flood-risk-related studies on national scales are based on data at the building level (e.g. Fuchs et al., 2015, 2017; Jongman et al., 2014; Röthlisberger et al., 2017). However, the individual monetary value of the buildings is usually not available due to data privacy restrictions and thus has to be estimated. There are different methods used in flood risk analyses to estimate individual building values (Jongman et al., 2014; Kleist et al., 2006). They range from uniform average value per building to sophisticated regression models considering different building features. Yet, the role of these value estimation methods in flood risk assessments has received even less attention than the effect of dasymetric mapping methods. To the best of our knowledge, no study has compared different object-based building value models, nor have these object-based methods ever been contrasted with the commonly used approaches of land-use-specific values per area within the context of regional or national risk analyses. To fill this gap, we investigate the influence of five different value estimation models (called M1 to M5; see Appendix A3 for an overview table of all abbreviations used in the text) on the resulting values of flood-exposed buildings in Switzerland. Four of these models (M1, M2, M4 and M5; see upper most row in Table 1) refer to individual buildings, whereas one model (M3) uses average values of buildings per area, differentiated by land use category. The five models' underlying concepts are widespread in risk management, construction industry and/or real estate management (see bottom row in Table 1). Apart from the concept, the five models mainly differ in their complexity and requirements on data resolution and differentiation.

However, this paper does more than evaluate the role of building value models within flood risk analyses. Our study also investigates the models' influence on flood risk management decisions. In the context of the above-mentioned need for prioritization, most current flood management policies aim for cost efficiency. With regard to cost-efficient measures, the actual monetary value of flood-exposed buildings is important, as are the statistical and spatial distributions of these values. While the spatial distributions suggest areas of priority for the implementation of cost-efficient protection measures, the monetary values of exposed buildings affect the upper cost limits of such measures. Thus, we investigate both the monetary values and their distributions. As for distributions and actual values, the extremely high values are particularly relevant for risk management. Therefore, our study analyses them in detail. The monetary values in this paper are insured values of buildings, which are replacement costs and correspond to the financial resources needed to reconstruct (flood) damaged buildings or building parts. Replacement costs are very common for cost-benefit analyses in Switzerland as the allocation of federal subsidies demands proof of the cost efficiency of measures using a tool with replacement values as default (Bründl et al., 2009). Moreover, a comprehensive review of flood loss models by Gerl

Table 1. Overview of concepts, data and applications of the five investigated models for building value estimation. BFP stands for building footprint polygons, BZP for building zone polygons and PIC for points of insurance contracts.

Model name and concept	M 1 uniform average value per building	M 2 uniform average value per building volume	M 3 average value of buildings per area, differentiated by land use category	M 4 average value per building volume, differentiated by building features	M 5 value per building, individually calculated based on linear regression
Parameter estimation and unit	Total value of buildings in an area divided by total number of buildings in the same area, (CHF)	Total volume of buildings in an area divided by total number of buildings in the same area, (CHF m ⁻³)	Total value of buildings within an area of a particular land use category divided by the size of the area, (CHF m ⁻²)	Total value of buildings with identical features divided by the volume of the buildings, (CHF m ⁻³)	Minimal adequate linear function of building features, (CHF)
Data for parameter estimation					
Minimal requirement	Global sums of values and numbers of buildings within a given area	Global sums of values and volumes of buildings within a given area	Global sum of building values within an area with particular land use size of the area	Global sums of values and volumes of buildings with identical features	Individual values and features of buildings
Used in this study	Complete data of eight cantons where entire portfolio insurance data are available: Total of insured buildings values in 529 224 PIC Total number of BFP (391 766)	Total of insured buildings values in 529 224 PIC Total volume of BFP (653 × 10 ⁶ m ³)	Total of insured buildings values in 529 224 PIC BZP of 12 408 km ² , covering the entire area	BFP of eleven cantons, reduced to polygons with joined PIC and matching volumes (n = 172 562) BFP including volume, summarized value of joined PIC and information on land use and building purpose	BFP including volume, summarized value of joined PIC and information on land use, municipality type, building purpose and use
Data for benchmark selection	The data must be spatially referenced at object level and complete within a given area. In this study, we use the 529 224 PIC of the eight cantons, where complete portfolio data of the cantonal insurance company for buildings are available.				
Data for model application					
Minimal requirement	Individual buildings: location only	Individual buildings: location and volume	Land use: spatially gapless information on land use categories	Individual buildings: location, volume and features	
Used in this study	BFP data set of 2 086 411 footprints	BFP data set of 2 086 411 footprints, including volume	BZP of 41 290 km ² , covering the whole of Switzerland	BFP data set of 2 086 411 footprints, including volume and information on land use and building purpose	
Frequent fields of applications	Default values in tools for cost–benefit analyses of flood protection measures		Widely used in flood risk analyses on regional to national scales	Mainly used in construction industry and real estate management for the estimation of individual building construction costs	
Examples	DEFRA (2001); Wagenaar et al. (2016); van Dyck and Willems (2013)	BAFU (2015); de Bruijn et al. (2015); Mobilair Lab (2016); Winter et al. (2018)	de Bubeck et al. (2011); Cammerer et al. (2013); ICPR (2001); Klijn et al. (2007); Thielen et al. (2008)	Hägi (1961); Naegeli and Wenger (1997); SVKG and SEK/SVIT (2002) Few applications in flood risk management, mainly at local level, e.g. Arrighi et al. (2013),	Lowe et al. (2006); Sonmez (2008) To our knowledge no application in flood risk management

et al. (2016) shows that replacement costs are in fact the most often indicated cost base. Yet, there are risk analyses which use other types of building values, e.g. property prices (Ernst et al., 2010) or depreciated construction values (ICPR, 2001). However, this paper's topic, which is the relevance of the model approach for the resulting value of exposed buildings, does not depend on the value type and we thus refer to the literature (Merz et al., 2010; Penning-Rowsell, 2015) for broader discussions on building values in risk analyses.

2 Methods applied and data used

The data and methods section is organized as follows. The first subsection (Sect. 2.1) generically explains the set-ups of the five building values models and the estimation of their parameter values. In Sect. 2.2, we describe subsequent steps towards values of flood-exposed buildings, namely the intersection with flood hazard maps and the spatial aggregation of the results. The models are compared in Sect. 2.3. The data used in this study are described in the last part of this section,

Sect. 2.4. Table 1 gives an overview of the five models with respect to their underlying concepts, data and applications.

2.1 Model set-up for value estimation

The five models in our study follow two different approaches. M3 is based on average value of buildings per area, differentiated by land use category. The other four models (M1, M2, M4 and M5) refer to individual buildings. These four models are defined as follows: M1 is uniform average value per building; M2 is uniform average value per building volume; M4 is average value per building volume, differentiated by building features; and M5 is value per building, individually calculated based on linear regression. From M1 to M5, the complexity of the five models increases, as well as the data and computational expenses required for the estimation of their parameter values (see Table 1). The selection of the five models is driven by the data, which are available throughout Switzerland, as this paper is focused on analyses on regional to national scales. An additional selection criteria is the current application in risk management, construction industry or real estate management (see bottom line in Table 1). In the following, we outline the concepts of the five models and the estimation of their parameter values.

Model M1: uniform average value per building

Model M1 takes a straightforward approach as it assigns the same uniform average building value to each building. The parameter estimation requires two quantities with the same spatial aggregation, e.g. administrative units: (1) the total cumulative value and (2) the total number of buildings within the same area. By dividing the total building value by the total number of buildings, we obtain the value of the model's only parameter. The parameter corresponds to the average value of the buildings situated within the observed area. The unit of the M1 parameter is monetary value per building, e.g. (CHF).

Model M2: uniform average value per building volume

Model M2 is based on the building volumes only. The data requirements for the parameter estimation are similar to the ones for M1. In place of the total number of buildings, M2 requires the total cumulative volume of buildings within a given area. To obtain the value of model's only parameter, the total building value is divided by the total building volume. Thus, the parameter of M2 is defined as the average value per building volume and is given in monetary value per unit volume, e.g. (CHF m⁻³).

Model M3: average building values per area, differentiated by land use category

Model M3 takes a very common approach to flood risk analyses on national scales. It makes use of average building val-

ues per unit area, differentiated by land use category. For the same given area, the parameter estimation requires two comprehensive data sets of comparable spatial resolution: (1) gapless polygons of land use types and (2) spatially referenced data on building values. The two data sets are spatially joined, and the total building values per land use category are then calculated. In a last step, the cumulative building values per each type of land use are divided by the respective total area. This results in land-use-specific values of the model's parameter. They correspond to the average monetary building value per area of each land use category, which is given in monetary value per unit area, e.g. (CHF m⁻²).

Model M4: average values per building volume, differentiated by land use category and building purpose

Model M4's parameter is the same as in M2, i.e. the average monetary value per building volume. In contrast, the parameter values of M4 are not uniform but differentiated according to building feature. In this study, land use category and building purpose are the criteria for differentiation. To estimate the specific parameter values of M4, we combine data on monetary value, volume, land use category and building purpose at the building level. These assignments at building level require inputting data of high spatial resolution and precise localization. To estimate M4's parameter values, the data assignments have to be complete for each individual building. However, in contrast to M1, M2 and M3, the input data for M4 do not need to be comprehensive within a given area. For M4, only buildings with complete information on value, volume and the differentiation criteria are considered, and the value and volume of all buildings from the same combination of differentiation criteria (e.g. same land use category and building purpose) are summed up. Finally, the cumulated monetary values are divided by the respective volumes, resulting in the model's parameter values. Thus, we obtain one specific value for each combination of differentiation criteria. The parameter's unit is monetary value per unit volume, e.g. (CHF m⁻³).

Model M5: value per building, individually calculated based on linear regression

M5 is a linear regression model and is set up with the same input data as M4. We develop M5 in an exploratory manner by starting with a maximal model, which includes all available explanatory variables, i.e. building features (Table 1 and Table A1) and their interactions. It is then reduced to simpler models by removing non-significant interactions and variables. In addition, models with transformed variables are set up. Out of this variety of models, we select the minimal adequate model. Namely, we follow the principle of parsimony and choose a model with a relatively small Akaike Information Criterion (AIC; Akaike, 1974), a high coefficient of determination (adjusted R^2) and a minimal number

of non-significant explanatory variables and interactions. In addition, we plot the model's residuals to check visually if principal assumptions of linear regression on residuals are satisfied. The result of this exploratory process is the minimal adequate model that makes it possible to calculate the expected monetary value of a building as a linear function of the selected buildings attributes and interactions. This value is given in monetary units, e.g. (CHF).

While the five applied models are conceptually different, the estimation of their parameter values in our study is based on the same data sets as much as possible. Nevertheless, the parameter estimation is based on two different kinds of data subsets. This is because the first three models (M1 to M3) require a data selection, which fulfils different criteria in comparison to the selection for M4 and M5. While the crucial prerequisite for M1, M2 and M3 is data completeness within a given area, the other two models require a high spatial accuracy of the input data, mirrored in matching data assignments on individual building levels. Figure 1 shows the workflow of the set-ups of the five models for building value estimation.

2.2 Intersection with flood hazard maps and spatial aggregation

Based on the five described models, it is possible to calculate the monetary value of individual buildings (M1, M2, M4 and M5) or mean building values within predefined areas (M3). To identify the values which are exposed to floods, the buildings or areas need to be spatially referenced and overlaid with flood hazard maps. The exposed values based on M3 are defined by the extent of flood-exposed areas and their respective monetary value per area. With regard to exposed values based on individual buildings, we classify a building as exposed to floods if it partially or entirely overlaps with a flood-prone area. From this exposed building, the entire monetary value is considered for the calculation of flood-exposed values. To compare the model based on areas (M3) with the other four models, we compile a map of regular hexagons with an area of 10 km² and calculate the sum of exposed values per hexagon for all five models.

The described intersection with flood hazard zones reduces the value of exposure to the buildings within flood-prone areas. In other contexts – in particular in the insurance industry, which provided data to this study (see Sect. 2.4.3) – exposure includes all assets or buildings, irrespective of the object's individual chance of being damaged.

2.3 Selection of benchmark model and model comparison

Because our study mainly focuses on comparing different modelling approaches rather than on model predictions, we follow a benchmark test instead of a strict validation procedure. In a first step, we select a benchmark model that best fits the direct application of provided portfolio data of can-

tonal insurance companies for buildings within eight Swiss cantons. In a second step, we compare the other four models with the benchmark model and examine the distributions of the extreme high values in more detail, including their spatial distributions. In contrast to the selection of the benchmark, the comparison of the benchmark model with the four other models covers the entire modelled area, i.e. the whole of Switzerland.

It is possible to select the model with the best fit in areas, where the data sets of the original building values are complete and spatially referenced on the building level. In our study, these areas correspond to the cantons, for which complete portfolio data of the cantonal insurance company for buildings are available; see Sect. 2.4.3. Within these cantons, we attribute the original building values from the portfolio data sets to the corresponding building geometries. Identifying flood-exposed buildings and summing the exposed values per hexagon are done in the same manner as for the building-based models. To identify the benchmark model, we examine differences and similarities between the model-based results and the results based on the original building values. For that matter, we calculate the root-mean-square errors (RMSE) and mean absolute errors (MAE) at the data aggregated to hexagons. We compile scatter plots of the hexagon values and compare the sum of exposed values over all hexagons within the validation area. As we are particularly interested in the distribution of the extreme high values, we further fit a generalized Pareto distribution (GPD) to the data above a certain consistent threshold. The threshold is the location parameter of the GPDs. The other two GPD parameters, the scale and shape, are estimated with the R package *fExtremes* (Wuertz, 2015) by applying the probability-weighted moment method. Furthermore, we compare the highest hexagon values of each data set within the validation area.

2.4 Data

Each of the five generic models makes it possible to estimate flood-exposed-building values based on data sets that are available in many countries. However, the model set-up, especially the estimation of the parameter values, requires data sets on monetary building values, which are either representative of a given area (M1 to M3) and/or spatially explicit (M3 to M5). In the following, Sect. 2.4.1, we present the input data of our study in Switzerland, and in Sect. 2.4.2 we detail the data selection for the parameter estimation. Section 2.4.3 shortly describes the data and area of model application and comparison.

2.4.1 Input data

The main three data sets which are used for the estimation of the model parameter values are (1) point of insurance contract (PIC), (2) building zone polygon (BZP) and (3) building footprint polygon (BFP). The latter two are also

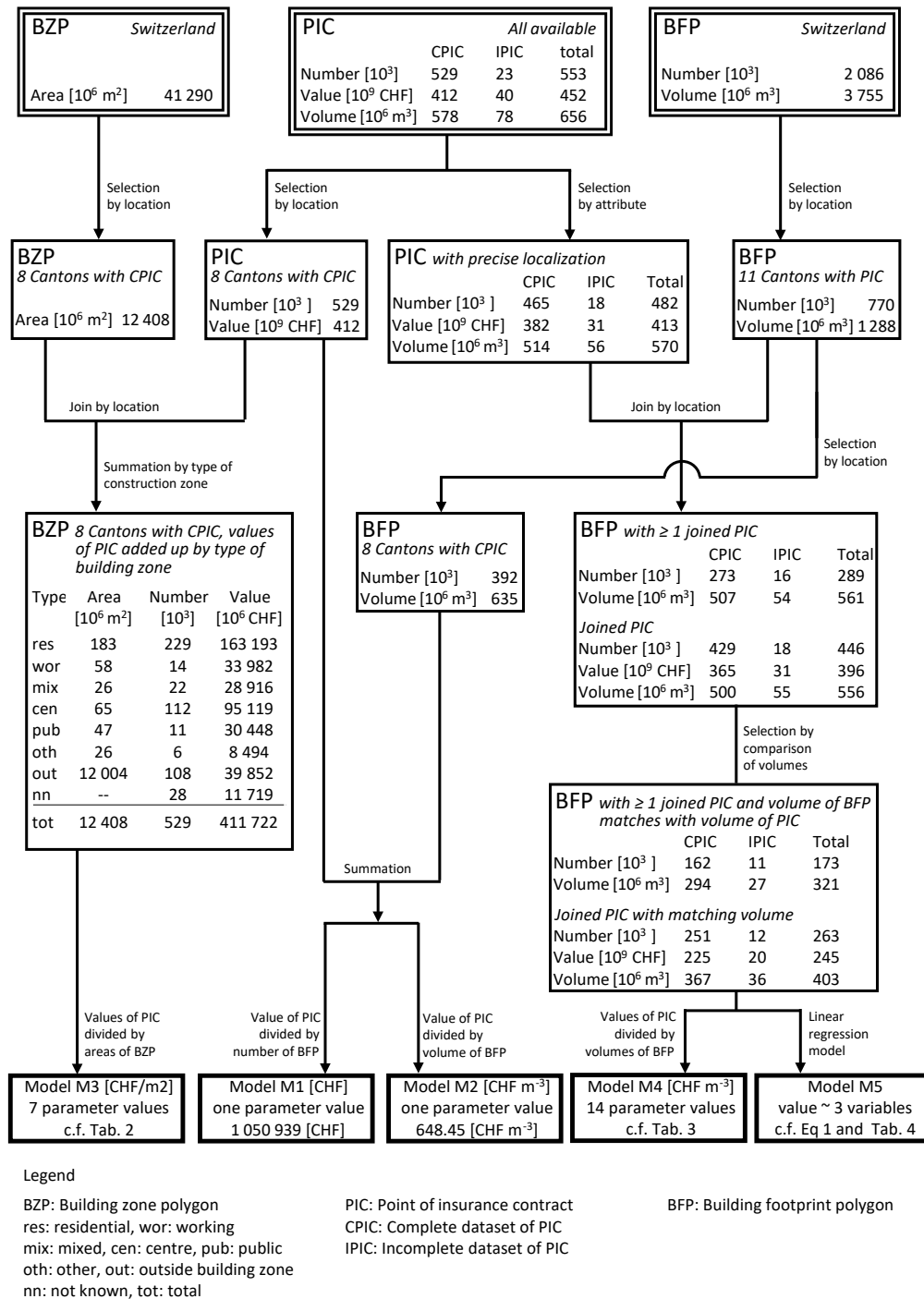


Figure 1. Workflow of the set-ups of the five investigated models for building value estimations.

used in the model application (see Table 1). The PIC data set is a compilation of 552 698 insurance contracts provided by eleven cantonal insurance companies for buildings (see Fig. 2), harmonized and expressed as values as per 2014. Of these eleven insurance companies, eight companies provided the whole portfolio data set from 2013, whereas the three re-

maining companies provided contract data, restricted to contracts, with at least one flood claim between 1999–2013 (two companies) and 1989–2013 (one company). All data are provided for the exclusive purpose of research and are subject to strict confidentiality.

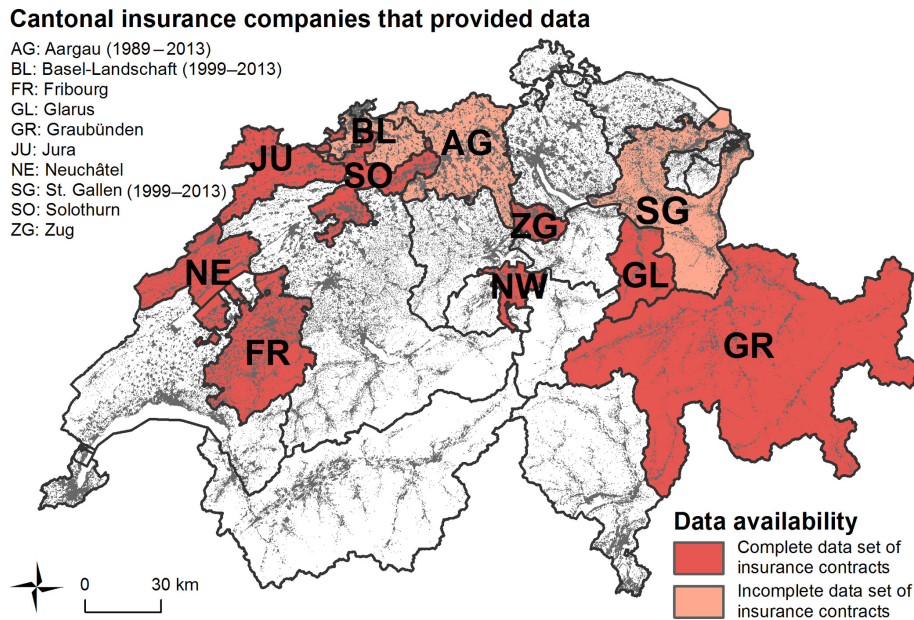


Figure 2. Overview of provided data by the cantonal insurance companies for buildings. Three insurance companies only provided data limited to contracts associated with at least one flood claim within the period indicated in brackets. The grey-shaded areas indicate the footprints of all buildings in Switzerland. Map source: Federal Office of Topography (swisstopo).

Table 2. Parameter values of the model M3, value per surface area (CHF m^{-2}) of seven types of land use, i.e. six types of building zones and the area outside of building zones, based on a complete portfolio data of eight cantonal insurance companies for buildings in Switzerland. Insured values of buildings, which are localized at least on street level, are directly assigned to a type of land use. Values of the remaining buildings are split over all types of land use according to the size of the area of each type. The results per type of land use, which are used for further analyses, are in bold. Table entries are ordered by rank of these results.

Type of land use	Area (10^3 m^2)	Value (10^3 CHF)	Value per area, directly assigned (CHF m^{-2})	Value per area, total (CHF m^{-2})
Centre	64 974	95 118 671	1463.94	1464.88
Mixed	25 705	28 915 610	1124.89	1125.84
Residential	182 593	163 193 242	893.76	894.70
Public	47 323	30 448 192	643.42	644.36
Working	57 652	33 982 269	589.44	590.38
Others	25 593	8 493 504	331.87	332.81
Outside building zone	12 003 959	39 851 666	3.32	4.26
Not directly assigned	–	11 719 182	–	0.94
Total	12 407 798	411 722 336	32.24	33.18

Cantonal insurance companies for buildings are present in 19 (of totally 26) Swiss cantons. In these 19 cantons, the insurance of buildings is compulsory and provided by the respective cantonal insurance company for buildings, which operates under a legal monopoly. The claims are compensated at replacement costs; thus, the premiums are calculated based on replacement values. Consequently, the portfolio data of a cantonal insurance company for buildings include the replacement value of virtually every building within the respective canton. In addition, most contracts are located on the building level – in this study, this is true for 87 % of the

provided contracts – and often contain the volume of the insured building or building part. In our case, 78 % of the contracts include this information. The replacement values used and provided by the cantonal insurance companies for buildings are object-specific estimates by experts. The values are based either (for new buildings) on documented construction costs such as invoices or (for older buildings) on on-site inspection and validation.

The second input data are the countrywide harmonized BZPs, provided by the Federal Office for Spatial Development (see Table A1 in the Appendix A). For our analysis,

Table 3. Parameter values of model M4, value per volume (CHF m⁻³) above ground, differentiated according to the area's land use where each building is located and by the purpose of the building. Calculations are based on insured values of 172 562 buildings, which are provided by eleven cantonal insurance companies in Switzerland. Table entries are ordered by the value per building volume of buildings with a residential purpose.

Type of land use	With residential purpose			Without residential purpose		
	Insured building values (10 ³ CHF)	Volume of buildings (10 ³ m ³)	Value per building volume (CHF m ⁻³)	Insured building values (10 ³ CHF)	Volume of buildings (10 ³ m ³)	Value per building volume (CHF m ⁻³)
Public	9 684 445	10 150	954	7 068 467	8640	818
Others	2 322 506	2446	950	866757	1187	730
Residential	110 421 355	123 056	897	2 263 843	2960	765
Centre	56 405 627	65 486	861	3 452 311	5351	645
Mixed	15 792 658	19 708	801	3 107 297	5321	584
Outside building zone	9 668 384	16 221	596	4 908 676	13 062	376
Working	7 702 381	15 259	505	12 140 152	32 234	377

Table 4. Parameter estimates, standard errors, and *t* and *p* values of the three explanatory variables (and their pairwise interaction) of model M5. The three explanatory variables are residential purpose (ResPur) with values yes and no, the building volume above ground in m³ (volume) and land use (LaUse) with values residential, working, mixed, centre, public, others and outside (i.e. area outside building zones). The intercept stands for the variable values of log₁₀ (volume) = 0 (i.e. volume = 1 m³); ResPur=no and LaUse=outside.

Parameter	Estimate	Standard error	<i>t</i> value	<i>Pr</i> (> <i>t</i>)
Intercept	3.097512	0.00633	489.334	< 2.00E-16
ResPur yes	0.793809	0.007992	99.323	< 2.00E-16
log ₁₀ (volume)	0.80819	0.002385	338.9	< 2.00E-16
LaUse residential	-0.51207	0.009017	-56.79	< 2.00E-16
LaUse working	-0.4035	0.016537	-24.4	< 2.00E-16
LaUse mixed	-0.65351	0.015906	-41.087	< 2.00E-16
LaUse centre	-0.70887	0.009651	-73.453	< 2.00E-16
LaUse public	-0.44107	0.017177	-25.678	< 2.00E-16
LaUse others	-0.6658	0.027504	-24.208	< 2.00E-16
ResPur yes × log ₁₀ (volume)	-0.15846	0.002694	-58.815	< 2.00E-16
ResPur yes × LaUse residential	-0.14691	0.003563	-41.23	< 2.00E-16
ResPur yes × LaUse working	-0.03614	0.005837	-6.192	5.95E-10
ResPur yes × LaUse mixed	-0.05128	0.005654	-9.071	< 2.00E-16
ResPur yes × LaUse centre	-0.0001	0.003439	-0.029	0.977
ResPur yes × LaUse public	-0.17378	0.006391	-27.19	< 2.00E-16
ResPur yes × LaUse others	-0.07611	0.011406	-6.673	2.52E-11
log ₁₀ (volume) × LaUse residential	0.258569	0.003217	80.371	< 2.00E-16
log ₁₀ (volume) × LaUse working	0.158917	0.004704	33.787	< 2.00E-16
log ₁₀ (volume) × LaUse mixed	0.26366	0.004834	54.542	< 2.00E-16
log ₁₀ (volume) × LaUse centre	0.263382	0.003448	76.397	< 2.00E-16
log ₁₀ (volume) × LaUse public	0.256911	0.005323	48.262	< 2.00E-16
log ₁₀ (volume) × LaUse others	0.282637	0.009382	30.127	< 2.00E-16

we reduce the nine provided building zone categories to six categories by merging the types “restricted building zones”, “zones for tourism and sports” and “transport infrastructure within building zones” to the type “other building zones”. Furthermore, we add the spatial complement of the building zones as “outside building zone” to the data set. Thus, we obtain a spatially gapless set of polygons with seven different types of building zones, namely “residential”, “working”, “mixed”, “centre”, “public”, “others” and “outside building zone”.

The third input data are data sets on buildings. In our study, we use the BFP of the swissTLM3D data set, provided by the Federal Office of Topography (see Table A1 in the appendix A) and harmonized as outlined in Röthlisberger et al. (2017). Three of our building value models consider not only the BFP positions but also various attributes which we assign to the polygons in preprocessing steps as described in Appendix A1. The complete set of attributes considered in the model set-up consists of six items: (1) building volume above ground, (2) type of building zone, (3) type of municipality within which the BFP is located, (4 and 5) binary in-

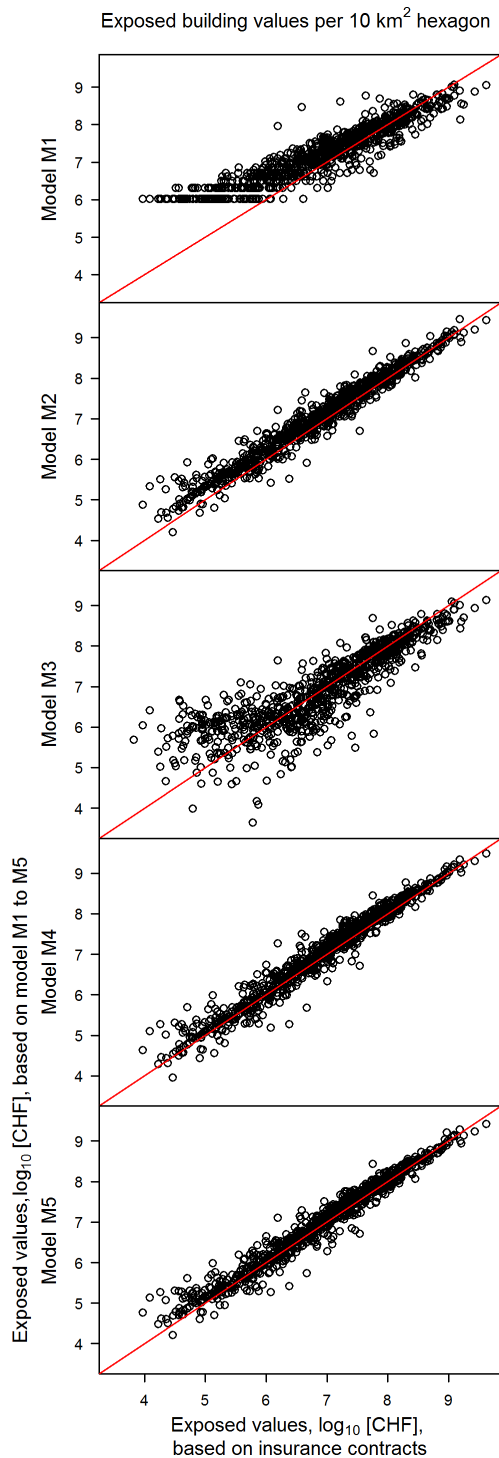


Figure 3. Scatter plot of flood-exposed-building values, aggregated to regular hexagons with a surface area of 10 km^2 . The sums based on models M1 to M5 (y axis) are plotted against the sums based on the direct application of the values from the spatially referenced building insurance contracts (x axis). The red lines indicate the 1 : 1 relation. The values are \log_{10} transformed and sums below 10^4 CHF are not shown.

formation about residential purpose and use and (6) building densities in the BFP’s surroundings.

The calculation of flood-exposed-building values does not only require information on building values, but also on flood-prone areas. To define the areas potentially prone to inundation in Switzerland, we combine two different types of flood maps. The main source is a compilation of all available communal flood hazard maps in Switzerland (Borner, 1999; de Moel et al., 2009). These maps are collected, harmonized and provided in agreement with the responsible cantonal authorities by the Swiss Mobiliar Insurance Company. We use the maps of December 2016, which cover 72 % of the buildings in Switzerland. In these maps, five different hazard levels are indicated, differentiated by the intensity (water depth and velocity) and probability of events (ARE et al., 2005). Out of the five hazard levels indicated in these maps, we consider the levels “major”, “moderate” and “low” as flood-prone areas. With the selection of these three levels, we include events up to a return period of 300 years. For the 28 % of the buildings in Switzerland that are not covered by the communal flood hazard maps, we use the coarser flood map called Aquaprotect. This data set is provided by the Federal Office for the Environment (Federal Office for the Environment, 2008). Aquaprotect is available for the whole of Switzerland and contains four different layers with recurrence periods of 50, 100, 250 and 500 years. For our study, we use the layer with the return period of 250 years. The compilation in GIS of the two map types follows the procedure described by Bernet et al. (2017) and results in a complete, nationwide map of flood-prone areas with return periods of up to 250 (territories not covered by communal hazard maps) and 300 years (territories covered by communal hazard maps).

2.4.2 Data selection for the parameter estimation

The workflow in Fig. 1 illustrates how the input data are combined and selected for the parameter estimation of the five models. The resulting data selection for each model is summarized in Table 1.

For M1 to M3, the two countrywide data sets (BFP for M1 and M2, BZP for M3) are reduced to the data entries, which are located within the eight cantons with complete building insurance data sets (left side of Fig. 1). In this way, the BZPs in the set-up of M3 cover 30 % of the data’s total coverage and the number of BFPs used for the parameter estimation of M1 and M2 correspond to 19 % of the total number of BFPs in Switzerland.

The selection of PIC is made in two ways. For the first three models (M1 to M3), we select all PICs within the eight cantons where complete portfolio data sets are available (see Fig. 1: PIC all available → selection by location → PIC eight cantons with CPIC). For M1 and M2, we directly use the total insured building value of these 529 224 contracts, which corresponds to CHF 412 billion. For M3, however, we fur-

Table 5. Indicators for the comparison of model M1 and M5 with the direct application of insurance data (insured values according to point-referenced building insurance contracts, PIC), in the eight cantons where complete portfolio data of the cantonal insurance companies for building are available. Sum represents the sum of exposed-building values over all 10 km² hexagons, RMSE and MAE represent the root-mean-square error and the mean-absolute error of exposed-building values per hexagon when comparing M1 to M5 with PIC. The generalized Pareto distribution (GPD) is fitted for hexagons with exposed-building values higher than 10⁸ CHF, which is equal to the location parameter of the GPD. Shape and scale represent the respective parameter of the fitted GPD. Max represents the highest sum of exposed-building values per hexagon. Bold numbers indicate the value (of M1–M5) nearest to the value based on PIC.

Method	Comparison over 1577 hexagons			Comparison of extreme values			
	Sum	RMSE	MAE	Fitted GPD for hexagons > 10 ⁸ (CHF)	Shape	Scale	Max
	(10 ⁶ CHF)	(10 ⁶ CHF)	(10 ⁶ CHF)		(10 ⁶)	(10 ⁶ CHF)	
M1	55 667	124	23	0.25639	128	1163	
M2	74 451	73	14	0.44574	151	2874	
M3	47 880	115	21	0.31655	117	1367	
M4	76 956	52	12	0.43464	162	3127	
M5	68 111	60	11	0.44709	143	2682	
PIC	67 375	–	–	0.49797	149	4157	

ther select the PICs that are localized at least at the street level, which is true for 95 % of the PICs in the eight cantons with complete portfolio data. These PICs are spatially joined with the BZPs within the respective eight cantons. The monetary values of these PICs (CHF 400 billion total) are summarized per BZP type, and the values of the remaining PICs (i.e. CHF 12 million; see Fig. 1: BZP eight cantons with CPIC, values of PIC added up by type of building zone) are split proportionally to the area of each BZP category and added to the respective sum per BZP categories.

For M4 and M5, we reduce the original PIC data provided by eleven insurance companies to the 87 % of points with a localization on building level, and then we assign these points to the nearest BFP with GIS software (see Fig. 1: PIC all available → selection by attribute → PIC with precise localization → join by location with BFP 11 cantons with PIC → BFP with ≥ 1 joined PIC). 92 % of the PICs with a localization on building level can be matched to a BFP within a distance of less than or equal to 5 m. The attributes of these PICs, i.e. the replacement values and volumes of the insured buildings or building parts, are summarized per BFP. With this summation, the BFP with at least one joined PIC contains the attributes of the preprocessing steps (see description in Appendix A1), as well as the insurance-sourced building values and volumes. In particular, each of these BFPs includes two types of building volume. The first type is the volume above ground, calculated, in preprocessing steps, based on BFP area and the average height above ground of the building. The second type is the sum of volumes recorded in all PICs, which are assigned to the BFPs. For M4 and M5, we select only those BFPs for which the two mentioned volumes are within a predefined range (see Fig. 1: BFP with ≥ 1 joined PIC → selection by comparison of volumes → BFP

with ≥ 1 joined PIC and volume of BFP matches with volume of PIC). For that matter, we calculate the volume ratio, i.e. the volume according to PIC divided by the BFP volume above ground. In the eight cantons, where we obtained complete portfolio data, we identify the volumes as matching if the volume ratio is equal to or more than 0.8 and less than or equal to 2.0. In the other three cantons, we set the lower criteria to equal to or more than 1.0. With this comparison of two independently derived volumes, we efficiently improve the quality of the BFP data. Particularly, we can exclude BFPs with inconsistencies in the calculation of the building volume above ground and BFPs with mistakenly (not) assigned PICs, which thus have monetary values that are too high (or low). The exclusion of these BFPs is crucial for the set-up of the regression model (M5) and cannot be done manually given the size of the data set. The described comparison of volumes reduces the BFPs and the joined PICs simultaneously and in a similar way. While 60 % of the BFPs to which a PIC is assigned are finally used for the set-up of M4 and M5, the respective ratio of PICs amounts to 59 %.

2.4.3 Data and area of model application and comparison

The estimation of the parameter values for all five models is restricted to territories or buildings for which specified building insurance data are available. In contrast to the parameter estimation, applying the models does not require any insurance data and is thus feasible for any territories or buildings with attributes that correspond to the model parameters. In our study, the building referenced models (M1, M2, M4, M5) are applied to the entire BFP data set of 2 086 411 polygons, while M3 is applied to the countrywide BZP data set with an

area of 41 290 km², thus covering all of Switzerland (see Table 1). The benchmark model is selected in the eight cantons where complete building insurance data sets are available; for the benchmark test, we again consider the entire territory of Switzerland.

3 Results and discussion

In this section, we first show the parameter values of the five building value models, M1 to M5 (Sect. 3.1), and then present the results of the benchmark selection and test. The overall discussion of the models in the last subsection (Sect. 3.4) complements the specific comments in the first three subsections.

3.1 Parameter values

M1 and M2

The parameter values of the two models with a single, uniform parameter are CHF 1 050 939 per building (M1) and 648.45 CHF m⁻³ per volume above ground (M2). These values are rather high compared to international literature data (DEFRA, 2001; de Bruijn et al., 2015; Wagenaar et al., 2016), mainly because of comparatively high building standards and construction costs in Switzerland. For instance, Diaz Muriel (2008) finds that the price level index for construction in Switzerland is 20 % higher than the average of the (at that time) 27 EU member states. In addition to and in contrast with these other studies, we count attached buildings like terraced houses as only one building, and the parameter of M2 refers to the building volume above ground but includes the costs for underground building volumes too.

M3 and M4

Table 2 shows the parameter values of M3, i.e. the monetary values of buildings per surface area (CHF m⁻²) of seven land use categories. Most notable are the value differences between the areas inside and outside building zones. The value for the areas outside the building zones is only a very low percentage of the building zones' values, i.e. between 0.3 % (for centre) and 1.3 % (for others). Within the building zones, the values show less variation; i.e. they differ by a maximal factor of 4.5 corresponding to the difference between the categories others and centre. Two aspects determine the parameter value of a specific land use class in M3: firstly, the density (built volume per unit area) of buildings in this land use class and, secondly, the monetary value per built unit volume. The second aspect is at the core of model M4, and the respective parameter values by land use type and building purpose (with or without residential purpose) are presented in Table 3. The monetary value per volume is higher for buildings with a residential purpose than for non-residential buildings, ranging between 17 % for residential and public building zones to

58 % for areas outside building zones. For residential buildings, the values for different land use types do not vary more than by a factor of 1.9 (working to public) and by a factor of up to 2.2 for buildings without a residential purpose. The ratio between the highest and the lowest M4 parameter value is 2.5. This is the ratio between the value per volume referring to residential buildings in public building zones and the value per volume, referring to non-residential buildings outside the building zone.

The remarkably smaller variation in parameter values in M4 compared to the variation in M3 and the differences between M3 and M4 in the ranking of land use types by parameter values all suggest that the differences in building densities have a much higher impact on the variation of M3 parameters than the differences in monetary value per volume. This is especially true for the areas outside building zones, where the M4 values per volume are comparable to the values within building zones. In contrast, the M3 parameter for the area outside building zones is not higher than 1.3 % of the lowest value within building zones. That low percentage reflects a similarly low ratio between building densities outside and inside building zones. However, the effect of building densities also dominates within building zones. For the centre and mixed building zones, the M4 values per volume are at rank four and five, while the M3 parameter values for these zones are at rank one and two. That means the M3 values per area for the centre and mixed building zones are highly ranked, not because of high monetary values per built volume, but because these building zones are densely built-up. In contrast, comparing M3 and M4 parameter values for the public and other zones suggests that the construction costs for the buildings in these zones are comparably high, but the built volume per area is rather low. In the international literature, the monetary values of buildings per surface area (M3, e.g. Bubeck et al., 2011; ICPR, 2001; Kljin et al., 2007) and the construction costs per building volume (M4, e.g. Arrighi et al., 2013; Fuchs et al., 2015) are remarkably lower than the values in this study. As in the case of M1 and M2, these differences can be explained mainly by differences in building standards and construction costs in Switzerland (Diaz Muriel, 2008). For M3, the relatively dense settlements within building zones in Switzerland are another reason for the comparably high values in our study.

Regression model M5

Based on our data, the minimal adequate linear regression model for the estimation of building values is

$$\log_{10}(\text{value}) = \text{ResPur} \times \log_{10}(\text{volume}) + \text{ResPur} \times \text{LaUse} + \log_{10}(\text{volume}) \times \text{LaUse}, \quad (1)$$

where value is the building value in (CHF), ResPur is the binary variable regarding residential purpose (yes/no), volume is the building volume above ground (m³), and LaUse is the categorical variable regarding land use (six types of building

Table 6. Hexagons of 10 km² grouped in decreasing order of monetary values of flood-exposed buildings in Switzerland. For each group of hexagons and each model (M1 to M5) the following entities are reported: the lower limit of exposed-building values per hexagon (in 10⁶ CHF), the sum (S* in 10⁹ CHF) of exposed-building values over all hexagons of the respective group, and the percentage (P* in %) of this sum per group in relation to the total value of flood-exposed buildings in Switzerland. The spatial distribution of six of these groups (highest 2%, lowest 65% and four groups in between) are shown in Fig. 4.

Hexagon group		Lower limit (10 ⁶ CHF) of exposed-building values per hexagon					Monetary value of exposed buildings per hexagon group: sum [10 ⁹ CHF] and percentage (%) of total									
Share (%)	Number	M1	M2	M3	M4	M5	M1		M2		M3		M4		M5	
							S*	P*	S*	P*	S*	P*	S*	P*	S*	P*
1	44	739	1518	827	1545	1409	48	14.1	112	21.9	57	18.4	127	23.6	107	22.8
2	89	590	1057	585	1114	980	77	23.0	168	32.8	88	28.4	185	34.4	158	33.6
5	222	353	550	344	565	500	137	40.8	268	52.4	146	47.0	287	53.5	248	52.8
10	444	224	303	197	306	274	200	59.4	358	70.1	204	65.7	380	70.7	330	70.2
20	889	108	129	88	134	119	270	80.3	447	87.3	264	85.2	471	87.8	412	87.5
35	1555	41	38	27	38	34	317	94.1	496	97.0	299	96.5	523	97.3	457	97.2
50	2222	12	7	5	6	6	333	99.0	509	99.6	308	99.5	536	99.7	469	99.7
100	4444	0	0	0	0	0	336	100	511	100	310	100	537	100	470	100

zones; see Sect. 2.4.1). The diagnostic plots of the model are presented in Appendix A2 and show that principal assumptions regarding the residuals are satisfied. The coefficient of determination, adjusted R^2 , equals 0.88. In other words, M5 explains 88% of the variance in the logarithmic monetary building values. The overall F statistic (60 000, on 21 and 172 degrees of freedom) results in a p value $< 2.2 \times 10^{-16}$, indicating an overall significance of the explanatory variables of M5. The estimates of the individual explanatory variables and their pairwise interactions are shown in Table 4, together with standard errors, t and p values. With one exception (ResPur yes \times LaUse centre), all parameters of M5 are significant.

The intercept of 3.098 (= CHF 1250) refers to the variable values of $\log_{10}(\text{volume}) = 0$, i.e. volume = 1 m³, ResPur = no and LaUse = outside. If the same theoretical building of 1 m³ has a residential purpose, the estimation of the monetary value increases by a factor between 4.2 ($10^{(0.793-0.173)}$) in public building zones and 6.2 ($10^{0.793}$) outside building zones or in centre zones. As building volume increases, however, this factor between buildings with and without a residential purpose decreases and drops below 1 for building volumes between 8200 m³ (public building zones) and 102 000 m³ (outside building zones). The effects of land use categories other than outside and their interaction with building volumes are similar to the ones with residential purposes, but in the opposite direction. A theoretical building with a volume of 1 m³ in a building zone has a lower building value by factors 0.18 ($10^{-(0.666+0.076)}$) for other building zones, residential purpose) to 0.39 ($10^{-0.404}$) for working zone, no residential purpose) compared to the same building outside building zones. With increasing building volumes, these factors increase and exceed 1 for building volumes between 52 m³ (public building zones, no res-

idential purpose) and 584 m³ (working building zones, residential purpose). In any case, a higher volume of buildings results in a higher building value, but for all buildings with a residential purpose, the increase in value is lower than the increase in volume. Consequently, the ratio of difference in value to difference in volume for residential buildings within the same building zone is below 1. In fact, the ratio ranges from $\Delta\text{volume}^{-0.350}$ for areas outside building zones to $\Delta\text{volume}^{-0.067}$ for other building zones. For non-residential buildings, however, the increase in value is higher than the increase in volume in all building zones (with maximal ratio of $\Delta\text{volume}^{0.091}$ for other building zones), except for working building zone ($\Delta\text{value} = \Delta\text{volume}^{-0.033}$) and for areas outside building zones where the difference in value equals $\Delta\text{volume}^{-0.192}$.

In summary, variable values that are different from the intercept generally increase the resulting monetary building values in M5:

- For ResPur, buildings with a residential purpose have a higher value than non-residential buildings, at least up to a volume of several thousand cubic metres.
- For LaUse, buildings in building zones are more expensive than comparable buildings outside building zones, but only if the buildings have a minimal volume of several dozen to a few hundred cubic metres, depending on land use and building purpose.
- Higher building volumes result in higher monetary building values, and for non-residential buildings in five building zones (residential, mixed, centre, public and others) the increase in value is higher than the increase in volume.

The above statement on ResPur in M5 is consistent with the relation of residential to non-residential parameter values in

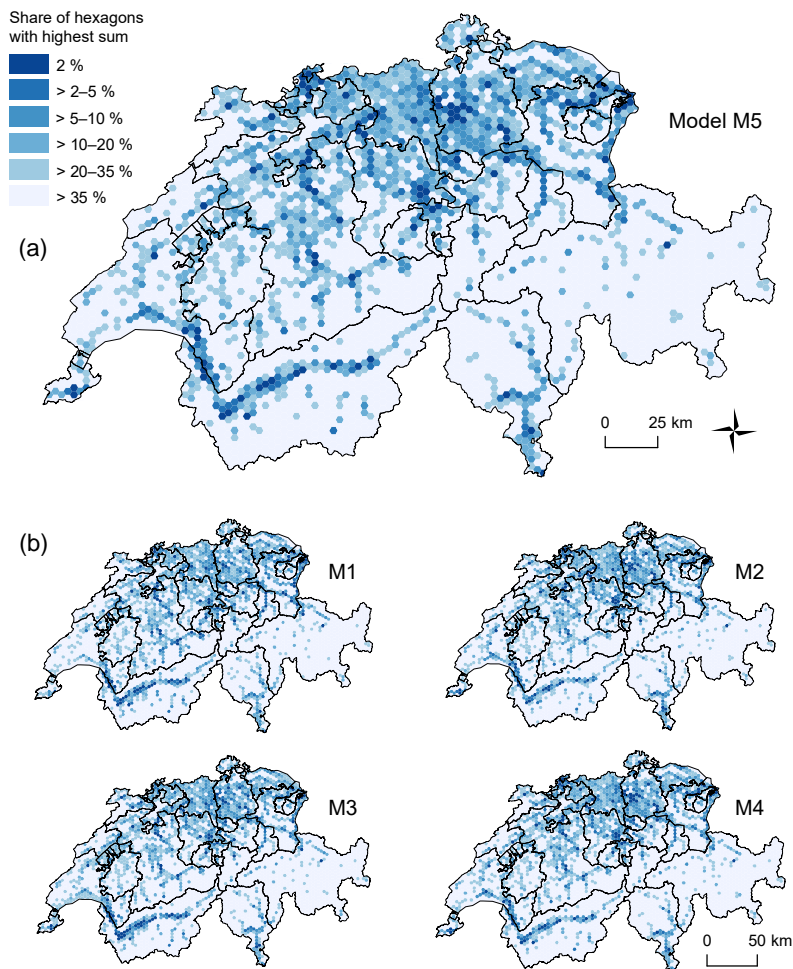


Figure 4. Spatial distribution of flood-exposed-building values based on benchmark model M5 (uppermost figure) in addition to models M1 to M4 (lower figures). Hexagons with a surface area of 10 km² are categorized according to their sum of flood-exposed-building values. The specific limits of each category and the corresponding sums of exposed values are presented in Table 6. Map sources: Federal Office of Topography (swisstopo).

M4. M4 and M5 also agree in terms of LaUse, apart from working building zones. However, the findings on the different Δ volume to Δ value relations in M5 do not support the concept of a constant value per volume ratio, which is used in M4.

In the following, we summarize the main reasons for excluding originally considered building features (building densities, residential use and municipality types) and for log-transforming the building volumes and values. The buildings densities are all highly correlated with building volume, but they explain less of the building values' variance than the volume (lower adjusted R^2 , higher AIC). The same holds for residential use with respect to residential purpose. Models that include municipality types and building zones contain many non-significant parameters. Models with municipality types (but without building zones) explain less than corresponding models with building zones (but without mu-

nicipality types). The building volumes and values are log-transformed since the untransformed values are right skewed and the residuals of models based on untransformed values are heteroscedastic.

3.2 Comparison of models with direct application of insurance data for benchmark model selection

The eight cantons with complete insurance portfolio data cover an area of 12 408 km². The corresponding layer of regular 10 km² hexagons contains 1577 hexagons. Each point in Fig. 3 represents one of these hexagons. The log₁₀ values of flood-exposed buildings summarized per hexagon based on value models M1 to M5 (y axis) are plotted against the exposed log₁₀ values based on the direct application of the values in the spatially referenced building insurance contracts (PIC, x axis). The red lines indicate a one-to-one relation.

Table 7. Indicators for the comparison of model M1 to M4 with benchmark model M5. Sum represents the sum of exposed-building values over all hexagons, RMSE and MAE represent the root-mean-square error and the mean-absolute error of exposed-building values per hexagon when comparing M1 to M4 with M5. The generalized Pareto distribution (GPD) is fitted for hexagons with exposed-building values higher than 10^8 (CHF), which is equal to the location parameter of the GPD. Shape and scale represent the respective parameter of the fitted GPD. Max represents the highest sum of exposed-building values per hexagon.

Model	Comparison over 4444 hexagons			Comparison of extreme values		
	Sum (10^6 CHF)	RMSE (10^6 CHF)	MAE (10^6 CHF)	Shape	Scale (10^6)	Max (10^6 CHF)
M1	336 460	214	47	0.20147	155	2912
M2	511 208	52	15	0.41285	207	7546
M3	309 794	191	44	0.30666	148	2634
M4	536 989	65	15	0.43357	211	9102
M5	470 420	–	–	0.42715	188	7201

The exposure values per hexagon based on the M2, M4 and M5 models differ hardly by more than a factor of 10^1 from the respective value based on direct PIC application. Moreover, the factors are homoscedastic. The results from M1 and M3, however, differ by up to a factor of 10^2 from the ones based on direct insurance data application. In addition, the factors for small values are clearly bigger than the factors for high values. Moreover, in M1 the values of hexagons with only a few exposed buildings are generally overestimated, and the hexagons with one or two exposed buildings appear as two horizontal lines (at 1.05×10^6 and 2.1×10^6 CHF), with only seven hexagons in which the direct application of PIC results in higher exposure values than based on M1. In contrast, the values in hexagons with the most exposed buildings are underestimated in M1. Hexagons with high exposure values are underestimated by the other four value models too, although this is less pronounced in the cases of M2, M4 and M5 than in M1 and M3.

The data in Table 5 support these findings quantitatively. Overall, the indicators for the models M1 and M3 show the least agreement with the values based on directly applied PICs. The sum of exposed values over all 1577 hexagons is closest to the PIC-based result in M5 (+1 %), and the sum differs most in M3 (–29 %). M4 shows the least RMSE and M5 the least MAE, and for both indicators, the values of M1 and M3 are approximately twice as high as the ones of the other three models. Comparing extremely high values again shows a clear division into two groups: M2, M4 and M5 versus M1 and M3. The GPD fitted for hexagons with exposed-building values higher than 10^8 CHF show the best match with PIC-based extreme values for M2 and M5. The shape parameter determines the weight of the tail in the GPD, and it is highest in the case of direct PIC application, followed by the ones based on M5 (–10.2 %) and M2 (–10.4 %). This general underestimation of extremely high values by the five models is also reflected in the maximal exposure values,

where the models result in –25 % (M4) to –72 % (M1) lower values compared to the direct PIC application.

Based on these results, we select M5 as the benchmark model for comparing the countrywide model applications presented in the following section.

3.3 Benchmark test: differences and similarities between the five models

The summarized value of all flood-exposed buildings in Switzerland is between 3.1×10^{11} (M3) and 5.4×10^{11} CHF (M4). Based on the benchmark model M5, it is 4.7×10^{11} CHF. The ratio between the highest and the lowest sums is thus 1.7, and the ratios to the benchmark model are between 0.7 and 1.1. Table 6 presents the exposure values per eight ranked groups of the total 4444 regular hexagons covering Switzerland. The table demonstrates that, for all five models, the distributions of exposed values per hexagon are clearly right skewed, but for M1 and M3 the skewness is less pronounced. This skew to the right implies that the exposure values of a few 10 km^2 hexagons represent an important part of the total value of flood-exposed buildings in Switzerland. For instance, the 2 % (89) hexagons with the highest exposure values based on M5 contain flood-exposed buildings with a value of 1.6×10^{11} CHF, which corresponds to 33.6 % of the total value exposed in the whole of Switzerland based on M5. This share of exposed values in the 98th percentile is comparable for values from M2 (32.8 %) and M4 (34.4 %), but remarkably lower for M1 (23 %) and M3 (28.4 %). Comparing the absolute values of the most exposed hexagons results in the division of the same two clusters, down to the 95th percentile, the exposure values based on M2, M4 or M5 are approximately twice as high as the ones based on M1 or M3.

Figure 4 shows the spatial distribution of six ranked groups of hexagons for all five models. The group limits in exposed-

Table 8. Overview of core features and suitable applications of the five models. Symbols of characteristics: + is positive, 0 is neutral and *minus* is negative. The key figure in the online version of the article is a graphical version of this table.

Model name and concept	M1 uniform average value per build- ing	M2 uniform average value per build- ing volume	M3 average value of buildings per area, differenti- ated by land use category	M4 average value per building volume, differentiated by building features	M5 value per build- ing, individually calculated based on linear regres- sion
Low data requirement for parameter estimation	++	+	0	-	--
Low computational expenses for parameter estimation	++	++	+	+	--
Low data requirement for model application	+	-	++	--	--
Agreement with direct application of insurance data	-	+	-	+	++
Suitable applications at national level					
Spatial distribution of exposed assets	++		++		
Absolute values of exposed assets		++		++	++

building values per hexagon are presented in columns three to seven in Table 6. The data again highlights the two groups: M2, M4 and M5 versus M1 and M3. However, the spatial distribution of the 1555 (35 %) hexagons with the highest exposure values is very similar, with each of the five applied value estimation models. These hexagons cover wide areas in the northern part of Switzerland, but appear as isolated points or lines only in the southern part. Overall, the pattern mirrors the spatial settlement structure (see Fig. 2) in Switzerland, but the areas in the west as well as in the most eastern canton (i.e. GR) seem to exhibit a disproportionally low exposure, which confirms results by Fuchs et al. (2017).

The log–log plots presented in Fig. 5 show the flood-exposed values per hexagon based on the benchmark model M5 (*x* axis) against the values based on the other four models (*y* axis), with the red line indicating a one-to-one relation. In M2 and M4, the exposed values differ by not more than a factor of 5 from the respective values based on M5, whereas this factor goes up to 2×10^2 in M3 and to 5×10^1 for M1. In addition, for M1 and M3, the factors are clearly bigger for lower exposure values than for higher ones, and high values in both are generally underestimated. In contrast, the low exposure values in M1 are overestimated, and the values of hexagons with only a few exposed buildings appear as horizontal lines, similar to the pattern shown in the panel M1 of Fig. 3, as discussed above. The M2 panel suggests a general overestimation of the values compared to M5. Moreover, the differences are more pronounced for the middle ranges than for the extreme values. For the absolute deviations of M4 values from M5, no such dependency from the value's rank can be detected, but the low values are underestimated, while high values are overestimated in M4.

Table 7 presents indicators when the M5 benchmark model is compared with the other four models. Overall, these indicators suggest that M2, closely followed by M4, best matches M5. In contrast, the exposure values based on M1 and M3 both agree much less with the M5 results. Compared to M5, M1 and M3 show a general underestimation of flood-exposed-building values, as well as an underestimation of the extreme high values. In contrast, M4 and, to a smaller degree, M2, overestimate the exposure values compared to M5. The parameters of the GPD fitted to hexagons with flood-exposed-building values higher than CHF 10^8 are very similar for M2, M4 and M5. Yet, the resulting empirical cumulative distribution functions presented in Fig. 6 for the highest two percent show that M2 matches better with M5 than M4.

3.4 Overall discussion of the five models

Based on the resulting values of flood-exposed buildings, the five models can be divided into two groups, one with M1 and M3 and another one with M2, M4 and M5 (see Table 8). Compared with the direct application of building values from PIC in eight cantons, M5 performs best. However, the results based on M2 and M4 are close, too, not only to the PIC results in the eight cantons (see Sect. 3.2), but also to the M5 results over all of Switzerland (see Sect. 3.3). These three high-performing models include the building volume to estimate the value, in contrast to M1 and M3. In other words, models which consider the building volume outperform the ones which do not include the volume, as long as there is a spread in the volume of the modelled building set.

With regard to data requirements for model parameter estimations (see Tables 1 and 8), M5 differs from the other four models, as it is the only model that needs data on an

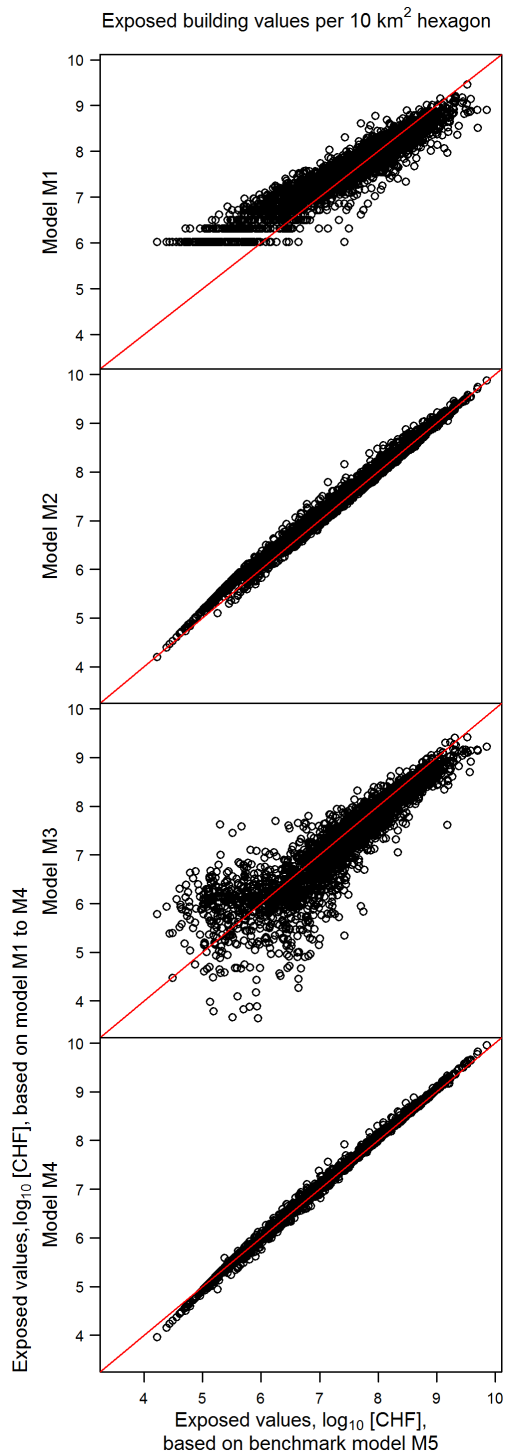


Figure 5. Scatter plot of flood-exposed-building values aggregated to regular hexagons with a surface area of 10 km^2 . The sums based on models M1 to M4 (y axis) are plotted against the sums based on the benchmark model M5 (x axis). The red lines indicate the 1 : 1 relation. All values are \log_{10} transformed and sums below 10^4 CHF are not shown.

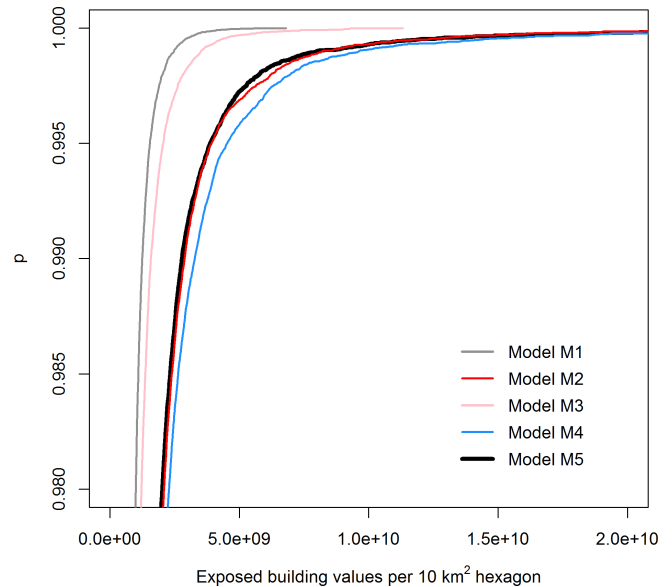


Figure 6. Empirical cumulative distribution function of flood-exposed-building values aggregated to hexagons with a surface area of 10 km^2 . Cumulative probabilities (p) are generated by 10^5 random values from GPD with the parameters shown in Table 7. To improve the readability, only probabilities over 98 % are shown.

individual building level. However, the less detailed data required in M1 to M4 differ too. While M1 and M2 require relatively simple data, i.e. global sums over a particular area such as administrative units, the sums of monetary building values required for M3 and M4 need to be differentiated to a higher degree. Consequently, the data requirements for the parameter estimation divide the models into three groups, with M1 and M2 in the group with the least requirements and M5 in the one with the most sophisticated requirements. The same grouping occurs when considering the computational expenses of the parameter estimations. While the parameter estimations in M1 and M2 each consist of one numerical division, and in M3 and M4 of several divisions, the set-up of a linear regression model in M5 is an iterative and time-consuming process.

Grouping the models based on data requirements for the model application results in a distinction between M3 and the other four models (see Tables 1 and 8). Applying M3 requires spatially gapless data on land use, whereas the other four models need information on individual building levels for application. Among these four models, M1 requires the least information (location only), while M4 and M5 require the most information about each individual building, i.e. location, volume and other features. With regard to computational expenses for the model application, the five models are similar.

The overall comparison of the five models reveals several things (see Table 8). On the one hand, M5 has the best matching exposure values when compared to the direct application

of existing individual building value. On the other hand, M5 requires the most data and computational resources. With M1 and M3, it is the opposite. In summary, all five models have advantages and disadvantages, and when selecting a model there is a need to balance them. However, selecting a model is often driven by data availability in real-world applications. As this study shows, selecting a model has consequences for resulting exposure values.

4 Conclusions

The paper illustrates the role of building value models in flood exposure analyses on regional to national scales. The presented findings are relevant for flood risk analyses too, as most risk analyses take the value of exposed assets into account in a linear way. The study is based on insurance data; the used monetary building values represent replacement costs. However, the insights of this paper into the relevance of the model approach for the resulting value of exposed buildings are valid as well for other value types, as depreciated construction costs or property prices.

With regard to the spatial distribution of exposed-building values, the models show widely uniform results. In contrast, the absolute values of exposure differ remarkably. The first finding implies that the spatial prioritization of flood protection measures would be similar with each of the applied value estimation methods. In practice, this means that the application of more sophisticated models does not generally provide a better basis for spatial prioritizations. Consequently, simpler models with lower requirements regarding data input and computational resources are preferable.

The second finding, however, suggests that decision-making processes that are based on cost–benefit criteria and thus rely on absolute monetary values are significantly influenced by which building value model one chooses. We find that models based on areas of land use classes, as commonly applied on regional to national scales, underestimate exposure values. The same is true for models based on individual buildings that do not take the building volumes into account. These two model types underestimate the overall exposure, but even more so the extremely high values on which risk management strategies generally focus. This underestimation of the exposure value by models not considering the volume of buildings indicates that flood-exposed buildings have in general a higher volume than buildings outside flood zones. By underestimating exposed values, the benefits of protection measures (i.e. avoided flood losses) are underestimated as well. In decision-making processes that are based on cost efficiency, this underestimation would result in suboptimal allocation of resources for protection measures. Consequently, we propose that estimating exposed-building values should be based on individual buildings rather than on areas of land use types. In addition, and provided that there is a spread in the volume of the modelled building set, the in-

dividual volumes of buildings have to be taken into account in order to provide a reliable basis for cost–benefit analyses. The consideration of other building features further improves the value estimation.

In our study for the whole of Switzerland, with a data aggregation on 10 km² hexagons, the optimal model for the estimation of absolute monetary building value is M5, i.e. a linear regression model considering the residential purpose and the building zone, in addition to building volume. In other contexts, where other data with different aggregations are available, the optimal building value model may be another one. For decisions that rely on absolute monetary building values, however, our results suggest using a value model based on individual building data that in any case includes the building volume. The concepts of the three respective value models presented in this study, i.e. M2, M4 and M5, are generic. Thus, these models are transferrable with minimal adjustments according to the application's purpose and the available data. However, within the context of flood risk management, the optimal value estimation model depends on the specific questions to be answered.

Growing availability of data with high resolution and spatial coverage in Switzerland and many other countries makes it possible to further develop complex multivariable building value models, e.g. based on machine learning methods as done by Wagenaar et al. (2017) for the modelling of absolute flood damage. Depending on future data availability, it is also possible to extend the presented analyses to other assets of interest such as population or infrastructure. The comparison between different nationwide exposure analyses based on object-specific data including monetary values would be another promising approach for further research.

Data availability. The data on which this study is based were provided by 11 different insurance companies. Each record contains confidential information on buildings such as the location (address and/or coordinates) and the insured value. Due to privacy protection, the data are subject to strict confidentiality and thus cannot be made accessible.

Appendix A

A1 Details on data and assignment of attributes to building polygons

Table A1 presents details on the data sets, which we use in our study aside from the insurance data described in Sect. 2.4. We assign the attributes to the building footprint polygons as follows.

A1.1 Building volume above ground

The building volume above ground is the product of the BFP area times the average building height above ground. While the calculation of a polygon's area is a standard procedure in GIS, the estimation of the building height based on the available data is a multistep process. First, the points of the digital elevation model (swissALTI3D) and the digital surface model (DSM) are assigned to the polygons and for each polygon the two means of the assigned swissALTI3D points and DSM points are calculated. The subtraction of the mean of the DSM points from the mean from the swissALTI3D points results in the building's average height above ground. If this height is ≥ 3.5 and ≤ 100 m (which is the case for 1 378 665 of total 2 086 411 BFPs) it is used in the volume calculation, otherwise ($n = 707 746$) it is adjusted as follows: for residential buildings (i.e. buildings with assigned residential units as explained further down, $n = 232 016$) the average numbers of floors of the assigned BDS points (attribute GASTWS in BDS) is calculated, and for the first floor the height is set to 3.5 m and for each additional floor 2.5 m is added. For non-residential buildings with a height < 3.5 m or > 100 m ($n = 475 730$) the value is set to 3.5 m.

A1.2 Type of building zone and type of municipality

For the assignment of the types of building zones and municipalities, the positions of the building polygons' centroids relative to the polygons in the data sets Bauzonen Schweiz and INFOFLAN-ARE are analysed. Prior to the assignment, in our study we reduce the types of building zones (attribute CH_BEZ_D in the data set Bauzonen Schweiz) from nine to seven types as described in Sect. 2.4.1. The types of municipalities (attribute TYP in INFOPLAN-ARE) are reduced from originally nine types down to six by merging the types "big centres" (code 1 in TYP), "secondary centres beside big centres" (2) and "middle centres" (4) to the type "big and middle centres" and by merging "belts of big centres" (3) and "belts of middle centres" (5) to the type "belts of big and middle centres". Furthermore, we add the areas of lakes to the type "agricultural" (code 8 in TYP) municipality if they are not part of a municipality but of a canton. We obtain a spatially gapless set of polygons with six types of municipality, namely "big and middle centres", "belts of big and middle centres", "small centres", "suburban rural municipal-

ities", "agricultural municipalities and cantonal lake areas" and "tourist municipalities".

A1.3 Binary information about residential purpose and use

The point data of residential units in the BDS ($n = 1 670 540$) are joined to the next BFP ($n = 2 086 411$) within 2 m. Ninety-seven percent (1 631 531) of the BDS points lay in or within a distance of 2 m to a BFP. We consider a BFP as a building with residential purpose if at least one BDS point is assigned to it ($n = 1 269 908$ BFPs.) The criteria for residential use is that at least one person with main residence (attribute GAPHW in the BDS data set) is assigned to the building polygon, which is true for 1 129 904 BFPs.

A1.4 Building densities in the BFP surroundings

For the calculation of the building density in the surrounding of a BFP we define circles of 50, 100, 200 and 500 m radius around the BFP's centroid. For each of these circles we calculate the area of all BFP (cut to the circle's edge) and divide it by the total area of the circle (cut to areas within Switzerland and not covered by lakes). This way, for each BFP we obtain the building density in a circle 50 m (100, 200 and 500 m) around its centroid.

A2 Diagnostic plots of linear regression model M5

Figure A1 shows the diagnostic plots of M5, the minimal adequate linear regression model presented in Sect. 3.1. The two plots of residuals versus fitted values suggest (Fig. A1a and c) that residuals fulfil the assumptions of homoscedasticity, as the residuals are spread equally along the ranges of the fitted values. The quantile–quantile plot (Fig. A1b) indicates that the tails of the residuals' distribution are heavier than in a normal distribution. Cook's distance plot (Fig. A1d) shows that all buildings are inside Cook's distance of 0.5, which means that no building significantly influences the resulting regression model. Overall it can be stated that the principal assumptions of linear regression modelling are reasonably satisfied.

A3 Abbreviations used in the text

Table A2 explains all abbreviations which are used in the text.

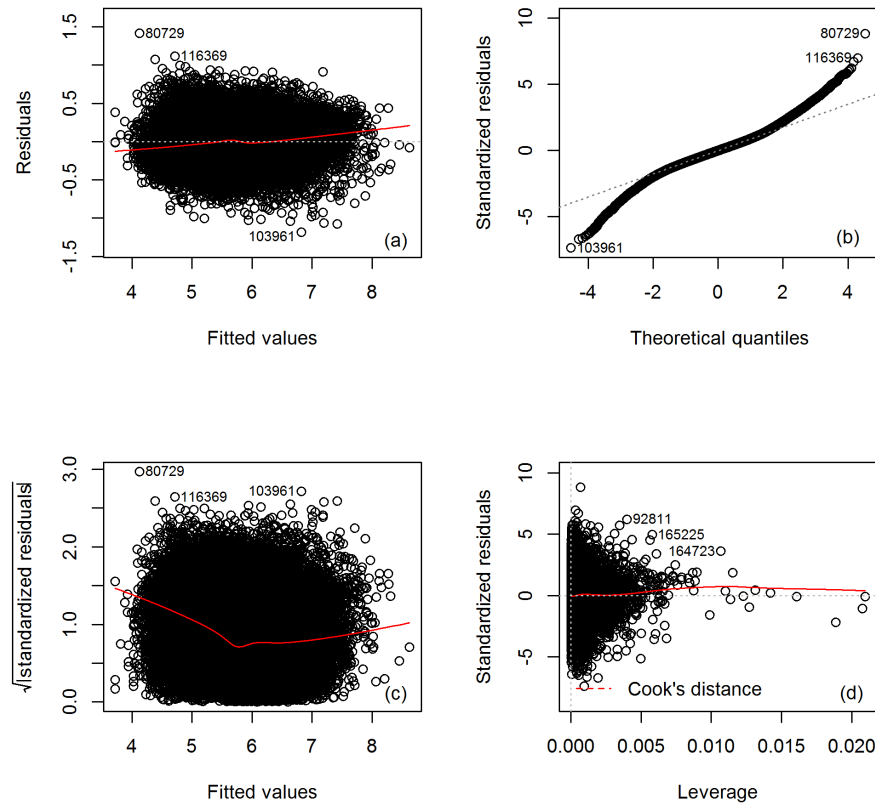


Figure A1. Diagnostic plots of model M5, namely residuals vs. fitted values (a), quantile–quantile plots of residuals vs. normally distributed quantiles (b), scale location plot (c) and Cook’s distance plot (d).

Table A1. Summary of data used in the set-up and/or application of the five building value models. All links were last checked on 7 September 2018.

Name	Consideration in model		Data set	Description	Source
	set-up	application			
Building footprints BFP	M1, M2, M4, M5	M1, M2, M4, M5	swissTLM3D	Feature TLM_GEBAEUDE_FOOTRPINT of the Swiss topographical landscape model, v1.4, as of 2016	Federal Office of Topography (swisstopo) https://shop.swisstopo.admin.ch/en/products/landscape/tlm3D
Polygons of building zones BZP	M2, M3, M4, M5	M2, M3, M4, M5	Bauzonen Schweiz (harmonized)	Polygons of building zones, 9 harmonized types, as of 2012	Federal Office for Spatial Development (ARE) http://www.kkgeo.ch/geodatenangebot/geodaten-bauzonen-schweiz.html
Digital elevation model	M2, M4, M5	M2, M4, M5	swissALT3D	High-precision digital elevation model of Switzerland, grid size of 2 × 2 m, as of 2013	swisstopo https://shop.swisstopo.admin.ch/en/products/height_models/alti3D
Digital surface model	M2, M4, M5	M2, M4, M5	DSM	Digital surface model, density of 1 point per 2 m ² , last updated in 2008	swisstopo https://shop.swisstopo.admin.ch/en/products/height_models/DOM
Municipality types	M4, M5		INFOPLAN-ARE	Typology of municipalities ARE, nine types based on municipality typology of FSO, as of 2014	ARE, Federal Statistical Office (FSO) and swisstopo data.geo.admin.ch/ch.are.gemeindetypen/data.zip
Residential purpose of buildings	M4, M5	M4, M5	BDS	No. of residential units in the Buildings and Dwellings statistics BDS, as of 2012	FSO https://www.bfs.admin.ch/bfs/en/home/statistics/construction-housing/surveys/gws2009.assetdetail.8521.html
Residential use of buildings	M4, M5		BDS	No. of people with main residence in BDS; see residential purpose	see residential purpose
Area of cantons	M1, M2, M3		SwissBOUN-DARIES3D	Polygons of the 26 Swiss cantons (districts), as of 2016	swisstopo https://shop.swisstopo.admin.ch/en/products/landscape/boundaries3D

Table A2. Abbreviations used in the text in alphabetical order.

Abbreviation	Meaning
AIC	Akaike Information Criterion
BFP	Building footprint polygon
BZP	Building zone polygon
CPIC	Complete data set of points of insurance contracts
M1	Model M1, uniform average value per building
M2	Model M2, uniform average value per building volume
M3	Model M3, average values per area, differentiated by land use category
M4	Model M4, average values per building volume, differentiated by land use category and building purpose
M5	Model M5, value per building, individually calculated based on linear regression
MAE	Mean absolute error
PIC	Point of insurance contract
RMSE	Root-mean-square error
swissTLM3D	Swiss topographical landscape model

Author contributions. VR and APZ designed the models and the computational framework and analysed the data. All authors discussed the results and contributed to the manuscript outline. VR wrote the manuscript with input from all authors. MK supervised the project.

Competing interests. The last author is a member of the editorial board of the journal. Otherwise, the authors declare that they have no conflict of interest.

Acknowledgements. We thank the natural hazards group at the Swiss Mobiliar Insurance Company “die Mobiliar AG” for acquiring and compiling the communal flood hazard maps. Furthermore, we would like to thank the public insurance companies for buildings of the cantons Aargau, Basel-Landschaft, Fribourg, Glarus, Graubünden, Jura, Neuchâtel, Nidwalden, St. Gallen, Solothurn and Zug for providing building-specific data and supporting us during the data harmonization process. Also, we would like to thank the Federal Office of Topography, the Federal Office for Spatial Development, the Federal Office for the Environment and the Federal Statistical Office for providing the corresponding spatial data. We thank Daniel Bernet for the joint effort in collecting and harmonizing the insurance data and for proofreading, Markus Mosimann for his support harmonizing the insurance data and Craig Hamilton for language editing. Last but not least, we would like to thank the two anonymous reviewers and the editor for their inputs which substantially improved this manuscript.

Edited by: Thomas Glade

Reviewed by: two anonymous referees

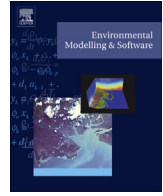
References

- Akaike, H.: A new look at the statistical model identification, *IEEE T. Automat. Contr.*, 19, 716–723, 1974.
- ARE Bundesamt für Raumplanung, BWG, Bundesamt für Wasser und Geologie, and BUWAL, Bundesamt für Umwelt, Wald und Landschaft: Empfehlung Raumplanung und Naturgefahren, 50 pp., 2005.
- Arnell, N. W. and Gosling, S. N.: The impacts of climate change on river flood risk at the global scale, *Climatic Change*, 134, 387–401, <https://doi.org/10.1007/s10584-014-1084-5>, 2016.
- Arrighi, C., Brugioni, M., Castelli, F., Franceschini, S., and Mazzanti, B.: Urban micro-scale flood risk estimation with parsimonious hydraulic modelling and census data, *Nat. Hazards Earth Syst. Sci.*, 13, 1375–1391, <https://doi.org/10.5194/nhess-13-1375-2013>, 2013.
- BAFU Bundesamt für Umwelt: EconoMe 4.0 Wirksamkeit und Wirtschaftlichkeit von Schutzmassnahmen gegen Naturgefahren: Handbuch/Dokumentation, available at: https://econome.ch/eco_work/doc/Handbuch_EconoMe_4.0_Version_Dez2016_D.pdf (last access: 7 September 2018), 2015.
- Barredo, J. I.: Normalised flood losses in Europe: 1970–2006, *Nat. Hazards Earth Syst. Sci.*, 9, 97–104, <https://doi.org/10.5194/nhess-9-97-2009>, 2009.
- Bernet, D. B., Prasuhn, V., and Weingartner, R.: Surface water floods in Switzerland: what insurance claim records tell us about the damage in space and time, *Nat. Hazards Earth Syst. Sci.*, 17, 1659–1682, <https://doi.org/10.5194/nhess-17-1659-2017>, 2017.
- Birkmann, J.: Risk, in: *Encyclopedia of Natural Hazards*, edited by: Bobrowsky, P. T., Springer, Dordrecht, 856–862, 2013.
- Borter, P.: Risikoanalyse bei gravitativen Naturgefahren: Methode, *Umwelt-Materialien*, Nr. 107/I, 117 pp., 1999.
- Bründl, M., Romang, H. E., Bischof, N., and Rheinberger, C. M.: The risk concept and its application in natural hazard risk management in Switzerland, *Nat. Hazards Earth Syst. Sci.*, 9, 801–813, <https://doi.org/10.5194/nhess-9-801-2009>, 2009.
- Bubeck, P., de Moel, H., Bouwer, L. M., and Aerts, J. C. J. H.: How reliable are projections of future flood damage?, *Nat. Hazards Earth Syst. Sci.*, 11, 3293–3306, <https://doi.org/10.5194/nhess-11-3293-2011>, 2011.
- Budiyono, Y., Aerts, J., Brinkman, J., Marfai, M. A., and Ward, P.: Flood risk assessment for delta mega-cities: A case study of Jakarta, *Nat. Hazards*, 75, 389–413, <https://doi.org/10.1007/s11069-014-1327-9>, 2015.
- Bundesrat: Umgang mit Naturgefahren in der Schweiz – Bericht des Bundesrates, Bern, 131 pp., 2016.
- Cammerer, H., Thieken, A. H., and Lammel, J.: Adaptability and transferability of flood loss functions in residential areas, *Nat. Hazards Earth Syst. Sci.*, 13, 3063–3081, <https://doi.org/10.5194/nhess-13-3063-2013>, 2013.
- Chen, K., McAneney, J., Blong, R., Leigh, R., Hunter, L., and Magill, C.: Defining area at risk and its effect in catastrophe loss estimation: A dasymmetric mapping approach, *Appl. Geogr.*, 24, 97–117, <https://doi.org/10.1016/j.apgeog.2004.03.005>, 2004.
- de Bruijn, K. M., Wagenaar, D. J., Slager, K., de Bel, M., and Burzel, A.: Updated and improved method for flood damage assessment: SSM2015, Version 2, Rijkswaterstaat Water, Verkeer en Leefomgeving, 1220043-003, 125 pp., 2015.
- de Moel, H. and Aerts, J. C. J. H.: Effect of uncertainty in land use, damage models and inundation depth on flood damage estimates, *Nat. Hazards*, 58, 407–425, <https://doi.org/10.1007/s11069-010-9675-6>, 2011.
- de Moel, H., van Alphen, J., and Aerts, J. C. J. H.: Flood maps in Europe – methods, availability and use, *Nat. Hazards Earth Syst. Sci.*, 9, 289–301, <https://doi.org/10.5194/nhess-9-289-2009>, 2009.
- DEFRA, Departement for Environment, Food and Rural Affairs: National Appraisal of Assets at Risk from Flooding and Coastal Erosion, including the potential impact of climate change: Final Report, Flood Management Division, London, 64 pp., 2001.
- Diaz Muriel, C.: Wide spread in construction prices across Europe in 2007, *Statistics in focus* 114, eurostat, 2008.
- Ernst, J., Dewals, B. J., Detrembleur, S., Archambeau, P., Erpicum, S., and Piroton, M.: Micro-scale flood risk analysis based on detailed 2D hydraulic modelling and high resolution geographic data, *Nat. Hazards*, 55, 181–209, <https://doi.org/10.1007/s11069-010-9520-y>, 2010.
- European Environment Agency: Economic losses from climate-related extremes, IND-182-en, CSI042, CLIM 039, 16 pp., 2017.
- European Parliament: Directive 2007/60/EC of the European Parliament and of the Council of 23 October 2007 on the assessment and management of flood risk: 2007/69/EC, 8 pp., 2007.

- Federal Office for the Environment: Terms of Use Aquaprotect, available at: <https://www.bafu.admin.ch/bafu/de/home/themen/naturgefahren/fachinformationen/naturgefahrensituation-und-raumnutzung/gefahregrundlagen/aquaprotect/nutzungsbedingungen-aquaprotect.html> (last access: 7 September 2018), 2008.
- Fuchs, S., Keiler, M., and Zischg, A.: A spatiotemporal multi-hazard exposure assessment based on property data, *Nat. Hazards Earth Syst. Sci.*, 15, 2127–2142, <https://doi.org/10.5194/nhess-15-2127-2015>, 2015.
- Fuchs, S., Röthlisberger, V., Thaler, T., Zischg, A., and Keiler, M.: Natural Hazard Management from a Coevolutionary Perspective: Exposure and Policy Response in the European Alps, *Ann. Am. Assoc. Geogr.*, 107, 382–392, <https://doi.org/10.1080/24694452.2016.1235494>, 2017.
- Gerl, T., Kreibich, H., Franco, G., Marechal, D., and Schröter, K.: A Review of Flood Loss Models as Basis for Harmonization and Benchmarking, *PloS one*, 11, e0159791, <https://doi.org/10.1371/journal.pone.0159791>, 2016.
- Glas, H., Jonckheere, M., Mandal, A., James-Williamson, S., Maeyer, P. de, and Deruyter, G.: A GIS-based tool for flood damage assessment and delineation of a methodology for future risk assessment: Case study for Annotto Bay, Jamaica, *Nat. Hazards*, 88, 1867–1891, <https://doi.org/10.1007/s11069-017-2920-5>, 2017.
- Hägi, A.: Die Bewertung von Liegenschaften, Zürich, 224 pp., 1961.
- Hatzikyriakou, A. and Lin, N.: Simulating storm surge waves for structural vulnerability estimation and flood hazard mapping, *Nat. Hazards*, 89, 939–962, <https://doi.org/10.1007/s11069-017-3001-5>, 2017.
- ICPR, International Commission for the Protection of the Rhine: Rhine-Atlas: Flood maps of extreme event, available at: <http://www.rheinatlas.de/> (last access: 7 September 2018), 2001.
- IPCC: Climate Change 2014. Synthesis Report. Summary for Policymakers, 32 pp., 2014.
- Jongman, B., Kreibich, H., Apel, H., Barredo, J. I., Bates, P. D., Feyen, L., Gericke, A., Neal, J., Aerts, J. C. J. H., and Ward, P. J.: Comparative flood damage model assessment: towards a European approach, *Nat. Hazards Earth Syst. Sci.*, 12, 3733–3752, <https://doi.org/10.5194/nhess-12-3733-2012>, 2012.
- Jongman, B., Koks, E. E., Husby, T. G., and Ward, P. J.: Increasing flood exposure in the Netherlands: implications for risk financing, *Nat. Hazards Earth Syst. Sci.*, 14, 1245–1255, <https://doi.org/10.5194/nhess-14-1245-2014>, 2014.
- Kleist, L., Thieken, A. H., Köhler, P., Müller, M., Seifert, I., Borst, D., and Werner, U.: Estimation of the regional stock of residential buildings as a basis for a comparative risk assessment in Germany, *Nat. Hazards Earth Syst. Sci.*, 6, 541–552, <https://doi.org/10.5194/nhess-6-541-2006>, 2006.
- Klijn, F., Baan, P., de Bruijn, K., and Kwadijk, J. C. J.: Overstromingsrisico's in Nederland in een veranderend klimaat, 165 pp., 2007.
- Koivumäki, L., Alho, P., Lotsari, E., Käyhkö, J., Saari, A., and Hyypä, H.: Uncertainties in flood risk mapping: A case study on estimating building damages for a river flood in Finland, *J. Flood Risk Manag.*, 3, 166–183, <https://doi.org/10.1111/j.1753-318X.2010.01064.x>, 2010.
- Kundzewicz, Z. W., Kanae, S., Seneviratne, S. I., Handmer, J., Nicholls, N., Peduzzi, P., Mechler, R., Bouwer, L. M., Arnell, N., Mach, K., Muir-Wood, R., Brakenridge, G. R., Kron, W., Benito, G., Honda, Y., Takahashi, K., and Sherstyukov, B.: Flood risk and climate change: Global and regional perspectives, *Hydrolog. Sci. J.*, 59, 1–28, <https://doi.org/10.1080/02626667.2013.857411>, 2014.
- Liu, J., Hertel, T. W., Diffenbaugh, N. S., Delgado, M. S., and Ashfaq, M.: Future property damage from flooding: sensitivities to economy and climate change, *Climatic Change*, 132, 741–749, 2015.
- Lowe, D. J., Emsley, M. W., and Harding, A.: Predicting Construction Cost Using Multiple Regression Techniques, *J. Constr. Eng. M.*, 132, 750–758, [https://doi.org/10.1061/\(ASCE\)0733-9364\(2006\)132:7\(750\)](https://doi.org/10.1061/(ASCE)0733-9364(2006)132:7(750)), 2006.
- Merz, B., Kreibich, H., Schwarze, R., and Thieken, A.: Review article “Assessment of economic flood damage”, *Nat. Hazards Earth Syst. Sci.*, 10, 1697–1724, <https://doi.org/10.5194/nhess-10-1697-2010>, 2010.
- Mobilier Lab: hochwasserrisiko.ch: Beschreibung Projekt und Vorgehen, available at: <http://www.hochwasserrisiko.ch/HochwassergefahrCH/Projekt.html> (last access: 7 September 2018), 2016.
- Molinari, D. and Scorzini, A. R.: On the Influence of Input Data Quality to Flood Damage Estimation: The Performance of the INSYDE Model, *Water*, 9, 688, <https://doi.org/10.3390/w9090688>, 2017.
- Naegeli, W. and Wenger, H.: Der Liegenschaftenschätzer, 4th Edn., Schulthess, Zürich, 328 pp., 1997.
- Penning-Rowsell, E., Johnson, C., Tunstall, S., Tapsel, S., Morris, J., Chatterton, J., and Green, C.: The Benefits of Flood and Coastal Risk Management: A Handbook of Assessment Techniques, 89 pp., 2005.
- Penning-Rowsell, E. C.: A realistic assessment of fluvial and coastal flood risk in England and Wales, *Trans. Inst. Br. Geogr.*, 40, 44–61, <https://doi.org/10.1111/tran.12053>, 2015.
- Röthlisberger, V., Zischg, A. P., and Keiler, M.: Identifying spatial clusters of flood exposure to support decision making in risk management, *Sci. Total Environ.*, 598, 593–603, <https://doi.org/10.1016/j.scitotenv.2017.03.216>, 2017.
- Sonmez, R.: Parametric Range Estimating of Building Costs Using Regression Models and Bootstrap, *J. Constr. Eng. M.*, 134, 1011–1016, [https://doi.org/10.1061/\(ASCE\)0733-9364\(2008\)134:12\(1011\)](https://doi.org/10.1061/(ASCE)0733-9364(2008)134:12(1011)), 2008.
- SVKG and SEK/SVIT: Das Schweizerische Schätzerhandbuch: Das umfassende und praxisorientierte Lehrbuch über die wichtigsten Immobilien-Bewertungsmethoden der Schweiz, 4th Edn., 382 pp., 2012.
- Thieken, A. H., Müller, M., Kleist, L., Seifert, I., Borst, D., and Werner, U.: Regionalisation of asset values for risk analyses, *Nat. Hazards Earth Syst. Sci.*, 6, 167–178, <https://doi.org/10.5194/nhess-6-167-2006>, 2006.
- Thieken, A. H., Olschewski, A., Kreibich, H., Kobsch, S., and Merz, B.: Development and evaluation of FLEMOps – a new Flood Loss Estimation Model for the private sector, in: *Flood Recovery, Innovation and Response*, edited by: Proverbs, D., Brebbia, C. A., and Penning-Rowsell, E., *WIT Trans. Ecol. Envir.*, 118, 315–324, 2008.

- van Dyck, J. and Willems, P.: Probabilistic flood risk assessment over large geographical regions, *Water Resour. Res.*, 49, 3330–3344, <https://doi.org/10.1002/wrcr.20149>, 2013.
- Wagenaar, D., de Jong, J., and Bouwer, L. M.: Multi-variable flood damage modelling with limited data using supervised learning approaches, *Nat. Hazards Earth Syst. Sci.*, 17, 1683–1696, <https://doi.org/10.5194/nhess-17-1683-2017>, 2017.
- Wagenaar, D. J., de Bruijn, K. M., Bouwer, L. M., and de Moel, H.: Uncertainty in flood damage estimates and its potential effect on investment decisions, *Nat. Hazards Earth Syst. Sci.*, 16, 1–14, <https://doi.org/10.5194/nhess-16-1-2016>, 2016.
- Winter, B., Schneeberger, K., Huttenlau, M., and Stötter, J.: Sources of uncertainty in a probabilistic flood risk model, *Nat. Hazards*, 91, 431–446, <https://doi.org/10.1007/s11069-017-3135-5>, 2018.
- Wuertz, D.: Package “fExtremes”: Description of package version 3010.81, 37 pp., 2015.
- Wünsch, A., Herrmann, U., Kreibich, H., and Thielen, A. H.: The role of disaggregation of asset values in flood loss estimation: a comparison of different modeling approaches at the Mulde River, Germany, *Environ. Manage.*, 44, 524–541, <https://doi.org/10.1007/s00267-009-9335-3>, 2009.
- Zhai, G., Fukuzono, T., and Ikeda, S.: Modeling Flood Damage: Case of Tokai Flood 2000, *J. Am. Water Resour. As.*, 4, 77–92, 2005.

Paper 12: Papathoma-Köhle, M., Zischg, A., Fuchs, S., Glade, T., Keiler, M., 2015. Loss estimation for landslides in mountain areas – An integrated toolbox for vulnerability assessment and damage documentation. *Environmental Modelling & Software* 63, 156–169. [10.1016/j.envsoft.2014.10.003](https://doi.org/10.1016/j.envsoft.2014.10.003).



Loss estimation for landslides in mountain areas – An integrated toolbox for vulnerability assessment and damage documentation



M. Papathoma-Köhle ^{a,*}, A. Zischg ^b, S. Fuchs ^c, T. Glade ^a, M. Keiler ^d

^a Department of Geography and Regional Research, University of Vienna, Universitätsstrasse 7, 1010 Vienna, Austria

^b Institute of Geography and Oeschger Centre for Climate Change Research, Mobiliar Lab for Natural Risks, University of Bern, Hallerstrasse 12, CH-3012 Bern, Switzerland

^c Institute of Mountain Risk Engineering, University of Natural Resources and Life Sciences, Peter-Jordan-Strasse 82, 1190 Vienna, Austria

^d Institute of Geography, University of Bern, Hallerstrasse 12, CH-3012 Bern, Switzerland

ARTICLE INFO

Article history:

Received 19 February 2014

Received in revised form

25 September 2014

Accepted 6 October 2014

Available online

Keywords:

Loss estimation

Vulnerability

Damage assessment

Landslides

Documentation

ABSTRACT

Global environmental change includes changes in a wide range of global scale phenomena, which are expected to affect a number of physical processes, as well as the vulnerability of the communities that will experience their impact. Decision-makers are in need of tools that will enable them to assess the loss of such processes under different future scenarios and to design risk reduction strategies. In this paper, a tool is presented that can be used by a range of end-users (e.g. local authorities, decision makers, etc.) for the assessment of the monetary loss from future landslide events, with a particular focus on torrential processes. The toolbox includes three functions: a) enhancement of the post-event damage data collection process, b) assessment of monetary loss of future events and c) continuous updating and improvement of an existing vulnerability curve by adding data of recent events. All functions of the tool are demonstrated through examples of its application.

© 2014 Elsevier Ltd. All rights reserved.

1. Introduction

Disaster costs are increasing globally. According to the European Environment Agency (EEA), as far as weather and climate related events are concerned, only in Europe and despite all the counter measures which have been taken, the overall damages have increased from EUR 9 billion in the 1980s, to more than EUR 13 billion in the 2000s (EEA, 2012). This is primarily due to increases in population, economic wealth and human activities in hazard-prone areas, as well as better reporting (EEA, 2012; Keiler, 2013). According to the Intergovernmental Panel on Climate Change (IPCC, 2012), the nature and the severity of the consequences following the occurrence of climate extremes or other hazardous phenomena depends not only on the process itself but also on the exposure and vulnerability of the elements at risk (Fig. 1). Climate change is responsible for changes in the frequency and magnitude of natural processes (Keiler et al., 2010), or actually, for changes in the inputs and the effect of processes (e.g. rainfall as an input to the process of flooding) and partially also for the occurrence locality, however,

socio-economic changes also result in alterations of the spatial and temporal pattern of exposure (Fuchs et al., 2005, 2013) and vulnerability (Fuchs et al., 2012a; Keiler et al., 2012). Therefore, strategies for risk reduction should not only focus on hazardous process and structural protection works, but also, on reducing the exposure and vulnerability of the exposed system. Consequently, appropriate tools are needed so that scientists, authorities and other stakeholders may assess the possible loss under different future scenarios (Papathoma-Köhle et al., 2011). According to IPCC (2012), vulnerability is a key factor in disaster losses; however, it is not yet well accounted for, since data on disasters at the local level are limited (Totschnig and Fuchs, 2013) and thus, improvements in local vulnerability reduction are constrained.

There have been numerous debates regarding the definition of “vulnerability”, since the specific term is used in various ways by scientists of different scientific backgrounds such as natural scientists, engineers, social scientists and climate change researchers (Glade (2003), Füssel (2007), Fuchs (2009), Hufschmidt and Glade (2010), Birkmann et al. (2013), Ciurean et al. (2013)). In natural science and as far as physical vulnerability is concerned, the most common definition of vulnerability is the one that was introduced by UNDRO (United Nations Disaster Relief Organisation) in 1984: “the degree of loss to a given element, or set of elements, within the area affected by a hazard. It is expressed on a scale of 0 (no loss) to 1

* Corresponding author.

E-mail addresses: maria.papathoma@gmail.com, maria.papathoma@univie.ac.at (M. Papathoma-Köhle).

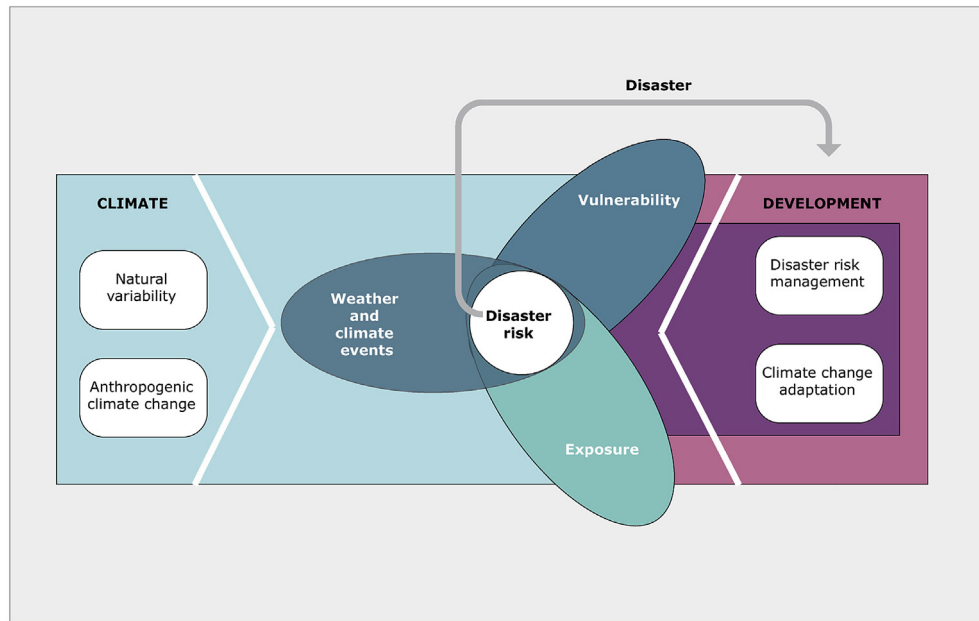


Fig. 1. Key concepts of disaster risk management and their interaction (modified from IPCC, 2012).

(total loss)". There is no universal method for assessing vulnerability (Fuchs et al., 2011); nevertheless, there are three dominant methods for assessing and assign values to it: vulnerability matrices (Papathoma-Köhle et al., 2012b), vulnerability indicators (Birkmann et al., 2013) and vulnerability curves (Fuchs et al., 2007a; Totschnig et al., 2011).

The use of vulnerability curves is common in the case of hazards that affect larger areas and a considerable number of buildings (e.g. floods and earthquakes, Apel et al., 2009). In these cases, the intensity of the process (water depth and ground acceleration respectively) can be assessed relatively easy for each building. Moreover, the reliability of the curve is high due to a rather high amount of available data. It is worth mentioning though, that a comparison of parametric (using indicators) and physically based modelling techniques (using curves) regarding flood vulnerability assessment showed that the parametric approaches are the most appropriate (Balica et al., 2013). Nevertheless, the authors of the specific comparative study indicated also the drawbacks of the parametric methods, such as high data requirements and high levels of uncertainty (Balica et al., 2013). On the other hand, for some types of hazards, such as rock falls or debris flows, the deduction of vulnerability curves is difficult due to the limited number of available damage data (Uzielli et al., 2008), the challenge in assessing the intensity of the process on individual buildings (Mazzorana and Fuchs, 2010) and the gaps in understanding the interaction between the process and the affected elements.

As far as debris flow and fluvial sediment transport (as one large group of landslides) are concerned, the main disadvantage of the vulnerability curves is the lack of reliable empirical data regarding building loss (Fuchs et al., 2012b; Papathoma-Köhle et al., 2012a, b). Although recently an increasing amount of studies focussing on vulnerability curves for this type of hazard can be found in the literature (see Fuchs et al., 2007a; Totschnig et al., 2011; Papathoma-Köhle et al., 2011 for an overview), these curves are mostly based on a limited amount of data related to building damages since such damages are rarely documented in detail (per building) or the information is not available due to e.g. data protection legislation. A second disadvantage is that, in order to develop a curve, information on the intensity of the process on a

detailed scale (intensity per building) is necessary. However, this information is challenging to be recorded and expressed since the intensity of a process depends on more than one factor (Keiler, 2011). For example, in the case of debris flow, the intensity is often expressed as the debris deposition height, although more factors, such as velocity, viscosity, pressure, direction and duration of impact might influence the overall intensity of the process (Jakob et al., 2012). Additionally, the process behaviour may change as it progresses over time and in space. Due to the temporal and spatial variability of sediment concentration during individual events the dominant process in the central part of the deposition zone is regularly used to define the entire event characteristics (Hungry et al., 2001). Moreover, the buildings that are considered for the development of a vulnerability curve should have similar characteristics. These characteristics, however, will not be fully considered in their assessment of vulnerability (Holub et al., 2012). This means that the computation of the curve provides us with information regarding the potential loss rather than information on how this loss can be reduced. Another important issue is the transferability of the method. Vulnerability curves developed for European mountain regions may be applied to other parts of the world only if the type of housing is similar to the one that was used for the development of the original curve (Fuchs et al., 2012c; Lo et al., 2012). In any other case, a new vulnerability curve has to be developed. Moreover, existing curves are based on reported (often tangible) damage and not comprehensively on a broader damage definition (e.g., with respect to tangible and intangible losses). It is, however, almost impossible to validate them (Meyer et al., 2013). For this reason, it is clear that there is a need for better detailed reporting of damages at local scale. Finally, vulnerability curves – if derived empirically – have to be regularly updated with data on losses from recent events, and to be consequently adjusted to the increased basic population. In order to achieve this goal, hence, there is an urge for automatization in the field of damage recording.

On the other hand, the advantage of the vulnerability curves, and the main reason why they are so popular among practitioners, is that they offer a quantitative rather than a qualitative result. By using vulnerability curves the potential economic loss may be expressed as an approximate value in relationship to the expected

hazard intensity for each element at risk (Kienholz et al., 2004). For this reason, vulnerability values may describe the susceptibility of elements at risk facing different natural processes with different spatial and temporal distributions of process intensities (e.g., flow depths, accumulation heights, flow velocities and pressures). Practitioners can use the results of vulnerability curves not only to assess the financial costs of future events under different scenarios, but also for cost benefit analysis for protection measures (e.g., Fuchs et al., 2007b; Markantonis et al., 2012; Fuchs, 2013) and for the impact assessment of alternative risk reduction strategies, such as land use planning (Greiving et al., 2006) or local structural protection (Holub and Fuchs, 2009).

In this paper, an innovative toolbox for assessing the loss of potential future landslide events is presented. The toolbox uses a vulnerability curve based on local past damage data in order to assess the monetary loss of future events and at the same time is targeted at reducing the disadvantages mentioned above. The new toolbox has three functions (tools): 1) it ensures the automatising of the recording of damages in an efficient way by supporting the damage documentation process after an event, 2) it can assess the monetary loss of potential future events, and 3) it improves and updates the curve by the inclusion of new damage data and a re-computation of the curve. Moreover, information on the condition and characteristics of the buildings is also recorded and may be used in the future to investigate the way that buildings with different characteristics react on the impact of debris flows or other torrential hazards.

2. State of the art

Loss estimation models have been developed in the past for various hazard types. The last decades, advances in information technology have significantly improved their functionality. Bendimerad (2001) suggests that loss estimation tools rely on the availability of two large datasets: data regarding the hazard itself (including information on the geology, geomorphology, soil conditions etc.) and data regarding the elements at risk (inventory of buildings and infrastructure, economic value of the elements, etc.). Bendimerad (2001), who focuses mainly on loss estimation tools for earthquake hazards, recognises also the central role of vulnerability curves within these tools. He defines these curves (sometimes referred to also as fragility curves) as “the functional relationship that provides the probability to reach or exceed a damage level as a function of the (earthquake) severity”. Finally, in the same study the advantages and possible uses of loss estimation tools are also listed: (1) accessibility (they can be used also by non-experts), (2) scenario analyses (the impact of different scenarios may be investigated), (3) special focus analyses (the focus may be on specific elements at risk or their components), and (4) customised applications (applications may be defined in order to satisfy specific user needs). In a review of methods for assessing the costs of natural hazards (including alpine hazards, drought, floods and coastal hazards), Meyer et al. (2013) underline the need for cost assessments for natural hazards, because they can be a powerful tool in the hands of decision makers, as well as insurance companies. They suggest that there is a variety of methods and terminologies for the estimation of costs related to natural hazards. As far as terminology is concerned, a glossary for cost categories was developed within the CONHAZ project. The CONHAZ project and cost assessments in general often include a variety of costs types (e.g. direct costs, business interruption costs, indirect costs, intangible costs or even risk mitigation costs). However, in the present paper the focus is clearly on direct costs related to property damage due to the direct physical contact with the hazard (Smith and Ward, 1998; in Meyer et al., 2013). Regarding direct costs, the review

(Meyer et al., 2013) refers also to the damage functions (elsewhere referred to also as fragility or vulnerability functions) for single or multi parameters as the most frequently applied method for cost assessment. They suggest that the functions may take into account one or more parameters. A thorough review of damage/vulnerability functions especially for alpine hazards (floods, landslides, rock falls and snow avalanches) is also provided by Papathoma-Köhle et al. (2011). Particularly for torrent hazards, a considerable number of vulnerability curves can be found in the literature. For example, Fuchs et al. (2007a) based on damage data from a debris flow event in Austria computed a vulnerability curve, Akbas et al. (2009) applied a similar method in Italy and Totschnig et al. (2011) modified the approach introducing the term “relative intensity” (intensity expressed as debris height in relation to building height). Moreover, Papathoma-Köhle et al. (2012a) computed a vulnerability curve for the valley of Martell, which was later improved by including additional data from debris flow events in South Tyrol, Italy (Papathoma-Köhle et al., 2012b). Finally, Quan Luna et al. (2011), based on intensity information derived by numerical modelling, provided three vulnerability curves for debris flows expressing intensity, not only as deposit height, but also as impact pressure and kinematic viscosity respectively.

There is an overall (and empirically-based) conclusion that low process intensities result in low damage ratios and, therefore, low vulnerability, whereas high process intensities result in high damage ratios and consequently high vulnerabilities (e.g., Totschnig and Fuchs, 2013). Nevertheless, there is only limited information available on spatial characteristics of vulnerability within the concept of risk (Fuchs et al., 2012b). As far as medium process intensities are concerned, it is evident that damage associated with medium process intensities (deposit height 1–2 m) may vary significantly (Fuchs et al., 2007a; Totschnig et al., 2011). Therefore, there may be a dependency other than between process intensity and the damage ratio of the buildings exposed. It has been shown that the spatial distribution of geographical locations with either high or low damage ratios is not only an effect of changing process intensities, but also an outcome of the general land use pattern on each individual torrent fan, and the overall constructive characteristics of the elements at risk (Fuchs et al., 2012b). Nevertheless, a further analysis of data, such as the type and year of construction, would enrich our understanding beyond space; such information would be of particular interest with respect to the overall discussion on multi-temporal and spatial assessment of risk (Fuchs and Bründl, 2005; Keiler et al., 2005, 2006; Zischg et al., 2005) and with respect to advances in multi-temporal vulnerability assessments (Fuchs et al., 2011; Papathoma-Köhle et al., 2011) and multi-hazard vulnerability studies (Kappes et al., 2012a, b).

A wide variety of different approaches is available for the assessment of hazard, risk and vulnerability. In the literature, individual studies may be found that set their focus on vulnerability models and loss estimation. Most of them aim at the development of tools and maps to provide information for or to support decision making of stakeholders involved in natural hazard mitigation. An example is the study of Samarasinghe and Strickert (2013) that developed fuzzy cognitive maps for adaptive policy formulation for earthquakes in mountain ski areas, allowing the participation of the stakeholders in the modelling process. Another example of participatory modelling is the study of Giupponi et al. (2013). They developed a tool for flood hazards that explores and communicates vulnerability to floods and climate change to stakeholders, such as representatives of public administrators, businesses and NGOs. The stakeholders of this study may actively participate by identifying the most relevant issues to be considered as input variables to the model. However, the specific tool considers a range of indicators that are relevant to many vulnerability dimensions (e.g. social) and

not only physical. On the other hand, there are studies and tools that concentrate not only on vulnerability but also on the hazard itself, such as a model developed by [Serra et al. \(2013\)](#) for wildfires in Spain. The model is focussing on the extent of clustering of wildfires and the development of risk maps that may provide a tool for preventing and managing vulnerability levels. In the literature, the elements at risk are usually the built environment and the population, however, there also studies concentrating on agriculture (e.g. [Pogson et al., 2012](#)). Last but not least, apart from a range of natural hazards, similar models have been also developed for man-made or technological hazards such as transportation of dangerous goods ([Tena-Chollet et al., 2013](#)).

Besides individual studies of different vulnerability assessments or loss estimation methodologies for specific hazards and areas, there are also loss estimation tools that include data for more than one hazard, as well as inventories for larger areas or countries such as the HAZUS model (USA), RiskScape (New Zealand), EconoMe (Switzerland) and CAPRA (Latin America).

HAZUS (Hazards United States) is a GIS (Geographic Information System) based on a loss estimation software package developed by FEMA (Federal Emergency Management Agency) for the USA that can identify and profile hazards, as well as estimating the losses and possible mitigation options considering the elements at risk in the hazardous areas. HAZUS contains inventories of buildings, essential facilities, transportation and utility facilities, as well as vehicles and agricultural products. It uses damage curves that can be chosen or developed by the user. HAZUS provides loss estimation for hurricanes, earthquakes and floods ([Scawthorn et al., 2006](#)).

RiskScape is an integrative risk assessment tool ([Schmidt et al., 2011](#)) which uses fragility functions for modelling risks from different natural hazards and for various elements at risk. The tool uses a software prototype for generating fragility functions from standard mathematical curves. Different types of fragility functions (empirical curves developed from historical data or synthetic functions (hypothetical curves) based on expert opinion developed independently) can be integrated in RiskScape. RiskScape uses a combination of both refining and adjusting the initial fragility curves to the situation for affected regions in New Zealand.

In Switzerland, an online risk assessment calculation tool EconoMe and its most recent version EconoMe-Develop have been developed for cost-benefit analysis of mitigation measures and have been in operation since 2008. The tool is used mainly for the prioritisation of mitigation projects by the Federal Office of the Environment (FOEN/BAFU) ([Bründl et al., 2009](#)). The specific tool is makes use of fixed (EconoMe) or user defined scenarios (EconoMe-Develop) regarding the hazard (avalanches, floods, debris flows, rock fall and landslides). The tool provides a calculation of exposure, consequence and risk analysis with and without mitigation measures ([Bründl, 2012](#)).

CAPRA (Comprehensive Approach to Probabilistic Risk Assessment) is a probabilistic risk assessment program developed for evaluating multi-hazard risk in Latin America. It is composed of modules of hazards, vulnerability and risk evaluation, as well as tools for cost benefit analysis and it is used for decision making. It provides disaster related information to a number of sectors such as health, education, transport, housing etc. ([Marulanda et al., 2013](#)).

Loss estimation tools like the ones described above require detailed damage datasets that may be derived only through adequate documentation of losses due to disastrous events. One of the main sources of uncertainty in the assessment of costs related to natural hazards is the lack of such datasets that may provide information not only about the past events and their characteristics (intensity, duration, extent, etc.), but also about the elements at risk, their condition prior to the event, the detailed amount of

damage and the intensity of the process associated with each damage. In this respect, several authors suggest (e.g. [Papathoma-Köhle et al., 2012b](#); [Meyer et al., 2013](#)) that improvements should be made in the collection of data following disastrous events and secondary data sets that may enable the calculation of natural hazard costs (e.g. object value). Many efforts have been done in the past for improvement and harmonisation of the collection of post event data such as DOMODIS ([Hübl et al., 2002](#)) and DIS-ALP ([Berger et al., 2007](#)), which focused on the documentation of mountain disasters. However, these initiatives gave an emphasis to the process and its characteristics rather to the consequences and detailed documentation of damage. Damage databases have been also developed by insurers or reinsurers (e.g. NATHAN of Munich Re and Swiss Re's Sigma; [Barredo, 2009](#)), as well as by national administrative bodies (e.g. StorMe; [Burren and Eyer, 2000](#)) at different scales. However, StorMe includes information regarding the event rather its consequences ([Burren and Eyer, 2000](#)). At global level, there is the EM-DAT database which is available on line and contains data on natural and technological disasters and their impact (casualties and costs). At national level, there are similar efforts: in Australia, the research team "Risk Frontiers" maintains a database with information regarding natural hazards and their impacts at national level and countries such as Germany (HOWAS) and countries from Latin America (DesInventar) also maintain databases for flood and natural/technological hazards respectively ([Hilker et al., 2009](#)). In Switzerland, there is the WSL damage database ([Hilker et al., 2009](#)) which focuses on economic damage and casualties. The recorded events are then available to official institutions responsible for land use planning, and protection measures. The financial damage is not only recorded for buildings but also for infrastructure, protective structures, forest and agricultural land ([Hilker et al., 2009](#)). The scale of the damage documentation is at community level ([Hilker et al., 2009](#)). However, to date, there is no standard for the documentation of losses related to natural hazards.

In Italy, the collection of natural hazards events and related information (damages and casualties) is made by means of the IFFI-system (Italian Landslide Inventory, [APAT, 2007](#)), particularly for landslides and rock falls. In the Autonomous Province of Bozen (South Tyrol), water related hazards and the related damage are documented by means of the ED30 system (event documentation for natural hazard events in the Department 30 – Hydraulic Engineering) ([Zischg et al., 2007](#)). Summarised information regarding affected persons, damages on buildings and infrastructure is inserted into the event documentation databases, in most cases without mentioning monetary values.

The main difference between the tool presented here and the existing approaches described above is that the presented tool is working on a local scale in contrast to HAZUS, RiskScape, etc. Moreover, the presented tool is tailored to the application in the European Alps due to the underlying loss data. Additionally, the tool can be used in the field by non-experts for rapid damage documentation and it can also improve itself automatically (updating of the existing vulnerability curve). However, the tool is focussing on the elements at risk and their characteristics without including hazard information (e.g. CAPRA). The presented tool contains not only damage information, but also (in contrast to HOWAS in Germany) information regarding characteristics of the buildings. This information is highly detailed and available on large scale. It includes information not only on the condition or floors of each building but also, on the presence of basement, characteristics of the surroundings and number, size and quality of openings, that is hardly available in any other existing database. RiskScape is currently developing such a database for New Zealand, still, the building characteristics are not as detailed as the ones presented

here (RiskScape Website). In the case of HAZUS, information on elements at risk is collected per Census Block, which, although it is the smallest geographical unit of the United States it includes several buildings.

Despite the fact that documentation methods are slowly improving taking full advantage of the increasingly available technology and loss estimation tools, there are still gaps to be filled, such as scale issues, degree of detail, relationship between damage pattern and process intensity on individual objects, etc. In order to address these issues, we have to improve first the quality and reliability of datasets allowing a more reliable assessment of physical vulnerability. In more detail, there is still the need for improving the vulnerability input within the risk assessment process, increase the quality of damage data and data on elements at risk, as well as the degree of detail. This can be done by continuously recording the consequences of natural processes adequately on the built environment. In this way, the interaction between process and consequences can be better understood and the gained knowledge may then be used for the design of vulnerability reduction strategies. The tool presented in this paper contributes significantly to the improvement of these datasets and, consequently, to the improvement of the vulnerability component of the risk assessment process. In other words, the tool contributes to the successful capture of damage information and its transfer to valuable and reliable datasets that may be used for vulnerability and risk assessment.

3. The vulnerability function

A vulnerability function was computed based on empirical damage data of buildings in South Tyrol, Italy, that have suffered the impact of debris flow or fluvial sediment transport in the past. Based on event documentation (photos), the heights of the deposits were estimated and the estimated monetary damage per building was analysed. The degree of loss per building was also calculated by comparing the value of the building (in terms of reconstruction costs) to the monetary damage caused by the event. At the beginning, Papathoma-Köhle et al. (2012a) conducted a pilot study in the municipality of Martell. A building-precise assessment of the debris flow intensities and the monetary loss of most of the affected

buildings of the 1987 debris flow event in the municipality of Martell was carried out. Overall, photographic documentation of 53 buildings was used out of the 69 buildings that were damaged or completely destroyed (Pfitscher, 1996), since, only for this amount of buildings adequate photographic documentation was available. By using photographic documentation, the extent of damage was translated into monetary loss, based on standard prices for renovation works (Kaswalder, 2009). The degree of loss for each building was then assessed, based on the overall building value (Papathoma-Köhle et al., 2012a). In order to improve the curve, more buildings that suffered damage due to debris flows or fluvial sediment transport in South Tyrol were added to the curve (52 additional buildings) in a later stage. The final curve, including all the buildings from the Italian Alps, is shown in Fig. 2 (Papathoma-Köhle et al., 2012b).

The vulnerability curve clearly shows that the higher the intensity of the process the greater the damage that an element at risk suffers. Papathoma-Köhle et al. (2012a, b) computed also a validation curve (blue curve in Fig. 2) using paid-out compensation data provided by the Department of Domestic Construction of the Autonomous Province of Bozen (South Tyrol) for the calculation of the degree of loss. The degree of loss for the development of the validation curve was expressed as the ratio of the estimated object value and the compensation that the building owners received in order to restore their building. The intensity values remained the same as the ones used for the initial vulnerability curve. The validation curve provided slightly higher degree of loss values for intensities 0–1.5 m and lower degree of loss values for intensities 1.5–3.5 m.

4. The toolbox

A toolbox was developed to support the risk management practice in regard to three main aims: (a) improvement of the damage data collection process on the field, (b) assessment of damage and loss for buildings prone to future events (scenarios), and (c) improvement of an existing vulnerability curve by using data of recent events.

Thus, the toolbox has three functions that were implemented as three separate but interlinked procedures (tools):

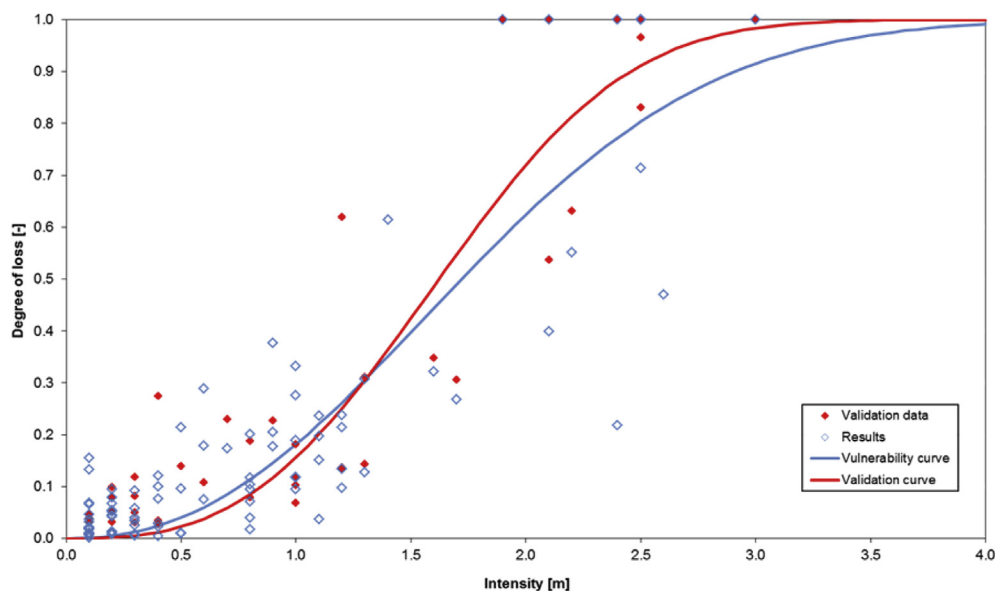


Fig. 2. The vulnerability function (blue curve) and the validation function (red curve) for debris flow events in South Tyrol (Papathoma-Köhle et al., 2012b). (For interpretation of the references to colour in this figure legend, the reader is referred to the web version of this article.)

1. A standardised method for improved and more efficient damage documentation and assessment in the field.
2. A method for damage and loss assessment of possible future events under different land use/hazard scenarios using the existing vulnerability curve.
3. Updating of the database and improvement of the curve by including additional empirical and well-documented damage data from recent events.

The toolbox considers mainly damage on residential buildings or buildings with similar characteristics without including specifications, such as sensitive inventories in industrial buildings. The three individual tools are connected to each other in terms of data and output exchange (Fig. 3). A starting menu prompts the user to the required tool, which is either damage documentation or damage calculation.

The first tool (damage documentation) offers a graphical user interface, which enables the documentation of physical damage on buildings caused by the impact of torrential hazards. With this tool, the majority of information regarding detailed damage patterns can be recorded into a database. On the basis of the input data, a mathematical function calculates the needed amount of restoration work and, eventually, the total monetary value of the restoration, as well as the total value of the building. In the calculation of the restoration costs, only the construction costs are calculated, based on the costs of an average building in South Tyrol. Content costs or special high value building features (e.g. expensive floors) are not considered. As a result, the loss ratio can be obtained for every assessed building. If, at a later stage, information on additional losses (from another hazard event) becomes available, the system re-calculates the existing vulnerability curve (third tool: update of existing curve), in order to take into account an enlarged sample of buildings and to increase the reliability of the function.

The second tool (loss assessment of future scenarios) calculates the monetary loss per building for a specific hazard scenario on the basis of the building value and the externally computed expected process intensity. The potential loss is subsequently calculated using the internal vulnerability curve, which is continuously updated by the third tool. Depending on the scale, this function can be used for individual objects but it can simultaneously be implemented into a GIS-procedure for loss assessment over wider regions. In the

following paragraphs, all three tools of the toolbox are described in detail.

4.1. Damage documentation tool

Following a debris flow event it is important to estimate the cumulative damage on buildings and infrastructure. The individual damage has to be documented and calculated in a short time window after the event because (a) damage is usually restored as soon as possible by the local population after the event and (b) the government needs information about the losses immediately for priority setting of intervention and restoration works and for the information of the media. In parallel, insurance companies would like to have an efficient instrument for the rapid documentation of the losses. If a larger area is affected by the event, the damage documentation should be made as efficient and precise as possible.

The damage documentation tool consists of a form, which is represented by a graphical user interface in the software environment (Fig. 4) and guides the user through the data input.

The process characteristics are usually described in detail in the (separate) event documentation database. Here, the process characteristics are expressed in terms of mean deposition heights around the building. If the deposit height varies around the building, a further input form supports the user to document the process characteristics on all sides of the building.

The input values are stored in the database and are, therefore, available for subsequent computation steps, such as the implemented mathematical function which calculates the monetary value of the total construction costs of the buildings based on the official price index of the Autonomous Province of Bozen-South Tyrol (Autonomous Province of Bozen-South Tyrol, 2012a). In 2012, the official prices of construction costs were € 342 per cubic metre of building volume, which is, respectively, € 1369 per square metre net living area. After the input of the ground plan area and the number of floors, the value of the building is calculated and inserted in the database.

Another mathematical function calculates the monetary value of the restoration costs by using the average hourly salaries and the general cost calculation guidelines for constructions of the Autonomous Province of Bozen-South Tyrol (2012b). This official database stores the necessary material costs and associated

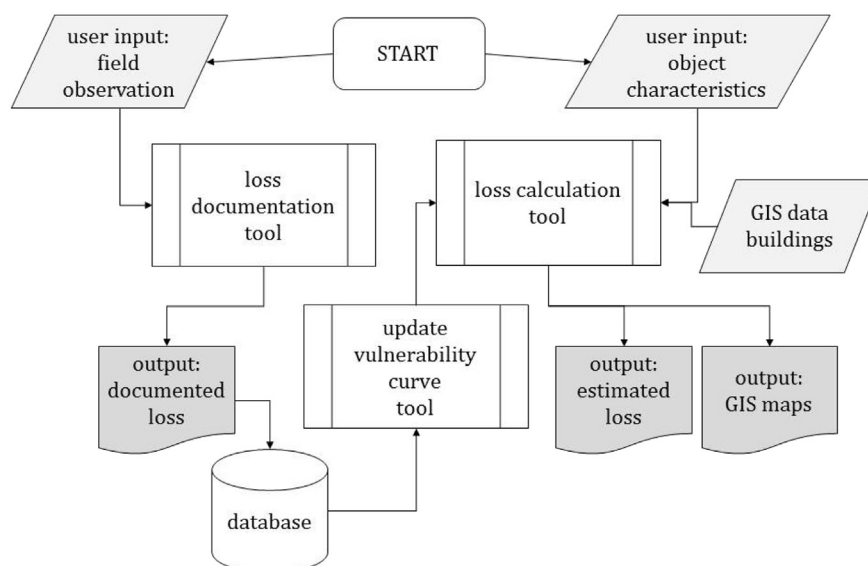


Fig. 3. The structure of the integrated toolbox.

Damage documentation



Impact to building - damage description

Community:

Locality, address, ID *:  

Functionality: residential
 auxiliary type:
 industrial/business type:
 public type:
 other type:

Construction: wood
 mixed
 mortar-built
 reinforced

Basement: no

Structures around the building: wall
 fence
 no

Vegetation around the building: trees
 hedge
 no

Protection works: yes Type:

Ground-plan area [m2]:
year of construction:
number of floors:

Apertures (hill side): type:
quantity:
quality:

Apertures (flank): type:
quantity:
quality:

garden destroyed
door of garage destroyed
garage destroyed:

area of exterior walls to be repainted [m2]: Building completely destroyed:

damaged area of exterior walls [m2]:
destroyed doors:

area of interior walls to be repainted [m2]: upper floors damaged

detr. heating or installations: damaged area of interior walls [m2]:
removing material: damaged windows: ground floor damaged

damage on accessories:

height of debris flow deposits above floor level [m]:

Impact process

detr. heating or installations:
removing material:
damage on accessories:
damaged doors:
removing material:
detr. heating or installations:
Additional damage total [€]:

basement damaged

--> CALCULATE DAMAGE

Damage [€]:

--> INPUT IN DATABASE

Fig. 4. The screen shot of the graphical user interface of the tool for damage documentation.

Table 1

Modified functional approaches for regression analysis of vulnerability. As Frechet distributions with different numbers of parameters were tested, a numeral suffix was used to distinguish between them. The RMSE for the Exponential, Weibull and Frechet functions is provided in the last column.

Distribution	Mathematical notation	Number of unknown parameters	Interval of the explaining variable	Root mean square error
Modified Weibull	$1 - e^{-a\left(\frac{x+b}{b}-1\right)^c}$	3 a, b, c	[0; +∞)	0.1318
Modified Exponential	$1 - e^{-a\left(\frac{x+b}{b}-1\right)}$	2 a, b	[0; +∞)	0.1437
Modified Frechet no. 1	$e^{-\left(\frac{x+b}{b}-1\right)^{-a}}$	2 a, b	[0; +∞)	0.1355
Modified Frechet no. 2	$e^{-c\left(\frac{x+b}{b}-1\right)^{-a}}$	3 a, b, c	[0; +∞)	0.1355

personnel working hours in standardised units. The data is accessible via an XML interface for use in any software, or in terms of a MS Access © database. The vulnerability tool uses the MS Access © tables of the price-index database for further computation. The official data sets were imported into the tool database representing the construction costs of this specific region. The mathematical function implemented in the tool considers the dimension of the building and the other input data (e.g. number of broken windows and doors, area of walls to be repainted, etc. see Table 1) to compute the necessary costs for each individual working step during the potential re-instatement of the building. Finally, the costs of each individual working step and the necessary material costs are summed up. After the input of the documented damages, the calculated costs are shown in the documentation form (Fig. 5). If the documented damage is connected with a GIS-dataset of the buildings, the results of the documentation tool can be shown in a map (Fig. 6).

The record set of the damage documentation for each building is subsequently complemented by two computed values: (a) the construction costs of the building and (b) the costs for repairing the damage due to the respective hazard event. These two values are then used by the tool for the assessment of loss of future events and for the update of the vulnerability function.

4.2. Loss assessment of future events

The tool for loss assessment of future events requires the input of information, such as the building category and functionality, the floor plan, the number of floors and the existence of a basement, the use of the ground floor and the upper floors, and additional information on auxiliary buildings such as garages, sheds and storerooms. Using this data, the tool calculates the total value of the construction costs using the official price index (Autonomous Province of Bozen-South Tirol, 2012a) as described above. Furthermore, since the expected process intensity is expressed as the height of debris deposits, this information is also needed. On the basis of this value, the tool computes the degree of loss using the vulnerability function (Fig. 5).

If the presence of a basement is unknown, the tool calculates two values. As a minimum value, the construction costs are calculated without considering a basement. In the maximum value, the construction costs of a basement the size of the first floor are considered. Additionally, based on the minimum and maximum construction costs, a mean value is also given. The tool calculates the potential damage by multiplying the degree of loss with the mean value of the construction costs.

This procedure was also incorporated as a GIS-procedure in the ArcGIS software environment. On the basis of an overlay of the GIS-dataset of the building characteristics (function, use of the building, ground plan area, floors) and the hazard maps (scenarios with process intensities), the potential losses caused by selected

scenarios can be computed over large areas. The GIS-procedure uses the vulnerability function computed from the tool database.

4.3. Update of the vulnerability curve

The vulnerability curve derives from the degree of loss associated with an expected process intensity. After recording the new damage documentation data (including information regarding the value of the buildings, the intensity of the process and the loss height), the update module of the tool re-calculates the parameters of the stored vulnerability function. The degree of loss is expressed as the ratio between repairing costs (monetary damage) and construction costs (object value) in terms of a Weibull function (Formula 1 (Totschnig et al., 2011; Papathoma-Köhle et al., 2012a, b)).

$$y = 1 - e^{a\left(\frac{x+b}{b}-1\right)^c} \quad (1)$$

Where:

y: degree of loss

a, b, c: factors describing the shape of the Weibull-function

x: process intensity

The factors describing the shape of the vulnerability curve (a,b,c) are recalculated based on the newly recorded datasets. The function itself does not change. It is assumed that with a growing dataset and detailed and improved documentation of damage of individual buildings, the vulnerability curve will become more and more reliable.

5. Implementation and practical use

The toolbox was used into three different applications. The three tools (damage documentation, loss assessment of future scenarios, and updating of the vulnerability curve) have been implemented into a Microsoft SQL Server and ESRI ArcGIS. The system offers the graphical user interface for data entry and output (as shown in Figs. 4 and 5); it contains the knowledge base for calculating the total amount and costs of restoration works (extract from the official price list of construction costs), and the database for the insertion of damage documentation. The routines and functions for the cost calculation and the calculation of the vulnerability curve are also implemented in the database as server functions. The database forms are accessible via internet.

5.1. Damage documentation

During the damage documentation in the field, shortly after a hazard event, a mobile internet connection is not always possible.

Fig. 5. Graphical user interface of the loss assessment tool.

Therefore, the tool was implemented into an MS Excel spreadsheet by using VBA and the same windows forms of the database. The spreadsheet contains the same graphical user interface as the database and stores the data in the same data format for an easy import into the database. The spreadsheet-based tool can be used on a tablet computer without internet connection.

The damage documentation tool was tested during the damage documentation in the consequences of numerous debris flow events in the area of Vipiteno/Sterzing, Autonomous Province of Bozen – South Tyrol, Italy (August 4th and 5th, 2012; refer to Zischg (2012) for details). A heavy rainfall event triggered more than ten debris flows. The debris flows damaged 52 mostly residential or residential/agricultural buildings. The physical characteristics of the debris flow events were documented by the official authorities of the Autonomous Province of Bozen – South Tyrol. The damage on the buildings and houses were documented during a field campaign five days after the event with the presented tool. The

damaged buildings were surveyed and the damage was recorded using the damage documentation form shown in Fig. 4. The tool was used on a tablet computer and supported an efficient documentation and time-saving damage assessment; the 52 buildings were documented and the related losses subsequently estimated within one day. Besides the photographic documentation, the tool did not require post-field processing.

5.2. Loss estimation

The total sum of incurring losses caused by the event was estimated by the tool to be 1.3 Mio. €. The process intensities impacting the building envelopes were locally very high with deposition heights of more than 2 m, with a mean of 0.7 m and a median of 0.3 m. Two thirds of the buildings affected by the debris flow did not experience structural damage. Two buildings were totally destroyed. Eleven buildings experienced damage in the

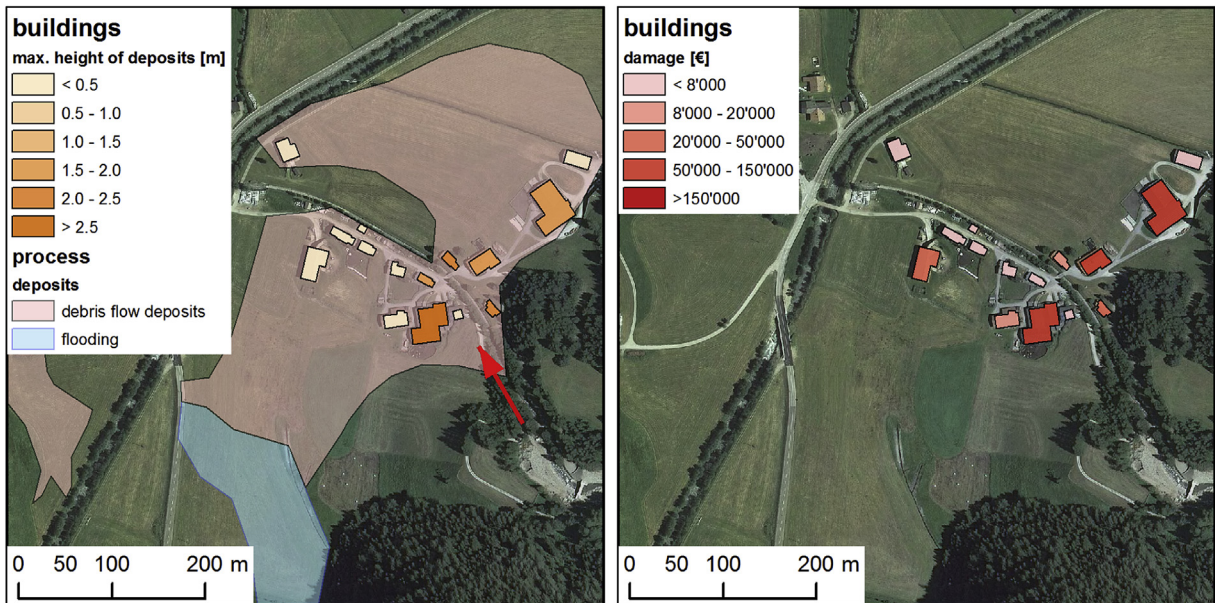


Fig. 6. Map of showing the spatial pattern of the process intensity distribution (left) and the monetary damage distribution (Fussendrass, community of Valle di Vizze/Pfisch).

interior because the debris entered into the building through broken windows or doors. The spatial pattern of the deposition height and flooding as well as the damage distribution in the specific area are shown in Fig. 6.

A comparison of the estimated loss (1.3 Mio. €) with the actual cost of this event is not possible because the estimation of the local authorities included also monetary losses regarding the content of the buildings and agricultural equipment.

5.3. Updating of the vulnerability curve

After recording the damage into the database, and after calculating the losses with the first two parts of the tool, the parameters of the vulnerability function were recalculated with the third part. The entire dataset consists of 271 documented damages: 136 from Austria (Totschnig and Fuchs, 2013), 34 from Martell valley (South Tirol, Italy) (Papathoma-Köhle et al., 2012a), and 100 damage from the Vipiteno/Sterzing and Pfisch/Val die Vizze areas as described above.

The dataset is divided into a training dataset (80% of the original data) and a test dataset (20% of the original data). The test dataset was stratified as such that both datasets contained the same amount of high and low values (Fig. 7).

The training dataset, composed from a total of 217 cases, was further divided randomly into ten subsets of equal size (22 cases

each) in order to cross-validate the different data models tenfold. Subsequently, we tested different possible loss functions for their power to fit best the training dataset. These functions had to comply with the mathematical requirements of (a) defining vulnerability as the dependent variable in a closed interval $[0; 1]$; (b) a steady and monotonic increase within the interval of its explaining variable (intensity); (c) steadiness with respect to higher orders within the defined interval; and (d) definition of its explaining variable either in the unbounded interval $(-\infty; +\infty)$ or in the half-open interval, bounded from below $[0; +\infty)$. Following Totschnig et al. (2011), an Exponential function, as well as a Weibull and two Frechet distributions were tested. These different functions were trained on the ten sub-samples of 22 data points (tenfold cross-validation), and as a result a Root Mean Square Error (RMSE) was obtained for each one of them (see Table 1).

As the modified Weibull distribution obtained the smallest RMSE (0.1318), this function was chosen to best represent the training dataset. In a second set of calculation, the Weibull function was tested taking the 20% residual test dataset. The RMSE increased slightly to 0.1358, which means that this function is able to project future (unknown) events with an accuracy of almost 87%.

In Fig. 8, the alteration of the Weibull distribution is presented in dependence on the amount of data considered. It is shown that, for the Martell event, the losses were slightly lower for small and medium process intensities up to 1.5 m deposition height, and

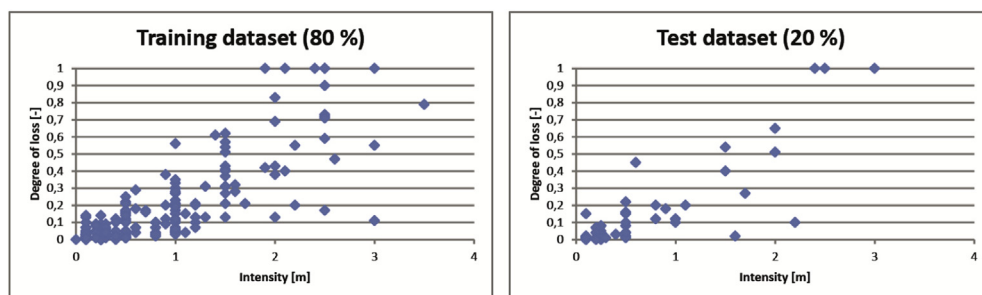


Fig. 7. The training and the test dataset used for the recalculation of the parameters of the vulnerability function.

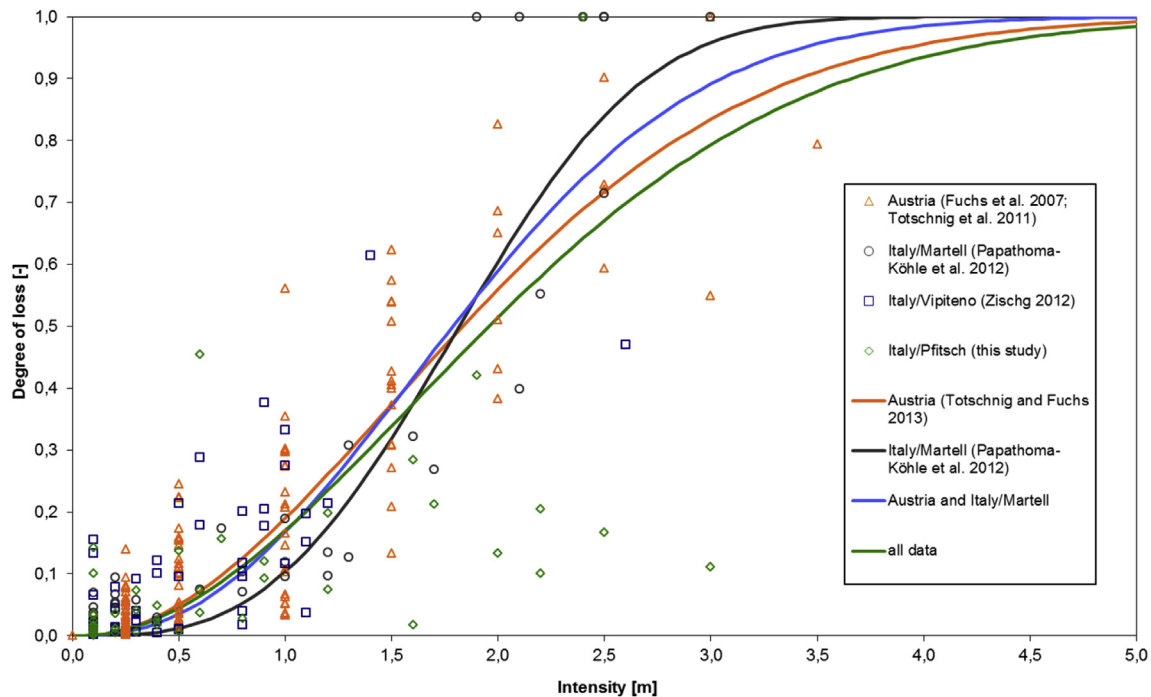


Fig. 8. Results of the recalculation of the vulnerability curve after the increase in the sample dataset. The green curve shows the vulnerability function calculated on the basis of all the data. (For interpretation of the references to colour in this figure legend, the reader is referred to the web version of this article.)

slightly above the population for higher process intensities. The combination of different sample data (Austria, Martell case study and the damage from Vipiteno/Sterzing and Pfitsch/Val die Vizze) shows how the shape of the function is altered due to different values of the parameters a , b and c calculated according to Equation (1). In Table 2, the values of the parameters describing the Weibull function (a , b , c) for the different case studies and respective curves are shown.

In general, the results also show that the spread is considerable for medium process intensities. Therefore, if the vulnerability function is used to calculate damage on single objects, the results may over- or underestimate the real losses. The method implies consideration of a minimum number of some objects in loss assessments. However, it is difficult to set a minimum number of data, as more factors may influence the reliability of the curve. For example, the data points should represent cases of the full spectrum of values. In other words, buildings that have suffered very high degree of loss should be used as well as others that have suffered minimum loss.

6. Discussion

The toolbox presented herein offers a number of solutions to various challenges that decision makers and planners have to deal with, such as: a) future change (climate and socio-economic) and associated increasing of damage costs, b) reliable vulnerability

assessment that will contribute to improved risk analysis, and c) better documentation of events and associated damage in large scale, etc. In the following paragraphs, the most important benefits and limitations of the present study are described. Finally, ideas for further development of the presented tool in the future are also outlined.

6.1. Benefits

The greatest benefit of the toolbox is its multi-functionality. The toolbox presented here can be used for loss estimation, rapid damage assessment and documentation at local level, and improvement through continuous updating of the existing core vulnerability curve. The tool has the ability to self-improve and to work against one of the greatest drawbacks in the field of risk analysis, which is the lack of reliable and adequate data. The tool improves the data collection procedure by providing a user-friendly and standardised data collection method that does not require a high number of qualified personnel. The data collection can take place on site within a short time period after the event. Depending on the availability of an internet connection, the data can be stored directly in the database or in a spreadsheet.

The toolbox can also be used as a basis for cost benefit analysis. Once the overall monetary loss of a hypothetical event is assessed, the alternative monetary loss by using mitigation measures may also be calculated. In this way, the best alternative risk mitigation and management strategies can be chosen. The implementation of the functions in a GIS-procedure is unproblematic when a dataset of buildings including their functionality and extent is available. Through the integrated functions, the reconstruction values of each building can be calculated on the basis of the attributes of the input dataset. The function delineates the vulnerability value from the intersection between the buildings dataset and the hazard intensity map and, therefore, calculates the expected loss for every object exposed to the hazard. Using GIS, not only the assessment of

Table 2
The parameters a , b , c for the Weibull function for the different case studies/curves shown in Fig. 8.

	Austria (orange curve)	Austria and Italy/Martell (blue curve)	Italy/Martell (black curve)	All data (green curve)
a	-1.253	-1.138	-0.27	-1.671
b	2.438	2.177	1.287	3.189
c	1.892	2.202	2.974	1.746

potential losses on buildings over large areas is possible, but also, the databases can be easily updated and the results can be visualised. The vulnerability of the elements at risk is not calculated in a static way, but, through the connection to GIS, the spatial pattern of the vulnerability may be also visualised and, in this way, the relationship between the natural process and its consequences may be better investigated. Moreover, databases including loss data may be exported and used in other applications.

An important benefit of the toolbox is that it can be used by multiple users that are not necessarily experts or experienced specialists. Decision makers and stakeholders with different backgrounds, such as, scientists, technicians, and administrative personnel, may all make use of the advantages of the toolbox. The situation and damage pattern following a disastrous event may change very quickly due to the need of the authorities and the local population to bring the situation back to normal. The tool offers a quick way of documenting damage directly on site, so that the original situation of the damaged elements following an event can be directly recorded. An innovative element of the toolbox is that, apart from the recorded damage, it also records (and creates a database of) building characteristics that influence its overall vulnerability (vulnerability indicators). In this way, two of the most commonly used methods for vulnerability assessment (vulnerability curves and vulnerability indicators) are integrated in the same tool supporting rather than opposing each other. Furthermore, the scale that the toolbox is used at offers a great detail of the damage pattern. Until now damage databases are maintained mostly at community level and they miss great detail (e.g. damage and intensity per building). The toolbox also offers possibilities of improvement and expansion such as additional elements at risks (infrastructure, agricultural areas, and open spaces) and hazard types. However, the most important benefit that the toolbox can demonstrate through the present study is its capacity to actively support risk reduction strategies and climate change adaptation efforts.

Finally, an additional strength of the tool is that, although the core vulnerability curve itself cannot be transferred and used in another area with different characteristics and type of built environment, the tool itself may be immediately used by local data and start performing by tuning itself automatically to the local context.

6.2. Limitations and improvement

One of the most significant limitations of the tool is the difficulty of recording information regarding the intensity of the process on each building. The intensity of the fluvial bedload transport or debris flow has been expressed in this paper as the height of debris deposits. However, in many cases this height was assumed by looking at the size of destruction or at the stains that material and water have left on the walls of the building. Moreover, the intensity of the process depends, apart from the deposition height, also on other factors, such as the velocity, the viscosity and the direction of the flow that approaches the building. These factors are generally challenging to record for each affected building. However, in some recent studies (Quan Luna et al., 2011; Jakob et al., 2012), information regarding the velocity and the viscosity of debris flows has been acquired through modelling of past events. In the case of the presented tool, intensity of the process is recorded through improved documentation, establishing the link between event and damage documentation. Nevertheless, during the development of the tool many assumptions had to be made which increased the level of uncertainty. There are uncertainties associated with the input data (e.g. object value, intensity assessment), and uncertainties associated with the model procedure (e.g. monetary loss assessment) that were not considered or quantified in this study. In more detail, sources of uncertainties are related to: a) the estimation of the

process intensity, b) the estimation of the degree of loss, c) the value of buildings and d) the credibility of the existing data. However, the quantification of these uncertainties within the tool and recommendations regarding their reduction could be one of the potential future improvements. The quantification of uncertainties is very important for the end-users of the tool that, in this way, may get an indication of how well the tool is expected to perform. The uncertainties related to the development of the vulnerability curve which formed the basis of the tool presented in this paper have been quantified in a recent study (Eidsvig et al., 2014). However, their quantification is not yet included as a function of the tool.

Furthermore, the tool may be transferable to areas with houses of similar type of construction and similar construction costs. However, if the building types are different, a new vulnerability curve has to be developed. The database of the construction costs can be easily adapted to other regions, if mean values for the single restoration works are available there in a standardized format. The development of the curve is often prevented by data limitations. However, the tool itself with its rapid damage assessment function is expected to improve data availability.

Moreover, since the database at the moment contains only a limited number of documented cases, the function is calculated based on all building types available. Nevertheless, in the future, a growing set of documented data will allow the development of more than one vulnerability functions for the different types of buildings (use, type of construction etc.).

6.3. Outlook

A future development of the tool, apart from its applications in other areas, must include more elements at risk. A similar toolbox could include critical infrastructure, such as powerlines, railway and road networks, industrial or other important buildings, such as airports and railway stations. Moreover, the tool could also be used for the loss estimation of agricultural areas, based on the intensity of the process and monetary loss, which includes for example the cleaning costs, replanting and the harvest loss. The tool could be also adequately modified to be used for other hazard types, such as floods. Although this paper is focussing mainly on direct losses to the built environment, the focus of the risk reduction strategies is always the protection of the human life. In this respect, the toolbox could be expanded to include data regarding the population e.g. number of inhabitants, population density, characteristics of the population, such as health condition, income, mobility, and density during different times of the year and the day. Information on people could also be included in the documentation process (e.g. number of casualties per building etc.). Nonetheless, one of the most important developments of the existing toolbox could be the possibility of quantifying its uncertainties in order to enable decision making. As it was mentioned in the previous paragraph, work concerning the quantification of uncertainties has already been done and the next step is the integration of the quantification of uncertainties in the tool. Finally, the tool could be used remotely from unqualified users as a phone or tablet application in order to populate a central database with data by ordinary people (non-experts) that are located on the spot during or right after an event and may assist in the post-damage data collection and documentation. This would be a step towards solving one of the biggest problems in the loss estimation and vulnerability assessment field, which is the one of data availability.

7. Conclusion

A toolbox for loss documentation for landslide hazards is presented. The toolbox can be used by decision makers to assess

potential losses of future debris flow events but also to document and record damage of real events in a rapid, sufficient and detailed way. The toolbox is a valuable instrument in the hands of stakeholders considering the on-going changes in the frequency and magnitude of hazardous events and also in the spatial pattern of the elements at risk. The tool offers also a solution to one of the most common challenges in risk assessment, which is the lack of adequate data. The databases included in the toolbox may be exported and used for other applications, but also the new data may be used to continuously update the tool and increase its reliability. Although the toolbox is an important step towards loss estimation at local level for debris flow hazards, there is still a need for continuous research in the field, in order to better understand the interactions between natural processes and the built environment, so that we are able to reduce the vulnerability of elements at risk and eventually the costs related to natural disasters.

Acknowledgements

The authors would like to thank Bruno Mazzorana from the Department of Hydraulic Engineering of the Autonomous Province of Bozen – South Tyrol, Italy. He supported the documentation of the damaged buildings following the debris flow events in August 2012 in the Vipiteno/Sterzing area and provided information on the process intensities. Furthermore, the authors would like to thank the reviewers and the editors for their valuable comments and suggestions to an earlier version of this paper. Funding for the presented research was provided by the Austrian Science Fund (FWF, L535-N10) and the EU project MOVE (Methods for the Improvement of Vulnerability Assessment in Europe; <http://www.move-fp7.eu>, contract number 211590).

References

- Akbas, S.O., Blahut, J., Sterlacchini, S., 2009. Critical assessment of existing physical vulnerability estimation approaches for debris flows. In: Malet, J.P., Remaitre, A., Bogaard, T. (Eds.), *Proceedings of Landslide Processes: from Geomorphologic Mapping to Dynamic Modeling*, Strasbourg, 6–7 Feb 2009, pp. 229–233.
- APAT – Agenzia per la Protezione dell'Ambiente e per i Servizi Tecnici, 2007. *Rapporto sulle frane in Italia. Il progetto IFFI- Metodologia, risultati e rapporti regionali*. Rapporti 78/2007. Roma. ISBN 978-88-448-0310-0.
- Apel, H., Aronica, G., Kreibich, H., Thieken, A., 2009. Flood risk analyses – how detailed do we need to be? *Nat. Hazards* 49 (1), 79–98.
- Autonome Provinz Bozen Südtirol, 2012a. *Beschluss der Landesregierung vom 18. Juni 2012, Nr. 904. Amtsblatt Nr. 26/I-II vom 27/06/2012*. <http://www.regione.taa.it/bur/pdf/I-II/2012/26/BO/BO26120179833.pdf>. access on July 2013.
- Autonome Provinz Bozen Südtirol, 2012b. *Resort Bauen. Abteilung 11: Hochbau und technischer Dienst. Richtpreisverzeichnis Hochbauarbeiten 2012*. Online database version. http://www.provinz.bz.it/Hochbau/downloads/hoed_2012.pdf. http://www.provinz.bz.it/Hochbau/browse_d.aspx. access on July 2013.
- Balica, S.F., Popescu, I., Beevers, L., Wright, N.G., 2013. Parametric and physically based modelling techniques for flood risk and vulnerability assessment: a comparison. *Environ. Model. Softw.* 41, 84–92.
- Barredo, J.I., 2009. Normalised flood losses in Europe: 1970–2006. *Nat. Hazards Earth Syst. Sci.* 9, 97–104.
- Bendimerad, F., 2001. Loss estimation: a powerful tool for risk assessment and mitigation. *Soil Dyn. Earthq. Eng.* 21, 467–472.
- Berger, E., Grisotto, S., Hübl, J., Kienholz, H., Kollarits, S., Leber, D., Loipersberger, A., Marchi, L., Mazzorana, B., Moser, M., Nössig, T., Riedler, W., Scheidl, C., Schmid, F., Schnetzer, I., Siegel, H., Volk, G., 2007. *DIS-alp: Disaster Information System of Alpine Regions Final report*, p. 96.
- Birkmann, J., Cardona, O.M., Carreño, M.L., Barbat, A.H., Pelling, M., Schneiderbauer, S., Kienberger, S., Keiler, M., Alexander, D., Zeil, P., Welle, T., 2013. Framing vulnerability, risk and societal responses: the MOVE framework. *Nat. Hazards* 67 (2), 193–211.
- Bründl, M., Romang, H.E., Bischof, N., Rheinberger, C.M., 2009. The risk concept and its application in natural hazard risk management in Switzerland. *Nat. Hazards Earth Syst. Sci.* 9, 801–813.
- Bründl, M., 2012. *Econo-Me-Develop – a software tool for assessing natural hazard risk and economic optimisation of mitigation measures*. In: *Proceedings, 2012 International Snow Science Workshop, Anchorage, Alaska*, pp. 639–643.
- Burres, S., Eyer, W., 2000. *STORME- ein Informationsgestützter Ereignis-Kataster der Schweiz*. Internationales Symposium Intrprävent 2000. Band 1, 25–37 (Villach: Kreiner Druck).
- Ciurean, R.L., Schröter, D., Glade, T., 2013. Conceptual frameworks of vulnerability assessments for natural disasters reduction. In: Tiefenbacher, J. (Ed.), *Approaches to Disaster Management – Examining the Implications of Hazards, Emergencies and Disasters*. InTech, pp. 3–32.
- EEA, 2012. *Climate Change, Impacts and Vulnerability in Europe 2012*. Office for Official Publications of the European Union, Luxembourg, p. 300.
- Eidsvig, U.M.K., Papathoma-Köhle, M., Du, J., Glade, T., Vangelsten, B.V., 2014. Quantification of model uncertainty in debris flow vulnerability assessment. *Eng. Geol.* 181, 15–26.
- Fuchs, S., 2009. Susceptibility versus resilience to mountain hazards in Austria – paradigms of vulnerability revisited. *Nat. Hazards Earth Syst. Sci.* 9 (2), 337–352.
- Fuchs, S., 2013. Cost-benefit analysis of natural hazard mitigation. In: Bobrowski, P. (Ed.), *Encyclopedia of Natural Hazards*. Springer, Dordrecht, pp. 121–125.
- Fuchs, S., Bründl, M., 2005. Damage potential and losses resulting from snow avalanches in settlements of the canton of Grisons, Switzerland. *Nat. Hazards* 34 (1), 53–69.
- Fuchs, S., Keiler, M., Zischg, A., Bründl, M., 2005. The long-term development of avalanche risk in settlements considering the temporal variability of damage potential. *Nat. Hazards Earth Syst. Sci.* 5 (6), 893–901.
- Fuchs, S., Heiss, K., Hübl, J., 2007a. Towards an empirical vulnerability function for use in debris flow risk assessment. *Nat. Hazards Earth Syst. Sci.* 7 (5), 495–506.
- Fuchs, S., Thöni, M., McAlpin, M.C., Gruber, U., Bründl, M., 2007b. Avalanche hazard mitigation strategies assessed by cost effectiveness analyses and cost benefit analyses – evidence from Davos. *Switz. Nat. Hazards* 41 (1), 113–129.
- Fuchs, S., Kuhlicke, C., Meyer, V., 2011. Editorial for the special issue: vulnerability to natural hazards – the challenge of integration. *Nat. Hazards* 58 (2), 609–619.
- Fuchs, S., Birkmann, J., Glade, T., 2012a. Vulnerability assessment in natural hazard and risk analysis: current approaches and future challenges. *Nat. Hazards* 64 (3), 1969–1975.
- Fuchs, S., Ornetmüller, C., Totschnig, R., 2012b. Spatial scan statistics in vulnerability assessment – an application to mountain hazards. *Nat. Hazards* 64 (3), 2129–2151.
- Fuchs, S., Tsao, T.-C., Keiler, M., 2012c. Quantitative vulnerability functions for use in mountain hazard risk management – the challenge of transfer. In: Koboltshg, G., Hübl, J., Braun, J. (Eds.), *Internationales Symposium Interpraevent, Genoble, April 23–26, 2012*. Internationale Forschungsgesellschaft Interpraevent, Klagenfurt, pp. 885–896.
- Fuchs, S., Keiler, M., Sokratov, S.A., Shnyarkov, A., 2013. Spatiotemporal dynamics: the need for an innovative approach in mountain hazard risk management. *Nat. Hazards* 68 (3), 1217–1241.
- Füssel, H.-M., 2007. Vulnerability: a generally applicable conceptual framework for climate change research. *Glob. Environ. Change* 17 (2), 155–167.
- Giupponi, C., Giove, S., Giannini, V., 2013. A dynamic assessment tool for exploring and communicating vulnerability to floods and climate change. *Environ. Model. Softw.* 44, 136–147.
- Glade, T., 2003. Vulnerability assessment in landslide risk analysis. *Die Erde* 134, 121–138.
- Greiving, S., Fleischhauer, M., Lückenköter, J., 2006. A methodology for an integrated risk assessment of spatially relevant hazards. *J. Environ. Plan. Manag.* 49 (1), 1–19.
- Hilker, N., Badoux, A., Hegg, C., 2009. The Swiss flood and landslide damage database 1972–2007. *Nat. Hazards Earth Syst. Sci.* 9, 913–925.
- Holub, M., Fuchs, S., 2009. Mitigating mountain hazards in Austria – legislation, risk transfer, and awareness building. *Nat. Hazards Earth Syst. Sci.* 9 (2), 523–537.
- Holub, M., Suda, J., Fuchs, S., 2012. Mountain hazards: reducing vulnerability by adapted building design. *Environ. Earth Sci.* 66 (7), 1853–1870.
- Hübl, J., Kienholz, H., Loipersberger, A., 2002. *DOMODIS-documentation of Mountain Disasters*, p. 40.
- Hufschmidt, G., Glade, T., 2010. Vulnerability analysis in geomorphic risk assessment. In: Alcántara-Ayala, I., Goudie, A.S. (Eds.), *Geomorphological Hazards and Disaster Prevention*. Cambridge University Press, pp. 233–243.
- Hungr, O., Evans, S., Bovis, M., Hutchinson, J., 2001. A review of the classification of landslides of the flow type. *Environ. Eng. Geoscience* 7 (3), 221–238.
- IPCC, 2012. *Managing the risks of extreme events and disasters to advance climate change adaptation. A Special Report of Working Groups I and II of the Intergovernmental Panel on Climate Change*. In: Field, C.B., Barros, V., Stocker, T.F., Qin, D., Dokken, D.J., Ebi, K.L., Mastrandrea, M.D., Mach, K.J., Plattner, G.-K., Allen, S.K., Tignor, M., Midgley, P.M. (Eds.), *Cambridge University Press, Cambridge, UK, and New York, NY, USA*, 582 pp.
- Jakob, M., Stein, D., Ulmi, M., 2012. Vulnerability of buildings to debris flow impact. *Nat. Hazards* 60 (2), 241–261.
- Kappes, M., Keiler, M., von Elverfeldt, K., Glade, T., 2012a. Challenges of analyzing multi-hazard risk: a review. *Nat. Hazards* 64 (2), 1925–1958.
- Kappes, M., Papathoma-Köhle, M., Keiler, M., 2012b. Assessing physical vulnerability for multi-hazards using an indicator-based methodology. *Appl. Geogr.* 32 (2), 577–590.
- Kaswalder, C., 2009. *Schätzungsstudie zur Berechnung des Schadenspotentials bei hochwasserereignissen durch die Rienz im Abschnitt Bruneck-St (Lorenzen)*. Autonome Provinz Bozen, Südtirol.
- Keiler, M., 2011. *Geomorphology and complexity – inseparable connected? Z. für Geomorphol.* 55 (Suppl. 3), 233–257.
- Keiler, M., Zischg, A., Fuchs, S., Hama, M., Stötter, J., 2005. Avalanche related damage potential – changes of persons and mobile values since the mid-twentieth century, case study Galtür. *Nat. Hazards Earth Syst. Sci.* 5 (1), 49–58.

- Keiler, M., Sailer, R., Jörg, P., Weber, C., Fuchs, S., Zischg, A., Sauer Moser, S., 2006. Avalanche risk assessment – a multi-temporal approach, results from Galtür, Austria. *Nat. Hazards Earth Syst. Sci.* 6 (4), 637–651.
- Keiler, M., Knight, J., Harrison, S., 2010. Climate change and geomorphological hazards in the eastern European Alps. *Philosophical Transactions of the Royal Society of London Series A: Mathematical. Phys. Eng. Sci.* 368, 2461–2479.
- Keiler, M., Kellereir-Pirklbauer, A., Otto, J.-C., 2012. Concepts and implications of environmental change and human impact: studies from Austrian geomorphological research. *Geografiska Annaler Series A. Phys. Geogr.* 94 (1), 1–5.
- Keiler, M., 2013. World-wide trends in natural disasters. In: Bobrowsky, P. (Ed.), *Encyclopaedia of Natural Hazards*. Springer, pp. 1111–1114.
- Kienholz, H., Krummenacher, B., Kipfer, A., Perret, S., 2004. Aspects of integral risk management in practice – considerations with respect to mountain hazards in Switzerland. *Österreichische Wasser- Abfallwirtsch.* 56 (3–4), 43–50.
- Lo, W.-C., Tsao, T.-C., Hsu, C.-H., 2012. Building vulnerability to debris flows in Taiwan: a preliminary study. *Nat. Hazards* 64 (3), 2107–2128.
- Markantonis, V., Meyer, V., Schwarze, R., 2012. Valuating the intangible effects of natural hazards. Review and analysis of the costing methods. *Nat. Hazards Earth Syst. Sci.* 12 (5), 1633–1640.
- Marulanda, M.C., Carreno, M.L., Cardona, O.D., Ordaz, M.G., Barbat, A.H., 2013. Probabilistic Earthquake Risk Assessment Using CAPRA: Application to the City of Barcelona, Spain. *Natural Hazards*, Online first. <http://dx.doi.org/10.1007/s11069-013-0685-z>.
- Mazzorana, B., Fuchs, S., 2010. Fuzzy Formative Scenario Analysis for woody material transport related risks in mountain torrents. *Environ. Model. Softw.* 25 (10), 1208–1224.
- Meyer, V., Becker, N., Markantonis, V., Schwarze, R., van den Bergh, J.C.J.M., Bouwer, L.M., Bubeck, P., Ciavola, P., Genovese, E., Green, C., Hallegatte, S., Kreibich, H., Lequeux, Q., Logar, I., Papyrakis, E., Pfuertscheller, C., Poussin, J., Przulski, V., Thieken, A., Viavattene, C., 2013. Review article: assessing the costs of natural hazards – state of the art and knowledge gaps. *Nat. Hazards Earth Syst. Sci.* 13 (5), 1351–1373.
- Papathoma-Köhle, M., Kappes, M., Keiler, M., Glade, T., 2011. Physical vulnerability assessment for alpine hazards: state of the art and future needs. *Nat. Hazards* 58 (2), 645–680.
- Papathoma-Köhle, M., Keiler, M., Totschnig, R., Glade, T., 2012a. Improvement of vulnerability curves using data from extreme events: debris flow event in South Tyrol. *Nat. Hazards* 64 (3), 2083–2105.
- Papathoma-Köhle, M., Totschnig, R., Keiler, M., Glade, T., 2012b. A new vulnerability function for debris flow – the importance of physical vulnerability assessment in alpine areas. In: Koboltschng, G., Hübl, J., Braun, J. (Eds.), *Internationales Symposium Interpraevent*, Grenoble, April 23–26, 2012. Klagenfurt, Internationale Forschungsgesellschaft Interpraevent, pp. 1033–1043.
- Pfitscher, A., 1996. *Wasserkatastrophen im Martelltal – Der 24./25. August 1987*. Municipality 23 Martell.
- Pogson, M., Hastings, A., Smith, P., 2012. Sensitivity of crop model predictions to entire meteorological and soil input datasets highlights vulnerability to drought. *Environ. Model. Softw.* 29, 37–43.
- Quan Luna, B., Blahut, J., Van Westen, C.J., Sterlacchini, S., Van Asch, T.W.J., Akbas, S., 2011. The application of numerical debris flow modelling for the generation of physical 26 vulnerability curves. *Nat. Hazards Earth Syst. Sci.* 11, 2047–2060.
- Samarasinghe, S., Strickert, G., 2013. Mixed-method integration and advances in fuzzy cognitive maps for computational policy simulations for natural hazard mitigation. *Environ. Model. Softw.* 39, 188–200.
- Scawthorn, C., Blais, N., Seligson, H., Tate, E., Mifflin, E., Thomas, W., Murphy, J., Jones, C., 2006. HAZUS-MH flood loss estimation methodology. I: overview and flood hazard characterization. *Nat. Hazards Rev.* 7, 60–71.
- Schmidt, J., Matcham, I., Reese, S., King, A., Bell, R., Henderson, R., Smart, G., Cousins, J., Smith, W., Heron, D., 2011. Quantitative multi-risk analysis for natural hazards: a framework for multi risk modelling. *Nat. Hazards* 58, 1169–1192.
- Serra, L., Juan, P., Varga, D., Mateu, J., Saez, M., 2013. Spatial pattern modelling of wildfires in Catalonia, Spain 2004–2008. *Environ. Model. Softw.* 40, 235–244.
- Smith, K., Ward, R., 1998. *Floods: Physical Processes and Human Impacts*. John Wiley & Sons, Chichester.
- Tena-Chollet, F., Tixier, J., Dusserre, G., Mangin, J.-F., 2013. Development of a spatial risk assessment tool for the transportation of hydrocarbons: mateology and implementation in a geographical information system. *Environ. Model. Softw.* 46, 61–74.
- Totschnig, R., Sedlacek, W., Fuchs, S., 2011. A quantitative vulnerability function for fluvial sediment transport. *Nat. Hazards* 58 (2), 681–703.
- Totschnig, R., Fuchs, S., 2013. Mountain torrents: quantifying vulnerability and assessing uncertainties. *Eng. Geol.* 155, 31–44.
- UNDRP, 1984. *Disaster Prevention and Mitigation – a Compendium of Current Knowledge*. United Nations, New York.
- Uzielli, M., Nadim, F., Lacasse, S., Kaynia, A., 2008. A conceptual framework for quantitative estimation of physical vulnerability to landslides. *Eng. Geol.* 102 (3–4), 251–256.
- Zischg, A., Fuchs, S., Keiler, M., Stötter, J., 2005. Temporal variability of damage potential on roads as a conceptual contribution towards a short-term avalanche risk simulation. *Nat. Hazards Earth Syst. Sci.* 5 (2), 235–242.
- Zischg, A., Macconi, P., Pollinger, R., Sperling, M., Mazzorana, B., Marangoni, N., Berger, E., Staffler, H.P., 2007. *Historische Überschwemmungs- und Murgangereignisse in Südtirol. Erhebung und Dokumentation*. Der Schlern 3, 3–16.
- Zischg, A., 2012. Systematische Erhebung der Gefährdungs- und Schadensbilder für die Objektkategorien Wohnhäuser, Wirtschaftsgebäude und Verkehrswege in ausgewählten Auswirkungssystemen des Großraumereignisses des 4. und 5. In: August 2012 Pfitscherbach – Oberer Eisack als planungsunterstützende Elemente des integralen Naturgefahr- und Risikomanagements im IREK – Projektgebiet. Projekt Interreg IVA Italien–Österreich IREK – Integrales Raumentwicklungskonzept für ausgewählte Lebensräume des Wipptals. Bozen.

Paper 13: Mosimann, M., Frossart, L., Keiler, M., Weingartner, R., Zischg, A., submitted. A robust and transferable model for the prediction of flood losses on household contents. *Water*.

Article

A robust and transferable model for the prediction of flood losses on household contents

Markus Mosimann^{1,2,3*}, Linda Frossard^{1,2,3}, Margreth Keiler^{1,2}, Rolf Weingartner^{1,2,3} and Andreas Paul Zischg^{1,2,3}

¹ Institute of Geography, University of Bern, Hallerstrasse 12, CH-3012 Bern, Switzerland

² Mobiliar Lab for Natural Risks, University of Bern, Hallerstrasse 12, CH-3012 Bern, Switzerland

³ Oeschger Centre for Climate Change Research, University of Bern, Falkenplatz 16, CH-3012 Bern, Switzerland

* Correspondence: markus.mosimann@giub.unibe.ch; Tel.: +41 31 631 88 39

Academic Editor: name

Version October 3, 2018 submitted to Water

Abstract: Beside the flood hazard analysis, a comprehensive flood risk assessment requires the analysis of the exposure of values at risk and their vulnerability. Currently, the main focus of such analysis is on losses on building structure. However, loss on household contents accounts for up to 30% of the total losses on buildings due to floods. Here, we present two functions for estimating flood losses on household contents based on flood losses on building structure. The models are constructed from and validated for insurance claim records. One model is based on a regression of the degree of loss for household content on the degree of loss for building structure. The second model is based on the same regression structure between the absolute losses of both types. Moreover, we tested our models for robustness, predictive power and transferability. Both models generate appropriate results with a comparative advantage of the relative over the absolute loss model. A detailed examination of the model residuals, shows that the Box-Cox transformation works well to accurately fit a standard regression model to general right-skewed loss data as the transformed data meet the assumptions of a regression model.

Keywords: Flood loss estimation; Vulnerability functions; Loss on household content; Flood impact modelling; Linear regression; Box-Cox transformation, Transferability

1. Introduction

The assessment of flood vulnerability and thus the analysis of losses due to floods constitutes a substantial public interest. Based on a database from 1946 to 2015, flood ranks third in the list of most fatal catastrophes related to natural hazards in Switzerland [1]. According to Swiss Re [2], floods accounted for 71 % of the total loss due to natural hazards in Switzerland over the period 1973 to 2011. Compared to windstorm (15 %), hailstorm (11 %) and other perils (3 %), this indicates the relevance of flood risk assessment. The destructive potential was also shown in August 2005, when floods and debris flows in Switzerland led to financial losses of more than CHF 3 billions [3, roughly EUR 2 billion].

The availability of flood models and the possibility to develop flood scenarios lead to new perspectives in detecting regions or even single buildings with a high loss potential. Especially, flood losses are increasingly estimated at the scale of single buildings [4–9]. Because inundations rarely lead to a total destruction of buildings, the term "(physical) vulnerability" [10] is used to describe the ratio of the monetary loss to the value of a building and thus describes the relative loss occurring on a building (loss divided by insurance sum). Synonymously, the term "degree of loss" is widely used [11,12]. Most

31 often mathematical functions are used to link parameters of flood magnitude (mainly flow depth,
32 less frequently flow velocity or duration of exposition) to empirical flood loss data, resulting in the
33 fitting of a vulnerability or stage-damage curve to observed data. The diversity of such functions is
34 manifold and ranges from univariate functions, e.g. based on Weibull distribution functions [13,14] or
35 root functions [15,16], over to multivariate functions, e.g. graduated models [17,18] or complex models
36 considering exposure variables like building type, footprint area etc. as well as hazard variables
37 [19,20].

38 Although such functions are mainly developed to assess building structure vulnerability, Dutta
39 *et al.* [16], Jonkman *et al.* [17], FOEN [18] and Kreibich *et al.* [20] also present stage-damage curves
40 for flood vulnerabilities of household contents. Especially univariate models or models considering
41 only hazard variables systematically neglect a possible effect of the structural vulnerability on the
42 vulnerability of contents.

43 Thielen *et al.* [21] examined the influence of several factors on flood loss on building structures
44 and contents for about 1000 flood-affected households, with information gained by computer-aided
45 telephone interviews. They analysed the influence of different variables in the lower and upper loss
46 quartiles by principle component analyses and the results indicate that flood impact variables (water
47 level, flood duration and contamination by sewage, chemicals or petrol/oil) are the most important
48 factors, followed by variables describing the size and value of the affected buildings or flats. Similar
49 significant variables were obtained for all combinations of loss type (monetary, relative loss) and
50 object type (contents, structure). Thielen *et al.* [21] also described an interrelation between content
51 and building structure losses, especially in the case of higher losses and degrees of loss. Although the
52 monetary loss was provided by the interviewed persons, the values of buildings and contents were
53 estimated by a model. Further it is shown that considering absolute household content loss is relevant,
54 since the mean absolute loss on contents (EUR 16 335) amounts to 39 % of the mean absolute loss on
55 building structures (EUR 42 093). Assuming the mean total loss on a building would consist of the
56 mean building structure loss and the mean household content loss, the share of the latter in the mean
57 total building loss is 28%, whereas the mean loss ratio for household contents (0.296) is more than
58 twice the mean loss ratio for buildings (0.123) [21].

59 In an analysis of the flood event in August 2005, FOWG [22] provide an overview of the estimated
60 losses based on insurance data. The report mentions an even larger fraction of the mean household
61 content loss of CHF 32 100 (EUR 20 700, calculated according to PSL [23]; total: CHF 700 (EUR 450)
62 millions; 21 783 claim records) relative to the mean building structure loss of CHF 55 800 (EUR 36 000;
63 total: CHF 250 (EUR 160) millions; 4483 claim records), resulting in a ratio of 58 % (share of the mean
64 household content loss in the mean total building loss, assumed to consist of the mean loss on building
65 structure and the mean loss on household contents: 36.5%).

66 Studies on flood losses on household contents are subject to restrictions concerning the availability
67 of empirical data needed for developing vulnerability functions or for assessing model reliability.
68 In case of missing loss data, proxies for values at risk and losses are used. One example are data
69 on flood losses compiled by interviews with persons affected by a flood event. Another example is
70 to model the values of building structure and household content and to derive relative losses from
71 these assumptions. Both approaches introduce uncertainties in the resulting flood loss models. The
72 developed models are mostly lacking information about model uncertainties, for instance in terms of
73 the (in)dependence of errors. In addition, most models are not tested for their robustness in prediction.
74 Another issue mentioned in literature [24,25] is the transferability of such models, meaning that they
75 are only valid for regions the data was collected in, or which at least show similar characteristics.

76 In summary, although putting effort in the estimation of losses on building structures, the role of
77 potential losses on household contents should not be underestimated. There is still a lack of knowledge
78 concerning the statistical correlation of losses on household contents with the corresponding losses
79 on building structures and in robustness and transferability of vulnerability functions for household
80 contents. Therefore, the main objective of this study is to develop a model for estimating flood losses on

81 household contents based on observed and reliable data. The main focus herein is to develop functions
82 which provide robustness in prediction and transferability to other regions. This also comprises the
83 question whether the loss on household contents can better be predicted by a relative loss model,
84 looking at the relation of the loss ratios occurring on buildings and contents, or by a direct loss model
85 connecting monetary loss on building structure with monetary loss on household contents.

86 Hereafter, we will use the terms "degree of loss" (= relative loss, vulnerability) and "monetary
87 loss" (= absolute loss). The "relative loss model" will describe the model, which predicts degrees of loss
88 on household contents based on degrees of loss on building structure. The "monetary loss model" will
89 predict monetary loss on household contents based on monetary loss on building structures.

90 2. Material and methods

91 This study relies on a data set from the private *Swiss Mobiliar Insurance Company*. In Switzerland,
92 19 out of 26 cantons have public insurance companies for buildings with monopoly positions. Hence,
93 different insurers are responsible for losses on building structures and for losses on household content.
94 Data about monetary losses on building structures and on household contents are only available for the
95 cantons without a monopoly position, namely Geneva, Uri, Schwyz, Ticino, Appenzell Inner-Rhodes,
96 Valais and Obwalden.

97 After the description of the data in the first subsection, we describe the development of the
98 vulnerability function in the subsequent section.

99 2.1. Data

100 The used data set (anonymised, as valid for December 2016) consists of the damage date, product
101 information (distinction between households, small enterprises and medium enterprises), type of
102 building describing its purpose (holiday homes, single-family house, apartment house with maximum
103 units or more than three units, etc.) and the type of construction (solid or not). The timespan of the
104 data covers January 2004 to December 2016. Here, we focus on household data only. As key elements
105 for this study, the data set includes information on the insurance sum of building structures and
106 household contents, as well as damage claim records on structures and contents at the time of the
107 occurrence of the loss. We did not correct the data with respect to inflation or modifications. The claim
108 data are distinguished by the cause of loss. Losses due to leakages in pipes and groundwater effects
109 are recorded as "water losses" and losses caused by riverine floods as "elementary losses". Based on
110 this distinction, losses due to water entering the structure at ground level (= "water losses") can be
111 identified and excluded. The availability of insurance sum and loss allows a more reliable calculation
112 of the degree of loss ($dol = \text{loss} / \text{insurance sum}$). As a contract ID and the address including
113 X-Y coordinates for a major part of the records are also available, it is possible to reliably link loss data
114 of building structures with those of household contents.

115 2.1.1. Quality check

116 Not all entries in the data set are valid for the proposed analysis. Thus, the data were preprocessed
117 and filtered to ensure a homogeneous data set. The loss data are provided separately for elementary
118 losses on building structures and household contents. To compare the degree of loss observed on a
119 building structure with that on household content, the single entries for structures and contents had to
120 be matched. For the data from the *Swiss Mobiliar Insurance Company*, this is possible by matching the
121 anonymous loss IDs. For every record, the address was used to check the accordance of the matched
122 entries. Residential buildings from single-family houses up to apartment buildings with maximum
123 three units and holiday homes were considered. Within the data set, buildings with more than three
124 apartments are defined as small and medium enterprises and were excluded from the analysis.

125 Some loss values in the claim records of the *Swiss Mobiliar Insurance Company* are remarkably and
126 implausibly low, resulting in outliers. These values might have been caused by e.g. the magnitude
127 of franchise or costs for administrative work. To exclude these outliers, only values above CHF 100

128 were taken into account for the analysis. In total, this concerns eight entries of the matched subsets.
 129 Furthermore, entries for on "household" products can include buildings like summer or bee houses
 130 with a very low insurance sum and systematically higher degrees of loss than residential buildings.
 131 In consultation with the experts from the *Swiss Mobiliar Insurance Company*, we excluded entries with
 132 insurance sums lower than CHF 100 000 (six cases). This ensures analysing a comparable class of
 133 buildings with residential purpose. After the quality check, there are 16 946 records of household
 134 content loss and 1662 records of building structure loss left. The number of loss records for building
 135 structure is the limiting data set for the number of claims occurring in combination because buildings
 136 are insured by monopolists in 19 out of 26 cantons, whereas for household contents this is only the
 137 case in the two cantons of Vaud and Nidwalden. For roughly one fourth (384) of all buildings insured
 138 by the *Swiss Mobiliar Insurance Company* with occurrence of structure loss, a loss claim of household
 139 content was recorded too. Hereafter, we only refer to those 384 *paired claim records*, where *paired*
 140 indicates buildings with a claim record for structure and content. As already mentioned, the loss data
 141 correspond to the amount of money paid by the insurance and thus the franchise is originally not
 142 included. Since the amounts and rates of franchise are legally anchored and the temporal information
 143 on the occurrence of the loss is provided, we are able to reproduce the effective loss.

144 2.1.2. Data distribution

145 Figure 1 shows the canton-wise distributions of all paired monetary flood losses and degrees of
 146 loss within the period from January 2004 to December 2016. The cantons of Geneva and Appenzell
 147 Inner-Rhodes are not shown because there were available only two and three records, respectively.
 148 One can observe that the distribution of monetary losses and degrees of loss is different among cantons.
 149 In Obwalden (OW) and Uri (UR), the cost of claim was highest, whereas in Ticino (TI) and Valais (VS)
 150 it was lowest. Compared to them, Schwyz (SZ) shows intermediate costs. This pattern is shown by the
 151 distributions of losses and degrees of loss on contents and in almost the same manner for structures.

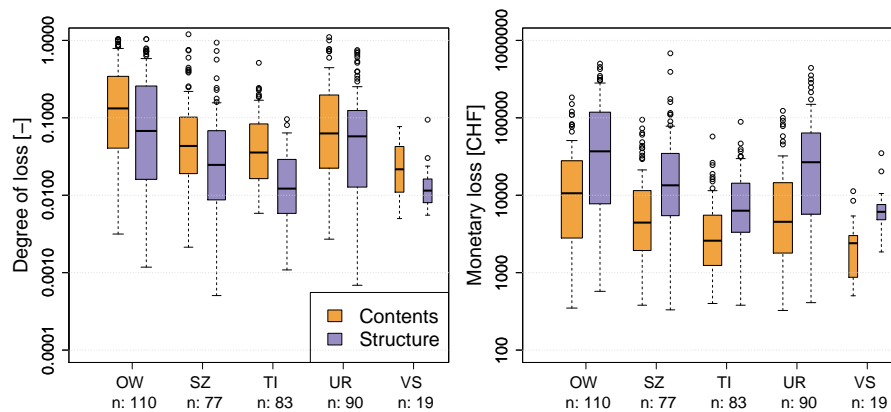


Figure 1. Canton-wise distribution of records in the data sets used for the analyses. Left: Degree of loss [-], right: monetary loss [CHF]; both on log-scale. Sample size is given by "n:" and illustrated by the width of the box plots. Due to the low number of claim records, data recorded in Geneva and Appenzell Inner-Rhodes are not presented.

152 As we are interested in the role of content losses and vulnerability compared to structural losses,
 153 we calculate as a first overview the shares of content losses and insurance sums on total (structure +
 154 content) building losses and building values (see Figure 2). This will help us to make comparisons
 155 with other studies and reports of past events.

156 2.2. Regression model

157 In this study, we used a linear regression [26,27] for the estimation of losses on household contents
 158 caused by flood events. The main objective of the regression analysis is to derive losses on household
 159 contents (as monetary [CHF] loss and as degree of loss [-]) from losses occurring on building structures
 160 at the same location and caused by the same event. Consequently, we use respectively the monetary
 161 loss and the degree of loss on household contents as the dependent variable and the corresponding
 162 type of loss on building structures as the only independent input.

163 2.2.1. Data transformation and fitting

164 As indicated by Figure 1, the distributions of monetary losses and degrees of loss are even on
 165 the log scale both characterized by a right skew and therefore not normally distributed, nor do they
 166 follow a log-normal distribution (i.e., the logarithm of a variable is normally distributed). As normality
 167 of the involved variables themselves is not a prerequisite in classical linear regression analysis [28,
 168 p. 92], we will not further comment on this. Instead we focus on the characteristics of the residuals
 169 produced by the linear model. This requires the consideration of heteroscedasticity, which is given
 170 when the variability of the response is not constant across the range of the explanatory variables. It can
 171 for example be addressed, visually with diagnostic plots or more formally by the Breusch-Pagan test
 172 [29]. Further, the assumption of normally distributed residuals has to be met as well [28,30] and will
 173 be tested by the Shapiro-Wilks test for normality ([31], implemented in the R software [32]). We will
 174 also use diagnostic plots as visual aids for interpretations. Gaussian linear regression models with
 175 non-normally distributed residuals might lead to inaccurate confidence and prediction intervals and
 176 biased predictions. Not considering either of these assumptions will lead to an inaccurate estimation
 177 of the regression parameters.

For data initially not satisfying these properties, power transformations are common methods to
 achieve normality and an approximately constant residual variance. Out of this family, the Box-Cox
 transformation, defined for $y \geq 0$ as

$$y^{(\lambda)} = \begin{cases} \frac{y^\lambda - 1}{\lambda}, & \lambda \neq 0, \\ \log(y), & \lambda = 0, \end{cases} \quad (1)$$

where $\lambda \in \mathbb{R}$ is the power parameter and $y^{(\lambda)}$ denotes the transformed version of y , is a special case
 [33–38]. To return to the original scale of the data, the values can be back-transformed by using

$$y = \begin{cases} \left(1 + \lambda y^{(\lambda)}\right)^{\frac{1}{\lambda}}, & \lambda \neq 0, \\ \exp\left(y^{(\lambda)}\right), & \lambda = 0. \end{cases} \quad (2)$$

The advantages of this transformation compared to other members of the power family are the
 systematic determination of the power parameter λ by maximum likelihood estimation [39, p. 278]
 and the continuity at $\lambda = 0$ [38, p. 67]. Consider the linear regression model with a single covariate x
 given by

$$y = \beta_0 + \beta_1 x + \varepsilon, \quad (3)$$

where y and x denote response and covariate respectively, β_0 and β_1 are the regression coefficients
 to be estimated and the error ε is assumed to be normally distributed with variance σ^2 . Originally
 the Box-Cox transformation would be applied to the response variable y so that y in equation (3)
 is replaced by $y^{(\lambda)}$, but an application to other non-negative quantities is of course also possible.
 Carroll and Ruppert [35] and Ruppert and Matteson [38] introduced the transform-both-sides (TBS) method,

which consists in transforming the response y and the deterministic part of the regression equation with the same power parameter λ so that the model equation (3) becomes

$$y^{(\lambda)} = (\beta_0 + \beta_1 x)^{(\lambda)} + \varepsilon.$$

This approach was actually developed for cases where the response y is known to theoretically satisfy a given non-linear function of x and some unknown parameters β_i , but where the residuals from the corresponding model on original scale would not satisfy normality and/or homoscedasticity. In our application of this model, we chose the linear structure because it does not seem too bad based on a scatterplot of the data and because we had no other a priori guess for the relation between y and x for the loss data. To nevertheless account for possible non-linearity between the two quantities, we also applied another model we termed pseudo-transform-both-sides (PTBS). It consists of the same linear regression structure applied to Box-Cox transformations of y and x , i.e.,

$$y^{(\lambda)} = \beta_0 + \beta_1 x^{(\lambda)} + \varepsilon.$$

In a first step we used the same power parameter λ for both transformations as given here, but due to slightly sub-optimal model diagnostics especially for the absolute loss data, we also fitted the following extension of the PTBS model with two different power parameters for x and y (later referred to as PTBS.seplam):

$$y^{(\lambda_y)} = \beta_0 + \beta_1 x^{(\lambda_x)} + \varepsilon.$$

178 For all three models, the complete parameter set can be estimated by maximum likelihood estimation,
179 so that standard errors and confidence intervals for all parameters are easily obtained.

180 The Bonferroni Outlier Test was used to detect exceptional data points [30]. We also calculated
181 Cook's distance, leverage and defined large residuals. Once the regression parameters are estimated
182 and all model assumptions verified, the edited regression has to be back-transformed to retrieve the
183 original and interpretable unit, resulting for the PTBS model in:

$$y = \left(1 + \lambda\beta_0 - \beta_1 + \beta_1 x^\lambda\right)^{\frac{1}{\lambda}}. \quad (4)$$

184 The back-transformation being non-linear for the PTBS and PTBS.seplam models, the residuals
185 are not any more normally distributed as they were in transformed form [39–42]. In addition,
186 mean and median of the back-transformed distribution no longer coincide. When $\lambda < 1$, the power
187 parameter for the back-transformation becomes > 1 which means that the normal distribution of
188 the residuals on the transformed scale gets right-skewed on the original scale [43]. The right skew
189 implies a discrepancy between the median and the mean of the back-transformed distribution such
190 that the former systematically underestimates the latter. Taylor [41] derived an approximation for the
191 conditional mean of the untransformed response variable y in terms of the model parameters β_0 , β_1 ,
192 σ^2 , λ for the original Box-Cox model, where $y^{(y)}$ is linear in x .

193 Adopted to the PTBS model it reads

$$E[Y|x] \approx \left(1 + \lambda\beta_0 + \lambda\beta_1 x^{(\lambda)}\right)^{\frac{1}{\lambda}} \times \left(1 + \frac{\sigma^2(1-\lambda)}{2(1 + \lambda\beta_0 + \lambda\beta_1 x^{(\lambda)})^2}\right) =: \psi \quad (5)$$

194 Replacing the parameters β_0 , β_1 , σ^2 , λ in (5) by their maximum likelihood estimates yields an
195 estimate $\hat{\psi}$ for the mean of the original variable Y . The variance of $\hat{\psi}$ can then be estimated by the delta
196 method (e.g. Weisberg [44]) and confidence intervals (and prediction intervals) for ψ can be based on
197 the asymptotic normality of the maximum likelihood estimator.

198 2.2.2. Cross-validation

199 To test the predictive accuracy of our models and their robustness in terms of variance and bias,
200 a leave-one-out cross-validation was applied [45,46]. For each model type (PTBS, PTBS.seplam, TBS
201 as well as relative or monetary loss), every single observation y_i is predicted as either the median
202 or the mean from the model fitted to the data set without observation y_i . For the resulting sample
203 of predictions, the aggregate prediction error is computed as the mean of the prediction errors for
204 the individual observations y_i . In addition we computed the standard deviations for each prediction
205 error sample as a measure of the spread of the individual prediction errors. To compare the prediction
206 quality and accuracy of the different models we considered four different error metrics for each case:
207 bias [CHF], relative bias [%], absolute error [CHF] and relative absolute error [%].

208 For comparisons in terms of accuracy, the results of both the monetary loss model and the model
209 based on degrees of loss need to describe the same unit and scale. We use the unit [CHF] for evaluating
210 the models. To do so, predicted degrees of loss on household contents are multiplied by the insurance
211 sum of the content, provided by the insurance company.

212 2.2.3. Assessment of transferability

213 Based on Wenger and Olden [47], who suggest non-random cross-validation by splitting data into
214 geographic regions, we analysed the performance of our models in terms of transferability. We applied
215 the non-random cross-validation based on monetary losses to data from five out of seven available
216 cantons. The cantons of Geneva and Appenzell Inner-Rhodes were neglected because only few claims
217 were found with both structure and content loss. The transferability assessment for our models was
218 tested for Obwalden ($n = 110$), Ticino (83), Uri (90), Schwyz (77) and Valais (19). To make sure that
219 the unbalanced sample sizes of the cantons do not impact the results, we applied non-random K -fold
220 cross-validation for several numbers of folds K between 2 and 20. In the last case, the fold sizes are
221 similar to the "outlying" Valais sample size. We used the same error metrics for this analysis as for the
222 leave-one-out cross-validation.

223 As a further assessment of transferability, we carried out an analysis of variance (anova) [44,48] on
224 the transformed data, assuming λ fixed. More particularly, we tested whether a model with individual
225 regression lines for each canton (differing either only in the intercept or in intercept and slope) fits the
226 data better than the simpler model with a single line. Good transferability of the current simple model
227 is then achieved if the more complex version with individual regression lines leads to *no* significantly
228 improve fit.

229 3. Results

230 3.1. On the role of household contents

231 Figure 2 a) shows the box plots of the shares of household content loss (left) and insurance sum
232 (right) on total building loss and insurance sum. The mean share of content loss amounts to 0.29 (=
233 29 %), whereas the median is roughly 25 %. With respect to the share on the total building value
234 (mean: 0.16; median: 0.15), this is disproportionately high. Thus, it is obvious that degree of loss of
235 contents is generally higher than the degree of loss of building structure, as we show in Figure 2b).
236 The interquartile range lies between 1.03 and 3.73 (median = 1.9, mean \approx 3.7), which implies that in
237 nearly three quarters of all losses, household content is more vulnerable than building structure.

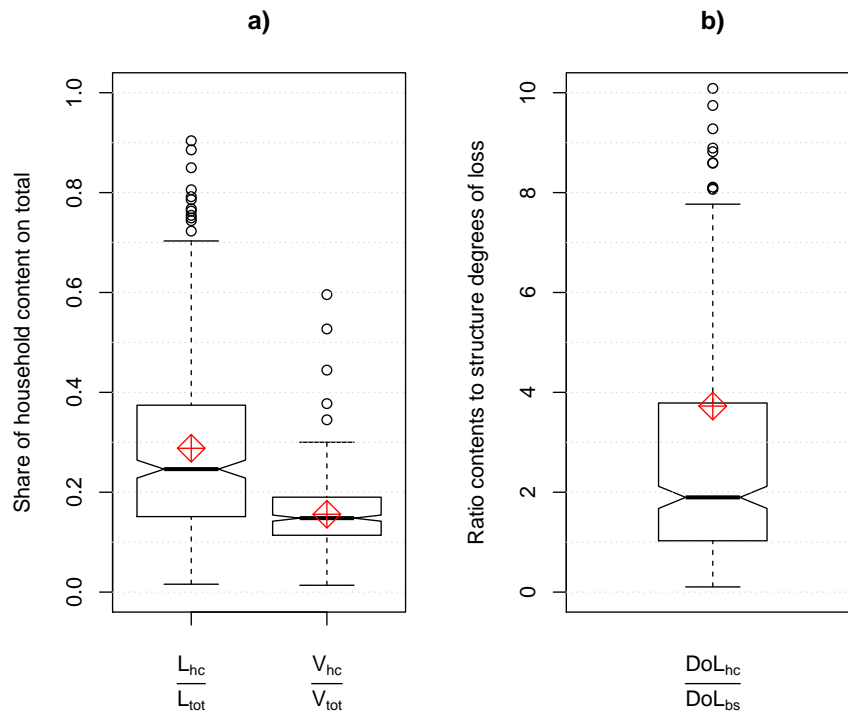


Figure 2. **a)** Left: Share of the household content loss (L_{hc}) on the total building loss (L_{tot} = structure loss + content loss). Right: Share of the insurance sum of household contents (V_{hc}) on the total insurance sum of a building (V_{tot}). **b)** Ratio of the degree of loss on household contents (DoL_{hc}) to the degree of loss on structure (DoL_{bs}) for the same building. The red diamond symbols indicate the corresponding mean values.

238 Table 1 shows the same quantities as seen in Figure 2, but instead of considering the complete
 239 data set, values are shown separately for each canton. We see that in Obwalden and Uri, contents show
 240 generally lower fractions and shares of content loss to total building loss.

Table 1. The role of household contents in five Swiss Cantons. OW: Obwalden, SZ: Schwyz, TI: Ticino, UR: Uri, VS: Valais. * Share of the summed content loss on the summed total (structure + content) loss per canton. ** Means and medians of observed shares of content loss on total loss. *** Means and medians of the observed ratios of degrees of loss of contents to degrees of loss of structure

	OW	SZ	TI	UR	VS
Share of content loss on total building loss*	0.22	0.23	0.32	0.21	0.26
Mean / median loss fraction**	0.27 / 0.22	0.31 / 0.28	0.33 / 0.28	0.25 / 0.24	0.28 / 0.24
Mean / median DoL ratio***	2.8 / 1.67	3.81 / 1.94	6.22 / 2.62	2.69 / 1.81	2.32 / 1.49

241 3.2. Model fitting

242 As mentioned in Section 2.2.1, we fitted different models to both types of loss data. Although the
 243 model fit is slightly advantageous for the TBS and the PTBS.seplam model, we define the PTBS model
 244 (regression function fitted after transformation by the same λ for both sides) as the best model, due to
 245 its better performance in terms of predictive power. Therefore, in the following two subsections, we
 246 will only present results for this specific model.

247 3.2.1. Data transformation

248 The 95 % confidence interval (CI) for λ obtained by profile maximum likelihood estimation
249 indicates a range with plausible values for λ . For degrees of loss, the method proposes to use $\lambda = 0.205$,
250 CI: (0.144, 0.265) as transformation parameter. Weisberg [36] recommends to use a rounded value
251 for λ . Because none of the suggested values $\{-1, -1/2, 0, 1/3, 1/2, 1\}$ lies within the range of our
252 confidence interval, we select the exact estimate of λ . Indeed we do not consider $y^{1/5}$, which would be
253 covered by the CI, to be more easily interpretable in terms of the original variable y than $y^{0.205}$.

254 For monetary loss, the best estimate and 95 % confidence interval of λ are 0.131 and (0.068, 0.193),
255 respectively. We use the exact value of λ for the same reasons as before.

256 3.2.2. Regression model

257 The result of the PTBS approach and the regression based on transformed degrees of loss can
258 be examined in Figure 3 a). Kendall's τ (0.556) and Spearman's ρ (0.746) suggest to reject the null
259 hypothesis of non-correlation of the degree of loss of building structure and household content. The
260 F -statistic of the model indicates significant linearity and the adjusted R^2 reaches 0.668. Here, the
261 confidence interval of the intercept parameter β_0 is $(-0.255, 0.060)$ which indicates that the regression
262 line goes roughly through the origin and the intercept parameter is not significant. A visual insight
263 into the diagnostic plots for the model based on degrees of loss is given in Figure A1 in the Appendix.
264 Based on the patternless scatter of the standardised residuals plotted against the fitted values (Figure
265 A1, top right), the standardized residuals following a normal distribution (Figure A1, top left) and
266 emphasized by the Shapiro-Wilks test (SW: p -value = 0.385), normality cannot be rejected. In addition,
267 the Breusch-Pagan test indicates that the null hypothesis of the residuals being homoscedastic cannot
268 be rejected either (BP: p -value = 0.742), which is also indicated by the scale-location plot (Figure
269 A1, bottom right) not showing severe changes in variance. The monetary loss model also meets
270 the requirements of a linear regression relatively reasonably. The model produces residuals which
271 are not significantly different from a normal distribution (SW: p -value = 0.245) and not significantly
272 heteroscedastic (BP: p -value = 0.221). Linearity is significant as well (adj. $R^2 = 0.618$, see Figure 3 c)),
273 the diagnostic plots are shown in Figure A3. Note that there is a slight pattern in residuals plotted
274 against the fitted values, indicating a minor lack of fit. Table A1 gives an overview of all parameter
275 estimates ($\hat{\beta}_0$, $\hat{\beta}_1$, $\hat{\sigma}$ and $\hat{\lambda}$), their confidence intervals (95 %-CI) and statistical measures for the resulting
276 models indicating the model quality (Shapiro-Wilks and Breusch-Pagan tests, Spearman's ρ , Kendall's
277 τ and the coefficient of determination (adj. R^2)).

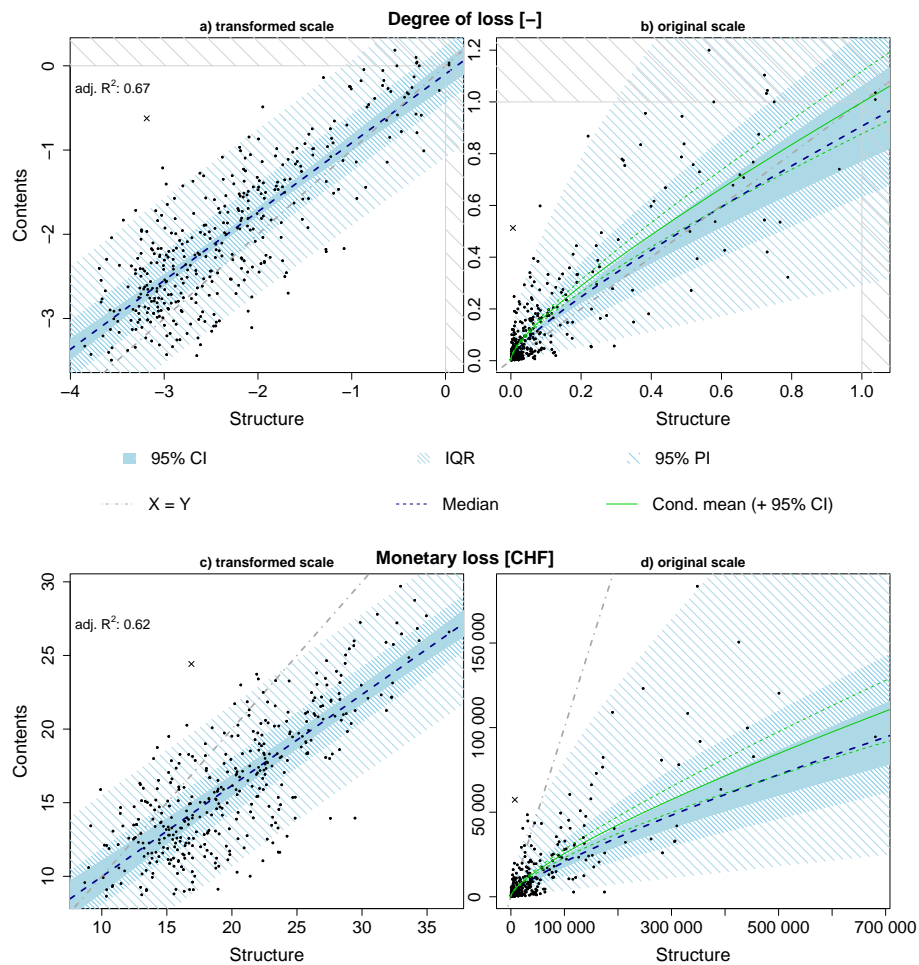


Figure 3. Loss models based on degrees of loss (a + b) and monetary loss in CHF (c + d). In plots a) + c), the models based on transformed input values are presented, whereas in b) + d) the model results are shown on the original scale after back-transformation. CI: Confidence Interval; IQR: Inter-Quartile Range; PI: Prediction Interval. Note that the mean in plots a) and c) coincides with the median. Cross symbol: Outlier excluded before model fitting.

278 After substitution of the model parameters in equation (4) and (5), respectively, the regression is
 279 not linear any more, because the back-transformation of the Box-Cox method leads to a non-linear
 280 function. Figure 3 b) and d) show the final results of the model optimization process on the original
 281 scale. In Figure 3 b), the concavity of the regression function points out that especially for objects
 282 where a low degree of loss was observed, the ratio of degree of loss of contents to the degree of loss of
 283 structure is generally higher than in cases, where high vulnerabilities were recorded. The major part of
 284 the household contents shows higher degrees of loss than the building structures.

285 The monetary loss model, which allows a direct estimation of loss on household contents based
 286 on the loss that occurred on building structure, shows that structure loss is in general considerably
 287 higher than the corresponding household content loss (see Figure 3 d). Poor predictive power is found
 288 on higher magnitudes (building structure losses > ca. 320 000 CHF). Here, the model underestimates
 289 the content loss.

290 3.3. Cross-validation

291 Figure 4 shows the metrics resulting from the leave-one-out cross-validation: i) bias, ii) relative
 292 bias, iii) mean absolute error and iv) relative absolute error. Here, results for the alternative models (TBS

293 and PTBS.seplam) are presented as well. The position of the black symbols indicates the aggregated
294 prediction error of the cross-validation, the dots along the dashed blue line indicate the standard
295 deviation of the individual prediction errors. To compare model accuracy in the same unit (CHF), the
296 predicted degrees of loss on household contents were multiplied by the insurance sum.

297 In terms of bias (Figure 4, i), we first of all see that there is a clear improvement from median to
298 mean estimation for both, the relative and absolute loss models. Second, we observe that the relative
299 loss model with median estimation performs better, whereas there is no clear "overall" pattern for
300 the mean estimates. Within the the groups (Loss.med, DoL.med, Loss.mean, DoL.mean), differences
301 in performance are rather small. Apparently, the relative loss models show lower mean absolute
302 prediction errors (Figure 4, iii). Regarding this particular metric, we can say that estimations by median
303 perform slightly better than by mean. Interestingly, the standard errors of the TBS and PTBS absolute
304 loss models and for the PTBS relative model lower mean prediction, whereas the metric itself gets
305 higher. Looking at the two relative metrics (Figure 4, ii + iv), we see that they are very similar to each
306 other. On one hand, we can observe that median prediction is in terms of these relative metrics more
307 accurate and on the other hand that the TBS and PTBS.seplam model supply roughly the same quality
308 - better than the PTBS model. Figure A5 also shows, that relative errors (Figure 4, ii + iv) are mainly
309 large for lower loss values, whereas large absolute errors (Figure 4, i, iii) rather occur in estimations of
310 high losses. This in turn is not surprising, as the loss is, relative to the loss magnitude, larger for smaller
311 losses. Hence a prediction of a small loss more easily misses the target by a few orders of magnitudes,
312 resulting in a relative prediction error of several hundred percent while its absolute prediction error in
313 CHF is still rather small compared to the larger loss values in the data. On the other hand, a small
314 percentage (relative error) of a large loss can correspond to a large amount of money (absolute error).
315 We also tested the behaviour of the Box-Cox transformation in the re-sampling process and found that
316 the estimation of λ is robust.

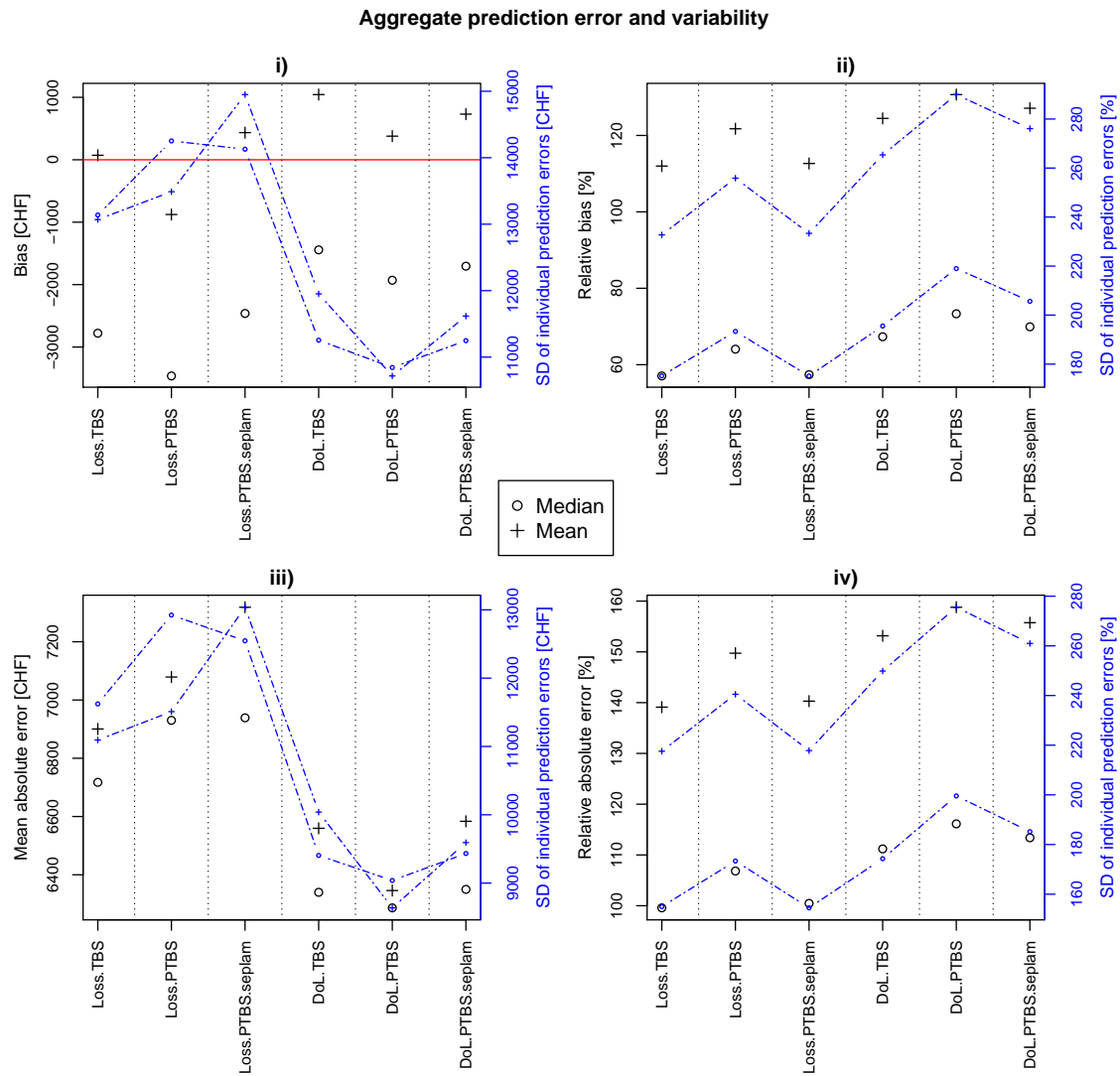


Figure 4. Cross-validation results for the model combinations based on leave-one-out cross-validation. ○: Aggregated prediction error with median prediction; +: Aggregated prediction error with mean prediction. The blue line indicates the standard deviation of the individual prediction errors; *i*): Bias [CHF]; *ii*): Relative bias [%]; *iii*): Mean absolute error [CHF]; *iv*): Relative absolute error [CHF].

317 In this study, we focus on the estimation of monetary flood losses. Therefore, we prioritize
 318 absolute to relative accuracy of the models. Therefore, in the following summary describing the major
 319 findings concerning the absolute and relative loss models, we just mention absolute bias and mean
 320 absolute error: a) The accuracy of predicting monetary loss is higher when derived by the relative loss
 321 model instead of the monetary loss model. b) The standard deviation in the error samples show that
 322 prediction variance is lower for the relative loss models which is accompanied by higher robustness. c)
 323 Although median estimation is able to compete with the mean estimation in terms of mean absolute
 324 error, it has clear disadvantages concerning bias. In the end, the fact that the PTBS model shows
 325 highest robustness and the best predictive accuracy, we selected this model to focus on and finally
 326 present in this study. We will use this model for the relative and absolute loss model although for the
 327 latter, the TBS model showed slight, for us not meaningful competitive advantages. Please also note
 328 that prioritization of relative metrics would lead to a different, but also plausible choice.

329 3.4. Transferability

330 The analysis of variance for the relative loss model on transformed scale indicates a significant
331 improvement in the overall fit for both PTBS models when separating the intercept according to
332 cantons (likelihood ratio test at 5% level) while such a separation is not significant for the TBS model.
333 However, this is not the case for the slope, meaning that there is only a shift of the regression line (on
334 transformed scale) along the vertical axis. The non-significance of the slope parameter implies that the
335 relative increase of the vulnerability of household contents to an increase of the vulnerability of the
336 building structure stays stable and is not significantly different across cantons.

337 In view of the apparently significant difference between the intercepts and thus the overall
338 magnitudes of degrees of loss for cantons, one would want to detect which cantons (or groups of
339 cantons) are most different from others. A first straightforward, but rather innocent approach would
340 be to assess the significance of all differences between pairs of intercepts by performing a *t*-test at a
341 given level for each of them. Yet we believe that properly answering this question involves so-called *a*
342 *posteriori* comparisons (Chapter 9 of Sokal and Rohlf [48]), all the more that we had no a priori guess
343 on which cantons might exhibit the largest differences before looking at the data. Performing such
344 comparisons falls into the large field of *multiple testing* or *multiple comparisons*, which roughly speaking
345 means that to reach an overall uncertainty level of α on several tests, the single sub-tests have to be
346 carried out at much smaller significance levels than α . This in turn means that less significances tend to
347 be found. We applied most approaches to this problem described in Sokal and Rohlf [48], but they did
348 not lead to coherent results. Moreover, the whole matter is complicated because the sample sizes of the
349 different cantons are not equal and their variances (still on transformed scale) seem to be significantly
350 different, whereas many multiple comparison methods do strictly speaking not apply without the
351 assumption of sample sizes and constant variances for all groups. We therefore do not present any
352 further "results" of this analysis here because they are in our opinion not sufficiently well-founded, but
353 refer to the discussion in Section 4. Interestingly, the difference in the intercept is only observed for the
354 relative and not for the absolute loss model, although both models rely on the same loss data set.

355 As our model with only one covariate is rather simple, the tendency for over-fitting as described
356 by Wenger and Olden [47] is expected to be rather small. This is indeed confirmed by the results
357 of the non-random cross-validation, which are very similar to those found with the leave-one-out
358 cross-validation (see Figure A6). Here, the models with high prediction accuracy thus also show the
359 best performance in terms of transferability.

4. Discussion

With approximately 29 %, the mean share of content loss on the total loss of residential buildings (structure + household contents) is similar to those found by Thielen *et al.* [21] (28 %) or FOWG [22] (36.5 %). Although we found comparable results in terms of the share of content loss on the total building loss, the data (monetary losses and degrees of loss) in our study were distributed over a lower range of magnitudes than in the analysis of Thielen *et al.* [21] for the Elbe and Danube floods. As mentioned in Section 3.1, regions with lower loss magnitudes showed in general a higher share of content loss on total building losses. This is emphasised by the facts, that the share on the loss is disproportionately high compared to the share of the content value to the total building value and, as seen by the linear regression in Figure 3 a) + b), the content loss to structure loss ratio is high especially for lower magnitudes. Therefore, as the loss magnitudes given by Thielen *et al.* [21] are higher, the mean share of content loss on the total building loss is rather high based on the findings in this study. Possible reasons are manifold and should be further studied, for instance different vulnerabilities of the buildings due to their type, differences of the hazard process (suspension load, dynamic or static inundation, caused by flooding of rivers in inclined topographies and inundation by a raising lake level, respectively, time of exposure, forecast accuracy of the event etc.). Preparedness may matter in this case as well: As insuring structure and contents in the regions analysed here is voluntary, contractors of insurance companies might be in general more sensitive to flood risks than others, and thus might be more resilient to such events. To our knowledge, this was not the case in the studies of Thielen *et al.* [21]. Another explanation for the differences in Thielen *et al.* [21] and FOWG [22] might be that in their studies content and structure losses need not necessarily be linked to each other. So the structure and content data sets do not have the same origin and thus, their results are not directly comparable with those of this study.

Uncertainty exists because information on the total number of flood-affected buildings and household contents is missing. This implies that we cannot make comparisons of loss frequency for building structure and household contents, respectively. Thus, we leave open the question of how probable a household content loss occurs when building structure is affected (and vice versa). Moreover we did not consider either that one building might consist of more than one household (in this study up to three). Depending on how the building is arranged, for instance with one apartment on the ground floor and two on upper floors (or vice versa), where water levels rarely rise to, content losses might get less (or more) relevant in the total building loss. Residents from upper floors storing contents on the underground floor might play a role in this context as well. We neglected those points and focused on examples where only both in combination, building structure and household content losses, occurred. In terms of total loss prediction, we point out that this is a crucial issue and that those points can make the difference between successful and failed predictions.

Furthermore, there are some methodical restrictions that have to be addressed. As we filtered the data by insurance sum, monetary loss and product type, the results are just valid for buildings with an insurance sum higher than CHF 100 000, losses above CHF 100 and with a residential purpose with maximum three apartments. Hence, attention has to be paid when comparing our results or applying the presented models to other data.

By applying the transform-both-sides (TBS) methodology after Carroll and Ruppert [35] to our data, we found a way to meet the assumptions of Gaussian linear regression models concerning homoscedasticity and normality in the distribution of the residuals. There is one minor disadvantage: Due to the challenges of the back-transformation to make inferences in the original scale, a correction factor has to be calculated to derive the estimated mean. This makes the equation more laborious than other approaches, but reproducibility is still given. Alternatively to the proposed method of our study to find a mean estimation, one could also try to fit a generalized linear model. In addition, a quantile regression approach (see Davino *et al.* [49]) could be potentially useful. So far, in vulnerability and flood loss prediction, the presented method was never used before and the benefits are shown by its reproducibility, the possibility for a systematic application in other study areas and considering the

410 prediction uncertainties. Our models indicate a high robustness of estimating λ , ensuring normality
411 and homoscedasticity for the residuals resulting from the subsequent linear regressions.

412 One objective of this study was to deduce whether the prediction of household content losses
413 performs better by a loss model based on degrees of loss, looking at the relation of loss ratio (loss /
414 insurance sum) occurring on content and structure or by a direct loss model connecting monetary loss
415 on household content with the loss on building structure. For the model based on degrees of loss, we
416 found one basic similarity as already presented by Jonkman *et al.* [17]: for the lower intensity level on
417 structure, with the increase of the degree of loss of structure, the degree of loss on household contents
418 comparatively increases following a concave function. This leads to a larger ratio of degrees of loss of
419 contents to degrees of loss of structure at low levels. This emphasises the findings mentioned above,
420 that especially for losses with low magnitudes, household contents are more vulnerable to floods than
421 building structure and here, the role of losses on household contents might be essential.

422 As a consequence of the model characteristics mentioned and as a punctuating element of this
423 statement, the regression of the monetary loss model shows a concave characteristic as well. This
424 implies that the ratio of the monetary household content losses relative to the building structure
425 losses is higher in low magnitudes compared to high ones. Although the model statistically meets
426 all demanded requirements (normality, homoscedasticity, robustness and, to some restrictions we
427 discuss afterwards, also transferability), we see in Figure 3 that for the highest structure losses, the
428 predicted content loss is underrated systematically. This could also be the reason that leads to the
429 (slight) tendency for negative bias and underestimation of the total loss we found in (non-)random
430 cross-validation. As these high values mainly occurred in the canton of Obwalden, we cannot clearly
431 say if this issue originates in methodical inadequacies or just local conditions.

432 Comparing the quality of the two PTBS models, the accuracy of the model based on degrees
433 of loss is advantageous as shown by the model fit, the absolute bias and the mean absolute error.
434 This includes tests for normality and homoscedasticity (Table A1 and Figure A1 + A3), robustness
435 (Figure 4) and transferability (Table A6, absolute errors). Concerning the analysis of variance, several
436 uncertainties remain. First of all, the application for the TBS approach turned out to be very complex
437 and there is still potential for improvement. We can clearly say that for the relative loss model based
438 on degrees of loss, a difference in the intercept parameter exists, but we cannot clearly define the
439 source that leads to the differences. With a variety of correction methods for the anova, we found
440 that only differences between a combination of three groups are significant, but not between any pair
441 of cantons. We mention that there are also uncertainties in the proceeding and methodical correct
442 utilization of the methods in detecting the relevant differences, not less because of unequal group
443 sizes and variances; see also Section 3.4. As mentioned, there is no improvement by distinguishing
444 the origin of the losses in the absolute loss model. Here, it is plausible that the higher variance and
445 the lower model fit prevents the intercept parameter from being significantly different. To conclude,
446 although uncertainties exist, we still would interpret the relative loss model as transferable, justified in
447 accordance with the intercept parameter statistically not being significant in model fitting, but we also
448 point out, that further analysis and improvements are required. In particular, we acknowledge that a
449 more in-depth statistical analysis of these uncertain aspects is not infeasible and would most likely
450 also lead to improved answers, but simply was beyond the scope of this study.

451 The random cross-validation underlines the relative loss model being more robust than the
452 monetary model, by returning lower error standard deviation and improved accuracy concerning
453 the absolute error types. In addition, we expect advantages of the relative loss model concerning
454 reliability, being independent of the value of an object. This means in detail that for the monetary loss
455 model a constant ratio of content and structure values is assumed, whereas the relative loss model
456 is independent of the variety of possible value-combinations, e.g. valuable contents being located in
457 low-priced buildings etc. The dependence of the monetary loss on the value is also shown by [21],
458 where variables describing value and size are highly relevant for monetary losses, whereas for the
459 degree of loss this effect is remarkably reduced by putting the monetary loss value in relation to the

460 monetary value of the object. We suppose that this could be the reason why variance and the model
461 fit in the relative loss model are more accurate. We point out that with degree of loss and monetary
462 loss of structure as only input variables, the relative and monetary models are able to explain 67%
463 and 62% of the variance in degrees of loss and monetary loss of contents, respectively. We explain
464 these high values with two out of three main components (flood variables and preparedness) found
465 by [21] being neutralized through our approach: As we analysed contents and structure being part
466 of the same building, the interacting flood variables are the same and thus neglectable. The same is
467 valid for preparedness: We linked contracts of contents and structure referring to the same person with
468 obviously the same preparedness.

469 5. Conclusions

470 Based on reliable data and established literature, we showed that household content loss is a
471 relevant factor in the estimation of flood losses and should be considered in future loss predictions
472 or flood risk assessments. In relation to the average total loss of a building including content and
473 structure loss, losses of household content contributes from 21% to 32% based on our data, whereas
474 contributions of up to 36 % are found in the literature. The results indicate that especially when low
475 degrees of loss or monetary losses are caused by floods, the vulnerability of contents is clearly higher
476 than the vulnerability of the corresponding building structure. Thus, assuming that generally high
477 flood intensities lead to high losses, it has to be considered that the share of household contents on the
478 total building loss is decreasing relatively in regions with comparatively high losses or degrees of loss.

479 We present two models, deduced from loss claims on residential buildings with maximum three
480 apartments, which allow to predict the degree of loss or the monetary loss for household contents
481 based only on corresponding losses on the building structure. Moreover, we tested and compared the
482 models in terms of robustness, transferability and predictive power. Both models generate appropriate
483 results with a comparative advantage of the relative over the monetary loss model. They meet the
484 statistical requirements of normally distributed residuals with constant variance which is the basis
485 for a robust model. As shown by random cross-validation, the absolute bias and standard deviation
486 is generally low for both, but lower for the relative loss model. As well, the relative loss model is
487 favourable being more transferable to new regions, as assessed by a non-random cross-validation.
488 Nevertheless, attention should be paid when applying the functions in regions where the major part of
489 degrees of loss or monetary losses is expected to scatter around the upper or lower range of our data
490 set or just a very small number of data is available. In this case, we presented a method that quantifies
491 uncertainties and supports the interpretation of the model accuracy.

492 The Box-Cox method is characterised by not insisting on a certain transformation. Instead, it
493 takes into account a multiple set of power transformations (including the log-transformation) to reach
494 normality and homoscedasticity of the residuals and suggests an appropriate λ -parameter based on
495 the quantitative and reproducible maximum likelihood method. By applying tests to the residual
496 distribution, we showed that this transformation method works well for general right-skewed loss
497 data, and meets model assumptions of a Gaussian linear regression. For both, the degree of loss and
498 monetary loss model, as the original data are strongly heteroscedastic, the uncertainties are rising with
499 increasing values of exposed assets and losses. We recommend to consider data transformation, as it is
500 providing a statistically correct estimation of the regression parameters and uncertainties.

501 **Supplementary Materials:** The Code and the data used in this paper
502 are available at <https://zenodo.org/record/1443238> or as git-repository at
503 https://bitbucket.org/MarMos90/houco_lossmodel/src/master/.

504 **Author Contributions:** Conceptualization, MM and AZ; Methodology, MM and LF; Validation and Formal
505 Analysis, LF and MM; Investigation, MM, LF and AZ; Data Curation, MM; Writing—Original Draft Preparation,
506 MM; Writing—Review & Editing, all; Visualization, MM, LF; Supervision, AZ, MK, RW

507 **Funding:** This research was funded by the Mobiliar Lab for Natural Risks.

508 **Acknowledgments:** The authors thank *Swiss Mobiliar Insurance Company* for providing the data and especially
 509 Luzius Thomi and Rouven Sturny for advice on the interpretation of the data.

510 **Conflicts of Interest:** The founding sponsors had no role in the design of the study; in the collection, analyses, or
 511 interpretation of data; in the writing of the manuscript, and in the decision to publish the results.

512 **Abbreviations**

513 The following abbreviations are used in this manuscript:

514

BP	Breusch-Pagan (test)
CI	Confidence Interval
DoL	Degree of Loss
515 PTBS	Pseudo-Transform-Both-Sides
PTBS.seplam	Pseudo-Transform-Both-Sides with separate transformation parameters λ for x and y
SW	Shapiro-Wilks (test)
TBS	Transform-Both-Sides

516 **Appendix A**

517 *Appendix A.1*

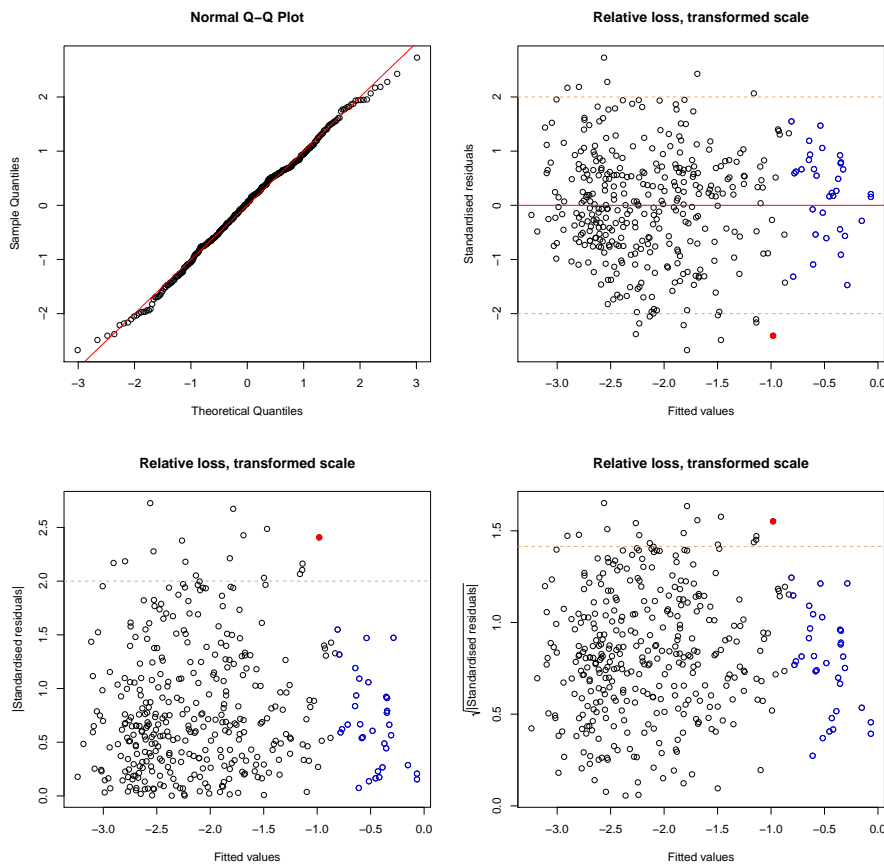


Figure A1. Diagnostic plots for the residuals (transformed degrees of loss) shown by Figure 3 a). Top left: Normal-Q-Q-plot, points along diagonal line don't reject normality (SW: normality with a p -value = 0.385). All other figures show the fitted values on X-axis against the standardised residuals on the Y-axis as normal (top right), absolute (bottom left) and the square root (bottom right) of the absolute values. Blue borders indicate high leverage points, red filled circles indicate high values for Cook's distance and the orange dashed lines indicate the borders to the definition of large residuals. Heteroscedasticity is not evident. One outlier (Bonferroni outlier test) is not shown in the plot.

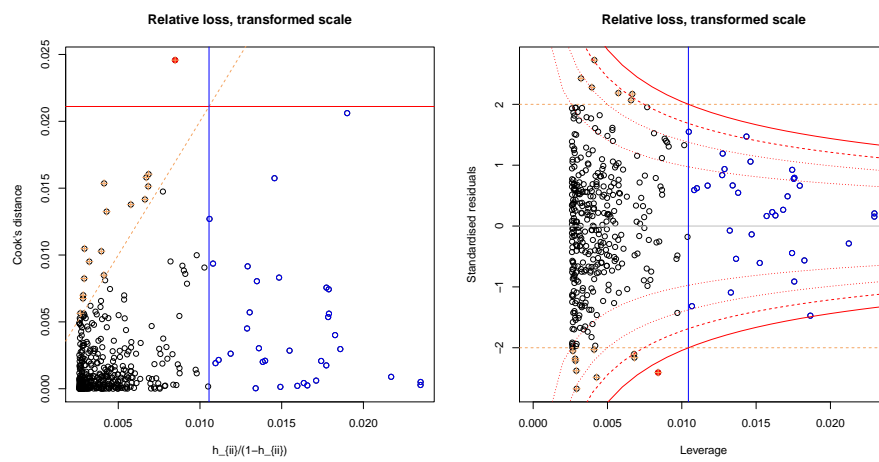
518 *Appendix A.2*

Figure A2. Leverage (X-axis) vs Cook's distance (left) and standardised residuals (right) for the relative loss model on the vertical axis. Blue borders indicate high leverage points, red filled circles indicate high values for Cook's distance and the orange dashed lines indicate the borders to the definition of large residuals. One outlier (Bonferroni outlier test) is not shown in the plot.

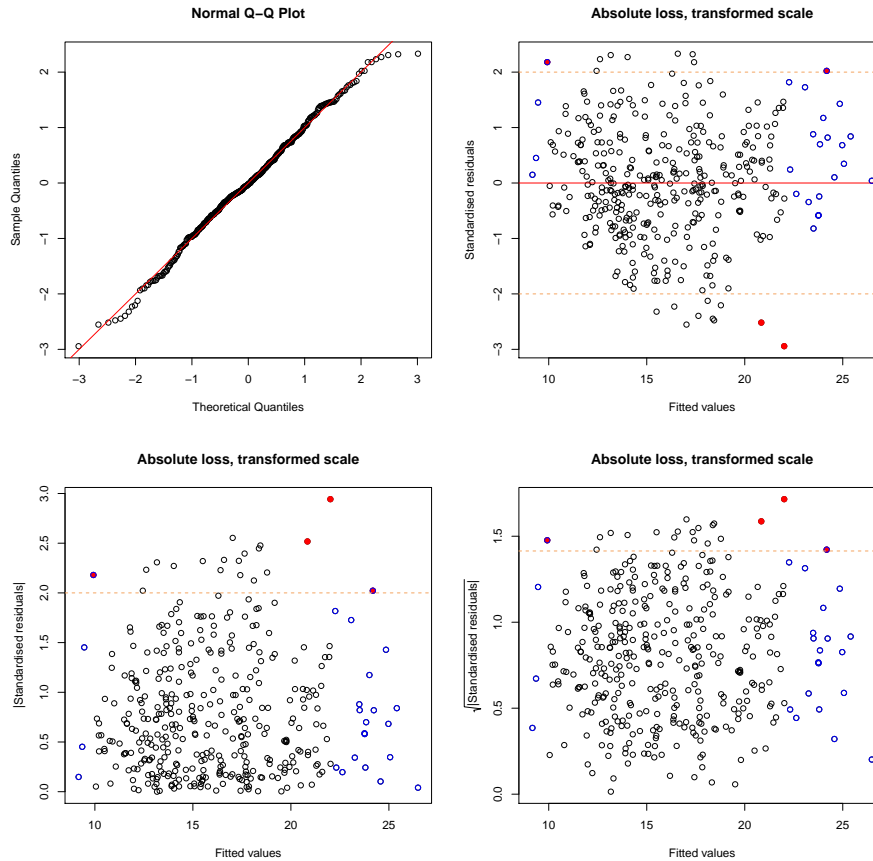
519 **Appendix B**520 *Appendix B.1*

Figure A3. Diagnostic plots for the regression showed in Figure 3 c). Top left: Normal-Q-Q-plot, points along diagonal line don't reject normality (SW: normality with a p -value = 0.245). All other figures show the fitted values on X-axis against the standardised residuals on the Y-axis as normal (top right), absolute (bottom left) and the square root (bottom right) of the absolute numbers. Blue borders indicate high leverage points, red filled circles indicate high values for Cook's distance and the orange dashed lines indicate the borders to the definition of large residuals. Heteroscedasticity is not evident. One outlier (Bonferroni outlier test) is not shown in the plot.

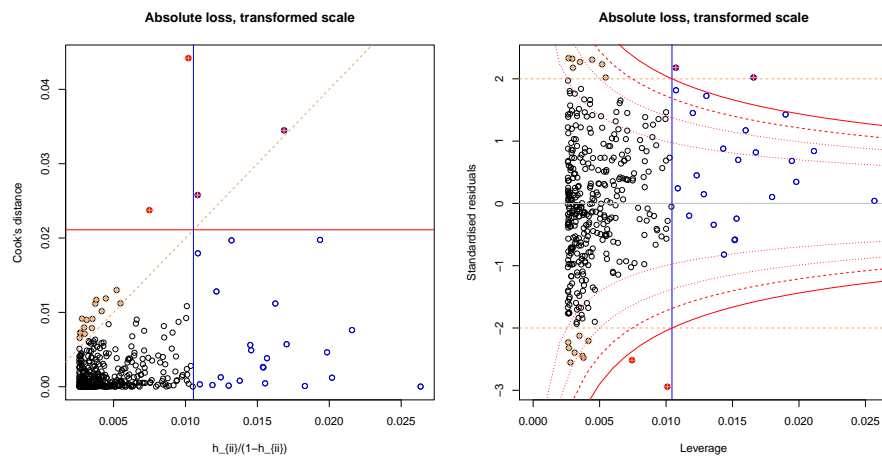
521 *Appendix B.2*

Figure A4. Leverage (X-axis) vs Cook's distance (left) and standardised residuals (right) of the relative loss model on the vertical axis. Blue borders indicate high leverage points, red filled circles indicate high values for Cook's distance and the orange dashed lines indicate the borders to the definition of large residuals. The outlier found for the relative loss model (Bonferroni outlier test) is not shown in the plot and was not used during the model fitting procedure.

522 **Appendix C**

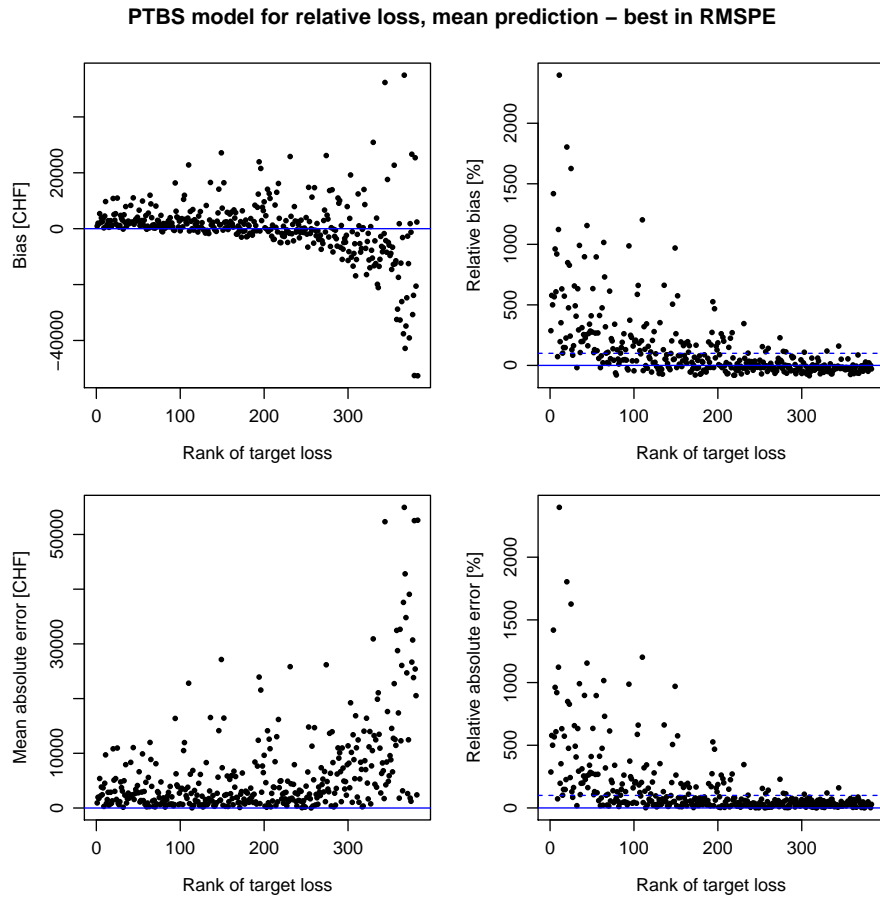


Figure A5. Dependence of single errors on ranking. Absolute errors show high variability in higher ranks of target loss (original scale), whereas relative errors are more variable in lower ranks.

523 **Appendix D**

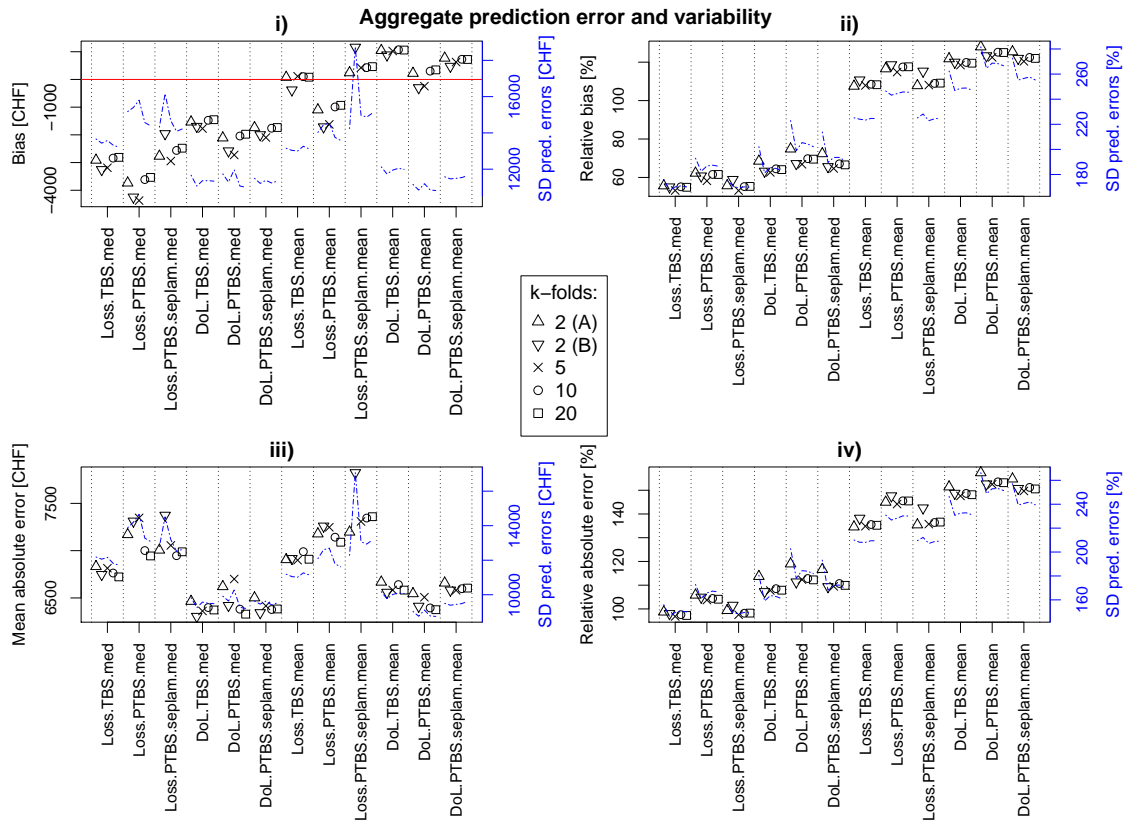


Figure A6. Non-random cross-validation. K -fold = 2, A: Obwalden + Ticino vs. Schwyz + Valais + Uri; B: Obwalden + Schwyz vs. Ticino + Valais + Uri. K -fold = 5: One group per canton. K -Fold = 10 / 20: Split Obwalden, Ticino, Schwyz and Uri into multiple groups such that all groups have approximately the same size

524 *Appendix D.1*

Table A1. Overview of the statistical evaluation and parameters of the two selected models. The estimates of β_0 , β_1 , λ and σ can be substituted in equation (4) or (5) to predict the median or mean of y , respectively. * 95 %-confidence interval

	relative loss model	monetary loss model
Spearman's ρ	0.746	0.72
Kendall's τ	0.556	0.527
λ Maximum Likelihood Estimate	0.205	0.131
$\hat{\lambda}$ CI*	(0.144, 0.265)	(0.068, 0.193)
$\hat{\sigma}$	0.495	2.745
$\hat{\beta}_0$	-0.098	3.798
β_0 CI*	(-0.255, 0.060)	(2.179, 5.416)
$\hat{\beta}_1$	0.817	0.618
β_1 CI*	(0.750, 0.884)	(0.560, 0.676)
adjusted R^2	0.668	0.618
Shapiro-Wilks p -value	0.385	0.245
Breusch-Pagan p -value	0.742	0.221

References

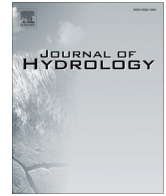
- 525 **References**
- 526 1. Badoux, A.; Andres, N.; Techel, F.; Hegg, C. Natural hazard fatalities in Switzerland from 1946 to 2015.
527 *Natural Hazards and Earth System Sciences* **2016**, *16*, 2747–2768. doi:10.5194/nhess-16-2747-2016.
- 528 2. Swiss Re. Floods in Switzerland - an underestimated risk **2012**.
- 529 3. Andres, N.; Badoux, A. Unwetterschäden in der Schweiz im Jahr 2016: Rutschungen, Murgänge,
530 Hochwasser und Sturzereignisse. *Wasser, Energie, Luft WEL* **2017**, *109*, 97–104.
- 531 4. Staffler, H.; Pollinger, R.; Zischg, A.; Mani, P. Spatial variability and potential impacts of climate change on
532 flood and debris flow hazard zone mapping and implications for risk management. *Natural Hazards and*
533 *Earth System Science* **2008**, *8*, 539–558. doi:10.5194/nhess-8-539-2008.
- 534 5. Ernst, J.; Dewals, B.J.; Detrembleur, S.; Archambeau, P.; Erpicum, S.; Piroton, M. Micro-scale flood risk
535 analysis based on detailed 2D hydraulic modelling and high resolution geographic data. *Natural Hazards*
536 **2010**, *55*, 181–209. doi:10.1007/s11069-010-9520-y.
- 537 6. Zischg, A.; Schober, S.; Sereinig, N.; Rauter, M.; Seymann, C.; Goldschmidt, F.; Bäk, R.; Schleicher, E.
538 Monitoring the temporal development of natural hazard risks as a basis indicator for climate change
539 adaptation. *Natural Hazards* **2013**, *67*, 1045–1058. doi:10.1007/s11069-011-9927-0.
- 540 7. Fuchs, S.; Keiler, M.; Zischg, A. A spatiotemporal multi-hazard exposure assessment based on property
541 data. *Natural Hazards and Earth System Science* **2015**, *15*, 2127–2142. doi:10.5194/nhess-15-2127-2015.
- 542 8. Fuchs, S.; Röthlisberger, V.; Thaler, T.; Zischg, A.; Keiler, M. Natural Hazard Management from a
543 Coevolutionary Perspective: Exposure and Policy Response in the European Alps. *Annals of the American*
544 *Association of Geographers* **2016**, pp. 1–11. doi:10.1080/24694452.2016.1235494.
- 545 9. Zischg, A.P.; Mosimann, M.; Bernet, D.B.; Röthlisberger, V. Validation of 2D flood models with insurance
546 claims. *Journal of Hydrology* **2018**, *557*, 350–361. doi:10.1016/j.jhydrol.2017.12.042.
- 547 10. Papathoma-Köhle, M.; Kappes, M.; Keiler, M.; Glade, T. Physical vulnerability assessment
548 for alpine hazards: State of the art and future needs. *Natural Hazards* **2011**, *58*, 645–680.
549 doi:10.1007/s11069-010-9632-4.
- 550 11. Fuchs, S.; Birkmann, J.; Glade, T. Vulnerability assessment in natural hazard and risk analysis: Current
551 approaches and future challenges. *Natural Hazards* **2012**, *64*, 1969–1975. doi:10.1007/s11069-012-0352-9.
- 552 12. Papathoma-Köhle, M. Vulnerability curves vs. vulnerability indicators: Application of an indicator-based
553 methodology for debris-flow hazards. *Natural Hazards and Earth System Sciences* **2016**, *16*, 1771–1790.
554 doi:10.5194/nhess-16-1771-2016.
- 555 13. Totschnig, R.; Sedlacek, W.; Fuchs, S. A quantitative vulnerability function for fluvial sediment transport.
556 *Natural Hazards* **2011**, *58*, 681–703. doi:10.1007/s11069-010-9623-5.
- 557 14. Papathoma-Köhle, M.; Zischg, A.; Fuchs, S.; Glade, T.; Keiler, M. Loss estimation for landslides in mountain
558 areas – An integrated toolbox for vulnerability assessment and damage documentation. *Environmental*
559 *Modelling & Software* **2015**, *63*, 156–169. doi:10.1016/j.envsoft.2014.10.003.
- 560 15. Hydrotec. Hochwasser-Aktionsplan Angerbach. Teil I: Berichte und Anlagen. Studie im Auftrag desStUA
561 Düsseldorf, Aachen. **2001**.
- 562 16. Dutta, D.; Herath, S.; Musiaka, K. A mathematical model for flood loss estimation. *Journal of Hydrology*
563 **2003**, *277*, 24–49. doi:10.1016/S0022-1694(03)00084-2.
- 564 17. Jonkman, S.N.; Bočkarjova, M.; Kok, M.; Bernardini, P. Integrated hydrodynamic and
565 economic modelling of flood damage in the Netherlands. *Ecological Economics* **2008**, *66*, 77–90.
566 doi:10.1016/j.ecolecon.2007.12.022.
- 567 18. FOEN. EconoMe 4.0. Wirksamkeit und Wirtschaftlichkeit von Schutzmassnahmen gegen Naturgefahren.
568 Handbuch / Dokumentation **2015**.
- 569 19. Dottori, F.; Figueiredo, R.; Martina, M.L.V.; Molinari, D.; Scorzini, A.R. INSYDE: A synthetic, probabilistic
570 flood damage model based on explicit cost analysis. *Natural Hazards and Earth System Sciences* **2016**,
571 *16*, 2577–2591. doi:10.5194/nhess-16-2577-2016.
- 572 20. Kreibich, H.; Seifert, I.; Merz, B.; Thielen, A.H. Development of FLEMOcs – a new model for the
573 estimation of flood losses in the commercial sector. *Hydrological Sciences Journal* **2010**, *55*, 1302–1314.
574 doi:10.1080/02626667.2010.529815.
- 575 21. Thielen, A.H.; Müller, M.; Kreibich, H.; Merz, B. Flood damage and influencing factors: New insights from
576 the August 2002 flood in Germany. *Water Resources Research* **2005**, *41*, 314. doi:10.1029/2005WR004177.

- 577 22. FOWG. Bericht über die Hochwasserereignisse 2005. *Federal Office for Water and Geology* **2005**.
- 578 23. PSL. Euro to Swiss Franc Spot Exchange Rates for 2005 from the Bank of England **2018**.
- 579 24. Cammerer, H.; Thielen, A.H.; Lammel, J. Adaptability and transferability of flood loss
580 functions in residential areas. *Natural Hazards and Earth System Science* **2013**, *13*, 3063–3081.
581 doi:10.5194/nhess-13-3063-2013.
- 582 25. Amadio, M.; Mysiak, J.; Carrera, L.; Koks, E. Improving flood damage assessment models in Italy. *Natural*
583 *Hazards* **2016**, *82*, 2075–2088. doi:10.1007/s11069-016-2286-0.
- 584 26. Weisberg, S. Simple Linear Regression. In *Applied Linear Regression*; John Wiley & Sons, Inc, 2005; pp. 19–46.
585 doi:10.1002/0471704091.ch2.
- 586 27. Good, P.I.; Hardin, J.W. Univariate Regression. In *Common Errors in Statistics (and How to Avoid Them)*; John
587 Wiley & Sons, Inc, 2003; pp. 127–143. doi:10.1002/0471463760.ch9.
- 588 28. Greene, W.H. *Econometric analysis*, 7th ed.; Pearson Addison Wesley: Harlow and New York, 2012.
- 589 29. Breusch, T.S.; Pagan, A.R. A Simple Test for Heteroscedasticity and Random Coefficient Variation.
590 *Econometrica* **1979**, *47*, 1287. doi:10.2307/1911963.
- 591 30. Weisberg, S. Outliers and Influence. In *Applied Linear Regression*; John Wiley & Sons, Inc, 2005; pp. 194–210.
592 doi:10.1002/0471704091.ch9.
- 593 31. Royston, J.P. An Extension of Shapiro and Wilk's W Test for Normality to Large Samples. *Applied Statistics*
594 **1982**, *31*, 115. doi:10.2307/2347973.
- 595 32. R Core Team. R: A Language and Environment for Statistical Computing, 2016.
- 596 33. Box, G.E.P.; Tidwell, P.W. Transformation of the Independent Variables. *Technometrics* **1962**, *4*, 531.
597 doi:10.2307/1266288.
- 598 34. Box, G.E.P.; Cox, D.R. An Analysis of Transformations. *Journal of the Royal Statistical Society. Series B*
599 *(Methodological)* **1964**, *26*, 211–252.
- 600 35. Carroll, R.J.; Ruppert, D. Power Transformations when Fitting Theoretical Models to Data. *Journal of the*
601 *American Statistical Association* **1984**, *79*, 321. doi:10.2307/2288271.
- 602 36. Weisberg, S. Nonlinear Regression. In *Applied Linear Regression*; John Wiley & Sons, Inc, 2005; pp. 233–250.
603 doi:10.1002/0471704091.ch11.
- 604 37. Maciejewski, R.; Pattath, A.; Ko, S.; Hafen, R.; Cleveland, W.S.; Ebert, D.S. Automated Box-Cox
605 Transformations for Improved Visual Encoding. *IEEE transactions on visualization and computer graphics*
606 **2013**, *19*, 130–140. doi:10.1109/TVCG.2012.64.
- 607 38. Ruppert, D.; Matteson, D.S. *Statistics and Data Analysis for Financial Engineering*; Springer New York: New
608 York, NY, 2015. doi:10.1007/978-1-4939-2614-5.
- 609 39. Perry, M.B.; Walker, M.L. A Prediction Interval Estimator for the Original Response When Using Box-Cox
610 Transformations. *Journal of Quality Technology* **2015**, *47*, 278–297.
- 611 40. Duan, N. Smearing Estimate: A Nonparametric Retransformation Method. *Journal of the American Statistical*
612 *Association* **1983**, *78*, 605. doi:10.2307/2288126.
- 613 41. Taylor, J.M.G. The Retransformed Mean after a Fitted Power Transformation. *Journal of the American*
614 *Statistical Association* **1986**, *81*, 114–118. doi:10.1080/01621459.1986.10478246.
- 615 42. Sakia, R.M. Retransformation bias: A look at the box-cox transformation to linear balanced mixed ANOVA
616 models. *Metrika* **1990**, *37*, 345–351. doi:10.1007/BF02613542.
- 617 43. Rothery, P. A cautionary note on data transformation: Bias in back-transformed means. *Bird Study* **1988**,
618 *35*, 219–221. doi:10.1080/00063658809476992.
- 619 44. Weisberg, S. Polynomials and Factors. In *Applied Linear Regression*; John Wiley & Sons, Inc, 2005; pp.
620 115–146. doi:10.1002/0471704091.ch6.
- 621 45. Davison, A.C.; Hinkley, D.V., Linear Regression. In *Bootstrap Methods and their Application*; Cambridge
622 Series in Statistical and Probabilistic Mathematics, Cambridge University Press, 1997; p. 256–325.
623 doi:10.1017/CBO9780511802843.007.
- 624 46. Hastie, T.; Tibshirani, R.; Friedman, J. Model Assessment and Selection. In *The Elements of Statistical*
625 *Learning*; Hastie, T.; Tibshirani, R.; Friedman, J., Eds.; Springer series in statistics, Springer New York: New
626 York, NY, 2009; pp. 219–259. doi:10.1007/978-0-387-84858-7.
- 627 47. Wenger, S.J.; Olden, J.D. Assessing transferability of ecological models: An underappreciated
628 aspect of statistical validation. *Methods in Ecology and Evolution* **2012**, *3*, 260–267.
629 doi:10.1111/j.2041-210X.2011.00170.x.

- 630 48. Sokal, R.; Rohlf, F. *Biometry; the principles and practice of statistics in biological research*; Series of books in
631 biology, W. H. Freeman, 1969.
- 632 49. Davino, C.; Furno, M.; Vistocco, D. *Quantile Regression*; John Wiley & Sons, Ltd: Oxford, 2014.
633 doi:10.1002/9781118752685.

634 © 2018 by the authors. Submitted to *Water* for possible open access publication under the terms and conditions
635 of the Creative Commons Attribution (CC BY) license (<http://creativecommons.org/licenses/by/4.0/>).

Paper 14: Zischg, A.P., Mosimann, M., Bernet, D.B., Röthlisberger, V., 2018. Validation of 2D flood models with insurance claims. *Journal of Hydrology* 557, 350–361. [10.1016/j.jhydrol.2017.12.042](https://doi.org/10.1016/j.jhydrol.2017.12.042).



Research papers

Validation of 2D flood models with insurance claims

Andreas Paul Zischg*, Markus Mosimann, Daniel Benjamin Bernet, Veronika Röthlisberger

University of Bern, Institute of Geography, Oeschger Centre for Climate Change Research, Mobiliar Lab for Natural Risks, Bern CH-3012, Switzerland



ARTICLE INFO

Article history:

Received 17 July 2017

Received in revised form 24 November 2017

Accepted 15 December 2017

Available online 19 December 2017

This manuscript was handled by Marco Borga, Editor-in-Chief, with the assistance of George Constantinescu, Associate Editor

Keywords:

2D flood model

Validation

Insurance claims

Model performance

ABSTRACT

Flood impact modelling requires reliable models for the simulation of flood processes. In recent years, flood inundation models have been remarkably improved and widely used for flood hazard simulation, flood exposure and loss analyses. In this study, we validate a 2D inundation model for the purpose of flood exposure analysis at the river reach scale. We validate the BASEMENT simulation model with insurance claims using conventional validation metrics. The flood model is established on the basis of available topographic data in a high spatial resolution for four test cases. The validation metrics were calculated with two different datasets; a dataset of event documentations reporting flooded areas and a dataset of insurance claims. The model fit relating to insurance claims is in three out of four test cases slightly lower than the model fit computed on the basis of the observed inundation areas. This comparison between two independent validation data sets suggests that validation metrics using insurance claims can be compared to conventional validation data, such as the flooded area. However, a validation on the basis of insurance claims might be more conservative in cases where model errors are more pronounced in areas with a high density of values at risk.

© 2017 Elsevier B.V. All rights reserved.

1. Introduction

Floods are one of the most damaging natural hazards, accounting for a majority of all economic losses from natural events worldwide (UNISDR 2015). Managing flood risk requires knowledge about the hazardous processes and about flood impacts. In recent years, flood inundation models have been remarkably improved and widely used for flood hazard simulation, flood exposure and flood loss analyses. A variety of models exist for different purposes and scales, reaching from global scale inundation models (Pappenberger et al. 2012, Ward et al. 2013, Sampson et al. 2015) to continental (Trigg et al. 2016), national (Merz et al. 2008) and finally regional and local scale models (Fewtrell et al. 2011, Neal et al. 2011, Pedrozo-Acuña et al. 2012, de Almeida et al., 2016, Garrote et al. 2016). Another increasing use of flood inundation models is the coupling of flood models with hydrologic and hydrometeorologic models within a model cascade or a coupled component modelling framework at the river basin scale (e.g., Biancamaria et al. 2009, Falter et al. 2015, Zhu et al. 2016, Felder et al. 2017). Thus, a variety of inundation models exist for different purposes (e.g., Horritt and Bates 2001a, Hunter et al. 2007, Chatterjee et al. 2008, Bates et al. 2010, Crispino et al. 2015, Courty et al. 2017). Developers are validating the models with a

broad set of validation techniques and data. Model validation here is defined after Hunter et al. (2007) as the “process of demonstrating that a given site-specific model is capable of making accurate predictions, defined with respect to the application in mind, for periods outside a calibration period”. If the accuracy and predictive capability in the validation period is proven to lie within an acceptable limit for a particular practical purpose, it is defined as being validated. Depending on the purpose of the model used and the available data, the validation methods vary remarkably. In 1D simulation frameworks, hydraulic models have been calibrated and validated with observed water levels at specific locations (Horritt and Bates 2002, Mark et al. 2004, Pappenberger et al. 2005, Hunter et al. 2007, Felder et al. 2017). However, with the development of 2D flood inundation models, spatially explicit model performance measures have been proposed and used for model validation. In many cases this is done by comparing the simulated inundation areas with observed ones as shown by Woodhead et al. (2007). Most likely, the main data used in the validation of inundation models is observation data of the wet/dry boundary. This leads to the comparison between modelled and observed inundation areas. Other validation data are aerial images and observed flood maps delineated thereof or satellite-based remote sensing data. Bates et al. (1997) describe a procedure for validating inundation models with remote sensing data. Especially synthetic aperture radar data have recently been used for calibration and validation (Horritt 2000, Horritt et al. 2007, Mason and Bates, 2009,

* Corresponding author.

E-mail address: andreas.zischg@giub.unibe.ch (A.P. Zischg).

Pappenberger et al., 2007, Tarpanelli et al. 2013). In contrast, Neal et al. (2009) and Savage et al. (2016) compared inundation models with a large set of water level measurements in a study area. This is probably the most reliable validation data (Segura-Beltrán et al. 2016). Furthermore, inundation models are also validated against stage-discharge relationships or time to peak (Horritt and Bates 2002). The latter is less often used if the main purpose of the inundation model is to provide the basis for flood loss analyses. For evaluating newly developed models, a benchmark test against established models or models that represent an industry standard is sometimes done (Neal et al., 2012a). The comparison of the flooded areas computed by different models is shown in several studies (Horritt and Bates 2001a, 2002, Tayefi et al. 2007, Chatterjee et al. 2008, Fewtrell et al. 2008, Castellarin et al. 2009, Neal et al., 2012a,b, Crispino et al. 2015, Trigg et al. 2016, Vozinaki et al. 2016, Lavoie and Mahdi, 2017). However, the main limiting factor for validating inundation models is often the lack of validation data (Neal et al., 2012a).

Beside model validation, the analyses of uncertainties or the sensitivities against model parameters are a fundamental step in model development (Pappenberger et al. 2006, Jakeman et al. 2006, Ratto et al. 2012, Freer et al. 2013, Pianosi et al. 2016, Teng et al. 2017). In sensitivity analysis, one focus is on the representation of the topography, especially the spatial resolution (Horritt and Bates 2001b, Cook and Merwade 2009, Dottori et al. 2013, Savage et al. 2015, 2016). Probabilistic models are able to incorporate a number of model runs with different parameterizations and different boundary conditions. Dottori et al. (2013) state that deterministic models and very high spatial resolution are potentially misleading as they could induce overconfidence derived from their spuriously precise results. This in turn may lead to wrong decisions in flood risk management. Thus, the choice of the modelling strategy depends on the main purpose of the study, the model complexity, the needed computational resources, and the available topographic data (Di Baldassarre et al., 2010, Dottori et al. 2013, Jonkman 2013, Refsgaard et al. 2016). A key point in the reliability of flood inundation models is the ability to represent flood protection measures (Merwade et al. 2008b, Neal et al. 2012b, Ward et al. 2013). On the reach scale, the inability to accurately represent river morphology is a disadvantage of raster based models. The increase in spatial resolution has a negative effect on the needed computing resources (Neal et al. 2012b, Savage et al. 2015). Solutions for dealing with this trade-off between spatial resolution and computing power are, for example, the use of subgrid approaches (i.e., modelling the flow in the river channel in 1D combined with floodplain routing in 2D) as exemplarily described by Neal et al. (2012b), the coupling of 1D and 2D simulation models (Vozinaki et al. 2016), or the use of nesting approaches as shown by Bermúdez et al. (2017). The latter nested a local scale flood inundation model based on irregular meshes into a basin scale model based on regular grids. A third group of models dealing with this topic is the simulation based on irregular meshes. These can have a high spatial resolution in the river channel and a coarser resolution in the floodplain (Horritt and Bates 2001a). Thus, these models are able to accurately represent river morphology and geometry. This includes the consideration of flood protection measures which is required for predicting flood patterns satisfyingly (Fewtrell et al. 2011). Consequently, the accurate consideration of flood protection measures must also be valid from the viewpoint of flood loss analyses as they increasingly consider single buildings (Zischg et al. 2013, Fuchs et al. 2015, Röthlisberger et al. 2017). However, 2D inundation models are often evaluated regarding the ability to accurately predicting flooded areas. In many cases, the flooded areas predicted by the model are compared with the observed wet areas of a specific flood event. However, such observations may not be an adequate validation dataset in all cases.

Especially for flood exposure and flood risk analyses, a model exhibiting a good overall fit regarding inundated areas in a large floodplain may not necessarily produce good results at locations of particular interest for risk assessment (Pappenberger et al. 2007b). Nevertheless, a method for validating 2D inundation models explicitly used for flood exposure and flood loss analyses has not been presented yet.

Therefore, the main aim of this study is to close this gap by developing a method for validating 2D flood inundation models used in flood exposure analyses. For that matter, the validation data and metrics need to be adapted to that particular purpose. Therefore, we propose alternative data for validating the model, i.e., a dataset of geo-localized insurance claims. Herein, the main question concerns the value of validating a 2D flood model on the basis of loss data rather than on the basis of inundated areas. This question is posed under the hypothesis that a validation based on insurance claims gives different weighting to urbanized areas in comparison to areas without values at risk. An additional question is, how the various validation metrics differ between each other when adopted to insurance claims.

The paper is structured as follows: in the methods chapter we first describe the study areas and the method for setting up the flood model. Following, we present the parameters and the boundary conditions for the model runs. Thereafter, we introduce the validation method and the data used. The results focus on both the performance of the model and the proposed validation method. In the discussions and conclusions, the results are discussed, and recommendations for using insurance claims in the validation of flood models are given.

2. Methods

We tested the validation approach on the basis of test cases for which insurance claims were available. All cases represent a complex flood topology with combined riverine and lake flooding. Two test cases have branching river morphologies. The validation is done by a full set of insurance claims in two test cases and by a sample set of claims in the other two test cases. We compare different metrics for validation of models that are based on binary validation data.

2.1. Study area

The four test cases are located in pre-Alpine areas of Switzerland (Fig. 1). The first two test cases are located in the Canton of Nidwalden. The western test case in the municipality of Stansstad is characterized by the Giesslibach torrent, the eastern part of Buochs and Ennetbürgen by the main river crossing the Canton of Nidwalden, the Engelberger Aa. Both river systems contribute to Lake Lucerne, which is a determining factor for flood risk in both study areas as well. Thus, the flooding is also influenced by lake flooding. The third test case is the floodplain in the city of Thun in the Canton of Bern. Here, the main process is lake flooding with combined riverine flooding downstream. The outflow of Lake Thun is the Aare River flowing through the city of Thun. The Aare River has two branches. During low flow conditions, the lake level is regulated by a weir. The fourth case is the floodplain of the city of Interlaken. This floodplain is a quaternary debris cone of the river Lütchine. The city is located between Lake Brienz (upstream) and Lake Thun (downstream). The Aare River connects the two lakes and is also regulated by two weirs during low flow conditions. Thus, this floodplain is affected by combined riverine and lake flooding. Fig. 1 shows the location of the study areas.

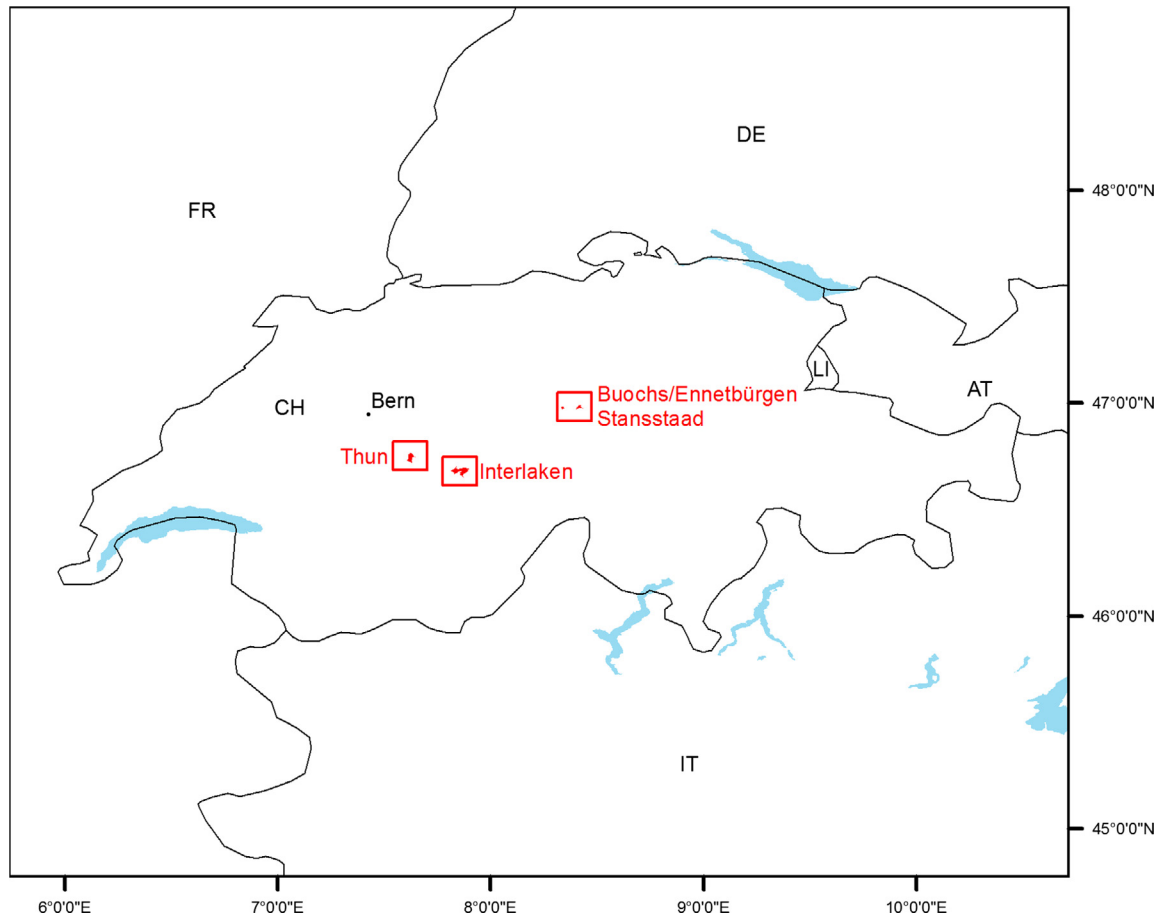


Fig. 1. Location of the four study areas.

2.2. Set up of the flood model

Flood loss analyses usually consist of flood scenarios around and above a river's discharge capacity. Consequently, the river's geometry has to be represented as accurately as possible. The river reaches of our case studies have lateral dams. Thus, the flood model has to represent not only the correct area for calculating the river carrying capacity but also the correct geometry. This means that the different heights of the left and right dams should be considered in the flood model. In our research, we are using the 2D inundation model (BASEMENT v2.6) because it is based on flexible irregular meshes and, thus, it allows to represent the river bed in a higher spatial resolution than the floodplains. BASEMENT stands for "Basic Simulation Environment". The model is developed and maintained by the Laboratory of Hydraulics, Hydrology and Glaciology (VAW) of the ETH Zurich. BASEMENT is described in detail by Vetsch et al. (2017) and has been validated analytically. It has been used for dam breach simulations (Vonwiller and Vetsch, 2015; Worni et al., 2012; Volz et al. 2012), in river restoration projects (Berchtold et al. 2012, Fah et al., 2007a,b, Bertoldi et al., 2014), and for the simulation of flash floods (Radice et al., 0000). The model is freely available and is widely used by consultants for flood risk analyses.

The first step in setting up the inundation model is the generation of the computational mesh. Within a predefined delimitation of the study area, we mapped the upper and lower shorelines of the river reaches and lakes. In the floodplains, only the most important hydraulic structures were represented by break lines. The triangulation was done with the TRIANGLE mesh generator

of Shewchuck (2002). This step is part of the pre-processing plug-in implemented in QGIS (BASEmesh, Vetsch et al. 2017). After generating the mesh, we directly attributed the z-coordinates to the nodes by using the local cell values of the digital terrain models. For the test sites in the Canton of Nidwalden we used the digital elevation model SwissALTI^{3D}, produced by the Federal Office of Topography (SWISSTOPO, 2017a). This terrain model is available for the whole of Switzerland and has a grid resolution of 2 m. The vertical accuracy is expected to be around ± 0.5 m. For the other study areas, we used a purely Lidar-derived digital elevation model provided by the Canton of Bern (KAWA 2015). This model has a grid resolution of 0.5 m and a vertical accuracy of ± 0.2 m. For the interpolation of the riverbed, we used surveyed cross sections with a mean distance of 100 m, provided by the Federal Office of Environment (FOEN, 2017a). We interpolated the riverbed levels between the cross sections by adapting the approaches proposed by Merwade et al. (2008a), Conner and Tonina (2014), and Costabile and Macchione (2015). The points of the cross sections were connected with 3D-polylines and the grid cells in between the cross sections were interpolated on the basis of the mean slope between the cross sections. Finally, we checked if the interpolated grid cells of the riverbed lay below the water surface measured by the Lidar. The terrain model of the riverbed was merged with the terrain model of the floodplain. The bottom of the lake was set to the minimum z-level of the connected river cells. From the merged digital terrain model, we computed a focal statistics raster of the maximum and minimum values within a 3×3 raster cell environment. The merged terrain model was the basis for attributing the z-values to the nodes of the mesh, except for the nodes located on an

upper shoreline of the river or a lake and the nodes located within the river channel. The z-values of the nodes representing the upper shorelines were attributed from the maximum focal statistics raster. The nodes within a river channel have been attributed with the z-values of the minimum raster. This leads to a smoothing of the river channel geometry and to a better representation of the river bank, and respectively the lake shorelines. The riverbed morphology is relatively simple since it is in all cases a totally anthropogenically modified river channel with approximately a trapezoidal form. Thus, we do not expect relevant problems arising from the effects of bathymetry interpolation on hydrodynamic results as shown by [Conner and Tonina \(2014\)](#). The roughness parameters (Manning/Strickler values) were delineated from the official guidelines of [BWG \(2001\)](#). We did not calibrate these parameters and no field investigations were made or retrospectively considered in this model setup. The weirs were considered as hydraulic obstacles in the river channel given by their geometries. The mesh has a maximum triangle area of 20 m² for river channel elements (50 m² in the case studies of Thun and Interlaken) and 100 m² for all other elements (1000 m² in case studies of Thun and Interlaken). The case studies of Thun and Interlaken have a coarser spatial resolution because these models are implemented in a model chain for the whole basin of the Aare River upstream of Bern (3000 km²) and thus are more focused on simulations at the river basin scale ([Zischg et al. 2016](#)). An extract of the mesh from the Buochs/Ennetbürgen case study is shown in [Fig. 2](#).

For the upper boundary conditions of the validation runs we used the hydrographs measured during the reference flood event in August 2005. The hydrographs of the lake levels of Lake Lucerne, Lake Thun and Lake Brienz, and the hydrographs of the rivers Engelberger Aa at Buochs and Lüttschine at Gsteig were delivered

by the Federal Office for Environment FOEN with a temporal resolution of 1 h ([FOEN, 2017b](#)). In the Lüttschine River, a dam breach occurred abruptly in the early morning of the 23rd of August 2005. We assumed that not considering the dam breach would lead to unrepresentative results. Thus, the breach of the left lateral dam of the Lüttschine River was considered by using two models with the same mesh structure but slightly different Z-values where the dam broke, as similarly shown by [Vorogushyn et al. \(2010\)](#). The first model with the intact dike at the Lüttschine River ran until the 23rd of August at 03:00 AM. Water surface elevations and flow velocities were conserved and used as a inputs for the second model with the considered dike breach, in addition with the continuative hydrograph. In contrast, the dike breach in the Engelberger Aa (case study Buochs/Ennetbürgen) is part of a flood corridor and, thus, a spillway. This situation is considered in the model by the dimension of the spillway after the overflow throughout the whole simulation.

2.3. Model validation with insurance claims

In all four case studies, a flood event occurred from the 22nd to 26th of August 2005. Depending on the site, the return period of this flood event was estimated by public authorities to be around 100–200 years. We used this flood event for the validation of the inundation model.

2.3.1. Validation data

If available, georeferenced data about flood-affected buildings and associated losses provide a validation dataset that is best suited for describing the performance of inundation models used for the analyses of exposure and flood losses at the level of the single

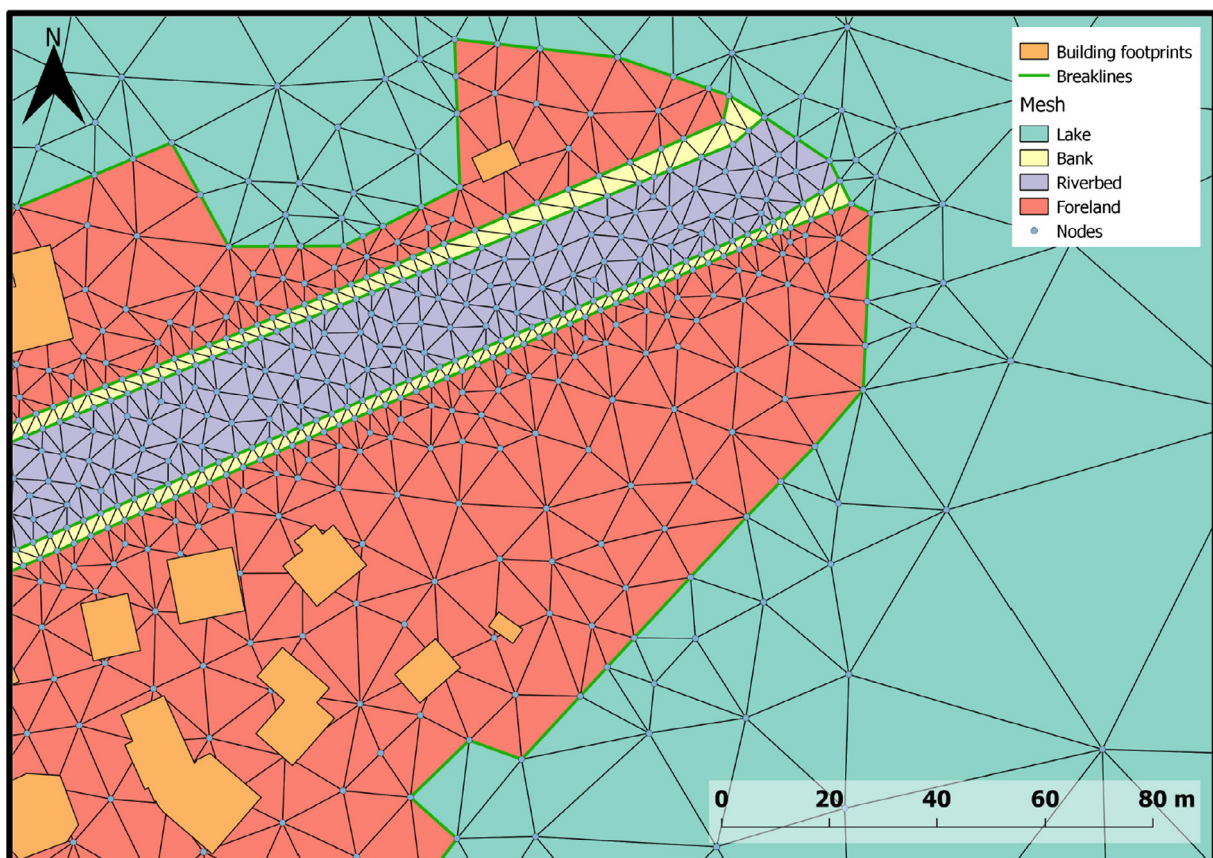


Fig. 2. Extract from the computation mesh in the Buochs/Ennetbürgen study area.

buildings. If insured, flood losses are being paid out by the insurance company to policyholders affected by a flood event. Due to direct financial interests, the claims are checked by experts and thus an overestimation of the number of cases is not expected. Losses that are smaller than a minimum threshold of reimbursements are not paid out but are still documented in the claims (franchise of 200 Swiss Francs in Nidwalden for residential buildings and 500–3000 Swiss Francs for industrial buildings). In a monopoly situation with a mandatory insurance for all house owners, a situation found in most Swiss cantons, the number of claims is very close to the number of affected buildings. Thus, for a settlement affected by a flood, it can be expected that a relevant number of insurance claims should be recorded. The claim records report the date and the amount of damage, as well as the type and address of the affected building. The address can be used for geocoding and, thereby, to localize the losses (Bernet et al. 2017). This results in a point dataset of geo-localized flood losses. The points can then be used to represent hits and non-hits. In a monopoly situation the “non-hits” are also known when the total dataset of insured values is made available by the insurance company. Together, the data provide binary information about which buildings were affected by a flood, and which ones were not, respectively. The access to these datasets is generally heavily restricted due to privacy regulations and due to commercial sensitivities in the case of free markets. In the Canton of Nidwalden, the insurance against natural hazards is mandatory. In this case, the public insurance company delivered anonymized insurance claims of the flood event in 2005 and the anonymized total stock of insured values (as valid per 01 January 2014). The damage data from the Public Insurance Company for Buildings (PICB) of Nidwalden were pre-processed as described in Bernet et al. (2017). During the flood event in August 2005 (period of 21st to 31st), the PICB received 1238 damage claims in the Canton of Nidwalden. Therefrom, only 26 claims do not include precise coordinates at the building level. 155 claims were rejected, or are still pending. These cases were not considered in the analysis. 206 data points are located within the study area of Stansstad, and 326 within Buochs and Ennetbürgen. Additionally, 95.1% of more than 1300 portfolio entries (Stansstad more than 450, Buochs and Ennetbürgen more than 800) within the study areas contain reliably localized data.

The buildings within the Canton of Bern are also insured by a PICB. In contrast, their data were not delivered due to privacy restrictions. Thus, the validation in the study areas of Thun and Interlaken has been done with data from the cooperative insurance company “Swiss Mobiliar”. These data contain anonymized claim records of building content and business inventory (excluding vehicles), as opposed to damages to buildings in the two case studies in the Canton of Nidwalden. This dataset, as well as the provided anonymized portfolio as per 31 December 2014, does not cover all buildings since the market for content and business inventory in the Canton of Bern is open to all private insurance companies. Thus, for the two case studies in the Canton of Bern, we cannot validate the inundation model with the basic population but only with a sample dataset. 311 damage claims are located in the study area of Thun, and 470 claims are located in the study area of Interlaken. In this study area, only the claims that could be localized at the building level were used for validation, i.e., 147 damage claims were not considered in the analysis because of an uncertain geo-localization.

One problem in attributing the exposure to floods and flow depths to vulnerable objects on a local scale is the spatial representation of the objects. An object represented by a point is probably less exposed than the same object represented by a polygon (e.g., building footprint, Röthlisberger et al. 2017). Thus, the point information from the insurance companies might not adequately represent the location of the building, especially in regards to the

exposition of floods near the outlines of the inundation area. Therefore, we aggregated the pointwise damage and portfolio information to the building footprints of the SwissTLM^{3D}, provided by the Federal Office of Topography (SWISSTOPO, 2017b). Because the portfolio data are valid from 01 January 2014, to 31 December 2014 and the flood event occurred in August 2005, a dissent in the datasets has to be assumed. For this issue, the precise dataset “Buildings and Dwellings statistic” (FSO 2014) from the Federal Statistical Office containing information about the period of construction was intersected with the building footprints as described by Fuchs et al. (2017) and Röthlisberger et al. (2016, 2017). By means of the known period of construction, buildings built after 2005 can be detected and dismissed. However, the construction period is available only for residential buildings. We assume that this removal of the buildings constructed after 2005 from all buildings better represents the situation at the time of the flood event.

In the case of Nidwalden, detailed information about the functionality of all buildings in the study area is given. 28.1% of all buildings defined as “minor constructions and auxiliary buildings” do not overlay a building footprint polygon and 95.2% of all such auxiliary buildings within the mapped flood event perimeter are themselves not documented as affected, whereas 77.6% show at least one entry with the same address but being exposed to the flood in contrary. In practice, the insurance company of the Canton of Nidwalden cumulates the information about losses for multiple buildings (including minor constructions and auxiliary buildings such as garages) from one owner to the home address of the owner. The obvious errors due to this practice are considered by deleting these footprints, as well as building footprint polygons not including any portfolio point. The information about the building purpose allows us to distinguish between residential and non-residential units. In Thun and Interlaken, where such information from the insurance company is lacking, the Buildings and Dwellings statistic is used for this differentiation. In the study areas of Nidwalden 17.8% of the exploitation information (residential or non-residential) provided by the insurance company is not consistent with the information from the Buildings and Dwellings statistics. Reasons can be found, for instance, in mixed usage within the same building or merged footprint polygons, due to spatial proximity.

The validation based on insurance claims was compared with a conventional validation approach. Namely, we used a second validation dataset, i.e., event documentations of the Cantons of Nidwalden and Bern. These datasets delimit the flooded areas of the flood event in August 2005 and are independent from the insurance claims.

2.3.2. Validation metric

The processed insurance data can be used to validate the model performance of the presented inundation models by adopting different metrics that allow for a spatially explicit application. The most used metrics to compare real and modelled values are i) the model fit measure, also named as the thread score, respectively the F statistics or the critical success index CSI (Bates and deRoo, 2000; Horritt and Bates 2002; Tayefi et al., 2007, see Eq. (1)), and ii) the flood area index FAI (Falter et al., 2013). Hereafter, we use the term “model fit” for the first metric. Other metrics that can be used on these data are accuracy statistics (Eq. (2)), the bias score (eq. 3), the probability of detection (Eq. (4)) or hit rate, the false alarm ratio (Eq. (5)), the probability of false detection or false alarm rate (Eq. (6)), and the success index (Eq. (7)). For a detailed description we refer to Bennett et al. (2013). We will compare the model fit with the other validation measures, with a focus on the comparison between the model fit and the FAI (Eq. (8)). Both metrics are based on the same equation but on different validation datasets. In our case, the model fit is calculated on the basis of specific points

in space, whereas the FAI is computed on the basis of areas. Before quantitatively analysing the model performance, a visual performance analysis is done.

The model prediction in terms of the number of exposed building footprint polygons are compared with the observed number of exposed polygons. A building is defined as exposed if its footprint intersects with a mesh element consisting of at least one node with a flow depth greater than 0 m. If the building is correctly predicted as inundated, it counts as a hit. Buildings predicted as dry by the model and observed as inundated, are counted as misses. Correct negatives are buildings that are predicted as dry by the model and are observed as dry in the insurance claims. Buildings predicted as wet by the model but observed as dry in the insurance claims are defined as false alarms.

$$F = \frac{\text{Num}(S_{\text{mod}} \cap S_{\text{obs}})}{\text{Num}(S_{\text{mod}} \cup S_{\text{obs}})} \quad (1)$$

S_{mod} is the set of buildings predicted as flooded, and S_{obs} is the set of buildings flooded. Num() denotes the number of members of the set. The following metrics are used for comparison with the model fit (Bennett et al., 2013).

$$\text{Accuracy} = \frac{\text{hits} + \text{correct negatives}}{\text{total}} \quad (2)$$

$$\text{Bias score} = \frac{\text{hits} + \text{false alarms}}{\text{hits} + \text{misses}} \quad (3)$$

$$\text{Probability of detection (hit rate)} = \frac{\text{hits}}{\text{hits} + \text{misses}} \quad (4)$$

$$\text{False alarm ratio} = \frac{\text{false alarms}}{\text{hits} + \text{false alarms}} \quad (5)$$

$$\begin{aligned} \text{Probability of false detection (false alarm rate)} \\ = \frac{\text{false alarms}}{\text{correct negatives} + \text{false alarms}} \end{aligned} \quad (6)$$

$$\text{Success index} = \frac{1}{2} \left(\frac{\text{hits}}{\text{hits} + \text{misses}} + \frac{\text{correct negatives}}{\text{correct negatives} + \text{false alarms}} \right) \quad (7)$$

$$\text{FAI} = \frac{\text{M1D1}}{\text{M1D1} + \text{M1D0} + \text{MOD1}} \quad (8)$$

In this equation, M1D1 is the area simulated as flooded and observed as wet, M1D0 is the predicted flooded area but observed as dry in the observation, and MOD1 is the predicted dry area but observed as wet.

3. Results and discussion

In this chapter, the results from the model validation are presented and discussed focussing on the model performance and on the validation metrics. The absolute values used for calculating the validation metrics are shown in Table 1. The values needed for calculating the FAI are shown in Table 2. The values of the

validation metrics are shown in Table 3. Regarding the model fit measure (Eq. (1)) including all types of buildings (see Table 3), only the simulation of Stansstad shows a satisfactory value above 0.7 which is commonly used as a threshold for good performance. In relation to insurance claims, the model runs have a model fit of 0.66 in Buochs/Ennetbürgen, 0.74 in Stansstad, 0.56 in Thun, and 0.47 in Interlaken. Only considering residential buildings which were constructed before the time of the flood event (values in brackets), the model fit measure is considerably higher for Buochs/Ennetbürgen and Stansstad, whereas this is not the case in Thun or Interlaken. This behaviour can be seen for every validation metric, out of the already mentioned model fit measure (Eq. (1)), the bias score (Eq. (3)), the hit rate (Eq. (4)) and the false alarm ratio (Eq. (5)) in the case of Thun. From now on, only results corresponding to all types of buildings are discussed. A difference in the values of the model fit measure can be found between the case studies with a complete damage and portfolio dataset in Nidwalden ($F = 0.66$ and 0.74 , respectively) and the two case studies in the Canton of Bern, where only a sample dataset was provided ($F = 0.56$ and 0.47 , respectively). It is still an open question whether this influences the validation results, and has to be addressed in the future. The highest accuracy value (Eq. (2)) can be found in Thun, where more than 90% of all buildings were predicted correctly with regard to hits (observed and modelled) and correct negatives (not observed and not modelled). In all other study areas, this value ranges from 77 to 79%.

The bias scores (Eq. (3)) show, that in Buochs/Ennetbürgen, Stansstad and Thun “false alarms” compared to “misses” are over-represented, leading to a bias score greater than 1. In these cases, the flood model showed a tendency to overestimate the number of exposed buildings. In Interlaken this relation is inverted and the bias score is below 1. The high amount of misses also influences the hit rate (Eq. (4)). In Interlaken, in comparison to the other model runs this value is low as well.

In Thun and Interlaken, 33–34% of all modelled events are false alarms (Eq. (5), false alarm ratio), which is more than 10% higher than in all other model regions. In the model region of Stansstad, more than half of all buildings not being observed as exposed to the flood were modelled as exposed (eq. 6, false alarm rate). In Buochs/Ennetbürgen, this is applicable for 24%, in Interlaken for 13% and in Thun for 7%. The metric shown in equation 7 equally weights the ability of the model to correctly detect occurrences and non-occurrences (Bennet et al. 2013). The model run of Stansstad shows the lowest values.

The ratio between the modelled area intersecting the observed area and the union of both (Eq. (8), flood area index) is showing the highest scores for Buochs/Ennetbürgen. Depending on whether the modelled river area is included and assumed as an M1D1 area (“hit”), this value again gets even higher (values in brackets, Table 3). Particularly in Thun, the flood area index is enhanced more than 10%. The corresponding maps are shown in Figs. 3–5.

In all case studies, differences between the modelled floods and the documented inundation areas can be observed. In the case of Buochs/Ennetbürgen, the model run resulted in an underestimation of the inundated area in the northern part of the study area (Fig. 3, left). This can be explained by the fact that a small tributary was neglected, which, according to the event documentation, lead

Table 1

Absolute values used for calculating the validation metrics of the four test cases (number of buildings). Values in brackets show metrics only considering residential buildings.

value	Buochs/Ennetbürgen	Stansstad	Thun	Interlaken
Hits	227 (198)	164 (144)	137 (111)	162 (137)
Misses	55 (45)	16 (12)	37 (30)	105 (87)
Correct negatives	194 (154)	35 (27)	975 (890)	528 (441)
False alarms	60 (36)	42 (29)	72 (59)	79 (65)

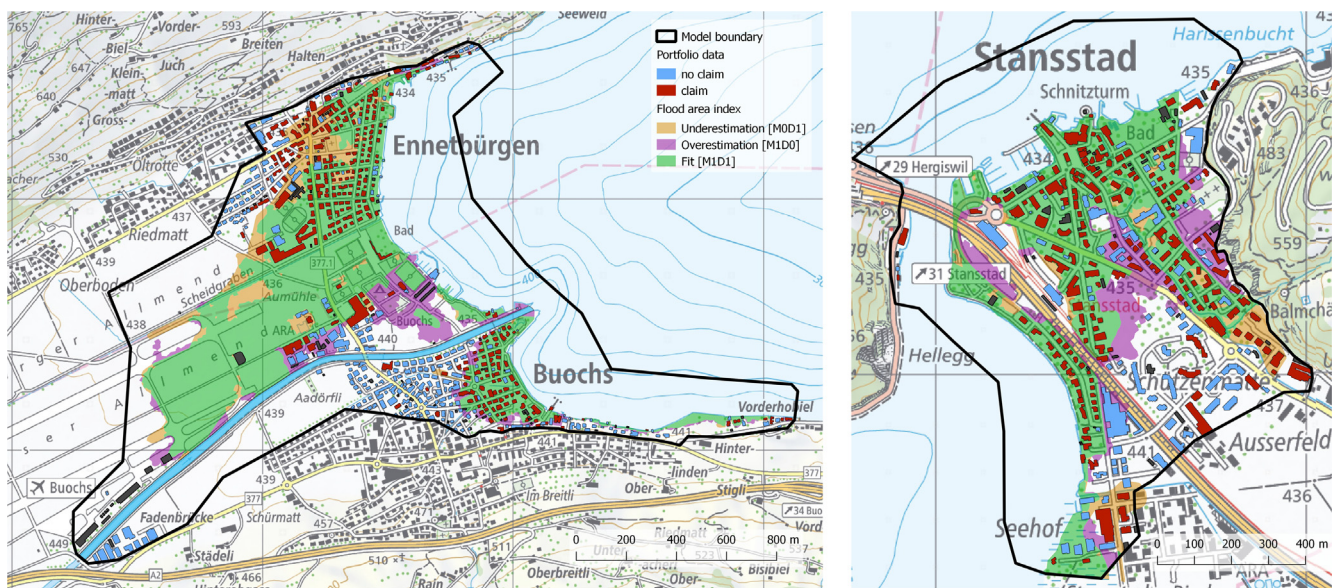
Table 2Absolute values used for calculating the flood area index FAI of the four test cases (m²). *Area of river reach included.

Value	Buochs/Ennetbürgen	Stansstad	Thun	Interlaken
M1D1	648,712 (62,823*)	267,452	752,937 (271,528*)	6,058,312 (679,770*)
M1D0	112,003	86,712	359,547	1,338,693
MOD1	131,638	42,788	120,445	1,756,338

Table 3

Validation metrics of the four test cases. Values in brackets show metrics only considering residential buildings. *River main channels count as an M1D1 ("hit"), lake areas are always excluded.

validation metric	Buochs/Ennetbürgen	Stansstad	Thun	Interlaken
model fit F	0.66 (0.71)	0.74 (0.78)	0.56 (0.56)	0.47 (0.47)
Accuracy	0.79 (0.81)	0.77 (0.81)	0.91 (0.92)	0.79 (0.79)
Bias score	1.02 (0.96)	1.14 (1.11)	1.20 (1.21)	0.90 (0.90)
Hit rate	0.81 (0.81)	0.91 (0.92)	0.79 (0.79)	0.61 (0.61)
False alarm ratio	0.21 (0.15)	0.20 (0.17)	0.34 (0.35)	0.33 (0.32)
False alarm rate	0.24 (0.19)	0.55 (0.52)	0.07 (0.06)	0.13 (0.13)
Success index	0.78 (0.81)	0.68 (0.70)	0.86 (0.86)	0.74 (0.74)
FAI	0.73 (0.74*)	0.67	0.61 (0.68*)	0.66 (0.69*)

**Fig. 3.** Map of the simulated inundation areas and insurance claims in Nidwalden. Map sources: SWISSTOPO (background map, reproduced by permission of SWISSTOPO (BA17073), Cantonal insurance Nidwalden (claims), Canton of Nidwalden (event documentation dataset).

to local flooding. Furthermore, the artificial breach in the lateral dam of the main river is a special invention of the Cantonal engineering administration. The discharge structures are designed in a way that they can overflow without being breached. In case of overflowing, the lee side of the dike is eroded and the excess flow is suddenly guided towards the flood corridor. In contrast to our simulation setup, the overflow was, in reality, withheld for a longer period and suddenly increased after the overflow. Thus, the peak discharge of the excess flow must have been slightly higher in reality than in our simulation. However, the flood corridor was not definitively implemented at the time of the flood and thus losses occurred in this study area. Another area that was underestimated by the model can be found in the case of Stansstad (Fig. 3, right). In the eastern part of the study area, a wider area is predicted as being dry, while documented as being wet according to the event documentation. This underestimation is the result of neglecting sediment transport in the small tributary Gieslibach. In the report of the event documentation, the tributary flooded the left side because the sediment retention basin was filled with sediment

and the water consequently flowed also towards the left in contrast to the evidence of the terrain model. Fig. 3 indicates a few of buildings that are located within the flooded areas while, according to the claim data, no damage had been caused during the event. These buildings are either associated with a low vulnerability against flooding or they are located above the water surface elevation at the micro-relief scale. In the case study of Thun (Fig. 4), the model remarkably overestimated the flooded area near the two branches of the Aare River in comparison with the event documentation dataset. However, the insurance dataset shows damages in this area. It is unknown, whether these damages resulted from excess rainfall, groundwater flooding or from riverine flooding. Note that we are not allowed to map single points of the losses in Figs. 4 and 5 due to privacy reasons. The overestimation near the lake outflow can be explained by micro-scale topographic features not present in the terrain model. The area in the south of Thun is underestimated by the model but mapped in the event documentation. In reality, this area was affected by groundwater flooding and not directly by lake flooding. In Interlaken, the

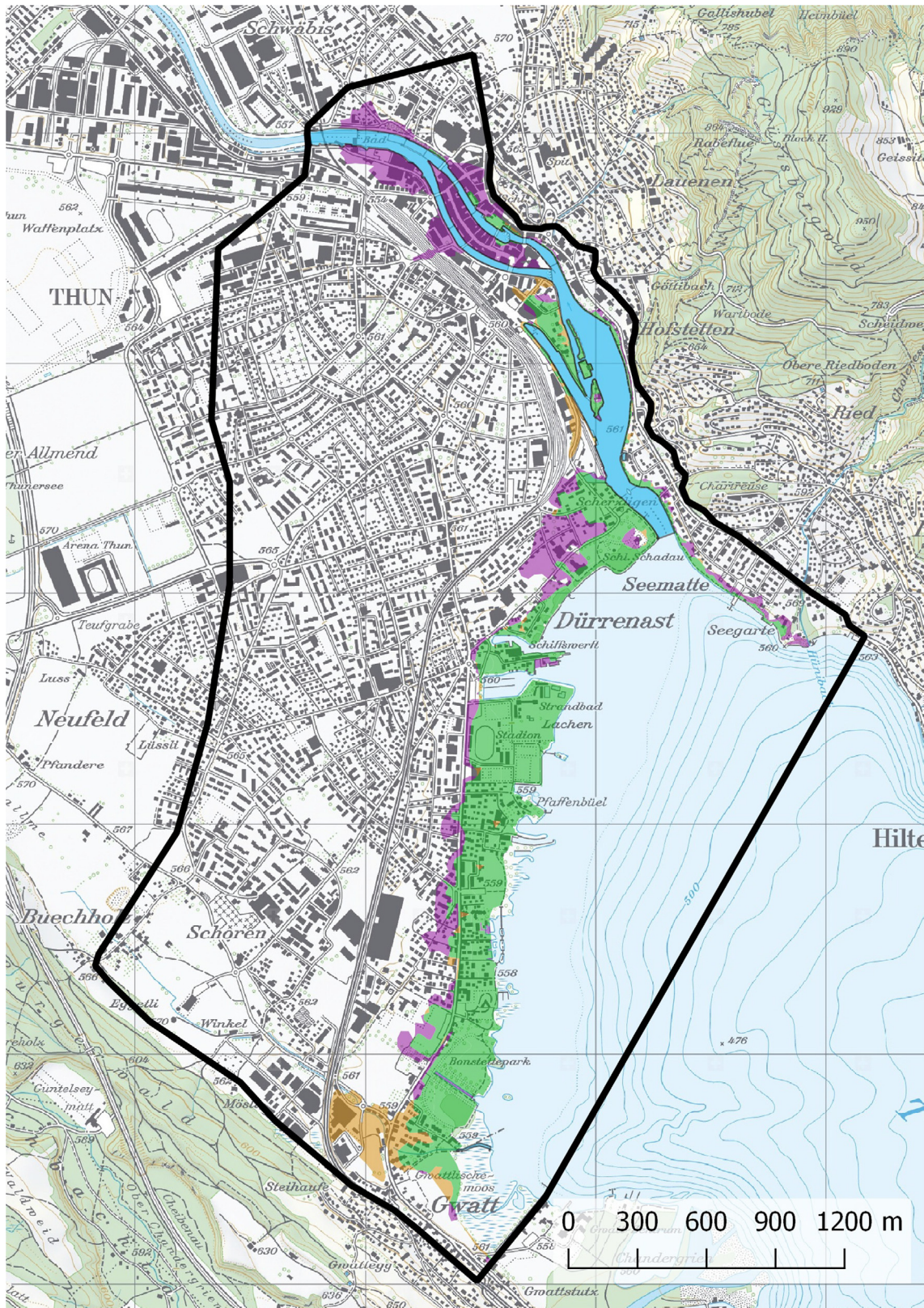


Fig. 4. Map of the simulated inundation areas and comparison with the event documentation data in Thun. The green colour shows the correctly predicted inundated areas, the violet colour shows the overestimation, and the yellow colour shows the underestimation. Map sources: SWISSTOPO (background map, reproduced by permission of SWISSTOPO (BA17073), Canton of Bern (event documentation dataset).

simulation resulted in a remarkable overestimation of the flooding north of the highway due to the dike breach on the Lütshine River (Fig. 5). However, the insurance claims show a considerable num-

ber of damages in this area. The model underestimated two weak points along the Lütshine River. The weak point downstream of the dam breach is not considered in the simulation because we

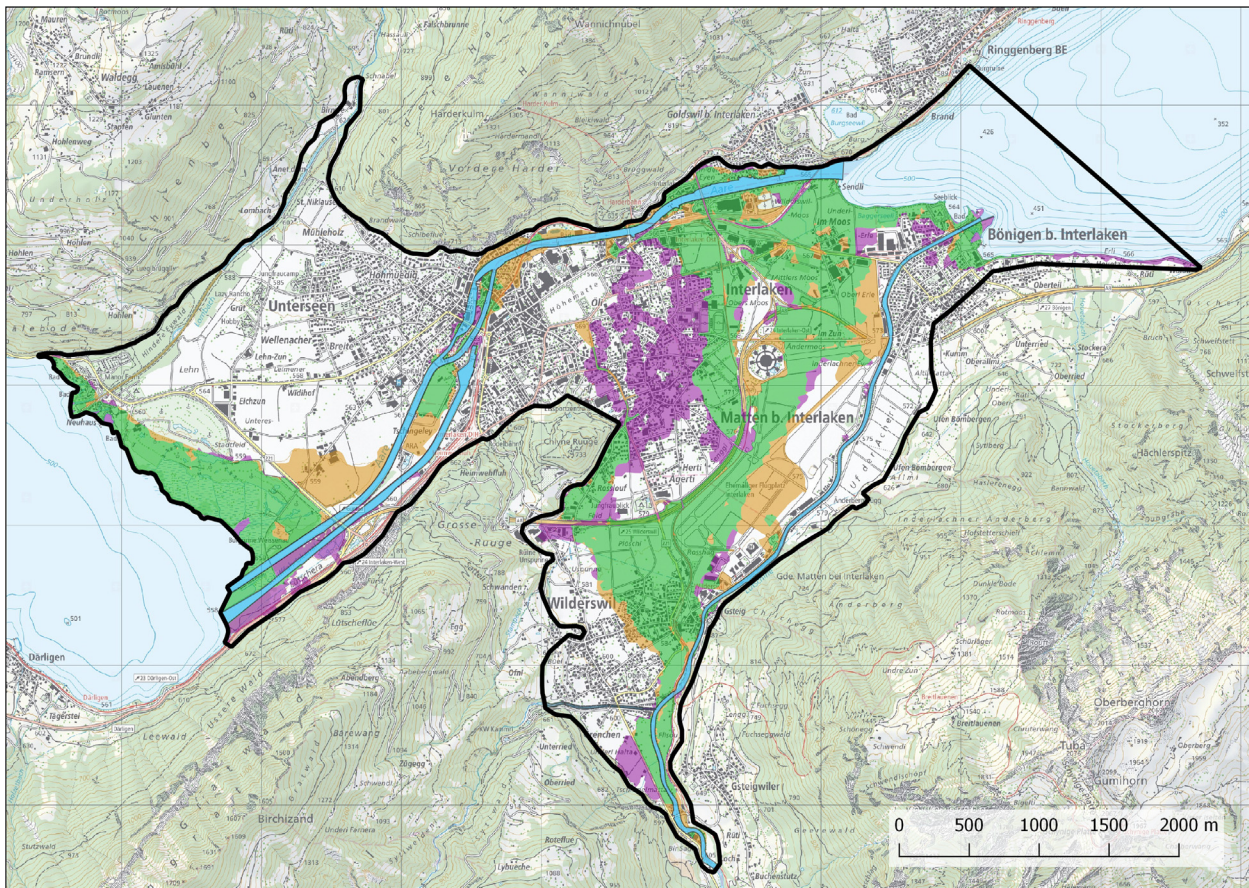


Fig. 5. Map of the simulated inundation areas and comparison with the event documentation data in Interlaken. The green colour shows the correctly predicted inundated areas, the violet colour shows the overestimation, and the yellow colour shows the underestimation. Map sources: SWISSTOPO (background map, reproduced by permission of SWISSTOPO (BA17073), Canton of Bern (event documentation dataset)).

used the river topography from 2014 with additional river widening and lateral dams implemented since 2005. However, the underestimation of flooded areas along the Aare River cannot be explained by simple topographical differences between 2014 and 2005. Here, the complex situation with two weirs and a branching river might not be represented with sufficient accuracy. In our model, the weirs are represented only as flow obstacles and not as weirs. This situation needs to be optimized for future work. In summary, most of the false predictions can be explained by micro-topographic structures and changes in the river channel due to flood prevention measures after the flood of 2005. Similar observations were made by Horritt and Bates (2001b), Bates et al. (2003), Fewtrell et al. (2008), Boettle et al. (2011), Dottori et al. (2013), and Almeida et al. (2016). Nevertheless, the results show an acceptable performance even without calibration (Wright et al. 2017), iterative corrections of the mesh (Jakeman et al. 2006), implementation of expert knowledge (Gharari et al. 2014), or the discussion of the uncertainty in the boundary conditions (Pappenberger et al. 2006). However, adapting the computational mesh or the reconstruction of the river geometry as present during the reference flood may result in a better performance. Furthermore, the flood event of 2005 was a remarkable but not extreme flood event. The peak discharge was not substantially higher than the channel carrying capacity. Thus, after Stephens et al. (2014) the validation values should be interpreted as conservative. In this study, we considered a building as exposed if it is affected by mesh nodes with a flow depth greater than 0 m. It remains an open question, if this assumption affects the validation metrics and has to be analysed in future works. The model fit cal-

culated on the basis of the insurance claims data differs from the one based on flooded areas. In Stansstad, the F value is higher than the FAI value. In this case study, claims are located in some areas predicted as wet by the model and observed as dry by the event documentation. In addition, a proportion of the areas predicted as wet but observed as dry do not contain buildings at all. This leads to an F value greater than the FAI value. In contrast, the F value is significantly lower than the FAI value in the other three case studies. Namely, relevant proportions of the areas that the model predicted well are located outside of the urbanized area while the deviations are located within the urbanized areas. In the case study of Interlaken, this is most apparent. The model erroneously predicted a relevant area in the centre of Interlaken as flooded (Fig. 5) that contains a high number of buildings. In contrast, in a relevant proportion of the accurately predicted wet areas, no buildings are located. This case demonstrates that the validation based on insurance claims is only considering points in space that are particularly relevant for flood risk assessment.

4. Conclusions and recommendations

The comparison between two independent validation data sets suggests that validation metrics using insurance claims can generally be compared to conventional validation data, e.g., the flooded area. Although the model fit computed on the basis of insurance claims gives similar results, the values are slightly lower than the ones computed on the basis of the observed inundation areas in three out of four test cases. Hence, it is shown that a model with

a good overall fit calculated on the basis of observed inundated areas does not necessarily exhibit a similarly good fit at locations of particular interest for risk assessment. Thus, a validation on the basis of insurance claims might be more conservative in cases where model errors are more pronounced in areas with a high density of values at risk. As insurance portfolios and loss data represent the most relevant target for a validation of flood models used for exposure assessments at the scale of the single buildings, this data can be recommended for validating inundation models.

However, the considered model fit metric based on insurance claim data penalizes both misses and false alarms. When a flood loss analysis aims at capturing the worst case, e.g., for portfolio analysis, the false alarms may have a lower weight, which is considered by the hit rate. The false alarm rate gives higher weights to false alarms but is sensitive to the correct negatives and thus to the delimitation of the study area. In summary, the use of additional validation metrics offers a more reliable base to assess specific aspects of the model performance rather than the model fit measure alone. Insurance claim data allow to calculate most of the binary validation metrics in a spatially explicit manner and, thus, allow to obtain more detailed insights regarding the advantages and the weak points of the selected 2D flood model. Nevertheless, the delimitation of the study area influences the proportion of the number of buildings within and outside the flooded areas and with it some of the described validation metrics.

Nevertheless, the insurance data have to be carefully pre-processed before being used for model validation. Special attention has to be given to examine whether the construction date of each building corresponds to the date of the reference flood event used for validation. The analysis showed that the removal of buildings constructed after the reference flood event influences the model fit. Another point to consider in pre-processing insurance claim data is to filter out claims associated to surface water flooding, as shown by Bernet et al. (2017) or claims associated with groundwater flooding. This has not been done in this study and should be addressed in future studies. Nevertheless, insurance claims constitute a potential validation dataset because of their consistent and relatively homogeneous records over time. In contrast to flood event documentation data sets, insurance claims are covering also small events and thus these data can remarkably extend the validation data, in general. Still, it remains an open question whether the flooded areas of past events can be reconstructed on the basis of insurance claims data.

Last but not least, the data availability constrained by privacy protection is a critical point. This will likely remain the main limitation of the presented approach. However, the presented validation approach can be adapted to situations where insurance claims are not available, when mapped flooded areas and a building dataset are obtainable. With an overlay between the flooded areas and the buildings' footprints, a binary validation dataset similar to a dataset of insurance claims could be created.

5. Code and/or data availability

The BASEMENT software is freely available at <http://www.basement.ethz.ch>. The validation data is under strict privacy rights and unfortunately it cannot be shared. The inundation models used for the validation are available under the creative commons attribution at [zenodo.org](https://www.zenodo.org/record/815136#.WUoJTIFpxhE) (<https://www.zenodo.org/record/815136#.WUoJTIFpxhE>), doi:<https://doi.org/10.5281/zenodo.815136>.

6. Authors' contributions

A. Zischg designed the study. M. Mosimann and A. Zischg prepared the simulation models and made the simulations. M. Mosi-

mann prepared the insurance claims for Thun and Interlaken and computed the validation. D.B. Bernet and V. Röthlisberger processed the insurance data of the Canton of Nidwalden. The manuscript was prepared by A. Zischg with contributions of all co-authors.

Acknowledgements

The authors declare that they have no conflict of interest. We acknowledge the Federal Statistical Office for Statistics FSO for providing the buildings and dwellings statistics, the Federal Office for Environment FOEN for providing the data of river cross sections, and the Federal Office for Topography swisstopo for providing the digital terrain model, the buildings dataset, and the topographic maps. Furthermore, we acknowledge the Canton of Bern for providing the Lidar data and the event documentation data, and the Canton of Nidwalden for the event document dataset. We especially thank the Cantonal public insurance company in Nidwalden and the Mobiliar insurance company for the provision of the validation dataset. The research was funded by the Swiss Mobiliar.

References

- Bates, P., de Roo, A., 2000. A simple raster-based model for flood inundation simulation. *J. Hydrol.* 236 (1–2), 54–77.
- Bates, P.D., Horritt, M.S., Smith, C.N., Mason, D., 1997. Integrating remote sensing observations of flood hydrology and hydraulic modelling. *Hydrol. Process.* 11, 1777–1795. [https://doi.org/10.1002/\(SICI\)1099-1085\(199711\)11:14<1777:AID-HYP543>3.0.CO;2-E](https://doi.org/10.1002/(SICI)1099-1085(199711)11:14<1777:AID-HYP543>3.0.CO;2-E).
- Bates, P.D., Marks, K.J., Horritt, M.S., 2003. Optimal use of high-resolution topographic data in flood inundation models. *Hydrol. Process.* 17, 537–557. <https://doi.org/10.1002/hyp.1113>.
- Bates, P.D., Horritt, M.S., Fewtrell, T.J., 2010. A simple inertial formulation of the shallow water equations for efficient two-dimensional flood inundation modelling. *J. Hydrol.* 387, 33–45. <https://doi.org/10.1016/j.jhydrol.2010.03.027>.
- Bennett, N.D., Croke, B.F., Guariso, G., Guillaume, J.H., Hamilton, S.H., Jakeman, A.J., Marsili-Libelli, S., Newham, L.T., Norton, J.P., Perrin, C., Pierce, S.A., Robson, B., Seppelt, R., Voinov, A.A., Fath, B.D., Andreassian, V., 2013. Characterising performance of environmental models. *Environ. Modelling Software* 40, 1–20. <https://doi.org/10.1016/j.envsoft.2012.09.011>.
- Berchtold, T., Vetsch, D., Weitbrech, V., Boes, R., 2012. Simulation of river-bed evolution due to channel widening. In: 34th Hydrology and Water Resources Symposium, Sydney, Australia, 19–22 Nov. 2012, 299–307.
- Bermúdez, M., Neal, J.C., Bates, P.D., Coxon, G., Freer, J.E., Cea, L., Puertas, J., 2017. Quantifying local rainfall dynamics and uncertain boundary conditions into a nested regional-local flood modeling system. *Water Resour. Res.* 50, 433. <https://doi.org/10.1002/2016WR019903>.
- Bernet, D.B., Prasuhn, V., Weingartner, R., 2017. Surface water floods in Switzerland. What insurance claim records tell us about the damage in space and time. *Nat. Hazards Earth Syst. Sci.* 17 (9), 1659–1682.
- Bertoldi, W., Siviglia, A., Tettamanti, S., Toffolon, M., Vetsch, D., Francalanci, S., 2014. Modeling vegetation controls on fluvial morphological trajectories. *Geophys. Res. Lett.* 41, 7167–7175. <https://doi.org/10.1002/2014GL061666>.
- Biancamaria, S., Bates, P.D., Boone, A., Mognard, N.M., 2009. Large-scale coupled hydrologic and hydraulic modelling of the Ob river in Siberia. *J. Hydrol.* 379, 136–150. <https://doi.org/10.1016/j.jhydrol.2009.09.054>.
- Boettle, M., Kropp, J.P., Reiber, L., Roithmeier, O., Rybski, D., Walther, C., 2011. About the influence of elevation model quality and small-scale damage functions on flood damage estimation. *Nat. Hazards Earth Syst. Sci.* 11, 3327–3334. <https://doi.org/10.5194/nhess-11-3327-2011>.
- BWG: Rauheiten in ausgesuchten schweizerischen Fließgewässern. Bern, 2001.
- Castellarin, A., Di Baldassarre, G., Bates, P., Brath, A., 2009. Optimal cross-sectional spacing in Preissmann Scheme 1D hydrodynamic models. *J. Hydraul. Eng.* 135, 96–105.
- Chatterjee, C., Förster, S., Bronstert, A., 2008. Comparison of hydrodynamic models of different complexities to model floods with emergency storage areas. *Hydrol. Process.* 22, 4695–4709. <https://doi.org/10.1002/hyp.7079>.
- Conner, J.T., Tonina, D., 2014. Effect of cross-section interpolated bathymetry on 2D hydrodynamic model results in a large river. *Earth Surface Processes Landforms* 39, 463–475. <https://doi.org/10.1002/esp.3458>.
- Cook, A., Merwade, V., 2009. Effect of topographic data, geometric configuration and modeling approach on flood inundation mapping. *J. Hydrol.* 377, 131–142. <https://doi.org/10.1016/j.jhydrol.2009.08.015>.
- Costabile, P., Macchione, F., 2015. Enhancing river model set-up for 2-D dynamic flood modelling. *Environ. Modelling Software* 67, 89–107. <https://doi.org/10.1016/j.envsoft.2015.01.009>.

- Courty, L.G., Pedrozo-Acuña, A., Bates, P.D., 2017. Itzi (version 17.1): an open-source, distributed GIS model for dynamic flood simulation, *Geosci. Model Dev.*, 10, 1835–1847, doi:10.5194/gmd-10-1835-2017.
- Crispino, G., Gisonni, C., Iervolino, M., 2015. Flood hazard assessment: comparison of 1D and 2D hydraulic models. *Int. J. River Basin Management* 13, 153–166. <https://doi.org/10.1080/15715124.2014.928304>.
- de Almeida, G.A.M., Bates, P., Ozdemir, H., 2016. Modelling urban floods at sub-metre resolution: challenges or opportunities for flood risk management? *J. Flood Risk Management*. <https://doi.org/10.1111/jfr3.12276>.
- Di Baldassarre, G., Schumann, G., Bates, P.D., Freer, J.E., Beven, K.J., 2010. Flood-plain mapping: a critical discussion of deterministic and probabilistic approaches. *Hydrol. Sci. J.* 55, 364–376. <https://doi.org/10.1080/02626661003683389>.
- Dottori, F., Di Baldassarre, G., Todini, E., 2013. Detailed data is welcome, but with a pinch of salt: accuracy, precision, and uncertainty in flood inundation modeling. *Water Resour. Res.* 49, 6079–6085. <https://doi.org/10.1002/wrcr.20406>.
- Fäh, R., Farshi, D., Müller, R., Rousselot, P., Vetsch, D., 2007. A comparison between a 1D- and a 2D-numerical modelling of a local river widening. In: *Proc. 32. IAHR-Congress Venice: 1270:1–10*, Venice.
- Fäh, R., Müller, R., Rousselot, P., Vetsch, D., 2007. Morphological development of river widening due to flood wave – comparison of field measurements and numerical modelling. In: *Proc. Symposium Mesures d'aménagement des cours d'eau pour la protection contre les crues, l'environnement, la société et l'économie, Communication LCH 33:67–78*. (in German).
- Falter, D., Vorogushyn, S., Lhomme, J., Apel, H., Gouldby, B., Merz, B., 2013. Hydraulic model evaluation for large-scale flood risk assessments. *Hydrol. Process.* 27 (9), 1331–1340.
- Falter, D., Schröter, K., Dung, N.V., Vorogushyn, S., Kreibich, H., Hundeda, Y., Apel, H., Merz, B., 2015. Spatially coherent flood risk assessment based on long-term continuous simulation with a coupled model chain. *J. Hydrol.* 524, 182–193. <https://doi.org/10.1016/j.jhydrol.2015.02.021>.
- Felder, G., Zischg, A., Weingartner, R., 2017. The effect of coupling hydrologic and hydrodynamic models on probable maximum flood estimation. *J. Hydrol.* <https://doi.org/10.1016/j.jhydrol.2017.04.052>.
- Fewtrell, T.J., Bates, P.D., Horritt, M., Hunter, N.M., 2008. Evaluating the effect of scale in flood inundation modelling in urban environments. *Hydrol. Process.* 22, 5107–5118. <https://doi.org/10.1002/hyp.7148>.
- Fewtrell, T.J., Duncan, A., Sampson, C.C., Neal, J.C., Bates, P.D., 2011. Benchmarking urban flood models of varying complexity and scale using high resolution terrestrial LiDAR data. *Phys. Chem. Earth Parts A/B/C* 36, 281–291. <https://doi.org/10.1016/j.pce.2010.12.011>.
- FOEN: Cross-sections Engelberger Aa. Federal Office of Environment FOEN, Hazard Prevention Division. Bern. Available at <https://www.bafu.admin.ch/bafu/en/home/office/divisions-sections/hazard-prevention-division.html>, last access 17 May 2017.
- FOEN: Hydrological data and forecasts. Federal Office of Environment FOEN. Bern. Available at <https://www.hydrodaten.admin.ch/en/stations-and-data.html>, last access 17 May 2017.
- Freer, J., Beven, K. J., Neal, J., Schumann, G., Hall, J., Bates, P., 2013. Flood risk and uncertainty. In: *Risk and uncertainty assessment for natural hazards*, Rougier, J., Sparks, R. S. J., Hill, L. J. (Eds.), Cambridge University Press, Cambridge, 190–233, 2013.
- FSO: Buildings and Dwellings statistic BDS, version 3.6. Federal Statistical Office FSO 2014.
- Fuchs, S., Röthlisberger, V., Thaler, T., Zischg, A., Keiler, M., 2017. Natural Hazard Management from a Coevolutionary Perspective. *Exposure and Policy Response in the European Alps*. *Ann. Am. Assoc. Geographers*, 1–11.
- Fuchs, S., Keiler, M., Zischg, A., 2015. A spatiotemporal multi-hazard exposure assessment based on property data. *Nat. Hazards Earth Syst. Sci.* 15 (9), 2127–2142.
- Garrote, J., Alvarenga, F.M., Díez-Herrero, A., 2016. Quantification of flash flood economic risk using ultra-detailed stage–damage functions and 2-D hydraulic models. *J. Hydrol.* 541, 611–625. <https://doi.org/10.1016/j.jhydrol.2016.02.006>.
- Gharari, S., Hrachowitz, M., Fenicia, F., Gao, H., Savenije, H.H.G., 2014. Using expert knowledge to increase realism in environmental system models can dramatically reduce the need for calibration. *Hydrol. Earth Syst. Sci.* 18, 4839–4859. <https://doi.org/10.5194/hess-18-4839-2014>.
- Horritt, M.S., 2000. Calibration of a two-dimensional finite element flood flow model using satellite radar imagery. *Water Resour. Res.* 36, 3279–3291. <https://doi.org/10.1029/2000WR900206>.
- Horritt, M.S., Bates, P.D., 2001a. Predicting floodplain inundation: Raster-based modelling versus the finite-element approach. *Hydrol. Process.* 15, 825–842. <https://doi.org/10.1002/hyp.188>.
- Horritt, M., Bates, P., 2001b. Effects of spatial resolution on a raster based model of flood flow. *J. Hydrol.* 253, 239–249. [https://doi.org/10.1016/S0022-1694\(01\)00490-5](https://doi.org/10.1016/S0022-1694(01)00490-5).
- Horritt, M.S., Bates, P.D., 2002. Evaluation of 1D and 2D numerical models for predicting river flood inundation. *J. Hydrol.* 268, 87–99. [https://doi.org/10.1016/S0022-1694\(02\)00121-X](https://doi.org/10.1016/S0022-1694(02)00121-X).
- Horritt, M.S., Di Baldassarre, G., Bates, P.D., Brath, A., 2007. Comparing the performance of a 2-D finite element and a 2-D finite volume model of floodplain inundation using airborne SAR imagery. *Hydrol. Process.* 21, 2745–2759. <https://doi.org/10.1002/hyp.6486>.
- Hunter, N.M., Bates, P.D., Horritt, M.S., Wilson, M.D., 2007. Simple spatially-distributed models for predicting flood inundation: a review. *Geomorphology* 90, 208–225. <https://doi.org/10.1016/j.geomorph.2006.10.021>.
- Jakeman, A.J., Letcher, R.A., Norton, J.P., 2006. Ten iterative steps in development and evaluation of environmental models. *Environ. Modelling Software* 21, 602–614. <https://doi.org/10.1016/j.envsoft.2006.01.004>.
- Jonkman, S.N., 2013. Advanced flood risk analysis required. *Nat. Clim. Change* 3, 1004. <https://doi.org/10.1038/nclimate2031>.
- KAWA: Lidar terrain model 2014. Canton of Bern, 2015.
- Lavoie, B., Mahdi, T.-F., 2017. Comparison of two-dimensional flood propagation models: SRH-2D and Hydro_AS-2D. *Nat. Hazards* 86, 1207–1222. <https://doi.org/10.1007/s11069-016-2737-7>.
- Mark, O., Weesakul, S., Apirumanekul, C., Aroonnet, S.B., Djordjević, S., 2004. Potential and limitations of 1D modelling of urban flooding. *J. Hydrol.* 299, 284–299. <https://doi.org/10.1016/j.jhydrol.2004.08.014>.
- Mason, D.C., Bates, P.D., Dall'Amico, J.T., 2009. Calibration of uncertain flood inundation models using remotely sensed water levels. *J. Hydrol.* 368, 224–236. <https://doi.org/10.1016/j.jhydrol.2009.02.034>.
- Merwade, V., Cook, A., Coonrod, J., 2008a. GIS techniques for creating river terrain models for hydrodynamic modeling and flood inundation mapping. *Environ. Modelling Software* 23, 1300–1311. <https://doi.org/10.1016/j.envsoft.2008.03.005>.
- Merwade, V., Olivera, F., Arabi, M., Edleman, S., 2008b. Uncertainty in flood inundation mapping: current issues and future directions. *J. Hydrol. Eng.* 13, 608–620. [https://doi.org/10.1061/\(ASCE\)1084-0699\(2008\)13:7\(608\)](https://doi.org/10.1061/(ASCE)1084-0699(2008)13:7(608)).
- Merz, R., Blöschl, G., Humer, G., 2008. National flood discharge mapping in Austria. *Nat. Hazards* 46, 53–72. <https://doi.org/10.1007/s11069-007-9181-7>.
- Neal, J.C., Bates, P.D., Fewtrell, T.J., Hunter, N.M., Wilson, M.D., Horritt, M.S., 2009. Distributed whole city water level measurements from the Carlisle 2005 urban flood event and comparison with hydraulic model simulations. *J. Hydrol.* 368, 42–55. <https://doi.org/10.1016/j.jhydrol.2009.01.026>.
- Neal, J., Schumann, G., Bates, P.D., 2012. A subgrid channel model for simulating river hydraulics and floodplain inundation over large and data sparse areas. *Water Resour. Res.*, 48, n/a-n/a, doi:10.1029/2012WR012514.
- Neal, J., Schumann, G., Fewtrell, T., Budimir, M., Bates, P., Mason, D., 2011. Evaluating a new LISFLOOD-FP formulation with data from the summer 2007 floods in Tewkesbury, UK. *J. Flood Risk Management* 4, 88–95. <https://doi.org/10.1111/j.1753-318X.2011.01093.x>.
- Neal, J., Villanueva, I., Wright, N., Willis, T., Fewtrell, T., Bates, P.D., 2012. How much physical complexity is needed to model flood inundation? *Hydrol. Process.* 26, 2264–2282. <https://doi.org/10.1002/hyp.8339>.
- Pappenberger, F., Beven, K., Horritt, M., Blazkova, S., 2005. Uncertainty in the calibration of effective roughness parameters in HEC-RAS using inundation and downstream level observations. *J. Hydrol.* 302, 46–69. <https://doi.org/10.1016/j.jhydrol.2004.06.036>.
- Pappenberger, F., Matgen, P., Beven, K.J., Henry, J.-B., Pfister, L., Fraipont, P., 2006. Influence of uncertain boundary conditions and model structure on flood inundation predictions. *Adv. Water Resour.* 29, 1430–1449. <https://doi.org/10.1016/j.advwatres.2005.11.012>.
- Pappenberger, F., Frodsham, K., Beven, K., Romanowicz, R., Matgen, P., 2007a. Fuzzy set approach to calibrating distributed flood inundation models using remote sensing observations. *Hydrol. Earth Syst. Sci.* 11, 739–752. <https://doi.org/10.5194/hess-11-739-2007>.
- Pappenberger, F., Beven, K., Frodsham, K., Romanowicz, R., Matgen, P., 2007b. Grasping the unavoidable subjectivity in calibration of flood inundation models. *A vulnerability weighted approach*. *J. Hydrol.* 333 (2–4), 275–287.
- Pappenberger, F., Dutra, E., Wetterhall, F., Cloke, H.L., 2012. Deriving global flood hazard maps of fluvial floods through a physical model cascade. *Hydrol. Earth Syst. Sci.* 16, 4143–4156. <https://doi.org/10.5194/hess-16-4143-2012>.
- Pedrozo-Acuña, A., Mariño-Tapia, I., Enriquez, C., Medellín Mayoral, G., González Villareal, F.J., 2012. Evaluation of inundation areas resulting from the diversion of an extreme discharge towards the sea: case study in Tabasco, Mexico. *Hydrol. Process.* 26, 687–704. <https://doi.org/10.1002/hyp.8175>.
- Pianosi, F., Beven, K., Freer, J., Hall, J.W., Rougier, J., Stephenson, D.B., Wagener, T., 2016. Sensitivity analysis of environmental models: A systematic review with practical workflow. *Environ. Modelling Software* 79, 214–232. <https://doi.org/10.1016/j.envsoft.2016.02.008>.
- Radice, A., Giorgetti, E., Brambilla D., Longoni L., Papini M., On integrated sediment transport modelling for flash events in mountain environments. *Acta Geophysica* 60, 191–213.
- Ratto, M., Castelletti, A., Pagano, A., 2012. Emulation techniques for the reduction and sensitivity analysis of complex environmental models. *Environ. Modelling Software* 34, 1–4. <https://doi.org/10.1016/j.envsoft.2011.11.003>.
- Refsgaard, J.C., Højberg, A.L., He, X., Hansen, A.L., Rasmussen, S.H., Stisen, S., 2016. Where are the limits of model predictive capabilities? *Hydrol. Process.* 30, 4956–4965. <https://doi.org/10.1002/hyp.11029>.
- Röthlisberger, V., Zischg, A., Keiler, M., 2016. Spatiotemporal aspects of flood exposure in Switzerland. In: *E3S Web Conf. 7*, S. 8008. doi:10.1051/e3sconf/20160708008.
- Röthlisberger, V., Zischg, A.P., Keiler, M., 2017. Identifying spatial clusters of flood exposure to support decision making in risk management. *Sci. Total Environ.* 598, 593–603. <https://doi.org/10.1016/j.scitotenv.2017.03.216>.
- Sampson, C.C., Smith, A.M., Bates, P.D., Neal, J.C., Alfieri, L., Freer, J.E., 2015. A high-resolution global flood hazard model. *Water Resour. Res.* 51, 7358–7381. <https://doi.org/10.1002/2015WR016954>.
- Savage, J. T. S., Bates, P., Freer, J., Neal, J., Aronica, G., 2015. When does spatial resolution become spurious in probabilistic flood inundation predictions? *Hydrol. Process.* n/a-n/a. doi:10.1002/hyp.10749.

- Savage, J., Pianosi, F., Bates, P., Freer, J., Wagener, T., 2016. Quantifying the importance of spatial resolution and other factors through global sensitivity analysis of a flood inundation model. *Water Resour. Res.* 52, 9146–9163. <https://doi.org/10.1002/2015WR018198>.
- Segura-Beltrán, F., Sanchis-Ibor, C., Morales-Hernández, M., González-Sanchis, M., Bussi, G., Ortiz, E., 2016. Using post-flood surveys and geomorphologic mapping to evaluate hydrological and hydraulic models: the flash flood of the Girona River (Spain) in 2007. *J. Hydrol.* 541, 310–329. <https://doi.org/10.1016/j.jhydrol.2016.04.039>.
- Shewchuk, J.R., 2002. Delaunay refinement algorithms for triangular mesh generation. *Comput. Geometry Theory Appl.* 22 (1–3), 21–74.
- Stephens, E., Schumann, G., Bates, P., 2014. Problems with binary pattern measures for flood model evaluation. *Hydrol. Process.* 28, 4928–4937. <https://doi.org/10.1002/hyp.9979>.
- SWISSTOPO: SwissALTI3D. Federal Office of Topography, swisstopo. Available online at https://shop.swisstopo.admin.ch/de/products/height_models/alti3D, last access 16 May 2017.
- SWISSTOPO: swissTLM3D. Federal Office of Topography, swisstopo. Available online at <https://shop.swisstopo.admin.ch/de/products/landscape/tlm3D>, last access 19 May 2017.
- Tarpanelli, A., Brocca, L., Melone, F., Moramarco, T., 2013. Hydraulic modelling calibration in small rivers by using coarse resolution synthetic aperture radar imagery. *Hydrol. Process.* 27, 1321–1330. <https://doi.org/10.1002/hyp.9550>.
- Tayefi, V., Lane, S.N., Hardy, R.J., Yu, D., 2007. A comparison of one- and two-dimensional approaches to modelling flood inundation over complex upland floodplains. *Hydrol. Process.* 21, 3190–3202. <https://doi.org/10.1002/hyp.6523>.
- Teng, J., Jakeman, A.J., Vaze, J., Croke, B., Dutta, D., Kim, S., 2017. Flood inundation modelling: a review of methods, recent advances and uncertainty analysis. *Environ. Modelling Software* 90, 201–216. <https://doi.org/10.1016/j.envsoft.2017.01.006>.
- Trigg, M.A., Birch, C.E., Neal, J.C., Bates, P.D., Smith, A., Sampson, C.C., Yamazaki, D., Hirabayashi, Y., Pappenberger, F., Dutra, E., Ward, P.J., Winsemius, H.C., Salamon, P., Dottori, F., Rudari, R., Kappes, M.S., Simpson, A.L., Hadzilacos, G., Fewtrell, T.J., 2016. The credibility challenge for global fluvial flood risk analysis. *Environ. Res. Lett.* 11, 94014.
- UNISDR: Making development sustainable: the future of disaster risk management, Global assessment report on disaster risk reduction, 4.2015, United Nations, Geneva, 311 pp., 2015.
- Vetsch, D., Siviglia, A., Ehrbar, D., Facchini, M., Gerber, M., Kammerer, S., Peter, S., Vonwiler, L., Volz, C., Farshi, D., Mueller, R., Rousselot, P., Veprek, R., Faeh, R., 2017. BASEMENT – Basic Simulation Environment for Computation of Environmental Flow and Natural Hazard Simulation., Zurich. Available at: www.basement.ethz.ch.
- Volz, C., Rousselot, P., Vetsch, D., Faeh, R., 2012. Numerical modelling of non-cohesive embankment breach with the dual-mesh approach. *J. Hydraul. Res.* 50 (6), 587–598.
- Vonwiller, L., Vetsch, D.F., Boes, R.M., 2015. On the role of modelling approach for simulation of bank erosion in straight, trapezoidal channel. In: Proceedings of the 36th IAHR World Congress 28 June - 3 July, The Hague, the Netherlands.
- Vorogushyn, S., Merz, B., Lindenschmidt, K.-E., Apel, H., 2010. A new methodology for flood hazard assessment considering dike breaches, *Water Resour. Res.* 46, n/a-n/a. doi:10.1029/2009WR008475.
- Vozinaki, A.-E.K., Morianou, G.G., Alexakis, D.D., Tsanis, I.K., 2016. Comparing 1D and combined 1D/2D hydraulic simulations using high-resolution topographic data: a case study of the Koiliaris basin, Greece. *Hydrol. Sci. J.* 1–15. <https://doi.org/10.1080/02626667.2016.1255746>.
- Ward, P.J., Jongman, B., Weiland, F.S., Bouwman, A., van Beek, R., Bierkens, Marc, F.P., Ligetvoet, W., Winsemius, H.C., 2013. Assessing flood risk at the global scale: model setup, results, and sensitivity. *Environ. Res. Lett.* 8, 44019. <https://doi.org/10.1088/1748-9326/8/4/044019>.
- Woodhead, S., Asselman, N., Zech, Y., Soares-Fraza, S., Bates, P., Kortenhaus, A., 2007. Evaluation of Inundation Models. Limits and capabilities of models, 34 pp.
- Worni, R., Stoffel, M., Huggel, C., Volz, C., Casteller, A., Luckman, B., 2012. Analysis and dynamic modeling of a moraine failure and glacier lake outburst flood at Ventisquero Negro, Patagonian Andes (Argentina). *J. Hydrol.* 444, 134–145.
- Wright, K.A., Goodman, D.H., Som, N.A., Alvarez, J., Martin, A., Hardy, T.B., 2017. Improving hydrodynamic modelling: an analytical framework for assessment of two-dimensional hydrodynamic models. *River Res. Appl.* 33, 170–181. <https://doi.org/10.1002/rra.3067>.
- Zhu, D., Echendu, S., Xuan, Y., Webster, M., Cluckie, I., 2016. Coupled hydro-meteorological modelling on a HPC platform for high-resolution extreme weather impact study. *Hydrol. Earth Syst. Sci.* 20, 4707–4715. <https://doi.org/10.5194/hess-20-4707-2016>.
- Zischg, A., Felder, G., Weingartner, R., Gómez-Navarro, J. J., Röthlisberger, V., Bernet, D., Rössler, O., Raible, C., Keiler, M., Martius, O., 2016. M-AARE - Coupling atmospheric, hydrological, hydrodynamic and damage models in the Aare river basin, Switzerland. In: 13th Congress INTERPRAEVENT 2016, 30 May to 2 June 2016, Lucerne, Switzerland. Conference proceedings, 444–451, 2016.
- Zischg, A., Schober, S., Sereinig, N., Rauter, M., Seymann, C., Goldschmidt, F., Bäk, R., Schleicher, E., 2013. Monitoring the temporal development of natural hazard risks as a basis indicator for climate change adaptation. *Nat. Hazards* 67 (3), 1045–1058.

Paper 15: Bermúdez, M., Zischg, A., 2018. Sensitivity of flood loss estimates to building representation and flow depth attribution methods in micro-scale flood modelling. *Nat Hazards* 92, 1633–1648. [10.1007/s11069-018-3270-7](https://doi.org/10.1007/s11069-018-3270-7).

Sensitivity of flood loss estimates to building representation and flow depth attribution methods in micro-scale flood modelling

María Bermúdez¹  · Andreas Paul Zischg² 

Received: 12 December 2017 / Accepted: 11 March 2018 / Published online: 17 March 2018
© Springer Science+Business Media B.V., part of Springer Nature 2018

Abstract Thanks to modelling advances and the increase in computational resources in recent years, it is now feasible to perform 2-D urban flood simulations at very high spatial resolutions and to conduct flood risk assessments at the scale of single buildings. In this study, we explore the sensitivity of flood loss estimates obtained in such micro-scale analyses to the spatial representation of the buildings in the 2D flood inundation model and to the hazard attribution methods in the flood loss model. The results show that building representation has a limited effect on the exposure values (i.e. the number of elements at risk), but can have a significant impact on the hazard values attributed to the buildings. On the other hand, the two methods for hazard attribution tested in this work result in remarkably different flood loss estimates. The sensitivity of the predicted flood losses to the attribution method is comparable to the one associated with the vulnerability curve. The findings highlight the need for incorporating these sources of uncertainty into micro-scale flood risk prediction methodologies.

Keywords Inundation modelling · Micro-scale · Building representation · Flood loss estimation

1 Introduction

Flood inundation numerical models are a well-established approach for conducting flood risk analysis. Although one-dimensional hydrodynamic models are still in widespread use for many applications, the use of two-dimensional models is required in built-up areas to reproduce the complex, multidirectional flow paths generated by urban features (Apel et al.

✉ María Bermúdez
mbermudez@udc.es

¹ Water and Environmental Engineering Group, University of A Coruña, A Coruña, Spain

² Institute of Geography, Oeschger Centre for Climate Change Research, Mobiliar Lab for Natural Risks, University of Bern, Bern 3012, Switzerland

2009). Thanks to modelling advances and the increase in computational resources in recent years, it is now feasible to perform 2-D urban flood simulations at resolutions as low as 10 cm (Ozdemir et al. 2013; de Almeida et al. 2016). Together with the increase in data availability, this has opened up the possibility of conducting flood risk analysis and assessing damages at the scale of the single building (micro-scale), without the need for spatial aggregation of elements at risk (Staffler et al. 2008; Merz et al. 2010; Zischg et al. 2013, 2018; Fuchs et al. 2015, 2017; Röthlisberger et al. 2017). In micro-scale risk analyses, flood hazard is estimated by means of spatially detailed models solving the 2D shallow water equations. In addition, fine-resolution geospatial datasets are exploited to characterize the reconstruction value and the vulnerability of each building. Such a detailed analysis is relevant to reliably assess the effectiveness of flood protection measures for reducing flood risk in individual areas (Ernst et al. 2010). It can be used to objectively evaluate the economic cost-effectiveness of individual precautionary measures on buildings (i.e. retrofitting methods) (Arrighi et al. 2013), or be part of decision support systems to evaluate flood risk (Qi and Altinakar 2011).

The adoption of a micro-scale flood modelling approach allows the representation of small-scale structural elements and small topographic variations explicitly in the hydrodynamic model, instead of parameterizing their effects via subgrid scale models or artificial roughness (Abdullah et al. 2012; Abily et al. 2016). The value of roughness coefficient in such a 2D hydrodynamic model is thus set to represent only small-scale roughness, its calibration being less important than for low spatial resolution models (Horritt and Bates 2002). This is relevant because of the lack of sufficient data for model calibration and validation in many locations. However, sensitivity to other model features, such as the mesh set-up in relation to the building pattern and the building representation, may have a significant impact on the hydrodynamic results and, in turn, on the flood loss results. A few studies deal with these effects in urban areas (Fewtrell et al. 2008, 2011; Sampson et al. 2012; Schubert and Sanders 2012). However, these aspects have received far less attention for rural and peri-urban situations and have been generally explored in isolation from evaluation of uncertainties in loss estimation approaches.

Several methods have been proposed in recent years to represent buildings in shallow water models. A first group of methods parameterizes the effects of buildings on flooding by means of porosity parameters (Cea and Vázquez-Cendón 2009; Schubert and Sanders 2012; Guinot 2012) or by building coverage and conveyance reduction factors (Chen et al. 2012a, b). This allows the simulation of urban flood flows with a relatively coarse mesh and hence a fast execution time. However, these methods are not suitable for micro-scale flood modelling, which aims at capturing the localized variability of flood depth and velocity around buildings. In this case, a so-called resolved approach, which explicitly considers the exact building geometries, is needed (Schubert and Sanders 2012). The building block (BB) method and the building hole (BH) method are among the most used methods of this type. In the BB method, a digital surface model that incorporates the heights of the rooftops is used to produce a local elevation rise of the grid cells within building footprints. In the BH method, the area within the building footprints is excluded from the model domain, and closed boundary conditions are enforced at building walls. As noted by Bellos and Tsakiris (2015), reservations have been expressed for the BB and BH methods, related to the fact that they do not simulate flood flow inside the building and therefore any possible storage effects of the buildings are not taken into account. However, alternative methods such as the representation of the exterior walls of each building with an inlet on the front wall (Bellos and Tsakiris 2015), so that water can slip into the house, are seldom used in practical applications.

A key component of any flood risk analysis is the vulnerability assessment (Fuchs et al. 2012; Papathoma-Köhle et al. 2017) which is frequently focused only on direct flood loss. Depth-damage functions, which denote the flood damage that would occur at specific water depths per asset or per land-use class, are typically applied for this purpose. Other factors such as flow velocity are presumed to influence flood damage, but their general consideration in monetary loss modelling is not recommended (Kreibich et al. 2009). From a practitioner's perspective, the application of depth-damage functions is, therefore, the standard approach to assessing urban flood loss. The development of site-specific depth-damage functions is not feasible at many locations, and the use of models developed elsewhere is common practice in the literature (Apel et al. 2006; Notaro et al. 2014). In fact, libraries of depth-damage curves are available for different regions (Davis and Skaggs 1992; Green 2003). In addition to the inherent uncertainty in the depth-damage curves, their extrapolation to regions where building characteristics are not necessarily the same raises concerns regarding their local representativeness (Cammerer et al. 2013; McGrath et al. 2015). Various studies have already acknowledged the uncertainty and limitations associated with the use of depth-damage curves in flood damage estimation (de Moel and Aerts 2011; Sampson et al. 2014). Freni et al. (2010) suggest that the use of highly detailed 2D hydraulic models in flood risk assessments might not be justified if depth-damage curves are used to assess damages, given the significant uncertainties of the later.

In addition to the selection of a suitable depth-damage curve, other modelling choices need to be made in flood risk assessments. It is necessary to define how the number of exposed buildings will be counted and how the inundation characteristics will be assigned to each exposed building. Exposure information is essentially provided through the overlapping of the building footprint and the hazard maps. The high spatial resolution of the hazard results in micro-scale flood assessments allows, however, for different exposure evaluation, i.e. building counting, methods. A building can be assumed to be affected by the inundation if water depths computed within its footprint are above a certain wet–dry threshold. More sophisticated methods consider a buffer distance between the building edges and the flooded areas or calculate the proportion of the external perimeter of a property that is wet in the case of partially flooded buildings (Environment Agency 2014). On the other hand, the assignment of flow characteristics (water depths in the general case) to each building may be performed in different ways. This is referred to as flow depth attribution method in this paper. In the micro-scale flood risk analysis performed by Ernst et al. (2010), the water depth in the building is obtained either by averaging the water depth in the neighbouring cells or by linearly interpolating the ground level and the free surface elevation inside the asset. The aforementioned differences in attribution methods can potentially result in very different flood damage estimates. Yet, to the best of our knowledge, there are no studies available that have quantified its impact on the flood loss predictions.

Hence, the main research question for this paper is how flood loss estimates are influenced by the building representation and the flow depth attribution methods. To answer this question, we conduct a micro-scale flood loss assessment in a low-density residential case study that is typical for rural and peri-urban hilly landscapes in Europe. The modelling framework comprises a flood inundation model and a flood loss model, which provide hazard and impact estimates for a given flood event at a high spatial resolution. We analyse the sensitivity of the predicted flood loss to the building representation in the flood inundation model and to the vulnerability function and attribution method in the flood loss model. The benefits and limitations of the different methods are evaluated, and the applicability for real-world case studies is discussed. The main aim of

this work is to contribute to the development of consistent frameworks for micro-scale flood risk assessments, with a balanced accuracy and spatial detail of the different steps of the modelling process.

2 Methods

The model experiment was set up on the basis of a flood inundation model and a flood loss model (Fig. 1). Both sub-modules were altered in the experiment. While we kept the upstream boundary condition of the flood inundation model constant, i.e. the inflow hydrograph, we varied the computational mesh with different representations of the buildings. In the flood loss module, the building dataset was kept constant while we varied the flow depth attribution methods and the vulnerability functions. The methodology is described in more detail below.

2.1 Study area

We set up the model experiment in the case study of Steffisburg, a community in the Canton of Bern in Switzerland. The study area covers an area of 4.8 km² and is located on the alluvial fan of the Zulg River (Fig. 2). The fan has an average slope of 1.3%. The Zulg River has a catchment area of 90 km². The main village of Steffisburg is located along the Zulg River sprawling towards south and the city of Thun. It has 15,700 inhabitants and 1682 buildings. The density of buildings is low in comparison with urban areas (~ 350 buildings per km²) but not as low as in rural areas. The average distance between three neighbouring buildings is 14.4 m with a standard deviation of 12.6 m. In comparison, Schubert and Sanders (2012) computed an average gap between buildings in an urban environment of 3.8 m. Hence, the village can be classified as a typical peri-urban settlement. The majority of the buildings are of residential and combined residential/commercial use. In the south and the north of the study area, two clusters of industrial/commercial buildings are located.

2.2 Flood inundation model

A flood inundation model of the area was set up using the software Iber (Bladé et al. 2014). The model solves the 2D depth-averaged shallow water equations by means of a finite

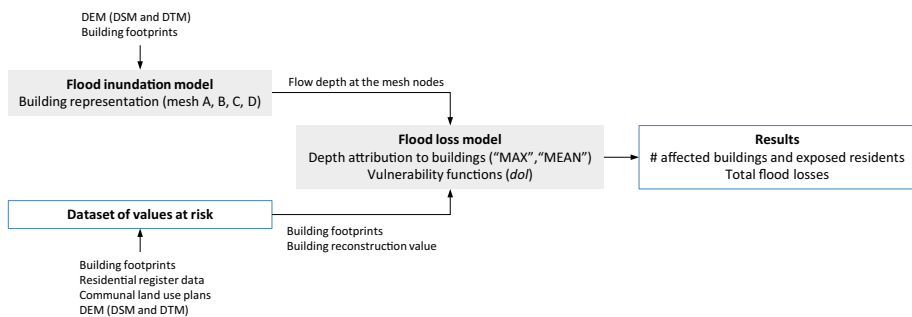


Fig. 1 Flow diagram of the methodology: flood inundation model, flood loss model and dataset of values at risk



Fig. 2 Extent of the study area. The Zulig River flows from NE to W through the village of Steffisburg

volume method. It computes the water depth and the two horizontal components of the depth-averaged velocity, the former constituting the basis for the flood hazard assessment in this work. The model Iber has been successfully applied in a wide range of flood modelling studies (Bodoque et al. 2016; González-Aguirre et al. 2016; Álvarez et al. 2017; Bonasia et al. 2017), including detailed flood assessments in urban areas, in which the flow depth field was evaluated at the scale of the streets and buildings (Garrote et al. 2016; Bermúdez et al. 2017). For a detailed description of the model and additional validation examples, we refer to Bladé et al. (2014) and Cea et al. (2016), and the references therein. The model is run in an uncalibrated mode using typical physical values for the Manning roughness coefficient, as proposed by Zischg et al. (2018). This is justified due to the low sensitivity of the model to the friction parameter and the absence of documented flood events that could be used for validation.

We set up the flood inundation model at the micro-scale, which implies that exposure and hazard must be assessed at the scale of individual elements at risk such as buildings or infrastructures. The flood model must, therefore, represent flows at this targeted spatial scale. The domain was discretized accordingly by an unstructured computational mesh at a very high spatial resolution, with mesh sizes of 2.5 m in the built-up areas and the river channel, and between 5 and 10 m in the non-urbanized areas. Element size is thus smaller than the critical length scales determined by building dimensions and building separation distances (Fewtrell et al. 2008). The total number of elements in the mesh is approximately 1,000,000, the exact number is depending on the mesh set-up explained below. We used a 0.5-m resolution digital elevation model (DEM) derived from LiDAR and a building footprint map to define the model geometry. Two different DEMs were used in this study: a “bare-earth” digital terrain model (DTM) and a digital surface model (DSM) which incorporates the elevation of the buildings (i.e. the heights of the rooftops). Four different

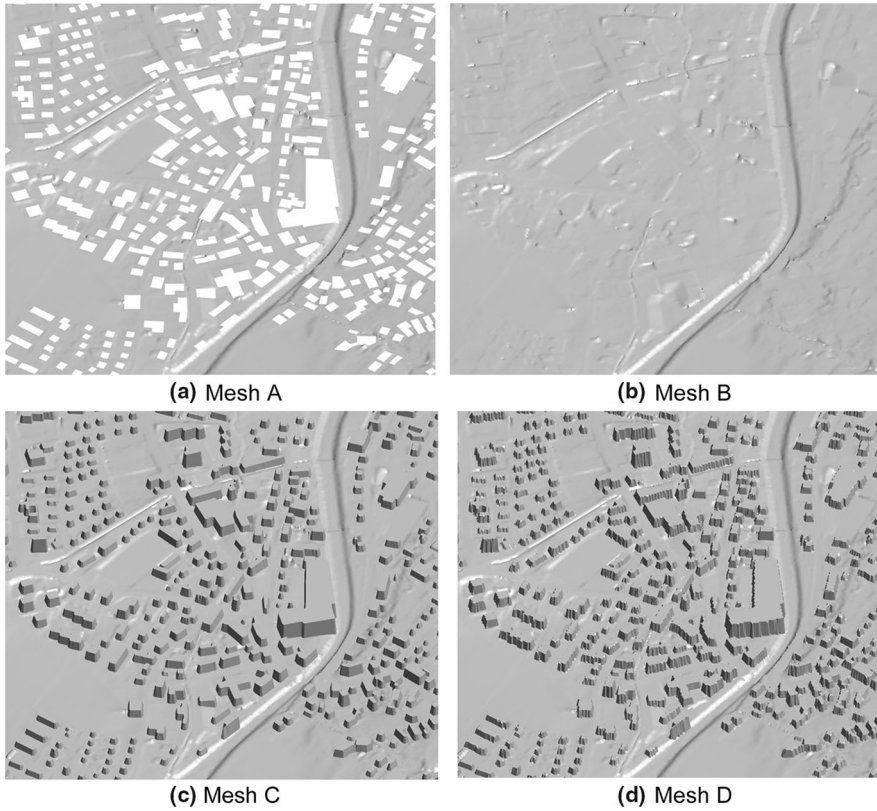


Fig. 3 Mesh geometries with different representations of the buildings (3D view). In **a**, buildings are represented as holes, while in **b–d** the area covered by the buildings is part of the mesh. The z -coordinates of the nodes within the building footprints equal the values of the DTM in **b** and the values of the DSM in **c** and **d**

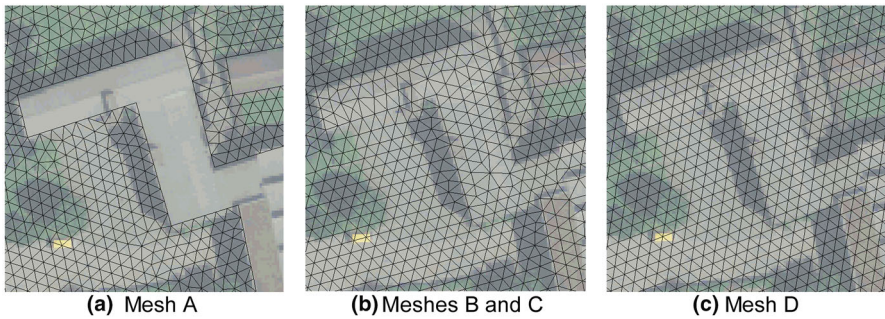


Fig. 4 Detail of the mesh around a building, overlaid on an aerial image. Meshes B and C are identical in this plan view, although elevations assigned to the nodes within the building footprint differ. Building footprints serve as constraints for mesh generation in meshes A, B and C

mesh configurations were considered (Figs. 3, 4), which differ on the building representation, as follows:

- *Mesh A* The building hole method BH is used to represent the buildings. Buildings are thus void areas in the mesh and buildings' walls fit exactly with numerical mesh edges.
- *Mesh B* Buildings are not represented in the model. For this purpose, the area covered by the buildings is not excluded from the calculation domain and the topography is defined from the DTM. The building footprint is still used to generate the mesh, so the mesh nodes located in the building walls stay at the same location as in mesh A.
- *Mesh C* The building block method BB is used to represent the buildings. This means that the buildings are not excluded from the calculation domain, and they appear as blocks with the height of the roofs in the mesh. The building footprint is used to generate the mesh, so building walls are aligned with internal element edges in the mesh (Fig. 4b). This allows a precise representation of the contours of the buildings in the mesh, as shown in Fig. 3c.
- *Mesh D* The building block method BB is used to represent the buildings, as in mesh C. However, the building footprint is not used to create the mesh, so mesh nodes are not forced to lie along the building footprint (Fig. 4c). As a consequence, the mesh cannot fit exactly the walls of the buildings, no matter how fine the resolution of the mesh is. Building walls are thus subject to an effect similar to the “staircase effect” that appears at curved and slanted interface boundaries on regular Cartesian grids (Kumar et al. 2009), as can be seen in Fig. 3d.

2.3 Values at risk

In this study, we focus on losses to buildings. Damages on house content, infrastructure or indirect losses are not considered. Hence, the dataset of the values at risk consists of a spatial dataset representing the buildings and their characteristics. The building is spatially represented by its footprint polygon. This basic dataset was extracted from the terrain model of the Federal Office for Topography (swisstopo). Adjacent polygons were merged to one polygon. We attributed the data of the residential register to the building footprints. These data were provided by the Federal Office for Statistics. This results in the number of residents per building. With this dataset, it was possible to classify all buildings with residential purpose. In a further step, we attributed the land-use categories of the communal land-use plans to each building. This leads to a distinction between buildings with residential, commercial, industrial and public purpose. Moreover, we attributed the volume of the building by computing the average difference between DSM and DTM and multiplying it with the footprint area. The reconstruction value of each building was successively computed on the basis of the volume and a typical price per volume differentiated by building category. The approach followed the methods presented in Fuchs et al. (2015, 2017) and Röthlisberger et al. (2017).

2.4 Flood loss model

The flood loss model combines the outcomes of the inundation model with the dataset of the values at risk. To allow the assessment of the uncertainties in the methods for representing the buildings in the mesh and in the methods for attributing flow depths to the buildings, the flood loss model has to be designed in a flexible way. The spatial representation of the buildings by their footprints is held constant in all methods for pre-

processing the mesh. However, depending on the representation of the buildings in the mesh, the flow depth attribution method changes. Thus, the flood loss model allows to consider different set-ups. In all set-ups, a building is counted as affected by the flood process if (a) a mesh node within the building footprint or (b) a mesh node at the border of the building footprint has a flow depth > 0 . In addition, the model allows the consideration of a building as affected if (c) a mesh node within a user-defined buffer distance is modelled as wet.

To account for the different building representation methods in one flood loss model, we set up the procedure described in the following steps. In a first step, the computational mesh of the Iber flood model is read in and a point dataset of nodes is created. Second, the nodes point dataset is intersected with the building footprint dataset and a topology table is created. Herein, two situations can be handled. The intersection between both datasets results in a new point dataset. This dataset contains all buildings that have nodes of the computational mesh located within its footprint polygon. All other buildings not having any nodes located within their footprints are considered in a further step. For these buildings, a near table is computed by considering a maximum buffer distance and a maximal number of nodes to consider in the neighbourhood analysis. This results in a table listing the mesh nodes that are relevant for attributing the flow depths to the building. The buffer distance and the maximum number of points to be considered in the analysis can be defined by the user. In our study, we defined a search radius of 0.5 m and a maximum number of 100 nodes to consider in the neighbourhood analysis. Third, the simulation outputs of the Iber model, i.e. the flow depths per mesh node and time step, are read into an array.

For each building, it is iteratively searched in the topology tables if the building intersects directly or indirectly (neighbourhood) with the mesh nodes. If the intersection between building and mesh nodes is a direct overlay, the flow depth is directly attributed to the building from the flow depths located within the building footprint. This can be done either by computing the average (MEAN) or the maximum flow depth of all nodes (MAX). If the building has no mesh nodes within its footprint, the flow depth is attributed from the neighbouring mesh nodes. Herein, also the average or the maximum could be defined depending on the research question. However, in the case of the “MEAN” attribution method, the average is computed by inversely weighting the distance between the building and the mesh nodes. The flow depth attribution is done for each time step of the flood inundation simulation. Consequently, a flow depth hydrograph is extracted for each building. In a subsequent step, the maximum flow depth over all time steps for each building is used to compute the degree of loss by means of the vulnerability function.

In this study, we used the vulnerability functions of Totschnig et al. (2011), Papathoma-Köhle et al. (2015), Hydrotec (2001), as cited in Merz and Thieken (2009), Jonkman et al. (2008) and Dutta et al. (2003). We used different vulnerability functions because, on the one hand, we aim at assessing the uncertainties in this part of the flood loss model and, on the other hand, we do not have loss data to validate the loss function or to choose the function with the highest fit. However, each of the selected vulnerability functions allows us to delineate a degree of loss for each building depending on the magnitude of the flood, i.e. the flow depth at the building scale in our case. The degree of loss *dol* resulting from the vulnerability function and the flow depth is used to compute the loss of the building. This is done by multiplying the *dol* with the reconstruction value of each building. Finally, all losses computed at single building level are summed up at the level of the study area.

With these specifications, the flood loss module is able to consider all four approaches for representing the buildings in the loss modelling. In mesh A, only the mesh nodes within

a distance of 0.5 m from the outline of the building footprint are considered in the flow depth attribution. In meshes B, C, and D, the mesh nodes within the building footprint or within a distance of 0.5 m from the outline are considered.

3 Results and discussion

The application of the flood loss model on the outcomes of four different flood inundation models, combined with two flow depth attribution methods and five vulnerability functions, resulted in forty simulation results. The number of affected buildings ranges from 572 to 618, and the number of exposed residents ranges from 3373 to 3502. The results of the exposure analyses are shown in Table 1. Mesh set-up D shows the lowest numbers of exposed buildings and residents, while mesh A shows the highest. Although the variability in the exposure is below 8%, this demonstrates that the procedure is sensitive to the mesh set-up and the approach of representing the buildings in the mesh.

Differences in flood extent between meshes A, C and D, which include different representations of the buildings, are below 0.3%. On the other hand, mesh B shows an increase in the flooded area of around 10% with respect to the other mesh configurations. However, given that buildings are not represented in mesh B, the internal area of affected buildings is counted as flooded area.

In contrast to the flood exposure, the flow depths at single building vary markedly with the mesh set-up and the flow depth attribution method. Figure 5 shows a comparison between the mesh set-ups and the flow depth attribution method. Obviously, the “MAX” flow depth attribution method results in higher flow depths at building scale than the “MEAN” method. The differences are particularly high for mesh C and mesh D, given that the dry nodes within the building footprint (nodes with the height of the rooftops) are used in the calculation of the mean depth of the building. In these cases, the “MEAN” method underestimates flow depths. In an additional calculation, we removed the nodes within the buildings and counted only the nodes at the outline of the building footprint in meshes B and C, or the neighbouring mesh nodes in mesh D. If the nodes within the building are excluded from the flood loss calculation, the flow depths are higher and more similar to the ones computed with mesh A (see Table 2). In the case of mesh B, the difference with the original mean depth value is very small, given that the nodes within the footprint are assigned the height of the ground and can thus be flooded. This leads to the conclusion that in averaging the flow depths (“MEAN” attribution method), the nodes within the building footprints should be excluded if their *z*-coordinates represent the building heights (BB method) and consequently do not exhibit relevant flow depths.

Table 1 Flood extent, number of exposed residents and number of affected buildings with the different mesh configurations

Mesh	Flood extent (m ²)	# Affected buildings	# Exposed residents
A	1,107,339	618	3502
B	1,242,711	592	3447
C	1,107,045	589	3391
D	1,110,062	572	3373

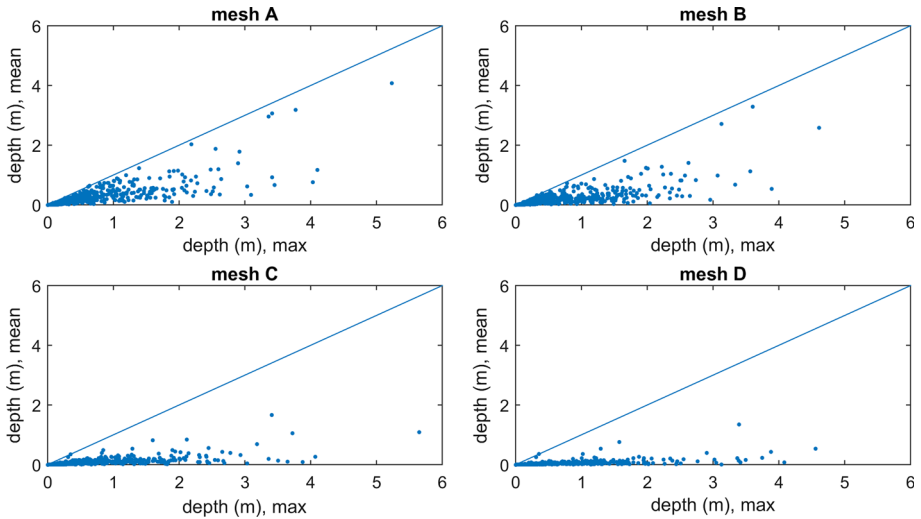


Fig. 5 Scatter plot of depth values assigned to each building with the different hazard attribution methods

Table 2 Average depth (m) attributed to buildings

Mesh	Flow depth (m) “MAX” attribution method	Flow depth (m) “MEAN” attribution method	Flow depth (m) “MEAN” attribution method (nodes within buildings excluded)
A	0.623	0.248	Not applicable
B	0.624	0.190	0.192
C	0.667	0.088	0.242
D	0.655	0.046	0.263

On average over all buildings, the flow depths attributed to the buildings by the “MAX” attribution method are systematically and markedly higher than the ones computed with the “MEAN” method. It should be noted that differences are also very relevant for mesh A, which has no nodes within the building footprints, and for mesh B, in which the nodes of the building footprint are assigned the height of the ground and can thus be flooded. In this relatively steep study area, the range of z -coordinates at the outlines of the building footprints (i.e. the difference between the minimum and maximum altitudes of the building footprint) is 0.78 m on average. Large buildings have a length of up to 80 m, which results in an altitude difference of up to 8.8 m. This significant variation in z -coordinates across the footprints results in variable flow depths within a single building. A significant portion of all buildings is only partially wet. It is concluded from the above that, as the flow depth is relevant for the computation of the degree of loss, the flood loss computation is highly sensitive to the flow depth attribution method.

When comparing the flow depths at building scale of the different mesh set-ups, the relevance of the flow depth attribution method becomes obvious again (see Fig. 6). However, the “MAX” attribution method has a relatively low sensitivity to the mesh set-up. The flow depths assigned to buildings are very similar for all four mesh set-ups. In

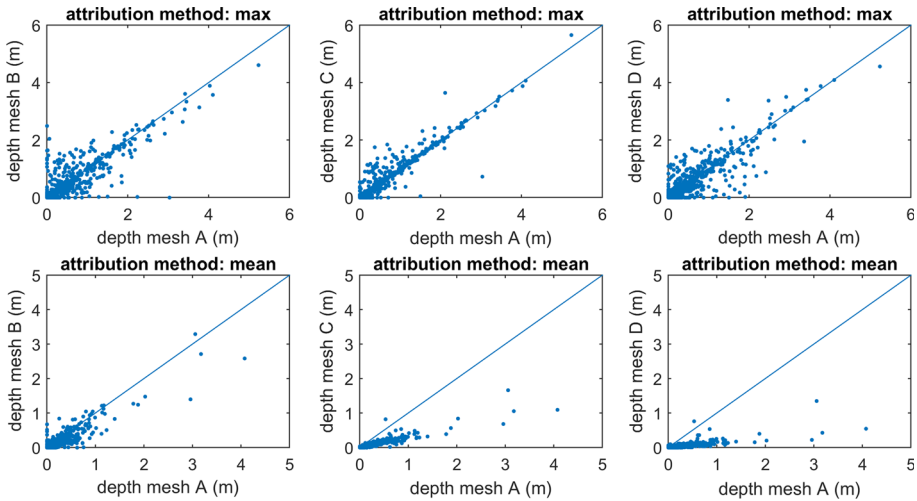


Fig. 6 Scatter plot of depth values assigned to each building with the different mesh configurations

contrast, the “MEAN” attribution method implies a higher sensitivity as meshes C and D result in significantly lower depths in buildings than meshes A and B. The averaged flow depths (“MEAN”) differ markedly between the mesh set-up, whereas the maximum flow depths (“MAX”) do not vary significantly. Hence, the latter flow depth assignment method produces robust estimations. It should be noted, however, that this robustness does not imply that the accuracy of the method is necessarily superior. If flow depths vary significantly across a single building, the depths obtained with the “MAX” attribution method might not be representative for damage assessment and produce an overestimation of losses.

The generally higher flow depths computed with the “MAX” assignment method result consequently in higher losses. Table 3 shows the computed flood losses on buildings summed up for the study area. The overall losses range from 800,000 CHF to 284 million

Table 3 Total flood losses in million Swiss Francs (CHF)

Mesh	Hazard attribution	Vulnerability function					Mean ± SD
		Totschnig et al. (2011)	Papathoma-Köhle et al. (2015)	Hydrotec (2001)	Jonkman et al. (2008)	Dutta et al. (2003)	
A	MAX	264.9	248.3	241.0	73.0	237.8	213.0 ± 78.9
	MEAN	33.2	41.9	123.5	14.0	100.1	62.5 ± 46.8
B	MAX	265.5	247.2	235.4	70.5	233.6	210.4 ± 79.3
	MEAN	21.9	28.6	103.5	10.6	81.5	49.2 ± 40.8
C	MAX	284.0	263.8	243.9	76.8	243.7	222.4 ± 83.1
	MEAN	2.9	5.0	60.5	4.9	42.3	23.1 ± 26.6
D	MAX	248.0	238.0	236.5	80.3	228.1	206.2 ± 70.7
	MEAN	0.8	1.6	38.5	2.9	26.9	14.2 ± 17.4

CHF. This is a remarkable uncertainty range and thus it underlines the importance of this sensitivity analysis. The flood loss computation is markedly sensitive to both the vulnerability function and the flow depth attribution method. While the first observation is in line with other studies (Apel et al. 2008, 2009; de Moel and Aerts 2011), the second observation adds new insights in the discussion of uncertainties in flood loss modelling. Depending on the flow depth attribution method, the total loss differs by two orders of magnitude. This can be explained by the differences in the flow depths at the single buildings. Especially, the consideration of mesh nodes within building footprint has to be avoided in averaging flow depths if these mesh nodes do not represent the z -coordinates of the ground floor but those of the roof top.

However, if only one vulnerability function and one flow depth attribution method is considered distinctly, but the mesh set-up is varied, the losses result as relatively robust. While mesh A is the most conservative in terms of number of exposed buildings and residents, it is not the most conservative in total losses. Mesh C with the “MAX” attribution method results in the highest losses.

From the viewpoint of the vulnerability functions, the one described by Jonkman et al. (2008) results in the lowest losses. This function was elaborated on data in the Netherlands. Still, the presented case study in an Alpine environment might differ markedly from a lowland situation in terms of process characteristics. The functions of Totschnig et al. (2011) and Paphoma-Köhle et al. (2015) consider torrential processes and sediment transport and might be more adequate for this case study. Nevertheless, as Cammerer et al. (2013) and Amadio et al. (2016) discussed, the transferability of vulnerability functions may be questioned in any case. However, the choice of the vulnerability function and a validation was out of scope of this study and the focus was laid on the comparison of different uncertainty sources.

From the view point of the real-world applicability, the four building representation methods applied in this work have distinct advantages and disadvantages, and the choice of method will depend on the available data and the particular application. All four methods result in computationally demanding simulations, given the grid size required to capture the complex flow between buildings. For applications that require multiple simulations or fast results, the development of computationally more efficient surrogates of these models might become necessary (Bermúdez et al. 2018). Model set-up complexity does vary significantly between the methods and is thus likely to be a more relevant criterion for choosing an approach. If a suitable DSM is available, the approach corresponding to mesh D (i.e. the BB method without building geometry data) is the easiest to implement, given that building footprints are not used to constrain the mesh. However, in order to capture precisely the contours of the buildings, a very fine grid is needed. On the other hand, methods which make use of building footprints to produce sharp elevation changes at building interfaces (meshes A and C in this work) are more demanding from a pre-processing perspective. However, they could potentially allow for a certain mesh size optimization, up to the critical grid sizes defined by building dimensions and separation distances, as noted by Fewtrell et al. (2008). This aspect is beyond the scope of this work, and no coarsening was applied in this study to ensure consistency between the four mesh configurations. The number of mesh elements can be further reduced if the buildings are represented as holes in the mesh (as in mesh A). However, this may be a disadvantage for certain applications, such as the computation of rainfall–runoff transformation from direct precipitation over the model domain. If the mesh excludes the areas covered by the buildings, the rainfall fields need to be modified to account for the artificial loss of area.

4 Conclusions

The presented model experiment allowed to assess and compare two uncertainty sources in flood loss modelling at the micro-scale. We analysed the sensitivity of a typical flood loss modelling set-up to the method for representing the buildings in the computational mesh of 2D flood models and to the method for assigning flow depths from the simulation outcomes to the single buildings.

The model experiment leads to the following main conclusions.

1. At the micro-scale, the topology between a building footprint and the computational mesh in a high spatial resolution is characterized by a high number of mesh nodes per building. Thus, the flow depths of the mesh nodes have to be interpolated in some way to assign the flow depth to the building since this parameter is needed for computing the degree of loss and consequently the loss at single building scale. As the flow depth attribution method can significantly influence the outcomes of flood loss analyses, we recommend that the chosen method is explicitly described in future studies.
2. The attribution of the maximum flow depth of all nodes within the building footprint and a specified buffer distance to the building is robust. With this attribution method, the mesh set-up (i.e. the method of representing the buildings in the computational mesh) does not significantly influence the loss estimation. In contrast, it becomes relevant when the flow depths are averaged over all nodes within the building. Herein, the nodes within the building footprint but representing the heights of the roof tops rather than the ground floor level result in flow depths of 0 m. Hence, these nodes should not be considered in averaging the flow depths. The mesh set-up should thus be designed so that it fits with the flow depth attribution method.
3. The exposure assessment is not highly sensitive to the building representation method. From this perspective, the benefits of using the more complex building representation methods in the flood inundation model are not clear. Results, however, showed that this low sensitivity to the mesh set-up is valid for the maximum flow depth attribution method only. Hence, in low-density peri-urban environments, the way how to consider the buildings in the mesh is dependent on the flow depth attribution method and thus it plays a role for exposure and flood loss estimations. Hence, further analyses should be aimed at finding a threshold for building density that acts as a proxy for areas in which the building representation method is relevant or not.

Software availability A free version of the model Iber is available for download at www.iberaula.es. The flood loss model and the procedure for processing the Iber simulation outcomes are incorporated in a Python script. The code with the functions used in this study is available at GitHub <https://github.com/zischg/IBERfloodlossmodel>. The functions follow mainly the procedure described in the method section.

Acknowledgements The authors thank the Swiss Federal Office for Statistics for providing the residential register, the Swiss Federal Office for Topography for providing the building dataset and the Canton of Bern, Switzerland for providing the Lidar terrain model. María Bermúdez gratefully acknowledges financial support from the Spanish Regional Government of Galicia (postdoctoral Grant reference ED481B 2014/156-0). Andreas Paul Zischg gratefully acknowledges financial support from the Swiss National Foundation (Grant No. IZK0Z2_170478/1).

Compliance with ethical standards

Conflict of interest The authors declare that they have no conflict of interest.

References

- Abdullah AF, Vojinovic Z, Price RK, Aziz NAA (2012) Improved methodology for processing raw LiDAR data to support urban flood modelling—accounting for elevated roads and bridges. *J Hydroinform* 14:253–269. <https://doi.org/10.2166/hydro.2011.009>
- Abily M, Bertrand N, Delestre O et al (2016) Spatial global sensitivity analysis of high resolution classified topographic data use in 2D urban flood modelling. *Environ Model Softw* 77:183–195. <https://doi.org/10.1016/j.envsoft.2015.12.002>
- Álvarez M, Puertas J, Peña E, Bermúdez M (2017) Two-dimensional dam-break flood analysis in data-scarce regions: the case study of Chipembe Dam, Mozambique. *Water* 9:432. <https://doi.org/10.3390/w9060432>
- Amadio M, Mysiak J, Carrera L, Koks E (2016) Improving flood damage assessment models in Italy. *Nat Hazards* 82:2075–2088. <https://doi.org/10.1007/s11069-016-2286-0>
- Apel H, Thielen AH, Merz B, Blöschl G (2006) A probabilistic modelling system for assessing flood risks. *Nat Hazards* 38:79–100. <https://doi.org/10.1007/s11069-005-8603-7>
- Apel H, Merz B, Thielen AH (2008) Quantification of uncertainties in flood risk assessments. *Int J River Basin Manag* 6:149–162. <https://doi.org/10.1080/15715124.2008.9635344>
- Apel H, Aronica GT, Kreibich H, Thielen AH (2009) Flood risk analyses—how detailed do we need to be? *Nat Hazards* 49:79–98. <https://doi.org/10.1007/s11069-008-9277-8>
- Arrighi C, Brugini M, Castelli F et al (2013) Urban micro-scale flood risk estimation with parsimonious hydraulic modelling and census data. *Nat Hazards Earth Syst Sci* 13:1375–1391. <https://doi.org/10.5194/nhess-13-1375-2013>
- Bellos V, Tsakiris G (2015) Comparing various methods of building representation for 2D flood modelling in built-up areas. *Water Resour Manag* 29:379–397. <https://doi.org/10.1007/s11269-014-0702-3>
- Bermúdez M, Neal JC, Bates PD et al (2017) Quantifying local rainfall dynamics and uncertain boundary conditions into a nested regional-local flood modeling system. *Water Resour Res* 53:2770–2785. <https://doi.org/10.1002/2016WR019903>
- Bermúdez M, Ntegeka V, Wolfs V, Willems P (2018) Development and comparison of two fast surrogate models for urban pluvial flood simulations. *Water Resour Manag*. <https://doi.org/10.1007/s11269-018-1959-8>
- Bladé E, Cea L, Corestein G et al (2014) Iber: herramienta de simulación numérica del flujo en ríos. *Rev Int Métodos Numéricos para Cálculo y Diseño en Ing* 30:1–10. <https://doi.org/10.1016/j.rimmi.2012.07.004>
- Bodoque JM, Amérgo M, Díez-Herrero A et al (2016) Improvement of resilience of urban areas by integrating social perception in flash-flood risk management. *J Hydrol* 541:665–676. <https://doi.org/10.1016/j.jhydrol.2016.02.005>
- Bonasia R, Areu-Rangel OS, Tolentino D et al (2017) Flooding hazard assessment at Tulancingo (Hidalgo, Mexico). *J Flood Risk Manag*. <https://doi.org/10.1111/jfr3.12312>
- Cammerer H, Thielen AH, Lammel J (2013) Adaptability and transferability of flood loss functions in residential areas. *Nat Hazards Earth Syst Sci* 13:3063–3081. <https://doi.org/10.5194/nhess-13-3063-2013>
- Cea L, Vázquez-Cendón ME (2009) Unstructured finite volume discretization of two-dimensional depth-averaged shallow water equations with porosity. *Int J Numer Methods Fluids*. <https://doi.org/10.1002/flid.2107>
- Cea L, Bermúdez M, Puertas J et al (2016) IberWQ: new simulation tool for 2D water quality modelling in rivers and shallow estuaries. *J Hydroinform* 18:816–830. <https://doi.org/10.2166/hydro.2016.235>
- Chen AS, Evans B, Djordjević S et al (2012a) A coarse-grid approach to representing building blockage effects in 2D urban flood modelling. *J Hydrol*. <https://doi.org/10.1016/j.jhydrol.2012.01.007>
- Chen AS, Evans B, Djordjević S, Savić DA (2012b) Multi-layered coarse grid modelling in 2D urban flood simulations. *J Hydrol* 470:1–11. <https://doi.org/10.1016/j.jhydrol.2012.06.022>
- Davis SA, Skaggs LL (1992) Catalog of residential depth-damage functions used by the army corps of engineers in flood damage estimation. IWR report 92-R-3, Institute for Water Resources, US Army Corps of Engineers, Ft. Belvoir, VA
- de Almeida GAM, Bates P, Ozdemir H (2016) Modelling urban floods at sub-metre resolution: challenges or opportunities for flood risk management? *J Flood Risk Manag*. <https://doi.org/10.1111/jfr3.12276>

- de Moel H, Aerts JCJH (2011) Effect of uncertainty in land use, damage models and inundation depth on flood damage estimates. *Nat Hazards* 58:407–425. <https://doi.org/10.1007/s11069-010-9675-6>
- Dutta D, Herath S, Musiak K (2003) A mathematical model for flood loss estimation. *J Hydrol* 277:24–49. [https://doi.org/10.1016/S0022-1694\(03\)00084-2](https://doi.org/10.1016/S0022-1694(03)00084-2)
- Environment Agency (2014) The updated flood map for surface water (uFMfSW) property points dataset. Bristol, UK. <https://data.gov.uk/dataset/risk-of-flooding-from-surface-water-suitability>
- Ernst J, Dewals BJ, Detrembleur S et al (2010) Micro-scale flood risk analysis based on detailed 2D hydraulic modelling and high resolution geographic data. *Nat Hazards* 55:181–209. <https://doi.org/10.1007/s11069-010-9520-y>
- Fewtrell TJ, Bates PD, Horritt M, Hunter NM (2008) Evaluating the effect of scale in flood inundation modelling in urban environments. *Hydrol Process* 22:5107–5118. <https://doi.org/10.1002/hyp.7148>
- Fewtrell TJ, Duncan A, Sampson CC et al (2011) Benchmarking urban flood models of varying complexity and scale using high resolution terrestrial LiDAR data. *Phys Chem Earth* 36:281–291. <https://doi.org/10.1016/j.pce.2010.12.011>
- Freni G, La Loggia G, Notaro V (2010) Uncertainty in urban flood damage assessment due to urban drainage modelling and depth–damage curve estimation. *Water Sci Technol* 61:2979–2993. <https://doi.org/10.2166/wst.2010.177>
- Fuchs S, Birkmann J, Glade T (2012) Vulnerability assessment in natural hazard and risk analysis: current approaches and future challenges. *Nat Hazards* 64:1969–1975. <https://doi.org/10.1007/s11069-012-0352-9>
- Fuchs S, Keiler M, Zischg A (2015) A spatiotemporal multi-hazard exposure assessment based on property data. *Nat Hazards Earth Syst Sci* 15:2127–2142. <https://doi.org/10.5194/nhess-15-2127-2015>
- Fuchs S, Röthlisberger V, Thaler T et al (2017) Natural hazard management from a coevolutionary perspective: exposure and policy response in the European Alps. *Ann Am Assoc Geogr* 107:382–392. <https://doi.org/10.1080/24694452.2016.1235494>
- Garrote J, Alvarenga FM, Díez-Herrero A (2016) Quantification of flash flood economic risk using ultra-detailed stage—damage functions and 2-D hydraulic models. *J Hydrol* 541:611–625. <https://doi.org/10.1016/j.jhydrol.2016.02.006>
- González-Aguirre JC, Vázquez-Cendón ME, Alavez-Ramírez J (2016) Simulación numérica de inundaciones en Villahermosa México usando el código IBER. *Ing del agua* 20:201. <https://doi.org/10.4995/ia.2016.5231>
- Green CH (2003) The handbook of water economics: principles and practice. Wiley, New York
- Guinot V (2012) Multiple porosity shallow water models for macroscopic modelling of urban floods. *Adv Water Resour* 37:40–72. <https://doi.org/10.1016/j.advwatres.2011.11.002>
- Horritt M, Bates PD (2002) Evaluation of 1D and 2D numerical models for predicting river flood inundation. *J Hydrol* 268:87–99. [https://doi.org/10.1016/S0022-1694\(02\)00121-X](https://doi.org/10.1016/S0022-1694(02)00121-X)
- Hydrotec (2001) Hochwasser-Aktionsplan Angerbach (Flood action plan for the river Angerbach). Teil I: Berichte und Anlagen. Studie im Auftrag des Stua Dusseldorf. Aachen, Germany
- Jonkman SN, Bočkarjova M, Kok M, Bernardini P (2008) Integrated hydrodynamic and economic modelling of flood damage in the Netherlands. *Ecol Econ* 66:77–90. <https://doi.org/10.1016/j.ecolecon.2007.12.022>
- Kreibich H, Piroth K, Seifert I et al (2009) Is flow velocity a significant parameter in flood damage modelling? *Nat Hazards Earth Syst Sci* 9:1679–1692
- Kumar B, Bhatt G, Duffy CJ (2009) An efficient domain decomposition framework for accurate representation of geodata in distributed hydrologic models. *Int J Geogr Inf Sci* 23:1569–1596. <https://doi.org/10.1080/13658810802344143>
- McGrath H, Stefanakis E, Nastev M (2015) Sensitivity analysis of flood damage estimates: a case study in Fredericton, New Brunswick. *Int J Disaster Risk Reduct* 14:379–387. <https://doi.org/10.1016/J.IJDRR.2015.09.003>
- Merz B, Thielen AH (2009) Flood risk curves and uncertainty bounds. *Nat Hazards* 51:437–458. <https://doi.org/10.1007/s11069-009-9452-6>
- Merz B, Kreibich H, Schwarze R, Thielen A (2010) Assessment of economic flood damage. *Nat Hazards Earth Syst Sci* 10:1697–1724. <https://doi.org/10.5194/nhess-10-1697-2010>
- Notaro V, De Marchis M, Fontanazza CM et al (2014) The effect of damage functions on urban flood damage appraisal. *Procedia Eng* 70:1251–1260. <https://doi.org/10.1016/J.PROENG.2014.02.138>
- Ozdemir H, Sampson CC, de Almeida GAM, Bates PD (2013) Evaluating scale and roughness effects in urban flood modelling using terrestrial LiDAR data. *Hydrol Earth Syst Sci* 17:4015–4030. <https://doi.org/10.5194/hess-17-4015-2013>

- Papathoma-Köhle M, Zischg A, Fuchs S et al (2015) Loss estimation for landslides in mountain areas—an integrated toolbox for vulnerability assessment and damage documentation. *Environ Model Softw* 63:156–169. <https://doi.org/10.1016/J.ENVSOF.2014.10.003>
- Papathoma-Köhle M, Gems B, Sturm M, Fuchs S (2017) Matrices, curves and indicators: a review of approaches to assess physical vulnerability to debris flows. *Earth Sci Rev* 171:272–288. <https://doi.org/10.1016/J.EARSCIREV.2017.06.007>
- Qi H, Altinakar MS (2011) Simulation-based decision support system for flood damage assessment under uncertainty using remote sensing and census block information. *Nat Hazards* 59:1125–1143. <https://doi.org/10.1007/s11069-011-9822-8>
- Röthlisberger V, Zischg AP, Keiler M (2017) Identifying spatial clusters of flood exposure to support decision making in risk management. *Sci Total Environ* 598:593–603. <https://doi.org/10.1016/j.scitotenv.2017.03.216>
- Sampson CC, Fewtrell TJ, Duncan A et al (2012) Use of terrestrial laser scanning data to drive decimetric resolution urban inundation models. *Adv Water Resour* 41:1–17. <https://doi.org/10.1016/j.advwatres.2012.02.010>
- Sampson CC, Fewtrell TJ, O’Loughlin F et al (2014) The impact of uncertain precipitation data on insurance loss estimates using a flood catastrophe model. *Hydrol Earth Syst Sci* 18:2305–2324. <https://doi.org/10.5194/hess-18-2305-2014>
- Schubert JE, Sanders BF (2012) Building treatments for urban flood inundation models and implications for predictive skill and modeling efficiency. *Adv Water Resour* 41:49–64. <https://doi.org/10.1016/j.advwatres.2012.02.012>
- Staffler H, Pollinger R, Zischg A, Mani P (2008) Spatial variability and potential impacts of climate change on flood and debris flow hazard zone mapping and implications for risk management. *Nat Hazards Earth Syst Sci* 8:539–558. <https://doi.org/10.5194/nhess-8-539-2008>
- Totschnig R, Sedlacek W, Fuchs S (2011) A quantitative vulnerability function for fluvial sediment transport. *Nat Hazards* 58:681–703. <https://doi.org/10.1007/s11069-010-9623-5>
- Zischg A, Schober S, Sereinig N et al (2013) Monitoring the temporal development of natural hazard risks as a basis indicator for climate change adaptation. *Nat Hazards* 67:1045–1058. <https://doi.org/10.1007/s11069-011-9927-0>
- Zischg AP, Mosimann M, Bernet DB, Röthlisberger V (2018) Validation of 2D flood models with insurance claims. *J Hydrol* 557:350–361. <https://doi.org/10.1016/J.JHYDROL.2017.12.042>

Paper 16: Bernet, D.; Zischg, A.; Prasuhn, V.; Weingartner, R., 2018: Modeling the extent of surface water floods in rural areas: lessons learned from the application of various uncalibrated models. *Environmental Modelling & Software*, 109, 134–151, doi:10.1016/j.envsoft.2018.08.005.



Modeling the extent of surface water floods in rural areas: Lessons learned from the application of various uncalibrated models



Daniel B. Bernet^{a,b,c,*}, Andreas Paul Zischg^{a,b,c}, Volker Prasuhn^d, Rolf Weingartner^{a,b,c}

^a Institute of Geography, University of Bern, CH-3012, Bern, Switzerland

^b Oeschger Centre for Climate Change Research, University of Bern, Falkenplatz 16, CH-3012, Bern, Switzerland

^c Mobiliar Lab for Natural Risks, University of Bern, Hallerstrasse 12, CH-3012, Bern, Switzerland

^d Agroscope, Research Division, Agroecology and Environment, Reckenholzstrasse 191, CH-8046, Zurich, Switzerland

ARTICLE INFO

Keywords:

Surface water flood
Rural environment
Flood inundation model
Uncalibrated
Validation

ABSTRACT

Surface water floods (SWFs) do not only increasingly threaten cities, but also affect rural areas. So far, little research has been dedicated to the prediction of SWFs in rural environments, although in practice the process is already being considered in deterministic flood hazard assessments. To test the validity of such assessments, we select four raster-based models with differing complexity and evaluate whether they reliably predict inundated areas by SWF in rural areas. The uncalibrated models are first applied to four artificial surfaces and second, to eight case studies covering manifold geographical and meteorological settings. For the case studies, the models' prediction skills are assessed based on inundated areas inferred from various sources. The models' performance is rather low for all case studies, which highlights the necessity for calibration and/or validation of such models. Moreover, the case studies provide more general conclusions concerning the modeling of SWFs in rural areas.

Software availability

- FLO-2D (cf. Sect. 2.1.1)
 - Details: FLO-2D Pro (Build No. 16.06.16)
 - Developers: FLO-2D Software Inc. (P.O. Box 66, Nutrioso, AZ 85932, United States)
 - Requirements: Windows 7 or higher
 - Cost: \$995.00
 - URL: <https://www.flo-2d.com/flo-2d-pro/>
- FloodArea (cf. Sect. 2.1.2)
 - Details: FloodArea^{HPC}-Desktop 10.3 (4 Cores) on ArcGIS[®]10.3.0.4322
 - Developers: geomer GmbH (Im Breitenspiel 11 b, 69126 Heidelberg, Germany)
 - Requirements: Windows 7 or higher and ArcGIS[®]10.3
 - Cost: €11'845.00 for 4 cores (€3'875.00 for 1 core)
 - URL: <http://www.geomer.de/en/software/floodarea>
- r.sim.water (cf. Sect. 2.1.3)
 - Details: Module r.sim.water in GRASS GIS 7.2.0 (2016)
 - Developers: H. Mitasova, J. Hofierka, C. Thaxton (and GRASS Development Team)
 - Requirements: Windows, Linux or Mac OSX

- Cost: Free of charge (GNU General Public Licence)
- URL: <https://grass.osgeo.org/grass72/manuals/r.sim.water.html>
- MFD (cf. Sect. 2.1.4)
 - Details: Tool Flow Accumulation (Top-Down) with option “Multiple Flow Direction” in SAGA GIS 4.1.0 (64-bit)
 - Developers: O. Conrad and T. Grabs
 - Requirements: Windows or Linux
 - Cost: Free of charge (GNU General Public Licence)
 - URL: http://www.saga-gis.org/saga_tool_doc/4.1.0/ta_hydrology_0.html

1. Introduction

Economic losses caused by floods have been heavily increasing over the past decades in absolute terms (Thieken et al., 2007; Kron et al., 2012; Grahn and Nyberg, 2017), mostly driven by societal development (e.g. Cutter and Emrich, 2005), but possibly exacerbated by climate change (Falconer et al., 2009; Barredo, 2009; Kundzewicz et al., 2014). In particular, the frequency and the intensity of heavy rainfall is expected to increase in many places in the future (Kundzewicz et al., 2014). This has drawn growing attention to surface water floods (SWFs), which are caused by intense rainfall that cannot be drained

Abbreviations: DEM, digital elevation model; GA, Green-Ampt; SWF, surface water flood; UAV, unmanned aerial vehicle

* Corresponding author. Institute of Geography, University of Bern, CH-3012, Bern, Switzerland.

E-mail address: daniel.bernet@giub.unibe.ch (D.B. Bernet).

<https://doi.org/10.1016/j.envsoft.2018.08.005>

Received 9 August 2017; Received in revised form 14 June 2018; Accepted 3 August 2018

Available online 07 August 2018

1364-8152/ © 2018 Elsevier Ltd. All rights reserved.

altogether by means of natural and/or artificial drainage systems, stem from surcharged sewers, channels, culverted watercourses or ground-water springs and, consequently, result in ponded water and overland flow (Hankin et al., 2008; Falconer et al., 2009). With a particular high percentage of impermeable areas, cities are particularly prone to SWFs, as exemplified by recent devastating flood events affecting urbanized areas in Western Europe, such as Hull, UK (Pitt, 2008; Coulthard and Frostick, 2010), Copenhagen, DK (Haghighatafshar et al., 2014), Amsterdam, NL (Gaitan et al., 2016; Spekkers et al., 2017) or Münster, DE (Spekkers et al., 2017). Cities in developing countries are even more severely impacted, as examples from Southeast Asia (Chan et al., 2012; Hénonin et al., 2013) or Africa (Di Baldassarre et al., 2010; Kundzewicz et al., 2014) illustrate.

Not surprisingly, a lot of research is dedicated to urban areas in terms of modeling SWFs (e.g. Maksivović et al., 2009; Chen et al., 2012; Sampson et al., 2013; de Almeida et al., 2016), flood loss estimation (e.g. Merz et al., 2010; Jongman et al., 2012; van Ootegem et al., 2015) as well as flood risk assessment and management (e.g. Kaźmierczak and Cavan, 2011; Blanc et al., 2012; Zhou et al., 2012; Löwe et al., 2017). In contrast, relatively little research has been dedicated to rural areas, in spite the fact that such areas are highly exposed to flooding, as examples from the European Alps point out (Fuchs et al., 2015, 2017; Röthlisberger et al., 2017). At the same time, these areas are not only affected by fluvial floods, but similarly by SWFs (Bernet et al., 2017). Moreover, overland flow generated on rural or peri-urban areas may be transferred into urbanized areas and thereby contribute to the adverse effects of SWFs within the urban environment, as well (Andrieu et al., 2004; Yu and Coulthard, 2015). Thus, scientific studies regarding the link between SWFs and assets at risk in rural areas are generally lacking.

In contrast, the topic of how to prepare for and manage SWFs has been discussed outside of academia (Bernet et al., 2017). This has led to a wide range of manuals and guidelines regarding SWF hazard assessment, risk management and awareness raising at the point scale (e.g. Egli, 2007; Rüttimann and Egli, 2010), as well as on communal and regional scales (e.g. Castro et al., 2008; DWA, 2013; LUBW, 2016; CEPRI, 2014). Therein, the focus lies generally on the built environment and, thus, the rural areas are considered, as well.

In practice, the tools used for SWF hazard assessments, consist mainly of single deterministic simulations with two-dimensional (2D) flood inundation models (cf. Meon et al., 2009; Tyrna and Hochschild, 2010; Kipfer et al., 2015; Tyrna et al., 2017). This circumstance has certainly been influenced by the heavily increasing availability of high-resolution digital elevation models (DEMs), driven by advancing data collection techniques (Wechsler, 2007; Fewtrell et al., 2008; Sampson et al., 2012; Chen et al., 2012; Neal et al., 2012; Dottori et al., 2013; de Almeida et al., 2016; Savage et al., 2016a). At the same time, the applicability of hydrodynamic flood inundation models to finer resolutions has been supported by increasing computational power (Fewtrell et al., 2008; Hunter et al., 2008; Dottori et al., 2013; Savage et al., 2016b). However, the exploitation of high-resolution DEMs is still limited by computational constraints (Chen et al., 2012; Sampson et al., 2012; de Almeida et al., 2016; Savage et al., 2016a; b; Tyrna et al., 2017). Thus, rather simple flood inundation models are applied in practice for SWF hazard assessments, as they usually encompass large areas.

In general, a compromise is inevitable when applying a model, balancing spatial resolution, model complexity and computational efficiency (Horritt and Bates, 2001; Cook and Merwade, 2009; Fewtrell et al., 2008, 2011; Sampson et al., 2012; Neal et al., 2012; Dottori et al., 2013; Savage et al., 2016a; b). At the same time, it is not obvious how the specific choice influences the models' performance. Moreover, recent studies have pointed out that the uncertainty associated with flood inundation models fed with high-resolution DEMs are more complex than previously thought (Abily et al., 2016; Savage et al., 2016b). Meanwhile, the models' extreme precisions may provoke

overconfidence in their results, which could ultimately lead to wrong decisions in flood risk management (Dottori et al., 2013; Savage et al., 2016a).

Wrong decisions can usually be prevented by rigorously evaluating the applied models (e.g. Jakeman et al., 2006; Bennett et al., 2013). However, appropriate data are crucial for this task. Yet, there is an eminent lack of observational data (Blanc et al., 2012; Neal et al., 2012; Spekkers et al., 2014; Yu and Coulthard, 2015; Gaitan et al., 2016; Rözer et al., 2016), which impairs the applicability of such deterministic modeling approaches. Even more so for SWFs in rural areas, where the lack of observational data is particularly pronounced (Yu and Coulthard, 2015). In practice, however, the lack of observational data does not appear to prevent the use of single deterministic simulations for SWF hazard assessments. On the contrary, examples of overland flow predictions in urban, peri-urban and rural areas indicate that it rather leads to the renouncement of model calibration and/or validation (cf. Meon et al., 2009; Tyrna and Hochschild, 2010; Kipfer et al., 2015; Tyrna et al., 2017). Such approaches are employed to produce large-scale SWF hazard maps, as the examples of Kipfer et al. (2015) and Tyrna et al. (2017) indicate. In practice, these maps are then being used to identify potentially affected assets, such as buildings, infrastructure, agricultural fields, etc.

Thus, the question arises whether the deterministic tools reportedly used today in hazard assessments, e.g., for compiling SWF maps, are fit for their purpose of predicting areas exposed to SWF under various conditions. In particular, it is unclear how well such a modeling approach performs if such tools are not conditioned and/or evaluated due to a lack of observational data. Using this starting point, the main goal of this study is to evaluate whether uncalibrated and unvalidated 2D models can reliably predict the extent of SWFs in rural environments, on which basis potentially exposed assets can be identified, for instance. Based on this evaluation, we are able to draw conclusions about the suitability of this modeling approach for assessing the extent of SWFs, as well as for modeling SWFs in rural areas, in general.

For that matter, we directly explore the models' predictive skills by comparing their outputs (Teng et al., 2017). In the style of other studies benchmarking 2D models (e.g. Fewtrell et al., 2011; Neal et al., 2012; Néelz and Pender, 2013), we apply the models to artificial and real-world test cases. As a first exercise, we apply the selected models to four artificial surfaces, inspired by Zhou and Liu (2002). In this highly controlled and simplified environment, the models can easily be compared and inherent model characteristics are revealed. In a second exercise, the models are applied to real-world case studies. To mimic the commonly used approach in practical SWF hazard assessments, we apply similar uncalibrated 2D models with varying complexity. Thereafter, we quantitatively assess the models' predictive skills regarding the flooded area using common binary pattern performance measures (Bennett et al., 2013). As there are no data about flow depths, flow velocities or flow dynamics available, we only compare the simulated with the observed SWF extents. For that matter, we have reconstructed inundated areas based on various observational data sources.

The seven study sites encompass various topographies, slopes, land use etc., while each of the eight case studies is associated with either relatively heavy or weak rainfall, respectively. Thus, for the purpose of this study, we relax the definition of SWFs and include not only events triggered by heavy rainfall, but also events associated with weak rainfall. All events have in common that overland flow was produced, which led or could have led to damages to the built and unbuilt environment along the flow paths. As per definition, the inundations did not originate from overtopping watercourses, but are directly triggered by effective rainfall (cf. Bernet et al., 2017, for a discussion of related terms).

Table 1

Model feature comparison. “Yes” indicates features or modules that can be directly assessed by the respective model, “no” highlights unavailable features, while “NA” describes features that are not applicable, i.e., the rainfall-related features for the flow accumulation algorithm MFD.

Feature, modules	FLO-2D	FloodArea	r.sim.water	MFD
Flow depth	yes	yes	yes	no
Flow velocity	yes	yes	no	no
Flow barrier	yes	yes	no	no
Unsteady rain	yes	yes	no	NA
Interception	yes	no	no	NA
Infiltration	yes	no	no	NA

2. Materials and methods

2.1. Models

In this study, we test three raster-based, 2D hydrodynamic flood inundation models, i.e., FLO-2D, FloodArea and r.sim.water. The models have been selected such that different levels of model complexity are covered, following Neal et al. (2012). From the wealth of available 2D hydrodynamic models (cf. Teng et al., 2017), we chose FloodArea and r.sim.water since they have reportedly been used in the field of flood hazard assessment covering large areas including rural environments (cf. Kipfer et al., 2015; Tyrna et al., 2017). FLO-2D was selected as it is a “hydro-inundation model”, using a term from Yu and Coulthard (2015) describing models that consider hydrological processes and overland flow routing, at the same time. Moreover, it has the most complex flow routing scheme among the selected models. Finally, the model selection was complemented by a flow accumulation algorithm, i.e., the multiple flow direction (MFD) algorithm introduced by Freeman (1991). Such flow algorithms have manifold applications due to their striking simplicity (cf. López-Vicente et al., 2014; Alder et al., 2015). An overview of the models’ features is provided by Table 1.

2.1.1. FLO-2D

FLO-2D is a distributed, physically based flood inundation model (O’Brian, 2009). Among the selected models, it is the most sophisticated one, as it makes use of the full dynamic wave approximation (O’Brian, 2009). FLO-2D has various modules which can be switched on or off, if desired. It incorporates an infiltration module with various available methods, whereas the Green-Ampt (GA) method based on Green and Ampt (1911) is the most sophisticated one.

2.1.2. FloodArea

FloodArea is a simplified hydrodynamic flood inundation model that is fully integrated into a Geographic Information System (GIS), i.e., ArcGIS[®] by ESRI, with the main purpose of calculating areas affected by floods (geomer, 2016). The model cannot directly account for losses such as interception and infiltration. Thus, these losses have to be considered by reducing the corresponding rainfall input (cf. Table 1 and Sect. 2.3.5).

2.1.3. r.sim.water

The hydrodynamic model r.sim.water simulates overland flow with a path sampling method, which is implemented as a module in the open source GIS software GRASS (Mitasova et al., 2004; Neteler et al., 2012). Similar to FloodArea, r.sim.water cannot directly account for losses such as interception and infiltration. Moreover, unsteady rainfall cannot be modeled (cf. Table 1 and Sect. 2.3.5).

2.1.4. MFD

MFD is a multiple flow direction algorithm that assesses the flow paths based solely on a digital elevation model (DEM) (Quinn et al., 1991). We use the algorithm implemented in the open source System

for Automated Geoscientific Analyses (SAGA) (Conrad et al., 2015). Among the selected models, MFD is the simplest approach that does not route any water, but instead assesses each cell’s relative catchment area. Consequently, the model does not predict any flow depths and velocities (cf. Table 1), but assesses a static characteristic of the topography, i.e., the distributed flow accumulation areas. Note that prior to applying MFD to real-world case studies, sinks and pits of the respective DEM were filled, as discussed by Wechsler (2007). For that matter, we used the algorithm by Planchon and Darboux (2002) with a value of 0.01° for the minimal slope.

2.2. Artificial surfaces

To assess the performance of flow routing algorithms, Zhou and Liu (2002) defined four different mathematical surfaces and compared the calculated specific catchment area with the theoretically true values. The application of such algorithms on smooth artificial surfaces reveals distinct patterns and characteristics reflecting the algorithm’s differing mathematical formulations (cf. Zhou and Liu, 2002; Seibert and McGlynn, 2007; Pilesjö and Hasan, 2014). We adapt this approach to flood inundation modeling. Even without a theoretically true value, the adaptation of this approach to SWF modeling reveals inherent model characteristics that might not be apparent otherwise. Therefore, as a first exercise, we apply the selected models to four artificial surfaces, i.e., to a plane (Eq. (1)), a concave (Eq. (2)), a convex (Eq. (3)) and to a combined concave/convex surface (Eq. (4)). We compiled corresponding raster DEMs of 250-by-250 cells and a resolution of 2 m. The elevations of the plane are given by

$$z = ax + by + c \quad (1)$$

where $a \approx -0.051$, $b \approx 0.141$, $c = 0$ for a prescribed slope of $s = 15^\circ$ and an aspect of $\alpha = 160^\circ$; $0 \leq x \leq 250$, $0 \leq y \leq 250$. The concave surface is defined as

$$\frac{x^2}{a} + \frac{y^2}{b} + \frac{z^2}{c} = 1 \quad z < 0 \quad (2)$$

where $a = 998$, $b = -748.5$, $c \approx 191.5$; $-250 \leq x \leq 0$ and $0 \leq y \leq 250$. The convex surface is given by

$$\frac{x^2}{a} + \frac{y^2}{b} + \frac{z^2}{c} = 1 \quad z > 0 \quad (3)$$

where $a = 998$, $b = -748.5$, $c \approx 191.5$; $0 \leq x \leq 250$, $-250 \leq y \leq 0$. Finally, the combined concave/convex surface is defined as

$$\frac{x^2}{a} + \frac{y^2}{b} = \frac{z}{c} \quad z < 0 \quad (4)$$

where $a = 998$, $b = -748.5$, $c \approx 191.5$; $-250 \leq x \leq 0$ and $-250 \leq y \leq 0$.

The artificial surfaces are further manipulated. Two rows of the corresponding DEMs are incised by a minimum of 0.3 m, in order to represent a 4 m wide street crossing the surfaces from West to East. This incision enables to test and visualize the influence of structures in the landscape that can have major effects on overland flow paths. The top views of the four artificial surfaces are shown in Fig. 1.

For the artificial surfaces, a rain event lasting 1 h with an intensity of 50 mmh^{-1} was simulated. Infiltration and interception losses were not considered. A Manning’s roughness coefficient of $n = 0.24 \text{ sm}^{-1/3}$ was chosen for all artificial surfaces, which corresponds to the value recommended for dense grass by McCuen (2016). A value of $n = 0.012 \text{ sm}^{-1/3}$ is chosen for the incised streets, which corresponds to the recommended value for asphalt (McCuen, 2016).

2.3. Real-world case studies

We elaborated eight real-world case studies at seven study sites, i.e., at one study site two different events were observed. The case studies’ characteristics are summarized in Tables 2 and 3, while their respective

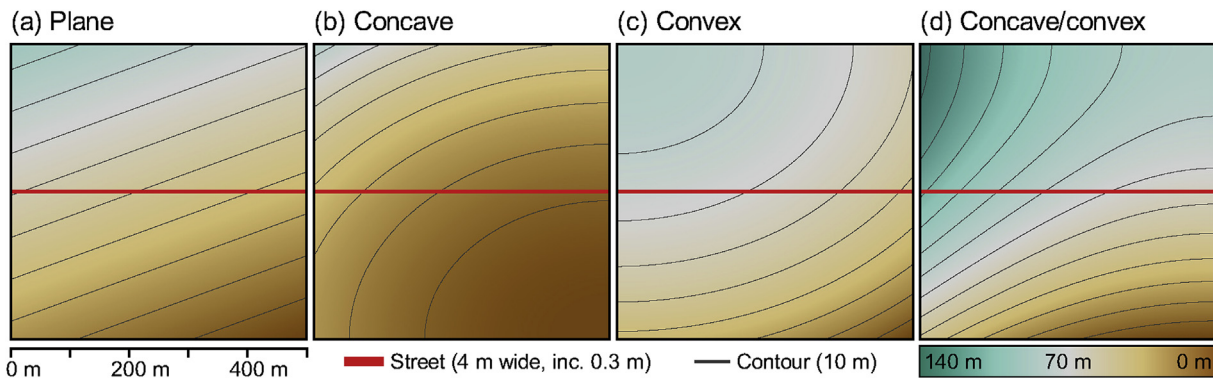


Fig. 1. A plane (a, mean slope = $14.9 \pm 1.6\%$), concave (b, mean slope = $12.6 \pm 6.5\%$), convex (c, mean slope = $12.6 \pm 6.5\%$) and a combined concave/convex (d, mean slope = $20.5 \pm 8.3\%$) artificial surface used for an initial test of the models.

location is shown in Fig. 2. In the following we introduce the delineation of the study perimeters, the gathered input data, the consideration of hydrological losses, the reconstruction of overland flow paths as well as the assessment of the model performance.

In terms of hydrological losses, we account for infiltration and interception losses, but neglect evaporation, as contributions of the latter are generally particularly low (cf. Yu and Coulthard, 2015). Furthermore, we assume that the influence of the sewer system on the flood extent is negligible. On the one hand, the fractions of built-up area are tiny in comparison to the rural areas for all case studies. On the other hand, the field observations indicated that the sewer systems were often either blocked (e.g., by eroded material, branches, leaves, hail, etc.) or surcharged. Thus, in this study, the interactions between overland flow and the sewer systems are neglected, as assumed similarly by e.g. Fewtrell et al. (2011) or Kipfer et al. (2012).

2.3.1. Domains

In order to delineate the study perimeter for each case study, the area is considered, within which documented observations regarding overland flow paths are available. The corresponding study perimeters were obtained by delineating the smallest respective watershed that still encompassed the reconstructed flow paths. Thereafter, these perimeters were buffered by at least 50 m to obtain a simulation domain that extends over the watershed's boundary. This ensures that the simulations' boundary effects within the study perimeters remain negligible. Thus, three different domains are differentiated for each case study:

- Observation domain (D_{obs}), within which all documented overland flow paths were reconstructed.
- Watershed domain (D_{wsd}) representing the smallest watershed that contains the observation perimeter. The model results were cropped to this area.
- Simulation domain (D_{sim}) representing the buffered watershed

Table 2

Characteristics of the five different case studies (at four study sites) triggered by relatively heavy rainfall.

Characteristic	E1	E2	E3a/E3b	E4
Date	20.07.2007	02.05.2013	12.07.2014/06.06.2015	08.06.2016
Town and Canton (abbr.)	Rubigen BE	Schleitheim SH	Mittelhausern BE	Dottikon AG
Slope: mean \pm sd (%)	7.7 ± 6.4	14.7 ± 9.3	18.1 ± 8.4	17.1 ± 10.1
Altitude: mean $\pm \Delta h/2$ (m)	571 ± 25	562 ± 62	727 ± 58	505 ± 82
Watershed domain D_{wsd} (km ²)	1.26	0.83	0.33	0.64
Observation domain D_{obs} (km ²)	0.61	0.22	0.33	0.33
Preconditions (-)	dry	normal	wet/dry	normal
Rainfall duration (h)	5	6	13/4	11
Rainfall sum (mm)	48.0	23.9	44.5/32.3	61.9
Max rainfall int. (mmh ⁻¹)	41.8	21.5	13.2/31.9	26.0
Mean rainfall int. (mmh ⁻¹)	9.6	4.0	3.4/8.1	5.6

Table 3

Characteristics of the three case studies triggered by relatively weak rainfall.

Characteristic	E5	E6	E7
Date	03.07.2007	13.05.2016	14.05.2016
Town and Canton (abbr.)	Bossonnens FR	Oberramsern SO	Oberflachs AG
Slope: mean \pm sd (%)	12.7 ± 10.9	22.1 ± 20	22.9 ± 11.5
Altitude: mean $\pm \Delta h/2$ (m)	765 ± 42	586 ± 92	614 ± 110
Perimeter P_{wsd} (km ²)	0.28	0.25	0.54
Perimeter P_{obs} (km ²)	0.04	0.03	0.09
Preconditions (-)	wet	wet	normal
Rainfall duration (h)	49	27	68
Rainfall sum (mm)	56.5	59.7	90.1
Max rainfall int. (mmh ⁻¹)	6.7	7.3	6.5
Mean rainfall int. (mmh ⁻¹)	1.2	2.2	1.3

domain, within which the simulations were carried out.

2.3.2. Primary input data

The main input for all four models is a DEM (Fig. 3). We used the DEM "swissALTI3D" as of 2013 with a regular grid size of 2-by-2 m, provided by the Swiss Federal Office of Topography (swisstopo, 2017a). Although, there are DEMs available with finer resolutions for some of the study sites, we used the aforementioned product, as it is homogeneous and available for whole Switzerland. As r.sim.water and MFD do not offer a direct option to integrate flow barriers such as buildings (cf. Table 1), the corresponding DEM was modified. All cells whose centroids were covered by a building were elevated by at least 10 m.

The land use was assessed between July 2014 and June 2016. As the land use was observed shortly after each event that falls into this period, i.e., E3a, E3b, E4, E6 and E7 (cf. Tables 2 and 3), the corresponding land use represent the conditions during these events. In contrast, the land use of the remaining case studies were assessed roughly three years after the date of occurrence, or more. Although there is a slight time shift, we assumed that the mapped land use is

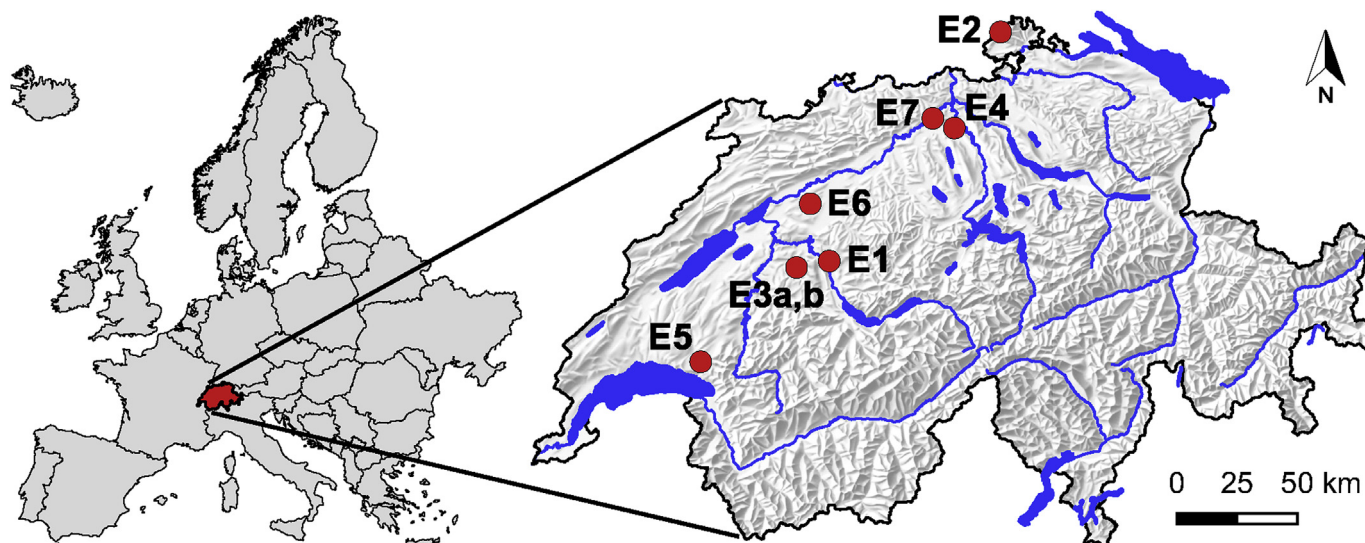


Fig. 2. Location of the seven study sites. Note the two case studies (E3a and E3b) were observed at the corresponding study site.

representative for the respective case study, as major land use changes are not expected at these study sites within the respective period. Firstly, the land use including buildings, streets, fields, etc. was digitized using orthophotos from the product “SWISSIMAGE” (swisstopo, 2017b). Secondly, the land use was adjusted and verified based on field observations.

The surface roughness values were obtained by linking the land use with literature tables, i.e., with the comprehensive collection from McCuen (2016), as indicated in Fig. 3. The corresponding values are listed in Table 4.

The hourly rainfall rate was extracted from the product “CombiPrecip” provided by the Federal Office of Meteorology and Climatology (MeteoSwiss, 2014). The product combines radar and rain gauge measurements by means of a co-kriging with external drift (e.g. Sideris et al., 2014; Panziera et al., 2016). It has a spatial resolution of 1-by-1 km, a temporal resolution of 1 h and is available from 2005 onwards (MeteoSwiss, 2014). As the case study sites are small, each study perimeter is covered by just a few cells. To reduce the influence of single cells that might contain outliers, the raster cells covering each perimeter were buffered by one cell. Thereafter, the mean of these cells were calculated for each time step. Next, the triggering rainfall events were extracted from the rainfall records by considering a minimum inter-event time of $t_{min} = 6$ h and a minimum intensity threshold of $i_{min} = 0.1$ mmh⁻¹, which are in line with common literature values (e.g. Dunkerley, 2008). Consequently, at the beginning of each event, the rain intensity had been <0.1 mmh⁻¹ for at least six consecutive time steps of 1 h each. Analogous, at the end of the event, it did not rain for at least 6 h with an intensity ≥ 0.1 mmh⁻¹.

2.3.3. Infiltration

Out of all four models only FLO-2D allows the user to account for infiltration directly, while it cannot be modeled explicitly by FloodArea and r.sim.water, whereas MFD is not dependent on rainfall altogether (Table 1). Therefore, the following approach was chosen: the full potential of FLO-2D was exploited by using the integrated GA infiltration module. To feed the other two models with similar input, as recommended by Neal et al. (2012), the GA method was implemented in R (R Core Team, 2016). Therewith, spatially and temporally variable cumulative infiltration rates were calculated. Based on these values, effective rainfall rates were obtained that were used as model inputs for FloodArea and r.sim.water (Sect. 2.3.5). Hereafter, the implementation and parametrization of the GA method are briefly outlined.

Based on Green and Ampt (1911), the cumulative infiltration $F(t)$

(mm) at time t (h) can be expressed as

$$F(t) = Kt + \Psi\Delta\Theta\left(\frac{F(t)}{\Psi\Delta\Theta} + 1\right), \quad (5)$$

whereas K is the hydraulic conductivity (mmh⁻¹), Ψ the wetting front soil suction head (mm), $\Delta\Theta = \Theta_f - \Theta_i$ (-) the difference between the final and initial soil moisture content. Thereby, an important assumption is that the water is ponded at the surface from the beginning of the steady rainfall. As this is generally not the case, Mein and Larson (1973) extended the GA infiltration method to account for the time until water starts to pond ($t = t_p$), at which time the cumulative infiltration depth equals the cumulative rainfall. Accordingly, the cumulative infiltration for steady rainfall after ponding time (i.e., $t > t_p$) is given by

$$F(t) = K(t - t_p) + F_p + \Psi\Delta\Theta\left(\frac{F(t)}{\Psi\Delta\Theta} + 1\right), \quad (6)$$

whereas t_p denotes the ponding time (h) and $F_p = F(t)$ the cumulative infiltration (mm) at ponding time $t = t_p$. We then implemented the GA method following Chu (1978), who expanded the method for unsteady rainfall events. The interested reader may refer to Chu (1978), who provides a detailed derivation and applied examples of the method.

The required GA infiltration parameters were obtained as follows: we estimated each study site's dominant soil texture based on expert knowledge, except for the case studies E4 and E6 for which soil maps including soil texture classes were available. We estimated the hydraulic conductivity K , the wetting front soil suction head Ψ and the effective porosity n_e using published regression parameter values from the comprehensive study by Rawls et al. (1983). Furthermore, it is assumed that the soils were saturated to a degree of $s_i = 30, 50$ or 80% before each event under dry, normal or wet conditions, respectively. Each respective condition was set according to the observed antecedent rainfall (cf. Tables 2 and 3). The change in soil moisture content was then estimated by $\Delta\Theta = n_e(s_f - s_i)$, while assuming that the soil's saturation after the event was $s_f = 100\%$.

2.3.4. Interception

Canopy storage capacity depends on various factors and roughly amounts 1 mm (e.g. Ward and Robinson, 2000). Thus, the depletion of this storage is tiny in comparison to the total rainfall volumes of the corresponding case studies (cf. Tables 2 and 3). Moreover, as the values of different land cover types are within the same order of magnitude, we simply considered a bulk interception loss of 1 mm. In FLO-2D this loss volume could be entered as a model parameter. For FloodArea and

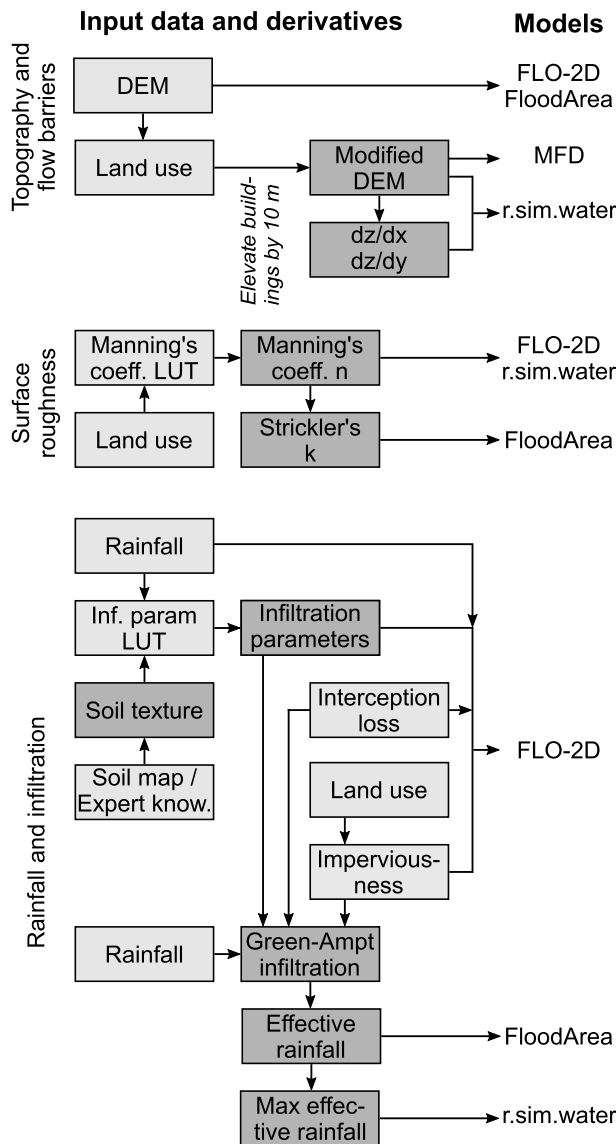


Fig. 3. Primary model input data (light gray boxes) as well as derivatives thereof (dark gray boxes). The look-up table (LUT) for Manning's coefficients is based on values from McCuen (2016), whereas the Strickler's values were obtained by taking their inverse, i.e., $k = 1/n$. The LUT for the infiltration parameters is based on Rawls et al. (1983) and O'Brian (2009). The Green-Ampt infiltration with ponding was implemented and calculated externally (cf. Sect. 2.3.3).

Table 4

Look-up table for relevant land use and corresponding Manning's roughness coefficients n , as recommended by McCuen (2016). The imperviousness is described by m (cf. Sect. 2.3.5). It indicates, whether the corresponding cell is considered as being fully impervious ($m = 1$, no infiltration), partially impervious ($m < 1$, reduced infiltration) or completely pervious ($m = 0$, normal infiltration). Note that the rain falling on buildings did not contribute to the overland flow.

Land use	Surface	n ($\text{sm}^{-1/3}$)	m (-)
Ley, meadow	Dense grass	0.240	0
Cropland	Conventional tillage without residue	0.090	0
Orchard	Woods without underbrush	0.200	0
Forest	Woods with light underbrush	0.400	0
Garden	Bermuda grass	0.410	0
Path, track	Graveled surface	0.012	0.75
Paved surface	Asphalt	0.012	1
Building	Smooth concrete	0.011	1

r.sim.water, we deducted the interception losses S (mm) from the total rainfall $P_t(t)$ (mm) to obtain a net rainfall $P_n(t)$ (mm) that reached the ground, as follows.

$$P_n(t) = \begin{cases} 0, & P_t(t) \leq S \\ P_t(t) - S, & P_t(t) > S \end{cases} \quad (7)$$

2.3.5. Effective rainfall

Infiltration cannot be modeled directly by FloodArea and r.sim.water (cf. Sect. 2.3.3). Thus, to account for infiltration and interception losses, we computed effective rainfall rates, which were then used as model inputs. The effective rainfall is given by

$$P_e(t) = P_n(t) - (1 - m)F(t), \quad (8)$$

whereas P_e is the cumulative effective rainfall (mm), P_n is the net rainfall that considers an initial interception loss (mm, cf. Eq. (7)), m is the imperviousness factor (cf. Table 4) and $F(t)$ is the cumulative infiltration (mm, Sect. 2.3.3). Note that an imperviousness factor can be set directly in FLO-2D's GA infiltration module for each individual cell (O'Brian, 2009). However, for FloodArea and r.sim.water, the imperviousness factors as specified in Table 4 were considered during the assessment of cell- and time-specific effective rainfall rates.

In FloodArea, spatial variable rainfall can be modeled by providing weighting factors (geomer, 2016), which can be thought of as runoff coefficients relating the hyetograph to cell-specific effective rainfall. Obviously, these coefficients are changing over time and space. They are defined as $c_{i,j,t} = P_e(i, j, t)/P_t(t)$. The spatially variable rainfall can then be modeled by creating a raster with cell values $c_{i,j}(t)$ for each time step t . The simulations can then be stopped after each time step and restarted with the runoff coefficients of the next time step. This procedure was automated with batch scripts.

For r.sim.water, this procedure is not straightforward, as the simulations cannot be restarted based on results from a previous time step. Therefore, we chose the time step with the highest effective rainfall rate and ran the model with only this single spatially variable rainfall field.

2.3.6. Reconstruction of overland flow paths

Data sources that possibly indicate past SWFs include insurance claim records, disaster databases, reports and recollections from affected people (Bernet et al., 2017, and references therein). However, for recent events, it is usually possible to reconstruct flow paths of SWFs based on their traces in the field, as exemplified by Fig. 4. Particularly in rural environments, overland flow usually leaves notable traces such as erosion marks, deposited sediments and flattened vegetation. For the purpose of this study, we have reconstructed discernible SWF traces based on field observations following the events of the case studies E3a, E3b, E4, E6 and E7, whereas for the remaining case studies, i.e., E1 and E2, the inundated areas were reconstructed based on external sources. Table 5 summarizes the source for the flow path reconstructions along with associated limitations, as well as a qualitative confidence level of the data quality.

Irrespective of the data source, the flow paths were reconstructed and spatially localized. Using standard GIS software, the field assessment were then digitally stored. All overland flow traces and paths were considered as being wet. To assess the performance of the models, these areas were compared to the model outputs, as outlined in the following section.

2.3.7. Model performance

Across various disciplines, map comparisons are a standard procedure to assess and compare model performances (e.g. Kuhnert et al., 2005; Foody, 2007; Bennett et al., 2013). However, there is not a single best method for this task. On the contrary, many tools including both quantitative as well as qualitative methods are recognized as being appropriate for this purpose (Kuhnert et al., 2005; Bennett et al., 2013).

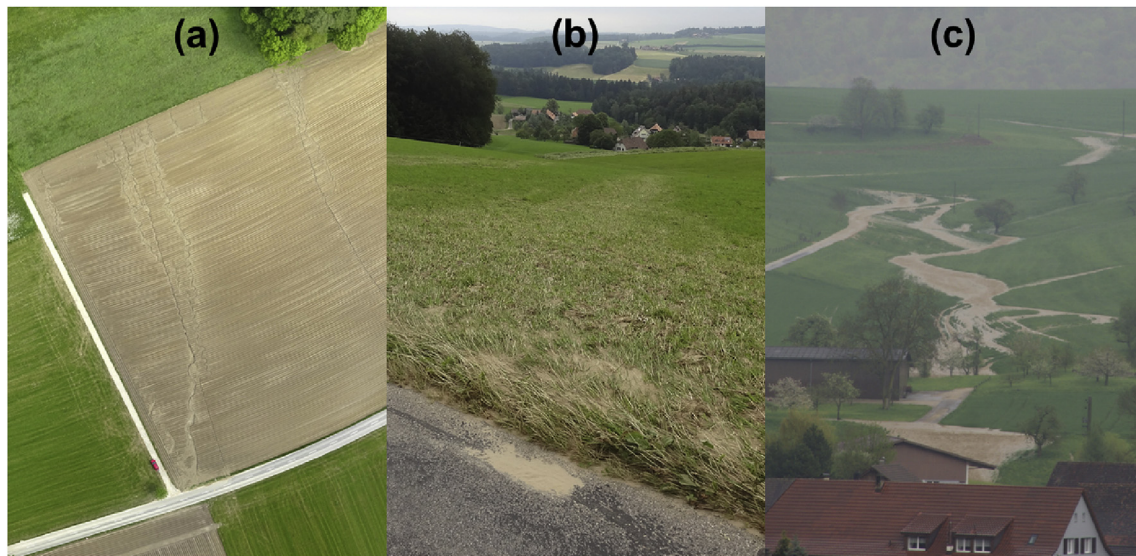


Fig. 4. Different sources used for reconstructing overland flow paths. (a) Orthophoto derived by means of a unmanned aerial vehicle (UAV) documenting traces of erosion in a field of the case study E6 (source: Elias Hodel, 16.05.2016). (b) Traces of overland flow in a field of the case study E3b that were mapped in the field (source: Daniel B. Bernet, 09.06.2015). (c) Photograph documenting actual overland flow of the case study E2 (source: Andrea Wanner-Staubesand, 02.05.2013).

Thus, the model performance assessment have to be adapted to the models’ objectives as well as to the characteristics of the available data, since the task is inherently case-specific (Bennett et al., 2013).

Along these lines, we compared the model outcomes and observations visually, as well as quantitatively. In terms of the latter, we used common binary pattern performance measures based on the contingency table (Table 6), which are widely being used for the comparison of simulated and observed flood extents (e.g. Aronica et al., 2002; Schumann et al., 2009; Stephens et al., 2014; Zischg et al., 2018). However, more recently, Stephens et al. (2014) pointed out that these performance measures are all subjected to a varying degree of bias, which should be considered in subsequent conclusions. As we are using different measures conjunctively in this study and are more interested in the broader picture, the influence of this circumstance on our conclusions is negligible.

The binary pattern performance measures are based on the assessment whether a cell was observed and/or simulated as wet or dry. All cells covered by an observed flow paths are considered as wet. For the simulation results, this information was inferred from the simulated maximum flow depths h_f (m) by applying an arbitrary threshold h_t (m). Thus, cells with a maximum flow depth below the threshold ($h_f < h_t$) are considered to be dry, while all other cells ($h_f \geq h_t$) are considered to be wet. We tested different threshold values and compared the performance of all models applied to all case studies using the observations as the reference. Based on these results, we empirically chose a value of $h_t = 0.02$ m as this threshold value maximized the performance of all models. Note that this threshold value is case-specific and, thus, might

Table 5

Exploited sources of information for reconstruction of inundated areas for each case study (cf. Tables 2 and 3).

ID	Source	Quantity	Limitations	Confidence
E1	External map	Ponded water and water on the streets	No indication of flow paths, assessment methods unknown	Low
E2	Photographs	Flow paths and flood extent	Spatial localization of depicted flow paths	high
E3a,b	Field visits, aerial photos	Traces of flow (sediments, flattened vegetation)	Impossible to identify flow that left no traces	high
E4	Field visit	Traces of flow (sediments, flattened vegetation)	Impossible to identify flow that left no traces; Flow traces in forest difficult to detect	medium
E5	Video	Flow dynamics and extent of flood	Coverage limited to small area, low resolution	medium
E6	Field visit, aerial photos	Traces of erosion in bare field	Impossible to identify flow that left no traces	medium
E7	Field visit	Traces of erosion in bare field	Impossible to identify flow that left no traces; small observation perimeter compared to watershed	medium

Table 6

Contingency table of model prediction or observation (A) versus model prediction (B).

	Present (wet) in A	Absent (dry) in A
Present (wet) in B	Hits: $a = A_1 B_1$	False alarms: $b = A_0 B_1$
Absent (dry) in B	Misses: $c = A_1 B_0$	Correct negatives $d = A_0 B_0$

be different for other models, observational data, resolutions, etc.

In the following, we compare the models’ results with observations, in addition to a comparison of the models among each other. The comparisons of the models with observations are constrained to the observation perimeter (D_{obs}), while the model comparison among each other is carried out within the whole watershed (D_{wsd} , cf. Sect. 2.3.1).

For the quantitative model comparison, we used the following binary pattern performance measures (e.g. Aronica et al., 2002; Pappenberger et al., 2007; Bennett et al., 2013), which are based on the contingency table (Table 6):

$$\text{Bias: } m_1 = \frac{a + b}{a + c} \quad m_1 \in [0, \infty] \quad \text{ideally } m_1 = 1 \quad (9)$$

$$\text{Critical success index: } m_2 = \frac{a}{a + b + c} \quad m_2 \in [0, 1] \quad \text{ideally } m_2 = 1 \quad (10)$$

$$\text{Hit rate: } m_3 = \frac{a}{a + c} \quad m_3 \in [0, 1] \quad \text{ideally } m_3 = 1 \quad (11)$$

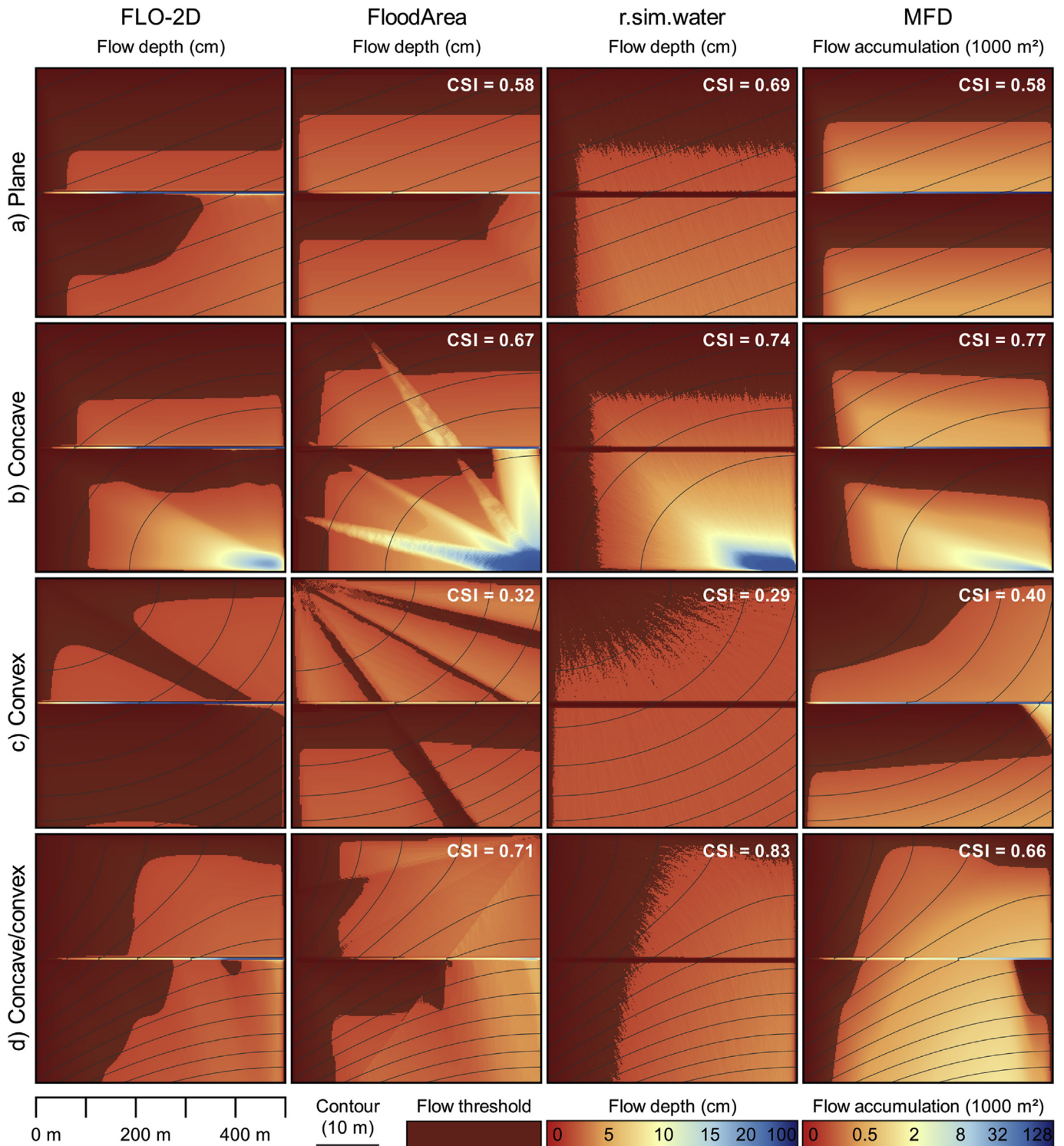


Fig. 5. Simulation results of the four different models on a plane (a), concave (b), convex (c) and a combination of a convex and concave (d) artificial surface. The flow threshold for the hydrodynamic models (FLO-2D, FloodArea, r.sim.water) is a flow depth of 0.02 m, whereas the flow threshold for the flow accumulation algorithm (MFD) is an accumulation area of 250 m². Cells with values below the respective flow threshold are considered to be dry (dark red cells), while all other cells are considered to be wet. The indicated critical success index (CSI, cf. Eq. (10)) was obtained by comparing the models' predicted wet and dry cells to the binary pattern produced by FLO-2D, which is used as a reference. (For interpretation of the references to colour in this figure legend, the reader is referred to the Web version of this article.)

False alarm rate: $m_4 = \frac{b}{b + d}$ $m_1 \in [0,1]$ ideally $m_4 = 0$ (12) et al., 2014).

Note that the critical success index (CSI) is also referred to as threat score or F^2 statistic in the literature (e.g. Bennett et al., 2013; Stephens

3. Results

3.1. Artificial surfaces

Despite the lack of a baseline, applying the models to the selected artificial surfaces reveals interesting characteristics (Fig. 5). First and foremost, the incised street represents a prominent topographical structure that has a significant influence on the flow pattern. The street acts like a channel, which can collect incoming water and can be overtopped, if the channel is full or if the incoming water is not sufficiently deflected. Whether the street is overtopped or not, is discernible by the amount of dry cells directly to the south of the incised street, i.e., cells with a flow depth or flow accumulation below the flow threshold (dark red cells in Fig. 5). For each artificial surface, the pattern of these dry cells varies significantly among the models. In contrast, the pattern of dry cells north of the street is more similar among the models for all but the convex surface, as discussed later. Thus, the street has a major influence on the distribution of dry and wet cells, respectively.

In more detail, *r.sim.water* does not predict a deflection of the water crossing the street on any surface. Quite the opposite is true for the flow accumulation calculated by MFD. For all but the combined concave/convex surface, the street poses a complete or nearly complete flow barrier. FLO-2D and FloodArea, on the other hand, show a more differentiated picture, as water is overtopping where ever the flow depths are exceeding the street's incision. This is most apparent on the concave surface, where FloodArea predicts a significant overtopping of the street's eastern end, unlike the other models. Thus, in this modeling exercise, the user's choice of a model does not only heavily influence the pattern of dry and wet cells south of the street, but also the corresponding flow paths.

The results of the hydrodynamic models do not only deviate substantially south of the street, but also on the street itself for each artificial surface. FLO-2D consistently predicts the highest flow depths on the street. FloodArea's results exhibit flow depths that lie mostly between the minimal values estimated by *r.sim.water* and the high values predicted by FLO-2D. However, as mentioned before, a striking difference of FloodArea compared to FLO-2D is the overtopping of the street's incision at the eastern side of the concave surface. Compared to the other hydrodynamic models, *r.sim.water* predicts by far the lowest flow depths on the street for all surfaces. In fact, the flow depths on the street predicted by *r.sim.water* are below the wet/dry threshold of 0.02 m for all surfaces. Thus, the flow patterns south of the street are heavily influenced of how the models predict the flow over this topographical structure.

However, the flow patterns are also dependent on how the models simulate flow over the four different topographical forms. Specifically, the flow patterns on the convex surface of each single model is strikingly different from the other ones, which is reflected by the particularly low CSI values indicated in Fig. 5. Also the flow patterns in the northern half of the combined concave/convex surface seem to deviate slightly more among the models than the produced patterns on the plane and the concave surface, respectively. This could be explained by the fact that the northern half of the concave/convex surface is characterized by convex forms that produce particularly different results among the models. Lastly, the flow pattern produced by FloodArea on the concave surface is characterized by striking flow paths. FloodArea produces also sharp-edged flow paths on the convex and the concave/convex surface, however not as pronounced as on the concave surface. These flow patterns stem from the limitation of flow directions to 16 fixed angles by FloodArea's flow routing scheme, which is described in e.g. Tyrna et al. (2017).

3.2. Real-world case studies

The performance of the models applied to each case study is depicted in Fig. 6. The obtained CSI (Eq. (10)) values are rather low and

indicate that, overall, all models have a low performance for all case studies. The respective maximal CSI of each model lies between 0.318 and 0.344, which stem from the case study E2. For the same case study, the models produce the highest hit rates (Eq. (11)), ranging between 0.566 and 0.788. Save a few exceptions, the hit rates are well below a value of 0.5 in all other case studies.

The bias is the fraction of simulated number of wet cells compared to the observed number of wet cells (Eq. (9)). Thus, a bias greater than one indicates an overestimation of the wet cells by the model, whereas a bias below one shows the opposite. As presented in Fig. 6, all models overestimate the number of reconstructed wet cells for some case studies, but heavily underestimate them for others. As depicted in Fig. 6, the bias is correlated with the false alarm rates (Eq. (12)). For each case study, models with a lower bias are also associated with a lower false alarm rate, and vice versa. The lowest absolute values are produced for the simulations with strong underestimations (bias \ll 1.0). This can be expected, since a particularly low bias value means that the number of modeled wet cells is much smaller than the observed number of wet cells. In this case, even if all modeled wet cells were misses, the false alarm rate would still be small, since the number of correct negatives is constantly high for all models. Hence, following Eq. (12), a low false alarm rate results.

Overall, we have identified three main issues limiting the models' performances, i.e., observational data of differing quality, insufficiently represented topographical structures and biased predictions of effective rainfall. In the following, we illustrate each of these issues with examples from the corresponding case studies.

The particularly low performance of all models applied to case study E1 can mainly be attributed to poor observational data. Namely, the derivation of observed wet cells are based on an external map (Jordi + Kolb AG, 2008). Therein, areas with ponded water as well as water on the streets are mapped, while overland flow paths in the agricultural fields are not indicated (Table 5). Thus, the observations only capture areas that are small compared to the whole area that must have been inundated, as depicted by Fig. 7. As a consequence, the wet cells are overestimated, the false alarm rates are high and the CSI values are low for all models. Moreover, the map by Jordi + Kolb AG (2008) does not provide any ancillary information such as the applied mapping methods. Therefore, the map turns out to be an unsuitable source of information for the purpose of validating the models.

Applying the models to artificial surfaces has highlighted that topographical structures such as streets can have major effects on the produced flow paths (Sect. 3.1). How the models are predicting flow on streets in real-world case studies and how this influences the prediction of subsequent flow paths, can best be shown with results from the case study E2. All models perform best in this case study, as indicated by Fig. 6. The CSI values are similarly high for all models, whereas the other scores vary slightly more. For instance, FLO-2D produces the highest hit rate, however, at the expense of the highest false alarm rate and the highest overestimation. In contrast, *r.sim.water* exhibits the smallest bias and false alarm rate, however, at the expense of a smaller hit rate. Depending on the situation, one or the other configuration might be more desirable. The visual comparison confirms that all four models produce plausible results. As an example for the simulation results, the maximal flow depth predicted by FLO-2D are depicted in Fig. 8.

Based on the similar performance of all four models, the case study E2 is best suited for comparing the simulated flow paths in more detail. Namely, in most of the other case studies the models are associated with a greater range of bias values, i.e., the number of wet cells varies more among the models, which impairs the attribution of model differences. Fig. 9 illustrates the model comparison of the observed and simulated wet cells, as categorized according to the contingency table (Table 6).

According to all models, water mainly accumulates in the thalweg, i.e., the path of lowest elevations along the hillslope (cf. Figs. 8 and 9). Thereby, the observed wet cells are captured well by all models, except

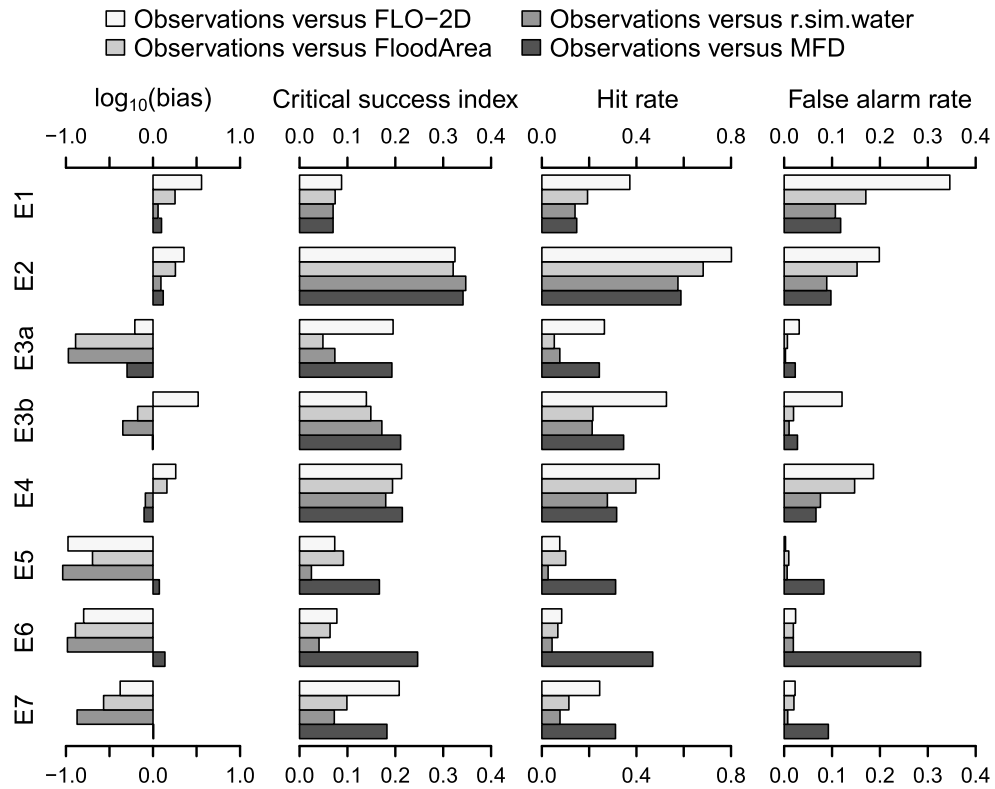


Fig. 6. Model performance of each model in comparison to the observed values evaluated within the observation domain (D_{obs} , Sect. 2.3.1). The binary pattern performance measures are defined in Eqs. (9)–(12). Note that not the bias itself, but the common logarithm of the bias is displayed. The IDs (E1-7) indicate the corresponding case study, as summarized in Tables 2 and 3

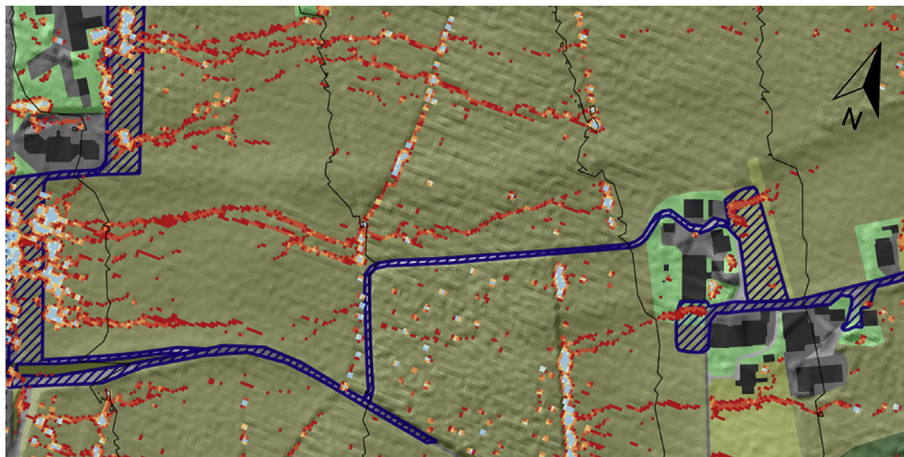
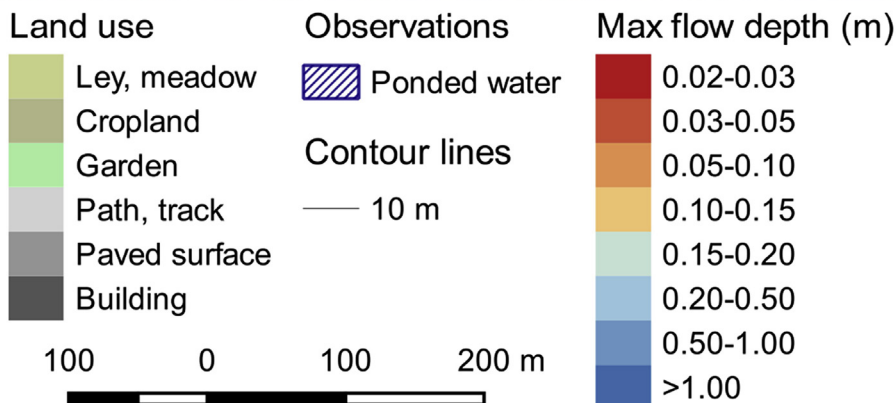


Fig. 7. Excerpt of the simulation results produced by r.sim.water applied to the case study E1. The observations inferred from an external map only capture areas where water was ponding or where the street's drainage system was overwhelmed, indicated by the hatched blue areas. Flow paths in the agricultural areas were not mapped. The accumulating water along what looks like trenches in the central part of the figure, are in fact caused by artifacts of the DEM, as visualized by the transparent land use on top of the DEM's hillshade image. Note that the north direction is slightly tilted, as indicated. (For interpretation of the references to colour in this figure legend, the reader is referred to the Web version of this article.)



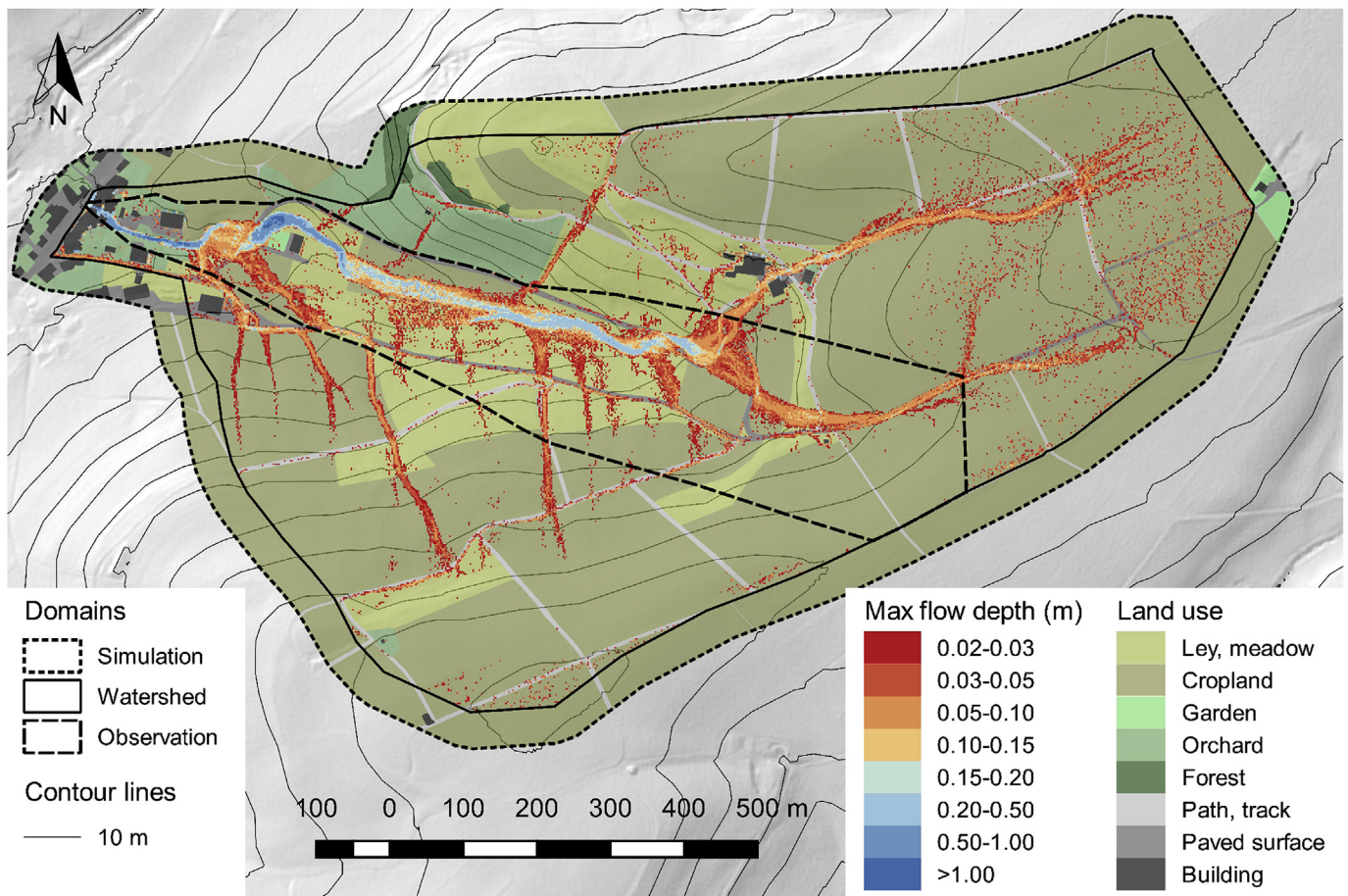


Fig. 8. Simulation result of FLO-2D applied to the case study E2. The maximal flow depths are categorized into discrete classes, as indicated in the legend. Considering the chosen water depth threshold, all cells that display a maximal water depth of $d \geq 0.02$ m are simulated as wet, whereas all other cells are predicted to remain dry.

MFD, which is not able to predict the ponding water towards the outlet of the observation domain. The main differences between the other models are that FLO-2D is overestimating the wet cells along the thalweg more than FloodArea, which in turn overestimates the wet cells to a larger degree than r.sim.water. This is reflected by the respective bias values indicated in Fig. 9.

Overall, the models have difficulties predicting the water flowing on the streets. Foremost, the streets in the upper part of the domain were inundated, but were not simulated as such, which is reflected by the numerous misses in this area (red cells, Fig. 9). Compared to the other models, FLO-2D predicts the observed wet street cells better. This behavior could be expected based on the results from the models applied to artificial surfaces, since FLO-2D predicted consistently larger flow depths on the street than the other models (Sect. 3.1). Along the same lines, r.sim.water predicts the lowest number of wet street cells, which is also supported by the findings of the artificial modeling exercise. Interestingly, all models predict roughly the same places where water overtops the street's confinement and joins the main flow path in the thalweg. Only one of these paths in the central part of the domain is predicted by FloodArea and FLO-2D, while the path is not indicated by r.sim.water and MFD. East thereof, a flow path could be observed that is not simulated by any model. Overall, this exemplifies that although the behavior may differ slightly between the models on a cell-by-cell basis, they all produce quite similar flow paths on a broader scale or, similarly fail to identify them.

As outlined introductorily, accurate predictions of effective rainfall are crucial for increased model performances, in addition to high-quality observational data and well-represented topographical

structures. If a model predicts too little runoff, it usually leads to an underestimation of wet cells and, consequently, to a rather low performance. This issue is nicely exemplified by the case studies E3a and E3b observed at the same study site (cf. Table 1). As shown in Fig. 6, the number of wet cells are underestimated by all models in the first event (E3a). In particular, FloodArea and r.sim.water predict a much lower number of wet cells than the number of wet cells inferred from the observations. Consequently, the performance of these two models is particularly low for this case study. The performances are more balanced for the second observed event (E3b). However, similarly to the case study E2, FLO-2D produces the highest hit rate, but also the highest false alarm rate, owed to the overestimated number of wet cells. Although, both case studies were triggered by thunderstorms, the rainfall intensities of E3a are moderate and the event spans 13 h, while E3b is associated with short and intense rainfall that is typical for thunderstorms (cf. Table 2).

Thus, we can observe that the hydrodynamic models, i.e., all except MFD, generally underestimate the number of wet cells for the case studies with low rainfall intensities. Namely, the said models exhibit an underestimation of the observed wet cells for the case studies E3a, E5, E6 and E7, as depicted in Fig. 6. This hints at the fact that the simulation of wet cells is less sensitive for case studies driven by intensive rainfall. In contrast, the mechanisms that lead to overland flow during the case studies with low rainfall intensities, are much more complex and badly captured by the chosen modeling approach of this study.

The model MFD is inherently different from the other three hydrodynamic models. It is not an event-based model, but assesses a static property of a catchment based solely on the DEM, i.e., the relative

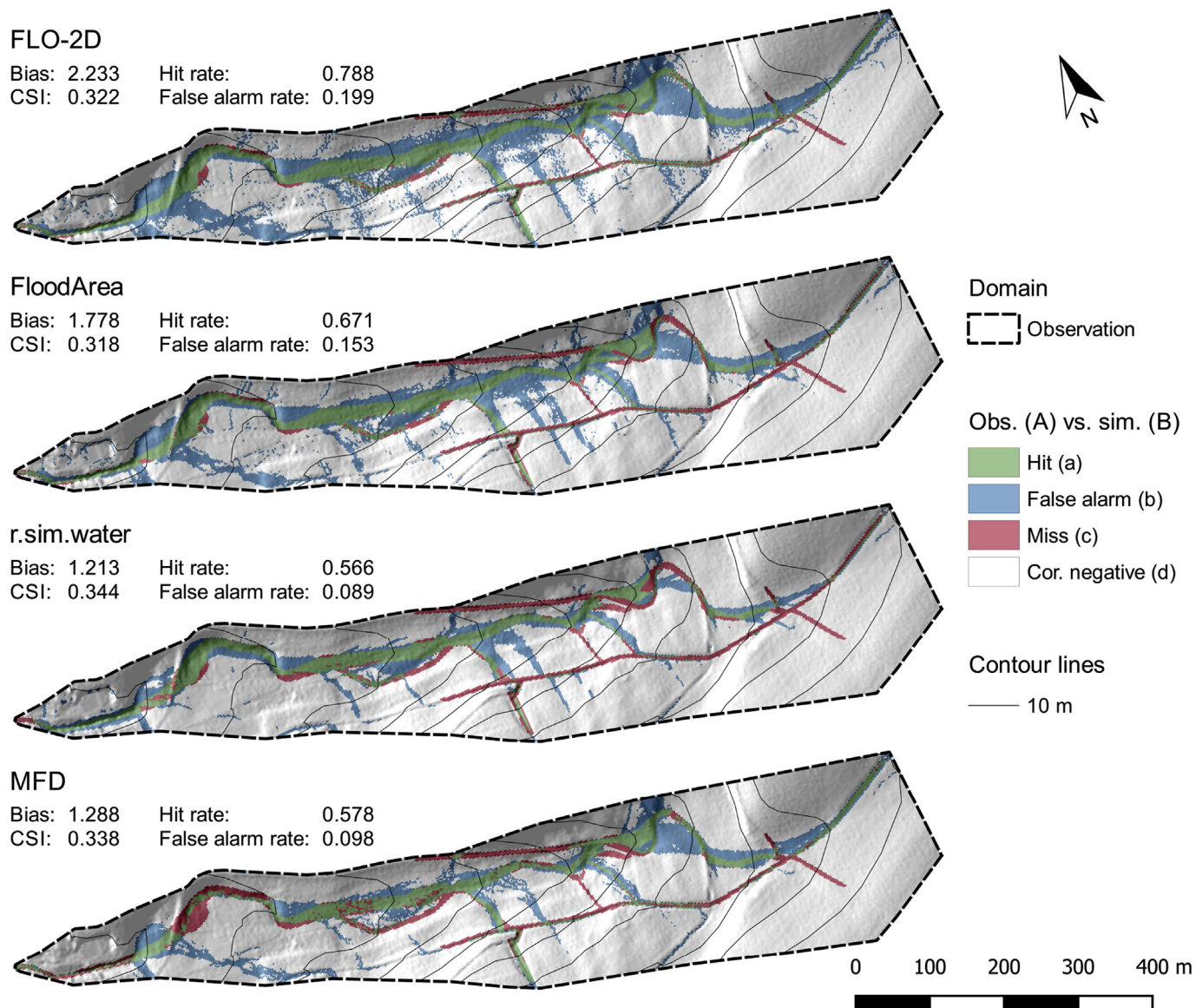


Fig. 9. Comparison of observed (obs.) and simulated (sim.) wet cells as categorized by the contingency table (Table 6) for each model applied to the case study E2. The definitions of hits, false alarms, misses and correct negatives can be found in Table 6. The whole study area (cf. Fig. 8) is clipped to the observation domain, as observations are unavailable outside of this domain. Note that the north direction is slightly tilted.

catchment area (Sect. 2.1.4). Applied to the considered case studies, MFD performs similarly or even better than the other models. This is most pronounced in the case study E6, further illustrated in Fig. 10.

As highlighted by Fig. 10, the number of wet cells predicted by FloodArea is particularly low for the case study E6 within the observation domain, which is reflected by the performance measures' low values (Fig. 10b). Although the flow paths in the middle of the observation domain are vaguely indicated, it is apparent that too little effective rainfall is predicted, which leads to the exhibited underestimation of wet cells. In contrast, the flow paths predicted by MFD are a function of the respective catchment area of each cell, irrespective of the rainfall. Thereby, the two flow paths in the middle of the observation domain are covered. Notably, the flow path at the western border of the observation domain is shifted slightly westwards in comparison to the observations. This behavior can be attributed to the specific land management of the corresponding potato field, i.e., furrows parallel to the slope, which promotes flow at western border of this field. The observed flow path at the eastern border of the observation domain is not captured by any model. Moreover, it should be

noted that the flow over the bare potato field led to erosion, as depicted in Fig. 4a, which in turn may have a significant influence on the flow patterns. However, such effects cannot be captured with this study's modeling approach.

Since in most case studies the observations only cover a rather small part of the whole simulated catchment (cf. D_{obs} and D_{wsd} in Tables 2 and 3) and the observations are associated with a varying degree of confidence (cf. Table 5), we additionally compare the model results within the whole simulation domain with each other independent of the observation data. By using the more sophisticated models as the reference, we can assess the capability of the simpler models to reproduce results of the more complex models. As Fig. 11 indicates, FloodArea as well as MFD reproduce the results stemming from FLO-2D rather well. At the same time, the false alarm rates are particularly low. However, we also recognize that FloodArea generally underestimates the wet cells in comparison to FLO-2D. r.sim.water slightly underestimates the wet cells in comparison to FloodArea. However, the underestimation is limited to a small range indicating that the underestimation is similar in all case studies.

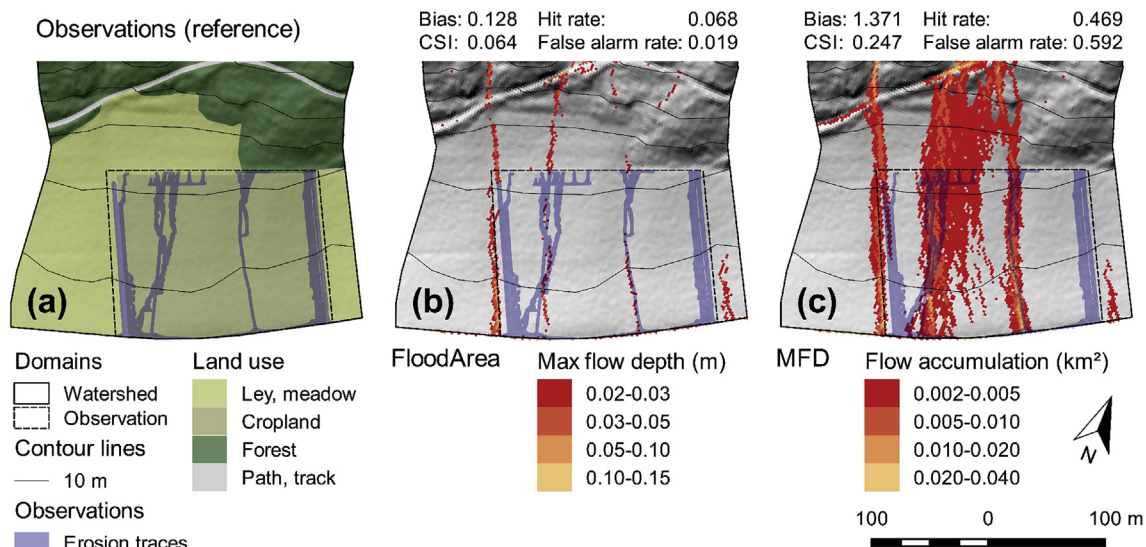


Fig. 10. Exemplary comparison of inundated areas inferred from documented traces of with flow depths predicted by FloodArea and flow accumulation calculated with MFD for the case study E6. (a) Flow paths inferred by means of a UAV in a potato field (cf. Fig. 4a). The land use is displayed in the background. (b) Maximal flow depth simulated by FloodArea. (c) Flow accumulation as predicted by MFD. Note that the north direction is slightly tilted for all sub-figures.

In addition to the comparison of the models among themselves, the first row and column of Fig. 11 also depicts the model performance in relation to the observations. Namely, it also displays the results shown in Fig. 6 in a different way, whereby the overall performance is better visualized. Thus, it depicts that the CSI of every model is rather low, as discussed before. Moreover, it visualizes that the CSI of the model MFD and FLO-2D is very similar, as well as the one of FloodArea and r.sim.water, but at a lower level. Moreover, it visualizes the stronger tendency of FloodArea and r.sim.water to underestimate the wet cells, compared to FLO-2D. In comparison, MFD is by far the least biased of all the models.

4. Discussions

In this study, we have followed the procedure employed in practice by current hazard assessments to produce SWF hazard maps, which are based on uncalibrated, single deterministic simulations (cf. Meon et al., 2009; Tyrna and Hochschild, 2010; Kipfer et al., 2015; Tyrna et al., 2017). The results from the models applied to artificial surfaces and eight real-world case studies suggest that the models' performance might be increased if the model were properly calibrated. For instance, the model exercise on artificial surfaces (cf. Sect. 3.1) exemplified the need to calibrate the surface roughness. Namely, FLO-2D predicts rather high flow depths on the incised street, while r.sim.water predicts flow depth that are even below the chosen flow threshold of 0.02 m. Simulations with altered roughness values indicated that r.sim.water is rather sensitive to the street's chosen roughness value. Similarly, the flow depths on the street predicted by FloodArea are generally below those predicted by FLO-2D. A calibration of the roughness value could also improve the match between FLO-2D and FloodArea. This circumstance is also exhibited by applying the models in real-world case studies, whereby FloodArea and r.sim.water predict lower flow depths on streets (cf. Fig. 9 and Sect. 3.2).

The results from applying the models to a broad range of different settings indicate that the models' performance would still vary significantly, even if the models were calibrated. Namely, all models perform similarly well in the case study E2 (cf. Fig. 6), whereas properly calibrated models might perform even better. Yet, it is clear that a calibration could not bring the models' performances to a similar level in all case studies. On the one hand, this indicates that calibration and/or validation based on one single case study might be misleading. Thus,

using various case studies covering a wide range of settings provides a more holistic picture of the models' performance. On the other hand, it also indicates that the models are not capable of capturing all relevant processes under diverse circumstances.

In fact, the results show that the hydrodynamic models tend to significantly underestimate the number of wet cells for the case studies associated with weak rainfall (cf. Figs. 6 and 10). Thus, the models do not predict sufficient runoff as compared to the observations, driven by an underestimation of the effective rainfall. More specifically, the results indicate that the considered infiltration assessment methods (cf. Sect. 2.3.5) are not capturing the governing processes well. Namely, saturation excess overland flow cannot be modeled by the applied methods, although this runoff generation mechanism is likely crucial for SWFs triggered by weak rainfall. Although SWFs are usually associated by heavy rainfall as mentioned before, results from Bernet et al. (2017) indicate that long lasting events with weak rainfall cause similar damage to buildings as short events with heavy rainfall. Thus, a model should be able to capture events characterized by heavy as well as weak rainfall to be suitable to reliably simulate SWFs in rural areas.

Along these lines, the two events observed at the same study site, i.e., case study E3a and E3b, exemplify that SWFs can be triggered by heavier and weaker rainfall at the same location (cf. Table 2). Moreover, the case studies exemplify that the flow paths are not a static function of the topography, but are dependent on soil characteristics, land use, land management in addition to the rainfall input, of course. Along these lines, Ferreira et al. (2015) highlighted for instance that runoff generation mechanism are spatially and temporally highly variable. Certainly, there are established and emerging methods that could represent the runoff generation processes better (e.g. Schmocker-Fackel et al., 2007; Antonetti et al., 2016; Steinbrich et al., 2016). However the consideration of such spatially highly variable processes are often impaired by the lack of appropriate data. Thus, for a better representation of the runoff generation processes, corresponding data are required. For the presented case studies such data were unavailable, as well as time-consuming and costly to collect.

The representation of topographical structures by the DEM is another aspect, which significantly influences the models' predictions (e.g. Sampson et al., 2012; de Almeida et al., 2016). As indicated by the model exercise on artificial surfaces, the models react sensitively on structures such as streets (Sect. 3.1). Moreover, applying the models to real-world case studies have pinpointed that the influence of such

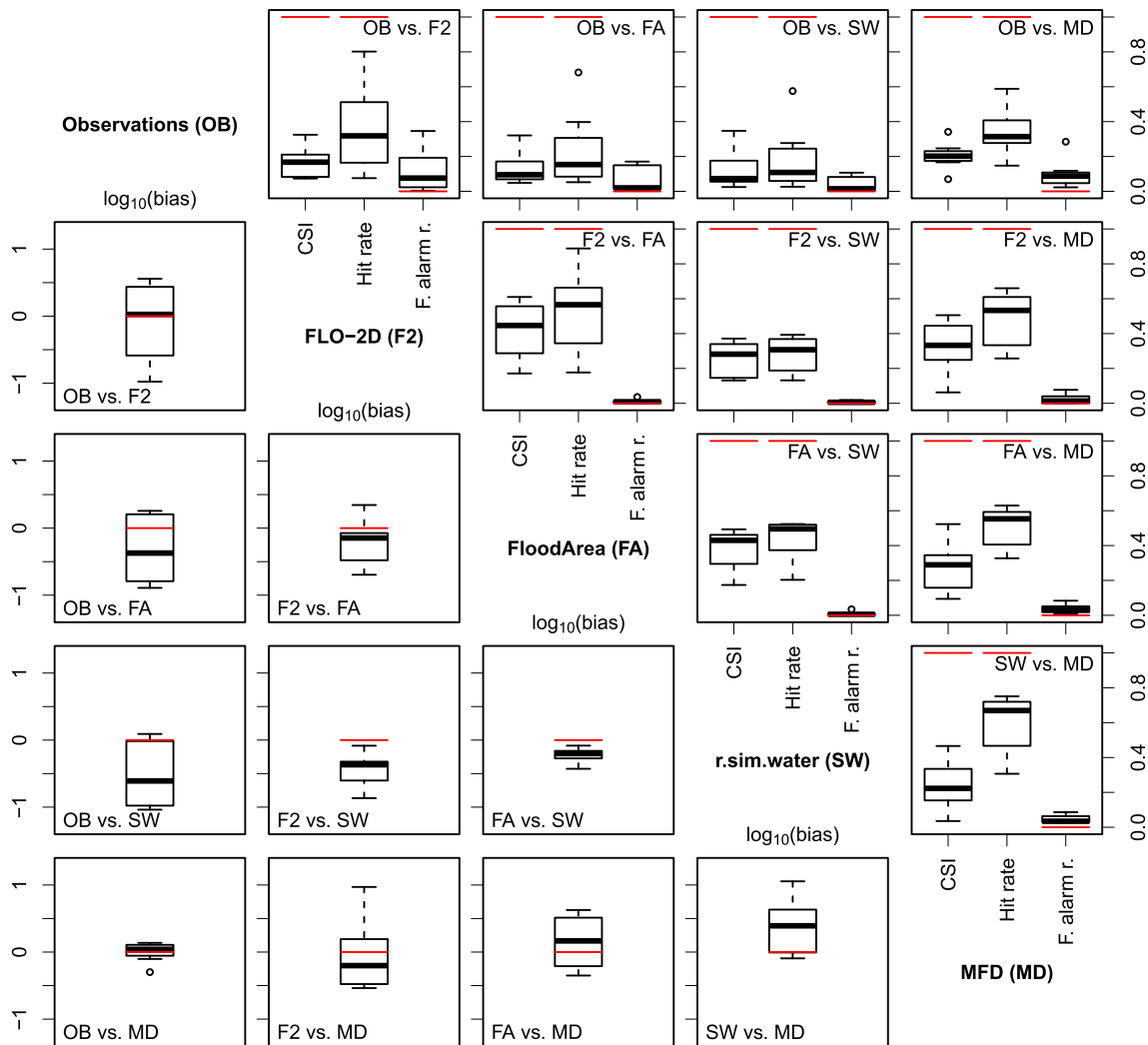


Fig. 11. Binary pattern performance measures of different pair-wise model and/or observation comparisons. Each box plot is built by eight values, i.e., one value for each case study. In the first row and the first column, the observations are compared with the model results within the observation domain (D_{obs} , Sect. 2.3.1). All other sub-figures show the comparison of different models within the watershed domain (D_{wsd} , Sect. 2.3.1). Each sub-figure is labeled with the abbreviated pairing, whereas the former label indicates the reference to which the latter is compared. As an example, the label “OB vs. SW” indicates the sub-figure, in which the observations are compared to the model results of r.sim.water. In the sub-figures above the diagonal, the performance measures are plotted, i.e., the critical success index (CSI, cf. Eq. (10)), the hit rate (cf. Eq. (11)) and the false alarm rate (f. alarm r., cf. Eq. (12)). The bias (cf. Eq. (9)) is plotted in the sub-figures below the diagonal. Note that not the bias itself, but the common logarithm of the bias is displayed. The ideal value of each performance measure (cf. Eqs. (9)–(12)) is indicated by the thin red line. The closer the box plots are to this red line, the more similar are the performance measures of the corresponding pairing. (For interpretation of the references to colour in this figure legend, the reader is referred to the Web version of this article.)

structures on the simulation results are governed more by the representation of such structures by the respective DEM than the choice of the model by the user. This is in line with findings stemming from more formal model comparisons, for instance from the benchmark study of urban flood label models by Fewtrell et al. (2011). This issue is illustrated by Fig. 9, which indicates that the models predict the streets' overtopping at the same locations, while numerous of these flow paths could not be observed in reality. Thus, this behavior suggests that the streets confinements are not represented accurately enough by the DEM, supported by the fact that the rural environment of the case study E2 is characterized by single-lane streets with width in the same order as the DEM's resolution. In consequence, the channelizing effect of overland flow on streets is rather poorly captured by the models. Confronted with the same issue, Kipfer et al. (2012) proposed to incise all streets by a fixed depth. However, this measure most likely incapacitate the model to correctly reproduce the street's overtopping. Thus, a more common solution is to use a DEM with a finer resolution, if available (Wechsler, 2007; Dottori et al., 2013). Generally, small-scale

structures such as narrow streets are certainly better represented by a DEM with finer resolutions (Wechsler, 2007; Fewtrell et al., 2011; de Almeida et al., 2016). Nevertheless, as has been pointed out before, finer resolutions might also lead to inadequate confidence in the extremely precise model outputs (Dottori et al., 2013). Along these lines, it is crucial to note that the DEM itself is an imperfect representation of the reality, irrespective of its resolution (Wechsler, 2007; Abily et al., 2016). Just as DEMs with coarser resolutions, topographical models with finer resolutions are not flawless either and contain artifacts, which may cause false results, as illustrated in Fig. 7. Therefore, the DEM needs to receive particular attention, i.e., it needs to be carefully pre- and post-processed in order to represent realistic flow paths, as other studies have highlighted as well (Hankin et al., 2008; Hunter et al., 2008; Tyrna et al., 2017).

The models may produce distinctly different results under certain circumstances, as highlighted by the models applied to the convex artificial surface characterized by diverging flow patterns (Fig. 5). However, in real-world applications such forms are likely less important in

comparison to plane and concave slopes, as exemplified by the case study E2 characterized by concave topography (cf. Fig. 8). On such slopes, the models exhibit better model agreement (Fig. 5). Thus, in real-world applications, the model choice seems to play an inferior role compared to the previously discussed issues including the appropriate representation of effective rainfall and topographical structures. In other words, the model choice is generally not the most important factor determining whether the observed inundation area can be predicted well by the corresponding model, at least for events associated with heavy rainfall. However, it should be noted that this statement might be different for the prediction of flow depths and/or flow velocities. As mentioned before, the hydrodynamic models, i.e., FLO-2D, FloodArea and r.sim.water, generally predict the number of wet cells less reliably for case studies associated with weak rainfall. An exception is the flow algorithm MFD, which produces the least biased results for all case studies (Fig. 11). At the downside, the algorithm cannot consider ponding or backwater, as exemplified by the model's distinct underestimation of the inundated area towards the outlet of the study site E2 (Fig. 9, MFD). Thus, MFD can be used for approximating the extent of inundated areas, but not for predicting flow depths, flow velocities, and flow dynamics in general.

Lastly, the model performance is also highly dependent on the used data. Therefore, it is crucial to account for the uncertainties introduced by the input data, for instance by carrying out a sensitivity analysis (e.g. Pianosi et al., 2016). At the same time, the uncertainties need to be considered, which stem from the observational data that are used to condition and/or evaluate the models. For instance, if the observational data are a bad representation of the models' simulated quantity, the performance of the models are inevitably low, as exemplified by the case study E1 (Fig. 7 and Sect. 3.2). Yet, as mentioned before, there is little high-quality observational data available, which exhibit appropriate spatial and temporal resolutions suitable for model calibration and/or validation (e.g. Hunter et al., 2008; Blanc et al., 2012; Neal et al., 2012; Yu and Coulthard, 2015). Consequently, in this study, it was necessary to exploit different data sources, including external maps, eye witnesses' photographs and videos, mapped flood traces based on field visits partly supported by aerial photographs (cf. Table 5 and Fig. 4). Yet, the mapped quantity is not the same for each source. While the exploited photographs and videos represent a snapshot of the flow pattern at a certain instant during the respective SWF, reconstructions based on flood marks are constrained to areas where the flood has left discernible traces. For instance, overland flow with few suspended particles might not leave identifiable traces. In consequence, this likely leads to an underestimation of the actual inundated area. Accordingly, we assigned this data source with a lower (medium) confidence level, as indicated in Table 5. Despite the increased confidence level for overland flow reconstructed from photographs and videos, a similar bias might apply to this data source, as well. Namely, a bias is introduced if the picture is not taken at the instant of the maximal flood extent.

Therefore, just as the simulation outputs, the observational data should be regarded as uncertain (Bennett et al., 2013; Stephens et al., 2014; Savage et al., 2016a). Thus, the representation of the observations and simulations as a crisp representation of the reality might be inappropriate. To address this issue, Pappenberger et al. (2007) applied a fuzzy set approach to measure the performance based on uncertain observational data. Thereby, slight shifts between observed and simulated wet cells could be accounted for. For simulated wet cells, it is straightforward to obtain a confidence level that a particular cell is wet by considering the simulated flow depths (Pappenberger et al., 2007). In contrast, this is not trivial for the observational data used in this study. Namely, ancillary data would be necessary. For instance, flood traces mapped in the field could be categorized according to the respective confidence that the corresponding area was in fact inundated.

In case only the flood extent is of interest, for instance when identifying potentially flooded assets, choosing a simple over a

hydrodynamic model might be advantageous: as exemplified by the real-world case studies, the extent of SWFs can be predicted similarly well with MFD as with the considered hydrodynamic models, while the associated computational demand is much smaller. Consequently, MFD could be applied to larger areas while exploiting the increasing availability of high-resolution DEMs. Moreover, there are other simple conceptual models, as termed by Teng et al. (2017), which may overcome some of the limitations of MFD, such as the incapability to simulate ponding water. Potential candidates include for instance the Rapid Flood Spreading Method (RFSM), as described by L'homme et al. (2008), or the model called HAND (height above the nearest drainage), as introduced by Nobre et al. (2011). Such approaches could be applied to (almost) any scale and area (Teng et al., 2017), which could make them interesting candidates for regional or even continental hazard assessments regarding SWFs. Moreover, such models are predestined to be used in probabilistic modeling approaches (e.g. Merwade et al., 2008; Aronica et al., 2012; Savage et al., 2016a). Thus, the applicability of a probabilistic modeling approach in relation to SWFs in rural areas should be investigated in the future, as well.

5. Conclusions and outlook

The main aim of this study was to test a SWF hazard assessment approach that is currently employed in practice and is based on single simulations with uncalibrated and/or unvalidated flood inundation models. For that matter, we applied four uncalibrated raster-based models to four characteristic artificial surfaces and eight real-world case studies. The models' application to the artificial surfaces exemplified that the flow patterns are heavily disturbed by streets, insofar as the prediction of inundated areas downslope of such structures are significantly influenced. Thus, there are large differences of how each model predicts these flow disturbances. Moreover, the modeling exercise has indicated that the models disagree most about the prediction of flow on the convex surface. The performance of the models applied to real-world case studies was assessed qualitatively as well as quantitatively in relation to inundated areas inferred from different sources. In summary, the performance of the selected grid-based models indicates that they are not (yet) suited to be employed in an uncalibrated mode to reliably and deterministically predict inundated areas caused by SWFs in rural areas. Mainly, the models' performances are impaired by biased predictions of effective rainfall and insufficient representation of topographical structures.

To improve the prediction of SWF hazards, various approaches seem prospective. First of all, the deterministic modeling approach could be improved by incorporating a better prediction of the complex runoff generation mechanisms under various conditions. Moreover, the representation of topographical structures could be improved by considering DEMs with finer resolutions. Alternatively, irregular meshes and corresponding models could be used for a better representation of structures such as streets. At the same time, this study indicates that the models' calibration and/or their results' validation is imperative. For this task, the uncertainties of the observations should be considered, which may vary significantly depending on the source and quality of the observations. In general, the quantification and communication of the models' associated uncertainties are crucial, as the models' extremely precise outputs have indeed the potential to provoke overconfidence in their results, which may lead to inappropriate decisions in flood risk management (Dottori et al., 2013).

A different way forward would be to exploit simple conceptual models such as MFD. Within the context of this study, MFD performed similarly well than the hydrodynamic models. Thus, similar conceptual models could be tested, which overcome some of the limitations of MFD, while providing similar results. The computational effort of such simple models is by far the least. Such approaches are therefore also interesting for the application to large areas, for instance in the context of regional, national or even continental SWF hazard assessments. Yet,

due to lower computational constraints, even the topographical data with the finest available resolutions might be exploited. Moreover, such models could be applied in a probabilistic simulation framework, which could potentially better handle the lack of observational data in comparison to the current deterministic approaches.

Finally, this study highlighted once more that observational data are crucial irrespective of the chosen way forward. Thus, a standardized method to document and report SWFs in rural and urban areas is required and should be developed. At the same time, systematic observations should be put in place to lie the ground for future research, which is certainly necessary.

Acknowledgments

Funding from the Mobiliar Lab for Natural Risks supported the completion of this research. We thank the Federal Office of Topography for providing the corresponding spatial data, as well as the Federal Office of Meteorology and Climatology for providing the rainfall data. We would also like to thank geomer GmbH for providing a FloodArea license under favorable terms, and in particular André Assmann for his assistance. Moreover, we thank Mirjam Stawicki for supporting the field work, David Thöni for his modeling efforts during the initial phase of the study, Simona Trefalt for proofreading, and Guido Felder for revising the manuscript.

Appendix A. Supplementary data

Supplementary data related to this article can be found at <https://doi.org/10.1016/j.envsoft.2018.08.005>.

References

- Abily, M., Bertrand, N., Delestre, O., Gourbesville, P., Duluc, C.-M., 2016. Spatial global sensitivity analysis of high resolution classified topographic data use in 2D urban flood modelling. *Environ. Model. Software* 77, 183–195. <https://doi.org/10.1016/j.envsoft.2015.12.002>.
- Alder, S., Prasuhn, V., Liniger, H., Herweg, K., Hurni, H., Candinas, A., Gujer, H.U., 2015. A high-resolution map of direct and indirect connectivity of erosion risk areas to surface waters in Switzerland — a risk assessment tool for planning and policy-making. *Land Use Pol.* 48, 236–249. <https://doi.org/10.1016/j.landusepol.2015.06.001>.
- de Almeida, G.A.M., Bates, P., Ozdemir, H., 2016. Modelling urban floods at sub-metre resolution: challenges or opportunities for flood risk management? *J. Flood Risk Manage.* 1–11. <https://doi.org/10.1111/jfr3.12276>.
- Andrieu, H., Browne, O., Laplace, D., 2004. Les crues en zone urbaine: des crues éclairs? *La Houille Blanche* 89–95. <https://doi.org/10.1051/lhb:200402010>.
- Antonetti, M., Buss, R., Scherrer, S., Margreth, M., Zappa, M., 2016. Mapping dominant runoff processes: an evaluation of different approaches using similarity measures and synthetic runoff simulations. *Hydrol. Earth Syst. Sci.* 20, 2929–2945. <https://doi.org/10.5194/hess-20-2929-2016>.
- Aronica, G., Bates, P.D., Horritt, M.S., 2002. Assessing the uncertainty in distributed model predictions using observed binary pattern information within GLUE. *Hydrol. Process.* 16, 2001–2016. <https://doi.org/10.1002/hyp.398>.
- Aronica, G.T., Franza, F., Bates, P.D., Neal, J.C., 2012. Probabilistic evaluation of flood hazard in urban areas using Monte Carlo simulation. *Hydrol. Process.* 26, 3962–3972. <https://doi.org/10.1002/hyp.8370>.
- Di Baldassarre, G., Montanari, A., Lins, H., Koutsoyiannis, D., Brandimarte, L., Blöschl, G., 2010. Flood fatalities in Africa: from diagnosis to mitigation. *Geophys. Res. Lett.* 37, L22402. <https://doi.org/10.1029/2010GL045467>.
- Barredo, J.I., 2009. Normalised flood losses in Europe: 1970–2006. *Nat. Hazards Earth Syst. Sci.* 9, 97–104. <https://doi.org/10.5194/nhess-9-97-2009>.
- Bennett, N.D., Croke, B.F., Guariso, G., Guillaume, J.H., Hamilton, S.H., Jakeman, A.J., Marsili-Libelli, S., Newham, L.T., Norton, J.P., Perrin, C., Pierce, S.A., Robson, B., Seppelt, R., Voinov, A.A., Fath, B.D., Andreassian, V., 2013. Characterising performance of environmental models. *Environ. Model. Software* 40, 1–20. <https://doi.org/10.1016/j.envsoft.2012.09.011>.
- Bernet, D.B., Prasuhn, V., Weingartner, R., 2017. Surface water floods in Switzerland: what insurance claim records tell us about the damage in space and time. *Nat. Hazards Earth Syst. Sci.* 17, 1659–1682. <https://doi.org/10.5194/nhess-17-1659-2017>.
- Blanc, J., Hall, J.W., Roche, N., Dawson, R.J., Cesses, Y., Burton, A., Kilsby, C.G., 2012. Enhanced efficiency of pluvial flood risk estimation in urban areas using spatial-temporal rainfall simulations. *J. Flood Risk Manage.* 5, 143–152. <https://doi.org/10.1111/j.1753-318X.2012.01135.x>.
- Castro, D., Einfalt, T., Frerichs, S., Friedeheim, K., Hatzfeld, F., Kubik, A., Mittelstädt, R., Müller, M., Seltmann, J., Wagner, A., 2008. Vorhersage und Management von Sturzfluten in urbanen Gebieten (URBAS): Schlussbericht des vom Bundesministerium für Bildung und Forschung geförderten Vorhabens. Hydrotec GmbH und Fachhochschule Aachen und Deutscher Wetterdienst, Aachen, Deutschland. <http://www.urbanesturzfluten.de>.
- CEPRI, 2014. Gérer les inondations par ruissellement pluvial — Guide de sensibilisation. Centre Européen de Prévention du Risque d'Inondation, Orléans, France. http://www.cepri.net/Ruissellement_pluvial.html.
- Chan, F.K.S., Mitchell, G., Adekola, O., McDonald, A., 2012. Flood risk in Asia's urban mega-deltas. In: *Environment and Urbanization ASIA* 3. pp. 41–61. <https://doi.org/10.1177/097542531200300103>.
- Chen, A.S., Evans, B., Djordjević, S., Savić, D.A., 2012. A coarse-grid approach to re-presenting building blockage effects in 2D urban flood modelling. *J. Hydrol.* 426–427, 1–16. <https://doi.org/10.1016/j.jhydrol.2012.01.007>.
- Chu, S.T., 1978. Infiltration during an unsteady rain. *Water Resour. Res.* 14, 461–466. <https://doi.org/10.1029/WR014i003p00461>.
- Conrad, O., Bechtel, B., Bock, M., Dietrich, H., Fischer, E., Gerlitz, L., Wehberg, J., Wichmann, V., Böhner, J., 2015. System for automated geoscientific Analyses (SAGA) v. 2.1.4. *Geosci. Model Dev. (GMD)* 8, 1991–2007. <https://doi.org/10.5194/gmd-8-1991-2015>.
- Cook, A., Merwade, V., 2009. Effect of topographic data, geometric configuration and modeling approach on flood inundation mapping. *J. Hydrol.* 377, 131–142. <https://doi.org/10.1016/j.jhydrol.2009.08.015>.
- Coulthard, T.J., Frostick, L.E., 2010. The Hull floods of 2007: implications for the governance and management of urban drainage systems. *J. Flood Risk Manage.* 3, 223–231. <https://doi.org/10.1111/j.1753-318X.2010.01072.x>.
- Cutter, S.L., Emrich, C., 2005. Are natural hazards and disaster losses in the U.S. increasing? *Eos Trans. AGU* 86, 381–389. <https://doi.org/10.1029/2005EO410001>.
- Dottori, F., Di Baldassarre, G., Todini, E., 2013. Detailed data is welcome, but with a pinch of salt: accuracy, precision, and uncertainty in flood inundation modeling. *Water Resour. Res.* 49, 6079–6085. <https://doi.org/10.1002/wrcr.20406>.
- Dunkerley, D., 2008. Identifying individual rain events from pluviograph records: a review with analysis of data from an Australian dryland site. *Hydrol. Process.* 22, 5024–5036. <https://doi.org/10.1002/hyp.7122>.
- DWA, 2013. Starkregen und urbane Sturzfluten — Praxisleitfaden zur Überflutungsvorsorge volume T1/2013 of DWA-Themen. Deutsche Vereinigung für Wasserwirtschaft, Abwasser und Abfall (DWA), Hennef, Deutschland.
- Egli, T., 2007. Wegleitung Objektschutz gegen meteorologische Naturgefahren. Vereinigung Kantonalen Feuerversicherungen, Bern, Schweiz. <http://vfk.ch/VKF/Downloads>.
- Falconer, R.H., Cobby, D., Smyth, P., Astle, G., Dent, J., Golding, B., 2009. Pluvial flooding: new approaches in flood warning, mapping and risk management. *J. Flood Risk Manage.* 2, 198–208. <https://doi.org/10.1111/j.1753-318X.2009.01034.x>.
- Ferreira, C., Walsh, R., Steenhuis, T.S., Shakesby, R.A., Nunes, J., Coelho, C., Ferreira, A., 2015. Spatiotemporal variability of hydrologic soil properties and the implications for overland flow and land management in a peri-urban Mediterranean catchment. *J. Hydrol.* 525, 249–263. <https://doi.org/10.1016/j.jhydrol.2015.03.039>.
- Fewtrell, T.J., Bates, P.D., Horritt, M., Hunter, N.M., 2008. Evaluating the effect of scale in flood inundation modelling in urban environments. *Hydrol. Process.* 22, 5107–5118. <https://doi.org/10.1002/hyp.7148>.
- Fewtrell, T.J., Duncan, A., Sampson, C.C., Neal, J.C., Bates, P.D., 2011. Benchmarking urban flood models of varying complexity and scale using high resolution terrestrial LiDAR data. *Phys. Chem. Earth* 36, 281–291. <https://doi.org/10.1016/j.pce.2010.12.011>.
- Foody, G.M., 2007. Map comparison in GIS. *Prog. Phys. Geogr.* 31, 439–445. <https://doi.org/10.1177/0309133307081294>.
- Freeman, T.G., 1991. Calculating catchment area with divergent flow based on a regular grid. *Comput. Geosci.* 17, 413–422. [https://doi.org/10.1016/0098-3004\(91\)90048-I](https://doi.org/10.1016/0098-3004(91)90048-I).
- Fuchs, S., Keiler, M., Zischg, A., 2015. A spatiotemporal multi-hazard exposure assessment based on property data. *Nat. Hazards Earth Syst. Sci.* 15, 2127–2142. <https://doi.org/10.5194/nhess-15-2127-2015>.
- Fuchs, S., Röthlisberger, V., Thaler, T., Zischg, A., Keiler, M., 2017. Natural hazard management from a coevolutionary perspective: exposure and policy response in the European Alps. *Ann. Assoc. Am. Geogr.* 107, 382–392. <https://doi.org/10.1080/24694452.2016.1235494>.
- Gaitan, S., van de Giesen, N.C., ten Veldhuis, J.A.E., 2016. Can urban pluvial flooding be predicted by open spatial data and weather data? *Environ. Model. Software* 85, 156–171. <https://doi.org/10.1016/j.envsoft.2016.08.007>.
- geomer, 2016. FloodAreaHPC-desktop: ArcGIS-extension for Calculating Flooded Areas — User Manual: Version 10.3. geomer GmbH and Ruiz Rodriguez + Zeisler + Blank, Heidelberg, Germany. <http://www.geomer.de/fileadmin/templates/main/res/downloads/UserManualFloodArea10.pdf>.
- Grahn, T., Nyberg, L., 2017. Assessment of pluvial flood exposure and vulnerability of residential areas. *Int. J. Disaster Risk Reduct.* 21, 367–375. <https://doi.org/10.1016/j.ijdrr.2017.01.016>.
- Green, W.H., Ampt, G.A., 1911. Studies on soil physics. *J. Agric. Sci.* 4, 1. <https://doi.org/10.1017/S002185960001441>.
- Haghighatafshar, S., la Cour Jansen, J., Aspegren, H., Lidström, V., Mattsson, A., Jönsson, K., 2014. Storm-water management in Malmö and Copenhagen with regard to climate change scenarios. *Vatten* 70, 159–168.
- Hankin, B., Waller, S., Astle, G., Kellagher, R., 2008. Mapping space for water: screening for urban flash flooding. *J. Flood Risk Manage.* 1, 13–22. <https://doi.org/10.1111/j.1753-318X.2008.00003.x>.
- Hénonin, J., Hongtao, M., Zheng-Yu, Y., Hartnack, J., Havno, K., Gourbesville, P., Mark, O., 2013. Citywide multi-grid urban flood modelling: the July 2012 flood in Beijing. *Urban Water J.* 12, 52–66. <https://doi.org/10.1080/1573062X.2013.851710>.
- Horritt, M., Bates, P., 2001. Effects of spatial resolution on a raster based model of flood

- flow. *J. Hydrol.* 253, 239–249. [https://doi.org/10.1016/S0022-1694\(01\)00490-5](https://doi.org/10.1016/S0022-1694(01)00490-5).
- Hunter, N.M., Bates, P.D., Neelz, S., Pender, G., Villanueva, I., Wright, N.G., Liang, D., Falconer, R.A., Lin, B., Waller, S., Crossley, A.J., Mason, D.C., 2008. Benchmarking 2D hydraulic models for urban flooding. *P. I. Civil Eng.-Wat. M.* 161, 13–30. <https://doi.org/10.1680/wama.2008.161.1.13>.
- Jakeman, A.J., Letcher, R.A., Norton, J.P., 2006. Ten iterative steps in development and evaluation of environmental models. *Environ. Model. Software* 21, 602–614. <https://doi.org/10.1016/j.envsoft.2006.01.004>.
- Jongman, B., Kreibich, H., Apel, H., Barredo, J.I., Bates, P.D., Feyen, L., Gericke, A., Neal, J., Aerts, J.C.J.H., Ward, P.J., 2012. Comparative flood damage model assessment: towards a European approach. *Nat. Hazards Earth Syst. Sci.* 12, 3733–3752. <https://doi.org/10.5194/nhess-12-3733-2012>.
- Jordi Kolb, A.G., 2008. Schadenkarte Unwetter 2007. Münsingen, Schweiz.
- Kazmierczak, A., Cavan, G., 2011. Surface water flooding risk to urban communities: analysis of vulnerability, hazard and exposure. *Landsc. Urban Plann.* 103, 185–197. <https://doi.org/10.1016/j.landurbplan.2011.07.008>.
- Kipfer, A., Kienholz, C., Liener, S., 2012. Ein neuer Ansatz zur Modellierung von Oberflächenabfluss. In: Koboltschnig, G., Hübl, J., Braun, J. (Eds.), INTERPRAEVENT 2012 — Conference Proceedings. International Research Society INTERPRAEVENT, pp. 179–189.
- Kipfer, A., Schönthal, E., Liener, S., Gsteiger, P., 2015. Oberflächenabflusskarte Kanton Luzern: Bericht. Bern, Schweiz: Geo7 AG.
- Kron, W., Steuer, M., Löw, P., Wirtz, A., 2012. How to deal properly with a natural catastrophe database — analysis of flood losses. *Nat. Hazards Earth Syst. Sci.* 12, 535–550. <https://doi.org/10.5194/nhess-12-535-2012>.
- Kuhnert, M., Voinov, A., Seppelt, R., 2005. Comparing raster map comparison algorithms for spatial modeling and analysis. *Photogramm. Eng. Rem. Sens.* 71, 975–984.
- Kundzewicz, Z.W., Kanae, S., Seneviratne, S.I., Handmer, J., Nicholls, N., Peduzzi, P., Mechler, R., Bouwer, L.M., Arnell, N., Mach, K., Muir-Wood, R., Brakenridge, G.R., Kron, W., Benito, G., Honda, Y., Takahashi, K., Sherstyukov, B., 2014. Flood risk and climate change: global and regional perspectives. *Hydrol. Sci. J.* 59, 1–28. <https://doi.org/10.1080/02626667.2013.857411>.
- López-Vicente, M., Pérez-Bielsa, C., López-Montero, T., Lambán, L.J., Navas, A., 2014. Runoff simulation with eight different flow accumulation algorithms: recommendations using a spatially distributed and open-source model. *Environ. Model. Software* 62, 11–21. <https://doi.org/10.1016/j.envsoft.2014.08.025>.
- Löwe, R., Ulrich, C., Sto Domingo, N., Mark, O., Deletic, A., Arnbjerg-Nielsen, K., 2017. Assessment of urban pluvial flood risk and efficiency of adaptation options through simulations — a new generation of urban planning tools. *J. Hydrol.* 550, 355–367. <https://doi.org/10.1016/j.jhydrol.2017.05.009>.
- LUBW, 2016. Leitfaden kommunales Starkregenrisikomanagement in Baden-Württemberg. Karlsruhe, Deutschland: Landesanstalt für Umwelt, Messungen und Naturschutz Baden-Württemberg (LUBW). <http://www.lubw.baden-wuerttemberg.de/servlet/is/261161>.
- L'homme, J., Sayers, P., Gouldby, B., Samuels, P., Wills, M., Mulet-Marti, J., 2008. Recent development and application of a rapid flood spreading method. In: Samuels, P., Huntington, S., Allsop, W., Harrop, J. (Eds.), *Flood Risk Management: Research and Practice Proceedings of the European Conference on Flood Risk Management Research into Practice*. Taylor and Francis Group, pp. 15–24.
- Maksimović, Č., Prodanović, D., Boonya-Aroonnet, S., Leitão, J.P., Djordjević, S., Allitt, R., 2009. Overland flow and pathway analysis for modelling of urban pluvial flooding. *J. Hydraul. Res.* 47, 512–523. <https://doi.org/10.3826/jhr.2009.3361>.
- McCuen, R.H., 2016. *Hydrologic Analysis and Design*, fourth ed. Pearson Higher Education, Hoboken, USA.
- Mein, R.G., Larson, C.L., 1973. Modeling infiltration during a steady rain. *Water Resour. Res.* 9, 384–394. <https://doi.org/10.1029/WR009i002p00384>.
- Meon, G., Stein, K., Förster, K., Riedel, G., 2009. Untersuchung Starkregengefährdeter Gebiete: Abschlussbericht Zum Forschungsprojekt. Technische Universität Braunschweig und Leichtweiß-Institut für Wasserbau, Braunschweig, Deutschland.
- Merwade, V., Olivera, F., Arabi, M., Edleman, S., 2008. Uncertainty in flood inundation mapping: current issues and future directions. *J. Hydrol. Eng.* 13, 608–620. [https://doi.org/10.1061/\(ASCE\)1084-0699\(2008\)13:7\(608\)](https://doi.org/10.1061/(ASCE)1084-0699(2008)13:7(608)).
- Merz, B., Kreibich, H., Schwarze, R., Thielen, A., 2010. Review article — “Assessment of economic flood damage”. *Nat. Hazards Earth Syst. Sci.* 10, 1697–1724. <https://doi.org/10.5194/nhess-10-1697-2010>.
- MeteoSwiss, 2014. Räumliche Daten CombiPrecip. Swiss Federal Office of Meteorology and Climatology. <http://www.meteoswiss.admin.ch/home/services-and-publications-produkte.subpage.html/en/data/products/2014/raeumliche-daten-combiprecip.html>, Accessed date: 3 July 2017.
- Mitasova, H., Thaxton, C., Hofierka, J., McLaughlin, R., Moore, A., Mitas, L., 2004. Path sampling method for modeling overland water flow, sediment transport, and short term terrain evolution in Open Source GIS. In: Miller, C.T., Farthing, M.W., Pinder, G.F., Gray, W.G. (Eds.), *Proceedings of the XVth International Conference on Computational Methods in Water Resources (CMWR XV)*. Elsevier, Chapel Hill, USA, pp. 1479–1490. [https://doi.org/10.1016/S0167-5648\(04\)80159-X](https://doi.org/10.1016/S0167-5648(04)80159-X).
- Neal, J., Villanueva, I., Wright, N., Willis, T., Fewtrell, T., Bates, P., 2012. How much physical complexity is needed to model flood inundation? *Hydrol. Process.* 26, 2264–2282. <https://doi.org/10.1002/hyp.8339>.
- Néelz, S., Pender, G., 2013. *Benchmarking the Latest Generation of 2D Hydraulic Modelling Packages: Report — SCI20002*. Environment Agency, Bristol, UK.
- Neteler, M., Bowman, M.H., Landa, M., Metz, M., 2012. GRASS GIS: a multi-purpose open source GIS. *Environ. Model. Software* 31, 124–130. <https://doi.org/10.1016/j.envsoft.2011.11.014>.
- Nobre, A.D., Cuartas, L.A., Hodnett, M., Rennó, C.D., Rodrigues, G., Silveira, A., Waterloo, M., Saleska, S., 2011. Height above the nearest drainage — a hydrologically relevant new terrain model. *J. Hydrol.* 404, 13–29. <https://doi.org/10.1016/j.jhydrol.2011.03.051>.
- van Ootegem, L., Verhofstadt, E., van Herck, K., Creten, T., 2015. Multivariate pluvial flood damage models. *Environ. Impact Assess.* 54, 91–100. <https://doi.org/10.1016/j.eiar.2015.05.005>.
- O'Brian, J.S., 2009. FLO-2D Reference Manual: Version 2009. FLO-2D Software Inc, Nutrioso, USA. <https://www.flo-2d.com/download/>.
- Panziera, L., Gabella, M., Zanini, S., Hering, A., Germann, U., Berne, A., 2016. A radar-based regional extreme rainfall analysis to derive the thresholds for a novel automatic alert system in Switzerland. *Hydrol. Earth Syst. Sci.* 20, 2317–2332. <https://doi.org/10.5194/hess-20-2317-2016>.
- Pappenberger, F., Frodsham, K., Beven, K.J., Romanowicz, R., Matgen, P., 2007. Fuzzy set approach to calibrating distributed flood inundation models using remote sensing observations. *Hydrol. Earth Syst. Sci.* 11, 739–752. <https://doi.org/10.5194/hess-11-739-2007>.
- Pianosi, F., Beven, K., Freer, J., Hall, J.W., Rougier, J., Stephenson, D.B., Wagener, T., 2016. Sensitivity analysis of environmental models: a systematic review with practical workflow. *Environ. Model. Software* 79, 214–232. <https://doi.org/10.1016/j.envsoft.2016.02.008>.
- Pilešjö, P., Hasan, A., 2014. A triangular form-based multiple flow algorithm to estimate overland flow distribution and accumulation on a digital elevation model. In: *T. GIS* 18, pp. 108–124. <https://doi.org/10.1111/tgis.12015>.
- Pitt, M., 2008. *The Pitt Review: Learning Lessons from the 2007 Floods: an Independent Review by Sir Michael Pitt*. Cabinet Office, London, UK.
- Planchon, O., Darboux, F., 2002. A fast, simple and versatile algorithm to fill the depressions of digital elevation models. *Catena* 46, 159–176. [https://doi.org/10.1016/S0341-8162\(01\)00164-3](https://doi.org/10.1016/S0341-8162(01)00164-3).
- Quinn, P., Beven, K., Chevallier, P., Planchon, O., 1991. The prediction of hillslope flow paths for distributed hydrological modelling using digital terrain models. *Hydrol. Process.* 5, 59–79.
- R Core Team, 2016. R: a Language and Environment for Statistical Computing. R Foundation for Statistical Computing, Vienna, Austria. <https://www.R-project.org>.
- Rawls, W.J., Brakensiek, D.L., Miller, N., 1983. Green-Ampt infiltration parameters from soils data. *J. Hydraul. Eng.-ASCE* 109, 62–70. [https://doi.org/10.1061/\(ASCE\)0733-9429\(1983\)109:1\(62\)](https://doi.org/10.1061/(ASCE)0733-9429(1983)109:1(62)).
- Röthlisberger, V., Zischg, A.P., Keiler, M., 2017. Identifying spatial clusters of flood exposure to support decision making in risk management. *Sci. Total Environ.* 598, 593–603. <https://doi.org/10.1016/j.scitotenv.2017.03.216>.
- Rözer, V., Müller, M., Bubeck, P., Kienzler, S., Thielen, A., Pech, I., Schröter, K., Buchholz, O., Kreibich, H., 2016. Coping with pluvial floods by private households. *Water* 8, 304. <https://doi.org/10.3390/w8070304>.
- Rüttimann, D., Egli, T., 2010. *Wegleitung Punktuelle Gefahrenabklärung Oberflächenwasser*. St. Gallen, Schweiz: Naturgefahrenkommission des Kantons St. Gallen.
- Sampson, C.C., Fewtrell, T.J., Duncan, A., Shaad, K., Horritt, M.S., Bates, P.D., 2012. Use of terrestrial laser scanning data to drive decimetric resolution urban inundation models. *Adv. Water Resour.* 41, 1–17. <https://doi.org/10.1016/j.advwatres.2012.02.010>.
- Sampson, C.C., Bates, P.D., Neal, J.C., Horritt, M.S., 2013. An automated routing methodology to enable direct rainfall in high resolution shallow water models. *Hydrol. Process.* 27, 467–476. <https://doi.org/10.1002/hyp.9515>.
- Savage, J.T.S., Bates, P., Freer, J., Neal, J., Aronica, G., 2016a. When does spatial resolution become spurious in probabilistic flood inundation predictions? *Hydrol. Process.* 30, 2014–2032. <https://doi.org/10.1002/hyp.10749>.
- Savage, J.T.S., Pianosi, F., Bates, P.D., Freer, J., Wagener, T., 2016b. Quantifying the importance of spatial resolution and other factors through global sensitivity analysis of a flood inundation model. *Water Resour. Res.* 52, 9146–9163. <https://doi.org/10.1002/2015WR018198>.
- Schmocker-Fackel, P., Naef, F., Scherrer, S., 2007. Identifying runoff processes on the plot and catchment scale. *Hydrol. Earth Syst. Sci.* 11, 891–906. <https://doi.org/10.5194/hess-11-891-2007>.
- Schumann, G., Bates, P.D., Horritt, M.S., Matgen, P., Pappenberger, F., 2009. Progress in integration of remote sensing-derived flood extent and stage data and hydraulic models. *Rev. Geophys.* 47, RG4001. <https://doi.org/10.1029/2008RG000274>.
- Seibert, J., McGlynn, B.L., 2007. A new triangular multiple flow direction algorithm for computing upslope areas from gridded digital elevation models. *Water Resour. Res.* 43. <https://doi.org/10.1029/2006WR005128>.
- Sideris, I.V., Gabella, M., Erdin, R., Germann, U., 2014. Real-time radar-rain-gauge merging using spatio-temporal co-kriging with external drift in the alpine terrain of Switzerland. *Q. J. R. Meteorol. Soc.* 140, 1097–1111. <https://doi.org/10.1002/qj.2188>.
- Spekkers, M.H., Kok, M., Clemens, F.H.L.R., ten Veldhuis, J.A.E., 2014. Decision-tree analysis of factors influencing rainfall-related building structure and content damage. *Nat. Hazards Earth Syst. Sci.* 14, 2531–2547. <https://doi.org/10.5194/nhess-14-2531-2014>.
- Spekkers, M., Rözer, V., Thielen, A., ten Veldhuis, M.-c., Kreibich, H., 2017. A comparative survey of the impacts of extreme rainfall in two international case studies. *Nat. Hazards Earth Syst. Sci.* 17, 1337–1355. <https://doi.org/10.5194/nhess-17-1337-2017>.
- Steinbrich, A., Leister, H., Weiler, M., 2016. Model-based quantification of runoff generation processes at high spatial and temporal resolution. *Environ. Earth Sci.* 75, 1423. <https://doi.org/10.1007/s12665-016-6234-9>.
- Stephens, E., Schumann, G., Bates, P., 2014. Problems with binary pattern measures for flood model evaluation. *Hydrol. Process.* 28, 4928–4937. <https://doi.org/10.1002/hyp.9979>.
- swisstopo, 2017a. swissALTI3D: the High Precision Digital Elevation Model of Switzerland. Swiss Federal Office of Topography. <https://shop.swisstopo.admin.ch/>

- [en/products/height_models/alti3D](#), Accessed date: 3 July 2017.
- swisstopo, 2017b. SWISSIMAGE: the Digital Color Orthophotomosaic of Switzerland. Swiss Federal Office of Topography. https://shop.swisstopo.admin.ch/en/products/images/ortho_images/SWISSIMAGE, Accessed date: 3 July 2017.
- Teng, J., Jakeman, A.J., Vaze, J., Croke, B., Dutta, D., Kim, S., 2017. Flood inundation modelling: a review of methods, recent advances and uncertainty analysis. *Environ. Model. Software* 90, 201–216. <https://doi.org/10.1016/j.envsoft.2017.01.006>.
- Thielen, A.H., Kreibich, H., Müller, M., Merz, B., 2007. Coping with floods: preparedness, response and recovery of flood-affected residents in Germany in 2002. *Hydrol. Sci. J.* 52, 1016–1037. <https://doi.org/10.1623/hysj.52.5.1016>.
- Tyrna, B.G., Hochschild, V., 2010. Modellierung von lokalen Überschwemmungen nach Starkniederschlägen. In: Strobl, J., Blaschke, T., Griesebner, G. (Eds.), *Angewandte Geoinformatik 2010*, pp. 325–334.
- Tyrna, B., Assmann, A., Fritsch, K., Johann, G., 2017. Large-scale high-resolution pluvial flood hazard mapping using the raster-based hydrodynamic two-dimensional model FloodAreaHPC. *J. Flood Risk Manage.* 42, 19. <https://doi.org/10.1111/jfr3.12287>.
- Ward, R.C., Robinson, M., 2000. *Principles of Hydrology*, fourth ed. McGraw-Hill, London, UK.
- Wechsler, S.P., 2007. Uncertainties associated with digital elevation models for hydrologic applications: a review. *Hydrol. Earth Syst. Sci.* 11, 1481–1500. <https://doi.org/10.5194/hess-11-1481-2007>.
- Yu, D., Coulthard, T.J., 2015. Evaluating the importance of catchment hydrological parameters for urban surface water flood modelling using a simple hydro-inundation model. *J. Hydrol.* 524, 385–400. <https://doi.org/10.1016/j.jhydrol.2015.02.040>.
- Zhou, Q., Liu, X., 2002. Error assessment of grid-based flow routing algorithms used in hydrological models. *Int. J. Geogr. Inf. Sci.* 16, 819–842. <https://doi.org/10.1080/13658810210149425>.
- Zhou, Q., Mikkelsen, P.S., Halsnæs, K., Arnbjerg-Nielsen, K., 2012. Framework for economic pluvial flood risk assessment considering climate change effects and adaptation benefits. *J. Hydrol.* 414–415, 539–549. <https://doi.org/10.1016/j.jhydrol.2011.11.031>.
- Zischg, A.P., Mosimann, M., Bernet, D.B., Röthlisberger, V., 2018. Validation of 2D flood models with insurance claims. *J. Hydrol.* 557, 350–361. <https://doi.org/10.1016/j.jhydrol.2017.12.042>.

Paper 17: Mazzorana, B., Zischg, A., Largiader, A., Hübl, J., 2009. Hazard index maps for woody material recruitment and transport in alpine catchments. *Natural Hazards and Earth System Sciences* 9, 197–209. [10.5194/nhess-9-197-2009](https://doi.org/10.5194/nhess-9-197-2009).

Hazard index maps for woody material recruitment and transport in alpine catchments

B. Mazzorana^{1,2}, A. Zischg^{3,4}, A. Largiader³, and J. Hübl²

¹Department of Hydraulic Engineering, Autonomous Province of Bolzano/Bozen South Tyrol, Bolzano, Italy

²Institute of Mountain Risk Engineering, University of Natural Resources and Applied Life Sciences, Vienna, Austria

³Abenis AG, Chur, Switzerland

⁴Abenis Alpinexpert srl, Bolzano, Italy

Received: 4 August 2008 – Revised: 5 February 2009 – Accepted: 9 February 2009 – Published: 19 February 2009

Abstract. A robust and reliable risk assessment procedure for hydrologic hazards deserves particular attention to the role of transported woody material during flash floods or debris flows. At present, woody material transport phenomena are not systematically considered within the procedures for the elaboration of hazard maps. The consequence is a risk of losing prediction accuracy and of underestimating hazard impacts. Transported woody material frequently interferes with the sediment regulation capacity of open check dams and moreover, when obstruction phenomena at critical cross-sections of the stream occur, inundations can be triggered. The paper presents a procedure for the determination of the relative propensity of mountain streams to the entrainment and delivery of recruited woody material on the basis of empirical indicators. The procedure provided the basis for the elaboration of a hazard index map for all torrent catchments of the Autonomous Province of Bolzano/Bozen. The plausibility of the results has been thoroughly checked by a backward oriented analysis on natural hazard events, documented since 1998 at the Department of Hydraulic Engineering of the aforementioned Alpine Province. The procedure provides hints for the consideration of the effects, induced by woody material transport, during the elaboration of hazard zone maps.

1 Introduction

In European mountain regions significant losses resulting from torrent processes occurred during the last decades (e.g., Oberndorfer et al., 2007; Autonome Provinz Bozen –

Südtirol, 2008), in spite of considerable efforts undertaken for the protection of endangered areas (Fuchs and McAlpin, 2005). A retrospective analysis on hazard maps highlighted a series of shortcomings with respect to torrential processes (Berger et al., 2007). In particular the effects of changing channel morphology and associated woody material transport phenomena were found to remarkably amplify process intensities (e.g., Diehl, 1997; Lyn et al., 2007). Considering the effects of woody material transport specifically, clear indications emerged from the analysis of the debris flow and flood events which recently occurred in several alpine regions (e.g., Rickli and Bucher, 2006). At critical channel geometry configurations such as bridge cross sections the transported woody material can be easily entrapped and subsequently partially or totally block the cross-sectional area for conveyance. In addition to increasing the loading conditions on the structural components of the bridges (e.g. piers and superstructure), overflowing becomes more frequent and therefore flood hazard impacts increase (Bezzola et al., 2003). Transported woody material frequently interferes directly with the sediment regulating capacity of open check dams (Lange et al., 2006). Clogging of the check dam openings during the early stages of debris flow events induces deposition when the intensity of the events is rather low. As a consequence, if the retention capacity is limited, a hazard mitigation performance can be expected which is far from optimum. In the procedures and regulations currently being used in hazard mapping, the assessment of such potential impacts is left to expert discretion. Decisions made in this way involve subjective assumptions concerning certain impact variables (e.g. woody material transport) and this affects the transparency, comparability and ultimately the quality of the hazard mitigation. In order to avoid such shortcomings in mitigation planning, we propose a procedure, which, based



Correspondence to: B. Mazzorana
(bruno.mazzorana@provinz.bz.it)

on empirical indicators, determines the relative propensity of mountainous streams to the entrainment and delivery of woody material.

While the ecological and morphological role of woody debris in mountain streams have been extensively studied (Abbe et al., 1997; Hildebrand et al., 1997; Keim et al., 2002; Gurnell et al., 2002; Montgomery and Piegay, 2003; Comiti et al., 2006), hazard related topics of woody material transport have been less systematically investigated. Nevertheless, some literature exists concerning in-stream structures. For example, Diehl (1997) studied the damage potential of transported woody material and Shields et al. (2001) analyzed the relation between flow resistance and increased inundation frequency due to the presence of large woody material. New insights into the dynamics of wood transport in streams have been achieved through flume experiments (Braudrick et al., 1997; Braudrick and Grant, 2000, 2001; Curran et al., 2003; Degetto, 2000; Rickenmann, 1997; Haga et al., 2002). The interaction of woody debris transport with protection measures has been investigated with a special focus on check dams (Bezzola et al., 2004; Lange et al., 2006; Uchiogi et al., 1996) and on rope nets (Rimböck, 2004). Furthermore, advanced tools for modelling woody material recruitment storage and dynamics for small streams and their watersheds have been developed (Lancaster et al., 2001).

This work addresses the following questions from a hazard assessment perspective: 1) For which mountain torrents do woody material recruitment and transport phenomena have been considered in hazard mapping? 2) Which mountain torrents are supposed to react in a sensitive way in terms of increasing hazard impacts if woody material transport occurs? 3) Which additional system loading and system response scenarios should be assumed, bearing in mind possible effects of woody material transport? 4) Can protection forest management policies be rationalized from a woody material transport hazard related perspective?

Based on these questions, the main objective of this study is to develop a procedure for generating hazard index maps (compare also Petraschek and Kienholz, 2003), in which the torrent catchments are classified according to their propensity to entrain and deliver woody material. Hazard index maps for debris flow and sediment transport and deposition processes already exist for the torrent catchments of the Autonomous Province of Bolzano/Bozen (Heinmann et al., 1998). These maps along with the newly created maps will constitute a reference on a hazard index level for the detection of the relevant hazard processes within each hazard assessment unit. In a successive analysis step the experts determine the hazard zones with more sophisticated procedures and can tailor the output maps to the requested level of detail.

2 Method

The proposed empirical method for the assessment of the hazard potential resulting from woody material recruitment and transport rests on the following outlined two step approach. In a first step the woody material recruitment areas are identified, localized and classified based on their capacity to increase the hazard potential of transport processes in alpine torrents. Woody material recruitment areas are defined as both vegetated torrent bed as well as wood-covered areas on hill slopes in close proximity or with a high connectivity to the torrent. In a second step an indicator for woody debris recruitment and transport is calculated for each torrent catchment. The application of a GIS based procedure, in which both aforementioned steps have been implemented, allowed for the generation of comprehensive hazard index maps for all torrential catchments of the Autonomous Province of Bolzano/Bozen. The level of detail of the procedure is restricted to the level of detail defined for hazard index maps (Petraschek and Kienholz, 2003).

2.1 A hazard process oriented view of woody material dynamics

As outlined by Rickli and Bucher (2006), the volume of the transported woody material in a defined torrent reach is a product of: 1) the transport process in the considered reach (e.g. inflow and outflow of woody material), 2) the potentially recruitable woody material along the banks and the channel bed, if vegetated (e.g. vegetated bars), and 3) the recruitment processes taking place on hill slopes. Rickli and Bucher (2006) identify the following relevant recruitment processes:

1. Bank erosion: Through the shear stress exerted on the wetted perimeter of the cross-section of the channel erosion processes occur along the banks altering the static equilibrium of the trees that can topple or slide into the channel. Hazard increasing conditions of synchronism between debris flow or flood events and the above mentioned woody material recruitment process is quite probable.
2. Wind-throw: strong wind conditions can either destabilize the trees that consequently fall as a whole into the channel, or lead to the recruitment of the epigeous parts, if their stems break under the wind loading. May and Gresswell (2003) point out that falling trees with a horizontal distance to the channel that exceeds their height can exert a destabilizing action on other trees (e.g. knock-on effect).
3. Snow loading: the pressure exerted by the snow, in particular wet snow in spring and autumn, can cause stability problems to broad-leaved trees increasing bending moments and shear forces. Through the concurring

cleaving action of ice, crowns of trees are susceptible to break off.

4. Landslides and other slope processes convey standing and lying woody material within the process perimeter towards the channel. Woody material temporarily stored in steep gullies on hill slope areas can also be conveyed toward the channel in connection with mass movements.
5. Avalanches are likely to incorporate and convey large volumes of woody material within the process perimeter.

As a general rule, in the case of debris flows, a large part of the available woody material within the discharge cross-section is likely to be entrained and transported. In the case of flood processes above a threshold discharge value, entrainment of woody material starts due to the fact that the destabilizing forces (drag and buoyancy forces) exceed the resisting forces (friction and the gravity component normal to the channel bed). It has been evidenced by flume experiments (Braudrick and Grant, 2000; Bezzola et al., 2003) that in larger mountainous streams, characterized by channel widths greater than the wood element length, entrainment depends on the orientation of the wood element in relation to a series of parameters. These parameters are the flow direction, the roughness of the wood element, the roughness of the stream bed, the density of the wood and the ratio between wood element diameter and flow depth. In smaller streams transport phenomena are characterized by a certain intermittency involving pivoting and jamming of the wood elements.

In the following sections, a classification scheme of the woody material recruitment areas is proposed (Sect. 2.2) and subsequently these areas are identified and spatially delimited (Sect. 2.3).

2.2 Classification of the woody material recruitment areas

Referring to the description of the dynamics of woody material briefly outlined in the previous section, the recruitment areas are classified according to the following criteria: 1) wood stand productivity, 2) activity/intensity of the recruitment processes, and 3) activity/intensity of torrential processes:

1. SIZ-areas (“stream influence zone”): The extent of these areas is determined by the wetted perimeter corresponding to the peak discharge of the considered extreme event of the debris flow or flood with intense bedload transport, depending on the dominant process (compare Sect. 2.3 for details). Hazard index maps for debris flows and floods with intense sediment transport for the torrent catchments of the Autonomous Province of Bolzano/Bozen have been produced (Staffler et al., 2008). The SIZ-areas include either the areas exposed to debris flows, overbank sedimentation or the channel

beds. Tree and shrub vegetation of the banks and the torrent bed which is directly exposed to the hydrodynamic forces is easily entrained. Vertical and lateral erosion can significantly reinforce the entrainment process (compare Fig. 1).

2. AWB-areas (“active wood buffer”): These active recruitment areas border the SIZ-areas. Toppling trees can directly reach the stream and considerably influence geomorphologic processes (compare Fig. 2). Autochthonous jams are made of woody material that has not been entrained from the point where it first entered the channel, although it may have rotated or the channel may have moved (Abbe and Montgomery, 1996). Up to a certain intensity of the flood process, the formation of these jams has a stabilizing effect on the stream bed, but for higher intensities mobilization of the woody material starts to occur.
3. RWB-Areas (“recharging wood buffer”): This forested band is directly connected to the outside of the AWB. Toppling trees cannot reach the stream bed directly, but as evidence from documented events underpins, they can destabilize other trees from the AWB (compare Fig. 2) or in extremely steep and cliffy areas they can slide into the stream bed. The parameters determining the width of the AWB and the RWB are the fundamental parameters of the forest stands and geomorphologic parameters. For most areas in the Autonomous Province of Bolzano/Bozen a georeferenced map of the potential forest types is available (Klosterhuber et al., 2007). The parameter which correlates well with the wood stand productivity is the dominant height or top height, which is relatively independent from thinning measures. The dominant stand height h_r is the predicted height of the quadratic mean of diameters of the 20% largest trees per stand (Kramer and Akça, 1995). The geomorphologic influence is represented by the inclination of the hill slope.
4. PRP (“preferential recruitment paths”): These are mainly steep stream channels in forested areas reaching the main channel. In these cases, transportation of woody material is possible even if the width of the AWB and the RWB is exceeded. The identification of these channels and areas is based on the hazard index map for debris flows and overbank sedimentation as well as on the event documentation of the Department of Hydraulic Engineering (Autonome Provinz Bozen – Südtirol – Abteilung Wasserschutzbauten, 2008).
 - d) PCA (“preferential contributing areas”): These are areas of potential shallow landslides in forested areas close to the stream channel (compare Fig. 3). Using models such as SHALSTAB (Dietrich and Montgomery, 1998) or SINMAP (Pack et al., 1998) to identify these areas enables the



Fig. 1. SIZ-zone: torrential processes with influence on entrainment and transport of woody material.



Fig. 3. PCA-areas: particularly active recruitment areas on hillslopes.



Fig. 2. AWB-areas and RWB-areas: recruitment mechanisms on hillslopes.

assessment of known and previously unknown areas of shallow landslides.

Regarding the fact that PRP and PCA provide particularly significant woody material recruitment, they are called “particularly active recruitment areas” (PARA). Figure 4 illustrates schematically the classification scheme adopted for the recruitment areas and the relevant processes involved. Figure 5 shows schematically the spatial distribution of the different recruitment areas.

2.3 Identification and spatial delimitation of the woody material recruitment areas

In this step, the woody debris recruitment areas were identified on the basis of existing datasets concerning forest cover, topography, hydrography and hydrology. The areas bordering the channel were selected. Furthermore, forested areas were identified which are prone to debris flows and shallow landslides and the connectivity of these areas to the stream bed was analysed. In a second step, the driftwood transport capacity of the stream is quantified using an indicator based on distinct topographic parameters. The combination of the delimited types of recruitment areas lead to the calculation of an index for the recruitment and transport capacity for woody debris of the torrent catchments.

The procedure used the following existing datasets:

- The *digital terrain model* of the Autonomous Province of Bolzano/Bozen with a resolution of 20 m.
- The *hazard index map for debris flow and overbank sedimentation* processes (Staffler et al. 2008). This dataset identifies and localizes the potential debris flow hazard zones. The map was elaborated on the basis of the digital elevation model, the vegetation map and the geological map following the procedure of Zimmermann et al. (1992 and 1997) and Heinimann et al. (1998).

- The *map of the classified land use* of the Autonomous Province of Bolzano/Bozen (Autonome Provinz Bozen – Südtirol 2004). The forest cover was extracted from this map.
- The map of the modelled *forest vegetation typologies* (Klosterhuber et al., 2007). From this map, the potential tree heights were delineated.
- The *map of the alpine torrent catchments*. This dataset delimitates the alpine torrent catchments with debris flow and overbank sedimentation processes.

In the first step, the torrent channels were derived from the digital terrain model. According to the formulas (1), (2) and (3), the areas of the active wood buffer (AWB) and the recharging wood buffer (RWB) along the torrent channels were determined.

(a) Calculation of the width of the active wood buffer (AWB) and the recharging wood buffer areas (RWB)

The probability of recruitment from a riparian forest on a plain surface is a function of a tree's height and distance from the stream, measured perpendicularly from the position of the tree to the nearest channel boundary (Robison and Beschta, 1990). The probability space for a tree falling is a disk centred on the tree with radius equal to the tree's height. Van Sickle and Gregory (1990) quantified the probability of a tree entering the stream as follows:

$$P_s = \frac{\cos^{-1}\left(\frac{z}{h}\right)}{180} \quad (1)$$

P_s – probability of entry; z – perpendicular distance to the nearest channel boundary (in our model the border of the SIZ-area); h – effective tree height.

The width of the AWB-areas on a plain surface w_{AWB} is obtained setting the probability of entry in Eq. (1) equal to zero and setting h equal to the top height of the forest type. Therefore, for hill slopes with slope inclination less than 40%, the width of the AWB-areas, is estimated as follows:

$$w_{AWB} = h_r \quad (2)$$

w_{AWB} – width of the AWB; h_r – top tree height.

As pointed out by Sobota et al. (2006), individual trees exhibit a stronger tendency to fall towards the channel on steep hillslopes (>40%) than on moderately sloped landforms (<40%). Integration of field data into an established recruitment model indicated that 1.5 to 2.4 times more large wood (by number of tree boles) would be recruited to stream reaches with steep hillslopes than to reaches with moderate side slopes or flat banks, if riparian forest conditions are assumed to be constant. They conclude that stream valley topography should be considered in models that use tree fall directions in predictions of large wood recruitment to streams.

For wood stands on hill slopes (slope $\geq 40\%$), the width of the active wood buffer was determined as follows:

$$w_{AWB} = k \cdot h_r \quad (3)$$

k – coefficient ($1.5 \leq k \leq 2.4$) for steep slopes (Sobota et al., 2006). On a hazard index level an average value of 1.95 has been chosen for the coefficient k .

Accounting for particular impact factors, such as wind throw or high forest dieback, the value of coefficient k in Eq. (3) should be increased, provided that experimental data is available.

As suggested by Harrington and DeBell (1996), in dense, spindly stands where the crowns support each other, trees can bend over and collapse entire sections of the stand (the domino effect).

After considering these impact factors, the additional buffer area (i.e. RWB) was identified. Due to falling trees within the RWB-area, destabilizing repercussions in the ABW-area can be expected. The width of the RWB-area was calculated analogously to the determination of the AWB-area as follows:

$$w_{RWB} = d \cdot h_r \quad (4)$$

d – coefficient for the knock-on effect.

On a hazard index level a value of 1 has been chosen for the coefficient d . Accounting for particular impact factors, such as wind throw or high forest dieback, the value of coefficient d in Eq. (4) should be increased, provided that experimental data is available.

A higher accuracy level in the determination of extents of the AWB and RWB areas, as required for the production of hazard maps rather than on a hazard index level, can be achieved deserving particular attention to connectivity (Borselli et al., 2008), that could influence the recruitment to stream. Using a high resolution digital elevation model (e.g. cell size of 2.5 m·2.5 m), all possible falling directions (max 8 directions) are determined for a tree (height equal to the top height), standing in the centre of the corresponding cell, that potentially permits recruitment (distance from SIZ-outward boundaries less than w_{AWB}). Connectivity is checked along each possible direction. The following connectivity criteria can be applied:

- 1) Connectivity is given along a possible tree fall direction, if the elevation profile along the tree fall direction does not exceed the linear elevation profile given by the straight line that connects the cell centre of the tree location with the cell centre of the cell identifying the SIZ-boundary.
- 2) If the elevation profile along the tree fall direction exceeds the linear elevation profile given by the straight line that connects the cell centre of the tree location with the cell centre of the SIZ-boundary cell the situation is different. It has to be checked whether or not the tree

WOODY DEBRIS RECRUITMENT – general scheme case: HILLSLOPE

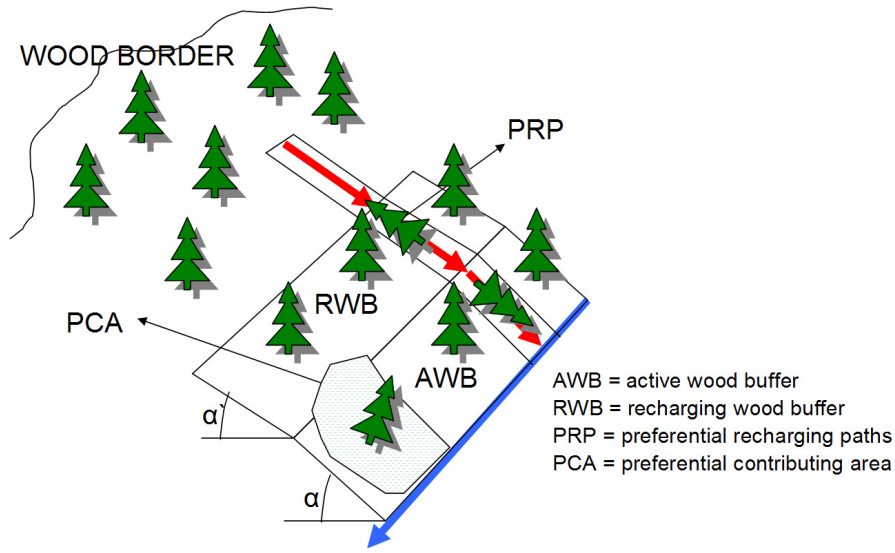


Fig. 4. Schematic illustration of the types of woody debris recruitment areas.

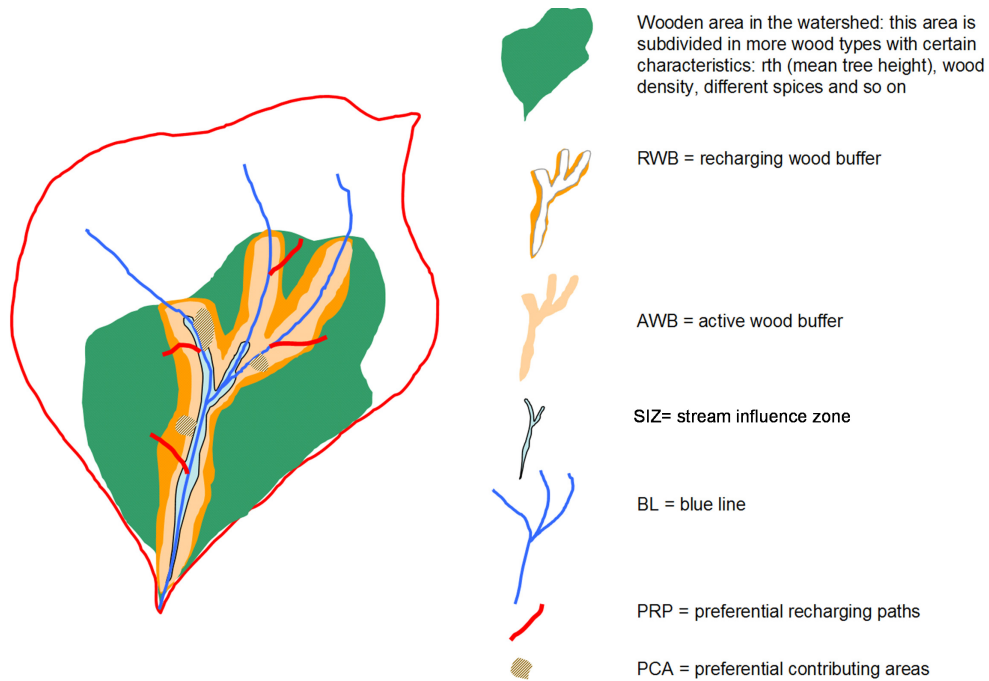


Fig. 5. Schematic illustration of the spatial delimitation of the different types of woody debris recruitment areas.

can tilt over the obstacles, which is defined here as the vertical props given by the cell centres with exceeding elevations with respect to the corresponding elevations of the straight connecting line.

In this way the tree fall directions which don't meet the connectivity criteria can be excluded.

It should be noted that the level of accuracy for hazard indexes uses a cell size of 20 m·20 m for computations. Moreover, if we consider that the top tree heights are not larger

than 40 m (Klosterhuber et al., 2007), only the case of one intermediary cell between the tree location cell and the SIZ boundary cell is possible. In this case a simplified connectivity check is proposed. Connectivity is assumed to be given along a certain tree fall direction if the elevation of the intermediary cell does not exceeds the elevation of the tree location cell.

(b) Identification of the preferential recruitment paths (PRP)

These areas were extracted from the hazard index maps for debris flows and overbank sedimentation processes. The preferential recruitment paths were identified and localized by geomorphic analyses of either the digital terrain model or the dataset of the superficial watercourses (after Zimmermann et al., 1992 and Heinimann et al., 1998). Steep and concave flowlines which are hydrologically connected with the SIZ areas were classified as PRP areas. Along these preferential recruitment paths woody material can be transported to the SIZ-areas from unstable forested areas despite that these recruitment areas are not topologically connected to the SIZ-areas themselves. If it is required, this information can be integrated with pre-existing maps from the event documentation database.

(c) Identification of the preferential contributing areas (PCA)

In a first step, the potentially unstable areas were identified and localized using the GIS-based approach for calculating the slope stability (SHALSTAB, Dietrich and Montgomery, 1998). The unstable areas resulting from this procedure were intersected with the forest cover. In a further step, the active landslides were extracted from the landslide inventory of the Autonomous Province of Bolzano/Bozen (IFFI). Both the evident and the potentially unstable forested areas bordering or being hydrologically connected with SIZ areas through the PRP areas were considered as PCA.

(d) Identification of the particularly active recruitment areas (PARA)

These areas result from the union of the PRP and the PCA.

(e) Identification of the torrent influence zones (SIZ)

In this study, the SIZ-zone was determined based on the hazard index maps for debris flow and for overbank sedimentation processes, including their transit and deposition areas (Staffler et al., 2008).

The analysis was made on a cell-by-cell basis for the whole territory of the Autonomous Province of Bolzano/Bozen – South Tyrol. The vector datasets were converted into raster datasets with the same resolution of the digital elevation model. Outputs of this step were the classified woody debris recruitment areas in the pre-defined torrent catchments.

2.4 A woody material recruitment indicator

After the identification of the potential woody debris recruitment areas, the indicator for the woody debris recruitment is calculated for each pixel and cumulated for each torrent catchment.

For every pixel in the stream channel the contributing woody debris recruitment areas are summarized using the following indicator:

$$RA_{hs,i} = a \cdot (AWB_{left,i} + AWB_{right,i}) + b \cdot (RWB_{left,i} + RWB_{right,i}) + c \cdot (PARA_{left,i} + PARA_{right,i}) \quad (5)$$

$RA_{hs,i}$ – recruitment areas on hill slopes connected to the i_{th} stretch of the stream.

The weighting coefficients a , b and c in Eq. (5) are calibration parameters which should be adapted according to the regional conditions. By means of an extensive analysis of the debris flow and overbank sedimentation events which occurred in the Autonomous Province of Bolzano/Bozen since 1998, the following procedure was used for the estimation of the parameter c . The process was based on visual inspection and image interpretation of adequately geo-referenced images. The active PARA-areas during the considered extreme events were localized and geo-referenced. On the basis of the high quality orthophoto-images from the year 2006, the ratio r_{V1} was estimated for wood volume V_{PARA}^t within the PARA-areas to the wood stand volume outside V_{WOOD}^t the PARA-areas (in the majority of the cases this involved the AWB- or RWB-areas). Additionally, pictures from the event documentation corresponding to the areas in the orthophotos were used to estimate the ratio r_{R1} of wood volume V_{PARA}^{t+1} still available after the event at time $t+1$ to the wood volume V_{PARA}^t present before the event at time t . The conditions of the wood in the PARA-areas before the event at time t were assumed to be comparable to those of the year 2006. The fact that V_{WOOD}^t can differ from the potential wood stand volume V_{POT}^t analyzed by Klosterhuber et al. (2007), the ratio r_{P1} of V_{WOOD}^t to V_{POT}^t should be recognized; however, assuming the requirements of the hazard index level $r_{P1}=1$, the coefficient c can be expressed in terms of r_{V1} and r_{R1} as follows:

$$c = r_{V1} (1 - r_{R1}) \quad (6)$$

In practice, a set of representative PARA-area were analyzed in different catchments and the above defined ratios were estimated. An area-weighted average value $c_{\mu}=0.48$ is used in the calculations.

A qualitative comparison between the recruitment processes occurring in PARA-areas and in AWB-areas of similar extent gave rise to the assumption that although recruitment from AWB-areas is an order of magnitude lower than recruitment from PARA-areas during extreme events, the recruitment from AWB-areas in the long term is a more continuous process. Taking into account the effects of wood degra-

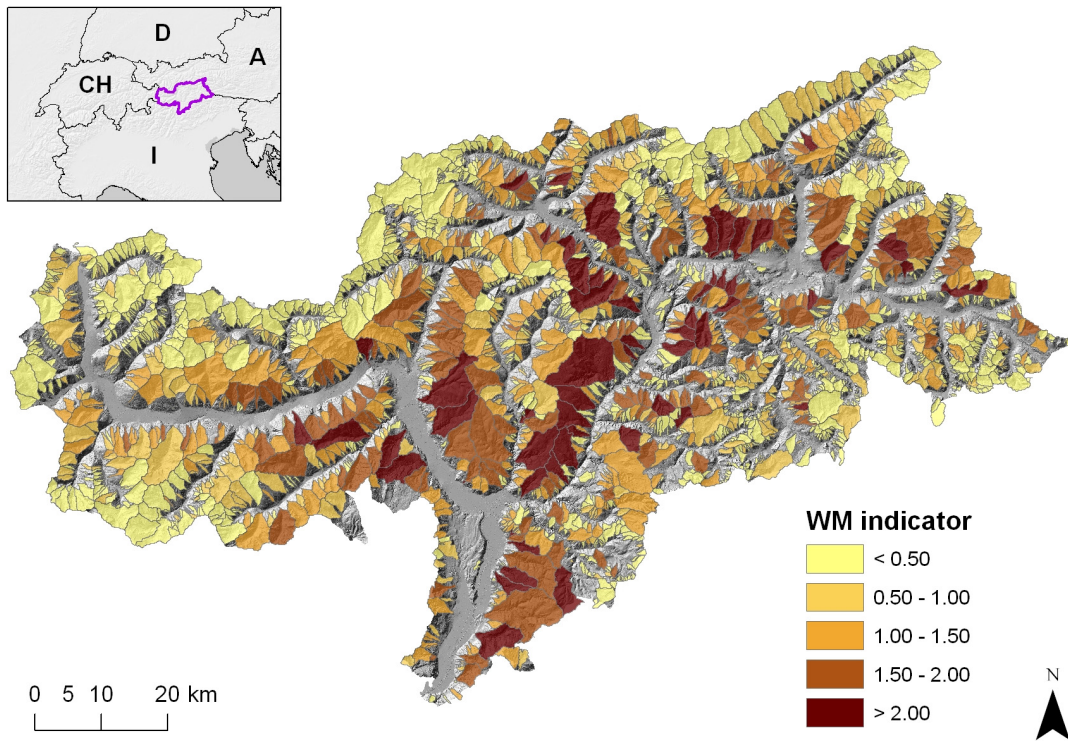


Fig. 6. Classification of the torrent catchments by the woody debris recruitment and transport indicator WM. Legend classification in equal intervals.

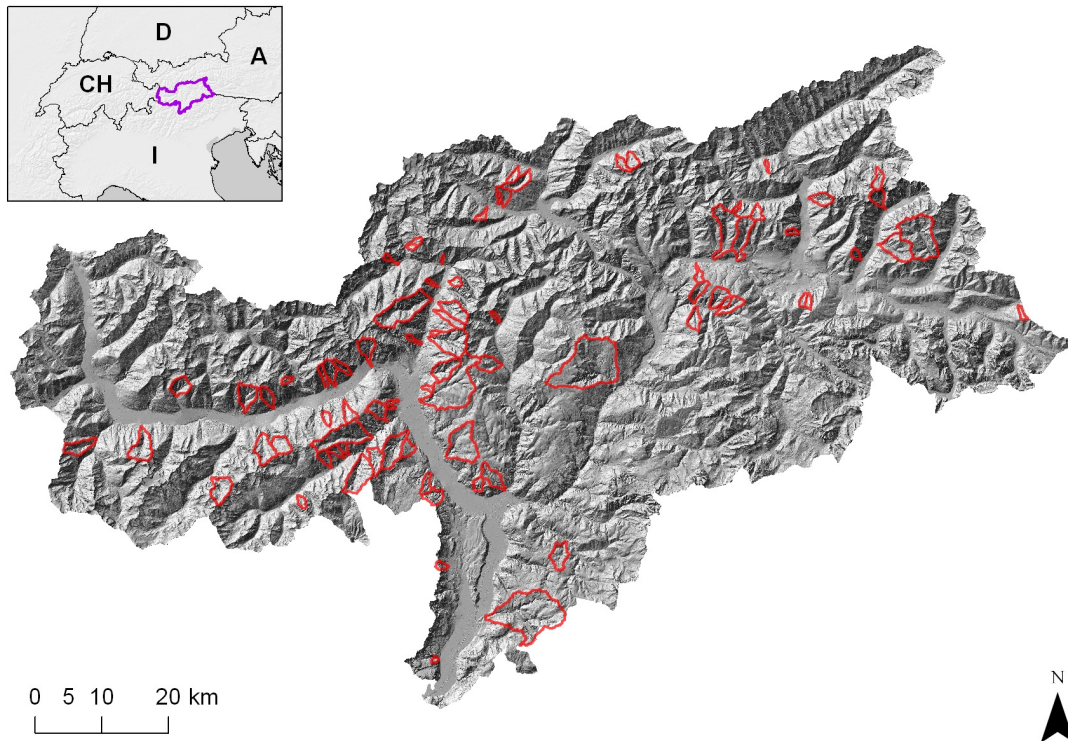


Fig. 7. Torrent catchments with observed woody material recruitment and transport during documented debris flow and overbank sedimentation processes.

dation in the long term, the weighting factor a for the recruitment contribution from the AWB-areas is chosen to be $a=0.5 \cdot c$. The indirect influence on the recruitment process of the RWB-areas justified the assumption $a > b$ and subsequently a value of $b=0.2 \cdot a$ was chosen.

Within the SIZ-areas more concurring processes take place: recruitment within the SIZ-area of tree and shrub vegetation of the banks and the torrent bed directly exposed to the hydrodynamic forces, entrainment, transport and deposition of the woody material. The recruitment process is modelled analogously to the above described processes occurring on the slopes as follows:

$$RA_{instream, i} = d \cdot (SIZ_i) \quad (7)$$

$RA_{instream, i}$ – in-stream recruitment areas corresponding to the i_{th} stretch of the stream.

The following ratios have been defined: a) ratio r_{V2} of wood volume V_{TIZ}^t within the SIZ-areas to the wood stand volume outside V_{WOOD}^t and b) ratio r_{R2} of wood volume V_{TIZ}^{t+1} still available after the event at time $t+1$ to the wood volume V_{TIZ}^t present before the event at time t . The coefficient d was qualitatively assessed as follows:

$$d = r_{V2} (1 - r_{R2}) \quad (8)$$

Due to the strong influence of the process type on in-stream recruitment, different coefficients for debris flows (d_1) and intense bedload transport processes with overbank sedimentation (d_2) have to be defined. A set of representative events were analyzed in different catchments and the above defined ratios were estimated. The area-weighted values of $d_{1, \mu}=0.46$ and $d_{2, \mu}=0.27$ were used in the calculations.

Subsequently the contributing in-stream recruitment areas were cumulated for each pixel in the stream channel as follows:

$$RA_{tot, i} = RA_{hs, i} + RA_{instream, i} \quad (9)$$

$RA_{tot, i}$ total recruitment areas connected to the i_{th} stretch of the stream.

2.5 An indicator for woody material entrainment and transport

Streams with a low longitudinal slope require a certain flow depth ($h \geq 2d_{BHD}$) and channel width ($b \geq L_{woody\ material}$) as well as an adequate radius of curvature in order to support woody material transport over major distances (Braudrick et al., 1997). In torrents with intense bedload transport the entrainment and transport process are facilitated by the coupled action of hydrodynamics and mobile bed dynamics. In torrents with debris flow activity the driftwood is easily entrained and incorporated in the mixture of solid material and water. In this process, the driftwood can be partially broken up and, in the absence of obstacles, it can be transported to the depositional area. The following parameters are relevant

to describe entrainment and transport of woody material on a hazard index level.

Q – peak total discharge (liquid and solid) at the closure section of the catchment for a 100-years return period event.

The liquid discharge Q for a 100-years return period event is given on a regionalized basis by the following expressions (Ferrari, 1996):

$$Q = 10.31 \cdot A^{0.593} \text{ in the Western Adige/Etsch basin} \quad (10a)$$

$$Q = 12.69 \cdot A^{0.606} \text{ in the Eastern Adige/Etsch basin} \quad (10b)$$

A – catchment area in [km^2].

Q_{tot} is derived specifically for either 1) floods with intense bedload transport and overbank sedimentation or 2) debris flows. For case 1), the solid discharge can be expressed according to Smart and Jaeggi's equation (1983):

$$q_s = 2.5qJ^{0.6} \left(J - \frac{d_m}{12.1h_m} \right) \quad (11)$$

q_s – solid discharge per unit width of the channel [$m^3/(m \cdot s)$], q – liquid discharge per unit width of the channel [$m^3/(m \cdot s)$], J – Channel slope [m/m], d_m – characteristic grain-size diameter [m], h_m – average flow depth [m].

Assuming that $d_m \ll 12.1h_m$ and that b is the channel width, Eq. (11) can be simplified to:

$$Q_s = 2.5QJ^{1.6} \quad (12)$$

$Q_s = q_s \cdot b$ – solid discharge [m^3/s], $Q = q \cdot b$ – liquid discharge [m^3/s].

Subsequently, in the bedload transport case, the total discharge Q_{tot} can be expressed by:

$$Q_{tot, bedload} = Q + 2.5QJ^{1.6} = (1 + 2.5J^{1.6}) Q \quad (13)$$

For case 2), the debris flow peak discharge is estimated through Takahashi's volumetric criterion (1978, 1980, 1991):

$$Q_{tot, df} = Q \frac{C^*}{C^* - C_{df}} \quad (14)$$

C_{df} – concentration of the granular mixture, $C^*=0.65$ – maximum possible concentration, C_{df} – can be expressed as follows:

$$C_{df} = \frac{\tan \alpha}{\Delta (\tan \phi - \tan \alpha)} \quad (15)$$

Δ – relative density of the submerged material, here assumed to be equal to 1.65, α slope angle of the channel, ϕ friction angle of the granular material, here assumed to be equal to 32° .

The following two additional parameters need to be defined:

– The average downstream longitudinal slope from the i_{th} section to the basin outlet section, $J_{ds, i}$.

The ratio $l_{Q,i}$ assigns a certain portion of the maximum discharge to every section of the channel depending on the location in the catchment, and is calculated as follows:

$$l_{Q,i} = \frac{Q_i}{Q} \quad (16)$$

Q_i – 100 years return period liquid discharge at the i_{th} section, Q – 100 years return period liquid discharge at the basin outlet section.

For the estimation of the woody material entrainment and transport potential the following indicator is proposed:

Indicator WM for the bedload transport case:

$$WM = Q_{\text{tot, bedload}} \cdot \frac{1}{A_{\text{tot}}} \cdot \sum_{i=1}^k (l_{Q,i} \cdot RA_{\text{tot},i}) \quad (17a)$$

Indicator WM for the debris flow case:

$$WM = Q_{\text{tot, df}} \cdot \frac{1}{A_{\text{tot}}} \cdot \sum_{i=1}^k (l_{Q,i} \cdot RA_{\text{tot},i}) \quad (17b)$$

k – number of control points, $i=1, \dots, k$, A_{tot} – catchment area, WM – hazard potential indicator for wood material delivery.

The expression $\frac{1}{A_{\text{tot}}} \cdot \sum_{i=1}^k (l_{Q,i} \cdot RA_{\text{tot},i})$ is an estimate of the relative availability of recruited woody material and is a synthetic indicator for the transport conditions along the channel. $Q_{\text{tot, bedload}}$ or $Q_{\text{tot, df}}$ estimate the relative propensity for entrainment and delivery of woody material under given transport conditions.

The WM indicator was calculated for each raster cell in the specified catchments. The value of the indicator at the basin outlet section of each torrent catchment was assigned to the particular catchment in the dataset.

3 Results

This procedure both delimited and classified woody material recruitment areas and computed recruitment and transport indicators for the pre-defined torrent catchments. The computed recruitment areas showed a high spatial variability within many of the catchments. Verifications in the field on control samples showed a significant correspondence of the modelled woody material recruitment areas with the mapped recruitment areas.

The computed indicator WM showed a high spatial variability (Fig. 6). For torrent catchments with a low percentage of forest cover, low values for the WM indicator resulted ($WM < 5 \text{ m}^3/\text{s}$). For steep and abundantly forested torrent catchments involving frequent debris flow processes, high values for the WM indicator resulted ($WM > 15 \text{ m}^3/\text{s}$). The relevance of the catchment area and therefore the relevance of the peak discharge is visible in the results of the procedure. In general, higher values of the WM indicator were

calculated in larger catchments; however, Fig. 6 shows that the weight $l_{Q,i}$ has an influence on these results. Small and steep catchments as well as large catchments with high discharge were associated with high values for the WM indicator, whereas in torrent catchments with a relatively low activity of torrential processes (small process areas), low values for the WM indicator were computed. Figure 6 shows that torrent catchments with a relatively high proportion of recruitment areas close to the end section had higher values for the WM indicators compared to catchments with a high proportion of recruitment areas in the upper parts of the catchments.

4 Discussion

Verifications in the field on control samples showed a significant correspondence of the modelled woody debris recruitment areas with the mapped recruitment areas. The developed procedure was validated on the basis of the event documentation database of the Department of Hydraulic Engineering of the Autonomous Province of Bolzano/Bozen. Figure 7 shows the torrent catchments with observed woody material transport by torrential processes. In a further step, the computed results have been shown to the local mountain torrent control and hydraulic engineering experts. High values for the WM indicator were computed for those catchments which were also considered susceptible to woody material transport phenomena in the opinion of the local experts. The calculated WM indicator was verified qualitatively and semi-quantitatively as described below. Although no systematic event documentation procedure exists regarding specific details of woody material transport during torrential events, the necessary data was reconstructed from database photographs of events. Nearly 1800 images showing woody material transported by debris flow and flood processes were extracted from this database and further georeferenced and analysed. On the basis of these images, the observed volume of transported material was estimated; however, these estimations were used for validation purposes in only a semi-quantitative way, since the analysed photographs show only a very small part of the torrent catchments. The validation procedure showed a reliable correspondence of the calculated woody debris recruitment and transport indicators with the analysed photographs. In general, catchments with high values of the WM indicator were found to be those catchments which, in reality, are documented as having events with significant transport and deposition of woody material (Figs. 5 and 6). In torrent catchments with values of the WM indicator $> 2 \text{ m}^3/\text{s}$, a minimum volume of 6 m^3 of woody material could be estimated from the photographs (range from 6 to 154 m^3 , mean 35 m^3 , $n=11$). In torrent catchments with values of the WM indicator between 1 and $2 \text{ m}^3/\text{s}$, a minimum volume of 3 m^3 of woody material could be estimated from the photographs (range from 3 to 130 m^3 , mean 25 m^3 ,

$n=51$). There was one exception in which a sizeable wood volume was observed ($\sim 3 \text{ m}^3$) despite a low calculated WM indicator ($0 \text{ m}^3/\text{s}$). This was due to the fact that the catchment was delimited at the upper end of the alluvial fan and the observed wood material was recruited in the area of the alluvial fan itself. Given that the outlined method delineates catchments by a lower boundary at the alluvial fan or debris flow cone, the recruitment of woody material downstream of these outlet points is overlooked. For such scenarios other approaches must be used (e.g. considering the hydrodynamic impacts on the wood stand).

A quantitative comparison between the computed values for the WM indicator and transported woody material volumes failed due to the following three reasons. Firstly, the photographs focused on deposited woody material in the areas where damages occurred and often neglected areas in the stream influence zones. Secondly, the frequency of torrential events in the considered catchments could not be estimated. Thus, the volume of debris in a given picture may not be an accurate indicator of volume if the frequency of events in the past decades is high (i.e. material has been transported downstream in previous events). Thirdly, the intensity/frequency relationship of the documented event is not known and therefore, the comparison of the documented events with the scenario of a return period of 100 years is difficult. Nevertheless, the comparison showed a noticeable spatial correlation between the WM indicator and observed transportation and deposition of woody material.

5 Conclusions

The questions stated in the introductory chapter were successfully answered. The procedure enables the identification of those torrent catchments susceptible to woody material recruitment and transport which must be considered in hazard mapping. The detection of hazards related to woody material transport is a fundamental prerequisite for a robust and reliable risk assessment procedure for hydrologic hazards. In catchments with high values of the woody material transport indicator (WM), a detailed analysis of torrential processes occurring at critical configurations (e.g. bridge locations) is highly recommended. The knowledge derived from the generated hazard index maps supports a hind- and foresighted conceptual planning process of functional and efficient protection systems. Due to the higher weight given to the recruitment areas close to the end section of a catchment, the procedure is able to identify those catchments for which forestry measures should be checked (e.g. thinning the wood stand within the relevant stream influence zone).

Detailed results on a catchment scale can be obtained using high resolution digital elevation and surface models, performing hydrological computations by means of distributed hydrological models and retrieving detailed forest cover datasets (e.g. tree heights, areas with different canopy

densities) and improving the parameter estimates for woody material recruitment and transport by ad hoc field surveys.

Regarding the young research stage of woody material transport processes, the possibility for further development of the application is a central aspect. In the authors' opinion, further improvements of the procedure could be attained by: a) introducing a probabilistic approach and connectivity indicators for the assessment of recruitment and b) using the results of 2-D hydrodynamic computations for the description of the time-dependent entrainment and transport processes within the SIZ-areas.

Acknowledgements. The project was co-financed by the European Union within the Interreg IIIA Italy-Switzerland project "Entwicklung und Anwendung eines Systems zur überregionalen Erkennung und Bewertung hydrogeologischer Risiken". The authors are indebted to Lorenzo Marchi for the hints and suggestions provided during the reviewing process that contributed to substantially improve the manuscript, to Omar Formaggioni for preparing the photographic material for the validation procedure and to Emily Procter for linguistically improving the text.

Edited by: F. Guzzetti

Reviewed by: L. Marchi and another anonymous referee

References

- Abbe, T. B. and Montgomery, D. R.: Large woody debris jams, channel hydraulics and habitat formation in large rivers, *Regul. River.*, 12, 2001–221, 1996.
- Abbe, T. B., Montgomery, D. R., and Petroff, C.: Design of stable in-channel wood debris structures for bank protection and habitat restoration: an example from the Cowlitz River, WA, in: *Management of Landscapes Disturbed by Channel Incision: Stabilization, Rehabilitation, Restoration*, edited by: Wang, S.S.Y., Langendoen, E. J., and Shields, F. D., University of Mississippi, Mississippi, 809–815, 1997.
- Autonome Provinz Bozen – Südtirol: Forst- und Landwirtschaftliche Realnutzungskarte, Bozen, 2004.
- Autonome Provinz Bozen – Südtirol – Abteilung Wasserschutzbauten: IHR – Informationssystem zu Hydrogeologischen Risiken, Methodischer Endbericht, Bozen, 2008.
- Berger, E., Grisotto, S., Hübl, J., Kienholz, H., Kollarits, S., Leber, D., Loipersberger, A., Marchi, L., Mazzorana, B., Moser, M., Nössing, T., Riedler, S., Scheidl, C., Schmid, F., Schnetzer, I., Siegel, H., and Volk, G.: DIS-ALP. Disaster information system of alpine regions, Final report, unpublished, 2007.
- Bezzola, G. R. and Lange, D.: Umgang mit Schwemmholz im Wasserbau, *Wasser Energie Luft*, 95(11/12), 360–363, 2003
- Bezzola, G. R., Sigg, H., and Lange, D.: Driftwood retention works in Switzerland, *Internationales Symposium Interpraevent 2004 – Riva del Garda*, 3, 29–40, 2004.
- Borselli, L., Cassi, P., and Torri, D.: Prolegomena to sediment and flow connectivity in the landscape: A GIS and field numerical assessment, *CATENA* 75 (Elsevier), 268–277, 2008.
- Braudrick, C. A., Grant, G. E., Ishikawa, Y., and Ikeda, H.: Dynamics of wood transport in streams: a flume experiment, *Earth Surface Proc. Land.*, 22, 669–683, 1997.

- Braudrick, C. A. and Grant G. E.: When do logs move in rivers?, *Water Resour. Res.*, 36(2), 571–583, 2000.
- Braudrick, C. A. and Grant, G. E.: Transport and deposition of large woody debris in streams: a flume experiment, *Geomorphology*, 41, 263–283, 2001.
- Comiti, F., Andreoli, A., Lenzi, M. A., and Mao, L.: Spatial density and characteristics of woody debris in five mountain rivers of the Dolomites (Italian Alps), *Geomorphology*, 78, 44–63, 2006.
- Curran, J. H. and Wohl, E. E.: Large woody debris and flow resistance in step-pool channels, Cascade Range, Washington, *Geomorphology*, 51, 141–157, 2003.
- Degetto, M.: Dinamica del legname in alveo e modellazione del suo comportamento in presenza di briglie filtranti, M.S. thesis, University of Padova, 2000.
- Diehl, T. H.: Potential Drift Accumulation at Bridges, US Department of Transportation, Federal Highway Administration Research and Development, Turner-Fairbank Highway Research Center, Virginia, Publication No. FHWA-RD-97-028, 1997.
- Dietrich, W. E. and Montgomery, D. R.: SHALSTAB: a digital terrain model for mapping shallow landslide potential, NCASI (National Council of the Paper Industry for Air and Stream Improvement) Technical Report, February 1998, 29 pp., 1998.
- Ferrari, R.: Censimento e sicurezza di piccoli invasi in provincia di Bolzano – relazione esplicativa, report for the office 30.6 of the Autonomous Province of Bolzano/Bozen, unpublished, 1996.
- Fuchs, S. and McAlpin, M. C.: The net benefit of public expenditures on avalanche defence structures in the municipality of Davos, Switzerland, *Nat. Hazards Earth Syst. Sci.*, 5, 319–330, 2005, <http://www.nat-hazards-earth-syst-sci.net/5/319/2005/>.
- Gurnell, A. M., Piegay, H., Gregory, S. V., and Swanson, F. J.: Large wood and fluvial processes, *Freshwater Biol.*, 47, 601–619, 2002.
- Haga, H., Kumagai, T., Otsuki, K., and Ogawa, S.: Transport and retention of coarse woody debris in mountain streams: An in situ field experiment of log transport and a field survey of coarse woody debris distribution, *Water Resour. Res.*, 38(8), 1126, doi:10.1029/2001WR001123, 2002.
- Harrington, C. A. and DeBell, D. S.: Above- and below-ground characteristics associated with wind toppling in a young *Populus* plantation, *Trees*, 11, 109–118, 1996.
- Heinimann, H., Hollenstein, K., Kienholz, H., Krummenacher, B., and Mani, P.: Methoden zur Analyse und Bewertung von Naturgefahren. Umweltmaterialien Bundesamt für Umwelt, Wald und Landschaft, Bern, 249 pp., 1998.
- Hildebrand, R. H., Cemly, A. D., Dolloff, C. A., and Harpster, K. L.: Effects of large woody debris placement on stream channel and benthic macroinvertebrate, *Can. J. Fish. Aquat. Sci.* 54, 931–939, 1997.
- Keim, R. F., Skaugset, A. E., and Bateman, D. S.: Physical aquatic habitat: II. Pools and cover affected by large woody debris in three western Oregon streams, *North American Journal of Fisheries Management*, 22, 151–164, 2002.
- Klosterhuber, R., Plettenbacher, T., Hotter, M., Schober, T., Aschaber, R., Vacik, H., Pircher, G., Gruber, G., and Ruprecht, H.: Ökologisches Handbuch zur Waldtypisierung und Waldstratifizierung Südtirol, Teil A, Zwischenbericht im Auftrag der Autonomen Provinz Bozen, Abteilung 32, Forstwirtschaft, 2007.
- Kramer, H. and Akça, A.: Leitfaden zur Waldmesslehre, J.D. Sauerländers Verlag, Frankfurt am Main, Germany, 1995 (in German).
- Lancaster, S. T. and Shannon, K. H.: Modelling Sediment and Wood Storage and Dynamics in Small Mountainous Watersheds, *Geomorphic Processes and Riverine Habitat Water Science and Application*, 4, 85–102, 2001.
- Lange, D. and Bezzola, G. R.: Schwemmholz, Probleme und Lösungsansätze, Mittlungen der Versuchsanstalt für Wasserbau, Hydrologie und Glaziologie (VAW), Zurich, 2006.
- Lyn, D., Cooper, T., Condon, D., and Gan, L.: Factors in debris accumulation at bridge piers, Washington, US Department of Transportation, Federal Highway Administration Research and Development, Turner-Fairbank Highway Research Center, 2007.
- May, C. L. and Gresswell, R. E.: Large wood recruitment and redistribution in headwater streams in the southern Oregon Coast Range, USA, *Can. J. Forest Res.*, 33(6), 1352–1362, 2003.
- Montgomery, D. R. and Piegay, H.: Wood in rivers: interactions with channel morphology and processes, *Geomorphology*, 51, 1–5, 2003.
- Oberndorfer, S., Fuchs, S., Rickenmann, D., and Andrecs, P.: Vulnerabilitätsanalyse und monetäre Schadensbewertung von Wildbacheignissen in Österreich, BFW, Wien, 2007.
- Pack, R.T., Tarboton, D.G., Goodwin, C.N.: The SINMAP approach to terrain stability mapping. Proceedings of the 8th Congress of the International Association of Engineering Geology, Vancouver, British Columbia, Canada, Vancouver, 21–25 September 1998.
- Petraschek, A. and Kienholz, H.: Hazard assessment and mapping of mountain risks in Switzerland, in: Debris-flow hazard mitigation: mechanics, prediction and assessment, edited by: Rickenmann, D. und Chen, C. L. (Hrsg.), Millpress, Rotterdam, 2003.
- Rickenmann, D.: Schwemmholz und Hochwasser, *Wasser Energie Luft*, 89, 115–119, 1997.
- Rickli, C. and Bucher, H.-U.: Schutzwald und Schwemmholz in Wildbacheinzugsgebieten, FAN-Agenda 1/06, 17–20, 2006.
- Rimböck, A.: Design of rope net barriers for woody debris entrapment, Introduction of a design concept, Proc. Int. Symp. Interpraevent 2004, Riva del Garda, Trento, Italy, 265–276, 2004.
- Robison, E. G. and Beschta, R. L.: Characteristics of coarse woody debris for several coastal streams of southeast Alaska, USA, *Can. J. Fish. Aquat. Sci.*, 47(9), 1684–1793, 1990.
- Shields, F. D., Morin, N., and Kuhnle, R. A.: Effects of large woody debris structures on stream hydraulics, Proc. Wetlands Engineering and River Restoration Conference, ASCE, Reston, VA, 2001.
- Smart, G. and Jaeggi, M.: Sediment transport on steep slopes, Mittlungen der Versuchsanstalt für Wasserbau, Hydrologie und Glaziologie, Zürich, Nr. 64, 1983.
- Sobota, D. J., Gregory, S. V., and Van Sickle, J.: Riparian tree fall directionality and modeling large wood recruitment to streams, *Can. J. Forest Res.*, 36(3), 1243–1254, 2006.
- Staffler, H., Pollinger, R., Zischg, A., and Mani, P.: Spatial variability and potential impacts of climate change on flood and debris flow hazard zone mapping and implications for risk management, *Nat. Hazards Earth Syst. Sci.*, 8, 539–558, 2008, <http://www.nat-hazards-earth-syst-sci.net/8/539/2008/>.
- Takahashi, T.: Mechanical characteristics of Debris Flow, *J. Hydr. Eng. Div.-ASCE*, 104(8), 1153–1169, 1978.

- Takahashi, T.: Debris Flow on prismatic open channel, *J. Hydr. Eng. Div.-ASCE*, 106(3), 381–396, 1980.
- Takahashi, T.: Debris flows, Rotterdam, Balkema, 1991.
- Uchiogi, T., Shima, J., Tajima, H., and Ishikawa, Y.: Design methods for wood-debris entrapment, *Proc. Int. Simp. Interpreaevent, Garmisch Partenkirchen*, 5, 279–288, 1996.
- Van Sickle, J. and Gregory, S. V.: Modeling inputs of large woody debris from falling trees, *Can. J. Forest Res.*, 20, 1593–1601, 1990.
- Zimmermann, M., Mani, P., and Gamma, P.: Murganggefahr und Klimaänderung – ein GIS-basierter Ansatz. vdf, Zurich, 161 pp., 1997.
- Zimmermann, M. and Haeberli, W.: Climatic change and debris flow activity in high mountain areas: a case study in the Swiss Alps, *Catena Supplement*, 22, 59–72, 1992.

Paper 18: Mazzorana, B., Hübl, J., Zischg, A., Largiader, A., 2011. Modelling woody material transport and deposition in alpine rivers. *Natural Hazards* 56, 425–449. [10.1007/s11069-009-9492-y](https://doi.org/10.1007/s11069-009-9492-y).

Modelling woody material transport and deposition in alpine rivers

B. Mazzorana · J. Hübl · A. Zischg · A. Largiader

Received: 6 December 2008 / Accepted: 19 December 2009 / Published online: 19 January 2010
© The Author(s) 2010. This article is published with open access at Springerlink.com

Abstract Recent flood events in Switzerland and Western Austria in 2005 were characterised by an increase in impacts and associated losses due to the transport of woody material. As a consequence, protection measures and bridges suffered considerable damages. Furthermore, cross-sectional obstructions due to woody material entrapment caused unexpected flood plain inundations resulting in severe damage to elements at risk. Until now, the transport of woody material is neither sufficiently taken into account nor systematically considered, leading to prediction inaccuracies during the procedure of hazard mapping. To close this gap, we propose a modelling approach that (1) allows the estimation of woody material recruitment from wood-covered banks and flood plains; (2) allows the evaluation of the disposition for woody material entrainment and transport to selected critical configurations along the stream and that (3) enables the delineation of hazard process patterns at these critical configurations. Results from a case study suggest the general applicability of the concept. This contribution to woody material transport analysis refines flood hazard assessments due to the consideration of woody material transport scenarios.

Keywords Woody material transport · Natural hazards · Hazard mapping · Risk assessment

B. Mazzorana (✉)

Department of Hydraulic Engineering, Autonomous Province of Bolzano South Tyrol, Bolzano, Italy
e-mail: bruno.mazzorana@provinz.bz.it

B. Mazzorana · J. Hübl

Institute of Mountain Risk Engineering, University of Natural Resources and Applied Life Sciences, Vienna, Austria

A. Zischg · A. Largiader

Abenis AG, Chur, Switzerland

A. Zischg

Abenis Alpinexpert srl, Bolzano, Italy

1 Introduction

Socio-economic developments in European mountain environments and related forelands are reflected in increasing settlement and economic activities in areas affected by natural hazards (Fuchs and Holub 2007). Consequently, considerable economic losses have resulted in recent years from events (Mitchell 2003; Autonome Provinz Bozen—Südtirol 2006; Oberndorfer et al. 2007) despite the efforts made towards the mitigation of flood hazards and the reduction of specific risks (Fuchs and McAlpin 2005). At critical stream geometry configurations in mountain streams (e.g., bridge cross sections), a remarkable increase in process intensities could be attributed to woody material transport phenomena (e.g., Diehl 1997; Lyn et al. 2007). Due to the general necessity of assessing natural hazards and risks in a reproducible manner, guidelines for hazard mapping were defined in European countries (e.g., BUWAL 1998; Autonome Provinz Bozen—Südtirol 2006), thereby providing milestones with respect to the quality of integral risk management. The major starting point for managing risk from an integral point of view is the deduction and systematic construction of consistent and reliable scenarios. However, subjective assumptions on relevant impact variables such as woody material transport intensities on the system-loading side and response mechanisms at critical configurations often cause biases and inaccuracies in the results. Considering the hazardous effects of woody material transport, clear indications emerged from the analyses of the debris flow and flood events that occurred recently in several Alpine regions (e.g., Bänziger 1990; Rickli and Bucher 2006). At critical stream geometry configurations (e.g., bridge locations), the transported woody material is repeatedly entrapped. In addition to increasing the loading conditions on the structural components of the bridges (e.g., piers, abutments and superstructure), overflowing is likely to occur more frequently. In order to assess these phenomena, this paper aims at contributing to a systematic investigation of woody material recruitment processes, an evaluation of the propensity for woody material entrainment and transport to critical configurations, and a detection of hazard process patterns at these critical configurations during extreme floods. The analysis of such elements is indispensable for comprehensive flood hazard assessments and for optimizing forest management strategies. Moreover, knowledge about the quantity of woody material, the main woody material pathways in the stream channel and the main places of deposition is fundamental for the design of resilient protection systems and for optimised emergency planning. In order to approach problems emerging from in-stream structures, a detailed study of the damage potential has been carried out by Diehl (1997). The relation between the flow resistance due to the presence of large woody debris (LWD) and increased inundation frequency has been analysed in detail by Shields et al. (2001). New insights into the dynamics of wood transport in streams have been achieved by flume experiments (Rickenmann 1997; Braudrick et al. 1997; Braudrick and Grant 2000, 2001; Degetto 2000; Haga et al. 2002; Curran and Wohl 2003; Bocchiola et al. 2006). The interaction of woody material transport with protection measures has been investigated with a special focus on check dams (Bezzola et al. 2004; Lange and Bezzola 2006) and on rope nets (Rimböck and Strobl 2002).

Acknowledging the fact that hazard impacts at critical configurations along the stream could be interpreted as effects of a complex process interaction field, the main objective of this paper is to propose a modelling concept for the analysis of the following key aspects in considering woody material transport in flood hazard mapping:

1. Disposition: Wood stand productivity and dead wood production in the recruitment areas are important factors that determine the disposition for woody transport phenomena in mountain streams.
2. Intensity of wood–flood interaction: Recruitment processes directly connected to the dynamics of wood–flood interaction become relevant. Recruitment processes due to wood–flood interaction can be attributed directly to hydrodynamic pressure loading and subsequent breakage of the stems. Moreover, morphodynamics such as stream bed erosion and aggradation and side erosion plays a relevant role (e.g., Abbe et al. 1997; Hildebrand et al. 1997; Gurnell et al. 2000; Keim et al. 2002; Montgomery and Piegay 2003; Comiti et al. 2006). In fact, the erosive action of the current is responsible for the scouring of root wads which in turn induces tree toppling.
3. Entrainment and transport of the woody material: The intensity of the flood process, in terms of flow depths and flow velocities, has to be considered as a critical parameter.
4. Interaction phenomena at critical channel geometry configurations: Significant in this context are woody material entrapment and the related consequences, e.g., bridge failures due to hydrostatic and hydrodynamic overloading. Because of the complexity of the involved process chains, magnitude-frequency-related considerations deserve close attention.

Given earlier, the developed conceptual structure comprises: (1) criteria for the localization and classification of woody material recruitment areas as well as the assessment of the woody material recruitment volumes; (2) a computational procedure for woody material entrainment processes; (3) a computational scheme for woody material transport, deposition and remobilization dynamics and (4) an analysis procedure of the interaction phenomena involving transported woody material occurring at critical stream configurations.

Data were implemented into a GIS environment. Subsequently, we tested the GIS application for reconstructing woody material recruitment, transport and deposition patterns during a design event with a reoccurrence period of 300 years and compared it with a flash-flood event occurred in 1987 in the Passirio/Passer River in South Tyrol (Northern Italy).

2 Theoretical background

Throughout the paper, we will consider a wood-covered flood plain region as a system, Ω , as shown in Fig. 1. The system is confined at the downstream side by the outflow boundaries, Γ_{out} , and at the upstream side by the inflow boundaries, Γ_{in} . To simplify matters, these boundaries are assumed to be invariant. Furthermore, it is supposed that the material flux exchanges (e.g., discharge, sediment rates and wood material amounts) within the environment are taking place at these boundaries. At the margins, the system is confined to lateral flood plain boundaries, namely the slopes of the mountains. The system consists of stocks or storage compartments and flows or fluxes. Three storage compartments are defined as (1) sediment storage, $(X_{\Omega}^1)^t$, (2) water storage, $(X_{\Omega}^2)^t$ and (3) wood material storage, $(X_{\Omega}^3)^t$. The corresponding fluxes within the system and at the inflow boundaries are: (1) sediment fluxes, $(\Delta_{\Omega}^1)^t$ and $(\Delta_{\Gamma}^1)^t$; (2) water fluxes, $(\Delta_{\Omega}^2)^t$ and $(\Delta_{\Gamma}^2)^t$; and (3) woody material fluxes, $(\Delta_{\Omega}^3)^t$ and $(\Delta_{\Gamma}^3)^t$.

Each flood can be intended as a disturbance of the system, and the effects of a certain flood event depend also on the settings given by the previous floods. As a consequence at

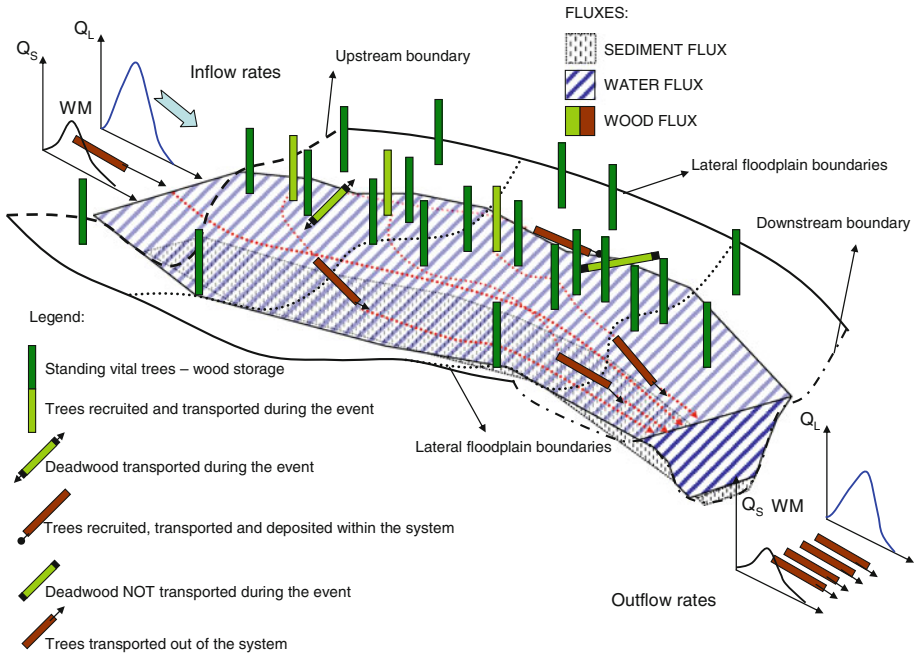


Fig. 1 Wood, sediment and fluxes and system dynamics

the beginning of each flood event, t_i^0 with $i = 1, \dots, N$, a specific set of initial conditions, $(X_{\Omega}^j)_{t_i^0}$ and $(\Delta_{\Omega}^j)_{t_i^0}$, with $j = 1, 2, 3$ and inflow boundary conditions, $(\Delta_{\Gamma}^j)_{t_i^0}$, have to be considered.

The simulations of the material fluxes taking place within the considered system during successive extreme events would require the solution of distinct boundary conditions and initial value problems. Between successive extreme events, the morphodynamical development as well as the growth of the wood stocks has to be monitored in order to correctly assess both the initial and boundary conditions. In the following subsections, a concise summary of the main findings regarding woody material recruitment, entrainment and transport are given.

2.1 Woody material recruitment

Rickli and Bucher (2006) identify the following relevant recruitment processes from hill slopes:

1. Bank erosion: through the shear stress exerted on the wetted perimeter of the cross section of the channel, erosion processes occur along the banks and alter the static equilibrium of the trees. Synchronisms between debris flows, flood events and the earlier mentioned woody material recruitment processes are quite probable.
2. Wind-throw: strong wind conditions can either destabilise the trees that consequently fall as a whole into the channel or lead to the recruitment of the epigeous parts if their stems break under the wind loading. May and Gresswell (2003) point out that falling trees with a horizontal distance to the channel that exceeds their height can exert a destabilizing action on other trees (e.g., knock-on effect).

3. Snow loading: the pressure exerted by snow, in particular wet snow in spring and autumn, can cause stability problems to broad-leaved trees, increasing bending moments and shear forces. Through the cleaving action of ice, crowns of trees are susceptible to break off.
4. Landslides and other slope processes convey standing and lying woody material towards the channel.
5. Avalanches are likely to incorporate and convey large volumes of woody material within the process perimeter.

Only a few exhaustive experimental results currently exist regarding woody material production and recruitment from different wood structures which are exposed to hydrodynamic impacts. Extensive experimental investigations have been carried out in order to study the hydraulic impact on vegetated riverbanks, e.g., the experiments carried out in the soil bioengineering test flume of the Vienna river (Rauch 2005). Furthermore, a series of 3D numerical simulations of vegetated Compound Channel Flows have been performed (Wilson et al. 2004). A second impact factor influencing woody material production is the wood structure itself. An analysis of recent flood events documented in the Province of Bolzano showed that wood vegetation in the river bed has a higher relative tendency to produce woody material (depending on wood stand volume) compared to wood vegetation on stream banks. In absolute terms, the amount of woody material recruited from the stream banks exceeded the volume recruited from the riverbank (Mazzorana et al. 2009). This fact can be attributed to the wood stand volume being on average larger on the bank slopes than in the river bed. In relation to the wood stand volume, wood vegetation located on the stream banks delivers more woody material due to lateral erosion phenomena than wood vegetation of the flood plain.

2.2 Woody material entrainment and transport

Theoretical models for woody material entrainment based on the balance of hydrodynamic (F) and resistance forces (R) on individual large woody material pieces have been developed by Braudrick et al. (1997) and Braudrick and Grant (2000). Assuming the shape of the woody debris pieces being cylindrical, and neglecting the influence of buoyancy, the hydrodynamic force can be expressed as follows (Haga et al. 2002):

$$F = \frac{1}{2}C_d\rho(lh \sin \theta + A_{\text{sub}} \cos \theta)U^2 \tag{1}$$

where C_d , drag coefficient for the woody material element in water; ρ , density of the water; l , length of the woody material element; h , flow depth given by hydrodynamic simulations; A_{sub} , submerged area of the log perpendicular to length; θ , angle of the element axis relative to the main flow direction; U , flow velocities given by hydrodynamic simulations as: $U = \sqrt{u^2 + v^2}$.

The resistance forces can be expressed as follows:

$$R = \left(g\sigma\frac{\pi d^2}{4} - g\rho A_{\text{sub}}l \right) (\mu \cos \alpha - \sin \alpha) \tag{2}$$

where d , diameter of the woody material element; μ , friction coefficient between the element and the channel bed; σ , density of the woody material element; α , channel bed slope; g , gravity acceleration.

Expressing the submerged area of the log perpendicular to its length can be defined as follows:

$$A_{\text{sub}} = d^2 \left\{ \frac{1}{4} \cos^{-1} \left(1 - \frac{2h}{d} \right) - \frac{1}{8} \sin \left[2 \cos^{-1} \left(1 - \frac{2h}{d} \right) \right] \right\} \quad (3)$$

Expressing the non-dimensional force $\Psi = \frac{F}{R}$ in terms of Eqs. 1 and 2, the following expression can be obtained (modified from Haga et al. 2002):

$$\Psi = \frac{F}{R} = \frac{\frac{1}{2} C_d \rho (lh \sin \theta + A_{\text{sub}} \cos \theta) U^2}{(g \sigma \frac{\pi d^2}{4} - g \rho A_{\text{sub}} l) (\mu \cos \alpha - \sin \alpha)} \quad (4)$$

Analysing Eq. 4, the dynamics of a single woody material element with known dimensions can be described within a simplified scheme as follows (Haga et al. 2002):

Floating condition:

$$\frac{h}{d} \geq 1 \quad (5)$$

Resting condition:

$$\Psi = \frac{F}{R} \leq 1 \quad \text{and} \quad \frac{h}{d} < 1 \quad (6)$$

Sliding or rolling condition:

$$\Psi = \frac{F}{R} > 1 \quad \text{and} \quad \frac{h}{d} < 1 \quad (7)$$

Field observations are in good agreement with the earlier outlined theory. According to those evidences, the entrainment condition for smooth wood logs with an approximate cylindrical form is $1 \leq \frac{h}{d} \leq 1.2$. The ratio, $\frac{h}{d}$, increases for wood logs with branches up to 1.5 and for wood logs with root wads up to 1.7.

The earlier outlined theoretical model does not consider the effects of morphodynamics. After Lange and Bezzola (2006), the entrainment is facilitated in the case of sediment transport due to the fact that the movable stream bed layer acts like a roller-bearing. In these conditions, the required flow depths, *ceteris paribus*, are 20–30% lower compared to the case without sediment transport.

The procedure for evaluating woody material dynamics from a hazard-related perspective relies on these theoretical principles and is described in the next section.

3 Modelling approach

This section provides a description of the developed modelling approach, which has been implemented into an ArcGIS-Esri[®] environment. The criteria for the identification, localization and classification of the woody material recruitment areas are explained, followed by the procedure for woody material volume assessment. Subsequently, the relevant aspects of woody material transport dynamics, namely the entrainment, transport and deposition and remobilization processes, are thoroughly discussed and a computational scheme is proposed. Finally, an analysis procedure of interactions at critical stream configurations is introduced.

3.1 Identification, localization and classification of woody material recruitment areas

Woody material recruitment areas are identified by the interpretation of aerial stereo images (photographs). According to the findings of Rauch (2005), an innovative *ad hoc* classification of the typologies of alluvial forests, lowland riparian forests and riverside woodland is proposed. The forested areas in the influence zone of the stream are classified into seven structural typologies according to their different behaviour when exposed to hydrodynamic loadings (Table 1). The classification criteria take into account the response of different vegetation and forest typologies to the hydraulic forces and impacts of flood processes. Figure 2 shows the interdependencies between woody material production (interpreted as “distance” from the point of origin in the coordinate system), the level of hydrodynamic impact forces (on the vertical axis), the position within the riparian zone (on the horizontal axis) and the vegetation structure (oblique axis). Table 1 also shows the potentially available volumes of woody material for each vegetation structure typology. In addition, Table 1 provides the description of the corresponding typical response mechanisms. The geomorphologic characteristics of the flood process areas have to be determined. These areas are classified as (1) stream bed, (2) stream bank and (3) process area of an extreme flood event.

The classification is made on the basis of digital elevation models, aerial photographs and a Lidar-based digital terrain model with a high spatial resolution. An output data set is obtained with the morphology of the stream influence zone.

3.2 Assessment of the recruited woody material volume

Three distinct computational procedures for the assessment of woody material recruitment volumes are presented for: the recruitment from (1) hill slopes, the recruitment from (2) tributaries, and (3) within the maximum extent of the flooded area.

Table 1 Structural classification of forested areas within the influence zone of the river (Blaschke et al. 2004)

ID	Structure characteristics	Assumed response characteristic	Response in case of flooding	Stand volume (m ³ /ha) Example: Passirio river	Dead wood volume (m ³ /ha)
1	Young-growth forest, dense	Flexible	Lie down, protect the soil	40	5
2	Young-growth forest, fragmentary	Flexible	Lie down, increased turbulences, rough, protect the soil	20	3
3	Multilayered structure, dense	Flexible and inflexible	Reduces flow velocity, rough, protect the soil	240	25
4	Even aged population, dense	Inflexible	Reduces flow velocity, protect the soil	400	40.2
5	Multilayered structure, fragmentary	Flexible and inflexible	Different velocities, turbulences, rough	120	18
6	Even aged population, fragmentary	Inflexible	Different velocities, turbulences, unruffled	200	24
7	Old growth, very patched	Inflexible	Elevated turbulences due to circulation around, leachate	150	20

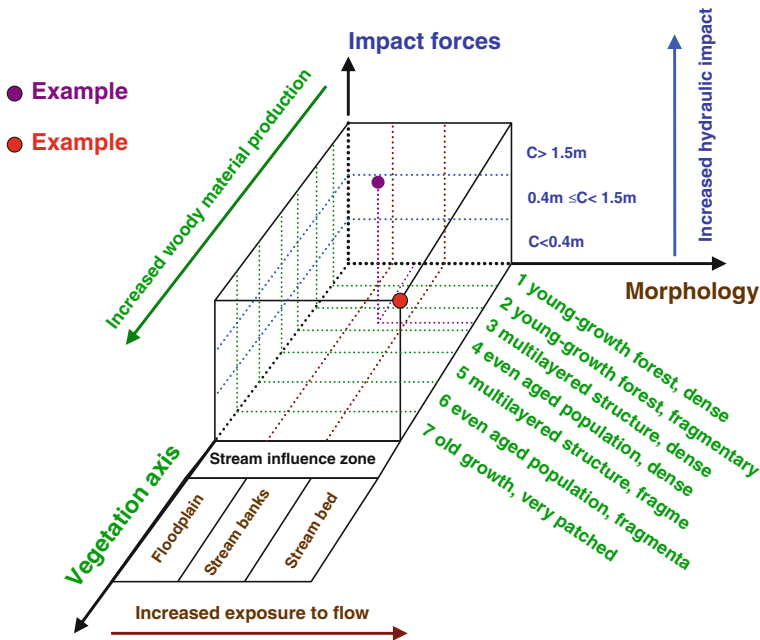


Fig. 2 Scheme for the assessment of the woody debris recruitment on regional scale

3.2.1 Assessment of the recruitment volumes from hill slopes

In this subsection, a procedure to assess the recruited woody material volumes from hill slopes is outlined. This assessment involves six steps:

- Step 1 Determination of the perimeter of the flooded areas of the considered extreme event from flow depth or velocity raster data sets. The flow depth or velocity data sets corresponding to the different time steps are given as output files of the hydrodynamic simulations performed with the 2D numerical model Sobek Rural (WL/Delft Hydraulics 2004). These raster data sets are overlaid in order to derive the perimeter identifying the maximum extent of the flood (see Fig. 3 for details).
- Step 2 A screening for the availability of wood-covered areas outside of the maximum flood boundaries. These wood-covered areas within a buffer width are categorised as active wood buffer (AWB) areas. This buffer width corresponds either to the potential tree height derived from the forest typology map (Klosterhuber et al. 2007) or to the real tree height retrieved from the Lidar-based digital surface model and the digital terrain model (Mazzorana et al. 2009). The difference between the surface model and the terrain model can give hints about the reference tree height and therefore about the width of the active wood buffer.
- Step 3 Identification of the recruitment wood buffer strips. Inside the delimitation polygon of the maximum extent flood area, buffer strips for the wood volumes, potentially recruited from the AWB areas, are identified in direct proximity to the AWB areas (see Fig. 3 for details). The width of these strips is half of the tree height of the adjacent AWB area and corresponds to the area of possible location of the centre of gravity of the recruited wood logs.

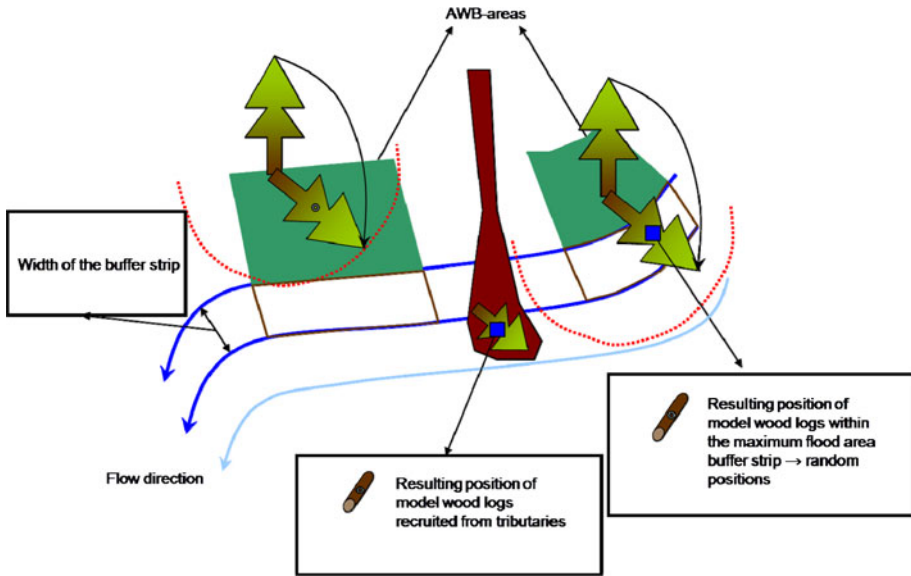


Fig. 3 Determination of the recruitment strips within the maximum extent buffer areas

- Step 4 Computation of the length of the contact boundary between the AWB areas and the buffer strips (identified in step 3). The user has to define the volume of recruited woody material per unit length of contact boundary for each AWB area. An estimation of recruitment volume scenarios is made on the basis of experimental data provided by inventories (Rickli and Bucher 2006). It should be noted that uncertainty is not negligible without detailed forest inventories and a precise estimation of dead wood volumes and forest stand stability conditions of the forest population. It is recommended to define a plurality of scenarios of recruitment volumes per unit length.
- Step 5 Specification of the dimension and number of the model wood logs. In this step, the dimensions of the “model wood log” (diameter and log length) are specified and the determination of the recruited number of model wood logs for each strip is straightforward, once known the volumes from the recruitment scenarios defined in the previous step. The position of the centre of gravity of the “model wood logs” is either chosen at random (see Fig. 3) or assessed by field investigations.
- Step 6 Determination of the starting position of the “model wood logs”. The volume of each recruited “model wood log” is assigned to the corresponding flow cell depending on the position of its centre of gravity (compare Fig. 3).

3.2.2 Assessment of the recruitment volumes from tributaries

This assessment involves the following two steps:

- Step 1 The recruitment scenarios of wood material volumes from the tributaries can be reliably defined only if a detailed documentation exists for events. If information

is missing, possible scenarios of recruited woody material volumes can be defined on the basis of empirical equations (Rickenmann 1997).

- Step 2 The number of “model wood logs” is calculated. Again the problem arises of the positioning of the “model wood logs” within the maximum extent flood area. In the case of accurate event documentations, the “model wood logs” can be placed within the geo-referenced depositional areas (see Fig. 3). Otherwise, engineering judgement is required to position the “model wood logs” by choosing, e.g., probable deposition sites.

3.2.3 Assessment of the recruitment volumes within the flooded area

Forests of different wood typologies produce determined amounts of dead wood ready for transport depending on the current stage in their “life cycle”. During the flood event itself, additional dead wood is produced as a consequence of either direct hydrodynamic impact on trees or destabilization of the trees’ anchorage through erosion phenomena (root wad scouring).

The vegetation structures are mapped and the morphology of the riverbank is overlaid with the outputs of the respective flood simulation. A woody material recruitment indicator is computed based on an impact-response assessment approach, which considers either the morphological characteristics or the flood intensity. This impact-response assessment approach has been developed on the basis of the findings of Rauch (2005) and Hübl et al. (2008). Experimental studies should further investigate the interplay of the following key factors: (1) Hydrodynamic impact: The hydrodynamic impact acts, on the one hand, through static and dynamic pressure forces on wood vegetation and, on the other hand, by yielding stress on the soil, weakening the root–soil anchorages. (2) Wood stand volume: A positive correlation between the recruited woody material volume and the wood stand volume is postulated. Average wood stand volume estimations for different wood stand structures are reported in Table 1. (3) Wood vegetation resistance–resilience: The influence of the aforementioned key factors cannot be understood and quantitatively estimated without assessing wood vegetation resistance–resilience mechanisms. These depend on both wood structural and species-specific characteristics. For the necessary accuracy level, the analysis is limited to the first type of characteristics underlining that resistance–resilience against hydrodynamic impact depends significantly on the flexibility of the wood and on recovery capacity. In addition, a very flexible vegetation structure protects the soil from erosion, while inflexible—old growth—population structures are weakened by erosion mechanisms and are also unstable due to an unfavourable slenderness (h/d) ratio. These interaction phenomena are described in Table 1.

The assessment scheme is shown in Fig. 2, where the energy indicator $C_{i,j}$ describes hydraulic impact on vegetation structures (see Eq. 8). The energy indicator is composed of a hydrostatic and a hydrodynamic pressure term and it is calculated as follows (Egli 2008, Holub and Hübl 2008):

$$Q_{i,j} = \rho g h_{i,j} + \frac{c_d \rho U_{i,j}^2}{2} \quad (8a)$$

where i,j , cell indices; $h_{i,j}$, flow depth [m]; $U_{i,j}$, flow velocity [m/s]; $Q_{i,j}$, pressure load; c_d , drag coefficient; ρ , density of the water.

Dividing both terms on the right hand side of Eq. 8a by ρg and assuming $c_d \approx 1$, we obtain the specific load:

$$C_{i,j} = \frac{Q_{i,j}}{\rho g} = h_{i,j} + \frac{U_{i,j}^2}{2g} \tag{8b}$$

The flow velocity is calculated from the velocities in direction x and y :

$$U_{i,j} = \sqrt{u_{x_{i,j}}^2 + u_{y_{i,j}}^2} \tag{9}$$

where $u_{x_{i,j}}$, flow velocity in x direction (m/s); $u_{y_{i,j}}$, flow velocity in y direction (m/s).

By a qualitative analysis of documented flood events (Mazzorana et al. 2009), the following assessment procedure for woody material recruitment could be established (see Fig. 4): (1) Identification and spatial delimitation of possible woody material recruitment areas, (2) assignment of these recruitment areas to the appropriate river morphology categories (e.g., stream bed, river banks, flood plain), (3) determination of the wood structure characteristics and definition of the respective structure typologies (see Table 1), (4) calculation of an indicator describing the hydraulic impact (Eq. 8a, 8b), (5) estimation of the recruitment volumes (recruited wood volume per hectare/stand volume per hectare), here referred to as woody material recruitment indicator (SVI) on the basis of the scheme shown in Fig. 4 and (6) quantification (see Eq. 10) of the absolute volume of recruited woody material (V_{SH}).

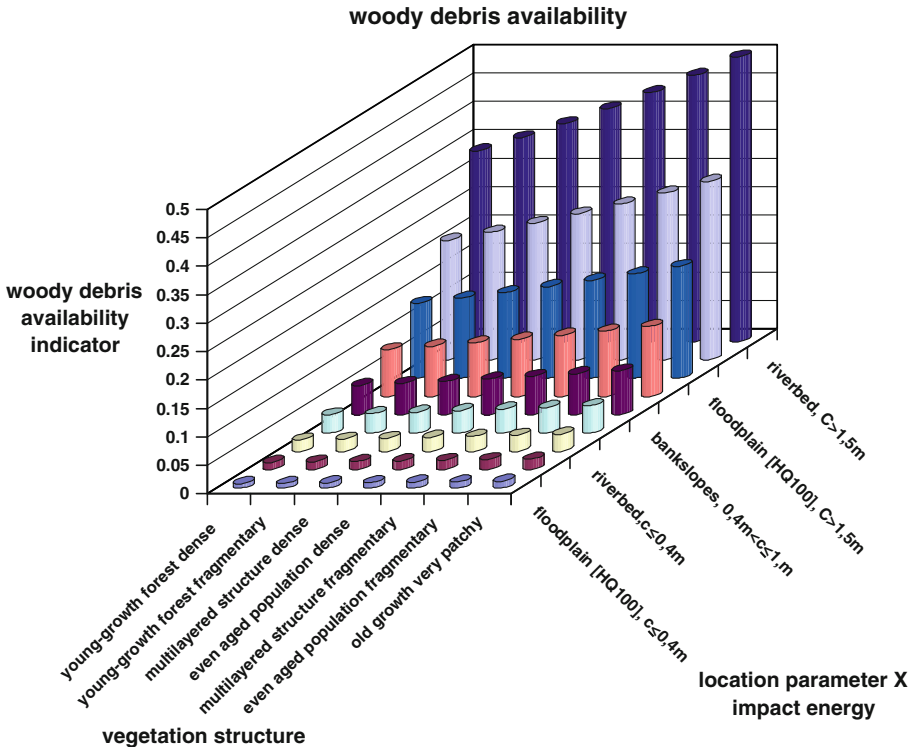


Fig. 4 Decision matrix for the quantification of the woody debris availability on a regional scale. Expert-based estimation of the woody material availability indicator

The parameter of the absolute volume of recruited woody material indicates the maximum volume of woody material that could be ripped at a given location by the flood process.

Finally, the recruited woody material volume for each cell is calculated as

$$V_{SH,ij} = SVI_{ij} \cdot V_{cell,ij} \tag{10}$$

Since the wood stand volume is given as a parameter showing values per hectares, Eq. 11 is used to calculate the woody material volume.

$$V_{SH,ij} = SVI_{ij} \cdot \left(\frac{A_{ij}}{10000} \right) \cdot V_{ha} \tag{11}$$

where $V_{cell,ij}$, wood stand volume for the cell ij ; V_{ha} , wood stand volume referred to an area of 1 ha; A_{ij} , area of the cell ij in m^2 .

The resulting output from this step is the calculated maximal volume of woody material that could be ripped out from each cell by the flood.

The estimations of the recruited wood volumes per hectare and the quantification of the absolute volume of recruited woody material (step 5 and 6 of the earlier outlined procedure, respectively) can be computed also following a slightly modified procedure, which explicitly accounts for the subdivision of the flood duration in time steps Δt . Two essential requirements are:

- a. Knowledge about the dead wood material available in each cell at time t^0 .
- b. Knowledge about the amount of greenwood, which, through either stem breakage or “uprooting” (and toppling) due to erosion, becomes dead wood ready for transport at the beginning of the successive time step.

Consequently, maximum estimated dead wood amounts for different forest typologies and predictions of the dead wood amounts produced in a given time step are required. Plausible values of dead wood volumes for different wood typologies range from 3 to 40.2 m^3/ha . In Table 1, estimations of possible dead wood volumes for different wood typologies are reported.

The prediction of the dead wood volumes, which are produced in a given time step in a determined forest typology exposed to determined hydrodynamic impacts and to determined river bed dynamics, is conducted with the following linear relationship:

$$V_{DW,ij}^{\Delta t} = k \cdot SVI_{ij}^t \cdot V_{GW,ij}^t \cdot \Delta t \tag{12}$$

where $V_{DW,ij}^{\Delta t}$, dead wood produced within the time step Δt in the cell ij ; SVI_{ij}^t , response class [1/s] (determined in full analogy to the first theory) for cell ij ; $V_{GW,ij}^t$, living wood volume in the cell at time step t [m^3] in cell ij ; Δt , time step (s); k , empirical constant, to be assessed on the basis observed extreme floods.

The amount of living wood at time step $t + 1$ is computed as follows:

$$V_{GW,ij}^{t+1} = V_{GW,ij}^t - V_{DW,ij}^{\Delta t} \tag{13}$$

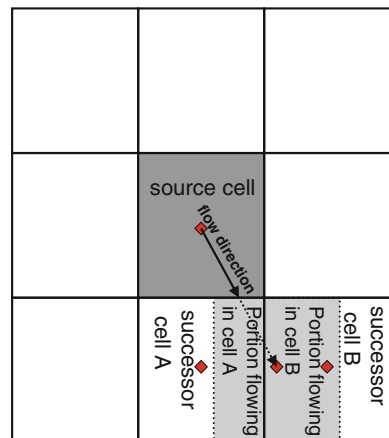
It should be noted that the influence of morphodynamics is not considered in its full complexity in this approach (e.g., no mobile bed or shear stress computations are performed). Morphodynamics are considered indirectly and in a simplified way in the estimation procedure of the woody material recruitment indicator (SVI_{ij}^t) by assigning a location attribute (i.e., stream bed, stream bank or flood plain) to each cell (compare Figs. 2, 4).

3.3 Woody material transport dynamics

Having defined and quantified the recruitment areas, the transport of material from these areas to the defined weak points or critical river locations and cross sections can be modelled. The modelling procedure is able to consider two different approaches for modelling the transport of woody material. If the main objective is the estimation of the pathways and the possible deposition zones, the transport of woody material is calculated on a cell-by-cell basis. This approach allows analysing the transportation and deposition dynamics either on a regional level or on a more detailed level. With this modelling approach, only one time step of the hydraulic modelling results can be considered. If the main objective is to study the interactions of transported woody material with obstacles such as bridges, the transport of woody material is calculated following an object-oriented approach. This approach allows for a consideration of more time steps of the hydraulic modelling and the deposition of woody material on sand banks during the falling limb of a flood hydrograph. In such a way, it is possible to keep track of the positions of the woody material elements from time step to time step.

The basics for the calculation of the transport dynamics are the same in the two approaches and are based on the following simplified model. This model delineates the possible pathways for woody material transport and computes for each of them the entrainment and transport conditions based on the theory outlined in Sect. 2.2 and on the following method. The input data are the raster results from a hydrodynamic 2D simulation of the design event (1 in 300 years return period) for water depths $h_{i,j}$ and flow velocities in x and y direction, $u_{x_{i,j}}$ and $u_{y_{i,j}}$. These rasters represent the state of the hydraulic simulation of different time steps. For each cell in the affected flood area, the flow direction is calculated according to the respective flow velocity in x and y directions, and given this flow direction, the source cell is moved until it is fitted into the next two neighbouring cells. The amount of woody material arriving from the source cell is divided into two portions according to the overlapping area of the moved source cell with the two neighbouring cells (Fig. 5). The particular portion of each subsequent cell is added, giving the total amount in this cell. The volumes passed through each cell are cumulated, and a grid data set of the woody material volume passed through each cell of the river influence zone is produced.

Fig. 5 Determination of the following cells (A and B) and their particular portion of the woody material from the source cell to receive



This approach is based on a further simplification of Eqs. 1 and 2 in order to precisely determine the woody material transport analysis conducted on a hazard index level (Petraschek and Kienholz 2003). Assuming that the woody material elements are positioned perpendicular to the flow direction ($\theta = 90^\circ$) and that the length of each element is expressed as a multiple of its diameter, $l = nd$, with $n \geq 1$; Eq. 14 is obtained from Eq. 1.

$$F = \frac{1}{2}C_d \cdot \rho \cdot k \cdot d \cdot h_{ij} \cdot U_{ij}^2 \tag{14}$$

Taking the hypothesis that the density of the wood element can be expressed as $\sigma = n \cdot \rho$ with $n \cong 1$ and that the local slope angle at the wood element locations is very small, $\alpha \cong 0^\circ$, Eq. 2 can be rewritten as:

$$R = \mu \rho g l \left(\frac{\pi d^2}{4} - A_{\text{sub}} \right) = g \rho k d \mu \left(\frac{\pi d^2}{4} - A_{\text{sub}} \right) \tag{15}$$

Based on Eqs. 3 and 4 can be rewritten as:

$$\begin{aligned} \Psi &= \frac{F}{R} = \frac{\frac{1}{2}C_d \rho k d h_{ij} U_{ij}^2}{g \rho k d \mu \left(\frac{\pi d^2}{4} - A_{\text{sub}} \right)} = \frac{\frac{1}{2}C_d h_{ij} U_{ij}^2}{g \mu \left(\frac{\pi d^2}{4} - A_{\text{sub}} \right)} \\ &= \frac{2C_d h_{ij} U_{ij}^2}{g \mu d^2 \left\{ \pi - \cos^{-1} \left(1 - \frac{2h_{ij}}{d} \right) + \frac{1}{2} \sin \left[2 \cos^{-1} \left(1 - \frac{2h_{ij}}{d} \right) \right] \right\}}. \end{aligned} \tag{16}$$

Subsequently, the velocity corresponding to $\Psi = \frac{F}{R} = 1$, here named as threshold velocity, U_{lim} , for the movement of the wood element, is determined accordingly by

$$\begin{aligned} U_{\text{lim},ij} &= \sqrt{\frac{2g\mu}{C_d h_{ij}} \left(\frac{\pi d^2}{4} - A_{\text{sub}} \right)} \\ &= \sqrt{\frac{g\mu d^2}{2C_d h} \left\{ \pi - \cos^{-1} \left(1 - \frac{2h_{ij}}{d} \right) + \frac{1}{2} \sin \left[2 \cos^{-1} \left(1 - \frac{2h_{ij}}{d} \right) \right] \right\}} \end{aligned} \tag{17}$$

Given these results and the conditions stated for expressions 5, 6 and 7, the cell-based transport inhibition parameter is defined as follows:

Case 1: If $h_{ij} \geq d$, the wood material element is floating and the associated specific transport inhibition parameter is $c_{ij}^* = 0$.

Case 2: If $h_{ij} < d$ and

$$\begin{aligned} 0 < U_{ij} &\leq \sqrt{\frac{g\mu_{ij}d^2}{2C_d h_{ij}} \left\{ \pi - \cos^{-1} \left(1 - \frac{2h_{ij}}{d} \right) + \frac{1}{2} \sin \left[2 \cos^{-1} \left(1 - \frac{2h_{ij}}{d} \right) \right] \right\}} \text{ or} \\ 0 < U_{ij} &\leq U_{\text{lim},ij} \end{aligned}$$

a condition of resting is imposed to the wood material element. The associated specific transport inhibition parameters $c_{ij}^* = 1$.

Case 3: If $h_{ij} < d$ and $U_{ij} > U_{\text{lim},ij}$ a condition of either sliding or rolling is imposed to the wood material element. The value of the associated transport inhibition parameter is expressed by:

$$c_{ij}^* = 1 - \frac{F_{ij}}{F_{ij}^*} = 1 - \frac{\frac{1}{2}C_d \rho k d h_{ij} U_{ij}^2}{\frac{1}{2}C_d \rho k d^2 U_{ij}^2} = 1 - \frac{h_{ij}}{d} \tag{18}$$

where c_{ij}^* , transport inhibition parameter of the cell ij (non-dimensional).

Observations noted by Diehl (1997) and Ng and Richardson (2001) indicate that woody material in ideal conditions is transported on the surface as individual pieces aligned with the flow and travelling at about the same velocity as the average water velocity at the surface.

Using the average velocity instead of the surface velocity as reference velocity for the moving woody material for a wide range of flow conditions, velocity along the transport trajectory for each moving woody material model log is estimated as follows:

$$U_{\text{wood},ij} = (1 - c_{ij}^*)U_{ij} \tag{19}$$

where $U_{\text{wood},ij}$, velocity of a wood log in the cell ij .

An analysis of the expression for the wood log velocity (Eq. 19) reveals that if the transport inhibition parameter tends to 1, coherently with resting or deposition conditions the velocity of the wood log tends to 0, whereas if the transport inhibition parameter tends to 0, the velocity of the wood log tends to U_{ij} . Through this method, it is possible to describe woody material transport pathways under unsteady flow conditions. A deposited woody material log can be remobilised in a successive time step under changed flow depth and flow velocity conditions.

3.4 Potential hazard impacts at critical stream configurations

The object-oriented approach for modelling the woody material transport dynamics as outlined in chapter 3.3 allows for an assessment of potential hazard impacts at critical stream configurations. This approach considers the model wood logs as points, representing the centre points of the model wood log. Each single object has information about log diameter, log length, diameter of root wads and impact-resistance characteristics as outlined in Fig. 2. The flowing of the model wood logs is computed following the procedure as proposed in Chap. 3.3.

A simplified assessment procedure for entrapment and deposition phenomena at special obstacles (e.g., bridges) is outlined. In Fig. 6a, a stream section with a crossing bridge is shown. Along the flow path, woody material can potentially interact with: (1) the superstructure of the bridge, (2) a single bridge pier and/or (3) two or more bridge piers.

Two types of obstacles are defined in order to model the interaction between these obstacles and the floating woody material:

- In-stream-obstacles Obstacles standing in the water such as piers or abutments. On these obstacles, transported logs can get entrapped upon collision at any stage of the flood.
- Crossing obstacles Obstacles crossing the stream at a given height on which the logs can get entrapped with their root plate when the flow depth approaches the object’s height i.e., lower chord of the superstructure of a bridge, see Fig. 6a.

Within the computational procedure, these obstacles are represented by polygonal objects. The following attributes are required to comprehensively describe these obstacles:

1. Retention probability (p_{ret}): Probability for each colliding log to get entrapped at the considered obstacle. This gives the expert the possibility to consider the geometry (e.g., profile) of an obstacle (e.g., inappropriately shaped piers) and estimate a proper retention probability

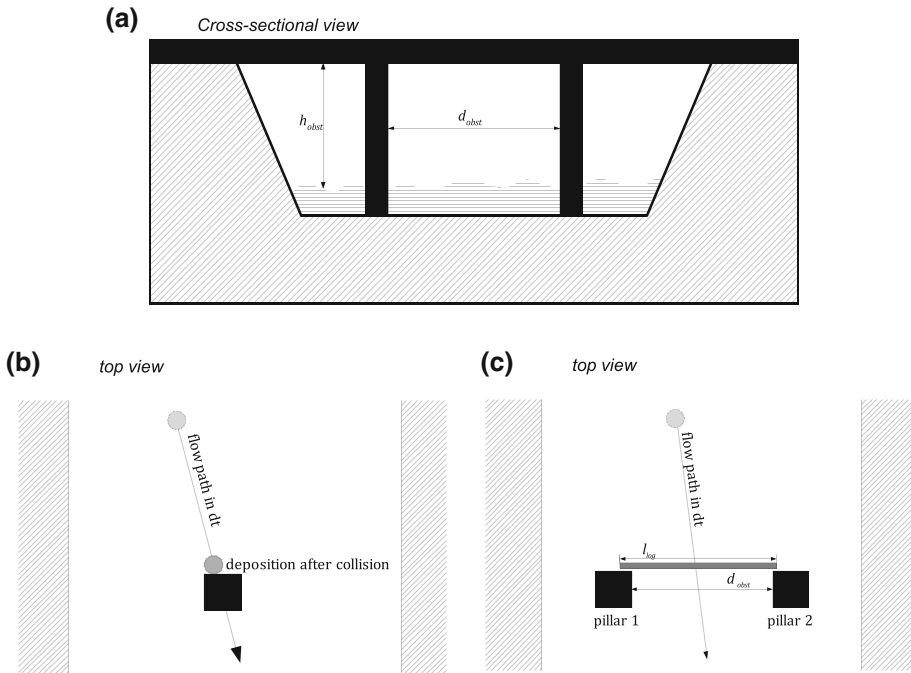


Fig. 6 **a** Example of a bridge as an obstacle consisting of two piers as in-stream-obstacles and the superstructure as a crossing obstacle d_{obst} indicates the minimum distance between the two piers and h_{obst} the height of the superstructure. **b** Example of a collision with an in-stream-object. The flow path intersects the shape of a pier. In this case, the floating log is entrapped at the first intersection point between the flow path and the shape of the pier. **c** Example of a woody material object floating between two piers of a bridge. The flow path does not cross any of the piers; however, the length (l_{log}) exceeds the minimum distance between the two pillars (d_{obst}) and the possibility of entrapment occurs

2. Obstacle height (h_{obst}): Height of the lower chord of a crossing obstacle above the initial water level. The obstacle type is defined using the obstacle height (Fig. 6a). In case the obstacle height equals zero, an object is treated as in-stream-obstacle, otherwise the object is handled as a crossing obstacle

A collision with an obstacle occurs when the flow path of a woody material log intersects an obstacle. If it is a crossing obstacle, the flow depth needs to reach a critical value. Above this value, the root plate can contact the lower chord of the obstacle. Depending on the retention probability of the obstacle, specified by expert judgement, the woody material logs may either be entrapped or flushed through (see Fig. 6b).

If an object is floating between two in-stream-obstacles, e.g., two piers, it is checked whether the length of the log exceeds the shortest distance (d_{obst}) between the two piers. If so, a spanning blockage can occur, provided that the log is unfavourably oriented. The corresponding probability (p_{ent}) is estimated through expert judgement.

The entrapped wood logs occlude part of the available flow section and become a part of the obstacle for wood logs subsequently approaching the critical configuration (see Fig. 6c).

4 Study site and test application

The Passer/Passirio River in the Autonomous Province of Bolzano—South Tyrol, Italy was chosen as test site for the application of the procedure described in the previous sections (Fig. 7). The Passer/Passirio River drains a catchment area of approximately 415 km² and opens to the receiving watercourse Etsch/Adige River near the city of Meran/Merano, Italy. The study area comprises the river bed and the extent of the simulated flooded areas of the Passer/Passirio River during a flood event with a return period of 1 in 300 years. A relevant volume of woody material arriving from the upper parts of the catchment is entrapped at the open check dam located in the upstream river reach. The upstream boundary of the simulation area is located at this open check dam near the community of St. Leonhard in Passeier. The upstream boundary of the simulation area is located at this open check dam near the community of St. Leonhard in Passeier. A high-magnitude flash flood occurred in the Passer/Passirio River in 1987 (Fig. 8), resulting in severe damage to regionally important bridges and roads. The downstream boundaries were defined near the locality of Saltaus/Saltusio at a bridge location (Fig. 7b). The cumulative volume of the transported woody material was calculated here. Within the studied river reach, the channel bed is characterised by twelve tributaries with relevant input of woody material. The material supplied by the tributaries was considered in this study. Figure 7c summarises the extent of the system.

The woody material volumes delivered by the tributaries were assessed and quantified by analysing recent debris flow events. Table 2 shows the assumed values for the available woody material inputs. The interceptors (e.g., bridges and check dams) within the river

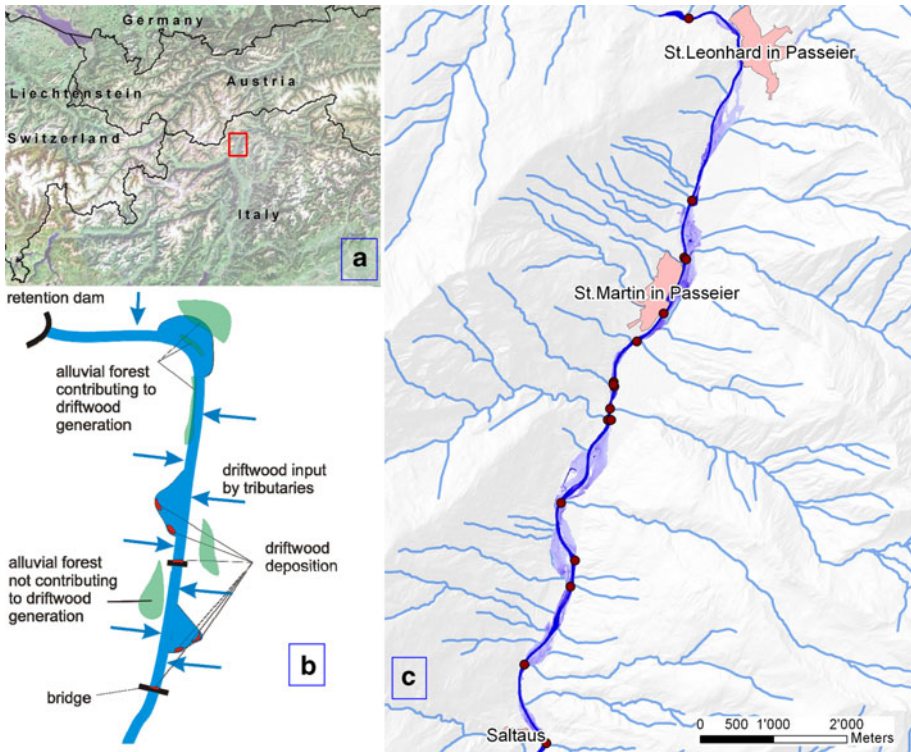


Fig. 7 a Localization, b system description and c extent and delimitation of the study area



Fig. 8 An aerial image of the study area after the flood event in 1987

influence zones were geo-referenced. For each of these critical configurations, the geometrical characteristics were assessed and a retention probability was assumed. This retention factor accounted for the woody material volumes retained by the obstacle. The simulation procedure was repeated with and without consideration of these weak points.

The inflow hydrograph (return period of 1 in 300 years) at the upstream boundaries of the study area was calculated with the GIS-based hydrologic modelling system BaSin 30 (AIDI 2005). The flood propagation computations were carried out with the hydrodynamic simulation model SOBEK Rural (WL/Delft Hydraulics 2004), which is capable of computing the full numerical solution of the shallow water equations. For a hazard indication analysis level, a pure 2D overland flow simulation was performed. Outputs included the flow depths and the flow velocities in x and y direction for the different time steps (e.g., 30 min for computations at the hazard index level). The flood simulation was performed on the basis of a digital elevation model delineated by airborne laser scanning technique with an original resolution of 2.5 m, upscaled to a resolution of 10 m.

For the calculation of the woody material transport dynamics, a reference diameter of the wood elements of $d = 0.3$ m was assumed. A drag coefficient of $C_d = 0.8$ and a friction coefficient of $\mu = 1.0$ were used during the sets of calculation. For an analysis conducted at a hazard index level, a value of 1.4×10^{-4} was chosen for the parameter k_1 in Eq. 12. A detailed analysis of transport dynamics at critical bridge locations has been carried out.

5 Simulation results

The application of the method outlined in Sect. 3.1 resulted in a map of the vegetation structures, a map of the morphological characteristics of the river influence zone and

Table 2 Assumed values for the input of woody debris from the tributaries

Torrent ID	Name of torrent	Woody debris volume (m ³)	Notes
G	Passer/Passirio	10	Initial condition: woody material passing through the retention dam
G.255	Keltalbach/Rio Lega	20	Torrent with debris flow processes
G.235	Talbach/Rio di Valle	2	Torrent with debris flow processes
G.230	Fartleisbach/Rio dell’Avas	5	Torrent with debris flow processes
G.220	Dorfbach/Rio Dorf	5	Torrent with debris flow processes
G.205	Schoenbichl (Kellerbach)/Rio di Belcolle	5	Torrent with debris flow processes
G.195	Heimatscheintal/Rio del Masso dei Tovi	5	Torrent with debris flow processes
		100	Lumbryhood in the neighbourhood upstream of the confluence of the Heimatscheintal/Rio del Masso dei Tovi torrent
		200	Lumbryhood in the neighbourhood upstream of the confluence of the Heimatscheintal/Rio del Masso dei Tovi torrent
G.190	Grafeisbach/Rio Graves	20	Torrent with debris flow processes
G.185	Kalbenbach/Rio della Clava	10	Torrent with debris flow processes
		40	Lumbryhood in the neighbourhood downstream of Grafeisbach/Rio Graves torrent
G.175	Prantlbach-Brandwaldbach/Rio Prantola	30	Torrent with debris flow processes
		20	Lumbryhood in the neighbourhood upstream of the confluence of the G.155 torrent
G.145	Widnerbach/Rio di Videna	2	Torrent with debris flow processes
G.120	Badbach/Rio di Bagno	4	Torrent with debris flow processes
G.110	Mainlechnerbach/Rio di Main	20	Torrent with debris flow processes

computed maximal volumes of recruited woody material within the considered system. Figure 9a shows an extract of the mapped vegetation structures within a channel section, indicating that a substantial part of the river influence zone in the study area is covered by vegetation. Thus, the recruitment of considerable amount of woody material is plausible. In Fig. 9b, the mapped geomorphologic classification of the river influence zone is shown, and in Fig. 10a, detail of the cell-by-cell simulation results is provided. The results show an increased concentration of woody material transport in the centre of the streamline. Additionally, the potential deposition areas of woody material are given; deposition primarily took place in flooded areas with low flow depths or low flow velocities outside of the river channel. Within the river channel, deposition of woody material was modelled at

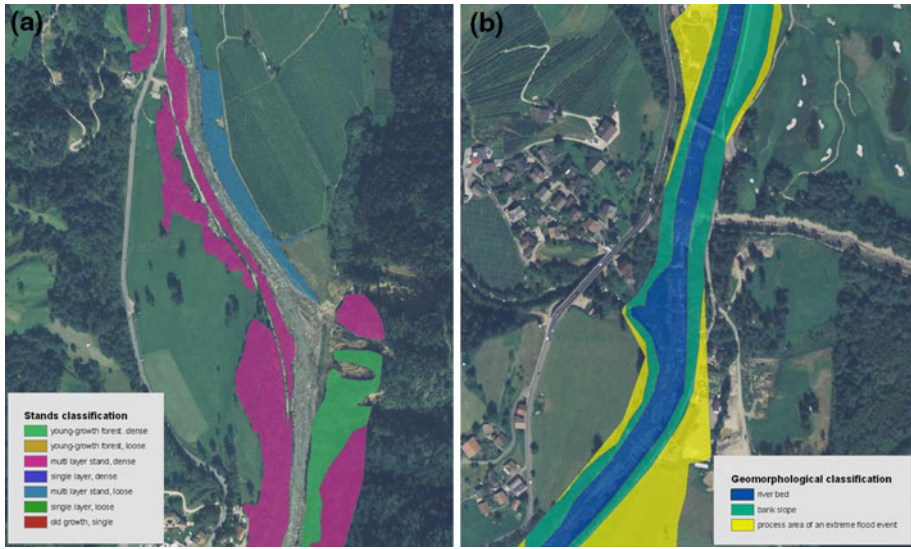


Fig. 9 a Extract of the mapped vegetation structure. b Extract of the mapped morphology of the river influence zones

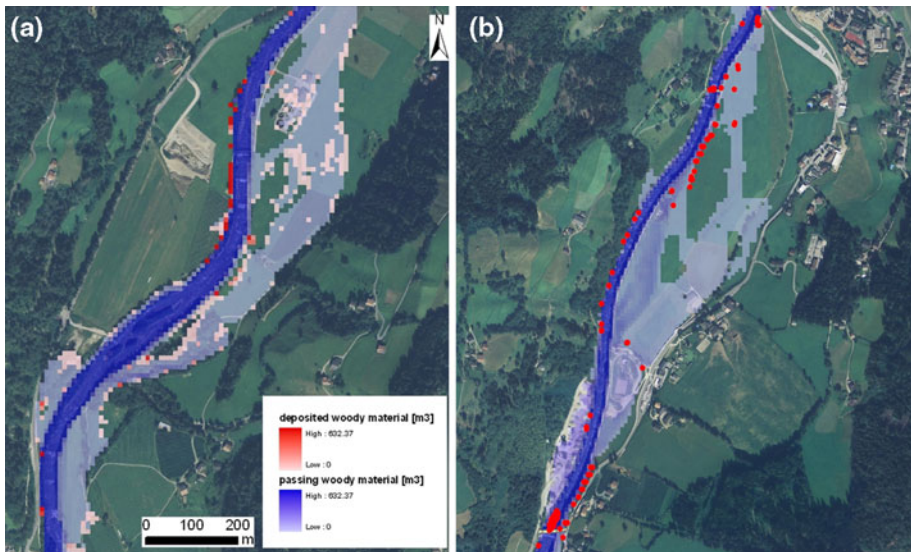


Fig. 10 a Results of the cell-by-cell simulation of the woody material transportation and deposition volumes. The red colours show the volume of deposited driftwood, the blue colours show the volume of passing driftwood at each cell. The maximum values are calculated at the outflow cell. b Results of the object-oriented simulation of the deposition of woody material. The red dots show the centre of gravity of the deposited model wood logs

the waterside slopes, at the waterside of river bends and at calm loops. The modelled woody material deposition areas corresponded accurately with the mapped potential deposition areas. The maximum of transported woody material was calculated as 632 m³ in

the last flow cell. This value indicates the maximum amount of transported woody material during a flood event with a reoccurrence period of 300 years at the outflow cell of the studied river reach. It corresponds with the dead wood volumes of 35 flooded hectares of different forest classes as shown in Table 1. This underlines that woody material transport and related phenomena are not negligible in the elaboration of the flood hazard zone map for the Passer/Passirio river. Additionally, the modelling results show the increase of transported driftwood along the river. At the upper reach of the river, small amounts of driftwood were computed; whereas downstream of each flooded wood stand with large dead wood volumes, the volume of transported driftwood increased. As expected, after a considerable deposition of driftwood, the volume of transported driftwood within the river channel decreased. Therefore, the modelling results lead to the identification of river reaches with significant driftwood transport. Since time dependency was not considered, the modelled design event had virtually an infinite duration, meaning that the entire amount of potentially removable wood stand volume was removed and mobilised. Thus, the computed woody material volumes represent the upper threshold in terms of potentially maximum values.

The cell-by-cell-based modelling procedure does not consider the rising and falling limb of the flood hydrograph as does the object-oriented modelling approach. Therefore, the results of the two approaches differ slightly. In general, the modelled deposition areas of both approaches are the same, but the computed deposition volumes differ slightly. Since the object-oriented approach considers different time steps of the flood process, it considers different process areas during the flood event. Therefore, the deposited volumes differ in situations where dead wood is re-mobilised after deposition due to the increase in the wetted perimeter or the increase in flow depth and/or velocities. The object-oriented approach outlines the track of each single model wood log and as such, the origin of the entrapped or deposited log could be assessed. Additionally, the consideration of more time steps of the flood simulation enables the tracking of the development of dead wood and the transport of the model wood logs in time. It was shown that most of the model wood logs flow repeatedly out from some of the flood forest areas. Only the flooding of a large area with the same wood stand characteristics and with high flood intensities led to a simultaneous burst of woody material into the river reach. The modelling procedure allows for the observation of these situations and the assessment of the consequences of the evolvment of log jams due to a simultaneous over-flooding. Figure 10b shows the woody material deposition areas computed by the object-oriented approach. Each red dot represents one model wood log. The results of the investigation of woody material dynamics at the selected weak point (i.e., bridge location) are shown in Fig. 11. The computed interaction process of the model wood logs showed that the log jams increased constantly at obstacles during the modelled flood event. After the modelled flood process, the net volume of the log jam at the selected bridge between Oberpsairer and Mörre was around 3 m³. Figure 11 shows the computed log jam at the bridge, and Fig. 12 show the bridge destroyed by the flood event in 1987. The picture does not allow reconstructing the total amount of driftwood entrapped at the bridge, as the bridge was over-flooded after the break of the left pillar and the entrapped woody material was transported away. However, Fig. 11 confirms the entrapment of driftwood with this obstacle. The procedure for modelling the interaction of the model wood logs with critical stream configurations calculates the volume of retained driftwood at every obstacle. The retention volume depends on the characteristics of the obstacle itself, and trapped driftwood necessarily reduces the volume which is transported downstream of the obstacle. This method allows for the identification of the systematically most relevant weak points in the system.

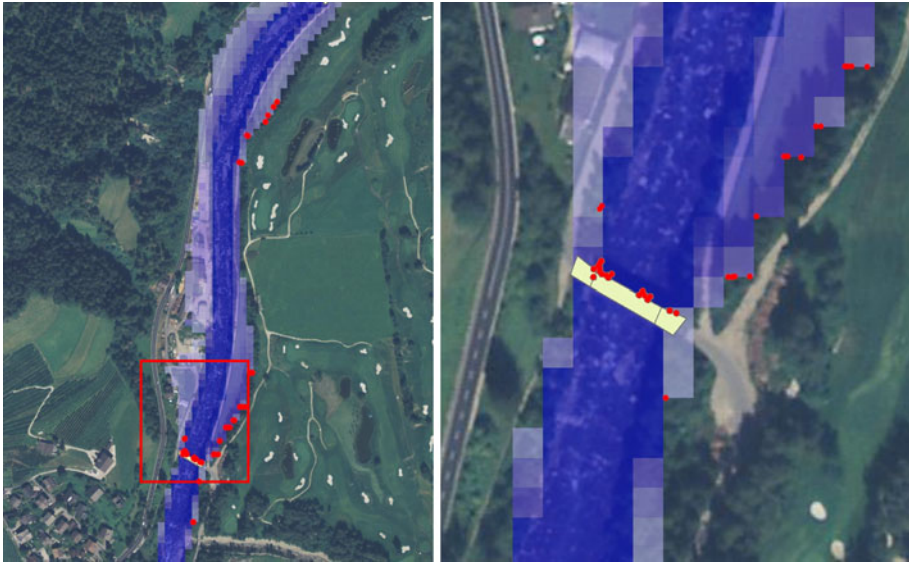


Fig. 11 Entrapment at a critical configuration. The graphic at the right side shows the entrapped driftwood on a more detailed scale



Fig. 12 Bridge destroyed across the Passer/Passirio river soon after the flood event in July 18th, 1987. The bridge was occluded with woody material and was destroyed after the outbreak of the river on the *left side*. The figure shows only the driftwood at the bridge that remained after the event

6 Discussion and conclusions

By the application of the developed method, valuable insights were provided regarding woody material recruitment processes and the propensity for entrainment and transport to critical configurations during extreme flood events. In particular, an overview of the

maximal amount of transported and deposited woody material in a defined river reach was given. Moreover, the main pathways of the woody material in the river channel were traced and subsequently the potential depositional areas were identified. Furthermore, the procedure provided the order of dimension of the woody material volume expected to pass through bridges during a flood event. Such quantified knowledge on woody material volume approaching a weak point location is crucial for a reliable scenario definition during hazard assessment, in particular with respect to a possible log jam formation, clogging or similar obstruction phenomena. Consequently, the transparency of hazard mapping procedure and the quality of the results are increased, and the supervision of the entire hazard mapping procedure by the respective public authorities is facilitated. The outcomes can also be used in order to support the definition of policies in riparian forest management and for defining particular measures such as thinning and other forest management actions. Nevertheless, the procedure presented earlier might still have certain limitations. The spatial resolution of the flood simulation has to be adapted and refined if the goal is a more detailed scale. With a grid size of 10 m, the river channel morphology is approximated with limited accuracy, resulting in a less precise calculation of the woody material flow paths. The procedure was found to be sensitive to the assumed wood stand volumes of different vegetation structures studied; however, a very detailed investigation on the wood structure might improve the procedure significantly. Additionally, the exposure time of the different vegetation structures to the flood event might be another relevant factor. During flood events with a relatively short duration, significantly smaller volumes are expected compared to long-duration flood events.

Despite these limitations, the developed method is of particular relevance to mitigate flood risk. The results of mapped recruitment areas with the respective forest structure typologies and identified transport paths with the transport dynamics for a determined critical configuration are essential indicators for hazard assessment.

The time-dependent modelling of woody material dynamics indicates whether or not the formation of log jams due to a simultaneous flooding of a large forested area with high flood intensities is plausible in the studied river reach. The assessment of the interaction processes induced at the considered critical configuration refines the hazard analysis and provides significantly more detailed input for the subsequent risk assessment. As shown during previous events, the critical configuration was repeatedly located at bridges; hence, the hypothetical debris accumulation for the entire bridge and the resulting consequences can be calculated according to the indications provided by Diehl (1997). This is fundamental information for effective risk mitigation strategies. Key elements of these strategies include: (1) the removal of those parts of the critical configuration that induce woody material accumulation, (2) the reconfiguration of the weak point to improve flow conditions and (3) the adherence to silvicultural measures in the respective recruitment areas in order to reduce the hazard source.

An application of the proposed model would allow enhanced emergency planning and preparations (e.g., excavating identified places in order to diminish accumulations at bridges; installation of temporary protection measures; implementation of local structural protection). These activities would introduce redundancies and buffer capacities into the system, thereby achieving an increased resilience of elements at risk.

Acknowledgments The development of the modelling approach was co-financed by the European Union within the Interreg IIIA project „Entwicklung eines Informationssystems für Naturraumpotentiale—Teil 2“. Afterwards, the procedure was refined within the Interreg IV B Alpine Space project “Adaptalp—Adaptation to Climate Change”, also co-financed by the EU. The authors express their sincere thanks to the two

anonymous reviewers and to Sven Fuchs and Francesco Comiti for valuable comments on an earlier version of the manuscript, to Emily Procter for improving the English manuscript and to Claudio Volcan for performing the hydrodynamic simulations.

Open Access This article is distributed under the terms of the Creative Commons Attribution Noncommercial License which permits any noncommercial use, distribution, and reproduction in any medium, provided the original author(s) and source are credited.

References

- Abbe TB, Montgomery DR, Petroff C (1997) Design of stable in-channel wood debris structures for bank protection and habitat restoration: an example from the Cowlitz River, WA. In: Wang SSY, Langedoen EJ, Shields FD (eds) Management of landscapes disturbed by channel incision: stabilization, rehabilitation, restoration. University of Mississippi, Mississippi, pp 809–815
- AIDI (Associazione Italiana di Idronomia) (2005) Procedura di calcolo dell'Idrogramma di piena a frequenza di superamento assegnata per il territorio della provincia Autonoma di Bolzano. Relazione tecnica, Bolzano
- Autonome Provinz Bozen—Südtirol (2006) Richtlinien für die Erstellung von Gefahrenzonenplänen und zur Klassifizierung des spezifischen Risikos. Bozen
- Bänziger R (1990) Schwemmholz im Unwettersommer 1987. Schweiz Ing Archit 47:1354–1358
- Bezzola G, Sigg H, Lange D (2004) Schwemmholzrückhalt in der Schweiz. In: Internationales Symposium „Interpraevent 2004“, Riva, Trient; Tagungspublikation, Band 3, pp 29–40
- Blaschke T, Tiede D, Heurich M (2004) 3D landscape metrics to modelling forest structure and diversity based on laser scanning data. In: The international archives of photogrammetry, remote sensing and spatial information sciences, vol XXXVI-8/W2, Freiburg, pp 129–132
- Bocchiola D, Rulli MC, Rosso R (2006) Transport of large woody debris in the presence of obstacles. *Geomorphology* 76:166–178
- Braudrick CA, Grant GE (2000) When do logs move in rivers? *Water Resour Res* 36(2):571–583
- Braudrick CA, Grant GE (2001) Transport and deposition of large woody debris in streams: a flume experiment. *Geomorphology* 41:263–283
- Braudrick CA, Grant GE, Ishikawa Y, Ikeda H (1997) Dynamics of wood transport in streams: a flume experiment. *Earth Surf Process Landf* 22:669–683
- BUWAL—Amt für Raumplanung Graubünden—Ufficio Cantonale di Pianificazione (1998) Grundlage zur FAN-Tagung vom 13-16 Oktober 1998 in Ittingen, 15 pp
- Comiti F, Andreoli A, Lenzi MA, Mao L (2006) Spatial density and characteristics of woody debris in five mountain rivers of the Dolomites (Italian Alps). *Geomorphology* 78:44–63
- Curran JH, Wohl EE (2003) Large woody debris and flow resistance in step-pool channels, Cascade Range, Washington. *Geomorphology* 51:141–157
- Degetto M (2000) Dinamica del legname in alveo e modellazione del suo comportamento in presenza di briglie filtranti. M.S. Thesis, University of Padova
- Diehl TH (1997) Potential drift accumulation at bridges. Publication No. FHWA-RD-97-028 U.S. Department of Transportation, Federal Highway Administration Research and Development, Turner-Fairbank Highway Research Center, Virginia
- Egli T (2008) Wegleitung Objektschutz gegen meteorologische Naturgefahren. Vereinigung Kantonalen Feuerversicherungen VKF, Bern
- Fuchs S, Holub M (2007) Risk management strategies for landslides in European mountain regions—current practice in Austria and future needs. *Geogr Forhum* 6:5–21
- Fuchs S, McAlpin M (2005) The net benefit of public expenditures on avalanche defence structures in the municipality of Davos, Switzerland. *Nat Hazards Earth Syst Sci* 5(3):319–330
- Gurnell AM, Petts GE, Hannah DM, Smith BPG, Edwards PJ, Kollmann J, Ward JV, Tockner K (2000) Wood storage within the active zone of a large European gravel-bed river. *Geomorphology* 34:55–72
- Haga H, Kumagai T, Otsuki K, Ogawa S (2002) Transport and retention of coarse woody debris in mountain streams: an in situ experiment of log transport and a field survey of coarse woody debris distribution. *Water Resour Res* 38:8
- Hildebrand RH, Cemly AD, Dolloff CA, Harpster KL (1997) Effects of large woody debris placement on stream channel and benthic macroinvertebrate. *Can J Fish Aquat Sci* 54:931–939
- Holub M, Hübl J (2008) Local protection against mountain hazards—state of the art and future needs. *Nat Hazards Earth Syst Sci* 8:81–99

- Hübl J, Anderschitz M, Florineth F, Gatterbauer H, Habersack H, Jäger E, Kogelnig A, Krepp F, Rauch JP, Schulev-Steindl E (2008) FLOODRISK II—Vertiefung und Vernetzung zukunftsweisender Umsetzungsstrategien zum integrierten Hochwasserschutz, Workpackage 2.3—Präventive Strategien für das Wildholzrisiko in Wildbächen. Bundesministerium für Land- und Forstwirtschaft, Umwelt und Wasserwirtschaft, Abteilung IV/5, Wildbach und Lawinenverbauung, 43
- Keim RF, Skaugset AE, Bateman DS (2002) Physical aquatic habitat: II. Pools and cover affected by large woody debris in three western Oregon streams. *North Am J Fish Manag* 22:151–164
- Klosterhuber R, Plettenbacher T, Hotter M, Schober T, Aschaber R, Vacik H, Pircher G, Gruber G, Ruprecht H (2007) Ökologisches Handbuch zur Waldtypisierung und Waldstratifizierung Südtirol, Teil A, Zwischenbericht im Auftrag der Autonomen Provinz Bozen, Abteilung 32, Forstwirtschaft. Bozen
- Lange D, Bezzola GR (2006) Schwemmholz, Probleme und Lösungsansätze, Mittellungen der Versuchsanstalt für Wasserbau, Hydrologie und Glaziologie (VAW), Zurich
- Lyn D, Cooper T, Condon D, Gan L (2007) Factors in debris accumulation at bridge piers, Washington, US Department of Transportation, Federal Highway Administration Research and Development, Turner-Fairbank Highway Research Center
- May CL, Gresswell RE (2003) Large wood recruitment and redistribution in headwater streams in the southern Oregon Coast Range, USA. *Can J For Res* 33(6):1352–1362
- Mazzorana B, Zischg A, Largiader A, Hübl J (2009) Hazard index maps for woody material recruitment and transport in alpine catchments. *Nat Hazards Earth Syst Sci* 9:197–209
- Mitchell JK (2003) European river floods in a changing world. *Risk Anal* 23:567–574
- Montgomery DR, Piegay H (2003) Wood in rivers: interactions with channel morphology and processes. *Geomorphology* 51:1–5
- Ng YLA, Richardson JR (2001) Transport mechanics of floating woody debris. Thesis, Faculty of the Graduate School, University of Missouri-Columbia
- Oberndorfer S, Fuchs S, Rickenmann D, Andrecs P (2007) Vulnerabilitätsanalyse und monetäre Schadensbewertung von Wildbachereignissen in Österreich. BFW, Wien
- Petraschek A, Kienholz H (2003) Hazard assessment and mapping of mountain risks in Switzerland. In: Rickenmann D, Chen CL (eds) Debris-flow hazard mitigation: mechanics, prediction and assessment. Millpress, Rotterdam
- Rauch HP (2005) Hydraulischer Einfluss von Gehölzstrukturen am Beispiel der ingenieurbiologischen Versuchsstrecke am Wienfluss. Dissertation, University of Life Sciences Vienna, Vienna
- Rickenmann D (1997) Schwemmholz und Hochwasser. *Wasser Energ Luft* 5(6):115–119
- Rickli C, Bucher H-U (2006) Schutzwald und Schwemmholz in Wildbacheinzugsgebieten. In: FAN-Agenda 1/06, pp 17–20
- Rimböck A, Strobl T (2002) Loads on rope net constructions for woody debris entrapment in torrents. International Congress “Interpraevent 2002 in the Pacific Rim”, Matsumoto, Japan; Congress publication, vol 2, pp 797–807
- Shields FD, Morin N, Kuhnle RA (2001) Effects of large woody debris structures on stream hydraulics. In: Proceedings of wetlands engineering and river restoration conference, ASCE, Reston
- Wilson CAME, Yagci O, Olsen NBR, Rauch HP (2004) 3D numerical modelling of vegetated compound channel flows. In: IAHR/IWA 6th international conference on hydroinformatics, Singapore
- WL Delft Hydraulics (2004) Release notes, SOBEK version v2.09.001. Delft

5.3 Synthesizing: Model coupling

Paper 19: Zischg, A., Felder, G., Weingartner, R., Gómez-Navarro, J.J., Röthlisberger, V., Bernet, D., Rössler, O., Raible, C., Keiler, M., Martius, O., 2016. M-AARE - Coupling atmospheric, hydrological, hydrodynamic and damage models in the Aare river basin, Switzerland, in: 13th Congress INTERPRAEVENT 2016, 30 May to 2 June 2016, Lucerne, Switzerland. Conference proceedings, 444–451.

M-AARE - Coupling atmospheric, hydrological, hydrodynamic and damage models in the Aare river basin, Switzerland

Andreas Paul Zischg, PhD^{1,2}; Guido Felder, MSc²; Rolf Weingartner, Prof.²; Juan José Gómez-Navarro, PhD²; Veronika Röthlisberger, MSc²; Daniel Bernet, MSc²; Ole Rössler, PhD³; Christoph Raible, Prof.⁴; Margreth Keiler, PD⁵; Olivia Martius, Prof.²

ABSTRACT

The triggering mechanism and the temporal evolution of large flood events, especially of worst-case scenarios, are not yet fully understood. Consequently, the cumulative losses of extreme floods are unknown. To study the link between weather conditions, discharges and flood losses it is necessary to couple atmospheric, hydrological, hydrodynamic and damage models. The objective of the M-AARE project is to test the potentials and opportunities of a model chain that relates atmospheric conditions to flood losses or risks. The M-AARE model chain is a set of coupled models consisting of four main components: the precipitation module, the hydrology module, the hydrodynamic module, and the damage module. The models are coupled in a cascading framework with harmonized time-steps. First exploratory applications show that the one way coupling of the WRF-PREVAH-BASEMENT models has been achieved and provides promising new insights for a better understanding of key aspects in flood risk analysis.

KEYWORDS

model coupling; worst-case flood; flood risk; Aare river; Switzerland

INTRODUCTION

In Switzerland, floods are the major cause of significant economic losses. The amplitude of flood peaks and the flood volume depend on the intensity and track of the triggering precipitation events, the topography and geology of the catchments, the wetness of the catchments prior to precipitation events as well as the hydro-morphologic conditions in the floodplains. However, the detailed triggering mechanism and the temporal evolution of large flood events, especially of worst-case scenarios, are not yet fully understood. Regarding mesoscale catchments, insights on the precipitation patterns leading to the most extreme floods are missing. Consequently, the cumulative losses of worst-case floods are unknown. The knowledge of the worst-case flood or of flood discharge return periods of up to 10'000 years are important for managing critical infrastructures as well as financial risks, e.g.,

1 University of Bern, Bern, SWITZERLAND, andreas.zischg@giub.unibe.ch

2 Mobiliar Lab for Natural Risks, Oeschger Centre for Climate Change Research, Institute of Geography, University of Bern

3 Oeschger Centre for Climate Change Research, Institute of Geography, University of Bern

4 Physics Institute, Oeschger Centre for Climate Change Research, University of Bern

5 Institute of Geography, University of Bern

for portfolio management of insurance companies. On a longer time scale, the question how the expected changes in precipitation intensities due to climatic changes influence the flood risk is of special interest. To study the link between weather conditions, discharges and flood losses it is necessary to couple atmospheric, hydrological, hydrodynamic and damage models. An attempt for coupling hydrologic with hydraulic models for flash flood predictions has been shown by Laganier et al. (2014). Various examples of coupling process models and vulnerability models were elaborated in the CRISMA project (Heikkilä et al. 2015). The focus in this project laid on the improvement of crisis management by simulating complex crisis scenarios of winter storm events, coastal submersion processes, earthquakes and for forest fires. An example of coupling hydrologic, hydrodynamic and damage models is given by Kourgialas and Karatzas (2013).

The objective of the project “M-AARE – Coupling atmospheric, hydrological, hydrodynamic and damage models in the Aare river basin” is to test the potentials and opportunities of a model chain that relates atmospheric conditions to flood risks. Thus, the main question is whether the coupling of atmospheric, hydrologic, hydrodynamic and damage models could potentially contribute to a better understanding of the formation of flood events and their consequences. Another aim of this explorative study is to quantify the resources needed for simulating these processes in a model chain.

With the model chain, the discharges from the catchments to the floodplains for selected precipitation scenarios and the retention effects in lakes and floodplains should be quantified. This allows to predict the flooded areas and the related losses to exposed residential buildings. Beside the hydro-meteorological characteristics, a key aspect of the method is to characterize and capture the non-linear effects of flood retention in the valley bottom and in the lakes. Furthermore, the model chain will allow the quantification of potential losses for given scenarios based on flow depths and flow velocities and therefore provide a sound basis for risk analysis.

The model chain was developed and tested in the watershed of the river Aare upstream of Bern, Switzerland, with an area of approx. 3000 km². This river basin is a complex network of sub-catchments with different runoff characteristics including two larger regulated lakes. Most of the rivers are trained since the 18th and 19th century.

METHODS

The M-AARE model chain is a set of coupled models consisting of four main components: the precipitation module, the hydrology module, the hydrodynamic module, and the damage module (see Fig. 1). The selected models in each module will be inter-changeable or can be used in an ensemble-framework for further sensitivity and uncertainty assessments.

Precipitation module

The precipitation module provides precipitation scenarios as inputs for the rainfall-runoff model. The latter is set up for each tributary and delivers the input hydrographs for the hydrodynamic model. The precipitation scenarios are formulated using two different approaches: a) by defining representative spatio-temporal precipitation patterns represented

in gridded datasets or b) by selecting extreme precipitation events from a long climate simulation of a Global Circulation Model (CESM1) and downscaling these selected cases with a Regional Climate Model (WRF). The first approach was used to estimate the probable maximum precipitation (PMP), which is done by applying a Monte Carlo approach. The identified spatio-temporal distributions with the most severe impacts feed subsequent models. For the second approach, a long-term climate simulation (a control simulation spanning more than 500 years) with the Earth System Model (ESM) provides a coarse-resolution dataset of several centuries of precipitation. From this data set, a number of case studies corresponding to extreme situations are selected as candidates for further analysis. However, the global model employs a coarse spatial resolution (1 degree) that precludes the accurate simulation of the precipitation in areas of complex topography such as Switzerland. Hence, these cases need to be dynamically downscaled with a Regional Climate Model (RCM). The applied RCM WRF implements a spatial resolution of 2 km over the entire alpine area, which allows a more realistic representation of precipitation induced by interactions between the large-scale forcing and orography. Outputs of both approaches in this module consist of gridded time series of temperature and precipitation of a selected number of scenarios.

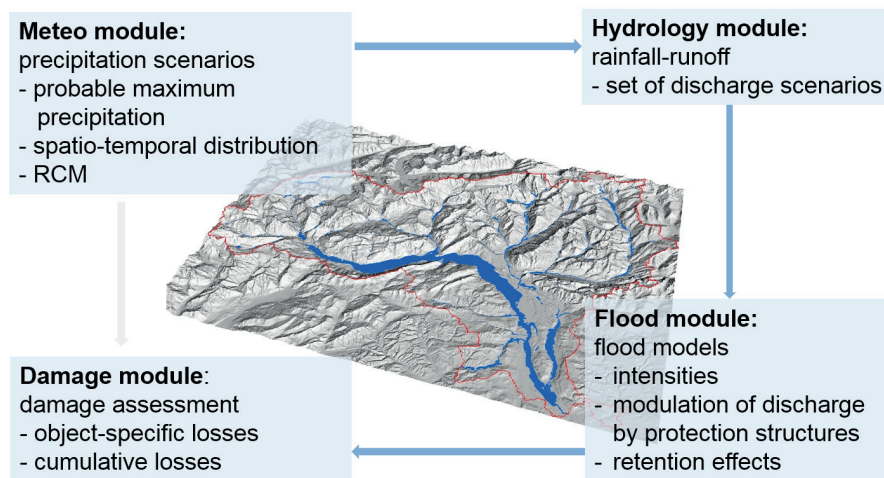


Figure 1. Conceptual setup of the model chain M-AARE in the Aare river basin.

Hydrologic module

For the rainfall-runoff modelling, we apply the hydrological model PREVAH (Viviroli et al. 2009). The model is set up for 15 sub-catchments that are located within the Aare basin with a spatial resolution of 1 km and hourly time steps. The delimitation of the catchments are presented in Fig. 2. The model is fed by the precipitation scenarios described above. The model output of the hydrologic module is used as the upper boundary condition of the hydrodynamic model.

Hydrodynamic module

The generated hydrographs are then routed with the hydrodynamic model BASEMENT-ETH (Vetsch et al. 2015) that accounts for the retention effects of lakes and floodplains. The hydraulic model was set up in two ways, a 1D- hydrodynamic model for all research questions regarding the flow routing only and a 2D-model used for coupling the damage module. The 1D model consists of cross sections along the whole valley bottom and considers the characteristics of the two lakes (lake Thun and lake Brienz) in modulating the flood hydrographs from the upper catchments. All of the main rivers considered in the 1D model were coupled in one integrated hydrodynamic model. This model consists of the Aare river from Meiringen to Bern including the two lakes and the area between the two lakes, the Gürbe valley, the Lütschine valley downstream from Gsteig, the Kander river downstream from the confluence with the Simme river. The river reaches in the main floodplains are implemented also in a 2D hydrodynamic model. Therefore, depending on the research question or on the damage model applied, these river reaches can either be modelled in 1D or in 2D, respectively. The 1D model was used for studying worst case discharges at the basin outlet in Bern. The 2D model was used to delimitate the flooded areas and as an input for the damage module. The spatial setup of the interface between the hydrologic and the hydraulic models is shown in Fig. 2.

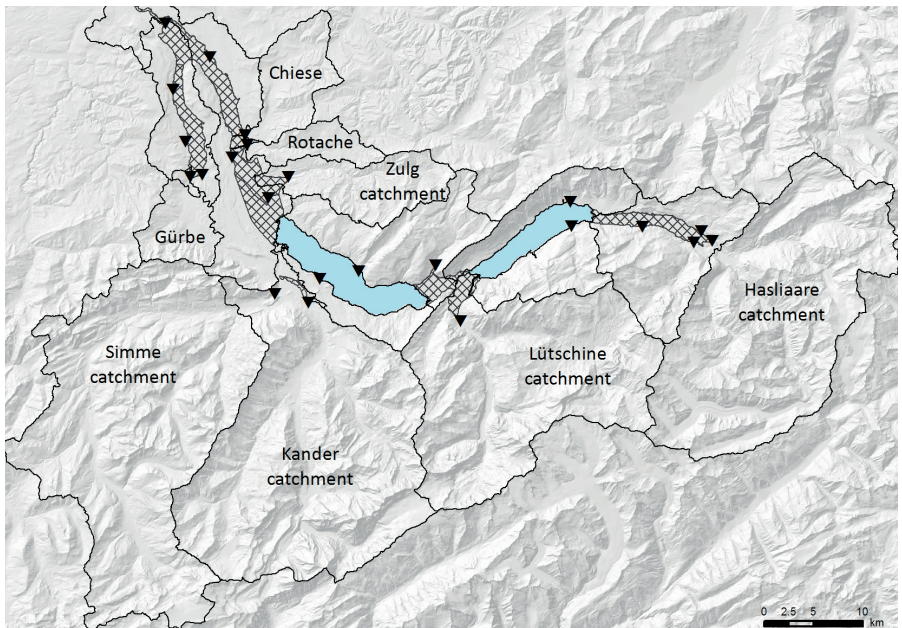


Figure 2. Spatial setup of the interface between hydrologic and hydrodynamic models. The black lines show the catchment delimitations. The calibrated catchments are indicated by labels. The black triangles indicate where the output of the hydrologic model will be used as input for the hydrodynamic model. The hatched areas represent the floodplains modelled in a 2D hydrodynamic model. The damage model is applied only in these areas.

Damage module

The hydrodynamic model – run in 2D mode – provides the basis for the damage module. This module consists of a dataset of buildings, each object classified by type, functionality, construction period, volume, reconstruction costs, and number of residents. The flood intensity maps resulting from the hydrodynamic module lead to the calculation of the object-specific vulnerability and therefore to the estimation of object-specific losses. The cumulative losses of a simulated precipitation scenario are summed up in a second step. Currently, a vulnerability function based on insurance data and reconstructed flood events is implemented. The method for the elaboration of the vulnerability curve follows the approach of Papathoma-Köhle et al. (2015), adopted to flood damages based on insurance data in Switzerland. The loss of life is calculated after Jonkman et al. (2008).

Coupling strategy

After Laganier et al. (2014), the model coupling strategy can either be of unidirectional or of bidirectional type. The first case is also called external coupling or a model cascade; the information is exchanged in one direction only. In the second case, the coupled sub-models interact between each other. In our case, the models are coupled in a cascading framework with harmonized time-steps. The coupling of the modules is controlled in a central timing and control device.

Calibration and validation

Each of the sub-models is calibrated and validated separately. The precipitation module is bias-corrected against gridded data sets of observations of precipitation in Switzerland. The hydrologic model is calibrated, if available, with observation data at the outflow of each sub-catchment (8 gauged sub-catchments). The models for the ungauged sub-catchments are regionalized by applying the parameter regionalization method proposed by Viviroli (2011). The hydrodynamic model was calibrated by empirically adjusting the friction coefficients. The values were adjusted by reconstructing observed flood events with particular regard to the water surface elevation in the main channel at peak discharge and the runtime of a peak discharge from one gauging station to another. The hydrodynamic model was validated based on watermarks along the rivers measured during the flood event in June 2014. The computed water surface elevations are within +/- 30 cm at nearly bankfull discharge. The 2D hydrodynamic model is calibrated in terms of reproducing the known channel capacity of the river reaches and in terms of reproducing the flooded areas of known flood events of 2005. The validation of the modelled flooded areas could not be quantified directly because the river geometry changed remarkably in some river reaches since the last observed floodings due to river training works. The damage model was validated in terms of reproducing the order of dimension of observed cumulative losses in past flood events. A direct validation of the damages to buildings was not possible because of lacking data at single objects level.

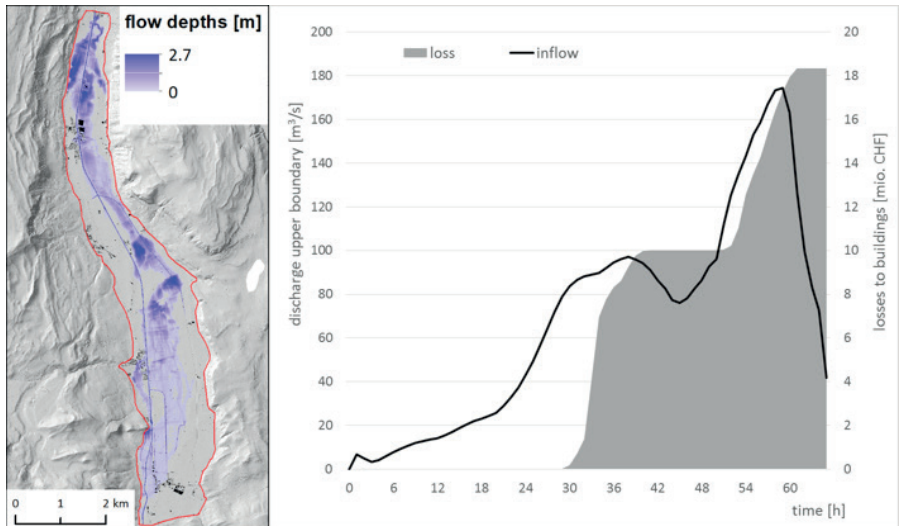


Figure 3. Flooded areas and losses to buildings in the subcatchment Gürbe related to a hydrograph resulting from one probable maximum precipitation scenario. The map at the left shows the flow depths at peak discharge, the diagram at the right shows the inflow hydrograph (continuous line) and the computed losses (grey area) over the time axis (hours).

RESULTS

The main result of the M-AARE project is the set up of a modelling chain of one-way coupled deterministic models. The first simulations of the model chain show that the chosen settings are suitable for modelling these natural processes, from precipitation to floods and flood losses. The meteo module provided numerous precipitation scenarios with different spatio-temporal distributions. These scenarios provide the input for the hydrologic model and the resulting discharges feed into the hydrodynamic model. The use of the downscaled global circulation model with a regional climate model showed that the latter is able to improve the simulation of precipitation compared to the GCM alone. Although, the large-scale flow and the location of the precipitation maxima is very similar at continental scales (as it is driven by the boundary conditions provided by the GCM) the spatial structure of the precipitation is refined at mesoscale scales, producing stronger precipitation gradients that allow to identify the main orographic barriers. Furthermore, much higher precipitation rates occur in some river catchments, which are indicative of potential disastrous situations at localised regions. The setting of the hydrodynamic model is able to consider retention capacities of lakes and floodplains, and to investigate the relationship between characteristics of process intensities and the related damages to residential buildings. The coupling between hydrologic and hydrodynamic models indicate that the relation between the input peak discharge and the modelled peak discharge at the outlet of the floodplains shows non-linear effects, which are usually neglected in extreme value statistical analyses. Further results of coupling the hydrologic and hydrodynamic models in probable maximum flood analyses are described in Felder et al. (subm.). Fig. 3 shows exemplarily the result of one of the simulated worst case

scenarios. The map in Fig. 3 shows the modelled flow depths at peak discharge. The diagram in Fig. 3 shows exemplarily a hydrograph of one probable maximum precipitation scenario in one of the subcatchments and the related losses on buildings. The evolution of the losses during the flood event is shown on the same time axis as the discharge.

CONCLUSIONS AND OUTLOOK

The results show that the one way coupling of the modules has been achieved and provides promising new insights for a better understanding of key aspects in flood risk analysis. The described model configuration allows to route the precipitation through different states of the river system and to take the retention effects of lakes and floodplains into account. The modelled magnitude of the effect of retention areas highlights the importance of considering such effects in extreme discharge estimations. First exploratory applications with the coupling of the WRF-PREVAH-BASEMENT models show the importance of clearly defined interfaces between the models. The coupling entails that all of the models are flexible enough to meet the requirements for the exchange of data, especially taking into account the different temporal resolution of each model. It is shown, that both the PREVAH model and the BASEMENT model are suited to be chained together and both are flexible enough to be operated by an external controller. In our case, the most important aspect is to harmonise the different time steps by using one framework. Therefore, the controller module is of strategic importance. Another important point is the definition of the location in space where the rainfall-runoff model delivers the computed discharges to the hydrodynamic model. These interfaces are located on the upper edges of floodplains in which remarkable effects of flood retention are to be supposed. The first applications of the damage model show that the vulnerability functions are crucial for calculating the damages. This module needs to be further improved and validated.

In conclusion, the M-AARE model chain has shown that the coupling of deterministic models offers a high potential to address further research questions and offers opportunities to provide a sound framework for different tasks in flood risk management. However, a successful implementation requires a high demand on specific knowledge and an interdisciplinary approach. Each of the modules needs knowledge and the coupling itself requires a rigorous definition of the interfaces between the models and an expertise in setting up of the controller module. Overall, the described model chain may provide the basis for further investigations:

- The model chain will simulate more scenarios of physically plausible peak discharges in the study area that are determined by the most extreme situations led by the large-scale circulation within the GCM. This will enable the analysis and characterization of worst-case floodings whose return period exceeds several centuries.
- With this model chain, it is possible to quantify the cumulative effects of all river training works or to assess the sensitivity of river reaches to the effects of climatic changes. This allows analysing the lake regulation procedures in case of a worst case flood.

- It allows forecasting flood damages on the basis of discharge forecasts in selected river reaches due to the analysed discharge-damage-relationships.
- The implementation of a multi-modelling approach in the hydrologic, hydrodynamic and damage modules will provide the possibility to quantify and describe the uncertainties in more detail.
- The M-AARE model chain may also provide a platform for planning of flood corridors and studying their effects in terms of flood hydrograph modulation on basin scale.
- Up to now, only buildings are considered in the computation of losses. The damage module has to be extended to other categories, e.g. losses to infrastructures etc.

REFERENCES

- Felder, G.; Zischg, A.; Weingartner, R. (subm.). The effect of a coupling of hydrologic and hydrodynamic models on PMF estimation.
- Heikkilä, A.-M.; Havlik, D.; Schlobinski, S. (2015). Modelling crisis management for improved action and preparedness. Espoo: VTT.
- Jonkman, S. N.; Vrijling, J. K.; Vrouwenvelder, A. C. W. M. (2008). Methods for the estimation of loss of life due to floods: a literature review and a proposal for a new method. In: *Nat Hazards* 46 (3), 353–389. DOI: 10.1007/s11069-008-9227-5.
- Kourgialas, Nektarios N.; Karatzas, George P. (2013). A hydro-economic modelling framework for flood damage estimation and the role of riparian vegetation. In: *Hydrol. Process.* 27 (4), S. 515–531. DOI: 10.1002/hyp.9256.
- Laganier, O.; Ayrat, P. A.; Salze, D.; Sauvagnargues, S. (2014). A coupling of hydrologic and hydraulic models appropriate for the fast floods of the Gardon River basin (France). In: *Nat. Hazards Earth Syst. Sci.* 14 (11), 2899–2920. DOI: 10.5194/nhess-14-2899-2014.
- Papathoma-Köhle, M.; Zischg, A.; Fuchs, S.; Glade, T.; Keiler, M. (2015). Loss estimation for landslides in mountain areas – An integrated toolbox for vulnerability assessment and damage documentation. In: *Environmental Modelling & Software* 63, 156–169. DOI: 10.1016/j.envsoft.2014.10.003.
- Viviroli, D.; Zappa, M.; Gurtz, J.; Weingartner, R. (2009). An introduction to the hydro-logical modelling system PREVAH and its pre- and post-processing-tools. In: *Environmental Modelling & Software* 24 (10), 1209–1222. DOI: 10.1016/j.envsoft.2009.04.001.
- Viviroli, D.; Weingartner, R. (2011). Umfassende hochwasserhydrologische Beurteilung ungemessener mesoskaliger Einzugsgebiete im Schweizerischen Rheineinzugsgebiet durch prozessorientierte Modellierung. In: *Hydrologie und Wasserbewirtschaftung*, 55(5), 258-272.
- Vetsch, D.; Siviglia, A.; Ehrbar, D.; Facchini, M.; Gerber, M.; Kammerer, S.; Peter, S.; Vonwiler, L.; Volz, C.; Farshi, D.; Mueller, R.; Rousselot, P.; Veprek, R.; Faeh, R. (2015). BASEMENT – Basic Simulation Environment for Computation of Environmental Flow and Natural Hazard Simulation. ETH Zürich.

Paper 20: Felder, G., Zischg, A., Weingartner, R., 2017. The effect of coupling hydrologic and hydrodynamic models on probable maximum flood estimation. *Journal of Hydrology* 550, 157–165. [10.1016/j.jhydrol.2017.04.052](https://doi.org/10.1016/j.jhydrol.2017.04.052).



Research papers

The effect of coupling hydrologic and hydrodynamic models on probable maximum flood estimation



Guido Felder*, Andreas Zischg, Rolf Weingartner

University of Bern, Institute of Geography & Oeschger Centre for Climate Change Research, Hydrology Group, Hallerstrasse 12, CH-3012 Bern, Switzerland

ARTICLE INFO

Article history:

Received 28 October 2016

Accepted 26 April 2017

Available online 3 May 2017

This manuscript was handled by A.

Bardossy, Editor-in-Chief, with the assistance of Roger Moussa, Associate Editor

Keywords:

Model coupling

Hydrodynamic model

PMP

PMF

ABSTRACT

Deterministic rainfall-runoff modelling usually assumes stationary hydrological system, as model parameters are calibrated with and therefore dependant on observed data. However, runoff processes are probably not stationary in the case of a probable maximum flood (PMF) where discharge greatly exceeds observed flood peaks. Developing hydrodynamic models and using them to build coupled hydrologic-hydrodynamic models can potentially improve the plausibility of PMF estimations. This study aims to assess the potential benefits and constraints of coupled modelling compared to standard deterministic hydrologic modelling when it comes to PMF estimation. The two modelling approaches are applied using a set of 100 spatio-temporal probable maximum precipitation (PMP) distribution scenarios. The resulting hydrographs, the resulting peak discharges as well as the reliability and the plausibility of the estimates are evaluated. The discussion of the results shows that coupling hydrologic and hydrodynamic models substantially improves the physical plausibility of PMF modelling, although both modelling approaches lead to PMF estimations for the catchment outlet that fall within a similar range. Using a coupled model is particularly suggested in cases where considerable flood-prone areas are situated within a catchment.

© 2017 Elsevier B.V. All rights reserved.

1. Introduction

Safety is a priority for communities when it comes to sensitive or potentially hazardous infrastructure like hydropower dams or nuclear power plants. In some cases, legal requirements define that such infrastructure has to be protected against any conceivable natural hazard that could occur. Therefore, governmental institutions as well as insurance companies are interested in a quantification of the possible worst-case scenario. Thus, various approaches for calculating the probable maximum flood (PMF) have been developed and applied in the course of the last several decades.

The World Meteorological Organization (WMO) defines the PMF as “the theoretical maximum flood that poses extremely serious threats to the flood control of a given project in a design watershed.” It is derived by converting the probable maximum precipitation (PMP) into runoff (WMO, 2009). The concept and the uncertainty of PMP estimation has been assessed in several recent studies (Micovic et al., 2015; Papalexiou et al., 2013; Salas et al., 2014). The PMP is usually converted to the PMF using deterministic hydrological models calibrated with observed data (e.g. Beauchamp et al., 2013; Kienzler et al., 2015; Zeimet et al.,

2015). This method assumes the hydrological system to remain steady, meaning that the system behaviour during the calibration period or the calibration event is presumed to be the same as it is during a PMF event. However, this assumption is questionable, since many protection measures are dimensioned to protect against design floods with return levels of 100 or 300 years. As soon as a catchment-specific threshold is reached, the system may no longer be steady (Sivakumar, 2009). At or beyond this threshold, new emerging retention areas (Lammersen et al., 2002), new flow paths (Huang et al., 2007; Vorogushyn et al., 2012) and changing runoff processes (Roger et al., 2012a, 2012b) can strongly affect the hydrograph shape and the peak discharge, due for example to failing protection measures or overflowing lateral dams. The peak discharge of a PMF is expected to exceed such catchment specific thresholds, making these factors relevant for PMF calculation. In the present study, we focus on such non-stationarities in the runoff process that are due to retention and inundation processes.

In contrast to a hydrologic model, a hydrodynamic model can be used to simulate the runoff process in complex terrain settings and wide floodplains in a more physically based way and may be more robust in cases when discharge exceeds the range of the observed data. This is due to the fact that in hydrodynamic modelling routing is calculated by solving the physically based Saint-Venant

* Corresponding author.

E-mail address: guido.felder@giub.unibe.ch (G. Felder).

equations at every calculation node within the model domain. In contrast, a hydrologic model calculates the routing rather conceptually, e.g. using a sequence of single linear storages in the HBV model (Bergström, 1995). The application of a hydrodynamic model allows for the consideration of the effects of retention areas, dykes, bridge piers and other physical obstacles. Numerous studies show that hydrodynamic models are particularly useful for considering retention effects due to floodplain inundation (Dutta et al., 2013; Meire et al., 2010; Skublics et al., 2014) and dyke breaches (Apel et al., 2009; Vorogushyn et al., 2010). Therefore the application of a hydrodynamic model potentially increases the plausibility of extreme flood estimations. Considering such retention effects in extreme flood estimations can be either trivial or of crucial importance, depending on catchment and riverbed characteristics. However, it is assumed that inundation and retention effects become non-negligible when it comes to PMF. This assumption can be checked by applying synthetic design hydrographs with various peak discharges (Serinaldi and Grimaldi, 2011) in a hydrodynamic model. This enables the identification of thresholds for the presence of widespread inundation and retention processes.

When calculating the PMF, the unsteadiness of the hydrological system that is induced by retention and inundation effects can be accounted for by coupling hydrologic and hydrodynamic models. This technique is particularly promising when the expected peak discharge may considerably exceed the observed maximum discharge or the river discharge capacity. A hydrologic model is used to determine the conversion from rainfall to runoff for a number of sub-catchments. The resulting hydrographs are used as upper boundary conditions of a hydrodynamic model. With computation power increasing over the past decade, coupled modelling approaches have been developed for flood estimation. Several case studies (e.g. Biancamaria et al., 2009; Bonnifait et al., 2009; Kim et al., 2012; Laganier et al., 2014; Lian et al., 2007) show the applicability of coupled hydrologic-hydrodynamic models in reconstructing observed flood events. A case study by Castro-Bolinaga and Diplas (2014) confirms the applicability of a hydrodynamic model for modelling extreme floods.

Despite the potential of coupling hydrologic and hydrodynamic models to increase the physical plausibility of PMF estimation, there is no systematic assessment of the effects of model coupling on PMF estimation. Although several above cited studies have shown that the application of a coupled hydrologic-hydrodynamic better represents inundation and retention processes than hydrological modelling alone, the influence of the choice of the modelling approach on PMF estimation itself remains unclear. The aim of the present study is therefore to evaluate whether coupling hydrologic and hydrodynamic models improves the plausibility of PMF estimation. This is done in three steps:

- The existence of catchment-specific thresholds for non-steady runoff processes is assessed by forcing a hydrodynamic model with a continuous series of synthetic design hydrographs. This process allows for the identification of catchment-specific thresholds for widespread inundations that lie beyond the design flood levels.
- The PMP is fed into a deterministic semi-distributed hydrologic model. This is the most common PMF estimation method (e.g. Beauchamp et al., 2013; Kienzler et al., 2015; Zeimet et al., 2015).
- The same PMP is fed into a deterministic semi-distributed hydrological model which is externally coupled to a hydrodynamic model.

The hydrographs generated with the coupled model are then compared to the hydrographs generated with the standard hydro-

logic model using the same precipitation input. In this way, the applicability of both modelling approaches in terms of PMF estimation can be compared. The results are interpreted through the identification of catchment-specific discharge thresholds for inundation and retention effects. This comparison of a hydrologic and a coupled hydrologic-hydrodynamic model in terms of PMF estimation contributes to a better understanding of the effect modelling approach selection on the resulting estimation, and therefore it informs the setup of future PMF studies and applied PMF estimations.

2. Study area

2.1. Physical characteristics and data availability

The study area is the Aare catchment at the northern edge of the Swiss Alps. It covers an area of about 3000 km² and its mean elevation is about 1600 m a.s.l. A map of the study area is shown in Fig. 1. The catchment can be roughly divided into an upper section and a lower section. The upper section of the catchment consists of a steep mountainous and partly glaciated landscape. The sub-catchments in this mountainous area drain directly into two connected lakes that cover 30 and 49 km² and that are partially regulated. The outflow of the lower lake crosses over into the lower part of the catchment, which is a relatively wide valley with extensive flood-prone areas.

The mean annual rainfall in the catchment amounts to 1500 mm, of which 500 mm evaporate and 1000 mm are discharged. The discharge regime is influenced by the presence of glaciers that cover about 8% of the total area, meaning that mean discharge is relatively low (70 m³ s⁻¹) in winter and relatively high (180 m³ s⁻¹) in summer. The catchment is well-researched and its hydrology is relatively well-known as a result of numerous studies that have been completed in the area (e.g. Roessler et al., 2014; Wehren, 2010). The highest observed peak discharges during the observation period 1918–2015 have been well documented and reconstructed by the Swiss Federal Office for the Environment (FOEN, 1991, 2000, 2008, 2009).

Meteorological data are provided by the Swiss Federal Office for Meteorology and Climatology (MeteoSwiss). Hourly time series from 30 stations that are situated within or near the catchment were used for calibration of the models. Discharge data are provided by the Swiss Federal Office for the Environment (FOEN) and the Bernese State Office for Water and Waste (AWA). For the catchment outlet, the time series covers 98 years (1918–2015) in daily resolution and 42 years (1974–2015) in hourly resolution. Within the catchment, there are 18 gauging stations with hourly resolutions, most of them covering more than 50 years. For the two lakes that are situated within the catchment, hourly resolved lake level time series are available from 1974 to 2015.

2.2. Division into sub-catchments

For modelling purposes, the catchment can be divided into 13 sub-catchments, as shown in Fig. 1. Eight of them are situated in the upper part of the catchment and drain into one of the two lakes. The other five sub-catchments are situated in the lower part of the catchment and drain directly into the Aare River. Two additional areas within the catchment are constituted by the two major lakes themselves. The main flood-prone areas are located around the two lakes and in the lower part of the catchment along the main river.

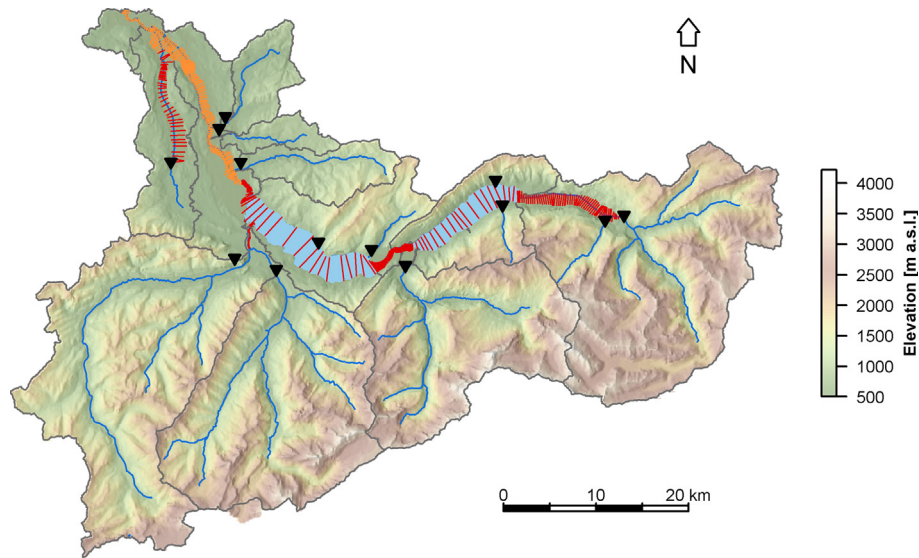


Fig. 1. The Aare catchment situated at the northern edge of the Swiss Alps, and the division of the catchment into 13 sub-catchments and the range of the hydrodynamic model. The black triangles indicate the coupling points between the hydrological and the hydrodynamic model. The red lines indicate cross sections of the hydrodynamic model. (For interpretation of the references to colour in this figure legend, the reader is referred to the web version of this article.)

3. Methods

This study was carried out in four steps. First, synthetic design hydrographs were calculated and modelled hydrodynamically, allowing for the examination and identification of catchment-specific thresholds for widespread inundation. Next, PMP scenarios that could be used to force the two different modelling approaches were generated. Finally, two modelling approaches were applied. The first approach entails the use of a deterministic hydrological model that was set up for the catchment. The second approach entails hydrological modelling of the sub-catchments within the catchment, where the hydrographs of the sub-catchments were used as upper boundary conditions for a subsequent hydrodynamic model. An overview of the river network, the coupling points between the hydrologic and hydrodynamic models and the spatial range of the hydrodynamic model is provided in Fig. 1.

3.1. Derivation and application of synthetic design hydrographs

Synthetic design hydrographs for the Aare catchment were derived using the guidelines proposed by Serinaldi and Grimaldi (2011). The synthetic unit hydrograph was calculated by fitting a two parametric gamma distribution as described by Nadarajah (2007) and Rai et al. (2008) to the structural hydrograph depicted by Serinaldi and Grimaldi (2011). The procedure was applied to generate synthetic design hydrographs for a continuous series of peak discharges in intervals of $50 \text{ m}^3 \text{ s}^{-1}$. The synthetic design hydrographs were used as upper boundary conditions for the lower part of the hydrodynamic model (lower 30 km of total 80 km, orange cross sections in Fig. 1). The application of synthetic design hydrographs in the hydrodynamic model is based on the assumption that the full discharge volume flows through the lower part of the hydrodynamic model, which is not necessarily the case due to lateral inflows between the upper and lower boundaries of the hydrodynamic model. However, it is assumed that possible discharge thresholds for the occurrence of inundation and retention effects can reasonably be identified. The synthetic design hydrographs that are used as upper boundary conditions can be directly compared to the according hydrograph that results as lower boundary condition. As long as the discharge stays in the riverbed,

the shape of the hydrograph is expected to stay unchanged, apart from a small temporal shift that results from the flow duration between the upper and the lower boundary of the hydrodynamic model and a slight flattening of the wave. As soon as the riverbed capacity at a certain point within the catchment is exceeded, new retention areas are wetted and new flow paths occur, changing the shape of the downstream hydrograph. By applying various hydrographs with differing peaks, thresholds for various points along the river at which the riverbed capacity is exceeded can be identified.

3.2. PMP estimation and spatio-temporal representation

The PMP for the event durations of 12 h, 24 h, 48 h, and 72 h were estimated following WMO guidelines (WMO, 2009). In order to identify the distributions that may cause the highest peak discharge at the study area outlet, the spatio-temporal distribution of the estimated PMP was deduced using a Monte-Carlo approach (Felder and Weingartner, 2016). Numerous randomly generated, physically plausible spatio-temporal distributions were tested by applying a hydrologic model where the random distribution was restricted to consider internal dependencies and correlations. In this case, approximately 10^6 PMP distributions were tested with the total precipitation amount held constant. The 100 physically plausible distributions that led to the highest peak discharges were considered most severe and are therefore applied in this study. The sample size of 100 spatio-temporal distributions is a compromise between the need for a large representative sample of distributions on the one hand and available computation power on the other. To ensure identical initial conditions for all model runs, the same observed meteorological environment was applied in modelling runs for each precipitation distribution. The meteorological environment represents medium summer conditions in terms of antecedent moisture. Summer conditions are used because the highest PMP estimation is based on summer atmospheric conditions.

This approach was chosen because it enables the derivation of a high number of slightly varying precipitation distributions. Applying a high number of varying PMP input scenarios allows for an assessment of the two different modelling approaches that is not dependent on how input data are chosen.

3.3. Hydrologic model PREVAH

The hydrologic modelling was done using PREVAH (Viviroli et al., 2009a), which is a deterministic, semi-distributed, HRU-based hydrological model that makes calculations on hourly time steps. The model structure is comparable to that of the well-known HBV model (Bergström, 1995) in which incoming precipitation in liquid or solid state passes a cascade of linear storages. Information about temperature, global radiation, sunshine duration, vapour pressure and wind speed are required for the calculation of the evapotranspiration. The model has been extensively tested and applied in studies that deal with extreme hydrological events (FOEN, 2009; Orth et al., 2015; Viviroli et al., 2009c; Zappa et al., 2015). These studies demonstrate the applicability of PREVAH to catchments like the Aare catchment. In the PREVAH model, the HRU's are directly routed to the catchment outlet. After modelling, additional routing can be applied by sequentially running several sub-models and incorporating intermediate lake modules that represent the lakes as single linear storages. In this study, the sub-catchments (see Fig. 1) were independently modelled. Sub-catchments that drain into a lake were fed into the respective lake module. The sub-catchments situated between the lower lake and the catchment outflow were fed into an additional routing module.

The model has 12 parameters to be calibrated. The gauged sub-catchments were calibrated using the PEST calibration tool developed by Doherty (2015). Information about parameter uncertainty and parameter sensitivity are provided by Viviroli et al. (2009b). The resulting NSE was between 0.70 and 0.92 for the calibration period (2001–2010) and between 0.65 and 0.88 for the validation period (2011–2014). The free parameters for the five ungauged contributing sub-catchments were estimated using the parameter regionalization approach developed by Viviroli et al. (2009c). Although it is not possible to evaluate this kind of parameter estimation specifically for ungauged catchments, Viviroli et al. (2009c) demonstrates that the parameter regionalization approach is appropriate.

3.4. Hydrodynamic model BASEMENT

The hydrodynamic model BASEMENT is a free hydrodynamic modelling system. The model is based on the continuity equation and solves the Saint-Venant equations for unsteady one-dimensional flow. A detailed derivation of the mathematical model applied in BASEMENT is illustrated in Vetsch et al. (2015).

In order to consider floodplains and storages outside the riverbed, the river cross sections were expanded to potential flood-prone areas. Cook and Merwade (2009) show that this procedure is advisable for modelling flood wave propagation, although the spatial details of the simulation of inundation depth and area are not as exact as in a 2D modelling environment. Cross sections of the riverbed and the directly adjacent levees were provided by the Swiss Federal Office of Environment FOEN. These cross sections were expanded to potential flood-prone areas beyond the levees using data from a digital elevation model with 0.5 m resolution and a vertical accuracy of 0.2 m. Considering the aim of this study, this resolution is sufficient for hydrodynamic modelling outside the riverbed because topographic details with major influence on flow paths and flow behaviour are sufficiently incorporated (Cook and Merwade, 2009; Mejia and Reed, 2011). The cross sections were set straight and perpendicular to the flow direction with average cross section spacing of approximately 150 m, as recommended in studies of other catchments (Ali et al., 2015; Castellarin et al., 2009; Samuels, 1990).

The hydrodynamic model was calibrated by empirically adjusting the Strickler coefficients (k_{str}). The values were adjusted by

reconstructing the water surface elevation and the propagation time of the peak discharge of observed flood events. Particular attention was given to the peak discharge and the time to peak at different gauging stations along the river. The k_{str} values were set between 33 and 45 in the riverbed and between 22 and 30 in the floodplains outside the riverbed. Additionally, hydrodynamic parameters that define the characteristics of weirs (factor μ of the Poleni equation) and pipes (contraction factor) were adjusted. The artificial lake management tools were set in a way that the discharge out of the lakes was maximized, as this is likely to be the case during flood events. The hydrodynamic model was then able to reconstruct the rating curve at the catchment outlet with an error of ± 2 cm in water level for observed flood events. In the range of a typical flood event, this corresponds to an error of approximately ± 5 m³ s⁻¹ or 1% of discharge, which is comparable to the error of the gauging station of about ± 1 cm (FOEN, 1998). The error is assumed to be slightly higher in the PMF case during which areas would be affected that were not flooded during the calibration flood events.

3.5. Model coupling

The outputs of the hydrologic model are fed into the hydrodynamic model as upper boundary conditions or as lateral inflows. The model coupling is external, which means that there is no direct interaction between the models and backwater effects are only involved within the spatial range of the hydrodynamic model. The range of the hydrodynamic model was set to incorporate all significant flood-prone areas and potential retention areas. It is assumed that minor retention areas inside the sub-catchments have a negligible effect on the peak flow at the catchment outlet.

The coupling points between the hydrological and the hydrodynamic model are shown in Fig. 1. There are two cases where a coupling point lies significantly upstream of the sub-catchment outflow (see the most eastern and the most western coupling points in Fig. 1). In these cases, areas situated downstream of the coupling points were separately modelled and then added to the hydrodynamic model, following the suggestions of Lerat et al. (2012). The hydrological model was not applied on the lakes within the catchment because they directly receive the precipitation that falls above them, and evaporation from the lakes was considered negligible. In these cases, precipitation was directly fed into the hydrodynamic model.

4. Results

4.1. Thresholds derived from the hydrodynamic modelling of synthetic design hydrographs

The calculated synthetic design hydrographs (see Section 3.1) and the results of the hydrodynamic modelling of these synthetic design hydrographs are shown in Fig. 2. The synthetic design hydrographs (on the left side of Fig. 2) that were used as upper boundary conditions are uniformly shaped. The hydrographs derived by hydrodynamic modelling (on the right side of Fig. 2) are identically shaped when peak discharges are below approximately 500 m³ s⁻¹. This corresponds to a peak discharge with a 30 year return period. Above that level, there are three clearly visible steps at approximately 570, 700 and 860 m³ s⁻¹. These thresholds indicate the occurrence of inundation and retention processes with significant influence on discharge processes. In consequence, the peak discharges of the synthetic design hydrographs on the model input side and the peak discharges of the calculated hydrographs on the model output side are no longer congruent. Two significant thresholds for emerging inundation and retention

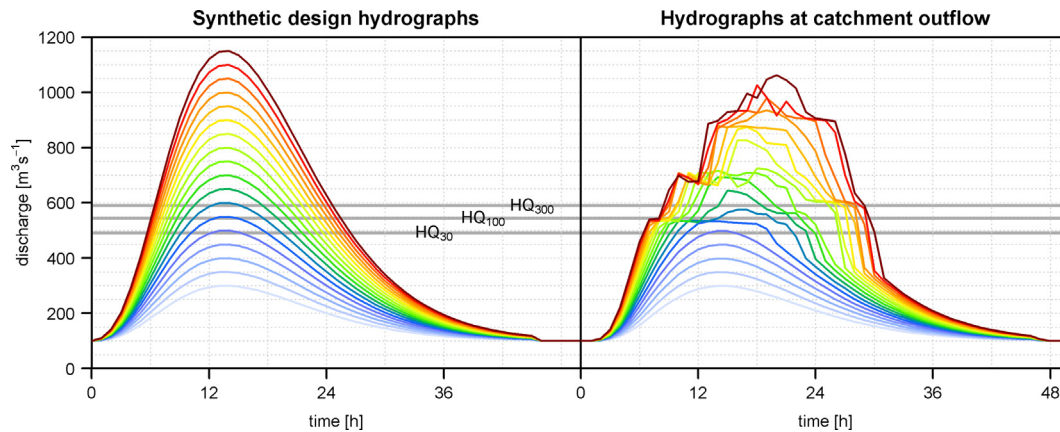


Fig. 2. Synthetic design hydrographs that were used as upper boundary conditions of the hydrodynamic model and the resulting hydrographs at the catchment outlet. The grey lines indicate discharges with return periods of 30, 100, and 300 years. The peak discharges of the given return levels are derived by fitting a GEV distribution to the annual maximum discharges (based on a discharge time series from 1918 to 2014). The data as well as the statistical estimation of the return levels are provided by the Swiss Federal Office of Environment FOEN.

processes (700 and $860 \text{ m}^3 \text{ s}^{-1}$) are considerably above the 300 year return level flood; hence these thresholds do not affect floods below the 300 year return level but are possibly of crucial importance for PMF estimation.

4.2. Modelling the PMF

The hydrographs that were derived by hydrological modelling are shown in Fig. 3. The hydrographs that were modelled by applying the coupled hydrological-hydrodynamic model are shown in Fig. 4. The hydrographs represent the modelled catchment response to the 100 PMP distributions described in Section 3.1, where the precipitation event lasts from hour 0 to hour 72 or less depending on the temporal distribution of the PMP.

4.2.1. Hydrograph behaviour before peak discharge

The hydrographs resulting from hydrological modelling generally increase relatively quickly at the beginning of the event. In contrast, the hydrographs resulting from the coupled model generally rise more slowly. Comparing the shapes of the hydrographs from the two modelling approaches shows that the hydrographs derived by hydrologic modelling increase constantly and relatively smoothly. The hydrographs derived by the coupled model reflect distinct steps at certain discharge levels, e.g. at $700 \text{ m}^3 \text{ s}^{-1}$. This

is due to the exceeded riverbed capacity and consequential inundations, which delay further water level rise at the outlet. The hydrologic model is not able to capture this effect.

4.2.2. Peak discharge and PMF estimate

The peak discharges are between 1010 and $1320 \text{ m}^3 \text{ s}^{-1}$ based on the hydrologic model and between 880 and $1220 \text{ m}^3 \text{ s}^{-1}$ based on the coupled model. A comparison of the modelled peak discharges of all model runs is shown in Fig. 5. The plot shows that the coupled model generates lower peak discharges than the hydrologic model for most of the PMP distributions. However, there are also some scenarios where the coupled model generates a higher peak discharge than the hydrologic model. This is due to the retarding effect of lakes that are situated within the catchment. Precipitation distributions for which the coupled model generates the highest peak discharge are the ones that lead to a superposition of sub-catchment reactions. In such cases, in the first phase of the event the most intense precipitation occurs in the sub-catchments that drain into a lake. Subsequently, the lake water level rises. In the course of the event, the most intense precipitation shifts to the sub-catchments that are situated between a lake and the catchment outlet. This leads to the superposition of maximum lake outflow and maximum discharge from other sub-catchments. The

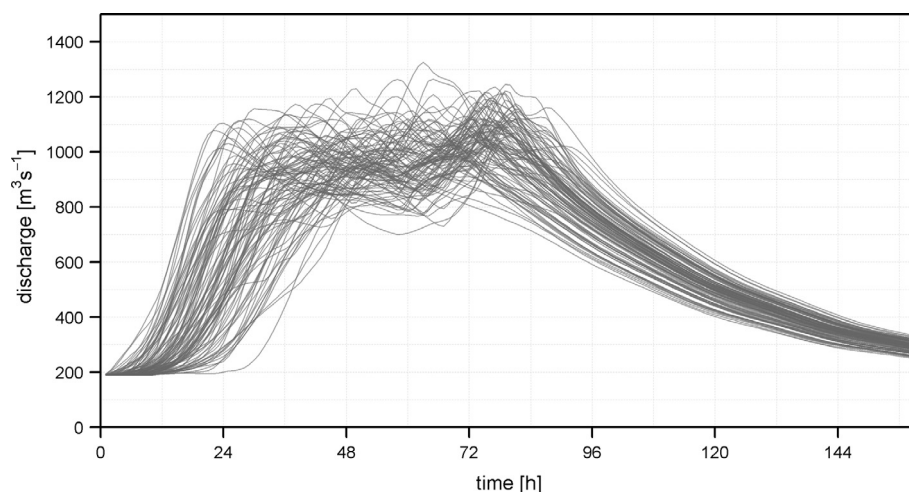


Fig. 3. Hydrographs generated by the hydrologic modelling of the 100 PMP scenarios at the outlet of the catchment.

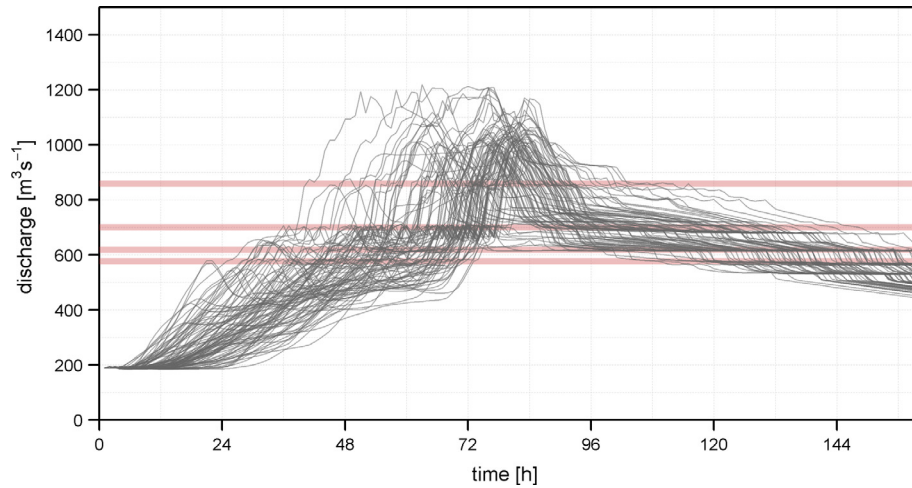


Fig. 4. Hydrographs generated by the coupled hydrologic-hydrodynamic modelling of the 100 PMP scenarios at the outlet of the catchment. The red lines indicate thresholds for the occurrence of significant retention effects.

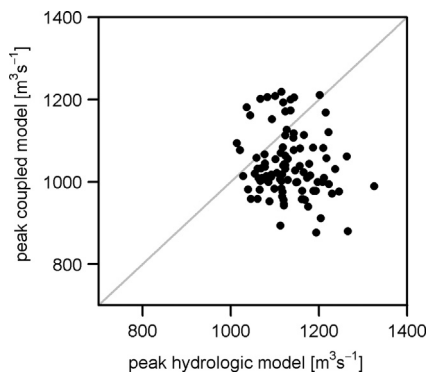


Fig. 5. Peak discharges that result from the two modelling approaches.

hydrological model, with its relatively simple representation of the lakes, is not able to reproduce this effect in detail.

The time between the beginning of the precipitation event and the peak discharge (time to peak) of each model run is shown in Fig. 6. As demonstrated by the hydrographs in Fig. 3 and Fig. 4, there are considerable differences in time to peak between the two modelling approaches. The hydrological model generates peaks that occur from 25 to 87 h after the start of precipitation, while the coupled model generates peaks between 48 and 85 h after the start of precipitation. There is less temporal variation in

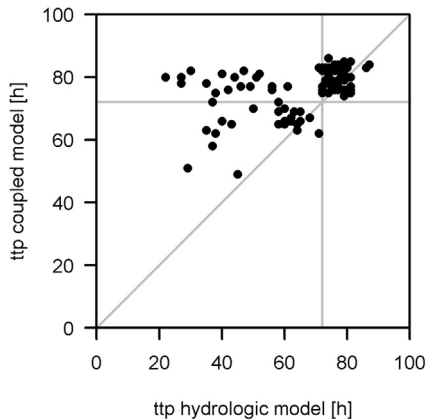


Fig. 6. Time to peak that result from the two modelling approaches in hours. The vertical and the horizontal lines indicate the end of the precipitation event.

the hydrographs generated by the coupled model than in those generated by the hydrological model. Considering that the total precipitation amount (PMP) was always held constant, Fig. 7 shows that the peak-to-volume ratios do not differ systematically.

4.2.3. Hydrograph behaviour after peak discharge

In both modelling approaches, the hydrographs drop considerably after the peak discharge is reached. In the coupled model, there are step changes visible again at various discharge levels toward the end of the events (570, 620, 700, 860 m³ s⁻¹). These levels correspond to thresholds of the riverbed capacity at various cross sections thus the step changes can be explained by the flooding of floodplains. In a first phase, the discharge at the catchment outlet is reduced due to the amount of water that exceeds the riverbed capacity and inundates surrounding areas. In a second phase, the discharge at the same cross section falls below the discharge capacity of the river reach, and the inundating water masses flow back into the riverbed. In a last phase, when the surrounding areas are drained they do not contribute to discharge anymore, leading to a distinctive kink in the hydrograph.

5. Discussion

The hydrodynamic modelling of synthetic design hydrographs shows that retention effects are more pronounced when the estimated discharge considerably exceeds the maximum discharge

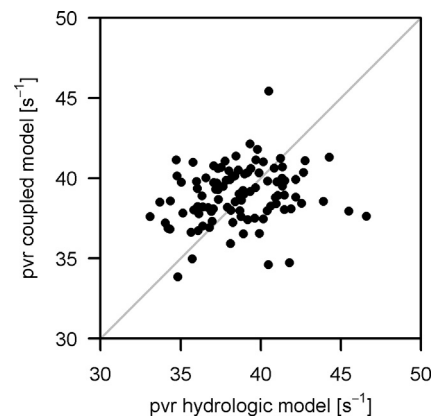


Fig. 7. Peak-to-volume ratios that result from the two modelling approaches.

of the calibration period. This is reasonable due to the fact that protection measures along the riverbed are often aligned to design floods of 30, 100 or 300 years, and not to floods with the magnitude of a PMF.

The hydrologic model and the coupled hydrologic-hydrodynamic model generate differently shaped hydrographs at the catchment outlet. The main difference in the two modelling approaches has to do with the representation of physical processes that occur within the catchment. The hydrological model represents the catchment reaction by using a set of calibrated parameters that usually define storage sizes, infiltration rates, evapotranspiration rates, and various other catchment characteristics. The calibrated model usually reproduces catchment behaviour that corresponds to catchment behaviour during the calibration period. However, the synthetic design hydrographs used in hydrodynamic modelling show that the catchment may deviate from its known behaviour due to the influence of effects that were absent during the calibration period. The deceleration of water flow due to changing riverbed characteristics, the storage and retention effects of inundated areas, as well as the depletion of lake storage capacity are possible reasons for such changing runoff characteristics. The hydrologic model does not consider non-stationary catchment behaviour that is caused by inundation and retention effects or the superimposing effects that occur when discharge considerably exceeds the highest observed peak discharges of the calibration period, which presumably would occur in the case of a PMF event. Therefore it quickly routes heavy precipitation input to the catchment outlet. In contrast, the coupled model approach is less dependent on the occurrence of extreme events within the calibration period as it captures and reproduces the effects of high precipitation on the watershed. The representation of non-linear retention effects in the coupled approach allows for a more verifiable and a physically more reliable PMF estimation.

The differences between the hydrologic and the coupled model in terms of the representation of runoff processes have direct consequences for the shapes of the hydrographs and for the PMF estimation. The coupled model simulates peak discharges that are slightly lower than the ones generated with the hydrologic model. The time to peak is generally lower for the outputs generated by the hydrologic model than for those generated by the coupled model due to the relatively immediate routing of the runoff to the catchment outflow and the neglect of runoff-delaying processes like inundations in the hydrologic model. As these differences are caused by the distinct representations of the routing process in the two modelling approaches, they are of general nature. However, the magnitude of these effects may vary from catchment to catchment. In case of simple channel geometries or riverbed capacities that continuously exceed the magnitude of the PMF, these differences are expected to decrease, although the application of a hydrodynamic model still increases the reliability of the estimation.

An additional benefit of the coupled model approach is that it allows for the identification and mapping of affected areas and floodplains within the catchment. This allows for a better estimation of the possible consequences of a PMF event. The additional information on possibly affected areas is highly important for insurance and re-insurance purposes as well as for the planning of sensitive infrastructure or protection measures. However, various studies show that identification and mapping of affected areas are uncertain due to several critical factors, i.e. the model calibration (Pappenberger et al., 2005, 2006; Remo et al., 2009; Di Baldassare et al., 2009), the lack of computation power limiting the consideration of various parameter sets (Altarejos-García et al., 2012), and uncertain design flood profiles (Brandimarte and Di Baldassare, 2012). Chatterjee et al. (2008) show that 1D-2D model coupling improves the modelling of areal extent, water

velocities, and the emptying process of retention areas in comparison to a 1D model, whereby it leads to comparable results in terms of peak discharge. However, such an approach requires significantly more computation power, a factor that limits the consideration of a high number of varying precipitation scenarios.

The setup and application of a coupled model is data-intensive and relatively time consuming. It usually requires pre-processing and calibration for every considered sub-catchment, the setup and calibration of a hydrodynamic model, and some effort for the coupling itself. Moreover, applying a coupled model involves a relatively long computation time. The availability of a high-resolution digital terrain model and river cross sections is required for coupled modelling. In contrast, the hydrological modelling approach only requires calibration of the sub-catchments, and the computation time is substantially lower than the computation time of a coupled model. Considering the similar range of peak discharges that were modelled by the two approaches, a hydrological model can reasonably be applied for rough PMF estimation in cases where only the catchment outlet is of interest or where the catchment is characterized by negligible potential retention areas. On the other hand, the coupled model better reflects physical reality when it comes to extreme floods. Using this approach is particularly imperative when retention areas in the catchment of interest may strongly influence PMF estimation.

6. Conclusion and perspectives

In this study, PMF estimations were derived by applying a hydrologic model and a coupled hydrologic-hydrodynamic model in order to assess the advantages and constraints of these two modelling approaches. The two modelling approaches were tested with 100 PMP scenarios with the same volume of precipitation but different spatio-temporal precipitation distributions. The resulting hydrographs can be used to assess the applicability of the modelling approaches for estimating PMF at the catchment outlet and to evaluate the representation of physical processes within the catchment. The hydrological model is suitable to roughly estimate a PMF, particularly in cases where no significant retention areas are situated in the catchment. The application of a coupled hydrologic-hydrodynamic model is recommended for a better understanding of the physical processes within the catchment, for mapping purposes, or for the planning of flood prevention measures. A PMF event comprises substantially larger discharge volumes and substantially higher peak discharges than observed events. In the case of a PMF, flood protection measures that are dimensioned for specific return levels fail; thus widespread floodplain inundation and non-linear processes occur. This calls for the incorporation of a physical perspective to make estimation more reliable and understandable. The difference in the model outputs indicates the importance of studying the benefits and constraints of modelling approaches applied for PMF estimation.

Acknowledgements

This study is funded by the University of Bern and the Mobiliar Lab for Natural Risks. The authors would like to thank the Federal Office of Environment (FOEN), the Federal Office for Meteorology and Climatology (MeteoSwiss) and the Department for Water and Waste of the Canton of Bern (AWA) for providing the necessary input data. Anne de Chastonay is acknowledged for her thoughtful comments.

References

- Ali, A., Di Baldassare, G., Solomatine, D.P., 2015. Testing different cross-section spacing in 1D hydraulic modelling: a case study on Johor River, Malaysia.

- Hydrol. Sci. J. 60 (2), 351–359. <http://dx.doi.org/10.1080/02626667.2014.889297>.
- Altarejos-García, L., Martínez-Chenoll, M.L., Escuder-Bueno, I., Serrano-Lombillo, A., 2012. Assessing the impact of uncertainty on flood risk estimates with reliability analysis using 1-D and 2-D hydraulic models. *Hydrol. Earth Syst. Sci.* 16, 1895–1914. <http://dx.doi.org/10.5194/hess/16-1895-2012>.
- Apel, H., Merz, B., Thieken, A.H., 2009. Influence of dike breaches on flood frequency estimation. *Comput. Geosci.* 35, 907–923. <http://dx.doi.org/10.1016/j.cageo.2007.11.003>.
- BASEMENT – Basic Simulation Environment for Computation of Environmental Flow and Natural Hazard Simulation. Version 2.5, © ETH Zurich, VAW, Vetsch D., Siviglia A., Ehrbar D., Facchini M., Gerber M., Kammerer S., Peter S., Vonwiller L., Volz C., Farshi D., Mueller R., Rousselot P., Veprek R., Faeh R., 2006–2015.
- Beauchamp, J.R., Leconte, R., Trudel, M., Brissette, F., 2013. Estimation of the summer-fall PMP and PMF of a northern watershed under a changed climate. *Water Resour. Res.* 49 (6), 3853–3862. <http://dx.doi.org/10.1002/wrcr.20336>.
- Bergström, S., 1995. The HBV model. In: Singh, V.P. (Ed.), *Computer Models of Watershed Hydrology*. Water Resources Publications, Highland Ranch, Colorado, U.S.A.
- Biancamaria, S., Bates, P., Boone, A., Mognard, N., 2009. Large-scale coupled hydrologic and hydraulic modelling of the Ob river in Siberia. *J. Hydrol.* 379, 136–150. <http://dx.doi.org/10.1016/j.jhydrol.2009.09.054>.
- Bonnifant, L., Delrieu, G., Le Lay, M., Boudevillain, B., Masson, A., Belleudy, P., Gaume, E., Saulnier, G.-M., 2009. Distributed hydrologic and hydraulic modelling with radar rainfall input: reconstruction of the 8–9 September 2002 catastrophic flood event in the Gard region, France. *Adv. Water Resour.* 32, 1077–1089. <http://dx.doi.org/10.1016/j.advwatres.2009.03.007>.
- Brandimarte, L., Di Baldassare, G., 2012. Uncertainty in design flood profiles derived by hydraulic modelling. *Hydrol. Res.* 43 (6). <http://dx.doi.org/10.2166/nh.2011.086>.
- Castellarin, A., Di Baldassare, G., Bates, P.D., Brath, A., 2009. Optimal cross-section spacing in Preissmann scheme 1D hydrodynamic models. *J. Hydraul. Eng.* 135, 96–105. [http://dx.doi.org/10.1061/\(ASCE\)0733-9429\(2009\)135:2\(96\)](http://dx.doi.org/10.1061/(ASCE)0733-9429(2009)135:2(96)).
- Castro-Bolinaga, C.F., Diplas, P., 2014. Hydraulic modeling of extreme hydrologic events: case study in Southern Virginia. *J. Hydraul. Eng.* 2014, 140.
- Chatterjee, C., Förster, S., Bronstert, A., 2008. Comparison of hydrodynamic models of different complexities to model floods with emergency storage areas. *Hydrol. Process.* 22, 4695–4709. <http://dx.doi.org/10.1002/hyp.7079>.
- Cook, A., Merwade, V., 2009. Effect of topographic data, geometric configuration and modelling approach on flood inundation mapping. *J. Hydrol.* 377, 131–142. <http://dx.doi.org/10.1016/j.jhydrol.2009.08.015>.
- Di Baldassare, G., Castellarin, A., Brath, A., 2009. Analysis of the effects of levee heightening on flood propagation: example of the River Po, Italy. *Hydrol. Sci. J.* 54 (6), 1007–1017. <http://dx.doi.org/10.1623/hysj.54.6.1007>.
- Doherty, J., 2015. Calibration and uncertainty analysis for complex environmental models. *Watermark Numerical Computing*, Brisbane, Australia, ISBN 978-0-9943786-0-6.
- Dutta, D., Teng, J., Vaze, J., Lerat, J., Hughes, J., Marvanek, S., 2013. Storage-based approaches to build floodplain inundation modelling capability in river system models for water resources planning and accounting. *J. Hydrol.* 504, 12–28. <http://dx.doi.org/10.1016/j.jhydrol.2013.09.033>.
- Felder, G., Weingartner, R., 2016. An approach for the determination of precipitation input for worst-case flood modelling. *Hydrol. Sci. J.* 61 (14), 2600–2609. <http://dx.doi.org/10.1080/02626667.2016.1151980>.
- FOEN (Federal Office for Environment), 1991. Event-analysis of the 1987 Flood. Nr. LHG-14-D. Bern, Switzerland.
- FOEN (Federal Office for Environment), 2000. Flood 1999. Data Analysis and Statistical Classification. Nr. LHG-28-D. Bern, Switzerland.
- FOEN (Federal Office for Environment), 2008. Event-analysis of the 2005 Flood. Part 2: Analysis of processes, measures and hazards. Nr. UW-0825-D. Bern, Switzerland.
- FOEN (Federal Office for Environment), 2009. Event-analysis of the August 2007 Flood. Nr. UW-0927-D. Bern, Switzerland.
- FOEN, 1998. Manual of streamflow gauging. LHG-26-D.
- Huang, S., Rauberg, J., Apel, H., Disse, M., Lindenschmidt, K.-E., 2007. The effectiveness of polder systems on peak discharge capping of floods along the middle reaches of the Elbe River in Germany. *Hydrol. Earth Syst. Sci.* 11, 1391–1401. <http://dx.doi.org/10.5194/hess-11-1391-2007>.
- Kienzler, P., Norina, A., Näf-Huber, D., Zappa, M., 2015. Derivation of extreme precipitation and flooding in the catchment of Lake Sihl to improve flood protection in the city of Zurich. *HyWa* 59, 48–58. http://dx.doi.org/10.5675/HyWa_2015_2_1.
- Kim, J., Warnoc, A., Ivanov, V., Katopodes, N., 2012. Coupled modeling of hydrologic and hydrodynamic processes including overland and channel flow. *Adv. Water Resour.* 37, 104–126. <http://dx.doi.org/10.1016/j.advwatres.2011.11.009>.
- Laganier, O., Ayrat, P.A., Salze, D., Sauvagnargues, S., 2014. A coupling of hydrologic and hydraulic models appropriate for the fast floods of the Gardon River basin (France). *Nat. Hazards Earth Syst. Sci.* 14, 2899–2920. <http://dx.doi.org/10.5194/nhess-14-2899-2014>.
- Lammersen, R., Engel, H., van de Langemheen, W., Buiteveld, H., 2002. Impact of river training and retention areas on flood peaks along the Rhine. *J. Hydrol.* 267, 115–124. [http://dx.doi.org/10.1016/S0022-1694\(02\)00144-0](http://dx.doi.org/10.1016/S0022-1694(02)00144-0).
- Lerat, J., Perrin, C., Andréassian, V., Loumagne, C., Ribstein, P., 2012. Towards robust methods to couple lumped rainfall-runoff models and hydraulic models: a sensitivity analysis on the Illinois River. *J. Hydrol.* 418–419, 123–135. <http://dx.doi.org/10.1016/j.jhydrol.2009.09.019>.
- Lian, Y., Chan, I., Sing, J., Demissie, M., Knapp, V., 2007. Coupling of hydrologic and hydraulic models for the Illinois River Basin. *J. Hydrol.* 344, 210–222. <http://dx.doi.org/10.1016/j.jhydrol.2007.08.004>.
- Meire, D., De Doncker, L., Declercq, F., Buis, K., Trosch, P., Verhoeven, R., 2010. Modelling river-foodplain interaction during flood propagation. *Nat. Hazards* 55 (1), 111–121. <http://dx.doi.org/10.1007/s11069-010-9554-1>.
- Mejia, A.I., Reed, S.M., 2011. Evaluating the effects of parameterized cross section shapes and simplified routing with a coupled distributed hydrologic and hydraulic model. *J. Hydrol.* 409, 512–524. <http://dx.doi.org/10.1016/j.jhydrol.2011.08.050>.
- Micovic, Z., Schaefer, M., Taylor, G., 2015. Uncertainty analysis for Probable Maximum Precipitation estimates. *J. Hydrol.* 521, 360–373. <http://dx.doi.org/10.1016/j.jhydrol.2014.12.033>.
- Nadarajah, S., 2007. Probability models for unit hydrograph derivation. *J. Hydrol.* 344, 185–189. <http://dx.doi.org/10.1016/j.jhydrol.2007.07.004>.
- Orth, R., Staudinger, M., Seneviratne, S., Seibert, J., Zappa, M., 2015. Does model performance improve with complexity? A case study with three hydrological models. *J. Hydrol.* 523, 147–159. <http://dx.doi.org/10.1016/j.jhydrol.2015.01.044>.
- Papalexioiu, S.M., Koutsoyiannis, D., Makropoulos, C., 2013. How extreme is extreme? An assessment of daily rainfall distribution tails. *Hydrol. Earth Syst. Sci.* 17, 851–862.
- Pappenberger, F., Beven, K., Horrit, M., Blazkova, S., 2005. Uncertainty in the calibration of effective roughness parameters in HEC-RAS using inundation and downstream level observations. *J. Hydrol.* 302, 46–69. <http://dx.doi.org/10.1016/j.jhydrol.2004.06.036>.
- Pappenberger, F., Matgen, P., Beven, K., Henry, J., Pfister, L., de Fraipont, P., 2006. Influence of uncertain boundary conditions and model structure on flood inundation predictions. *Adv. Water Resour.* 29, 1430–1449. <http://dx.doi.org/10.1016/j.advwatres.2005.11.012>.
- Rai, R.K., Sarkar, S., Singh, V.P., 2008. Evaluation of the adequacy of statistical distribution functions for deriving unit hydrograph. *Water Resour. Manage.* 23, 899–929. <http://dx.doi.org/10.1007/s11269-008-9306-0>.
- Remo, J., Pinter, N., Heine, R., 2009. The use of retro- and scenario-modeling to assess effects of 100+ years river of engineering and land-cover change on Middle and Lower Mississippi River flood stages. *J. Hydrol.* 376, 403–416. <http://dx.doi.org/10.1016/j.jhydrol.2009.07.049>.
- Roessler, O., Froidevaux, P., Börst, U., Rickli, R., Martius, O., Weingartner, R., 2014. Retrospective analysis of a nonforecasted rain-on-snow flood in the Alps – a matter of model limitations or unpredictable nature? *Hydrol. Earth Syst. Sci.* 18, 2265–2285. <http://dx.doi.org/10.5194/hess-18-2265-2014>.
- Rogger, M., Kohl, B., Pirkl, H., Viglione, A., Komma, J., Kirnbauer, R., Merz, R., Blöschl, G., 2012a. Runoff models and flood frequency statistics for design flood estimation in Austria – do they tell a consistent story? *J. Hydrol.* 456–457, 30–43. <http://dx.doi.org/10.1016/j.jhydrol.2012.05.068>.
- Rogger, M., Pirkl, H., Viglione, A., Komma, J., Kohl, B., Kirnbauer, R., Merz, R., Blöschl, G., 2012b. Step changes in the flood frequency curve: Process controls. *Water Resour. Res.* 48 (5). <http://dx.doi.org/10.1029/2011WR011187>.
- Salas, J.D., Gaviñán, G., Salas, F.R., Julien, P.Y., Abdullah, J., 2014. *Uncertainty of the PMP and PMF*. In: Eslamian, S. (Ed.), *Handbook of Engineering Hydrology, Book II: Modeling, Climate Change and Variability*. CRC Press. Taylor & Francis Group, Boca Raton, FL, pp. 575–603.
- Samuels, P.G., 1990. Cross section location in one-dimensional models. In: White, W.R. (Ed.), *Int. Conf. on River Flood Hydraulics*. John Wiley & Sons Ltd., Chichester, UK, pp. 339–350.
- Serinaldi, F., Grimaldi, S., 2011. Synthetic design hydrographs based on distribution functions with finite support. *J. Hydrol. Eng.* 16, 434–446. [http://dx.doi.org/10.1061/\(ASCE\)HE.1943-5584.0000339](http://dx.doi.org/10.1061/(ASCE)HE.1943-5584.0000339).
- Sivakumar, B., 2009. Nonlinear dynamics and chaos in hydrologic systems: latest developments and a look forward. *Stoch. Environ. Res. Risk Assess.* 23, 1027–1036. <http://dx.doi.org/10.1007/s00477-008-0265-z>.
- Skublics, D., Seibert, S., Ehret, U., 2014. Modelling flood retention with hydrological and hydrodynamic models under different boundary conditions – sensitivity analysis on the Danube reach from Neu-Ulm to Donauwörth. *HyWa* 58, 178–189. http://dx.doi.org/10.5675/HyWa_2014_3_1.
- Vetsch, D., Siviglia, A., Ehrbar, D., Facchini, M., Gerber, M., Kammerer, S., Peter, S., Vonwiller, L., Volz, C., Farshi, D., Mueller, R., Rousselot, P., Veprek, R., Faeh, R., 2015. System Manuals of BASEMENT, Version 2.5. Laboratory of Hydraulics, Glaciology and Hydrology (VAW), ETH Zurich. Available from <http://www.basement.ethz.ch> [Access 21.09.2016].
- Viviroli, D., Zappa, M., Gurtz, J., Weingartner, R., 2009a. An introduction to the hydrological modelling system PREVAH and its pre- and post-processing tools. *Environ. Modell. Software* 24, 1209–1222. <http://dx.doi.org/10.1016/j.envsoft.2009.04.001>.
- Viviroli, D., Zappa, M., Schwanbeck, J., Gurtz, J., Weingartner, R., 2009b. Continuous simulation for flood estimation in ungauged mesoscale catchments of Switzerland – Part I: modelling framework and calibration results. *J. Hydrol.* 377, 191–207. <http://dx.doi.org/10.1016/j.jhydrol.2009.08.023>.
- Viviroli, D., Mittelbach, H., Gurtz, J., Weingartner, R., 2009c. Continuous simulation for flood estimation in ungauged mesoscale catchments of Switzerland – Part II: parameter regionalisation and flood estimation results. *J. Hydrol.* 377, 208–225. <http://dx.doi.org/10.1016/j.jhydrol.2009.08.022>.
- Vorogushyn, S., Merz, B., Lindenschmidt, K.-E., Apel, H., 2010. A new methodology for flood hazard assessment under consideration of dike breaches. *Water Resour. Res.* 46 (8), W08541. <http://dx.doi.org/10.1029/2009WR008475>.
- Vorogushyn, S., Lindenschmidt, K.-E., Kreibich, H., Apel, H., Merz, B., 2012. Analysis of a detention basin impact on dike failure probabilities and flood risk for a

- channel-dike-floodplain system along the river Elbe, Germany. *J. Hydrol.* 436–437, 120–131. <http://dx.doi.org/10.1016/j.jhydrol.2012.03.006>.
- Wehren, B., 2010. *The Hydrology of the Kander River - Yesterday, Today, Tomorrow. Analysis and Modelling of the Floods and Their Spatio-Temporal Dynamics Thesis (PhD). University of Bern, Switzerland.*
- WMO (World Meteorological Organization), 2009. *Manual on Estimation of Probable Maximum Precipitation (PMP)*. Nr. 1045. Geneva, Switzerland.
- Zappa, M., Andres, N., Kienzler, P., Näf-Huber, D., Marti, C., Oplatka, M., 2015. Crash tests for forward-looking flood control in the city of Zürich (Switzerland). *Proc. IAHS 370*, 235–242. <http://dx.doi.org/10.5194/piahs-370-235-2015>.
- Zeimetz, F., Garcia-Hernández, J., Schleiss, A.J., 2015. Extreme flood estimations on a small alpine catchment in Switzerland, the case study of Limmerboden. *Proc. IAHS 370*, 147–152. <http://dx.doi.org/10.5194/piahs-370-147-2015>.

Paper 21: Zischg, A., Felder, G., Weingartner, R., Quinn, N., Coxon, G., Neal, J., Freer, J., Bates, P., 2018. Effects of variability in probable maximum precipitation patterns on flood losses. *Hydrol. Earth Syst. Sci.* 22, 2759–2773. [10.5194/hess-22-2759-2018](https://doi.org/10.5194/hess-22-2759-2018).



Effects of variability in probable maximum precipitation patterns on flood losses

Andreas Paul Zischg^{1,2}, Guido Felder¹, Rolf Weingartner¹, Niall Quinn³, Gemma Coxon², Jeffrey Neal², Jim Freer², and Paul Bates²

¹University of Bern, Institute of Geography, Oeschger Centre for Climate Change Research, Mobiliar Lab for Natural Risks, Bern, 3012, Switzerland

²School of Geographical Sciences, University of Bristol, Bristol, BS8 1SS, UK

³Fathom Ltd., Bristol, BS1 6QF, UK

Correspondence: Andreas Paul Zischg (andreas.zischg@giub.unibe.ch)

Received: 29 December 2017 – Discussion started: 31 January 2018

Revised: 19 April 2018 – Accepted: 24 April 2018 – Published: 8 May 2018

Abstract. The assessment of the impacts of extreme floods is important for dealing with residual risk, particularly for critical infrastructure management and for insurance purposes. Thus, modelling of the probable maximum flood (PMF) from probable maximum precipitation (PMP) by coupling hydrological and hydraulic models has gained interest in recent years. Herein, we examine whether variability in precipitation patterns exceeds or is below selected uncertainty factors in flood loss estimation and if the flood losses within a river basin are related to the probable maximum discharge at the basin outlet. We developed a model experiment with an ensemble of probable maximum precipitation scenarios created by Monte Carlo simulations. For each rainfall pattern, we computed the flood losses with a model chain and benchmarked the effects of variability in rainfall distribution with other model uncertainties. The results show that flood losses vary considerably within the river basin and depend on the timing and superimposition of the flood peaks from the basin's sub-catchments. In addition to the flood hazard component, the other components of flood risk, exposure, and vulnerability contribute remarkably to the overall variability. This leads to the conclusion that the estimation of the probable maximum expectable flood losses in a river basin should not be based exclusively on the PMF. Consequently, the basin-specific sensitivities to different precipitation patterns and the spatial organization of the settlements within the river basin need to be considered in the analyses of probable maximum flood losses.

1 Introduction

Floods are one of the most damaging natural hazards, accounting for a majority of all economic losses from natural events worldwide (UNISDR, 2015). Managing flood risks requires knowledge about hazardous processes and the impacts of floods. Typically the impacts of design floods with a certain (extreme) return period (IPCC, 2012) or the impacts of worst-case floods are required for sound risk analysis and for the planning of risk reduction measures. In particular, for portfolio risk analyses of insurance companies, the estimation of the probable maximum loss is important for fulfilling financial regulations and stability criteria. Furthermore, critical infrastructure, such as power stations, has to be protected against extreme floods. Since floods are expected to increase due to climatic changes (Asadieh and Krakauer, 2015; Arnell and Gosling, 2016; Beniston et al., 2007; Bouwer, 2013; Fischer and Knutti, 2016; Millán, 2014; Pfahl et al., 2017; Rajczak et al., 2013; Scherrer et al., 2016), flood risk analyses and the management of extreme events will become even more relevant (Smolka, 2006; Yuan et al., 2017). Hence, insurance companies and governmental institutions are increasingly interested in quantifying flood risks, and especially in estimating the impacts of probable maximum floods leading to high cumulative losses (Burke et al., 2016; Morrill and Becker, 2017) or the destruction of critical infrastructure (Hasan and Foliente, 2015; Mechler et al., 2010; Michaelides, 2014).

An important aspect in flood risk analysis is the modelling of worst-case floods and their impacts (Büchle et al., 2006). One main question herein is the search for the upper physical limits of discharge in a river basin, i.e. the maximum outflow from a catchment that is possible with the given catchment characteristics and the maximum rainfall in the climate region (Felder and Weingartner, 2017). Here, the hydrological modelling undertaken to derive probable maximum flood (PMF) from probable maximum precipitation (PMP) is an important first step as a basis for inundation modelling (Felder et al., 2017). The PMP is defined as “the theoretical maximum precipitation for a given duration under modern meteorological conditions” (World Meteorological Organization, 2009). Differently, the PMF is defined as “the theoretical maximum flood that poses extremely serious threats to the flood control of a given project in a design watershed” (World Meteorological Organization, 2009). The PMF is estimated on the basis of the PMP and is commonly used in practice for the planning of hydropower dams. However, there is still a controversial discussion on the underlying concept of PMP, particularly on the assumption that the upper tail of flood distributions is bounded (Micovic et al., 2015). Comprehensive summaries of this discussion are provided by Salas et al. (2015) and by Rouhani and Leconte (2016). Nevertheless, PMP/PMF estimation methods have been continuously developed and improved. Beauchamp et al. (2013), Lagos-Zuniga and Vargas (2014), and Felder and Weingartner (2016) discuss the role of the spatio-temporal distribution of the PMP on the PMF, while Rousseau et al. (2014) and Stratz and Hossain (2014) discuss climate change and stationarity issues. Hence, Faulkner and Benn (2016), Micovic et al. (2015), Rouhani and Leconte (2016), and Salas et al. (2014) have proposed incorporating uncertainty bands into the PMP estimation.

Nevertheless, the detailed triggering mechanism and the temporal evolution of large flood events, specifically of worst-case scenarios, are not yet fully understood. An important question concerns how the peak discharge and the volume of a flood depend on the intensity and track of the triggering precipitation events, i.e. the spatio-temporal pattern of precipitation (Adams et al., 2012; Bruni et al., 2015; Cristiano et al., 2017; Emmanuel et al., 2015, 2016; Ochoa-Rodriguez et al., 2015; Paschalis et al., 2014; Rafieeinassab et al., 2015; Zhang and Han, 2017). In addition to the storm track dynamics, the peak flow depends on the watershed characteristics (Singh, 1997). In mountainous catchments with high topographical complexity, the storm track and the precipitation pattern are influenced by the mountain ranges. Furthermore, the river network is influenced by geological and tectonic structures and is thus more complex in mountainous terrain than in low-lying areas. Thus, in upland areas high variability in the spatio-temporal pattern of a probable maximum precipitation event and the resulting river flows has to be assumed. The definition of the spatio-temporal characteristics of PMP scenarios is a crucial step in the anal-

ysis of the impacts of extreme flood events. Hence, different approaches in distributing PMP in space and time over a catchment have been developed recently (Beauchamp et al., 2013; Dodov and Foufoula-Georgiou, 2005; Foufoula-Georgiou, 1989; Franchini et al., 1996; Felder and Weingartner, 2016). Regarding mountainous meso-scale catchments with an area of a few thousand km², insights into precipitation patterns leading to the most extreme floods are rather rare. The precipitation pattern leads to a specific pattern of the outflows from the sub-catchments. Depending on the geometry of the main river network, this timing of the outflows from the sub-catchments influences peak discharge in the individual river reaches. Hence, the relative timing of peak discharge arrivals in river confluences as a consequence of the spatio-temporal distribution of the rainfall pattern has to be addressed (Nicótina et al., 2008; Nikolopoulos et al., 2014; Pattison et al., 2014; Emmanuel et al., 2016; Zoccatelli et al., 2011). Thus, sound analysis of extreme floods in a complex river basin requires an assessment of the variability of chronological superimpositions of flood waves in tributaries and the effect of this on the probability of inundation. Neal et al. (2013) highlight the importance of spatial dependence between tributaries in terms of inundation probability and magnitude. Consequently, the amount of flood losses is also expected to vary with the timing of peak flows in the tributaries. Ochoa-Rodriguez et al. (2015) also stated that the temporal variation of rainfall inputs affects hydrodynamic modelling results remarkably. Emmanuel et al. (2015) showed that the spatio-temporal organization of rainfall plays an important role in the discharge at the outlet of the catchment and stated that a simulation approach is needed to study the effects of rainfall variability in complex river basins. The effects vary with the catchment size and its characteristics. Nevertheless, they state that there is a knowledge gap in this field. Probably the study that is most clearly focused on the role of the tributary relative timing and sequencing for extreme floods is presented by Pattison et al. (2014). They showed that tributary relative timing and synchronization is important in the determination of flood peak downstream. Thus, the distribution of extreme rainfall in space and time must play a critical role in determining the PMF and the peak discharge at the catchment outlet.

While the influence of rainfall variability on catchment response is under investigation, the further influence on flood losses is rarely investigated. To our knowledge, so far only Sampson et al. (2014) have analysed the effects of different precipitation scenarios on flood losses in depth. However, the Sampson et al. study focused on an urban area and on a (relatively) small scale. Thus far, no studies have been conducted in mountainous river basins to our knowledge.

In addition to the variability in precipitation patterns, other uncertainties have to be considered in flood loss estimation. Besides uncertainties in hydrological modelling that are not considered in this study, other factors lead to uncertainties in inundation modelling and in flood loss estimation. Uncer-

tainties in inundation modelling and flood risk analysis are addressed by Apel et al. (2008), Di Baldassarre et al. (2010), Gai et al. (2017), Merz and Thielen (2009), and Neal et al. (2013). Savage et al. (2015) and Fewtrell et al. (2008) describe the effects of spatial scale on inundation modelling. Altarejos-García et al. (2012), Chatterjee et al. (2008), Horritt and Bates (2001, 2002), Kvočka et al. (2015), and Neal et al. (2012b) discuss the effects of the chosen inundation model, its parametrization, and the role of input data on flood modelling results. Other uncertainties in flood modelling outputs are related to uncertainties in levee heights (Sanyal, 2017) or digital elevation models (Saksena and Merwade, 2015). Beside the uncertainties in flood modelling, observational uncertainties also need to be recognized with recent studies highlighting the importance of observational errors in rainfall and discharge data (McMillan et al., 2012; Coxon et al., 2015).

Furthermore, uncertainties in the economic models used to estimate flood losses and flood damages are relevant (de Moel et al., 2015). Herein, the input data, the choice of the impact indicators, the scale, and the vulnerability models are relevant sources of uncertainty (Ward et al., 2013; Apel et al., 2008; Merz and Thielen, 2009; de Moel and Aerts, 2011). In particular, vulnerability functions are considered as one of the most relevant sources of uncertainty in flood loss estimation (Ward et al., 2013; Sampson et al., 2014). Thus, uncertainty analysis is a key aspect in flood risk assessment. Some of the limitations and uncertainties mentioned above are addressed by several recent studies. Especially with regard to coupled models, uncertainty and sensitivity analyses are important for assessing the propagation of cascading uncertainties to the final result (Ward et al., 2013; Rodríguez-Rincón et al., 2015). Uncertainty analysis focuses on quantifying the spread of uncertainty in the model input on the model outputs, i.e. the forward propagation of the uncertainties to the prediction variables. In contrast, sensitivity analysis focuses on apportioning output uncertainty to the different sources of uncertainty (input factors). A global sensitivity analysis investigates how the variation in the output of a numerical model can be attributed to variations of its input factors (Pianosi et al., 2016). However, uncertainty analyses and sensitivity analyses of coupled models or model chains are rarely investigated topics.

In summary, we identify a research gap in our understanding of the effects of spatio-temporal precipitation patterns on the amount of flood losses in a river basin. The main goals of this study are to analyse the effects of variability in probable maximum precipitation patterns on flood losses, and to compare these effects with other uncertainties in flood loss modelling in a complex mountain catchment (i.e. choice of inundation models or vulnerability functions). One important question is whether the variability in precipitation patterns is more or less influential than other uncertainties in flood loss estimation. A second question is whether the maximum dis-

charge at the catchment outlet is a reliable proxy indicator for identifying the scenario(s) for worst case flood loss.

2 Methods

To address the above questions using a numerical experiment we constructed an inundation modelling framework composed of several coupled modules. The model chain was developed for the Aare River basin in Switzerland (3000 km²) and consists of five main components: a precipitation module, a hydrology module, a hydrodynamic routing module, a hydrodynamic inundation module, and a damage module. The model chain computes the flood losses (model output) on the basis of a specified rainfall event (model input). In the following, the setup of the model chain is described. The uncertainties related to the precipitation pattern were subsequently compared with selected other uncertainty factors in the model chain, i.e. uncertainties related to the inundation modelling approach and to the chosen vulnerability functions. Hence, we conducted a global sensitivity analysis of the model chain with the objective to rank the uncertainty in the rainfall pattern and the uncertainties in the model setup (choice of sub-models) according to their relative contribution to the output variability after Pianosi et al. (2016). The uncertainties in the model setup are considered in the sensitivity analysis by varying the setup of the submodules for flood modelling and loss modelling.

2.1 Probable maximum precipitation and probable maximum discharge

The probable maximum precipitation PMP for the whole catchment was estimated using the guidelines of World Meteorological Organization (2009). The method for distributing the PMP in space and time is based on a Monte Carlo approach proposed by Felder and Weingartner (2016). This approach aims at identifying a PMP pattern leading to the PMF by testing a high number of randomly generated spatio-temporal patterns considering physical plausibility criteria. To consider the spatio-temporal patterns of precipitation in the river basin, the same amount of areal precipitation in the PMP scenario (300 mm for a 72 h event over 3000 km²) was distributed in different spatio-temporal patterns across the entire river basin in a Monte Carlo simulation framework after Felder and Weingartner (2016). We focused on a precipitation event lasting 3 days, since this timespan corresponds to the typical event duration within the river basin and leads to the highest floods. The PMP scenarios are assumed to occur during the summer season with a height of the freezing level above the maximal altitudes. This means that snowfall is not considered. In the first step, a random temporal distribution of the total precipitation for the chosen duration was generated. The variation of rainfall between one time step and the following was limited to 20 % at maximum. This avoids im-

plausible temporal distributions. In the second step, the temporal pattern of the rainfall was distributed spatially in three meteorological regions, and in the sub-catchments within each meteorological region. The sub-catchments and the meteorological regions were defined to consider the relatively independent behaviour of specific parts of the catchment, e.g. lowlands and mountainous regions, in terms of precipitation amount and intensity. The randomly created precipitation pattern was checked against the spatial dependencies to fulfil a spatial consistency within neighbouring catchments. Intensive precipitation must be concentrated in adjacent meteorological regions and affiliated sub-catchments. The concentration of intense rainfall in meteorological regions and thus in adjacent sub-catchments implicitly allows taking into account the storm movement and the effects of the mountain crests. For further details see Felder and Weingartner (2016). From a set of 10^6 Monte Carlo simulations with a simplified but computationally efficient hydrological model based on unit hydrographs, we selected 150 scenarios with the highest discharge at the basin outlet in Bern. The number of scenarios is chosen to allow for analysing the variability of PMP patterns but at the same time allowing to be computationally feasible. These precipitation scenarios are then used as inputs for the detailed rainfall–runoff model, which is set up for each tributary and delivers the input hydrographs for the hydrodynamic model. For the rainfall–runoff modelling, we used the hydrological model PREVAH (Viviroli et al., 2009b), which is a deterministic, semi-distributed model based on hydrological response units (HRU) that are directly routed to the catchment outlet. The model is set up for 15 sub-catchments that are located within the Aare River basin upstream of Bern using an hourly time steps. The calibration and validation of the hydrological model is described in Felder et al. (2017). The output of the hydrological model of each sub-catchment is used as an upper boundary condition for the hydrodynamic model, in this case the 1-D hydrodynamic model BASEMENT-ETH (Vetsch et al., 2017) that accounts for the retention effects of lakes and floodplains. The model is based on the continuity equation and solves the Saint-Venant equations for unsteady 1-D flow. Lakes and their outlet weirs are considered in the hydrodynamic model. Here, we considered only the discharge from the lakes with maximal open weirs. No lake or reservoir regulation is considered, since lake regulation can be assumed to be irrelevant in case of extreme floods. The hydrologic and the hydrodynamic models were calibrated and validated separately, and then again together in the coupled version. The hydrological model was calibrated with all available gauged observation data at the outflow of 8 out of the 15 sub-catchments. The models for the ungauged sub-catchments were regionalized by applying the parameter regionalization method proposed by Viviroli et al. (2009a). The 1-D hydrodynamic model was calibrated by empirically adjusting the friction coefficients in the river channels with particular regard to the water surface elevation in the main channel at peak discharge. However, the

coupled hydrological–hydraulic model was validated against the observation at the catchment outlet. In the validation period 2011–2014, the coupled hydrological–hydraulic model has a NSE value of 0.85 (Nash–Sutcliffe efficiency; Nash and Sutcliffe, 1970), and a KGE value of 0.85 (Kling–Gupta efficiency; Gupta et al., 2009; Kling et al., 2012).

2.2 Inundation modelling

The coupled simulations of the 150 rainfall patterns provide the basis for the inundation modelling. The 1-D hydrodynamic model routes the water flow from the sub-catchments towards the catchment outlet. We defined the coupling points between the hydrological and the hydraulic model with a bottom-up approach: first, we delimited the floodplains for which the flood loss estimation will be valid (system delimitation). Second, we defined the upper boundary conditions of these floodplains. Third, we delimited the upstream catchments for the hydrological model based on the coupling points. However, the location of the gauging stations was also considered in the definition of the coupling points in order to calibrate and validate the hydrological model. The 1-D hydrodynamic model computes the level of the lakes and the outflow from the lakes. However, we used a 2-D inundation model as reference model for estimating the flow depths in the floodplains required for flood loss analysis. We nested the 2-D inundation models into the 1-D hydrodynamic model (see schematic of the approach in Fig. 1) to avoid the computationally demanding simulation of the lake retention with the 2-D model. We simulated all scenarios with the 1-D model and nested the 2-D model into the outcomes of the 1-D model at specific locations (boundary conditions). Hence, the 2-D model is always started after the simulation with the 1-D model in a cascading approach. The lake outflow hydrographs and lake level hydrographs from the 1-D hydrodynamic model and the hydrographs computed by the hydrological model that are directly flowing into the floodplains considered by the 2-D models were used as upper or lower boundary conditions for the 2-D flood inundation modelling. Minor tributaries are neglected as upper boundary condition. However, the outflows from their catchments are taken into account by aggregating all minor tributaries to sub-catchment level. The spatial setup of the model experiment, as well as the interfaces between the hydrological model and the floodplains modelled in 2-D, are shown in Fig. 2. In the 1-D model, the outflow from the sub-catchments is fed directly in the main river without considering flooding in the alluvial fans of the tributaries. In contrast, the outflows from the sub-catchments are fed into the 2-D model at the coupling points as shown in Fig. 2. Thus, the 2-D model considers flooding of the alluvial fans of the tributaries.

We used the LISFLOOD-FP model for the 2-D inundation simulation and as a basis for flood loss modelling. The model and its validation is described by Bates and de Roo (2000), Bates et al. (2010), and Neal et al. (2009, 2011, 2012a). The

model was set up with a subgrid representation of the channel and a spatial resolution on the floodplain of 50 m. The digital terrain model (DTM) was upscaled from a lidar DTM with high spatial resolution (0.5 m). The basis of this terrain data is a digital terrain model (DTM) provided by the Canton of Bern. This terrain model was created from lidar measurements collected in 2014 and 2015 with a resolution of about four points per m^2 . The lidar data were processed by the data provider to create a raster DTM with a cell size of 0.5 m. The buildings and the most important hydraulic structures in the main rivers (main bridges) were removed by this process. We corrected this raw raster model by (a) manually eliminating the remaining hydraulic obstacles in the river reaches, (b) correcting the height of the riverbanks in the Aare and Gürbe rivers reaches on the basis of DGPS measurements along the riverbanks, and (c) interpolating the altitudes of the raster cells of the river bed on the basis of surveyed bathymetric cross sections provided by the Federal Office for the Environment (BAFU). The result is a DTM with a spatial resolution of 0.5 m and the above mentioned corrections. This hydraulically correct DTM provides the basis for the aggregation at coarser spatial resolution for the flood inundation models.

The subgrid channel module requires the heights of the river bed and of the lateral dams, the river width, and the shape of the river bed. These data were computed at high resolution and aggregated onto the target resolution of the inundation model by conserving the cross-sectional area of the river channel from the high-resolution terrain model.

The 2-D hydrodynamic model was calibrated in terms of reproducing the stage–discharge relationships at the gauging stations and the known channel capacity along the river reaches. The model was validated on the basis of documented flooding. The fit of the inundation model (after Bates and de Roo, 2000) computed on the basis of observed discharges of the flood event in August 2005 and a comparison between modelled and observed inundation extents ranges between 0.5 and 0.9, depending on the floodplain. The lower values can be explained by dam breaks that occurred in reality but are not considered in the model, or by recent changes in the river geometry since the last flood event (implementation of new flood defence measures).

In addition to the 2-D inundation model, we elaborated inundation maps from the 1-D hydrodynamic simulations. We constructed water surface elevation (WSE) maps by interpolating the WSE values at the cross sections of the 1-D model. The projection of these WSE maps onto the digital terrain model (spatial resolution of 10 m) and the comparison with the DTM subsequently lead to a map of flow depths.

2.3 Flood loss modelling

In this study, we focused on structural damage to buildings (residential, public, and industrial buildings) without considering losses to mobile assets, building contents, and infras-

structure. The flood loss module of this model chain consists of a dataset of buildings similar to that described in Röthlisberger et al. (2017) and Fuchs et al. (2015). Each building is represented by a polygon and is classified by type, functionality, construction period, volume, reconstruction costs, and number of residents. Furthermore, we delineated the height of the ground floor above sea level of each building on the basis of a lidar terrain model with sub-metre resolution.

The resulting flow depths (FDs) and WSEs from the hydrodynamic module were attributed to each building (exposure analysis) and used for deriving the object-specific degree of loss from the vulnerability functions and consequently for the estimation of object-specific losses. The flow depth was attributed to the building following two different approaches. The first approach is a direct attribution of the flow depth from the FD maps to each building. The second approach is an indirect attribution where the flow depth at each building results from the difference between the WSE raster of the flood simulation and the minimum ground floor level of the building. The idea behind this approach is to take into account local small-scale elevations of the houses. If a building footprint covers more than one cell, we used the maximum flow depth of all relevant cells of the inundation map (Bermúdez and Zischg, 2018). The flow depth was used to calculate the degree of loss on the basis of a vulnerability function. The degree of loss resulting from the flow depth and the vulnerability function was subsequently multiplied with the reconstruction value of the building. This results in the expected loss to the building structure. The object-specific losses were subsequently summed to give the cumulative losses of a simulated precipitation scenario.

Five vulnerability functions were considered in the damage calculation procedure. We used the functions of Totschnig et al. (2011; V1), Papathoma-Köhle et al. (2015; V2), Hydrotec (2001; V3) as cited in Merz and Thielen (2009), Jonkman et al. (2008; V4), and Dutta et al. (2003; V5). We used different vulnerability functions because there is no regionally adopted and validated vulnerability function available for Switzerland, and because we aimed explicitly at exploring the range of uncertainties related to the choice of the function and its relevance for the maximum uncertainties in the outcomes. A direct validation of the vulnerability functions was not possible because of a lack of loss data at the level of single objects due to privacy restrictions. The selected vulnerability functions consider flow depths as the only input variable for the estimation of the degree of loss. We did not consider flow velocity because the inundation models used in this study do not provide flow velocities and we wanted to use comparable loss models.

2.4 Benchmarking against other selected uncertainty factors

The effects of variability in probable maximum precipitation patterns on flood losses are compared with selected other

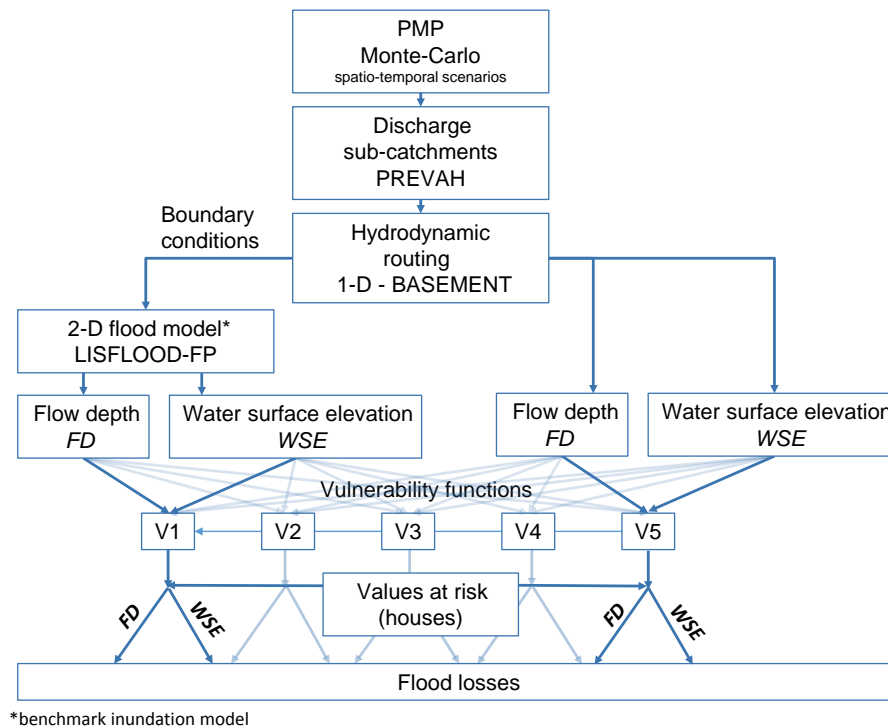


Figure 1. Schematic of the nesting approach. The 2-D flood inundation models and the loss models are nested in a 1-D routing model.

uncertainty factors. The comparison was made by following the parallel models approach first presented by Visser et al. (2000) for the example of climate simulations. Merz and Thielen (2009) adopted this approach for the identification of principal uncertainty sources in flood risk calculations. In summary, this approach computes a number of model runs with varying input parameters. In the first step, the minimum and maximum values of all simulation outcomes (flood losses in financial units in this study) were extracted. The difference between both is defined as the maximum uncertainty range (MUR). In the second step, the uncertainty range (UR_{sub}) of a specific subset of model runs was computed. The subsets from all model runs can be defined by specific criteria, e.g. a subset of all model runs with the same flood model or a subset of model runs using the same vulnerability function. The uncertainty range of this subset is given by the difference between the minimum and maximum values of all simulation outcomes of this specific subset. Third, the reduced uncertainty range (RUR) was computed according to Eq. (1). This indicator describes the relative role of an uncertainty source to the maximum uncertainty range of all model runs.

$$RUR = \frac{(MUR - UR_{\text{sub}})}{MUR} \cdot 100\% \quad (1)$$

The RUR is related to the maximum uncertainty range of all models but is not relative to the RUR of other subsets. Furthermore, Eq. (1) does not isolate all the contributions of the

different components to the maximum uncertainty range but they remain intertwined, except the selected uncertainty factor. However, the RUR values of the subsets are comparable. A high value of RUR means that the subset contributes significantly to the maximum uncertainty range. Alternatively, a small value of RUR ($RUR \ll 100\%$) indicates that the subset has a reduced effect on the overall uncertainty (Visser et al., 2000). In the model experiment for this study, we analysed the relative contribution of (a) the spatio-temporal rainfall pattern, (b) the choice of the inundation model and the exposure analysis approach, and (c) the choice of the vulnerability function. Hence, we followed a hierarchical approach for the selection of the subsets. For assessing the contribution of the spatio-temporal rainfall pattern to the overall uncertainty, we analysed 150 rainfall scenarios (hierarchical level 1 – precipitation). For each of these rainfall scenarios, the losses were computed with two different flood inundation models (LISFLOOD-FP and BASEMENT-1D) in combination with two different exposure modelling approaches (FD and WSE; hierarchical level 2 – flood model) and five different vulnerability functions identified previously (hierarchical level 3 – vulnerability). For each PMP scenario, 20 loss estimations were computed (four flood models times five vulnerability functions). Overall, the whole ensemble amounts to 3000 model runs (i.e. flood loss estimations). The RUR values were computed on the basis of subsets selected by the hierarchical levels representing the uncertainty factors considered in this analysis.

3 Study area

We set up the flood inundation models for the main valley of the Aare River basin upstream of Bern, Switzerland. The catchment elevation ranges from 500 to 4200 m a.s.l., with a mean elevation of 1600 m a.s.l. The southern part of the river basin consists of relatively high alpine mountains. Several alpine peaks within this area exceed 4000 m a.s.l., and parts of it are glaciated (8 % of the total catchment area). The main valley of the Aare River basin consists of a relatively flat floodplain with two lakes, where widespread flooding can occur. The lakes are natural but artificially managed, and are oriented along an approximately east–west axis in the lowland part of the catchment. The study area covers 3000 km², and the following main river reaches are considered in the model chain (see Fig. 2):

1. Hasliaare river, from Meiringen to Lake Brienz (floodplain: 15 km²; contributing area: 451 km²);
2. Lake Brienz static inundation model (lake area: 31 km²; contributing area: 1138 km²);
3. Interlaken, area between Lake Brienz and Lake Thun and the fan of the Lütischine River (floodplain: 28 km²);
4. Lake Thun static inundation model (lake area: 50 km²; contributing area: 2450 km²);
5. Thun (floodplain: 8 km²);
6. Aare River reach between Thun and Bern (floodplain: 42 km²);
7. Gürbe River reach between Burgistein and Belp (floodplain: 15 km²; contributing area: 116 km²).

4 Results

The main results of the coupled model simulations are the discharges at the outlet of each of the sub-catchments, the discharge at the outlet of the Aare River basin at Bern, and the flood losses for 150 PMP simulations. Figure 3 shows the hydrographs of the 150 PMP scenarios at the outlet of the river basin in Bern. The outflow from the river basin varies remarkably in peak discharge and time to peak. The peak discharges for each ensemble member were in the range 906 to 1296 m³ s⁻¹. Thus, the highest peak discharge is 43 % higher than the lowest in the selected set of scenarios. Moreover, Fig. 3 shows the discharges of the tributaries downstream of Lake Thun during peak flow of the Aare River at Bern. It is shown that the highest peak discharge at Bern depends on both a high flow in the main river and high flows in the tributaries. Upstream of Thun, the synchronization of flood peaks is represented by the lake levels.

The flood inundation modelling resulted in a set of flood maps representing the 150 PMP scenarios. The overlay of

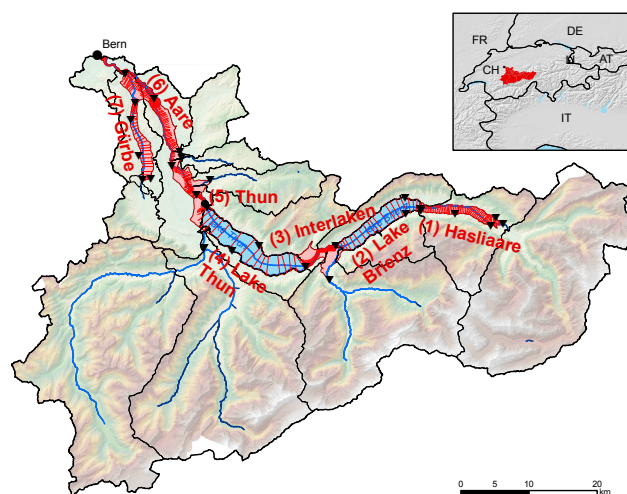


Figure 2. The Aare River catchment upstream of Bern, Switzerland. The sub-catchments of the hydrological model are divided by black lines. The black triangles indicate the coupling points between the hydrologic and the 2-D inundation model. The 1-D routing model covers all floodplains (red lines) and the lakes (blue). The floodplains that are covered by the individual 2-D inundation models nested into the 1-D routing model are marked and labelled in red.

these flood maps leads to an inundation extent map that estimates a spatial probability of inundation, conditional on the rainfall sum of a PMP event in the river basin. Each inundation map is treated as equally weighted in the probabilistic map. This map represents the probability that a model grid cell is flooded in one PMP scenarios. An extract of this map is shown in Fig. 4. The map shows that not all of the PMP scenarios lead to flooding of the same areas. Thus, despite the narrow framing of floodplains in mountainous areas by topography, high variability in flood extent can be observed. The discharge in the Lütischine River at Interlaken and the lake levels of both lakes, Lake Brienz and Lake Thun, have the strongest influence on the inundation probability map. In particular, the level of Lake Thun and the flooding by the Lütischine River determine a remarkable portion of the flooded area.

Depending on the chosen approach for inundation modelling and exposure analysis, the number of affected buildings varies remarkably. At minimum 2423 buildings and at maximum 5371 buildings are affected across the whole domain (not shown). The high variability between the PMP patterns is also shown by the number of exposed residents (Fig. 5). The exposure shows a bimodal distribution in the case of the 2-D model and a unimodal distribution in the case of the 1-D model. This is related to the exposure of houses at the alluvial fan of the Lütischine River. This floodplain is flooded only in some of the scenarios but when flooded, the number of affected buildings increases remarkably. This is not the case in the 1-D model because this model

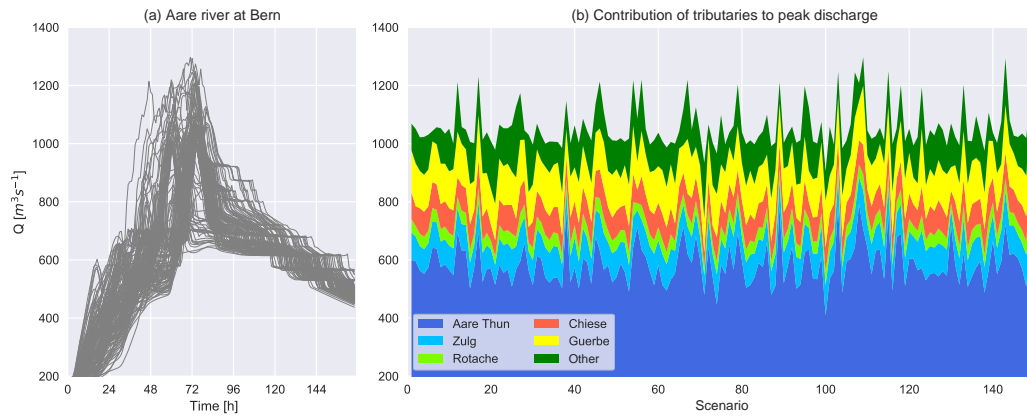


Figure 3. (a) Hydrographs at the outlet of the Aare River basin in Bern resulting from the coupled hydrologic-hydrodynamic modelling of the 150 PMP scenarios. (b) Superimposition of the tributaries downstream of Lake Thun during peak flow of the Aare River at Bern.

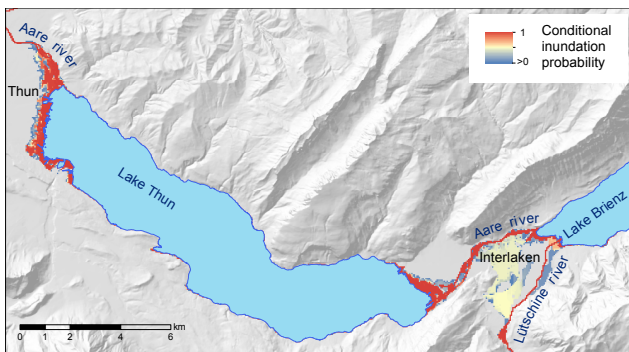


Figure 4. Detailed example of the conditional probability flood map for the floodplains of Thun and Interlaken. Predicted flood inundation extents can change significantly depending on the specific spatial properties of a few of the PMP scenarios and hence have lower mapped inundation probabilities.

only considers flooding by the main river Aare and neglects the tributaries.

The flood simulation mapped outputs (flow depth maps and water surface elevation maps) were used separately to calculate the flood losses at the individual building level. Subsequently, the flood losses at building scale were aggregated at a catchment level. Figure 6 shows the distribution of the aggregated flood losses. It is shown that – depending on the model ensemble member – the losses vary between CHF 0.06 and 2.87 billion. Thus, the losses are remarkably influenced by all the experimental uncertainty factors previously discussed in the modelling chain. However, even if the effect of the vulnerability function and the choice of the exposure analysis approach are not considered, the losses still vary markedly depending on the PMP scenario. Maximum losses are still approximately 3–5 times the minimum losses for some of the vulnerability functions. The vulnerability function V4 (Jonkman et al., 2008) results in the lowest

losses. This function was calibrated for lowland floodplains and thus has generally lower degrees of loss. However, this vulnerability function might be more representative for the areas affected by lake flooding than the others. In the 2-D FD model runs, the exposure is higher compared to the 2-D WSE model runs. In contrast, the losses are higher in the 2-D WSE run. This relates to the mean flow depths at the buildings. The mean flow depth over all affected buildings is 0.54 m in the 2-D FD model runs and 0.87 m in the 2-D WSE model runs. This results in higher losses although the number of exposed buildings is lower. The flow depths in the 1-D FD and 1-D WSE model runs are 1.08 and 1.36 m respectively. This explains the generally higher losses in the 1-D model runs compared to the 2-D model runs.

The benchmark against other uncertainties such as the flood modelling in combination with the exposure analysis approach and the vulnerability functions shows that the uncertainties considered in the model experiment contribute significantly to the sensitivity of the model chain to the assumptions made. Each member of the ensemble runs represents a rainfall pattern and a resulting flood loss computed on a basis of a combination of a specific flood model with a specific loss model. The difference between the ensemble member with the absolute minimum and the member with the absolute maximum of flood losses represents the maximum uncertainty range MUR. The total number of runs was divided into subsets that represents in each case the uncertainty range of a specific combination of the variables. The difference between the member with the absolute minimum of this subset and the member with the absolute maximum of this subset represents the reduced uncertainty range UR_{sub} . Consequently, the reduced uncertainty range RUR is computed after Eq. (1). The reduced uncertainty range RUR of all subsets ranges between 14 and 92 % of the maximum uncertainty range MUR. The reduced uncertainty range of the subset of ensemble members considering only the vari-

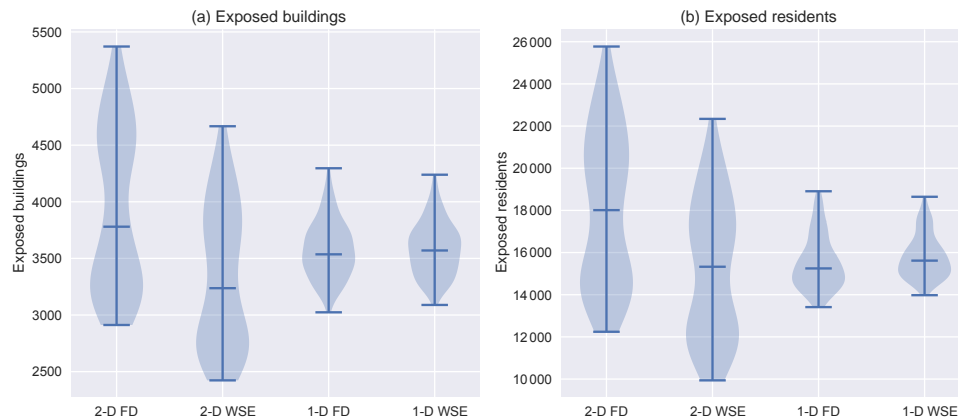


Figure 5. Exposed buildings (a) and residents (b) aggregated at river basin level. Flood losses aggregated at river basin level. The variation between the PMP scenarios is shown on the y axis, whereas the x axis shows the variability inherent to the choice of the flood model (2-D: LISFLOOD-FP; 1-D: BASEMENT-1D) in combination with the approach for attributing flow depths to the buildings (FD: flow depths are calculated on the basis of flow depths maps; WSE: flow depths are calculated on the basis of water surface elevation maps and the object-specific ground floor level).

ability in rainfall scenarios lies between 42 and 92 % with a median of 72 %. Hence, the highest RUR of all subsets is dominated by the subsets regarding the variability in probable maximum precipitation pattern. Figure 7 shows the comparison between the RUR values of the subsets in which the variability of one of the three considered uncertainty factors was analysed. This analysis makes evident that the rainfall pattern contributes most to the maximum uncertainty range.

In Fig. 8 (left column), we plotted the results of all model outcomes with focus on the 2-D inundation model in terms of exposed number of buildings and persons, and in terms of flood losses against the peak discharge of the respective precipitation pattern at the catchment outlet. The hypothesis that the flood losses increase with peak discharge at the outlet of the river basin can be verified in the sense that there is a significant correlation. This relationship is weaker for exposed buildings and residents than for the flood losses. However, the rainfall scenario leading to the highest peak discharge at the basin outlet does not correspond with the highest flood losses. Instead, the flood losses are more correlated with high lake levels in Lake Thun (see Fig. 8, right column). The correlation between flood losses and the level of Lake Thun (Spearman's rank correlation coefficient ranges from 0.54 to 0.94, depending on the flood model and the vulnerability function) is stronger than between losses and the peak discharge at the catchment outlet (Spearman's rank correlation coefficient ranging from 0.43 to 0.71). Thus, in the Aare River basin, the level of Lake Thun is a more relevant proxy indicator for the amount of flood losses in the whole river basin than the peak discharge at the outlet of the river basin (i.e. the so-called PMF of the river basin). This can be explained by the local situation of the city of Thun where the density of the building stock is very high along the shoreline of Lake Thun and along the Aare River. The major area

of the Aare River basin contributes to the lakes. Only 20 % of the catchment area is located downstream of Lake Thun. Although the area of Lake Thun covers only about 2 % of its contributing area, this means that the river basin has relevant retention areas that attenuate the outflow from the river basin and thus the PMF. Vice versa, this retention effect increases flood losses because a relevant number of buildings are located in neighbourhood of the lake shorelines. Likewise, not all of the PMP scenarios lead to flooding by the Lüttschine River in Interlaken. As shown in Fig. 4, the floodplain of this river is flooded only in a minority of the ensemble runs. Depending on whether this floodplain is flooded or not, up to 1500 exposed buildings and therefore up to one-third of the total number of maximally exposed buildings in the whole river basin could be affected. Thus, the highest loss of all simulated scenarios is related to a combination of a high lake level in Thun with high river discharge of the Lüttschine River. This shows that the maximum loss depends on both the spatio-temporal pattern of the rainfall and the internal organization of the river basin in terms of the spatial distribution of the values at risk (i.e. exposure) within the floodplains.

5 Discussion and conclusions

In this study, we set up a coupled component model for estimating flood losses of extreme flood events in a complex mountainous river basin. On the basis of a Monte Carlo approach, we computed an ensemble of extreme flood events for different precipitation patterns of a 3-day probable maximum precipitation scenario. With this model experiment, we analysed the effects of the spatial distribution of the rainfall within a mountainous river basin on flood losses. Further-

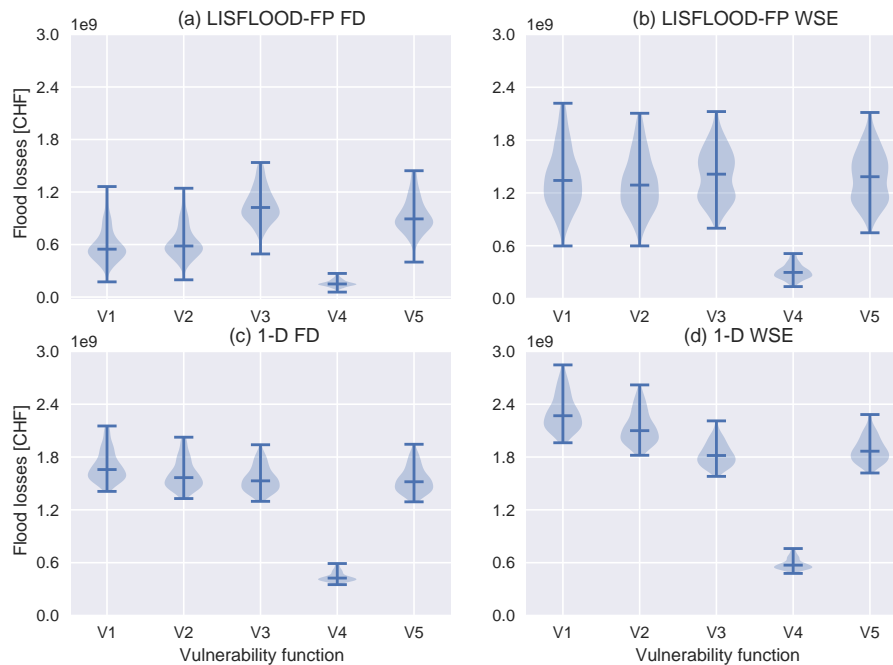


Figure 6. Flood losses aggregated at river basin level. The variation between the PMP scenarios is shown in the y axis, whereas the x axis shows the variability inherent to the vulnerability functions. The diagram in (a) shows flood losses that are calculated based on the flow depths as modelled by LISFLOOD-FP, the diagram in (b) shows the flood losses that are calculated based on the water surface elevation and the object-specific ground floor level. The flood losses estimated by the 1-D model are shown in (c) and (d).

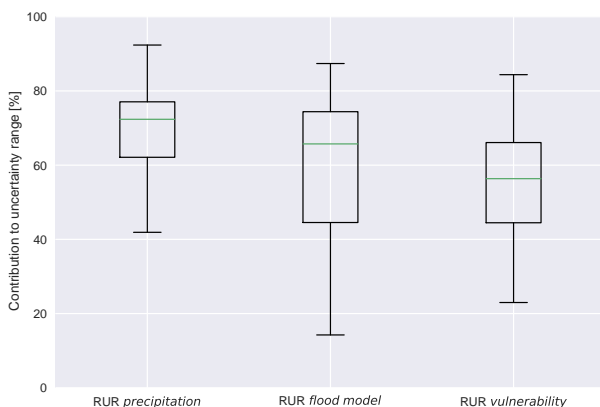


Figure 7. Reduced uncertainty ranges RUR of the subsets of model runs representing the three main uncertainty sources.

more, we benchmarked these effects with other uncertainties in flood loss modelling.

The model experiment showed that the sensitivity of flood losses to the variability of spatial distribution of rainfall within a river basin with a complex topography is larger than for the other considered uncertainty factors. The PMP pattern determines the magnitude and timing of the flood peaks coming from the sub-catchments and flowing through the floodplains along the main valleys and the lakes. Thus, the rainfall

pattern could lead to a superimposition of flood waves as described by the model experiments of Neal et al. (2013) and Pattison et al. (2014). In addition to the superimposition of flood waves, it is shown that lake levels, as a proxy for the water volumes coming from different sub-catchments, are also relevant for the determination of flood losses. This complements the findings of Sampson et al. (2014) on the impacts of precipitation variability on insurance loss estimates. With the present study, we extended the Sampson et al. study, which was focussed on urban environments, with a focus on complex mountainous river basins.

Furthermore, the model experiment showed that the peak flow coming from a single sub-catchment can be responsible for a relevant share of the total sum of exposed buildings and flood losses. Thus, the physical variability of the river basin is coupled with the topological situation of the main settlements within the floodplains, i.e. the spatial pattern of exposure. The inundation probability maps and the variability in flood losses show that two floodplains are mainly responsible for a high amount of flood losses. This documents that flood losses depend on both the spatio-temporal pattern of the rainfall and the internal organization of the river basin in terms of the spatial distribution or aggregation of the values at risk within the floodplains. Moreover, the spatial setup of the values at risk within the floodplains leads to its specific sensitivity to flood magnitude and lake level. However, these specific sensitivities of the single floodplains together with

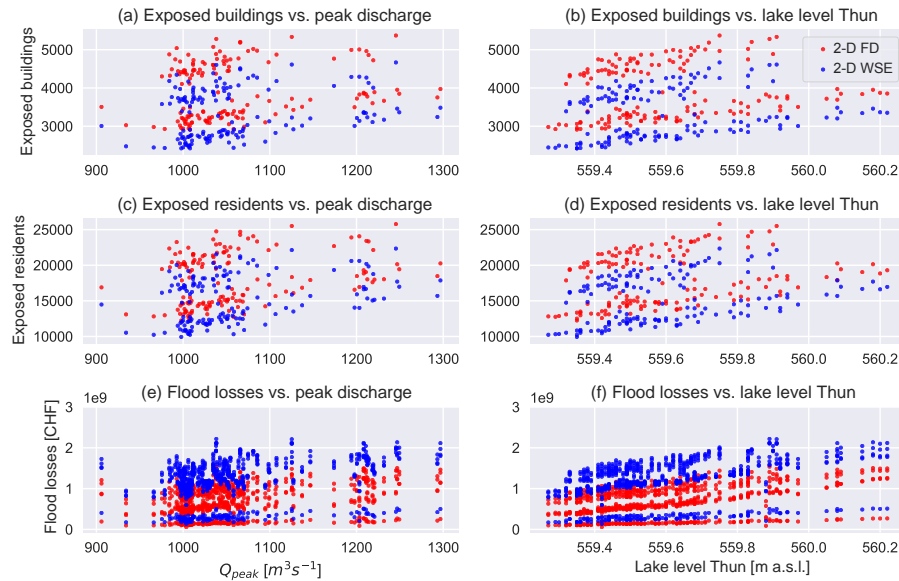


Figure 8. This figure shows the aggregated flood losses for the 150 PMP scenarios. The red dots show the exposed entities and losses that are computed based on the flow depths, the blue dots show the exposed entities and losses that are computed based on water surface elevation. The figures in the last row show the losses resulting from all vulnerability functions.

the variability in rainfall pattern lead to a specific sensitivity of the whole river basin to a certain pattern of rainfall. This behaviour has to be analysed and generalized in further studies and considered in the estimation of probable maximum flood losses.

Despite the topographical confinement of the floodplains by the mountain hillslopes, the flooded areas vary markedly with different rainfall patterns. Thus, the probabilistic map shows high spatial variability, caused by a few of the PMP scenarios significantly increasing inundation areas. Hence, the flow depths even at the individual building level, and consequently the total flood losses, vary remarkably with rainfall scenario. This case study in a mountainous environment and in an environment with remarkable retention capacities due to the presence of lakes may even lead to an attenuated illustration of this effect. These retention effects attenuate the PMF on one side but control the flood losses on the other side if settlements are located alongside the lakes. However, in mountain areas without lakes, the effects of spatio-temporal variability in precipitation patterns on flood losses may be even more accentuated. However, a modelling approach is needed to analyse these effects as stated by Emmanuel et al. (2015).

Nevertheless, the other uncertainty factors considered in this study, i.e. the role of the flood model, the exposure assessment approach and the vulnerability functions, are also contributing markedly to the maximum uncertainty range. This is in line with the findings of other studies (Jongman et al., 2012; de Moel and Aerts, 2011). Consequently, these

uncertainties also have to be taken into account in portfolio analysis or in the analysis of probable maximum flood losses.

In summary, we conclude that the analysis of a broader set of extreme floods with different precipitation patterns leads to more a comprehensive view of flood losses in a river basin compared to standard deterministic PMP/PMF methods. The spatio-temporal characteristics of rainfall patterns must be considered in complex mountainous river basins. Moreover, the analysis of the probable maximum flood losses in a river basin should consider the systemic vulnerability of the floodplains or the behaviour of floodplains as human–water systems as stated by Di Baldassarre et al. (2013, 2014). This involves the identification of key locations of exposure that contribute most to the overall flood losses. Probabilistic inundation maps provide a first overview of key locations of flooded areas with high sensitivity against the rainfall pattern. Furthermore, it is shown that the presented model experiment provides a valuable instrument for the consideration of all components in the analysis of the variability of rainfall patterns to flood losses in a river basin, from hazard to exposure to vulnerability.

However, the approach for simulating rainfall patterns presented here has its limitations. Although it has been shown that it can reproduce past flood events (Felder and Weingartner, 2016) and results in more robust PMF estimations than a uniform rainfall distribution (Felder and Weingartner, 2017), it is not comparable to a regional climate model or weather forecast model. In future research, an inverse modelling approach may be followed by searching the worst case precipitation pattern leading to the worst case flood losses on the

basis of the system characteristics of the river basin (sensitivities of floodplains and spatial setup of the river system). The calculation of the maximum expectable flood losses in a river basin should not be based exclusively on the PMF. In contrast to the initial hypothesis, we observed that other catchment characteristics in combination with the PMF could remarkably influence the flood losses. Consequently, in complex river basins it is recommended to analyse the sensitivity of the most relevant floodplains before analysing the probable maximum flood losses.

Code availability. Data of cross section surveys were provided the Federal Office for the Environment. The lidar terrain model was provided by the Canton of Bern. Basic GIS data were provided by the Federal Office for Topography swisstopo. The residential register was provided by the Federal Office for Statistics. The data about values at risk are restricted by privacy regulations. All other data produced in this study and the codes for the model experiment are available from the leading author on request. The inundation model LISFLOOD-FP is available at <http://www.bristol.ac.uk/geography/research/hydrology/models/lisflood/> (Bates, 2018).

Author contributions. The study was designed by APZ, JF, PB, and RW. The hydrological model was set up and run by GF. Model coupling and the set up of the hydraulic model were done by APZ, NQ, GC, and JN. The loss model was developed by APZ. The analyses were performed by APZ with the support of all co-authors. The manuscript was prepared by APZ with the contribution of all co-authors.

Competing interests. The authors declare that they have no conflict of interest.

Acknowledgements. The work was partially funded by the Swiss National Foundation (grant no. IZKOZ2_170478/1), by the Swiss Mobiliar, by NERC grant SINATRA (Susceptibility of catchments to INTense RAInfall and flooding, grant no. NE/K008781/1), and by NERC grant MaRIUS (Managing the Risks, Impacts and Uncertainties of droughts and water Scarcity, grant no. NE/L010399/1). We thank the Federal Government of Switzerland and the Canton of Bern for providing the data.

Edited by: Erwin Zehe

Reviewed by: two anonymous referees

References

Adams, R., Western, A. W., and Seed, A. W.: An analysis of the impact of spatial variability in rainfall on runoff and sediment predictions from a distributed model, *Hydrol. Process.*, 26, 3263–3280, <https://doi.org/10.1002/hyp.8435>, 2012.

Altarejos-García, L., Martínez-Chenoll, M. L., Escuder-Bueno, I., and Serrano-Lombillo, A.: Assessing the impact of uncertainty

on flood risk estimates with reliability analysis using 1-D and 2-D hydraulic models, *Hydrol. Earth Syst. Sci.*, 16, 1895–1914, <https://doi.org/10.5194/hess-16-1895-2012>, 2012.

Apel, H., Merz, B., and Thielen, A. H.: Quantification of uncertainties in flood risk assessments, *Int. J. River Basin Manage.*, 6, 149–162, <https://doi.org/10.1080/15715124.2008.9635344>, 2008.

Arnell, N. W. and Gosling, S. N.: The impacts of climate change on river flood risk at the global scale, *Clim. Change*, 134, 387–401, <https://doi.org/10.1007/s10584-014-1084-5>, 2016.

Asadih, B. and Krakauer, N. Y.: Global trends in extreme precipitation: climate models versus observations, *Hydrol. Earth Syst. Sci.*, 19, 877–891, <https://doi.org/10.5194/hess-19-877-2015>, 2015.

Bates, P.: LISFLOOD-FP. Model description and download, available at: <http://www.bristol.ac.uk/geography/research/hydrology/models/lisflood/>, last access: 4 May 2018.

Bates, P. D. and de Roo, A. P. J.: A simple raster-based model for flood inundation simulation, *J. Hydrol.*, 236, 54–77, [https://doi.org/10.1016/S0022-1694\(00\)00278-X](https://doi.org/10.1016/S0022-1694(00)00278-X), 2000.

Bates, P. D., Horritt, M. S., and Fewtrell, T. J.: A simple inertial formulation of the shallow water equations for efficient two-dimensional flood inundation modelling, *J. Hydrol.*, 387, 33–45, <https://doi.org/10.1016/j.jhydrol.2010.03.027>, 2010.

Beauchamp, J., Leconte, R., Trudel, M., and Brissette, F.: Estimation of the summer-fall PMP and PMF of a northern watershed under a changed climate, *Water Resour. Res.*, 49, 3852–3862, <https://doi.org/10.1002/wrcr.20336>, 2013.

Beniston, M., Stephenson, D. B., Christensen, O. B., Ferro, C. A. T., Frei, C., Goyette, S., Halsnaes, K., Holt, T., Jylhä, K., Koffi, B., Palutikof, J., Schöll, R., Semmler, T., and Woth, K.: Future extreme events in European climate: An exploration of regional climate model projections, *Clim. Change*, 81, 71–95, <https://doi.org/10.1007/s10584-006-9226-z>, 2007.

Bermúdez, M. and Zischg, A. P.: Sensitivity of flood loss estimates to building representation and flow depth attribution methods in micro-scale flood modelling, *Nat. Hazards*, 14, 253, <https://doi.org/10.1007/s11069-018-3270-7>, 2018.

Bouwer, L. M.: Projections of future extreme weather losses under changes in climate and exposure, Risk analysis an official publication of the Society for Risk Analysis, 33, 915–930, <https://doi.org/10.1111/j.1539-6924.2012.01880.x>, 2013.

Bruni, G., Reinoso, R., van de Giesen, N. C., Clemens, F. H. L. R., and ten Veldhuis, J. A. E.: On the sensitivity of urban hydrodynamic modelling to rainfall spatial and temporal resolution, *Hydrol. Earth Syst. Sci.*, 19, 691–709, <https://doi.org/10.5194/hess-19-691-2015>, 2015.

Büchle, B., Kreibich, H., Kron, A., Thielen, A., Ihringer, J., Oberle, P., Merz, B., and Nestmann, F.: Flood-risk mapping: contributions towards an enhanced assessment of extreme events and associated risks, *Nat. Hazards Earth Syst. Sci.*, 6, 485–503, <https://doi.org/10.5194/nhess-6-485-2006>, 2006.

Burke, N., Rau-Chaplin, A., and Varghese, B.: Computing probable maximum loss in catastrophe reinsurance portfolios on multi-core and many-core architectures, *Concurrency Computat.: Pract. Exper.*, 28, 836–847, <https://doi.org/10.1002/cpe.3695>, 2016.

Chatterjee, C., Förster, S., and Bronstert, A.: Comparison of hydrodynamic models of different complexities to model floods

- with emergency storage areas, *Hydrol. Process.*, 22, 4695–4709, <https://doi.org/10.1002/hyp.7079>, 2008.
- Coxon, G., Freer, J., Westerberg, I. K., Wagener, T., Woods, R., and Smith, P. J.: A novel framework for discharge uncertainty quantification applied to 500 UK gauging stations, *Water Resour. Res.*, 51, 5531–5546, <https://doi.org/10.1002/2014WR016532>, 2015.
- Cristiano, E., ten Veldhuis, M.-C., and van de Giesen, N.: Spatial and temporal variability of rainfall and their effects on hydrological response in urban areas – a review, *Hydrol. Earth Syst. Sci.*, 21, 3859–3878, <https://doi.org/10.5194/hess-21-3859-2017>, 2017.
- de Moel, H. and Aerts, J. C. J. H.: Effect of uncertainty in land use, damage models and inundation depth on flood damage estimates, *Nat. Hazards*, 58, 407–425, <https://doi.org/10.1007/s11069-010-9675-6>, 2011.
- de Moel, H., Jongman, B., Kreibich, H., Merz, B., Penning-Rowsell, E., and Ward, P. J.: Flood risk assessments at different spatial scales, *Mitig. Adapt. Strateg. Glob. Change*, 20, 865–890, <https://doi.org/10.1007/s11027-015-9654-z>, 2015.
- Di Baldassarre, G., Schumann, G., Bates, P. D., Freer, J. E., and Beven, K. J.: Flood-plain mapping: A critical discussion of deterministic and probabilistic approaches, *Hydrol. Sci. J.*, 55, 364–376, <https://doi.org/10.1080/02626661003683389>, 2010.
- Di Baldassarre, G., Kooy, M., Kemerink, J. S., and Brandimarte, L.: Towards understanding the dynamic behaviour of floodplains as human-water systems, *Hydrol. Earth Syst. Sci.*, 17, 3235–3244, <https://doi.org/10.5194/hess-17-3235-2013>, 2013.
- Di Baldassarre, G., Kemerink, J. S., Kooy, M., and Brandimarte, L.: Floods and societies: the spatial distribution of water-related disaster risk and its dynamics, *WIREs Water*, 1, 133–139, <https://doi.org/10.1002/wat2.1015>, 2014.
- Dodov, B. and Fofoula-Georgiou, E.: Incorporating the spatio-temporal distribution of rainfall and basin geomorphology into nonlinear analyses of streamflow dynamics, *Adv. Water Resour.*, 28, 711–728, <https://doi.org/10.1016/j.advwatres.2004.12.013>, 2005.
- Dutta, D., Herath, S., and Musiak, K.: A mathematical model for flood loss estimation, *J. Hydrol.*, 277, 24–49, [https://doi.org/10.1016/S0022-1694\(03\)00084-2](https://doi.org/10.1016/S0022-1694(03)00084-2), 2003.
- Emmanuel, I., Andrieu, H., Leblois, E., Janey, N., and Payrastré, O.: Influence of rainfall spatial variability on rainfall–runoff modelling: Benefit of a simulation approach?, *J. Hydrol.*, 531, 337–348, <https://doi.org/10.1016/j.jhydrol.2015.04.058>, 2015.
- Emmanuel, I., Payrastré, O., Andrieu, H., Zuber, F., Lang, M., Klijn, F., and Samuels, P.: Influence of the spatial variability of rainfall on hydrograph modelling at catchment outlet: A case study in the Cevennes region, France, *E3S Web Conf.*, 7, 18004, <https://doi.org/10.1051/e3sconf/20160718004>, 2016.
- Faulkner, D. and Benn, J.: Reservoir Flood Estimation: Time for a Re-think, in: *Dams – Benefits and Disbenefits; Assets or Liabilities?*, edited by: Pepper, A., ICE Publishing, London, 2016.
- Felder, G. and Weingartner, R.: An approach for the determination of precipitation input for worst-case flood modelling, *Hydrol. Sci. J.*, 61, 2600–2609, <https://doi.org/10.1080/02626667.2016.1151980>, 2016.
- Felder, G. and Weingartner, R.: Assessment of deterministic PMF modelling approaches, *Hydrol. Sci. J.*, 62, 1591–1602, <https://doi.org/10.1080/02626667.2017.1319065>, 2017.
- Felder, G., Zischg, A., and Weingartner, R.: The effect of coupling hydrologic and hydrodynamic models on probable maximum flood estimation, *J. Hydrol.*, 550, 157–165, <https://doi.org/10.1016/j.jhydrol.2017.04.052>, 2017.
- Fewtrell, T. J., Bates, P. D., Horritt, M., and Hunter, N. M.: Evaluating the effect of scale in flood inundation modelling in urban environments, *Hydrol. Process.*, 22, 5107–5118, <https://doi.org/10.1002/hyp.7148>, 2008.
- Fischer, E. M. and Knutti, R.: Observed heavy precipitation increase confirms theory and early models, *Nat. Clim. Change*, 6, 986–991, <https://doi.org/10.1038/nclimate3110>, 2016.
- Foufoula-Georgiou, E.: A probabilistic storm transposition approach for estimating exceedance probabilities of extreme precipitation depths, *Water Resour. Res.*, 25, 799–815, <https://doi.org/10.1029/WR025i005p00799>, 1989.
- Franchini, M., Helmlinger, K. R., Foufoula-Georgiou, E., and Todini, E.: Stochastic storm transposition coupled with rainfall–runoff modeling for estimation of exceedance probabilities of design floods, *J. Hydrol.*, 175, 511–532, [https://doi.org/10.1016/S0022-1694\(96\)80022-9](https://doi.org/10.1016/S0022-1694(96)80022-9), 1996.
- Fuchs, S., Keiler, M., and Zischg, A.: A spatiotemporal multi-hazard exposure assessment based on property data, *Nat. Hazards Earth Syst. Sci.*, 15, 2127–2142, <https://doi.org/10.5194/nhess-15-2127-2015>, 2015.
- Gai, L., Baartman, J. E. M., Mendoza-Carranza, M., Wang, F., Ritsema, C. J., and Geissen, V.: A framework approach for unravelling the impact of multiple factors influencing flooding, *J. Flood Risk Manage.*, published online first, <https://doi.org/10.1111/jfr3.12310>, 2017.
- Gupta, H. V., Kling, H., Yilmaz, K. K., and Martinez, G. F.: Decomposition of the mean squared error and NSE performance criteria: Implications for improving hydrological modelling, *Hydrology Conference 2010*, 377, 80–91, <https://doi.org/10.1016/j.jhydrol.2009.08.003>, 2009.
- Hasan, S. and Foliente, G.: Modeling infrastructure system interdependencies and socioeconomic impacts of failure in extreme events: emerging R&D challenges, *Nat. Hazards*, 78, 2143–2168, <https://doi.org/10.1007/s11069-015-1814-7>, 2015.
- Horritt, M. S. and Bates, P. D.: Effects of spatial resolution on a raster based model of flood flow, *J. Hydrol.*, 253, 239–249, [https://doi.org/10.1016/S0022-1694\(01\)00490-5](https://doi.org/10.1016/S0022-1694(01)00490-5), 2001.
- Horritt, M. S. and Bates, P. D.: Evaluation of 1D and 2D numerical models for predicting river flood inundation, *J. Hydrol.*, 268, 87–99, [https://doi.org/10.1016/S0022-1694\(02\)00121-X](https://doi.org/10.1016/S0022-1694(02)00121-X), 2002.
- Hydrotec: Hochwasser-Aktionsplan Angerbach, Teil I: Berichte und Anlagen, Studie im Auftrag des Stua Dusseldorf, Aachen, Germany, 2001.
- IPCC: Managing the risks of extreme events and disasters to advance climate change adaptation: Special report of the Intergovernmental Panel on Climate Change, Cambridge University Press, New York, x, 582, 2012.
- Jongman, B., Kreibich, H., Apel, H., Barredo, J. I., Bates, P. D., Feyen, L., Gericke, A., Neal, J., Aerts, J. C. J. H., and Ward, P. J.: Comparative flood damage model assessment: towards a European approach, *Nat. Hazards Earth Syst. Sci.*, 12, 3733–3752, <https://doi.org/10.5194/nhess-12-3733-2012>, 2012.
- Jonkman, S. N., Bočkarjova, M., Kok, M., and Bernardini, P.: Integrated hydrodynamic and economic modelling of flood damage in the Netherlands, Special Section: Integrated Hydro-Economic

- Modelling for Effective and Sustainable Water Management, 66, 77–90, <https://doi.org/10.1016/j.ecolecon.2007.12.022>, 2008.
- Kling, H., Fuchs, M., and Paulin, M.: Runoff conditions in the upper Danube basin under an ensemble of climate change scenarios, Hydrology Conference 2010, 424–425, 264–277, <https://doi.org/10.1016/j.jhydrol.2012.01.011>, 2012.
- Kvočka, D., Falconer, R. A., and Bray, M.: Appropriate model use for predicting elevations and inundation extent for extreme flood events, Nat. Hazards, 79, 1791–1808, <https://doi.org/10.1007/s11069-015-1926-0>, 2015.
- Lagos-Zuniga, M. A. and Vargas, M. X.: PMP and PMF estimations in sparsely-gauged Andean basins and climate change projections, Hydrol. Sci. J., 59, 2027–2042, <https://doi.org/10.1080/02626667.2013.877588>, 2014.
- McMillan, H., Krueger, T., and Freer, J.: Benchmarking observational uncertainties for hydrology: Rainfall, river discharge and water quality, Hydrol. Process., 26, 4078–4111, <https://doi.org/10.1002/hyp.9384>, 2012.
- Mechler, R., Hochrainer, S., Aaheim, A., Salen, H., and Wreford, A.: Modelling economic impacts and adaptation to extreme events: Insights from European case studies, Mitig. Adapt. Strateg. Glob. Change, 15, 737–762, <https://doi.org/10.1007/s11027-010-9249-7>, 2010.
- Merz, B. and Thielen, A. H.: Flood risk curves and uncertainty bounds, Nat. Hazards, 51, 437–458, <https://doi.org/10.1007/s11069-009-9452-6>, 2009.
- Michaelides, S.: Vulnerability of transportation to extreme weather and climate change, Nat. Hazards, 72, 1–4, <https://doi.org/10.1007/s11069-013-0975-5>, 2014.
- Micovic, Z., Schaefer, M. G., and Taylor, G. H.: Uncertainty analysis for Probable Maximum Precipitation estimates, J. Hydrol., 521, 360–373, <https://doi.org/10.1016/j.jhydrol.2014.12.033>, 2015.
- Millán, M. M.: Extreme hydrometeorological events and climate change predictions in Europe, J. Hydrol., 518, 206–224, <https://doi.org/10.1016/j.jhydrol.2013.12.041>, 2014.
- Morrill, E. P. and Becker, J. F.: Defining and Analyzing the Frequency and Severity of Flood Events to Improve Risk Management from a Reinsurance Standpoint, Hydrol. Earth Syst. Sci. Discuss., <https://doi.org/10.5194/hess-2017-167>, in review, 2017.
- Nash, J. E. and Sutcliffe, J. V.: River flow forecasting through conceptual models part I – A discussion of principles, J. Hydrol., 10, 282–290, 1970.
- Neal, J., Schumann, G., Fewtrell, T., Budimir, M., Bates, P., and Mason, D.: Evaluating a new LISFLOOD-FP formulation with data from the summer 2007 floods in Tewkesbury, UK, J. Flood Risk Manage, 4, 88–95, <https://doi.org/10.1111/j.1753-318X.2011.01093.x>, 2011.
- Neal, J., Schumann, G., and Bates, P. D.: A subgrid channel model for simulating river hydraulics and floodplain inundation over large and data sparse areas, Water Resour. Res., 48, 1–16, <https://doi.org/10.1029/2012WR012514>, 2012a.
- Neal, J., Villanueva, I., Wright, N., Willis, T., Fewtrell, T., and Bates, P. D.: How much physical complexity is needed to model flood inundation?, Hydrol. Process., 26, 2264–2282, <https://doi.org/10.1002/hyp.8339>, 2012b.
- Neal, J., Keef, C., Bates, P., Beven, K., and Leedal, D.: Probabilistic flood risk mapping including spatial dependence, Hydrol. Process., 27, 1349–1363, <https://doi.org/10.1002/hyp.9572>, 2013.
- Neal, J. C., Bates, P. D., Fewtrell, T. J., Hunter, N. M., Wilson, M. D., and Horritt, M. S.: Distributed whole city water level measurements from the Carlisle 2005 urban flood event and comparison with hydraulic model simulations, J. Hydrol., 368, 42–55, <https://doi.org/10.1016/j.jhydrol.2009.01.026>, 2009.
- Nicotina, L., Alessi Celegon, E., Rinaldo, A., and Marani, M.: On the impact of rainfall patterns on the hydrologic response, Water Resour. Res., 44, 311, <https://doi.org/10.1029/2007WR006654>, 2008.
- Nikolopoulos, E. I., Borga, M., Zoccatelli, D., and Anagnostou, E. N.: Catchment-scale storm velocity: Quantification, scale dependence and effect on flood response, Hydrol. Sci. J., 59, 1363–1376, <https://doi.org/10.1080/02626667.2014.923889>, 2014.
- Ochoa-Rodriguez, S., Wang, L.-P., Gires, A., Pina, R. D., Reinoso-Rondinel, R., Bruni, G., Ichiba, A., Gaitan, S., Cristiano, E., van Assel, J., Kroll, S., Murlà-Tuyls, D., Tisserand, B., Schertzer, D., Tchiguirinskaia, I., Onof, C., Willems, P., and ten Veldhuis, M.-C.: Impact of spatial and temporal resolution of rainfall inputs on urban hydrodynamic modelling outputs: A multi-catchment investigation, J. Hydrol., 531, 389–407, <https://doi.org/10.1016/j.jhydrol.2015.05.035>, 2015.
- Papathoma-Köhle, M., Zischg, A., Fuchs, S., Glade, T., and Keiler, M.: Loss estimation for landslides in mountain areas – An integrated toolbox for vulnerability assessment and damage documentation, Environ. Modell. Softw., 63, 156–169, <https://doi.org/10.1016/j.envsoft.2014.10.003>, 2015.
- Paschalis, A., Faticchi, S., Molnar, P., Rimkus, S., and Burlando, P.: On the effects of small scale space?: Time variability of rainfall on basin flood response, J. Hydrology, 514, 313–327, <https://doi.org/10.1016/j.jhydrol.2014.04.014>, 2014.
- Pattison, I., Lane, S. N., Hardy, R. J., and Reaney, S. M.: The role of tributary relative timing and sequencing in controlling large floods, Water Resour. Res., 5444–5458, <https://doi.org/10.1002/2013WR014067>, 2014.
- Pfahl, S., O’Gorman, P. A., and Fischer, E. M.: Understanding the regional pattern of projected future changes in extreme precipitation, Nat. Clim. Change, 7, 423–427, <https://doi.org/10.1038/nclimate3287>, 2017.
- Pianosi, F., Beven, K., Freer, J., Hall, J. W., Rougier, J., Stephenson, D. B., and Wagener, T.: Sensitivity analysis of environmental models: A systematic review with practical workflow, Environ. Modell. Softw., 79, 214–232, <https://doi.org/10.1016/j.envsoft.2016.02.008>, 2016.
- Rafieenasab, A., Norouzi, A., Kim, S., Habibi, H., Nazari, B., Seo, D.-J., Lee, H., Cosgrove, B., and Cui, Z.: Toward high-resolution flash flood prediction in large urban areas – Analysis of sensitivity to spatiotemporal resolution of rainfall input and hydrologic modeling, J. Hydrol., 531, 370–388, <https://doi.org/10.1016/j.jhydrol.2015.08.045>, 2015.
- Rajczak, J., Pall, P., and Schär, C.: Projections of extreme precipitation events in regional climate simulations for Europe and the Alpine Region, J. Geophys. Res.-Atmos., 118, 3610–3626, <https://doi.org/10.1002/jgrd.50297>, 2013.
- Rodríguez-Rincón, J. P., Pedrozo-Acuña, A., and Breña-Naranjo, J. A.: Propagation of hydro-meteorological uncertainty in a model cascade framework to inundation prediction, Hydrol. Earth Syst.

- Sci., 19, 2981–2998, <https://doi.org/10.5194/hess-19-2981-2015>, 2015.
- Röthlisberger, V., Zischg, A. P., and Keiler, M.: Identifying spatial clusters of flood exposure to support decision making in risk management, *Sci. Total Environ.*, 598, 593–603, <https://doi.org/10.1016/j.scitotenv.2017.03.216>, 2017.
- Rouhani, H. and Leconte, R.: A novel method to estimate the maximization ratio of the Probable Maximum Precipitation (PMP) using regional climate model output, *Water Resour. Res.*, 52, 7347–7365, <https://doi.org/10.1002/2016WR018603>, 2016.
- Rousseau, A. N., Klein, I. M., Freudiger, D., Gagnon, P., Frigon, A., and Ratté-Fortin, C.: Development of a methodology to evaluate probable maximum precipitation (PMP) under changing climate conditions: Application to southern Quebec, Canada, *J. Hydrol.*, 519, 3094–3109, <https://doi.org/10.1016/j.jhydrol.2014.10.053>, 2014.
- Saksena, S. and Merwade, V.: Incorporating the effect of DEM resolution and accuracy for improved flood inundation mapping, *J. Hydrol.*, 530, 180–194, <https://doi.org/10.1016/j.jhydrol.2015.09.069>, 2015.
- Salas, J. D., Gavilán, G., Salas, F. R., Julien, P. Y., and Abdullah, J.: Uncertainty of the PMP and PMF, in: *Handbook of Engineering Hydrology*, vol. 2: Modeling, Climate Change and Variability, 575–603, 2014.
- Salas, J. D., Tarawneh, Z., and Biondi, F.: A hydrological record extension model for reconstructing streamflows from tree-ring chronologies, *Hydrol. Process.*, 29, 544–556, <https://doi.org/10.1002/hyp.10160>, 2015.
- Sampson, C. C., Fewtrell, T. J., O’Loughlin, F., Pappenberger, F., Bates, P. B., Freer, J. E., and Cloke, H. L.: The impact of uncertain precipitation data on insurance loss estimates using a flood catastrophe model, *Hydrol. Earth Syst. Sci.*, 18, 2305–2324, <https://doi.org/10.5194/hess-18-2305-2014>, 2014.
- Sanyal, J.: Uncertainty in levee heights and its effect on the spatial pattern of flood hazard in a floodplain, *Hydrol. Sci. J.*, 62, 1483–1498, <https://doi.org/10.1080/02626667.2017.1334887>, 2017.
- Savage, J. T. S., Bates, P., Freer, J., Neal, J., and Aronica, G.: When does spatial resolution become spurious in probabilistic flood inundation predictions?, *Hydrol. Process.*, 30, 2014–2032, <https://doi.org/10.1002/hyp.10749>, 2015.
- Scherrer, S. C., Fischer, E. M., Posselt, R., Liniger, M. A., Croci-Maspoli, M., and Knutti, R.: Emerging trends in heavy precipitation and hot temperature extremes in Switzerland, *J. Geophys. Res.-Atmos.*, 121, 2626–2637, <https://doi.org/10.1002/2015JD024634>, 2016.
- Singh, V. P.: Effect of spatial and temporal variability in rainfall and watershed characteristics on stream flow hydrograph, *Hydrol. Process.*, 11, 1649–1669, [https://doi.org/10.1002/\(SICI\)1099-1085\(19971015\)11:12<1649::AID-HYP495>3.0.CO;2-1](https://doi.org/10.1002/(SICI)1099-1085(19971015)11:12<1649::AID-HYP495>3.0.CO;2-1), 1997.
- Smolka, A.: Natural disasters and the challenge of extreme events: Risk management from an insurance perspective, *Philos. T. R. Soc. A*, 364, 2147–2165, <https://doi.org/10.1098/rsta.2006.1818>, 2006.
- Stratz, S. A. and Hossain, F.: Probable Maximum Precipitation in a Changing Climate: Implications for Dam Design, *J. Hydrol. Eng.*, 19, 6014006, [https://doi.org/10.1061/\(ASCE\)HE.1943-5584.0001021](https://doi.org/10.1061/(ASCE)HE.1943-5584.0001021), 2014.
- Totschnig, R., Sedlacek, W., and Fuchs, S.: A quantitative vulnerability function for fluvial sediment transport, *Nat. Hazards*, 58, 681–703, <https://doi.org/10.1007/s11069-010-9623-5>, 2011.
- UNISDR: Making development sustainable: The future of disaster risk management, Global assessment report on disaster risk reduction, 4.2015, United Nations, Geneva, 311 p., 2015.
- Vetsch, D., Siviglia, A., Ehrbar, D., Facchini, M., Gerber, M., Kammerer, S., Peter, S., Vonwiler, L., Volz, C., Farshi, D., Mueller, R., Rousselot, P., Veprek, R., and Faeh, R.: BASEMENT – Basic Simulation Environment for Computation of Environmental Flow and Natural Hazard Simulation, Zurich, 2017.
- Visser, H., Folkert, R. J. M., Hoekstra, J., and de Wolff, J. J.: Identifying Key Sources of Uncertainty in Climate Change Projections, *Clim. Change*, 45, 421–457, <https://doi.org/10.1023/A:1005516020996>, 2000.
- Viviroli, D., Mittelbach, H., Gurtz, J., and Weingartner, R.: Continuous simulation for flood estimation in ungauged mesoscale catchments of Switzerland – Part II: Parameter regionalisation and flood estimation results, *J. Hydrology*, 377, 208–225, <https://doi.org/10.1016/j.jhydrol.2009.08.022>, 2009a.
- Viviroli, D., Zappa, M., Gurtz, J., and Weingartner, R.: An introduction to the hydrological modelling system PREVAH and its pre- and post-processing-tools, *Environ. Modell. Softw.*, 24, 1209–1222, <https://doi.org/10.1016/j.envsoft.2009.04.001>, 2009b.
- Ward, P. J., Jongman, B., Weiland, F. S., Bouwman, A., van Beek, R., Bierkens, M. F. P., Ligtoet, W., and Winsemius, H. C.: Assessing flood risk at the global scale: Model setup, results, and sensitivity, *Environ. Res. Lett.*, 8, 44019, <https://doi.org/10.1088/1748-9326/8/4/044019>, 2013.
- World Meteorological Organization: Manual on estimation of probable maximum precipitation (PMP), 3rd ed., WMO, no. 1045, World Meteorological Organization, Geneva, xxxii, 259, 2009.
- Yuan, X.-C., Wei, Y.-M., Wang, B., and Mi, Z.: Risk management of extreme events under climate change, *J. Clean. Prod.*, 166, 1169–1174, <https://doi.org/10.1016/j.jclepro.2017.07.209>, 2017.
- Zhang, J. and Han, D.: Assessment of rainfall spatial variability and its influence on runoff modelling: A case study in the Brue catchment, UK, *Hydrol. Process.*, 31, 2972–2981, <https://doi.org/10.1002/hyp.11250>, 2017.
- Zoccatelli, D., Borga, M., Viglione, A., Chirico, G. B., and Blöschl, G.: Spatial moments of catchment rainfall: rainfall spatial organisation, basin morphology, and flood response, *Hydrol. Earth Syst. Sci.*, 15, 3767–3783, <https://doi.org/10.5194/hess-15-3767-2011>, 2011.

Paper 22: Zischg, A., Felder, G., Mosimann, M., Röthlisberger, V., Weingartner, R., 2018. Extending coupled hydrological-hydraulic model chains with a surrogate model for the estimation of flood losses in complex river systems. *Environmental Modelling & Software*, 108, 174–185, doi:10.1016/j.envsoft.2018.08.009.



Extending coupled hydrological-hydraulic model chains with a surrogate model for the estimation of flood losses

Andreas Paul Zischg*, Guido Felder, Markus Mosimann, Veronika Röthlisberger, Rolf Weingartner

Institute of Geography, Oeschger Centre for Climate Change Research, University of Bern, CH-3012 Bern, Switzerland



ARTICLE INFO

Keywords:

Model coupling
Surrogate model
Flood loss estimation
Complex river system
River basin-scale

ABSTRACT

In comparison to a local-scale flood risk analysis, modeling flood losses and risks at the river basin scale is challenging. Particularly in mountainous watersheds, extreme precipitation can be distributed spatially and temporally with remarkable variability. Depending on the topography of the river basin and the topological characteristics of the river network, certain rainfall patterns can lead to a synchronization of the flood peaks between tributaries and the main river. Thus, these complex interactions can lead to high variability in flood losses. In addition, flood inundation modeling at the river basin scale is computationally resource-intensive and the simulation of multiple scenarios is not always feasible. In this study, we present an approach for reducing complexity in flood-risk modeling at the river basin scale. We developed a surrogate model for flood loss analysis in the river basin by decomposing the river system into a number of subsystems. A relationship between flood magnitude and flood losses is computed for each floodplain in the river basin by means of a flood inundation and flood loss model at sub-meter resolution. This surrogate model for flood-loss estimation can be coupled with a hydrological-hydraulic model cascade, allowing to compute a high number of flood scenarios for the whole river system. The application of this model to a complex mountain river basin showed that the surrogate model approach leads to a reliable and computationally fast analysis of flood losses in a set of probable maximum precipitation scenarios. Hence, this approach offers new possibilities for stress test analyses and Monte-Carlo simulations in the analysis of system behavior under different system loads.

1. Introduction

Floods are one of the most damaging natural hazards, accounting for a majority of all economic losses from natural events worldwide (UNISDR, 2015). Managing flood-risk requires knowledge about hazardous processes and the impact of floods. Although flood-risk management practice is rapidly changing, the primary approach at present is the prevention of floods by means of constructing flood defense works, such as lateral dams along rivers. Flood protection measures are typically designed on a local-basis and the most optimized solution in terms of cost-benefit analysis (Mechler, 2016; Shreve and Kelman, 2014). The insurance of flood risks is also part of flood-risk management practices. Both the design of flood prevention measures and portfolio risk analyses require sound knowledge of flood hazards within a particular area (Burke et al., 2016). The complex processes occurring in river basins that lead to flooding can be simulated with a cascade of dedicated models (Biancamaria et al., 2009; Felder et al., 2017; Wagner et al., 2016). Thus atmospheric, hydrological, flood inundation and

flood-loss models are run subsequently on the basis of precipitation scenarios (with a certain probability). Recently, remarkable progress was made for developing model chains from atmospheric to hydrological and hydraulic models, either on global-scale (Sampson et al., 2015), continental-scale (e.g., Trigg et al., 2016) or river basin-scale (Lian et al., 2007; Biancamaria et al., 2009; Paiva et al., 2013; Laganier et al., 2014; Falter et al., 2015; Nguyen et al., 2016; Felder et al., 2017).

However, the coupling of atmospheric, hydrological and hydraulic models mostly ends with the hydraulic model. The extension of a model cascade with flood impact models has been rare to date. Thus, only a small number of studies extend the model chains towards a coupled-component model from rainfall to flood-losses. Examples of full model chains from rainfall to flood losses are shown by Alfieri et al. (2016a), Ward et al. (2013, 2015) at global scale, by Alfieri et al. (2016b) at continental scale, by Falter et al. (2014), Falter et al. (2015), Qiu et al. (2017), Schumann et al. (2013), van Dyck and Willems (2013) at large river basin scale, and by McMillan and Brasington (2008), Foudi et al. (2015), Koivumäki et al. (2010) at regional and local scale. In most

* Corresponding author.

E-mail address: andreas.zischg@giub.unibe.ch (A.P. Zischg).

<https://doi.org/10.1016/j.envsoft.2018.08.009>

Received 22 June 2017; Received in revised form 3 July 2018; Accepted 3 August 2018

Available online 04 August 2018

1364-8152/ © 2018 Elsevier Ltd. All rights reserved.

cases, of risk analysis, a cascading modeling approach is followed.

The complexity of the processes triggering floods is determined by spatio-temporal patterns in precipitation (Emmanuel et al., 2015), by the geomorphic characteristics of the sub-catchments of the river basin, and by the synchronization of the flood peaks between the tributaries and the main river channel (Pattison et al., 2014). Particularly in mountainous catchments with a high topographical complexity, the storm track and the precipitation pattern are influenced by the mountain ranges. Thus, the relative timing of peak discharges in river confluences as a consequence of the spatio-temporal distribution of the rainfall pattern have to be addressed (Emmanuel et al., 2016; Zoccatelli et al., 2011). Furthermore, in mountainous areas, the runoff is also determined by the 0 °C isothermal altitude and thus by the share of areas with snowfall rather than rainfall (Zeimet et al., 2017). Hence, an integrated modeling approach and the coupling of specific simulation models is needed to assess the processes leading to floods in river basins with a complex river topology. In addition, if the impacts of floods have to be assessed, the simulation models have to be extended with impact models.

Feasible solutions for impact modeling address the interactions between natural and social/technological systems and include integrated modeling approaches (Kelly et al., 2013; Laniak et al., 2013; Welsh et al., 2013), coupled natural and human systems (Liu et al., 2007; O'Connell and O'Donnell, 2014), or coupled component models (Strasser et al., 2014).

In the case of flood impact modeling, there is a lack of computationally efficient flood-loss models that can be coupled with hydrologic models and used in wider areas at a higher spatial resolution. However, the availability of data needed for flood risk analysis at the river basin scale is constantly improving and with it, the level of detail is rising. Consequently, this non-linearly increases the required computing power. In many cases, probabilistic approaches are required to simulate a high number of flood scenarios (e.g., in Monte-Carlo simulations). Here, a model chain from atmosphere to rainfall-runoff, flood inundation and flood losses reaches its limits due to the lengthy amount of computing time necessary. In addition to the computationally demanding inundation models, the flood loss models require computational resources too, if targeted at single-object scale but applied in a whole river basin. Therefore, the study design of flood risk analysis at the river basin scale has always required a trade-off between the level of detail (spatial resolution) and the size of the study area (Fewtrell et al., 2008; Savage et al., 2016). Usually, with an increasing size of the study area, the spatial resolution decreases (Savage et al., 2015). Thus, there is a gap in methods available for representing a river basin system at a high spatial resolution while contemporaneously maintaining the ability to study the complex interactions between the physical processes and the impact on the values at risk.

However, there are other approaches for dealing with computational demands in integrated environmental models than the variation of the model's spatial resolution. Such approaches include metamodeling strategies, the use of model emulators and surrogate models. Metamodels, model emulators, response surface modeling and surrogate modeling are often used as synonyms (Ratto et al., 2012; Razavi et al., 2012a). The principal idea behind surrogate models is emulate and to replace the complex simulation model requiring high computational resources with a simplified and fast-to-run model (Castelletti et al., 2012; Yazdi and Salehi Neyshabouri, 2014). A surrogate model can be derived by simplifying the process-based model structure, or by generalizing the studied system's behavior with a low-order approximation of a set of outcomes of a model experiment with the complex model (Castelletti et al., 2012). Dynamic emulation modeling aims at preserving the dynamic nature of the original process-based model and is, thus, preferably used for reducing complexity (Castelletti et al., 2012). Surrogate models are often used in applications that require a large number of model runs, e.g. in sensitivity analysis, in scenario analysis, and in optimization. In flood management applications,

surrogate models have been used for reservoir operation (Castro-Gama et al., 2014; Tsoukalas and Makropoulos, 2015), water resources management (Tsoukalas et al., 2016) and for reducing the complexity in hydraulic simulations (Gama et al., 2014; Meert et al., 2016; Wolfs et al., 2015). A review of surrogate modeling in hydrology is given by Razavi et al. (2012b). Nevertheless, Saint-Geours et al. (2014) and Marrel et al. (2011) stated that the development of surrogate models with spatially distributed inputs and outputs is still an open research question. This also applies to object-based flood loss modeling, where a 2D inundation model computes flow depths for each affected building and the loss model computes the damages on the basis of the flow depths, a vulnerability function, and the building value.

Hence, the question arises if a surrogate modeling approach is suitable to represent the inherent complexities of flood processes that lead to flood losses within a river basin. Specifically, we aim to assess whether the surrogate modeling approach is able to represent the flood processes and their impacts at the river basin scale with a spatial resolution at street level. Thus, the main aim of this work is to develop a surrogate model for flood loss analysis and to evaluate its applicability in the context of a model experiment with multiple scenarios covering different spatiotemporal patterns of rainfall over a river basin with a complex topography. Within this context, the hypothesis is that a river system can be divided into subsystems which are connected within a topological river network (Wolfs et al., 2015). The reaction of the whole system to a flood scenario can then be deduced from the reactions and interactions of the subsystems. Thereby, we aim at contributing to the discussion about the use of surrogate models in model simplification (Crout et al., 2009; van Nes et al., 2005) and in flood risk analyses (Wolfs et al., 2015; Wolfs and Willems, 2013).

2. Methods

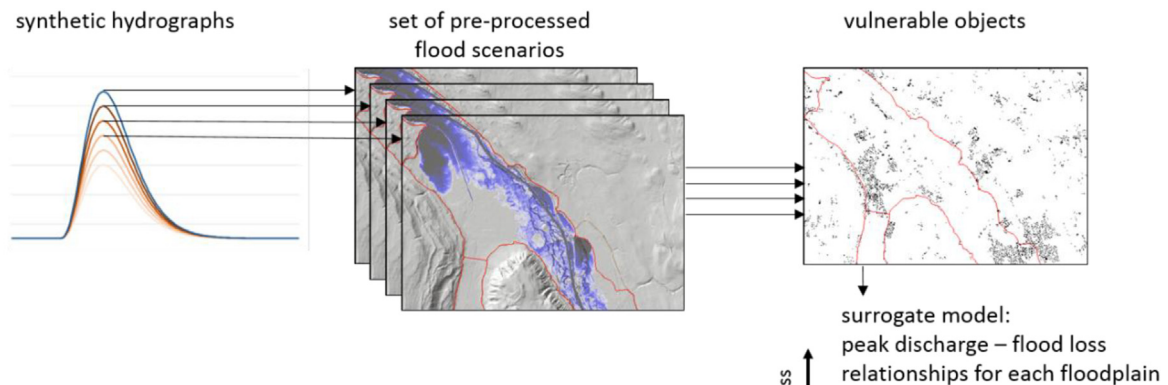
The main goal of flood risk analysis at the river basin scale is to analyze the potential consequences of a selected precipitation scenario or a set of scenarios. This is done by a model cascade of rainfall-runoff models with 2D hydraulic models producing the flow depths for the flood loss models. Here, we propose a different method, where the last two models are substituted. The 2D hydraulic model and the flood loss model are replaced by a 1D hydraulic model with a surrogate model for flood loss computation nested into the 1D hydraulic model. This requires two main steps. First, the surrogate model has to be developed. Then, the surrogate model is introduced into the model chain with reduced complexity. We tested this method on the Aare River basin, located upstream of Bern, Switzerland.

This chapter is organized as follows. First, the case study and the definition of the system under consideration are described in detail. Second, the development of the surrogate model is described. The interrelation between the two main steps is shown in Fig. 1. Third, we describe the model evaluation procedure. The methods chapter is concluded with a description of the setup and the application of the model chain for flood loss analyses.

2.1. System definition and system delimitation

The study area is the watershed of the Aare River located upstream of Bern, Switzerland (see Fig. 2). The river basin has an area of approximately 3000 km² and thus is defined as a mesoscale catchment. The river network consists of 26 tributary catchments (sub-catchments), with confluence into the floodplains of the main valley. The main valley is divided into seven floodplains. These are the floodplains of the river reaches “Hasliaare”, between Meiringen and Lake Brienz (1), the coastal areas of “Lake Brienz” (2), the flood plain of the city “Interlaken” and the river Lüttschine (3), the coastal areas of “Lake Thun” (4), the floodplain of the city “Thun” (5), the river “Aare”, between Thun and Bern (6), and the tributary “Gürbe”, between Burgstein and Belp (7). The flooding processes in the Aare River basin are dominated by

A. Development of the surrogate model



B. Implementation of the surrogate model in a model chain

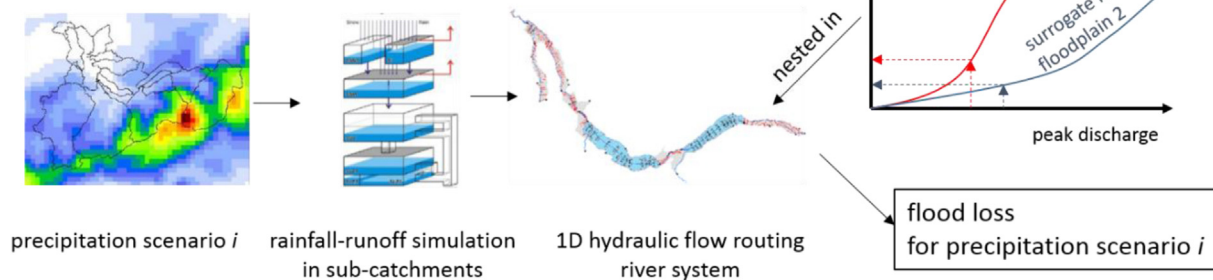


Fig. 1. Overview of the method. The first step is to develop the surrogate model. The second step is to nest the surrogate model into a model chain from the meteorological model to a rainfall-runoff and 1D hydraulic routing model.

both riverine and lake flooding. The Hasliaare floodplain is dominated mainly by riverine flooding. However, the delta of the Hasliaare floodplain is also affected by flooding from Lake Brienz. The lateral shorelines of Lake Brienz and Lake Thun are exposed to lake flooding only. In contrast, the city of Interlaken is exposed to four different flooding processes. In the eastern part, this floodplain is exposed to lake flooding from Lake Brienz. The western part is exposed to lake flooding from Lake Thun. A high water-level in Lake Brienz leads to a high discharge in the Aare River, between the two lakes. Consequently, the central part of the city of Interlaken is exposed to riverine flooding. From the southern boundary of the floodplain, the tributary Lüttschine River flows into Lake Brienz with the occurrence of riverine flooding possible. The city of Thun is exposed to both lake flooding from Lake Thun and riverine flooding from the Aare River at high lake levels. The floodplain of the Aare River between Thun and Bern and the floodplain of the Gürbe River are exposed to riverine flooding. The discharge of the Aare River downstream of Thun is dominated mainly by the outflow from Lake Thun and secondarily by its tributaries. Transport and deposition of sediment and woody debris were not considered in this analysis.

The physical processes in the river system considered here are principally defined as flood processes leading to losses at buildings. The main driver for the amount of losses due to flooding is the flood magnitude (i.e., peak discharge and lake level), with the related flow depths at the location of the exposed buildings. Thus, we assume here that there is a relevant relationship between the flood magnitude and the values at risk. In addition to the flood magnitude, this relationship also depends upon the hydromorphic characteristics of the floodplain (i.e., how the building stock is topographically and topologically located within or outside the flooded areas) and the characteristics of the building stock (economic values and vulnerabilities). This relationship can also be named as the exposure “footprint” of a floodplain (Rougier

et al., 2013). This approach was described by Hubbard et al. (2014) for an urban area exposed to flooding. Here, this approach is extended to a number of floodplains. Each floodplain is defined as a subsystem of the whole river basin. The input of the upper boundary condition of a subsystem is the inflow of water. The magnitude of the boundary condition is defined by the peak discharge in a river reach in the case of riverine flooding and by the lake level in case of lake flooding. The fluxes (flood flows) between the subsystems are modelled with the hydrodynamic model BASEMENT in 1D (BASEchain, Vetsch et al., 2017). Fig. 3 shows the spatial setup of the river system and the topology between the subsystems.

2.2. Development of the surrogate model

The surrogate model is built in three steps. First, for each subsystem (i.e., floodplain), the range of system loads at the upper boundary condition were defined. On the basis of an observed discharge time-series, typical flood hydrographs, i.e. a synthetic design hydrograph, were derived using the guidelines proposed by Serinaldi and Grimaldi (2011). For each river gauging station in the study area, observed hydrographs were normalized in terms of event duration and peak discharge. The resulting dimensionless event hydrographs were superimposed, and centered around the peak position. A two parametric gamma distribution function was fitted to represent the typical shape of the event hydrographs, as described by Nadarajah (2007) and Rai et al. (2009). This resulted in a synthetic unit hydrograph that represents a typical hydrograph shape of flood events in the corresponding catchment. The synthetic unit hydrograph was scaled to various peak discharges, whereas an empirical peak-volume-ratio was used to determine the corresponding event duration. Recently developed techniques for the determination of flood-type-specific synthetic design hydrographs, as for example proposed by Brunner et al. (2017), were

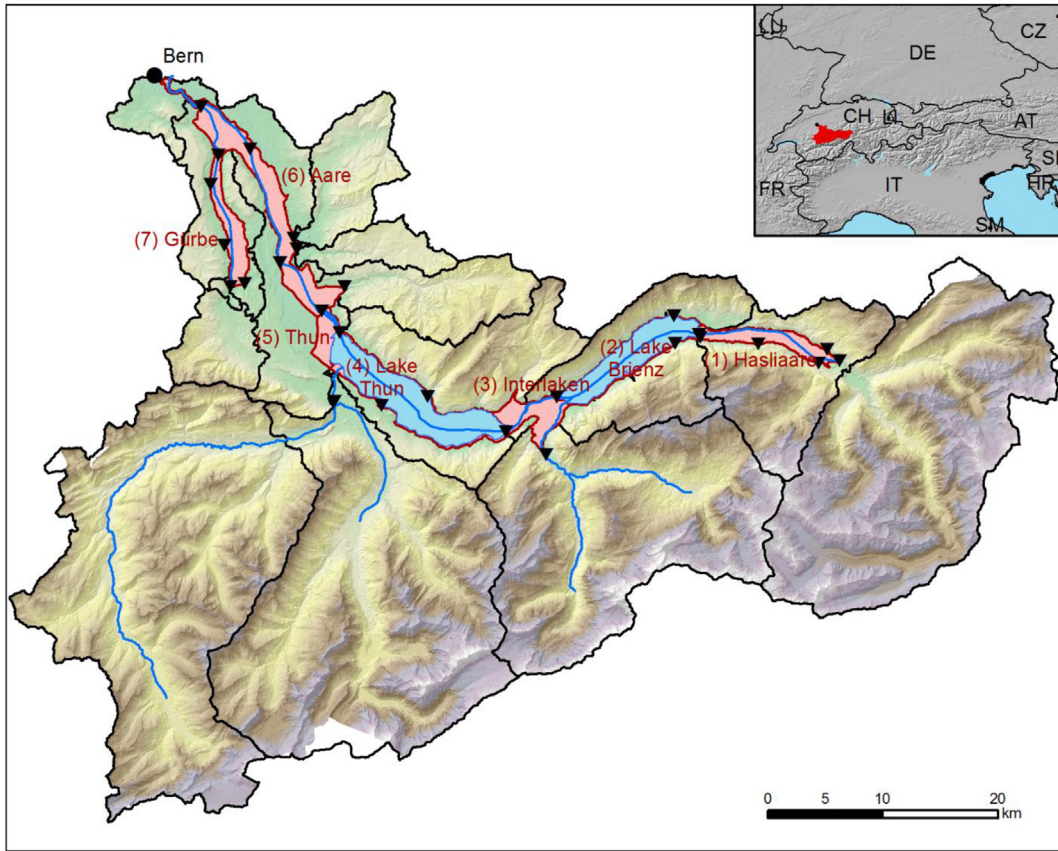


Fig. 2. Aare river basin upstream of Bern, Switzerland. The sub-catchments of the hydrological model are divided by black lines. The black triangles are indicating the points where the outflow from the subcatchments is used as a system load at the upper boundary conditions of the floodplains. The floodplains that are represented by the surrogate model are marked in red. (For interpretation of the references to colour in this figure legend, the reader is referred to the Web version of this article.)

not considered in this study. The procedure was applied to generate synthetic design hydrographs for a continuous series of peak discharges for each of the floodplains affected by riverine flooding (Hasliaare River, Lütschine River, Aare River between Thun and Bern, Gürbe River). The synthetic design hydrographs were used as upper boundary conditions for the 2D inundation model of each floodplain.

In the second step, we developed a flood inundation model in 2D for each floodplain. We used the flood inundation model BASEMENT in 2D (BASEplane) to represent the water fluxes through the river systems (Vetsch et al., 2017). It is a numerical model solving the shallow water equations on the basis of an irregular mesh. The mesh was generated on the basis of a digital terrain model (DTM) of the year 2015, with a

spatial resolution of 0.5 m and a maximum error of ± 0.2 m in the z-axis orientation. In the river courses, the DTM was corrected on the basis of topographical surveys of the riverbed. These data were delivered by the Federal Office for the Environment, FOEN. The heights and location of the lateral dams were surveyed by dGPS. Together, all data sources result in a high-resolution terrain model. In the flood models, the roughness coefficients in the river channels were calibrated with existing stage-discharge relationships. The roughness coefficients in the floodplains were estimated based on literature. The floodplains are delimited by the lateral dimensions of the floodplains (i.e., the confining hillslopes). The upper system boundaries are the main river courses flowing into the floodplains. The lower system boundary is

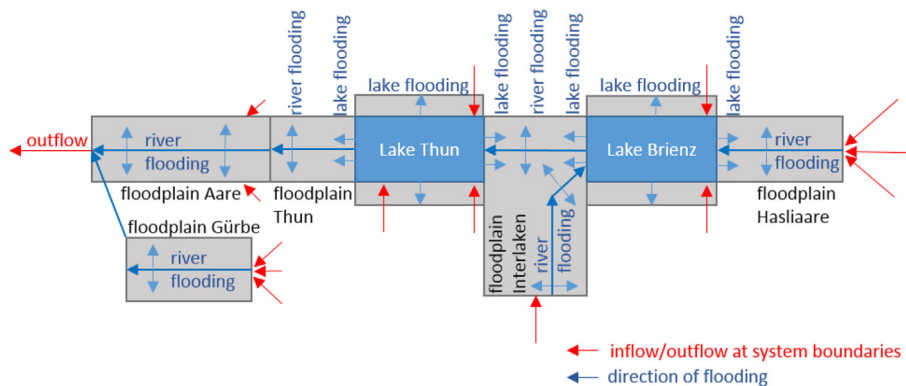


Fig. 3. Simplified representation of the river system. The floodplains are represented in gray. The type of flooding process is represented by blue arrows. (For interpretation of the references to colour in this figure legend, the reader is referred to the Web version of this article.)

determined by the lakes, or other topographic or geomorphologic constraints delimiting the floodplains.

The 2D hydrodynamic model provides the basis for the flood-loss model. In this study, we focus only on structural damages to buildings (i.e., residential, public and industrial buildings). Damages to mobile assets, building content, movables and infrastructure are not considered here. The loss model consists of a dataset of buildings with attributes and a set of vulnerability functions. Each building is represented by a polygon and classified by type, functionality, construction period, volume, reconstruction costs, altitude level of ground floor and number of residents. The dataset of the values at risk was elaborated on the basis of the SwissBuildings^{3D} dataset of the Federal Office for Topography SWISSTOPO, based on the approaches of Fuchs et al. (2017); Röthlisberger et al. (2017), and Röthlisberger et al. (2016). The reconstruction values of the buildings were calculated on the basis of the volume (derived by the Lidar surface and terrain models) and the mean prices per cubic meter and building function (SVKG-SEK/SVIT, 2012), accordingly to the practice in Switzerland. The flood intensity maps (flow depths), resulting from the hydrodynamic models, lead to the calculation of the object-specific vulnerability and therefore to the estimation of object-specific losses (Fuchs et al., 2012; Zischg et al., 2013). Vulnerability functions provide a degree of loss on the basis of the flow depth at the location of the house. The value ranges from 0 (no damage) to 1 (total loss). This degree of loss is subsequently multiplied by the specific reconstruction value of the building. Currently, three vulnerability functions are considered in the damage calculation procedure. We used the functions of Hydrotec (2001), Jonkman et al. (2008), and Dutta et al. (2003), shown in Fig. 4. The multiplication of the reconstruction value of the house with the degree of loss leads to the flood-loss for a specific exposed object (e.g., a single house). The sum of all losses in the floodplain enters into the “flood peak – flood loss” relationship of the floodplain.

We modelled the inundation for each floodplain and specific set of synthetic hydrographs. This results in a number of simulations ranging from the river discharge capacity to a worst case flood. Each model run was overlain with the building dataset and the degree of loss was calculated for each single building on the basis of the flow depth at the building, as well as the resulting loss. Thus, for each synthetic hydrograph, a sum of flood losses in the floodplain is computed. Furthermore, the number of exposed buildings and the number of exposed residents are summarized. Generally speaking, this follows the dynamic emulation modeling approach of Castelletti et al. (2012). With peak discharge (flood magnitude), the resulting flood losses and exposed buildings/residents increases. For each floodplain, the shape of this relationship between flood magnitude and flood losses is calculated. These

floodplain-specific curves are the basis of the meta-model, or surrogate model for further analyses. The surrogate model can then be used to extend coupled hydrological-hydraulic model chains by nesting it into the 1D hydrodynamic model.

2.3. Model evaluation

The complexity of the model chain requires a validation of the surrogate model and of the surrogate model coupled with the hydrologic/hydraulic model. In addition, the 2D inundation model used for the elaboration of the surrogate model has also to be validated separately. Thus, the coupled hydrologic-hydraulic model, the 2D inundation model, and the surrogate model were validated separately and in the coupled version.

First, the coupled hydrologic hydraulic model (1D) was validated against the observed discharge at the catchment outlet in the validation period from 2011 to 2014. For this, we computed the Nash-Sutcliffe-Efficiency NSE (Nash and Sutcliffe, 1970) and the Kling-Gupta-Efficiency KGE (Gupta et al., 2009; Kling et al., 2012).

Second, the 2D inundation models used to elaborate the surrogate model were validated with post-event data of the floods in May 1999, and August 2005 (Table 1). The main purpose of the 2D inundation model is to predict the number of affected buildings and to predict the flow depths at the buildings. Thus, a validation of this model should weight the populated areas higher than the areas without values at risk (Stephens et al., 2014). As the surrogate model gives the number of exposed buildings and the flood losses as outputs, we adapted a validation approach proposed by (Zischg et al., 2018) that explicitly focuses on the validity of the flood models in populated areas. They proposed to adapt binary performance measures to be used with insurance claims for validating flood models. Hence, we validated the model performance with the model fit measure F (Bennett et al., 2013, eq. (1), also defined as critical success index CSI or flood area index FAI). This measure can be computed by either considering the predicted and observed flooded areas or the number of affected and not affected buildings. If based on the flooded areas, this performance measure requires a comparison of the spatial pattern of the observed and the modelled wet and dry areas. If the populated areas should be weighted higher, this performance measure can be computed by overlaying the map of the observed flood extent with the dataset of the buildings. The buildings within the observed flood extent represent the reference observation dataset. Subsequently, these buildings are compared with the buildings located in the modelled flood extent. Buildings correctly predicted as inundated, count as hits. Buildings predicted as dry by the model and observed as inundated, are counted as misses. Buildings predicted as wet by the model but observed as dry are defined as false alarms. Correct negatives are buildings that are predicted and observed as dry (outside of observed flood extent). The validation of the 2D inundation model of the floodplains of Interlaken and Thun is described in Zischg et al. (2018).

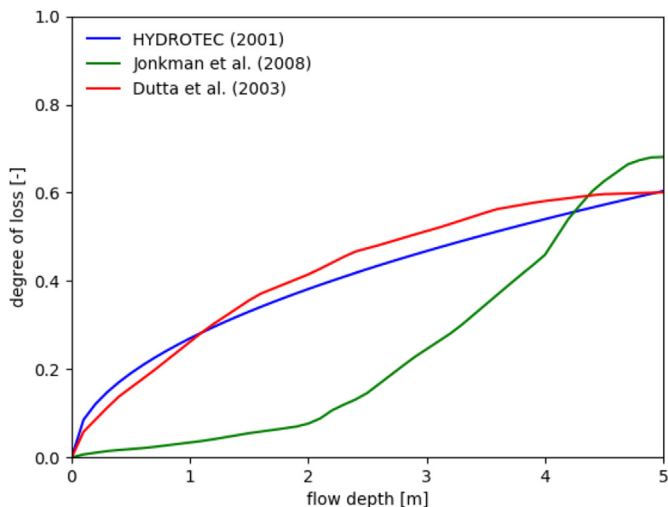


Fig. 4. Vulnerability functions used for flood loss estimation.

Table 1
Peak discharges and return levels of the flood events used for model evaluation. Source: FOEN (2018).

River reach	May 12–16, 1999	August 22–23, 2005	October 10–11, 2011	Peak discharge of a 100-year flood
Hasliaare River	228 m ³ /s < 10 yy	444 m ³ /s 47 yy	367 m ³ /s 22 yy	538 m ³ /s
Lütschine River	126 m ³ /s < 2 yy	254 m ³ /s > 150 yy	226 m ³ /s 68 yy	239 m ³ /s
Aare River at Bern	613 m ³ /s > 150 yy	605 m ³ /s > 150 years	416 m ³ /s < 10 yy	551 m ³ /s
Gürbe River	44.6 m ³ /s < 10 yy	52.1 m ³ /s 20 yy	8.08 m ³ /s < 1 yy	60.7 m ³ /s

$$F = \frac{\text{hits}}{\text{hits} + \text{false alarms} + \text{misses}} \quad (1)$$

Third, the surrogate model was coupled with the hydrologic/hydraulic model chain and validated with event documentations from three past flood events based on the number of affected buildings. We counted the number of buildings that are located within the areas that were reportedly flooded during the flood events in May 1999 August 2005, and October 2011, respectively. The characteristics of these reference flood events are summarized in Table 1. Subsequently, we computed the number of affected buildings in these three flood events with the surrogate model. For the flood event of 1999, we used the observed discharges for calculating the number of affected buildings with the surrogate model. In contrast, we used both the observed and modelled discharges of the hydrologic/hydraulic model chain to calculate the number of affected buildings during the flood events of 2005 and 2011. Consequently, we compared the modelled number of affected buildings with the observed ones.

Fourth, we analyzed the relative error of the surrogate model. Depending on the range of peak discharges - from the river conveyance to the probable maximum flood - we selected different intervals of the synthetic hydrographs used for computing the surrogate model. In the Aare River reach, we used intervals of $100 \text{ m}^3/\text{s}$ to compute the surrogate model, while in the other floodplains we used intervals of $50 \text{ m}^3/\text{s}$, except in the Gürbe River reach. In this floodplain, we used intervals of $5 \text{ m}^3/\text{s}$. To estimate the interpolation error, we doubled the intervals of the peak discharges for deriving the surrogate model and compared the interpolated value of the coarser surrogate model with the values of the original surrogate model. The interpolation error is represented here by the root mean square error (RSME). However, the surrogate models of the lakes are based on a continuous simulation and thus we did not analyze the sensitivity of these models to an increase of the interval.

Fifth, we modelled one out of the 150 model runs with the full 2D simulation model. We selected the model run with the highest peak discharge at the river basin outlet at Bern, corresponding to the probable maximum flood. This model run was used as a benchmark to evaluate the performance of the surrogate model for this scenario.

A validation of the loss module was not possible, as corresponding loss data are protected by privacy regulations of the corresponding Cantonal insurance company. However, the predicted flood losses were validated in another case study using the same model setup with observed loss data delivered by the Cantonal insurance company for buildings (Zischg et al., 2018). In the river reach of the Engelberger Aa River in the Canton of Nidwalden, the flood event of August 2005 led to losses of around 22 million Swiss Francs. The vulnerability function of Jonkman et al. (2008) underestimated the losses (26% of documented losses), whereas the vulnerability function of Hydrotec (2001) overestimated the losses by a factor of 2.7, and the vulnerability function of Dutta et al. (2003) by a factor of 2.1. Thus, we assume that the three different vulnerability functions should quantify a range of possible outcomes and the most reliable loss estimation lays in between different outcomes.

2.4. Computing the system behavior and the flood losses during probable maximum precipitation scenarios

We tested the applicability of the surrogate model with a set of extreme flood scenarios based on the probable maximum precipitation (PMP). The PMP is often used for the analysis of residual risks and furthermore for identifying the probable maximum flood (PMF) in a river basin. The PMP in the study area was estimated after the guidelines of WMO (World Meteorological Organization, 2009). To consider the spatio-temporal patterns of precipitation in the river basin, the same amount of areal precipitation in the PMP scenario (300 mm in 3 days) was distributed in different spatio-temporal patterns across the entire

river basin in a Monte-Carlo-simulation framework after Felder and Weingartner (2016). In a first step, a random temporal distribution of the total precipitation for the chosen duration was generated. In a second step, the temporal pattern of the rainfall was distributed spatially in three meteorological regions, and in five sub-catchments within each meteorological region. The sub-catchments and the meteorological regions were defined to consider the relatively independent behavior of specific parts of the catchment, e.g. lowlands and mountainous regions, in terms of precipitation amount and intensity. A set of plausibility criteria evaluates the physical reliability of the randomly generated rainfall pattern. For further details we refer to Felder and Weingartner (2016). From a set of physically valid 10^6 iterations, we extracted 150 scenarios that lead to the highest discharge at the catchment outlet. These rainfall scenarios were fed subsequently into the hydrological model (Felder et al., 2017). The rainfall scenarios were modelled in 15 sub-catchments with the hydrological model PREVAH (Viviroli et al., 2009). The discharge at the outlets of the sub-catchments was routed through the river system with the hydraulic model BASEMENT in 1D (Vetsch et al., 2017). The hydrodynamic model is based on the St. Venant equations and computes the water fluxes in 1D. This model allows for simulation of the weirs at the outlets of the lakes within the river network and thus is able to simulate lake levels. The 1D hydrodynamic model was calibrated by empirically adjusting the friction coefficients in the river channels with particular regard to the water surface elevation in the main channel at peak discharge. The setup of this system is described in detail by Felder et al. (2017) and Felder and Weingartner (2017). The surrogate model described in chapter 2.2 is nested into this 1D hydraulic model. The 1D hydraulic model provides the upper boundary conditions for the single floodplain models. The peak discharge is then extracted from the modelled inflow hydrographs and used for interpolating the flood losses from the surrogate models of each floodplain. The losses of the single sub-models are then summed up for each precipitation scenario. We computed the number of exposed buildings and residents and the flood losses for 150 scenarios. Out of 10^6 simulations, these scenarios had the highest discharge at the outlet of the river basin in Bern. Thus, this can be assumed as a set of extreme floods. The scenario with the highest discharge at Bern was modelled with the 2D simulation model as a reference run. In the 2D simulation, the tributaries flowing into the floodplains from the lateral boundaries are considered, as well as in the loss model. The same scenario was then simulated with the surrogate model. Finally, the reliability of the surrogate model was evaluated by comparing it with the reference model run.

3. Results

3.1. Surrogate model

The primary result of the first part is the “flood magnitude – flood exposure” relationship for each floodplain. In Fig. 5, these relationships are presented for riverine floods. Here, the sensitivity of the floodplain against peak discharges is shown in terms of the number of exposed buildings and people. The figure shows that the floodplain of the Lüttschine River reach is the sub-model with the highest sensitivity to an increasing peak discharge. The Lake Thun sub-model is that which has the highest sensitivity against a rising lake level (Fig. 6). It is shown that the exposure of residents is increasing, on average, by 38 residents per cm of rising lake level.

Regarding flood losses, the “flood magnitude – flood loss” relationships exhibit shapes similar to that of the “flood magnitude – flood exposure” relationships. In contrast to the exposed buildings and residents, the figures for the losses show the uncertainty in flood loss estimation in relation to the vulnerability functions. The vulnerability function of Jonkman et al. (2008) results in remarkably low losses (Figs. 7 and 8). Fig. 8 shows that the floodplain of Thun is the sub-system with the highest sensitivity to increasing flood magnitudes.

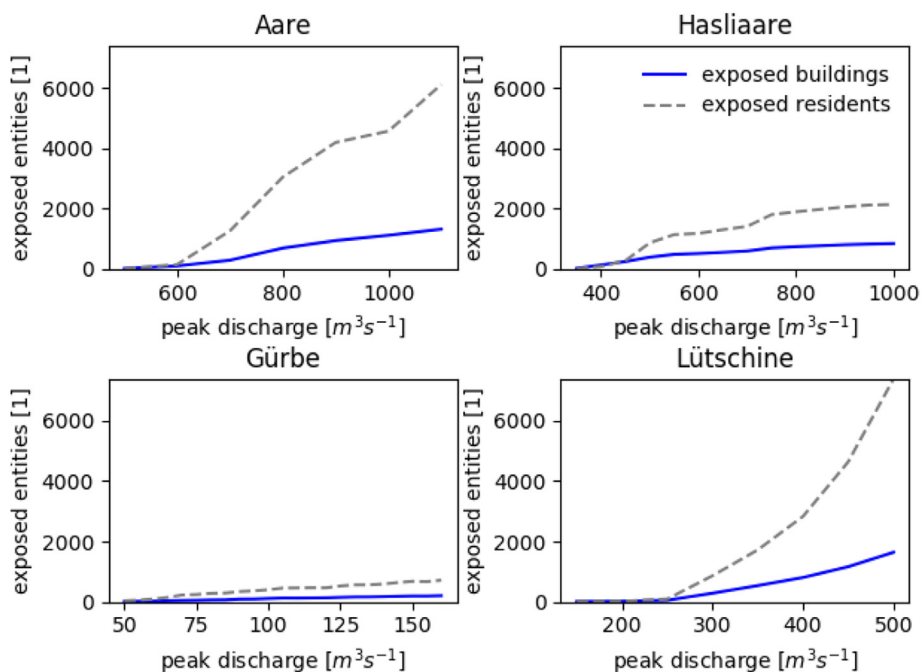


Fig. 5. “Peak discharge – flood exposure” relationships for the floodplains with riverine flooding.

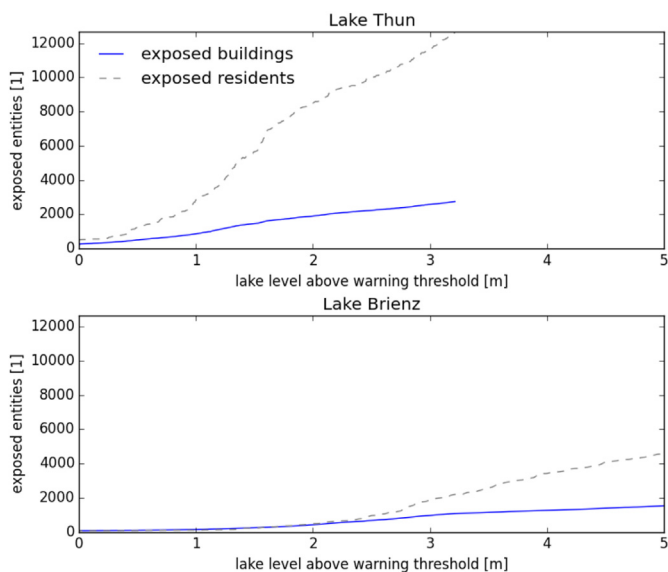


Fig. 6. “Lake level – flood exposure” relationships for the floodplains with lake flooding. Warning thresholds for Lake Thun: 558.3 m a.s.l.; warning threshold for Lake Brienz: 563.9 m a.s.l.

3.2. Model evaluation

The model evaluation showed that both the single modules and the model chain can be used reliably in this study. The coupled hydrologic-hydraulic model has a NSE value of 0.85 and a KGE value of 0.85 in the validation period 2011–2014.

The 2D inundation model was validated with the flood event in August 2005. Based on the observed discharges and flooded areas of the flood event in August 2005, the 2D flood model of the Aare and Gürbe river reaches exhibit a model fit of 0.62, the model of the floodplain in Thun has a model fit of 0.61, and the model of the floodplain in Interlaken has a model fit of 0.68 (with consideration of the dam break in the Lütschine River). In the Hasliaare river reach, a dam break occurred and thus the observed flooded areas are remarkably higher than

the modelled ones. In contrast to the Lütschine river reach, this dam break was not modelled in the validation run and thus no validation was possible for this river reach and this flood event. Calculating the model fit on the basis of the modelled discharges (model chain of the coupled hydrological-hydraulic model based on precipitation as the model input, and whole study area), gives a model fit of 0.46 when considering flooded areas in the validation metric and a model fit of 0.49 when considering the number of exposed buildings, respectively.

The output of the surrogate model in terms of number of exposed buildings was compared with the observed number of affected buildings. However, in the corresponding simulation, the dam breaks that occurred in the Hasliaare river reach and in the floodplain of the Lütschine river during the flood event in 2005 were not considered and, thus, the surrogate model underestimates the number of exposed buildings. The surrogate model nested into the full model chain predicted 1643 affected buildings, while 2366 buildings were actually located in the flooded areas of the 2005 event (Table 2). In contrast, when run with the observed discharges of the flood event in May 1999, the surrogate model predicts 995 affected buildings, while 1059 buildings were actually located in the flooded areas. This corresponds to an underestimation of 6%. However, the surrogate model neglects a dam break in the Aare River reach during the flood event in 1999 and, thus, underestimates the exposed buildings in this area. For the 2011 flood event, the surrogate model predicts 132 and 38 affected buildings with observed and modelled discharges, respectively. At river basin scale, the full 2D model nearly predicts the exact number of buildings affected by the 2011 flood. However, when looking at the detail, there is a slight underestimation in the Hasliaare River reach and a slight overestimation in the Lütschine River reach. The hydrological model underestimates the peak discharges during this rain-on-snow flood event (Rössler et al., 2014) and thus the surrogate model underestimates the number of affected buildings when implemented into the full model chain.

A comparison of the presented surrogate models with coarsened surrogate models shows that the number of simulations for elaborating the surrogate model and thus the intervals between the considered flood magnitudes is relevant for the robustness. The submodels have an RMSE of 54 buildings in the Aare River reach, 16 in the Hasliaare River reach, 28 in the Lütschine River reach, and 7 in the Gürbe River reach.

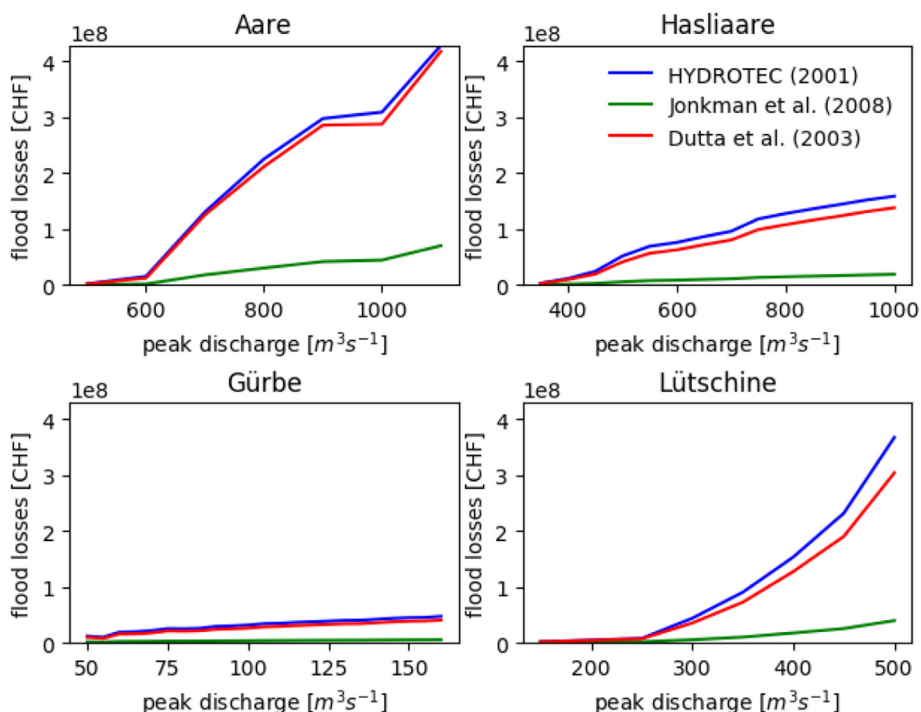


Fig. 7. “Peak discharge – flood loss” relationships for the floodplains with riverine flooding.

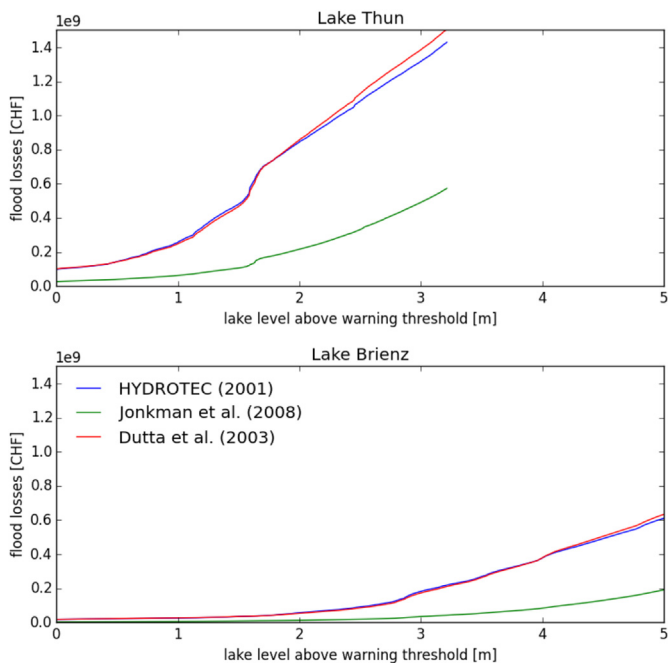


Fig. 8. “Lake level – flood loss” relationships for the floodplains with lake flooding. Warning thresholds for Lake Thun: 558.3 m a.s.l.; warning threshold for Lake Brienz: 563.9 m a.s.l.

For the 2005 flood event, the RSME lays in the order of 48% of the exposed buildings in the Aare River reach and of 0.5–3.9% in the other river reaches. In terms of flood losses, the RMSE is 43.5, 1.5, 1.8, and 1.4 million Swiss Francs, respectively. While the RMSE is highly relevant for the Aare River reach, it is less relevant for the other river reaches. The surrogate model of the Aare River reach is already based on wide intervals of the peak discharges and thus a coarsening of the intervals leads to remarkable model errors. In contrast, narrow intervals increase the robustness. This is especially relevant for peak discharges

around the river conveyance capacity.

The benchmark test with the selected scenario run in full 2D mode shows the applicability of the surrogate model in the case of extreme floods. The surrogate model predicts 3294 exposed buildings and 15413 residents, whereas the full 2D simulation predicts 3720 exposed buildings and 17261 residents. Thus, the losses are underestimated in the surrogate model in comparison to a full 2D simulation. The simplified model underestimates the number of exposed buildings and the number of exposed residents by 11%, and the computed losses by 13–23%, depending on the vulnerability function. The deviation can be explained by the flooding of smaller lateral tributaries, which the reference model considers in contrast to the surrogate model. These smaller tributaries did not lead to flooding in the validation runs. In the Hasliaare River reach, the reference model run simulates flooding that is mainly due to the tributaries. Thus, in this river reach, the surrogate model does not consider the flooding of more than 200 buildings. In the Aare River and Gürbe River reaches, the surrogate model underestimates the exposure of 188 and 275 buildings respectively for the same reason.

3.3. Model application

The combination of the single surrogate models was used in a Monte-Carlo framework for modeling flood losses of probable maximum precipitation scenarios. This results in a high number of outcomes, rather than a single value in a deterministic framework (Fig. 9). The number of exposed buildings range from 2181 to 3661 depending on the precipitation scenario, with a median of 2768. Thereby, a minimum of 8569 and a maximum of 16175 residents are exposed as a result. The median of the exposed residents is 11079. However, the histogram of the losses (Fig. 9) shows a double peak. This double peak is a consequence of the different vulnerability functions. While two vulnerability functions (Dutta et al., 2003; Hydrotec, 2001) have relatively similar shapes, the third vulnerability function (Jonkman et al., 2008) shows remarkable differences to the others up to flow depths of 3 m. The left peak in the histogram at the right of Fig. 9 shows the losses calculated with the vulnerability function of Jonkman et al. (2008), the

Table 2

Number of exposed buildings in the flooded areas of the flood events of May 1999, August 2005, and October 2011. *surrogate model based on observed discharges and lake levels. **surrogate model based on observed precipitation and, thus, based on modelled discharges and lake levels. ***No consideration of levee breaches.

floodplain	1999 obs.	1999 surrogate model*	2005 obs.	2005 surrogate model*	2005 surrogate model**	2011 obs.	2011 2D*	2011 surrogate model*	2011 surrogate model**
Hasliaare River and Lake Brienz	3	33	412	***265	***191	31	16	60	1
Interlaken (Lütschine River and both Lakes)	110	93	941	***161	***141	13	33	38	12
Thun (Aare River and Lake Thun)	308	353	408	397	723	0	0	0	0
Aare River between Thun and Bern	258	***126	111	110	137	0	0	0	0
Gürbe River	0	0	14	16	0	0	0	0	0
lateral lake shorelines	380	390	480	406	451	31	34	34	25
whole study area	1059	995	2366	1355	1643	86	83	132	38

right peak in the histogram shows the losses of the other two vulnerability functions. Consequently, the losses range from 129 to 1499 million Swiss Francs, with a median of 782 million Swiss Francs. The loss footprint of the floodplains allows us to understand which precipitation pattern leads to the highest losses. High losses are associated with a high level of Lake Thun and a high discharge in the Lütschine River.

4. Discussion

The presented meta-modeling approach in a river basin is a combination of surrogate models. The main benefit of this approach is that it enables analysis of the behavior of a complex river system under varying system loads. The basis of the model is a 1D hydrodynamic routing model (Vetsch et al., 2017) that routes the inflow fluxes from the sub-catchments, provided by the hydrological model through the connected floodplains. The flood loss sub-models are nested into this hydrodynamic routing model, similar to Alarcon et al. (2014), Mani et al. (2014) and Bermúdez et al. (2017), except in the form of surrogate models. Since the 1D hydrodynamic routing model is remarkably (~2000–4000 times) faster than the 2D flood inundation model with a high spatial resolution, the combination of the 1D hydrodynamic model with the surrogate for flood loss computation offers a high potential in scenario-based flood risk analyses and in other applications that demand low computational costs. This is in line with the conclusions of Wolfs and Willems (2013) and Wolfs et al. (2015). Because the meta-

model is derived from a flood inundation model in a very high spatial resolution (accuracy at the sub-meter resolution), the high spatial accuracy can be brought to the river basin scale in a computationally efficient framework. Hence, the presented model can be used in Monte-Carlo simulations, targeting flood loss analyses, as shown in the example of probable maximum precipitation scenarios. If the number of scenarios to be simulated remarkably exceeds the number of synthetic hydrographs required for building the surrogate model, the simplified model is able to reduce the computational costs.

However, the presented surrogate model has still notable uncertainties. In comparison to a full 2D simulation, it introduces an interpolation error. This error depends on the intervals of flood magnitudes that are as reference simulations needed for elaborating the meta-model. This is especially relevant for flood events with a high frequency but it can be solved by increasing the number of simulations with a magnitude slightly below and above river conveyance capacity. Furthermore, the surrogate model represents the errors of the 2D model and the loss model. A crucial factor is the spatial representation and attribution of the buildings. Uncertainties in the building dataset are directly relevant for the prediction capability of the surrogate model. Both errors, either caused by the model simplification or by the 2D inundation and flood loss models, contribute to the total error. While the first is more easily to consider by increasing the number of simulations in the pre-processing and elaboration of the surrogate model, the errors in the inundation and flood loss models are in many cases difficult to detect and to quantify because of lacking documentation of

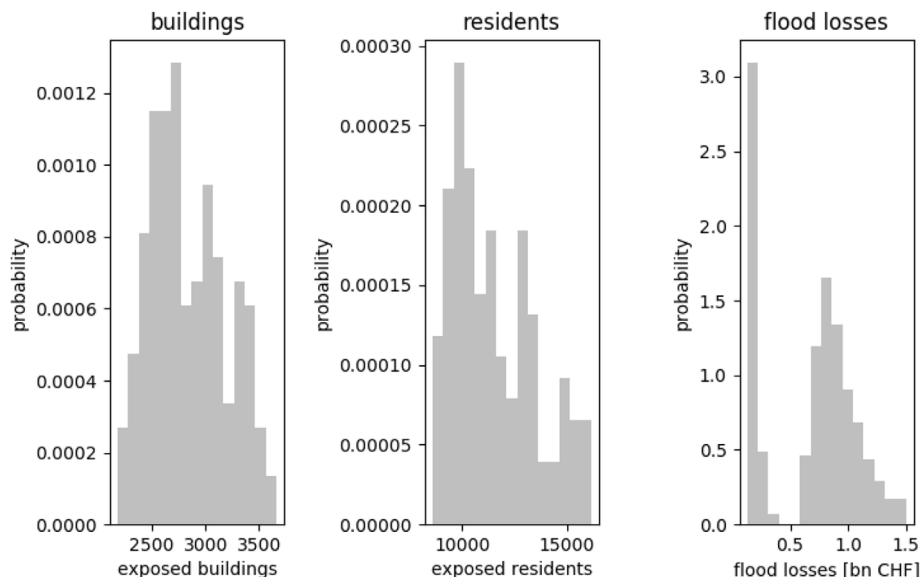


Fig. 9. Histograms of exposed buildings and residents, and flood losses in 150 PMP scenarios.

historic flood events and their impacts. Last but not least, the surrogate model depends on reliable predictions of peak discharges and thus it heavily depends on the reliability of the coupled hydrologic/hydraulic model. A comparison of the loss estimations that are based either on observed or modelled discharges showed that the uncertainty in the prediction of the peak discharges is still the one of the most relevant contributions to the overall uncertainty.

In general, the surrogate models show the effects of an increase in river discharge on the flood exposure. Nevertheless, the surrogate models do not consider the smaller tributaries yet. The reference run shows that, in the study area, the lateral tributaries play a relevant role in causing flood losses and producing the peak discharge in the main river reach. In other cases than those presented, the lateral tributaries may be a less significant driver for flood losses than the main river reach. With the consideration of more tributaries, the system could potentially be better represented by surrogate models. In principle, the presented approach can be extended with consideration of the tributaries. However, the problem of duple exposures arises, i.e., buildings that are affected by both the main river and a tributary should not be counted twofold. This remains to be addressed. It could be solved by developing spatially distributed surrogate models, e.g. meta-models that show the relationship between the peak-discharge of the main river or the nearby tributary and the flow depths for each single building. In such a simulation, duple exposure of buildings from the main river and the tributary can be identified and considered. However, the level of complexity increases and with it the required pre-processing work needs to be considered. Consequently, one has to ask for the practicability and efficiency of the approach (Crout et al., 2009; Wolfs et al., 2015). Furthermore, discharge time series, which are needed for the elaboration of the tributaries' synthetic design hydrographs are often not available. Moreover, at the confluence of two river reaches, the synchronization of the peak discharges in both rivers plays a determinant role in flood loss estimation (Neal et al., 2013). Thus, the surrogate modeling approach must be extended by considering multiple scenarios that depend upon each other. Another approach to overcome this critical issue is to scrupulously define the validity of the model predictions by a rigorously dedicated spatial delimitation of the study area. This can be done either by bounding the system to the floodplains in the valley bottoms only, by inserting the flood hydrographs directly into the main river rather than in the lateral border of the floodplains, or by restricting the data containing the buildings explicitly to the ones the flood prediction should be valid for.

The loss computation model was not validated on the basis of loss data in the study area. For this purpose, another study area had to be chosen, where reliable data about flood losses was available. However, the vulnerability functions used in this work can easily be exchanged with other ones, as presented by Jongman et al. (2012) or Merz et al. (2013). The uncertainty inherent in the chosen vulnerability function has to be estimated (Merz et al., 2004; Merz and Thielen, 2009; Wagenaar et al., 2016), as this appears to be one of the most sensitive factors in flood loss estimations (Moel and Aerts, 2011). Furthermore, the transferability of vulnerability functions from one region to another is questionable (Cammerer et al., 2013) but is out of the scope of this study.

The results of the scenario runs show a high variability in the resulting numbers of exposed buildings and residents, as well as flood losses. The high variability is in line with the findings of Sampson et al. (2014). Furthermore, it must be mentioned that the floodplains in the case study do not show a very high sensitivity to the volume of a flood event in terms of flood loss estimation. High flood volumes are represented in this study by high lake levels. In cases where the volume of a flood is a remarkable factor for the amount of flood losses, the presented approach has to be extended with different forms of synthetic hydrographs. Other points are not discussed here, such as the propagation of the uncertainties in the model cascade framework, as discussed by McMillan and Brasington (2008) and Rodríguez-Rincón et al.

(2015). This, as well as the questions regarding the limitations of the use of surrogate models must be analyzed next.

5. Conclusions

With the development and application of a surrogate model, we present an approach for reducing complexity in flood risk modeling at the river basin scale without losing the ability to study the complex interactions between the physical processes and the impacts on the values at risk. We can verify our hypothesis of decomposing the river system into a number of subsystems and deriving the reaction of the whole system to a rainfall scenario by modeling the behavior of the subsystems in the form of relationships between flood magnitude and flood exposure/losses for each subsystem. The presented approach is a feasible way to overcome the trade-off between the spatial resolution of the inundation model and the accuracy of flood loss prediction. We have shown that the use of a surrogate model can bridge different scales by maintaining a high spatial resolution, while simultaneously allowing the simulation of a high number of flood scenarios. This approach offers new possibilities for stress test analyses and Monte-Carlo simulations demanding low computational resources in order to analyze the system behavior under different system loads. It has been shown that the surrogate model approach leads to a reliable and computationally fast analysis of flood losses in a set of probable maximum precipitation scenarios in a river basin. Thus, the approach may be implemented in coupled-component models, in portfolio risk assessments, and in the identification of the hot spots in a river basin. Furthermore, the presented approach may offer a high potential to couple it with real-time discharge forecast systems. Thus, this approach may be a basis for making a step forward from short-term discharge forecast towards short-term loss forecasts. In addition, the sensitivity analyses of the subsystem may also provide a basis for an inverse modeling approach that searches for the spatio-temporal precipitation pattern and leads to the worst-case scenario losses.

Software Availability

The hydraulic model BASEMENT is available at <http://www.basement.ethz.ch/>.

Acknowledgments

The authors acknowledge the Federal Office for Environment FOEN for providing the data of river cross-sections, the Federal Office for Topography SWISSTOPO for providing the buildings dataset, the Federal Office for Statistics FOS for providing the residential statistics, and the Canton of Bern for providing the Lidar data and the event documentation data. This work was financially supported by the Mobililar Lab for Natural Risks.

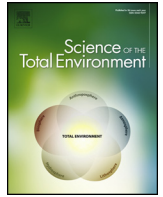
References

- Alarcon, V.J., Johnson, D., McAnally, W.H., van der Zwaag, J., Irby, D., Cartwright, J., 2014. Nested hydrodynamic modeling of a coastal river applying dynamic-coupling. *Water Resour. Manag.* 28, 3227–3240. <https://doi.org/10.1007/s11269-014-0671-6>.
- Alfieri, L., Bisselink, B., Dottori, F., Naumann, G., de Roo, A., Salamon, P., Wyser, K., Feyen, L., 2016a. Global projections of river flood risk in a warmer world. *Earth's Future*. <https://doi.org/10.1002/2016EF000485>.
- Alfieri, L., Feyen, L., Salamon, P., Thielen, J., Bianchi, A., Dottori, F., Burek, P., 2016b. Modelling the socio-economic impact of river floods in Europe. *Nat. Hazards Earth Syst. Sci.* 16, 1401–1411. <https://doi.org/10.5194/nhess-16-1401-2016>.
- Bennett, N.D., Croke, B.F.W., Guariso, G., Guillaume, J.H.A., Hamilton, S.H., Jakeman, A.J., Marsili-Libelli, S., Newham, L.T.H., Norton, J.P., Perrin, C., Pierce, S.A., Robson, B., Seppelt, R., Voinov, A.A., Fath, B.D., Andreassian, V., 2013. Characterising performance of environmental models. *Environ. Model. Software* 40, 1–20. <https://doi.org/10.1016/j.envsoft.2012.09.011>.
- Bermúdez, M., Neal, J.C., Bates, P.D., Coxon, G., Freer, J.E., Cea, L., Puertas, J., 2017. Quantifying local rainfall dynamics and uncertain boundary conditions into a nested regional-local flood modeling system. *Water Resour. Res.* 50, 433. <https://doi.org/10.1002/2016WR019903>.

- Biancamaria, S., Bates, P.D., Boone, A., Mognard, N.M., 2009. Large-scale coupled hydrologic and hydraulic modelling of the Ob river in Siberia. *J. Hydrol.* 379, 136–150. <https://doi.org/10.1016/j.jhydrol.2009.09.054>.
- Brunner, M.I., Viviroli, D., Sikorska, A.E., Vannier, O., Favre, A.-C., Seibert, J., 2017. Flood type specific construction of synthetic design hydrographs. *Water Resour. Res.* 53, 1390–1406. <https://doi.org/10.1002/2016WR019535>.
- Burke, N., Rau-Chaplin, A., Varghese, B., 2016. Computing probable maximum loss in catastrophe reinsurance portfolios on multi-core and many-core architectures. *Concurrency Comput. Pract. Ex.* 28, 836–847. <https://doi.org/10.1002/cpe.3695>.
- Cammerer, H., Thieken, A.H., Lammel, J., 2013. Adaptability and transferability of flood loss functions in residential areas. *Nat. Hazards Earth Syst. Sci.* 13, 3063–3081. <https://doi.org/10.5194/nhess-13-3063-2013>.
- Castelletti, A., Galelli, S., Ratto, M., Soncini-Sessa, R., Young, P.C., 2012. A general framework for Dynamic Emulation Modelling in environmental problems. *Environ. Model. Software* 34, 5–18. <https://doi.org/10.1016/j.envsoft.2012.01.002>.
- Castro-Gama, M.E., Popescu, I., Li, S., Mynett, A., van Dam, A., 2014. Flood inference simulation using surrogate modelling for the Yellow River multiple reservoir system. *Environ. Model. Software* 55, 250–265. <https://doi.org/10.1016/j.envsoft.2014.02.002>.
- Crout, N.M.J., Tarsitano, D., Wood, A.T., 2009. Is my model too complex?: Evaluating model formulation using model reduction. *Environ. Model. Software* 24, 1–7. <https://doi.org/10.1016/j.envsoft.2008.06.004>.
- Dutta, D., Herath, S., Musiak, K., 2003. A mathematical model for flood loss estimation. *J. Hydrol.* 277, 24–49. [https://doi.org/10.1016/S0022-1694\(03\)00084-2](https://doi.org/10.1016/S0022-1694(03)00084-2).
- Emmanuel, I., Andrieu, H., Leblois, E., Janey, N., Payrastré, O., 2015. Influence of rainfall spatial variability on rainfall-runoff modelling: benefit of a simulation approach? *J. Hydrol.* 531, 337–348. <https://doi.org/10.1016/j.jhydrol.2015.04.058>.
- Emmanuel, I., Payrastré, O., Andrieu, H., Zuber, F., Lang, M., Kljif, F., Samuels, P., 2016. Influence of the spatial variability of rainfall on hydrograph modelling at catchment outlet: a case study in the Cevennes region. France. *E3S Web Conf.* 7, 18004. <https://doi.org/10.1051/e3sconf/20160718004>.
- Falter, D., Dung, N.V., Vorogushyn, S., Schröter, K., Hundecha, Y., Kreibich, H., Apel, H., Theisselmann, F., Merz, B., 2014. Continuous, large-scale simulation model for flood risk assessments: proof-of-concept. *J. Flood Risk Manage.* n/a. <https://doi.org/10.1111/jfr3.12105>.
- Falter, D., Schröter, K., Dung, N.V., Vorogushyn, S., Kreibich, H., Hundecha, Y., Apel, H., Merz, B., 2015. Spatially coherent flood risk assessment based on long-term continuous simulation with a coupled model chain. *J. Hydrol.* 524, 182–193. <https://doi.org/10.1016/j.jhydrol.2015.02.021>.
- Felder, G., Weingartner, R., 2016. An approach for the determination of precipitation input for worst-case flood modelling. *Hydrol. Sci. J.* 61, 2600–2609. <https://doi.org/10.1080/02626667.2016.1151980>.
- Felder, G., Weingartner, R., 2017. Assessment of deterministic PMF modelling approaches. *Hydrol. Sci. J.* <https://doi.org/10.1080/02626667.2017.1319065>.
- Felder, G., Zischg, A., Weingartner, R., 2017. The effect of coupling hydrologic and hydrodynamic models on probable maximum flood estimation. *J. Hydrol.* 550, 157–165. <https://doi.org/10.1016/j.jhydrol.2017.04.052>.
- Fewtrell, T.J., Bates, P.D., Horritt, M., Hunter, N.M., 2008. Evaluating the effect of scale in flood inundation modelling in urban environments. *Hydrol. Process.* 22, 5107–5118. <https://doi.org/10.1002/hyp.7148>.
- Foudi, S., Osés-Eraso, N., Tamayo, I., 2015. Integrated spatial flood risk assessment: the case of Zaragoza. *Land Use Pol.* 42, 278–292. <https://doi.org/10.1016/j.landusepol.2014.08.002>.
- Fuchs, S., Birkmann, J., Glade, T., 2012. Vulnerability assessment in natural hazard and risk analysis: current approaches and future challenges. *Nat. Hazards* 64, 1969–1975. <https://doi.org/10.1007/s11069-012-0352-9>.
- Fuchs, S., Röthlisberger, V., Thaler, T., Zischg, A., Keiler, M., 2017. Natural hazard management from a coevolutionary perspective: exposure and policy response in the European alps. *Ann. Assoc. Am. Geogr.* 107, 382–392. <https://doi.org/10.1080/24694452.2016.1235494>.
- Gama, M.C., Popescu, I., Shengyang, L., Mynett, A., 2014. Modeling the inference between upstream inflow hydrographs and downstream flooded areas in a reservoir driven system. *Procedia - Social and Behavioral Sciences* 108, 207–218. <https://doi.org/10.1016/j.sbspro.2013.12.832>.
- Gupta, H.V., Kling, H., Yilmaz, K.K., Martinez, G.F., 2009. Decomposition of the mean squared error and NSE performance criteria: implications for improving hydrological modelling. *Hydrology Conference* 377, 80–91. <https://doi.org/10.1016/j.jhydrol.2009.08.003>. 2010.
- Hubbard, S., Stewart, K., Fan, J., 2014. Modeling spatiotemporal patterns of building vulnerability and content evacuations before a riverine flood disaster. *Appl. Geogr.* 52, 172–181. <https://doi.org/10.1016/j.apgeog.2014.05.006>.
- Hydrotec, 2001. Hochwasser-Aktionsplan Angerbach. Teil I: Berichte und Anlagen. Studie im Auftrag des Stua Dusseldorf, Aachen, Germany.
- Jongman, B., Kreibich, H., Apel, H., Barredo, J.I., Bates, P.D., Feyen, L., Gericke, A., Neal, J., Aerts, J.C.J.H., Ward, P.J., 2012. Comparative flood damage model assessment: towards a European approach. *Nat. Hazards Earth Syst. Sci.* 12, 3733–3752. <https://doi.org/10.5194/nhess-12-3733-2012>.
- Jonkman, S.N., Bočkarjova, M., Kok, M., Bernardini, P., 2008. Integrated hydrodynamic and economic modelling of flood damage in The Netherlands. *Special Section: Integrated Hydro-Economic Modelling for Effective and Sustainable Water Management* 66, 77–90. <https://doi.org/10.1016/j.ecolecon.2007.12.022>.
- Kelly, R.A., Jakeman, A.J., Barreteau, O., Borsuk, M.E., ElSawah, S., Hamilton, S.H., Henriksen, H.J., Kuikka, S., Maier, H.R., Rizzoli, A.E., van Delden, H., Voinov, A.A., 2013. Selecting among five common modelling approaches for integrated environmental assessment and management. *Environ. Model. Software* 47, 159–181. <https://doi.org/10.1016/j.envsoft.2013.05.005>.
- Kling, H., Fuchs, M., Paulin, M., 2012. Runoff conditions in the upper Danube basin under an ensemble of climate change scenarios. *Hydrology Conference* 424–425, 264–277. <https://doi.org/10.1016/j.jhydrol.2012.01.011>. 2010.
- Koivumäki, L., Alho, P., Lotsari, E., Käyhkö, J., Saari, A., Hyyppä, H., 2010. Uncertainties in flood risk mapping: a case study on estimating building damages for a river flood in Finland. *Journal of Flood Risk Management* 3, 166–183. <https://doi.org/10.1111/j.1753-318X.2010.01064.x>.
- Laganier, O., Ayrat, P.A., Salze, D., Sauvagnargues, S., 2014. A coupling of hydrologic and hydraulic models appropriate for the fast floods of the Gardon River basin (France). *Nat. Hazards Earth Syst. Sci.* 14, 2899–2920. <https://doi.org/10.5194/nhess-14-2899-2014>.
- Laniak, G.F., Olchin, G., Goodall, J., Voinov, A., Hill, M., Glynn, P., Whelan, G., Geller, G., Quinn, N., Blind, M., Peckham, S., Reaney, S., Gaber, N., Kennedy, R., Hughes, A., 2013. Integrated environmental modeling: a vision and roadmap for the future. *Environ. Model. Software* 39, 3–23. <https://doi.org/10.1016/j.envsoft.2012.09.006>.
- Lian, Y., Chan, I.-C., Singh, J., Demissie, M., Knapp, V., Xie, H., 2007. Coupling of hydrologic and hydraulic models for the Illinois River Basin. *J. Hydrol.* 344, 210–222. <https://doi.org/10.1016/j.jhydrol.2007.08.004>.
- Liu, J., Dietz, T., Carpenter, S.R., Folke, C., Alberti, M., Redman, C.M., Ouyang, Z., Deadman, P., Kratz, T., Provencher, W., 2007. Coupled human and natural systems. *Ambio* 639–649.
- Mani, P., Chatterjee, C., Kumar, R., 2014. Flood hazard assessment with multiparameter approach derived from coupled 1D and 2D hydrodynamic flow model. *Nat. Hazards* 70, 1553–1574. <https://doi.org/10.1007/s11069-013-0891-8>.
- Marrel, A., Iooss, B., Jullien, M., Laurent, B., Volkova, E., 2011. Global sensitivity analysis for models with spatially dependent outputs. *Environmetrics* 22, 383–397. <https://doi.org/10.1002/env.1071>.
- McMillan, H.K., Brasington, J., 2008. End-to-end flood risk assessment: a coupled model cascade with uncertainty estimation. *Water Resour. Res.* 44, 295. <https://doi.org/10.1029/2007WR005995>.
- Mechler, R., 2016. Reviewing estimates of the economic efficiency of disaster risk management: opportunities and limitations of using risk-based cost-benefit analysis. *Nat. Hazards* 81, 2121–2147. <https://doi.org/10.1007/s11069-016-2170-y>.
- Meert, P., Pereira, F., Willems, P., 2016. Computationally efficient modelling of tidal rivers using conceptual reservoir-type models. *Environ. Model. Software* 77, 19–31. <https://doi.org/10.1016/j.envsoft.2015.11.010>.
- Merz, B., Kreibich, H., Lall, U., 2013. Multi-variate flood damage assessment: a tree-based data-mining approach. *Nat. Hazards Earth Syst. Sci.* 13, 53–64. <https://doi.org/10.5194/nhess-13-53-2013>.
- Merz, B., Kreibich, H., Thieken, A., Schmidtke, R., 2004. Estimation uncertainty of direct monetary flood damage to buildings. *Nat. Hazards Earth Syst. Sci.* 4, 153–163.
- Merz, B., Thieken, A.H., 2009. Flood risk curves and uncertainty bounds. *Nat. Hazards* 51, 437–458. <https://doi.org/10.1007/s11069-009-9452-6>.
- de Moel, H., Aerts, J.C.J.H., 2011. Effect of uncertainty in land use, damage models and inundation depth on flood damage estimates. *Nat. Hazards* 58, 407–425. <https://doi.org/10.1007/s11069-010-9675-6>.
- Nadarajah, S., 2007. Probability models for unit hydrograph derivation. *J. Hydrol.* 344, 185–189. <https://doi.org/10.1016/j.jhydrol.2007.07.004>.
- Nash, J.E., Sutcliffe, J.V., 1970. River flow forecasting through conceptual models part I - A discussion of principles. *J. Hydrol.* 10, 282–290.
- Neal, J., Keef, C., Bates, P., Beven, K., Leedal, D., 2013. Probabilistic flood risk mapping including spatial dependence. *Hydrol. Process.* 27, 1349–1363. <https://doi.org/10.1002/hyp.9572>.
- Nguyen, P., Thorstensen, A., Soroshian, S., Hsu, K., AghaKouchak, A., Sanders, B., Koren, V., Cui, Z., Smith, M., 2016. A high resolution coupled hydrologic-hydraulic model (HiResFlood-UCI) for flash flood modeling. *J. Hydrol.* 541, 401–420. <https://doi.org/10.1016/j.jhydrol.2015.10.047>.
- O'Connell, P.E., O'Donnell, G., 2014. Towards modelling flood protection investment as a coupled human and natural system. *Hydrol. Earth Syst. Sci.* 18, 155–171. <https://doi.org/10.5194/hess-18-155-2014>.
- de Paiva, R.C.D., Buarque, D.C., Collischonn, W., Bonnet, M.-P., Frappart, F., Calmant, S., Bulhões Mendes, C.A., 2013. Large-scale hydrologic and hydrodynamic modeling of the Amazon River basin. *Water Resour. Res.* 49, 1226–1243. <https://doi.org/10.1002/wrcr.20067>.
- Pattison, I., Lane, S.N., Hardy, R.J., Reaney, S.M., 2014. The role of tributary relative timing and sequencing in controlling large floods. *Water Resour. Res.* 5444–5458. <https://doi.org/10.1002/2013WR014067>.
- Qiu, L., Du, Z., Zhu, Q., Fan, Y., 2017. An integrated flood management system based on linking environmental models and disaster-related data. *Environ. Model. Software* 91, 111–126. <https://doi.org/10.1016/j.envsoft.2017.01.025>.
- Rai, R.K., Sarkar, S., Singh, V.P., 2009. Evaluation of the adequacy of statistical distribution functions for deriving unit hydrograph. *Water Resour. Manag.* 23, 899–929. <https://doi.org/10.1007/s11269-008-9306-0>.
- Ratto, M., Castelletti, A., Pagano, A., 2012. Emulation techniques for the reduction and sensitivity analysis of complex environmental models. *Environ. Model. Software* 34, 1–4. <https://doi.org/10.1016/j.envsoft.2011.11.003>.
- Razavi, S., Tolson, B.A., Burn, D.H., 2012a. Numerical assessment of metamodelling strategies in computationally intensive optimization. *Environ. Model. Software* 34, 67–86. <https://doi.org/10.1016/j.envsoft.2011.09.010>.
- Razavi, S., Tolson, B.A., Burn, D.H., 2012b. Review of surrogate modeling in water resources. *Water Resour. Res.* 48, 559. <https://doi.org/10.1029/2011WR011527>.
- Rodríguez-Rincón, J.P., Pedrozo-Acuña, A., Breña-Naranjo, J.A., 2015. Propagation of hydro-meteorological uncertainty in a model cascade framework to inundation prediction. *Hydrol. Earth Syst. Sci.* 19, 2981–2998. <https://doi.org/10.5194/hess-19-2981-2015>.
- Rössler, O., Froidevaux, P., Börst, U., Rickli, R., Martius, O., Weingartner, R., 2014.

- Retrospective analysis of a nonforecasted rain-on-snow flood in the Alps – a matter of model limitations or unpredictable nature? *Hydrol. Earth Syst. Sci.* 18, 2265–2285. <https://doi.org/10.5194/hess-18-2265-2014>.
- Röthlisberger, V., Zischg, A., Keiler, M., 2016. Spatiotemporal aspects of flood exposure in Switzerland. *E3S Web Conf.* 7, 8008. <https://doi.org/10.1051/e3sconf/20160708008>.
- Röthlisberger, V., Zischg, A.P., Keiler, M., 2017. Identifying spatial clusters of flood exposure to support decision making in risk management. *Sci. Total Environ.* 598, 593–603. <https://doi.org/10.1016/j.scitotenv.2017.03.216>.
- Rougier, J., Sparks, R.S.J., Hill, L.J. (Eds.), 2013. *Risk and Uncertainty Assessment for Natural Hazards*. Cambridge University Press, Cambridge 1 online resource (xi, 574).
- Saint-Geours, N., Bailly, J.-S., Grelot, F., Lavergne, C., 2014. Multi-scale spatial sensitivity analysis of a model for economic appraisal of flood risk management policies. *Environ. Model. Software* 60, 153–166. <https://doi.org/10.1016/j.envsoft.2014.06.012>.
- Sampson, C.C., Fewtrell, T.J., O'Loughlin, F., Pappenberger, F., Bates, P.B., Freer, J.E., Cloke, H.L., 2014. The impact of uncertain precipitation data on insurance loss estimates using a flood catastrophe model. *Hydrol. Earth Syst. Sci.* 18, 2305–2324. <https://doi.org/10.5194/hess-18-2305-2014>.
- Sampson, C.C., Smith, A.M., Bates, P.D., Neal, J.C., Alfieri, L., Freer, J.E., 2015. A high-resolution global flood hazard model. *Water Resour. Res.* 51, 7358–7381. <https://doi.org/10.1002/2015WR016954>.
- Savage, J.T.S., Bates, P., Freer, J., Neal, J., Aronica, G., 2015. When does spatial resolution become spurious in probabilistic flood inundation predictions? *Hydrol. Process.* <https://doi.org/10.1002/hyp.10749>. n/a-n/a.
- Savage, J.T.S., Pianosi, F., Bates, P., Freer, J., Wagener, T., 2016. Quantifying the importance of spatial resolution and other factors through global sensitivity analysis of a flood inundation model. *Water Resour. Res.* 52, 9146–9163. <https://doi.org/10.1002/2015WR018198>.
- Schumann, G.J.-P., Neal, J.C., Voisin, N., Andreadis, K.M., Pappenberger, F., Phanthuwongpakdee, N., Hall, A.C., Bates, P.D., 2013. A first large-scale flood inundation forecasting model. *Water Resour. Res.* 49, 6248–6257. <https://doi.org/10.1002/wrcr.20521>.
- Serinaldi, F., Grimaldi, S., 2011. Synthetic design hydrographs based on distribution functions with finite support. *J. Hydrol. Eng.* 16, 434–446. [https://doi.org/10.1061/\(ASCE\)HE.1943-5584.0000339](https://doi.org/10.1061/(ASCE)HE.1943-5584.0000339).
- Shreve, C.M., Kelman, I., 2014. Does mitigation save? Reviewing cost-benefit analyses of disaster risk reduction. *International Journal of Disaster Risk Reduction* 10, 213–235. <https://doi.org/10.1016/j.ijdrr.2014.08.004>.
- Stephens, E., Schumann, G., Bates, P., 2014. Problems with binary pattern measures for flood model evaluation. *Hydrol. Process.* 28, 4928–4937. <https://doi.org/10.1002/hyp.9979>.
- Strasser, U., Vilsmaier, U., Prettenhaler, F., Marke, T., Steiger, R., Damm, A., Hanzer, F., Wilcke, R.A.I., Stötter, J., 2014. Coupled component modelling for inter- and transdisciplinary climate change impact research: dimensions of integration and examples of interface design. *Environ. Model. Software* 60, 180–187. <https://doi.org/10.1016/j.envsoft.2014.06.014>.
- SVKG-SEK/SVIT Schweizerische Vereinigung kantonaler Grundstückbewertungsexperten, Schweizerische Schätzungsexperten-Kammer, 2012. *Das Schweizerische Schätzerhandbuch: Das umfassende und praxisorientierte Lehrbuch über die wichtigsten Immobilien-Bewertungsmethoden der Schweiz*, fourth ed. Sekretariat SVK c/o Kantonales Steueramt Aargau, Sektion Grundstückschätzung, Aarau 383 S.
- Trigg, M.A., Birch, C.E., Neal, J.C., Bates, P.D., Smith, A., Sampson, C.C., Yamazaki, D., Hirabayashi, Y., Pappenberger, F., Dutra, E., Ward, P.J., Winsemius, H.C., Salamon, P., Dottori, F., Rudari, R., Kappes, M.S., Simpson, A.L., Hadzilacos, G., Fewtrell, T.J., 2016. The credibility challenge for global fluvial flood risk analysis. *Environ. Res. Lett.* 11, 94014.
- Tsoukalas, I., Kossieris, P., Efstratiadis, A., Makropoulos, C., 2016. Surrogate-enhanced evolutionary annealing simplex algorithm for effective and efficient optimization of water resources problems on a budget. *Environ. Model. Software* 77, 122–142. <https://doi.org/10.1016/j.envsoft.2015.12.008>.
- Tsoukalas, I., Makropoulos, C., 2015. Multiobjective optimisation on a budget: Exploring surrogate modelling for robust multi-reservoir rules generation under hydrological uncertainty. *Environ. Model. Software* 69, 396–413. <https://doi.org/10.1016/j.envsoft.2014.09.023>.
- UNISDR, 2015. *Making Development Sustainable: the Future of Disaster Risk Management*. United Nations, Geneva, pp. 311.
- van Dyck, J., Willems, P., 2013. Probabilistic flood risk assessment over large geographical regions. *Water Resour. Res.* 49, 3330–3344. <https://doi.org/10.1002/wrcr.20149>.
- van Nes, Egbert, H., Scheffer, M., 2005. A strategy to improve the contribution of complex simulation models to ecological theory. *Ecol. Model.* 185, 153–164. <https://doi.org/10.1016/j.ecolmodel.2004.12.001>.
- Vetsch, D., Siviglia, A., Ehrbar, D., Facchini, M., Gerber, M., Kammerer, S., Peter, S., Vonwiler, L., Volz, C., Farshi, D., Mueller, R., Rousselot, P., Veprek, R., Faeh, R., 2017. BASEMENT – Basic Simulation Environment for Computation of Environmental Flow and Natural Hazard Simulation. (Zurich).
- Viviroli, D., Zappa, M., Gurtz, J., Weingartner, R., 2009. An introduction to the hydrological modelling system PREVAH and its pre- and post-processing-tools. *Environ. Model. Software* 24, 1209–1222. <https://doi.org/10.1016/j.envsoft.2009.04.001>.
- Wagenaar, D.J., de Bruijn, K.M., Bouwer, L.M., Moel, H. de, 2016. Uncertainty in flood damage estimates and its potential effect on investment decisions. *Nat. Hazards Earth Syst. Sci.* 16, 1–14. <https://doi.org/10.5194/nhess-16-1-2016>.
- Wagner, S., Fersch, B., Yuan, F., Yu, Z., Kunstmann, H., 2016. Fully coupled atmospheric-hydrological modeling at regional and long-term scales: development, application, and analysis of WRF-HMS. *Water Resour. Res.* 52, 3187–3211. <https://doi.org/10.1002/2015WR018185>.
- Ward, P., Jongman, B., Weiland, F.S., Bouwman, A., van Beek, R., Bierkens, M., Ligetvoet, W., Winsemius, H.C., 2013. Assessing flood risk at the global scale: model setup, results, and sensitivity. *Environ. Res. Lett.* 8, 44019. <https://doi.org/10.1088/1748-9326/8/4/044019>.
- Ward, P.J., Jongman, B., Salamon, P., Simpson, A., Bates, P., Groeve, T. de, de Muis, S., Coughlan, Erin, Rudari, R., Trigg, M.A., Winsemius, H.C., 2015. Usefulness and limitations of global flood risk models. *Nat. Clim. Change* 5, 712–715. <https://doi.org/10.1038/nclimate2742>.
- Welsh, W.D., Vaze, J., Dutta, D., Rassam, D., Rahman, J.M., Jolly, I.D., Wallbrink, P., Podger, G.M., Bethune, M., Hardy, M.J., Teng, J., Lerat, J., 2013. An integrated modelling framework for regulated river systems. *Environ. Model. Software* 39, 81–102. <https://doi.org/10.1016/j.envsoft.2012.02.022>.
- Wolfs, V., Meert, P., Willems, P., 2015. Modular conceptual modelling approach and software for river hydraulic simulations. *Environ. Model. Software* 71, 60–77. <https://doi.org/10.1016/j.envsoft.2015.05.010>.
- Wolfs, V., Willems, P., 2013. A data driven approach using Takagi-Sugeno models for computationally efficient lumped floodplain modelling. *J. Hydrol.* 503, 222–232. <https://doi.org/10.1016/j.jhydrol.2013.08.020>.
- World Meteorological Organization, 2009. *Manual on Estimation of Probable Maximum Precipitation (PMP)*, third ed. World Meteorological Organization, Geneva, xxxii, pp. 259.
- Yazdi, J., Salehi Neyshabouri, S.A.A., 2014. Adaptive surrogate modeling for optimization of flood control detention dams. *Environ. Model. Software* 61, 106–120. <https://doi.org/10.1016/j.envsoft.2014.07.007>.
- Zeimet, F., Schaeffli, B., Artigue, G., García Hernández, J., Schleiss, A.J., 2017. Relevance of the correlation between precipitation and the 0 °C isothermal altitude for extreme flood estimation. *J. Hydrol.* 551, 177–187. <https://doi.org/10.1016/j.jhydrol.2017.05.022>.
- Zischg, A., Schober, S., Sereinig, N., Rauter, M., Seymann, C., Goldschmidt, F., Bäk, R., Schleicher, E., 2013. Monitoring the temporal development of natural hazard risks as a basis indicator for climate change adaptation. *Nat. Hazards* 67, 1045–1058. <https://doi.org/10.1007/s11069-011-9927-0>.
- Zischg, A.P., Mosimann, M., Bernet, D.B., Röthlisberger, V., 2018. Validation of 2D flood models with insurance claims. *J. Hydrol.* 557, 350–361. <https://doi.org/10.1016/j.jhydrol.2017.12.042>.
- Zoccatelli, D., Borga, M., Viglione, A., Chirico, G.B., Blöschl, G., 2011. Spatial moments of catchment rainfall: rainfall spatial organisation, basin morphology, and flood response. *Hydrol. Earth Syst. Sci.* 15, 3767–3783. <https://doi.org/10.5194/hess-15-3767-2011>.

Paper 23: Felder, G., Gómez-Navarro, J.J., Zischg, A., Raible, C.C., Röthlisberger, V., Bozhinova, D., Martius, O., Weingartner, R., 2018. From global circulation to local flood loss: Coupling models across the scales. *Science of The Total Environment* 635, 1225–1239. [10.1016/j.scitotenv.2018.04.170](https://doi.org/10.1016/j.scitotenv.2018.04.170).



From global circulation to local flood loss: Coupling models across the scales



Guido Felder^{a,b,*}, Juan José Gómez-Navarro^c, Andreas Paul Zischg^{a,b}, Christoph C. Raible^d, Veronika Röthlisberger^{a,b}, Denica Bozhinova^d, Olivia Martius^{a,b}, Rolf Weingartner^{a,b}

^a Institute of Geography, University of Bern, Hallerstrasse 12, Bern 3012, Switzerland

^b Mobiliar Lab for Natural Risks, Oeschger Centre for Climate Change Research, University of Bern, Hallerstrasse 12, Bern 3012, Switzerland

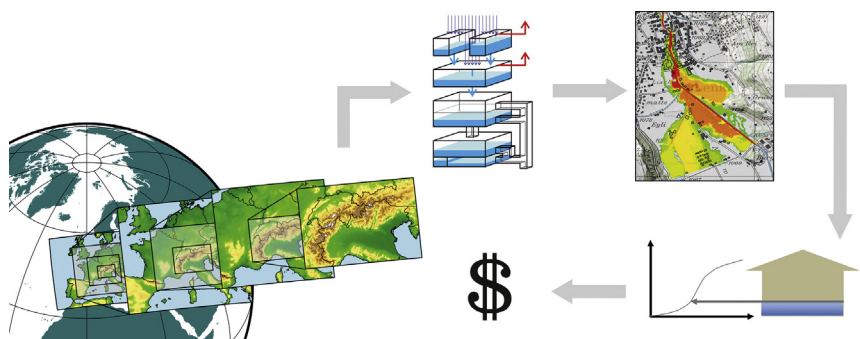
^c Facultad de Química, Department of Physics, University of Murcia, Campus de Espinardo, Murcia 30100, Spain

^d Climate and Environmental Physics, Oeschger Centre for Climate Change Research, University of Bern, Sidlerstrasse 5, Bern 3012, Switzerland

HIGHLIGHTS

- An assessment of a model chain from atmosphere to local flood loss is presented.
- Special attention is paid on deterministic process representation.
- Scale differences from atmospheric processes to local impact need to be considered.
- The setup allows for a good representation of hydrometeorological extremes.
- Several technical and methodical constraints have been identified.

GRAPHICAL ABSTRACT



ARTICLE INFO

Article history:

Received 26 October 2017

Received in revised form 5 March 2018

Accepted 12 April 2018

Available online 12 April 2018

Editor: R. Ludwig

Keywords:

GCM
RCM
Model coupling
Downscaling
Flood risk
Flood loss

ABSTRACT

Comprehensive flood risk modeling is crucial for understanding, assessing, and mitigating flood risk. Modeling extreme events is a well-established practice in the atmospheric and hydrological sciences and in the insurance industry. Several specialized models are used to research extreme events including atmospheric circulation models, hydrological models, hydrodynamic models, and damage and loss models. Although these model types are well established, and coupling two to three of these models has been successful, no assessment of a full and comprehensive model chain from the atmospheric to local scale flood loss models has been conducted. The present study introduces a model chain setup incorporating a GCM/RCM to model atmospheric processes, a hydrological model to estimate the catchment's runoff reaction to precipitation inputs, a hydrodynamic model to identify flood-affected areas, and a damage and loss model to estimate flood losses. Such coupling requires building interfaces between the individual models that are coherent in terms of spatial and temporal resolution and therefore calls for several pre- and post-processing steps for the individual models as well as for a computationally efficient strategy to identify and model extreme events. The results show that a coupled model chain allows for good representation of runoff for both long-term runoff characteristics and extreme events, provided a bias correction on precipitation input is applied. While the presented approach for deriving loss estimations for particular extreme events leads to reasonable results, two issues have been identified that need to be considered in further applications: (i) the identification of extreme events in long-term GCM simulations for downscaling and (ii) the representativeness of the vulnerability functions for local conditions.

© 2018 Elsevier B.V. All rights reserved.

* Corresponding author at: Institute of Geography, University of Bern, Hallerstrasse 12, 3012 Bern, Switzerland.
E-mail address: guido.felder@giub.unibe.ch (G. Felder).

1. Introduction

Floods are a natural hazard whose frequency is expected to rise in many areas due to ongoing anthropogenic climate change (IPCC, 2014). In addition, flood impacts are projected to increase due to increasing exposure (Bouwer, 2013; Hirabayashi et al., 2013; Kundzewicz et al., 2013). Since the occurrence of flood events cannot be prevented, society has to take action to increase its resilience to these changing conditions. This requires planning adaptation strategies and realizing flood mitigation measures. Knowledge on potentially flood-affected areas is needed to reduce impacts of future flood events. This calls for greater understanding of possible meteorological scenarios, hydrological processes, flooding probability, and the vulnerability of the assets within flood affected areas.

A prominent approach to gaining insight into atmospheric processes, and therefore meteorological extremes leading to severe impacts, is based on numerical models. Using a modeling approach to identify potential flood-affected areas and the damages that could incur requires coupling several models to a model chain. The first element in such a model chain is a meteorological component that provides precipitation and temperature data, the key inputs for the rest of the model chain. These variables can be generated with stochastic weather generators. However, there are some known issues regarding the representation of extreme events, such as capturing the dependence between variables, and the dependence of variables in space (Furrer and Katz, 2008; Semenov, 2008; Vandenberghé et al., 2010). Alternatively, the variables can be simulated in dynamical models by combining a Global Circulation Model (GCM) and a higher resolution Regional Climate Model (RCM). This is necessary when dealing with areas characterized by complex topography since the explicit simulation of topographically influenced processes leads to a more reliable simulation of extreme precipitation events (Keller et al., 2016).

The meteorological variables serve as input for a hydrological model, which simulates the runoff. The runoff can lead to flooding, which is simulated with hydrodynamic models. Eventually, a damage and loss model is used to estimate damages that result from simulated inundations. Although the individual parts of these modeling components are well established and commonly used in their respective research communities, a coupling of all these elements such as the one presented in this study has not been reported so far.

Coupling GCMs and RCMs to hydrological models has been the topic of numerous recent studies. In terms of spatial scales, such applications bridge calculations made for a global scale (10^4 km) to calculations made for the mesoscale (10^2 km). Most of these studies focused on a particular application of linked GCM and hydrological models. Several studies reviewed downscaling methods for hydrological applications (e.g. Fowler et al., 2007; Kundzewicz and Stakhiv, 2010; Teng et al., 2012; Wilby, 2010). More recent studies focused on specific methodological problems in this procedure, namely on scale effects (Piniewski et al., 2013), rainfall statistics (Langousis et al., 2016), and hydro-meteorological extremes (Madsen et al., 2014; Toftiq and Guven, 2014; Sunyer et al., 2015). The results of these studies have confirmed the applicability of linking GCMs to hydrological models via RCMs. Such model chains have been extensively used to assess climate change impacts on hydrological variables (e.g. Camici et al., 2014; Chen et al., 2013; Das et al., 2013; Fiseha et al., 2014; Kara et al., 2016; Li et al., 2014; Salathé et al., 2014; Xu et al., 2015).

Coupling a hydrological model with a hydrodynamic model has also been applied and evaluated in numerous studies. This part of the model chain couples the mesoscale (1000 to 100 km) to the micro-scale (1 km to 10 m). Such coupled models have been assessed by Brandimarte and Di Baldassarre (2012), Cook and Merwade (2009), Lerat et al. (2012), and Kim et al. (2012), among others and have been extensively applied in studies that estimate flood wave propagation (e.g. Laganier et al., 2014), retention effects (e.g. Felder et al., 2017; Skublics et al., 2014; Vorogushyn et al., 2012),

and flood probabilities (Altarejos-García et al., 2012; Dutta et al., 2013; Felder and Weingartner, 2017).

Finally, hydrodynamic models have been coupled to loss models to estimate flood losses. This approach has been applied in several case studies where the input was mainly estimated using observed hydrographs rather than modeled ones (e.g. Apel et al., 2009; Cammerer et al., 2013; Ernst et al., 2010; Falter et al., 2015). The scale of the models depends mainly on the aim of the respective study, and it typically encompasses the micro-scale (1–10 m). A rough assessment of global flood risk using GCM and hydrodynamic models with relatively coarse resolution has been conducted in several studies (e.g. Winsemius et al., 2015). A recent study by Thielen et al. (2016) complements this approach with statistical downscaling to better represent local climate variables.

A review of studies in the recent literature is further summarized in Table 1. It is apparent how all parts of the end-to-end model chain have been covered by the literature. However, the coupling of all models that are needed for a deterministic local flood loss estimation using one single model chain has not been accomplished yet to our knowledge. Therefore, the aim of the present study is to assess the applicability, strengths, and weaknesses of a coupled model chain that covers all of the above-mentioned models. The first focus is on the general applicability of the model chain, i.e. what modeling strategy is feasible considering the available computational resources. The second question is whether such a model chain sufficiently represents physical processes. This is assessed in terms of long-term characteristics and in terms of extreme events. Third, the model chain is assessed regarding its applicability for spatial and temporal scales that range across various orders of magnitude. With this approach, new opportunities and constraints of model coupling across many scales can be evaluated, and sensitive interfaces between the models can be identified. This is important in order to develop a smooth transition of model variables across the scales and in terms of identifying technical constraints. The applicability test is conducted in view of the research question on identifying extreme precipitation scenarios in order to delineate their financial impacts (i.e. flood losses to buildings).

2. Description of the model chain

The approach followed in this study entails selecting extreme events within a long climate simulation, applying the full model chain to such cases, and comparing the results with recent events, with the aim of gaining insight into physically plausible extreme precipitation scenarios over a time frame beyond the short instrumental record. Compared to resampling approaches or the use of stochastic weather generators, the main advantage of the proposed approach is that it is less dependent on the period and the quality of the instrumental record.

The study design is shown schematically in Fig. 1. The meteorological inputs into the model chain are the results of three different modeling approaches: dynamical downscaling based on ERA-Interim reanalysis, dynamical downscaling based on a GCM, and the latter followed by a statistical bias correction. These three precipitation modeling approaches are used separately for the model assessment. First, the model chain is calibrated and validated using input from ERA-interim. This enables an assessment of the model chain's ability to represent the natural system. In a second step, the precipitation modeled by a downscaled free GCM run is used as input both in an uncorrected and in a quantile-mapped mode. A comparison with observed precipitation and runoff data allows for an assessment of the model chain regarding long-term system behavior. It is assumed that if the model is able to represent the long-term characteristics of hydrological variables, it is also applicable for extreme events. As a showcase, the model is driven by a set of downscaled

Table 1

Model types and their characteristic spatial resolution and a non-exhaustive overview of studies in which coupled models have been applied. The characteristic resolution is understood as a rough statement on the magnitude and differs from model to model. Studies that remarkably differ from these characteristic resolutions, e.g. flood risk assessments on a global scale, are not considered.

	GCM	RCM	Hydrological model	Hydrodynamic model	Loss model
Characteristic spatial res.	10 ⁵ m	10 ⁴ m	10 ³ m	10 m	10 m
Characteristic temporal res.	Day	Day	Hour	Second	–
Sunyer et al. (2015)	x	x			
Langousis et al. (2016)	x	x			
Fowler et al. (2007)	x	x	x		
Kundzewicz and Stakhiv (2010)	x	x	x		
Wilby (2010)	x	x	x		
Teng et al. (2012)	x	x	x		
Madsen et al. (2014)	x	x	x		
Tofiq and Guven (2014)	x	x	x		
Camici et al. (2014)	x	x	x		
Piras et al. (2016)	x	x	x		
Duan et al. (2017)		x	x	x	
Cook and Merwade (2009)			x	x	
Di Baldassarre et al. (2010)			x	x	
Kim et al. (2012)			x	x	
Lerat et al. (2012)			x	x	
Vorogushyn et al. (2012)			x	x	
Laganier et al. (2014)			x	x	
Skublics et al. (2014)			x	x	
Altarejos-García et al. (2012)			x	x	
Falter et al. (2015)			x	x	x
Thieken et al. (2016)	x		x	x	x
Apel et al. (2009)				x	x
Ernst et al. (2010)				x	x
Cammerer et al. (2013)				x	x
Winsemius et al. (2015)				x	x
Current study	x	x	x	x	x

and bias corrected extreme events. For this particular purpose, a number of candidates to precipitation events within a 400-year GCM simulation are downscaled and fed into the model chain. This enables the assessment of the model chain when it comes to extreme events and losses.

2.1. Climate modeling

The input required by the hydrological component of the model chain is the precipitation flux, as well as the temperature. These variables are produced in our study using two different RCM simulations, the first driven by a GCM and the second by a reanalysis product. The resolution of the final downscaled fields is 2 km in both cases.

2.1.1. Reanalysis

ERA-Interim is a reanalysis product from the European Centre for Medium Range Weather Forecast. It is produced running the IFS model at a spectral resolution of T255 and 60 vertical levels (Dee et al., 2011). The setup includes a number of observational datasets that are assimilated in the model with a 4-D variational analysis. This dataset covers the period from 1979 up to the present day. To drive the RCM, a selection of this data spanning 1979–2013 with a 6-hour temporal resolution was used. The highest spatial resolution was used, with data interpolated to 0.75° × 0.75°.

2.1.2. GCM

The GCM data used in this study consist of a simulation carried out with the first version of the Community Earth System Model (CESM, Hurrell et al., 2013). The model is a fully coupled GCM considering components of the atmosphere, land, sea ice, ocean, and the carbon cycle. The model is run with a horizontal resolution of about 1° for all components.

Two different simulations were performed in the process. First, a so-called control simulation, where forcings are kept constant to 850 CE conditions, was run for 500 years. Only the last 400 years are used in this study to identify extreme precipitation events

(see details in the following section). Second, the latter simulation was branched from a preindustrial (1850 CE) simulation provided by the NCAR and continued until 2005. Details on the forcing used and a description of the simulated climate is given in Lehner et al. (2015). Note, however, that from the latter simulation only the period 1986 to 2005 is used in this study to deduce the bias correction of the GCM-RCM part of the chain.

2.1.3. RCM

The RCM is version 3.5 of the Weather Research and Forecasting Model (WRF) (Skamarock et al., 2008). This is a limited area model that solves the non-hydrostatic equations of atmospheric dynamics over a terrain-following coordinate system. It is a state-of-the-art RCM that is customarily used for both meteorological and climate purposes (García-Valdecasas Ojeda et al., 2017; Gómez-Navarro et al., 2015; Stucki et al., 2016; Messmer et al., 2017, among others). The model setup employed in this study is nearly the same as that described by Gómez-Navarro et al. (2015), and implements four nested domains that downscale the large-scale driving data from either ERA-Interim or CESM to 2 km in its innermost domain (Fig. 2). More recently, Gómez-Navarro et al. (2018) performed a validation of this model configuration regarding its ability to simulate the precipitation regimes over Switzerland. The high resolution in its innermost domain has been selected as it minimizes the scale gap in the coupling with the next model chain, therefore minimizing systematic errors. Further, it enables the explicit simulation of convective processes, rendering the parametrization of such processes unnecessary. A growing body of literature supports the increased performance of simulations with such high-resolution (e.g. Ban et al., 2014; Keller et al., 2016; Zittis et al., 2017). Prein et al. (2015) reviewed the recent bibliography about convection permitting simulations. They report how the added value of this type of simulations is especially notable at sub-daily scale and in summer. This makes this setup especially suitable for reproducing summer extreme events in areas of complex orography, precisely the phenomena most relevant for the area of interest of this study. Further,

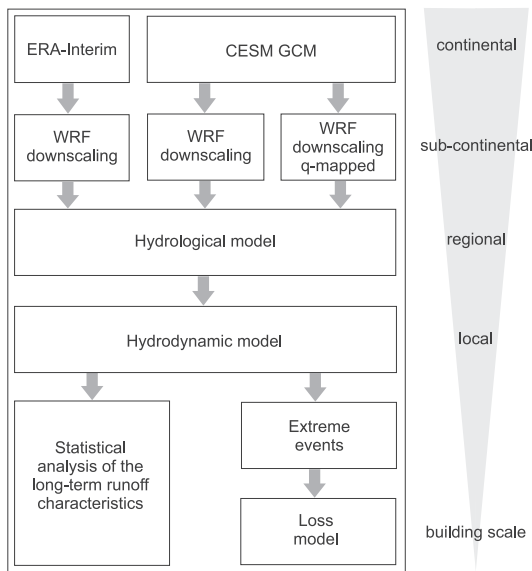


Fig. 1. Chain of coupled models used in this study. The process representations range from hundreds of kilometers (top) to a few meters (bottom). On the right, the characteristic scale of the process representation is indicated.

this high resolution facilitates the explicit simulation of the physical links between the large-scale circulation, the mesoscale processes responsible for regional patterns of precipitation, and eventually the discharge processes, which is the main purpose of the proposed model chain. Such high-resolution has the drawback of a huge computational cost that precludes the downscaling of the entire 400-year period, therefore the emphasis in case studies emerges as an alternative.

The only difference between the model configuration in the simulations driven by ERA-Interim (hereafter WRF-ERA) and those driven by CESM (hereafter WRF-CESM) is that in the latter no nudging scheme is employed, whereas in the former horizontal wind, temperature, and humidity are nudged above the boundary layer. The rationale behind this procedure is that the GCM should not be regarded as accurately as the reanalysis product, especially accounting for the overestimation of zonal circulation (Bracegirdle et al., 2013)

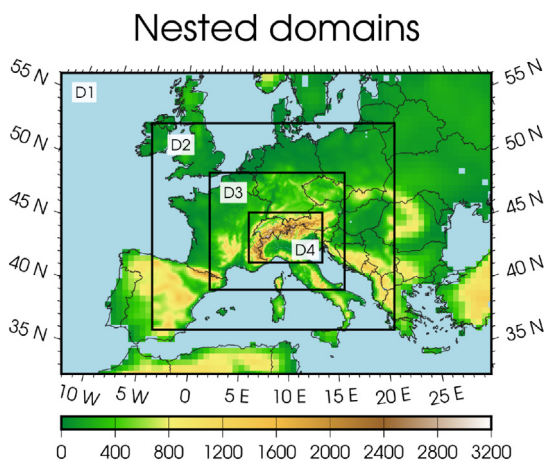


Fig. 2. Configuration of the four two-way nested domains. The spatial resolutions are 54, 18, 6, and 2 km, for domains D1 to D4, respectively. The figure depicts the orography and land sea mask implemented in the simulations. (For interpretation of the references to color in this figure legend, the reader is referred to the web version of this article.)

and other biases reported for this particular model setup (Lehner et al., 2015).

Thus, in total, three different sets of RCM simulations are used in this study – one continuous run driven by ERA-Interim in the period of 1979–2013 using nudging, a second continuous run driven by CESM for the period of 1986–2005, which is used for the bias correction, and finally a set of short runs around extreme cases which are selected from a long 400-year CESM run according to the criteria detailed in Section 3.3. Temperature data were directly derived from the model output without further processing, after confirming that there is no systematic bias (shown in Fig. 5).

2.2. Hydrological and hydrodynamic modeling

The deterministic, semi-distributed hydrological model PREVAH (Viviroli et al., 2009b) was applied for the hydrological modeling component. Various studies in areas similar to the present study area confirm the applicability of the model, particularly for modeling extreme events (Felder and Weingartner, 2017; FOEN, 2009; Orth et al., 2015; Viviroli et al., 2009a; Zappa et al., 2015). The model uses hydrological response units (HRUs) that are directly routed to the catchment outlet. For the present case, the HRUs are built based on catchment characteristics (altitude zone, slope, aspect, land use, soil type and glaciation) at a 2 km resolution. Twelve parameters are calibrated (14 in case of glaciated catchments). Fourteen sub-catchments with an average area of 200 km² were independently modeled; their location is shown in Fig. 3. For 9 out of these 14 sub-catchments calibration was performed using hourly resolved discharge data, leading to NSE skill-scores between 0.70 and 0.92. The other 5 sub-catchments were parametrized using the regionalization approach proposed by Viviroli et al. (2009a).

The outflow from the sub-catchments has to be routed through the floodplains towards the river basin outlet. The output of the hydrological model is fed into the hydrodynamic model as the upper boundary condition or as lateral inflow. In this study, the 1D hydrodynamic model BASEMENT (Vetsch et al., 2016) was used, which is based on the continuity equation and solves the Saint-Venant equations for unsteady one-dimensional flow. The model structure and its mathematical foundations are described in detail by Vetsch et al. (2016). BASEMENT simulates water fluxes through floodplains with their topography represented by cross-sections. For each time step and cross-section, the model computes flow velocity and water surface elevation. The hydrodynamic model is set up to incorporate all significant flood-prone areas and potential retention areas in the main river valley. Riverbed cross-sections were provided by the Swiss Federal Office of Environment (FOEN). These cross-sections are expanded to the whole valley ground based on a 0.5 m laser scan digital elevation model. This procedure enables the effects of widespread inundation and retention processes on discharge routing to be captured (Cook and Merwade, 2009; Mejia and Reed, 2011). A cross section spacing of 150 m and a perpendicular orientation is chosen based on recommendations made by Ali et al. (2015), Castellarin et al. (2009), and Samuels (1990). With this, the lake regulation and the retention effects of the lakes and the floodplains are considered.

The hydrodynamic model is calibrated on observed data. The calibration is based on an adjustment of the roughness (Strickler) coefficients (k_{str}) of the single cross-sections. Separate values are set for the riverbed, the adjacent levees, and the hinterland, aiming to reconstruct observed propagation times and peak flows. The roughness parameters are calibrated by representing the stage-discharge curves of all available river gauging stations in the study area. These coefficients are transferred to the neighboring cross-sections. The behavior of the lake outflows is described using the Poleni equation, whereas the dimensionless factor μ is empirically adjusted in order to reconstruct observed flood events. A more detailed description of the applied

hydrological and hydrodynamic model as well as a comprehensive explanation of the calibration strategy is provided in Felder et al. (2017). The model validation on observed flood events shows an error of ± 2 cm in terms of water level (mean flow depth: 2 m) or ± 5 m³ s⁻¹ in terms of discharge (mean runoff: 122 m³ s⁻¹). The model coupling with the hydrological model is external, which means that there is no direct interaction between the models and backwater effects are only treated within the spatial domain of the hydrodynamic model.

2.3. Loss modeling

A flood loss model is nested into the 1D hydrodynamic model and consists of a 2D flood inundation model for each floodplain, a building dataset, and a set of vulnerability functions. The flood loss model computes losses to buildings (structural damages), fatalities, damages to infrastructure or house content, and indirect damages due to business interruption are not considered in this study.

Flood dynamics in the floodplains are modeled with the 2D inundation model LISFLOOD-FP (Bates and de Roo, 2000). This two-dimensional hydrodynamic model is designed to simulate dynamic flooding in complex terrains in a computationally efficient way. The model computes water depths for each grid cell and time step. In this study, the model was set up with a spatial resolution of 50 m. The digital terrain model (DTM) is upscaled from a Lidar DTM with a high spatial resolution (0.5 m). The channel flow is computed in a subgrid mode (Neal et al., 2012). This subgrid channel module requires information on the heights of the river bed and of the lateral levees, on the river width, and on the shape of the river bed. These data are computed at high resolution and aggregated onto the target resolution by conserving the cross-sectional area of the river channel from the high-resolution terrain model. The 2D hydrodynamic model is calibrated in terms of reproducing the stage-discharge relationships at the gauging stations at bank-full discharge and the known channel capacity along the river reaches. As in the 1D hydrodynamic model, the roughness coefficients calibrated at the river gauging stations are transferred to the remaining river reaches. The model is validated on the basis of documented flooding. The fit of the inundation model (Bates and de Roo, 2000) computed on the basis of observed discharges of the flood event in August 2005 and a comparison between modeled and observed inundation extents ranges between 0.5 and 0.9, depending on the river reach. The lower values can be explained by dam breaks that occurred in reality but are not considered in the model.

The 1D hydrodynamic model provides the boundary conditions (primary and lateral inflows and lake levels) for the 2D inundation

model. Hence, the 2D inundation model is nested into the 1D hydrodynamic model. The 2D inundation model provides the flow depths during floods in the floodplains as the input for the loss computation module. The loss module consists of a dataset of buildings, each object classified by type, functionality, volume, reconstruction costs, and number of residents (Röthlisberger et al., 2017). The building footprints were provided by the Federal Office for Topography Swisstopo. The volume of the buildings is derived from LIDAR data provided by the Canton of Bern. The monetary values of the buildings (reconstruction costs) are calculated based on the above-ground building volume by means of a heuristic determination of mean values for reconstruction costs per cubic meter (regional construction costs according to SVKG (2012)). In addition, the number of residents is attributed to each building using the residential statistics of the Federal Office for Statistics.

The flow depths resulting from a model simulation were attributed to each building and provide the basis for estimating an object-specific degree of loss. The degree of loss is the ratio between the loss and the total reconstruction cost of the building. It depends on the flow depth and is used to compute the damage to the building by multiplying it with the reconstruction value of the building. The relationship between the degree of loss and the flow depth is described by an empirically derived vulnerability function. A vulnerability function is needed to determine losses based on the flow depths according to the characteristics of the individual buildings. Currently, no specific vulnerability function is available for Switzerland, and there is no dataset available to validate the flood loss module due to data privacy regulations in the study area. Hence, a selection of different flood vulnerability functions was applied to consider the uncertainties in the flood loss estimation and to capture a range of possible outcomes in the flood loss estimations. For the present study, vulnerability functions suggested by Dutta et al. (2003), Hydrotec (2001), Papathoma-Köhle et al. (2015), and Totschnig et al. (2011) are used in the flood loss computation module. In summary, the flood loss module in this model chain computes the damages on the single-building scale and aggregates the losses to the basin scale for each model simulation.

3. Data and methods

3.1. Study area and data availability

The study was conducted for the catchment of the Aare River up to Bern (see Fig. 3). The catchment is located at the northern edge of the Swiss alps and covers about 3000 km². The catchment's elevation ranges from 500 to 4200 m a.s.l., with a mean elevation of 1600 m a.s.l. The southern part of the catchment consists of alpine

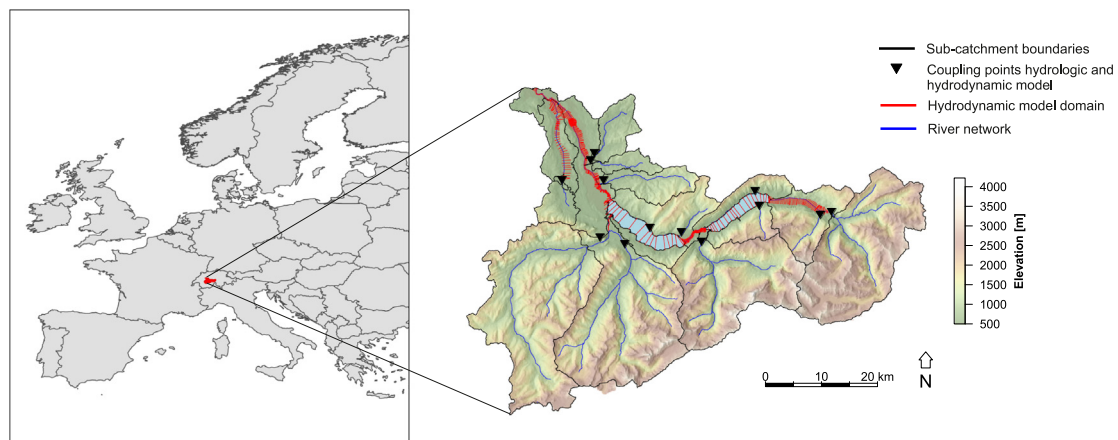


Fig. 3. Study area and sub-catchments. (For interpretation of the references to color in this figure legend, the reader is referred to the web version of this article.)

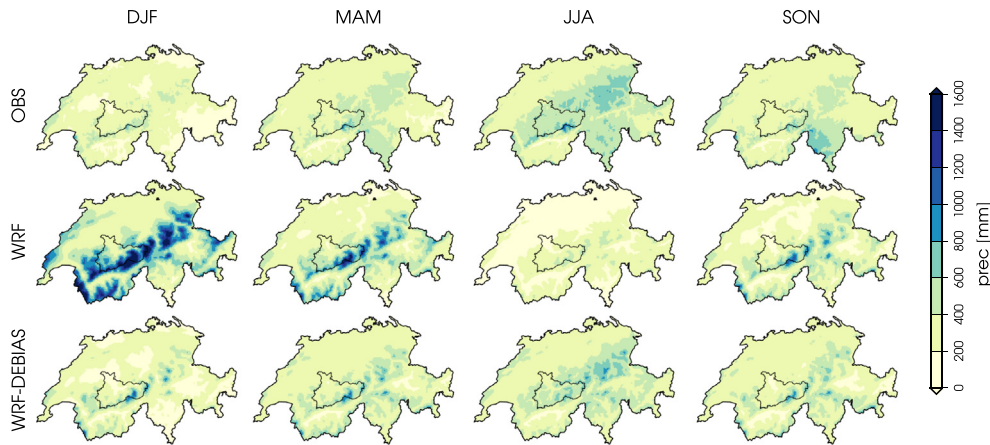


Fig. 4. Seasonally accumulated precipitation over Switzerland for the period of 1985–2005 in the OBS dataset (top), the raw WRF-CESM simulation (middle), and the former after QM correction (bottom). The Aare catchment is highlighted in the maps as the focus of this study. (For interpretation of the references to color in this figure legend, the reader is referred to the web version of this article.)

mountains. Several alpine peaks within this area exceed 4000 m a.s.l., and parts of it are glaciated (8% of the total catchment area). The northern part of the catchment consists of a relatively flat valley, where widespread potential floodplains are present. Two natural but artificially managed lakes are located between the northern and the southern part of the catchment. The alpine (southern) part of the catchment can roughly be subdivided into four major sub-catchments that each cover approximately 500 km² and drain into one of the lakes. The lakes have a balancing effect since they dampen peak discharges and attenuate low flow situations. The alpine sub-catchments determine the regime of the whole study area, which is driven by glacier- and snow melt, with high flows in summer and low flows in winter. The northern sub-catchments cover about 500 km² in total; their outflow is mainly driven by rainfall. Since they directly contribute to the catchment's runoff without draining into a lake, they can significantly influence the peak discharge of the catchment. The typical response time of the whole catchment amounts to 1–2 days. The complex physiographic setup of the catchment bears considerable consequences for atmospheric modeling as the complex topographic structure is not captured by the spatial resolution in the CESM. This drawback justifies the necessity of dynamically downscaling the GCM in order to produce physically realistic meteorological fields suitable for this complex catchment.

Further, the presence of lakes and widespread potential floodplains calls for a hydrodynamic model that is able to capture retention and inundation effects on discharge behavior.

3.2. Observational dataset

Discharge time series in a 10 min temporal resolution covering at least 30 years were available for nine sub-catchments, as well as for the catchment outflow. Data were provided by the Swiss Federal Office of Environment. The discharge time series of the sub-catchments are used for the calibration and validation of the hydrological model. The discharge time series gauged at the catchment outflow is used for the calibration of the hydrodynamic model, as well as for the validation of the coupled hydrologic-hydrodynamic model.

To validate the simulated precipitation and to carry out a bias correction, a gridded observational dataset is used. It consists of the RhiresD dataset, provided by [MeteoSwiss \(2015\)](#). This observational dataset, hereafter referred as OBS, is based on daily precipitation sums measured by the MeteoSwiss high-resolution rain-gauge network. The dataset is provided on a 2 km resolution, and has been spatially matched onto the 2 km grid of the WRF simulation's innermost domain.

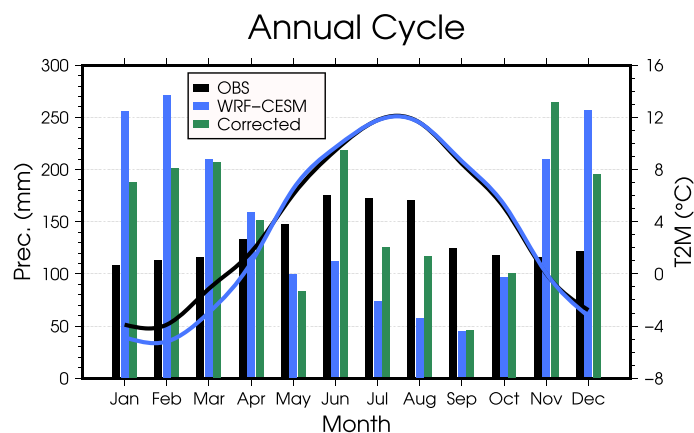


Fig. 5. Annual precipitation cycle in the Aare catchment in the observational dataset, as simulated by WRF, and then after correction taking into account precipitation over the same region. The bold line represents the monthly mean temperature for the period from 1979 to 2013.

3.3. Selection of extreme cases

Although the aim of this study relies on showing the feasibility of the full model chain, we showcase it with an application in the simulation of meteorological extreme events. Such events are selected within the 400-year control run conducted with CESM.

The proposed method is based on the assumption that the precipitation simulated by the GCM is related to the one obtained in the RCM. Thus, the precipitation averaged over a region that encompasses Switzerland (12 grid points in the GCM) is evaluated. A set of grid points is used in order to avoid misinterpretations, as the GCM uses subgrid parametrizations (in particular for precipitation) that could lead to artifacts at single grid points nearby or above topography. Out of this time series, the most extreme cases are selected according to the following selection procedure:

- The selection is carried out separately and for each season independently.
- The daily precipitation series are aggregated in running windows of variable length (1, 2, 3, 5 and 10 days). The resulting series are considered independently.
- The series corresponding to each window are inspected, and the 4 single most extreme events for each temporal frame are selected.

Note that this algorithm does not explicitly exclude days where precipitation leads to multiple events, i.e. the precipitation which occurred on the most extreme day may also have contributed to a 2-day extreme event, etc. All in all, the selection comprises $5 \times 4 \times 4 = 80$ events that require the simulation of $4 \times 4 \times (1 + 2 + 3 + 5 + 10) = 336$ days. Thus, the selected number of events leads to a feasible number of days to be downscaled with the RCM with the available computational resources. Also, the use of various temporal windows accounts for the fact that some extreme floods are not always produced by one heavy, isolated precipitation event, but are rather caused by precipitation accumulation over several days. Furthermore, selecting extremes separately by season aims to minimize problems due to seasonality improperly reproduced by the GCM. That is, extremes in all seasons are studied, regardless of when, across the annual cycle, the GCM produces the strongest precipitation.

It can be argued that these events might not necessarily correspond to extreme episodes in the real, externally forced climate. To demonstrate that this is not a bottleneck for this selection, the control simulation has been compared to a transient simulation for the 1000–2010 period (Lehner et al., 2015) in terms of extreme precipitation over Switzerland. Both simulations were carried out with the same CESM configuration. The results (not shown) indicate that the severity of extreme events is hardly distinguishable between control and transient simulations, and that the severity of these episodes remains stationary during the last millennium. Therefore, the extreme events within the control simulation are a sensible surrogate for the ones that can be expected in more realistic externally forced simulations. In any case, these cases are selected to serve as test bed for the model chain, and its value resides in its intrinsic physical consistency. Therefore, the interpretation of what type of events they represent is a consideration that does not affect the generality of the results regarding the model chain that is presented hereafter.

3.4. Bias correction of precipitation

The data produced by the GCM are not as accurate as those produced by reanalysis products (Wang et al., 2014). A prominent, well known bias is the overestimation of zonal circulation over Europe (e.g., Bracegirdle et al., 2013). These biases are introduced in the RCM through the domain boundaries, and they induce systematic biases in the precipitation flux simulated in the innermost domain of the

RCM. In addition, the RCM itself is a source of errors and uncertainties arising both from the parametrization of certain sub-grid processes and from a limited understanding of some components of the climate system. It is important to acknowledge and assess systematic biases, although they are to some extent inherent in all areas of climate modeling. A comprehensive analysis of the model performance in both the WRF-CESM and WRF-ERA simulations is presented in Gómez-Navarro et al. (2018). They identify biases in WRF-CESM associated to wrong seasonality in the driving model, which leads to an underestimation (overestimation) of precipitation in summer (winter). Such biases play a key role in this study, as the hydrological processes simulated in the following steps of the model chain exhibit non-linear behavior that makes them very sensitive to small deviations in precipitation fluxes. Therefore, some relevant results regarding the ability of the RCM to simulate observed climate are presented. These are relevant for the discussion of the outcome of the rest of the model chain.

As a mean to compensate for systematic biases in the output of the RCM, a bias correction technique was applied, generating adjusted precipitation fluxes that are in principle more representative of the observed precipitation rates than those in the raw RCM output. This so-called Quantile Mapping (QM) technique (Gudmundsson et al., 2012; Jakob Themeßl et al., 2011) calibrates a non-parametric statistical model that can be used to adjust the simulated events, with the underlying assumption being that the biases found during the calibration period are consistent across different time periods and even during unobserved extreme events. In a nutshell, bias correction is based on using a climate simulation and an observational product to obtain the sampling quantiles of both datasets independently. Then, this information is used to map the daily simulated precipitation onto the distribution of observed precipitation (Jakob Themeßl et al., 2011).

This simple method ensures that the sampling distribution of the corrected values mimics the one in the observations. Thereby, not only the mean and variance but also higher-level moments of the distribution are reproduced. It relies however on two important assumptions. The first assumption is that the corrected dataset inherits the properties of the observational product, which is considered a perfect surrogate of actual precipitation. Second, the sampling distributions of quantiles in the simulation and observations is assumed to be an accurate estimation of the actual, unknown, distributions, which is closely related to the length of the period used. This transient 20-year simulation spans the period of 1986–2005 with exactly the same configuration as the one used to simulate the extreme events. Clearly, some extreme cases exceed the precipitation range covered by the 20-year simulation, so extrapolation becomes necessary. The underlying assumption is that the bias in percentiles beyond 95% is constant, which is equivalent to assuming a straight line of slope 1 in a quantile-quantile diagram.

The use of QM needs to be accompanied by a word of caution. Post-processing techniques are in the focus of recent and intense debate (Maraun, 2016). As described above, QM establishes a relationship between two probability distributions. Therefore, a choice must be made regarding the data to be used to calculate such distributions, e.g. the precipitation in each grid point or the precipitation average in a certain area of interest. Using either of these data, QM (and more generally every bias-correction technique) has the effect of a statistical downscaling, which breaks down the physical consistency of the model. This is the case when the spatial structure of the simulated field is disturbed due to the different corrections carried out in different grids. To minimize this side effect, a less aggressive correction is applied, namely using the single couple of distributions obtained from the daily precipitation averaged over the Aare catchment in both the WRF-CESM and in OBS for the period 1985–2005. Then, both distributions are used to correct each grid cell independently. The use of just one general transformation is meant

to minimize the risk of statistical over-fitting, which might disturb the intended physical consistency with the RCM. Furthermore, it should be considered that although this procedure ensures that the correction is accurate across all distribution moments in the area used to establish the distributions, it may lead to worse corrections when it is applied in areas away from it, as shown in the following sections. This effect implies that the correction is especially suited for the Aare catchment, although it may lead to erroneous corrections in other areas that are not considered in the rest of the model chain. Finally, note that QM is applied in this study twice, first for the continuous 1985–2005 run and then for the selected events. Daily PDFs are used to correct daily series of precipitation in the former case, in which all days without a minimum threshold are considered. However, to correct the selected events the PDFs are obtained for the precipitation aggregated over the corresponding temporal windows, e.g. 5-day events are corrected according to the PDFs obtained for precipitation in chunks of 5 days.

3.5. Initial conditions for the hydrological and the hydrodynamic model

As explained in Section 3.3, the number of days that can be downscaled is limited due to limited computational resources. Such event-based modeling is based on several assumptions on the initial catchment conditions. The initial state of the hydrological model was set to average seasonal conditions in terms of storage levels, soil moisture, and snow-water-equivalent. Therefore, four sets of initial conditions were defined. The same procedure was applied to define the initial conditions of the 1D hydrodynamic model, namely the initial lake levels and the tributary inflows. The model was run for a period of 12 days. Therefore, at least 2 days after the precipitation event were modeled as well (exact number depends on the length of the scenario). This ensures that no peak discharges are missed, even when they occur after the actual precipitation event.

4. Results

First, an evaluation of the model chain regarding long-term runoff characteristics is presented, since acceptable model performance on a long-term basis is required for a reliable assessment of extreme event characterization. Then, the evaluation focuses on the modeling and reconstruction of extreme events, which is of particular importance for further applications of similar model chains for flood loss modeling.

4.1. Long-term characteristics of precipitation simulation

Precipitation biases in the WRF-CESM simulation illustrate how the bias correction procedure applied on a daily basis to the full simulated period (Section 3.4) adjusts the precipitation values over the Aare catchment. Fig. 4 illustrates the systematic biases present in the WRF-CESM simulation showing the maps of accumulated precipitation for each season in the observations (top), the raw WRF-CESM simulation (middle), and the bias-corrected one (bottom). A comprehensive discussion of these biases, as well as a comparison with biases of the WRF-CESM and WRF-ERA simulations and deficiencies in the simulation of the large-scale circulation within CESM, is provided by Gómez-Navarro et al. (2018). Fig. 4 demonstrates how WRF systematically overestimates winter and spring precipitation, while it underestimates summer precipitation. The deviations of the modeled precipitation amounts from the observed ones are not constant over the different seasons. This calls for studying extreme events independently for each season. These biases can be removed to a great extent applying QM, as depicted in the bottom row. The deficiencies regarding the annual precipitation cycle are apparent in Fig. 5, where the precipitation averaged over the Aare catchment for each month is shown for the simulation as well as for the output of the

QM correction. Clearly, the bias correction adjusts the representation of the annual cycle, increasing (decreasing) their values in the warm (cold) seasons and narrowing differences with the observations. The bold lines represent the monthly mean temperature derived from the WRF-ERA simulation and from the observed dataset. They confirm that the seasonal pattern of the mean temperature is well represented by the WRF-ERA simulation, which is important for a reliable modeling of snow accumulation or snow melt.

The overall performance of the three precipitation products under consideration is further shown in Fig. 6, where the quantiles of the modeled 1-day areal mean precipitation intensities are compared to the quantiles of the observed mean areal precipitation. The areal mean precipitation based on the downscaled reanalysis data is congruent with the observed quantiles in low-intensity cases. However, it systematically overestimates the observed quantiles above an intensity of 20 mm, and particularly above 60 mm. This means that mean areal precipitation derived from this dataset is systematically too high in the upper range of quantiles. A similar pattern is observed in the downscaled but uncorrected CESM data (WRF-CESM-RAW). The overestimation of quantiles between 50 mm and 80 mm is even more distinct in the WRF-ERA-based dataset. The quantile mapping of these data corrects the overestimation of these quantiles, as shown on the right hand side of Fig. 6. Although the fit is not perfect, there is no systematic under- or overestimation of the observed quantiles, even in the upper range of precipitation intensities.

The bias correction procedure has been applied to each event individually, and is illustrated for one particular case in Fig. 7, which shows the precipitation accumulated in a 1-day extreme event in the summer. This event led to heavy precipitation in the central part of Switzerland, and thus it is a good case for our consideration of severe flooding in the area of interest. WRF-CESM underestimates summer precipitation; therefore this event is corrected towards higher precipitation by the bias correction method. The effect of the correction is shown in the map (Fig. 7, right panel) leading to extensive areas where precipitation exceeds 170 mm in 24 h, whereas in the original model output precipitation barely reaches 120 mm.

4.2. Long-term characteristics of runoff simulation

The discharge quantiles derived through the coupled hydrological-hydrodynamic modeling of the corresponding precipitation datasets are shown in Fig. 8. As the WRF-ERA based precipitation dataset is used to calibrate the hydrological model, the systematic overestimation of medium and high quantiles in the WRF-ERA precipitation is corrected to a certain degree, meaning that the overestimation of higher runoff quantiles is not as distinct as it is with precipitation. As depicted in the study design shown in Fig. 1, the same WRF-ERA-based calibration is applied for the hydrological modeling of the WRF-CESM-based data. In the case of raw WRF-CESM, this procedure leads to good representation of observed runoff quantiles with respect to low and medium flows, and to an underestimation of extreme flows that exceed $400 \text{ m}^3 \text{ s}^{-1}$. Using the corrected version, the distribution of the runoff quantiles scatters around the observed quantiles. Although the flows between 350 and $450 \text{ m}^3 \text{ s}^{-1}$ are slightly underrepresented, there is no systematic over- or underestimation. Comparing the runoff quantiles of the WRF-CESM-RAW and the WRF-CESM-QM data shows the benefit of applying a quantile mapping procedure on the precipitation dataset, as this clearly improves the representation of the runoff quantiles.

4.3. Hydrometeorological extremes

The representation of extremely high flows can be assessed by comparing the annual maximum floods estimated using hydrological-hydrodynamic modeling based on the three different precipitation datasets with the observed annual maximum floods.

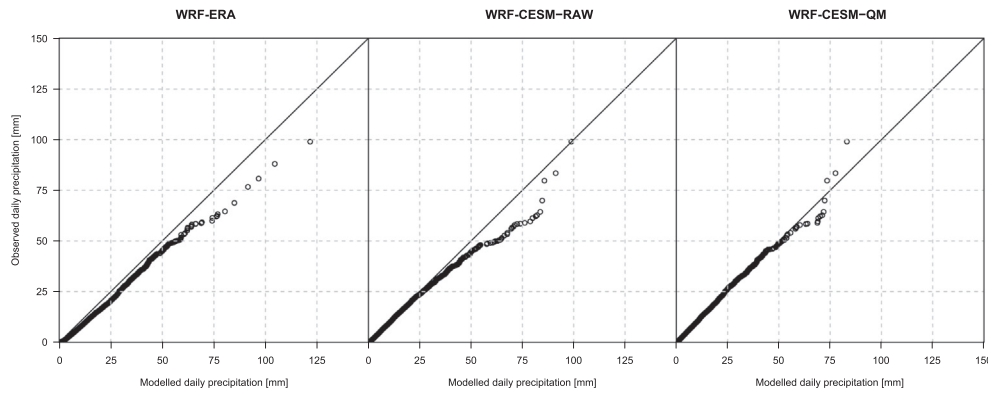


Fig. 6. Quantiles of the 1-day areal mean precipitation sums of the WRF-ERA dataset, the uncorrected downscaled WRF-CESM dataset and the quantile-mapped downscaled WRF-CESM-QM dataset for the study area. Each dataset covers a period of 20 years.

For this purpose, a generalized extreme value (GEV) distribution was fitted to the annual maximum peak flows using a maximum likelihood approach for parameter estimation and a Weibull approach to determine the empirical plotting positions, following the recommendations of Makkonen (2008) and DWA (2012). The uncertainty bounds were calculated based on the residual distribution as proposed by Coles (2004). The comparison of the resulting GEV distributions is shown in Fig. 9. The WRF-ERA based annual maximum floods lie systematically above the observed ones, which is in line with the quantile analysis in Fig. 8. Accordingly, the corresponding tail distribution of the fitted GEV distribution is not congruent with the empirical distribution. The annual maximum floods based on the raw WRF-CESM precipitation dataset are systematically too low, and the corresponding GEV-distribution fitted to these data lies significantly below the empirically derived one. Furthermore, fitting a distribution function on annual maximum floods based on the WRF-CESM dataset leads to a negative shape parameter ξ and therefore to an upper-bounded distribution function, which is clearly not in line with the empirical distribution. Again, these findings correspond with the quantile comparison in Fig. 8. The annual maximum floods based on the corrected WRF-CESM dataset are shown in the right part of Fig. 9. Although the modeled annual maximum floods slightly deviate from the observed ones, the corresponding fitted GEV distribution function is nearly congruent with the distribution of the observed values. This particularly applies for the tails of the distributions. This means that the hydrological and hydrodynamic modeling of the WRF-CESM-QM precipitation dataset allows for the

reconstruction of both long-term runoff characteristics and extreme events, which enables the further analyses.

The seasonal distribution of the annual maximum floods is mainly determined by the catchment characteristics presented in Section 3.1. The highest extreme flows usually occur in summer. This can be explained by the high snowfall line, the glacier contribution, and the relatively high initial lake levels during summer and low initial lake levels during winter. Therefore, extreme flows during winter are rather exceptional due to these initial conditions, and the seasonal bias in the precipitation inputs shown in Fig. 5 is not directly transferred to the seasonal distribution of extreme runoffs.

The next step, following the scheme shown in Fig. 1, is the identification of extreme events in the 400-year GCM simulation. Based on the criteria detailed in Section 3.3, a number of situations potentially leading to extreme values have been selected for downscaling. Unfortunately, not all cases selected by the algorithm could be downscaled in the end due to a purely technical reason: in two cases (a 3-day event and a 10-day event, both in summer) numerical instabilities precluded the execution of the RCM. The magnitude of the precipitation as simulated by the RCM is shown for winter and summer in Fig. 10.

The PDFs of precipitation are presented for the several temporal windows used in the case selection algorithm (the results for spring and autumn are not shown for the sake of brevity, although they exhibit similar behavior and support similar conclusions). Firstly, a comparison of the blue and orange curves demonstrates once again, but from a different point of view, the systematic biases and

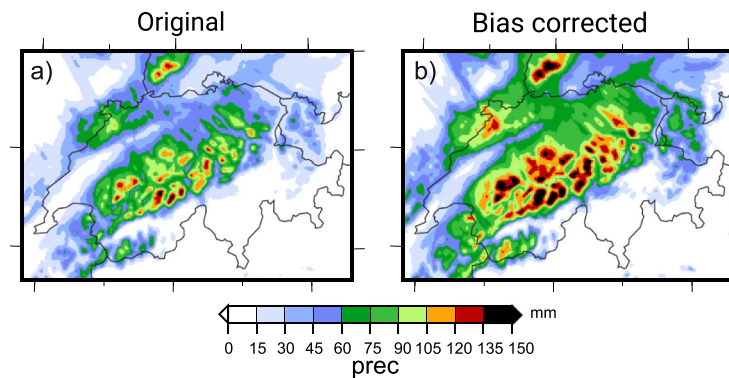


Fig. 7. Example of extreme precipitation event in the summer. The panel on the left (a) shows the 1-day accumulated precipitation for an extreme event in the control simulation. The panel on the right (b) shows the precipitation field after QM correction. (For interpretation of the references to color in this figure legend, the reader is referred to the web version of this article.)

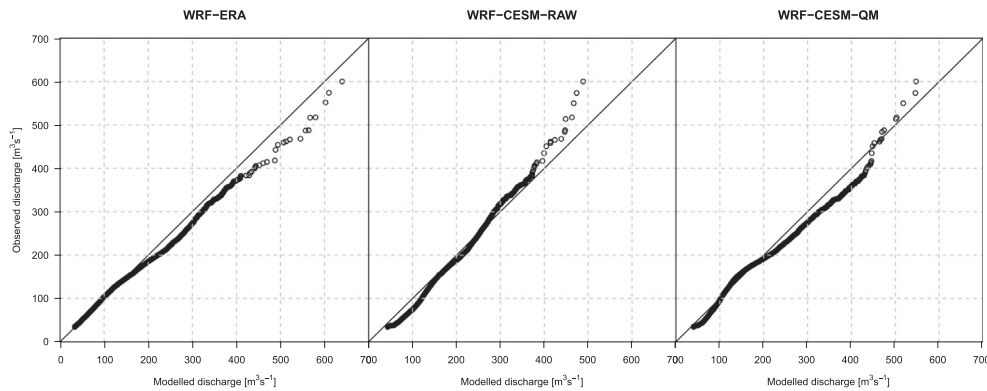


Fig. 8. Long-term runoff quantiles estimated with the WRF-ERA dataset, the uncorrected downscaled CESM dataset (WRF-CESM-RAW), and the quantile-mapped downscaled CESM dataset (WRF-CESM-QM) for the study area. The quantiles are compared with quantiles of the observed data.

seasonality issues discussed in Section 4.2. The WRF-CESM-RAW simulation underestimates precipitation for the summer and overestimates it for the winter. This is consistent across temporal windows from 1- to 10-day PDFs. Still, it should be noted that this systematic bias is corrected for each event with QM using the corresponding distributions derived for each temporal frame. This figure allows the selected events to be placed in a climatic context. Once down-scaled, in all cases the precipitation values are extreme compared to the climatological mean. However, the precipitation values for these events are far lower than the expected values above the 99th percentile. The values are lower because the selected events were the four most extreme within a 400-year period, which should represent the far right tail of the 20-year climatological precipitation shown by the blue curve in each panel. As this is not always the case, it can be concluded that the events cannot be regarded as extremes with return periods of hundred of years, i.e. the event selection procedure seems to have missed such situations. This situation becomes more problematic when the spatial structure of precipitation is evaluated (not shown). In some cases the precipitation is severe when spatially averaged over a large area, as demonstrated in Fig. 10. However, due to the complexity of the topography, it occurs in areas beyond the boundaries of our area of interest, which renders the situation uninteresting for our analysis. These drawbacks do not represent a bottleneck of the model chain, as the criteria still lead to situations

that are certainly extreme and of interest, but it severely limits the scope of the conclusions that can be drawn regarding the event duration these extremes represent. This issue is further discussed in the following sections.

4.4. Damage and loss estimation

The flood losses in the precipitation scenarios are shown in Fig. 11. Generally, the selected precipitation scenarios show high loss variability. The flood losses are in the range between 0.1 and ca. 3 billion Swiss Francs. This is related to the exposure of 800–7600 buildings associated with 3500–36000 residents, with a total value of 19,000 buildings and 98,000 residents. Several factors explain the high variability in flood losses. The estimated loss depends not only on the precipitation sum, but also on the spatio-temporal pattern in rainfall, the characteristics of the values at risk in the floodplains, and the applied vulnerability functions. The precipitation event leading to the highest loss estimation has a total precipitation sum of 144 mm over 5 days. This is a flood event in August. Thus, the altitude of the rainfall-snowfall limit leads to a high amount of rainfall and no snowfall. In comparison, the historic flood event that caused the most flood losses in the Canton of Bern was the Flood of August 2005 with a mean areal precipitation of 160 mm over the study area in 48 h. This flood event resulted in 341.3 mio. Swiss Francs

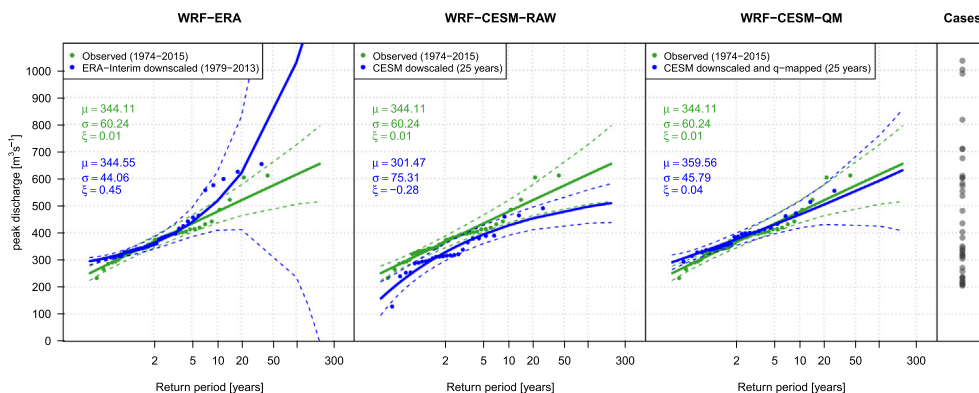


Fig. 9. Comparison of annual maximum floods and corresponding fits of a generalized extreme value (GEV) distribution function. The return level plots are either based on observed data (indicated in black) or on modeled data (indicated in blue). The annual maximum floods that result from the ERA-interim dataset lie systematically above the observed ones, leading to a distinct overestimation of floods with return levels above 5 years. The annual maximum floods based on the uncorrected WRF-CESM-RAW dataset are systematically too low, leading to an underestimation of high return level floods. Applying a downscaling procedure and using the resulting WRF-CESM-QM dataset leads to good correspondence of observed and modeled annual maximum floods, and therefore to a nearly congruent fitted distribution function. The gray dots on the right side indicate the peak discharges that result from the downscaled precipitation scenarios from the 400-year GCM-run. The distribution and the magnitudes of these peak flows confirm the plausibility of the modeled events. (For interpretation of the references to color in this figure legend, the reader is referred to the web version of this article.)

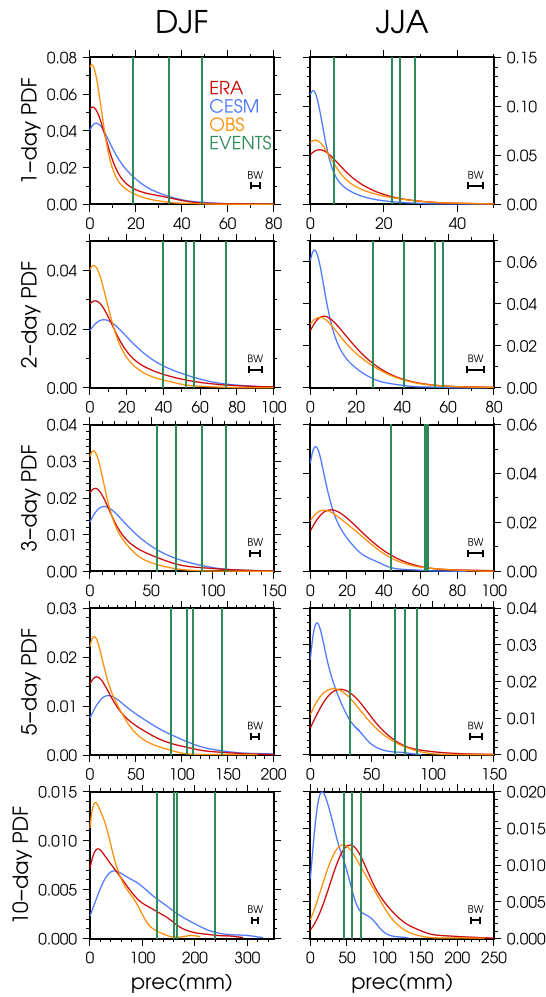


Fig. 10. Probability density functions of precipitation in different temporal windows over the Aare catchment derived from WRF-ERA (red), the WRF-CESM-RAW simulation (blue), and observed data OBS (orange). To estimate the curves, Gaussian kernel density estimators are used with a bandwidth that is illustrated in the bottom-right corner of each panel. Row by row, the different panels show the winter (left) and summer (right) results for the five temporal windows considered based on the procedure described in Section 3.3. The green vertical bars represent the precipitation obtained in the selected events. Although there should be 4 bars per panel, one corresponding to each event, computational instabilities were found in some events that hampered their simulation. Intermediate seasons exhibit similar behavior and are therefore not shown. (For interpretation of the references to color in this figure legend, the reader is referred to the web version of this article.)

in flood losses to buildings (FOEN, 2008). The discharge in Bern had a return period of approximately 150 years. Based on this comparison, the scenarios simulated here are indeed extreme events. However, the total aerial precipitation is below the probable maximum precipitation in the area as indicated by WMO (2009). The second highest losses simulated here are due to a flood event in winter. This shows that extreme precipitation events in winter combined with warm air temperatures could lead to extreme flooding despite the rather dampening initial conditions in winter. However, such a scenario is beyond observed flood events in the observation period. Due to the topographic complexity of the study area, a certain variability in flood losses is related to the varying spatio-temporal characteristics of the derived precipitation events (Pattison et al., 2014; Emmanuel et al., 2015). This is significant because of the spatial distribution of the values at risk, i.e. the buildings. In the present study, numerous buildings are located alongside the shorelines of lake Thun and in the floodplain of Interlaken. Thus, flood loss is relatively high in case of precipitation distributions that lead to

high flows in these particular areas. In addition, the estimated losses vary depending on the choice of vulnerability functions. This is in agreement with previous studies on uncertainties related to vulnerability functions (Apel et al., 2008, 2004; Merz et al., 2004; Merz and Thielen, 2009). The present modeling approach accounts for these factors influencing extreme flood loss estimations.

5. Discussion

The presented model chain including simulations from atmospheric processes to local flood risk covers several orders of magnitude in space and time. Its application yielded useful information with regard to its general applicability and the modeling strategies, process representation, and issues related to the scale gap between globally running GCMs and locally occurring flood losses. These three topics are further discussed in the subsections below.

5.1. General applicability and modeling strategy

From a technical point of view, the results prove that coupling several models from GCM to damage models is feasible. It allows for a realistic assessment of floods and flood-prone areas, provided that each model component sufficiently represents the involved processes. Here, process representation is checked separately for each model (except the loss model) by applying an independent model calibration and validation. Once the single models are properly calibrated and validated, the performance of coupled models can be assessed using long-term characteristics of intermediate variables like precipitation and runoff.

However, a complete description of the flood risk (including frequent and extreme events) would require downscaling the full transient GCM run, which is impossible with the currently available computational resources. Therefore, a comprehensive validation of the full model chain in terms of flood risk is hardly achievable. Nevertheless, the selected scenarios provide a basis for identifying flood scenarios that exceed the protection goals of the flood defenses in the study area. In the presented case study, the flood defenses are dimensioned by aiming to protect against flood events with return periods of roughly 80–100 years. It is shown that several precipitation scenarios lead to flow discharges higher than the carrying capacity of the river channels and thus lead to severe flooding. Thus, the presented method could complement the existing approaches for delineating residual risks, i.e. the risk that remains after the implementation of protective measures. The uncertainty in the flood loss estimation procedure can be overcome to a certain degree by applying several differing vulnerability functions, which provides some information about the model sensitivity to vulnerability functions. It can be stated that the derived flood loss estimations lie within a reasonable range when compared to the highest observed events.

The GCM simulation that serves as a basis for identifying extreme precipitation events spans 400 years of control run. Current computational resources do not allow such a long time period to be downscaled. Therefore, a few sub-samples of interest must be selected from the total GCM time series. A crucial point in this strategy is that the time frames for downscaling have to be chosen before downscaling is applied, therefore without certainty that the pre-selected event will correspond to an extreme situation once downscaled. It is assumed that the amount of precipitation modeled by the GCM and averaged over the study area is a good indicator for downscaled extreme precipitation. This is qualitatively true, as can be observed in Fig. 10, where the selected events are found in the right tail of the rainfall distribution. However, the events correspond to lower percentiles than expected (in all cases below the 99th). This is in part because in some cases the downscaled extreme precipitation takes place outside the area of interest, i.e. outside the Aare catchment, but also because in few events there is no extreme precipitation event at all.

Loss estimations for downscaled extreme events

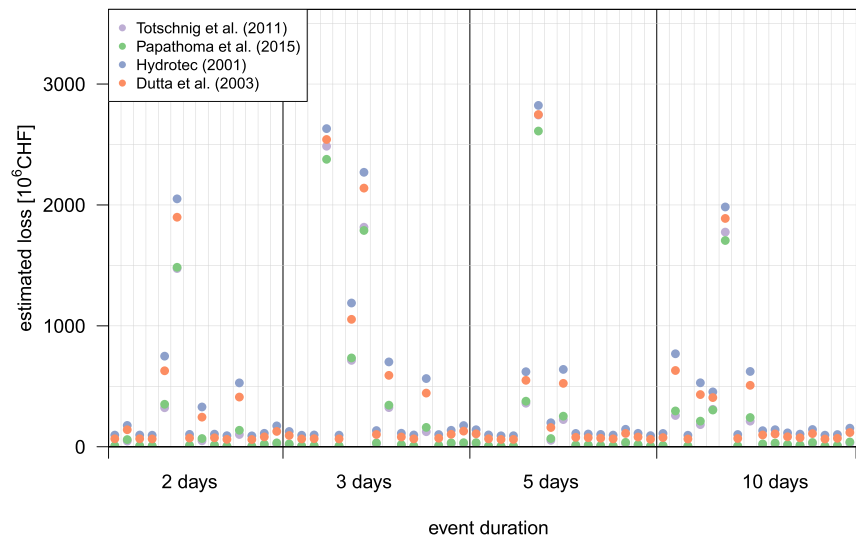


Fig. 11. Loss estimations based on the hydrological and hydrodynamic modeling of the identified extreme events. The different colors indicate the applied vulnerability function. Multiple functions were applied to assess the sensitivity of the lack of validation data. (For interpretation of the references to color in this figure legend, the reader is referred to the web version of this article.)

The efficiency of case selection using the much shorter but available continuous simulation in the period 1986–2005 can be estimated to some extent. The correlation between the GCM averaged series and the downscaled precipitation for the Aare catchment is 0.21. Further, the days within this period whose precipitation is above the 90th percentile in both datasets are identified. It turns out that only 20% of days belong simultaneously to the GCM and the downscaled series, i.e. about 80% of days whose actual precipitation was above the 90th percentile in the downscaled control period were not flagged by the selection algorithm described in Section 3.3. This simple analysis clearly illustrates the important differences between the GCM and RCM outputs, and points out severe limitations in the method used to identify candidates to severe precipitation episodes. At the same time it demonstrates the necessity of downscaling strategies. Therefore, the identification of events in the long-term GCM simulation for downscaling is a crucial step in overcoming the scale gap between globally running GCMs and local flood impacts that deserves important improvements. If the aim of future modeling exercises is to characterize situations that are realistically representative of extreme events with long return periods, then this difficulty can become an important bottleneck of the case study approach. Therefore, further research is needed to refine the selection of candidates for extreme events at regional scales.

The aim of this study, which has conditioned the chosen modeling strategy, is to keep the physical consistency over all modeling steps from atmospheric to flood loss modeling. Unfortunately all climate models are affected by structural limitations that lead to biases of different intensities that can condition its use in certain applications. Bias-correction techniques minimize such problems, but at the expense of affecting the physical consistency (Maraun, 2016). Therefore a compromise has to be established. The biases present in the WRF-CESM simulation pertain especially the representation of the annual cycle, and are noticeable enough to call for the use of bias-correction techniques. However, the QM method has not been applied in a per-grid basis. This minimizes the risk of over-fitting of the raw precipitation product to the observations, which would otherwise destroy the spatial coherence provided by the dynamical downscaling, being an important issue further discussed by Gómez-Navarro et al. (2018). The spatio-temporal structure as well as the magnitude of the modeled precipitation is physically determined.

No further assumptions have to be made, and no further processing steps beyond the calibration of the models to fit observations have to be applied. This is a clear benefit compared to other precipitation modeling approaches, e.g. stochastic weather generators (e.g. Leander et al., 2005; Semenov, 2008) or similar stochastic approaches (e.g. Foufoula-Georgiou, 1989; Vandenberghe et al., 2010).

The hydrological and hydrodynamic models can be calibrated and validated using observed discharge data, which is a widely accepted and well-researched approach. However, assessing the long-term runoff characteristics of a meso-scale catchment requires modeling a time series of several years, which calls for the application of a 1D hydrodynamic model. To model long time series with a more detailed 2D hydrodynamic model would exponentially increase computation time and is therefore not feasible. A 2D representation, however, incorporates lateral flows and therefore remarkably increases the accuracy of estimating flooding extent on building scale and improves the loss estimation. One way to overcome the tradeoff between computation time and degree of detail is to combine a 1D model with a 2D model. The 1D model is used to model the long-term runoff characteristics. The 2D model is only used for inundation modeling in case of extreme events, where the 1D model outputs serve as boundary conditions. Eventually, the output of the 2D model builds the basis for loss estimation. Such a modeling approach combines reasonable computation times for modeling long-term runoff characteristics and detailed model outputs as a basis for loss modeling.

The limitation of loss modeling lies in the unknown uncertainty of the vulnerability functions. This issue can be resolved by increasing the quantity and quality of observational data, which provide the basis for empirically deducing vulnerability functions. Alternatively, Schröter et al. (2014) showed that the predictive capability of the loss model can be improved by incorporating more explanatory variables or by choosing a Bayesian network-based loss modeling approach. However, these approaches do not help overcome the issues associated with a lack of validation data.

5.2. Representation of atmospheric and hydrological processes

The atmospheric processes in the GCM are explicitly resolved based on basic, well-established physical laws and are therefore

coherently structured in space and time according to physical boundaries and climate forcings. However, the coarse resolution of global models hampers their direct application in areas with complex topography. Likewise, the dynamical downscaling step solves similar sets of equations as the GCM, therefore maintaining this coherent structure. RCMs have the advantage of improving the representation of simulated physical processes in case of strong topographic influences since the underlying model topography is more finely resolved and directly incorporated. Thus, fields produced by a GCM and down-scaled by a RCM are coherent in their spatio-temporal behavior. However, model deficiencies and errors attributable to a great extent to uncertainty in parametrized sub-grid processes lead to certain systematic errors that have to be addressed.

In this particular application, the comparison of precipitation intensity quantiles showed that the downscaled WRF-CESM-RAW precipitation time series does not sufficiently represent the observed long-term rainfall characteristics over the study area in a 20-year climatic simulation. Therefore, a variant of quantile mapping correction is applied in order to minimize perturbations in the physical consistency while compensating for systematic biases. The WRF-CESM-QM dataset is more appropriate for a description of the rainfall characteristics for all intensities, even in a topographically complex study area, and therefore leads to plausible precipitation event estimations in mountainous regions, which justifies the application of such a complex model chain. This is certainly in line with other applications of downscaled rainfall data (Bowden et al., 2016; García-Valdecasas Ojeda et al., 2017; Gudmundsson et al., 2012; Maule et al., 2013; Jakob Themeßl et al., 2011, among others). Applications based on CESM datasets are spatially and temporally coherent on a large scale. Furthermore, the empirical frequencies of particular synoptic situations and seasonal patterns are inherently incorporated and do not have to be taken into additional consideration.

The simulation of hydrological processes by conceptual hydrological modeling is well established for normal flows as well as for extreme events. For the present study, the appropriateness of conceptual hydrological modeling is demonstrated by the good skill scores that resulted from the model calibration and validation for each sub-catchment. However, the hydrological model PREVAH (Viviroli et al., 2009b) applied in this study is a conceptual, semi-deterministic model. This means that many processes, e.g. evapotranspiration or soil water flows, are incorporated using empirical formulas rather than deterministic calculations. Furthermore, the primary model output is a discharge time series for the outlet of a pre-defined catchment, with no direct deterministic flow representation inside the catchment. In consequence, the presented approach does not allow for loss estimations for areas lying within the hydrologically modeled sub-catchments described in Section 3.1 and shown in Fig. 3. The hydrodynamic model provides a better physical representation of the flows within and around the riverbed. In this way, runoff conditions are calculated precisely in terms of water level and flow durations. In case of extreme events, inundation and retention effects that may be crucial for runoff determination (Felder et al., 2017) are also incorporated. This model set-up calls for careful planning of the spatial arrangement of the hydrological and hydrodynamic models. The hydrological model shall be applied in areas where runoff formation takes place and where ideally the damage potential is low. The hydrodynamic model must be applied in all potentially flood-prone areas and in areas with a high damage potential.

The actual setup of the 2D inundation model nested into the hydrologic-hydrodynamic model chain reliably represents the flooding processes in the floodplains and allows for flow depths to be attributed to the individual buildings. Thus, this setup allows for flood losses to be estimated at building scale with an aggregation of the object-related losses to the basin scale. However, the deterministic approach of the model chain ends with the attribution

of flow depths to buildings. The subsequent loss estimation is partly based on empirical stage-damage functions, and thus the last step in the model chain differs from the previous physically based approaches.

5.3. Temporal and spatial scales

As indicated in Table 1, the resolutions of the applied models range from 100 km to 10 m in space and from days to seconds in time. The present study presents two key considerations for overcoming these scale gaps. Firstly, incorporating intermediate models enables capturing flood-triggering processes that occur on intermediate scales. In the present case, the hydrological model simulates the catchment reaction to the precipitation events on an hourly resolution in time and on a 2 km resolution in space. The hydrodynamic model covers the next scale gap, as it simulates the runoff processes at a resolution of 10 s and 10 m. Secondly, the application of a dynamic downscaling technique followed by QM is important and, when necessary, the long-term characteristics of precipitation fields should be debiased.

The presented model chain has a relatively high level of flexibility when it comes to temporal scale. As soon as all sub-modules are to be run on sub-daily temporal scales, the time steps of all subsequent models can be adapted to the necessary time step. In practice, the small catchments (below 200 km²) require an hourly time step for reliable estimation of peak river discharges.

6. Conclusions

This paper presents a model chain able to bridge the spatial scales from global circulation down to the building scale and from hundreds of years to single flood events. To our knowledge, this is the first study dealing with such a wide range of scales. The presented approach is suited for the identification of extreme flood events. A model chain from the atmosphere to flood risk is a potentially useful additional method for characterizing design floods with very low return periods in planning disaster risk reduction. With this temporal flexibility and the coherence of the spatio-temporal rainfall patterns, the approach is promising for future flood risk assessments. A coupled model chain, linking atmospheric processes and synoptic situations to local flood losses, is particularly promising for risk identification for insurance portfolios. In contrast to approaches using weather generators, the presented approach is physically more consistent in mountainous regions where topographical effects are relevant for locally high precipitation intensities. Although the approach is promising, further improvements are required before it is suitable for practical application. First, the use of bias-correction techniques is necessary to remove prominent biases in downscaled precipitation, which precludes the pure physical consistency of the model chain. Second, the process of selecting extreme events to be dynamically downscaled is critical for the extrapolability of the results from few cases to conclusions regarding the full period spanned by the GCM. The simple selection procedure applied in this study leads to downscaled events that are not as extreme as expected, indicating that the event selection strategy should be improved in future studies.

Acknowledgments

We thank the Federal Office of Topography for providing the corresponding spatial data, the Federal Office for Statistics for providing residential statistics, as well as the Federal Office of Meteorology and Climatology for providing rainfall data and access to the ERA-Interim dataset, and the Mobiliar Lab for Natural Risks for supporting the study. JJGN acknowledges the CARM for the funding provided through the Seneca Foundation (project 20022/SF/16).

References

- Ali, A., Di Baldassarre, G., Solomatine, D.P., 2015. Testing different cross-section spacing in 1D hydraulic modelling: a case study on Johor River, Malaysia. *Hydrol. Sci. J.* 60, 351–360. <https://doi.org/10.1080/02626667.2014.889297>.
- Altarejos-García, L., Martínez-Chenoll, M.L., Escudé-Bueno, I., Serrano-Lombillo, A., 2012. Assessing the impact of uncertainty on flood risk estimates with reliability analysis using 1-D and 2-D hydraulic models. *Hydrol. Earth Syst. Sci.* 16, 1895–1914. <https://doi.org/10.5194/hess-16-1895-2012>.
- Apel, H., Aronica, G.T., Kreibich, H., Thielen, A.H., 2009. Flood risk analyses—how detailed do we need to be? *Nat. Hazards* 49, 79–98. <https://doi.org/10.1007/s11069-008-9277-8>.
- Apel, H., Merz, B., Thielen, A.H., 2008. Quantification of uncertainties in flood risk assessments. *Int. J. River Basin Manag.* 6, 149–162. <https://doi.org/10.1080/15715124.2008.9635344>.
- Apel, H., Thielen, A.H., Merz, B., Blöschl, G., 2004. Flood risk assessment and associated uncertainty. *Nat. Hazards Earth Syst. Sci.* 4, 295–308. <https://doi.org/10.5194/nhess-4-295-2004>.
- Ban, N., Schmidli, J., Schr, C., 2014. Evaluation of the convection-resolving regional climate modeling approach in decade-long simulations. *J. Geophys. Res.-Atmos.* 119, 7889–7907. <https://doi.org/10.1002/2014JD021478>.
- Bates, P., de Roo, A., 2000. A simple raster-based model for flood inundation simulation. *J. Hydrol.* 236, 54–77. [https://doi.org/10.1016/S0022-1694\(00\)00278-X](https://doi.org/10.1016/S0022-1694(00)00278-X).
- Bouwer, L.M., 2013. Projections of future extreme weather losses under changes in climate and exposure. *Risk Anal.* 33, 915–930. <https://doi.org/10.1111/j.1539-6924.2012.01880.x>.
- Bowden, J.H., Talgo, K.D., Spero, T.L., Nolte, C.G., 2016. Assessing the added value of dynamical downscaling using the standardized precipitation index. *Adv. Meteorol.* 2016, 1–14. <https://doi.org/10.1155/2016/8432064>.
- Bracegirdle, T.J., Shuckburgh, E., Sallee, J.-B., Wang, Z., Meijers, A.J.S., Bruneau, N., Phillips, T., Wilcox, L.J., 2013. Assessment of surface winds over the Atlantic, Indian, and Pacific ocean sectors of the southern ocean in CMIP5 models: historical bias, forcing response, and state dependence. *J. Geophys. Res.-Atmos.* 118, 547–562. <https://doi.org/10.1002/jgrd.50153>.
- Brandimarte, L., Di Baldassarre, G., 2012. Uncertainty in design flood profiles derived by hydraulic modelling. *Hydrol. Res.* 43, 753. <https://doi.org/10.2166/nh.2011.086>.
- Camicci, S., Brocca, L., Melone, F., Moramarco, T., 2014. Impact of climate change on flood frequency using different climate models and downscaling approaches. *J. Hydrol. Eng.* 19, 04014002. [https://doi.org/10.1061/\(ASCE\)HE.1943-5584.0000959](https://doi.org/10.1061/(ASCE)HE.1943-5584.0000959).
- Cammerer, H., Thielen, A.H., Lammel, J., 2013. Adaptability and transferability of flood loss functions in residential areas. *Nat. Hazards Earth Syst. Sci.* 13, 3063–3081. <https://doi.org/10.5194/nhess-13-3063-2013>.
- Castellari, A., Di Baldassarre, G., Bates, P.D., Brath, A., 2009. Optimal cross-sectional spacing in Preissmann scheme 1D hydrodynamic models. *J. Hydraul. Eng.* 135, 96–105. [https://doi.org/10.1061/\(ASCE\)0733-9429\(2009\)135:2\(96\)](https://doi.org/10.1061/(ASCE)0733-9429(2009)135:2(96)).
- Chen, J., Brissette, F.P., Chaumont, D., Braun, M., 2013. Performance and uncertainty evaluation of empirical downscaling methods in quantifying the climate change impacts on hydrology over two North American river basins. *J. Hydrol.* 200–214. <https://doi.org/10.1016/j.jhydrol.2012.11.062>.
- Coles, S., 2004. *An Introduction to Statistical Modelling of Extreme Values*. Springer Press, London, UK.
- Cook, A., Merwade, V., 2009. Effect of topographic data, geometric configuration and modeling approach on flood inundation mapping. *J. Hydrol.* 377, 131–142. <https://doi.org/10.1016/j.jhydrol.2009.08.015>.
- Das, T., Maurer, E.P., Pierce, D.W., Dettinger, M.D., Cayan, D.R., 2013. Increases in flood magnitudes in California under warming climates. *J. Hydrol.* 501, 101–110. <https://doi.org/10.1016/j.jhydrol.2013.07.042>.
- Dee, D.P., Uppala, S.M., Simmons, A.J., Berrisford, P., Poli, P., Kobayashi, S., Andrae, U., Balmaseda, M.A., Balsamo, G., Bauer, P., Bechtold, P., Beljaars, A.C.M., van de Berg, L., Bidlot, J., Bormann, N., Delsol, C., Dragani, R., Fuentes, M., Geer, A.J., Haimberger, L., Healy, S.B., Hersbach, H., Hólm, E.V., Isaksen, I., Kållberg, P., Köhler, M., Matricardi, M., McNally, A.P., Monge-Sanz, B.M., Morcrette, J.-J., Park, B.-K., Peubey, C., de Rosnay, P., Tavolato, C., Thépaut, J.-N., Vitart, F., 2011. The ERA-Interim reanalysis: configuration and performance of the data assimilation system. *Q. J. R. Meteorol. Soc.* 137, 553–597. <https://doi.org/10.1002/qj.828>.
- Di Baldassarre, G., Schumann, G., Bates, P.D., Freer, J.E., Beven, K.J., 2010. Flood-plain mapping: a critical discussion of deterministic and probabilistic approaches. *Hydrol. Sci. J.* 55, 364–376. <https://doi.org/10.1080/02626661003683389>.
- Duan, J.G., Bai, Y., Dominguez, F., Rivera, E., Meixner, T., 2017. Framework for incorporating climate change on flood magnitude and frequency analysis in the upper Santa Cruz river. *J. Hydrol.* 549, 194–207. <https://doi.org/10.1016/j.jhydrol.2017.03.042>.
- Dutta, D., Herath, S., Musiak, K., 2003. A mathematical model for flood loss estimation. *J. Hydrol.* 277, 24–49. [https://doi.org/10.1016/S0022-1694\(03\)00084-2](https://doi.org/10.1016/S0022-1694(03)00084-2).
- Dutta, D., Teng, J., Vaze, J., Lerat, J., Hughes, J., Marvanek, S., 2013. Storage-based approaches to build floodplain inundation modelling capability in river system models for water resources planning and accounting. *J. Hydrol.* 504, 12–28. <https://doi.org/10.1016/j.jhydrol.2013.09.033>.
- DWA, 2012. *Ermittlung von Hochwasserwahrscheinlichkeiten*. DWA-M 552, ISBN 978-3-942964-25-8.
- Emmanuel, I., Andrieu, H., Leblois, E., Janey, N., Payrastra, O., 2015. Influence of rainfall spatial variability on rainfall-runoff modelling: Benefit of a simulation approach? *J. Hydrol.* 531, 337–348. <https://doi.org/10.1016/j.jhydrol.2015.04.058>.
- Ernst, J., Dewals, B.J., Detrembleur, S., Archambeau, P., Epicum, S., Piroton, M., 2010. Micro-scale flood risk analysis based on detailed 2D hydraulic modelling and high resolution geographic data. *Nat. Hazards* 55, 181–209. <https://doi.org/10.1007/s11069-010-9520-y>.
- Falter, D., Schröter, K., Dung, N.V., Vorogushyn, S., Kreibich, H., Hundscha, Y., Apel, H., Merz, B., 2015. Spatially coherent flood risk assessment based on long-term continuous simulation with a coupled model chain. *J. Hydrol.* 524, 182–193. <https://doi.org/10.1016/j.jhydrol.2015.02.021>.
- Felder, G., Weingartner, R., 2017. Assessment of deterministic PMF modelling approaches. *Hydrol. Sci. J.* 62, 1591–1602. <https://doi.org/10.1080/02626667.2017.1319065>.
- Felder, G., Zischg, A., Weingartner, R., 2017. The effect of coupling hydrologic and hydrodynamic models on PMF estimation. *J. Hydrol.* 550, 157–165. <https://doi.org/10.1016/j.jhydrol.2017.04.052>.
- Fiseha, B.M., Setegn, S.G., Melesse, A.M., Volpi, E., Fiori, A., 2014. Impact of climate change on the hydrology of upper tiber river basin using bias corrected regional climate model. *Water Resour. Manag.* 28, 1327–1343. <https://doi.org/10.1007/s11269-014-0546-x>.
- FOEN, 2008. *Event-analysis of the 2005 Flood: Part 2: Analysis of Processes, Measures and Hazards*.
- FOEN, 2009. *Event-analysis of the August 2007 Flood*.
- Foufoula-Georgiou, E., 1989. A probabilistic storm transposition approach for estimating exceedance probabilities of extreme precipitation depths. *Water Resour. Res.* 25, 799–815.
- Fowler, H.J., Blenkinsop, S., Tebaldi, C., 2007. Linking climate change modelling to impacts studies: recent advances in downscaling techniques for hydrological modelling. *Int. J. Climatol.* 27, 1547–1578. <https://doi.org/10.1002/joc.1556>.
- Furrer, E.M., Katz, R.W., 2008. Improving the simulation of extreme precipitation events by stochastic weather generators. *Water Resour. Res.* 44, <https://doi.org/10.1029/2008WR007316>.
- García-Valdecasas Ojeda, M., Gámiz-Fortis, S.R., Castro-Díez, Y., Esteban-Parra, M.J., 2017. Evaluation of WRF capability to detect dry and wet periods in Spain using drought indices. *J. Geophys. Res. Atmos.* 122, 1569–1594. <https://doi.org/10.1002/2016JD025683>.
- Gómez-Navarro, J.J., Raible, C.C., Bozhinova, D., Martius, O., Garca Valero, J.A., Montvez, J., 2018. A new region-aware bias correction method for simulated precipitation in the Alpine region. *Geosci. Model Dev.* <https://doi.org/10.5194/gmd-2017-329>.
- Gómez-Navarro, J.J., Raible, C.C., Dierer, S., 2015. Sensitivity of the WRF model to PBL parametrisations and nesting techniques: evaluation of wind storms over complex terrain. *Geosci. Model Dev.* 8, 3349–3363. <https://doi.org/10.5194/gmd-8-3349-2015>.
- Gudmundsson, L., Bremnes, J.B., Haugen, J.E., Engen-Skaugen, T., 2012. Technical note: downscaling RCM precipitation to the station scale using statistical transformations - a comparison of methods. *Hydrol. Earth Syst. Sci.* 16, 3383–3390. <https://doi.org/10.5194/hess-16-3383-2012>.
- Hirabayashi, Y., Mahendran, R., Koirala, S., Konoshima, L., Yamazaki, D., Watanabe, S., Kim, H., Kanae, S., 2013. Global flood risk under climate change. *Nat. Clim. Chang.* 3, 816–821. <https://doi.org/10.1038/nclimate1911>.
- Hurrell, J.W., Holland, M.M., Gent, P.R., Ghan, S., Kay, J.E., Kushner, P.J., Lamarque, J.-F., Large, W.G., Lawrence, D., Lindsay, K., Lipscomb, W.H., Long, M.C., Mahowald, N., Marsh, D.R., Neale, R.B., Rasch, P., Vavrus, S., Vertenstein, M., Bader, D., Collins, W.D., Hack, J.J., Kiehl, J., Marshall, S., 2013. The community earth system model: a framework for collaborative research. *Bull. Am. Meteorol. Soc.* 94, 1339–1360.
- Hydrotec, 2001. *Hochwasser-aktionsplan angerbach. teil 1: Berichte und anlagen*.
- IPCC, 2014. *Climate Change 2014: The Physical Science Basis: Summary for Policymakers*. Geneva, Switzerland.
- Jakob Themeßl, M., Gobiet, A., Leuprecht, A., 2011. Aug. Empirical-statistical downscaling and error correction of daily precipitation from regional climate models. *Int. J. Climatol.* 31, 1530–1544. <https://doi.org/10.1002/joc.2168>.
- Kara, F., Yuçel, I., Akurek, Z., 2016. Climate change impacts on extreme precipitation of water supply area in Istanbul: use of ensemble climate modelling and geostatistical downscaling. *Hydrol. Sci. J.* 61, 2481–2495. <https://doi.org/10.1080/02626667.2015.1133911>.
- Keller, M., Fuhrer, O., Schmidli, J., Stengel, M., Stockli, R., Schaer, C., 2016. Evaluation of convection-resolving models using satellite data: the diurnal cycle of summer convection over the alps. *Meteorol. Z.* 25, 165–179.
- Kim, J., Warnock, A., Ivanov, V.Y., Katopodes, N.D., 2012. Coupled modeling of hydrologic and hydrodynamic processes including overland and channel flow. *Adv. Water Resour.* 37, 104–126. <https://doi.org/10.1016/j.advwatres.2011.11.009>.
- Kundzewicz, Z.W., Kanae, S., Seneviratne, S.I., Handmer, J., Nicholls, N., Peduzzi, P., Mechler, R., Bouwer, L.M., Arnell, N., Mach, K., Muir-Wood, R., Brakenridge, G.R., Kron, W., Benito, G., Honda, Y., Takahashi, K., Sherstyukov, B., 2013. Flood risk and climate change: global and regional perspectives. *Hydrol. Sci. J.* 59, 1–28. <https://doi.org/10.1080/02626667.2013.857411>.
- Kundzewicz, Z.W., Stakhiv, E.Z., 2010. Are climate models “ready for prime time” in water resources management applications, or is more research needed? *Hydrol. Sci. J.* 55 (7), 1085–1089. <https://doi.org/10.1080/02626667.2010.513211>.
- Laganier, O., Ayrat, P.A., Salze, D., Sauvagnargues, S., 2014. A coupling of hydrologic and hydraulic models appropriate for the fast floods of the Gardon River Basin (France). *Nat. Hazards Earth Syst. Sci.* 14, 2899–2920. <https://doi.org/10.5194/nhess-14-2899-2014>.
- Langousis, A., Matalakis, A., Deidda, R., Marrocu, M., 2016. Assessing the relative effectiveness of statistical downscaling and distribution mapping in reproducing rainfall statistics based on climate model results. *Water Resour. Res.* 52, 471–494. <https://doi.org/10.1002/2015WR017556>.
- Leander, R., Buishand, A., Aalders, P., Wit, M.D., 2005. Estimation of extreme floods of the River Meuse using a stochastic weather generator and a rainfall-runoff

- model/Estimation des crues extrêmes de la meuse à l'aide d'un générateur stochastique de variables météorologiques et d'un modèle pluie-débit. *Hydrol. Sci. J.* 50, <https://doi.org/10.1623/hysj.2005.50.6.1089>.
- Lehner, F., Joos, F., Raible, C.C., Mignot, J., Born, A., Keller, K.M., Stocker, T.F., 2015. Climate and carbon cycle dynamics in a CESM simulation from 850 to 2100 CE. *Earth Syst. Dynam.* 6, 411–434.
- Lerat, J., Perrin, C., Andréassian, V., Loumagne, C., Ribstein, P., 2012. Towards robust methods to couple lumped rainfall-runoff models and hydraulic models: a sensitivity analysis on the illinois river. *J. Hydrol.* 418–419, 123–135. <https://doi.org/10.1016/j.jhydrol.2009.09.019>.
- Li, F., Xu, Z., Liu, W., Zhang, Y., 2014. The impact of climate change on runoff in the Yarlung Tsangpo River Basin in the Tibetan Plateau. *Stoch. Env. Res. Risk A.* 28, 517–526. <https://doi.org/10.1007/s00477-013-0769-z>.
- Madsen, H., Lawrence, D., Lang, M., Martinkova, M., Kjeldsen, T.R., 2014. Review of trend analysis and climate change projections of extreme precipitation and floods in Europe. *J. Hydrol.* 519, 3634–3650. <https://doi.org/10.1016/j.jhydrol.2014.11.003>.
- Makkonen, L., 2008. Bringing closure to the plotting position controversy. *Comput. Stat. Theory Methods* 37, 460–467. <https://doi.org/10.1080/03610920701653094>.
- Maraun, D., 2016. Bias correcting climate change simulations - a critical review. *Curr. Clim. Chang. Rep.* 2, 211–220. <https://doi.org/10.1007/s40641-016-0050-x>.
- Maule, C.F., Thejll, P., Christensen, J.H., Svendsen, S.H., Hannaford, J., 2013. Jan. Improved confidence in regional climate model simulations of precipitation evaluated using drought statistics from the ENSEMBLES models. *Clim. Dyn.* 40, 155–173. <https://doi.org/10.1007/s00382-012-1355-7>.
- Mejia, A.I., Reed, S.M., 2011. Evaluating the effects of parameterized cross section shapes and simplified routing with a coupled distributed hydrologic and hydraulic model. *J. Hydrol.* 409, 512–524. <https://doi.org/10.1016/j.jhydrol.2011.08.050>.
- Merz, B., Kreibich, H., Thielen, A., Schmidtke, R., 2004. Estimation uncertainty of direct monetary flood damage to buildings. *Nat. Hazards Earth Syst. Sci.* 4, 153–163. <https://doi.org/10.5194/nhess-4-153-2004>.
- Merz, B., Thielen, A.H., 2009. Flood risk curves and uncertainty bounds. *Nat. Hazards* 51, 437–458. <https://doi.org/10.1007/s11069-009-9452-6>.
- Messmer, M., Gomez-Navarro, J.J., Raible, C.C., 2017. The impact of Vb-cyclones to ocean temperature and soil moisture changes in sensitivity experiments with WRF. *Earth Syst. Dynam.* 8, 477–493. <https://doi.org/10.5194/esd-8-477-2017>.
- MeteoSwiss, 2015. Documentation of Meteoswiss Grid-data Products: Daily Precipitation (final analysis): Rhiresd. http://www.ifu.ethz.ch/hydrologie/research/research_data/proddochrhiresd.pdf.
- Neal, J., Schumann, G., Bates, P., 2012. A subgrid channel model for simulating river hydraulics and floodplain inundation over large and data sparse areas. *Water Resour. Res.* 48, 619. <https://doi.org/10.1029/2012WR012514>.
- Orth, R., Staudinger, M., Seneviratne, S.I., Seibert, J., Zappa, M., 2015. Does model performance improve with complexity? A case study with three hydrological models. *J. Hydrol.* 523, 147–159. <https://doi.org/10.1016/j.jhydrol.2015.01.044>.
- Papathoma-Köhle, M., Zischg, A., Fuchs, S., Glade, T., Keiler, M., 2015. Loss estimation for landslides in mountain areas - an integrated toolbox for vulnerability assessment and damage documentation. *Environ. Model Softw.* 63, 156–169. <https://doi.org/10.1016/j.envsoft.2014.10.003>.
- Pattison, I., Lane, S.N., Hardy, R.J., Reaney, S.M., 2014. The role of tributary relative timing and sequencing in controlling large floods. *Water Resour. Res.* 50, 5444–5458. <https://doi.org/10.1002/2013WR014067>.
- Piniewski, M., Voss, F., Bärlund, I., Okruszko, T., Kundzewicz, Z.W., 2013. Effect of modelling scale on the assessment of climate change impact on river runoff. *Hydrol. Sci. J.* 58, 737–754. <https://doi.org/10.1080/02626667.2013.778411>.
- Piras, M., Mascaro, G., Deidda, R., Vivoni, E.R., 2016. Impacts of climate change on precipitation and discharge extremes through the use of statistical downscaling approaches in a mediterranean basin. *Sci. Total Environ.* 543, 952–964. <https://doi.org/10.1016/j.scitotenv.2015.06.088>.
- Prein, A.F., Langhans, W., Fossler, G., Ferrone, A., Ban, N., Goergen, K., Keller, M., Tlle, M., Gutjahr, O., Feser, F., Brisson, E., Kollet, S., Schmidli, J., van Lipzig, N.P.M., Leung, R., 2015. A review on regional convection-permitting climate modeling: demonstrations, prospects, and challenges. 53. <https://doi.org/10.1002/2014RG000475>. 2014RG000475.
- Röthlisberger, V., Zischg, A.P., Keiler, M., 2017. Identifying spatial clusters of flood exposure to support decision making in risk management. *Sci. Total Environ.* 598, 593–603. <https://doi.org/10.1016/j.scitotenv.2017.03.216>.
- Salathé, E.P., Hamlet, A.F., Mass, C.F., Lee, S.-Y., Stumbaugh, M., Steed, R., 2014. Estimates of twenty-first-century flood risk in the pacific northwest based on regional climate model simulations. *J. Hydrometeorol.* 15, 1881–1899. <https://doi.org/10.1175/JHM-D-13-0137.1>.
- Samuels, P.G., 1990. Cross section location in one-dimensional models. In: Ltd, H.R. (Ed.), *Int. Conf. on River Flood Hydraulics*. pp. 339–350. Wallingford, Oxfordshire.
- Schröter, K., Kreibich, H., Vogel, K., Riggelsen, C., Scherbaum, F., Merz, B., 2014. How useful are complex flood damage models? *Water Resour. Res.* 50, 3378–3395. <https://doi.org/10.1002/2013WR014396>.
- Semenov, M.A., 2008. Simulation of extreme weather events by a stochastic weather generator. *Clin. Res.* 35, 203–212. <https://doi.org/10.3354/cr00731>.
- Skamarock, W.C., Klemp, J.B., Dudhia, J., Gill, D.O., Barker, D.M., Wang, W., Powers, J.G., 2008. A description of the advanced research WRF version 3. Technical Report TN475+STR. National Center for Atmospheric Research.
- Skublics, D., Seibert, S., Ehret, U., 2014. Modelling flood retention with hydrological and hydrodynamic models under different boundary conditions - sensitivity analysis on the danube reach from Neu-Ulm to Donauwörth. *Hydrol. Wasserbewirtsch.* 178–189. https://doi.org/10.5675/HyWa_2014.
- Stucki, P., Dierer, S., Welker, C., Gómez-Navarro, J.J., Raible, C.C., Martius, O., Brnnimann, S., 2016. Evaluation of downscaled wind speeds and parameterised gusts for recent and historical windstorms in Switzerland. *Tellus A* 68, <http://www.tellusa.net/index.php/tellusa/article/view/31820>. <https://doi.org/10.3402/tellusa.v68.31820>.
- Sunyer, M.A., Hundedcha, Y., Lawrence, D., Madsen, H., Willems, P., Martinkova, M., Vormoor, K., Bürger, G., Hanel, M., Kriaučiuniene, J., Loukas, A., Osuch, M., Yücel, I., 2015. Inter-comparison of statistical downscaling methods for projection of extreme precipitation in Europe. *Hydrol. Earth Syst. Sci.* 19, 1827–1847. <https://doi.org/10.5194/hess-19-1827-2015>.
- SVKG, 2012. *Das Schweizerische Schätzerhandbuch*. Aarau.
- Teng, J., Vaze, J., Chiew, F.H.S., Wang, B., Perraud, J.-M., 2012. Estimating the relative uncertainties sourced from GCMs and hydrological models in modeling climate change impact on runoff. *J. Hydrometeorol.* 13, 122–139. <https://doi.org/10.1175/JHM-D-11-058.1>.
- Thielen, A.H., Kammerer, H., Dobler, C., Lammel, J., Schöberl, F., 2016. Estimating changes in flood risks and benefits of non-structural adaptation strategies - a case study from Tyrol, Austria. *Mitig. Adapt. Strateg. Glob. Chang.* 21, 343–376. <https://doi.org/10.1007/s11027-014-9602-3>.
- Tofiq, F.A., Guven, A., 2014. Prediction of design flood discharge by statistical downscaling and general circulation models. *J. Hydrol.* 1145–1153. <https://doi.org/10.1016/j.jhydrol.2014.06.028>.
- Totschnig, R., Sedlacek, W., Fuchs, S., 2011. A quantitative vulnerability function for fluvial sediment transport. *Nat. Hazards* 58, 681–703. <https://doi.org/10.1007/s11069-010-9623-5>.
- Vandenbergh, S., Verhoest, N.E.C., Buyse, E., de Baets, B., 2010. A stochastic design rainfall generator based on copulas and mass curves. *Hydrol. Earth Syst. Sci.* 14, 2429–2442. <https://doi.org/10.5194/hess-14-2429-2010>.
- Vetsch, D., Siviglia, A., Ehrbar, D., Facchini, M., Gerber, M., Kammerer, S., Peter, S., Vonwiller, L., Volz, C., Farshi, D., Mueller, R., Rousset, P., Veprek, R., Faeh, R., 2016. Basement: basic simulation environment for computation of environmental flow and natural hazard simulation. www.basement.ethz.ch.
- Viviroli, D., Mittelbach, H., Gurtz, J., Weingartner, R., 2009a. Continuous simulation for flood estimation in ungauged mesoscale catchments of Switzerland - part II: parameter regionalisation and flood estimation results. *J. Hydrol.* 377, 208–225. <https://doi.org/10.1016/j.jhydrol.2009.08.022>.
- Viviroli, D., Zappa, M., Gurtz, J., Weingartner, R., 2009b. An introduction to the hydrological modelling system Preval and its pre- and post-processing-tools. *Environ. Model. Softw.* 24, 1209–1222. <https://doi.org/10.1016/j.envsoft.2009.04.001>.
- Vorogushyn, S., Lindenschmidt, K.-E., Kreibich, H., Apel, H., Merz, B., 2012. Analysis of a detention basin impact on dike failure probabilities and flood risk for a channel-dike-floodplain system along the River Elbe, Germany. *J. Hydrol.* 120–131. <https://doi.org/10.1016/j.jhydrol.2012.03.006>.
- Wang, C., Zhang, L., Lee, S.-K., Wu, L., Mechoso, C.R., 2014. A global perspective on CMIP5 climate model biases. *Nat. Clim. Chang.* 4, 201–205. <http://www.nature.com/nclimate/journal/v4/n3/full/nclimate2118.html?foxtrotcallback=true>. <https://doi.org/10.1038/nclimate2118>.
- Wilby, R.L., 2010. Evaluating climate model outputs for hydrological applications. *Hydrol. Sci. J.* 55, 1090–1093. <https://doi.org/10.1080/02626667.2010.513212>.
- Winsemius, H.C., Aerts, J.C.J.H., van Beek, L.P.H., Bierkens, M.F.P., Bouwman, A., Jongman, B., Kwadijk, J.C.J., Ligtoet, W., Lucas, P.L., van Vuuren, D.P., Ward, P.J., 2015. Global drivers of future river flood risk. *Nat. Clim. Chang.* 6, 381–385. <https://doi.org/10.1038/nclimate2893>.
- WMO, 2009. *Manual on Estimation of Probable Maximum Precipitation (PMP)*.
- Xu, Y.-P., Gao, X., Zhu, Q., Zhang, Y., Kang, L., 2015. Coupling a regional climate model and a distributed hydrological model to assess future water resources in Jinhua River Basin, East China. *J. Hydrol. Eng.* 20, 04014054. [https://doi.org/10.1061/\(ASCE\)HE.1943-5584.0001007](https://doi.org/10.1061/(ASCE)HE.1943-5584.0001007).
- Zappa, M., Andres, N., Kienzler, P., Näf-Huber, D., Marti, C., Oplatka, M., 2015. Crash tests for forward-looking flood control in the city of Zürich (Switzerland). *Proc. Int. Assoc. Hydrol. Sci.* 235–242. <https://doi.org/10.5194/piabs-370-235-2015>.
- Zittis, G., Bruggeman, A., Camera, C., Hadjicicolaou, P., Lelieveld, J., 2017. The added value of convection permitting simulations of extreme precipitation events over the Eastern Mediterranean. 191, 20–33. <https://doi.org/10.1016/j.atmosres.2017.03.002>.

Paper 24: Zischg, A., Hofer, P., Mosimann, M., Röthlisberger, V., Ramirez, J.A., Keiler, M., Weingartner, R., 2018. Flood risk (d)evolution: Disentangling key drivers of flood risk change with a retro-model experiment. *Science of the Total Environment* 639, 195–207. [10.1016/j.scitotenv.2018.05.056](https://doi.org/10.1016/j.scitotenv.2018.05.056).



Flood risk (d)evolution: Disentangling key drivers of flood risk change with a retro-model experiment



Andreas Paul Zischg^{a,b,*}, Patrick Hofer^b, Markus Mosimann^{a,b}, Veronika Röthlisberger^{a,b}, Jorge A. Ramirez^b, Margreth Keiler^{a,b}, Rolf Weingartner^{a,b}

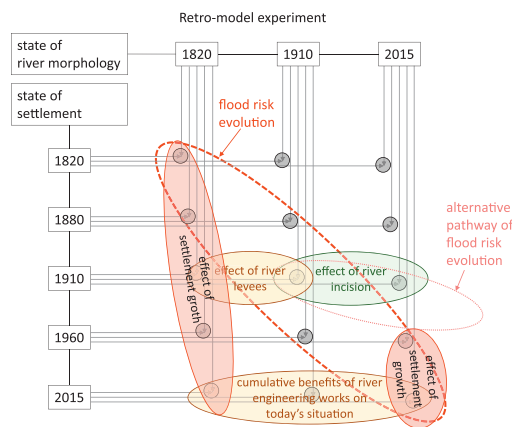
^a Oeschger Centre for Climate Change Research, University of Bern, Falkenplatz 16, 3012 Bern, Switzerland

^b Institute of Geography, University of Bern, Hallerstrasse 12, 3012 Bern, Switzerland

HIGHLIGHTS

- A novel approach for disentangling spatio-temporal dynamics in flood risk change
- River levees, river incision and urbanization as drivers of flood risk considered
- Flood risks markedly change at decadal and centennial time scale.
- Construction of levees and consecutive river incision are main drivers.
- Rebound effect due to settlement growth after levee construction quantified

GRAPHICAL ABSTRACT



ARTICLE INFO

Article history:

Received 26 February 2018

Received in revised form 4 May 2018

Accepted 4 May 2018

Available online xxxx

Keywords:

Model experiment

Flood risk change

Spatio-temporal dynamics of flood risk

Floodplain

Settlement development

River engineering

ABSTRACT

Flood risks are dynamically changing over time. Over decades and centuries, the main drivers for flood risk change are influenced either by perturbations or slow alterations in the natural environment or, more importantly, by socio-economic development and human interventions. However, changes in the natural and human environment are intertwined. Thus, the analysis of the main drivers for flood risk changes requires a disentangling of the individual risk components. Here, we present a method for isolating the individual effects of selected drivers of change and selected flood risk management options based on a model experiment. In contrast to purely synthetic model experiments, we built our analyses upon a retro-model consisting of several spatio-temporal stages of river morphology and settlement structure. The main advantage of this approach is that the overall long-term dynamics are known and do not have to be assumed. We used this model setup to analyse the temporal evolution of the flood risk, for an ex-post evaluation of the key drivers of change, and for analysing possible alternative pathways for flood risk evolution under different governance settings. We showed that in the study region the construction of lateral levees and the consecutive river incision are the main drivers for decreasing flood risks over the last century. A rebound effect in flood risk can be observed following an increase in settlements since the 1960s. This effect is not as relevant as the river engineering measures, but it will become increasingly relevant in the future with continued socio-economic growth. The presented approach could provide a methodological framework for studying pathways for future flood risk evolution and for the

* Corresponding author at: University of Bern, Oeschger Centre for Climate Change Research, Bern 3012, Switzerland.
E-mail address: andreas.zischg@giub.unibe.ch (A.P. Zischg).

formulation of narratives for adapting governmental flood risk strategies to the spatio-temporal dynamics in the built environment.

© 2018 Elsevier B.V. All rights reserved.

1. Introduction

Floods are one of the most damaging natural hazards, accounting for a majority of all economic losses from natural hazards worldwide (UNISDR, 2015). Managing flood risks requires knowledge about hazardous processes and their impacts. Risk resulting from floods is defined as a function of the probability of a flood event or scenario, respectively, and the related extent of damage (Fuchs et al., 2005). The latter is computed by a function of the monetary value of the object affected by the flood and its vulnerability against process magnitude.

However, the single factors of the risk formula are evolving over time, as well as the resulting risk. Consequently, flood risks are being more frequently analysed from a dynamical perspective rather than from a static one (Merz et al., 2010; Mazzorana et al., 2012). Hence, many studies are dealing with changes of natural risks over recent decades and centuries (Keiler et al., 2005; Hufschmidt et al., 2005; Keiler et al., 2006; Himmelsbach et al., 2015; Achleitner et al., 2016). In addition, research on climate change and their impacts is focusing on future changes in risks (Hundecha and Merz, 2012; Beckers et al., 2013; Hirabayashi et al., 2013; Merz et al., 2014; Alfieri et al., 2015a, 2015b; Devkota and Bhattarai, 2015; Alfieri et al., 2016; Arnell and Gosling, 2016; Kundzewicz et al., 2014). Only a few studies consider both, the impacts of climatic changes to river flows and the future dynamics in the elements at risk (Bouwer et al., 2010; Jongman et al., 2012; Liu et al., 2015; Winsemius et al., 2015; Löschner et al., 2016). However, most studies focus on the future increase of flood risk. To our knowledge, a closer look at the dynamics of the change itself is rather rare.

Several intertwined natural and anthropogenic drivers influence the spatio-temporal evolution of flood risk in floodplains. Floods are either caused by direct rainfall on the floodplain (pluvial floods, surface water floods) or rainfall on river catchments resulting in catchment outflow. The latter is causing floods in downstream floodplains (riverine floods, lake floods). Thus, the boundary conditions of floods in a floodplain can either be rainfall or river flow, or both. Consequently, changes in flood processes, i.e. changes in frequency and magnitude of floods in a floodplain, are determined by these external influencing factors. In several studies, the changes in rainfall frequency and intensity are investigated, with a special focus on the effects of climatic changes (Gobiet et al., 2014; Arheimer and Lindström, 2015). Thus, changes in the incoming flow hydrographs are external drivers of change in floodplains (Hollis, 1975; Hooke, 2006; Muñoz et al., 2017). In mountainous areas, flood losses are also influenced by sediment transport and deposition processes (Staffler et al., 2008; Keiler et al., 2010).

River morphology changes over time (Marani and Rigon, 1994; Pinter et al., 2001; Sear and Newson, 2003; Brierley and Fryirs, 2016; Slater et al., 2015) and this can include natural and gradual changes in the river morphology and flood regime (Church and Ferguson, 2015; Coulthard and Van De Wiel, 2007; Hall et al., 2014; Herget et al., 2007; Marchese et al., 2017; Vorogushyn and Merz, 2013; Arnaud-Fassetta, 2003), changes in the adjacent vegetation (Corenblit et al., 2014), or disruptive changes by flood events (Guan et al., 2016), e.g. by levee failures (Croke et al., 2015). Also important are anthropogenic interventions that are relevant drivers of flood risk in a floodplain, for example the construction of flood defences such as levees and dams (Pinter et al., 2000; Belz et al., 2001; Surian and Rinaldi, 2003; Bronstert et al., 2007; Di Baldassarre et al., 2009; Ernst et al., 2010; Bergillos et al., 2016) or river restoration projects (Kiss et al., 2008; Dixon et al., 2016). Changes in river morphology can be captured by reconstructing the morphology of historic states of the river and comparing it with the present state. This concept of retro-modelling was first defined by Remo and Pinter

(2007) and Remo et al. (2009). Retro-modelling provided a methodological framework for some of these mentioned studies. However, the construction of levees as flood protection measures in one floodplain can have adverse effects in downstream floodplains (Tobin, 1995; Pinter et al., 2006; Gregory, 2006; Zhao and Shao, 2015; van Triet et al., 2017) and can result in trade-offs in flooding between upstream and downstream floodplains (Ryffel et al., 2014; Salzmann et al., 2016). Likewise, land use changes impart an effect on catchment hydrology and floods (Burby and French, 2007; O'Connell et al., 2007; Rogger et al., 2017). For example, drainage of land for settlement or agriculture can incur subsidence that results in increasing flood hazards and flood risk (Carisi et al., 2017).

Beside changes in the natural environment, i.e. the fluvial aspect of the floodplain, flood risk is also changing due to variations in the exposed elements at risk and their vulnerability. One of the most relevant drivers of flood risk is the increase in the elements at risk due to socio-economic development (Elmer et al., 2012; Fuchs et al., 2015). The growth of settlements and thus the increase of residential buildings is related to population growth (Cammerer and Thielen, 2013). Infrastructure is increasing in parallel with population growth. This has wider impacts on the socio-economic system. For example, in economically active areas, floodplains are increasingly occupied by production facilities, as these require relatively flat areas for their construction (Nicholls and Crompton, 2017). Recent studies in Austria show an increase in the number of buildings potentially affected by floods of up to 700% in the last century (Fuchs et al., 2015; Fuchs et al., 2016). With economic development, the elements at risk and the infrastructure in floodplains are increasing in quantity and monetary value. Last but not least, higher object vulnerabilities (Adger, 2006; Posey, 2009; Boudou et al., 2016) due to changes in the construction techniques result in increasing flood risks. Increasing values at risk compete with the opposing drivers of flood risk reduction measures by individuals and the public (Wiering et al., 2017). Hence, changes in exposure and vulnerability are influenced by governmental interventions and regulations and by the actions of individuals (Noël and Cai, 2017). On the one hand, local governments regulate land use with spatial planning instruments. In many countries, the occupation and utilization of areas potentially affected by floods is not allowed or restricted. Moreover, governmental institutions and legislative entities are providing the basic principles and legislative frameworks for land use (planning) in floodplains (Gober and Wheeler, 2015). Thereby, land use regulations are dictating the actions of the individuals and businesses. Governments and insurance companies are increasingly enforcing individuals to protect their houses against floods with object protection measures.

In summary, the built environment in floodplains, whether the settlement area or the river channel, is subject to changes and co-evolutionary dynamics in both spheres of society and nature (Di Baldassarre et al., 2013a; Di Baldassarre et al., 2015). Floodplains are influenced by flood events and subsequent changes in the society, by governmental decisions as adaptation to these flood events, and individual agents (Di Baldassarre et al., 2013b). These dynamics between society and nature influences past and future risk pathways. Moreover, the spatio-temporal development of all these drivers for change in flood risk leads to difficulties in predicting flood risk. Consequently, recent studies have extended the framework of risk analysis towards a spatio-temporal framework as drivers for flood risk changes are varying in space and time (Ahmad and Simonovic, 2013; Aubrecht et al., 2013; Cammerer et al., 2013; Fuchs et al., 2013; Früh-Müller et al., 2015; Fuchs et al., 2016; Röthlisberger et al., 2016).

The main problem in estimating future risks and spatio-temporal dynamics in risk components is that a study design has to be based on assumptions of the future development of societal and natural drivers of flood risk. Thus, the future pathways of evolving flood risks could be remarkably diverse and risk predictions might be uncertain. We aim at closing this gap by proposing a model experiment, in which the evolution of the considered drivers for flood risk is known. The main research questions are how to set up the model experiment in a way that it enables a disentangling of the main drivers of change and how alternative pathways of flood risk evolution could be simulated. Essentially, we want to know how flood risk would have developed over the last 100 years if society had implemented nature based solutions for flood risk management rather than technical solutions involving river corrections. Herein, our hypothesis is that a multi-temporal (retro-) model of the floodplain allows to capture flood risk change in a spatially explicit way and to disentangle the main drivers of change.

2. Study area and methods

The key for disentangling the different drivers of change is to elaborate spatial datasets representing different states in time of each selected driver. In our model experiment, we consider the following drivers of change as they evolved through the time period 1820–2015: a) the river morphology and b) the size and structure of the settlement. Two processes, the construction of levees and the consecutive river incision influence the first driver. The model experiment is set up in a multi-temporal mode. This includes the creation of digital elevation models that represent historic states of the river morphology. In the model experiment, the different states of the river morphology (retro-models) are combined with different states of the building dataset. In addition, alternative development pathways are analysed by assuming the introduction of selected land use regulation strategies at an early point in time. The combination of the temporal states of the river and the settlement leads to the isolated quantification of the effects of

each selected driver of change. An overview of the method is given in Fig. 1.

2.1. Study area

The proposed approach of isolating the key drivers of flood risk change in a model experiment was developed in a case study where the necessary multi-temporal datasets of both river morphology and settlement structure are available. In Switzerland, the technology for river engineering and corrections spread in the early 19th century. One of the first relevant river corrections took place as early as in 1714 with the Kander River deviation (Wirth et al., 2011). In 1807 the Linth River was corrected (Vischer, 2003), and in 1824 the Aare River was corrected following the general zeitgeist of the era of river engineering. In the framework of preparatory planning of these river correction works, the engineers measured mean water flows at many cross sections and made astonishingly exact surveys of the natural river topography. These data are available in the archives of the public authorities.

In our study, we focus on the floodplain of the Emme River between Burgdorf and Gerlafingen (Canton of Bern, Switzerland, see Fig. 2). The Emme River drains a river catchment of 963 km² upstream of the study area. The mean altitude of the pre-alpine catchment is about 860 m a.s.l. The size of the study area is 55 km².

2.1.1. Historic development of river morphology and settlements in the study area

The floodplain experienced a devastating and well-documented flood event in 1764. After this flood event, the authorities began with the installation of simple wooden river stabilisation measures. Moreover, after the flood events 1868 and 1876, the federal and cantonal authorities decided to regulate the main river course of the Emme, and in 1884 they began with the construction of lateral dikes. In the following decade, the narrowed riverbed incised by up to 2.4 m. Consequently, soon after the first anthropogenic modifications the erosion had to be

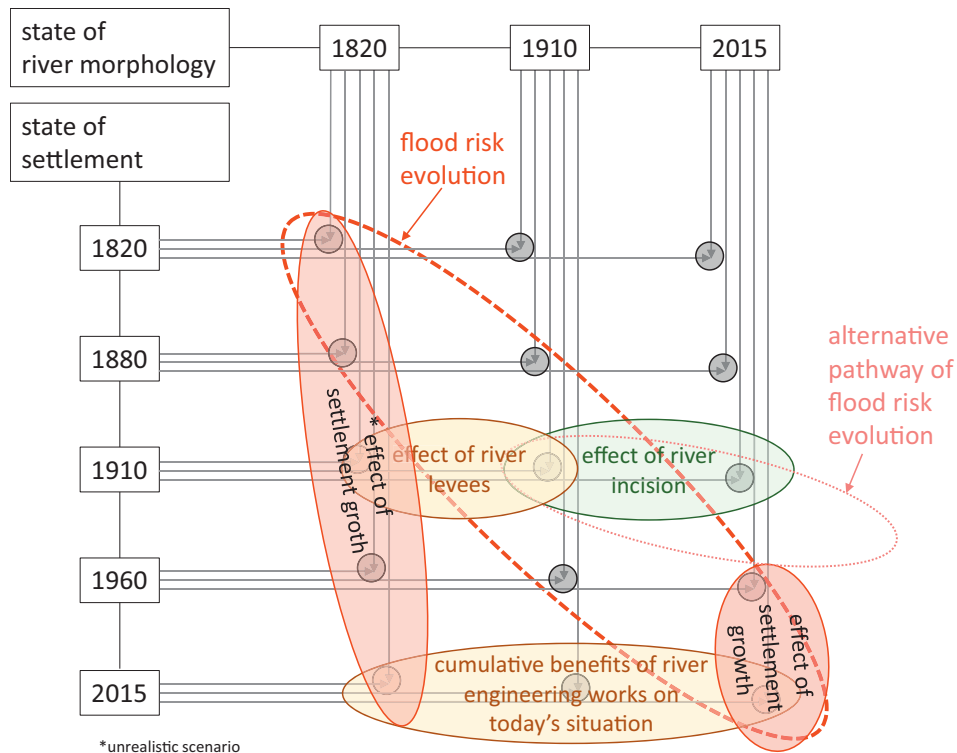


Fig. 1. Overview of the model experiment. The different states of the river morphology are combined with different states of the settlement. The combinations allow analysing the key drivers of flood risk change in isolation. The timesteps are defined by the availability of historic data sources and maps.

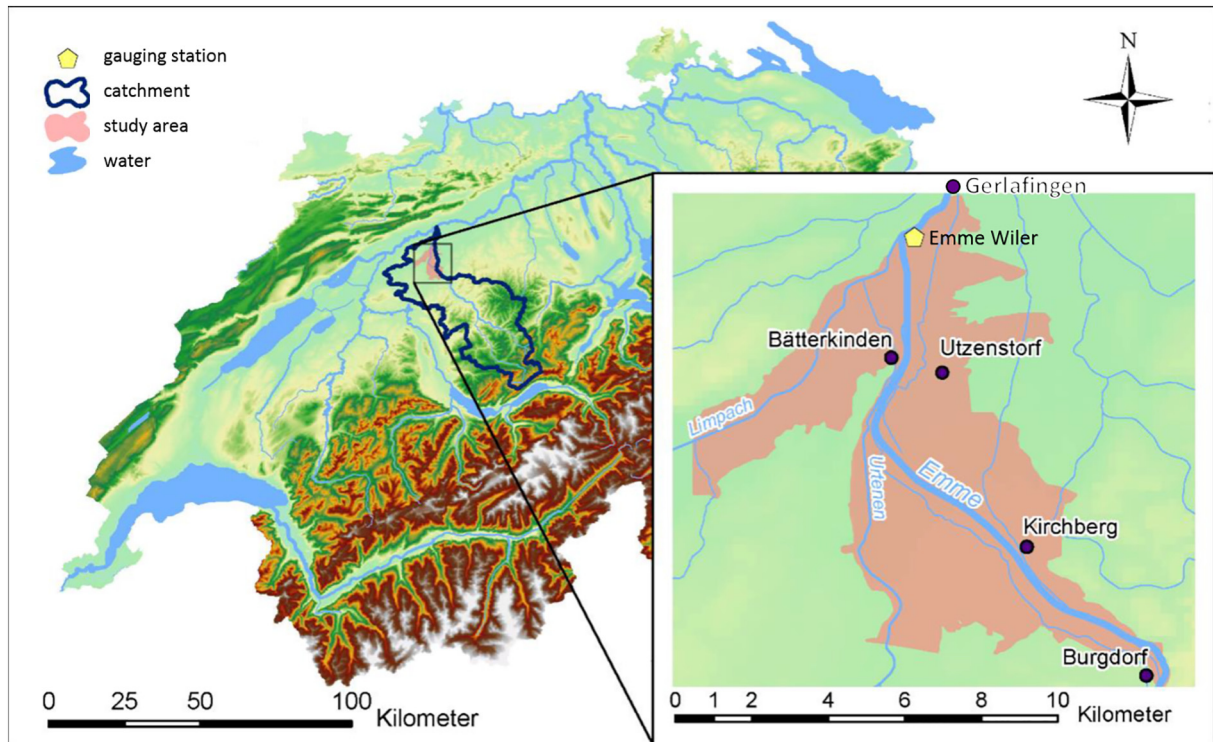


Fig. 2. Overview of the study area, the floodplain of the Emme River downstream of Burgdorf, Switzerland.

stopped by the construction of riverbed stabilisation measures. Hence, this case study shows exemplarily a highly dynamic evolution of a natural river towards an anthropogenically modified river. Additionally, the floodplain experienced a considerable economic growth in the late 19th and throughout the 20th century. This has been reflected by a population increase as well as by the number of houses.

The dates for the reconstruction of the historic states of the floodplain are mainly determined by the availability of reliable historic sources and relevant dates with abrupt changes in parts of the study area. The present day situation represents the status of the river morphology and the status of the settlements in the year 2015. The most recent datasets are available for this year. The furthest point back in time with reliable data for reconstructing the natural state of the floodplain is the year 1820. For this year, reliable historic surveys were available. A map from the year 1820 allowed the reconstruction of the settlements. Between 1880 and 1910, the river corrections took place with the construction of lateral levees. Hence, a map dated by 1910 allowed reconstructing both the river and the settlement models. After the construction of lateral levees, the riverbed incised remarkably. The incision stopped only in the 1960s after the construction of transverse structures for riverbed stabilisation. Since then, the river morphology did not change substantially. We reconstructed the state of the settlements in 1960 to capture the relevant increase of the settlements in this economically prosperous period.

2.2. Model experiment

The model experiment was based on the combination of different states of the floodplain in time. We focused on the evolution of flood risk since 1820 and on the comparison of the effects of selected driving forces for flood risk change, i.e. the effects of changing river morphology and the effect of settlement growth. From now on, we use the abbreviation SRS for the state of the river morphology and SSS for the state of

the settlement. We used the following combinations of specific states of these factors for answering the research questions:

- The **evolution of flood risk** is quantified by analysing the flood risk in the years 1820 (SRS 1820 \cap SSS 1820), 1880 (SRS 1820 \cap SSS 1880), 1910 (SRS 1910 \cap SSS 1910), 1960 (SRS 2015 \cap SSS 1960), and 2015 (SRS 2015 \cap SSS 2015). According to the historic maps, the river morphology was relatively stable before the river corrections and after 1960. Between these selected points in time, we assumed a linear trajectory of flood risk evolution because temporal states in between the selected ones are unknown.
- The **effects of river levees** are analysed by comparing the states before and after the construction works, i.e. comparing the combination SRS 1820 \cap SSS 1910 with the combination SRS 1910 \cap SSS 1910.
- To analyse the **effects of river incision** on flood risk, we compared the two following states: SRS 1910 \cap SSS 1910 and SRS 2015 \cap SSS 1910. This scenario isolates the effect of river incision by ignoring the effect of the increasing settlements.
- To capture the **effects of urbanization** in the 1960s and thereafter, we compared the states of the settlements in 1960 and 2015 in a constant river morphology (SRS 2015 \cap SSS 1960 vs. SRS 2015 \cap SSS 2015).

In addition to the analysis of the actual development of flood risk, we hypothesized **alternative pathways of flood risk development**. For these analyses, we used the following hypothetical combinations of specific states of river morphology and settlement:

- **Do-nothing:** In a baseline hypothetical scenario of the model experiment we explored no interventions for flood risk management. This scenario consists of the river morphology in 1910 with present day buildings (SRS 1910 \cap SSS 2015) and represents a 'do-nothing' policy. For comparison, this scenario is trialled with the combination SRS 2015 \cap SSS 2015 to answer the question of how many buildings are

benefitting today from the decisions made more than 100 years ago. In other words, this comparison quantifies the cumulative benefits of historic river engineering works on today's situation.

Moreover, we analysed the effects of an introduction of land use planning at an early point in time and thus the long-term effect of this kind of risk management policy. The municipalities in Switzerland have to consider hazard maps in their land use regulation plans. Depending on the hazard zone, the construction of houses is regulated or restricted. A description of the land use regulation policy is given in [Appendix A](#). The actual hazard maps have been incorporated into the municipal land use regulation plans in the period 2009–2015. The effect of this relatively recent intervention can only be quantified several years after implementation. Thus, we analysed the effects of an early implementation of the hazard maps on flood risk reduction. Considering hazard maps and land use regulation policy the following scenarios were developed:

- **Hypothetical land use regulation scenario 1: Land use regulation only.** In this experiment, we asked how many buildings occupied by people would not have been built in restricted areas (red hazard zones) if the hazard mapping regulation had been introduced in 1910 instead of in the 2000s. We elaborated a hazard map for the river morphology in 1910 following the actually valid guidelines for hazard mapping in Switzerland (see [Appendix A](#)). From the buildings dataset, we removed all the buildings that had been constructed in the red hazard zone (high hazard level) after the hypothetical implementation of the hazard map in 1910. This scenario shows an alternative pathway of flood risk development under strict land-use regulation over 100 years, starting from a relatively natural state of the river and following a nature-based flood risk management strategy.
- **Hypothetical land use regulation scenario 2: Land use regulation combined with object protection measures.** This scenario is based on the same assumptions as hypothetical scenario 1, but in addition we assumed that house owners in the blue hazard zones (medium hazard) implement object protection measures reducing the vulnerability of buildings by 50%, e.g. by sealing of house entrances or cellar windows to reduce the probability of water entering the house.
- **Hypothetical land use regulation scenario 3: Alternative policy.** This scenario hypothesizes the effects of an alternative land use regulation policy. Here, we implemented an alternative to the Swiss hazard mapping approach, by hypothetically adopting the Bavarian policy for hazard mapping. The main aspect of this policy is to avoid construction of houses in the area flooded by a 100-year flood event, irrespectively of the flow depths. As in the first and second hypothetical scenarios, we removed all the buildings that had been constructed in the regulated perimeter after the hypothetical implementation of this policy in 1910.

2.3. Analyses and models required for conducting the model experiment

To conduct the model experiment, three principal components must be prepared. The multi-temporal setup based on a) the retro-models of the river morphology, b) the retro-models of the houses, and c) the flood simulation and flood loss analysis module. In the following, we describe the main components of the model experiment.

2.3.1. Retro-models of the river morphology

The starting point of the multi-temporal analysis of changes in the river morphology is the actual situation. We elaborated a hydraulically correct digital elevation model (DEM) on the basis of a Lidar-based DEM with a spatial resolution of 0.5 m ([KAWA Amt für Wald des Kantons Bern, 2015](#)). We corrected the heights of the lateral levees with dGPS measurements. Hydraulic obstacles in the river channel (e.g. bridges) were removed, and the river bed below the water surface

was interpolated by using surveyed cross sections from the Federal Office for the Environment (FOEN) as described in [Zischg et al. \(2018b\)](#). The result is a DEM that reflects the anthropogenically modified river and its floodplain in 2015 (SRS 2015).

In total contrast to SRS 2015, we created a river channel that closely represents the morphology prior to any human interventions. We reconstructed this relatively natural state of the river by means of historic topographic maps (maps of Dufour and Siegfried from the federal Office for Topography SWISSTOPO) and contemporary topographic surveys ([Ritter, 1804](#); [Anonymous, 1780–1820, 1820a, 1820b, 1898](#)). The historic terrain models were reconstructed by georeferencing and digitalizing historic maps and historic cross-sections combined with the mapping of the geomorphologic evidences of former river structures in areas not modified by anthropogenic activities ([Zischg, 2016](#)). The historic maps and surveys are in a different coordinate system. Thus, we georeferenced the digitalized images with reference points and landmarks that are visible in both the historic and present day maps (see [Fig. 3](#)). We used the high-resolution digital elevation model for georeferencing the historic maps, because the abandoned channels and old branches indicated in the old maps are still visible in the present day DEM. The comparison of the historic maps with the landmarks in the DEM showed a high reliability and accuracy of the historic sources. From the georeferenced historic maps, we digitized the planform of the natural river course. In a subsequent step, we mapped all recent anthropogenic modifications of the terrain in the riverbed and the floodplain and erased these areas from the present day terrain model. In the resulting holes in the DEM, we interpolated a mean surface based on the elevation values at the lateral borders of the erased areas. This results in a terrain model free from artificial and hydraulically relevant landscape modifications. Afterwards, we incised the digitized areas of the historic riverbeds into the historic terrain model. The incision depth was delineated from the historic topographic surveys of cross section geometries. The resulting DEM represents the relatively natural river channel and floodplain in 1820 (SRS 1820, see [Fig. 4](#)). We repeated the procedure to elaborate the DEM of 1910 (SRS 1910) based on the maps of [Goldschmied \(1913\)](#) and [Luder \(1928\)](#). The reconstructed terrain models provided the basis for the creation of the computational mesh for a hydrodynamic model. In 1820, the river course was on average 90 m wide and the riverbed was about 1–3 m below the surrounding floodplain. In contrast, the present day DEM has a river width of 42 m and is on average 3 m below the natural river bed.

2.3.2. Retro-models of the elements at risk

In the analysis of flood risk, we focus explicitly on buildings and houses. In a multi-temporal exposure analysis, the building data set has to be elaborated for selected temporal states. For the present day situation, we used the building dataset elaborated by [Röthlisberger et al. \(2017\)](#). This dataset spatially represents the building's footprints, to which their building value and the number of inhabitants were attributed (SSS 2015). This dataset is based on the digital terrain model of the Federal Office for Topography SWISSTOPO and the residential statistics of the Federal Office for Statistics (FOS). The building value was calculated based on each building's volume, which has been derived from LIDAR measurements. The monetary value was calculated based on average construction prices. This present day situation provided the basis for the retro-models of the settlements. From a copy of this dataset, we removed the buildings which were not present in the topographic maps of 1959 and 1960 (SWISSTOPO). This results in a dataset representing the settlement in 1960 (SSS 1960). The historic Siegfried maps of 1915, 1916, and 1917 lead to a dataset of the settlements in 1910 (SSS 1910). The historic maps of 1871, 1879, 1880 lead to a dataset representing the year 1880 (SSS 1880). Finally, we used the historic Dufour map of the year 1845 (SWISSTOPO) and the maps of [Finsler \(1978\)](#) for reconstructing the status of settlements in 1820 (SSS 1820).

However, we let the reconstruction values, the type of functionality, and the vulnerability of the houses constant over the whole period in

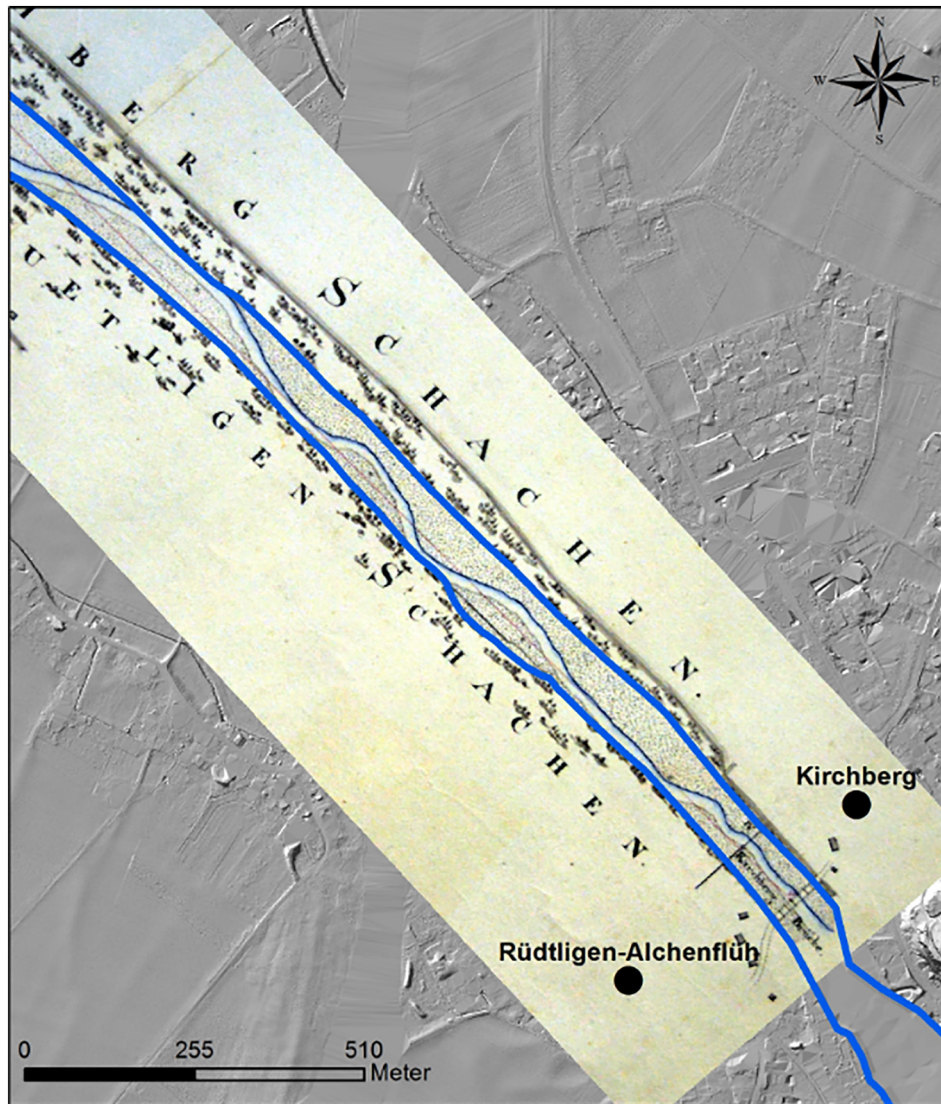


Fig. 3. Extract of the historic map of 1820 of the Emme river reach near Kirchberg, Switzerland.

the model experiment. This means that the losses vary only with the number of houses exposed to floods and not with the inflation or extension of building values over time.

2.3.3. Flood simulation and flood loss analyses

The selected spatio-temporal states of the digital terrain models and the buildings provided the basis for a flood loss analysis. For each temporal status of the river morphology, we simulated several flood events ranging from the mean annual flood to an extreme flood.

An important step in this procedure is the preparation of the hydrographs for flood simulation. On the basis of an observed discharge time-series, typical flood hydrographs, i.e. a synthetic design hydrograph, were derived using the guidelines proposed by Serinaldi and Grimaldi (2011). Based on measurements at the river gauging station in the study area, observed hydrographs were normalized in terms of event duration and peak discharge. The resulting dimensionless event hydrographs were superimposed and centered on the peak position. A two parametric gamma distribution function was fitted to represent the typical shape of the event hydrographs, as described by Nadarajah (2007) and Rai et al. (2009). This resulted in a synthetic unit hydrograph that represents a typical hydrograph shape of flood events in the corresponding catchment. The synthetic unit hydrograph was scaled to various peak discharges, whereas an empirical peak-

volume-ratio was used to determine the corresponding event duration. The procedure was applied to generate synthetic design hydrographs for a continuous series of peak discharges in intervals of $50 \text{ m}^3/\text{s}$ (Fig. 5). The occurrence probability of each hydrograph was delineated from the extremal statistics of the gauging station Emme Wiler (provided by FOEN). In general, the delineated synthetic hydrographs represent a typical flood hydrograph. Nevertheless, other event types could potentially occur, as for instance long lasting rainfall events (Brunner et al., 2018). These may have a higher volume than the one assumed while having the same peak discharge. In these cases, the flood losses may be higher.

In a further step, we developed a flood inundation model in two dimensions (2D) for each floodplain. We used the 2D flood inundation model BASEMENT to represent the water fluxes through the river and its floodplain (Vetsch et al., 2017). It is a numerical model solving the shallow water equations on the basis of an irregular mesh. An irregular mesh was generated from each of the reconstructed DEMs. The model has been validated with insurance claims in nearby case studies and reproduced well historic flood events (Zischg et al., 2018b). We calibrated the friction values of the SRS 2015 inundation model with the stage-discharge relationship at the gauging station at Emme-Wiler (FOEN). The friction value of $31 \text{ m}^{1/3}/\text{s}$ (Strickler coefficient) results in a maximum deviation of the model from the stage-discharge

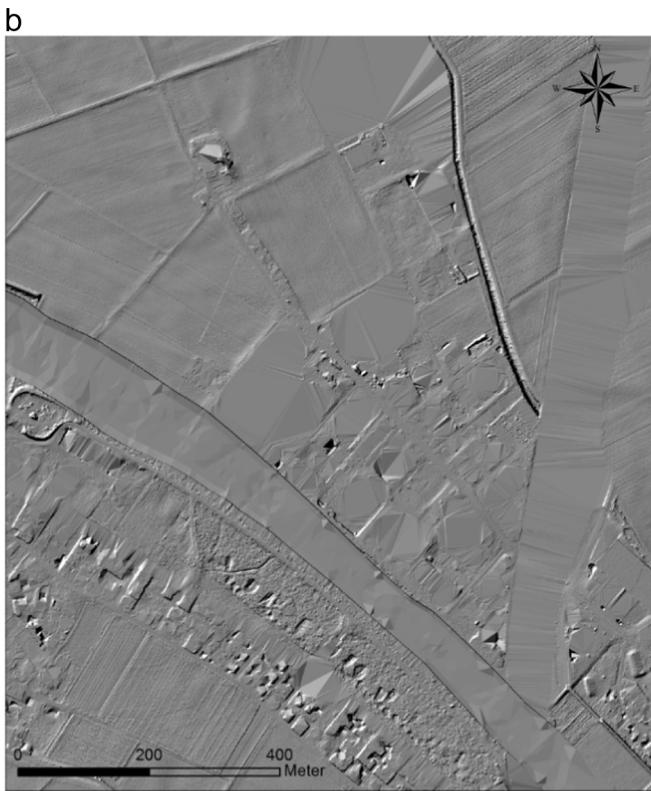
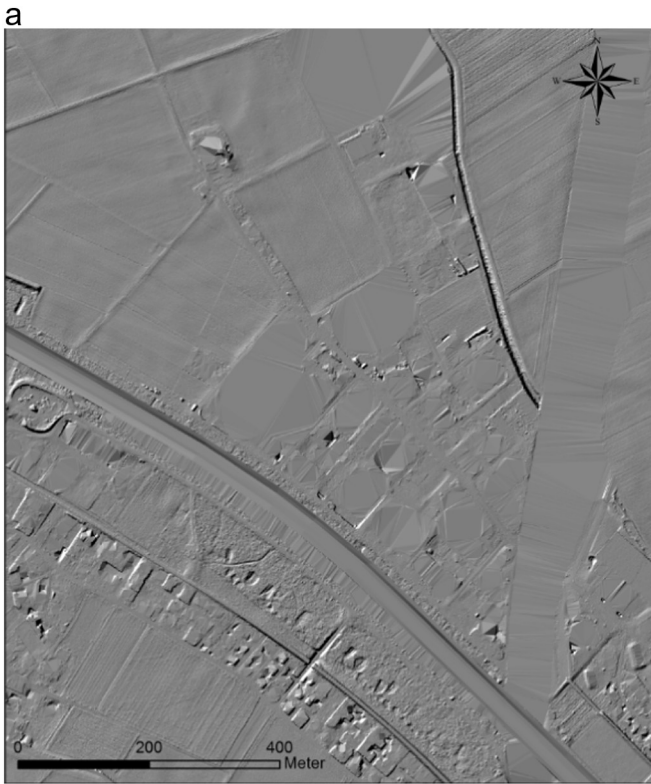


Fig. 4. Hillshades of the present day DEM (SRS 2015, left) and historic DEM of 1820 (SRS 1820, right).

relationship of 5 cm along the range of observations. The river structure is relatively homogeneous along the river reach. Thus, we assumed the same friction value for the riverbed across the whole river reach. The average size of the mesh elements is approximately 32 m² in the river channel and 279 m² in the floodplain. The main linear structures are considered in the mesh as break lines.

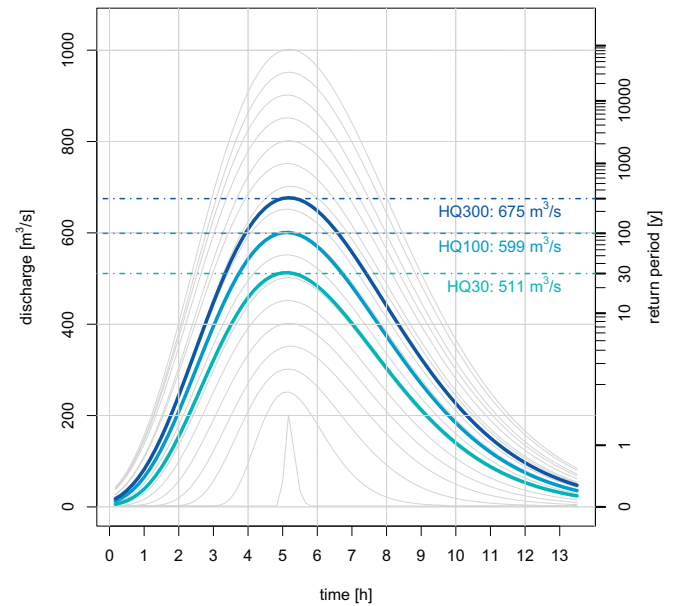


Fig. 5. Synthetic hydrographs with an interval of 50 m³/s used for the flood simulations. In addition, the three hydrographs used for the elaboration of the hazard maps are shown in bold lines.

As there are no flood events in the floodplains recorded in the past years but a few bank-full discharge flood events, we validated the hydraulic model with the flood events on 08th August 2007 and 24th July 2014. As in reality, the model simulated a bank-full discharge with no overtopping and consequently no flooding in the floodplain. Hence, the model reproduces the bank-full discharge (water surface elevations max. 15 cm below dam heights) without overtopping the lateral levees. Moreover, we checked if the simulation model reproduces the weak points known by the official hydraulic engineering authorities, i.e. the locations along the river where water is first overtopping the levees in case of a flood. These weak points have been reproduced by the model and overflowing of the dams is beginning at known locations.

The synthetic design hydrographs were used as upper boundary conditions for the 2D inundation model of each terrain model. The lower boundary condition is defined as where the water flows out of the model. The flow depths resulting from the hydrodynamic models were attributed to each building by identifying the maximum flow depth of all nodes within the footprint of the building (Bermúdez and Zischg, 2018). This leads to the calculation of the object-specific vulnerability and estimation of object-specific losses (Zischg et al., 2013; Zischg et al., 2018a). Vulnerability functions provide a degree of loss on the basis of the flow depth at the location of the house. The value ranges from 0 (no damage) to 1 (total loss). This degree of loss is subsequently multiplied by the specific reconstruction value of the building. Currently, five vulnerability functions are considered in the damage calculation procedure. We used the functions of Hydrotec (2001), Dutta et al. (2003), Jonkman et al. (2008), Totschnig et al. (2011), and Paphoma-Köhle et al. (2015). The multiplication of the building value of the house with the degree of loss leads to the flood-loss for a specific exposed object (e.g., a single house). The multi-model ensemble of losses calculated with different vulnerability functions was aggregated to an average loss at single building level, as proposed by Figueiredo et al. (2017). The sum of all losses of each flood scenario in the floodplain enters into the “flood peak – flood loss” relationship of the floodplain. The aggregated losses are subsequently multiplied with the probability of the scenario. The flood risk over all scenarios until a return period of 100 years results from the integration of all scenario-related risks (Fig. 10). Applying a range of scenarios covering the

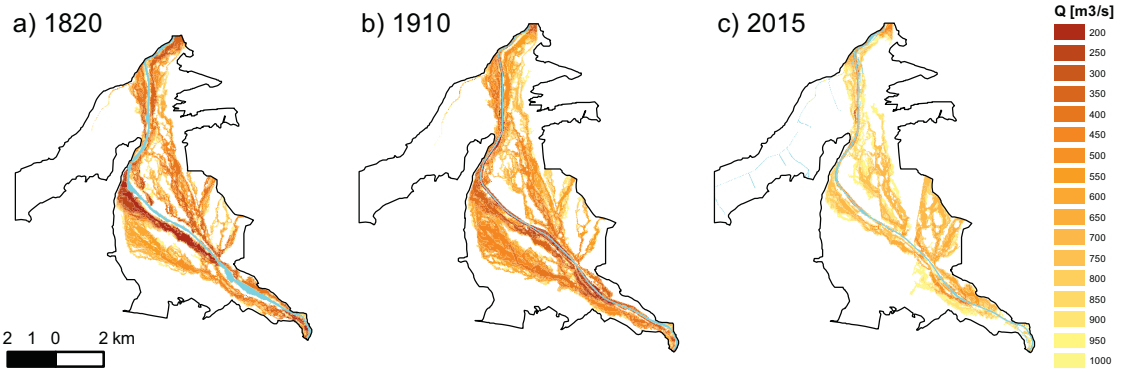


Fig. 6. Minimal peak discharge needed for flooding specific locations in the floodplain: a) Flood map of a natural river morphology in 1820, b) flood map of the river morphology in 1910, c) flood map of the present day situation (2015).

expected flood magnitudes in the river reach offers a differentiated sensitivity analysis of the floodplain against the flood magnitude, and thus non-linear behavior in the flood peak – flood loss relationship can be detected if present.

3. Results and discussion

The multi-temporal retro-model consists of three states in time of the river morphology and five states in time of the settlement structure.

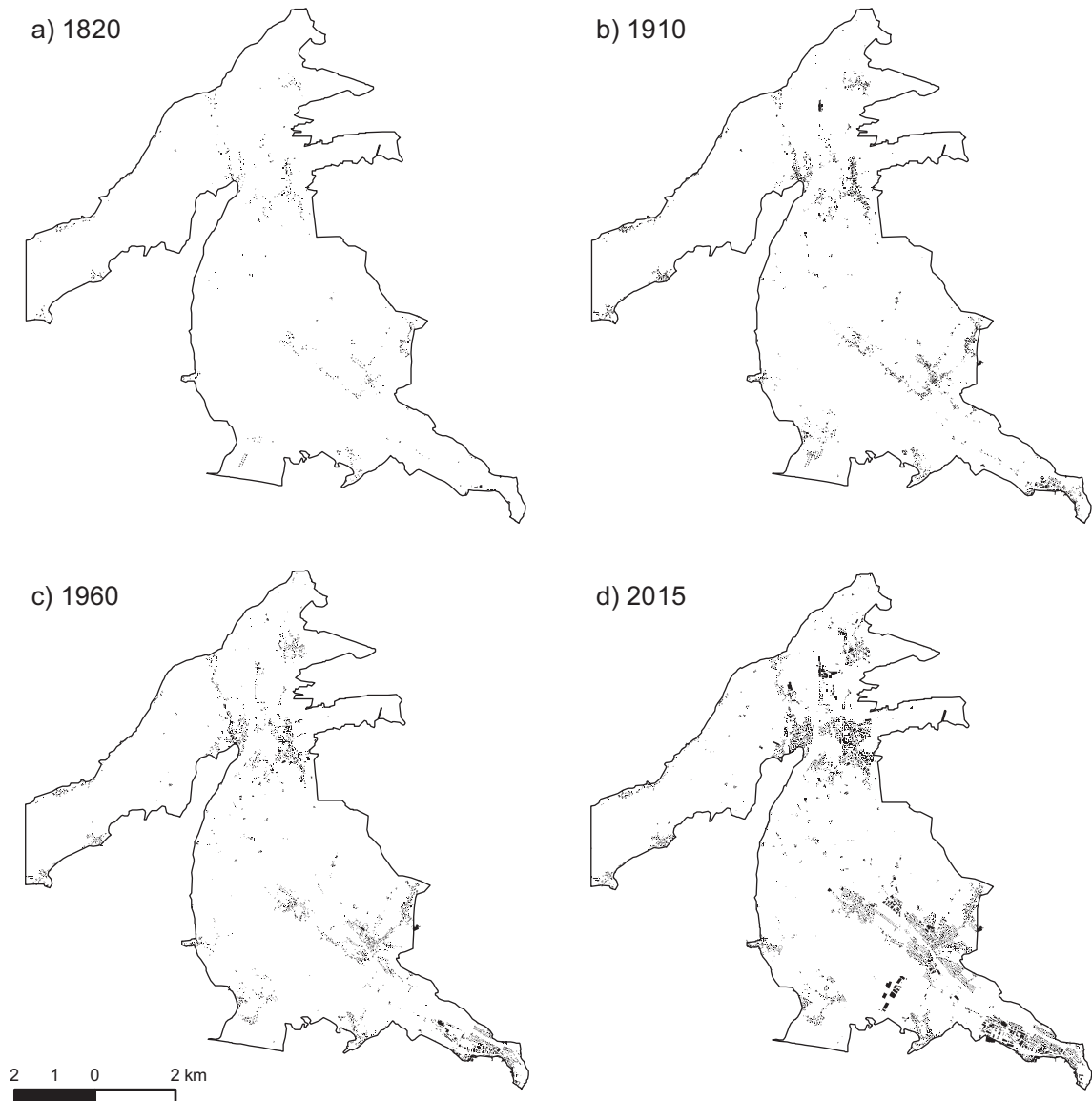


Fig. 7. Overview of the spatio-temporal evolution in settlement structure.

The hydraulic simulations result in three sets of flood scenarios based on the DEMs of the river models. The simulations show the spatial pattern of the floodplain's sensitivity against the flood magnitude. In Fig. 6, the set of scenarios are shown in a generalized way. For each mesh triangle, the minimum peak discharge is shown that is needed to flood the respective part of the floodplain. The figure shows the effectiveness of the levees in terms of reducing flooded areas from 1820 (Fig. 6a), to 1910 (Fig. 6b) and 2015 (Fig. 6c). The maximum flood considered in this study (with a peak discharge of 1000 m³/s, corresponding to a return period of 81,800 years) covers an area of 19.5 km² in the original state of the river while only 13.7 km² are being flooded in the present day DEM. The river incision reduces the flooded areas by 7.5 km². This means that the river correction is also remarkably effective in an extreme flood event. More important from the risk point of view, the reduction of flooded areas is more effective in frequent floods. For instance, a flood event with a return period of 30 years (peak discharge of 511 m³/s) covers 11.47 km² in 1910 while it covers only 0.96 km² today.

In addition to the changes in the river morphology, the settlement structure co-evolved with the river. Fig. 7 shows the time stamps of the settlement structure. The settlement in the study area grew by a factor of 10.6 in the period 1820–2015, by a factor of 3.6 in the period 1820–1910, and by a factor of 2.9 in the period 1910–2015. Fig. 8 demonstrates the temporal evolution of the settlement aggregated for the whole floodplain of the Emme River.

3.1. Flood risk evolution and drivers of flood risk change

The shown spatio-temporal dynamics allows the quantification of the flood risk change (Fig. 10, right). Flood risk in 1820 was in the order of 6.2 mio. CHF/year. It increased to 21.6 mio. CHF/year in 1880, because of the settlement growth. After the construction of the levee, flood risk decreased to 17.3 mio. CHF/year in 1910 and further to 0.6 mio. CHF/year in 1960 due to the consecutive river incision. After 1960, flood risk increased again to 3 mio. CHF/year until 2015. In summary, flood risk in 2015 is half (48.4%, 3.2 mio. CHF/year less) of that in 1820. Surprisingly, flood risk decreased overall in the period 1820–2015, with a rebound effect since 1960.

When looking at the main drivers, the river engineering measures are the most important driver for flood risk change (−42.4 mio. CHF/year, calculated as shown in Fig. 10b). However, an important part of this flood risk reduction is due to the incision after the construction of the levees. The river incision between 1910 and 1960 increased the river conveyance and resulted in a flood risk reduction of 16.7 mio. CHF/year when assuming SSS 1910 as constant. This is 40.3% of the total flood risk reduction by the river engineering measures (flood risk change in the period 1880–1960). The engineering works are effective in the full range of peak discharges, meaning that they reduce the losses also in the extremal range of peak of flood magnitudes. Herein, the 'peak discharge – flood loss' relationship, i.e. the loss footprint of the floodplain, allows a closer look at the sensitivity of the floodplain against flood magnitudes (Fig. 9).

When looking at the effect of the growing settlements, we can observe that this factor constrains the effects of the river engineering measures. From 1960 to 2015, flood risk increased by 2.4 mio. CHF/year (a factor of 5) after a period with decreasing risk. As shown in Fig. 9, exposure increases mostly in the extremal range of flood magnitudes. This diagram shows that the river engineering measures introduce a threshold behavior into the floodplain's loss footprint. In the river morphology of 2015, there are no losses until a certain threshold in flood magnitude. However, beyond this threshold losses increase with a high rate. This means that losses are sensitive against an increase in peak discharge in the upper range of return periods. In contrast, the natural state of the river is less responsive to increasing flood magnitude (Figs. 9 and 10). Especially in the upper range of floods, the rate of increase in

flood losses with peak discharge is much lower than in the present day state. However, the overall losses are much higher.

3.2. Alternative pathways of flood risk evolution

In addition to the identification of the main drivers, we analysed the effects of alternative policies as exemplarily demonstrated by Thaler et al. (2018) for prioritization strategies. The do-nothing strategy, based on the assumption that no interventions are taken, results in a flood risk that is 45.6 times higher than the present day risk (Fig. 10). Thus, the cumulative effect of all river engineering measures of the present day state is a flood risk reduction of 133.9 mio. CHF/year when considering SSS 2015 as the baseline. In absolute numbers, 1950 houses are protected from a 100-year flood when compared with a relatively natural river morphology (SRS 1820). The losses of a 100-year flood are reduced by 84.5% in comparison to the do-nothing strategy. When assuming the state of settlement in 1820 as constant over time in combination with a changing river morphology, the number of exposed buildings decreased by 85%.

The first hypothetical land use regulation scenario on alternative pathways shows that an introduction of the hazard mapping policy as early as 1910 would have resulted in a flood risk that is 25.5 times higher than the present day risk reduced by river engineering works, but 28.2% less than in a do-nothing scenario (hypothetical land use regulation scenario 2). In contrast, if an average reduction of the vulnerability of houses against flooding in blue hazard zones by 50% is considered, this results in a further risk reduction of 28.7% (in total 56.9% less than the do-nothing scenario, hypothetical land use regulation scenario 2). Thus, the effectiveness of the actual hazard mapping policy markedly depends on the implementation of object protection measures. Interestingly, the hypothetical consideration of an alternative land use regulation policy (hypothetical land use regulation scenario 3), e.g. the Bavarian land use regulation policy (Drost and Ell, 2016), shows that the effectiveness of different kinds of policies would be remarkably diverse. Under the Bavarian policy the model suggests that risk reduction is in the same range as technical measures. Both technical measures and this policy is aiming at protecting elements at risk up to a design event of a 100-year flood. Thus, non-technical interventions can compete with engineering measures (Thieken et al., 2016), but they have to be implemented in a long time horizon, as shown by Fig. 10.

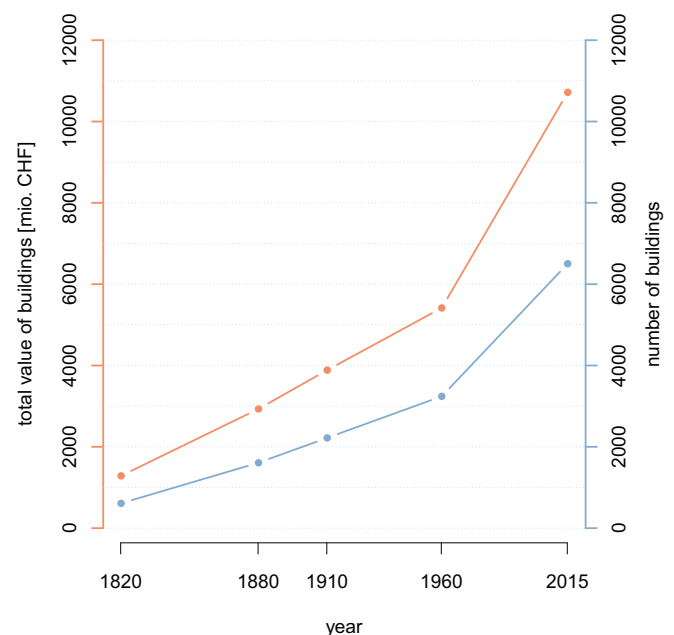


Fig. 8. Settlement growth in the study area in the period 1820–2015.

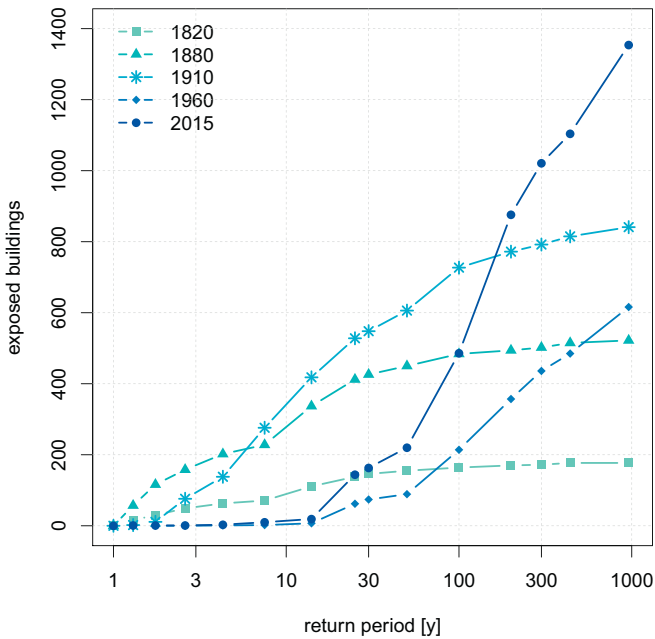


Fig. 9. Peak discharge – flood exposure relationships in different states of the floodplain.

4. Conclusions

In the model experiment, we showed that the most relevant of the considered drivers of change in the study region is the human intervention on the river morphology. However, changes of river morphology by the construction of the lateral dams are not the only driver for decreasing risk. The levees alone are effective for flood risk reduction only in the range of frequent floods up to a peak discharge 450 m³/s (return period ~14 years). In contrast, a relevant driver for flood risk reduction is the incision of the river following the construction of the levees. The incision

markedly increases the river conveyance and consequently reduces the frequency of flooding in the floodplain. Thus, this secondary effect of the human interventions has also a high relevance for reducing flood risks.

The effects of river morphology that decrease flood risk are partly rebound by an increase of the elements at risk since the 1960s. However, the effects of the drivers that reduce flood risks are more relevant than the effects of the drivers that increase risks. Overall, a decrease in flood risk results.

While the results of the model experiment are case-specific, the described retro-modelling experiment approach demonstrated a suitable method for disentangling the main drivers of change in flood risk. Besides disentangling drivers of change, the presented model experiment allows the analysis of alternative pathways. We have shown the isolated effect of land use regulation that restricts the construction of houses in hazard zones. Nevertheless, land use regulation aiming at limiting flood exposure needs a long-term time horizon to become effective. Furthermore, the actual hazard mapping policy is less effective than other concepts of land use regulation, e.g. keeping the flooded area of a 100-year flood event totally free from new constructions. The latter has a higher effectiveness, especially in combination with the strategy of reserving room for rivers, and is applied in other European regions as for example in Bavaria, Germany (Drost and Ell, 2016). If in 1910 this policy had been implemented instead of the river corrections with the following river incision, the risk would only slightly be higher than in the present day situation. Thus, keeping the floodplains free from houses for a long period is nearly as effective as constructive protection measures. Nonetheless, the costs of this policy in terms of missed opportunities due to unrealised economic land use have to be discussed before a final conclusion can be drawn.

We showed that the flood risk is evolving considerably and that it is not necessarily increasing. In contrast, the presented examples show a relevant decrease of the flood risk in the past 200 years. Furthermore, the presented example confirms the so called levee effect (White, 1945), caused by the increase of settlement in floodplains protected by levees. Mainly, overall flood risk in engineered river systems is only increasing due to an increase in residual risks.

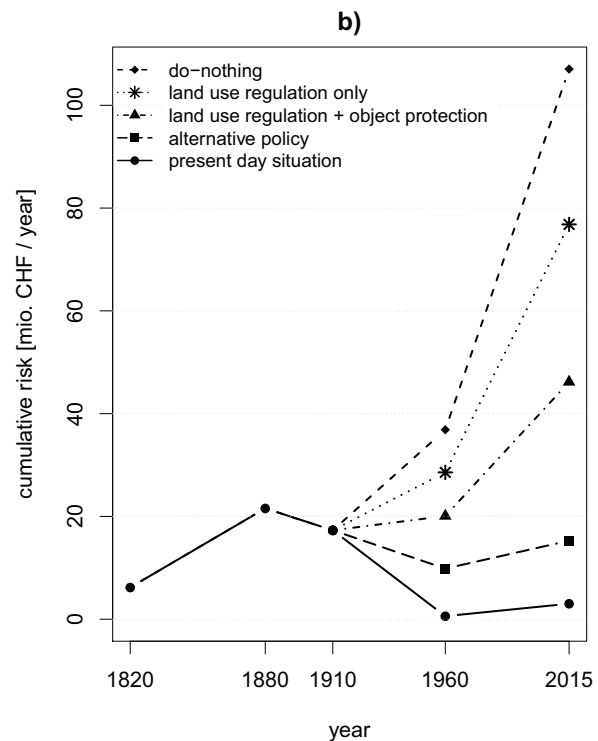
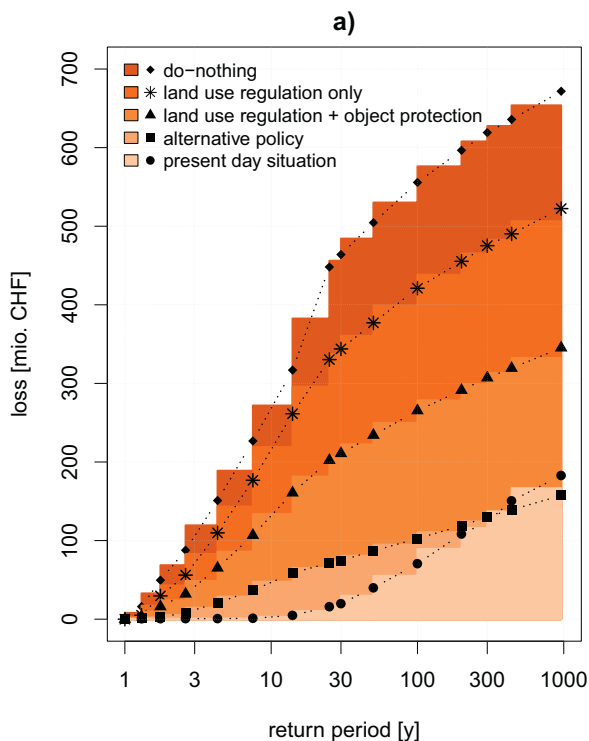


Fig. 10. a) Flood loss footprint of the floodplain. b) Trajectory of flood risk evolution and alternative pathways. Hypothetical scenario 1 considers land use regulation only.

In comparison to fully synthetic model experiments, the study design of the retro-model experiment is based on real data. This means that such a model experiment must not necessarily contain highly uncertain assumptions that are inherent in fully synthetic model experiments. Examples for such assumptions are the growth factor of the settlement, the intervention of governments in the form of hydraulic engineering works, or the spatio-temporal dynamics of settlement evolution after the introduction of land use maps. All of these dynamics are unknown in prospective experiments. Nevertheless, a retro-model experiment allows analysing alternative pathways of floodplain evolution, by altering one model parameter while letting the others constant.

The retro-model has a potential for analysing feedbacks between physical and social processes. With this, the approach may help to understand perspectives for the future by considering the feedback mechanisms between the drivers of flood risk change in the past. This may provide a basis for developing coupled component models of the full flood risk chain from climate, precipitation, floods and losses that consider the spatio-temporal dynamics in both physical and socio-economic components, e.g. considering adaptation efforts in future projections of flood risk. This should eventually lead to sophisticated model chains that consider at least partially the complexity in flood risk evolution. The approach may be furthermore adapted for a risk monitoring program as demanded by Zischg et al. (2013). By quantitatively observing the spatio-temporal dynamics of the single factors in the risk formula, the evolution of flood risk can be monitored as well.

Last but not least, a retro-model is a reliable basis for the formulation of narratives in climate adaptation (Dessai and Hulme, 2004). They can provide good examples for successful adaptation pathways (Wise et al., 2014) in history. Furthermore, they could be used in risk communication for demonstrating undesired effects of the sum of individual decisions over a long period, and for illustrating how undesired side effects could be avoided by the design of natural flood management options (Lane, 2017; Thieken et al., 2016). However, projections of future adaptation pathways should not be based on past trends identified by retro-models. Furthermore, the presented approach has other important limitations. First, it requires reliable and accurate historic spatial data over a long period and second, the spatio-temporal dynamics of flood risk between the selected time steps are unknown.

Acknowledgments

The authors acknowledge the Federal Office for Environment FOEN for providing the data of river cross-sections and gauging station data, the Federal Office for Topography SWISSTOPO for providing basic GIS data, the Federal Office for Statistics FOS for providing the residential statistics, and the Canton of Bern for providing the Lidar data and the event documentation data. This work was financially supported by the Mobilier Lab for Natural Risks.

Appendix A. Hazard mapping and land use planning in Switzerland

In Switzerland, all municipalities are obliged to elaborate a hazard map. This hazard map classifies an examined area into five categories with respect to the magnitude and frequency of potential flood events (Fuchs et al., 2017). Red zones (high hazard) indicate areas where residents are at risk both inside and outside of buildings and sudden destruction of a building is possible upon impact with process-related forces. Blue zones (moderate hazard) indicate those areas where people are at risk outside of buildings and moderate destruction of buildings may be possible. Yellow zones (low hazard) delimit areas where flood hazard may lead to considerable monetary loss at buildings, but people are rarely at risk. The main criteria for classification of the hazard is the flood intensity with thresholds at 0.5 m or 0.5 m²/s (yellow and blue), between 0.5 m and 2.0 m or 0.5 m²/s and 2.0 m²/s (yellow and blue), or exceeding 2.0 m or 2.0 m²/s (red). The probability of occurrence of

the underlying flood hazard is used to further distinguish the hazard zones for up to 30 year (blue and red), 30–100 year (yellow, blue and red) and 100 to 300 year (yellow and red) return periods. Areas within the investigation focus but without a potential hazard are coloured as white. Areas susceptible to a residual risk are coloured in yellow-white striped, i.e. areas in which the probability of occurrence of a flood event is less than one in 300 years. The hazard maps were elaborated in a target scale of 1:2000 to 1:10,000.

When implemented into the legally binding land use regulation plan of the municipality, the hazard map becomes relevant for homeowners and landowners. The Guidelines for the Consideration of the Hydrological Hazards in Land-Use Planning Activities were approved in 1997 (BWW, BRP, and BUWAL, 1997). In red zones, the authorities are obliged to restrict any construction of new houses. Thus, land parcels within red zones cannot be sold with a value of land suitable for construction. Houses that are located in red zones before the implementation of the hazard map are not allowed to be extended, nor their type of use could be modified. In blue zones, new houses are only permitted to be constructed if their constructor guarantees to implement protection measures that prevent losses from flooding. Existing houses have to be adapted in case of a planned modification or extension. In yellow zones, the construction of critical buildings, e.g. schools and public buildings, is allowed only after a specific sensitivity analysis of the planned project (Kanton Zürich, 2014).

References

- Achleitner, S., Huttenlau, M., Winter, B., Reiss, J., Plörer, M., Hofer, M., 2016. Temporal development of flood risk considering settlement dynamics and local flood protection measures on catchment scale: an Austrian case study. *Int. J. River Basin Manag.* 14: 273–285. <https://doi.org/10.1080/15715124.2016.1167061>.
- Adger, W.N., 2006. Vulnerability. *Glob. Environ. Chang.* 16:268–281. <https://doi.org/10.1016/j.gloenvcha.2006.02.006>.
- Ahmad, S.S., Simonovic, S.P., 2013. Spatial and temporal analysis of urban flood risk assessment. *Urban Water J.* 10:26–49. <https://doi.org/10.1080/1573062X.2012.690437>.
- Alfieri, L., Burek, P., Feyen, L., Forzieri, G., 2015a. Global warming increases the frequency of river floods in Europe. *Hydrol. Earth Syst. Sci.* 19:2247–2260. <https://doi.org/10.5194/hess-19-2247-2015>.
- Alfieri, L., Feyen, L., Dottori, F., Bianchi, A., 2015b. Ensemble flood risk assessment in Europe under high end climate scenarios. *Glob. Environ. Chang.* 35:199–212. <https://doi.org/10.1016/j.gloenvcha.2015.09.004>.
- Alfieri, L., Feyen, L., Di Baldassarre, G., 2016. Increasing flood risk under climate change: a pan-European assessment of the benefits of four adaptation strategies. *Clim. Chang.* <https://doi.org/10.1007/s10584-016-1641-1>.
- Anonymous, 1780–1820. Plan der Güter, die zwischen der Wynigenbrücke und der Kirchbergbrücke an der Emme liegen. Massstab: k.A. Aus: BAB PP 220.
- Anonymous, 1820a. Plan des Emmen-Bettes von Kirchberg bis Zuchwyl-Brücke. Massstab: 1:5000 (in Bern-Fuss). Aus: StAB AA V 189a-b.
- Anonymous, 1820b. Querprofile Emme. StAB AA V 189a-h.
- Anonymous, 1898. Emme, Mittellauf: Querprofile der beiden Ufer von km 15–34. Aus: StAB AA V 199a.
- Arheimer, B., Lindström, G., 2015. Climate impact on floods: changes in high flows in Sweden in the past and the future (1911–2100). *Hydrol. Earth Syst. Sci.* 19: 771–784. <https://doi.org/10.5194/hess-19-771-2015>.
- Arnaud-Fassetta, G., 2003. River channel changes in the Rhone Delta (France) since the end of the Little Ice Age: geomorphological adjustment to hydroclimatic change and natural resource management. *Catena* 51:141–172. [https://doi.org/10.1016/S0341-8162\(02\)00093-0](https://doi.org/10.1016/S0341-8162(02)00093-0).
- Arnell, N.W., Gosling, S.N., 2016. The impacts of climate change on river flood risk at the global scale. *Clim. Chang.* 134:387–401. <https://doi.org/10.1007/s10584-014-1084-5>.
- Aubrecht, C., Fuchs, S., Neuhold, C., 2013. Spatio-temporal aspects and dimensions in integrated disaster risk management. *Nat. Hazards* 68:1205–1216. <https://doi.org/10.1007/s11069-013-0619-9>.
- Beckers, A., Dewals, B., Epicum, S., Dujardin, S., Detrembleur, S., Teller, J., Piroton, M., Archambeau, P., 2013. Contribution of land use changes to future flood damage along the river Meuse in the Walloon region. *Nat. Hazards Earth Syst. Sci.* 13: 2301–2318. <https://doi.org/10.5194/nhess-13-2301-2013>.
- Belz, J.U., Busch, N., Engel, H., Gasber, G., 2001. Comparison of river training measures in the Rhine?: catchment and their effects on flood behaviour. *Marit. Eng.* 148: 123–132. <https://doi.org/10.1680/maen.148.3.123.40103>.
- Bergillos, R.J., Rodriguez-Delgado, C., Millares, A., Ortega-Sánchez, M., Losada, M.A., 2016. Impact of river regulation on a Mediterranean delta: assessment of managed versus unmanaged scenarios. *Water Resour. Res.* 52:5132–5148. <https://doi.org/10.1002/2015WR018395>.
- Bermúdez, M., Zischg, A.P., 2018. Sensitivity of flood loss estimates to building representation and flow depth attribution methods in micro-scale flood modelling. *Nat. Hazards* 14, 253. <https://doi.org/10.1007/s11069-018-3270-7>.

- Boudou, M., Danière, B., Lang, M., 2016. Assessing changes in urban flood vulnerability through mapping land use from historical information. *Hydrol. Earth Syst. Sci.* 20: 161–173. <https://doi.org/10.5194/hess-20-161-2016>.
- Bouwer, L.M., Bubeck, P., Aerts, J.C.J.H., 2010. Changes in future flood risk due to climate and development in a Dutch polder area. *Glob. Environ. Chang.* 20:463–471. <https://doi.org/10.1016/j.gloenvcha.2010.04.002>.
- Brierley, G.J., Fryirs, K.A., 2016. The use of evolutionary trajectories to guide 'moving targets' in the management of river futures. *River Res. Appl.* 32:823–835. <https://doi.org/10.1002/rra.2930>.
- Bronstert, A., Bárdossy, A., Bismuth, C., Buiteveld, H., Disse, M., Engel, H., Fritsch, U., Huntech, Y., Lammensen, R., Niehoff, D., Ritter, N., 2007. Multi-scale modelling of land-use change and river training effects on floods in the Rhine basin. *River Res. Appl.* 23:1102–1125. <https://doi.org/10.1002/rra.1036>.
- Brunner, M.I., Seibert, J., Favre, A.-C., 2018. Representative sets of design hydrographs for ungauged catchments: a regional approach using probabilistic region memberships. *Adv. Water Resour.* 112:235–244. <https://doi.org/10.1016/j.advwatres.2017.12.018>.
- Burby, R.J., French, S.P., 2007. Coping with floods: the land use management paradox. *J. Am. Plan. Assoc.* 47:289–300. <https://doi.org/10.1080/01944368108976511>.
- BWW, BRP, and BUWAL, 1997. Berücksichtigung der Hochwassergefahren bei raumwirksamen Tätigkeiten. Biel und Bern: Bundesamt für Wasserwirtschaft, Bundesamt für Raumplanung, Bundesamt für Umwelt, Wald und Landschaft.
- Cammerer, H., Thieken, A.H., 2013. Historical development and future outlook of the flood damage potential of residential areas in the Alpine Lech Valley (Austria) between 1971 and 2030. *Reg. Environ. Chang.* 13:999–1012. <https://doi.org/10.1007/s10113-013-0407-9>.
- Cammerer, H., Thieken, A.H., Verburg, P.H., 2013. Spatio-temporal dynamics in the flood exposure due to land use changes in the Alpine Lech Valley in Tyrol (Austria). *Nat. Hazards* 68:1243–1270. <https://doi.org/10.1007/s11069-012-0280-8>.
- Carisi, F., Domeneghetti, A., Gaeta, M.G., Castellarin, A., 2017. Is anthropogenic land subsidence a possible driver of riverine flood-hazard dynamics?: a case study in Ravenna, Italy. *Hydrol. Sci. J.* 6:1–16. <https://doi.org/10.1080/02626667.2017.1390315>.
- Church, M., Ferguson, R.L., 2015. Morphodynamics: rivers beyond steady state. *Water Resour. Res.* <https://doi.org/10.1002/2014WR016862> (n/a).
- Corenblit, D., Davies, N.S., Steiger, J., Gibling, M.R., Bornette, G., 2014. Considering river structure and stability in the light of evolution: feedbacks between riparian vegetation and hydrogeomorphology. *Earth Surf. Process. Landf.* <https://doi.org/10.1002/esp.3643> (n/a).
- Coulthard, T.J., Van De Wiel, Marco J., 2007. Quantifying fluvial non linearity and finding self organized criticality?: insights from simulations of river basin evolution. *Geomorphology* 91:216–235. <https://doi.org/10.1016/j.geomorph.2007.04.011>.
- Croke, J., Denham, R., Thompson, C., Grove, J., 2015. Evidence of self-organized criticality in riverbank mass failures: a matter of perspective? *Earth Surf. Process. Landf.* 40: 953–964. <https://doi.org/10.1002/esp.3688>.
- Dessai, S., Hulme, M., 2004. Does climate adaptation policy need probabilities? *Clim. Pol.* 4:107–128. <https://doi.org/10.1080/14693062.2004.9685515>.
- Devkota, R.P., Bhattarai, U., 2015. Assessment of climate change impact on floods from a techno-social perspective. *J. Flood Risk Manage.* <https://doi.org/10.1111/jfr3.12192> (n/a-n/a).
- Di Baldassarre, G., Castellarin, A., BRATH, A., 2009. Analysis of the effects of levee heightening on flood propagation: example of the River Po, Italy. *Hydrol. Sci. J.* 54: 1007–1017. <https://doi.org/10.1623/hysj.54.6.1007>.
- Di Baldassarre, G., Kooy, M., Kemerink, J.S., Brandimarte, L., 2013a. Towards understanding the dynamic behaviour of floodplains as human-water systems. *Hydrol. Earth Syst. Sci.* 17:3235–3244. <https://doi.org/10.5194/hess-17-3235-2013>.
- Di Baldassarre, G., Viglione, A., Carr, G., Kuil, L., Salinas, J.L., Blöschl, G., 2013b. Socio-hydrology: conceptualising human-flood interactions. *Hydrol. Earth Syst. Sci.* 17: 3295–3303. <https://doi.org/10.5194/hess-17-3295-2013>.
- Di Baldassarre, G., Viglione, A., Carr, G., Kuil, L., Yan, K., Brandimarte, L., Blöschl, G., 2015. Debates-perspectives on socio-hydrology: capturing feedbacks between physical and social processes. *Water Resour. Res.* 51:4770–4781. <https://doi.org/10.1002/2014WR016416>.
- Dixon, S.J., Sear, D.A., Odoni, N.A., Sykes, T., Lane, S.N., 2016. The effects of river restoration on catchment scale flood risk and flood hydrology. *Earth Surf. Process. Landf.* 41: 997–1008. <https://doi.org/10.1002/esp.3919>.
- Drost, U., Ell, M., 2016. Das neue Wasserrecht: Ein Lehrbuch für Ausbildung und Praxis in Bayern, 2., vollständig überarbeitete Auflage, Boorberg, Stuttgart, München, Hannover, Berlin, Weimar, Dresden, 323 Seiten.
- Dutta, D., Herath, S., Musiak, K., 2003. A mathematical model for flood loss estimation. *J. Hydrol.* 277:24–49. [https://doi.org/10.1016/S0022-1694\(03\)00084-2](https://doi.org/10.1016/S0022-1694(03)00084-2).
- Elmer, F., Hoymann, J., Duthmann, D., Vorogushyn, S., Kreibich, H., 2012. Drivers of flood risk change in residential areas. *Nat. Hazards Earth Syst. Sci.* 12:1641–1657. <https://doi.org/10.5194/nhess-12-1641-2012>.
- Ernst, J., Dewals, B.J., Detrembleur, S., Archambeau, P., Erpicum, S., Piroton, M., 2010. Micro-scale flood risk analysis based on detailed 2D hydraulic modelling and high resolution geographic data. *Nat. Hazards* 55:181–209. <https://doi.org/10.1007/s11069-010-9520-y>.
- Figueiredo, R., Schröter, K., Weiss-Motz, A., Martina, M.L.V., Kreibich, H., 2017. Improving accuracy and quantifying uncertainty in flood loss estimations through the use of multi-model ensembles. *Nat. Hazards Earth Syst. Sci. Discuss.* 1–34 <https://doi.org/10.5194/nhess-2017-349>.
- Finsler, H.C., 1978. Das Amt Fraubrunnen um 1820–1830, Blätter 3, 6 und 9, Landschaftswandel und wirtschaftliche Umstrukturierung seit dem frühen 19. Jahrhundert, Fraubrunnen.
- Früh-Müller, A., Wegmann, M., Koellner, T., 2015. Flood exposure and settlement expansion since pre-industrial times in 1850 until 2011 in north Bavaria, Germany. *Reg. Environ. Chang.* 15:183–193. <https://doi.org/10.1007/s10113-014-0633-9>.
- Fuchs, S., Keiler, M., Zischg, A., Bründl, M., 2005. The long-term development of avalanche risk in settlements considering the temporal variability of damage potential. *Nat. Hazards Earth Syst. Sci.* 5:893–901. <https://doi.org/10.5194/nhess-5-893-2005>.
- Fuchs, S., Keiler, M., Sokratov, S., Shnyarkov, A., 2013. Spatiotemporal dynamics: the need for an innovative approach in mountain hazard risk management. *Nat. Hazards* 68:1217–1241. <https://doi.org/10.1007/s11069-012-0508-7>.
- Fuchs, S., Keiler, M., Zischg, A., 2015. A spatiotemporal multi-hazard exposure assessment based on property data. *Nat. Hazards Earth Syst. Sci.* 15:2127–2142. <https://doi.org/10.5194/nhess-15-2127-2015>.
- Fuchs, S., Röthlisberger, V., Thaler, T., Zischg, A., Keiler, M., 2016. Natural hazard management from a coevolutionary perspective: exposure and policy response in the European Alps. *Ann. Am. Assoc. Geogr.* 1–11 <https://doi.org/10.1080/24694452.2016.1235494>.
- Fuchs, S., Röthlisberger, V., Thaler, T., Zischg, A., Keiler, M., 2017. Natural hazard management from a coevolutionary perspective: exposure and policy response in the European Alps. *Ann. Am. Assoc. Geogr.* 1–11 <https://doi.org/10.1080/24694452.2016.1235494>.
- Gober, P., Wheat, H.S., 2015. Debates-perspectives on socio-hydrology: modeling flood risk as a public policy problem. *Water Resour. Res.* 51:4782–4788. <https://doi.org/10.1002/2015WR016945>.
- Gobiet, A., Kotlarski, S., Beniston, M., Heinrich, G., Rajczak, J., Stoffel, M., 2014. 21st century climate change in the European Alps—a review. *Sci. Total Environ.* 493:1138–1151. <https://doi.org/10.1016/j.scitotenv.2013.07.050>.
- Goldschmid, H., 1913. Emmekorrektion 1. Sektion Kantonsgrenze Bern/Solothurn bis Grenze Burgdorf. Situationsplan km. 0–14. Massstab 1:5000. Aus: StAB BB 06.7.371, KantonBern.
- Gregory, K.J., 2006. The human role in changing river channels. 37th Binghamton Geomorphology Symposium the Human Role in Changing Fluvial Systems 79: pp. 172–191. <https://doi.org/10.1016/j.geomorph.2006.06.018>.
- Guan, M., Carrivick, J.L., Wright, N.G., Sleigh, P.A., Staines, K.E.H., 2016. Quantifying the combined effects of multiple extreme floods on river channel geometry and on flood hazards. *J. Hydrol.* 538:256–268. <https://doi.org/10.1016/j.jhydrol.2016.04.004>.
- Hall, J., Arheimer, B., Borga, M., Brázdil, R., Claps, P., Kiss, A., Kjeldsen, T.R., Kriaučiūnienė, J., Kundzewicz, Z.W., Lang, M., Llasat, M.C., Macdonald, N., McIntyre, N., Mediero, L., Merz, B., Merz, R., Molnar, P., Montanari, A., Neuhold, C., Parajka, J., Perdigão, R.A.P., Plavcová, L., Rogger, M., Salinas, J.L., Sauquet, E., Schär, C., Szolgay, J., Viglione, A., Blöschl, G., 2014. Understanding flood regime changes in Europe: a state-of-the-art assessment. *Hydrol. Earth Syst. Sci.* 18:2735–2772. <https://doi.org/10.5194/hess-18-2735-2014>.
- Herget, J., Dikau, R., Gregory, K.J., Vandenberghe, J., 2007. The fluvial system — research perspectives of its past and present dynamics and controls. *Geomorphology* 92: 101–105. <https://doi.org/10.1016/j.geomorph.2006.07.034>.
- Himmelsbach, I., Glaser, R., Schoenbein, J., Riemann, D., Martin, B., 2015. Flood risk along the upper Rhine since AD 1480. *Hydrol. Earth Syst. Sci. Discuss.* 12:177–211. <https://doi.org/10.5194/hessd-12-177-2015>.
- Hirabayashi, Y., Mahendran, R., Koirala, S., Konoshima, I., Yamazaki, D., Watanabe, S., Kim, H., Kanae, S., 2013. Global flood risk under climate change. *Nat. Clim. Chang.* 3: 816–821. <https://doi.org/10.1038/nclimate1911>.
- Hollis, G.E., 1975. The effect of urbanization on floods of different recurrence interval. *Water Resour. Res.* 11:431–435. <https://doi.org/10.1029/WR011i003p00431>.
- Hooke, J.M., 2006. Human impacts on fluvial systems in the Mediterranean region. 37th Binghamton Geomorphology Symposium the Human Role in Changing Fluvial Systems 79: pp. 311–335. <https://doi.org/10.1016/j.geomorph.2006.06.036>.
- Hufschmidt, G., Crozier, M., Glade, T., 2005. Evolution of natural risk: research framework and perspectives. *Nat. Hazards Earth Syst. Sci.* 5:375–387. <https://doi.org/10.5194/nhess-5-375-2005>.
- Huntech, Y., Merz, B., 2012. Exploring the relationship between changes in climate and floods using a model-based analysis. *Water Resour. Res.* 48, 3331. <https://doi.org/10.1029/2011WR010527>.
- Hydrotec, 2001. Hochwasser-Aktionsplan Angerbach. Teil I: Berichte und Anlagen. Studie im Auftrag des Stua Dusseldorf, Aachen, Germany.
- Jongman, B., Ward, P.J., Aerts, J.C.J.H., 2012. Global exposure to river and coastal flooding: long term trends and changes. *Glob. Environ. Chang.* 22:823–835. <https://doi.org/10.1016/j.gloenvcha.2012.07.004>.
- Jonkman, S.N., Bočkarjova, M., Kok, M., Bernardini, P., 2008. Integrated hydrodynamic and economic modelling of flood damage in the Netherlands. Special Section: Integrated Hydro-economic Modelling for Effective and Sustainable Water Management. 66: pp. 77–90. <https://doi.org/10.1016/j.jecolecon.2007.12.022>.
- Kanton Zürich, 2014. Gefahrenkarte Kanton Zürich – Lesehilfe. Zürich.
- KAWA Amt für Wald des Kantons Bern, 2015. LiDAR Bern – Airborne Laserscanning. Gesamtbericht Befliegung – Befliegung Kanton Bern 2011–2014.
- Keiler, M., Zischg, A., Fuchs, S., Hama, M., Stötter, J., 2005. Avalanche related damage potential - changes of persons and mobile values since the mid-twentieth century, case study Galtür. *Nat. Hazards Earth Syst. Sci.* 5:49–58. <https://doi.org/10.5194/nhess-5-49-2005>.
- Keiler, M., Sailer, R., Jörg, P., Weber, C., Fuchs, S., Zischg, A., Sauermoser, S., 2006. Avalanche risk assessment; a multi-temporal approach, results from Galtür, Austria. *Nat. Hazards Earth Syst. Sci.* 6:637–651. <https://doi.org/10.5194/nhess-6-637-2006>.
- Keiler, M., Knight, J., Harrison, S., 2010. Climate change and geomorphological hazards in the eastern European Alps. *Philos. Transact. A Math. Phys. Eng. Sci.* 368:2461–2479. <https://doi.org/10.1098/rsta.2010.0047>.
- Kiss, T., Fiala, K., Sipos, G., 2008. Alterations of channel parameters in response to river regulation works since 1840 on the Lower Tisza River (Hungary). *Geomorphology* 98:96–110. <https://doi.org/10.1016/j.geomorph.2007.02.027>.
- Kundzewicz, Z.W., Kanae, S., Seneviratne, S.I., Handmer, J., Nicholls, N., Peduzzi, P., Mechler, R., Bouwer, L.M., Arnell, N., Mach, K., Muir-Wood, R., Brakenridge, G.R., Kron, W., Benito, G., Honda, Y., Takahashi, K., Sherstyukov, B., 2014. Flood risk and

- climate change: global and regional perspectives. *Hydrol. Sci. J.* 59:1–28. <https://doi.org/10.1080/02626667.2013.857411>.
- Lane, S.N., 2017. Natural flood management. *WIREs Water* 4, e1211. <https://doi.org/10.1002/wat2.1211>.
- Liu, J., Hertel, T.W., Diffenbaugh, N.S., Delgado, M.S., Ashfaq, M., 2015. Future property damage from flooding: sensitivities to economy and climate change. *Clim. Chang.* 132:741–749. <https://doi.org/10.1007/s10584-015-1478-z>.
- Löschner, L., Herrnegger, M., Apperl, B., Senoner, T., Seher, W., Nachtnebel, H.P., 2016. Flood risk, climate change and settlement development: a micro-scale assessment of Austrian municipalities. *Reg. Environ. Chang.* 42, 125. <https://doi.org/10.1007/s10113-016-1009-0>.
- Luder, F., 1928. Situationsplan von Burgdorf, erstellt nach dem Kataster (Druck). *Masstab: 1:2000. Aus: BAB PP 315*.
- Marani, M., Rigon, R., 1994. Self-organized River Basin Landscapes - Fractal and Multifractal Characteristics. <https://doi.org/10.1029/94WR01493>.
- Marchese, E., Scropio, V., Fuller, I., McColl, S., Comiti, F., 2017. Morphological changes in alpine rivers following the end of the Little Ice Age. *Geomorphology* <https://doi.org/10.1016/j.geomorph.2017.07.018>.
- Mazzorana, B., Levaggi, L., Keiler, M., Fuchs, S., 2012. Towards dynamics in flood risk assessment. *Nat. Hazards Earth Syst. Sci.* 12:3571–3587. <https://doi.org/10.5194/nhess-12-3571-2012>.
- Merz, B., Hall, J., Disse, M., Schumann, A., 2010. Fluvial flood risk management in a changing world. *Nat. Hazards Earth Syst. Sci.* 10:509–527. <https://doi.org/10.5194/nhess-10-509-2010>.
- Merz, B., Aerts, J., Arnbjerg-Nielsen, K., Baldi, M., Becker, A., Bichet, A., Blöschl, G., Bouwer, L.M., Brauer, A., Cioffi, F., Delgado, J.M., Gocht, M., Guzzetti, F., Harrigan, S., Hirschboeck, K., Kilsby, C., Kron, W., Kwon, H.-H., Lall, U., Merz, R., Nissen, K., Salvatti, P., Swierczynski, T., Ulbrich, U., Viglione, A., Ward, P.J., Weiler, M., Wilhelm, B., Nied, M., 2014. Floods and climate: emerging perspectives for flood risk assessment and management. *Nat. Hazards Earth Syst. Sci.* 14:1921–1942. <https://doi.org/10.5194/nhess-14-1921-2014>.
- Muñoz, L.A., Olivera, F., Giglio, M., Berke, P., 2017. The impact of urbanization on the streamflows and the 100-year floodplain extent of the Sims Bayou in Houston, Texas. *Int. J. River Basin Manag.* 7:1–9. <https://doi.org/10.1080/15715124.2017.1372447>.
- Nadarajah, S., 2007. Probability models for unit hydrograph derivation. *J. Hydrol.* 344: 185–189. <https://doi.org/10.1016/j.jhydrol.2007.07.004>.
- Nicholls, S., Crompton, J.L., 2017. The effect of rivers, streams, and canals on property values. *River Res. Appl.* 36:773. <https://doi.org/10.1002/rra.3197>.
- Noël, P.H., Cai, X., 2017. On the role of individuals in models of coupled human and natural systems: lessons from a case study in the Republican River Basin. *Environ. Model. Softw.* 92:1–16. <https://doi.org/10.1016/j.envsoft.2017.02.010>.
- O'Connell, P.E., Ewen, J., O'Donnell, G., Quinn, P., 2007. Is there a link between agricultural land-use management and flooding? *Hydrol. Earth Syst. Sci.* 11:96–107. <https://doi.org/10.5194/hess-11-96-2007>.
- Papathoma-Köhle, M., Zischg, A., Fuchs, S., Glade, T., Keiler, M., 2015. Loss estimation for landslides in mountain areas – an integrated toolbox for vulnerability assessment and damage documentation. *Environ. Model. Softw.* 63:156–169. <https://doi.org/10.1016/j.envsoft.2014.10.003>.
- Pinter, N., Thomas, R., Wlosinski, J.H., 2000. Regional impacts of levee construction and channelization, Middle Mississippi River, USA. In: Marsalek, J., Watt, W.E., Zeman, E., Sieker, F. (Eds.), *Flood Issues in Contemporary Water Management*. NATO Science Series, Series 2. Environment Security 71. Springer, Netherlands, Dordrecht, pp. 351–361.
- Pinter, N., Thomas, R., Wlosinski, J.H., 2001. Assessing flood hazard on dynamic rivers. *Eos Trans. AGU* 82:333. <https://doi.org/10.1029/01EO00199>.
- Pinter, N., van der Ploeg, Rienk R., Schweigert, P., Hofer, G., 2006. Flood magnification on the River Rhine. *Hydrol. Process.* 20:147–164. <https://doi.org/10.1002/hyp.5908>.
- Posey, J., 2009. The determinants of vulnerability and adaptive capacity at the municipal level: evidence from floodplain management programs in the United States. *Glob. Environ. Chang.* 19:482–493. <https://doi.org/10.1016/j.gloenvcha.2009.06.003>.
- Rai, R.K., Sarkar, S., Singh, V.P., 2009. Evaluation of the adequacy of statistical distribution functions for deriving unit hydrograph. *Water Resour. Manag.* 23:899–929. <https://doi.org/10.1007/s11269-008-9306-0>.
- Remo, J.W.F., Pinter, N., 2007. Retro-modeling the Middle Mississippi River. *J. Hydrol.* 337: 421–435. <https://doi.org/10.1016/j.jhydrol.2007.02.008>.
- Remo, J.W.F., Pinter, N., Heine, R., 2009. The use of retro- and scenario-modeling to assess effects of 100+ years river of engineering and land-cover change on Middle and Lower Mississippi River flood stages. *J. Hydrol.* 376:403–416. <https://doi.org/10.1016/j.jhydrol.2009.07.049>.
- Ritter, J., 1804. Plan der Emmenkorrektur von Joseph Ritter: Abschnitt der Emme zwischen Ziegelbrücke und Eysteg (nach dem Emmenplan von J. A. Riediger). *Masstab k.A. Aus: BAB PP 151*.
- Rogger, M., Agnoletti, M., Alaoui, A., Bathurst, J.C., Bodner, G., Borga, M., Chaplot, V., Gallart, F., Glatzel, G., Hall, J., Holden, J., Holko, L., Horn, R., Kiss, A., Kohnová, S., Leitinger, G., Lennartz, B., Parajka, J., Perdigão, R., Peth, S., Plavcová, L., Quinton, J.N., Robinson, M., Salinas, J.L., Santoro, A., Szolgyai, J., Tron, S., van den Akker, J.J.H., Viglione, A., Blöschl, G., 2017. Land-use change impacts on floods at the catchment scale – challenges and opportunities for future research. *Water Resour. Res.* <https://doi.org/10.1002/2017WR020723>.
- Röthlisberger, V., Zischg, A., Keiler, M., 2016. Spatiotemporal aspects of flood exposure in Switzerland. *E3S Web Conf.* 7:8008. <https://doi.org/10.1051/e3sconf/20160708008>.
- Röthlisberger, V., Zischg, A.P., Keiler, M., 2017. Identifying spatial clusters of flood exposure to support decision making in risk management. *Sci. Total Environ.* 598: 593–603. <https://doi.org/10.1016/j.scitotenv.2017.03.216>.
- Ryffel, A.N., Rid, W., Grêt-Regamey, A., 2014. Land use trade-offs for flood protection: a choice experiment with visualizations. *Ecosyst. Serv.* 10:111–123. <https://doi.org/10.1016/j.ecoser.2014.09.008>.
- Salzmann, N., Huggel, C., Nussbaumer, S.U., Ziervogel, G., 2016. *Climate Change Adaptation Strategies – An Upstream-downstream Perspective*. Springer International Publishing (Imprint; Springer, Cham, 1 online resource (x, 292)).
- Sear, D.A., Newson, M.D., 2003. Environmental change in river channels: a neglected element. *Towards geomorphological typologies, standards and monitoring*. *Detecting Environmental Change: Science and Society.* 310:pp. 17–23. [https://doi.org/10.1016/S0048-9697\(02\)00619-8](https://doi.org/10.1016/S0048-9697(02)00619-8).
- Serinaldi, F., Grimaldi, S., 2011. Synthetic design hydrographs based on distribution functions with finite support. *J. Hydrol. Eng.* 16:434–446. [https://doi.org/10.1061/\(ASCE\)HE.1943-5584.0000339](https://doi.org/10.1061/(ASCE)HE.1943-5584.0000339).
- Slater, L.J., Singer, M.B., Kirchner, J.W., 2015. Hydrologic versus geomorphic drivers of trends in flood hazard. *Geophys. Res. Lett.* 42:370–376. <https://doi.org/10.1002/2014GL062482>.
- Staffler, H., Pollinger, R., Zischg, A., Mani, P., 2008. Spatial variability and potential impacts of climate change on flood and debris flow hazard zone mapping and implications for risk management. *Nat. Hazards Earth Syst. Sci.* 8:539–558. <https://doi.org/10.5194/nhess-8-539-2008>.
- Surian, N., Rinaldi, M., 2003. Morphological response to river engineering and management in alluvial channels in Italy. *Geomorphology* 50:307–326. [https://doi.org/10.1016/S0169-555X\(02\)00219-2](https://doi.org/10.1016/S0169-555X(02)00219-2).
- Thaler, T., Zischg, A., Keiler, M., Fuchs, S., 2018. Allocation of risk and benefits-distributional justices in mountain hazard management. *Reg. Environ. Chang.* <https://doi.org/10.1007/s10113-017-1274-6>.
- Thieken, A.H., Cammerer, H., Dobler, C., Lammell, J., Schöberl, F., 2016. Estimating changes in flood risks and benefits of non-structural adaptation strategies – a case study from Tyrol, Austria. *Mitig. Adapt. Strateg. Glob. Chang.* 21:343–376. <https://doi.org/10.1007/s11027-014-9602-3>.
- Tobin, G.A., 1995. The levee love affair: a stormy relationship? *J. Am. Water Resour. Assoc.* 31:359–367. <https://doi.org/10.1111/j.1752-1688.1995.tb04025.x>.
- Totschnig, R., Sedlacek, W., Fuchs, S., 2011. A quantitative vulnerability function for fluvial sediment transport. *Nat. Hazards* 58:681–703. <https://doi.org/10.1007/s11069-010-9623-5>.
- UNISDR, 2015. *Making development sustainable: The future of disaster risk management*. Global Assessment Report on Disaster Risk Reduction, 4.2015. United Nations, Geneva (311 pp.).
- van Triet, N.K., Dung, N.V., Fujii, H., Kummu, M., Merz, B., Apel, H., 2017. Has dyke development in the Vietnamese Mekong Delta shifted flood hazard downstream? *Hydrol. Earth Syst. Sci.* 21:3991–4010. <https://doi.org/10.5194/hess-21-3991-2017>.
- Vetsch, D., Siviglia, A., Ehrbar, D., Facchini, M., Gerber, M., Kammerer, S., Peter, S., Vonwiler, L., Volz, C., Farshi, D., Mueller, R., Rousselot, P., Veprek, R., Faeh, R., 2017. *BASEMENT – Basic Simulation Environment for Computation of Environmental Flow and Natural Hazard Simulation* (Zurich).
- Vischer, D., 2003. *Die Geschichte des Hochwasserschutzes in der Schweiz, Berichte des BWG, Serie Wasser, 5, Bern* (209 pp.).
- Vorogushyn, S., Merz, B., 2013. Flood trends along the Rhine: the role of river training. *Hydrol. Earth Syst. Sci.* 17:3871–3884. <https://doi.org/10.5194/hess-17-3871-2013>.
- White, G., 1945. *Human Adjustment to Floods*. Department of Geography, University of Chicago, USA.
- Wiering, M., Loefflerink, D., Crabbé, A., 2017. Stability and change in flood risk governance: on path dependencies and change agents. *J. Flood Risk Manag.* <https://doi.org/10.1111/jfr3.12295>.
- Winsemius, H.C., Aerts, Jeroen C.J.H., van Beek, Ludovicus P.H., Bierkens, Marc F.P., Bouwman, A., Jongman, B., Kwadijck, J.C.J., Ligtoet, W., Lucas, P.L., van Vuuren, D.P., Ward, P.J., 2015. Global drivers of future river flood risk. *Nat. Clim. Chang.* <https://doi.org/10.1038/nclimate2893>.
- Wirth, S.B., Girardclos, S., Rellstab, C., Anselmetti, F.S., 2011. The sedimentary response to a pioneer geo-engineering project: tracking the Kander River deviation in the sediments of Lake Thun (Switzerland). *Sedimentology* 58:1737–1761. <https://doi.org/10.1111/j.1365-3091.2011.01237.x>.
- Wise, R.M., Fazy, I., Stafford Smith, M., Park, S.E., Eakin, H.C., van Archer Garderen, E.R.M., Campbell, B., 2014. Reconceptualising adaptation to climate change as part of pathways of change and response. *Glob. Environ. Chang.* 28:325–336. <https://doi.org/10.1016/j.gloenvcha.2013.12.002>.
- Zhao, T., Shao, Q., 2015. Detecting floodplain inundation based on the upstream-downstream relationship. *J. Hydrol.* 530:195–205. <https://doi.org/10.1016/j.jhydrol.2015.09.056>.
- Zischg, A., 2016. River corrections and long-term changes in flood risk in the Aare valley, Switzerland. *E3S Web Conf.* 7, 11010. <https://doi.org/10.1051/e3sconf/20160711010>.
- Zischg, A., Schober, S., Sereinig, N., Rauter, M., Seymann, C., Goldschmidt, F., Bäk, R., Schleicher, E., 2013. Monitoring the temporal development of natural hazard risks as a basis indicator for climate change adaptation. *Nat. Hazards* 67:1045–1058. <https://doi.org/10.1007/s11069-011-9927-0>.
- Zischg, A.P., Felder, G., Weingartner, R., Quinn, N., Coxon, G., Neal, J., Freer, J., Bates, P., 2018a. Effects of variability in probable maximum precipitation patterns on flood losses. *Hydrol. Earth Syst. Sci. Discuss.* 1–24. <https://doi.org/10.5194/hess-2017-758>.
- Zischg, A.P., Mosimann, M., Bernet, D.B., Röthlisberger, V., 2018b. Validation of 2D flood models with insurance claims. *J. Hydrol.* 557:350–361. <https://doi.org/10.1016/j.jhydrol.2017.12.042>.

Paper 25: Zischg, A.; Galatioto, N.; Deplazes, S.; Weingartner, R.; Mazzorana, B., 2018: Modelling spatiotemporal dynamics of large wood recruitment, transport and deposition at river reach scale during extreme floods. *Water* 10(9), 1134. [10.3390/w10091134](https://doi.org/10.3390/w10091134).

Article

Modelling Spatiotemporal Dynamics of Large Wood Recruitment, Transport, and Deposition at the River Reach Scale during Extreme Floods

Andreas Paul Zischg ^{1,*} , Niccolo Galatioto ¹, Silvana Deplazes ¹, Rolf Weingartner ¹ and Bruno Mazzorana ²

¹ Oeschger Centre for Climate Change Research, Institute of Geography, University of Bern, Bern CH-3012, Switzerland; nicc.gal@hotmail.com (N.G.); silvana.deplazes@bs.ch (S.D.); rolf.weingartner@giub.unibe.ch (R.W.)

² Faculty of Sciences, Instituto de Ciencias de la Tierra, Universidad Austral de Chile, Valdivia 5090000, Chile; bruno.mazzorana@uach.cl

* Correspondence: andreas.zischg@giub.unibe.ch; Tel.: +41-31-631-8839

Received: 22 June 2018; Accepted: 23 August 2018; Published: 25 August 2018



Abstract: Large wood (LW) can lead to clogging at bridges and thus cause obstruction, followed by floodplain inundation. Moreover, colliding logs can cause severe damage to bridges, defense structures, and other infrastructure elements. The factors influencing spatiotemporal LW dynamics (LWD) during extreme floods vary remarkably across river basins and flood scenarios. However, there is a lack of methods to estimate the amount of LW in rivers during extreme floods. Modelling approaches allow for a reliable assessment of LW dynamics during extreme flood events by determining LW recruitment, transport, and deposition patterns. Here, we present a method for simulating LWD on a river reach scale implemented in R (LWDsimR). We extended a previously developed LW transport model with a tree recognition model on the basis of Light Detection and Ranging (LiDAR) data for LW recruitment simulation. In addition, we coupled the LWD simulation model with the hydrodynamic simulation model Basic Simulation Environment for Computation of Environmental Flow and Natural Hazard Simulation (BASEMENT-ETH) by adapting the existing LW transport model to be used on irregular meshes. The model has been applied in the Aare River basin (Switzerland) to quantify mobilized LW volumes and the associated flow paths in a probable maximum flood scenario.

Keywords: large wood; rivers; extreme flood; recruitment; transport; deposition; coupled component modelling

1. Introduction

Riverine floods in many parts of the world are a threat to people, settlements, and infrastructure and thus a major cause of significant losses [1]. Analyzing flood events is therefore a prerequisite for risk management. Floods are triggered by precipitation events of high intensity or long duration. However, the local flood magnitude also depends on catchment characteristics, land use, river morphology, and the status of flood defense measures [2–4]. Especially in mountainous areas, the impacts of floods can be accentuated by sediment transport or large wood (LW) transport. Both sediment and LW transport can lead to bridge clogging with subsequent channel outbursts [5]. Concomitantly, bridges may be severely damaged and flood magnitude may be increased in the floodplain [5–9]. If sediment deposition in the river channel and subsequent riverbed aggradation or LW jam formation potentially occur in a specific site, obstruction of bridges due to these processes has to be considered in the

prediction of flooded areas and the associated adverse consequences [10]. In addition, the destruction of flood defenses or other infrastructure due to colliding trunks plays a relevant role in flood consequence analysis. The factors influencing the process magnitude and the course of a flood event are often considered in risk analyses by defining different scenarios that potentially lead to an aggravation of the flood and related consequences [11–13]. Hence, the amount of sediment or LW is an important aspect in scenario definition and thus risk analysis. These estimations are a prerequisite for the design of flood mitigation measures. Furthermore, it is important to know which processes can occur at a specific point of interest and how these processes will evolve spatially and temporally under different circumstances. Considering sediment dynamics during floods is becoming more frequent in flood risk analysis. In recent years, various simulation models have been developed for modelling this process [14–16]. In contrast, methods and simulation models for assessing the recruitment, transport, and deposition of LW during floods still need to be substantially improved. The topic of in-stream LW has been extensively investigated within the domains of ecology, geomorphology, and hydromorphology. Here, the focus is placed on the relevance of wood for river habitats and river morphology [17–24], wood budgets [25–28], wood storage [29,30], and wood transport rates in rivers [23,31,32] in the long term. Only a few studies describe methods for quantifying LW volumes and fluxes in rivers in the short term [33–37], e.g., by remote sensing [38–40], radio frequency identification (RFID) and Global Positioning System (GPS) techniques [36,41], time-lapse photography [34], or video monitoring [42–44]. On the other hand, the spatiotemporal dynamics of LW in rivers has been analyzed from the risk management perspective with a focus on extreme floods only in recent years. Comiti et al. [45] stated that the current knowledge of LW dynamics (LWD; i.e., recruitment, transport, and deposition) during high-magnitude floods is still limited since extreme floods are, by definition, rare events and thus the opportunity to study these processes in reality is very limited. Practically, during extreme weather events, observing and monitoring hazardous processes is logistically complex and temporally challenging. Another reason for these knowledge limitations is that these highly complex processes differ substantially across river basins [23,27,45–48]. Due to remarkable variability of catchments in terms of land use, geology, forested area, and river hydromorphology, empirical estimations of LW volumes during large floods are uncertain. Furthermore, other geomorphologic processes play an important role in wood recruitment. The flood hydrograph is one of the main factors influencing LW volume [49]. Thus, transferring the analysis from one catchment to others is questionable. In addition, the recruitment of trees and entrainment into the river flow is influenced by riverbank erosion, landslides in forested areas near the riverbed, and debris flows bringing eroded trees from tributary catchments into the main river channel [45,50–53]. Moreover, small mountain torrents, wide gravel-bed rivers, and regulated rivers exhibit pronounced differences in LW dynamics [45].

In summary, LWD are complex and consist of different subprocesses. Different models for simulating LW transport and deposition have been developed so far. Abbe et al. [54] described LW patterns and processes of LW and woody debris at the micro scale, with a focus on jam formation. Amicarelli et al. [55] and Albano et al. [56] modeled LWD with a smoothed particle hydrodynamics approach. Bragg et al. [57] modeled the ecological disturbance in riparian forests at the single tree scale. Bocchiola et al. [58] presented a simplified numerical approach to model LW transport in one dimension (1D). Models that consider the movement of single trees on the basis of a hydrodynamic two-dimensional (2D) model have been proposed by Mazzorana et al. [59] and Ruiz-Villanueva et al. [60]. The latter is, to our knowledge, the most complex model for simulating LW transport, deposition, and jamming at bridges or other obstacles. The model is implemented in a 2D hydraulic model (Iber) that solves the shallow water equations with a finite volume method [61,62]. The LW transport model simulates incipient motion of single pieces of wood, performing a balance of the forces acting on it. Interactions between logs and the channel configuration and among the logs themselves, with subsequent influence on the hydrodynamics, are also taken into account. The logs are represented by cylindrical objects. This model is the most advanced in terms of process representation at the micro scale. However, the LW fluxes at the upper boundary condition have to be estimated.

In contrast, Mazzorana et al. [59] presented an approach that also considers the recruitment process. The erosion of standing trees is considered by analyzing the hydrodynamic forces. The transport of the logs is coupled with a 2D hydrodynamic model and the dynamics of single floating wood are computed on the basis of flow forces [63–65]. However, the coupling is of unidirectional type and therefore the influence of wood jams on the hydrodynamics is neglected. The logs are represented by points and the interaction between the logs and obstacles and among the logs themselves is more generalized than in the approach of Ruiz-Villanueva et al. [60]. However, this approach is, to our knowledge, the only one that considers the whole process chain of LW recruitment, transport, and deposition. The approach of Mazzorana et al. [59] requires the locations of standing trees or lying trees or logs as input data. Thus, the trees in floodplains have to be localized and classified, and their volume must be estimated. For this task, some approaches have only recently been developed. Besides the interpretation of aerial images [66] or geographic information system (GIS) analysis [26,59], a number of approaches for single-tree detection and classification on the basis of Light Detection and Ranging (LiDAR) data have been published [67–75]. These approaches significantly facilitate the preprocessing of the input data needed for LW transport models.

In summary, if risk management options have to be designed at a specific point of interest where LWD are expected to significantly influence the flood process, engineers can use simulation models explicitly dedicated to analyzing the clogging of LW at bridges while considering the interactions between the logs and a two-way coupling with the hydrodynamic model (i.e., [60]). Regarding the estimation of upper boundary conditions for simulations of the clogging process, there is a lack of methods for (a) estimating potential LW volume standing in the flood influence zones upstream of the object at risk, (b) assessing the spatiotemporal dynamics of LW within a flood event (i.e., a time series of wood fluxes), and (c) identifying the most relevant recruitment areas that deliver LW to the point of interest (e.g., a planned bridge or weir). The latter includes the transport and deposition processes along the river reach. However, a single tool for answering all these questions is still missing. In particular, estimating wood load in terms of LW volume during extreme floods is difficult, because statistical methods are not feasible due to the rarity of observation data.

The main goal of this work was therefore to develop a tool for quantifying incoming LW fluxes at a specific point of interest in a river network as a basis for the design of wood-retention structures in a river basin. This requires the full consideration of LWD—from recruitment to transport and deposition—along the river reach upstream of the point of interest. Apart from the approach of Mazzorana et al. [59], there are no applicable or extendable models to cover the full “process cascade” at the required spatial scale. However, the latter approach is implemented in raster-based software. As modelling LWD requires high spatial resolution, the raster approach limits the application of the model to restricted sizes of the study area. The approach of Mazzorana et al. [59] does not allow simulating LWD at the river reach scale with the required spatial resolution.

Thus, the main research question here relates to the applicability of a full model chain to simulate LWD during an extreme flood at river reach scale. Our hypothesis is that implementing the model in a vector-based, object-oriented modelling approach on the basis of irregular triangular computational meshes allows simulating LWD at the required scale and spatial resolution. Consequently, this requires modelling LW as objects (floating logs). Hence, the secondary research question relates to the development of a tree detection and volume estimation approach.

Accordingly, this paper first describes the general framework for LW recruitment and transport modelling. Second, the model is evaluated by comparing the simulation results with well-documented flood events. After this evaluation, a model application for assessing LWD during an extreme flood event is described. Finally, the results are discussed and conclusions on the use of the proposed model in flood risk management are drawn from the model evaluation and application.

2. Methods

The presented approach is based on the following steps: detection and characterization of trees, hydraulic modelling, modelling of the recruitment of LW, and modelling of the transportation and deposition processes. Hence, this section is structured along this concept (Figure 1). First, we present the overall modelling approach. Herein, an introduction to the basic framework of LWD simulation is given. Second, the method for identifying single trees in forested areas and classifying the vegetation is described. After an explanation of the procedure for simulating hydrodynamics with Basic Simulation Environment for Computation of Environmental Flow and Natural Hazard Simulation (BASEMENT-ETH), we describe the implementation of the relevant processes of LW dynamics, i.e., recruitment, mobilization, transport, deposition, and entrapment at bridges. Herein, the basic idea and the implementation of the model are explained. The whole procedure was implemented in a set of functions programmed in R (LWDsimR (see Supplementary Materials)). The software was developed in the framework of the present study.

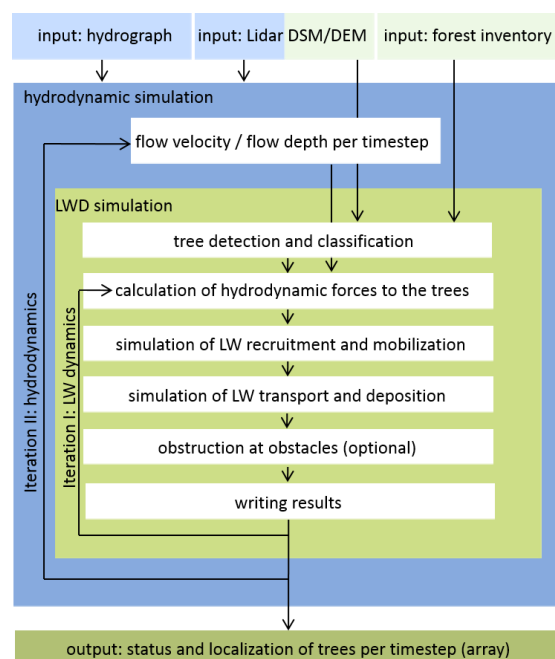


Figure 1. General framework of large wood dynamics (LWD) simulation in LWDsimR. DSM, digital surface model; DEM, digital elevation model; LW, large wood.

2.1. Basic Framework of LWD Modelling

The basic concept of LWDsimR follows the approach of Mazzorana et al. [59] and was extended with a tree recognition and classification module. LWD during a flood is simulated in a spatially (upper, lower, and lateral boundaries) and temporally (duration of the event) delimited system. Water flow entering the system at the upper system boundary and leaving it at the lower system boundary is simulated by a two-dimensional hydrodynamic model. The vegetated area in the system is represented in single-tree resolution. The trees are extracted from LiDAR data and classified on the basis of forest inventory data. Single trees are represented as cylindrical objects, which may have rootstock in the form of a disc and a specific diameter. Branches, crown, and rejuvenation are neglected. Every tree is considered by the model as a point feature in space with certain attributes describing its characteristics and status during the simulation time. During the simulation, every tree has a “status” that defines whether it is rooted, lying, transported, or jammed at a bridge. Under given conditions at every time step, standing trees can therefore be recruited (eroded and mobilized) and transported into the channel. The lying trees (greenwood and deadwood) can be transported by the flood, depending

on the hydrodynamic conditions. During the simulation, the trees can be deposited, remobilized, or entrapped at bridges, or can leave the system at the lower system boundary (LSB). Only trees that are standing in the influence zone of the flood (flooded areas) and are directly influenced by hydrodynamic forces are considered for recruitment. All trees outside of the flooding perimeter are neglected or have to be inserted into the system border (e.g., contributions of tributaries or provided by hillslope processes). The main input data needed for simulation are hydrographs at the upper boundary conditions, digital surface and elevation models, and data about local forest characteristics (forest inventory). While the hydrodynamic simulation is done with BASEMENT-ETH, LWD simulation and postprocessing are performed with LWDsimR.

2.2. Identification and Classification of Trees

The detection of single trees in the forested areas is based on digital surface models (DSMs) and digital elevation models (DEMs) with a spatial resolution of 0.5 m [76]. A normalized surface model (NSM) is calculated by subtracting the DEM from the DSM. The forested area is defined by a predefined vegetation mask extracted from the land cover map LK25 of the Federal Office for Topography (SWISSTOPO). It is assumed that tree crowns are represented as local maxima in the NSM [77]. Therefore, they can be detected using a moving window approach. Here, we used a window of 3.5×3.5 m. A grid cell is defined as a local maximum if all of its neighbors in the window have a lower height value. To be identified as a tree, a cell has to exceed a predefined minimum height, in our case 3 m. This approach is sensitive to the size of the window. A small window generally leads to the detection of more local maxima, which can cause erroneous multidetections of large trees with big crowns and several smaller tops. With an increasing window size, the risk of multidetection decreases, but smaller and dense standing trees might be neglected. Hence, the size of the window must be chosen carefully and with regard to the prevalent vegetation structure. We used sample areas for calibration in which we measured the location and height of each tree.

After detecting the trees, the necessary attributes of every tree, namely diameter at breast height (DBH), tree height, diameter of rootstock, forest structure [78,79], and slope, are determined. The height of the trees can be directly derived from the NSM, whereas DBH has to be calculated on the basis of height using a regional tariff function [80]. The diameter of the rootstock can be defined as a multiple of DBH with a factor between 2 and 3 [38] or 5 [59]. The attribute “structure” represents the vegetation structure concerning the age and density according to [59]. The tree density (443 trees with a $DBH \geq 12$ cm per hectare) was delineated from the forest inventory of the region “Northern Alps, West” [78,79]. Moreover, it is necessary to determine whether a tree is standing in an area unit with predominant young vegetation and if the tree density in this area unit is above or below a predefined threshold. The attribute “slope” determines, over a threshold, whether a tree is standing in a steep or rather flat area. The threshold for defining steep slopes is 25° . Subsequently, we estimated the volume of every tree according to the function proposed by Denzin [81] (Equation (1)). We used a form factor f of 0.5. l is the tree height.

$$vol = \frac{\pi}{4} \times DBH^2 \times f \times l \quad (1)$$

The location of deadwood is generated as a set of random points within the forested area. The amount of deadwood (i.e., the point density for the study region) can be estimated on the basis of forest inventories. In our study, we used a density of 24 trees/hectare. We deduced the length and diameter of the deadwood from the relative frequency distribution of samples from field studies in the riparian forests of Belp, Elfenau, Rubigen, and Uttigen ($n = 149$). Finally, the generated greenwood and deadwood are merged into a point shapefile with a unique ID and the corresponding attributes.

2.3. Hydrodynamic Simulation

For the hydrodynamic simulation, the freely available BASEMENT-ETH software was used [14]. BASEMENT-ETH consists of 2 numerical subsystems: BASEchain for 1-dimensional numerical

simulations of river reaches based on cross-section and BASEplane for 2-dimensional numeric simulation of river reaches and flood plains based on an unstructured mesh. In both subsystems, sediment transport can be considered [14]. This tool basically solves shallow water equations. The topography is represented in an unstructured flexible mesh, whereas single triangles have an assigned roughness represented by Strickler values. During the simulation, flux takes place on the edges between 2 elements in finite volume methods and the water level and velocity in the x and y directions are calculated. This hydraulic model has been extensively used and validated in the study area [82–87]. The calculated flow variables for different time steps form the basis for the subsequent simulation of LW dynamics.

The simulation on the basis of an unstructured mesh offers some benefits for LWD modelling. In comparison to approaches based on regular grids, the size of the study area can be extended without losing too much detail within the river channel. Thus, the approach of irregular meshes is expected to be more adaptable, especially at locations with relevant discontinuities [56]. In contrast, the approach of Mazzorana et al. [59] for LWD simulation is based on regular grids. Hence, there is a trade-off between the spatial resolution of the grid and the extent of the study area. As a consequence of increased grid size, a loss in the robustness of in-stream LW transport simulation has to be expected. Therefore, here we adapted the original approach of Mazzorana et al. [59] for LWD simulation to be used on irregular meshes.

2.4. LWD Simulation

The following section explains the functionality of LWDsimR in detail. The program was written in the R programming language [88]. The transport simulation was extended with capabilities for input generation (tree identification and classification). The results of hydrodynamic simulations were used as the basis for the LWD simulation. The 2 models were unilaterally coupled and the influence of LW on the hydrodynamics was neglected. However, a simplified approach for considering the retention of LW volume by bridges was implemented.

Basically, the simulation of LWD is calculated in 2 nested loops. The function of the outer loop is to load the results of the different time steps from the hydrodynamic simulation (flow depth and velocity in the x and y directions) into the model. The function of the inner loop is to calculate the processes of LWD in a specific number of time steps during one time step of the hydrodynamic simulation. Hence, the number of iterations of the inner loop defines the number of time steps and therefore the temporal resolution of the LWD simulation. This procedure allows LWD to be simulated with a higher temporal resolution than the hydrodynamics.

During every time step of the inner loop, the following procedure is executed to calculate the LWD processes:

- **Localization:** For every tree, its closest 3 mesh-nodes of the hydrodynamic model are identified. On these nodes, the hydrodynamic conditions of the particular time step are read out. The conditions are interpolated at the position of the tree using the inverse distance weighting interpolation method.
- **Recruitment and mobilization:** Whether standing trees are standing or have fallen into the channel is checked. For standing trees, the hydrodynamic forces are analyzed to estimate the recruitment. For uprooted trees, the recruitment analysis is not needed and the flow conditions are analyzed; only recruitment processes from soil erosion in the influence zone of the flood are considered. Lateral erosion of river banks and subsequent river widening or other changes of the channel morphology are not considered. Since there is still a lack of detailed knowledge with respect to possible recruitment mechanisms, a probabilistic approach is considered. Depending on the hydrodynamic forces acting on a tree, a recruitment probability is determined on the basis of the vegetation structure and the local slope according to [59]. In a first step, the hydraulic impact C is calculated on the basis of flow depth h and flow velocity U (Equation (2)).

$$C = h \times \frac{U^2}{2g} \quad (2)$$

- On the basis of the classified hydraulic impact, the wood structure, and the slope, a probability factor of recruitment is assigned (Figure 2). The probability of mobilization is calculated for each time step, divided by the total number of time steps. For each tree, it is randomly defined if the status of the tree changes from “standing” to “recruited,” depending on the assigned probability. A “recruited” tree is defined as an uprooted tree that has fallen due to hydrodynamic forces.
- Entrainment, transport, and deposition: For all lying trees (uprooted greenwood and deadwood), it is checked whether the conditions for entrainment are fulfilled. For simplicity, it is assumed that the density of all trees is lower than 1 and their orientation is parallel to the flow. Interactions between trees and breaking of logs are neglected. The transport process can take place under floating or rolling/sliding conditions [89]. Depending on these conditions, the transport velocity differs from a velocity equal to the streamflow for floating trees to reduced velocity for sliding or rolling trees. For a comprehensive description of the physical foundations of the transport dynamics, we refer to the literature [59]. Using the information about velocity and flow direction, the new positions for every transported log are calculated for every time step. A transported log can be deposited at a particular time step if the conditions for transportation are not fulfilled anymore, and it can be remobilized at a later time step. Transported trees that are not deposited or entrapped at a bridge reach the lower system boundary (LSB) and are not considered in the further simulation.
- Bridge clogging: Bridges can optionally be considered in the model as polygon geometries with information about their height above the riverbed and length. If 1 or more of the 3 closest mesh-nodes of a transported tree lies within such a polygon, it is assumed that the tree is passing a bridge. In this case, it can collide with 1 or more piers or interact with the bridge deck and cause clogging [90]. As a simplification, the specific bridge structure and the flow conditions are neglected. Furthermore, if log jams are formed, they do not interact with other trees and cannot break. With regard to the randomness of this process and the lack of physical knowledge, a probabilistic approach is applied. According to [90], the probability of a log being jammed at a bridge is the sum of all blocking probabilities on single bridge elements. The blocking probability for the piers is calculated following [91] since only the bottom width and log length are considered in the equation. The clogging probability at the bridge piers is calculated according to [92] (Equation (3)) and at the bridge deck according to [93] for trees with (Equation (4)) and without (Equation (5)) rootstocks. The total blocking probability of a tree at a bridge is the sum of the single probabilities. A random generator is used to determine, with the given probability, whether a tree is jammed or passes the bridge normally. For a detailed description of the clogging probabilities, we refer to [91]. This feature considering LW retention by clogging is optional.

$$prob_{pier} = -\frac{1}{15} + \frac{2l}{15 \times B_{min}} \quad (3)$$

$$prob_{deck\ log} = -3.5 + 2.56 \times \frac{h + \frac{d_R}{2}}{H} \quad (4)$$

$$prob_{deck\ root} = -0.074 + 0.88 \times \frac{l}{B_{min}} \times \frac{h + \frac{d}{2}}{H} \quad (5)$$

Where l is the log length; B_{min} is the minimal distance between bridge piers; h is the flow depth; H is the distance between river bed and lowermost edge of the bridge; d_R is the diameter of rootstock; d is the diameter of log.

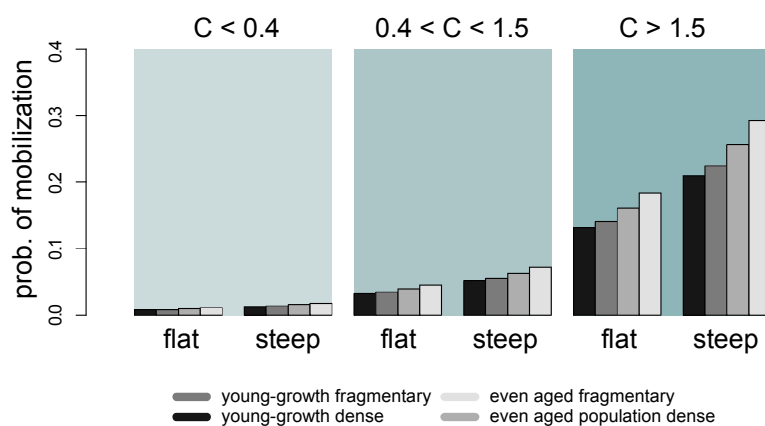


Figure 2. Probabilities of mobilization used in the recruitment module.

The results are saved and the LWD processes are calculated again for the next time step. The final result consists of a 3-dimensional array showing the status and location (x , y coordinates) of each log. From this, the tracking of the logs during the simulation, a video of the simulation, or the analysis of the LWD dynamics along the river reach can be derived. The volume of LW is quantified in solid form, i.e., considering the wood mass only.

2.5. Model Test

To test and validate LWDsimR, we compared model runs with observations. We reconstructed 2 well-documented flood events with the model. The first test was done in the Aare River reach from Thun to Bern, Canton of Bern, Switzerland (see Figure 2). We reconstructed the flood event of August 22, 2005, and compared the simulated LW volume at the lower system boundary with the observed volume. During this flood event, the Aare River had a peak discharge of $605 \text{ m}^3/\text{s}$ and an estimated return period of >150 years [94]. Approximately 2300 m^3 of loose and $600\text{--}900 \text{ m}^3$ of solid woody material blocked the weir [95]. The flood event led to inundation of the Matte district, generating 50×10^6 Swiss Francs of damages [96]. Second, we tested whether the LW input delivered from the tributary Zulg River in the flood event of June 7, 2015, could be transported toward Bern as documented. Here, we first modelled recruitment and transport within the Zulg River catchment. Subsequently, we used the LW volume coming from the tributary as input to the main river and modelled the transport of LW along the Aare River toward Bern.

2.6. Modelling LWD during an Extreme Flood

Large quantities of LW transported by the Aare River to Bern pose a severe problem, since clogging of the Mattenschwelle weir can lead to severe inundation of the Matte district in the city of Bern due to backwater effects. This happened during the flood event in 2005. For sound risk management, knowledge about LWD in the Aare River and an estimation of the maximum volumes of woody material in the worst case scenario are paramount. Therefore, the focus of our attention in modelling an extreme flood scenario that explicitly takes into account LWD is the city of Bern (see Figure 3). The main LW recruitment areas are located in the floodplain of the river Aare between Thun and Bern. In this floodplain, we considered LW recruitment due to erosion of root wads by hydrodynamic forces. Hence, we simulated LW dynamics in the Aare between Thun and Bern during an extreme flood event. This is a flood scenario of a probable maximum precipitation event [97], with a peak discharge of $1100 \text{ m}^3/\text{s}$ and a duration of 40 h. The outcome of the hydrodynamic model has a temporal resolution of 20 min and the time step of LWDsimR is set to 5 s. Bridge clogging in the upstream river reaches is neglected, because only pierless and high bridges span the Aare River. The Zulg River tributary can potentially deliver relevant LW quantities to the main river. The confluence of the Zulg and Aare rivers is in Steffisburg, 3 km downstream of Thun. It is considered an important source of woody

material and therefore was modelled separately first. Logs transported from the upper Zulg catchment to Steffisburg were used as input for the simulation of LWD in the Aare River. The other tributaries of the river downstream of Lake Thun do not have any relevant forests in the flood influence zones and thus do not deliver LW to the main river. LW delivered by the tributaries upstream of Lake Thun is entrapped by the lake and thus is not relevant to the point of interest.

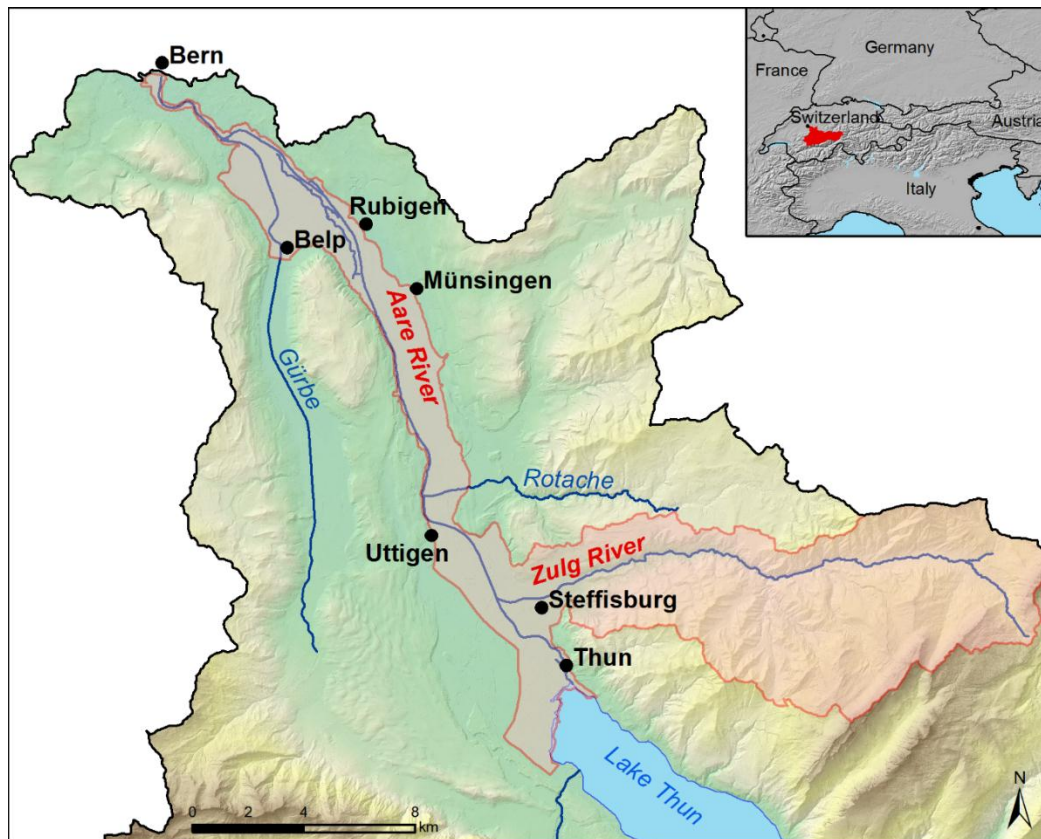


Figure 3. Overview of the study area. Background data: Canton of Bern.

3. Results

The reconstruction of the flood event in August 2005 resulted in a LW volume of 1774 m³ at the lower boundary condition in Bern. This is remarkably higher than the observed volume of 600–900 m³. However, the latter takes into account clogged wood only. The volume of LW that passed the weir during the flood is unknown. In contrast, the simulated volume represents the volume of LW that passed the LSB. Thus, the results of simulated LW volume must be above the observed value.

The second model test showed that during the 2015 flood in the Zulg River, an LW volume of 343 m³ was recruited in the catchment and transported to the confluence with the Aare River. This is in line with the estimation of <<600 m³ that was observed and documented by public authorities [98]. In contrast to our simulation, landslides also contributed to LW during this flood in the Zulg River catchment. Here, we do not consider the recruitment of LW by landslides, therefore the simulated volume has to be lower than the observed volume. Logs coming from the Zulg tributary follow the thalweg of the Aare River and no implausible deposition of LW along the river banks was simulated. Along its flow in the Aare River, LW coming from the Zulg River was dispersed into a more or less dense layer. From the total LW volume of the Zulg River, 98.5% was transported to Bern in this test case. Only a small volume of LW was deposited in the confluence between the Zulg and Aare rivers. This is in line with observations along the Aare River after this flood event.

Applying the model to an extreme flood event gives the expected LW volume at the point of interest, in our case the Matteschwelle weir in Bern. An overview concerning the volume of the simulated LWD is shown in Table 1. From the alluvial forests between Thun and Bern, with a total stock of 112,661 m³ in the direct flood influence zone, 11,841 m³ was recruited in the simulation; 7288 m³ was deposited within the system and did not reach Bern, whereas 3933 m³ was transported through the system toward the LSB, including the 343 m³ from the Zulg River catchment.

Table 1. Modelled solid LW volumes during an extreme flood in the Aare River.

LW Class	LW Volume (m ³)
Forest stock in inundated areas	112,661
Total mobilized wood	11,841
Mobilized in Zulg tributary	343
Mobilized living wood	5732
Mobilized deadwood	6109
Deposited after mobilization	7288
Volume passing the lower system boundary in Bern	3933

The temporal distribution of the simulated LWD in the Aare River is shown in Figure 4. The hydrodynamic simulation starts with a bankfull discharge and partially flooded alluvial forests within the river bed as the initial condition. Thus, the initial recruitment rate is very high and there is a high share of deadwood. The mobilization rate soon falls to 25 m³/20 min and then increases again with the rising limb of the hydrograph. The share of greenwood increases, whereas the recruitment of deadwood is reduced constantly over time. The mobilization rate peaks at 250 m³/20 min after 5 h with flooding of the alluvial forests in the floodplain. The mobilization rate drops after the peak discharge is reached after 14 h. LW reaches Bern in 2 pulses; the first pulse occurs 5 h after the simulation start. A decrease of the rate follows before it starts to increase again around peak discharge and peaks a second time at hour 13. After a further peak, it decreases strongly. In all, 61% of the mobilized wood is deposited within the system, mostly on spots close to artificial buildings in the floodplains, such as driveways to the road that bridge over the Aare River. These hydraulic obstacles that perpendicularly cross the floodplain also act as an obstacle for LW, as well as the highway that is partially built on an earth dam (Figure 5).

The recruited trees are mostly located along the banks and dams and close to the main channel. This is especially valid for the recruitment areas of LW that reach Bern (Figure 6). Trees located on banks, islands, and areas close to the main channel are most exposed to the hydrodynamics. Once LW reaches the main channel, it can be transported over long distances without being deposited. Only a few selected alluvial forests (Elfenau, Zopfen, Raintalau, and Vorder Jaberg) deliver LW that reaches the LSB. The LW delivered by the Zulg River is transported to Bern.

The spatial pattern of the deposition process is different from that of the recruitment process, although deposition is also simulated along the whole river reach. The simulation of LW deposition reveals much more scattered and spotty patterns, with relevant depositions in particular areas. This can be clearly seen in the deposition map in Figure 7. Important locations for deposition of LW within the floodplain are the Aare River bridge near Rubigen (see Figure 5), the heightened highway between Rubigen and Münsingen, the railway bridge near Uttigen, and several spots mostly along the banks or edges of the wetted area. Major depositions are simulated mainly on 2 spots along the highway north and south of the bridge with different deposition patterns. North of the bridge, the woody material was deposited along a zone 400 m in length with shallow water depth, whereas south of the bridge the deposition accumulated on a single spot on the highway. Other specific deposition spots can be found on the left- and right-hand sides of the bridge in the upstream direction. Deposition of smaller volumes occurred in the entire floodplain.

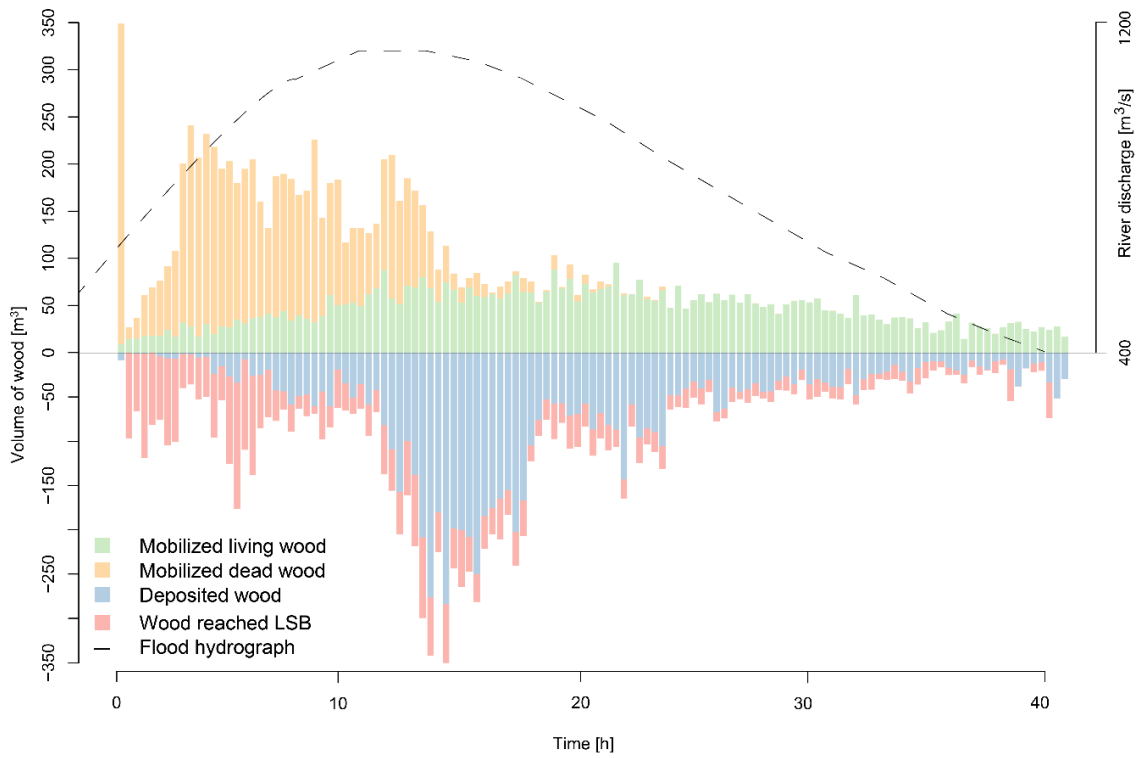


Figure 4. Simulated temporal distribution of LW dynamics in a worst case flood along the Aare River. Time step of the hydrodynamic model = 1200 s, time step of LWDsimR = 5 s.

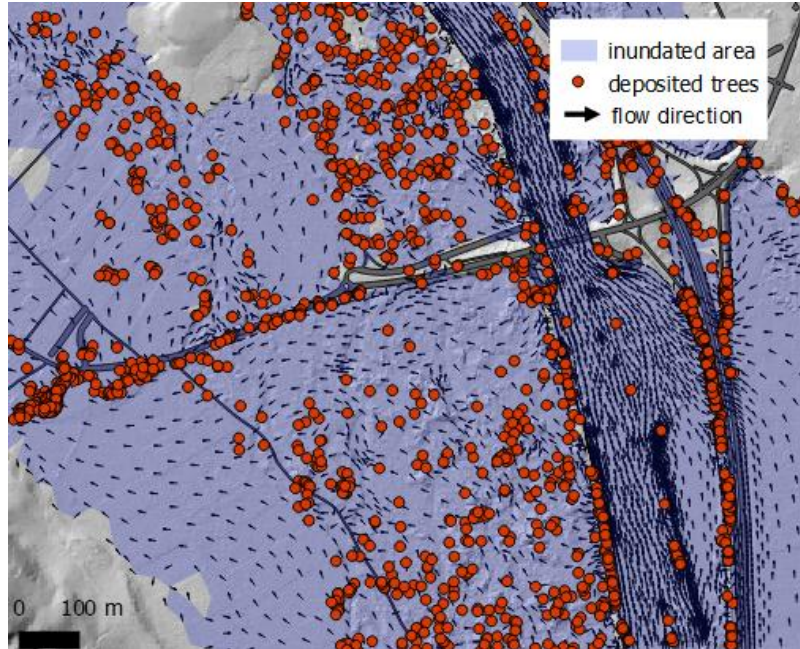


Figure 5. Extract of the map of the deposition areas in the Aare River floodplain near Rubigen. Background map: Federal Office of Topography SWISSTOPO.

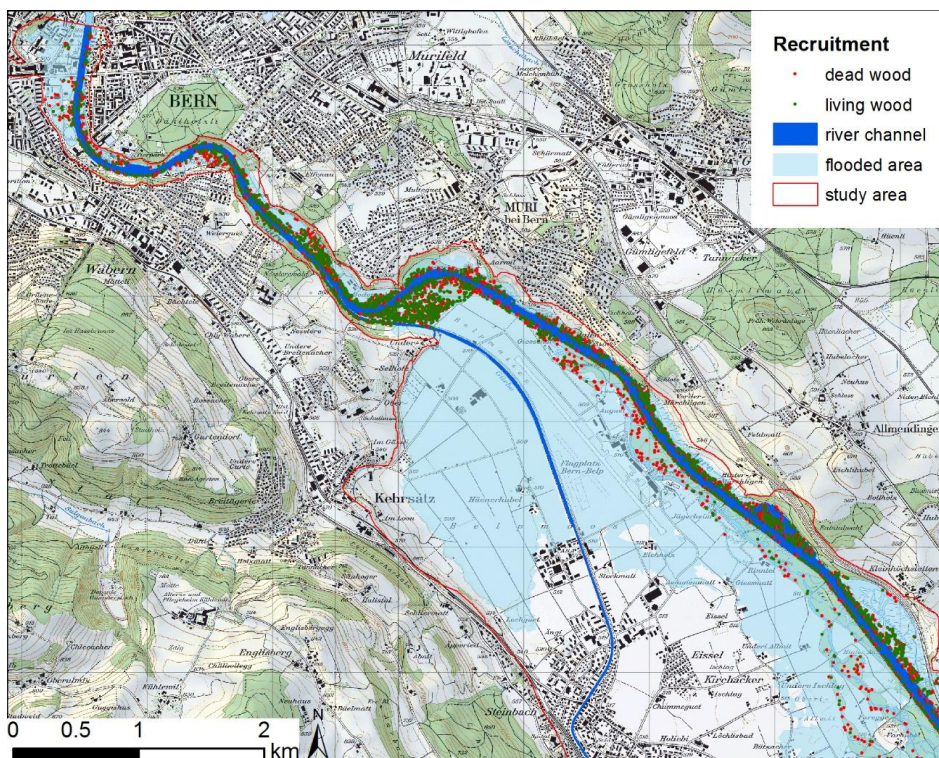


Figure 6. Extract of the map of the recruitment areas of LW that reached the lower system boundary at Bern during the simulation. The dots show the initial locations of the wood logs. Background map: Federal Office of Topography SWISSTOPO.

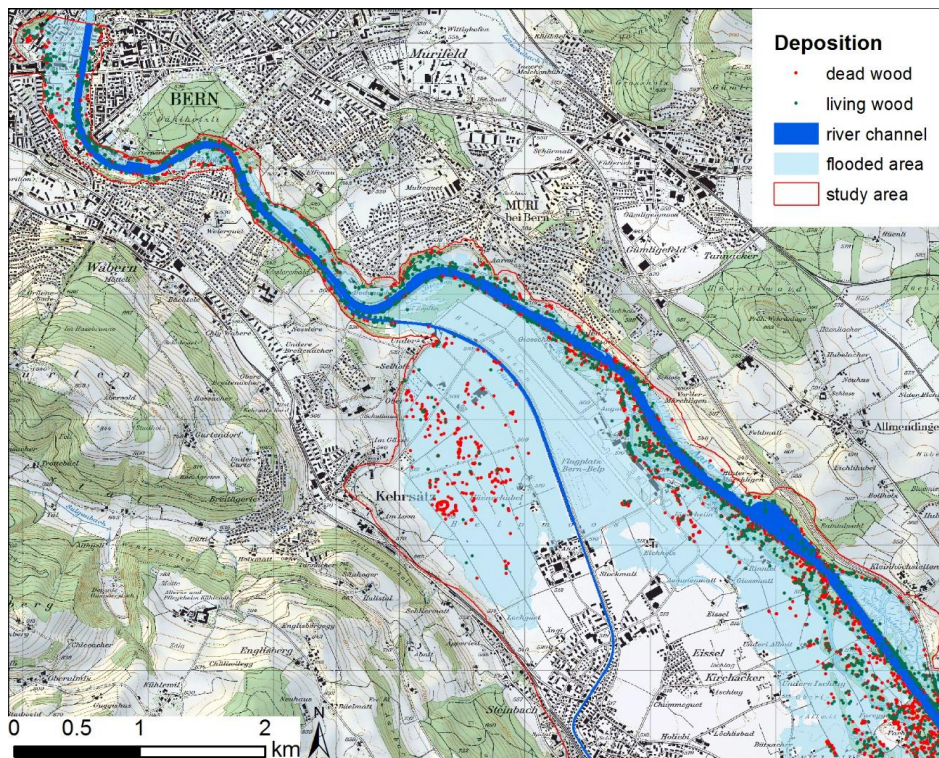


Figure 7. Extract of the map of the deposition areas in the Aare River floodplain upstream of Bern. The dots show the locations of the wood logs at the end of the simulation. Background map: Federal Office of Topography SWISSTOPO.

4. Discussion and Conclusions

Comiti et al. [45] raised the question of whether we are able to reliably and quantitatively predict LW recruitment, transport, and deposition within a given river basin during a selected flood scenario of a given magnitude/frequency. In this paper, we presented the LWDsimR modelling tool, which enabled us to answer this question quantitatively to a certain extent in the Aare River basin upstream of Bern, Switzerland.

With the presented approach, it is possible to quantify LW dynamics as a better-informed guess. The procedure could help to estimate the amount of LW volume at a specific point in a river system, especially in areas where no flood events occurred, which helps to assess LW volume empirically by analyzing past events. Implementing the simulation model on an irregular computational mesh allows the simulation of LWD in larger areas, i.e., at a river reach or basin scale. In comparison, a raster-based approach would be limited by the trade-off between spatial resolution and extent of the study area.

The comparison between the simulated and observed volumes of LW at Bern during the flood event of 2005 shows that the model may overestimate predicted LW volume. Despite the uncertainties in the observation, the model tests showed that the approach is applicable to river reaches up to 30 km in length. Moreover, the model correctly simulated the transport path of LW delivered by tributaries in the main river.

In comparison to the LW volume that obstructed the weir in Bern during the flood of 2005, the LW volume to be expected in a worst case flood is considerably higher. A flood event of a probable maximum precipitation scenario produces threefold more LW than the hitherto known most extreme flood. However, it can be assumed that the simulated LW volume transported to the LSB in Bern is rather an upper limit for several reasons. First, the total amount of recruited trees in the floodplains is likely to be overestimated due to high flow depths but relatively low flow velocities. The implemented recruitment algorithm gives large weight to flow depth. Second, a significant part of the recruited wood is not deposited within the system and therefore reaches the lower system boundary at Bern. Standing trees often function as flow obstacles for floating trees. This is not considered here. Moreover, if one flood event occurs, a share of the forest stock will be transported out of the floodplains. A subsequent flood of the same magnitude will have less LW available for recruitment. This leads to the presented approach being sensitive to the date of the forest inventory, i.e., the date of the LiDAR scan. Regarding the recruitment areas, it must furthermore be considered that the Zulg tributary likely plays a considerably more important role than in the simulation results because of the highly probable activity of landslides during an extreme flood.

Nevertheless, the simulation allows the identification of areas prone to recruitment processes of LW due to soil erosion by hydrodynamic forces and shows the ability to transport recruited logs from source areas over long distances to the LSB. Therefore, from a forest management point of view, it may be worthwhile to closely inspect the identified areas, especially those in the upstream vicinity of the point of interest, and to consider preventing massive recruitment of LW.

However, the validation and application of LWDsimR showed some limitations of the tool. The recruitment process is based on a probabilistic approach. Future developments should implement physical-based approaches that fully consider the hydrodynamic forces on vegetation and the resistance of vegetation. Furthermore, we cannot validate the number of recruited trees, because only LW volumes are given in the observation data. Moreover, the clogging process at bridges could not be validated at the time of the study. In LWDsimR, this process is considered only for the purpose of LW budgeting along the river reaches. The modelling of the clogging process has to be improved in the future. Recently, some experiments showed possible ways to improve the modelling of this process [99–102]. For this question, we recommend using more detailed and fully coupled models, i.e., those in [60].

Another open question is the transferability of the model to smaller alpine rivers and torrents. In rivers with a width on the order of a tree length or less, the transport module may overestimate the deposition and underestimate the transportation of logs toward the lower system boundary. Underestimation may also be caused by neglecting other processes like sediment transport and

morphology changes during the flood. Furthermore, it has to be noted that the model neglects the input of LW into a river reach by debris flow from tributaries, by landslides, or by bank erosion and the remobilization of LW that was deposited in the channel during previous floods. These recruitment processes play an important role [52,103–105] and have to be implemented in future versions. Thus, future developments should focus on modelling LW recruitment by these geomorphic processes. Moreover, the uncertainties in the model and the sensitivity against input data and model parameters should be analyzed thoroughly in the future. For this, implementing a parallelization scheme in the model is a prerequisite. Another limitation of the model is the requirement of reliable input data, i.e., single trees with their locations and different characteristics. These data are lacking in many regions, and hence transferability may be limited to regions with available data.

Overall, the simulation results of the LW dynamics, both the temporal and spatial dynamics, in a river reach during an extreme flood event provide important information for flood risk management. LWDsimR allows the expected volume of LW on a certain point in the river basin to be assessed by considering the actual conditions of vegetation and a specific flood scenario. This provides a basis for the design of bridges or wood-retention structures and for quantitatively assessing LWD during a worst case flood. Thus, model experiments with LWDsimR could provide a range of values of LW delivery under different flood magnitudes, providing a basis for assessing catchment behavior in terms of LW delivery and dynamics.

Analyzing the trade-off between the ecological benefits of wood in rivers and flood risk management [106], another reason was found for using LWDsimR. With the presented model, one can identify the areas from which LW is recruited and transported toward the lower system boundary and those from which the recruited LW is not transported downstream. With this, areas that are important for ecology and for flood discharge improvement can be prioritized on the basis of a transparent and reproducible method. Therefore, the unnecessary use of wood cuts as a flood prevention measure can be avoided.

Supplementary Materials: The code of LWDsimR used in this paper and a user manual are available at <https://zenodo.org/record/1296733>. The code used to simulate the case study is available at <https://github.com/zischg/LWDsimAare>. The data of the case study are available at <http://dx.doi.org/10.17632/kchsr5tjw5.1>.

Author Contributions: Conceptualization: all; methodology: all; software: N.G.; validation: N.G. and A.Z.; writing—original draft: A.Z.; writing—review and editing: all.

Funding: This research was funded by the Mobiliar Lab for Natural Risks and partially by the Swiss National Foundation (Grant No. IZK0Z2_170478/1).

Acknowledgments: The authors are grateful to Philipp Mösch, who provided insightful expertise and data for tree classification.

Conflicts of Interest: The authors declare no conflict of interest.

References

- Desai, B.; Maskrey, A.; Peduzzi, P.; De Bono, A.; Herold, C. *Making Development Sustainable: The Future of Disaster Risk Management, Global Assessment Report on Disaster Risk Reduction*; United Nations Office for Disaster Risk Reduction (UNISDR): Geneva, Switzerland, 2015.
- Weingartner, R.; Barben, M.; Spreafico, M. Floods in mountain areas—An overview based on examples from Switzerland. *Mt. Hydrol. Water Resour.* **2003**, *282*, 10–24. [[CrossRef](#)]
- Zischg, A. Floodplains and Complex Adaptive Systems—Perspectives on Connecting the Dots in Flood Risk Assessment with Coupled Component Models. *Systems* **2018**, *6*, 9. [[CrossRef](#)]
- Zischg, A.P.; Hofer, P.; Mosimann, M.; Röthlisberger, V.; Ramirez, J.A.; Keiler, M.; Weingartner, R. Flood risk (d)evolution: Disentangling key drivers of flood risk change with a retro-model experiment. *Sci. Total Environ.* **2018**, *639*, 195–207. [[CrossRef](#)] [[PubMed](#)]
- Ruiz-Villanueva, V.; Wyżga, B.; Mikuś, P.; Hajdukiewicz, M.; Stoffel, M. Large wood clogging during floods in a gravel-bed river: The Długopole bridge in the Czarny Dunajec River, Poland. *Earth Surf. Process. Landf.* **2017**, *42*, 516–530. [[CrossRef](#)]

6. Kim, H.J.; Lee, J.W.; Yoon, K.S.; Cho, Y.S. Numerical analysis of flood risk change due to obstruction. *KSCE J. Civ. Eng.* **2012**, *16*, 207–214. [[CrossRef](#)]
7. Ruiz-Villanueva, V.; Bodoque, J.M.; Díez-Herrero, A.; Eguibar, M.A.; Pardo-Igúzquiza, E. Reconstruction of a flash flood with large wood transport and its influence on hazard patterns in an ungauged mountain basin. *Hydrol. Process.* **2013**, *27*, 3424–3437. [[CrossRef](#)]
8. Ruiz-Villanueva, V.; Bodoque, J.M.; Díez-Herrero, A.; Bladé, E. Large wood transport as significant influence on flood risk in a mountain village. *Nat. Hazards* **2014**, *74*, 967–987. [[CrossRef](#)]
9. Hajdukiewicz, H.; Wyżga, B.; Mikuś, P.; Zawiejska, J.; Radecki-Pawlik, A. Impact of a large flood on mountain river habitats, channel morphology, and valley infrastructure. *Floods Mt. Environ.* **2016**, *272*, 55–67. [[CrossRef](#)]
10. Loat, R.; Petraschek, A. *Consideration of Flood Hazards for Activities with Spatial Impact*; Federal Office for the Environment (FOEN): Bern, Switzerland, 1997.
11. Mazzorana, B.; Fuchs, S. Fuzzy Formative Scenario Analysis for woody material transport related risks in mountain torrents. *Environ. Model. Softw.* **2010**, *25*, 1208–1224. [[CrossRef](#)]
12. Mazzorana, B.; Comiti, F.; Scherer, C.; Fuchs, S. Developing consistent scenarios to assess flood hazards in mountain streams. *J. Environ. Manag.* **2012**, *94*, 112–124. [[CrossRef](#)] [[PubMed](#)]
13. Schmocker, L.; Weitbrecht, V. Driftwood: Risk Analysis and Engineering Measures. *J. Hydraul. Eng.* **2013**, *139*, 683–695. [[CrossRef](#)]
14. Vetsch, D.; Siviglia, A.; Ehrbar, D.; Facchini, M.; Gerber, M.; Kammerer, S.; Peter, S.; Vonwiler, L.; Volz, C.; Farshi, D.; et al. *BASEMENT—Basic Simulation Environment for Computation of Environmental Flow and Natural Hazard Simulation*; Eidgenössische Technische Hochschule (ETH) Zurich: Zurich, Switzerland, 2017.
15. Horton, P.; Jaboyedoff, M.; Rudaz, B.; Zimmermann, M. Flow-R, a model for susceptibility mapping of debris flows and other gravitational hazards at a regional scale. *Nat. Hazards Earth Syst. Sci.* **2013**, *13*, 869–885. [[CrossRef](#)]
16. Coulthard, T.J.; Neal, J.C.; Bates, P.D.; Ramirez, J.; de Almeida, G.A.M.; Hancock, G.R. Integrating the LISFLOOD-FP 2D hydrodynamic model with the CAESAR model: Implications for modelling landscape evolution. *Earth Surf. Process. Landf.* **2013**, *38*, 1897–1906. [[CrossRef](#)]
17. Gurnell, A.M.; Piegay, H.; Swanson, F.J.; Gregory, S.V. Large wood and fluvial processes. *Freshw. Biol.* **2002**, *47*, 601–619. [[CrossRef](#)]
18. Wohl, E. Of wood and rivers: Bridging the perception gap. *WIREs Water* **2015**, *2*, 167–176. [[CrossRef](#)]
19. Wohl, E. Bridging the gaps: An overview of wood across time and space in diverse rivers. *Geomorphology* **2017**, *279*, 3–26. [[CrossRef](#)]
20. Moulin, B.; Schenk, E.R.; Hupp, C.R. Distribution and characterization of in-channel large wood in relation to geomorphic patterns on a low-gradient river. *Earth Surf. Process. Landf.* **2011**, *36*, 1137–1151. [[CrossRef](#)]
21. Sear, D.A.; Millington, C.E.; Kitts, D.R.; Jeffries, R. Logjam controls on channel-floodplain interactions in wooded catchments and their role in the formation of multi-channel patterns. *Geomorphology* **2010**, *116*, 305–319. [[CrossRef](#)]
22. Senter, A.E.; Pasternack, G.B.; Piégay, H.; Vaughan, M.C.; Lehyan, J.S. Wood export varies among decadal, annual, seasonal, and daily scale hydrologic regimes in a large, Mediterranean climate, mountain river watershed. *Geomorphology* **2017**, *276*, 164–179. [[CrossRef](#)]
23. Seo, J.I.; Nakamura, F. Scale-dependent controls upon the fluvial export of large wood from river catchments. *Earth Surf. Process. Landf.* **2009**, *34*, 786–800. [[CrossRef](#)]
24. Seo, J.I.; Nakamura, F.; Nakano, D.; Ichiyanaagi, H.; Chun, K.W. Factors controlling the fluvial export of large woody debris, and its contribution to organic carbon budgets at watershed scales. *Water Resour. Res.* **2008**, *44*. [[CrossRef](#)]
25. Kramer, N.; Wohl, E. Rules of the road: A qualitative and quantitative synthesis of large wood transport through drainage networks. *Geomorphology* **2017**, *279*, 74–97. [[CrossRef](#)]
26. Ruiz-Villanueva, V.; PIEGAY, H.; Stoffel, M.; Gaertner, V.; Perret, F. Analysis of Wood Density to Improve Understanding of Wood Buoyancy in Rivers. In *Engineering Geology for Society and Territory-Volume 3*; Lollino, G., Arattano, M., Rinaldi, M., Giustolisi, O., Marechal, J.C., Grant, G.E., Eds.; Springer International Publishing: Cham, Switzerland, 2015; pp. 163–166.

27. Ruiz-Villanueva, V.; Piégay, H.; Gurnell, A.A.; Marston, R.A.; Stoffel, M. Recent advances quantifying the large wood dynamics in river basins: New methods and remaining challenges. *Rev. Geophys.* **2016**, *54*, 611–652. [[CrossRef](#)]
28. Ruiz-Villanueva, V.; Wyżga, B.; Hajdukiewicz, H.; Stoffel, M. Exploring large wood retention and deposition in contrasting river morphologies linking numerical modelling and field observations. *Earth Surf. Process. Landf.* **2016**, *41*, 446–459. [[CrossRef](#)]
29. Gurnell, A.M.; Petts, G.E.; Hannah, D.M.; Smith, B.P.G.; Edwards, P.J.; Kollmann, J.; Ward, J.V.; Tockner, K. Wood storage within the active zone of a large European gravel-bed river. *Geomorphology* **2000**, *34*, 55–72. [[CrossRef](#)]
30. Gurnell, A.M.; Petts, G.E.; Harris, N.; Ward, J.V.; Tockner, K.; Edwards, P.J.; Kollmann, J. Large wood retention in river channels: The case of the Fiume Tagliamento, Italy. *Earth Surf. Process. Landf.* **2000**, *25*, 255–275. [[CrossRef](#)]
31. Wohl, E.; Cenderelli, D.A.; Dwire, K.A.; Ryan-Burkett, S.E.; Young, M.K.; Fausch, K.D. Large in-stream wood studies: A call for common metrics. *Earth Surf. Process. Landf.* **2010**, *35*, 618–625. [[CrossRef](#)]
32. Seo, J.I.; Nakamura, F.; Chun, K.W.; Kim, S.W.; Grant, G.E. Precipitation patterns control the distribution and export of large wood at the catchment scale. *Hydrol. Process.* **2015**, *29*, 5044–5057. [[CrossRef](#)]
33. MacVicar, B.J.; Piégay, H.; Henderson, A.; Comiti, F.; Oberlin, C.; Pecorari, E. Quantifying the temporal dynamics of wood in large rivers: Field trials of wood surveying, a-ting, tracking, and monitoring techniques. *Earth Surf. Process. Landf.* **2009**, *34*, 2031–2046. [[CrossRef](#)]
34. Kramer, N.; Wohl, E. Estimating fluvial wood discharge using time-lapse photography with varying sampling intervals. *Earth Surf. Process. Landf.* **2014**, *39*, 844–852. [[CrossRef](#)]
35. Ravazzolo, D.; Mao, L.; Picco, L.; Sitzia, T.; Lenzi, M.A. Geomorphic effects of wood quantity and characteristics in three Italian gravel-bed rivers. *Geomorphology* **2015**, *246*, 79–89. [[CrossRef](#)]
36. Schenk, E.R.; Moulin, B.; Hupp, C.R.; Richter, J.M. Large wood budget and transport dynamics on a large river using radio telemetry. *Earth Surf. Process. Landf.* **2014**, *39*, 487–498. [[CrossRef](#)]
37. Bertoldi, W.; Ashmore, P.; Tubino, M. A method for estimating the mean bed load flux in braided rivers. *Geomorphology* **2009**, *103*, 330–340. [[CrossRef](#)]
38. Bertoldi, W.; Gurnell, A.A.; Welber, M. Wood recruitment and retention: The fate of eroded trees on a braided river explored using a combination of field and remotely-sensed data sources. *Geomorphology* **2013**, *180*, 146–155. [[CrossRef](#)]
39. Brown, C.G.; Sarabandi, K.; Pierce, L.E. Model-Based Estimation of Forest Canopy Height in Red and Austrian Pine Stands Using Shuttle Radar Topography Mission and Ancillary Data: A Proof-of-Concept Study. *IEEE Trans. Geosci. Remote Sens.* **2010**, *48*, 1105–1118. [[CrossRef](#)]
40. Henshaw, A.J.; Bertoldi, W.; Harvey, G.L.; Gurnell, A.M.; Welber, M. Large Wood Dynamics Along the Tagliamento River, Italy: Insights from Field and Remote Sensing Investigations. In *Engineering Geology for Society and Territory-Volume 3*; Lollino, G., Arattano, M., Rinaldi, M., Giustolisi, O., Marechal, J.C., Grant, G.E., Eds.; Springer International Publishing: Cham, Switzerland, 2015; pp. 151–154.
41. Ravazzolo, D.; Mao, L.; Picco, L.; Lenzi, M.A. Tracking log displacement during floods in the Tagliamento River using RFID and GPS tracker devices. *Geomorphology* **2015**, *228*, 226–233. [[CrossRef](#)]
42. MacVicar, B.; Piégay, H. Implementation and validation of video monitoring for wood budgeting in a wandering piedmont river, the Ain River (France). *Earth Surf. Process. Landf.* **2012**, *37*, 1272–1289. [[CrossRef](#)]
43. Benacchio, V.; Piégay, H.; Buffin-Bélanger, T.; Vaudor, L. A new methodology for monitoring wood fluxes in rivers using a ground camera: Potential and limits. *Geomorphology* **2017**, *279*, 44–58. [[CrossRef](#)]
44. Wyżga, B.; Mikuś, P.; Zawiejska, J.; Ruiz-Villanueva, V.; Kaczka, R.J.; Czech, W. Log transport and deposition in incised, channelized, and multithread reaches of a wide mountain river: Tracking experiment during a 20-year flood. *Geomorphology* **2017**, *279*, 98–111. [[CrossRef](#)]
45. Comiti, F.; Lucía, A.; Rickenmann, D. Large wood recruitment and transport during large floods: A review. *Geomorphology* **2016**, *269*, 23–39. [[CrossRef](#)]
46. Mazzorana, B.; Zischg, A.; Largiader, A.; Hübl, J. Hazard index maps for woody material recruitment and transport in alpine catchments. *Nat. Hazards Earth Syst. Sci.* **2009**, *9*, 197–209. [[CrossRef](#)]
47. Wohl, E. Threshold-induced complex behavior of wood in mountain streams. *Geology* **2011**, *39*, 587–590. [[CrossRef](#)]

48. Staffler, H.; Pollinger, R.; Zischg, A.; Mani, P. Spatial variability and potential impacts of climate change on flood and debris flow hazard zone mapping and implications for risk management. *Nat. Hazards Earth Syst. Sci.* **2008**, *8*, 539–558. [[CrossRef](#)]
49. Ruiz-Villanueva, V.; Wyzga, B.; Mikuś, P.; Hajdukiewicz, H.; Stoffel, M. The role of flood hydrograph in the remobilization of large wood in a wide mountain river. *J. Hydrol.* **2016**, *541*, 330–343. [[CrossRef](#)]
50. Ruiz-Villanueva, V.; Díez-Herrero, A.; Ballesteros, J.A.; Bodoque, J.M. Potential large woody debris recruitment due to landslides, bank erosion and floods in mountain basins: A quantitative estimation approach. *River Res. Appl.* **2014**, *30*, 81–97. [[CrossRef](#)]
51. Ruiz-Villanueva, V.; Wyzga, B.; Zawiejska, J.; Hajdukiewicz, M.; Stoffel, M. Factors controlling large-wood transport in a mountain river. *Geomorphology* **2016**, *272*, 21–31. [[CrossRef](#)]
52. Lucía, A.; Comiti, F.; Borga, M.; Cavalli, M.; Marchi, L. Dynamics of large wood during a flash flood in two mountain catchments. *Nat. Hazards Earth Syst. Sci.* **2015**, *15*, 1741–1755. [[CrossRef](#)]
53. Rigon, E.; Comiti, F.; Lenzi, M.A. Large wood storage in streams of the Eastern Italian Alps and the relevance of hillslope processes. *Water Resour. Res.* **2012**, *48*. [[CrossRef](#)]
54. Abbe, T.B.; Montgomery, D.R. Patterns and processes of wood debris accumulation in the Queets river basin, Washington. *Geomorphology* **2003**, *51*, 81–107. [[CrossRef](#)]
55. Amicarella, A.; Albano, R.; Mirauda, D.; Agate, G.; Sole, A.; Guandalini, R. A Smoothed Particle Hydrodynamics model for 3D solid body transport in free surface flows. *Comput. Fluids* **2015**, *116*, 205–228. [[CrossRef](#)]
56. Albano, R.; Sole, A.; Mirauda, D.; Adamowski, J. Modelling large floating bodies in urban area flash-floods via a Smoothed Particle Hydrodynamics model. *J. Hydrol.* **2016**, *541*, 344–358. [[CrossRef](#)]
57. Bragg, D.C. Simulating catastrophic and individualistic large woody debris recruitment for a small riparian system. *Ecology* **2000**, *81*, 1383–1394. [[CrossRef](#)]
58. Bocchiola, D.; Catalano, F.; Menduni, G.; Passoni, G. An analytical–numerical approach to the hydraulics of floating debris in river channels. *J. Hydrol.* **2002**, *269*, 65–78. [[CrossRef](#)]
59. Mazzorana, B.; Hübl, J.; Zischg, A.; Largiader, A. Modelling woody material transport and deposition in alpine rivers. *Nat. Hazards* **2011**, *56*, 425–449. [[CrossRef](#)]
60. Ruiz-Villanueva, V.; Bladé, E.; Sánchez-Juny, M.; Martí-Cardona, B.; Díez-Herrero, A.; Bodoque, J.M. Two-dimensional numerical modeling of wood transport. *J. Hydroinformatics* **2014**, *16*, 1077–1096. [[CrossRef](#)]
61. Cea, L.; Bladé, E. A simple and efficient unstructured finite volume scheme for solving the shallow water equations in overland flow applications. *Water Resour. Res.* **2015**, *51*, 5464–5486. [[CrossRef](#)]
62. Bermúdez, M.; Zischg, A.P. Sensitivity of flood loss estimates to building representation and flow depth attribution methods in micro-scale flood modelling. *Nat. Hazards* **2018**, *92*, 1633–1648. [[CrossRef](#)]
63. Braudrick, C.A.; Grant, G.E. When do logs move in rivers? *Water Resour. Res.* **2000**, *36*, 571–583. [[CrossRef](#)]
64. Braudrick, C.A.; Grant, G.E. Transport and deposition of large woody debris in streams: A flume experiment. *Geomorphology* **2001**, *41*, 263–283. [[CrossRef](#)]
65. Braudrick, C.A.; Grant, G.E.; Ishikawa, Y.; Ikeda, H. Dynamics of Wood Transport in Streams: A Flume Experiment. *Earth Surf. Process. Landf.* **1997**, *22*, 669–683. [[CrossRef](#)]
66. Atha, J.B. Identification of fluvial wood using Google Earth. *River Res. Appl.* **2014**, *30*, 857–864. [[CrossRef](#)]
67. Næsset, E. Determination of mean tree height of forest stands using airborne laser scanner data. *ISPRS J. Photogramm. Remote Sens.* **1997**, *52*, 49–56. [[CrossRef](#)]
68. Lim, K.; Treitz, P.; Wulder, M.; St-Onge, B.; Flood, M. LiDAR remote sensing of forest structure. *Prog. Phys. Geogr.* **2003**, *27*, 88–106. [[CrossRef](#)]
69. Hollaus, M.; Dorigo, W.; Wagner, W.; Schadauer, K.; Höfle, B.; Maier, B. Operational wide-area stem volume estimation based on airborne laser scanning and national forest inventory data. *Int. J. Remote Sens.* **2009**, *30*, 5159–5175. [[CrossRef](#)]
70. Forzieri, G.; Guarnieri, L.; Vivoni, E.R.; Castelli, F.; Preti, F. Multiple attribute decision making for individual tree detection using high-resolution laser scanning. *For. Ecol. Manag.* **2009**, *258*, 2501–2510. [[CrossRef](#)]
71. Kasprak, A.; Magilligan, F.J.; Nislow, K.H.; Snyder, N.P. A LiDAR-derived evaluation of watershed-scale large woody debris sources and recruitment. Coastal Maine, USA. *River Res. Appl.* **2012**, *28*, 1462–1476. [[CrossRef](#)]
72. Kwak, D.-A.; Cui, G.; Lee, W.-K.; Cho, H.-K.; Jeon, S.W.; Lee, S.-H. Estimating plot volume using lidar height and intensity distributional parameters. *Int. J. Remote Sens.* **2014**, *35*, 4601–4629. [[CrossRef](#)]

73. Mücke, W.; Deák, B.; Schroiff, A.; Hollaus, M.; Pfeifer, N. Detection of fallen trees in forested areas using small footprint airborne laser scanning data. *Can. J. Remote Sens.* **2014**, *39*, S32–S40. [[CrossRef](#)]
74. Atha, J.B.; Dietrich, J.T. Detecting Fluvial Wood in Forested Watersheds using LiDAR Data: A Methodological Assessment. *River Res. Appl.* **2016**, *32*, 1587–1596. [[CrossRef](#)]
75. Yao, W.; Krzystek, P.; Heurich, M. Tree species classification and estimation of stem volume and DBH based on single tree extraction by exploiting airborne full-waveform LiDAR data. *Remote Sens. Environ.* **2012**, *123*, 368–380. [[CrossRef](#)]
76. KAWA Amt für Wald des Kantons Bern. *LiDAR Bern-Airborne Laserscanning. Gesamtbericht Befliegung –Befliegung Kanton Bern 2011–2014*; Kanton Bern: Bern, Switzerland, 2015.
77. Koch, B.; Heyder, U.; Weinacker, H. Detection of individual tree crowns in airborne lidar data. *Photogramm. Eng. Remote Sens.* **2006**, *72*, 357–363. [[CrossRef](#)]
78. Brändli, U.B. *Schweizerisches Landesforstinventar. Ergebnisse der dritten Erhebung 2004–2006*; Eidgenössische Forschungsanstalt für Wald, Schnee und Landschaft WSL: Birmensdorf, Switzerland, 2010.
79. Schweizerisches Landesforstinventar LFI. *Daten der Erhebung 2009/13 (LFI4b)*; Swiss Federal Research Institute (WSL): Birmensdorf, Switzerland, 2016.
80. KAWA Amt für Wald des Kantons Bern. *Erläuterungen zu den LiDAR Bestandesinformationen Wald BE. Technischer Bericht*; Kanton Bern: Bern, Switzerland, 2014.
81. Denzin, A. Schätzung der Masse stehender Waldbäume. *Forstarchiv* **1929**, *5*, 382–384.
82. Zischg, A.; Felder, G.; Weingartner, R.; Gómez-Navarro, J.J.; Röthlisberger, V.; Bernet, D.; Rössler, O.; Raible, C.; Keiler, M.; Martius, O. M-AARE-Coupling atmospheric, hydrological, hydrodynamic and damage models in the Aare river basin, Switzerland. In Proceedings of the 13th Congress INTERPRAEVENT 2016, Lucerne, Switzerland, 30 May–2 June 2016; pp. 444–451.
83. Zischg, A.P.; Mosimann, M.; Bernet, D.B.; Röthlisberger, V. Validation of 2D flood models with insurance claims. *J. Hydrol.* **2018**, *557*, 350–361. [[CrossRef](#)]
84. Zischg, A. River corrections and long-term changes in flood risk in the Aare valley, Switzerland. *E3S Web Conf.* **2016**, *7*, 11010. [[CrossRef](#)]
85. Felder, G.; Zischg, A.; Weingartner, R. The effect of coupling hydrologic and hydrodynamic models on probable maximum flood estimation. *J. Hydrol.* **2017**, *550*, 157–165. [[CrossRef](#)]
86. Felder, G.; Gómez-Navarro, J.J.; Zischg, A.P.; Raible, C.C.; Röthlisberger, V.; Bozhinova, D.; Martius, O.; Weingartner, R. From global circulation to local flood loss: Coupling models across the scales. *Sci. Total Environ.* **2018**, *635*, 1225–1239. [[CrossRef](#)] [[PubMed](#)]
87. Zischg, A.P.; Felder, G.; Mosimann, M.; Röthlisberger, V.; Weingartner, R. Extending coupled hydrological-hydraulic model chains with a surrogate model for the estimation of flood losses. *Environ. Model. Softw.* **2018**, *108*, 174–185. [[CrossRef](#)]
88. R Development Core Team. *R: A Language and Environment for Statistical Computing*; R Foundation for Statistical Computing: Vienna, Austria, 2008.
89. Haga, H.; Kumagai, T.O.; Otsuki, K.; Ogawa, S. Transport and retention of coarse woody debris in mountain streams: An in situ field experiment of log transport and a field survey of coarse woody debris distribution. *Water Resour. Res.* **2002**, *38*. [[CrossRef](#)]
90. Diehl, T.H. *Potential Drift Accumulation at Bridges*; Publication No. FHWA-RD-97-028; U.S. Department of Transportation, Federal Highway Administration Research and Development, Turner-Fairbank Highway Research Center: McLean, VA, USA, 1997.
91. Lange, D.; Bezzola, G.R. *Schwemmholz: Probleme und Lösungsansätze*; Versuchsanst. für Wasserbau, Hydrologie und Glaziologie (VAW-ETHZ): Zürich, Switzerland, 2006.
92. Bezzola, G.R.; Gantenbein, S.; Hollenstein, R.; Minor, H.E. Verklausung von Brückenquerschnitten. In Proceedings of the Internationales Symposium Moderne Methoden und Konzepte im Wasserbau, Zurich, Switzerland, 7–9 October 2002; VAW, ETH-Zentrum: Zurich, Switzerland, 2002.
93. Schmocker, L.; Hager, W.H. Probability of Drift Blockage at Bridge Decks. *J. Hydraul. Eng.* **2011**, *137*, 470–479. [[CrossRef](#)]
94. River Discharge Measurements in Switzerland. 2018. Available online: <https://www.hydrodaten.admin.ch/> (accessed on 16 August 2018).

95. Waldner, P.; Köchli, D.; Usbeck, T.; Schmocker, L.; Sutter, F.; Rickli, C.; Rickenmann, D.; Lange, D.; Hilker, N.; Wirsch, A.; et al. *Schwemmholz des Hochwassers 2005—Schlussbericht des WSL-Teilprojekts Schwemmholz der Ereignisanalyse BAFU/WSL des Hochwassers 2005*; Eidgenössische Forschungsanstalt für Wald, Schnee und Landschaft WSL: Birmensdorf, Switzerland, 2005.
96. Bezzola, G.R.; Hegg, C. *Ereignisanalyse Hochwasser 2005. Teil 1—Prozesse, Schäden und erste Einordnung*; Bundesamt für Umwelt BAFU, Eidgenössische Forschungsanstalt WSL: Bern, Switzerland, 2007.
97. Zischg, A.P.; Felder, G.; Weingartner, R.; Quinn, N.; Coxon, G.; Neal, J.; Freer, J.; Bates, P. Effects of variability in probable maximum precipitation patterns on flood losses. *Hydrol. Earth Syst. Sci.* **2018**, *22*, 2759–2773. [[CrossRef](#)]
98. Hunziker, G. *Schwemmholz Zulg. Untersuchungen zum Schwemmholzaufkommen in der Zulg und deren Seitenbächen*; Kanton Bern: Bern, Switzerland, 2016.
99. Bocchiola, D.; Rulli, M.C.; Rosso, R. A flume experiment on the formation of wood jams in rivers. *Water Resour. Res.* **2008**, *44*. [[CrossRef](#)]
100. Davidson, S.L.; MacKenzie, L.G.; Eaton, B.C. Large wood transport and jam formation in a series of flume experiments. *Water Resour. Res.* **2015**, *51*, 10065–10077. [[CrossRef](#)]
101. Gschnitzer, T.; Gems, B.; Mazzorana, B.; Aufleger, M. Towards a robust assessment of bridge clogging processes in flood risk management. *Geomorphology* **2017**, *279*, 128–140. [[CrossRef](#)]
102. Gschnitzer, T.; Gems, B.; Aufleger, M.; Mazzorana, B.; Comiti, F. On the Evaluation and Modelling of Wood Clogging Processes in Flood Related Hazards Estimation. In *Engineering Geology for Society and Territory—Volume 3*; Lollino, G., Arattano, M., Rinaldi, M., Giustolisi, O., Marechal, J.C., Grant, G.E., Eds.; Springer International Publishing: Cham, Switzerland, 2015; pp. 139–142.
103. Iroumé, A.; Mao, L.; Andreoli, A.; Ulloa, H.; Ardiles, M.P. Large wood mobility processes in low-order Chilean river channels. *Geomorphology* **2014**, *228*, 681–693. [[CrossRef](#)]
104. Ruiz-Villanueva, V.; Díez-Herrero, A.; Bodoque, J.M.; Bladé, E. Large wood in rivers and its influence on flood hazard. *Cuadernos de Investigación Geográfica* **2014**, *40*, 229–246. [[CrossRef](#)]
105. Ruiz Villanueva, V.; Bladé Castellet, E.; Díez-Herrero, A.; Bodoque, J.M.; Sánchez-Juny, M. Two-dimensional modelling of large wood transport during flash floods. *Earth Surf. Process. Landf.* **2014**, *39*, 438–449. [[CrossRef](#)]
106. Iacob, O.; Rowan, J.S.; Brown, I.; Ellis, C. Evaluating wider benefits of natural flood management strategies: An ecosystem-based adaptation perspective. *Hydrol. Res.* **2014**, *45*, 774. [[CrossRef](#)]



© 2018 by the authors. Licensee MDPI, Basel, Switzerland. This article is an open access article distributed under the terms and conditions of the Creative Commons Attribution (CC BY) license (<http://creativecommons.org/licenses/by/4.0/>).

Paper 26: Staffler, H., Pollinger, R., Zischg, A., Mani, P., 2008. Spatial variability and potential impacts of climate change on flood and debris flow hazard zone mapping and implications for risk management. *Natural Hazards and Earth System Sciences* 8, 539–558. [10.5194/nhess-8-539-2008](https://doi.org/10.5194/nhess-8-539-2008).

Spatial variability and potential impacts of climate change on flood and debris flow hazard zone mapping and implications for risk management

H. Staffler¹, R. Pollinger², A. Zischg^{3,4}, and P. Mani⁵

¹Department of Civil Protection, Autonomous Province of Bolzano South Tyrol, Bolzano, Italy

²Department of Hydraulic Engineering, Autonomous Province of Bolzano South Tyrol, Bolzano, Italy

³Abenis AG, Chur, Switzerland

⁴Abenis Alpinexpert srl, Bolzano, Italy

⁵geo7 AG, Berne, Switzerland

Received: 18 February 2008 – Revised: 7 May 2008 – Accepted: 13 May 2008 – Published: 12 June 2008

Abstract. The main goals of this study were to identify the alpine torrent catchments that are sensitive to climatic changes and to assess the robustness of the methods for the elaboration of flood and debris flow hazard zone maps to specific effects of climate changes. In this study, a procedure for the identification and localization of torrent catchments in which the climate scenarios will modify the hazard situation was developed. In two case studies, the impacts of a potential increase of precipitation intensities to the delimited hazard zones were studied.

The identification and localization of the torrent and river catchments, where unfavourable changes in the hazard situation occur, could eliminate speculative and unnecessary measures against the impacts of climate changes like a general enlargement of hazard zones or a general over dimensioning of protection structures for the whole territory. The results showed a high spatial variability of the sensitivity of catchments to climate changes. In sensitive catchments, the sediment management in alpine torrents will meet future challenges due to a higher rate for sediment removal from retention basins. The case studies showed a remarkable increase of the areas affected by floods and debris flow when considering possible future precipitation intensities in hazard mapping. But, the calculated increase in extent of future hazard zones lay within the uncertainty of the methods used today for the delimitation of the hazard zones. Thus, the consideration of the uncertainties laying in the methods for the elab-

oration of hazard zone maps in the torrent and river catchments sensitive to climate changes would provide a useful instrument for the consideration of potential future climate conditions. The study demonstrated that weak points in protection structures in future will become more important in risk management activities.

1 Introduction

The assessment of dangerous processes and the delimitation of hazard zones is a fundamental task in risk analysis and risk management. In general, the assessment and evaluation of geomorphologic processes and hazards could be made using the reconstruction of historical processes (backward directed indication) or using simulation models (forward directed indication, Kienholz et al., 2004). In practice, both approaches mostly are combined. Usually, the hazard assessment is made for the actual state of the studied system (e.g. torrent catchment, landslide area, etc.). Natural hazards are described by the process intensity of a given design event with a certain reoccurrence interval (e.g. 30, 100, 300 years). The actual system status is described by the statistical system behaviour of the last decades.

Due to impacts of climate changes, slight changes in the future system could be assumed. Once changes in the environmental system occurred, the future geomorphologic processes must not occur exactly in the same way as in the past. E.g. shifts in altitude levels or system constellations never observed before could be expected. Thus, backward directed indication of natural hazards and the interpretation



Correspondence to: A. Zischg
(a.zischg@abenis.ch)

of the past geomorphologic processes also named as “silent witnesses” and statistical analyses of time series for assessing actual processes will increasingly be subjected to uncertainties. Past observation data (e.g. precipitation data series) could probably not represent the future system status. As a consequence, the statistically described natural hazard situation and the reoccurrence intervals of design flood discharges or design parameters for the planning of hydraulic protection structures could only partially be valid under future climate conditions (e.g. Caspary 1996, 2004, Caspary and Bardossy 1995, Bardossy and Pakosch 2005, Frei et al. 2006, Katzenberger 2004, Hennegriff et al. 2006).

But, most of the decisions made in risk prevention have to be made for a period of almost 30–50 years. E.g. hazard zone maps do influence land use planning over a long period. In Austria or in Switzerland, some of the hazard zone maps made in the 1980ies are still now valid documents for land use planning. Technical construction measures such as river dams or flood retention basins have an average lifespan of almost 50 years. In practice, today’s decisions for long-term risk management activities such as the planning of technical protection measures do not consider the future system status but are reactions after damaging events.

Since a few years, the Autonomous Province of Bolzano – South Tyrol, Italy is beginning to elaborate hazard zone maps. Because of the high relevance of the elaborated hazard zone maps for land use planning and the planning of risk reduction measures, the institutions responsible for the elaboration of these decision bases are interested to know, if these documents will be valid also under future climate conditions. Thus, this study aims not at making a contribution to the quantitative assessment of the impacts of climate change to natural hazards. But, the main goal of this study was to assess the robustness or sensitivity of the commonly used procedures for the delimitation of flood and debris flow hazard zone maps to climatic changes. The question should be answered, if, where and how the practices for hazard mapping and risk management must be adapted to potential impacts of climatic changes.

The focus of this case study lied not on the exact representation of the environmental systems by means of detailed process and climate models but on the resulting differences of the hazard assessment representing different climate conditions. Thus, only the potential impacts of climate change to specific input parameters should be studied.

In this study, a procedure

- for identifying the alpine torrent catchments that are sensitive to climatic changes and
- for assessing the robustness of the methods for the elaboration of flood and debris flow hazard zone maps to specific effects of climate changes

should be developed.

The targeted time frame for the assessment of the potential effects of climate changes to the flood risk situation in the Autonomous Province of Bolzano - South Tyrol is the second half of the 21st century (2050–2100). The results of the procedure should lead to formulate recommendations for the adaptation of risk management practices to specific effects of climate changes.

Natural hazards are mostly defined as natural conditions or phenomena which cause undesired consequences for persons, settlements, infrastructures and goods. In some definitions, natural hazards are described as natural geomorphologic processes that are considered as hazards only in intersection with human activities. These processes are characterized as the probability of occurrence of a potentially damaging phenomenon (United Nations, 2004). The physical process itself is characterized by the parameters intensity/magnitude and occurrence probability. The risk resulting from natural hazards is defined as a quantifying function of the probability of occurrence of a dangerous process and the related degree of damage. The latter is specified by the damage potential and the vulnerability of the endangered object (Fuchs et al., 2007).

$$R_{i,j} = p_{Si} \cdot A_{Oj} \cdot p_{Oj,Si} \cdot v_{Oj,Si} \quad (1)$$

According to the definition of United Nations (2004), the specifications for the probability of the defined scenario (p_{Si}), the monetary value of the object affected by this scenario (A_{Oj}), the probability of exposure of object j to scenario i ($p_{Oj,Si}$), and the vulnerability of object j in dependence on scenario i ($v_{Oj,Si}$) are required for the quantification of risk ($R_{i,j}$).

The methods for the description and characterization of the natural hazards in the Alps are based on the intensity and frequency of events. Thus, the concept of the legally binding hazard maps is based on the return period and the intensity of processes. Usually, natural hazards are described in hazard maps by threshold classes of the process intensity for different design events with a given reoccurrence interval (e.g. 30, 100, 300 years, resp. 200 years for rivers with engineering measures). The relative consequences for the land use and the corresponding legally binding restrictions are also based on this concept. Risk analyses are made on the basis of this concept of hazard maps. Furthermore, the planning and design of permanent countermeasures are based on specific design events with a legally defined return period and the related process intensity.

The Autonomous Province Bolzano – South Tyrol adapted the methods for the elaboration of hazard maps of Heinemann et al. (1998) and combined this approach with the Italian national framework legislative of the laws no. 267 of 3 August 1998, no. 365 of 11 December 2000 and the D.P.C.M. of 29 September 1998 (Gius, 2005). The guidelines for the delimitation of hazard zone maps are described in Gius (2005), Stötter and Zischg (2007) and Autonome Provinz Bozen – Südtirol (2006).

Because of these practices in risk management, the deduction of the most critical factors for hazard assessment under changing environmental conditions is relatively obvious: At least for natural hazards related to precipitation, the most relevant changes in the environmental parameters due to climatic changes are to be expected in the intensity/frequency relation of precipitation events (rainfall, snowfall). Indirect effects are shifts in altitude levels due to rising temperatures, e.g. rising of the altitude of the limit between snowfall and rainfall or rising of the lower boundary of permafrost zones. Seasonal and regional changes in precipitation patterns are to be expected as follows: In Autumn, extreme values for daily precipitations are expected to increase by 10% in the Northern Alps and by 20% in the Southern Alps. In winter and spring, an increase between 0% and 20% is expected for both regions (KOHS, 2007). Brunetti et al. (2001) observed a trend for an increase in frequency of extreme precipitation events in Northeastern Italy. Under the most unfavourable conditions, a 100-year event of today could in the future become a 20-year event (Frei et al., 2006). Similar trends were calculated for the rivers Donau, Enz, Kocher and Alp in South West Germany (Casparly, 2004). Casparly (2004) underlines that the discharge regimes of these rivers show statistical instationarities in their time series because of the relative accumulation of extreme events since the 1990ies. E.g. a discharge event with a reoccurrence interval of 100 years in the reference period 1932–1976 of the river Enz at the gauge of Pforzheim equals a discharge event with a reoccurrence interval of 30 years in the reference period 1932–2002. Remarkably increases in runoff and discharge volumes were also computed for the Lavanttal region (Austria) when considering possible effects of climate changes (Regional Office of Carinthia, Department of Water Economy 2008).

An indirect effect of the increase of mean temperature is the rising altitude level for the limit between rainfall and snowfall. In areas of the Northern Alps below 1500 m a.s.l., an increase of flood peaks is expected in winter due to higher soil water contents, the rising of the rainfall/snowfall limit level and due to an increased liquid precipitation (KOHS, 2007). In the pre-Alpine regions, the increase of precipitation in winter and the rising of the snowfall limit will have consequences for the activities of landslides in winter and spring. The increase in saturation leads to an increase in landslide activity and to an increase in sediment load in alpine torrent catchments (Schädler et al., 2007). Due to the rising altitude level of glacier retreat and permafrost degradation, the sediment transport in the areas between approximately 2300 and 2800 m a.s.l. and with relevant bed load source areas in this altitude level is expected to increase (KOHS, 2007). Since in these areas more precipitation will fall in liquid form, this trend is expected to be remarkably.

Discussions with experts for hazard zone mapping in different workshops resulted, that the following climatological parameters used in the assessment of flood and debris flow hazards are at most sensitive to climate changes

- Intensity of precipitation
- Frequency of precipitation of a certain intensity/magnitude

Other parameters such as the altitude of snowfall limit, the altitude of snowmelt level, the antecedent precipitation, the retreating of glaciers or the degradation of permafrost are considered only in a generalized way in the common procedures for hazard zone mapping. Certain parameters needed for hazard mapping are assumed as worst case scenarios, e.g. the assumption that the altitude of the limit between snowfall and rainfall during extreme precipitation events is higher than the mountain crests and all precipitation contributes to runoff. Thus, in this study only the impacts of a potential increase in the intensities of extreme precipitation events (>50 mm/d) to the delimitation of hazard zones were analyzed. On the basis of a literature review, a possible increase in the precipitation intensity of at maximum of 20% for all design events as indicated by Frei et al. (2006) for the Southern Alps was assumed for this sensitivity analysis. The assumption is consistent with the observed trend in the reduction of the return period between extreme precipitation events in Northeastern Italy (Brunetti et al., 2001). Due to the main focus on the robustness of the procedures for hazard zone mapping, in this study no downscaling procedures from global and regional climate models to the local conditions were followed. It was assumed that the effects of an increase in precipitation intensity of less than 20% are laying within the uncertainties of the procedures for the delimitation of hazard zones. Therefore, it was expected that an increase of less than 20% will not show remarkably effects to the increase in the extent of the hazard zones.

2 Method

The study was made in three main steps. Firstly, the sensitivity of the alpine torrent catchments to climate changes was analysed qualitatively on the regional scale. Secondly, the possible effects of climate changes to the delimitation of flood hazard zones were analysed in a case study. In another case study, the possible effects of climate changes to the delimitation of debris flow hazard zones were analysed. Finally, conclusions and recommendations for the adaptation of the risk management practices have been elaborated on the basis of the results of the previous three steps.

2.1 Identification and localisation of alpine torrent and river catchments sensitive to climate changes

In this part of the study, the sensitivity of the alpine torrent catchments to climate changes was analysed on the regional scale. The focus of this study lied on the identification of the torrent catchments in which the future climate scenarios

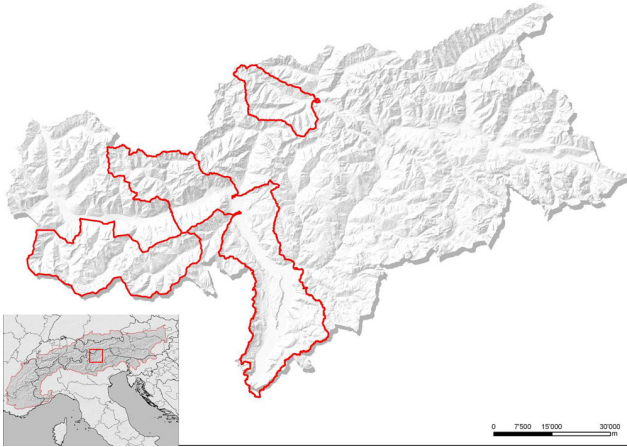


Fig. 1. Study area in the Autonomous Province of Bolzano South Tyrol, Italy.

described above will modify the hazard situation (flood and debris flows).

The first step of the procedure was to match the environmental parameters relevant for hazard assessment on the regional scale with the existing spatial datasets. On the basis of the identified parameters and the existing datasets, an approach for the classification of the torrent catchments of different dimensions and for the qualitative assessment of the sensitivity of the catchments to assumed climatic changes was developed. The catchments were classified into three catchment classes: mountain torrents, torrential rivers and alpine rivers (see Table 1). The results of the study were the delineated catchments classified by the sensitivity to the changes in the selected environmental parameters.

The activities of flood and debris flow processes in alpine torrents are mainly driven by the discharge, the sediment budget and the sediment transport capacity. The sediment transport capacity is influenced either by short precipitation events (thunderstorms) or by longer precipitation events. Because of the steepness of alpine torrent catchments, the hydrological characteristics in the runoff formation are less important. In torrential river catchments both the sediment budget and the hydrological characteristics in the runoff formation are important. In river catchments, the hydrological characteristics in the runoff formation are important. Because of the larger catchment area, the characteristics of the sediment budget are evened.

The sensitivity analysis was made in a pilot area of the Autonomous Province of Bolzano – South Tyrol (Fig. 1). The delimitation of the torrent and river catchments was made on the basis of the classification scheme for public watercourses of the Autonomous Province of Bolzano. The basic assumptions for potential future climate conditions were the following:

- The daily mean temperatures in summer and winter are increasing (Heimann and Sept, 2000; OcCC, 2007)
- The mean sum of precipitation in summer is decreasing or remains constant
- The mean sum of precipitation in winter is increasing (OcCC, 2007)
- The intensity and frequency of short extreme rainfall events in summer and autumn is increasing (Christensen and Christensen, 2003)

It was assumed that the following factors are varying spatially and are relevant for the sensitivity of the torrent catchments to climate changes:

- Percentage of areas located between 1000 and 2000 m a.s.l.: It is expected that the snow cover in these areas will be reduced and the frequency of combined snowmelt/rainfall events will increase (KOHS, 2006). A threshold value of 50% of these areas respective to the total catchment area was chosen. This information layer was extracted from the digital elevation model. The value for this parameter was found by a statistical analysis of the catchments assessed as sensitive to climatic changes by local experts.
- Characteristics of bed load source areas: Bed load source areas could be divided into recent and older deposits. Recent deposits are alimeted by recent weathering and denudation processes. The quantity of mobilizeable sediment storages in torrents eroding recent deposits is depending on the intensity of the sediment delivery processes and the period between extreme discharge events transporting the weathered material downstream (Zimmermann et al. 1997). Older deposits were composed by relict geomorphologic deposition processes (e.g. glacial moraines, holocene alluvial sediments, landslides). The quantity of mobilizeable sediment storages in torrents eroding older deposits is mainly unlimited. If the percentage of areas with older deposits to the total bed load source area exceeds 30% of the total catchment area, the torrent catchments were classified as torrents eroding older deposits, otherwise as torrents eroding recent deposits. The value for this parameter was found by a statistical analysis of the catchments assessed as sensitive to climatic changes by local experts. Landslides do influence the quantity of mobilizeable sediment. An increase in precipitation could increase the activity of landslides, especially in winter and spring (Bader and Kunz 1998). If the percentage of landslide areas with respective to the total bed load source area exceeds 30%, the torrent catchments were classified as torrents mainly influenced by landslide activity. This information layer was extracted from the dataset of the hazard index map for debris

Table 1. Classification of alpine torrent catchments.

Torrent classification	Catchment area	Description
(a) mountain torrents	<20 km ²	torrents, torrential processes mainly driven by discharge and bed load transport processes
(b) torrential rivers	20–100 km ²	torrential rivers, processes mainly driven by hydrology and partially by bed load transport
(c) Alpine rivers	100–1 000 km ²	rivers, processes mainly driven by runoff processes

flows and from the landslide inventory of the Geological Survey of the Autonomous Province of Bolzano (IFFI – Italian National Landslide Inventory).

- Available bed load source areas: The bed load sediment budget of alpine torrents depends on the quantity of bed load source areas available for sediment transport and the sediment transport capacity. The sensitivity of torrent activity against climate changes increases with a higher proportion of bed load source areas respective to the total catchment area. During the elaboration of the hazard index map for debris flow, the available bed load source areas were computed and weighted on the basis of the relevance for torrential processes (geo7 2006, Heinimann et al. 1998). For this analysis, a minimum threshold for the weighted bed load source areas per catchment was used for the identification of sensitive catchments. This information layer was extracted from the dataset of the hazard index map for debris flows.
- Permafrost degradation and glacier retreat areas: Permafrost influences the hydrology and stability of steep scree slopes, since ice-rich permafrost acts as a barrier to groundwater percolation and can imply local saturation within non-frozen debris (Zimmermann and Haeberli, 1992). Permafrost thawing in non-consolidated material leads to an increase of pore water pressure and a loss of cohesion (Harris et al., 2001). The disappearance of ground ice bodies in scree slopes leaves caverns and destabilizes parts of these disintegrated slope areas. With accelerated permafrost thawing, the susceptibility of these slope areas for landslide and debris flows and the triggered volumes is expected to rise (Zimmermann et al., 1997; Rebetz et al., 1997). Catchments were classified as sensitive, if more than 30% of the total catchment area is subjected to permafrost degradation. The value for this parameter was found by a statistical analysis of the catchments assessed as sensitive to climatic changes by local experts. This information layer was created by modelling the permafrost distribution of 1850, 1990 and 2100 (after Stötter, 1994; Zischg, 2007). The difference between the datasets of the permafrost distribution of 1850 and 2100 was classified as permafrost degradation areas. Because of a lack in multitemporal glacier datasets, glacier retreat areas were not considered in this study.

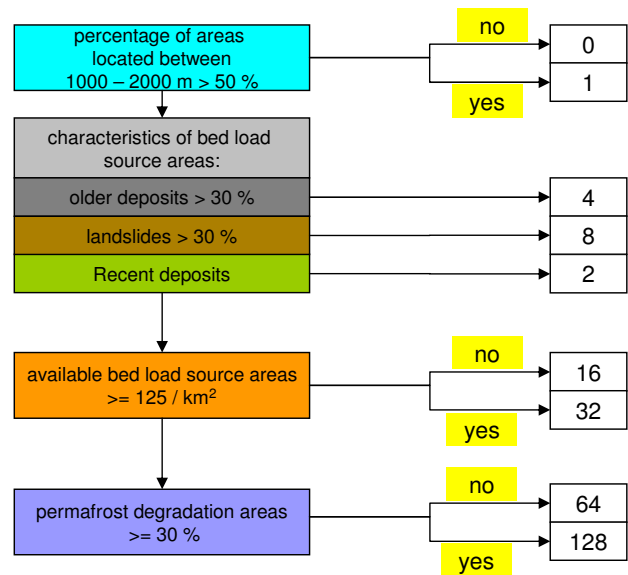


Fig. 2. Decision tree for the identification and localisation of alpine torrent catchments sensitive against climate changes.

- Areas with elevated surface runoff: Areas with reduced water storage capacities increase the surface runoff. The sensitivity of torrential rivers and rivers to climate changes increases with a higher proportion of areas with reduced water storage capacities respective to the total catchments area. This information layer was created by modelling the Topindex after Beven et al. (1995) under consideration of the geological permeability. This index describes the susceptibility of areas for saturated surface runoff.

The delimited torrent, torrential river and river catchment areas were classified by the combination of these factors influencing the sensitivity of mountain torrents and rivers to climate changes. The classification was made by means of a decision tree implemented into a GIS-based procedure (Figs. 2, 3, 4). The results of the classification procedure are different classes of torrent and river catchments reacting in different ways to potential climate changes (Figs. 5, 6, 7). The classification of the catchment types are shown in Tables A1–A3.

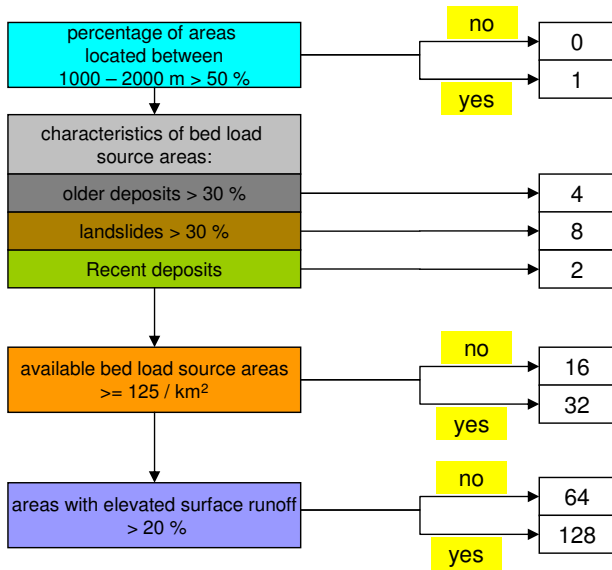


Fig. 3. Decision tree for the identification and localisation of torrential river catchments sensitive against climate changes.

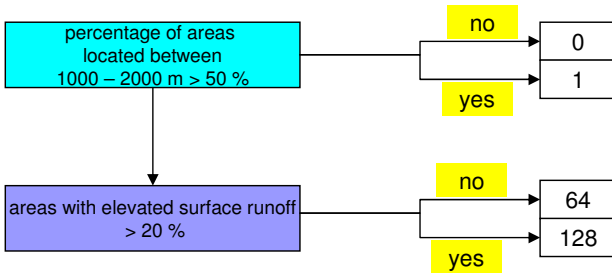


Fig. 4. Decision tree for the identification and localisation of alpine river catchments sensitive against climate changes.

2.2 Potential impacts of climate changes to the delimitation of flood hazard zones, case study Rio Ridanna/Mareiter Bach

In this part of the study, the sensitivity of the common methods and procedures for the delimitation of flood hazard zone maps to climate changes was analysed. The focus of this case study lied not on the exact representation of the environmental systems by means of detailed process and climate models but on testing the robustness of the methods and procedures for hazard mapping to changes of the needed input parameters. On the basis of a literature review, a possible increase of 20% of the precipitation intensity for each design event (recurrence interval 30, 100, 200 years) was assumed for this sensitivity analysis. The hazard induced by bed load transport and overbank sedimentation was not considered.

The Rio Ridanna/Mareiter Bach basin lies in the north of the Autonomous Province of Bolzano – South Tyrol (Fig. 8). The river endangers parts of the Vipiteno/Sterzing Basin and

	catchment type	available bed load source areas	discharge summer	discharge winter	bed load transport capacity summer	bed load transport capacity winter	frequency of small events	frequency of medium events	frequency of extreme events
WB01 (082)									
WB02 (146)									
WB03 (098)									
WB04 (162)									
WB05 (084)									
WB06 (148)									
WB07 (100)									
WB08 (164)									
WB09 (088)									
WB10 (152)									
WB11 (104)									
WB12 (168)									
WB13 (083)									
WB14 (147)									
WB15 (099)									
WB16 (163)									
WB17 (085)									
WB18 (149)									
WB19 (101)									
WB20 (165)									
WB21 (089)									
WB22 (153)									
WB23 (105)									
WB24 (169)									

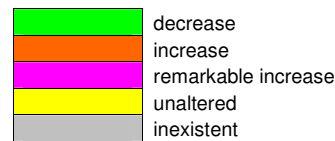


Fig. 5. Synthesis of the considered potential impacts of climate changes to alpine torrent catchments (WB01 to WB24). The identification number of the torrent catchment type resulting from the decision tree is shown in the brackets

the city of Vipiteno/Sterzing and confluences with the Isarco/Eisack River. The catchment area is 210 km². This study area is a representative example for an alpine river with hazard potential for settlements.

For the assessment of the present flood hazard situation of the Rio Ridanna/Mareiter Bach for the Vipiteno/Sterzing basin, this procedure was followed:

- statistical analyses of the precipitation time series of the measurement stations in the study area and calculation of the characteristics of precipitation events relevant for the hazard scenarios with a return period of 30, 100 and 200 years,
- preparation and calibration of the rainfall-runoff model,
- simulation of the inundation processes for each return period,

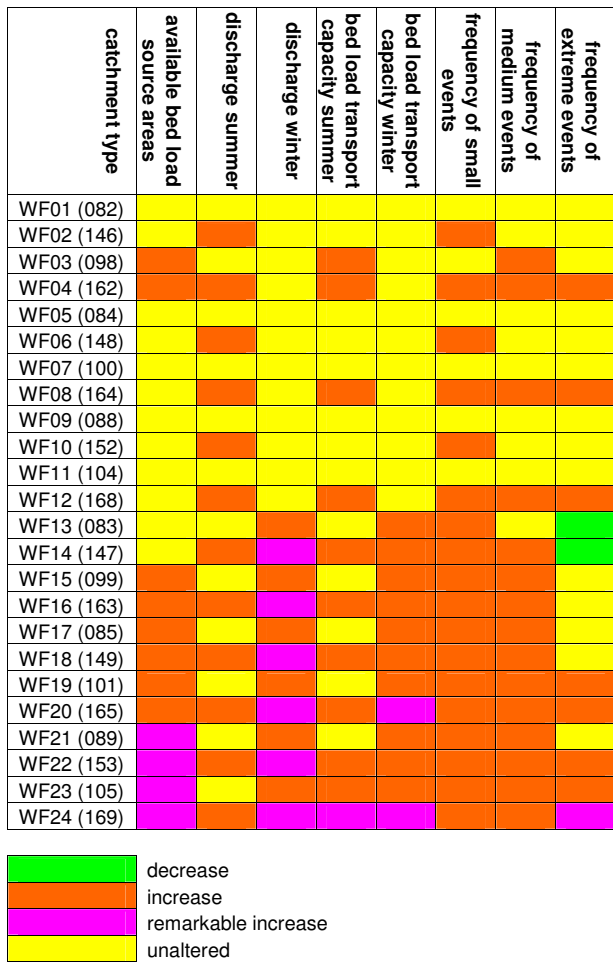


Fig. 6. Synthesis of the considered potential impacts of climate changes to torrential river catchments (WF01 to WF24). The identification number of the torrential river catchment type resulting from the decision tree is shown in the brackets.

- delimitation of the hazard zone map,
- analysis of the exposed buildings.

The results of the procedures described above were the hazard maps describing the hazard situation on the basis of simplified assumptions representing present (scenario 2000) and future (2050–2100) climate conditions (scenario +20%). The main focus laid more on the comparison of the two hazard situations rather than on the single hazard assessment itself.

The statistical analysis of the precipitation time series was based on the measurement stations of Ridanna/Ridnaun (31 measurement years). In the analysis, precipitation events with a duration of 24 h were considered (Scherer and Mazzorana, 2007). The calculated precipitation values of a rainfall event with a duration of 24 hours representing reoccurrence intervals of 30, 100 and 200 years are shown in Table 2. For the representation of the design precipitation events under

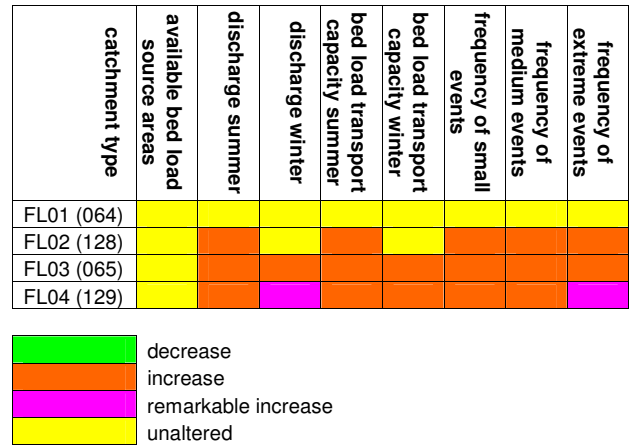


Fig. 7. Synthesis of the considered potential impacts of climate changes to alpine river catchments (FL01 to FL04). The identification number of the river catchment type resulting from the decision tree is shown in the brackets.

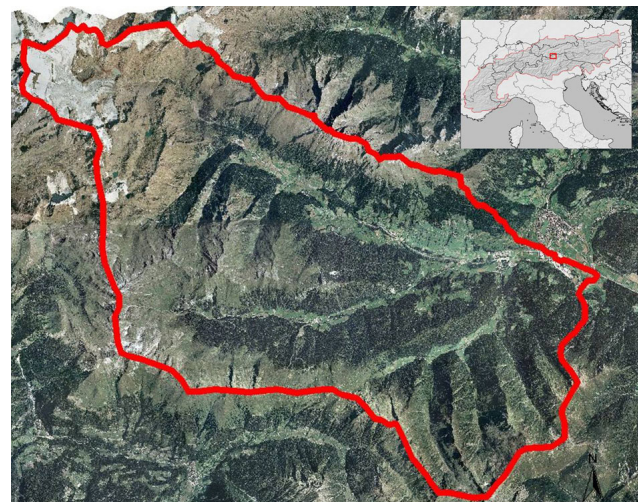
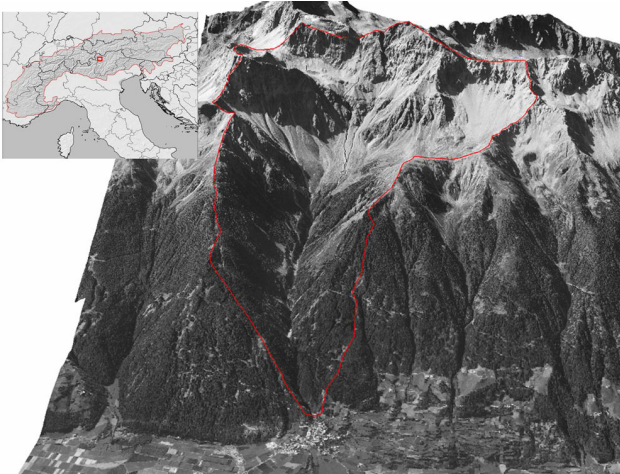


Fig. 8. Localisation and delimitation of the Rio Ridanna/Mareiter Bach catchment.

future climate conditions (scenario +20%) 20% of these calculated values were added (see Table 2). For the discharge prediction, the rainfall-runoff model Hec-HMS and the SCS-approach was used and adapted to the catchment characteristics of the Rio Ridanna/Mareiter Bach. The calibration of the model was made within the Interreg IIIB project “River Basin Agenda” (Scherer and Mazzorana, 2005a; Scherer and Mazzorana, 2005b). The model was calibrated with the precipitation events of 1996 and 1997. For the simulation of the inundation process, the simulation model SOBEK of WL Delft Hydraulics was used. The flood hazard zone map was made by following the guidelines for hazard zone mapping of the Autonomous Province of Bolzano – South Tyrol (Autonome Provinz Bozen – Südtirol, 2006) and Heinimann et

Table 2. Calculated rainfall and runoff values for relevant return periods and different climate conditions (Scherer and Mazzorana, 2007).

return period of a rainfall event, duration 24 h	N _{tot} (precipitation) [mm]		Q _{max} (discharge) at confluence [m ³ /s]	
	scenario 2000	scenario +20%	scenario 2000	scenario +20%
30 years	106.6	127.9	212.5	299.6
100 years	125.7	150.8	272.6	383.9
200 years	136.6	164.0	333.3	431.8

**Fig. 9.** Localisation and delimitation of the Rio Cengles/Tschenglsler Bach catchment.

al. (1998). The resulting hazard maps were overlaid with the buildings in the settlement areas. Thus, the changes in the hazard situation were demonstrated by the changes in the extent of the hazard zones and by the changes in the number of the endangered buildings. The related damages were estimated by multiplying the number of endangered buildings with a mean value of expected losses per building. This value represents a combination of the terms A_{Oj} and $v_{Oj,si}$ in Eq. 1. For residential buildings, a mean value of expected losses of about € 45 000 was used, and for industry buildings a mean value of expected losses of about € 80 000 was used for the estimation of the potential damages regarding flood events.

2.3 Potential impacts of climate changes to the delimitation of debris flow hazard zones, case study Rio Cengles/Tschenglsler Bach

The Rio Cengles/Tschenglsler Bach torrent lies in the western part of the Autonomous Province of Bolzano South Tyrol. The Rio Cengles/Tschenglsler Bach torrent confluent with the river Adige/Etsch. The catchment area is 11 km². This study area is a representative example for systematized alpine torrents eroding older deposits in permafrost degradation ar-

reas (Fig. 9). The hazard potential of these kinds of torrents is mainly driven by the sediment mobilization and bedload transport capacity because of the unlimited sediment source areas. The sediment transport capacity is driven by the runoff and the discharge. The upper catchment area is characterized by the disappearance of a small glacier in the recent years and the erosion of oversteepened scree slopes supposed to permafrost degradation. The Rio Cengles/Tschenglsler Bach is systematized by sediment retention basins and check dams.

For the assessment of the actual situation of debris flow hazards in the Rio Cengles/Tschenglsler Bach catchment, the following procedure was followed (IPP 2007):

- characteristics of precipitation events relevant for the hazard scenarios with a return period of 30, 100 and 300 years,
- preparation and verification of the rainfall-runoff model,
- simulation of the bed load transport in the transit area and in the sediment retention basins,
- simulation of the debris flow processes in the deposition area for each return period,
- delimitation of the hazard zone map,
- analysis of the exposed buildings.

Since no meteorological station is located in the catchment area or in the neighbourhood of 20 km, the calculation of the rainfall characteristics representing the present climate conditions (scenario 2000) was made following the procedures of VAPI (Valutazione delle portate in Italia, Villi and Bacchi 2001). Villi and Bacchi (2001) made a regionalization of the precipitation intensities for given reoccurrence intervals. The results of the procedure were the needed input parameters for the hydrologic and hydraulic simulations representing precipitation events with reoccurrence intervals of 30, 100 and 300 years and a duration of 1 hour (scenario 2000, see Table 5). Because of the steepness of the catchment, intensive rainfall events with a duration of one hour are the most relevant precipitation scenarios. These values fit with the values of the precipitation time series of the meteorological station in Prato/Prad. For the representation of future

climate conditions (scenario +20%), 20% of these precipitation values were added (IPP, 2007; Table 5). For the discharge prediction, the rainfall-runoff model Hec-HMS and the SCS-approach was used and adapted to the catchment characteristics of the Rio Cengles/Tschenglsler Bach. The calibration of the model was made with well documented debris flow events (Gostner, 2002). For the simulation of the bed load transport in the transit area and in the sediment retention basins, the simulation model DAMBRK of the US National Weather Service was used. For the simulation of the debris flow processes in the runout area, the simulation model Flow-2D (O'Brian, 2001) was used. The flood hazard zone map was made following the guidelines for hazard zone mapping of the Autonomous Province of Bolzano – South Tyrol (Autonome Provinz Bozen – Südtirol, 2006) and Heinimann et al. (1998).

3 Results

3.1 Identification and localisation of alpine torrent and river catchments sensitive to climate changes

The main results of the procedure were the classification of the torrent catchments into different reaction typologies and the classification into different sensitivity typologies (Fig. 10). The datasets could be queried under different aspects. Figure 10 show a high spatial variability of the sensitivity of the torrent catchments to specific impacts of climatic changes. This underlines the observations made in the Ecrin massif (Jomelli et al., 2004; Jomelli et al., 2007). The procedure was made also for torrential river and river catchments. The results showed that the runoff of nearly all torrent catchments is expected to increase in summer (Fig. 10a). The runoff in winter is expected to increase only in torrent catchments having a high percentage of their total surface area below 2000 m (Fig. 10b). The bed load transport in summer is expected to increase in high mountain areas and is expected to decrease in catchments at submontane levels (Fig. 10c). In some catchments eroding younger deposits (weathered material), a decrease in extreme events is highlighted (Fig. 10f). This is consistent with the observations of Jomelli et al. (2004), Jomelli et al. (2007) and Stoffel and Beniston (2006). In some catchments eroding older deposits an increase in extreme events is pointed out (Fig. 10f). This seems consistent with the observations of Rebetez et al. (1997). The bed load transport in winter increases in a few mountain torrent catchments and does not change in the most catchments (Fig. 10d). The frequency of small scale debris flow and sediment transport processes is expected to increase in most of the torrent catchments (Fig. 10e).

Table 3. Number of buildings endangered by flood processes of the Rio Ridanna/Mareiter Bach and per hazard zones.

hazard zone	number of exposed buildings			
	scenario 2000		scenario + 20%	
	habitation	production	habitation	production
yellow	12	30	13	6
blue	3	7	9	35
red	0	1	2	2

3.2 Potential impacts of climate changes to the delimitation of flood hazard zones, case study Rio Ridanna/Mareiter Bach

By increasing the rainfall intensities for the design events describing the basic assumptions for the delimitation of the hazard zone maps by 20%, the parameters needed for hazard evaluation changed as shown in Table 2. Figure 11 show the spatial changes of the inundation processes. The modelling results (flow depth and flow velocity) were classified following the guidelines for hazard zone mapping of the Autonomous Province of Bolzano – South Tyrol (Autonome Provinz Bozen – Südtirol, 2006) and Heinimann et al. (1998). Figure 12 shows the impacts of climate changes to the delimitation of the compiled hazard zone maps (synthesis of all design events) by considering flow depth and flow velocity without further on-site investigations.

The study confirmed the results of prior analyses that the discharge capacity of the Rio Ridanna/Mareiter Bach in the Vipiteno/Sterzing basin is lower than the discharge of a design event with a return period of 30 years. Either considering the effects of climate changes to the hazard situation or not, this fact leads to the endangerment of parts of the Vipiteno/Sterzing basin also during relatively frequent events. The historical analyses of flooding events in the Vipiteno/Sterzing basin confirmed this fact (Zischg, 2005).

The analyses of the possible impacts of climate changes showed that the flooded areas of a design event with a return period of 30 years representing the assumed future climate conditions (scenario +20%) have a larger extent than the flooded areas of a design event with a return period of 100 years representing the actual climate conditions (scenario 2000). The hazard zones delimited and classified following the guidelines for hazard zone mappings show remarkable changes if considering the assumed changes in precipitation intensities due to climate changes. The hazard zones representing the assumed future climate conditions show a shift from the yellow zones to the blue zones. In this case study, the extent of the blue zones increased significantly. The changes in the extent of the hazard zones implicate changes in the number of exposed buildings (see Table 3). Under the assumptions made in this study, the buildings exposed to

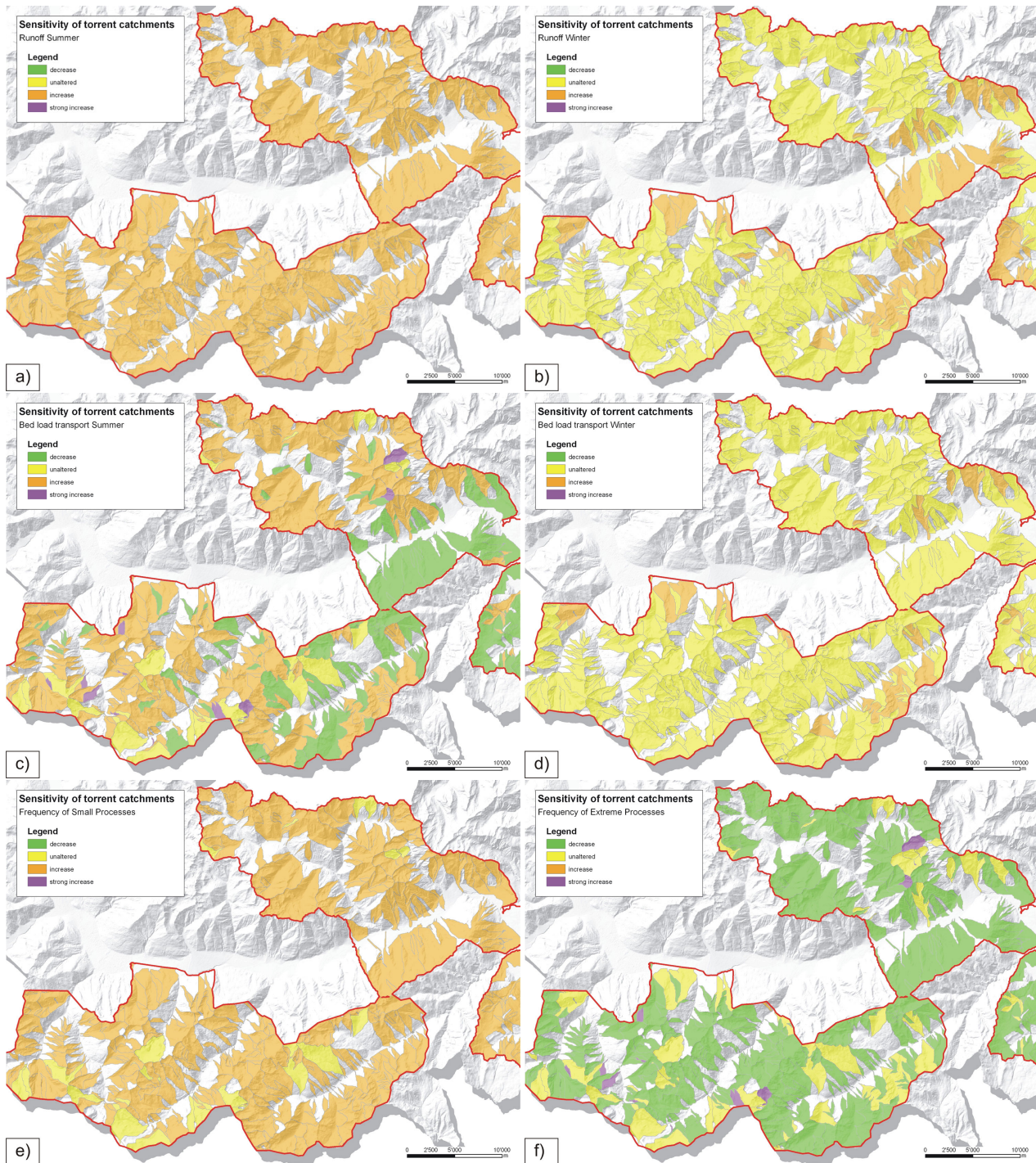


Fig. 10. Classified torrent catchments and their qualitative sensitivity to the assumed changes in the environmental parameters influencing the hazard situation. **(a)** Sensitivity of torrent catchments to climate changes: Runoff in summer. **(b)** Runoff in winter. **(c)** Bed load transport in summer. **(d)** Bed load transport in winter. **(e)** Frequency of small scale processes. **(f)** Frequency of extreme events.

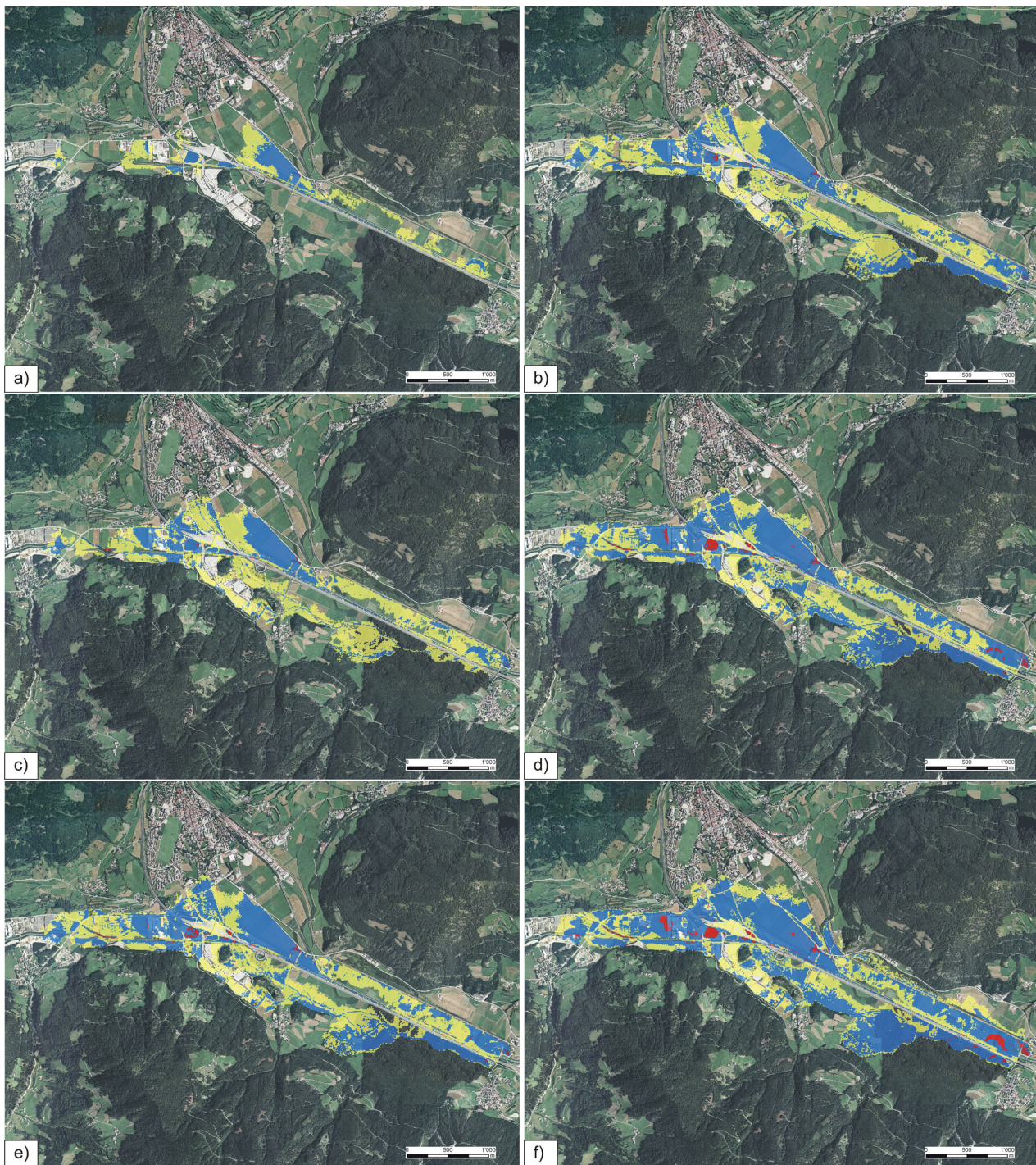


Fig. 11. Changes in flow depths and affected area of the inundation process in the Vipiteno/Sterzing basin. The maps show the classified flow depth. Flow depths from 0 to 0.5 m are shown in yellow, flow depths from 0.5 to 2 m are shown in blue, flow depths of more than 2 m are shown in red. **(a)** Flooded area of a discharge with a return period of 30 years (HQ30) representing scenario 2000. **(b)** Flooded area of a discharge with a return period of 30 years (HQ30) representing scenario +20%. **(c)** Flooded area of a discharge with a return period of 100 years (HQ100) representing scenario 2000. **(d)** Flooded area of a discharge with a return period of 100 years (HQ100) representing scenario +20%. **(e)** Flooded area of a discharge with a return period of 200 years (HQ200) representing scenario 2000. **(f)** Flooded area of a discharge with a return period of 200 years (HQ200) representing scenario +20%.

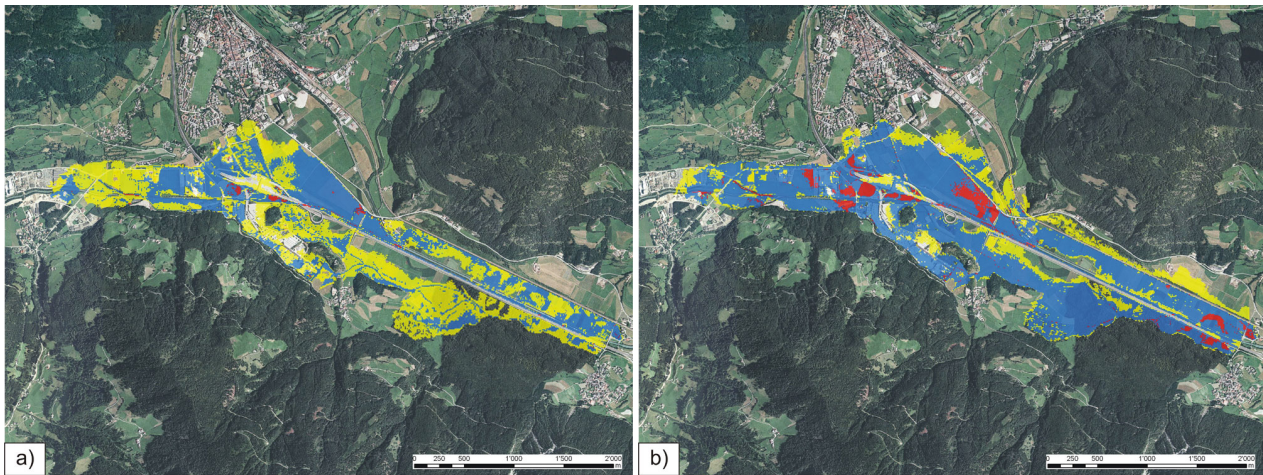


Fig. 12. Results of inundation modelling reclassified following the guidelines for hazard zone mapping (Autonome Provinz Bozen – Südtirol 2006; in red hazard zones, the construction of new buildings is restricted; in blue hazard zones, the construction of new buildings is regulated; in yellow hazard zones prevail hazards with low intensities). **(a)** Flood hazard map representing scenario 2000. **(b)** Flood hazard map representing scenario +20%.

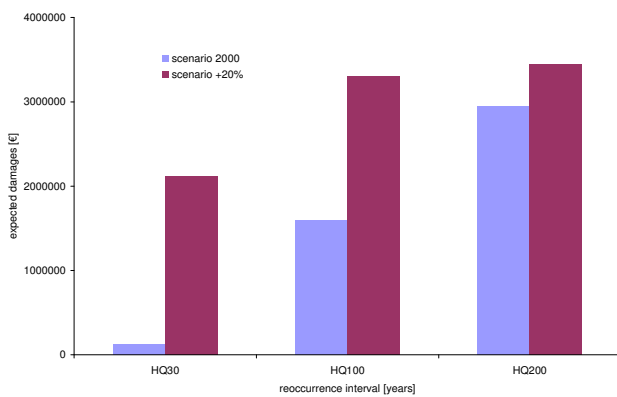


Fig. 13. Changes in expected damages due to flood events in the Vipiteno/Sterzing Basin for the scenario representing the present climate conditions and for the scenario representing possible future climate conditions.

flood hazards with a low intensity (yellow hazard zones) in future may be exposed to blue hazard zones. This is valid especially for the industrial buildings constructed during the last decade in the free spaces in the neighbourhood of the rivers, avoided for settlement in the decades before. The potential shifts from blue hazard zones to red hazard zones do not show significant consequences for buildings. The related risks increased for each scenario (Table 4 and Fig. 13). The expected damages of a flood event with a return period of 30 years (scenario +20%) increased up to 1700% (in comparison to the scenario 2000). The expected damages of a flood event with a return period of 100 years increased up to 207% and up to 117% for an event with a return period of 200 years.

3.3 Potential impacts of climate changes to the delimitation of debris flow hazard zones, case study Rio Cengles/Tschenglser Bach

By increasing the rainfall intensities for the design rainfall events for the delimitation of the hazard zone maps of 20%, the parameters needed for hazard evaluation changed as shown in Table 5. The assumed increase of 20% of the input parameter rainfall intensity for the design events (scenario +20%) lead to an increase of the water discharge of about 37% for a return period of 30 years, of about 45% for a return period of 100 years and of about 31% for a return period of 300 years. The transported volumes increased about 36% for a return period of 30 years, about 51% for a return period of 100 years and of about 43% for a return period of 300 years relative to the design events representing the actual climate conditions. The peak discharge of a design event with a return period of 30 years representing the assumed future climate conditions has nearly the same dimension as a design event with a return period of 100 years representing the actual climate conditions (Table 5). The areas affected by debris flows increases of about 4–30% if the assumed future climate conditions are considered in the simulation model (Fig. 14). The changes in the extent of the hazard zones do not have consequences for the settlements and do not influence the risk situation (if the case of an occlusion of the channel in the settlement area due to wood debris etc. and resulting overflow of the river banks is not considered).

Table 4. Number of buildings endangered by flood processes of the Rio Ridanna/Mareiter Bach and expected damages per design events.

reoccurrence interval	number of exposed buildings and related damages					
	scenario 2000			scenario +20%		
	habitation	production	damages [€]	habitation	production	damages [€]
30	1	1	125 000	8	22	2 120 000
100	7	16	1 595 000	13	34	3 305 000
200	12	30	2 940 000	16	34	3 440 000

Table 5. Calculated rainfall and runoff values and bed load transport in the Rio Cengles/Tschenglsler Bach torrent for relevant return periods and different climate conditions (IPP, 2007).

return period of a rainfall event, duration 60 min	N_{tot} (precipitation) [mm]		Q_{max} (discharge) at confluence [m^3/s]		VB (volume of transported material) [m^3]	
	scenario 2000	scenario +20%	scenario 2000	scenario +20%	scenario 2000	scenario +20%
30 years	55.6	66.7	31.5	44.4	59 000	80 000
100 years	74.2	89.0	47.3	70.4	73 000	110 000
300 years	81.2	97.5	63.5	86.5	83 000	119 000

4 Conclusions

The results of the approach for assessing and classifying the sensitivity of mountain torrent and torrential river catchments against the assumed climate changes showed where the future scenarios of natural hazards are expected to occur more likely. The analyses pointed out that the impacts of climate changes to the hazard situation of torrential and river systems have a high spatial variability. The identification and localization of the torrent catchments, where unfavourable changes in the hazard situation occur could eliminate speculative and unnecessary measures against the impacts of climate changes like a general enlargement of hazard zones or a general over dimensioning of protection structures for the whole territory (e.g. as suggested by Hennegriff et al., 2006). Thus, the procedure could support the discussion about future strategies for adaptation to alternated climate conditions by providing the trends for the development of the hazard situation in a higher spatial resolution.

At the moment, the procedure for the identification and localization of torrent catchments does not consider quantitatively future climate scenarios (e.g. global and regional climate models). This weakness in fact could be eliminated in future, but the qualitative approach allows the transfer of the approach to other areas. The dataset about the classified torrent and torrential river catchments and their sensitivity to climate changes provides the basis for the identification and localization of settlement areas, where increases in the future risk potential have to be expected.

As an example for the use of the dataset, the hazard index map for debris flow processes (geo7, 2006; Zimmermann et al., 1997) was overlaid with the sensitive catchments and the settlement areas. The intersection of these two databases

leads to the identification and localisation of potential debris flow processes starting in catchments that are sensitive to changes due to permafrost degradation. The settlement areas potentially affected by these debris flow processes were pointed out. The potential debris flow processes starting in catchments that are sensitive to permafrost degradation are endangering only insignificant parts of the settlements in the Autonomous Province of Bolzano. Thus, only these settlement areas are sensitive to this specific impact of climate change. But, the environmental changes in the starting areas of the debris flows endangering these sensitive areas must be observed and monitored.

The procedure for the identification and localisation of alpine torrent and torrential river catchments that are sensitive to climate changes provide an information basis for the identification of these cases, where the risk potential tends to increase. Because the impacts of climate changes to natural hazards show remarkably regional differences, the knowledge about where the expected changes in the natural hazard situation have consequences to the risk situation is crucial for the consideration of the impacts of climate change in land use planning and risk management. The presented procedure provides a further information basis for decision-making in land use planning and natural hazard and risk management with a long-term planning horizon. Furthermore, it provides a methodological framework for further refinement and enhancement of the consideration of the effects of climate changes in natural hazards and risk management.

The case study of the Rio Ridanna/Mareiter Bach river showed possible consequences of climate changes to the hazard situation of an alpine river. The study showed that the assumed increase of the precipitation intensities has

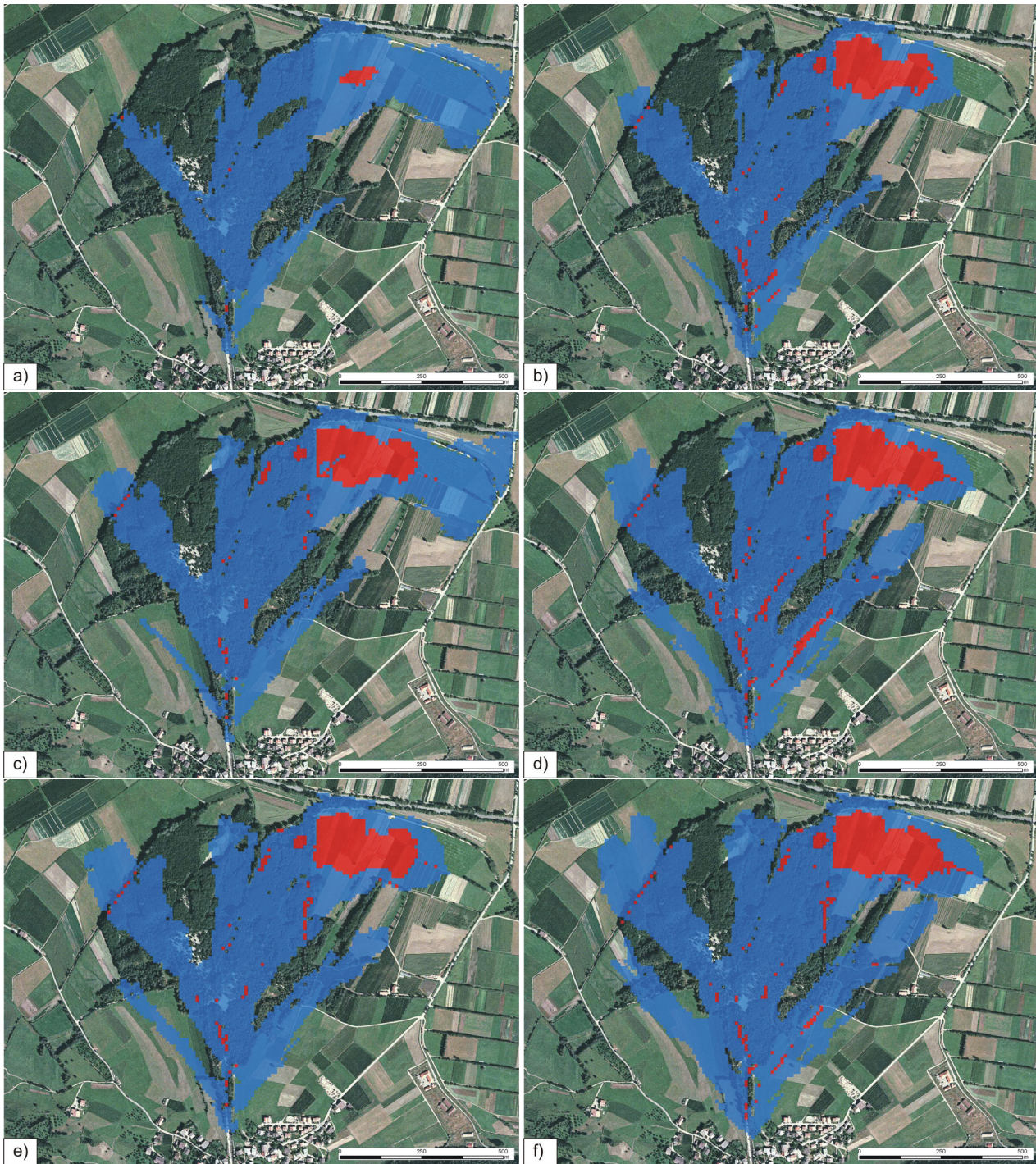


Fig. 14. Changes in flow depths and affected area of the debris flow processes of the Rio Cengles/Tschenglsler Bach torrent. The maps show the classified flow depth following the guidelines for hazard zone mapping (Autonome Provinz Bozen – Südtirol, 2006). Flow depths from 0 to 1 m are shown in blue, flow depths greater than 1 m are shown in red. Critical shear stress parameter of 400 Pa. **(a)** Flow depths for a design event with a return period of 30 years (scenario 2000). **(b)** Flow depths for a design event with a return period of 30 years (scenario +20%). **(c)** Flow depths for a design event with a return period of 100 years (scenario 2000). **(d)** Flow depths for a design event with a return period of 100 years (scenario +20%). **(e)** Flow depths for a design event with a return period of 300 years (scenario 2000). **(f)** Flow depths for a design event with a return period of 300 years (scenario +20%).

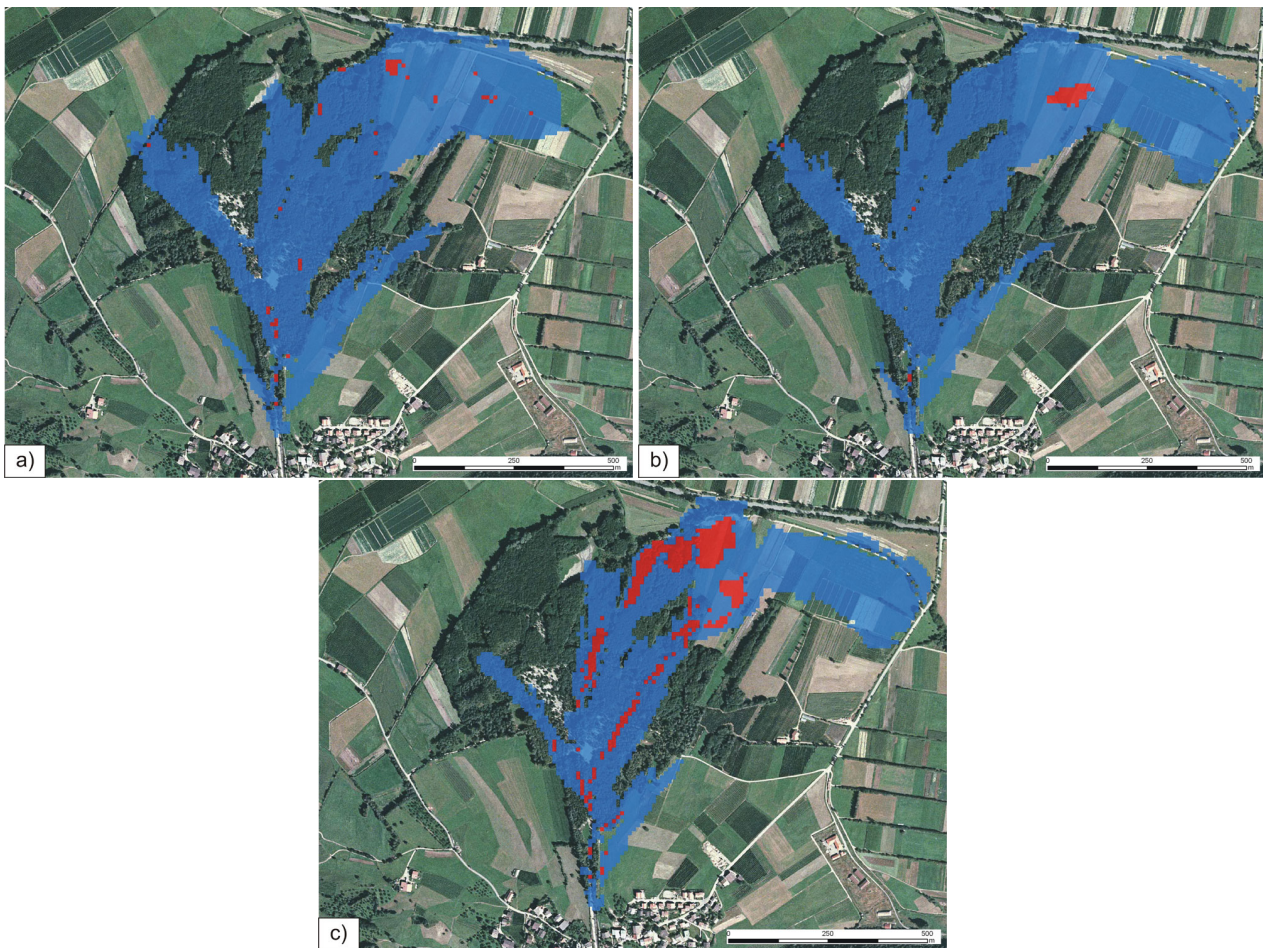


Fig. 15. Variations in flow depth and extent of a design event with a return period of 30 years (actual climate conditions) using different input parameters for the critical shear stress. **(a)** Flow depths for a design event with a return period of 30 years (scenario 2000). Critical shear stress parameter of 200 Pa. **(b)** Flow depths for a design event with a return period of 30 years (scenario 2000). Critical shear stress parameter of 400 Pa. **(c)** Flow depths for a design event with a return period of 30 years (scenario 2000). Critical shear stress parameter of 800 Pa.

remarkable impacts on the natural hazard situation (process intensities). The calculated increase of discharge due to the assumed increase in rainfall intensity showed a significant accentuation of the already existing weak points in the protection structures and the resulting hazard situation. The modelling results showed a remarkably increase in the flooded areas and an increase in flow depths. The hazard zones changed one “level” of hazard classification. Generally, the “yellow” zones delineated on the basis of the actual climate conditions tended to become “blue” zone. This could lead to significant restrictions for land use. The study demonstrated that already known weak points in risk reduction systems as protection structures in future will become more important in risk management activities. This means that the stress-strain behaviour of these weak points in cases of discharges exceeding the channel capacity must be stud-

ied. The knowledge about the behaviour of protection structures in loading case could provide a decision base for the elaboration of and the training of crisis management plans.

The potential effects of changed input parameters as the precipitation intensity to the extent of the hazard zones are not negligible for land use planning purposes. Usually, the hazard assessment of floods is based on the statistical analysis of relatively short data series for precipitation and discharge measurements. As shown in this case study, the analysis of the flood processes bases on a data series of about 31 years. Because of the curtness of the available data series, the calculated intensity values for the future design rainfall event (+20%) representing the future climate conditions (2050–2100) are laying within the 95% confidence interval of the data series representing the present climate conditions. Thus, the assumed future changes in the input

parameter “precipitation intensity” lay within the uncertainty of the methods used today for the delimitation of the hazard zones. Thus, the consideration of the uncertainties laying in the methods used for the elaboration of hazard zone maps would provide a useful instrument for the consideration of potential future climate conditions in sensitive catchments.

The case study of the Rio Cengles/Tschenglser Bach torrent confirmed the hypothesis that the bed load transport capacity of torrents eroding older deposits increases with a potential increase in rainfall intensity. Due to the unlimited predisposition of mobilizable material for debris flows, the process intensity of these torrents increases with the increase of bed load transport capacity because of higher discharges. The changes in process intensity in the deposition area of the debris flow are remarkable, but are lying within the uncertainties due to mostly poorly known process characteristics and models. The ranges of the modelling results due to changes in the input parameters of rheology and critical shear stresses of the debris flow simulation model exceed the ranges of the modelling results due to changes in the input parameter for rainfall intensity (Fig. 15).

The case study showed that possible effects of climate changes are not relevant for torrents that have been systemized with remarkably efforts and where the runout and deposition areas of the torrential processes have been kept free from settlements and infrastructures. Nevertheless, the analyses showed that an assumed increase of rainfall intensity lead to a nonlinear increase of the process intensities. Especially the volume transported by debris flows due to the increase in discharge and transport capacity increased remarkably when considering possible future climate conditions.

This lead to the conclusion that the sediment management in alpine torrents will meet future challenges. In future, the costs for maintenance of existing protection structures will increase due to higher deposition volumes and a higher frequency of removal of debris flow deposits from sediment retention basins. Thus, cost-benefit analyses made within the planning of new protection structures must consider the future higher operating expenses.

The study showed that an increase in the intensity and frequency of flood and debris flow hazards has to be expected as a consequence of climate changes in sensitive catchments. But, the effects of these changes in the hazard situation to the risk situation depend also on other factors in the risk equation. The future changes in the extent of the damage potential and the vulnerability of endangered objects to natural hazard processes would also influence the future risk potential. Thus, the consideration of impacts of climate changes in natural hazard and risk management must be made using a holistic approach combining all the available instruments and possibilities from risk prevention to land use planning and crisis management activities.

The conceptional approach for assessing the impacts of climate changes on risks showed that especially the factor of the vulnerability mostly unconsidered in risk analyses points out the uncertainties in this assessment. But, the consideration of this risk factor opens new possibilities for risk reduction. With the reduction of the vulnerability of endangered buildings against the dangerous processes, a remarkable increase in the hazard potential as an impact of climate changes must not stringently conduct in an increase in risk.

Appendix A

Table A1. Types of Alpine torrent catchments.

catchment type	ID decision tree	Description
WB01	082	Higher located mountain torrent catchments with minor bed load source areas, mainly recent deposits.
WB02	146	Higher located mountain torrent catchments with minor bed load source areas, mainly recent deposits. Important areas affected by permafrost degradation or glacier retreat.
WB03	098	Higher located mountain torrent catchments with major bed load source areas, mainly recent deposits.
WB04	162	Higher located mountain torrent catchments with major bed load source areas, mainly recent deposits. Important areas affected by permafrost degradation or glacier retreat.
WB05	084	Higher located mountain torrent catchments with minor bed load source areas, mainly older deposits.
WB06	148	Higher located mountain torrent catchments with minor bed load source areas, mainly older deposits. Important areas affected by permafrost degradation or glacier retreat.
WB07	100	Higher located mountain torrent catchments with major bed load source areas, mainly older deposits.
WB08	164	Higher located mountain torrent catchments with major bed load source areas, mainly older deposits. Important areas affected by permafrost degradation or glacier retreat.
WB09	088	Higher located mountain torrent catchments with minor bed load source areas and active landslides.
WB10	152	Higher located mountain torrent catchments with minor bed load source areas and active landslides. Important areas affected by permafrost degradation or glacier retreat.
WB11	104	Higher located mountain torrent catchments with major bed load source areas and active landslides.
WB12	168	Higher located mountain torrent catchments with major bed load source areas and active landslides. Important areas affected by permafrost degradation or glacier retreat.
WB13	083	Lower located mountain torrent catchments with minor bed load source areas, mainly recent deposits.
WB14	147	Lower located mountain torrent catchments with minor bed load source areas, mainly recent deposits. Important areas affected by permafrost degradation or glacier retreat. Not existing!
WB15	099	Lower located mountain torrent catchments with major bed load source areas, mainly recent deposits.
WB16	163	Lower located mountain torrent catchments with major bed load source areas, mainly recent deposits. Important areas affected by permafrost degradation or glacier retreat. Not existing!
WB17	085	Lower located mountain torrent catchments with minor bed load source areas, mainly older deposits.
WB18	149	Lower located mountain torrent catchments with minor bed load source areas, mainly older deposits. Important areas affected by permafrost degradation or glacier retreat. Not existing!
WB19	101	Lower located mountain torrent catchments with major bed load source areas, mainly older deposits.
WB20	165	Lower located mountain torrent catchments with major bed load source areas, mainly older deposits. Important areas affected by permafrost degradation or glacier retreat. Not existing!
WB21	089	Lower located mountain torrent catchments with minor bed load source areas and active landslides.
WB22	153	Lower located mountain torrent catchments with minor bed load source areas and active landslides. Important areas affected by permafrost degradation or glacier retreat. Not existing!
WB23	105	Lower located mountain torrent catchments with major bed load source areas and active landslides.
WB24	169	Lower located mountain torrent catchments with major bed load source areas and active landslides. Important areas affected by permafrost degradation or glacier retreat. Not existing!

Table A2. Types of torrential river catchments.

catchment type	ID decision tree	Description
WF01	082	Higher located torrential river catchments with minor bed load source areas, mainly recent deposits. Limited susceptibility to surface runoff.
WF02	146	Higher located torrential river catchments with minor bed load source areas, mainly recent deposits. Increased susceptibility to surface runoff.
WF03	098	Higher located torrential river catchments with major bed load source areas, mainly recent deposits. Limited susceptibility to surface runoff
WF04	162	Higher located torrential river catchments with major bed load source areas, mainly recent deposits. Increased susceptibility to surface runoff.
WF05	084	Higher located torrential river catchments with minor bed load source areas, mainly older deposits. Limited susceptibility to surface runoff
WF06	148	Higher located torrential river catchments with minor bed load source areas, mainly older deposits. Increased susceptibility to surface runoff.
WF07	100	Higher located torrential river catchments with major bed load source areas, mainly older deposits. Limited susceptibility to surface runoff
WF08	164	Higher located torrential river catchments with major bed load source areas, mainly older deposits. Increased susceptibility to surface runoff.
WF09	088	Higher located torrential river catchments with minor bed load source areas and active landslides. Limited susceptibility to surface runoff
WF10	152	Higher located torrential river catchments with minor bed load source areas and active landslides. Increased susceptibility to surface runoff.
WF11	104	Higher located torrential river catchments with major bed load source areas and active landslides. Limited susceptibility to surface runoff
WF12	168	Higher located torrential river catchments with major bed load source areas and active landslides. Increased susceptibility to surface runoff.
WF13	083	Lower located torrential river catchments with minor bed load source areas, mainly recent deposits. Limited susceptibility to surface runoff.
WF14	147	Lower located torrential river catchments with minor bed load source areas, mainly recent deposits. Increased susceptibility to surface runoff.
WF15	099	Lower located torrential river catchments with major bed load source areas, mainly recent deposits. Limited susceptibility to surface runoff
WF16	163	Lower located torrential river catchments with major bed load source areas, mainly recent deposits. Increased susceptibility to surface runoff.
WF17	085	Lower located torrential river catchments with minor bed load source areas, mainly older deposits. Limited susceptibility to surface runoff
WF18	149	Lower located torrential river catchments with minor bed load source areas, mainly older deposits. Increased susceptibility to surface runoff.
WF19	101	Lower located torrential river catchments with major bed load source areas, mainly older deposits. Limited susceptibility to surface runoff
WF20	165	Lower located torrential river catchments with major bed load source areas, mainly older deposits. Increased susceptibility to surface runoff.
WF21	089	Lower located torrential river catchments with minor bed load source areas and active landslides. Limited susceptibility to surface runoff
WF22	153	Lower located torrential river catchments with minor bed load source areas and active landslides. Increased susceptibility to surface runoff.
WF23	105	Lower located torrential river catchments with major bed load source areas and active landslides. Limited susceptibility to surface runoff
WF24	169	Lower located torrential river catchments with major bed load source areas and active landslides. Increased susceptibility to surface runoff.

Table A3. Types of river catchments.

catchment type	ID decision tree	Description
FL01		Higher located alpine river catchments. Limited susceptibility to surface runoff.
FL02		Higher located alpine river catchments. Increased susceptibility to surface runoff.
FL04		Lower located alpine river catchments. Limited susceptibility to surface runoff.
FL02		Lower located alpine river catchments. Increased susceptibility to surface runoff.

Acknowledgements. The project was co-financed by the European Union within the Interreg IIIB Alpine Space project “ClimChAlp – Climate Change, Impacts and Adaptation strategies for the Alps”. The authors thank to C. Scherer and B. Mazzorana for the simulation of the flood processes, A. Waldner and W. Gostner for modelling the debris flow processes and M. Eschgfäller for the literature review. Furthermore, the authors thank to V. Jomelli and another anonymous referee for their constructive remarks.

Edited by: F. Castelli

Reviewed by: V. Jomelli and another anonymous referee

References

- Autonome Provinz Bozen – Südtirol: Richtlinien für die Erstellung von Gefahrenzonenplänen und zur Klassifizierung des spezifischen Risikos, Bozen, 2006.
- Bader, S. and Kunz, P.: Klimarisiken – Herausforderung für die Schweiz, Zurich, 1998.
- Bardossy, A. and Pakosch, S.: Wahrscheinlichkeiten extremer Hochwasser unter sich ändernden Klimaverhältnissen, *Wasserwirtschaft*, 97, 58–64, 2005.
- Beven, K. J., Lamb, R., Quinn, P., Romanowicz, R., and Freer, J.: TOPMODEL. In: *Computer Models of Watershed Hydrology*, edited by: Singh, V. P., Water Resources Publications, 1995.
- Brunetti, M., Maugeri, M., and Nanni, T.: Changes in total precipitation, rainy days and extreme events in northeastern Italy, *Pure and Applied Geophysics*, 21, 861–871, 2001.
- Caspary, H. J.: Recent winter floods in Germany caused by changes in the atmospheric circulation across Europe, *Physics and Chemistry of the Earth*, 20, 459–462, 1996.
- Caspary, H. J.: Zunahme “kritischer” Wetterlagen als Ursache für die Entstehung extremer Hochwasser in Südwestdeutschland, in: *Klimaveränderung und Konsequenzen für die Wasserwirtschaft – Fachvorträge beim KLIWA-Symposium am 3. und 4.5.2004 in Würzburg*, 135–151, 2004.
- Caspary, H. J. and Bardossy, A.: Markieren die Winterhochwasser 1990 und 1993 das Ende der Stationarität in der Hochwasserhydrologie infolge Klimaänderungen? *Wasser & Boden*, 47, 18–24, 1995.
- Christensen, J. H. and Christensen, O. B.: Climate modelling: Severe summertime flooding in Europe, *Nature*, 421, 805–806, 2003.
- Frei, C., Schöll, R., Fukutome, S., Schmidli, J., and Vidale, P. L.: Future change of precipitation extremes in Europe: Intercomparison of scenarios from regional climate models, *J. Geophys. Res.*, 111, D06105, doi:10.1029/2005JD005965, 2006.
- Fuchs, S., Heiss, K., and Hübl, J.: Towards an empirical vulnerability function for use in debris flow risk assessment. *Nat. Hazards Earth Syst. Sci.*, 7, 495–506, 2007, <http://www.nat-hazards-earth-syst-sci.net/7/495/2007/>.
- geo7: Gefahrenhinweiskarte Murgang und Übersarung. Technischer Bericht. Unpublished project report within the Interreg IIIA Italy-Switzerland project “Entwicklung und Anwendung eines Systems zur überregionalen Erkennung und Bewertung hydrogeologischer Risiken”, Bozen, 27 pp., 2006.
- geo7: Gefahrenhinweiskarte Murgang und Übersarung: Auswertung im Hinblick auf die Klimaänderung. Erläuterungen zum Entscheidungsbaum, Unpublished report within the project Interreg IIIB Alpine Space “ClimChAlp - Climate Change, Impacts and Adaptation Strategies in the Alpine Space”, Bozen, 34 pp., 2007.
- Gius, S.: Die Gefahrenzonenplanung in Südtirol, *Wildbach- und Lawenverbau* 152, 49–61, 2005.
- Gostner, W.: Integrale Analyse eines murfähigen Wildbaches anhand einer Fallstudie. Unpublished M.S. thesis, ETH Lausanne, Lausanne, 203 pp., 2002.
- Harris, C., Davies, M. C. R., and Etzelmüller, B.: The assessment of potential geotechnical hazards associated with mountain permafrost in a warming global climate. *Permafrost Periglac.*, 12, 145–156, 2001.
- Heimann, D. and Sept, V.: Climate change estimates of summer temperature and precipitation in the Alpine region. *Theor. Appl. Climatol.*, 66, 1–12, 2000.
- Heinimann, H., Hollenstein, K., Kienholz, H., Krummenacher, B., and Mani, P.: Methoden zur Analyse und Bewertung von Naturgefahren. *Umweltmaterialien Bundesamt für Umwelt, Wald und Landschaft*, Bern, 249 pp., 1998.
- Hennegriff, W., Kolokotronis, V., Weber, H., and Bartels, H.: Klimawandel und Hochwasser. Erkenntnisse und Anpassungsstrategien beim Hochwasserschutz. *Wasser, Abfall*, 53, 770–779, 2006.
- IPP Ingenieure Patscheider and Partner GmbH: Untersuchungen zur Sensitivität der Murganggefahr des Tschenglsler Baches gegenüber möglichen Klimaveränderungen. Unpublished report within the project Interreg IIIB Alpine Space “ClimChAlp - Climate Change, Impacts and Adaptation Strategies in the Alpine Space”, Bozen, 2007.
- Jomelli, V., Pech, V., Chochillon, C., and Brunstein, D.: Geomor-

- phic Variations of Debris Flows and Recent Climatic Change in the French Alps, *Climatic Change*, 64(1), 77–102, 2004.
- Jomelli, V., Brunstein, D., Grancher, D., and Pech, P.: Is the response of hill slope debris flows to recent climate change univocal? A case study in the Massif des Ecrins (French Alps), *Climatic Change*, 85(1), 119–137, 2007.
- Katzenberger, B.: Bisherige Erkenntnisse aus KLIWA - Handlungsempfehlungen. In: KLIWA, (ed.): Klimaveränderung und Konsequenzen für die Wasserwirtschaft – Fachvorträge beim KLIWA-Symposium am 3 und 4 Mai 2004 in Würzburg, 197–204, 2004.
- Kienholz, H., Krummenacher, B., Kipfer, A., and Perret, S.: Aspects of integral risk management in practice - Considerations with respect to mountain hazards in Switzerland, *Österreichische Wasser- und Abfallwirtschaft*, 3–4, 43–50, 2004.
- KOHS – Kommission Hochwasserschutz im Schweizerischen Wasserwirtschaftsverband: Auswirkungen der Klimaänderung auf den Hochwasserschutz in der Schweiz. Ein Standortpapier der Kommission Hochwasserschutz im Schweizerischen Wasserwirtschaftsverband (KOHS), *Wasser, Energie, Luft*, 99(1), 55–59, 2007.
- O'Brien, J. S. and Julien, P. Y.: FLO-2D, Users Manual, Version 2001.06, 2001.
- OcCC: Klimaänderung und die Schweiz 2050, Erwartete Auswirkungen auf Umwelt, Gesellschaft und Wirtschaft, Bern, 172 pp., 2007.
- Rebetez, M., Lugon, R., and Baeriswyl, P.-A.: Climatic Change and debris Flows in High Mountain Regions: The Case Study of the Ritigraben Torrent (Swiss Alps), *Clim. Change*, 36, 371–389, 1997.
- Regional Office of Carinthia, Department of Water Economy: Rainfall/Runoff Model for small catchment areas in the Lavant Valley for determination of potential future effects through assessment of regional climate change scenario. Interreg IIB Alpine Space project ClimChAlp – Climate Change, Impacts and Adaptation Strategies in the Alpine Space, Project report of WP 5 – Climate Change and Resulting Natural Hazards, Klagenfurt, 2008.
- Schädler, B., Frei, C., Grebner, D., and Willi, H. P.: Grundlagen zum Klima, *Wasser-Energie-Luft*, 1, 58–59, 2007.
- Stoll, C.: Schätzung des Schadenpotenzials bei Hochwasserereignissen durch die Ahr bei Uttenheim und St. georgen und durch die Rienz im Bereich Bruneck bis St. Lorenzen. Unpublished report for the Interreg IIB project "River Basin Agenda", Bruneck, 80 pp., 2004.
- Scherer, C. and Mazzorana, B.: Schutzwasserbau für den Oberen Eisack, Bericht zur Hydraulik. Unpublished report within the project Interreg IIB Alpine Space "River Basin Agenda", Bozen, 66 pp., 2005a.
- Scherer, C. and Mazzorana, B.: Schutzwasserbau für den Oberen Eisack. Bericht zur Hydrologie. Unpublished report within the project Interreg IIB Alpine Space "River Basin Agenda", Bozen, 117 pp., 2005b.
- Scherer, C. and Mazzorana, B.: Gefahrenszenarien im Einzugsgebiet des Mareiter Baches. Unpublished report within the project Interreg IIB Alpine Space "ClimChAlp - Climate Change, Impacts and Adaptation Strategies in the Alpine Space", Bozen, 129 pp., 2007.
- Stötter, J.: Veränderungen der Kryosphäre in Vergangenheit und Zukunft sowie Folgeerscheinungen. Habilitation thesis, University of Munich, Munich, 264 pp., 1994.
- Stötter, J. and Zischg, A.: Alpines Risikomanagement – theoretische Ansätze, erste Umsetzungen, in: *Naturrisiken und Sozialkatastrophen*, edited by: Felgentreff, C. and Glade, T., Berlin, Heidelberg, 297–310, 2007.
- United Nations: Living with risk. United Nations, Geneva, 2004.
- Villi, V. and Bacchi, B.: Valutazione delle piene nel Triveneto, CNR-GNDCI Consiglio nazionale delle ricerche – Gruppo nazionale per la difesa dalle catastrofi idrogeologiche, Padova, Brescia, 2001.
- Zimmermann, M., Mani, P., and Gamma, P.: Murganggefahr und Klimaänderung – ein GIS-basierter Ansatz. vdf, Zurich, 161 pp. 1997.
- Zimmermann, M. and Haerberli, W.: Climatic change and debris flow activity in high mountain areas: a case study in the Swiss Alps. *Catena Supplement*, 22, 59–72, 1992.

Paper 27: Zischg, A., Schober, S., Sereinig, N., Rauter, M., Seymann, C., Goldschmidt, F., Bäk, R., Schleicher, E., 2013. Monitoring the temporal development of natural hazard risks as a basis indicator for climate change adaptation. *Natural Hazards* 67, 1045–1058. [10.1007/s11069-011-9927-0](https://doi.org/10.1007/s11069-011-9927-0).

Monitoring the temporal development of natural hazard risks as a basis indicator for climate change adaptation

A. Zischg · S. Schober · N. Sereinig · M. Rauter · C. Seymann ·
F. Goldschmidt · R. Bäk · E. Schleicher

Received: 29 October 2010 / Accepted: 5 August 2011 / Published online: 23 August 2011
© Springer Science+Business Media B.V. 2011

Abstract The potential effects of climatic changes on natural risks are widely discussed. But the formulation of strategies for adapting risk management practice to climate changes requires knowledge of the related risks for people and economic values. The main goals of this work were (1) the development of a method for analysing and comparing risks induced by different natural hazard types, (2) highlighting the most relevant natural hazard processes and related damages, (3) the development of an information system for the monitoring of the temporal development of natural hazard risk and (4) the visualisation of the resulting information for the wider public. A comparative exposure analysis provides the basis for pointing out the hot spots of natural hazard risks in the province of Carinthia, Austria. An analysis of flood risks in all municipalities provides the basis for setting the priorities in the planning of flood protection measures. The methods form the basis for a monitoring system that periodically observes the temporal development of natural hazard risks. This makes it possible firstly to identify situations in which natural hazard risks are rising and secondly to differentiate between the most relevant factors responsible for the increasing risks. The factors that most influence the natural risks could be made evident

A. Zischg (✉)
Abenis AG, Chur, Switzerland
e-mail: a.zischg@abenis.ch

S. Schober · N. Sereinig
Department of Water Resources Management, Provincial Government of Carinthia,
Klagenfurt, Austria

M. Rauter
School of Geoinformation, Carinthia University of Applied Sciences, Klagenfurt, Austria

C. Seymann
Torrent and Avalanche Control Service, Klagenfurt, Austria

F. Goldschmidt · R. Bäk
Department of Geology and Soil Protection, Provincial Government of Carinthia, Klagenfurt, Austria

E. Schleicher
Department of Land Use Planning, Provincial Government of Carinthia, Klagenfurt, Austria

and eventual climate signals could be pointed out. Only with this information can the discussion about potential increases in natural risks due to climate change be separated from other influencing factors and be made at an objective level.

Keywords Integral natural hazards and risk management · Climate change adaptation · Risk analysis

1 Introduction

The management of natural hazards has a long tradition in Austria and in the Alps. For a decade, the former practice of managing floods, debris flows, avalanches, rock falls and landslides has been more or less transformed into a practice of integrated risk management. Integrated risk management is the process of finding the most efficient solutions and combinations of measures for risk reduction throughout all phases of risk management (prevention, intervention and restoration). The focus in natural hazard management has shifted from the construction of protective measures as the principal solution to the defence against natural hazards to a more holistic approach, which views risk management as integrating a variety of individual but coordinated activities from different disciplines and different administrative levels (Zischg 2010). One principle of integrated risk management is the consideration of the results of quantitative risk analysis and therefore risk-based decision-making.

The risk resulting from natural hazards is defined as a quantifying function of the probability of occurrence of a dangerous process and the related degree of damage. The latter is specified by the damage potential and the vulnerability of the endangered object (United Nations 2004).

$$R_{i,j} = p_{Si} \cdot A_{Oj} \cdot p_{Oj,Si} \cdot v_{Oj,Si}$$

According to the United Nations (2004) definition, the specifications for the probability of the defined scenario (p_{Si}), the monetary value of the object affected by this scenario (A_{Oj}), the probability of exposure of object j to scenario i ($p_{Oj,Si}$) and the vulnerability of object j in dependence on scenario i ($v_{Oj,Si}$) are required for the quantification of risk ($R_{i,j}$).

The risks induced by natural hazards change over time with the changing environment (Keiler et al. 2006; Fuchs et al. 2005). On the one hand, the probability of occurrence and the magnitudes of natural hazard processes may be altered by the effects of climate change. These effects vary remarkably between process types and between specific local situations (Keiler et al. 2010). Whereas the effects of rising temperatures on natural hazard processes related to glacier and permafrost degradation may be identified and constrained locally, the effects of climate change on precipitation and, therefore, on precipitation-related processes are more difficult to assess. The occurrence probability of natural hazard processes related to precipitation, such as floods, debris flows and avalanches, is expected to increase (Frei et al. 2006; Caspary 2004). Other analyses point out a possible decrease in the occurrence probability of debris flows depending on their type of sediment delivery for transportation (Staffler et al. 2008; Jomelli et al. 2004, 2007). While the direct effects of climate change on natural hazard processes can be assessed and monitored, indirect effects or feedbacks in process chains are less well known (Keiler et al. 2010). In mountainous areas, natural hazard processes are strongly influenced by the topographical, geological and microclimatological conditions and evolve in a downward slope from the headwater catchment area

towards the floodplain areas. This means that natural hazard processes in the flood plains are influenced by processes in higher areas. This interrelation depends on the characteristics of transport processes and leads to a high spatial and temporal variability in the domain of natural hazard processes (Keiler et al. 2010; Staffler et al. 2008). The topographical, climatical and geomorphological diversity of the Alps require a locally differentiated view of the potential effects of climatic changes on natural hazards. There will be areas likely to be affected by natural hazards related to climate change, and there will be others without any changes in the actual natural hazard situation (Staffler et al. 2008).

Besides the probability of occurrence and the intensity of potential natural hazards that can be affected by climatic changes, the extent of damage and the vulnerability of endangered objects also affect the level of risks (e.g., Fuchs et al. 2007). In comparison to the potential effects of climate change on natural hazards, the latter parameter of the risk formula affects the resulting risks more significantly. Economic development leads to the spread of settlements and infrastructure towards endangered zones. At the same time, the values of houses and goods and the requirements for mobility are increasing (Keiler 2004; Keiler et al. 2005). The functioning of local economies is based on the functioning of infrastructures for transport, communication, water provision and electricity supply. This leads to an increased dependency of human activities on the continuous functioning of infrastructures and, therefore, to an increase in vulnerability to the effects of natural hazards. Society's demand for absolute safety in the area of natural hazards is increasing while, at the same time, individual responsibility is increasingly denied (Fuchs 2009; Zischg 2010). The increasing demands for higher safety standards will also put greater pressure on public finances.

Due to the dimensionality and the aggregation of these trends in increasing natural hazard risks, the practice of risk management in general has to be adapted to these new situations and the challenges must be faced by the relevant stakeholders (PLANALP 2010). The resulting rapid changes in both the number of exposed people or values of goods and the changing characteristics of natural hazards due to climate change require a new approach to managing this complex system of risk and safety. Although the effects of climate change are only one of several factors influencing natural hazard risks, they should be monitored and evidenced. But this factor has to be considered separately from the others. At the moment, the common agreement in natural hazard risk management practice is to avoid a general consideration of simplified effects of climate change on natural hazards equally over wide areas without any local differentiation. The common agreement of most relevant stakeholders in natural hazard risk management in the Alps is to monitor the further development of natural hazard risks influenced by climate change. And in cases where the effects of climate change on a specific risk situation become evident or can be reliably assessed, these effects are faced by an integrated risk management approach (Greminger and Zischg 2011). A general update of hazard zone maps over large areas on the basis of today's climate projections is not considered.

The monitoring of the long-term development of natural hazard risks requires a monitoring system that is able to differentiate between the main factors influencing the risks. The pre-condition for the monitoring of the effects of climate change on natural hazard risks is the knowledge of the existing risks. The effects of climate change on the existing risk situation can only be quantified if existing risks in the whole study area are known.

The main aim of this work was to elaborate a method for analysing and comparing natural hazard risks induced by different processes in a wider area. The method should meet the following requirements:

- the actual risks induced by floods, debris flows, avalanches, rock falls and landslides should be analysed on the basis of the existing data (hazard maps and land-use maps)
- the procedure should be able to analyse the natural hazard risks on a community level but the risks should be summarisable at the regional level (province)
- the procedure should highlight the communities in the study area with the highest values of natural hazard risks (hot spots)
- the procedure should make it possible distinguish between different factors influencing the risks (hazard-related or vulnerability-related factors)
- the procedure should be made on the basis of the methodological framework of risk analysis for cost-benefit analyses (binding guidelines for cost-benefit analyses in Austria), the damage functions and object-related vulnerability functions should be incorporated as variables that can be adapted to new findings
- the procedures should allow periodic updates and the analysis of the historic development of risks
- the results of the risk analysis should be visualised for the wider public

One aim of this study was to show which hazardous processes (floods, debris flows, avalanches, rock-fall processes and landslides) produce the most relevant exposure of people and property. This comparative analysis should provide the basis for pointing out the hot spots of natural hazard risks in the province of Carinthia (Bundesland Kärnten), Austria. The method should provide the basis for a control system that periodically observes whether the effects of climate change are increasing the risks of flooding.

2 Method

The achievement of the goals set requires a close collaboration between the various responsible institutions in the province of Carinthia. In Carinthia, the authority responsible for flood protection is the Department of Water Resources Management. The authority responsible for protection against torrential hazards and avalanches is the Torrent and Avalanche Control Service. The Department of Geology and Soil Protection is responsible for the management of rock fall and landslide threats. The Department of Land Use Planning is responsible for land use planning.

The first step towards the goals was the definition of a common dataset of object categories to be considered in exposure and risk analysis (elements at risk). The second step was the elaboration and compilation of datasets for the different natural hazard processes. On the basis of a dataset of elements at risk and subsequently compiled damage maps, an exposure analysis for all processes and a risk analysis for flood processes were made. The results of exposure analyses of individual single process types were compared, and the communities with the highest number of elements at risk have been pointed out. Finally, the results of this comparative analysis were prepared for visualisation and for use as a basis for communicating risks.

2.1 Definition of the classes of elements at risk

The European Water Framework Directive and the Guidelines for cost-benefit analyses in hydraulic engineering and in torrent and avalanche control (BMLFUW 2006a, 2008) define the classes of elements at risk that are to be considered in risk analyses. In general, this study followed the definitions for elements at risk in these guidelines with adaptations to

local particularities, especially due to classification schemes of existing datasets. A catalogue of elements at risk was prepared for the whole region of Carinthia on the basis of existing datasets and without additional field work. The elaboration of the catalogue of elements at risk was supported by an interdisciplinary working group with people from different administrative units. The result of this work was a jointly accepted catalogue of elements at risk that have to be considered in the exposure and risk analyses of all relevant natural hazard types. The standardisation of the classes of elements at risk was one precondition to make exposure and risk analyses of different natural hazard processes comparable. The following classes of elements at risk were considered in exposure and risk analysis:

Buildings

- Buildings with one domicile
- Buildings with two or more domiciles
- Buildings for apartment-sharing communities
- Buildings with tourist functions
- Industrial buildings
- Public buildings
- Schools or hospitals
- Others

Infrastructure

- Motorways
- Main roads with regional function
- Municipal roads
- Secondary access roads
- Bridges
- Areas with industrial functions
- Airports
- Railways
- Power stations and electricity substations
- Sewage management infrastructure
- Water supply infrastructure
- Power lines
- Gas supply stations and lines

Agriculture and forestry

- Grassland
 - Farmland
 - Forest
-

There is a variety of different datasets in the study area that provide the databases to be used within a GIS-based analysis of the elements at risk. The datasets range from land-use maps, information systems for water resource management, roads and railways, to datasets of power- and water-supply companies. The procedure for the compilation of a database of

elements at risk from many different datasets was combined into a software package that guarantees a standardisation of the procedure and saves time resources. Most of the existing datasets are suited for the compilation of the dataset of object categories for risk analysis. But in the study area at the moment, there is no specific dataset of buildings with attributes useable directly for risk analysis. The building categories therefore had to be extracted and classified combining two different datasets: (1) the land registry, without any information on the function of the buildings and (2) the dataset of the location of household addresses. These two datasets are not related and were provided from different institutions. The procedure takes the extent and the localisation of the buildings from the land registry, which contains only the surface area of the building itself. The classification of the functionality of the building was derived from the address dataset that is available as a point file. The point datasets of the addresses and of the schools were combined with the polygon datasets of the building layer. The attributes of the point layers were attributed to the polygon layer by means of different rules for spatial relationships. All address points related spatially to a building were used to classify the building itself. If a single address point of a private household falls into a single building or is situated in the vicinity of the building, then the building itself was classified as a domicile for one household. In cases where a building polygon is overlaid by more than one address point, the building was classified as multi-functional depending on the type of use. After classifying the functionality of each building, the next step was to attribute the number of residents or the number of workplaces to each building. The number of people and workplaces for each building were calculated on the basis of the Austrian statistics dataset. This provides information on the type of household and employment within grid cells with a resolution of 125 m. The total sum of workplaces and inhabitants of each grid cell of the statistics dataset was divided by the number of buildings of the respective functions within this raster cell. The resulting value was attributed to the individual buildings of each class of buildings. In cases where the grid cells indicate the number of workplaces, this number could be divided by the number of buildings with industrial functions.

2.2 Compilation of the hazard information

There are different datasets that can be used to describe information on natural hazard processes in the study area. Three different datasets exist for flood processes, and there are different datasets for rock falls, debris flows and landslides. There are hazard zone maps for flood hazards on the major rivers, which were elaborated following the guidelines for the hazard zone maps of the BMLFUW (2006b). The maps drawn up before 2006 show two classes of intensity of a flood event with a return period of 100 years. More recent maps differentiate between flood events with return periods of 30, 100 and 300 years. These maps consist of intensity maps for each of the selected scenarios and return periods. The hazard zone maps do not cover all areas. Hazard maps are being drawn up for the missing areas. Furthermore, a nationwide map of flood events of a return period of 30, 100 and 200 years (HORA, see <http://www.wassernet.at/article/articleview/74694/1/13524/>) is available. In areas where there are no regional authority hazard zone maps, the HORA flood hazard maps of an event with a return period of 100 years were considered for risk analysis. A simplified modelling procedure was used to map the extent of potential flood areas for a few areas where there are no hazard zone maps of the regional authority or HORA flood hazard maps. This procedure uses a digital elevation model to demarcate any areas that can be flooded due to the topographic condition. This does not consider the quantity of the discharge but defines all areas potentially affected by flooding from the

main rivers. It was assumed that all rivers overflow their banks or breach the dams. The resulting map therefore does not contain any information on probability of occurrence or intensity. This map was used only for a small number of river reaches. For the other hazardous processes considered in the comparative exposure analysis, the existing datasets compiled to one harmonised map for each process. The hazard zone maps for torrential hazards were prepared by the Torrent and Avalanche Control Service following the Austrian guidelines (BMLFUW 2011). These hazard zone maps define the areas potentially affected by flood or debris-flow processes from torrential catchments of a return period of 150 years. The hazard zones are classified into two categories of process intensity. The same guidelines also describe the procedure for drawing up hazard zone maps for avalanches. The hazard zone maps of avalanches also consider a return period of 150 years and classify two categories of intensity. The hazard maps for rock fall and landslide processes were compiled and provided by the Department of Geology and Soil Protection. These hazard maps do not consider a certain return period or occurrence probability but classify the evident and potential hazard areas in three categories: potential hazard area, area with identified hazard and area with identified hazard of a high probability or intensity. One hazard map was compiled for each process type.

2.3 Comparative exposure analysis

In a further step, the catalogue of elements at risk was intersected with the hazard maps. The hazard information was attributed to the buildings dataset. The information of the process type, the related intensity class and the return period of the respective scenario were attributed to every single building. If a building was located on the border of two classes of hazard intensity, the intensity class with the higher grade was attributed to it. Afterwards, the number of exposed buildings was summarised at municipality level for each process type and intensity class. The other categories of elements at risk such as streets and infrastructure were intersected with all hazard maps of each process type. The units describing the quantity of the exposed elements were summarised at municipality level. This resulted in a table for each municipality that summarises the number of exposed objects or the length/area of all categories of the catalogue of elements at risk. The results of the exposure analysis for each process type were compared at municipality level.

2.4 Flood risk analysis

The analysis of flood risk was made on the BMLFUW (2006a, 2008) guidelines. These contain functions for the estimation of the damages on endangered objects. The risk analysis was made only for flood processes of the main rivers. The analysis of damage and risks due to torrential processes, avalanches, rock-fall processes and landslides was not made within this study but it is planned for the near future.

The damage to buildings was calculated using the following formula (1):

$$S = S_{\min} + 1000 * B * \sqrt{W} \quad (1)$$

where S is damage in €, S_{\min} minimal damage in € and B factor depending on the functionality of the building. Damage in k€ with an inundation depth of 1 m (without S_{\min}), W water depth in m above floor level of the building.

The values of the parameters used for the calculation of the damages are described in Table 1. The water depths were extracted from the hazard zone maps. The transformation

Table 1 Parameters and their values used for the calculation of damages to buildings due to flooding

Functionality of the building	Smin cellar	B cellar	Smin ground floor	B ground floor
Buildings with one domicile	3,250	11.0	13,360	30.0
Buildings with two or more domiciles	2,800	11.0	11,800	29.0
Buildings for apartment-sharing communities	1,000	5.0	8,000	25.0
Buildings with tourist functions	10,000	20.0	20,000	62.5
Industrial buildings	12,000	21.3	26,000	216.0
Public buildings	12,000	21.3	30,000	168.8
Schools or hospitals	12,000	21.3	30,000	168.8
Others	1,000	8.0	7,000	20.0

of inundation water depths to the water depth above floor level of the building was made by using mean values for the factor W . The mean values were extracted from a reverse analysis of a detailed study in the catchment of the river Glan. For yellow hazard zones (low and medium intensity), a medium water depth above floor level of 0.15 m was assumed and for red hazard zones (high intensity) 0.77 m. A value of 0.16 m was used for the factor W to calculate flood damage on the basis of the HORA flood hazard maps.

We did not use a vulnerability factor to calculate damage on other classes of the catalogue of elements at risk because the existing hazard maps do not make it possible to deduce the required details of process intensity for the assessment of the vulnerability factor of infrastructures. For both intensity classes, we used medium damage values instead of the vulnerability factor. The values are shown in Table 2. The results of the risk analysis were summarised at communal and regional administrative level.

2.5 Visualisation of the results of the comparative exposure analysis and of the risk analysis for decision-makers and the wider public

The results of comparative exposure analysis and the flood risk analysis were summarised at municipal level and subsequently published on a website of the provincial authorities of Carinthia. A fact sheet showing the results of the comparative exposure analyses was prepared for each municipality (see Fig. 1). These fact sheets contain the most relevant information about the municipality with the characteristics of the different process types, the hazard maps, and the number of the exposed objects and the results of the flood risk analyses. The number of elements at risk of each hazard type (flood processes, debris flows, rock-fall processes and landslides) was visualised in tables and in summary charts or diagrams. The diagrams show the number of elements at risk of different categories. The results of the flood risk analysis are summarised in a table. For each category of the catalogue of elements at risk, the potential damage of a flood event with a return period of 100 years is summarised in the table. The comparison between potential damages of different categories of elements at risk is shown in common diagrams (see Fig. 2).

2.6 Combination into an information system for monitoring the temporal development of natural hazard risks

The procedure for the comparative exposure analysis and the flood risk analysis was combined into the information system of the Carinthian provincial authorities. This system

Table 2 Mean values of damage to infrastructure due to flooding

Element at risk	Unit	Value
Motorways	€/m	2575
Main roads with regional function	€/m	527
Secondary access roads	€/m	527
Municipal roads	€/m	527
Bridges	€/m	16000
Railways	€/km	3.51
Power stations and electricity substations	€	10,000.00
Sewage infrastructure management	€	10,000.00
Water supply infrastructure	€	10,000.00
Electricity lines 20 kV	€/m	149
Electricity lines 110 kV	€/m	702
Grassland	€/m ²	2453
Farmland	€/m ²	3271

includes all relevant information for the procedure, either as static maps or periodically updated maps. The hazard zone maps are updated regularly after a period of 10–15 years. If significant system changes that influence either the probability or the intensity of hazard processes occur, the hazard zone maps will be updated, for example, after significant system changes due to the effects of climate change or due to the construction of protection measures.

3 Results

The result of the approach is a database with the information about the numbers of elements at risk for different process types and the potential damages of a flood event with a return period of 100 years. The information can be queried at local level (hazard zone), at a communal or regional level. The database provides an overview of the expected damages or losses. It allows the aggregation of data on different levels and provides the basis for a comparative analysis of the risks in the municipalities of Carinthia. The summarised data are presented in the form of fact sheets on the internet. These fact sheets for each municipality highlight the critical hazards in their territory.

The comparative exposure analysis shows the spatial distribution of the elements at risk exposed to the different process types within Carinthia and highlights the municipalities with the highest number of exposed buildings, people and infrastructure. It shows that the municipalities in the valleys of the study area are mostly affected by flood and debris-flow processes on the alluvial fans. The municipalities with the highest number of elements at risk are located in the wider flood plains potentially affected by flooding. These risks are concentrated within a few municipalities (see Fig. 3). In total, more than 52,000 inhabitants are potentially affected by a flood event with a return period of 100 years in the study area. Almost 50% of the total number of inhabitants affected by flood processes are located in two municipalities. Totally, of 35,455 buildings are potentially exposed by flood processes. This is 14% of the total building stock. The comparison between the number of elements at risk exposed to the different process types shows a high variability (see Fig. 3). In comparison to flood processes, torrential processes (debris flows and flood process of

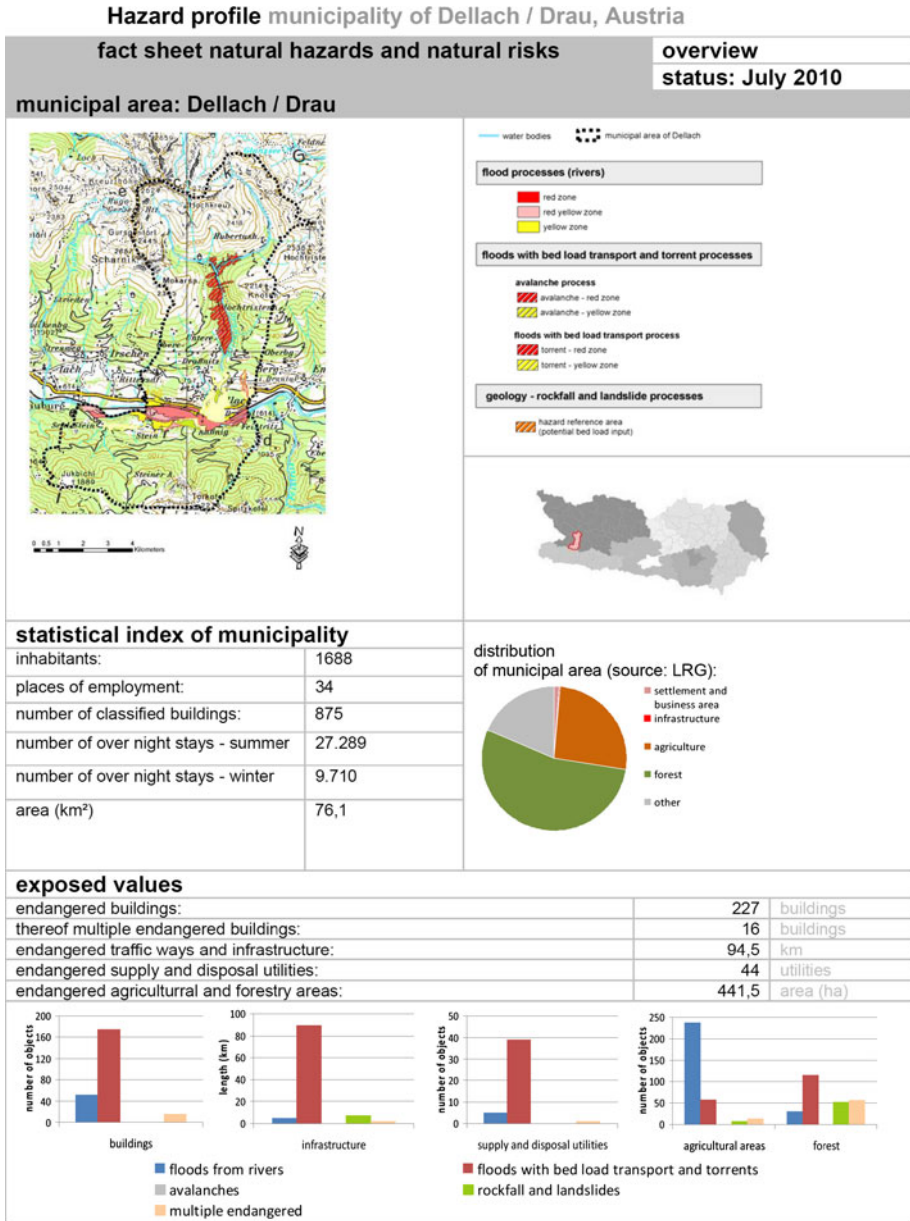


Fig. 1 Example of a factsheet showing the results of the comparative exposure analysis. Example of the municipality of Dellach im Drautal

mountain torrents) potentially affect 39,897 inhabitants and 19,287 buildings. Avalanches potentially affect 1,249 inhabitants and 660 buildings. Figure 4 shows the spatial distribution of potential damages due to flooding. In mountainous regions, the damage to infrastructure is higher than the damage to buildings. This contrasts to the situation in the floodplains, where the potential damage to buildings is higher.

	red hazard zone (high intensity)	red-yellow hazard zone (high intensity)	yellow hazard zone (low and medium intensity)	sum HQ100
damages on buildings	789.000 €	307.000 €	1.377.000 €	2.473.000 €
buildings with residential function	0 €	0 €	575.000 €	575.000 €
public buildings, industrial buildings, schools	789.000 €	307.000 €	802.000 €	1.898.000 €
infrastructure	2.428.000 €	1.002.000 €	6.056.000 €	9.486.000 €
roads	663.000 €	228.000 €	923.000 €	1.814.000 €
bridges	---	---	---	---
railroads	1.765.000 €	774.000 €	5.133.000 €	7.672.000 €
utilities	505.000 €	109.000 €	198.000 €	812.000 €
agriculture	356.000 €	112.000 €	191.000 €	659.000 €
number of exposed persons	39			
number of exposed working places	16			

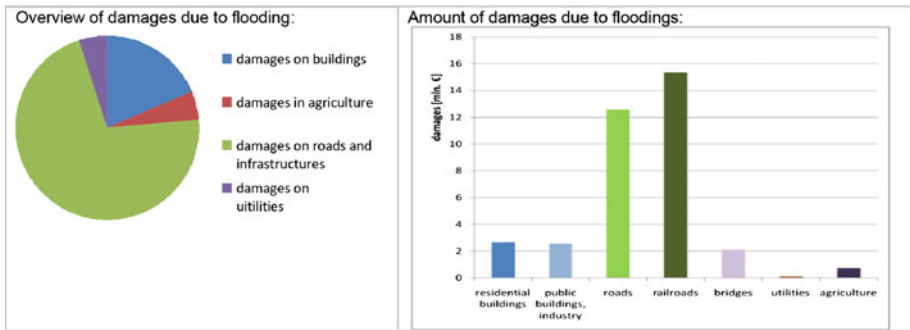


Fig. 2 Example of one part of a fact sheet showing the results of the flood risk analysis. Example of the municipality of Dellach im Drautal

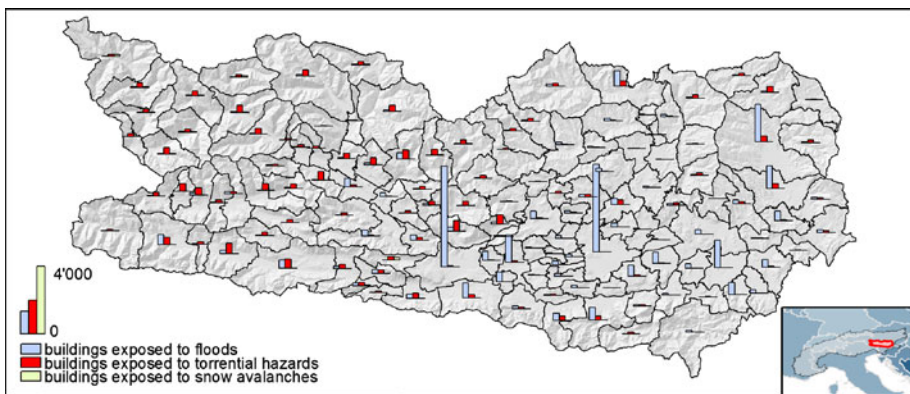


Fig. 3 Number of buildings exposed to floods, torrent hazards and avalanches in the municipalities of Carinthia

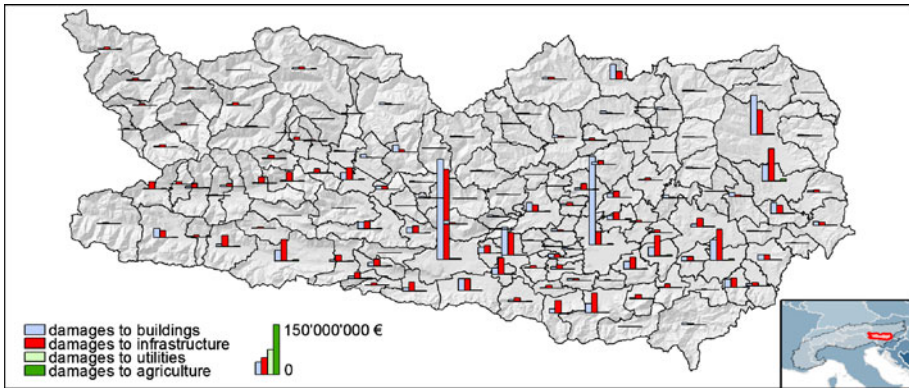


Fig. 4 Potential damage to buildings, infrastructure, utilities and agriculture due to flooding in the municipalities of Carinthia. The damage is calculated for a flood event with a return period of 100 years and is summarised at municipality level

4 Discussion and conclusions

The procedure provides the number of different classes of elements at risk exposed to floods, torrential hazards and avalanches. This comparative exposure analysis highlights the most critical processes in each municipality in Carinthia. The information is published in the form of fact sheets for each municipality, which summarise and visualise the results in a comprehensible form at municipality level. The number and units of exposed categories of elements at risk and the expected damage are values that are used in everyday management tasks and routines. The fact sheets allow a differentiated view of natural hazards at municipality level and a comparison of potential damage between different process types and between different categories of elements at risk. They therefore represent a kind of “risk portfolio” of the municipalities.

But the comparison between the different hazard types is limited, because of (1) different return periods of the hazard scenarios on which the hazard zone maps are based, (2) the spatial probability of occurrence was not considered in the exposure analysis, (3) the vulnerability of the elements at risk was not considered in the exposure analysis and (4) the spatial and temporal coherence of natural hazard events was not considered. Whereas flooding is likely occur in a greater area at the same time, debris-flow processes are in most cases spatially and temporally dispersed. This limits the comparability of the results of exposure analysis. This gap could only be bypassed by analysing the risks for all processes by means of a detailed risk analysis.

Nevertheless, the comparative exposure analysis highlights the order of dimension of elements at risk, and it is therefore suited to highlighting the hot spots in the region and in each municipality. With this, the results could provide indications for investing public funds most efficiently across administrative borders. The differentiation between damage of different categories of elements at risk makes it possible to analyse which type of stakeholder could contribute most to risk reduction. In municipalities in which damage to buildings is potentially the most relevant factor in the total sum of damages, private households can contribute significantly to risk reduction (in addition to flood protection measures). In these municipalities, raising citizens’ awareness should be supported and promoted. In this sense, the information basis provides a tool for communicating risks and

therefore for improving self-responsibility in a long-term time scale. In municipalities in which only infrastructure or utilities are affected by natural hazards, the public authorities responsible for the maintenance of the affected infrastructure should be involved in risk reduction activities.

The result of the flood risk analysis provides a tool for setting the priorities in the planning and construction of flood reduction measures. The responsible authority therefore becomes an objective decision base for the investment of public funds.

5 Outlook

With the elaborated information system, a point of origin for setting up an indicator system to monitor the effects of climate change on the natural hazard situation has been created. In Carinthia, the potential damage caused by natural hazards and the hot spots are now known. The monitoring system is able to run the procedure for different time steps, and the changes in the values have been archived. On the basis of historic data, the historic development of the damage potential and the resulting risks have been reconstructed. In future, the monitoring system will update the fact sheets once a new version of an information layer is available. If the procedure is repeated regularly after an update of the hazard maps or of the database of elements at risk, the trends in the temporal development of natural hazard risks could be monitored and highlighted. The differentiation between the temporal development of risks and elements at risk allows the extraction of an eventual climate signal. This climate signal could be evidenced in future if the trend in the development of natural hazard risks is remarkably different from the trend of the economic values of elements at risks (see Fig. 5). The factors that influence the temporal development of natural hazard risks have mostly been made evident. This leads to the identification of areas in which an increasing natural hazard risk is influenced by a climate signal and not by the increase in the economic value of elements at risk. Only in these areas, adaptation measures are necessary. With this information, the discussion of potential increases in natural risks due to climate change has been made at an objective level for a whole region. But the comparative analysis of different hazard types should in future be based on a detailed risk analysis rather than on an exposure analysis.

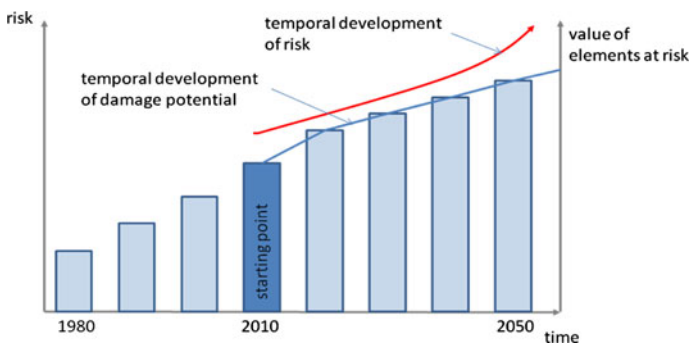


Fig. 5 Simplified concept for monitoring the temporal development of the economic values at risk and the related risks. The dark bar shows the situation of 2010, the light bars show hypothetical values of future and historic trends

Acknowledgments The work this article describes was partially financed by the project “AdaptAlp—Adaptation to Climate Change in the Alps”. The AdaptAlp project is part of the European Territorial Cooperation and co-funded by the European Regional Development Fund (ERDF) in the scope of the Alpine Space Programme www.alpine-space.eu.

References

- BMLFUW (2006a) Richtlinien für die Wirtschaftlichkeitsuntersuchung und Priorisierung von Maßnahmen der Wildbach- und Lawinerverbauung gemäß § 3 Abs. 2 Z 3 Wasserbautenförderungsgesetz 1985. Teil I: Kosten-Nutzen-Untersuchung (KNU) und standardisierte Nutzenuntersuchung. Teil II: Leitfadens-Prioritätenreihung. Wien
- BMLFUW (2006b) Richtlinien zur Gefahrenzonenplanung der Bundeswasserbauverwaltung, Fassung 2006. Wien
- BMLFUW (2008) Kosten-Nutzenuntersuchungen im Schutzwasserbau. Richtlinie, Wien
- BMLFUW (2011) die.wildbach—Richtlinie für die Gefahrenzonenplanung, BMLFUW-LE.3.3.3/0185-IV/5/2007, Fassung vom 04. February 2011. Wien. <http://www.forstnet.at/filemanager/download/71592/>. Accessed 05 April 2011
- Caspary HJ (2004) Zunahme “kritischer” Wetterlagen als Ursache für die Entstehung extremer Hochwasser in Südwestdeutschland. In: KLIWA (ed) Klimaveränderung und Konsequenzen für die Wasserwirtschaft-Fachvorträge beim KLIWA-Symposium am 3. und 4.5.2004 in Würzburg, pp 135–151
- Frei C, Schöll R, Fukutome S, Schmidli J, Vidale PL (2006) Future change of precipitation extremes in Europe: intercomparison of scenarios from regional climate models. *J Geophys Res* 111:D06105
- Fuchs S (2009) Susceptibility versus resilience to mountain hazards in Austria—Paradigms of vulnerability revisited. *Nat Hazards Earth Syst Sci* 9(2):337–352
- Fuchs S, Keiler M, Zischg A, Bründl M (2005) The long-term development of avalanche risk in settlements considering the temporal variability of damage potential. *Nat Hazards Earth Syst Sci* 5:893–901
- Fuchs S, Heiss K, Hübl J (2007) Towards an empirical vulnerability function for use in debris flow risk assessment. *Nat Hazards Earth Syst Sci* 7:495–506
- Greminger P, Zischg A (2011) Risk management and risk prevention. Final Report WP6, Alpine Space 2007–2013 project “AdaptAlp—Adaptation to climate change in the Alpine Space”. Berne. <http://www.adaptalp.org>. Accessed 05 April 2011
- Jomelli V, Pech V, Chochillon C, Brunstein D (2004) Geomorphic variations of debris flows and recent climatic change in the French Alps. *Clim Change* 64(1):77–102
- Jomelli V, Brunstein D, Grancher D, Pech P (2007) Is the response of hill slope debris flows to recent climate change univocal? A case study in the Massif des Ecrins (French Alps). *Clim Change* 85(1):119–137
- Keiler M (2004) Development of the damage potential resulting from avalanche risk in the periode 1950–2000, case study Galtür. *Nat Hazards Earth Syst Sci* 4:249–256
- Keiler M, Zischg A, Fuchs S, Hama M, Stötter J (2005) Avalanche related damage potential—changes of persons and mobile values since the mid-twentieth century, case study Galtür. *Nat Hazards Earth Syst Sci* 5:49–58
- Keiler M, Sailer R, Jörg P, Weber C, Fuchs S, Zischg A, Sauermoser S (2006) Avalanche risk assessment—a multi-temporal approach, results from Galtür, Austria. *Nat Hazards Earth Syst Sci* 6:637–651
- Keiler M, Knight J, Harrison S (2010) Climate change and geomorphological hazards in the eastern European Alps. *Phil Trans R Soc* 368:2461–2479
- PLANALP (2010) Integral natural hazard risk management: recommendations. Alpine Convention, Innsbruck
- Staffler H, Pollinger R, Zischg A, Mani P (2008) Spatial variability and potential impacts of climate change on flood and debris flow hazard zone mapping and implications for risk management. *Nat Hazards Earth Syst Sci* 8:539–558
- Zischg A (2010) Transnational collaboration in natural hazards and risk management in the Alpine Space. In: Nota G (ed) *Advances in risk management*. SCIYO, Rijeka, pp 255–270

5.4 Concluding remarks: Perspectives of coupled component modelling

Paper 28: Thaler, T., Zischg, A., Keiler, M., Fuchs, S., 2018. Allocation of risk and benefits—distributional justices in mountain hazard management. *Regional Environmental Change* 18, 353–365. [10.1007/s10113-017-1229-y](https://doi.org/10.1007/s10113-017-1229-y).

Allocation of risk and benefits—distributional justices in mountain hazard management

Thomas Thaler¹  · Andreas Zischg^{2,3} · Margreth Keiler^{2,4} · Sven Fuchs¹

Received: 22 November 2016 / Accepted: 22 September 2017

© The Author(s) 2017. This article is an open access publication, corrected publication [January/2018]

Abstract As financing protection against mountain hazards becomes increasingly challenging and therefore investments have to be prioritized, dilemmas of justice emerge: some local governments and individuals benefit from natural hazard protection schemes, whereas others loose. Decisions on whom to protect often caused contradicting concepts of political understanding, which differ in interpretations of fair resource allocation and distribution. This paper analyses the impact of different philosophical schools of social justice on mountain hazard management in Austria. We used data from a spatially explicit, object-based assessment of elements at risk and compared potential distributional effects of three political jurisdictions. We found that—depending on the respective political direction—various local governments gain and others loose within the actual distributional system of mitigation strategies. The implementation of a utilitarian policy approach would cause that high income communities in hazard-prone areas would mainly benefit. Consequently, this policy direction would encourage the public administration to ignore their own failure in the past natural hazards management and

prevention. On the other hand, following a Rawlsians approach mainly peripheral communities would gain from new policy direction who often show besides natural hazards problem mainly large socio-economic challenges. Finally, the most radical change would include the implementation of a liberalism policy, whereabouts the state only provides hazard information, but no further mitigation measures. These findings highlight the distributional consequences of future mountain hazard management strategies and point to the crucial selection of policy direction in navigating the selection of various adaptation schemes.

Keywords Social justice · Political economy · Risk reduction · Distributional consequences · Mountain hazards

Introduction

Since the beginning of 2000s, the Austrian natural hazard funding policy is following a mixture of egalitarianism and utilitarianism social justices' direction (see also Thaler and Hartmann 2016). The national government introduced to prioritise the investment based on cost-benefit analysis, where the highest benefit-cost ratio gets implemented first (Sinabell and Url 2007; BMLFUW 2009). One reason for this result is that the overall budget and the resource distribution over the federal states is mainly disaster-driven (Thaler 2014), which means that after major strikes investments for mitigation and adaptation are repeatedly shifted towards these federal states (Raschky and Weck-Hannemann 2007). However, the allocation of flood protection measures is equally distributed in terms of protection level and also in terms of funding between nine different federal states. However, several natural hazard events, such as those that occurred in 2002, 2005, and 2013 in Austria, caused high damages for the environment and

Electronic supplementary material The online version of this article (<https://doi.org/10.1007/s10113-017-1229-y>) contains supplementary material, which is available to authorized users.

✉ Thomas Thaler
thomas.thaler@boku.ac.at

¹ Institute of Mountain Risk Engineering, University of Natural Resources and Life Sciences, Vienna, Austria

² Mobiliar Laboratory for Natural Risks, Oeschger Centre for Climate Change Research, Institute of Geography, University of Bern, Bern, Switzerland

³ School of Geographical Sciences, University of Bristol, Bristol, UK

⁴ Institute of Geography, University of Bern, Bern, Switzerland

humanity, and losses for the economy (Habersack et al. 2004, 2009; Blöschl et al. 2013). This has focused the attention of policy makers and other stakeholders of how to approach the topic of natural hazard protection, which is that not everyone is threatened equally by hazard events. This has led to an increasing discussion on changes beyond that of vulnerability and natural hazards (Fuchs 2009; Giupponi and Biscaro 2015). This change has driven a transformation in the role of the state in terms of responsibility sharing and increased individual responsibilities for mitigation and adaptation (Adger et al. 2013, 2016; Thaler and Levin-Keitel 2016). Additionally, the transformation of responsibility has been encouraged with the implementation of the EU Floods Directive in 2007, such as the introduction of Areas of Potentially Significant Flood Risk (APSFR),¹ insurance companies, or international risk-averse investors which request a re-thinking of the current financial distribution within hazard management (EC 2007; BMLFUW 2011, 2014; Penning-Rowsell 2015; Husby et al. 2016). One key question refers to the problem of social justice and injustice within this new policy direction, which plays a central role in the ongoing natural hazard management policy (Collins 2010; Grineski et al. 2012).

Debates on social justices and equity in managing natural hazards and risk became more prominent in the past 10 years (Fielding and Burningham 2005; Colton 2007; Johnson et al. 2007; Walker and Burningham 2011; Thaler and Hartmann 2016). In particular, after Hurricane Katrina in 2005, various publications addressed the question about social and spatial inequality with the aim to understand the impact of natural disasters on low-income households (such as Dixon and Ramutsindela 2006; Elliott and Pais 2006; Bullard and Warf 2009; Walker and Burningham 2011). The research mainly concentrated on the question of which parts of a population (racial/ethnic or low-income individuals) are significantly higher exposed to natural hazards than others (Fielding and Burningham 2005; Colton 2007; Chakraborty et al. 2014; Grineski et al. 2015; Montgomery and Chakraborty 2015; Maldonado et al. 2016). These studies, however, strongly followed the tradition of the 1980s discourse on environmental injustices, where authors argued that environmental injustice is mainly based on the socio-economic status leading to a disproportionate and unequal exposure of individuals (Walker 2012; Harrison 2014). Similar discussion can be found in the discussion within climate justices, whereabouts the focus of

climate justices lie on unequal distribution of the effects of climate change (Schlosberg and Collins 2014; Schlosberg et al. 2017). In recent years, the research focus concentrated on the challenge of inequality within the post-event phase, such as unequal distribution of federal resources after an event in terms of psychological assistance or financial support (Elliott and Pais 2006; Munoz and Tate 2016).

The latter shifted the debate on distributional consequences (e.g., priorities, resource allocation) of current policy strategies in climate change adaptation (Holland 2017). Local climate adaptation strategies often confront the challenge of prioritisation of resources in adaptation strategies. The main reason is that some social groups are excluded from the planning and implementation process through lack of empowerment (e.g., resources or knowledge). Climate change adaptation strategies are highly technical-oriented with the goal to protect one group, which might include larger negative consequences for others (Thaler and Priest 2014; Holland 2017; Schlosberg et al. 2017). Above all studies from the UK analysed the impact of policy changes within natural hazard management on the society, to demonstrate who gains and who loses from this change (Penning-Rowsell and Pardoe 2012a, b, 2015). This debate again encouraged the question of how funding for natural hazard and risk management should be distributed within a country, and how a respective policy should look like (spatially approach). Hence, future policy might change in either direction, especially if the financial situation of a state is not strong enough to rise the share in investments of state expenditures (Thaler and Priest 2014; Thaler et al. 2016). Besides, a study by Röthlisberger et al. (2017) showed potential approaches for prioritisation in risk reduction and natural hazards management strategies in Switzerland. However, these studies are mainly ex-post oriented with the limitation to show changes from past decisions. In this paper, we provide an ex-ante view of potential impacts by government changes. In particular, to show the potential consequences and implications for the society.

Social justices in natural hazard management

The concept of justice has a broad understanding and interpretation (Elster 1992; Mill 2010; Patrick 2014). Basically, justice concerns questions on the allocation of wealth (resources), participation, and recognition across different members of a society (Schlosberg 2007). Various models and methods can be distinguished, which allow for different interpretations. Neoclassic approaches, for example, have a strong focus on fair distribution and allocation within a market system (Thaler and Hartmann 2016). Nevertheless, studies also report on injustice resulting from a combination between socio-economic and cultural injustice (Schlosberg 2007). Cultural factors

¹ The current Austrian flood risk management plan insist the prioritisation of natural hazards mitigation for Areas of Potentially Significant Flood Risk (APSFR) across the country. The designation of the Areas of Potentially Significant Flood Risk (APSFR) is mainly based on four categories: (1) number of people per river mile; (2) infrastructure; (3) industrial complexes with major accidents treats, such as Seveso II industries; and (4) cultural heritage. However, the most important variable was number of people (more than 600 per km) which counted 79% in the overall designation of the APSFR areas (BMLFUW 2015).

are reflected in discrimination of nationality, sexuality, gender, or/and ethnicity (Fraser 1995), and they are characterised in a cultural domination of one or more groups with the result of not recognising and disrespecting minor groups. Therefore, material unequal distribution reflects income and property ownership of each individual citizen. Unequal economic distribution means barriers to access at labour market, education system, and health care and also unequal access to living space with the effect that marginalised population more often inhabits hazard-prone areas based on socio-economic inequality. To overcome these effects, Honneth (2001) suggested the institutional framework as a key driver in the question of social justice and equity. As a result, social justice can be addressed as a link between ‘how, and in what way, individuals recognise on another reciprocally’ (ibid: 45), and the rules of distribution (material and cultural) are mirrors of society and their institutions. Additionally, ‘rules of distribution cannot simply be derived from the relations of production, but are rather to be seen as the institutional expression of a socio-cultural dispositive that determines in what esteem particular activities are held at a specific point in time’ (ibid: 54). Conflicts over distribution can be only understood as ‘symbolic struggles over the legitimacy of the sociocultural dispositive’ (ibid: 54). To achieve a fair distribution, the political discussion and especially institutions (formal and informal) have to be changed. Justice in natural hazard and risk management demands more than just a fair socio-economic distribution or recognition of cultural roots (Campbell 2012; May and Morrow 2012; Neal et al. 2014; Zwarteveen and Boelens 2014). Justice also relates to the process by which a certain distribution is selected (procedural justice), but this aspect is not covered by this paper. Instead, the type of justice (and philosophical tradition) discussed in this article will concern questions of allocation and distribution of resources and, further, capital and wealth across different members of society.

The key contribution of this study is to examine the potential impacts of changing the current natural hazard management policy in Austria on distributional effects in showing possible impacts of three philosophical schools (utilitarianism, Rawlsians, libertarianism, see also [appendix A](#)). The focus lies on the question of the impact on the distributional effects when following strictly one of the three philosophical schools in natural hazard management. Thus, the main aim is to demonstrate how various directions within the social justice debate potentially affect the national hazard mitigation policy in Austria. Accordingly, we focus on the question of how distributional effects can be organised within the country based on three theoretical schools within the social justice debate. The selected schools focus their key concept and main arguments around distributional effects of new

policy concepts and strategies. The key questions surrounding those problems include the following:

- What are the potential impacts of changing national risk mitigation strategies in Austria based on different justice frameworks?
- Which regions would profit from a change in the national risk mitigation strategy towards a more Rawlsians understanding of social justice?

This paper is distinguished in two main sections. The first part focuses on the theoretical discussion of social justices, which provided the analytical framework for our study. In the second part, we present results of our experimental study. The focus is on the question of distributional impacts if the Austrian natural hazard management policy would change for the period 2016–2045.

Data and methods

The study was conducted in three consecutive steps. The first step was the identification of buildings exposed to snow avalanches and flood hazards (from the year 2012). The actual state of exposure to natural hazards provided the starting point for the experimental analysis of the impacts of different policies. In the second step, we developed a method for considering the different hierarchical units in the impact analysis. On the basis of this framework, the third step included the evaluation of the outcome of each policy for the period 2016–2045.

Assessing natural hazard exposure

In this paper, assessed hazards included river and torrential flooding in mountain areas as well as snow avalanches. The Austrian legislation foresees the introduction of hazard zones in land use planning to regulate the land use development; these are mandatory mainly for the upper part of the catchments. The method for delimiting hazard zones is regulated by a national legal act (Republic of Austria 1975) and an associated decree (Republic of Austria 1976; compare Holub and Fuchs 2009). Hazard maps are based on a design event with a frequency of 1 in 150 years, and an event occurring more frequent with a return period of 1 in 10 years (ibid.). The underlying magnitude is related to the expected impact pressure and flow height, respectively. In overall, red hazard zones indicate those areas where the permanent utilisation for settlement and traffic purposes is not possible or only possible with extraordinary efforts for mitigation measures. Yellow hazard zones indicate those areas where a permanent utilisation for settlement and traffic purposes is impaired by hazard processes. However, main critique includes (i) that hazard maps show only the actual situation, without taking into account future

developments, such as process dynamics resulting from climate change (Auer et al. 2007; Keiler et al. 2010; Huggel et al. 2012) as well as (ii) that the focus is on the actual hazard extent in the respective run-out areas (mainly residential areas) and excludes a broader view of the space, e.g. with respect to agricultural land use in the drafting process of hazard maps.

We defined exposed buildings as built structures that are susceptible to mountain hazards. Therefore, we overlaid the national building inventory data with the hazard maps in a geographic information system (GIS) (Fuchs et al. 2015, 2017). The Austrian building and residents inventory was provided by the Federal Ministry of Agriculture, Forestry, Environment, and Water Management. We classified each building by 14 categories based on its main use and calculated the economic value of each building. The economic valuation is conducted by an economic module based on building type as well as average construction costs based on Kranewitter (2002) and Keiler et al. (2006). Further, the construction costs were analysed based on replacement value (Fuchs and McAlpin 2005). The dataset including the buildings, their functionality and values, and their number of residents was delineated from the Austrian residential register. This dataset and the method for processing the data are described in-depth by Fuchs et al. (2015). Each building was overlaid with the hazard maps to know the current exposure in Austria. Furthermore, we aggregated the numbers of exposed and non-exposed buildings for the areal units of local governments. With these numbers, we computed the share of exposed buildings, and the ratio of the average building values of exposed and non-exposed buildings.

Hierarchical units of analysis

For the exposure analysis, the analysis was done on an object-based level (individual house in a hazard zone), and the data were aggregated at the required level, depending on the chosen policy scenario.

- The first level refers to the building data. A building object is represented spatially by a point and has the following attributes: the type of functionality, the reconstruction value of the building, and the number of principal residents. Each building object is member of (i) an administrative unit (i.e. of a local government and of a region) and (ii) of a hazard zone.
- The second level refers to the hazard zones in Austria. A hazard zone is represented by a polygon. The different classes of hazard zones (red and yellow zones depending on the process intensities) and overlapping or neighbouring hazard zones are merged into one polygon representing a hazard zone. Therefore, the hazard process type and the process intensities are not differentiated in this study. A hazard zone polygon is member of an

administrative unit (of a local government and of a region) and provides the reference unit for the future investigation in our analysis.

- The third level refers to the local administrative unit. The main aggregation and reference unit is the smallest administrative unit at local level, i.e. the area of responsibility of a local government. All financial projects invested in risk prevention at hazard zone level are summed up at local level.

With this topological setting, the analysis was done on an object-based level (individual house in a hazard zone), and the data were aggregated at the required level, depending on the chosen policy scenario.

Implementation of policy scenarios

The concept of utilitarianism, developed by classical economists, such as John Stuart Mill and Graham Bentham, understands justice and equity as the sum of individual benefits. The aim of utilitarianism is to ‘maximise the total potential happiness of society as a whole through the aggregation of individual happiness’ (Johnson et al. 2007: 376). Thereby, the focus is on benefits of each individual (Bartel 2002), and consequently, policy discussion should ensure maximal benefit of society (‘greatest benefit to the greatest number’, Hunold and Young 1998: 84). In natural hazard management, utilitarianism develops criteria which should be chosen to secure the highest risk reduction per unit of resource input. Natural hazard risk management strategies provided to those areas within country, where the benefits offer the greatest gain to the society (Johnson et al. 2007).

Rawls (2005) defined justice as the equal distribution of basic rights and duties within a society. Justices will be defined by the society, who defines a common understanding of what social justice is, as well as which actions insurance the basic needs for each individual within the society. Based on this understanding, Rawls tolerates injustices, if unequal developments in society increase the overall benefit (wealth) of a society. However, if the outcome reflects injustice, individuals will not be punished/discriminated in another aspect. Referring to natural hazard and risk management, an application of Rawls’ concept of justice requests to distribute resources to most vulnerable people and objectives (Johnson et al. 2007). Therefore, the key objective is to select risk management strategies not only and inevitably for high-value assets and areas of high-value aggregation (Johnson et al. 2008).

The main focus of liberalism is in general a concept of free market thinking, with a particular focus on competition, availability of full information, equilibrium in market processes, and freedom of individual self-decision (economic freedom, Hayek 1991; Harrison 2014). Key aspects include the availability of full information, which are mainly pre-defined rules

equally to each individual (Hayek 1991). The allocation of goods and services is based on equilibrium (Pareto) principles. In natural hazard management policy, the strategies are organised and planned by the sum of individual preferences which are based on rational choice decisions (Varian 1975; Harvey 1999; Bowen and Wells 2002). Consequently, there is a limited influence of the public sector on the natural hazard management policies. As a result, the state would be reduced towards providing hazard information to individuals (Thaler and Hartmann 2016), but the individuals have to manage their risk individually, such as through local structural protection measures or insurance (Holub and Fuchs 2009; Penning-Rowsell 2015). The overlaying and aggregation procedures depend on the respectively policy scenario.

Utilitarianism

For the first policy scenario (utilitarianism), we conducted the following steps:

1. The hazard maps were overlaid with the building dataset.
2. For each hazard zone, we summed up the reconstruction values of the exposed buildings.
3. Hazard maps with the aggregated exposed building values were sorted in a descending order. This resulted in a priority list for investments by the sum of exposed values at risk per hazard zone.
4. It was assumed that following the priority list, in each year, the buildings in a specific number of hazard zones would be protected by defence structures. We assumed a total number of 60 projects² per year for a period of 30 years (2016–2045).
5. At the end of the period, the number of new protection schemes invested following the priority list was summed up at local level. A principal assumption in this study is that from now until the end of the reference period, no more houses will be built in exposed areas. Risk reduction measures will be focused on existing exposed assets only. This showed spatial locations where investment in natural hazard management would be distributed in 30 years following this policy.

Rawlsians

For the second policy scenario (Rawlsians), we conducted the following steps:

² The Austrian Torrent and Avalanche Control Authority invests between 60 and 70 million € per year in new protection measures (BMF 2016). We assumed that an average cost of 1 mio. € for a project that reduces the hazards in one single hazard zone. The government implemented 60 mitigation strategies per hazard zone per year.

1. The hazard maps were overlaid with the buildings dataset.
2. Local governments were classified by their vulnerability. Because there is no dataset for classifying the vulnerability and the coping capacity of the Austrian local governments, respectively, we elaborated simple indicators for a vulnerability classification (Papathoma-Köhle et al. 2017). We used more than one indicator to demonstrate challenges and uncertainties within the decision-making process. The first indicator (i) was the share of the number of exposed buildings in comparison to the total number of buildings per local authority (Fuchs et al. 2015). The higher the number of exposed buildings was in relation to the total number of buildings within the local government, the higher was the vulnerability. As a second indicator, we selected the share of the sum of exposed building values to the total sum of monetary building values (ii) for each local government (Fuchs et al. 2017). The third indicator was based on the average monetary value of the exposed buildings compared to the average monetary value of all buildings in each local government (iii). A value > 1 means that exposed buildings are more costly than the average of all buildings in the local government. A value < 1 means that the exposed buildings are less worth than the average of the total building stock in the local authority. The highest ranking in terms of vulnerability had the local government with the lowest value for this indicator. It is assumed that local government where the exposed buildings have a lower monetary value than the average are more vulnerable than others. Hence, this indicator represents an important factor to classify social vulnerability of each local government (Cutter et al. 2003). The local government were classified and ranked by each of these three indicators in a descending order.
3. Classification of the vulnerability of Austrian local governments for the Rawlsians policy is depending on how we define vulnerability. In this paper, we distinguish between three different possibilities: option a, classification based on the share between the number of exposed buildings and the total number of buildings; option b, classification based on the sum of exposed building values to the total sum of monetary building values; and option c, classification based on the mean monetary value of the exposed buildings in comparison to the mean monetary value of all buildings in the respective local authority.
4. As for the utilitarianism approach, we assumed that 60 projects for natural hazard risk reduction would be financed per year and invested accordingly to the priority list based on step 2.
5. At the end of the period, the investments following the priority list of vulnerable local governments were

summed up at local level. This shows the distributional effects in the 30 years period.

Liberalism

For the third policy scenario (liberalism), we assume that the Austrian natural hazards system change towards a self-oriented risk management policy; including no public funding from the national government. The citizens living in the hazard-prone areas have to organise their individual protection scheme. For the third policy scenario (Liberalism), we conducted the following steps:

1. The hazard maps were overlaid with the buildings dataset.
2. We elaborated a map of the exposed building values, aggregated at the level of the local governments. This map—together with the hazard maps—should provide the information of the relevance of natural hazards for the public and for stakeholders in the economy.
3. Evaluation of distribution of hazard maps in Austria.

Results

Current situation in the Austrian natural hazards management

Figure 1 provides information on the monetary values exposed to mountain hazards. The datasets of exposed buildings, monetary values, and residents provided the input for the analyses of distributional effects. The highest monetary values of buildings exposed to mountain hazards—except from a few outliers—can be found among touristic hotspots in Austria, mainly in the Federal states of Salzburg and Tyrol, where many tourist infrastructure in the various skiing areas can be found in hazard-prone areas (Fuchs et al. 2015). The starting point for the model experiment is shown in Fig. 1. In overall, out of a total of 2,399,500 buildings, 120,682 buildings are exposed to mountain hazards within 9978 hazard zones distributed across the nine Federal States. Based on the topography and the characteristic geomorphic processes acting on the land surface, the eastern part of Austria shows a low number of hazard zones defined under the degree of hazard zoning (Republic of Austria 1976) compared to the western part.

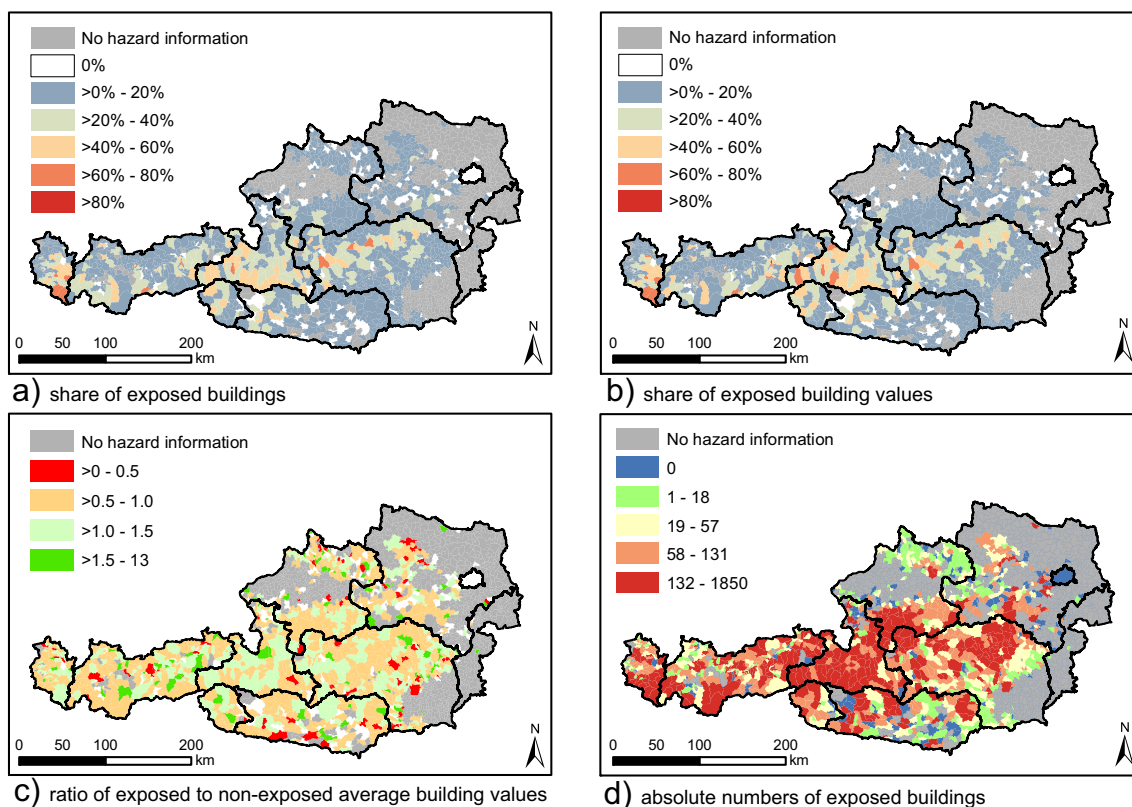


Fig. 1 The actual state of exposure to mountain hazards and the starting point of the experimental study for the policy impact analysis. **a** The share of exposed buildings to the total number of buildings in the administrative units of the local governments in Austria. **b** The share of the exposed building values to the total building values. The highest shares are found in the central and western parts of the country (especially in the federal

states Salzburg, Tyrol, and Vorarlberg). **c** The spatial distribution of the ratio of average building values. Local governments with an average building value of exposed buildings less than the average building value within the areal unit are preferably located in rural and remote areas. In **d**, the absolute numbers of exposed buildings are shown (quantiles)

Spatial distribution of funding under a utilitarianism policy framework

The implication of the introduction of a strict utilitarianism policy approach within the Austrian natural hazard management system would have large impacts on the current funding distribution in Austria. The system would look like the English flood risk management policy (Johnson et al. 2007; Thaler and Hartmann 2016). In Fig. 2, the spatial and temporal analysis of the distribution of funding for the Austrian mountain hazards policy is presented. Between 2016 and 2045, the utilitarianism approach would allow investments into 1800 projects to reduce future impacts of hazard events. At the end of the period, 83,848 buildings with 264,285 residents and with roughly 46.7 billion € of building values would have gained from this policy in terms of the implementation of new structural protection measures. The mean stock of assets secured per hazard zone is about 256 million €. The range of choice for the Austrian investment projects show that the concentration of funding would be mainly around the touristic hot spots in Austria (federal state of Salzburg and Tyrol) as well as the federal state of Styria, where a large amount of residential and industrial buildings can be found in hazard-prone areas. On the other hand, the federal states of Vorarlberg, Lower and Upper Austria would loose from the new direction within the funding policy. The main reason is the settlement pattern in these federal states, where building pattern are more dispersed in contrast to other federal states in Austria.

Remarkable differences emerged between the different local governments in Austria. Analysing the local level, the

main winners of this policy would be local governments in Salzburg and Tyrol, such as (1) Sankt Leonhard im Pitztal (federal state of Tyrol) with 15 projects for the period 2016–2045, (2) Kapfenberg (federal state of Styria) with 11 projects for the period 2016–2045, (3) Bad Hofgastein (federal state of Salzburg) for 10 projects for the period 2016–2045, and (4) Kappl (federal state of Tyrol) with 10 projects for the same period. Key targets are again the touristic hotspots in Austria, where the tourism sector has the main contribution to the local economy, except of the city of Kapfenberg. The local authority Kapfenberg includes a large amount of residential buildings as well as industry complexes in the hazard-prone areas. Using the relative relationship (number of projects to the total number of hazard zones in the federal state), the main winners would be the Federal State of Salzburg followed by the federal states of Tyrol and Carinthia (see Table 1).

Spatial distribution of funding under a Rawlsians policy framework

Analysing the distributional effects under the Rawlsians policy estimates different results in dependence on the selection of indicators. In Fig. 2 and Table 1, the potential implications for the Austrian natural hazard policy are presented. Like the utilitarianism policy framework, under the Rawlsians system, the Austrian government would realise 1800 projects across the country within the time period between 2016 and 2045. By the end of this period, in overall under Rawl's investment policy, the government would protect 157,603, 155,264, and 71,547 residents based on the option a, b, and c.

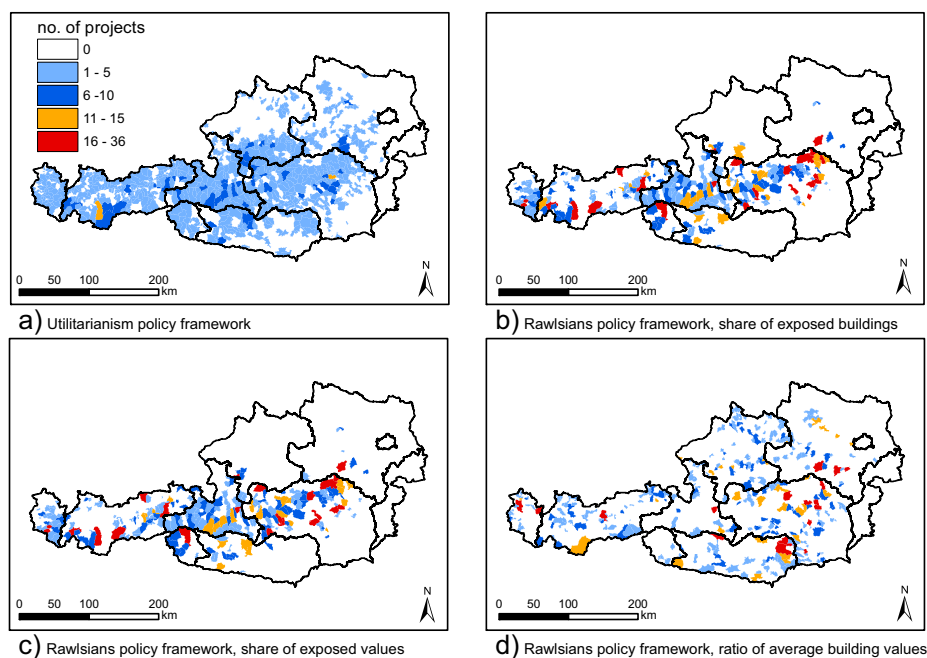


Fig. 2 Sum of projects invested in local governments following **a** the utilitarianism policy framework for investments in risk reduction measures in the period 2016–2045 in Austria and **b**, **c**, **d** the Rawlsians policy framework in the period 2016–2045 in Austria

Table 1 Number of projects invested in the communities following the utilitarianism and Rawlsians policy in the period 2016–2045 in Austria, aggregated on regional level

Federal State	Utilitarianism	Rawlsians		
	% No. of projects in comparison to total hazard zones in the region	No. of projects in comparison to total hazard zones in the region for option (a) [%]	No. of projects in comparison to total hazard zones in the region for option (b) [%]	No. of projects in comparison to total hazard zones in the region for option (c) [%]
Burgenland	12.50	13.11	14.89	27.60
Carinthia	17.40	5.13	5.85	21.23
Lower Austria	15.70	48.21	46.77	17.74
Upper Austria	12.90	22.77	22.77	19.19
Salzburg	47.80	22.57	22.81	13.89
Styria	14.00	4.44	3.19	19.38
Tyrol	23.10	0.00	0.00	0.00
Vienna	0.00	14.92	15.03	10.59
Vorarlberg	14.10	13.11	14.89	27.60

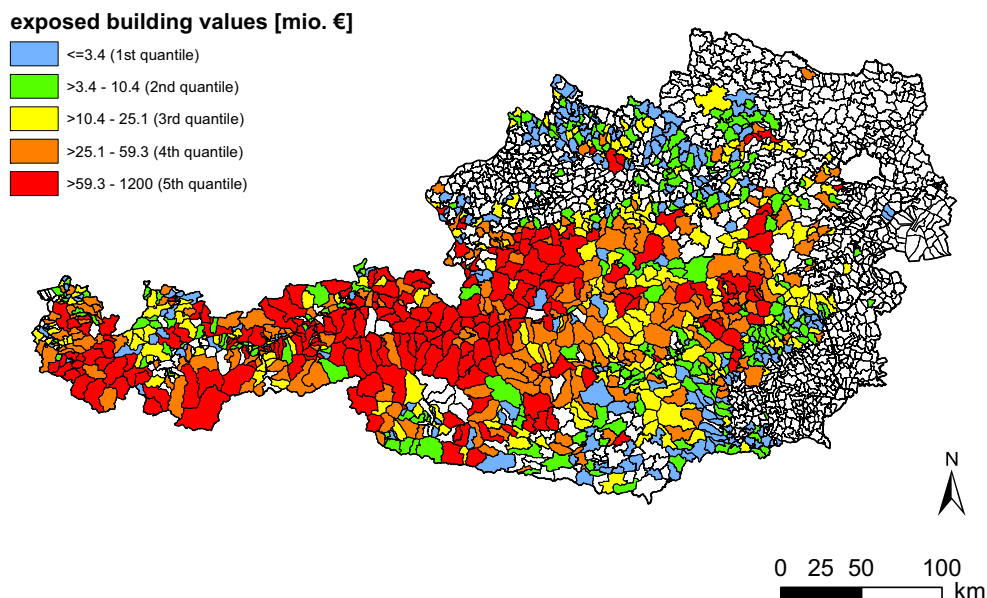
In terms of building reconstruction values, the Rawlsians funding policy would protect 28.5, 29.4 respectively 9.5 billion €. Following the different policy options, the results show a wide range of spatial distribution within the funding system. In particular, selecting option c in the distribution of funding would refer mainly to peripheral local governments with a lower economic activity and with a strong focus on agriculture, respectively. Large differences were also found at regional scale in the relative comparison between numbers of projects and total hazard zones (Table 1). Under options a and b, the main winners would be the federal states of Lower Austria, Salzburg, and Styria. The numbers and consequently the spatial distribution of profiteers drastically change if option c is chosen, which would distribute the funding towards the federal states of Burgenland, Tyrol, and Vorarlberg. Such disparities in the results strongly depend on the method chosen and show that these federal states have mainly buildings with a low value at risk in hazard-prone areas.

Looking at the local scale, options a and b showed similar results in terms of the locations benefitting from this policy perspective (Stumm and Fügen in the federal state of Tyrol, St. Anton im Montafon and Innerbraz in the federal state of Vorarlberg). The main reason for this similarity is the large number of detached houses, moreover, tourism dominates areas which results in a high number of exposed hotels. On the other hand, option c would move the funding towards low-income families in hazard-prone areas, such as householders in the local governments Zell am Ziller (federal state of Tyrol), Stolzalpe (federal state of Styria), Mannersdorf am Leithagebirge (federal state of Lower Austria), and St. Jakob im Rosental (federal state of Carinthia). Main winners would be local governments in former industrial areas with structural economic problems or peripheral-rural areas.

Spatial distribution of funding under a liberalism policy framework

Hazard reduction under a liberalism approach would throughout restructure the Austrian natural hazards system towards a self-oriented risk management policy, including strengthening of self-responsibility (Holub and Fuchs 2009). A first transformation would refer to the implementation of a free market mechanism in terms of compensation, such as the introduction of risk-based insurance systems without public compensation and subvention (Ungern-Sternberg 2004; Fuchs 2009). A second change would affect the realisation of structural measures such as investments in flood-proofing measures instead of large embankments and would transfer the responsibility to individual householders. Consequently, this step would reframe the question of who pays and who gains, because only house owners in hazard-prone zones would have to invest in natural hazard management (Fig. 3). A third change would refer to the provision of information. Hayek (1991), for example, had foreseen the availability and provision of full information as the central characteristic for individual decision behaviour. This means that hazard information has to be very transparent and has to show the individual risk at each location (at individual building level) within the country (Penning-Rowse 2015). In Austria, for example, such policy would require the design of local-scale hazard and object-specific risk maps. So far, this kind of information is partly available for the country. Nevertheless, various federal states in the eastern part of Austria show a lack of realisation of local-scale hazard maps providing the basis for elaborating risk maps (see also appendix B). The challenge might be that the public administration cannot ensure the necessary information for the individuals.

Fig. 3 Reconstruction values of buildings exposed to mountain hazards in Austria



Discussion

Implications of different national risk mitigation strategies

In overall, the existing Austrian system of natural hazard and risk management ensures a high level of protection which is equally distributed within the country (Thaler and Hartmann 2016). Nevertheless, the analyses and the debate of the distributional consequences were largely ignored in the current policy, such as in many other countries (Penning-Rowsell and Pardoe 2015). However, in the past years, we observe a first change in the Austrian natural hazard management system, which is mainly based on various interests and external developments, such as the implementation of EU legislation (EC 2007), an increase of exposed buildings within hazard-prone areas in some regions of the country (Fuchs et al. 2015, 2017) and economic and financial crises with the consequence of a change within the current spatial distribution on subsidies for natural hazard mitigation. This paper debated and showed the potential implications if the national government would shift the current system towards a more risk-based and vulnerability-based policy, respectively. Such a shift would have large implications for the different householders (positively and negatively depending on the new policy direction). The access to state-provided funding for natural hazard management under a utilitarianism framework would implicate that economic attractive local governments, especially in the tourism hotspots of Austria, would again gain mainly from this policy direction. The resulting governmental focus on high building values in hazard-prone areas would be on one side understandable; on the other hand, the government would encourage the increase of potential losses (Fuchs et al. 2015, 2017). This would generate a situation of moral hazard within

the society, because the Austrian policy so far is based on cost-benefit analysis when structural mitigation is implemented, which results in securing clusters of high values by structural protection measures (Tarlock 2012). Rawlsian justices as fairness funding policy would instead focus the distribution towards the most vulnerable groups within the society (Cutter et al. 2003; Johnson et al. 2007; Thaler and Hartmann 2016). A central question remains who are the most vulnerable within a society (Cutter 2003; Wisner et al. 2004; Fuchs et al. 2007). In general, focussing on the average building value (option c average monetary value of the exposed buildings), householders with low building values would gain mainly from the new policy direction. The outcome demonstrates that peripheral local governments would benefit disproportionately from new structural protection measures. Such a governmental activity would protect householders who are often socially excluded and have a lack of opportunity to protect themselves (Jacobs 1961; Sen 2010; Lejano and Funderburg 2016). However, if the Austrian government would choose option a (number of exposed buildings) or b (sum of the exposed building values) of the Rawlsian approach, the results provide a different picture. The public authorities would be able to provide protection schemes for higher building values and would secure similar local governments like the utilitarianism, which contradicts the original idea of Rawls to provide a concept of social justices as an alternative to the ideas from Graham Bentham and John Stuart Mill (Lyons 1972; Zerbe and Plotnick 1988). The main reason is that within options a and b, the local governments allowed in the past high-value buildings to be constructed in hazard-prone areas in contrast to option c, where high-value buildings, such as hotels or commercial buildings, were built outside the hazard zones. Consequently, this policy direction would encourage the

public administration to ignore their own failure in natural hazards management (Jongman et al. 2012, 2014; Fuchs et al. 2017; Röthlisberger et al. 2017). Lastly, the implementation of a liberalism understanding within the Austrian natural hazard management policy would be the most radical shift within the society in terms of responsibility (Johnson and Priest 2008; Thaler and Priest 2014; Mostert 2015; Reese and Jacob 2015). The central responsibility within the natural hazard management discourse would be organised by individuals instead of the public administration. The changes would request that the private property owners have to strengthen the individual resilience capacity to response to future natural hazard events, also in terms of collecting information about the risk (Djordjevic et al. 2011; Kuhlicke et al. 2011; Babčický and Seebauer 2017). The consequences were that main losers would be householders with a high social vulnerability and a low individual capacity to response to natural hazard events (Chakraborty et al. 2014; Montgomery and Chakraborty 2015; Maldonado et al. 2016) or especially tenants without any possibilities for implementing risk reduction measures, while utilitarian and libertarian principles show similar static implications. Although the latter indicate less financial resources from public administration dedicated for mitigation, there is clearly a different dynamic implication. Utilitarian framework would incentivise building on risky places, while the libertarian principle would deter it and possibly alter relative value of properties.

Limitations of the study

However, the results have to be interpreted under consideration of the main limitations. Firstly, the experiment is based on a static assumption, i.e. the building stock is assumed to be static over the time period, while in reality, it is remarkably dynamic (Fuchs et al. 2013). Future improvements may consider the growing building stock (exposed and non-exposed buildings). With a growing building stock, the indicators and therefore the priority lists may change over time and a monitoring of the development may be required to continuously adapt the policy (e.g. as proposed by Zischg et al. 2013). Furthermore, the hazard zones will change over time because of changes in the flood defence structures or because of climatic changes (e.g. Staffler et al. 2008; Keiler et al. 2010).

Conclusion

This study examined the different impacts of different social justice traditions might change the spatial distribution of funding for natural hazard protection schemes. This implicates a strong political debate on the question whom to protect, or on differentiating between upstream and downstream local governments

or different economic or cultural regions, which raises a central but barely discussed conflict: who (or rather what) should be protected against hazard events with highest priority? Such changes showed not only a transformation within the public administration but also affected the individual behaviour in responding to natural hazard events. Consequently, our key findings showed several implications not only for the national policy on natural hazard management in Austria but also for the discussion on social justices. We found that depending on the selection of philosophical tradition, the winners and losers will remarkably change. For instance, prioritisation of structural protection measures based on utilitarianism would mainly support the tourism hotspots as well as industrial complexes in the mountain areas. The consequences would be that the public administration would acknowledge and encourage constructing new and more high-value buildings in hazard-prone areas. This would result in an increase of potential losses across the country. On the other hand, focus on the most vulnerable groups (based on mean values of buildings) would mainly support local governments in peripheral areas. As such, this policy would mainly support the main losers from a utilitarianism economic thinking. Yet, the number of individuals who gain from this policy would be much lower in comparison to the other potential options. But in the end, the main question is if the selected philosophical traditions used in this paper should be adopted by the Austrian natural hazards management system, or if disaster risk reduction in Austria needs different/additional instruments and supports. Therefore, the selected approach for the future policy requires not only a scientific but also a political debate. In this way, both the requirements of the EU floods directive and the overall aim to decrease vulnerability and increase resilience for the reduction of social exclusion may be considered.

Acknowledgements Open access funding provided by University of Natural Resources and Life Sciences Vienna (BOKU). This project has been funded by the Austrian Climate and Energy Fund project SHARED (project number KR16AC0K13268). The authors kindly acknowledge data provision by the Austrian Federal Ministry of Agriculture, Forestry, Environment, and Water Management. Furthermore, we would like to thank the two anonymous reviewers for their valuable comments and suggestions to an earlier version of this paper.

Open Access This article is distributed under the terms of the Creative Commons Attribution 4.0 International License (<http://creativecommons.org/licenses/by/4.0/>), which permits unrestricted use, distribution, and reproduction in any medium, provided you give appropriate credit to the original author(s) and the source, provide a link to the Creative Commons license, and indicate if changes were made.

References

- Adger N, Quinn T, Lorenzoni I, Murphy C (2016) Sharing the pain: perceptions of fairness affect private and public response to hazard. *Annals of American Association of Geographers* 5:1079–1096. <https://doi.org/10.1080/24694452.2016.1182005>

- Adger N, Quinn T, Lorenzoni I, Murphy C, Sweeney J (2013) Changing social contracts in climate-change adaptation. *Nat Clim Chang* 3: 330–333. <https://doi.org/10.1038/nclimate1751>
- Auer I, Böhm R, Jurkovic A, Lipa W, Orlik A, Potzmann R, Schöner W, Ungersböck M, Matulla C, Briffa K, Jones P, Efthymiadis D, Brunetti M, Nanni T, Maugeri M, Mercalli L, Mestre O, Moisselin JM, Begert M, Müller-Westermeier G, Kveton V, Bochnicek O, Stastny P, Lapin M, Szalai S, Szentimrey T, Cegnar T, Dolinar M, Gajic-Capka M, Zaninovic K, Mastorovic Z, Nieplova E (2007) HISTALP—Historical instrumental climatological surface time series of the Greater Alpine Region. *Int J Climatol* 27:17–46. <https://doi.org/10.1002/joc.1377>
- Babcicky P, Seebauer S (2017) The two faces of social capital in private flood mitigation: opposing effects on risk perception and response capacity. *J Risk Res* 20:1017–1037. <https://doi.org/10.1080/13669877.2016.1147489>
- Bartel R (2002) Neo-/Liberalismus und öffentliche Finanzen. *Das Öffentliche Haushaltswesen Österreich* 43:26–45
- Blöschl G, Nester T, Komma J, Parajka J, Perdigo RAP (2013) The June 2013 flood in the Upper Danube Basin, and comparisons with the 2002, 1954 and 1899 floods. *Hydrol Earth Syst Sci* 17:5197–5212. <https://doi.org/10.5194/hess-17-5197-2013>
- BMF (2016): Bundesfinanzgesetz 2016 und Detaildokumente. https://service.bmf.gv.at/BUDGET/Budgets/2016/bfg/teilhefte/_start_teilhefte.htm [last access: 15/08/2016]
- BMLFUW (2009): Kosten-Nutzen-Untersuchungen im Schutzwasserbau. Richtlinie. Vienna: Bundesministerium für Land- und Forstwirtschaft, Umwelt und Wasserwirtschaft
- BMLFUW (2011): Vorläufige Bewertung des Hochwasserrisikos 2011. Bericht zur Umsetzung in Österreich. Vienna: Bundesministerium für Land- und Forstwirtschaft, Umwelt und Wasserwirtschaft
- BMLFUW (2014) Maßnahmenkatalog des Hochwassermanagementplans. Bundesministerium für Land- und Forstwirtschaft, Umwelt und Wasserwirtschaft, Vienna
- BMLFUW (2015): Nationaler Hochwasserrisikomanagementplan. RMP 2015. Vienna: Bundesministerium für Land- und Forstwirtschaft, Umwelt und Wasserwirtschaft
- Bowen WM, Wells MV (2002) The politics and reality of environmental justice: a history and considerations for public administrators and policy makers. *Public Adm Rev* 62:688–698. <https://doi.org/10.1111/1540-6210.00251>
- Bullard RD, Wright B (2009) Race, place, and environmental justice after Hurricane Katrina: struggles to reclaim, rebuild, and revitalize New Orleans and the Gulf coast. Westview Press, Boulder, CO
- Campbell T (2012) Theories of justice. Ashgate, Farnham
- Chakraborty J, Collins TW, Montgomery MC, Grineski SE (2014) Social and spatial inequities in exposure to flood risk Miami, Florida. *Nat Hazard Rev* 15:04014006. [https://doi.org/10.1061/\(ASCE\)NH.1527-6996.0000140](https://doi.org/10.1061/(ASCE)NH.1527-6996.0000140)
- Collins TW (2010) Marginalization, facilitation, and the production of unequal risk: the 2006 Paso Del Norte floods. *Antipode* 42:258–288. <https://doi.org/10.1111/j.1467-8330.2009.00755.x>
- Colton C (2007) Environmental justice in a landscape of tragedy. *Technol Soc* 29:173–179. <https://doi.org/10.1016/j.techsoc.2007.01.006>
- Cutter S (2003) The vulnerability of science and the science of vulnerability. *Ann Assoc Am Geogr* 93:1–12. <https://doi.org/10.1111/1467-8306.93101>
- Cutter SL, Boruff BJ, Shirley WL (2003) Social vulnerability to environmental hazards. *Soc Sci Q* 84:242–261. <https://doi.org/10.1111/1540-6237.8402002>
- Dixon J, Ramutsindela M (2006) Urban resettlement and environmental justice in Cape Town. *Cities* 23:129–139. <https://doi.org/10.1016/j.cities.2005.08.003>
- Djordjevic S, Butler D, Gourbesville P, Ole E, Pasche E (2011) New policies to deal with climate change and other drivers impacting on resilience to flooding in urban areas: the CORFU approach. *Environ Sci Pol* 14:864–873. <https://doi.org/10.1016/j.envsci.2011.05.008>
- EC (2007) Directive 2007/60/EC of the European Parliament and of the Council of 23 October 2007 on the assessment and management of flood risks. European Parliament, Brussels
- Elliott JR, Pais J (2006) Race, class, and Hurricane Katrina: social differences in human responses to disaster. *Soc Sci Res* 35:295–321. <https://doi.org/10.1016/j.ssresearch.2006.02.003>
- Elster J (1992) Local justice: how institutions allocate scarce goods and necessary burdens. Russell Sage Foundation, New York
- Fielding J, Burningham K (2005) Environmental inequality and flood hazard. *Local Environ* 10:379–395. <https://doi.org/10.1080/13549830500160875>
- Fraser N (1995): From redistribution to recognition? Dilemmas of justice in a ‘post-socialist’ age. *New Left Review* 1/212
- Fuchs S (2009) Susceptibility versus resilience to mountain hazards in Austria—paradigms of vulnerability revisited. *Nat Hazards Earth Syst Sci* 9:337–352. <https://doi.org/10.5194/nhess-9-337-2009>
- Fuchs S, Heiss K, Hübl J (2007) Towards an empirical vulnerability function for use in debris flow risk assessment. *Nat Hazards Earth Syst Sci* 7:495–506. <https://doi.org/10.5194/nhess-7-495-2007>
- Fuchs S, Keiler M, Sokratov S, Shnyarkov A (2013) Spatiotemporal dynamics: the need for an innovative approach in mountain hazard risk management. *Nat Hazards* 68:1217–1241. <https://doi.org/10.1007/s11069-012-0508-7>
- Fuchs S, Keiler M, Zischg A (2015) A spatiotemporal multi-hazard exposure assessment based on property data. *Nat Hazards Earth Syst Sci* 15:2127–2142. <https://doi.org/10.5194/nhess-15-2127-2015>
- Fuchs S, McAlpin MC (2005) The net benefit of public expenditures on avalanche defence structure in the municipality of Davos, Switzerland. *Nat Hazards Earth Syst Sci* 5:319–330. <https://doi.org/10.5194/nhess-5-319-2005>
- Fuchs S, Röthlisberger V, Thaler T, Zischg A, Keiler M (2017) Natural hazard management from a co-evolutionary perspective: exposure and policy response in the European Alps. *Ann Am Assoc Geogr* 107:382–392. <https://doi.org/10.1080/24694452.2016.1235494>
- Giupponi C, Biscaro C (2015) Vulnerabilities—bibliometric analysis and literature review of evolving concepts. *Environ Res Lett* 10:123002. <https://doi.org/10.1088/1748-9326/10/12/123002>
- Grineski SE, Collins TW, Chakraborty J, Montgomery MC (2015) Hazardous air pollutants and flooding: a comparative interurban study of environmental injustice. *GeoJournal* 80:145–158. <https://doi.org/10.1007/s10708-014-9542-1>
- Grineski SE, Collins TW, Ford P, Fitzgerald R, Aldouri R, Velazquez-Angulo G, de Lourdes Romo Aguilar M, Lu D (2012) Climate change and environmental injustice in a bi-national context. *Appl Geogr* 33:25–35. <https://doi.org/10.1016/j.apgeog.2011.05.013>
- Habersack H, Bürgel J, Kanonier A (2009) FloodRisk II Vertiefung und Vernetzung zukunftsweisender Umsetzungsstrategien zum integrierten Hochwassermanagement, Synthese. Eigenverlag Bundesministerium für Land- und Forstwirtschaft, Umwelt und Wasserwirtschaft, Vienna
- Habersack HM, Bürgel J, Petraschek A (2004) Analyse der Hochwasserereignisse vom August 2002—Floodrisk, Synthese. Eigenverlag Bundesministerium für Land- und Forstwirtschaft, Umwelt und Wasserwirtschaft, Vienna
- Harrison JL (2014) Neoliberal environmental justice: mainstream ideas of justice in political conflict over agricultural pesticides in the United States. *Environmental Politics* 23:650–669. <https://doi.org/10.1080/09644016.2013.877558>
- Harvey D (1999) The environment of justice. In: Fischer F, Hajer M (eds) *Living with nature: environmental politics as cultural discourse*. Oxford University Press, Oxford, pp 153–185
- Hayek FA (1991) *The road to serfdom*. Routledge, London

- Holland B (2017) Procedural justice in local climate adaptation: political capabilities and transformational change. *Environmental Politics* 26: 391–412. <https://doi.org/10.1080/09644016.2017.1287625>
- Holub M, Fuchs S (2009) Mitigating mountain hazards in Austria—legislation, risk transfer, and awareness building. *Nat Hazards Earth Syst Sci* 9:523–537. <https://doi.org/10.5194/nhess-9-523-2009>
- Honneth A (2001) Invisibility: on the epistemology of ‘recognition’. *Aristotelian Society Supplementary* 75:111–126. <https://doi.org/10.1111/1467-8349.00081>
- Huggel C, Clague J, Korup O (2012) Is climate change responsible for changing landslide activity in high mountains? *Earth Surf Process Landf* 37:77–91. <https://doi.org/10.1002/esp.2223>
- Hunold C, Young IM (1998) Justice, democracy, and hazardous siting. *Political Studies* 46:82–95. <https://doi.org/10.1111/1467-9248.00131>
- Husby TG, Mechler R, Jongman B (2016) What if the Dutch started worrying about flood risk? Implications for disaster risk reduction. *Reg Environ Chang* 16:565–574. <https://doi.org/10.1007/s10113-015-0769-2>
- Jacobs J (1961) *The death and life of great American cities*. Random House, New York
- Johnson C, Penning-Rowsell E, Parker D (2007) Natural and imposed injustices: the challenges in implementing ‘fair’ flood risk management policy in England. *Geogr J* 173:374–390. <https://doi.org/10.1111/j.1475-4959.2007.00256.x>
- Johnson C, Priest S (2008) Flood risk management in England: a changing landscape of risk responsibility. *Int J Water Resour Dev* 24:513–525. <https://doi.org/10.1080/07900620801923146>
- Johnson C, Tunstall S, Priest S, McCarthy S, Penning-Rowsell E (2008) Social justice in the context of flood and coastal erosion risk management: a review of policy and practice. Department for Environment, Food & Rural Affairs, London
- Jongman B, Koks EE, Husby TG, Ward PJ (2014) Increasing flood exposure in the Netherlands: implications for risk financing. *Nat Hazards Earth Syst Sci* 14:1245–1255. <https://doi.org/10.5194/nhess-14-1245-2014>
- Jongman B, Ward PJ, Aerts JCJH (2012) Global exposure to river and coastal flooding: Long term trends and changes. *Glob Environ Chang* 22:823–835. <https://doi.org/10.1016/j.gloenvcha.2012.07.004>
- Keiler M, Knight J, Harrison S (2010) Climate change and geomorphological hazards in the eastern European Alps. *Phil Trans R Soc A* 368:2461–2479. <https://doi.org/10.1098/rsta.2010.0047>
- Keiler M, Zischg A, Fuchs S (2006) Methoden zur GIS-basierten Erhebung des Schadenspotentials für naturgefahreninduzierte Risiken. In: Strobl J, Roth C (eds) *GIS und Sicherheitsmanagement*. Wichmann, Heidelberg, pp 118–128
- Kranewitter H (2002) *Liegenschaftsbewertung*. Gescio-Publisher, Vienna
- Kuhlicke C, Steinführer A, Begg C, Bianchizza C, Bründl M, Buchecker M, De Marchi B, Di Masso Tarditti M, Höppner C, Komac B, Lemkow L, Luther J, McCarthy S, Pellizzoni L, Renn O, Scolobig A, Supramaniam M, Tapsell S, Wachinger G, Walker G, Whittle R, Zorn M, Faulkner H (2011) Perspectives on social capacity building for natural hazards: outlining an emerging field of research and practice in Europe. *Environ Sci Pol* 14:804–814. <https://doi.org/10.1016/j.envsci.2011.05.001>
- Lejano RP, Funderburg R (2016) Geographies of risk, the regulatory state, and the ethic of care. *Ann Assoc Am Geogr* 106:1097–1113. <https://doi.org/10.1080/24694452.2016.1179565>
- Lyons D (1972) Rawls versus utilitarianism. *J Philos* 64:535–545. <https://doi.org/10.2307/2025370>
- Maldonado A, Collins TW, Grineski SE, Chakraborty J (2016) Exposure to flood hazards in Miami and Houston: are Hispanic immigrants at greater risk than other social groups? *Int J Environ Res Public Health* 17:E775. <https://doi.org/10.3390/ijerph13080775>
- May L, Morrow P (2012) *Procedural justice*. Ashgate, The library of essays on justice. Farnham
- Mill JS (2010) *Utilitarianism, liberty and representative government*. Wildside Press, Milton Keynes
- Montgomery MC, Chakraborty J (2015) Assessing the environmental justice consequences of flood risk: a case study in Miami, Florida. *Environ Res Lett* 10:095010. <https://doi.org/10.1088/1748-9326/10/9/095010>
- Mostert E (2015) Who should do what in environmental management? Twelve principles for allocating responsibilities. *Environ Sci Pol* 45: 123–131. <https://doi.org/10.1016/j.envsci.2014.10.008>
- Munoz CE, Tate E (2016) Unequal recovery? Federal resource distribution after a Midwest flood disaster. *Int J Environ Res Public Health* 17:E507. <https://doi.org/10.3390/ijerph13050507>
- Neal MJ, Lukaszewicz A, Syme GJ (2014) Why justice matters in water governance: some ideas for a ‘water justice framework’. *Water Policy* 16:1–18. <https://doi.org/10.2166/wp.2014.109>
- Papathoma-Köhle M, Gems B, Sturm M, Fuchs S (2017) Matrices, curves and indicators: a review of approaches to assess physical vulnerability to debris flows. *Earth Sci Rev* 171:272–288. <https://doi.org/10.1016/j.earscirev.2017.06.007>
- Patrick MJ (2014) The cycles and spirals of justice in water-allocation decision making. *Water Int* 39:63–80. <https://doi.org/10.1080/02508060.2013.863646>
- Penning-Rowsell E (2015) Flood insurance in the UK: a critical perspective. *WIREs Water* 2:601–608. <https://doi.org/10.1002/wat2.1104>
- Penning-Rowsell E, Pardoe J (2012a) Who loses if flood risk is reduced: should we be concerned? *Area* 44:152–159. <https://doi.org/10.1111/j.1475-4762.2012.01085.x>
- Penning-Rowsell E, Pardoe J (2012b) Who benefits and who loses from flood risk reduction? *Environ Plann C: Gov Policy* 30:448–466. <https://doi.org/10.1068/c10208>
- Penning-Rowsell E, Pardoe J (2015) The distributional consequences of future flood risk management in England and Wales. *Environ Plann C: Gov Policy* 33:1301–1321. <https://doi.org/10.1068/c13241>
- Raschky PA, Weck-Hannemann H (2007) Charity hazard—a real hazard to natural disaster insurance? *Environ Hazard* 7:321–329. <https://doi.org/10.1016/j.envhaz.2007.09.002>
- Rawls J (2005) *A theory of justice*. Harvard University Press, Cambridge
- Reese G, Jacob L (2015) Principles of environmental justice and pro-environmental action: a two-step process model of moral anger and responsibility to act. *Environ Sci Pol* 51:88–94. <https://doi.org/10.1016/j.envsci.2015.03.011>
- Republic of Austria (1975) *Forstgesetz 1975*. Vienna: BGBl. 440/1975
- Republic of Austria (1976) *Verordnung des Bundesministers für Land- und Forstwirtschaft vom 30. Juli 1976 über die Gefahrenzonenpläne*. Vienna: BGBl 436/1976
- Röthlisberger V, Zischg A, Keiler M (2017) Identifying spatial clusters of flood exposure to support decision making in risk management. *Science of Total Environment* 598, 593–603. <https://doi.org/10.1016/j.scitotenv.2017.03.216>
- Schlosberg D (2007) *Defining environmental justice: theories, movements, and nature*. Oxford University Press, New York
- Schlosberg D, Collins LB (2014) From environmental to climate justice: climate change and the discourse of environmental justice. *WIREs Climate Change* 5:359–374. <https://doi.org/10.1002/wcc.275>
- Schlosberg D, Collins LB, Niemeyer S (2017) Adaptation policy and community discourse: risk, vulnerability, and just transformation. *Environmental Politics* 26:413–437. <https://doi.org/10.1080/09644016.2017.1287628>
- Sen A (2010) *The idea of justice*. Penguin Publisher, London
- Sinabell F, Url T (2007) Effizientes Risikomanagement für Naturgefahren am Beispiel von Hochwasser. *WIFO Monatsberichte* 6(2007):537–547
- Staffler H, Pollinger R, Zischg A, Mani P (2008) Spatial variability and potential impacts of climate change on flood and debris flow hazard

- zone mapping and implications for risk management. *Nat Hazards Earth Syst Sci* 8:539–558. <https://doi.org/10.5194/nhess-8-539-2008>
- Tarlock DA (2012) Takings, water rights, and climate change. 36 *Vermont Law Review* 731. http://scholarship.kentlaw.iit.edu/cgi/viewcontent.cgi?article=1675&context=fac_schol. [last accessed 02 Mar 2016]
- Thaler T (2014) Developing partnership approaches for flood risk management: implementation of inter-local co-operations in Austria. *Water Int* 39:1018–1029. <https://doi.org/10.1080/02508060.2014.992720>
- Thaler T, Hartmann T (2016) Justice and flood risk management: reflecting on different approaches to distribute and allocate flood risk management in Europe. *Nat Hazards* 83:129–147. <https://doi.org/10.1007/s11069-016-2305-1>
- Thaler T, Levin-Keitel M (2016) Multi-level stakeholder engagement in flood risk management—a question of roles and power: lessons from England. *Environ Sci Pol* 55:292–301. <https://doi.org/10.1016/j.envsci.2015.04.007>
- Thaler T, Priest S (2014) Partnership funding in flood risk management: new localism debate and policy in England. *Area* 46:418–425. <https://doi.org/10.1111/area.12135>
- Thaler T, Priest S, Fuchs S (2016) Evolving interregional co-operation in flood risk management: distances and types of partnership approaches in Austria. *Reg Environ Chang* 16:841–853. <https://doi.org/10.1007/s10113-015-0796-z>
- Ungern-Sternberg T (2004) *Efficient monopolies—the limits of competition in the European property insurance market*. Oxford University Press, Oxford
- Varian HR (1975) Distributive justice, welfare economics, and the theory of fairness. *Philos Public Aff* 4:223–247
- Walker G (2012) *Environmental justice: concepts, evidence and politics*. Routledge, Abingdon
- Walker G, Burningham K (2011) Flood risk, vulnerability and environmental justice: evidence and evaluation of inequality in a UK context. *Critical Social Policy* 31:216–240. <https://doi.org/10.1177/0261018310396149>
- Wisner B, Blaikie P, Cannon T, Davis I (2004) *At risk: natural hazards, people's vulnerability and disasters*. Routledge, London
- Zerbe RO, Plotnick RD (1988) Rawlsian difference principles and economic utilitarianism. *Soc Justice Res* 2:207–222. <https://doi.org/10.1007/BF01054557>
- Zischg A, Schober S, Sereinig N, Rauter M, Seymann C, Goldschmidt F, Bäk R, Schleicher E (2013) Monitoring the temporal development of natural hazard risks as a basis indicator for climate change adaptation. *Nat Hazards* 67:1045–1058. <https://doi.org/10.1007/s11069-011-9927-0>
- Zwarteveen MZ, Boelens R (2014) Defining, researching and struggling for water justice: some conceptual building blocks for research and action. *Water Int* 39:143–158. <https://doi.org/10.1080/02508060.2014.891168>

Paper 29: Zischg, A., 2018. Floodplains and Complex Adaptive Systems—Perspectives on Connecting the Dots in Flood Risk Assessment with Coupled Component Models. *Systems* 6(9). [10.3390/systems6020009](https://doi.org/10.3390/systems6020009).

Review

Floodplains and Complex Adaptive Systems— Perspectives on Connecting the Dots in Flood Risk Assessment with Coupled Component Models

Andreas Paul Zischg 

Oeschger Centre for Climate Change Research, Institute of Geography, University of Bern,
3012 Bern, Switzerland; andreas.zischg@giub.unibe.ch; Tel.: +41-31-631-8839

Received: 10 December 2017; Accepted: 30 March 2018; Published: 5 April 2018



Abstract: Floodplains, as seen from the flood risk management perspective, are composed of co-evolving natural and human systems. Both flood processes (that is, the hazard) and the values at risk (that is, settlements and infrastructure built in hazardous areas) are dynamically changing over time and influence each other. These changes influence future risk pathways. The co-evolution of all of these drivers for changes in flood risk could lead to emergent behavior. Hence, complexity theory and systems science can provide a sound theoretical framework for flood risk management in the 21st century. This review aims at providing an entry point for modelers in flood risk research to consider floodplains as complex adaptive systems. For the systems science community, the actual problems and approaches in the flood risk research community are summarized. Finally, an outlook is given on potential future coupled component modeling approaches that aims at bringing together both disciplines.

Keywords: flood risk; floodplains; sensitivity analysis; coupled component modeling; complex adaptive systems

1. Introduction

Floods are one of the most damaging natural hazards, accounting for a majority of all economic losses from natural events worldwide [1]. Managing flood risks requires knowledge about hazardous processes and their impacts. Hence, risks resulting from floods are defined as functions of the probability of a flood event or scenario, respectively, and the related extent of damage [2,3]. The latter is computed in most cases by a function of the monetary value of the object affected by the flood and its vulnerability against the magnitude of the process scenario. In floodplains, these main factors of flood risk, the flood process, and the values at risk meet each other locally. From a physical perspective, floodplains are defined as areas of land adjacent to and formed by flowing water in times of floods. In addition, from a socioeconomic perspective, floodplains provide land for settlement, infrastructure, and other human activities. Floodplains and the main drivers for flood risks are evolving over time. Consequently, in natural hazards and risk research, an actual change in the paradigms can be observed. Risks are being more frequently analyzed from a dynamic rather than a static perspective [4,5]. Hence, many studies are dealing with changes of natural risks over recent decades and centuries [2,6–10]. In addition, research on climate changes and its impact is the focus of future changes in risks [11–20]. A few studies consider both the impacts of climatic changes to river flows and the future dynamics in the values at risk [21–26]. As drivers for changes in risk are not only varying in time, recent studies extend the dynamic framework of risk analysis toward a spatiotemporal framework [27–34]. Herein, the drivers of flood risk vary in space and time. Consequently, a few studies adopted the system dynamics approach to a spatial system dynamics approach for water resources systems and flood

risk analyses [35–37]. Beside flood risk research, system dynamics modeling is also becoming an increasingly attractive approach in social sciences and earth system modeling [38–42].

In summary, the built environment in floodplains, whether the settlement area or the river channel, is subject to changes and co-evolutionary dynamics in both spheres. Floodplains are influenced by flood events and subsequent disruptive changes in the society, by governmental decisions as adaptation to these flood events, and individual agents. These co-evolutionary dynamics in the drivers for changes in flood risk influence future risk pathways, and could lead to emergent behavior. Hence, complexity theory and systems science potentially provide a sound theoretical framework for flood risk management as postulated by Helbing et al. [43] for other risks.

This short review aims at summarizing recent attempts in analyzing and modeling spatiotemporal changes in flood risk from a complex systems perspective and at giving an explorative outlook of future perspectives in considering floodplains as complex adaptive systems. With this, I am aiming at providing a summary of the prospective approaches for modeling the co-evolutionary dynamics and emergent behavior of floodplains and thus, an entry point for flood risk modelers to consider floodplains as complex adaptive systems. Moreover, I am aiming at providing a collection of relevant literature from the flood risk research community, and thus an entry point for the systems science community into flood risk research. The focus is placed on the approaches for modeling the co-evolutionary and spatiotemporal dynamics in the evolution of flood risks in floodplains.

2. Main Drivers of Evolving Risks in Floodplains

The spatiotemporal evolution of flood risk in floodplains is composed of several drivers that are intertwined with each other. In a reductionist approach, flood risk research is focusing on a single aspect of flood risk and their changes in space and time. However, constructivist perspectives in flood risk research are rather rare, and are more frequently present in the systems sciences. In this paper, I will summarize the main drivers of evolving flood risks in floodplains.

2.1. Changes in Flood Processes

Floods are either caused directly by rainfall onto the system under investigation (pluvial floods and surface water floods, for example) or by falling onto river catchments, resulting in a catchment outflow. The latter causes floods in downstream floodplains (riverine floods and lake floods). Thus, the boundary condition of floods in floodplains can either be rainfall, river flows, or both. Consequently, changes in flood processes, that is, changes in the frequency and magnitude of floods, are determined by these external influencing factors. In many studies, the changes in rainfall frequency and intensity are investigated, with a special focus on the effects of climatic changes [44,45]. In addition, changes in the incoming flow hydrographs are drivers of change in floodplains [46–48]. In mountainous areas, flood losses are also influenced by sediment transport and deposition processes [49].

However, the rivers themselves and their floodplains change over time [50–53]. These can be natural and gradual changes in the river morphodynamics and flood regime [54–57], changes in the adjacent vegetation [58], or disruptive changes by flood events [59], for example by levee failures [60]. Last but not least, anthropogenic interventions are more or less the most relevant driver of flood risk in a floodplain; that is, the construction of flood defenses such as levees and dams [61–63] or river restoration projects [64–66]. Furthermore, the construction of levees as flood protection measures in one floodplain can have adverse effects in downstream floodplains [67–71], and thus result in trade-offs between upstream and downstream floodplains [72,73]. Reviews on the impacts of land use changes and regulations on floods are given by Rogger et al. [74], Burby et al. [75], and O’Connell et al. [76]. Moreover, floodplains can be affected by land subsidence due to drainage or groundwater extraction. This results in increasing flood hazards and consequently, increasing flood risk [77].

2.2. Changes in Exposure and Vulnerability

In addition to changes in the natural environment (that is, the fluvial aspect of the floodplain), flood risks also change due to variations in the exposed values at risk and in their vulnerability. First of all, one of the most relevant drivers of flood risk is the increase in the values that are at risk due to economic development [78,79]. The growing of settlements and thus, the increase of residential buildings is related to population growth [80]. With it, the infrastructure increases as well. Infrastructure failures have wider impacts on the socioeconomic systems, and thus exhibit relevant interdependencies [81–84]. In economically active areas, floodplains are increasingly occupied by production facilities, as these require relatively flat compound areas for their construction that are not available in hilly areas [85]. Recent studies show that the number of buildings potentially affected by floods increased by up to 700% in the last century [31,78]. With economic development, the objects at risk and the infrastructure in the floodplains increase in terms of monetary value. This and higher object vulnerabilities [86,87] result in increased flood risks. Both factors compete with the opposing drivers of flood risk reduction measures by individuals and the public.

2.3. Adaptation in Governance

Changes in exposure and vulnerability are influenced by the action of individuals and by governmental interventions and regulations. On the one hand, local governments regulate land use with planning instruments. In several countries, the occupation and utilization of areas potentially affected by floods are not allowed or restricted. Moreover, governmental institutions and legislative entities are defining the basic principles and legislative frameworks for spatial planning in floodplains. On the other hand, land use regulations are binding the actions of the individuals and businesses. Hence, both the actions of individual agents and the public composed by a collection of agents result in the key interfering driving forces for changes in flood risk [88]. Often, the actions of individuals and governments are an adaptation to flooding events [89–92]. When a flood affects a relevant share of a house or the infrastructure of the floodplain, individuals urge the government to act. As a reaction to the flood event and requests by the population, the local government invests in flood protection measures [93–95]. If many communities are affected, the regional or national governments react by adapting the legislative or financial framework for flood risk management [96–99]. Individuals experiencing a flood event become aware and sensible to the hazard, and adapt by protecting their homes and workplaces from floods with object-based flood protection measures [100,101]. Moreover, governments try to inform and to sensitize residents in floodplains by aiming at increasing risk awareness [102]. These adaptations can be seen as social learning. Consequently, the following flood event will result in fewer losses. Hence, the vulnerability of values at risk and socioeconomic activities in floodplains might decrease due to the adaptation measures. Overall, this complexity calls for adaptive flood risk management strategies and integrative governance [103–117].

3. Characterization of Floodplains from the Viewpoint of Complex Adaptive Systems

Flood risk—as a quantitative variable of hazard, exposure, and vulnerability—is evolving in space and time. However, the quantification of flood risk in terms of expected losses in a specified time period summarizes all of the factors into one lumped variable. As the single factors in the risk formula are supposed to be co-evolutionary dynamics, it is interesting to have a look at the spatiotemporal evolution of the single drivers first and second to the evolution of the floodplain as a whole. The classical risk formula and the approaches in risk analyses enable a monitoring of the temporal development of the risks by periodically repeating a risk analysis [118]. However, these approaches do not provide a theoretical framework for a deeper understanding and for delineating management options from the behavior of the floodplain, including all drivers of change. As shown in Section 2, the factors influencing flood risk exhibit co-evolutionary dynamics with positive and negative feedback between each other. Moreover, signals from the natural process shaping floodplains as well as information

processing between the local human agents and its collective in the form of governmental institutions in the floodplain lead to the complex behavior of a floodplain. Both the natural and the human systems adapt their behavior after flood events. The social system changes their behavior by learning from accidents and continuously adapting flood risk management strategies. Consequently, this adaptation leads to an emerging behavior of floodplains. Behavior in terms of vulnerability against floods and resilience changes remarkably with time. Following the overall complexity of the co-evolutionary dynamics in the drivers of flood risk and the emergent behavior, floodplains can be defined as complex adaptive systems [119,120]. As the actions of the individuals are difficult to predict, the future development paths of such a complex system as floodplains are difficult to predict as well. Hence, complex systems science might provide a helpful theoretical framework for the analysis and simulation of future development pathways of floodplains. However, the identification of emergent behavior, self-organization, and adaptation, as well as mapping complexity, remain a key challenge in flood risk research [121–124].

4. Prospective Approaches in Modeling Co-Evolutionary Dynamics in Floodplains

As the co-evolution of natural–human systems became more evident recently, the disciplines involved in flood risk research tried to collaborate with social sciences to implement human behavior in their models for analysis and prediction. There are mainly two research foci to mention in regard to the co-evolutionary dynamics in floodplains and the interactions between human and natural systems: the coupled human–natural systems approach, and the socio-hydrology approach [125]. The latter is a sub-discipline of socio-ecological systems research [126].

The research topic “coupled human–natural systems” (CHANS) mainly focus on wildlife habitats and landscape evolution [127]. An overview is given by Liu et al. [128]. However, there are some studies dealing with evolving floodplains and the role of individuals [129]. One focus in these models is an analysis of the resilience of the social systems in floodplains [130]. Another focus lays on vulnerability analysis, as exemplarily shown by Turner et al. [131]. The approach is also used to model flood protection investments [132]. The CHANS approach focuses on spatially explicit simulations of changes in systems by considering feedback mechanisms between human activities and the natural environment.

In 2013, the International Association of Hydrological Sciences launched a decade of focused research with the theme “Panta Rhei: Change in Hydrology and Society” [133–135]. Consequently, hydrological science attempted to analyze and model human behavior and their interlinkages with the natural environment, as well as co-evolutionary dynamics. These attempts are often termed as “socio-hydrology”. This new focus aims at understanding the dynamics and co-evolution of coupled human–water systems [136] and the relationships between society and floods [137]. Soon after, conceptual articles followed and sharpened the research topic [138–148]. A review is given by Blair and Buytaert [125].

In parallel, different case studies described typically complex problems in floodplains from the “socio-hydrology” perspective [149–156]. A debate on socio-hydrology describes different points of views and discussions between research groups in this field [157–163]. In the wider field of socio-hydrology, a few studies focused on the dynamic behavior of floodplains as human–water systems [164] and on conceptualizing human–flood interactions [165,166]. The main topic herein is the relationship between the development paths of settlements and the construction of levees. In contrast to the CHANS approach, socio-hydrological models are based on system dynamics, and simulate system behavior mainly in a lumped way (that is, a way that is not spatially explicit). In geomorphology, similar tendencies in capturing and analyzing the co-evolution of socio-natural systems and the effects of human interventions on river morphology can be observed [167–169]. Hydrologic and geomorphic drivers in flood hazard evolution are compared by Slater et al. [170].

The unresolved challenges in socio-hydrology lie in the parameterization and validation of the models [163]. Spatially explicit models for the prediction of future pathways in floodplain evolution

are still lacking [138,171,172]. Furthermore, there is still a lack of models that can predict potential adverse consequences for flood risk due to unintentional developments in the areas protected by levees [164]. This cannot be studied until the models explicitly consider space and time.

In the following sections, I will give a short overview of the three selected approaches that enable the consideration of the interactions between natural processes and human activities and describe the complex behavior of floodplains. I exemplarily selected one top–down modeling approach, one bottom–up modeling approach, and an approach that offers, in my opinion, a promising way to combine the two first mentioned options. The selection of modeling approaches is based on the classification of Kelly et al. [173]. The top–down modeling approaches aim to represent the system as a whole. The system behavior is represented by the interactions between the system components. Its design is mostly inferred by studying the overall behavior of the system. A model designed in this way can produce only deterministic results, and processes within the system are usually hard to analyze. In contrast, the bottom–up approach mainly focuses on representing the processes in a system. The overall behavior of the whole system results from the processes and their interactions. The latter approach is implemented mainly by explicitly considering space and time. A typical example of the first modeling technique is system dynamics. The most typical bottom–up modeling approach is agent-based models. A prospective approach of combining the benefits of both approaches is coupled component modeling.

4.1. System Dynamics

System dynamics (SD) is a computer simulation problem-solving approach with a foundation in the concepts of system feedbacks with the purpose of gaining insight into real-world system behavior [174]. System dynamics is based on the first computational experiments of Forrester [175] and on the system theory of Luhmann [176]. These approaches have recently been used in conceptualizing human–flood interactions [165], in vulnerability analyses [177], in modeling the feedbacks between flooding and economic growth [178], and to analyze upstream–downstream trade-offs in the internalization and externalization of flood risks [179].

However, system dynamic models are in most cases lumped models. Only a few studies deal with a spatial discretization of system dynamic models [180–183]. In flood risk research, these either deal with structural changes in flood risks [174] in general, the management of flood risk [111], or disaster management [184].

These approaches provide a potential for system conceptualization and thus a holistic analysis of floodplains. However, there is still a lack of methods for incorporating physically-based process models and linking them with the other modules in complex models. Moreover, the consideration of changes over time in system dynamic models is still a challenge. As an example, in studying the evolution of the flood risk of a specific floodplain, a modeler would build a system model at the macro level that incorporates the main drivers that change risk, such as river morphology, river engineering works, the dynamics in the exposure of houses, and finally, the risk management strategies. The modeler must know the present state of the system, the changes in these drivers, and the effects of the different risk reduction options. The system dynamics model would then quantitatively simulate the change in the overall flood risk in the floodplain within a certain time period. Thus, the outcome is quantitative, but aggregated in a lumped variable. The processes on the ground, that is, the spatiotemporal dynamics, are not modeled explicitly. However, the adaptive capacity can be studied because of the ability to consider flood risk management options and their effects.

4.2. Agent-Based Modeling

Agent-based modeling techniques (ABM) aim at simulating the behavior and decision-making of individuals (agents) and groups of individuals or institutions explicitly in space and time at the micro scale [125,173,185]. In (multi)agent models, the interactions between the agents are considered as well. The behavior of the agents is mostly determined by a set of rules. Agents can share common resources,

compete, or react to a changing environment. Moreover, agents could be simulated as learning entities. The overall system behavior results in the sum of all actions, reactions, and interactions of the agents. Thus, this approach is preferably used in modeling complex adaptive systems. In hierarchical agent-based models, the effects of regulations by institutions could also be simulated [186]. Another benefit of this approach is the ability to consider time lags, memory, and legacy effects. Major challenges in developing agent-based models lie in their calibration and validation. In regards to flood risk management, agent-based models are being used for simulating the behavior of people in case of flooding. An example is the planning of evacuations [187–189], where pedestrians, cars, and crowding are considered. Another example is the assessment of flood risk management strategies under future climate changes [190]. In this example, institutional behavior is also modeled. In regards to the co-evolutionary dynamics and emergence in floodplains, ABMs can be used to model how individuals and institutions react to a changing environment. Exemplarily, which house owner is taking precautionary measures into account to protect their homes against increasing floods can be simulated. Herein, experience with former flood events, the availability bias, or other incentives could be considered. Furthermore, the role of institutions in changing the environment as a reaction to a flood event could be modeled in space and time. For example, where do governments invest in river engineering works?

4.3. Coupled Component Modeling

Coupled component models (CCM) are composed of specialized disciplinary models representing the parts of the system. Coupled models integrate sub-models to form a model chain that represents a whole system [125]. Synonymously, this type of model is often defined as an integrated environmental model [191,192]. Coupled component models have an advantage in that they are flexible regarding the level of integration, and are relatively transparent because the sub-models are in most cases validated in their specific discipline. Moreover, coupled component models are generally able to combine system dynamics and agent-based models. In such cases, the disciplinary and spatially explicit process models can simulate the (changing) boundary conditions of agent-based models. The outcomes of both results in the system behavior. The design of a CCM can be based on a causal loop diagram of SDs. Hence, instead of using stocks and flows, CCMs simulates the processes directly. However, the sub-models often use different spatial and temporal scales. Thus, the bridging of different scales in model coupling is challenging. Another advantage is that coupled component models can potentially combine both lumped and spatially explicit models. An overview of common coupled or integrated modeling approaches is given by Kelly et al. [173]. However, there is still a lack of integrating process-based models with socio-environmental models. As an example, a few studies showed how to couple system dynamics with agent-based models [193], physically-based models [194], or expert systems [195]. In regards to flood risk analysis, models for weather forecasts are coupled with hydrological models, inundation models, and with flood impact models (for example, flood loss models). An example of a complex modeling chain from rainfall to flood risk is given by Falter et al. [196] or Zischg et al. [197]. In addition, Saint-Geours et al. [198] and Thaler et al. [199] present an approach of incorporating risk management policies in coupled component models.

5. Conclusions and Outlook from a Modeler's Perspective

In this short review, I summarized the literature on modeling floodplains as complex adaptive systems. Beside this, there are other approaches that might be applicable in this context such as Bayesian networks, network theory, or knowledge-based models (that is, expert systems). I focused here on approaches that are applicable in predicting future pathways of flood risk evolution in floodplains. The literature review results in the first overview of modeling floodplains in their complexity and provides a few conclusions for further research that is needed in order to simulate the complex interactions between the natural processes and human actions. Flood risk is determined by several factors, and thus the coupling of models that are specified for selected drivers of flood risk change is needed.

Hitherto, in flood risk research, two main approaches of coupling models prevail. One of the most common approaches is the coupling of different models across specific domains. This is either done in a cascading approach or in a coupled modeling approach. In the first approach, changes in the boundary conditions of the model changes are analyzed from the viewpoint of the impacts to the studied system represented by the model chain. However, the studied system itself, which is represented by the sub-models in the model chain, changes contemporarily with the boundary conditions. In many cases, top-down model chains represent a system behavior that is relatively constant in time. One example of such a shortage is to study future flood risks without implementing the future system status of floodplains with their values at risk and the adaptation of flood risk management strategies over time. Moreover, the development of the studied system over time is influenced by its sensitivity to changes in the boundary conditions. This means that both changes in the boundary conditions and internal changes in the system predetermine the development path of a changing floodplain. Both drivers of change are interwoven, and a sound analysis of changes in complex environmental systems needs to consider them. Thus, a second main approach in model coupling is to study the sensitivity of floodplains. In this bottom-up approach, the focus is laid more on the internal behavior and change of the system rather than on the boundary conditions. In the coupled models, this is studied on the one hand by sensitivity analyses of the sub-modules in an isolated way, and on the other hand by sensitivity analyses of the whole model chain.

While both top-down and bottom-up modeling approaches offer a high potential for the development of methods and tools for the analysis of changes in complex environmental systems, a research gap is identified in bridging both approaches. Therefore, the main aim of future research in modeling floodplains as complex adaptive systems should be to integrate both approaches. This should lead to an extension of the capabilities of coupled component modeling. If the sensitivity of a hydro-geomorphic system is analyzed in detail and a model of adaptive behavior is developed (bottom-up approach), a subsequent analysis of the impacts of changing the boundary conditions (top-down), and consequently, a prediction of future development paths can be done more satisfyingly. This means that changes over time in the boundary conditions meet system-specific sensitivities and adaptive capabilities. Figure 1 schematizes a possible combination of top-down and bottom-up approaches in modeling floodplains as complex adaptive systems with a coupled component model.

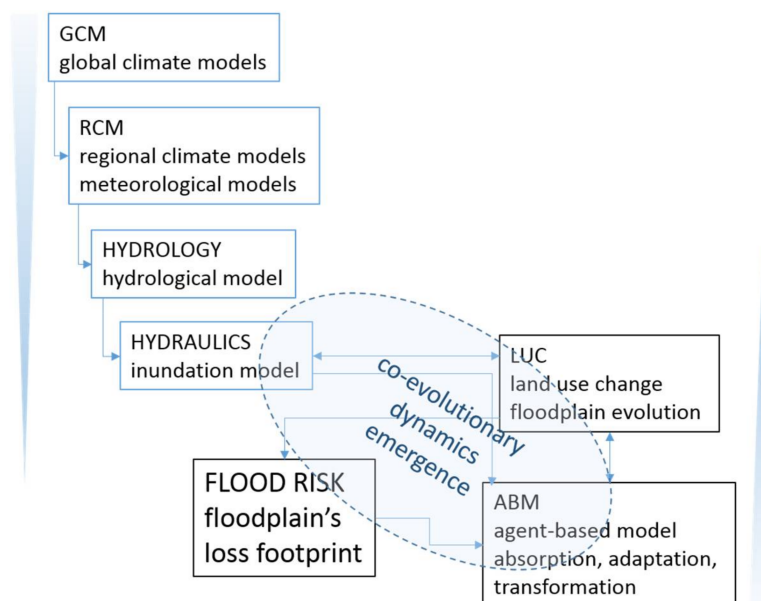


Figure 1. The proposed schema for merging top-down and bottom-up approaches in the framework of coupled component models.

Herein, coupled component models seem to promise the most flexible and robust approach for the prediction of future pathways of floodplain development. This modeling approach is modular; thus, the model chains can be extended step by step with sub-models that have already been validated in their specific domain of application. This modularity makes coupled component models more transparent, robust, and interpretable than lumped specific-purpose models. However, the coupling of already existing models remains a challenge, as they potentially address different scales in space and time. Moreover, coupled component models are preferred, as they consider explicitly spatial phenomena.

Before being applied in floodplain modeling, coupled component models have to be extended remarkably. In my opinion, especially the coupling of process models with agent-based models that simulate the interactions of individuals and institutions with the changing environment, offer a huge potential for extending the capabilities for simulating complex adaptive systems such as floodplains. Thus, the inclusion of the bottom-up modeling approach leads to a more holistic application for prediction purposes than process models alone. The combination of physics-based process models and ABMs offer a thorough simulation of the spatiotemporal dynamics in floodplains. In conclusion, the coupled component models have to be extended with agent-based models representing adaptive behavior sub-modules, and with capabilities for modeling the interactions between the sub-modules, such as feedbacks. This might lead to the capability of modeling adaptive behavior and emergent phenomena.

Acknowledgments: The research of the author is funded by the Swiss Mobiliar insurance.

Conflicts of Interest: The author declares no conflicts of interest. The funding sponsors had no role in the design of the study; in the collection, analyses, or interpretation of data; in the writing of the manuscript, and in the decision to publish the results.

References

1. United Nations International Strategy for Disaster Reduction (UNISDR). *Making Development Sustainable: The Future of Disaster Risk Management*; United Nations: Geneva, Switzerland, 2015.
2. Fuchs, S.; Keiler, M.; Zischg, A.; Bründl, M. The long-term development of avalanche risk in settlements considering the temporal variability of damage potential. *Nat. Hazards Earth Syst. Sci.* **2005**, *5*, 893–901. [[CrossRef](#)]
3. Haimes, Y.Y. On the complex definition of risk: A systems-based approach. *Risk Anal. Off. Publ. Soc. Risk Anal.* **2009**, *29*, 1647–1654. [[CrossRef](#)] [[PubMed](#)]
4. Mazzorana, B.; Levaggi, L.; Keiler, M.; Fuchs, S. Towards dynamics in flood risk assessment. *Nat. Hazards Earth Syst. Sci.* **2012**, *12*, 3571–3587. [[CrossRef](#)]
5. Merz, B.; Hall, J.; Disse, M.; Schumann, A. Fluvial flood risk management in a changing world. *Nat. Hazards Earth Syst. Sci.* **2010**, *10*, 509–527. [[CrossRef](#)]
6. Keiler, M.; Zischg, A.; Fuchs, S.; Hama, M.; Stötter, J. Avalanche related damage potential—Changes of persons and mobile values since the mid-twentieth century, case study Galtür. *Nat. Hazards Earth Syst. Sci.* **2005**, *5*, 49–58. [[CrossRef](#)]
7. Keiler, M. Development of the damage potential resulting from avalanche risk in the period 1950–2000, case study Galtür. *Nat. Hazards Earth Syst. Sci.* **2004**, *4*, 249–256. [[CrossRef](#)]
8. Keiler, M.; Sailer, R.; Jörg, P.; Weber, C.; Fuchs, S.; Zischg, A.; Sauermoser, S. Avalanche risk assessment; a multi-temporal approach, results from Galtür, Austria. *Nat. Hazards Earth Syst. Sci.* **2006**, *6*, 637–651. [[CrossRef](#)]
9. Achleitner, S.; Huttenlau, M.; Winter, B.; Reiss, J.; Plörer, M.; Hofer, M. Temporal development of flood risk considering settlement dynamics and local flood protection measures on catchment scale: An Austrian case study. *Int. J. River Basin Manag.* **2016**, *14*, 273–285. [[CrossRef](#)]
10. Himmelsbach, I.; Glaser, R.; Schoenbein, J.; Riemann, D.; Martin, B. Flood risk along the upper Rhine since AD 1480. *Hydrol. Earth Syst. Sci. Discuss.* **2015**, *12*, 177–211. [[CrossRef](#)]
11. Alfieri, L.; Bisselink, B.; Dottori, F.; Naumann, G.; de Roo, A.; Sa Iamon, P.; Wyser, K.; Feyen, L. Global projections of river flood risk in a warmer world. *Earth Futur.* **2016**. [[CrossRef](#)]

12. Alfieri, L.; Burek, P.; Feyen, L.; Forzieri, G. Global warming increases the frequency of river floods in Europe. *Hydrol. Earth Syst. Sci.* **2015**, *19*, 2247–2260. [[CrossRef](#)]
13. Alfieri, L.; Feyen, L.; Di Baldassarre, G. Increasing flood risk under climate change: A pan-European assessment of the benefits of four adaptation strategies. *Clim. Chang.* **2016**. [[CrossRef](#)]
14. Arnell, N.W.; Gosling, S.N. The impacts of climate change on river flood risk at the global scale. *Clim. Chang.* **2016**, *134*, 387–401. [[CrossRef](#)]
15. Devkota, R.P.; Bhattarai, U. Assessment of climate change impact on floods from a techno-social perspective. *J. Flood Risk Manag.* **2015**. [[CrossRef](#)]
16. Hirabayashi, Y.; Mahendran, R.; Koirala, S.; Konoshima, L.; Yamazaki, D.; Watanabe, S.; Kim, H.; Kanae, S. Global flood risk under climate change. *Nat. Clim. Chang.* **2013**, *3*, 816–821. [[CrossRef](#)]
17. Hundecha, Y.; Merz, B. Exploring the relationship between changes in climate and floods using a model-based analysis. *Water Resour. Res.* **2012**, *48*, 3331. [[CrossRef](#)]
18. Kundzewicz, Z.W.; Kanae, S.; Seneviratne, S.I.; Handmer, J.; Nicholls, N.; Peduzzi, P.; Mechler, R.; Bouwer, L.M.; Arnell, N.; Mach, K.; et al. Flood risk and climate change: Global and regional perspectives. *Hydrol. Sci. J.* **2014**, *59*, 1–28. [[CrossRef](#)]
19. Merz, B.; Aerts, J.; Arnbjerg-Nielsen, K.; Baldi, M.; Becker, A.; Bichet, A.; Blöschl, G.; Bouwer, L.M.; Brauer, A.; Cioffi, F.; et al. Floods and climate: Emerging perspectives for flood risk assessment and management. *Nat. Hazards Earth Syst. Sci.* **2014**, *14*, 1921–1942. [[CrossRef](#)]
20. Alfieri, L.; Feyen, L.; Dottori, F.; Bianchi, A. Ensemble flood risk assessment in Europe under high end climate scenarios. *Glob. Environ. Chang.* **2015**, *35*, 199–212. [[CrossRef](#)]
21. Bouwer, L.M.; Bubeck, P.; Aerts, J.C.J.H. Changes in future flood risk due to climate and development in a Dutch polder area. *Glob. Environ. Chang.* **2010**, *20*, 463–471. [[CrossRef](#)]
22. Jongman, B.; Koks, E.E.; Husby, T.G.; Ward, P.J. Increasing flood exposure in the Netherlands: Implications for risk financing. *Nat. Hazards Earth Syst. Sci.* **2014**, *14*, 1245–1255. [[CrossRef](#)]
23. Jongman, B.; Ward, P.J.; Aerts, J.C.J.H. Global exposure to river and coastal flooding: Long term trends and changes. *Glob. Environ. Chang.* **2012**, *22*, 823–835. [[CrossRef](#)]
24. Liu, J.; Hertel, T.W.; Diffenbaugh, N.S.; Delgado, M.S.; Ashfaq, M. Future property damage from flooding: Sensitivities to economy and climate change. *Clim. Chang.* **2015**, *132*, 741–749. [[CrossRef](#)]
25. Löschner, L.; Herrnegger, M.; Apperl, B.; Senoner, T.; Seher, W.; Nachtnebel, H.P. Flood risk, climate change and settlement development: A micro-scale assessment of Austrian municipalities. *Reg. Environ. Chang.* **2016**, *42*, 125. [[CrossRef](#)]
26. Winsemius, H.C.; Aerts, J.C.J.H.; van Beek, L.P.; Bierkens, M.F.; Bouwman, A.; Jongman, B.; Kwadijk, J.C.; Ligtoet, W.; Lucas, P.L.; van Vuuren, D.P.; et al. Global drivers of future river flood risk. *Nat. Clim. Chang.* **2015**, *6*, 381–385. [[CrossRef](#)]
27. Ahmad, S.S.; Simonovic, S.P. Spatial and temporal analysis of urban flood risk assessment. *Urban Water J.* **2013**, *10*, 26–49. [[CrossRef](#)]
28. Aubrecht, C.; Fuchs, S.; Neuhold, C. Spatio-temporal aspects and dimensions in integrated disaster risk management. *Nat. Hazards* **2013**, *68*, 1205–1216. [[CrossRef](#)]
29. Cammerer, H.; Thieken, A.H.; Verburg, P.H. Spatio-temporal dynamics in the flood exposure due to land use changes in the Alpine Lech Valley in Tyrol (Austria). *Nat. Hazards* **2013**, *68*, 1243–1270. [[CrossRef](#)]
30. Früh-Müller, A.; Wegmann, M.; Koellner, T. Flood exposure and settlement expansion since pre-industrial times in 1850 until 2011 in north Bavaria, Germany. *Reg. Environ. Chang.* **2015**, *15*, 183–193. [[CrossRef](#)]
31. Fuchs, S.; Röthlisberger, V.; Thaler, T.; Zischg, A.; Keiler, M. Natural Hazard Management from a Coevolutionary Perspective: Exposure and Policy Response in the European Alps. *Ann. Am. Assoc. Geogr.* **2016**, *107*, 1–11. [[CrossRef](#)] [[PubMed](#)]
32. Röthlisberger, V.; Zischg, A.; Keiler, M. Spatiotemporal aspects of flood exposure in Switzerland. *E3S Web Conf.* **2016**, *7*, 8008. [[CrossRef](#)]
33. Röthlisberger, V.; Zischg, A.P.; Keiler, M. Identifying spatial clusters of flood exposure to support decision making in risk management. *Sci. Total Environ.* **2017**, *598*, 593–603. [[CrossRef](#)] [[PubMed](#)]
34. Fuchs, S.; Keiler, M.; Sokratov, S.; Shnyparkov, A. Spatiotemporal dynamics: The need for an innovative approach in mountain hazard risk management. *Nat. Hazards* **2013**, *68*, 1217–1241. [[CrossRef](#)]

35. Ahmad, S.; Simonovic, S.P. Modeling Dynamic Processes in Space and Time—A Spatial System Dynamics Approach. In Proceedings of the World Water and Environmental Resources Congress 2001, Orlando, FL, USA, 20–24 May 2001; pp. 1–20.
36. Ahmad, S.S.; Simonovic, S.P. System dynamics and hydrodynamic modelling approaches for spatial and temporal analysis of flood risk. *Int. J. River Basin Manag.* **2015**, *13*, 443–461. [[CrossRef](#)]
37. Ahmad, S.; Simonovic, S.P. Spatial System Dynamics: New Approach for Simulation of Water Resources Systems. *J. Comput. Civ. Eng.* **2004**, *18*, 331–340. [[CrossRef](#)]
38. Bentley, R.A.; Maddison, E.J.; Ranner, P.H.; Bissell, J.; Caiado, C.; Bhatanacharoen, P.; Clark, T.; Botha, M.; Akinbami, F.; Hollow, M.; et al. Social tipping points and Earth systems dynamics. *Front. Environ. Sci.* **2014**, *2*. [[CrossRef](#)]
39. Brinke, W.B.M.; Knoop, J.; Muilwijk, H.; Ligtvoet, W. Social disruption by flooding, a European perspective. *Int. J. Disaster Risk Reduct.* **2017**, *21*, 312–322. [[CrossRef](#)]
40. Von Elverfeldt, K.; Embleton-Hamann, C.; Slaymaker, O. Self-organizing change? On drivers, causes and global environmental change. *Geomorphology* **2016**, *253*, 48–58. [[CrossRef](#)]
41. Fraternali, P.; Castelletti, A.; Soncini-Sessa, R.; Vaca Ruiz, C.; Rizzoli, A.E. Putting humans in the loop: Social computing for Water Resources Management. *Environ. Model. Softw.* **2012**, *37*, 68–77. [[CrossRef](#)]
42. Donges, J.F.; Winkelmann, R.; Lucht, W.; Cornell, S.E.; Dyke, J.G.; Rockström, J.; Heitzig, J.; Schellnhuber, H.J. Closing the loop: Reconnecting human dynamics to Earth System science. *Anthr. Rev.* **2017**, *4*, 151–157. [[CrossRef](#)]
43. Helbing, D.; Brockmann, D.; Chadeaux, T.; Donnay, K.; Blanke, U.; Woolley-Meza, O.; Moussaid, M.; Johansson, A.; Krause, J.; Schutte, S.; et al. Saving Human Lives: What Complexity Science and Information Systems can Contribute. *J. Stat. Phys.* **2015**, *158*, 735–781. [[CrossRef](#)] [[PubMed](#)]
44. Gobiet, A.; Kotlarski, S.; Beniston, M.; Heinrich, G.; Rajczak, J.; Stoffel, M. 21st century climate change in the European Alps—A review. *Sci. Total Environ.* **2014**, *493*, 1138–1151. [[CrossRef](#)] [[PubMed](#)]
45. Arheimer, B.; Lindström, G. Climate impact on floods: Changes in high flows in Sweden in the past and the future (1911–2100). *Hydrol. Earth Syst. Sci.* **2015**, *19*, 771–784. [[CrossRef](#)]
46. Hollis, G.E. The effect of urbanization on floods of different recurrence interval. *Water Resour. Res.* **1975**, *11*, 431–435. [[CrossRef](#)]
47. Hooke, J.M. Human impacts on fluvial systems in the Mediterranean region. *Geomorphology* **2006**, *79*, 311–335. [[CrossRef](#)]
48. Muñoz, L.A.; Olivera, F.; Giglio, M.; Berke, P. The impact of urbanization on the streamflows and the 100-year floodplain extent of the Sims Bayou in Houston, Texas. *Int. J. River Basin Manag.* **2017**, *7*, 1–9. [[CrossRef](#)]
49. Staffler, H.; Pollinger, R.; Zischg, A.; Mani, P. Spatial variability and potential impacts of climate change on flood and debris flow hazard zone mapping and implications for risk management. *Nat. Hazards Earth Syst. Sci.* **2008**, *8*, 539–558. [[CrossRef](#)]
50. Sear, D.A.; Newson, M.D. Environmental change in river channels: A neglected element. Towards geomorphological typologies, standards and monitoring. *Detect. Environ. Chang. Sci. Soc.* **2003**, *310*, 17–23. [[CrossRef](#)]
51. Brierley, G.J.; Fryirs, K.A. The Use of Evolutionary Trajectories to Guide ‘Moving Targets’ in the Management of River Futures. *River Res. Appl.* **2016**, *32*, 823–835. [[CrossRef](#)]
52. Marani, M.; Rigon, R. Self-Organized River Basin Landscapes—Fractal and Multifractal Characteristics. *Water Resour. Res.* **1994**, *30*, 3531–3539. [[CrossRef](#)]
53. Pinter, N.; Thomas, R.; Wlosinski, J.H. Assessing flood hazard on dynamic rivers. *Eos Trans. AGU* **2001**, *82*, 333. [[CrossRef](#)]
54. Church, M.; Ferguson, R.I. Morphodynamics: Rivers beyond steady state. *Water Resour. Res.* **2015**, *51*, 1883–1897. [[CrossRef](#)]
55. Coulthard, T.J.; Van De Wiel, M.J. Quantifying fluvial non linearity and finding self organized criticality? Insights from simulations of river basin evolution. *Geomorphology* **2007**, *91*, 216–235. [[CrossRef](#)]
56. Hall, J.; Arheimer, B.; Borga, M.; Brázdil, R.; Claps, P.; Kiss, A.; Kjeldsen, T.R.; Kriaučiūnienė, J.; Kundzewicz, Z.W.; Lang, M.; et al. Understanding flood regime changes in Europe: A state-of-the-art assessment. *Hydrol. Earth Syst. Sci.* **2014**, *18*, 2735–2772. [[CrossRef](#)]
57. Herget, J.; Dikau, R.; Gregory, K.J.; Vandenberghe, J. The fluvial system—Research perspectives of its past and present dynamics and controls. *Geomorphology* **2007**, *92*, 101–105. [[CrossRef](#)]

58. Corenblit, D.; Davies, N.S.; Steiger, J.; Gibling, M.R.; Bornette, G. Considering river structure and stability in the light of evolution: Feedbacks between riparian vegetation and hydrogeomorphology. *Earth Surf. Process. Landf.* **2014**, *40*, 189–207. [[CrossRef](#)]
59. Guan, M.; Carrivick, J.L.; Wright, N.G.; Sleight, P.A.; Staines, K.E.H. Quantifying the combined effects of multiple extreme floods on river channel geometry and on flood hazards. *J. Hydrol.* **2016**, *538*, 256–268. [[CrossRef](#)]
60. Croke, J.; Denham, R.; Thompson, C.; Grove, J. Evidence of Self-Organized Criticality in riverbank mass failures: A matter of perspective? *Earth Surf. Process. Landf.* **2015**, *40*, 953–964. [[CrossRef](#)]
61. Di Baldassarre, G.; Castellarin, A.; Brath, A. Analysis of the effects of levee heightening on flood propagation: Example of the River Po, Italy. *Hydrol. Sci. J.* **2009**, *54*, 1007–1017. [[CrossRef](#)]
62. French, J.R. Hydrodynamic Modelling of Estuarine Flood Defence Realignment as an Adaptive Management Response to Sea-Level Rise. *J. Coast. Res.* **2008**, *2*, 1–12. [[CrossRef](#)]
63. Pinter, N.; Thomas, R.; Wlosinski, J.H. Regional Impacts of Levee Construction and Channelization, Middle Mississippi River, USA. In *Flood Issues in Contemporary Water Management*; Marsalek, J., Watt, W.E., Zeman, E., Sieker, F., Eds.; Springer: Dordrecht, The Netherlands, 2000; pp. 351–361.
64. Dixon, S.J.; Sear, D.A.; Odoni, N.A.; Sykes, T.; Lane, S.N. The effects of river restoration on catchment scale flood risk and flood hydrology. *Earth Surf. Process. Landf.* **2016**, *41*, 997–1008. [[CrossRef](#)]
65. Surian, N.; Rinaldi, M. Morphological response to river engineering and management in alluvial channels in Italy. *Geomorphology* **2002**, *50*, 307–326. [[CrossRef](#)]
66. Kiss, T.; Fiala, K.; Sipos, G. Alterations of channel parameters in response to river regulation works since 1840 on the Lower Tisza River (Hungary). *Geomorphology* **2008**, *98*, 96–110. [[CrossRef](#)]
67. Pinter, N.; van der Ploeg, R.R.; Schweigert, P.; Hoefler, G. Flood magnification on the River Rhine. *Hydrol. Process.* **2006**, *20*, 147–164. [[CrossRef](#)]
68. Ward, P.J.; Renssen, H.; Aerts, J.C.J.H.; van Balen, R.T.; Vandenberghe, J. Strong increases in flood frequency and discharge of the River Meuse over the late Holocene: Impacts of long-term anthropogenic land use change and climate variability. *Hydrol. Earth Syst. Sci.* **2008**, *12*, 159–175. [[CrossRef](#)]
69. Gregory, K.J. The human role in changing river channels. *Geomorphology* **2006**, *79*, 172–191. [[CrossRef](#)]
70. Tobin, G.A. The Levee Love Affair: A Stormy Relationship? *J. Am. Water Resour. Assoc.* **1995**, *31*, 359–367. [[CrossRef](#)]
71. Van Triet, N.K.; Dung, N.V.; Fujii, H.; Kummu, M.; Merz, B.; Apel, H. Has dyke development in the Vietnamese Mekong Delta shifted flood hazard downstream? *Hydrol. Earth Syst. Sci.* **2017**, *21*, 3991–4010. [[CrossRef](#)]
72. Ryffel, A.N.; Rid, W.; Grêt-Regamey, A. Land use trade-offs for flood protection: A choice experiment with visualizations. *Ecosyst. Serv.* **2014**, *10*, 111–123. [[CrossRef](#)]
73. Salzmann, N.; Huggel, C.; Nussbaumer, S.U.; Ziervogel, G. *Climate Change Adaptation Strategies—An Upstream-Downstream Perspective*; Springer: Cham, Switzerland, 2016.
74. Rogger, M.; Agnoletti, M.; Alaoui, A.; Bathurst, J.C.; Bodner, G.; Borga, M.; Chaplot, V.; Gallart, F.; Glatzel, G.; Hall, J.; et al. Land-use change impacts on floods at the catchment scale—Challenges and opportunities for future research. *Water Resour. Res.* **2017**, *53*, 5209–5219. [[CrossRef](#)] [[PubMed](#)]
75. Burby, R.J.; French, S.P. Coping With Floods: The Land Use Management Paradox. *J. Am. Plan. Assoc.* **2007**, *47*, 289–300. [[CrossRef](#)]
76. O’Connell, P.E.; Ewen, J.; O’Donnell, G.; Quinn, P. Is there a link between agricultural land-use management and flooding? *Hydrol. Earth Syst. Sci.* **2007**, *11*, 96–107. [[CrossRef](#)]
77. Carisi, F.; Domeneghetti, A.; Gaeta, M.G.; Castellarin, A. Is anthropogenic land subsidence a possible driver of riverine flood-hazard dynamics? A case study in Ravenna, Italy. *Hydrol. Sci. J.* **2017**, *6*, 1–16. [[CrossRef](#)]
78. Fuchs, S.; Keiler, M.; Zischg, A. A spatiotemporal multi-hazard exposure assessment based on property data. *Nat. Hazards Earth Syst. Sci.* **2015**, *15*, 2127–2142. [[CrossRef](#)]
79. Elmer, F.; Hoymann, J.; Düthmann, D.; Vorogushyn, S.; Kreibich, H. Drivers of flood risk change in residential areas. *Nat. Hazards Earth Syst. Sci.* **2012**, *12*, 1641–1657. [[CrossRef](#)]
80. Morales, A.P.; Gil-Guirado, S.; Cantos, J.O. Housing bubbles and the increase of flood exposure. Failures in flood risk management on the spanish south-eastern coast (1975–2013). *J. Flood Risk Manag.* **2015**, *11*, S302–S313. [[CrossRef](#)]

81. Hasan, S.; Foliente, G. Modeling infrastructure system interdependencies and socioeconomic impacts of failure in extreme events: Emerging R & D challenges. *Nat. Hazards* **2015**, *78*, 2143–2168. [[CrossRef](#)]
82. Little, R.G. Controlling Cascading Failure: Understanding the Vulnerabilities of Interconnected Infrastructures. *J. Urban Technol.* **2002**, *9*, 109–123. [[CrossRef](#)]
83. Gonzva, M.; Barroca, B.; Gautier, P.-É.; Diab, Y. Modeling disruptions causing domino effects in urban guided transport systems faced by flood hazards. *Nat. Hazards* **2017**, *86*, 183–201. [[CrossRef](#)]
84. Pescaroli, G.; Alexander, D. Critical infrastructure, panarchies and the vulnerability paths of cascading disasters. *Nat. Hazards* **2016**, *82*, 175–192. [[CrossRef](#)]
85. Nicholls, S.; Crompton, J.L. The effect of rivers, streams, and canals on property values. *River Res. Appl.* **2017**, *36*, 773. [[CrossRef](#)]
86. Adger, W.N. Vulnerability. *Glob. Environ. Chang.* **2006**, *16*, 268–281. [[CrossRef](#)]
87. Posey, J. The determinants of vulnerability and adaptive capacity at the municipal level: Evidence from floodplain management programs in the United States. *Glob. Environ. Chang.* **2009**, *19*, 482–493. [[CrossRef](#)]
88. Wiering, M.; Liefferink, D.; Crabbé, A. Stability and change in flood risk governance: On path dependencies and change agents. *J. Flood Risk Manag.* **2017**. [[CrossRef](#)]
89. Kreibich, H.; Müller, M.; Thieken, A.H.; Merz, B. Flood precaution of companies and their ability to cope with the flood in August 2002 in Saxony, Germany. *Water Resour. Res.* **2007**, *43*, 41. [[CrossRef](#)]
90. Kuhlicke, C. The dynamics of vulnerability: Some preliminary thoughts about the occurrence of ‘radical surprises’ and a case study on the 2002 flood (Germany). *Nat. Hazards* **2010**, *55*, 671–688. [[CrossRef](#)]
91. Guthrie, R. The catastrophic nature of humans. *Nat. Geosci.* **2015**, *8*, 421–422. [[CrossRef](#)]
92. Reilly, A.C.; Guikema, S.D.; Zhu, L.; Igusa, T. Evolution of vulnerability of communities facing repeated hazards. *PLoS ONE* **2017**, *12*, e0182719. [[CrossRef](#)] [[PubMed](#)]
93. Thomi, L.; Zischg, A.; Suter, H. *Was Macht Hochwasserschutzprojekte Erfolgreich? Eine Evaluation der Risikoentwicklung, des Nutzens und der Rolle privater Geldgeber*; Geographisches Institut: Bern, Switzerland, 2015.
94. White, G. *Human Adjustment to Floods*; University of Chicago: Chicago, IL, USA, 1945.
95. James, L.A.; Marcus, W.A. The human role in changing fluvial systems: Retrospect, inventory and prospect. *Geomorphology* **2006**, *79*, 152–171. [[CrossRef](#)]
96. Hartmann, T. *Clumsy Floodplains: Responsive Land Policy for Extreme Floods/by Thomas Hartmann*; Ashgate: Farnham, UK, 2011.
97. Ison, R.L.; Collins, K.B.; Wallis, P.J. Institutionalising social learning: Towards systemic and adaptive governance. *Environ. Sci. Policy* **2015**, *53*, 105–117. [[CrossRef](#)]
98. Kjeldsen, T.R.; Prosdocimi, I. Assessing the element of surprise of record-breaking flood events. *J. Flood Risk Manag.* **2016**, *19*, 83. [[CrossRef](#)]
99. Wiering, M.; Kaufmann, M.; Mees, H.; Schellenberger, T.; Ganzevoort, W.; Hegger, D.L.T.; Larrue, C.; Matczak, P. Varieties of flood risk governance in Europe: How do countries respond to driving forces and what explains institutional change? *Glob. Environ. Chang.* **2017**, *44*, 15–26. [[CrossRef](#)]
100. Collenteur, R.A.; Moel, H.; de Jongman, B.; di Baldassarre, G. The failed-levee effect: Do societies learn from flood disasters? *Nat. Hazards* **2015**, *76*, 373–388. [[CrossRef](#)]
101. Gallopín, G.C. Linkages between vulnerability, resilience, and adaptive capacity. *Glob. Environ. Chang.* **2006**, *16*, 293–303. [[CrossRef](#)]
102. White, G.F.; Kates, R.W.; Burton, I. Knowing better and losing even more: The use of knowledge in hazards management. *Environ. Hazards* **2001**, *3*, 81–92.
103. Klijn, F.; Kreibich, H.; Moel, H. de; Penning-Rowsell, E. Adaptive flood risk management planning based on a comprehensive flood risk conceptualisation. *Mitig. Adapt. Strateg. Glob. Chang.* **2015**, *20*, 845–864. [[CrossRef](#)]
104. Klinke, A.; Renn, O. Adaptive and integrative governance on risk and uncertainty. *J. Risk Res.* **2012**, *15*, 273–292. [[CrossRef](#)]
105. Koontz, T.M.; Gupta, D.; Mudliar, P.; Ranjan, P. Adaptive institutions in social-ecological systems governance: A synthesis framework. *Environ. Sci. Policy* **2015**, *53*, 139–151. [[CrossRef](#)]
106. Kruse, S.; Pütz, M. Adaptive Capacities of Spatial Planning in the Context of Climate Change in the European Alps. *Eur. Plan. Stud.* **2013**, *22*, 2620–2638. [[CrossRef](#)]
107. Hurlimann, A.C.; March, A.P. The role of spatial planning in adapting to climate change. *WIREs Clim. Chang.* **2012**, *3*, 477–488. [[CrossRef](#)]

108. Hasselman, L. Adaptive management intentions with a reality of evaluation: Getting science back into policy. *Environ. Sci. Policy* **2017**, *78*, 9–17. [[CrossRef](#)]
109. Lawrence, J.; Reisinger, A.; Mullan, B.; Jackson, B. Exploring climate change uncertainties to support adaptive management of changing flood-risk. *Environ. Sci. Policy* **2013**, *33*, 133–142. [[CrossRef](#)]
110. Mori, K.; Perrings, C. Optimal management of the flood risks of floodplain development. *Sci. Total Environ.* **2012**, *431*, 109–121. [[CrossRef](#)] [[PubMed](#)]
111. Simonovic, S.P. Managing flood risk, reliability and vulnerability. *J. Flood Risk Manag.* **2009**, *2*, 230–231. [[CrossRef](#)]
112. Priest, S.J.; Penning-Rowsell, E.C.; Suykens, C.; Lang, M.; Klijn, F.; Samuels, P. Promoting adaptive flood risk management: The role and potential of flood recovery mechanisms. *E3S Web Conf.* **2016**, *7*, 17005. [[CrossRef](#)]
113. Prenger-Berninghoff, K.; Cortes, V.J.; Sprague, T.; Aye, Z.C.; Greiving, S.; Głowacki, W.; Sterlacchini, S. The connection between long-term and short-term risk management strategies for flood and landslide hazards: Examples from land-use planning and emergency management in four European case studies. *Nat. Hazards Earth Syst. Sci.* **2014**, *14*, 3261–3278. [[CrossRef](#)]
114. Smit, B.; Wandel, J. Adaptation, adaptive capacity and vulnerability. *Glob. Environ. Chang.* **2006**, *16*, 282–292. [[CrossRef](#)]
115. Thaler, T. Moving away from local-based flood risk policy in Austria. *Reg. Stud. Reg. Sci.* **2016**, *3*, 329–336. [[CrossRef](#)]
116. Van der Pol, T.D.; van Ierland, E.C.; Gabbert, S. Economic analysis of adaptive strategies for flood risk management under climate change. *Mitig. Adapt. Strateg. Glob. Chang.* **2015**. [[CrossRef](#)]
117. Birkmann, J.; Bach, C.; Vollmer, M. Tools for Resilience Building and Adaptive Spatial Governance. *Raumforsch. Raumordn.* **2012**, *70*, 293–308. [[CrossRef](#)]
118. Zischg, A.; Schober, S.; Sereinig, N.; Rauter, M.; Seymann, C.; Goldschmidt, F.; Bäk, R.; Schleicher, E. Monitoring the temporal development of natural hazard risks as a basis indicator for climate change adaptation. *Nat. Hazards* **2013**, *67*, 1045–1058. [[CrossRef](#)]
119. Miller, J.H.; Page, S.E. *Complex Adaptive Systems: An Introduction to Computational Models of Social Life*; Miller, J.H., Page, S.E., Eds.; Princeton University Press: Princeton, NJ, USA, 2007.
120. Mitchell, M. *Complexity: A Guided Tour*; Oxford University Press: Oxford, UK, 2009.
121. Birdsey, L.; Szabo, C.; Falkner, K. Identifying Self-Organization and Adaptability in Complex Adaptive Systems. In Proceedings of the 2017 IEEE 11th International Conference on Self-Adaptive and Self-Organizing Systems (SASO), Tucson, AZ, USA, 18–22 September 2017; pp. 131–140.
122. Bras, R.L. Complexity and organization in hydrology: A personal view. *Water Resour. Res.* **2015**. [[CrossRef](#)]
123. Kirschke, S.; BORCHARDT, D.; Newig, J. Mapping Complexity in Environmental Governance: A comparative analysis of 37 priority issues in German water management. *Environ. Policy Gov.* **2017**, *3*, 101. [[CrossRef](#)]
124. Weis, S.W.M.; Agostini, V.N.; Roth, L.M.; Gilmer, B.; Schill, S.R.; Knowles, J.E.; Blyther, R. Assessing vulnerability: An integrated approach for mapping adaptive capacity, sensitivity, and exposure. *Clim. Chang.* **2016**, *136*, 615–629. [[CrossRef](#)]
125. Blair, P.; Buytaert, W. Socio-hydrological modelling: A review asking “why, what and how?”. *Hydrol. Earth Syst. Sci.* **2016**, *20*, 443–478. [[CrossRef](#)]
126. Schlüter, M.; Mcallister, R.R.J.; Arlinghaus, R.; Bunnefeld, N.; Eisenack, K.; Hölker, F.; Milner-Gulland, E.J.; Müller, B. New horizons for managing the environment: A review of coupled social-ecological systems modeling. *Nat. Resour. Model.* **2012**, *25*, 219–272. [[CrossRef](#)]
127. Werner, B.T.; McNamara, D.E. Dynamics of coupled human-landscape systems. *Geomorphology* **2007**, *91*, 393–407. [[CrossRef](#)]
128. Liu, J.; Dietz, T.; Carpenter, S.R.; Folke, C.; Alberti, M.; Redman, C.M.; Ouyang, Z.; Deadman, P.; Kratz, T.; Provencher, W. Coupled human and natural systems. *Ambio* **2007**, 639–649.
129. Noël, P.H.; Cai, X. On the role of individuals in models of coupled human and natural systems: Lessons from a case study in the Republican River Basin. *Environ. Model. Softw.* **2017**, *92*, 1–16. [[CrossRef](#)]
130. Folke, C. Resilience: The emergence of a perspective for social-ecological systems analyses. *Glob. Environ. Chang.* **2006**, *16*, 253–267. [[CrossRef](#)]

131. Turner, B.L.; Matson, P.A.; McCarthy, J.J.; Corell, R.W.; Christensen, L.; Eckley, N.; Hovelsrud-Broda, G.K.; Kasperson, J.X.; Kasperson, R.E.; Luers, A.; et al. Illustrating the coupled human-environment system for vulnerability analysis: Three case studies. *Proc. Natl. Acad. Sci. USA* **2003**, *100*, 8080–8085. [[CrossRef](#)] [[PubMed](#)]
132. O’Connell, P.E.; O’Donnell, G. Towards modelling flood protection investment as a coupled human and natural system. *Hydrol. Earth Syst. Sci.* **2014**, *18*, 155–171. [[CrossRef](#)]
133. McMillan, H.; Montanari, A.; Cudennec, C.; Savenije, H.; Kreibich, H.; Krueger, T.; Liu, J.; Mejia, A.; van Loon, A.; Aksoy, H.; et al. Panta Rhei 2013–2015: Global perspectives on hydrology, society and change. *Hydrol. Sci. J.* **2016**, 1–18. [[CrossRef](#)]
134. Kreibich, H.; Krueger, T.; van Loon, A.; Mejia, A.; Liu, J.; McMillan, H.; Castellarin, A. Scientific debate of Panta Rhei research—How to advance our knowledge of changes in hydrology and society? *Hydrol. Sci. J.* **2016**, 1–3. [[CrossRef](#)]
135. Montanari, A.; Young, G.; Savenije, H.H.G.; Hughes, D.; Wagener, T.; Ren, L.L.; Koutsoyiannis, D.; Cudennec, C.; Toth, E.; Grimaldi, S.; et al. “Panta Rhei—Everything Flows”: Change in hydrology and society—The IAHS Scientific Decade 2013–2022. *Hydrol. Sci. J.* **2013**, *58*, 1256–1275. [[CrossRef](#)]
136. Sivapalan, M.; Savenije, H.H.G.; Blöschl, G. Socio-hydrology: A new science of people and water. *Hydrol. Process.* **2012**, *26*, 1270–1276. [[CrossRef](#)]
137. Di Baldassarre, G.; Kemerink, J.S.; Kooy, M.; Brandimarte, L. Floods and societies: The spatial distribution of water-related disaster risk and its dynamics. *WIREs Water* **2014**, *1*, 133–139. [[CrossRef](#)]
138. Pande, S.; Sivapalan, M. Progress in socio-hydrology: A meta-analysis of challenges and opportunities. *WIREs Water* **2016**, *4*, e1193. [[CrossRef](#)]
139. Elshafei, Y.; Sivapalan, M.; Tonts, M.; Hipsey, M.R. A prototype framework for models of socio-hydrology: Identification of key feedback loops and parameterisation approach. *Hydrol. Earth Syst. Sci.* **2014**, *18*, 2141–2166. [[CrossRef](#)]
140. Gupta, H.V.; Nearing, G.S. Debates-the future of hydrological sciences: A (common) path forward? Using models and data to learn: A systems theoretic perspective on the future of hydrological science. *Water Resour. Res.* **2014**, *50*, 5351–5359. [[CrossRef](#)]
141. Liu, D.; Tian, F.; Lin, M.; Sivapalan, M. A conceptual socio-hydrological model of the co-evolution of humans and water: Case study of the Tarim River basin, western China. *Hydrol. Earth Syst. Sci.* **2015**, *19*, 1035–1054. [[CrossRef](#)]
142. Garcia, M.; Portney, K.; Islam, S. A question driven socio-hydrological modeling process. *Hydrol. Earth Syst. Sci.* **2016**, *20*, 73–92. [[CrossRef](#)]
143. Mount, N.J.; Maier, H.R.; Toth, E.; Elshorbagy, A.; Solomatine, D.; Chang, F.-J.; Abrahart, R.J. Data-driven modelling approaches for socio-hydrology: Opportunities and challenges within the Panta Rhei Science Plan. *Hydrol. Sci. J.* **2016**, *61*, 1192–1208. [[CrossRef](#)]
144. Seidl, R.; Barthel, R. Linking scientific disciplines: Hydrology and social sciences. *J. Hydrol.* **2017**, *550*, 441–452. [[CrossRef](#)]
145. Sivapalan, M.; Konar, M.; Srinivasan, V.; Chhatre, A.; Wutich, A.; Scott, C.A.; Wescoat, J.L.; Rodríguez-Iturbe, I. Socio-hydrology: Use-inspired water sustainability science for the Anthropocene. *Earth Futur.* **2014**, *2*, 225–230. [[CrossRef](#)]
146. Sivapalan, M.; Blöschl, G. Time scale interactions and the coevolution of humans and water. *Water Resour. Res.* **2015**, *51*, 6988–7022. [[CrossRef](#)]
147. Viglione, A.; Di Baldassarre, G.; Brandimarte, L.; Kuil, L.; Carr, G.; Salinas, J.L.; Scolobig, A.; Blöschl, G. Insights from socio-hydrology modelling on dealing with flood risk—Roles of collective memory, risk-taking attitude and trust. *J. Hydrol.* **2014**, *518*, 71–82. [[CrossRef](#)]
148. Wesseling, A.; Kooy, M.; Warner, J. Socio-hydrology and hydrosocial analysis: Toward dialogues across disciplines. *WIREs Water* **2016**, *4*, e1196. [[CrossRef](#)]
149. Fuchs, S.; Karagiorgos, K.; Kitikidou, K.; Maris, F.; Paparrizos, S.; Thaler, T. Flood risk perception and adaptation capacity: A contribution to the socio-hydrology debate. *Hydrol. Earth Syst. Sci.* **2017**, *21*, 3183–3198. [[CrossRef](#)]
150. Lu, Z.; Wei, Y.; Xiao, H.; Zou, S.; Xie, J.; Ren, J.; Western, A. Evolution of the human–water relationships in the Heihe River basin in the past 2000 years. *Hydrol. Earth Syst. Sci.* **2015**, *19*, 2261–2273. [[CrossRef](#)]

151. Di Baldassarre, G.; Saccà, S.; Aronica, G.T.; Grimaldi, S.; Ciullo, A.; Crisci, M. Human-flood interactions in Rome over the past 150 years. *Adv. Geosci.* **2017**, *44*, 9–13. [[CrossRef](#)]
152. Gaál, L.; Szolgay, J.; Kohnová, S.; Parajka, J.; Merz, R.; Viglione, A.; Blöschl, G. Flood timescales: Understanding the interplay of climate and catchment processes through comparative hydrology. *Water Resour. Res.* **2012**, *48*, 383. [[CrossRef](#)]
153. Mao, F.; Clark, J.; Karpouzoglou, T.; Dewulf, A.; Buytaert, W.; Hannah, D. HESS Opinions: A conceptual framework for assessing socio-hydrological resilience under change. *Hydrol. Earth Syst. Sci.* **2017**, *21*, 3655–3670. [[CrossRef](#)]
154. Reynard, E.; Bonriposi, M.; Graefe, O.; Homewood, C.; Huss, M.; Kauzlaric, M.; Liniger, H.; Rey, E.; Rist, S.; Schädler, B.; et al. Interdisciplinary assessment of complex regional water systems and their future evolution: How socioeconomic drivers can matter more than climate. *WIREs Water* **2014**, *1*, 413–426. [[CrossRef](#)]
155. Sofia, G.; Roder, G.; Dalla Fontana, G.; Tarolli, P. Flood dynamics in urbanised landscapes: 100 years of climate and humans' interaction. *Sci. Rep.* **2017**, *7*, 40527. [[CrossRef](#)] [[PubMed](#)]
156. Westerberg, I.K.; Di Baldassarre, G.; Beven, K.J.; Coxon, G.; Krueger, T. Perceptual models of uncertainty for socio-hydrological systems: A flood risk change example. *Hydrol. Sci. J.* **2017**. [[CrossRef](#)]
157. Di Baldassarre, G.; Viglione, A.; Carr, G.; Kuil, L.; Yan, K.; Brandimarte, L.; Blöschl, G. Debates-Perspectives on socio-hydrology: Capturing feedbacks between physical and social processes. *Water Resour. Res.* **2015**, *51*, 4770–4781. [[CrossRef](#)]
158. Gober, P.; Wheeler, H.S. Debates-Perspectives on socio-hydrology: Modeling flood risk as a public policy problem. *Water Resour. Res.* **2015**, *51*, 4782–4788. [[CrossRef](#)]
159. Loucks, D.P. Debates-Perspectives on socio-hydrology: Simulating hydrologic-human interactions. *Water Resour. Res.* **2015**, *51*, 4789–4794. [[CrossRef](#)]
160. Montanari, A. Debates-Perspectives on socio-hydrology: Introduction. *Water Resour. Res.* **2015**, *51*, 4768–4769. [[CrossRef](#)]
161. Sanderson, M.R.; Bergtold, J.S.; Heier Stamm, J.L.; Caldas, M.M.; Ramsey, S.M. Bringing the “social” into socio-hydrology: Conservation policy support in the Central Great Plains of Kansas, USA. *Water Resour. Res.* **2017**, *53*, 6725–6743. [[CrossRef](#)]
162. Sivapalan, M. Debates-Perspectives on socio-hydrology: Changing water systems and the “tyranny of small problems”-Socio-hydrology. *Water Resour. Res.* **2015**, *51*, 4795–4805. [[CrossRef](#)]
163. Troy, T.J.; Pavao-Zuckerman, M.; Evans, T.P. Debates-Perspectives on socio-hydrology: Socio-hydrologic modeling: Tradeoffs, hypothesis testing, and validation. *Water Resour. Res.* **2015**, *51*, 4806–4814. [[CrossRef](#)]
164. Di Baldassarre, G.; Kooy, M.; Kemerink, J.S.; Brandimarte, L. Towards understanding the dynamic behaviour of floodplains as human-water systems. *Hydrol. Earth Syst. Sci.* **2013**, *17*, 3235–3244. [[CrossRef](#)]
165. Di Baldassarre, G.; Viglione, A.; Carr, G.; Kuil, L.; Salinas, J.L.; Blöschl, G. Socio-hydrology: Conceptualising human-flood interactions. *Hydrol. Earth Syst. Sci.* **2013**, *17*, 3295–3303. [[CrossRef](#)]
166. Ciullo, A.; Viglione, A.; Castellarin, A.; Crisci, M.; Di Baldassarre, G. Socio-hydrological modelling of flood-risk dynamics: Comparing the resilience of green and technological systems. *Hydrol. Sci. J.* **2016**, *62*, 880–891. [[CrossRef](#)]
167. Ashmore, P. Towards a sociogeomorphology of rivers. *Geomorphology* **2015**, *251*, 149–156. [[CrossRef](#)]
168. Keiler, M. Geomorphology and Complexity—inseparably connected? *Z. Geomorphol. Suppl. Issues* **2011**, *55*, 233–257. [[CrossRef](#)]
169. Temme, A.J.A.M.; Keiler, M.; Karszenberg, D.; Lang, A. Complexity and non-linearity in earth surface processes—Concepts, methods and applications. *Earth Surf. Process. Landf.* **2015**, *40*, 1270–1274. [[CrossRef](#)]
170. Slater, L.J.; Singer, M.B.; Kirchner, J.W. Hydrologic versus geomorphic drivers of trends in flood hazard. *Geophys. Res. Lett.* **2015**, *42*, 370–376. [[CrossRef](#)]
171. Srinivasan, V.; Sanderson, M.; Garcia, M.; Konar, M.; Blöschl, G.; Sivapalan, M. Prediction in a socio-hydrological world. *Hydrol. Sci. J.* **2016**, *62*, 338–345. [[CrossRef](#)]
172. Lane, S.N. Acting, predicting and intervening in a socio-hydrological world. *Hydrol. Earth Syst. Sci.* **2014**, *18*, 927–952. [[CrossRef](#)]
173. Kelly, R.A.; Jakeman, A.J.; Barreteau, O.; Borsuk, M.E.; ElSawah, S.; Hamilton, S.H.; Henriksen, H.J.; Kuikka, S.; Maier, H.R.; Rizzoli, A.E.; et al. Selecting among five common modelling approaches for integrated environmental assessment and management. *Environ. Model. Softw.* **2013**, *47*, 159–181. [[CrossRef](#)]

174. Neuwirth, C.; Peck, A.; Simonović, S.P. Modeling structural change in spatial system dynamics: A Daisyworld example. *Environ. Model. Softw.* **2015**, *65*, 30–40. [[CrossRef](#)] [[PubMed](#)]
175. Forrester, J.W. *Urban Dynamics*; Massachusetts Institute of Technology Press: Boston, MA, USA, 1969.
176. Luhmann, N. *Soziale Systeme*; Suhrkamp: Frankfurt, Germany, 1987.
177. Rougé, C.; Mathias, J.-D.; Deffuant, G. Vulnerability: From the conceptual to the operational using a dynamical system perspective. *Environ. Model. Softw.* **2015**, *73*, 218–230. [[CrossRef](#)]
178. Grames, J.; Prskawetz, A.; Grass, D.; Blöschl, G. Modelling the interaction between flooding events and economic growth. *Proc. IAHS* **2015**, *369*, 3–6. [[CrossRef](#)]
179. Roos, M.M.D.; Hartmann, T.T.; Spit, T.T.J.M.; Johann, G.G. Constructing risks—Internalisation of flood risks in the flood risk management plan. *Environ. Sci. Policy* **2017**, *74*, 23–29. [[CrossRef](#)]
180. Wingo, P.; Brookes, A.; Bolte, J. Modular and spatially explicit: A novel approach to system dynamics. *Environ. Model. Softw.* **2017**, *94*, 48–62. [[CrossRef](#)]
181. Neuwirth, C. System dynamics simulations for data-intensive applications. *Environ. Model. Softw.* **2017**, *96*, 140–145. [[CrossRef](#)]
182. Neuwirth, C.; Hofer, B.; Peck, A. Spatiotemporal processes and their implementation in Spatial System Dynamics models. *J. Spat. Sci.* **2015**, *60*, 277–288. [[CrossRef](#)]
183. ElSawah, S.; Pierce, S.A.; Hamilton, S.H.; van Delden, H.; Haase, D.; Elmahdi, A.; Jakeman, A.J. An overview of the system dynamics process for integrated modelling of socio-ecological systems: Lessons on good modelling practice from five case studies. *Environ. Model. Softw.* **2017**, *93*, 127–145. [[CrossRef](#)]
184. Simonovic, S.P. *Systems Approach to Management of Disasters*; John Wiley & Sons: Hoboken, NJ, USA, 2011.
185. Heppenstall, A.; Malleson, N.; Crooks, A. “Space, the Final Frontier”: How Good are Agent-Based Models at Simulating Individuals and Space in Cities? *Systems* **2016**, *4*, 9. [[CrossRef](#)]
186. Malanson, G.P.; Walsh, S.J. Agent-based models: Individuals interacting in space. *Appl. Geogr.* **2015**, *56*, 95–98. [[CrossRef](#)]
187. Dawson, R.J.; Peppe, R.; Wang, M. An agent-based model for risk-based flood incident management. *Nat. Hazards* **2011**, *59*, 167–189. [[CrossRef](#)]
188. Lumbroso, D.; Davison, M. Use of an agent based model and Monte Carlo analysis to estimate the effectiveness of emergency management interventions to reduce loss of life during extreme floods. *J. Flood Risk Manag.* **2016**, *11*, S419–S433. [[CrossRef](#)]
189. Dressler, G.; Müller, B.; Frank, K.; Kuhlicke, C. Towards thresholds of disaster management performance under demographic change: Exploring functional relationships using agent-based modeling. *Nat. Hazards Earth Syst. Sci.* **2016**, *16*, 2287–2301. [[CrossRef](#)]
190. Jenkins, K.; Surminski, S.; Hall, J.; Crick, F. Assessing surface water flood risk and management strategies under future climate change: Insights from an Agent-Based Model. *Sci. Total Environ.* **2017**, *595*, 159–168. [[CrossRef](#)] [[PubMed](#)]
191. Laniak, G.F.; Olchin, G.; Goodall, J.; Voinov, A.; Hill, M.; Glynn, P.; Whelan, G.; Geller, G.; Quinn, N.; Blind, M.; et al. Integrated environmental modeling: A vision and roadmap for the future. *Environ. Model. Softw.* **2013**, *39*, 3–23. [[CrossRef](#)]
192. Welsh, W.D.; Vaze, J.; Dutta, D.; Rassam, D.; Rahman, J.M.; Jolly, I.D.; Wallbrink, P.; Podger, G.M.; Bethune, M.; Hardy, M.J.; et al. An integrated modelling framework for regulated river systems. *Environ. Model. Softw.* **2013**, *39*, 81–102. [[CrossRef](#)]
193. Martin, R.; Schlüter, M. Combining system dynamics and agent-based modeling to analyze social-ecological interactions—An example from modeling restoration of a shallow lake. *Front. Environ. Sci.* **2015**, *3*, 1166. [[CrossRef](#)]
194. Malard, J.J.; Inam, A.; Hassanzadeh, E.; Adamowski, J.; Tuy, H.A.; Melgar-Quiñonez, H. Development of a software tool for rapid, reproducible, and stakeholder-friendly dynamic coupling of system dynamics and physically-based models. *Environ. Model. Softw.* **2017**, *96*, 410–420. [[CrossRef](#)]
195. Zischg, A.; Fuchs, S.; Keiler, M.; Meißl, G. Modelling the system behaviour of wet snow avalanches using an expert system approach for risk management on high alpine traffic roads. *Nat. Hazards Earth Syst. Sci.* **2005**, *5*, 821–832. [[CrossRef](#)]
196. Falter, D.; Schröter, K.; Dung, N.V.; Vorogushyn, S.; Kreibich, H.; Hündecha, Y.; Apel, H.; Merz, B. Spatially coherent flood risk assessment based on long-term continuous simulation with a coupled model chain. *J. Hydrol.* **2015**, *524*, 182–193. [[CrossRef](#)]

197. Zischg, A.P.; Felder, G.; Weingartner, R.; Quinn, N.; Coxon, G.; Neal, J.; Freer, J.; Bates, P. Effects of variability in probable maximum precipitation patterns on flood losses. *Hydrol. Earth Syst. Sci. Discuss.* **2018**, in review. [[CrossRef](#)]
198. Saint-Geours, N.; Bailly, J.-S.; Grelot, F.; Lavergne, C. Multi-scale spatial sensitivity analysis of a model for economic appraisal of flood risk management policies. *Environ. Model. Softw.* **2014**, *60*, 153–166. [[CrossRef](#)]
199. Thaler, T.; Zischg, A.; Keiler, M.; Fuchs, S. Allocation of risk and benefits—Distributional justices in mountain hazard management. *Reg. Environ. Chang.* **2018**, *18*, 353–365. [[CrossRef](#)]



© 2018 by the author. Licensee MDPI, Basel, Switzerland. This article is an open access article distributed under the terms and conditions of the Creative Commons Attribution (CC BY) license (<http://creativecommons.org/licenses/by/4.0/>).

6 References

- Ahmad, S.S., Simonovic, S.P., 2013. Spatial and temporal analysis of urban flood risk assessment. *Urban Water Journal* 10, 26–49. 10.1080/1573062X.2012.690437.
- Alfieri, L., Bisselink, B., Dottori, F., Naumann, G., Roo, A. de, Salamon, P., Wyser, K., Feyen, L., 2016a. Global projections of river flood risk in a warmer world. *Earth's Future*. 10.1002/2016EF000485.
- Alfieri, L., Burek, P., Feyen, L., Forzieri, G., 2015a. Global warming increases the frequency of river floods in Europe. *Hydrol. Earth Syst. Sci.* 19, 2247–2260. 10.5194/hess-19-2247-2015.
- Alfieri, L., Dottori, F., Betts, R., Salamon, P., Feyen, L., 2018. Multi-Model Projections of River Flood Risk in Europe under Global Warming. *Climate* 6, 6. 10.3390/cli6010006.
- Alfieri, L., Feyen, L., Di Baldassarre, G., 2016b. Increasing flood risk under climate change: A pan-European assessment of the benefits of four adaptation strategies. *Climatic Change*. 10.1007/s10584-016-1641-1.
- Alfieri, L., Feyen, L., Dottori, F., Bianchi, A., 2015b. Ensemble flood risk assessment in Europe under high end climate scenarios. *Global Environmental Change* 35, 199–212. 10.1016/j.gloenvcha.2015.09.004.
- Armbruster, S., Hintermann, B., Zischg, A., 2018. The effects of flood events on land and housing value: Evidence from the Swiss real estate market: SURED 2018 - Monte Verità Conference on Sustainable Resource Use and Economic Dynamics, June 3-7, 2018, Ascona/Switzerland. ETH Zurich, Zurich, 39 pp.
- Arnell, N.W., Gosling, S.N., 2016. The impacts of climate change on river flood risk at the global scale. *Climatic Change* 134, 387–401. 10.1007/s10584-014-1084-5.
- Beniston, M., Farinotti, D., Stoffel, M., Andreassen, L.M., Coppola, E., Eckert, N., Fantini, A., Giacomoni, F., Hauck, C., Huss, M., Huwald, H., Lehning, M., López-Moreno, J.-I., Magnusson, J., Marty, C., Morán-Tejeda, E., Morin, S., Naaim, M., Provenzale, A., Rabatel, A., Six, D., STÖTTER, J., Strasser, U., Terzago, S., Vincent, C., 2018. The European mountain cryosphere: A review of its current state, trends, and future challenges. *The Cryosphere* 12, 759–794. 10.5194/tc-12-759-2018.
- Bermúdez, M., Zischg, A.P., 2018. Sensitivity of flood loss estimates to building representation and flow depth attribution methods in micro-scale flood modelling. *Nat Hazards* 92, 1633–1648. 10.1007/s11069-018-3270-7.
- Bernet, D.B., Zischg, A.P., Prasuhn, V., Weingartner, R., 2018. Modeling the extent of surface water floods in rural areas: Lessons learned from the application of various uncalibrated models. *Environmental Modelling & Software* 109, 134–151. 10.1016/j.envsoft.2018.08.005.
- Blair, P., Buytaert, W., 2016. Socio-hydrological modelling: A review asking "why, what and how?". *Hydrol. Earth Syst. Sci.* 20, 443–478. 10.5194/hess-20-443-2016.
- Boeckli, L., Brenning, A., Gruber, S., Noetzli, J., 2012a. A statistical approach to modelling permafrost distribution in the European Alps or similar mountain ranges. *The Cryosphere* 6, 125–140. 10.5194/tc-6-125-2012.
- Boeckli, L., Brenning, A., Gruber, S., Noetzli, J., 2012b. Permafrost distribution in the European Alps: Calculation and evaluation of an index map and summary statistics. *The Cryosphere* 6, 807–820. 10.5194/tc-6-807-2012.

- Bouwer, L.M., Bubeck, P., Aerts, J.C.J.H., 2010. Changes in future flood risk due to climate and development in a Dutch polder area. *Global Environmental Change* 20, 463–471. 10.1016/j.gloenvcha.2010.04.002.
- Calvin, K., Bond-Lamberty, B., 2018. Integrated human-earth system modeling—state of the science and future directions. *Environ. Res. Lett.* 13, 63006. 10.1088/1748-9326/aac642.
- Clark, M.P., Fan, Y., Lawrence, D.M., Adam, J.C., Bolster, D., Gochis, D.J., Hooper, R.P., Kumar, M., Leung, L.R., Mackay, D.S., Maxwell, R.M., Shen, C., Swenson, S.C., Zeng, X., 2015. Improving the representation of hydrologic processes in Earth System Models. *Water Resour. Res.* 51, 5929–5956. 10.1002/2015WR017096.
- Cremonese, E., Gruber, S., Phillips, M., Pogliotti, P., Boeckli, L., Noetzli, J., Suter, C., Bodin, X., Crepez, A., Kellerer-Pirklbauer, A., Lang, K., Letey, S., Mair, V., Morra di Cella, U., Ravel, L., Scapozza, C., Seppi, R., Zischg, A., 2011. Brief Communication: "An inventory of permafrost evidence for the European Alps". *The Cryosphere* 5, 651–657. 10.5194/tc-5-651-2011.
- Di Baldassarre, G., Kooy, M., Kemerink, J.S., Brandimarte, L., 2013a. Towards understanding the dynamic behaviour of floodplains as human-water systems. *Hydrol. Earth Syst. Sci.* 17, 3235–3244. 10.5194/hess-17-3235-2013.
- Di Baldassarre, G., Viglione, A., Carr, G., Kuil, L., Salinas, J.L., Blöschl, G., 2013b. Socio-hydrology: conceptualising human-flood interactions. *Hydrol. Earth Syst. Sci.* 17, 3295–3303. 10.5194/hess-17-3295-2013.
- Di Baldassarre, G., Viglione, A., Carr, G., Kuil, L., Yan, K., Brandimarte, L., Blöschl, G., 2015. Debates-Perspectives on socio-hydrology: Capturing feedbacks between physical and social processes. *Water Resour. Res.* 51, 4770–4781. 10.1002/2014WR016416.
- Donges, J.F., Heitzig, J., Barfuss, W., Kassel, J.A., Kittel, T., Kolb, J.J., Kolster, T., Müller-Hansen, F., Otto, I.M., Wiedermann, M., Zimmerer, K.B., Lucht, W., 2018a. Earth system modelling with complex dynamic human societies: The copan: CORE World-Earth modeling framework. *Earth Syst. Dynam. Discuss.*, 1–27. 10.5194/esd-2017-126.
- Donges, J.F., Lucht, W., Heitzig, J., Barfuss, W., Cornell, S.E., Lade, S.J., Schlüter, M., 2018b. Taxonomies for structuring models for World-Earth system analysis of the Anthropocene: Subsystems, their interactions and social-ecological feedback loops. *Earth Syst. Dynam. Discuss.*, 1–30. 10.5194/esd-2018-27.
- Donges, J.F., Winkelmann, R., Lucht, W., Cornell, S.E., Dyke, J.G., Rockström, J., Heitzig, J., Schellnhuber, H.J., 2017. Closing the loop: Reconnecting human dynamics to Earth System science. *The Anthropocene Review* 4, 151–157. 10.1177/2053019617725537.
- Dottori, F., Szewczyk, W., Ciscar, J.-C., Zhao, F., Alfieri, L., Hirabayashi, Y., Bianchi, A., Mongelli, I., Frieler, K., Betts, R.A., Feyen, L., 2018. Increased human and economic losses from river flooding with anthropogenic warming. *Nature Climate change* 5, 171. 10.1038/s41558-018-0257-z.
- Elmer, F., Hoymann, J., Düthmann, D., Vorogushyn, S., Kreibich, H., 2012. Drivers of flood risk change in residential areas. *Nat. Hazards Earth Syst. Sci.* 12, 1641–1657. 10.5194/nhess-12-1641-2012.
- Felder, G., Gómez-Navarro, J.J., Zischg, A.P., Raible, C.C., Röthlisberger, V., Bozhinova, D., Martius, O., Weingartner, R., 2018. From global circulation to local flood loss: Coupling models across the scales. *Science of The Total Environment* 635, 1225–1239. 10.1016/j.scitotenv.2018.04.170.
- Felder, G., Weingartner, R., 2017. Assessment of deterministic PMF modelling approaches. *Hydrological Sciences Journal*. 10.1080/02626667.2017.1319065.

- Felder, G., Zischg, A., Weingartner, R., 2017. The effect of coupling hydrologic and hydrodynamic models on probable maximum flood estimation. *Journal of Hydrology* 550, 157–165. 10.1016/j.jhydrol.2017.04.052.
- Feyen, L., Dankers, R., Bódis, K., Salamon, P., Barredo, J.I., 2012. Fluvial flood risk in Europe in present and future climates. *Climatic Change* 112, 47–62. 10.1007/s10584-011-0339-7.
- Flato, G.M., 2011. Earth system models: An overview. *WIREs Clim Change* 2, 783–800. 10.1002/wcc.148.
- Forrester, J.W., 1969. *Urban dynamics*. Massachusetts Institute of Technology Press, Boston.
- Fuchs, S., Heiss, K., Hübl, J., 2007. Towards an empirical vulnerability function for use in debris flow risk assessment. *Nat. Hazards Earth Syst. Sci.* 7, 495–506. 10.5194/nhess-7-495-2007.
- Fuchs, S., Keiler, M., Zischg, A., 2015. A spatiotemporal multi-hazard exposure assessment based on property data. *Nat. Hazards Earth Syst. Sci.* 15, 2127–2142. 10.5194/nhess-15-2127-2015.
- Fuchs, S., Keiler, M., Zischg, A., Bründl, M., 2005. The long-term development of avalanche risk in settlements considering the temporal variability of damage potential. *Nat. Hazards Earth Syst. Sci.* 5, 893–901. 10.5194/nhess-5-893-2005.
- Fuchs, S., Röthlisberger, V., Thaler, T., Zischg, A., Keiler, M., 2017. Natural Hazard Management from a Coevolutionary Perspective: Exposure and Policy Response in the European Alps. *Annals of the American Association of Geographers* 107, 382–392. 10.1080/24694452.2016.1235494.
- Giorgi, F., Avissar, R., 1997. Representation of heterogeneity effects in Earth system modeling: Experience from land surface modeling. *Rev. Geophys.* 35, 413–437. 10.1029/97RG01754.
- Grames, J., Prskawetz, A., Grass, D., Blöschl, G., 2015. Modelling the interaction between flooding events and economic growth. *Proc. IAHS* 369, 3–6. 10.5194/piahs-369-3-2015.
- Himmelsbach, I., Glaser, R., Schoenbein, J., Riemann, D., Martin, B., 2015. Flood risk along the upper Rhine since AD 1480. *Hydrol. Earth Syst. Sci. Discuss.* 12, 177–211. 10.5194/hessd-12-177-2015.
- Hirabayashi, Y., Mahendran, R., Koirala, S., Konoshima, L., Yamazaki, D., Watanabe, S., Kim, H., Kanae, S., 2013. Global flood risk under climate change. *Nature Climate change* 3, 816–821. 10.1038/nclimate1911.
- Hufschmidt, G., Crozier, M., Glade, T., 2005. Evolution of natural risk: Research framework and perspectives. *Nat. Hazards Earth Syst. Sci.* 5, 375–387. 10.5194/nhess-5-375-2005.
- Hundecha, Y., Merz, B., 2012. Exploring the relationship between changes in climate and floods using a model-based analysis. *Water Resour. Res.* 48, 3331. 10.1029/2011WR010527.
- Jongman, B., Ward, P.J., Aerts, J.C.J.H., 2012. Global exposure to river and coastal flooding: Long term trends and changes. *Global Environmental Change* 22, 823–835. 10.1016/j.gloenvcha.2012.07.004.
- Jonkman, S.N., 2013. Advanced flood risk analysis required. *Nature Climate change* 3, 1004. 10.1038/nclimate2031.
- Keiler, M., Zischg, A., Fuchs, S., Hama, M., Stötter, J., 2005. Avalanche related damage potential - changes of persons and mobile values since the mid-twentieth century, case study Galtür. *Nat. Hazards Earth Syst. Sci.* 5, 49–58. 10.5194/nhess-5-49-2005.
- Kelly, R.A., Jakeman, A.J., Barreteau, O., Borsuk, M.E., ElSawah, S., Hamilton, S.H., Henriksen, H.J., Kuikka, S., Maier, H.R., Rizzoli, A.E., van Delden, H., Voinov, A.A., 2013. Selecting among five common modelling approaches for integrated environmental assessment and management. *Environmental Modelling & Software* 47, 159–181. 10.1016/j.envsoft.2013.05.005.

- Kenner, R., Chinellato, G., Iasio, C., Mosna, D., Cuozzo, G., Benedetti, E., Visconti, M.G., Manunta, M., Phillips, M., Mair, V., Zischg, A., Thiebes, B., Strada, C., 2016. Integration of space-borne DInSAR data in a multi-method monitoring concept for alpine mass movements. *Cold Regions Science and Technology* 131, 65–75. 10.1016/j.coldregions.2016.09.007.
- Kundzewicz, Z.W., Kanae, S., Seneviratne, S.I., Handmer, J., Nicholls, N., Peduzzi, P., Mechler, R., Bouwer, L.M., Arnell, N., Mach, K., Muir-Wood, R., Brakenridge, G.R., Kron, W., Benito, G., Honda, Y., Takahashi, K., Sherstyukov, B., 2014. Flood risk and climate change: global and regional perspectives. *Hydrological Sciences Journal* 59, 1–28. 10.1080/02626667.2013.857411.
- Liu, J., Dietz, T., Carpenter, S.R., Alberti, M., Folke, C., Moran, E., Pell, A.N., Deadman, P., Kratz, T., Lubchenco, J., Ostrom, E., Ouyang, Z., Provencher, W., Redman, C.L., Schneider, S.H., Taylor, W.W., 2007a. Complexity of coupled human and natural systems. *Science (New York, N.Y.)* 317, 1513–1516. 10.1126/science.1144004.
- Liu, J., Dietz, T., Carpenter, S.R., Folke, C., Alberti, M., Redman, C.M., Ouyang, Z., Deadman, P., Kratz, T., Provencher, W., 2007b. Coupled human and natural systems. *Ambio*, 639–649.
- Liu, J., Hertel, T.W., Diffenbaugh, N.S., Delgado, M.S., Ashfaq, M., 2015. Future property damage from flooding: Sensitivities to economy and climate change. *Climatic Change* 132, 741–749. 10.1007/s10584-015-1478-z.
- Löschner, L., Herrnegger, M., Apperl, B., Senoner, T., Seher, W., Nachtnebel, H.P., 2016. Flood risk, climate change and settlement development: A micro-scale assessment of Austrian municipalities. *Reg Environ Change* 42, 125. 10.1007/s10113-016-1009-0.
- Luhmann, N., 1987. *Soziale Systeme*. Suhrkamp, Frankfurt am Main.
- Mair, V., Zischg, A., Lang, K., Tonidandel, D., Krainer, K., Kellerer-Pirklbauer, A., Deline, P., Schoeneich, P., Cremonese, E., Pogliotti, P., Gruber, S., Boeckli, L., 2011. PermaNET - Permafrost Long-term Monitoring Network. Synthesis report. International Research Society INTERPRAEVENT, Klagenfurt.
- Mazzorana, B., Hübl, J., Zischg, A., Largiader, A., 2011. Modelling woody material transport and deposition in alpine rivers. *Nat Hazards* 56, 425–449. 10.1007/s11069-009-9492-y.
- Mazzorana, B., Levaggi, L., Keiler, M., Fuchs, S., 2012. Towards dynamics in flood risk assessment. *Nat. Hazards Earth Syst. Sci.* 12, 3571–3587. 10.5194/nhess-12-3571-2012.
- Mazzorana, B., Zischg, A., Largiader, A., Hübl, J., 2009. Hazard index maps for woody material recruitment and transport in alpine catchments. *Nat. Hazards Earth Syst. Sci.* 9, 197–209. 10.5194/nhess-9-197-2009.
- Merz, B., Hall, J., Disse, M., Schumann, A., 2010. Fluvial flood risk management in a changing world. *Nat. Hazards Earth Syst. Sci.* 10, 509–527. 10.5194/nhess-10-509-2010.
- Mosimann, M., Frossart, L., Keiler, M., Weingartner, R., Zischg, A., in revision. A robust and transferable model for the prediction of flood losses on household contents. *Water*.
- Müller-Hansen, F., Schlüter, M., Mäs, M., Donges, J.F., Kolb, J.J., Thonicke, K., Heitzig, J., 2017. Towards representing human behavior and decision making in Earth system models – an overview of techniques and approaches. *Earth Syst. Dynam.* 8, 977–1007. 10.5194/esd-8-977-2017.
- Munoz, S.E., Dee, S.G., 2017. El Niño increases the risk of lower Mississippi River flooding. *Scientific reports* 7, 1772. 10.1038/s41598-017-01919-6.
- Munoz, S.E., Giosan, L., Therrell, M.D., Remo, Jonathan W. F., Shen, Z., Sullivan, R.M., Wiman, C., O'Donnell, M., Donnelly, J.P., 2018. Climatic control of Mississippi River flood hazard amplified by river engineering. *Nature* 556, 95–98. 10.1038/nature26145.

- Nazemi, A., Wheater, H.S., 2015a. On inclusion of water resource management in Earth system models – Part 1: Problem definition and representation of water demand. *Hydrol. Earth Syst. Sci.* 19, 33–61. 10.5194/hess-19-33-2015.
- Nazemi, A., Wheater, H.S., 2015b. On inclusion of water resource management in Earth system models – Part 2: Representation of water supply and allocation and opportunities for improved modeling. *Hydrol. Earth Syst. Sci.* 19, 63–90. 10.5194/hess-19-63-2015.
- Neuwirth, C., 2017. System dynamics simulations for data-intensive applications. *Environmental Modelling & Software* 96, 140–145. 10.1016/j.envsoft.2017.06.017.
- Neuwirth, C., Peck, A., Simonović, S.P., 2015. Modeling structural change in spatial system dynamics: A Daisyworld example. *Environmental Modelling & Software* 65, 30–40. 10.1016/j.envsoft.2014.11.026.
- Palmer, P.I., Smith, M.J., 2014. Earth systems: Model human adaptation to climate change. *Nature* 512, 365–366. 10.1038/512365a.
- Papathoma-Köhle, M., Zischg, A., Fuchs, S., Glade, T., Keiler, M., 2015. Loss estimation for landslides in mountain areas – An integrated toolbox for vulnerability assessment and damage documentation. *Environmental Modelling & Software* 63, 156–169. 10.1016/j.envsoft.2014.10.003.
- Paprotny, D., Sebastian, A., Morales-Nápoles, O., Jonkman, S.N., 2018. Trends in flood losses in Europe over the past 150 years. *Nature communications* 9, 1985. 10.1038/s41467-018-04253-1.
- Pinter, N., Jemberie, A.A., Remo, Jonathan W. F., Heine, R.A., Ickes, B.S., 2008. Flood trends and river engineering on the Mississippi River system. *Geophys. Res. Lett.* 35, 1080. 10.1029/2008GL035987.
- Pinter, N., Jemberie, A.A., Remo, Jonathan W. F., Heine, R.A., Ickes, B.S., 2009. Cumulative impacts of river engineering, Mississippi and Lower Missouri rivers. *River Res. Applic.* 189, n/a-n/a. 10.1002/rra.1269.
- Pinter, N., van der Ploeg, Rienk R., Schweigert, P., Hofer, G., 2006. Flood magnification on the River Rhine. *Hydrol. Process.* 20, 147–164. 10.1002/hyp.5908.
- Probst, T., Wicki, W., Zischg, A., Pichler, A., 2013. Alpine strategy for adaptation to climate change in the field of natural hazards: Developed by the Platform on Natural Hazards of the Alpine Convention PLANALP. Alpine Convention, Innsbruck.
- Roos, M.M.D., Hartmann, T.T., Spit, T.T.J.M., Johann, G.G., 2017. Constructing risks – Internalisation of flood risks in the flood risk management plan. *Environmental Science & Policy* 74, 23–29. 10.1016/j.envsci.2017.04.007.
- Röthlisberger, V., Zischg, A., Keiler, M., 2016. Spatiotemporal aspects of flood exposure in Switzerland. *E3S Web Conf.* 7, 8008. 10.1051/e3sconf/20160708008.
- Röthlisberger, V., Zischg, A.P., Keiler, M., 2017. Identifying spatial clusters of flood exposure to support decision making in risk management. *Science of The Total Environment* 598, 593–603. 10.1016/j.scitotenv.2017.03.216.
- Röthlisberger, V., Zischg, A.P., Keiler, M., 2018. A comparison of building value models for flood risk analysis. *Nat. Hazards Earth Syst. Sci.* 18, 2431–2453. 10.5194/nhess-18-2431-2018.
- Rougé, C., Mathias, J.-D., Deffuant, G., 2015. Vulnerability: From the conceptual to the operational using a dynamical system perspective. *Environmental Modelling & Software* 73, 218–230. 10.1016/j.envsoft.2015.07.018.
- Sattler, K., Keiler, M., Zischg, A., Schrott, L., 2011. On the Connection between Debris Flow Activity and Permafrost Degradation: A Case Study from the Schnalstal, South Tyrolean Alps, Italy. *Permafrost and Periglac. Process.* 22, 254–265. 10.1002/ppp.730.

- Simonovic, S.P., 2009. Managing flood risk, reliability and vulnerability. *Journal of Flood Risk Management* 2, 230–231. 10.1111/j.1753-318X.2009.01040.x.
- Simonovic, S.P., 2011. *Systems Approach to Management of Disasters: Methods and Applications*, 1st ed. Wiley, s.l., 312 pp.
- Staffler, H., Pollinger, R., Zischg, A., Mani, P., 2008. Spatial variability and potential impacts of climate change on flood and debris flow hazard zone mapping and implications for risk management. *Nat. Hazards Earth Syst. Sci.* 8, 539–558. 10.5194/nhess-8-539-2008.
- Stoffel, M., Tiranti, D., Huggel, C., 2014. Climate change impacts on mass movements—case studies from the European Alps. *Sci. Total Environ.* 493, 1255–1266. 10.1016/j.scitotenv.2014.02.102.
- Thaler, T., Zischg, A., Keiler, M., Fuchs, S., 2018. Allocation of risk and benefits—distributional justices in mountain hazard management. *Reg Environ Change* 18, 353–365. 10.1007/s10113-017-1229-y.
- Tobin, G.A., Montz, B.E., 1994. THE FLOOD HAZARD AND DYNAMICS OF THE URBAN RESIDENTIAL LAND MARKET. *J Am Water Resources Assoc* 30, 673–685. 10.1111/j.1752-1688.1994.tb03322.x.
- UNISDR, 2015. *Making development sustainable: The future of disaster risk management*. United Nations, Geneva, 311 pp.
- Verburg, P.H., Dearing, J.A., Dyke, J.G., van der Leeuw, S., Seitzinger, S., Steffen, W., Syvitski, J., 2016. Methods and approaches to modelling the Anthropocene. *Global Environmental Change* 39, 328–340. 10.1016/j.gloenvcha.2015.08.007.
- Vitousek, P.M., 1997. Human Domination of Earth's Ecosystems. *Science (New York, N.Y.)* 277, 494–499. 10.1126/science.277.5325.494.
- Voinov, A., Shugart, H.H., 2013. 'Integronsters', integral and integrated modeling. *Environmental Modelling & Software* 39, 149–158. 10.1016/j.envsoft.2012.05.014.
- Werner, B.T., McNamara, D.E., 2007. Dynamics of coupled human-landscape systems. *Geomorphology* 91, 393–407. 10.1016/j.geomorph.2007.04.020.
- Wingo, P., Brookes, A., Bolte, J., 2017. Modular and spatially explicit: A novel approach to system dynamics. *Environmental Modelling & Software* 94, 48–62. 10.1016/j.envsoft.2017.03.012.
- Winsemius, H.C., Aerts, Jeroen C. J. H., van Beek, Ludovicus P. H., Bierkens, Marc F. P., Bouwman, A., Jongman, B., Kwadijk, J.C.J., Ligtoet, W., Lucas, P.L., van Vuuren, D.P., Ward, P.J., 2015. Global drivers of future river flood risk. *Nature Climate change*. 10.1038/nclimate2893.
- Zischg, A., 2016. River corrections and long-term changes in flood risk in the Aare valley, Switzerland. *E3S Web Conf.* 7, 11010. 10.1051/e3sconf/20160711010.
- Zischg, A., 2018. Floodplains and Complex Adaptive Systems—Perspectives on Connecting the Dots in Flood Risk Assessment with Coupled Component Models. *Systems* 6, 9. 10.3390/systems6020009.
- Zischg, A., Felder, G., Weingartner, R., Gómez-Navarro, J.J., Röthlisberger, V., Bernet, D., Rössler, O., Raible, C., Keiler, M., Martius, O., 2016. M-AARE - Coupling atmospheric, hydrological, hydrodynamic and damage models in the Aare river basin, Switzerland, in: 13th Congress INTERPRAEVENT 2016, 30 May to 2 June 2016, Lucerne, Switzerland. Conference proceedings, vol. 2016, pp. 444–451.
- Zischg, A., Galatioto, N., Deplazes, S., Weingartner, R., Mazzorana, B., 2018a. Modelling Spatio-temporal Dynamics of Large Wood Recruitment, Transport, and Deposition at the River Reach Scale during Extreme Floods. *Water* 10, 1134. 10.3390/w10091134.

-
- Zischg, A., Mair, V., Lang, K., 2012a. PROALP - Kartierung und Monitoring von Permafrost in der Autonomen Provinz Bozen Südtirol, Italien. Conference proceedings INTERPRAEVENT 2012, Grenoble, France 12, 1–12.
- Zischg, A., Mair, V., Lang, K., Deline, P., Ravanel, L., Schoeneich, P., Kellerer-Pirklbauer, A., 2012b. Consideration of permafrost and permafrost degradation in natural hazards assessment. Conference proceedings INTERPRAEVENT 2012, Grenoble, France 12, 1–12.
- Zischg, A., Schober, S., Sereinig, N., Rauter, M., Seymann, C., Goldschmidt, F., Bäk, R., Schleicher, E., 2013. Monitoring the temporal development of natural hazard risks as a basis indicator for climate change adaptation. *Nat Hazards* 67, 1045–1058. 10.1007/s11069-011-9927-0.
- Zischg, A.P., Felder, G., Mosimann, M., Röthlisberger, V., Weingartner, R., 2018b. Extending coupled hydrological-hydraulic model chains with a surrogate model for the estimation of flood losses. *Environmental Modelling & Software* 108, 174–185. 10.1016/j.envsoft.2018.08.009.
- Zischg, A.P., Felder, G., Weingartner, R., Quinn, N., Coxon, G., Neal, J., Freer, J., Bates, P., 2018c. Effects of variability in probable maximum precipitation patterns on flood losses. *Hydrol. Earth Syst. Sci.* 22, 2759–2773. 10.5194/hess-22-2759-2018.
- Zischg, A.P., Hofer, P., Mosimann, M., Röthlisberger, V., Ramirez, J.A., Keiler, M., Weingartner, R., 2018d. Flood risk (d)evolution: Disentangling key drivers of flood risk change with a retro-model experiment. *Sci. Total Environ.* 639, 195–207. 10.1016/j.scitotenv.2018.05.056.
- Zischg, A.P., Mosimann, M., Bernet, D.B., Röthlisberger, V., 2018e. Validation of 2D flood models with insurance claims. *Journal of Hydrology* 557, 350–361. 10.1016/j.jhydrol.2017.12.042.

References
